Vol. 19, No. 4, December, 2020
ISSN (Print): 0972-6268; ISSN (Online) : 2395-3454

# Nature Environment & Pollution Technology

A Multidisciplinary, International Journal on Diverse Aspects of Environment

Technoscience Publications
website: www.neptjournal.com

Technoscience Publications
A-504, Bliss Avenue, Balewadi,
Opp. SKP Campus, Pune-411 045
Maharashtra, India

www.neptjournal.com

# Nature Environment and Pollution Technology

**(An International Quarterly Scientific Research Journal)**



**Published by** : Mrs. T. P. Goel, B-34, Dev Nagar, Tonk Road, Jaipur-302 018 Rajasthan, India

**Managing Office** : Technoscience Publications, A-504, Bliss Avenue, Balewadi, Pune-411 045, Maharashtra, India

**E-mail** : contact@neptjournal.com; journalnept@gmail.com

## INSTRUCTIONS TO AUTHORS

### Scope of the Journal

The Journal publishes original research/review papers covering almost all aspects of environment like monitoring, control and management of air, water, soil and noise pollution; solid waste management; industrial hygiene and occupational health hazards; biomedical aspects of pollution; conservation and management of resources; environmental laws and legal aspects of pollution; toxicology; radiation and recycling etc. Reports of important events, environmental news, environmental highlights and book reviews are also published in the journal.

### Format of Manuscript

- The manuscript (*mss*) should be typed in double space leaving wide margins on both the sides.
- First page of mss should contain only the title of the paper, name(s) of author(s) and name and address of Organization(s) where the work has been carried out along with the affiliation of the authors.

*Continued on back inner cover...*

# Nature Environment and Pollution Technology

**Vol. 19, No. (4), December 2020**


## CONTENTS

# The Journal is Currently Abstracted and Indexed in:

- International Scientific Indexing (UAE) with Impact Factor 2.236 (2018)
- NAAS Rating of the Journal (2019) = 3.85
- Scopus®, SJR (0.127) 2019
- Index Copernicus (2018) = 135.97
- EI Compendex of Elsevier
- Indian Science Abstracts, New Delhi, India
- Chemical Abstracts, U.S.A.
- Elsevier Bibliographic Databases
- Pollution Abstracts, U.S.A.
- Paryavaran Abstract, New Delhi, India
- Zoological Records
- Indian Citation Index (ICI)
- Scopus CiteScore (2019) = 0.5
- Electronic Social and Science Citation Index (ESSCI)
- EBSCO: Environment Index™
- Ulrich's (Refereed) database
- CrossRef (DOI)
- DOAJ
- Zetoc
- Google Scholar
- ProQuest, U.K.
- J-Gate
- Environment Abstract, U.S.A.
- British Library
- Centre for Research Libraries
- WorldCat (OCLC)
- JournalSeek
- Connect Journals (India)
- CSA: Environmental Sciences and Pollution Management
- Research Bible (Japan)
- Indian Science
- Geobase
- Elektronische Zeitschriftenbibliothek (EZB)
- SHERPA/RoMEO
- Directory of Science
- CNKI Scholar (China National Knowledge Infrastructure)
- Access to Global Online Research in Agriculture (AGORA)
- AGRIS (UN-FAO)
- Full papers are available on the Journal's Website: www.neptjournal.com
- UDL-EDGE (Malaysia) Products like *i*-Journals, *i*-Focus and *i*-Future

**www.neptjournal.com**

# Nature Environment and Pollution Technology

Nature Environment and Pollution Technology
An International Quarterly Scientific Journal

p-ISSN: 0972-6268
(Print copies up to 2016)
e-ISSN: 2395-3454

Vol. 19 | No. 4 | pp.1343-1354 | 2020

Original Research Paper

https://doi.org/10.46488/NEPT.2020.v19i04.001

Open Access Journal

# Realistic Decontamination of $Fe^{2+}$ Ions from Groundwater Using Bentonite/ Chitosan Composite Fixed Bed Column Studies

**M.E.M. Hassouna*† and M. H. Mahmoud****
*Chemistry Department, Faculty of Science, Beni-Suef University 62514, Beni-Suef, Egypt
**Potable Water & Sanitation Company, Beni-Suef, Egypt
†Corresponding author: M.E.M. Hassouna; mhassouna47@hotmail.com; mohamed.hassona@science.bsu.edu.eg

**Nat. Env. & Poll. Tech.**
**Website: www.neptjournal.com**

*Received:* 21-11-2019
*Revised:* 13-12-2019
*Accepted:* 01-03-2020

**Key Words:**
Bentonite
Chitosan
Adsorption
Fixed bed column

## ABSTRACT

Bentonite/chitosan composite was synthesized and characterized by different techniques including XRD, FT-IR, SEM and TEM to detect its physicochemical properties. The composite was introduced in realistic purification application to reduce the dissolved iron content in raw groundwater sample by fixed-bed column system. The plotted breakthrough curves and the related mathematical parameters revealed that the column achieves iron removal percentage of about 69% from 6.6 L of water after adjusting the factors affecting the system at 3 cm bed thickness, 5 mL/min flow rate, 5 mg/L concentration and pH 6. Applying the column system to remove iron from groundwater under the same conditions can achieve iron removal percentage of about 69% from a total volume of 8.2 L of water. The interaction of the metal on the column was attained after 18 hours and the saturation time was attained after 27.5 hours which revealed the high performance of the composite in the designed column system for the purification of groundwater.

## INTRODUCTION

In later periods, the contamination of the water supplies represents the main challenge that faces the modern communities and the contemporary world to provide safe water for populations (Mohamed et al. 2018). One of the commonly recorded water pollutants is the presence of dissolved metal ions that are reported as toxic, non-degradable and having a high tendency to accumulate in the living tissues (Abukhadra et al. 2019a). $Fe^{+2}$ and $Mn^{+2}$ ions are dissolved salts detected extensively in the groundwater wells, especially in the deep ones that are poor in dissolved oxygen.

It was reported that iron ions can be present as dissolved $Fe^{2+}$ or as undissolved species such as $Fe(OH)_3$ (Hassouna et al. 2017, Barloková & Ilavsky 2010). The existence of $Fe^{2+}$ pollutants within the water supplies at high concentrations can reduce the water purity and affect negatively the human health (Ehssan 2012, Al-Anber 2010). Additionally, the common oxidation of $Fe^{2+}$ ions resulted in precipitation of hydroxide suspensions that produce unpleasant colour and taste. Their role in the turbidity of the water supplies was reported (Homoncik et al. 2010). Moreover, the precipitated hydroxide species can cause the generation of some toxic derivatives that commonly resulted in several types of diseases including neoplasia, arthropathy, cardiomyopathy, oliguria, anorexia, neurological disorder and biphasic shock (Sarin et al. 2004, Takeda 2003). The accepted value for the concentrations of $Fe^{2+}$ is recommended not to exceed 0.3 mg/L due to the previous side effects (Abd ElSalam et al.2019). However, the European Union set 0.2 mg/L of iron as the maximum limit in drinking water (European Union 1998).

Biological treatment, oxidation, ion exchange, adsorption and membrane filtrations are the commonly investigated methods in the decontamination of $Fe^{2+}$ (Pathania et al. 2016). Among all the stated technologies, the use of low-cost adsorbents was recommended by numerous researchers as simple and highly effective techniques (Yang et al. 2017, Albadarin et al. 2017). Therefore, several types of natural and synthetic materials were introduced for this target as heulandite, clinoptilolite, bentonite, kaolinite, activated carbon, synthetic zeolite, fly ash, metal oxide and mesoporous silica (Hethnawi et al. 2018, Mohamed et al. 2018).

Bentonite is a common type of clays that can be identified as fine-grained sedimentary rocks and is composed mainly of smectite clay minerals in addition to quartz, and feldspar as associated impurities (Li et al. 2016). It was applied widely as an adsorbent for metal ions as well as other inorganic and organic contaminants. This was attributed to its reported unique properties of flexible chemical and crystalline structure, remarkable surface area, superior adsorption capacities and proved environmental value (Abukhadra et al. 2019 b). Although previous studies were reported about the decon-

tamination of metals by bentonite, numerous studies were conducted to upgrade its adsorption capacities by chemical or physical modification processes (Amadio et al. 2017).

Integration between bentonite and biogenic polymers in hybrid material or composite was investigated as a potential technique to improve the bentonite properties and maximize its uptake capacity (Wang et al. 2016, Jaymand 2014, Bober et al. 2010). Kamińska (2018) has performed efficient removal of organic micro pollutants with different properties from WWTP (wastewater treatment plant) effluent in fixed bed columns packed with several combinations of sand, granular activated carbon (GAC), and granular clay-carbonaceous composite. Two types of bentonite-powder activated carbon-based granules (Ben-AC) were prepared with different calcination temperatures. It was found that higher calcination temperature enhanced the surface porosity and adsorption potential versus studied micro pollutants due to dehydroxylation resulting in higher chemical activity.

Chitosan was studied as one of the best used biogenic polymers that can be integrated with clays in effective and eco-friendly composite (Abukhadra et al. 2019b). Chitosan is a common natural polyaminosaccharide that can be extracted from chitan and has several environmental and technical advantages. It has the advantages of nontoxicity, biocompatibility, biodegradability, bioactivity, high adsorption properties, high physical and mechanical performance (Ngah et al. 2010). Thus, the integration between chitosan and bentonite can be resulted in the development of novel materials of higher adsorption properties than the individual phases (Liu et al. 2014, Tirtom et al. 2012).

Fixed-bed column using chitosan immobilized on bentonite has been used for the removal of copper (Futalan et al. 2011a) and Ni (Futalan et al. 2011b). Chitosan/bentonite/MnO composite beads in fixed-bed operation has been used for manganese removal from water (Muliwa et al. 2018). Adsorption of Pb (II), Cu (II), and Ni (II) from aqueous solution using Chitosan-Coated Bentonite has been performed using fixed bed (Futalan et al. 2012, Tsai et al. 2016). It has been, also, used for the removal of nitrates (Golie et al. 2018). Giannakas & Pissanou (2018) reviewed the use of Chitosan/Bentonite Nanocomposites for wastewater treatment.

Kaolinite nanotubes (KNTs) were synthesized from kaolinite by ultrasonic scrolling (Abukhadra et al. 2019c). KNTs were used as adsorbents for $Zn^{2+}$, $Cd^{2+}$, $Pb^{2+}$, and $Cr^{6+}$ with uptake capacities of 103 mg/g, 116 mg/g, 89 mg/g, and 91 mg/g, respectively.

Arsenic removal has received much attention all over the world because of its toxicity and carcinogenicity (Barakan et al. 2019). As (V) has been adsorbed from aqueous solution onto Fe(III)-impregnated bentonite (Fe-Bent).

Thus, this study aims to introduce realistic treatment and purification of raw groundwater from iron pollutants through fixed bed column based on synthetic bentonite/chitosan composite as low cost and eco-friendly adsorbent. The controlling factors including the pH, bed thickness, flow rate and initial concentrations were studied in details to set the best operating conditions. Moreover, two kinetic models were evaluated to describe the studied system.

## MATERIALS AND METHODS

The used bentonite was collected as representative sample from bentonite quarry, Northern Western Desert, Egypt. Chitosan was delivered as a commercial polymer material by Winlab Company. The used standard iron certified reference (CRM) was obtained from Merck Co. (Germany). Glacial acetic acid (Sigma-Aldrich, 99.8%) was used as dissolvent for chitosan. NaOH pellets and hydrochloric acid solution were used as pH modifiers and were delivered by El-Nasr Company, Egypt for chemical products. The incorporated chemicals in all the experimental tests are of analytical grade and were applied directly without purification.

### Synthesis of Bentonite/Chitosan Composite

The fabrication of the composite has involved the grinding of the raw bentonite by ball mill to fine particles in the size range of 100 μm to 20 μm followed by mechanical mixing with chitosan gel according to (Abukhadra et al. 2019a). This was accomplished by dispersion of 5 g of bentonite powder in about 100 mL of distilled water for 1 h under speed stirring (1000 rpm). Then the bentonite mixture was mixed with chitosan gel that was formed by dissolving 2.5 g of chitosan in about 50 mL of acetic acid (0.1M) and stirred for another 2 h fixing the speed at 1000 rpm. After that, the mixture was treated by ultrasonic waves for (5 h) to accelerate and confirm the intercalation of bentonite sheets by chitosan chains (Fig. 1). Finally, the product was separated and dried at 60°C for 10 h and kept for further characterization and application.

### Characterization Techniques

The crystalline properties were studied based on the obtained X-ray diffraction patterns of bentonite, chitosan and bentonite/chitosan composite using X-ray diffractometer [PANalytical (Empyrean)]. External morphological properties and the internal structure after the intercalation process were studied using Scanning-Electron Microscope (Gemini, Zeiss-Ultra 55) and Transmission-Electron Microscope (JEOL-JEM2100). The change in the active functional groups before and after the intercalation process was inspected by Bruker spectrometer FT-IR (Vertex 70).

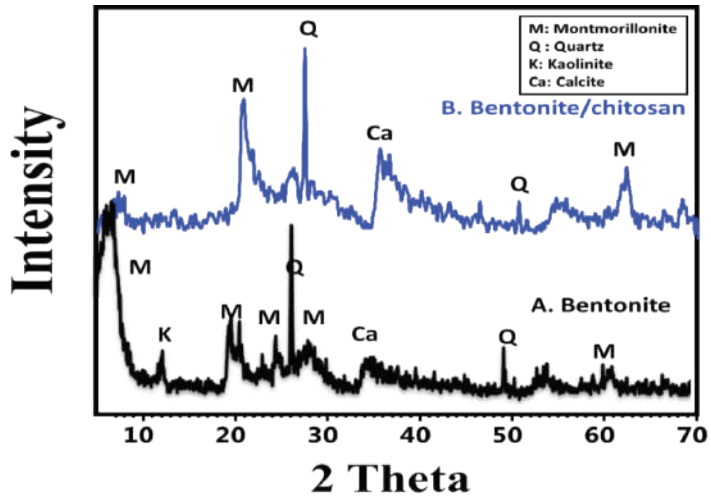


Fig. 1: XRD patterns of bentonite (A) and bentonite/chitosan composite (C).

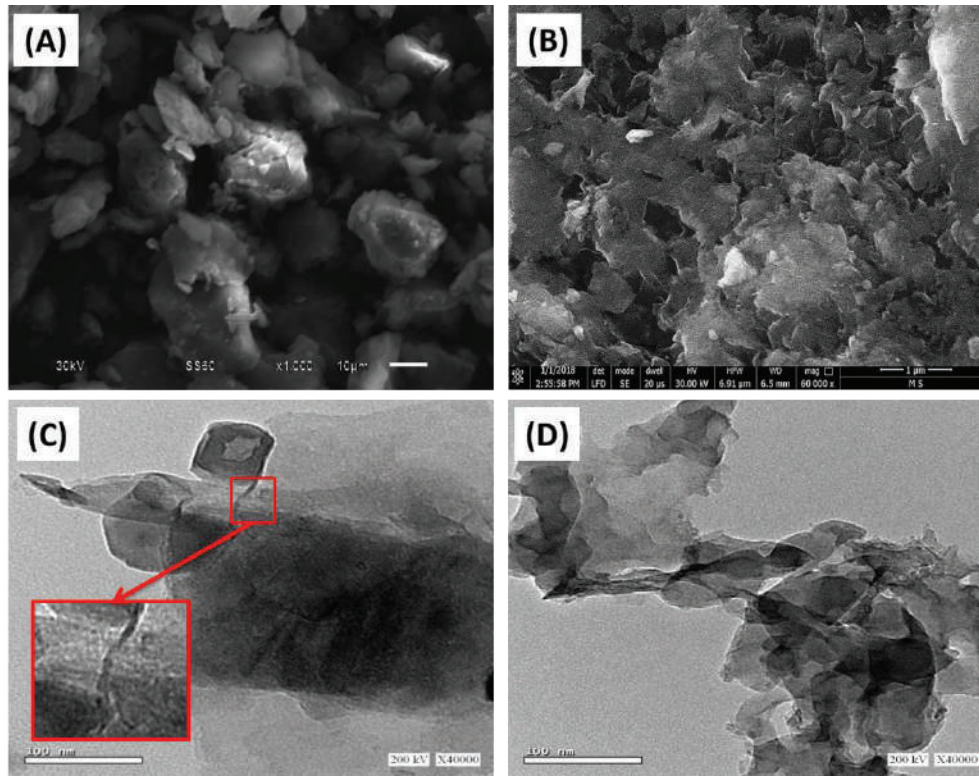


Fig. 2: SEM images of bentonite (A) and bentonite/chitosan composite (B); and the TEM images (C) and (D).

The residual iron concentrations after the test were estimated using inductively coupled plasma mass spectrometer (ICP-MS; Perkin Elmer) with detection limit of about 0.1 mg/L. The reference solutions which were used match the requirements of CRM standard iron of the National institute of standard and technology. The measured results are the average values obtained after triplicate tests with a standard deviation lower than 6 %.

### Adsorption Tests

**Collecting the raw water samples:** The groundwater samples were collected from different groundwater wells in Beni-Suef Governorate, Middle Egypt. The samples were set in polypropylene containers that were washed using dilute nitric acid and then rinsed using distilled water. Then, water samples were acidified by nitric acid to reduce the pH value to be less than 2 as critical step to avoid the possible adsorption of $Fe^{2+}$ on the polypropylene walls of the used containers (APHA 1999). Then the preserved samples were kept in a refrigerator at about 4°C to avoid the predicted evaporation at room temperature.

### Fixed Bed Column Study

**Designing the column system:** The used column system was composed of glass cylinder with 2 cm internal diameter and 15 cm length ending with an outlet leading to a pump (Fig. 4). The bentonite/chitosan bed was packed and inserted in the glass between two separated layers of polyethylene wool supported by plastic mesh to avoid the leaching of the adsorbent particles.

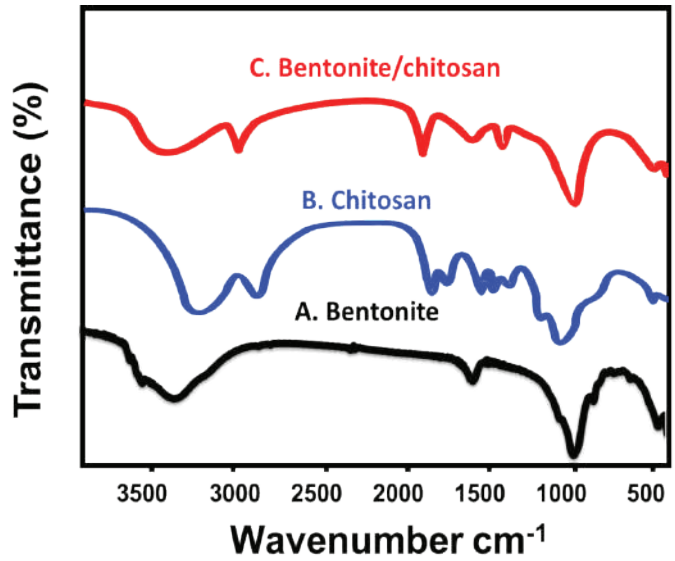


Fig. 3: FT-IR spectra of bentonite (A), chitosan (B) and bentonite/chitosan composite (C).

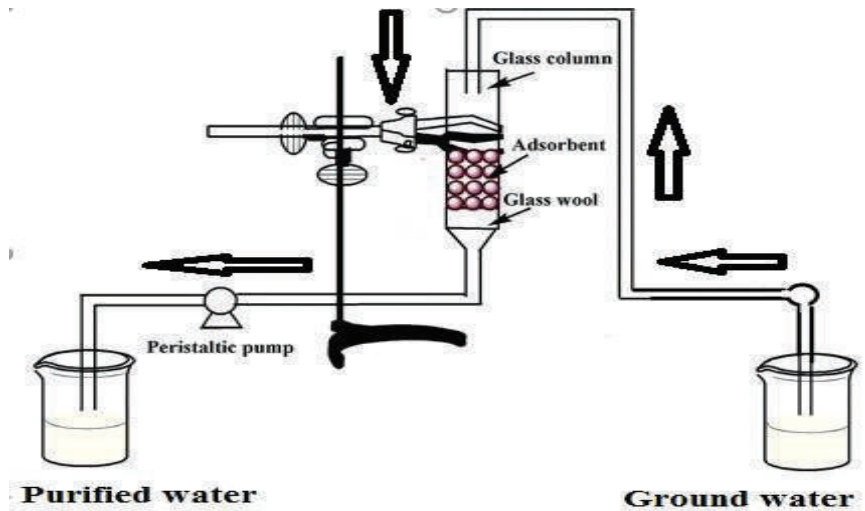


Fig. 4: Fixed-bed column.

Water samples were pumped through the column and after regular intervals of (60 min), the filtrated waters were collected to measure the residual metal concentrations. The controlling factors were studied considering pH within a range from (3 to 7), and the other factors were adjusted at 0.02 g of bentonite/chitosan mass, 100 mL solution volume, time of 120 min and 10 mg/L concentration. The bed height (thickness) was studied within a range from 1-3 cm after fixing the other conditions at 10 mg/L concentration, 5 mL/min flow rate and 1440 min total filtration time. Also, the influence of flow rate was studied within a range from 5 mL/min to 15 mL/min at fixed values of 3 cm bed thickness, 10 mg/L concentration and 24 hours total time. Finally, the effect of concentration was studied within a range from 5 mg/L to 15 mg/L at fixed values of 3 cm thickness, 5 mL/min flow rate and 24 hours total filtration time.

**Fixed bed column data analysis:** The performance of bentonite/chitosan-based column system was checked according to the theoretical parameters of the plotted curves for residual concentration ($C_{eff}$)/ initial concentration ($C_o$) versus the filtration time. The breakthrough points and exhausted points of the curves were estimated at $C_{eff}$ of about 10 % and $C_o$ of about 95 %, respectively. The obtained volumes of the effluents ($V_{eff}$ (mL)) were measured from Eq.(1) (Zhang et al. 2015):

$$V_{eff} = Q\ x\ t_{total} \quad \ldots(1)$$

Where Q denotes the volumetric flow rate in mL/min and $t_{total}$ is the flow time. All the mathematical parameters of the system were estimated according to the linear equations from Eq.(2) to Eq.(6) (Abukhadra et al. 2019b).

$$C_{ad} = C_o - C_{eff} \quad \ldots(2)$$

$$q_{total}(mg) = \frac{QA}{1000} = \frac{Q}{1000}\int_{t=0}^{t=t_{total}} C_{ad}\, dt \quad \ldots(3)$$

$$M_{total}(mg) = \frac{CQt_{total}}{1000} \quad \ldots(4)$$

$$q_{eq}(mg/g) = \frac{q_{total}}{X} \quad \ldots(5)$$

$$Total\ removal\ .,\%\ (R.,\%) = \frac{q_{total}}{M_{total}}\ 100 \quad \ldots(6)$$

Where the symbols denote the adsorbed ions ($C_{ad}$), total adsorbed ions ($q_{total}$), the area of the plotted breakthrough curves (A), the total pumped ions in the system ($M_{total}$), the uptake equilibration ($q_{eq}$) and the used bentonite/chitosan mass (X).

## RESULTS AND DISCUSSION

### Characterization

**Structural properties:** The structural and crystalline properties of bentonite and bentonite/chitosan composite were inspected based on the obtained XRD pattern (Fig.1). The used raw sample of bentonite showed XRD pattern with characteristic peaks of montmorillonite as the main clay mineral of the smectite group and as the dominant component of the sample in addition to other crystalline phases of kaolinite, calcite and quartz minerals that can be identified as impurities. Montmorillonite minerals were detected with their identification peaks at different temperatures as 6.54°C, 19.84°C, 25°C and 28.34°C, respectively that are related to the lattice planes of (002), (020) and (105), respectively (card No: 00-003-0010).

The intercalation of chitosan chains between bentonite layers was reflected in the resulted XRD pattern as the peaks that were deviated from their normal positions and the main peak was detected at 6.3° with low diffraction intensity. The recorded increase in the d-spacing to 13.91Å for bentonite/chitosan composite as compared to 13.486Å for raw bentonite revealed successful fabrication of the bentonite/chitosan composite by intercalation process.

**Morphological properties:** The morphological properties of bentonite and bentonite/chitosan composite were studied using SEM and TEM images. The SEM images reflected the presences of bentonite as compacted sheets of montmorillonite and decorated by tiny nudes related to the associated mineral impurities (Fig. 2A). The intercalation of montmorillonite sheets by chitosan revealed considerable changes in the surface morphology of bentonite. The surface of the composite exhibits a network structure of noticeable interstitial microspores in addition to irregular fibrous particles related mainly to the admixed chitosan (Fig. 2B). The integration between bentonite and chitosan also was confirmed by TEM images (Fig. 3). The studied bentonite particles are of multi-layered structure and showed characteristic lattice fingers (Fig. 3B). After the integration between it and chitosan chains, the composite appeared as hybrid material composed of bentonite sheets and fibrous particles of chitosan (Fig. 3C).

However, several studies revealed the reduction in the specific area after the modification of bentonite by chitosan, the synthetic composite in the introduced study declared slight enhancement in it as it increased from 91 $m^2/g$ for raw bentonite to 98.44 $m^2/g$ for bentonite/chitosan composite, respectively. This can be explained by the reported formation of bentonite/chitosan composite as an interlocked network structure forming a secondary porous matrix.

**Chemical functional groups:** The changes in the chemical functional groups were monitored based on the FT-IR spectra of bentonite and bentonite/chitosan composite, the main groups are displayed in Table 1. The main chemical groups of

clay minerals were identified in the bentonite sample as OH, Si-O-Si, and Al-O (Table 1). Also, chitosan as single-phase was identified by its characteristic amide, aliphatic C-H, N-H, and C-O groups. The integration between the bentonite layers and chitosan chains also was reflected in the FT-IR results. The obtained bands revealed the formation of hybrid material of heterogeneous functional groups related to both bentonite and chitosan (Table 1). Additionally the appearance of such mixed bands associated with clear deviation from their normal positions confirming the successful intercalation of bentonite layer by chitosan (Fig. 3 and Table 1).

## Fixed Bed Column Studies

The initial pH plays a vital role in controlling the surface properties of the adsorbent as well as the speciation of the dissolved metals (Seliem et al. 2016, Ozdes et al. 2009). The influence of pH on the uptake properties of bentonite chitosan for $Fe^{2+}$ ions was studied within the pH range from 2 to 7 to avoid the possible precipitation of iron at the high alkaline conditions (Ehssan 2012). The experimental results declared continuous enhancement in the removal percentages of iron with the regular expanding in the pH value achieving the best results at the highest pH 7. The removal percentages were augmented by 26 %, 40 %, 64 %, 78 % and 80 % with the increment of pH.

This makes it a promising material for realistic purification of polluted water resources. The previous behaviour can be elucidated based on the proton-competitive adsorption phenomenon at the different studied pH conditions. The regular increase in the value of pH associated with a noticeable reduction in the concentration of the present hydronium ions that act as competitors with adsorbed metal ions and in turn promotes the uptake of $Fe^{2+}$ ions by bentonite/chitosan composite (Sprynskyy et al. 2006). Moreover, the alkaline conditions can accelerate the dissociation of the counter ions within the clay matrix which can reduce the uptake capacities (Hassouna et al. 2014). Fig. 4 shows a detailed diagram for the fixed bed column.

## Effect of Bed Thickness

The obtained breakthrough curves with the different thicknesses of the bentonite/chitosan bed are illustrated in Fig. 5B. Generally, the column performance shows noticeable enhancing with the regular increment in the bed thickness. The obtained breakthrough time ($t_b$) for the treated solutions was enhanced by 27, 37.5 and 42.5 hours with the regular increment in the bentonite/chitosan bed thickness by 1, 2 and 3 cm, respectively. Also, this was reflected in the obvious increment in the required time till saturation or the exhausting of the column to be 45, 52.5 and 55 hours, for the same thickness in order (Table 1). The previous observations reflected the possible enhancing in the lifetime and the operation of bentonite/chitosan-based column with the regular increase in its thickness of the bed as well as the treated water volumes.

The quantities of the adsorbed $Fe^{2+}$ ions by bentonite/chitosan bed of 1, 2 and 3 cm thicknesses were 592, 737 and 947 mg, respectively, which was reflected in the total removal percentage of iron ions. The resulted total removal percentages by the end of the filtration time were 40.8 %, 50.75 % and 65.2% corresponding to bentonite/chitosan beds with thicknesses of 1, 2 and 3 cm, respectively. This was related to the role of the high bed thickness in reducing the axial dispersions of mass transfer and in turn, promote the diffusion of $Fe^{2+}$ ions onto the synthetic bentonite/chitosan

Table 1: FT-IR spectral bands and the related functional groups of bentonite, chitosan, and bentonite/chitosan composite.

| Band Positions ($cm^{-1}$) | | | Chemical functional group |
|---|---|---|---|
| BE | CH | BE/CH | |
| 3480 | - | 3494 | Attributed to the OH group of the crystal structure and water absorbed by bentonite (Abukhadra et al. 2019) |
| - | 3387.5 | - | Overlap between OH and N-H (Zhu et al. 2009) |
| - | 2911 | 2916.3 | Stretching of aliphatic C-H (Zhu et al. 2009) |
| - | 1653 | 1651.4 | Bending of N-H group (Liu et al. 2015) |
| 1640.6 | - | 1644.5 | Water within the interlayers |
| - | 1452 | 1455 | Bending of N-H group (Abukhadra et al. 2019) |
| - | 1373 | - | Bending of C-H group (Abukhadra et al. 2019) |
| - | 1084 | - | Stretching of C-O group (Liu et al. 2015) |
| 1000 | - | 1022.4 | Si-O group (Hassouna et al. 2017) |
| 918 | - | - | Al-O groups (Abukhadra et al. 2018) |
| 400-1000 | - | 400-100 | Mg-$Fe^{2+}$-OH, Si-O-Al and Si-O-Mg groups (Abukhadra et al. 2018) |

composite as an adsorbent (Mohan et al. 2017). Therefore, the pumped polluted solutions spent high time intervals in close contact with the bentonite/chitosan composite. Also, using high bed thickness increases the number of active uptake sites which increase the quantities of captures of iron ions.

**Determination of Adsorption Isotherm Parameters**

At room temperature, the required quantity (in gram) of the investigated adsorbent is added to a 1 L of the contaminated water sample.

The adsorption was performed with constant stirring of the reaction medium using jar test Phipps bride stirrer (Model 7790-402, USA). After a certain time, the solution with dispersed adsorbent was filtered. The experiment was carried out using different doses of the adsorbent (10-1000 ppm) for different time intervals. An aliquot of 10 mL was taken for the ICP measurements. Adsorption isotherm of the investigated metal ions ($Fe^{+2}$) by the prepared column was determined over a wide range of metal ion concentrations. The adsorption isotherm curves and adsorption parameters were calculated using Langmuir and Freundlich models (Dada et al. 2012).

$$q_e = \frac{Q_m\, bC_e}{1+ C_e}$$ Non-linear form $$\frac{C_e}{q_e} = \frac{C_e}{Q_m} + \frac{1}{Q_m\, b}$$ linear form

Both $Q_m$ and b are calculated from the slope and intercept of the linear relationship between $C_e/q_e$ and $C_e$ respectively.

Freundlich adsorption model is $q_e = Kf\, C_e 1/n$ nonlinear form but the linear form is

$$\log q_e = \log Kf + (1/n) \log C_e.$$

Both Kf and n are calculated from the intercept and slope of the linear relationship of double logarithmic of $q_e$ and $C_e$.

Where, $q_e$ is the equilibrium concentration of adsorbed metal ion on polymer surface (mg/g). $C_e$ is the bulk concentration of metal ion at equilibrium (mg/L). $Q_m$ is the monolayer adsorption capacity (mg/g), b is a constant related to the adsorption equilibrium constant and Kf & n are dimensionless constants refer to the adsorption capacity and adsorption intensity respectively.

**Adsorption isotherms**: The effect of metal ion concentrations on the removal efficiency of the investigated polymeric sample was studied. The quantity of the polymers was kept constant at 50 ppm at room temperature. Both, the Langmuir model which describes the monolayer adsorbate on

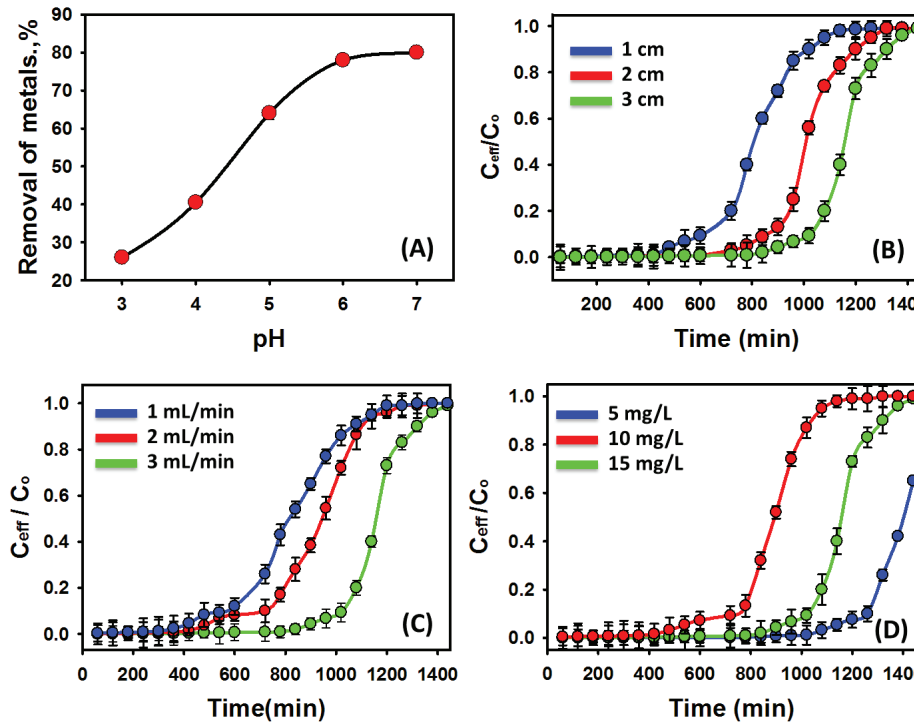


Fig. 5: Effect of solution pH on the removal of iron from water (A), removal of iron at different bed thickness (B), at different operating flow rates (C) and at different initial bentonite/chitosan concentrations (D).

the surface of the adsorbent and Freundlich model which describes the multilayer adsorptions have been investigated. The linear relationships of both isotherm models are graphically presented in Figs. 6 and 7, from which the Langmuir and Freundlich isotherm parameters were calculated and given in Table 3.

**Effect of Flow Rate**

The performance of bentonite/chitosan-based column system using different flow rates for the studied iron polluted solutions was presented graphically in Fig.5C and the related theoretical parameters are listed in Table 1. The performance of the system was largely affected by increasing the solution flow rate, as the time was decreased by 42.5, 30 and 25 hours by expanding the flow rate by 5, 10 and 15 mL/min, respectively. Additionally, the saturation time or the column exhaustion interval was reduced significantly by 57, 50 and 47.5 hours for the same studied flow rates in the order which will reduce the lifetime of the system.

However, on increasing the flow rates of the pumped solution associated with an observable increment in the total purified volumes, there was a noticeable reduction in the total removal percentage of $Fe^{2+}$ ions, upon which 5 mL/min was set as the best flow rate for the bentonite/chitosan fixed-bed column system (Table 2). The reported results for the influence of higher flow rates in reducing the residence time between the composite bed and iron polluted solution have affected negatively the required contact time for promising uptake of dissolved $Fe^{2+}$ ions (Nazaria et al. 2016). The slower flow rates provide long residence times for effective diffusion of $Fe^{2+}$ ions between the composite grains which increase the uptake chances by more active adsorption sites (Abdolali et al. 2017).

**Effect of Initial Concentration**

The influence of iron concentrations on the studied bentonite/chitosan-based column system was investigated using three different concentrations (5, 10, 15 mg/L). The results were plotted in breakthrough curves (Fig. 5D) and the related theoretical parameters were estimated and listed in Table 1. The plotted curves emphasized the obvious reduction in breakthrough as well as the saturation time with the increment in $Fe^{2+}$ concentration from 5 mg/L to 15 mg/L. Such behaviour was explained by several authors to be a result of the large concentration gradient and the low mass transfer resistance that is associated with using high concentrations of the inspected pollutants in addition to the expected saturation of the composite adsorption sites by the adsorbed $Fe^{2+}$ ions (Abdolali et al. 2017). Therefore, the performance of the column and its lifetime affected negatively the over increase in the concentrations of the dissolved water pollutants.

**Purification of Raw Groundwater Samples**

The purification of real groundwater sample was performed after adjusting the controlling factors at 3 cm for the bentonite/chitosan composite bed thickness, 5mL/min as flow rate and pH 7 for total filtration time of 7 hours. The chemical analysis of the studied real groundwater sample

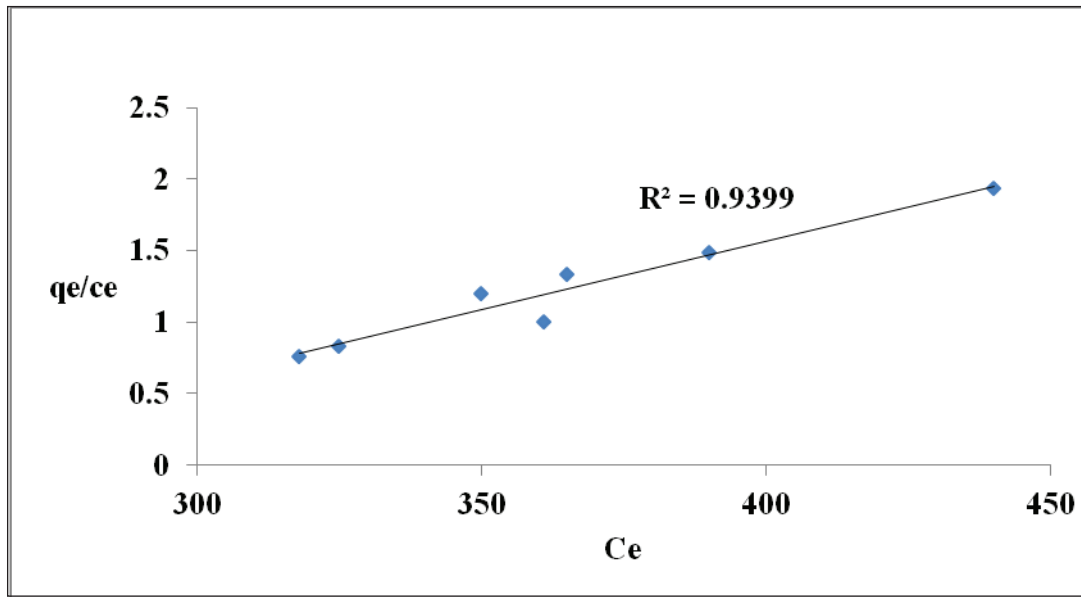


Fig. 6: Langmuir isotherm plot of iron adsorption.

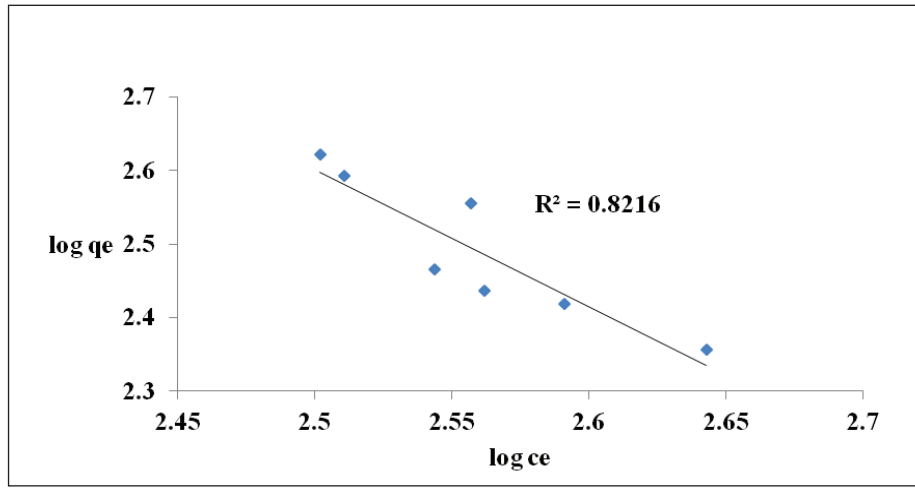


Fig. 7: Freundlich isotherm plot of iron adsorption

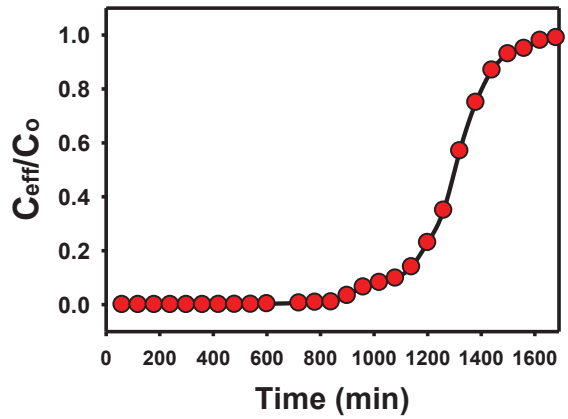


Fig. 8: The removal of iron from raw groundwater samples.

Table 2: Mathematical parameters of bentonite/chitosan continuous fixed-bed column system.

| Bed height | Flow rate | Conc. | $C_{ad}$ (mg/L) | q ($_{total}$) mg | $q_{eq}$ (mg/) | M $_{(total)}$ Mg | R. (%) | $t_b$ (min) | $t_s$ (min) | $V_{eff}$ (mL) |
|---|---|---|---|---|---|---|---|---|---|---|
| Aqueous solutions | | | | | | | | | | |
| 1cm | 5mL/min | 10 mg/L | 318 | 592 | 418 | 1452 | 40.8 | 650 | 1080 | 5400 |
| 2cm | 5mL/min | 10 mg/L | 350 | 737 | 292 | 1452 | 50.75 | 900 | 1260 | 6000 |
| 3cm | 5mL/min | 10 mg/L | 390 | 947 | 263 | 1452 | 65.2 | 1020 | 1380 | 6300 |
| 3cm | 10mL/min | 10 mg/L | 325 | 1516 | 391 | 2904 | 52.2 | 720 | 1200 | 11400 |
| 3cm | 15mL/min | 10 mg/L | 361 | 1376 | 360 | 4356 | 31.6 | 600 | 1140 | 15300 |
| 3cm | 5mL/min | 5mg/L | 365 | 982 | 273 | 1089 | 90.2 | 1260 | --- | 6600 |
| 3cm | 5mL/min | 15 mg/L | 440 | 778 | 227 | 2541 | 30.6 | 720 | 1080 | 5100 |
| Raw groundwater | | | | | | | | | | |
| The sample | | | 85 | 112.5 | 70.4 | 163 | 69 | 1080 | 1560 | 8200 |

Table 3: Langmuir and Freundlich isotherm parameters.

| Ce | qe | Ln ce | Ln qe | ce/qe | log ce | log Qe |
|---|---|---|---|---|---|---|
| 318 | 418 | 5.76 | 6.03 | 0.760766 | 2.502 | 2.621 |
| 350 | 292 | 5.85 | 6.83 | 1.19863 | 2.544 | 2.465 |
| 390 | 263 | 5.96 | 5.57 | 1.48289 | 2.591 | 2.419 |
| 325 | 391 | 5.78 | 5.96 | 0.831202 | 2.511 | 2.592 |
| 361 | 360 | 5.88 | 5.88 | 1.002778 | 2.557 | 2.556 |
| 365 | 273 | 5.89 | 5.60 | 1.336996 | 2.562 | 2.436 |
| 440 | 227 | 6.08 | 5.42 | 1.938326 | 2.643 | 2.356 |

Table 4: The chemical composition of the studied raw groundwater.

| Parameters | Sample value |
|---|---|
| Turbidity (NTU) | 45 |
| pH | 7.49 |
| Alkalinity (mg/L ) | 189 |
| Conductivity (Us/cm) | 1315 |
| Total hardness (mg/L) | 191 |
| Ca hardness (mg/L) | 112 |
| Mg hardness (mg/L) | 79 |
| Chloride (mg/L) | 103 |
| Sulfate (mg/L) | 150 |
| Ammonia (mg/L) | 0.62 |
| Nitrite (mg/L) | 0.009 |
| Nitrate (mg/L) | 7.05 |
| Iron (mg/L) | 0.4 |
| Manganese (mg/L) | 0.91 |
| Cu (mg/L) | 0.009 |
| Zn (mg/L) | 0.02 |

showed the presence of different types of dissolved contaminants (Table 4). The iron content was 0.4 mg/L which exceeds the accepted limit; this also was recorded for the contents of manganese and ammonia which can affect the adsorption trend of iron in the system (Table 2). The resulted curve for fixed-bed purification of the groundwater sample from dissolved iron appears in Fig. 8 and the performance mathematical parameters are presented in Table 1.

The breakthrough time and saturation time were attained after 45 and 65 hours, respectively. The detected reduction in the obtained breakthrough time as well as the saturation time for groundwater as compared to the prepared aqueous solution of 5 mg/L concentration related the existence of other dissolved elements and compounds that affect the affinity of bentonite/chitosan composite for the dissolved iron. The results reflected that the column has capacity to adsorb about 112 mg as total adsorbed iron and the equilibrium capacity is 70 mg/g. This was associated with total removal percentage of about 69% for the total treated volume of 8200 mL.

## CONCLUSION

Bentonite/chitosan composite was synthesized as an adsorbent for iron ions from water. Its adsorption properties were studied by continuous fixed-bed column system. The mathematical parameters of the breakthrough curves showed removal percentage of about 90% from 6.6 L of the aqueous solution after adjusting the factors of the system at 3 cm bed thickness, 5 mL/min flow rate, 5 mg/L concentration and at pH 6. For the groundwater at the same conditions, iron removal percentage reached 69% for 8.2 L of treated water. The breakthrough and the saturation times were attained after 45 and 68.5 hours, respectively.

## REFERENCES

Abukhadra, M.R., Dardir, F.M., Ahmed, E.A. and Soliman, M.F. 2019a. Efficient removal of Sr ions from water utilizing a novel Ni/$Fe^{+2}$-doped spongy apatite through fixed-bed column system: optimization and realistic application. Clean Technologies and Environmental Policy, 21: 69-80. doi.org/10.1007/s10098-018-1616-1.

Abukhadra, M.F., Adlii, A. and Bakry, B.M. 2019b. Green fabrication of bentonite/chitosan cobalt oxide composite (BE/CHCo) of enhanced adsorption and advanced oxidation removal of Congo red dye and Cr(VI) from water. International Journal of Biological Macromolecules, 126: 402-413. doi.org/10.1016/j.ijbiomac.2018.12.225.

Abukhadra, M.R., Bakry, B.M., Adlii, A., Yakout, S.M. and El-Zaidy, M.E. 2019c. Facile conversion of kaolinite into clay nanotubes (KNTs) of enhanced adsorption properties for toxic heavy metals ($Zn^{2+}$, $Cd^{2+}$, $Pb^{2+}$ and $Cr^{6+}$) from water. J. Hazard. Mater., 374: 296-308. doi: 10.1016/j.jhazmat.2019.04.047.

Abukhadra, M.R., Shaban, M., Sayed, F. and Saad, I. 2018. Efficient photocatalytic removal of safarnin-O dye pollutants from water under sunlight using synthetic bentonite/polyaniline $Ni_2O_3$ photocatalyst of enhanced properties. Environmental Science and Pollution Research, 25(33): 33264-33276. doi.org/10.1007/s11356-018-3270-x.

Albadarin, A.B., Collins, M.N., Naushad, M., Shirazian, S., Walker, G. and Mangwandi, C. 2017. Activated lignin-chitosan extruded blends for efficient adsorption of methylene Blue. Chemical Engineering Journal, 307: 264-272. doi.org/10.1016/j.cej.2016.08.089.

Abd ElSalam, H.M., Kamal, E.H.M. and Ibrahim, M. S. 2018. Cleaning of wastewater from total coliform using chitosan-grafted-poly (2-methy-

laniline). Journal of Polymers and the Environment, 26(8): 3412-3421. https://doi.org/10.1007/s10924-018-1225-4.

Abdolali, A., Ngo, H.H., Guo, W., Zhou, J.L., Zhang, J., Liang, S., Chang, S.W., Nguyen, D.D. and Liu, Y. 2017. Application of a breakthrough biosorbent for removing heavy metals from synthetic and real wastewaters in a lab-scale continuous fixed-bed column. Biores. Technol., 229: 78-87. doi: 10.1016/j.biortech.2017.01.016.

Al-Anber, M.A. 2010. Removal of high-level $Fe^{3+}$ from aqueous solution using natural inorganic materials: Bentonite (NB) and quartz (NQ). Desalination, 250(3): 885-891. doi:10.1016/j.desal.2009.06.071.

Amadio, T. M., Hotza, D., Neto, J.B.R., Blosi, M., Costa, A.L. and Dondi, M. 2017. Bentonites functionalized by impregnation with $TiO_2$, Ag, Pd and Au nanoparticles. Applied Clay Science, 146: 1-6.

APHA 1999. Standard Methods for the Examination of Water and Wastewater, Amer Public Health Assn; 20th edition.

Barakan, S., Aghazadeh, V., Samiee, A. and Mohammadi, S. 2019. Thermodynamic, kinetic and equilibrium isotherm studies of As(V) adsorption by Fe(III)-impregnated bentonite. Environment Development and Sustainability, 10.1007/s10668-019-00424-2.

Barloková, D. and Ilavský, J. 2010. Removal of iron and manganese from water using filtration by natural materials of disposers. J. Environ. Stud., 19(6): 1117-1122.

Bober, P., Stejskal, J., Spírková, M., Trchová, M., Varga, M. and Proke, J. 2010. Conducting polyaniline-montmorillonite composites. Synthetic Metals, 160: 2596-2604.

Dada, A.O, Olalekan, A.P., Olatunya, A.M. and Dada, O. 2012. Langmuir, Freundlich, Temkin and Dubinin-Radushkevich isotherms studies of equilibrium sorption of $Zn^{2+}$ unto phosphoric acid modified rice husk. IOSR Journal of Applied Chemistry (IOSR-JAC), 3(1): 38-45. http://dx.doi.org/10.9790/5736-0313845.

Ehssan, M.N. 2012. Utilization of bentonite as an adsorbent material in the removal of iron. Int. J. Eng. Sci. Technol., 4: 4480-4489.

European Union 1998. Richtlinie 98/83/EG des Rates.

Futalan, C., Kan, C., Dalida, M.L. and Pascua, C. 2011a. Fixed-bed column studies on the removal of copper using chitosan immobilized on bentonite. Carbohydrate Polymers, **83**(2): 697-704. DOI: 10.1016/j.carbpol.2010.08.043.

Futalan, C.M., Kan, C.C., Dalida, M.L.P, Pascua, C., Hsien, K.J. and Wan, M.W. 2011b. Nickel removal from aqueous solution in fixed bed using chitosan-coated Bentonite. Sustain. Environ. Res., 21(6): 361-367.

Futalan, C.M., Tsai, W.C., Lin, S.S., Dalida, M.L. and Wan, M.W. 2012. Copper, nikel and lead adsorption from aqueous solution using chitosan-immobilized on bentonite in ternary system. Sustain. Environ. Res., 22: 345-355.

Giannakas, A. and Pissanou, M. 2018. Chitosan/bentonite nanocomposites for wastewater treatment: a review. SF J. Nanochem. Nanotechnol., 1(1): 1010-1021.

Golie, W.M., Ambethkar, Y. and U. Sreedevi, U. 2018. Recovery of nitrate from water using chitosan/bentonite biocomposite in a continuous stirred tank reactor. J. Environ. Bio. Res., 2(1): 1-3.

Hassouna, M.E.M., Shaban, M. and Nassif, F.M. 2017. Adsorptive removal of iron and manganese from groundwater using CNTs clay and organo-clay nano composites. International Journal of Chemistry and Aquatic Sciences (IJCA), 3(1): 1-21.

Hassouna, M.E.M., Shaban, M. and Nassif, F.M. 2014. Removal of iron and manganese ions from ground water using kaolin sub micro powder and its modified forms. Int. J. Bioassays, 3(07): 3137-3145. DOI:10.21746/ijbio.2014.07.006.

Hethnawi, A., Manasrah, D. A., Vitale, G. and Nassar, N.N. 2018. Fixed-bed column studies of total organic carbon removal from industrial wastewater by use of diatomite decorated with polyethylenimine functionalized pyroxene nanoparticles. Journal of Colloid and Interface, 513: 28-42. DOI: 10.1016/j.jcis.2017.10.078.

Homoncik, S.C., MacDonald, A.M., Heal, K.V., Dochartaigh, B.E.O. and Ngwenya, B.T. 2010. Manganese concentrations in Scottish groundwater. Sci. Total Environ., 408: 2467-2473. doi: 10.1016/j.scitotenv.2010.02.017.

Jaymand, M. 2014. Conductive polymers/zeolite (nano-) composites: under-exploited materials. RSC Adv., 4: 33935-33954. doi: 10.1039/C4RA03067B.

Kamińska, G. 2018. Removal of organic micropollutants by grainy bentonite-activated carbon adsorbent in a fixed bed column. Water, 10(12): 1791-1804. doi:10.3390/w10121791.

Kumar, M. and Puri1, A. 2012. A review of permissible limits of drinking water. Indian J. Occup. Environ. Med., 16(1): 40-44. doi: 10.4103/0019-5278.99696.

Li, N., Yang, B., Xu, L., Xu, G., Sun, W. and Yu, S. 2016. Simple synthesis of $Cu_2O$/Na-bentonite composites and their excellent photocatalytic properties in treating methyl orange solution. Ceramics International, 42(5): 5979-5984. doi: 10.1016/j.ceramint.2015.12.145.

Liu, Q., Yang, B., Lujie, Z. and Huang, R. 2014. Adsorption of an anionic azo dye by cross-linked chitosan/bentonite composite. International Journal of Biological Macromolecules, 72: 1129-1135. doi: 10.1016/j.ijbiomac.2014.10.008.

Mohamed, F. M.R., Abukhadra, M.R. and Shaban, M. 2018. Removal of safranin dye from water using polypyrrole nanofiber/Zn-$Fe^{+2}$ layered double hydroxide nanocomposite (Ppy NF/Zn-$Fe^{+2}$ LDH) of enhanced adsorption and photocatalytic properties. Science of the Total Environment, (640-641): 352-363. https://doi.org/10.1016/j.scitotenv.2018.05.316.

Mohan, S., Singh, D.K., Kumar, V. and Hasan, S.H. 2017. Effective removal of fluoride ions by rGO/$ZrO_2$ nanocomposite from aqueous solution: fixed bed column adsorption modelling and its adsorption mechanism. J. Fluor. Chem., 194: 40-5.

Muliwa, A., Leswifi, T.Y., Maity, A., Ochieng, A. and Onyango, M. 2018. Fixed-bed operation for manganese removal from water using chitosan/bentonite/MnO composite beads. Environmental Science and Pollution Research, 25(4). doi: 10.1007/s11356-018-1993-3.

Nazaria, G., Abolghasemi, H., Esmaieli, M. and Pouya, E.S. 2016. Aqueous phase adsorption of cephalexin by walnut shell-based activated carbon: a fixed-bed column study. Appl. Surf. Sci., 375: 144-153. doi.org/10.1016/j.apsusc.2016.03.096.

Ngaha, W.S.W., Teonga, L.C. and Hanafiah, M.A.K.M. 2011. Adsorption of dyes and heavy metal ions by chitosan composites. Carbohydrate Polymers, 83: 1446-1456. doi:10.1016/j.carbpol.2010.11.004.

Ozdes, D., Gundogdu, A., Kemer, B., Duran, C., Senturk, H.B. and Soylak, M. 2009. Removal of Pb (II) ions from aqueous solution by a waste mud from copper mine industry: equilibrium, kinetic and thermodynamic study. J. Hazard. Mater., 166: 1480-1487. doi: 10.1080/19443994.2012.669161.

Pathania, D., Gupta, D., Al-Muhtaseb, A.H., Sharma, G., Kumar, A., Naushad, M., Ahamad, T. and Alshehri, S.M. 2016. Photocatalytic degradation of highly toxic dyes using chitosan-g-poly(acrylamide)/ZnS in presence of solar irradiation. Journal of Photochemistry and Photobiology A: Chemistry, 329: 61-68. doi: 10.1016/j.jphotochem.2016.06.019.

Sarin, P., Snoeyink, V.L., Bebee, J., Jim, K.K., Beckett, M.A., Kriven, W.M. and Clement, J.A. 2004. Iron release from corroded iron pipes in drinking water distribution systems. Water Res., 38(5): 1259-1269. doi:10.1016/j.watres.2003.11.022.

Seliem, M. K., Komarneni, S. and Abukhadra, M. R. 2016. Phosphate removal from solution by composite of MCM-41 silica with rice husk: kinetic and equilibrium studies. Microporous and Mesoporous Materials, 224: 51-57. https://doi.org/10.1016/j.micromeso.2015.11.011

Sprynskyy, M., Buszewski, B., Terzyk, A.P. and Namiesnik, J. 2006. Study of the selection mechanism of heavy metal ($Pb^{2+}$, $Cu^{2+}$, $Ni^{2+}$, and $Cd^{2+}$) adsorption on clinoptilolite. J. Colloid Interface Sci., 304: 21-28. doi.org/10.1016/j.jcis.2006.07.068.

Takeda, A. 2003. Manganese action in brain function. Brain. Res. Rev., 41: 79-87. doi: 10.1016/S0165-0173(02)00234-5.

Tirtom, V.N., Dinçer, A., Becerik, S., Aydemir, T. and Çelik, A. 2012. Removal of lead (II) ions from aqueous solution by using crosslinked chitosan-clay beads. Desalination and Water Treatment, 39(1-3): 76-82.http://dx.doi.org/10.1080/19443994.2012.669161.

Tsai, W.C, de Luna, M.D.G., Bermillo-Arriesgado, H.LP. Futalan, C.M., James I. Colades, J.I. and Wan, M.W. 2016. Competitive fixed-bed adsorption of Pb (II), Cu (II), and Ni (II) from aqueous solution using chitosan-coated bentonite. International Journal of Polymer Science, 1-11. http://dx.doi.org/10.1155/2016/1608939.

Wang, G., Zhang, S., Wang, J., Ma, S., Lu, X. and Komarneni, S. 2016. Synthesis of porous Al pillared montmorillonite after preintercalation with dodecylamine: textural and thermal properties. Journal of Porous Materials, 23(6): 1687-1694. doi: 10.1007/s10934-016-0276-y.

Yang, M., Liu, X., Qi, Y., Sun, W. and Men, Y. 2017. Preparation of-carrageenan/graphene oxide gel beads and their efficient adsorption for methylene blue. Journal of Colloid and Interface Science, 506: 669-677. doi.org/10.1016/j.jcis.2017.07.093.

Zhang, Y., Li, J. and Li, W. 2015. Effect of particle size on removal of sunset yellow from aqueous solution by chitosan modified diatomite in a fixed bed column. RSC Adv., 5: 85673-85681. doi: 10.1039/c5ra13645h.

Zhua, H., Jiang, R., Xiao, L., Chang, Y., Guan, Y., Li, X. and Zeng, G. 2009. Photocatalytic decolorization and degradation of Congo Red on innovative crosslinked chitosan/nano-CdS composite catalyst under visible light irradiation. Journal of Hazardous Materials, 169(1-3): 933-40. doi: 10.1016/j.jhazmat.2009.04.037.

Nature Environment and Pollution Technology
An International Quarterly Scientific Journal

p-ISSN: 0972-6268
(Print copies up to 2016)
e-ISSN: 2395-3454

Vol. 19 | No. 4 | pp. 1355-1165 | 2020

Original Research Paper

https://doi.org/10.46488/NEPT.2020.v19i04.002

Open Access Journal

# The Kinetic Model for Decolourization of Commercial Direct Blue 2 Azo Dye Aqueous Solution by the Fenton Process and the Effect of Inorganic Salts

**Hasan F. Al-Rubai*, Ahmed K. Hassan* and Bahaa M. Altahir**†**

*Environment and Water Directorate, Ministry of Science and Technology, Baghdad, Iraq

**Department of Biology, University of Baghdad, Baghdad, 10071, Iraq

†Corresponding author: Bahaa M. Altahir; baha782004@gmail.com

**Nat. Env. & Poll. Tech.**
**Website: www.neptjournal.com**

*Received:* 18-11-2019
*Revised:* 29-12-2019
*Accepted:* 16-01-2020

**Key Words:**
Azo dye
Degradation
Fenton process
Adsorption kinetics

## ABSTRACT

The study of Fenton's oxidation and degradation of Direct Blue 2 (DB2) as the commercial azo dye in synthetic aqueous solution has been accomplished. The optimum oxidative degradation reaction conditions were achieved as follows: pH = 3.50, $[H_2O_2]$ = $1.1\times10^{-3}$ M, $[Fe^{2+}]$ = $1.0\times10^{-4}$ M for [DB 2] = $1.0\times10^{-4}$ M. Under optimal conditions, 80% of decolouration efficiency was carried out within 15 min of reaction. An engagement between the kinetics of the colour removal rates (ln $k_2$) versus $L_{azo\ bond}$ was carried out at the different pH levels. The colour removal rate was increased with decreasing of $L_{azo\ bond}$, in the order of pH: 3.5 > 5.0 > 2.5. The second-order kinetic model provided the best correlation of the data. Effects of various inorganic anions (such as $Cl^-$, $SO_4^{2-}$, $CO_3^{2-}$, etc.) was studied to enhance the oxidation efficiency of Fenton reaction. Advanced oxidation technologies were developed in this study especially with dealing with contaminated textile wastewater over the use of chemical treatment.

## INTRODUCTION

The textile industry is a major source of outflowing industrial wastewater due to more exhaustion of water during process operations. This industrial wastewater contains chemicals such as alkalis, acids, dyes, surfactants and matter high in biochemical oxygen demand (Razzak & Hossain 2016). As the textile industry uses more water than any other industry globally, virtually all wastewater discharged is highly polluted. Water consumption of an average-sized textile mill about 50 gals per kg of fabric manufactured daily (Luo et al. 2016). The most plentiful of these compounds are azo dyes, which exemplify 70% of the world dye product. Large volumes of industrial wastewater with high scales of azo dyes (about 250 $mg.L^{-1}$) are every day vacuous by many industries around the world in the surface water. The stability and complexity of the dye structure make it more difficult to degrade when it is present in the textile wastewater (Garcia-Segura & Brillas 2016). Therefore, the mineralization of dyes generated by the textile industry is the main challenge and environmental concern (Holkar et al. 2016). There are several methods currently used to remove wastewater contamination in the fabric, but they are not universally applicable and are not cost-effective for all dyes (Nidheesh et al. 2013). In the last years, the problem of a high toxic level of wastewater has been tried by Advanced Oxidation Processes (AOPs) (Sharma et al. 2018). AOPs are based on the in-situ generation of hydroxyl radical ($HO^{\bullet}$, $E^{\circ}$ ($HO^{\bullet}/H_2O$) = 2.80V) (Dewil et al. 2017). The Fenton system is one of the most used techniques to degrade different organic pollutants such as azo-dyes by hydroxyl free radical generated from the hydrogen peroxide molecules reduction with $Fe^{2+}$ ions at acidic pH (Jin et al. 2017).

$$Fe^{2+} + H_2O_2 \rightarrow Fe^{3+} + HO^{\bullet} + HO^- \quad \ldots(1)$$

$$Fe^{3+} + H_2O_2 \rightarrow Fe(OOH)^{2+} + H^+ \quad \ldots(2)$$

$$Fe(OOH)^{2+} \rightarrow Fe^{2+} + HO_2^{\bullet} \quad \ldots(3)$$

In Fenton oxidation process, hydroxyl free radical prefer to attack the azo bond (–N=N–) of the dye molecule by cleaving it to produce aromatic amines and inorganic ions such as $NH_4^+$ (Trovó et al. 2016). For the treatment of industrial textile wastewater containing dyes; the AOPs are effective techniques for degradation of aromatic compounds consequent to the electrophilic aromatic exchange of $HO^{\bullet}$ which then leads to open the aromatic ring (Mousset et al. 2014). The goal of the other treatment is reducing the chemical oxygen demand of the industrial textile wastewater. Typically, these two targets require various chemical reagents like $H_2O_2$ and $Fe^{2+}$ coincide to either azo bond or chemical oxygen demand loadings (Dehghani et al. 2016). This manuscript reports the colour removal or COD removal kinetics of the DB 2 which contains diazo bond, by Fenton oxidation process. The goals of this study were: (1) to determine the best molar ratio of

$H_2O_2/Fe^{2+}$ through Fenton oxidation process of DB 2 at optimum pH according to the colour removal kinetics with constant $Fe^{2+}$ and variable $H_2O_2$; (2) at the optimum conditions, estimation of the effects of either azo bond loading factor ($L_{azobond}$) or COD loading factor ($L_{COD}$) at different pH values in relation to the colour removal kinetic classify and COD removal of DB2 by Fenton oxidation process; (3) at optimum conditions on degradation of DB2, study the effect of the inorganic anions such as sulphate, carbonate chloride and bicarbonate

## MATERIALS AND METHODS

### Chemicals

Direct Blue 2 (DB2) (Ciba Specialty Chemicals Inc). $H_2O_2$ (30%W/W), $Na_2SO_3$ and $FeSO_4.7H_2O$ were obtained from Merck and BDH. NaOH (99%) and $H_2SO_4$ (99%) were used to adjust the pH which was purchased from Appli Chem (GmbH). To estimate the concentration of hydrogen peroxide, a solution of ammonium metavanadate $NH_4VO_3$ (BDH) was prepared. Its molar concentration was 0.062 M dissolved in sulfuric acid, with a concentration of 0.058 M. KCl (99%), NaCl (99%), $Na_2CO_3$ (99.0%), $NaHCO_3$ (98%), $Na_2SO_4$ (99%) and $K_2SO_4$ (99%) were obtained from Fluka. All solutions were prepared with distilled water. The main characteristics and chemical structure of DB 2 dye are as shown in Table 1 and Fig. 1.

### Experimental Procedure

The colour removal of the azo dye DB 2 solutions was followed quantitatively by measuring the decrease in absorbance at max = 570 nm using (UV/VIS, Model SP-3000 OPTIMA) spectrophotometer. The chemical oxygen demand (COD) was determined by the method described in EPA method 410.4 (Luo et al. 2016, Razzak & Hossain 2016). $H_2O_2$ was quantified spectrophotometrically as described by Nogueira (Nogueira et al. 2005). The degradation of DB 2 was carried out by the Fenton process using a batch reactor (total volume of 1 L) under constant agitation with a magnetic stirrer and room temperature ranged from 35±2°C. The experiments were conducted as the following:

1. To determine the effect of the primary concentration of $H_2O_2$ ($0.22 \times 10^{-4}$ to $4.4 \times 10^{-3}$ M) on the removal kinetics of DB 2 ($1 \times 10^{-4}$ M). The experiments were conducted with a constant concentration of iron ions ($1 \times 10^{-4}$ M) and pH 3.5. A desired amount of $FeSO_4.7H_2O$ was added to each experiment. Either 1 M $H_2SO_4$ or 1 M NaOH was used to adjust the pH at the specified value, the proper amount of $H_2O_2$ was added to each batch reactor. To estimate the dye decolourization, 10 mL of sample was immediately analysed at 1, 3, 5, 7, 10, 15, 20, 30, 45 and 60 min.
2. For this step of oxidation, the effect of $[H_2O_2]$ was in the range of $1.0 \times 10^{-5}$ to $2.5 \times 10^{-4}$ M, the stock solution of $[H_2O_2]$ was $1.1 \times 10^{-3}$ M and pH of the dye solution was constant at 3.5 on decolourization rate of [DB 2] = $1.0 \times 10^{-4}$ M.
3. The most favourable molar ratio $H_2O_2/Fe^{2+}$ was experimentally determined by changing either $H_2O_2$ or $Fe^{2+}$ concentrations as described in the first and second steps. In the literature review, $H_2O_2$ and $Fe^{2+}$ doses were determined by carrying out several experiments at different ratios of $H_2O_2$ and $Fe^{2+}$ doses (Kehinde & Abdul Aziz 2014, Garcia-Segura & Brillas 2016, Luo et al. 2016).
4. Experiments were achieved at three pH values (2.5, 3.5 and 5.0) and different $L_{azobond}$ for the Fenton oxidation process. The colour removal (decolourization) kinetic

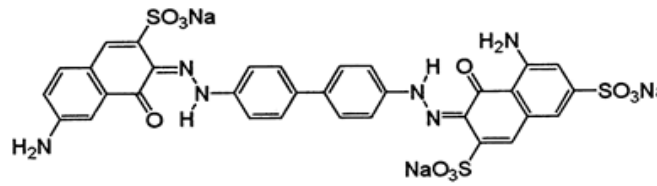


Fig. 1: Chemical structure of DB2.

Table 1: Characteristics of DB 2.

| Properties | Value |
|---|---|
| Chemical formula | $C_{32}H_{12}N_6Na_3O_{11}S_3$ |
| Molar Mass | 831 g/mol |
| Functional group | Diazo |
| Color, λ max (nm) | Deep Purple, 570 |

of $1.0\times10^{-4}$ M of DB 2, was studied at different $L_{azo\ bond}$ (1.0, 0.75, 0.5 and 0.25) which are equivalent to $H_2O_2$ concentrations ($2.0\times10^{-4}$, $2.7\times10^{-4}$, $4.0\times10^{-4}$ and $8.0\times10^{-4}$ M), respectively for the demolition of azo group bond at a constant $H_2O_2/Fe^{2+}$ molar ratio of 11.

5. The COD removal of DB 2, was studied at different $L_{COD}$ (1.0, 0.75, 0.5, and 0.25) at $H_2O_2/Fe^{2+}$ molar ratio equal to 11. Different $H_2O_2$ concentrations: $1.4\times10^{-2}$, $1.9\times10^{-2}$, $2.8\times10^{-2}$ and $5.6\times10^{-2}$ M equivalent to $L_{COD}$ (1.0, 0.75, 0.5, and 0.25) were used for the COD removal, for the reason that the empirical COD concentration gained at $1.0\times10^{-4}$ M DB 2 solution was 224 mg $O_2$ $L^{-1}$ (COD = $7.0\times10^{-3}$ M).
6. The effect of 1.0 % of inorganic salts on decolourization of DB 2 at ($1.0\times10^{-4}$ M) was investigated. 10 g of inorganic salt was added to 1 L batch reactor for each experiment.
7. To ensure the removal of residual hydrogen peroxide $H_2O_2$, 100 µL of 1.0 M sodium sulphate $Na_2SO_3$ solution, was added to all samples before the analysis by UV-Vis. Thus, the residual of $H_2O_2$ was destroyed and Fenton reactions were stopped (Holkar et al. 2016). While, to measure the COD concentration in the treated water, the interference from residual $H_2O_2$ was removed by addition of $Na_2CO_3$ (20 g/L) and placed in a water bath at 90°C for 60 min (Wu and Englehardt 2012, Nidheesh et al. 2013).

## RESULTS AND DISCUSSION

Results presented here are based on the batch system of degradation of DB 2 by Fenton oxidation. The parameters for colour removal (decolourization) efficiencies such as loading azo bond factor ($L_{azo\ bond}$) or COD loading factor ($L_{COD}$) were studied; which are defined by Eqs. 4 and 5, respectively (Trovó et al. 2016, Sharma et al. 2018). In oxidation processes using the Fenton's reagent, the amount of oxygen $O_2$ available in $H_2O_2$ must be measured to produce free hydroxyl radicals $HO^{\bullet}$ responsible for the breakdown of the azo bond and the intermediate organic compounds (Sharma et al. 2018). Therefore, the dosage of $H_2O_2$ required should be based on the initial $L_{azo\ bond}$, $L_{COD}$ of DB 2, and $O_2$ supplied by $H_2O_2$, respectively.

$$L_{azo\ bond} = \{[DB\ 2]_{initial}\ (M)\}/O_{2\ available}\ (M) \quad \ldots(4)$$

$$L_{COD} = \{COD_{initial}\ (M)\}/O_{2available}\ (M) \quad \ldots(5)$$

Where, $DB2_{initial}$ and $COD_{initial}$ are the initial concentration and the chemical oxygen demand of DB 2 dye, respectively. Dye decolourization efficiency was calculated as follows:

$$(\%)\ \text{Dye colour removal efficiency} = (1 - C_t / C_0) \times 100 \quad \ldots(6)$$

Where, $C_t$ and $C_0$ (mol.$L^{-1}$) are the concentrations of DB 2 dye at reaction time t and 0, respectively. The chemical oxygen demand removal percentage was calculated as follows:

$$(\%)\ \text{COD removal} = (1 - COD_t / COD_0) \times 100 \quad \ldots(7)$$

Where, $COD_t$ and $COD_0$ are the chemical oxygen demand of DB 2 dye at reaction time t and 0, respectively.

### Effect of the $H_2O_2$ Dose on the Removal of DB 2

In the Fenton process, hydrogen peroxide plays an essential role in contaminant removal efficiency. Therefore, it was necessary to find the optimum hydrogen peroxide concentrations. The decolourization of $1.0\times10^{-4}$ M DB 2 was evaluated in the range of ($0.22\times10^{-4}$ and $4.5\times10^{-3}$ M) $H_2O_2$ and constant amount of ferrous iron ($1\times10^{-4}$ M or 5.6 mg/L) to find the optimal oxidant dosage. The effect of hydrogen peroxide

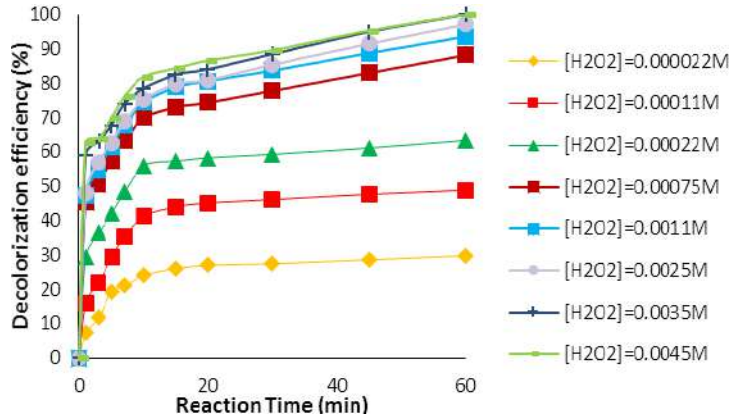


Fig. 2: DB 2 reaction time effect on decolourization of dye by Fenton oxidation at various $H_2O_2$ doses. Experimental conditions: [DB 2] = $1.0\times10^{-4}$ M, [$Fe^{2+}$] = $1.0\times10^{-4}$ M and pH = 3.5.

concentration and reaction time are shown in Fig. 2. At the concentration of $0.22 \times 10^{-4}$ M, the colour removal of DB 2 was 24.0 % after 10 min of the reaction. However, the increment of peroxide dosage till $1.1 \times 10^{-3}$ M, a colour removal was reached at a higher level of 74.0%. The concentration of $1.1 \times 10^{-3}$ M $H_2O_2$ was selected as the best concentration and used in all experiments to estimate the effects of $Fe^{2+}$ concentration on DB 2. At $H_2O_2$ concentration of higher than $1.1 \times 10^{-3}$ M, the decolourization efficiency of dye solution showed little considerable efficiency, which may be due to the reaction of hydroxyl radicals with $H_2O_2$, and scavenging of $HO^{\bullet}$ radicals takes place as shown in Eq. 8 (Liu et al. 2017).

$$HO^{\bullet} + H_2O_2 \rightarrow H_2O + HO_2^{\bullet} \quad k_1 = 2.7\times10^7\ M^{-1}.\ S^{-1} \ldots(8)$$

## The kinetics of influence of $H_2O_2$ concentration on DB 2 decolourization

Because of different side reactions occurring at the same time, the kinetic study of Fenton oxidation is highly complicated. Two models of kinetic studies were experimented to achieve the kinetics parameters. The first and second-order reaction, have been tested to fit the experimental data obtained from the colour removal experiments. The correlation coefficient ($R^2$) was used in the comparison of the two models. The data of Table 2 illustrate that the first-order model was not useful enough for proper parameter selection may due to the low correlation parameters, while the second-order reaction was much better. The results illustrated that the colour removal kinetics of DB 2 followed the second-order model very well.

Fig. 3 shows that the DB 2 colour removal kinetic rates at constant iron ions of $1.0 \times 10^{-4}$ M increase with the $H_2O_2$ concentration in two steps. The first step was at the small amount of $H_2O_2$ ranged $0.22 \times 10^{-4}$ to $1.1 \times 10^{-3}$ M, the DB 2 colour removal kinetics increased slowly with a rate constant, $k = 2 \times 10^6\ [H_2O_2] + 416.97$ and with higher correlation coefficient value of $R^2 = 0.9715$. The second step was at the concentration of $H_2O_2$ was increased from $1.1 \times 10^{-3}$ to $4.5 \times 10^{-3}$ M, DB 2 colour removal kinetics was increased, and a rate constant $K = 372437\ [H_2O_2] + 2014.7$ and correlation coefficient $R^2$ was decreased to a value of 0.8561 (Fig. 3). The positive effect of DB 2 colour removal kinetics values was observed with a high concentration of $H_2O_2$ may be due to the high production of hydroxyl free radical. When $H_2O_2$ concentration was larger than $1.1 \times 10^{-3}$ M (Fig. 3), the DB 2 colour removal kinetics was linearly increased, the

Table 2: First and second orders kinetic parameters and correlation coefficients for each $H_2O_2$ concentration. Experimental conditions: $[Fe^{2+}] = 1.0 \times 10^{-4}$ M, pH= 3.5 and [DB 2] = $1.0 \times 10^{-4}$ M.

| $[H_2O_2]$ (M) | $H_2O_2/Fe^{+2}$ | First-order | | Second-order | |
|---|---|---|---|---|---|
| | | $K_1$ ($min^{-1}$) | $R^2$ | $K_2$ ($M^{-1}.min^{-1}$) | $R^2$ |
| $4.5 \times 10^{-3}$ | 45 | 0.1355 | 0.7649 | 3890 | 0.9233 |
| $3.5 \times 10^{-3}$ | 35 | 0.1227 | 0.7472 | 3171 | 0.9124 |
| $2.5 \times 10^{-3}$ | 25 | 0.1171 | 0.8322 | 2714 | 0.9547 |
| $1.1 \times 10^{-3}$ | 11 | 0.1148 | 0.8418 | 2604 | 0.9567 |
| $7.5 \times 10^{-4}$ | 7.5 | 0.0994 | 0.8186 | 2035 | 0.9343 |
| $2.2 \times 10^{-4}$ | 2.2 | 0.0704 | 0.8799 | 1128 | 0.9468 |
| $1.1 \times 10^{-4}$ | 1.1 | 0.0737 | 0.8786 | 556 | 0.9332 |
| $0.22 \times 10^{-4}$ | 0.22 | 0.0268 | 0.9168 | 312 | 0.9323 |

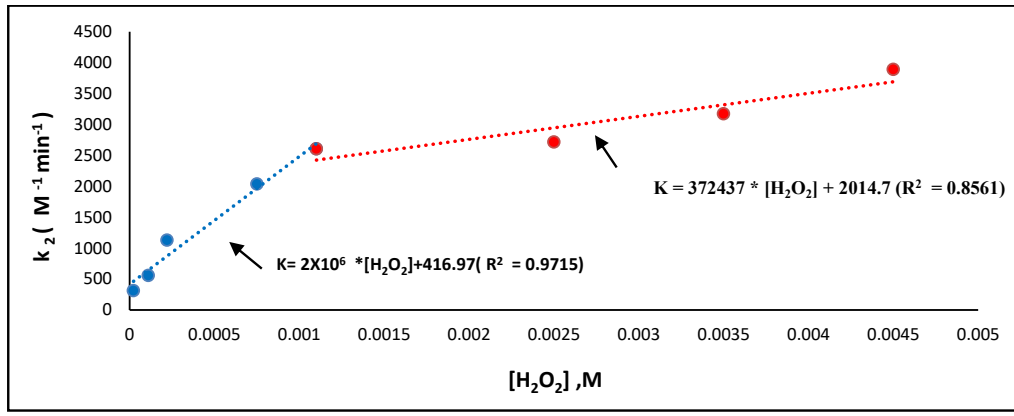


Fig. 3: Correlations among the second order kinetic constants versus $H_2O_2$ used, obtained during DB 2 decolourization by Fenton process. Initial conditions: $[Fe^{2+}] = 1 \times 10^{-4}$ M, pH= 3.5 and [DB 2] = $1.0 \times 10^{-4}$ M.

regression coefficient value was decreased at the same time. It suggests that the overdosed $H_2O_2$ was scavenging hydroxyl free radicals excessively (Eq. 8). Consequently, $1.1 \times 10^{-3}$ M $H_2O_2$ was selected as the optimum concentration on DB 2 colour removal kinetics.

### Effect of $Fe^{2+}$ Doses on the Removal of DB 2

The influence of $Fe^{2+}$ stimulation on the removal of DB 2 was examined using the different $Fe^{2+}$ concentrations. The [$Fe^{2+}$] were in range of $1.0 \times 10^{-5}$ to $2.5 \times 10^{-4}$ M with constant $H_2O_2$ concentration of $1.1 \times 10^{-3}$ M. Increase of the concentration of [$Fe^{2+}$] from $1.0 \times 10^{-5}$ to $1.0 \times 10^{-4}$ M had the positive effect on the removal rate for DB 2 (Fig. 4). The colour removal was increased from 22.0 % to74.0 % at 10 min of the reaction, that effect may be due to the activity of $Fe^{2+}$ in initiating the degradation of $H_2O_2$ to generate hydroxyl free radicals as a part of Fenton process. These radicals can reacted with DB 2 instantly, that lead to DB 2 degradation (Lucas & Peres 2006). When the concentration of $Fe^{2+}$ was increased to higher than $1.0 \times 10^{-4}$ M, a slight increase in the decomposition rate may have occurred and that improved the function of $Fe^{2+}$ as a scavenger of $HO^*$ (Eq. 9). Hence, the optimum $Fe^{2+}$ concentration of the removal of DB 2 was selected as $1.0 \times 10^{-4}$ M.

$$Fe^{2+} + HO^{\bullet} \quad Fe^{3+} + OH^{-} \quad k_2 = 3 \times 10^8 \ M^{-1}.S^{-1} \quad \ldots(9)$$

### The Kinetics of Influence of $Fe^{2+}$ Concentration on DB 2 Colour Removal

Two kinetic models were studied to estimate the effect of $Fe^{2+}$ concentrations on the decomposition kinetics of DB 2. Table 3 shows the kinetic parameters of the study. The regression coefficient ($R^2$) values of the second-order reaction were higher than the first-order and we concluded that the colour removal kinetics of DB 2 obeys to the second-order kinetics model. The correlation between the second-order kinetics of the DB 2 colour removal and different $Fe^{2+}$ concentrations (from $1.5 \times 10^{-5}$ to $2.5 \times 10^{-4}$ M) are presented in Fig. 5. Fig. 5 elucidates that the DB 2 colour removal kinetic average increase with the increase of $Fe^{2+}$ in two varied steps as well: (1) At low concentration of $Fe^{2+}$ ranged from $1.5 \times 10^{-5}$ to $1.0 \times 10^{-4}$ M, the DB 2 colour removal kinetics was increased clearly with a slope of $3.0 \times 10^7$. (2) At high concentration of $Fe^{2+}$ (from $1.5 \times 10^{-4}$ to $2.5 \times 10^{-4}$ M), DB 2 colour removal kinetics increased also but the slope ($9.0 \times 10^6$) was decreased. At low colour removal kinetics in the second step in comparison with the first step, the proposition may lead to that $Fe^{2+}$ was higher than the need for consumption amount of $HO^{\bullet}$ (Eq. 10). Thus, the amount of hydroxyl free radicals available to oxidize DB 2 dye became very low. The positive effect of $Fe^{2+}$ on the DB 2 colour removal kinetics assured that $Fe^{2+}$ stimulate by fast dissociation of $H_2O_2$ into $HO^{\bullet}$ radicals;

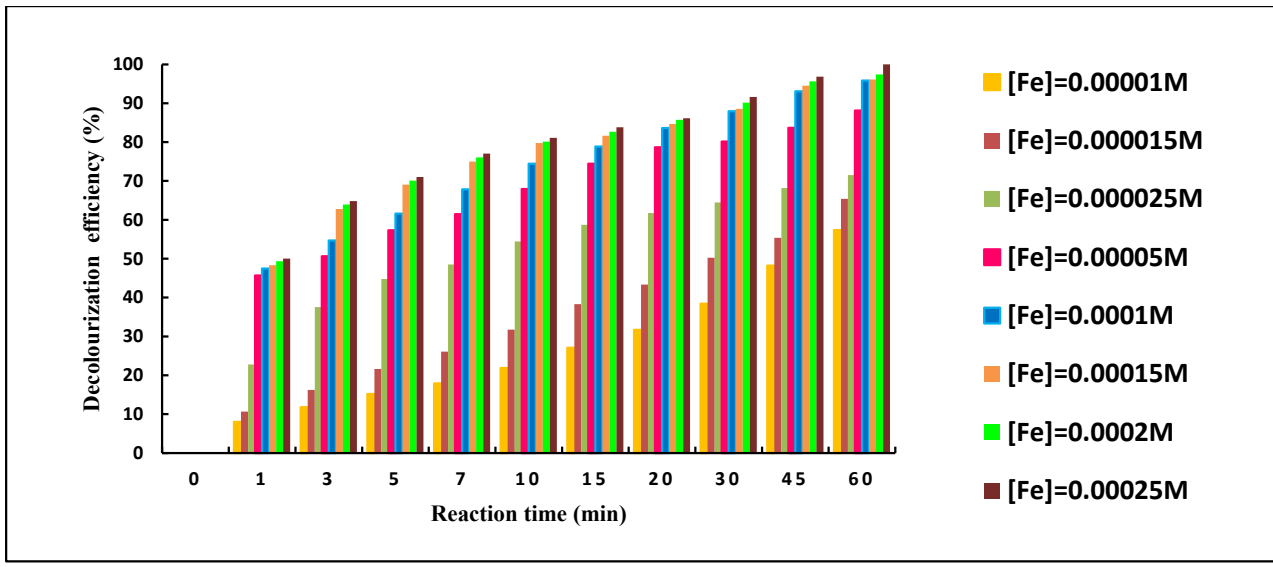


Fig. 4: DB 2 Decolourization by Fenton's reagent oxidation at different $Fe^{+2}$ concentrations. Experimental conditions: [$H_2O_2$] = $1.1 \times 10^{-3}$ M, pH=3.5 and [DB 2] = $1.0 \times 10^{-4}$ M.

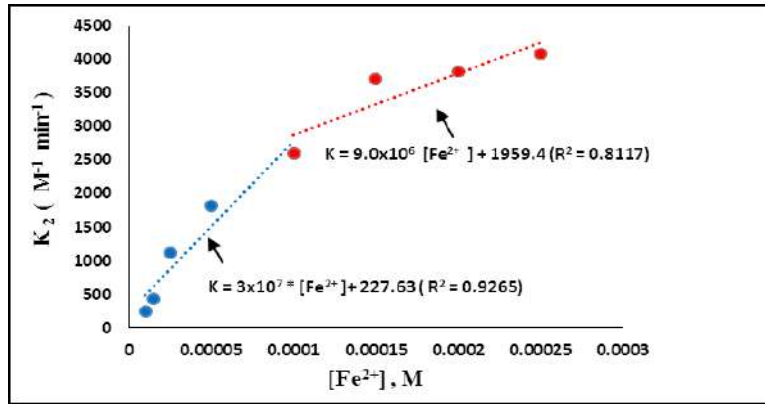


Fig. 5: Correlation between the second-order kinetic constants versus $Fe^{2+}$ used found during DB 2 decolourization by Fenton process. Primary conditions: $[H_2O_2] = 1.1\times10^{-3}$ M, pH = 3.5 and [DB 2] = $1.0\times10^{-4}$ M

Table 3: First and second-order kinetic parameters and regression coefficients for each $Fe^{2+}$ concentrations. Experimental conditions: [DB 2] = $1.0 \times 10^{-4}$ M, $[H_2O_2] = 1.1 \times 10^{-3}$ M and pH = 3.5.

| $[Fe^{+2}]$ (M) | $H_2O_2/Fe^{2+}$ | First-order | | Second-order | |
|---|---|---|---|---|---|
| | | $K_1$ ($min^{-1}$) | $R^2$ | $K_2$ ( $M^{-1}. min^{-1}$ ) | $R^2$ |
| $1.0\times10^{-5}$ | 110 | 0.0223 | 0.9259 | 255 | 0.9446 |
| $1.5\times10^{-5}$ | 73 | 0.0353 | 0.9524 | 435 | 0.9733 |
| $2.5\times10^{-5}$ | 44 | 0.0719 | 0.8826 | 1126 | 0.9449 |
| $5.0\times10^{-5}$ | 22 | 0.0922 | 0.7821 | 1820 | 0.9064 |
| $1.0\times10^{-4}$ | 11 | 0.1148 | 0.8418 | 2604 | 0.9567 |
| $1.5\times10^{-4}$ | 7.3 | 0.1403 | 0.8541 | 3707 | 0.9765 |
| $2.0\times10^{-4}$ | 5.5 | 0.1422 | 0.8443 | 3820 | 0.9724 |
| $2.5\times10^{-4}$ | 4.4 | 0.1471 | 0.8489 | 4085 | 0.9764 |

that may be due to the $Fe^{2+}$ not capable to oxidize organic molecules. When $Fe^{2+}$ dose is more than $1.0 \times 10^{-4}$ M (Fig. 5); the DB 2 colour removal kinetics rate increased linearly with lower intensity by scavenging $HO^{\bullet}$ radicals. Thus, $1.0 \times 10^{-4}$ M $Fe^{2+}$ was selected as the optimum concentration.

## $H_2O_2/Fe^{2+}$ Molar Ratio Effect on DB 2 Decolourization Kinetics

Concentrations of $H_2O_2$ over $Fe^{2+}$ are important parameters to optimize for the determination of the ratio $H_2O_2/Fe^{2+}$ to achieve the maximum Decolourization efficiency of DB 2 from aqueous solutions. The ratio has been used in the following experiments. Several studies have reported that the effect of the optimum molar ratio of Fenton reagent $H_2O_2/Fe^{2+}$ was disparate for colour removal of azo dyes. For a perfect example, the ratio of $H_2O_2$ /$Fe^{2+}$ was 20:1 for C.I. Reactive Blue 4 and C.I. Reactive Red 2 (Agustina and Ang 2012), while the ratio was 40:1 for Reactive Black 5 (Lucas & Peres 2006, Dewil et al. 2017). These variations likely attributed to different proposed oxidation mechanisms during the Fenton oxidation process of different azo dyes. Table 2 and Table 3 show the results obtained in this study, the optimum concentrations of $H_2O_2$ and $Fe^{2+}$ were $1.1\times10^{-3}$ M and $1.0\times10^{-4}$ M, respectively. Consequently, the experimental optimum $H_2O_2/Fe^{2+}$ molar ratio of 11 was selected for the next experiments.

## Effect of pH and $L_{azo\ bond}$ on DB 2 Color Removal Kinetics

The pH effect on the Decolourization of DB 2 was achieved by a series of experiments conducted at three initial pH values 2.5, 3.5 and 5 (Fig. 6). The reaction time was 60 min and constant concentration of $H_2O_2 = 1.1\times10^{-3}$ M and $Fe^{2+} = 1.0\times10^{-4}$ M. pH of 2.5 had the negative effect on $HO^{\bullet}$ radical production in the reaction of $H_2O_2$ with $Fe^{2+}$ Eq. (1), This may be attributed to $HO^{\bullet}$ scavenging by $H^+$ ions; which elucidate the decrease of the colour removal efficiency at pH 2.5 (Esteves et al. 2016, Jin et al. 2017). On the other hand, at pH 3.5, the Decolourization efficiency of DB 2 rapidly increased with the increase in pH, at pH 3.5 almost

100% of Decolourization efficiency was achieved (Fig. 6). The main reason is that more $Fe(OH)^{+}$ is formed, which has much higher activity compared to $Fe^{2+}$ in the Fenton process (Lopez-Alvarez et al. 2012, Trovó et al. 2016). Besides, at higher pH (pH 5), the precipitation of ferric hydroxide happen, causing the reduction in the dissolving $Fe^{3+}$ ions. Aside from, in such circumstances, $H_2O_2$ is less stable, resulting in less $HO^{\bullet}$ radicals formed, decreasing the removal efficiency of Fenton oxidation (Mousset et al. 2014, Jin et al. 2017). Therefore, the pH 3.5 was chosen the optimum pH of Fenton oxidation process. At molar ratio of $H_2O_2/Fe^{2+}$ equal to 11, the effect of four $L_{azo\ bond}$ operator values (0.25, 0.5, 0.75, and 1.0) was evaluated.

Table 4 shows four levels of $L_{azo\ bond}$ and symbolized well by the second-order kinetic model. The results elucidate the significant difference in DB 2 colour removal rates at every pH and $L_{azo\ bond}$. The results in Table 4 approved the selection of pH 3 in Decolourization rates of DB 2 dye. The data were in harmony with previous literatures for assessment of the colour removal of Amido black 10B and Terasil Red R (Dehghani et al. 2016). The best DB 2 colour removal rates were found at the smallest $L_{azo\ bond}$ factor of 0.25 and higher

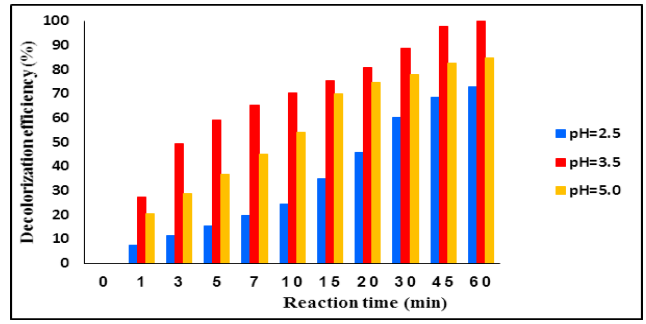


Fig. 6: Effect of pH on the colour removal efficiency of DB 2 by Fenton process. Experimental conditions; $[Fe^{2+}] = 1.0\times10^{-4}$ M, $[H_2O_2] = 1.1\times 10^{-3}$ M and $[DB2] = 1.0\times10^{-4}$ M.

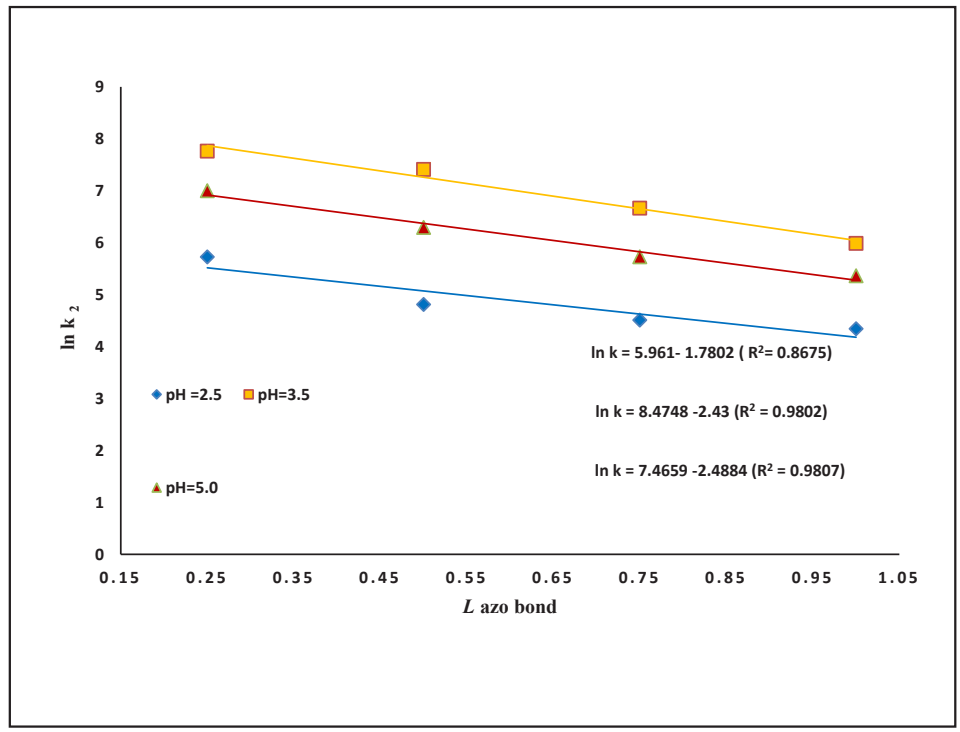


Fig. 7: Correlations between ln $k_2$ of the colour removal rates versus $L_{azo\ bond}$ at different pH values obtained during Fenton oxidation of $1.0 \times 10^{-4}$ M DB 2.

Table 4: Second–order kinetic model and regression parameters for every pH and $L_{azo\ bond}$ value during Fenton oxidation of $1.0 \times 10^{-4}$ M DB 2.

| pH | $L_{azo\ bond}$ 1.0 | $L_{azo\ bond}$ 0.75 | $L_{azo\ bond}$ 0.5 | $L_{azo\ bond}$ 0.25 |
|---|---|---|---|---|
| 2.5 | $k_2$ =77 $R^2$=0.8967 | $k_2$ = 91 $R^2$=0.970 | $k_2$ = 123 $R^2$=0.929 | $k_2$ = 307 $R^2$=0.8675 |
| 3.5 | $k_2$ = 398 $R^2$=0.9895 | $k_2$ = 784 $R^2$= 0.989 | $k_2$ =1654 $R^2$ =0.986 | $k_2$ = 2351 $R^2$ = 0.98 |
| 5.0 | $k_2$ = 1098 $R^2$= 0.920 | $k_2$ = 542 $R^2$ =0.94 | $k_2$ = 308 $R^2$ = 0.933 | $k_2$ = 214 $R^2$=0.911 |

$k_2$ values, due to the smaller $L_{azo\ bond}$ factor represented a greater amount of $H_2O_2$ concentration per mole of DB 2 and coincides with the larger $O_2$ concentration able to be used for oxidizing the DB 2 dye. Fig. 7 presents a linear relation between the second-order kinetic ln $k_2$ value and the $L_{azo\ bond}$ at each pH value.

## COD Removal of RR120 at Different $L_{COD}$ Factors

Although homogeneous catalytic process decolorized the DB 2, the DB 2 azo dye was not completely mineralized. For this reason it is necessary to consider complementary information about the degradation of the organic pollutants (O'Dell 1939, Holkar et al. 2016). Chemical oxygen demand (COD) gives an average measure of the oxidation state of the organic by-products generated during the degradation of DB 2 (Orhon & Çokgör 1997) . Under the optimal conditions of pH 3.5 and $H_2O_2/Fe^{2+}$ ratio of 11, experiments using four varied $L_{COD}$ values (0.25, 0.5, 0.75, 1.0) were performed to examine the efficiency of Fenton reagent on COD removal kinetics of DB 2 (Fig. 8). The COD removal increases with decreasing $L_{COD}$ because the hypothetical amount of the concentration of $H_2O_2$ and $Fe^{2+}$ was increased. At the

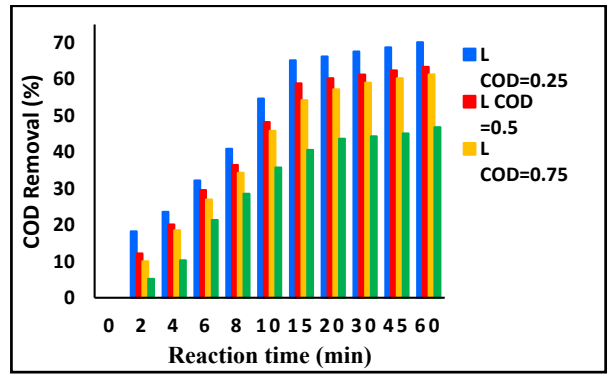


Fig . 8: Correlation between the COD removal of $1.0 \times 10^{-4}$ M DB 2 (COD = 224 mg $O_2$ . $L^{-1}$) versus reaction time. Experimental conditions: pH = 3.5 and molar ratio $H_2O_2$ /$Fe^{2+}$ = 11.

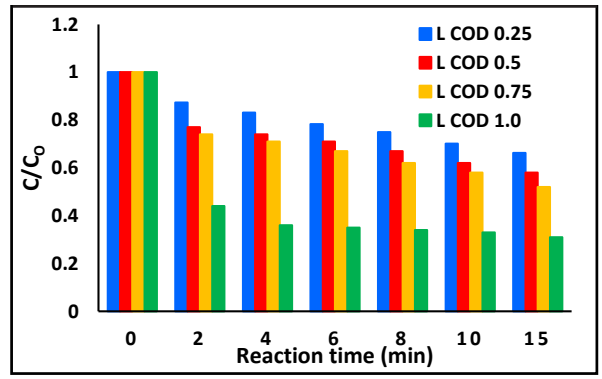


Fig. 9: The consumption of $H_2O_2$ using different. $L_{COD\ factor}$ Experimental conditions [DB2] = $1.0 \times 10^{-4}$ M pH = 3.5.

maximum ($L_{COD}$ = 1.0) 41% of COD was removed at 15 min while at the minimum ($L_{COD}$ = 0.25) 65% of COD was removed at the same time. These results approved that there was a residual amount of $H_2O_2$ in solution after 15 min of Fenton's oxidation reaction (Fig. 9). Although, all the $Fe^{2+}$ was transformed to $Fe^{3+}$, and that may decrease the reaction rate of $Fe^{2+}$ with $H_2O_2$, low amount of $H_2O_2$ was consumed (Fig. 9). The results of consuming the $H_2O_2$ showed that the 82 % $H_2O_2$ was consumed after 15 min at $L_{COD}$ = 1.0 while only about 43% $H_2O_2$ was consumed at $L_{COD}$ = 0.25.

### Effect of DB 2 Concentration on Colour Removal Kinetics

The colour removal efficiency at different concentrations of DB 2 was studied. The result was observed that the decolourization of dye increases with the decrease of primary DB 2 concentration (Fig. 10). As the concentration of dye decreased from $1.5\times10^{-4}$ M to $5.0\times10^{-5}$ M, the decolourization efficiency of dye increased from 43% to 93 % within the first 10 min of reaction. A decrease in the concentration of DB 2 dye reveals that lesser dye molecules will be available to scavenging by $HO^{\bullet}$ radicals which lead to an increase in the colour removal efficiency of DB 2 (Javaid & Qazi 2019) . Table 5 represents the second-order kinetic rates of colour removal of DB 2 at various DB 2 concentrations. Also, Table 5 shows the effect of different $[H_2O_2]$/[DB 2] ratios with an increase of colour removal kinetics combined with fact that the colour removal kinetics inversely proportional with DB 2 concentration in two varied steps.

A tenuous increase in colour removal kinetic rate (from 407 to 2604 $M^{-1}$ $min^{-1}$) occurred when the ratio $H_2O_2$/dye increases from 7.3 to 11. However, increasing the $H_2O_2$/dye ratio from 11 to 22, there was an acute increase in colour removal kinetic rate (from 2604 to 23415 $M^{-1}$ $min^{-1}$). Furthermore, the efficiency of DB2 colour removal increases with decreasing $H_2O_2$/DB 2 molar ratio, which points out that a higher concentration of DB 2 was removed by using a smaller dose of $H_2O_2$ (Fig. 10).

### The Influence of Inorganic Ions on DB 2 Colour Removal by Fenton Oxidation

The influence of some inorganic anions on the colour removal of DB 2 was tested at the optimum conditions. The experiments were designed to decompose ($1.0 \times 10^{-4}$ M) DB 2 in the presence of 1.0 % of inorganic salt used in this study.

Due to the expectation of the existence of a large number of anions in industrial textile wastewater, consequently, we intend to assess the decolourization of DB 2 in high doses of selected inorganic salts. The existence of inorganic anions

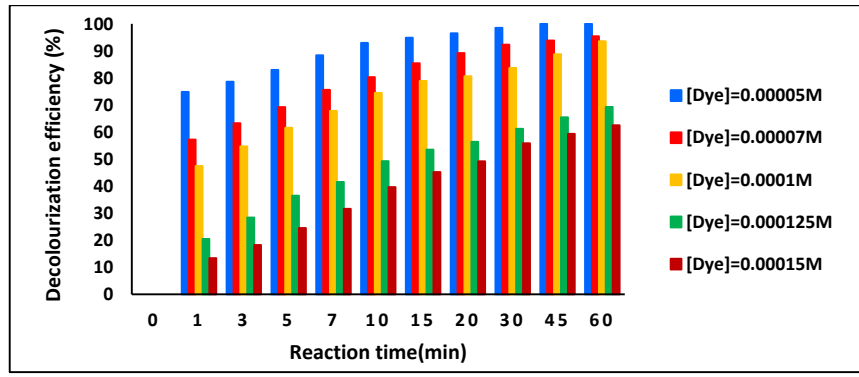


Fig. 10: Effect of initial DB 2 concentration on its colour removal efficiency during Fenton oxidation. Experimental conditions: $[H_2O_2]$ =$1.1\times10^{-3}$M, $[Fe^{2+}]$ =$1.0\times10^{-4}$ M and pH = 3.5.

Table 5: Second-order kinetic constants and regression coefficients for each DB 2 concentration during Fenton oxidation Experimental conditions: $[Fe^{2+}]$ = $1.0\times10^{-4}$ M, $[H_2O_2]$ = $1.1\times10^{-3}$ M and pH=3.5.

| [DB 2] (M) | $[H_2O_2]$/[DB 2] | $K_2$ ($M^{-1}$ $min^{-1}$) | $R^2$ |
|---|---|---|---|
| $1.5 \times 10^{-4}$ | 7.3 | 407 | 0.9819 |
| $1.25 \times 10^{-4}$ | 8.8 | 716 | 0.9714 |
| $1.0 \times 10^{-4}$ | 11 | 2604 | 0.9567 |
| $7.0 \times 10^{-5}$ | 15.7 | 7326 | 0.9501 |
| $5.0 \times 10^{-5}$ | 22 | 23415 | 0.94 |

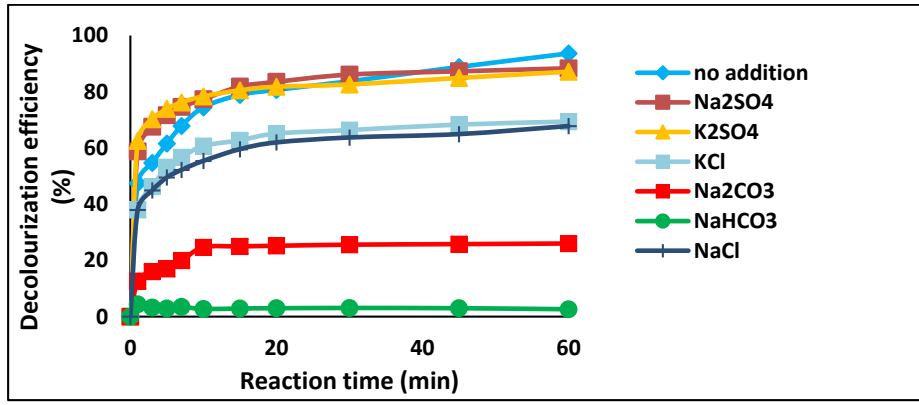


Fig: 11: Effect of addition of 1.0% inorganic anionic on DB 2 colour removal efficiency. Experimental conditions: pH = 3.5, [DB 2] = 1.0 $\times 10^{-4}$M, $[H_2O_2] = 1.1\times10^{-3}$ M and $[Fe^{2+}] = 1.0\times10^{-4}$ M.

in the aqueous solution had a high effect on Fenton oxidation (Oliveira et al. 2015). In this research, the influence of carbonate, bicarbonate, sulphate and chloride on the Fenton process was evaluated. Fig. 11 shows the effect of the studied anions on the DB 2 degradation by Fenton oxidation process. Anions inhibit the degradation of DB 2 in the following order: $HCO_3^- > CO_3^{2-} > Cl^- > SO_4^{2-}$

The addition of inorganic salts displayed various suppressed behaviours in Fenton process treatment. The influence of the addition of $HCO_3^-$ and $CO_3^{2-}$ may be attributed to a decrease in the average of production of $HO^\bullet$ because of the formation of $CO_3^{\bullet-}$ as shown in Eqs. (10) and (11).

$$HO^\bullet + HCO_3^- \rightarrow H_2O + CO_3^{\bullet-} \quad \ldots(10)$$

$$HO^\bullet + CO_3^{2-} \rightarrow OH^- + CO_3^{\bullet-} \quad \ldots(11)$$

The radical $CO_3^{\bullet-}$ is less reactive than $HO^\bullet$ radicals. In the case of $Cl^-$, it also has a great effect on the decomposition of DB 2 because it reacts with $Fe^{2+}$ forming complex and free radical less effective than the radical of hydroxyl as shown in Eqs. (12) and (13).

$$Fe^{2+} + Cl^- \rightarrow FeCl^+ \quad \ldots(12)$$

$$Cl^- + HO^\bullet \rightarrow ClOH^{\bullet-} \quad \ldots(13)$$

The salts of the sulphate ion appear to have less effect on the Fenton process, where sulphate ion reacts with $Fe^{2+}$ and $HO^\bullet$, a component $HO^\bullet$ [Eqs. (14) and (15)] (Kehinde and Abdul Aziz 2014).

$$Fe^{2+} + SO_4^{2-} \rightarrow FeSO_4 \quad \ldots(14)$$

$$HSO_4 + HO^* \rightarrow SO_4^{\bullet-} + H_2O \quad \ldots(15)$$

## CONCLUSIONS

The parameters for loading azo bond factor ($L_{azo\ bond}$) or COD loading factor ($L_{COD}$) were highly effective parameters of colour removal (decolourization) efficiencies using the batch system by Fenton oxidation. The results obeyed that the overdosed $H_2O_2$ was scavenging hydroxyl free radicals. The influence of the addition of $HCO_3^-$ and $CO_3^{2-}$ may be attributed to a decrease in the average of production of $HO^\bullet$ because of the formation of $CO_3^{\bullet-}$. The radical $CO_3^{\bullet-}$ is less reactive than $HO^\bullet$ radicals and the salts of the sulphate ion appear to have less effect on the Fenton process.

## REFERENCES

Agustina, T. E. and Ang, H. M. 2012. Decolourization and mineralization of C.I. reactive blue 4 and C.I. reactive red 2 by Fenton oxidation process. International Journal of Chemical and Environmental Engineering, 3(3): 142-148.

Dehghani, M., Mosleheyan, M., Karimiyan, S., Faramarzi, Z., Ansari, M., Shamsedini, N., Reza Javaheri, M. and Shahsavani, S. 2016. Efficiency of the photo Fenton process for Decolourization of direct red 81 dye from the aqueous solution. Jundishapur J. Health Sci., 8(4): e34951.

Dewil, R., Mantzavinos, D., Poulios, I. and Rodrigo, M. A. 2017. New perspectives for advanced oxidation processes. Journal of Environmental Management, 195: 93-99.

Esteves, B. M., Rodrigues, C. S., Boaventura, R. A., Maldonado-Hodar, F. J. and Madeira, L. M. 2016. Coupling of acrylic dyeing wastewater treatment by heterogeneous Fenton oxidation in a continuous stirred tank reactor with biological degradation in a sequential batch reactor. J. Environ. Manage., 166: 193-203.

Garcia-Segura, S. and E. Brillas. 2016. Combustion of textile monoazo, diazo and triazo dyes by solar photoelectro-Fenton: Decolorization, kinetics and degradation routes. Applied Catalysis B: Environmental, 181: 681-691.

Holkar, C. R., Jadhav, A. J., Pinjari, D. V., Mahamuni, N. M. and Pandit, A. B. 2016. A critical review on textile wastewater treatments: Possible approaches. Journal of Environmental Management, 182: 351-366.

Javaid, R. and U. Y. Qazi. 2019. Catalytic oxidation process for the degradation of synthetic dyes: An overview. International Journal of Environmental Research and Public Health, 16: 2066.

Jin, H., Tian, X., Nie, Y., Zhou, Z., Yang, C., Li, Y. and Lu, L. 2017. Oxygen vacancy promoted heterogeneous Fenton-like degradation of ofloxacin at pH 3.2-9.0 by Cu substituted magnetic Fe3O4@FeOOH nanocomposite. Environ. Sci. Technol., 51(21): 12699-12706.

Kehinde, F. and Abdul Aziz, H. 2014. Textile wastewater and the advanced oxidative treatment process, an overview. International Journal of Innovative Research in Science, Engineering and Technology, 3(8): 15310-15316.

Liu, Y., Jin, W., Zhao, Y., Zhang, G. and Zhang, W. 2017. Enhanced catalytic degradation of methylene blue by αFe2O3/graphene oxide via heterogeneous photo-Fenton reactions. Applied Catalysis B: Environmental, 206: 642-652.

Lopez-Alvarez, B., Torres-Palma, R. A., Ferraro, F. and Penuela, G. 2012. Solar photo-Fenton treatment of carbofuran: analysis of mineralization, toxicity, and organic by-products. J. Environ. Sci. Health A Tox. Hazard. Subst. Environ. Eng., 47(13): 2141-50.

Lucas, M. S. and Peres, J. A. 2006. Decolourization of the azo dye reactive black 5 by Fenton and photo-Fenton oxidation. Dyes and Pigments, 71(3): 236-244.

Luo, L., Yao, Y., Gong, F., Huang, Z., Lu, W., Chen, W. and Zhang, L. 2016. Drastic enhancement on Fenton oxidation of organic contaminants by accelerating Fe(iii)/Fe(ii) cycle with l-cysteine. RSC Advances, 6(53): 47661-47668.

Mousset, E., Oturan, N., van Hullebusch, E. D., Guibaud, G., Esposito, G. and Oturan, M. A. 2014. Treatment of synthetic soil washing solutions containing phenanthrene and cyclodextrin by electro-oxidation. Influence of anode materials on toxicity removal and biodegradability enhancement. Applied Catalysis B: Environmental, 160-161: 666-675.

Nidheesh, P. V., Gandhimathi, R. and Ramesh, S. T. 2013. Degradation of dyes from aqueous solution by Fenton processes: A review. Environmental Science and Pollution Research, 20(4): 2099-2132.

Nogueira, R. F. P., Oliveira, M. C. and Paterlini, W. C. 2005. Simple and fast spectrophotometric determination of H2O2 in photo-Fenton reactions using metavanadate. Talanta, 66(1): 86-91.

O'Dell, J. W. 1939. Determination of Chemical Oxygen Demand by Semi-Automated Colorimetry, U.S. Environmental Protection Agency.

Oliveira, T. D. D., Martini, W. S., Santos, M. D. R., Matos, M. A. C. and Rocha, L. L. D. 2015. Caffeine oxidation in water by Fenton and Fenton-like processes: Effects of inorganic anions and ecotoxicological evaluation on aquatic organisms. Journal of the Brazilian Chemical Society, 26: 178-184.

Orhon, D. and E. U. Çokgör. 1997. COD Fractionation in Wastewater Characterization—The State of the Art. Journal of Chemical Technology & Biotechnology 68:283-293.

Razzak, N. R. B. and Hossain, D. 2016. Characterization and advanced oxidation treatment of dyeing effluent by Fenton's reagent. Water Resources, 43(3): 559-564.

Sharma, A., Ahmad, J. and Flora, S. J. S. 2018. Application of advanced oxidation processes and toxicity assessment of transformation products. Environmental Research, 167: 223-233.

Trovó, A. G., Hassan, A. K., Sillanpää, M. and Tang, W. Z. 2016. Degradation of acid blue 161 by Fenton and photo-Fenton processes. International Journal of Environmental Science and Technology, 13(1): 147-158.

Wu, T. and Englehardt, J. D. 2012. A new method for removal of hydrogen peroxide interference in the analysis of chemical oxygen demand. Environmental Science & Technology, 46(4): 2291-2298.

Nature Environment and Pollution Technology
An International Quarterly Scientific Journal

p-ISSN: 0972-6268
(Print copies up to 2016)
e-ISSN: 2395-3454

Vol. 19 | No. 4 | pp. 1367-1378 | 2020

Original Research Paper

https://doi.org/10.46488/NEPT.2020.v19i04.003

Open Access Journal

# Groundwater Recharge Potential Sites in Semi-Arid Region of Man River Basin, Maharashtra State, India: A Geoinformatic Approach

**V. M. Dikshit†**
Department of Geology, D.B.F. Dayanand College of Arts and Science, Solapur, 413 002, India
†Corresponding author: V. M. Dikshit; vinay09dikshit@gmail.com

**Nat. Env. & Poll. Tech.**
**Website: www.neptjournal.com**

*Received:* 19-11-2019
*Revised:* 20-12-2019
*Accepted:* 03-01-2020

**Key Words:**
Watershed development
Geoinformatics
Overlay analysis
Groundwater recharge

## ABSTRACT

The prosperity of the entire biotic community depends on two broad components of nature; land and water. The basaltic rock is known to have poor storage and transmission capability. It gets fully saturated during monsoon but a situation of rejected recharge results in post-monsoon and early summer months. These aquifers also drain naturally due to high water table gradient formed by sloping and undulating topography. The available and new groundwater recharge potential zones can better augment by adopting a scientific and multi-sectoral approach for making the future plan. The study area encompasses Manganga River basin, bounded between Lat. 17°54' N to 17°00' N and Long. 74°27' E to 75°31' E. The study area is in basaltic terrain with undulating topography. The spatial and non-spatial data generated based on various thematic maps such as geology, lineament density, geomorphology, slope, drainage buffer, land-use land-cover, soil texture and soil erodibility have been prepared using satellite data. The groundwater prospects maps generated by overlay analysis of the spatial thematic maps were grouped into five classes and their distribution are: very good/excellent, good, moderate, poor and very poor. The results show that a major portion of the study area falls in the category 'poor' followed by 'very poor'. Based on the outputs derived from groundwater recharge potential zones, an action plan for watershed development in the study area has been suggested like the development of percolation/water retention ponds at the identified sites and tube/bore/open wells along the dense lineament zones. The aspect related to conjunctive use, groundwater legislation, the involvement of NGO'S, women and community participation, mass awareness, adoption of advanced irrigation system etc. will play an important role in conserving and developing the precious water resources. .

## INTRODUCTION

Geoinformatics has been described as "the science and technology dealing with the structure and character of spatial information, its capture, its classification and qualification, its storage, processing, portrayal and dissemination, including the infrastructure necessary to secure optimal use of this information" or "the art, science or technology dealing with the acquisition, storage, processing production, presentation and dissemination of geoinformation". Geoinformatics is integrated studies of remote sensing, Geographic Information System (GIS) and Global Positioning System (GPS). Remote sensing is the art and science of acquiring images of the earth using sensors on aeroplanes or satellites. These images have capabilities for manipulating, analysing and visualizing in a remote sensing software. Remote sensed imagery is integrated within a GIS. A geographic information system (GIS) is a computer-based tool for mapping and analysing feature events on the earth. GIS technology integrates common database operations, such as query and statistical analysis, with maps. GIS manages location-based information and provides tools for display and analysis of various statistics, including population characteristics, economic development opportunities, and vegetation types. GIS allows linking databases and maps to create dynamic displays. Additionally, it provides tools to visualize, query, and overlay those databases in ways not possible with traditional spreadsheets. These abilities distinguish GIS from other information systems and make it valuable to a wide range of public and private enterprises for explaining events, predicting outcomes, and planning strategies. GPS is a satellite-based radio navigation system that provides geolocation and time information to a GPS receiver anywhere on or near the Earth where there is an unobstructed line of sight to four or more GPS satellites. In this paper, a geoinformatics approach has been taken to delineate groundwater recharge zones in the study area.

## STUDY AREA

Man River is the right bank tributary of the south-easterly flowing Bhima River. The Man River basin spatially occupies parts of Sangli, Satara and Solapur districts of Maharashtra

state and is situated between 17°00' to 17°52' N latitude and 74°25' to 75°30' E longitude (Fig. 1). Man River has its origin (head) in the Mahadeva Hills at an altitude of 1054m ASL. The total catchment area of the basin is about 4,626km$^2$ and the stream length is 154km. It is flowing over basaltic stratum, known as Deccan Plateau which is the eastern part of Western Ghats (Sahyadri Mountain) formed by Quaternary cymatogenic upwarp during the formation of West Coast Fault (WCF) system in the Arabian Sea (Powar 1993). The sea-facing scarp of the eastern fault block of WCF recedes eastward due to weathering, and forms a strip of a low-lying area known as Konkan Coastal Belt (KCB). Hence, Western

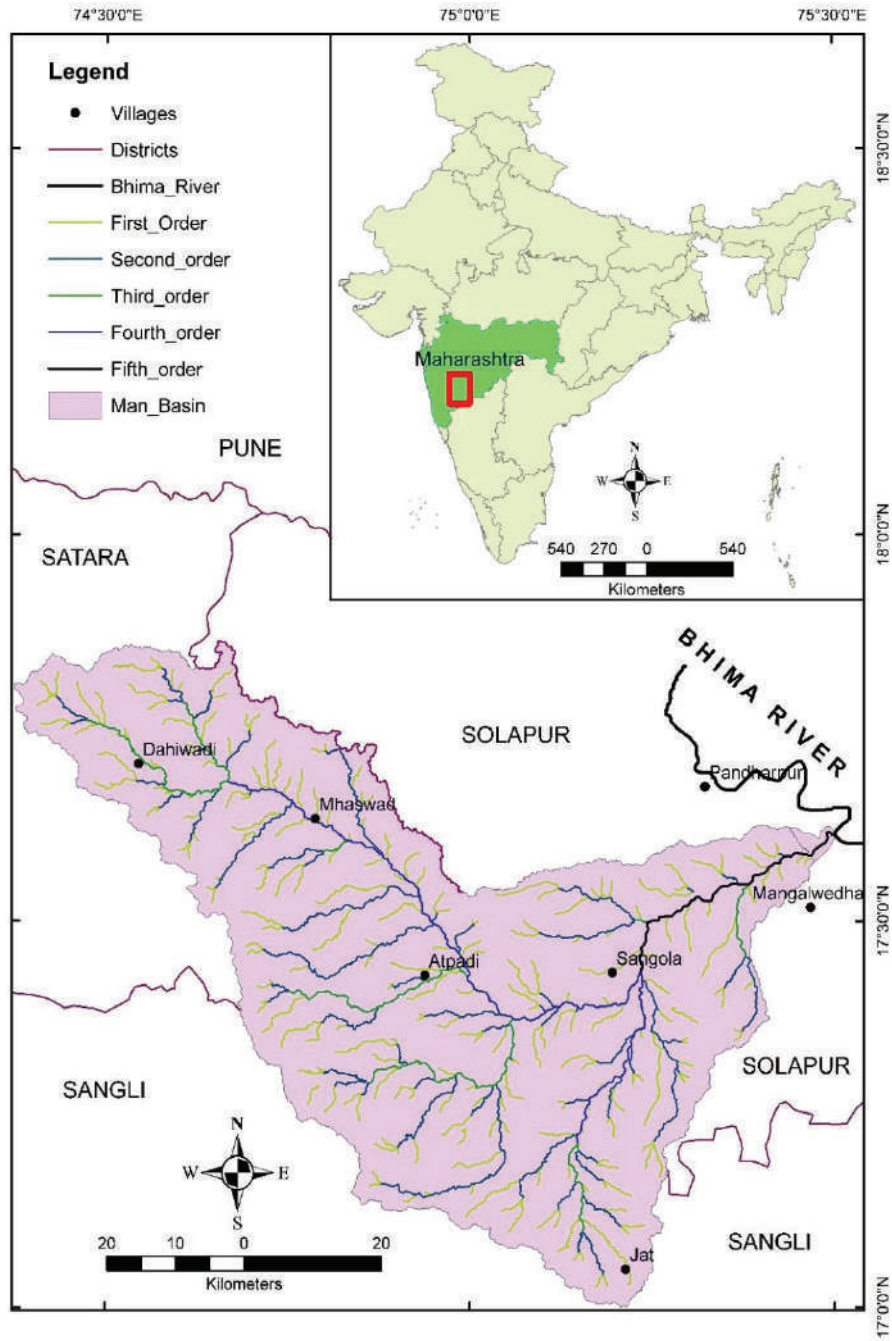


Fig. 1: Location map of Man River basin.

Ghats forms a major drainage divide between westward and eastward flowing river systems. The eastward flowing rivers are longer than westward flowing rivers, which ultimately join Arabian Sea (west coast) and Bay of Bengal (east coast) respectively. The Western Ghats develops rain shadow zone of SW monsoon in the major parts of central and eastern Maharashtra state.

Being a part of the rain shadow zone, the Man River basin experiences dry, semi-arid tropical monsoon type of climate (IMD 2005). According to agro-climatic classification, the study area falls in scarcity zone (Kalamkar 2011). The Man River basin receives annual rainfall between 500 and 700mm, of which 90% precipitation received during June to October months of the SW monsoon season. About 50% precipitation is received during September to October. The monsoonal rainfall pattern is bimodal. The potentially high evapotranspiration rate is because of the high temperature throughout the year. Occasionally flash flood generates and recharges the groundwater. Characteristically, the Man River basin is in the zone of lowest annual rainfall (<600mm) and highest annual water deficit (>900mm) and has its source (head) in lowest rainfall zone, admits it in the class of chronic to the severe drought-prone zone of the semi-arid river basin. The vegetation cover is sparse and is dominated by thorny vegetation, shrubs and grasses. *Acacia* is the most common naturally growing species in the area.

Lithologically, the Man River basin constitutes horizontally disposed "aa type simple" basaltic lava flows of Upper Cretaceous to Lower Miocene origin. At some places, two flows are separated by red bole bed. The red bole bed comprises clay which was deposited between two lava eruptions, and forms a district hydrogeological unit as it can receive, stock and transmit water due to the inherent physical characteristics like porosity and permeability. Recent alluvial formations (2 to 12m thick) overlie basaltic traps. The detrital material consists of silt, clay, silt, sand and gravel, occurring as lenses or patches along the major stream courses. Due to its limited areal extent alluvium do not constitute as potential aquifers.

The basaltic flows derive its status as an aquifer based on its secondary porosity in the form of vesicles, fractures, well developed interconnected jointing pattern, cooling joints and decomposed material (murum) (Powar 1981). Characteristically, a flow has an upper vesicular and amygdaloidal part, a middle part with horizontal and vertical sets of joins and massive and un-jointed lower part. The top-soil overlie on decomposed basaltic material. Factors playing the vital role in the occurrence and movement of groundwater are topography, nature and extent of weathering, jointing and fracture pattern, thickness and depth of occurrence of vesicular basalts. The shallow aquifers in the area are phreatic and unconfined and occur at the depth of 10 to 15m. At places, potential zones encounter at deeper levels in the interconnected fractured zone, which are generally confined down to 60-90m.

Hydromorphologically, the study area has been classified as highly dissected undulating highlands, moderately dissected gently sloping terrain, poorly dissected plain and low land valley fills. Highly dissected undulating highlands (hillocks) forms major run-off zones, moderately dissected gently sloping terrain unit forms recharge zones and poorly dissected plain and low land valley fills are groundwater storage zones (Fig. 2).

The Man River basin is tectonically disturbed (Chandrasekhar 1991), which is dictated by the evidences such as 1. Presence of the combination of dendritic and rectangular drainage pattern, 2. River flows through the structurally controlled valley throughout its course after Najre village, 3. Lengths of right side tributaries are more than lengths of left tributaries is indicative of asymmetric drainage basin and eastward tilt of the drainage basin, 4. The Man river flowing all along its course in south-easterly direction but abruptly changes its course halfway to follow north-easterly direction suggesting stream capture, 5. River has palaeo-channels throughout its course between Najre and Kadlus as well as abandoned channels are observed at Hatid, Shegaon, and Walekhind villages, 6. Thick alluvium covered black cotton soil has been observed near Mangalvedha village at the confluence of Man River and Bhima River and 7. Presence of Sangola gravity 'high'. The Man River basin shows high-level erosional surfaces than the surrounding tributaries of Bhima River and Krishna River. This uniqueness may be one of the causes of groundwater scarcity. The palaeo-channels located in the basin at Mangewadi, Kadlus, Sonand, Baldongi and Balgaon could be the potential recharge zones. These tectonic weaknesses could be the best groundwater recharge zones.

## MATERIALS AND METHODS

Delineation of groundwater recharge zones has been carried out using geoinformatics techniques for Man River basin. The groundwater occurrence and movement are directly or indirectly controlled by terrain characteristics such as lithological units, structural disposition, geomorphic set-up, surface water condition, vegetation, etc. Groundwater occurrence being a subsurface phenomenon, its identification is indirectly based on the analysis of some directly observable terrain features. These can be well understood with the help of remote sensing (RS). The revolution in computer technology, the advent of Remote Sensing (RS) and Geographic Information System

(GIS) offers great scope for handling and analysing spatial data including the delineation of groundwater recharge zones (Prasad et al. 2008).

Visual interpretation and digital image analysis of satellite data help in the indication of groundwater recharge zones through 1) Identification of geological structures and the hydrophysical properties, 2) Water-bearing geological formations and water enrichment, 3) Areas of recharge, 4) Places of discharge, 5) Nature of outlet of groundwater to the surface, 6) Depth and conditions for the occurrence of groundwater and 7) Direction of movement.

Although remote sensing (RS) data do not directly detect deeper subsurface resources, it has been effectively used in groundwater exploration as RS data aid in drawing inferences on groundwater potentiality of the region indirectly. The freshwater surface resources are normally considered to form subsurface water resources. These sources of surface water are directly detected by satellite RS data as water absorbs most of the radiation in the infrared region, which helps in the delineation of even smaller water bodies. Vegetation, which is easily detected through spectral reflectance, is indicative of the water saturation and moisture of the ground. RS data help indirectly by giving certain ground information that aid in drawing inferences on groundwater recharge zones of the area.

Primarily, the infiltration capacity of the soil determines the groundwater potentiality. The speed of infiltration is dependent upon mainly on porosity and permeability of the soil and the velocity of the surface run-off. Infiltration reduces to a great extent for the steeply sloping ground

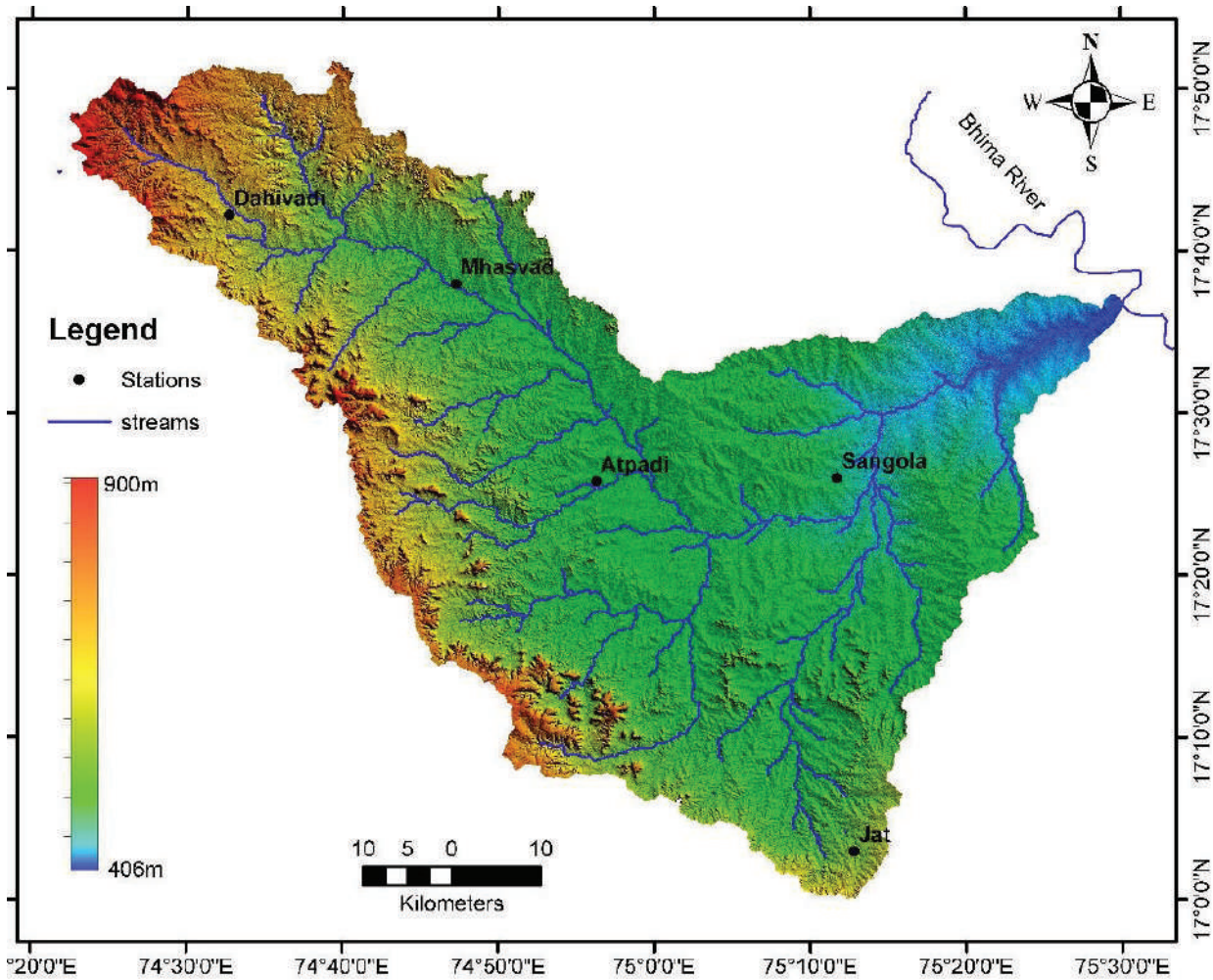


Fig. 2: Colour coded Digital Elevation Model (DEM) of Man River Basin with locations of rain gauge stations.

surface as the velocity of surface run-off increases sharply. Also, a vegetative cover gives a higher infiltration capacity compared to barren lands. Factors which help in the storage of groundwater are 1. infiltration capacity, 2) porosity and permeability of the soil, 3) velocity of the surface run-off, 4) vegetation (vegetative cover increases infiltration capacity) and 5) thickness of the porous and permeable zone.

Digitally enhanced products of the LANDSAT 7 ETM+ satellite images have been used in this study for the delineation of land-use/land cover and geomorphology of the study area. Survey Map of India (1:50,000) have been used to delineate the drainage and contour lines. The orders were designated to each stream following Strahler stream ordering technique (Strahler 1964). Buffers were generated for each stream proportional to their groundwater prospects. DEM was generated through 20m contour lines and used to derive the slope (%). The Soil map published by National Bureau of Soil Survey (scale 1:5,00,000) and the geological map published by Geological Survey of India (scale 1:2,50,000) were used to generate the soil and geology map of the study area. Various thematic maps prepared for the study area were verified in the field with the help of handheld GPS instrument. The spatial database layers like geomorphology, lineament density, slope in degrees, land use/land cover, rainfall erosivity and soil type were used to delineate the groundwater recharge zones. Appropriate weightage was assigned to each of the map layers based on their groundwater prospects. Ranks were also assigned to each subclasses of the thematic maps (Table 1). Lithologically the entire study area exposes basalt stratum uniformly and there is no change in lithology, hence lithological thematic map has not been prepared.

All the thematic maps were converted into raster maps (30 x 30 m grid) and superimposed by weighted overlay method (rank and weightage wise thematic maps), for the delineation of the groundwater recharge zones. The groundwater recharge zones were grouped into five classes; very high, high, moderate, low, and very low. Dug well inventory has been carried during the pre and post-monsoon to understand the hydrogeology of the study area. The wells were located in the field using a Garmin handheld GPS. Fig. 3 depicts the illustration of the methodology of the study.

## RESULTS AND DISCUSSION

The results of thematic maps prepared from the special database are as follows.

Table 1: Weightage and scores assigned to various parameters and subclasses for assessing groundwater recharge zones.

| Sr No. | Parameters | Sub Classes (map units) | Score | Weight % |
|---|---|---|---|---|
| | | Man River Channel | 5 | |
| 1 | Geomorphology | Valley | 4 | 30 |
| | | Lower Plateau | 3 | |
| | | 0.0 to 0.25 | 2 | |
| 2 | Lineament density | 0.26 to 0.50 | 4 | 20 |
| | | 0.51 to 0.75 | 5 | |
| | | < 5 Gentle | 5 | |
| 3 | Slope (degree) | 5- 20 Moderate | 3 | 20 |
| | | >20 Steep | 0 | |
| | | Perennial river / Sand Riverine | 5 | |
| | | Irrigated crop land | 3 | |
| 4 | Landuse/ Land cover | Rainfed cropland | 2 | 10 |
| | | Shrubs / grasses | 1 | |
| | | Bare areas | 1 | |
| | | 425-450 | 2 | |
| 5 | Rainfall erosivity | 451-470 | 4 | 10 |
| | | 471-490 | 5 | |
| | | Deep black | 5 | |
| 6 | Soil Type | Medium black | 3 | 10 |
| | | Coarse shallow | 3 | |

**Geomorphology:** Geomorphologically the area represents rolling topography by residual hillocks formed by denudational processes 800mto 1054m ASL covered by basaltic lava flows. The hill slopes are gentle to steep in nature. The intermittent valleys or pediment zones are represented by stream courses and agriculture fields. The lower plateau, valleys and river channel are the predominant geomorphic units (Figs. 1 and 2). The lower plateau (76.5%) indicates moderate groundwater recharge. The valleys (21.86%) are landforms formed by fluvial activity proved to be good recharge potential zones. They show recent sediments deposited by the streams. This geomorphic unit possesses high groundwater recharge potential. The geomorphic unit containing river channels (1.64%) in alluvial formation possesses very high groundwater recharge potential.

**Lineament density:** Features of structural origin are structural hills, ridges and valleys. Structural ridges are poor groundwater recharge zones. Whereas subsurface fractures

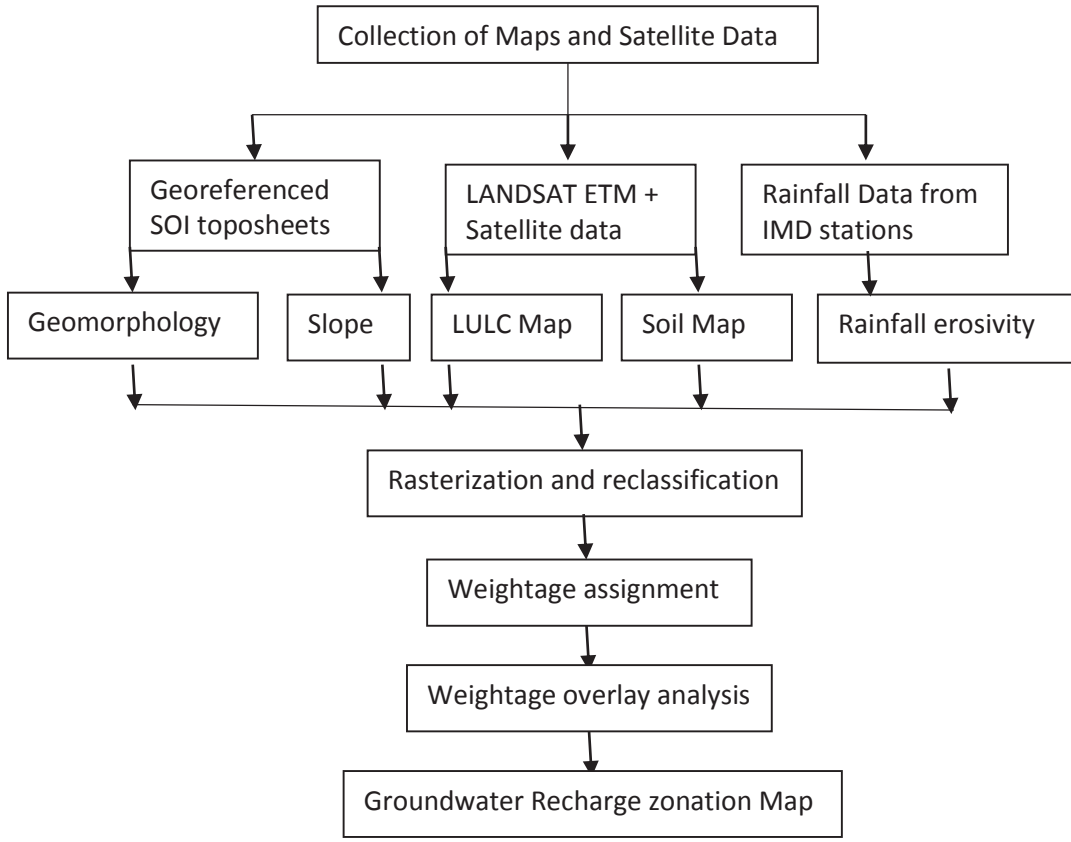


Fig. 3: Flow Chart of the methodology adopted in the present study.

Table 2: R-factor (Rainfall erosivity) in the study area.

| Sr. No. | Rain gauge stations | Rainfall intensity (I) in inches/30 min/year | | | | | | R-Factor |
|---|---|---|---|---|---|---|---|---|
| | | 2012 | 2013 | 2014 | 2015 | 2016 | 2017 | |
| 1. | Jat | 0.18 | 0.63 | 0.38 | 0.15 | 0.58 | 0.42 | 426 |
| 2. | Atpadi | 0.18 | 0.36 | 0.36 | 0.23 | 0.27 | 0.56 | 475 |
| 3. | Sangola | 0.25 | 0.36 | 0.36 | 0.23 | 0.24 | 0.56 | 466 |
| 4. | Dahiwadi | 0.90 | 0.23 | 0.32 | 0.22 | 0.20 | 0.39 | 489 |
| 5. | Mhaswad | 0.90 | 0.23 | 0.32 | 0.22 | 0.20 | 0.39 | 489 |

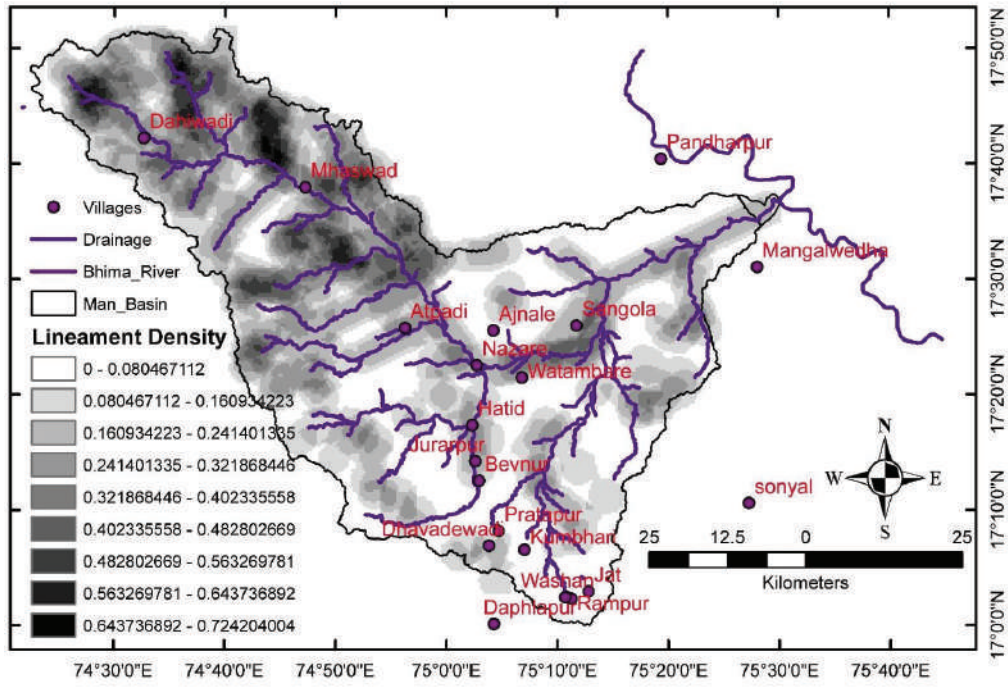


Fig. 4: Lineament density map.

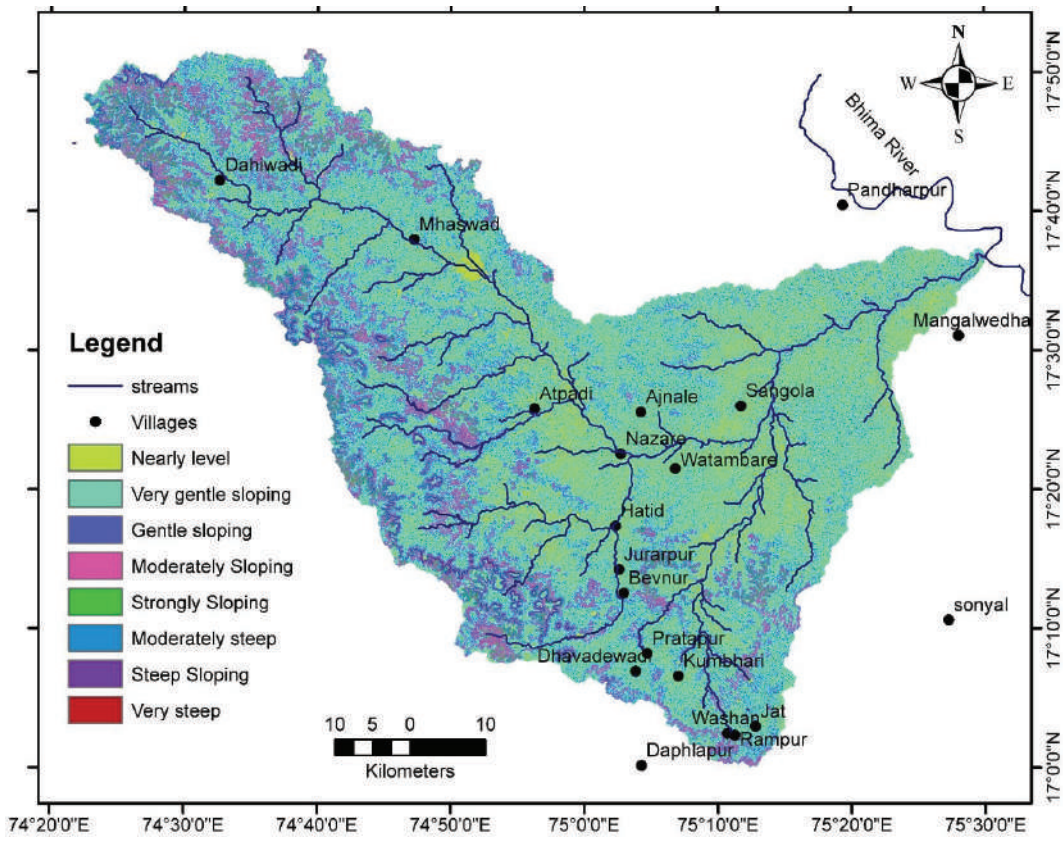


Fig. 5: Classified slope map of the study area.

and joints qualify as good groundwater recharge zones. The lineaments are surface expressions of subsurface weak zones such as fractures, joints, faults, etc. and are observed as faint lines of straight or curved nature, change in grey level tones, linear growth of vegetation and abnormal straight course of the stream, which can be accurately mapped after ground check. Mapping of lineaments can be achieved by the edge enhancement process called "spatial filtering" of satellite data. Prasad & Sivaraj (2000) used IRS LiSS-III satellite data and aerial photographs to locate structurally controlled weaker zones, i.e. lineaments suitable for groundwater accumulation. The density variation of lineaments was achieved in the ArcGIS environment and presented as a thematic map (Fig. 4). The region of higher lineament density is in the dark shade which is considered as potential groundwater recharge zones.

**Slope:** Slope plays a key role in the groundwater occurrence as infiltration is inversely related to the slope (Mondal et al. 2009). A major portion (84.21%) of the Man River basin falls under 'Gentle slope' class (0 to 5 per cent). 'Moderate slope' (5 to 20 percent) constitute 15.69% and 'Steep slope' (> 20 percent) form only 0.1% of the total area (Fig. 5). The dominance of the lower slope classes (0 to 20 %) is a favourable feature for groundwater recharge and its potential depends on underlying lithology as well as geomorphology. A break in the slope *(i.e.* steep slope followed by gentle slope) generally promotes an appreciable groundwater infiltration (Saraf et al. 1998)

**Land use land cover:** The land use in the study area is classified in to nine types (Fig. 6). The major area is covered by mosaicked vegetation, shrubs and grasses (35.24%), followed by irrigated cropland (24.39%) and rain-fed and mosaicked

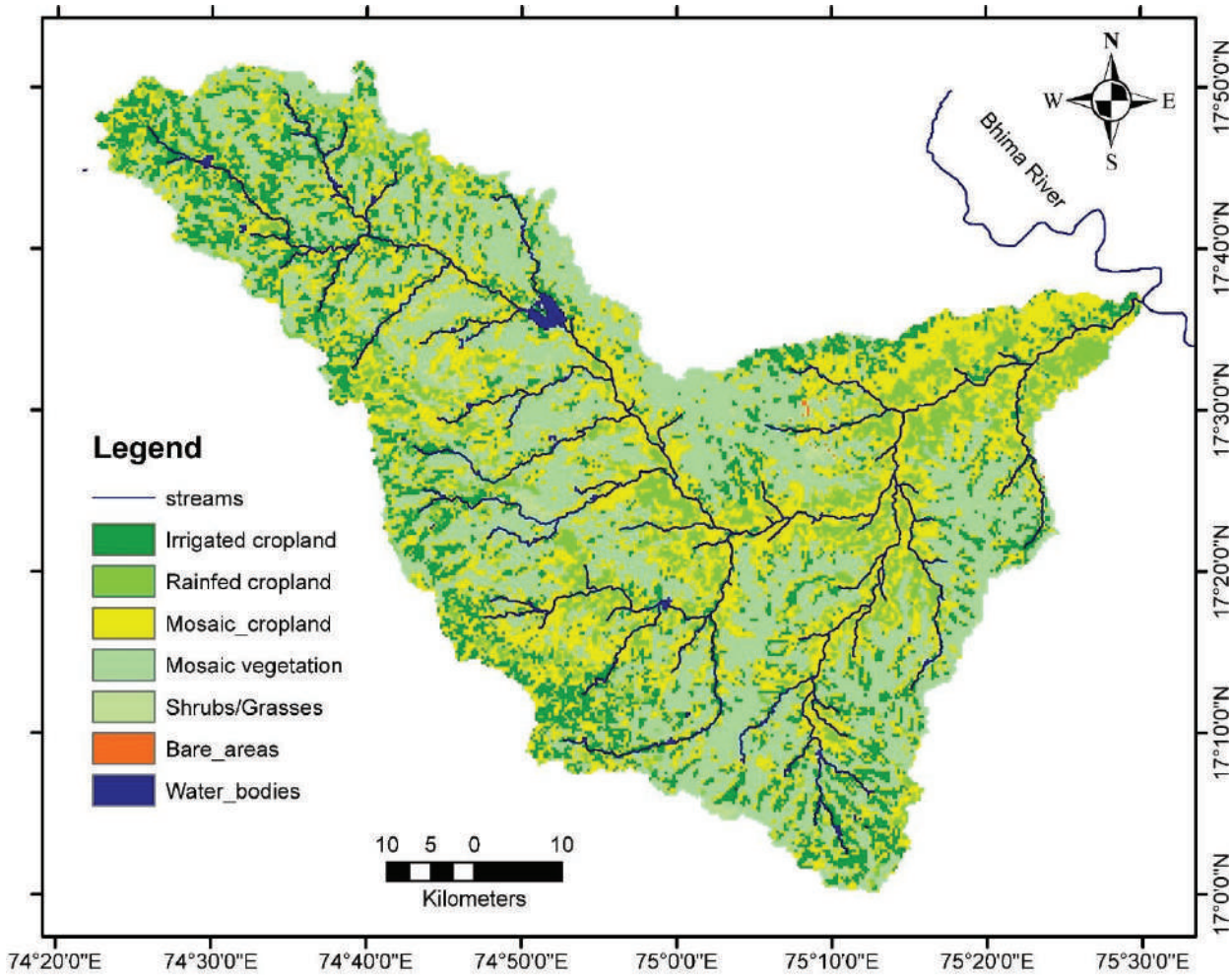


Fig. 6: Land Use Land Cover (LULC) map of the study area.

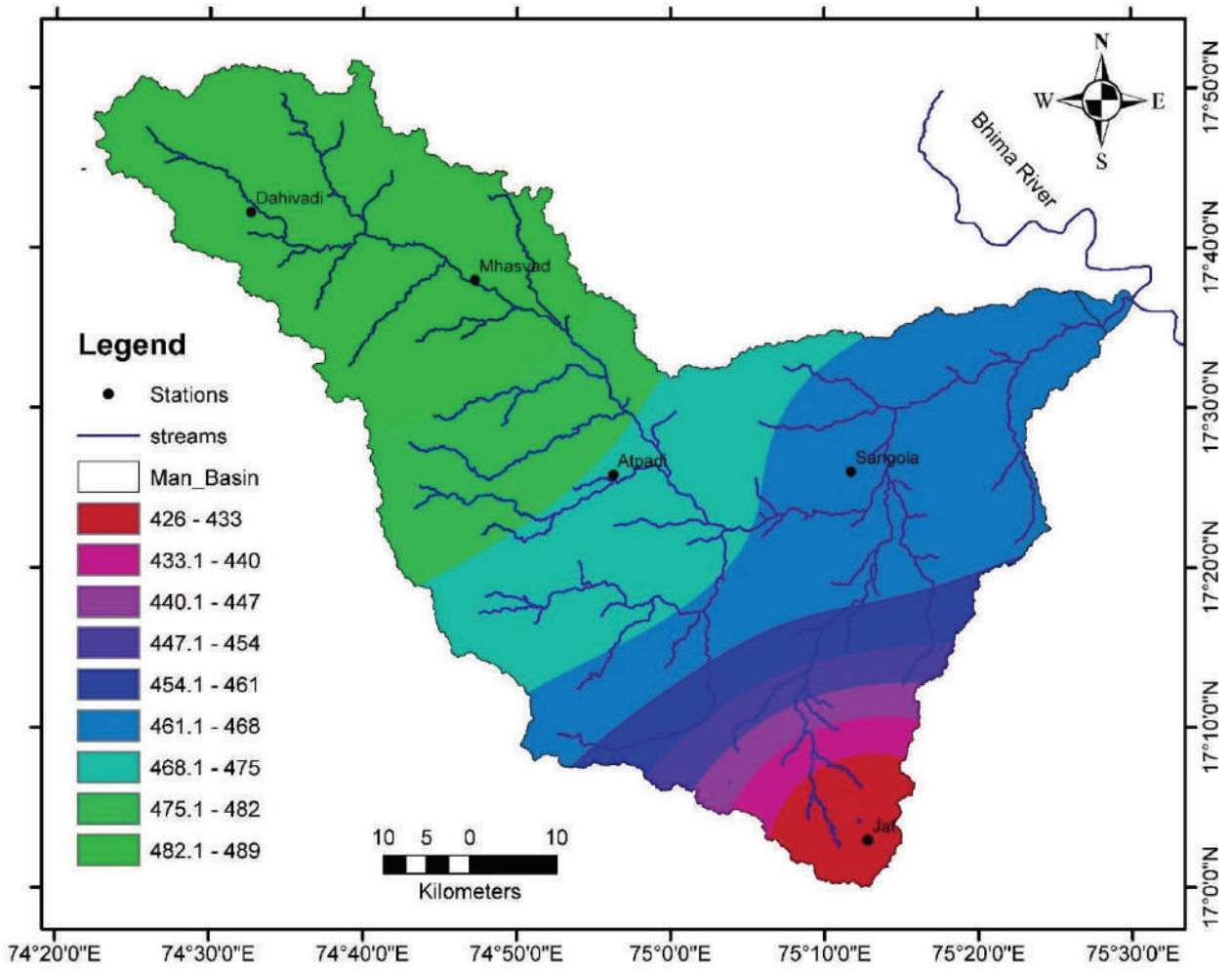


Fig. 7: Rainfall erosivity (R-factor) map of the study area.

cropland (11.40%) of very good water potential, and barren land (10.23%), etc.

**Rainfall erosivity (R):** It is the annual total value of the erosion index ($EI_{30}$) for a particular location. Computation of $EI_{30}$ from recording type rain gauge chart is described by Singh et al. (1981). It is the average annual summation (EI) values in a normal year's rain. The erosion-index is a measure of the erosion force of specific rainfall. When other factors are constant, storm losses from rainfall are directly proportional to the product of the total kinetic energy of the storm (E) times its maximum 30-minute intensity (I). Storms less than 0.5 inches are not included in the erosivity computations because these storms generally add little to the total R value. R factors represent the average storm EI values over a 22-year record. R is an indication of the two most important characteristics of a storm determining its erosivity, the amount of rainfall and peak intensity sustained over an extended period. The erosivity of rainfall varies greatly by location. The rainfall record for six years was collected from rain gauge stations (Jat, Atpadi, Sangola, Dahiwadi and Mhaswad) in the Man River basin. The obtained data were calculated for rainfall erosivity using equation 1 and presented in Table 2.

After determining the E and $I_{30}$ values for each storm throughout the record, they are to be multiplied by each other and then summed on a per year basis. The average of these annual sums over the period of record is the R-factor.

$$R = \frac{1}{n}\sum_{j=1}^{n}\left[\sum_{K=1}^{m}(E)(I_{30})\right]_j \qquad \ldots(1)$$

Where, K is the number of the individual storms up to m which is the total number of storms in a year, and j is the

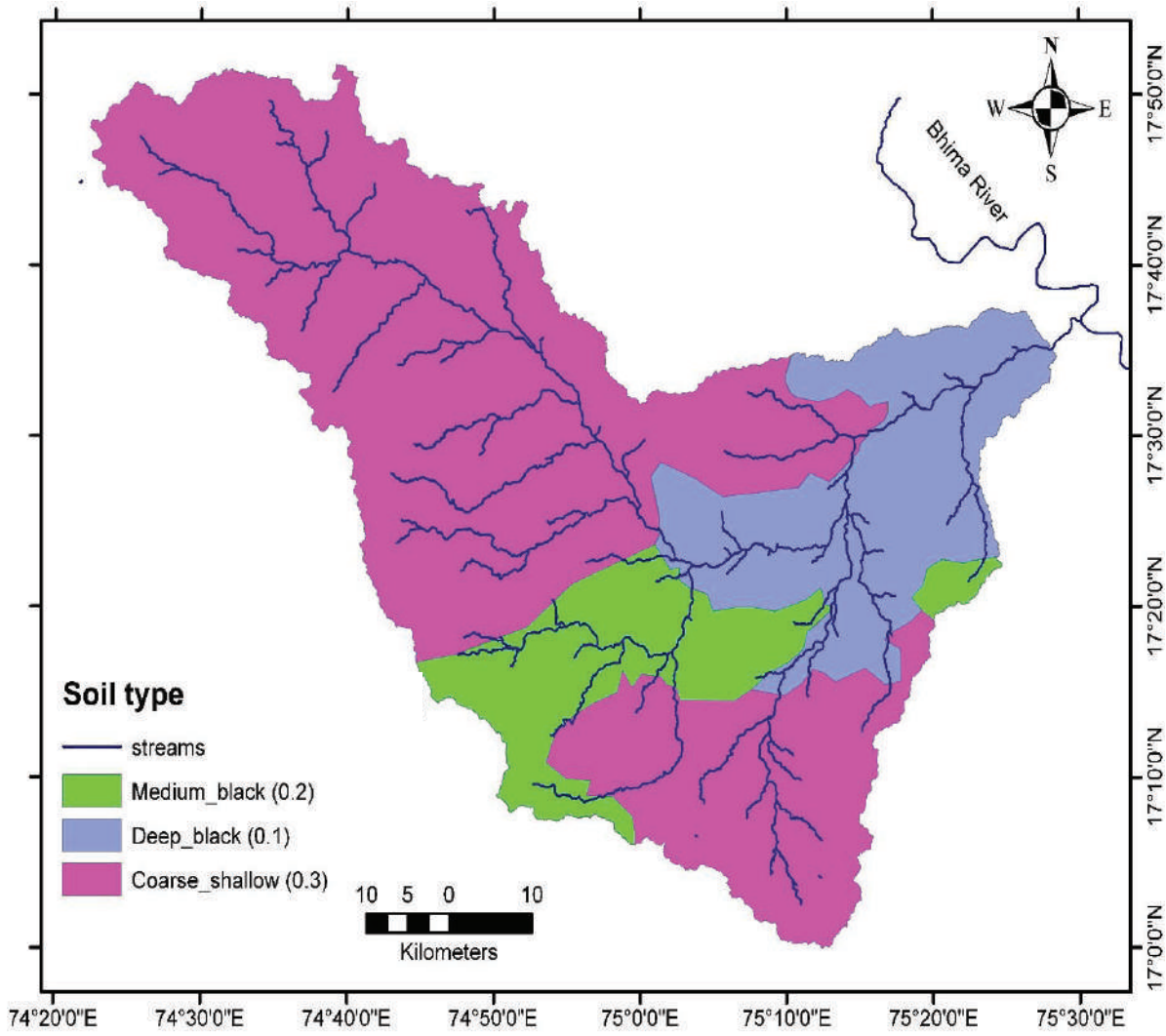


Fig. 8: Soil map of the study area.

number of the year up to n which is the total number of the years over which data was collected.

The thematic map of rainfall erosivity is prepared (Fig. 7) using the data from Table 2. The region of higher rainfall erosivity resist infiltration, hence, found to be non-potential groundwater recharge zone. Soil conservation practices should be undertaken in these regions to increase the infiltration rate.

**Soil type:** Three types of soils are generally seen in the Man River Basin, namely; medium black, deep black and coarse shallow (Fig. 8). Coarse shallow type of soil constitutes the most predominant region in the study area. The topsoil and the subsoil are highly pervious and facilitate good recharge. Riverine alluvium soil is seen all along the banks of Man River. They predominantly contain sand fraction. Brown hydromorphic soil is mostly confined to valley bottoms of the undulating portions. They have been formed as a result of transportation and deposition of material from the adjoining hills and slopes, and also through deposition by rivers. The deep black soil has a high water holding capacity which facilitates infiltration, while medium black and coarse shallow soils have moderate to low infiltration capacities respectively.

**Potential groundwater recharge zones:** Groundwater recharge zones (Fig. 9) were delineated through the integration of the reclassified raster map layers of geomorphology, lineament density, slope, landuse/land cover, soil erosivity and soil type using the weighted overlay analysis in Arc-GIS platform. The result shows that the distribution of groundwa-

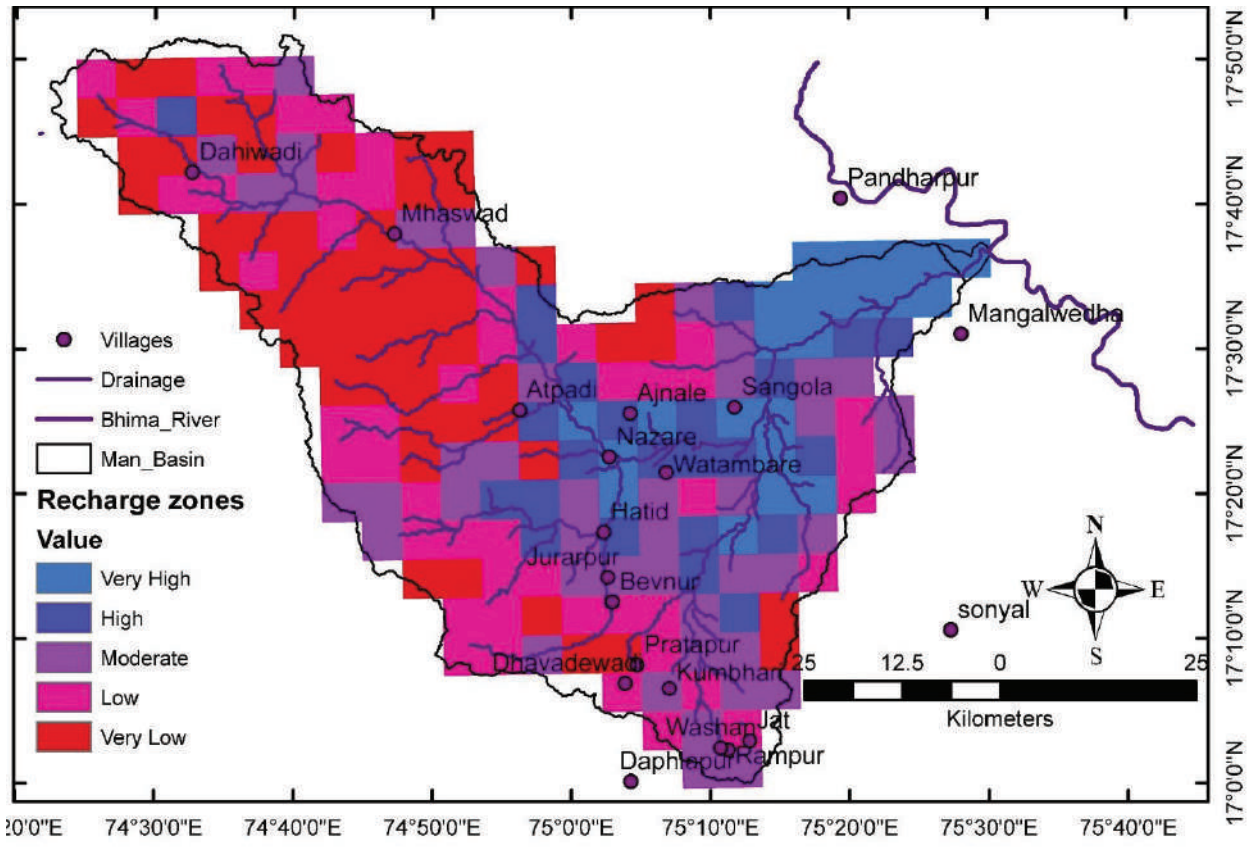


Fig. 9: Potential groundwater recharge zones in the Man River basin.

ter prospect 'very high and high' is confined to only 16.49% of the study area, falls in valleys close to the perennial higher order streams at lower reaches of the Man river. The major portion of the study area falls in 'moderate' (41.09%) class followed by 'low to very low' (42.42%).

## CONCLUSIONS AND RECOMMENDATIONS

The occurrence and movement of groundwater in an area are largely controlled by rainfall, and the characteristics of the terrain features like landforms, lineaments or structural control, soil type, topography, landuse/land cover, soil erosivity, etc. The study demonstrated the utility of RS and GIS technique in delineating potential groundwater recharge zones for a geographical area of the semi-arid region. The groundwater prospect zones delineated for Man River basin will serve as a base for further artificial recharging, water shade management and soil conservation for planners.

Following recommendations are suggested:

- Hilly areas and foothills should follow both soil and water conservation activities such as continuous contour trenching (CCT), Nala bunds, Gabion structure, Vegetative bunds, Loose boulder bunds, Terracing etc. The construction of medium and minor irrigation project at foothills are also feasible with lined or pipe canal system.
- Plain or pediment: This area requires groundwater augmentation by constructing percolation tanks, cement plugs and K.T.Weirs, at appropriate and need-based locations on scientific lines.
- The area showing rising water level trend and having shallow water level ranging from 3m to 6 m bgl during pre-monsoon needs groundwater development at favourable locations.
- Semi critical and over-exploited watersheds intensive site-specific artificial recharge measures coupled with public awareness at every level is the need of the hour.
- Town/City/Urban areas: the rooftop rainwater harvesting for artificial recharge should be made mandatory. So that the available resources for drinking water supply should remain sustainable.

- Women and community participation, mass awareness, adoption of advanced irrigation system etc will play an important role in conserving and developing the precious water resources.

## REFERENCES

Chandrasekhar B.S. 1991. Hydrological Studies of Part Areas of Solapur, Sangli Districts of Maharashtra and Bijapur, Belgaum District of Karnataka Through Remote Sensing Analysis. Ph.D. Thesis, University of Poona, Pune.

IMD 2005. Climate of Maharashtra. India Meteorological Department, Pune.

Kalamkar, S. S. 2011. Agricultural Growth and Productivity in Maharashtra: Trends and Determinants. Allied Publishers Pvt. Ltd., New Delhi.

Mondal, Md. Surabuddin, Pandey, A. C. and Garg, R. D 2009. Groundwater prospects evaluation based on hydrogeomorphological mapping using high resolution satellite images: A case study in Uttarakhand. Journal of Indian Society of Remote Sensing, 36: 69-76

Powar, K.B. 1981. Lineament fabric and dyke patterns in the western part of the Deccan Volcanic Province. Mem. Geol. Soc. India, 3: 45–57.

Powar, K.B. 1993. Geomorphological evolution of Konkan coastal belt and adjoining Sahyadri uplands with reference to quaternary uplift. Curr. Sci., 64(11 &12): 793-796.

Prasad, R. K., Mondal, N. C., Banerjee, Pallavi, Nandakumar, M. V. and Singh, V. S. 2008. Deciphering potential groundwater zone in hard rock through the application of GIS. Environmental Geology, 55/3: 467-475.

Saraf, A.K. and Choudhary, P.R. 1998. Integrated remote sensing and GIS for groundwater exploration and identification of artificial recharge sites. International Journal of Remote Sensing, 19(10): 1825-1841.

Singh, G., Ram Babu and Chandra, S. 1981. Soil loss prediction research in Indian. Bull. No. T-121D-9, CSWCRTI, Dehradun.

Strahler, A. N. 1964. Quantitative Geomorphology of Drainage Basins and Channel Networks. Handbook of Applied Hydrology. Edited by V.T Chow, McGraw Hill, New York, pp 411.

Nature Environment and Pollution Technology
An International Quarterly Scientific Journal

p-ISSN: 0972-6268
(Print copies up to 2016)
e-ISSN: 2395-3454

Vol. 19 | No. 4 | pp.1379-1390 | 2020

Original Research Paper

https://doi.org/10.46488/NEPT.2020.v19i04.004

Open Access Journal

# Comparative Study: The Adsorption Disparity for Tetracycline and Cefradine on Cornstalk Biochar

**Khan Ahmad Ali*, Guoting Li**† and Wenchuan Wang***

*School of Water Conservancy, North China University of Water Resources and Electric Power, Zhengzhou 450011, China

**School of Environmental and Municipal Engineering, North China University of Water Resources and Electric Power, Zhengzhou 450011, China

†Corresponding author: Guoting Li; lipsonny@126.com

**Nat. Env. & Poll. Tech.**
**Website: www.neptjournal.com**

*Received:* 20-12-2019
*Revised:* 03-01-2020
*Accepted:* 28-03-2020

**Key Words:**
Adsorption
Cornstalk
biochar
Cefradine
Tetracycline

## ABSTRACT

The study gives the elimination of two kinds of antibiotics, tetracycline (TC) and cefradine (CF) by adsorption process, on the biochar derived from cornstalk. Dense, multifaceted and thick fragments of raw cornstalk almost all vanished at a pyrolytic temperature above 400°C. The carbon content increased from 60.48% of the raw cornstalk to 75.5% of the cornstalk biochar pyrolyzed at 600°C (BC600), while the oxygen content decreased from 17.31% to 6.94%. The uptake of each TC and CF on the cornstalk biochar was highly pH-dependent. The maximum adsorption capacities of TC and CF at 298 K calculated from the Langmuir mannequin have been 28.0 and 38.0 mg/g, respectively. The Columbic interaction and π–π electron-donor-acceptor interaction between cornstalk biochar and CF/TC molecules played the main role. The experimental records were well outfitted by way of the ability of the pseudo-second-order kinetics model, indicating a possible chemisorption process to some extent. Isotherm result implied that both adsorption and partitioning contributed to the uptake of TC and CF onto BC600.

## INTRODUCTION

For wastewater treatment, adsorption technology has become the most familiar, attractive and effective. For, adsorption technology, without production of any other toxic by-products or intermediates pollutants, contaminants could be attached on the adsorptive materials surface area and can be easily removed or separated from treated water by filtration or centrifugation (Ali et al. 2012, Qu 2008). As such, many adsorbents have been found and synthesized for eliminating inorganic pollutants (e.g. heavy metals, arsenic and fluoride etc.) and organic pollutants (e.g. antibiotics, dyes, PPCP's, pesticides, etc.) from wastewater. Carbon-containing adsorbents are usually the most useful for eliminating organic pollutants due to their large surface area, high affinity towards organic compounds, and easy to reuse and regeneration. For wastewater treatment, low-cost and efficient biochars, which are mostly derived from agricultural wastes or natural biomass, have attracted increasing preference. The preparation of biochar offers the chance to turn bioenergy into a carbon-negative industry, with carbon sequestration and gas capture, which are expected to be a carbon-neutral energy source (Lehmann 2007, Lee et al. 2010). Also, biochar has proved an important role in climate change extenuation, energy production, waste management, soil improvement and environmental management (Ahmad et al. 2014, Zhou et al. 2015, Ge & Qu 2003). For adsorptive elimination of inorganic/organic pollutants from wastewater and soil, the biochars are particularly considered as an environment friendly adsorbent (Rokhina et al. 2013, Kim et al. 2005, Polubesova et al. 2006). Adsorption capability of different pollutants depends on their chemical and physical properties, factors affecting are pyrolysis conditions, pyrolysis technologies and feedstock even raw biochar has the low capability to remove pollutants from wastewater (Figueroa et al. 2004). The use of agricultural by-products or wastes for environmental protection has received marvellous consideration as they are low-cost, abundant in source and renewable (Chen et al. 2018, Peng et al. 2017, Wang et al. 2017). There was 7.18 hundred million tons of crop straw in 2015 and corn stalks were account for 34.2% by Statistical data of Chinese Academy of Agricultural Sciences (Da-li et al. 2018), which shows an enormous amount of cornstalk biomass. Biochar formed by combusting corn stalks (composed of lignin, cellulose, and hemicelluloses) under limited oxygen environments encompasses high specific surface area, stable structures, and a large amount of surface sites, which can be utilized to eliminate ecological contaminants (Yang et al. 2017a,

Yang et al. 2017b, Yang et al. 2017c). Direct application of raw cornstalk for the adsorptive elimination of organic pollutants is lack of practical application potential since the likely organic leaching from cornstalk results secondary pollution problem. As unique characteristics of cornstalk, the biochar synthesized from cornstalk is considered to have a new porous microstructure and large surface area, resulting in improvement of the adsorptive elimination of pollutants.

Due to not easily degradable, the antibiotics can cause a lot of environmental problems in marine environments, the antibiotics resistance of bacteria has been increased due to remaining antibiotics, aquatic organisms face bioaccumulation and biomagnification by the impact of residue antibiotics (Bai et al. 2014,four quinolones, three tetracyclines and two macrolides in water, sediment, and biota samples from the Liao River Basin, China were investigated in the present study. The samples were collected in May 2012, and laboratory analyses revealed that antibiotics were widely distributed in the Liao River Basin. Macrolides made up the majority of antibiotics in the water ranging from not detected (ND Gao et al. 2012,distribution and bioaccumulation of 22 antibiotics, including eight fluoroquinolones (FQs Kim et al. 2014)the freshwater crustacean Daphnia magna. D. magna was exposed to algal food (Pseudokirchneriella subcapitata. Tetracycline (TC) and cefradine (CF) have different functional groups but have similar molecular weight. To find out some important results and comparing the adsorption capacity of TC and CF will be motivating. In this study, cornstalk biochar was synthesized through a simple and cost-effective pyrolysis method, and innovatively applied for adsorptive elimination of the two usual emerging PPCPs. To determine and compare the adsorption capacity of TC and CF on cornstalk biochar a series of batch adsorption experiments were directed and adsorption mechanism was discussed as well.

## MATERIALS AND METHODS

### Materials

Tetracycline hydrochloride (TC, molecular weight 444) was purchased from Solarbio Lifesciences Company (Beijing, China), and Cefradine (CF, A.R.) from Tianjin Fengfan Chemical Reagent Company (Tianjin Province, China). All the chemicals used were of analytical grade. Deionized (DI) water was used to prepare all the solutions.

### Preparation of Cornstalk Biochar

Raw cornstalk was collected from the farmland of Zhengzhou (Henan Province). After washing, drying, crushing and sieving (using a 40 mesh sieve) the cornstalk biomass was put into a ceramic pot with pressed state and enclosed with a fitting lid. The cornstalk was pyrolyzed at different temperatures for 3 h under an oxygen-limited condition. After it was treated with HCl for 12 hours and then after filtration, the residues were rinsed with DI water to neutral pH and dried in an oven at 80°C overnight. Prepared biochar was preserved in a desiccator for further use. The cornstalk biochars pyrolyzed at 400°C and 600°C were designated as BC400 and BC600, respectively.

### Characterization

By using Philips Quanta-2000 scanning electron microscope (SEM) combined with an energy dispersive X-ray (EDX) spectrometer, the morphology of the raw cornstalk and cornstalk biochars pyrolyzed at different temperatures were recorded. To analyse the zeta potential of the cornstalk biochar pyrolyzed at 600°C, a zeta potential analyser (Zetasizer 2000, Malvern Co., UK) was used. Nicolet NEXUS 470 FTIR spectrophotometer was used for recording spectra of Fourier transform infrared spectroscopy (FTIR) in a range of 400 to 4000 $cm^{-1}$. By using surface area and pore-size analyser (NOVA 2200 e, USA) and Brunauer, Emmett and Teller (BET) method the specific surface area of biochars was measured.

### Batch Adsorption Experiment

A fresh stock solution of TC and CF was prepared by dissolving (500 mg/L) in DI water and stored in a refrigerator at 277 K. For experimental work the stock solution was used for the preparation of required concentration solutions of CF and CF by diluting with DI water of each. In experimental work to find out the adsorption isotherms and pH effect, the 20.0 mg/L concentration of TC or CF was used with the 0.4 g/L dose of cornstalk biochar. At a constant temperature of 298 K shaking at 145 rpm for 24 h, samples were collected and filtered through a 0.45 μm syringe membrane filter before concentration measurement. The pH of the solution was adjusted by using diluted $HNO_3$ or NaOH at neutral pH except during the pH effect study itself. For the kinetics study, 400 mg of cornstalk biochar was added into 1000 mL of 20.0 mg/L TC or CF solution.

### Concentration Analyses

A UVmini-1240 spectrophotometer (Shimadzu, Japan) was used to analyse the concentrations of TC and CF at the wavelength of maximum absorption at 360 and 264 nm, respectively (Gao et al. 2012,distribution and bioaccumulation of 22 antibiotics, including eight fluoroquinolones (FQs Kim et al. 2014)the freshwater crustacean Daphnia magna. D. magna was exposed to algal food (Pseudokirchneriella subcapitata. The adsorption capacities were calculated as follows:

$$q_e = (C_o - C_e)V/W \quad \ldots(1)$$

$$q_t = (C_o - C_t)V/W \quad \ldots(2)$$

Where, $q_e$ and $q_t$ (mg/g) are the adsorption capacities at equilibrium and time $t$ (min); $C_0$ (mg/L) is the initial concentration of TC or CF in solution, while $C_e$ and $C_t$ (mg/L) are the concentrations of TC or CF at equilibrium and $t$ (min), respectively; V (L) is the volume of solution, and W (g) is the mass of the cornstalk biochar used.

## RESULTS AND DISCUSSION

### Characterization of Cornstalk and Cornstalk Biochar

***SEM and EDX*:** Fig.1 shows the SEM images of the raw cornstalk and the cornstalk biochars pyrolyzed at 400°C (BC400) and 600°C (BC600). From Fig.1(a,b), it can be seen that the cornstalk mainly consisted of dense and multifaceted fragments. After pyrolysis at 400°C, thin flecks outweighed and the thick fragments nearly all vanished confirming that pyrolysis slashed the natural films of the cornstalk compared with the raw cornstalk. The fragments of BC400 and BC600 became smaller as showed in Fig.1(c,d), so the increase in pyrolytic temperature produced a more condensed structure of cornstalk biochar. By EDX the contents of C, N and O, molar ratios of O/N, (O+N)/C and wt. % values in the raw cornstalk and cornstalk biochar are represented in Fig. 2. Cornstalk and cornstalk biochar pyrolyzed at 400°C and 600°C were all carbon-rich, with C (carbon) contents increasing from 60.5% of the cornstalk to 75.5% of the cornstalk biochar pyrolyzed at 600°C. The carbon content of cornstalk biochar (75.5%) in this research were especially close to that of cornstalk biochar treated by pyrolysis in an $N_2$ environment at 600°C as shown by elemental analysis (Yao et al. 2014). Also, the N content increased gradually from 3.1% of the raw cornstalk to 6.0% of the cornstalk biochar BC600. The increased N content was also observed by other researchers (Sun et al. 2014, Avilez 2012, Al-Wabel et al. 2013)ash content, pH, electrical conductivity, basic functional groups, carbon stability, and total content of C, N, P, K, Ca, and Mg increased while biochar yield, total content of O, H and S, unstable form of organic C and acidic functional groups decreased. The ratios of O/C, H/C, (O. +. N and in specific, the O contents dropped from 17.3% of the raw cornstalk to 6.9% of the cornstalk biochar.

Before and after pyrolysis treatment the relative molar ratios of O/C and (O+N)/C could imitate the change to some extent of surface hydrophilicity and functional groups of the raw cornstalk and biochars. The molar ratios of O/N and (O+N)/C decreased from 21.5% to 6.9% and from 25.9% to 13.7%, respectively on BC600. The decrease of (O+N)/C molar ratio showed the loss of the surface polar functional groups while the fall of O/N molar ratio showed that the biochar surface became less hydrophilic (Chen & Chen 2009, Chun et al. 2004, Cornelissen & Gustafsson 2005). Above discussion signifies that biochar derived from cornstalk could have a certain amount of polar functional groups on the

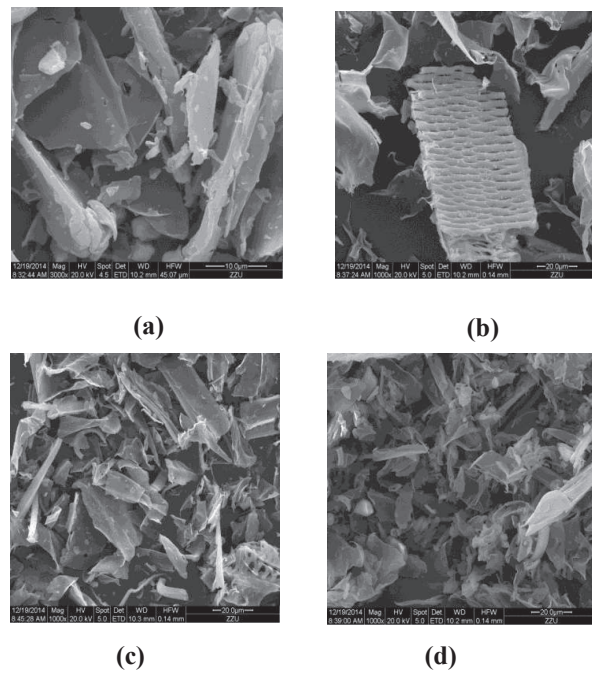


Fig. 1: Scanning electron microscopy images of the raw cornstalk (a, b) and cornstalk biochars BC400 (c) and BC600 (d).

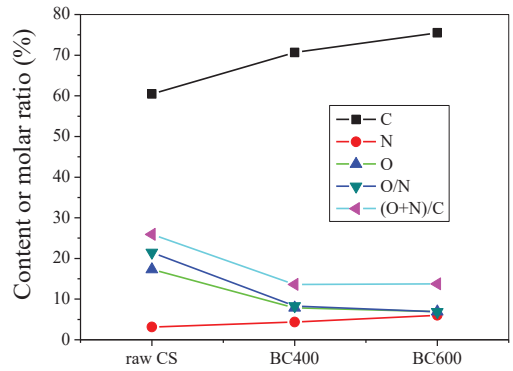


Fig. 2: Changes in element contents (wt%) of C, N, O and the molar ratios (%) of O/N and (O+N)/C in the raw cornstalk, and cornstalk biochars BC400 and BC600.

surface and facilitate the diffusion and adsorption of polar organic pollutants on the biochar surface.

**BET surface area:** Specific surface area and pore structure characteristics of the biochar were measured by BET method as illustrated in Fig. 3. The surface area of cornstalk biochar was 315.8 $m^2$/g, and pore size 5.58 nm, respectively, while the raw cornstalk surface area was 1.3 $m^2$/g, and pore size 1.98 nm. The results of the analysis suggested that the cornstalk biochar contained high surface area and total pore volume compared with other sludge-based activated carbon materials (Li et al. 2011)specific surface area, zeta potential, scanning electron microscope and X-ray diffraction. Adsorption experiments were conducted as function of particle size, SAC dosage, pH, salt concentration, contact time and initial concentration. Desorption of dyes on SAC was studied in deionized water with different pH values and the dye-exhausted carbon was regenerated by thermal treatment. The results showed that the equilibrium adsorption data were well represented by the Langmuir isotherm equation. The maximum adsorption capacity (263.16. mg/g for MB and 34.36. mg/g for RR 24. It was reported that specific surface area of activated carbon prepared from paper mill sewage sludge by carbonization at low temperature was about 130-140 $m^2$/g (Monsalvo et al. 2011), while BET surface areas of activated carbons prepared from dried sewage sludge using $CO_2$, air and KOH as activating agents were below 100 $m^2$/g. Even though, the biochar usually has a lower specific surface area than commercial activated carbons, which typically have a specific surface area of about 400~1,500 $m^2$/g. The biochar was classified as mesoporous material with an average pore size falling in the range of 2-50 nm (Chen et al. 2011). These results suggested that biochar with higher surface area and more pore volume may be used as potential adsorbent.

**FTIR:** The FTIR spectra of cornstalk and cornstalk biochar samples prepared at different pyrolytic temperatures are shown in Fig. 4. First, the strong band at 3,420 $cm^{-1}$ represents the stretching vibration of the hydroxyl group (OH), which became weaker with increasing pyrolytic temperature. This indicated the significant loss of moisture and water of hydration, as a consequence of pyrolysis. Secondly, the bands at 2,903 $cm^{-1}$ (aliphatic C-H stretching), at 1,035 $cm^{-1}$ and 1,105 $cm^{-1}$ (C-O-C), at 1,247 $cm^{-1}$ ($CH_2$) and (C-O in the acetyl group) almost disappeared after heating to 400°C simultaneously, while the intensity at 1,607 $cm^{-1}$ (aromatic C=C and C=O), faded (Chen & Chen 2009, Zhu et al. 2014, Luo et al. 2014). The FTIR data study behaviour coordinat-

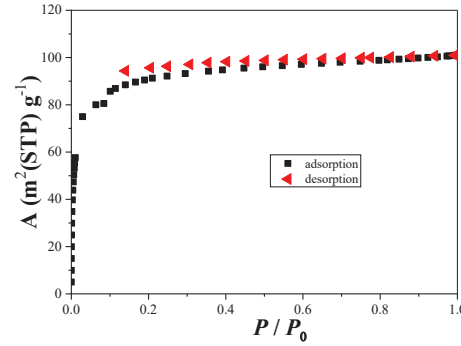


Fig. 3: BET surface areas and average pore sizes of the raw cornstalk, cornstalk biochars BC400 and BC600.

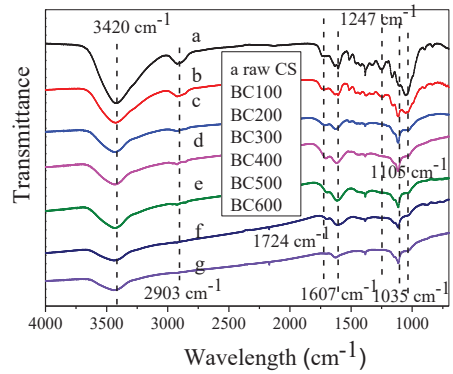


Fig. 4: FTIR spectra of the raw cornstalk, and cornstalk biochars samples prepared under pyrolysis temperatures from 100°C to 600°C.

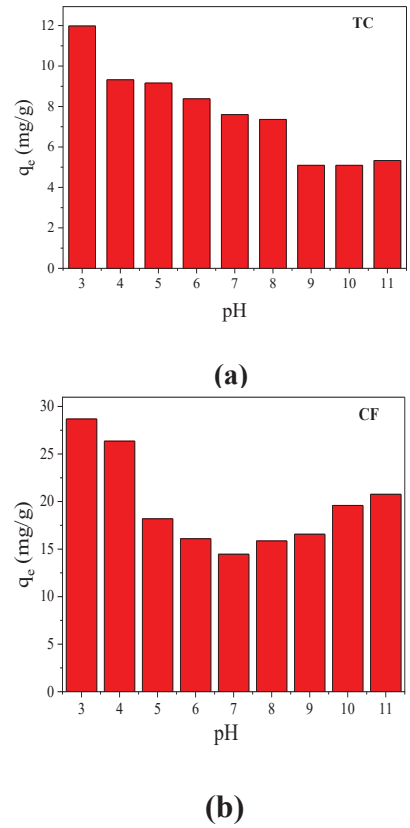


Fig. 5: Effect of solution pH on the adsorption of TC (a) and CF (b) by using BC600.

ed with EDX observations. Finally, the band at 1,700 $cm^{-1}$ (C=O) eliminated, which is in accordance with other studies, as the elimination of the band at 1,700 $cm^{-1}$ was observed by other researchers (Zhu et al. 2014, Luo et al. 2014, Carvalho et al. 2011). This implied that the content of C=N functional groups among oxygen-containing functional groups increased while the concentration of other oxygen-containing functional groups diminished concurrently.

## Effect of Solution pH on the Adsorption of TC and CF

To eliminate the TC and CF from wastewater, cornstalk biochar BC600 was preferred based on the stability and surface properties. The uptake of CF was higher than that of TC at a low adsorbate concentration, and the removal of both TC and CF decreased gradually with increasing solution pH (Song et al. 2019). Fig.5(a, b) shows the effect of

solution pH in the pH range of 3.0 to 11.0. It is found that the removal efficiency of TC and CF from wastewater was highly pH-dependent and was higher in acidic condition as compared to alkaline condition, which was the indication of H-bond formation during adsorption. The experimental results show that the optimum adsorption for both TC and CF was achieved at pH 3.0 with the adsorption capacities of 12.0 and 28.7 mg/g, respectively which decreased with the increase in solution pH. The adsorption of TC was less than that of CF in the testing pH range. Commonly, the surface charge of the biochar should be significantly pretentious by solution pH and a more negatively-charged biochar surface is hypothetically promising for the adsorption of positively charged contaminants due to Columbic attraction (Ahmadzadeh et al. 2015). Fig. 6 represents the Zeta potential of the biochar BC600 as a function of solution pH. With the increasing solution pH, the surface charge of BC600 in the pH range of 3.0~10.0 turned to be more negative. Though TC and CF have alike molecular weight, they would be in different ionic forms in water due to protonation or deprotonation of their unlike functional groups at different pHs. Amphoteric TC molecules may mostly exist in a cationic form at pH < 3.3, resulting from the protonation of dimethyl ammonium group. At the pH ranging from 3.3 to 7.68, it would present as a zwitterion due to the loss of a proton from the phenolic diketone moiety. At pH > 7.68, it mostly occurs as an anion when the tricarbonyl system and phenolic diketone moiety deprotonated (Kulshrestha et al. 2004, Liu et al. 2012). In comparison, the CF molecules having characteristic functional groups, including amino group and a carboxyl group, have pKa values of 7.3 and 2.5. It was thus assumed that CF molecules could become more negatively charged at lower solution pH than TC. Compared to TC, minor adsorption of CF was estimated as an importance of a greater Columbic repulsion force between CF and BC600. But, it was examined that the uptake of CF was higher than that of TC within the whole pH range. Moreover, there was same alteration on the adsorption presentation of BC 600 for both CF and TC at pH > 7 in which the Columbic repulsion between BC600 and CF/TC molecules should be higher with the increasing pH. So it could be determined that the Columbic interaction among cornstalk biochar and CF/TC molecules would somewhat affect the adsorption process. Meanwhile, the cornstalk biochar BC600 could work as π electron donors because it had a highly graphitized surface with relatively high π electron density. The TC and CF molecules were usually observed as π electron acceptors, prominent to a mechanism of π-π electron-donor-acceptor (EDA) interaction involved in the improvement of adsorption onto BC600 (Teixidó et al. 2011, Zheng et al. 2013, Jing et al. 2014). Also, based on the results of pH effect, the zeta potential of biochar and species distribution of TC/CF under different solution pH, the effect of Coulombic force between biochar and TC/CF on the adsorption should be neglectable. The π-π electron-donor-acceptor (EDA) interaction between BC600 and CF was stronger than TC, yielding a comparatively higher adsorption capacity of CF on BC600 (Song et al. 2019). As the protonated and neutral species of TC and CF were more effective π electron acceptors, a slight reduction in TC and CF uptake was expected under alkaline conditions. This was consistent with results from the pH effect study. Thereby, it was deduced that the EDA interaction between BC600 and

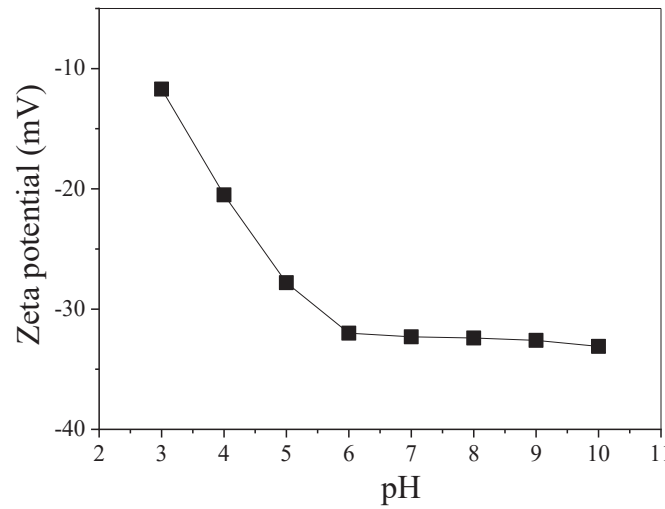


Fig. 6: Zeta potentials of cornstalk biochar BC600. Biochar dose = 200 mg/L, ionic strength 0.01 M $NaNO_3$, equilibrium time 48 h.

CF was stronger than that between BC600 and TC, yielding a comparatively higher uptake of CF on BC600.

## Adsorption Kinetics

Adsorption kinetics of TC and CF onto the cornstalk biochar BC600 was investigated at pH 5.0, 7.0 and 9.0, respectively. Similar adsorption kinetics performances were observed for both the antibiotics. For simplicity, only the adsorption kinetics of TC and CF are presented in Figs. 7 and 8. Two kinetic models including pseudo-first-order and pseudo-second-order models were used to fit the kinetics data. The mathematical equations of the linear and non-linear models of the pseudo-first-order and the pseudo-second-order kinetics are those available in the literature (Lagergren 1898, Ho & McKay 1999):

$$q_t = q_e\,(1 - e^{-k_1 t}) \quad \ldots(3)$$

$$ln(q_e - q_t) = lnq_e - k_1 t \quad \ldots(4)$$

$$q_t = \frac{k_2 q_e^{\,2} t}{(1 + k_2 q_e t)} \quad \ldots(5)$$

$$\frac{t}{q_t} = \frac{1}{k_2 q_e^{\,2}} + \frac{t}{q_e} \quad \ldots(6)$$

Where, $q_e$ and $q_t$ are the adsorption capacities (mg/g) at equilibrium and at time $t$ (minutes), respectively; and $k_1$ ($min^{-1}$)and $k_2$ (g/mg.min) are the related adsorption rate constants for the pseudo-first-order and the pseudo-second-order model, respectively. Based on the correlation coefficients ($R^2$), the experimental data can be better fitted by the pseudo-second-order kinetics model in both linear and nonlinear forms, indicating that the uptake of TC onto the cornstalk biochar might be a chemisorption process to some extent. According to the values of $k_2$, the adsorption of TC on cornstalk biochar BC600 at pH 7.0 was relatively faster than that at pH 5 and 9. This was beneficial for its practical application on the treatment of contaminated natural water (pH at around 6.8).

## Adsorption Isotherms

Adsorption isotherms are the basis for analysing adsorption

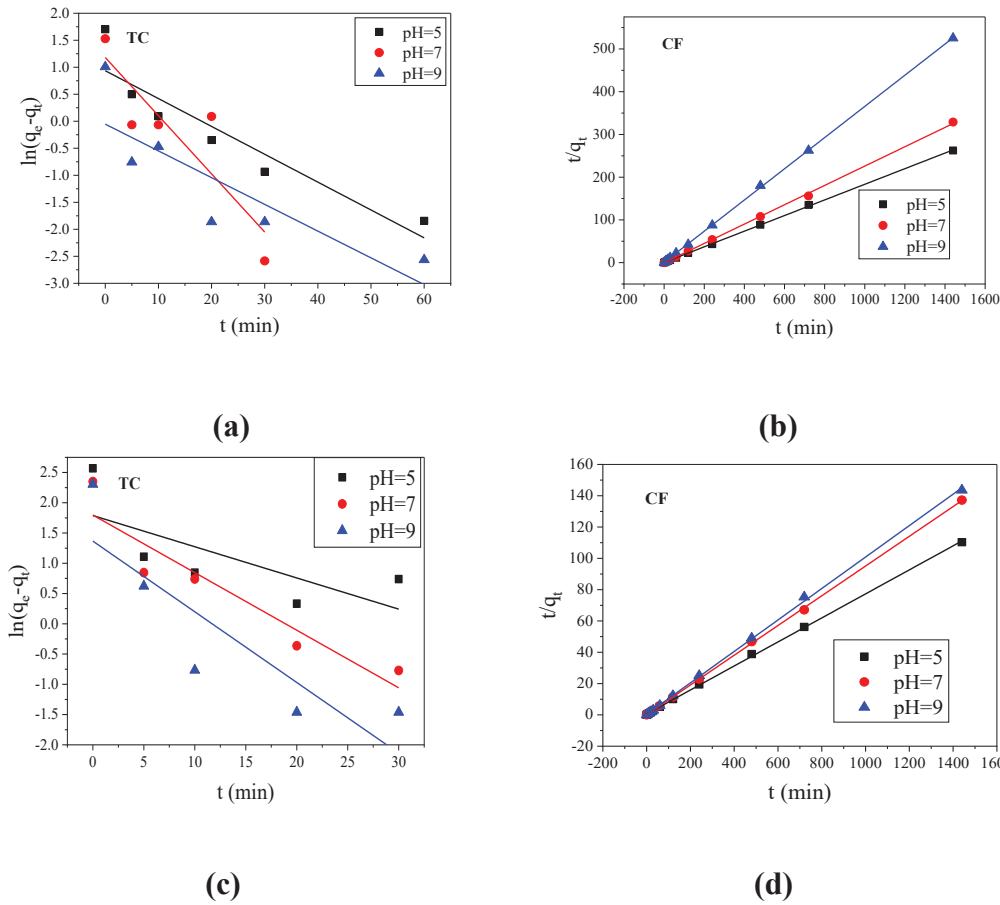


Fig. 7: Linear adsorption kinetics (a, c) and (b, d) for the pseudo-first-order and the pseudo-second-order models for TC and CF respectively.

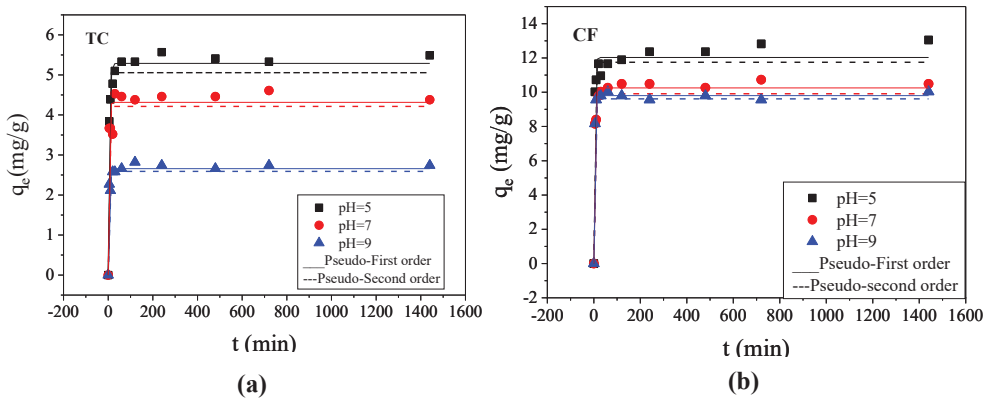


Fig. 8: Nonlinear pseudo-first-order and pseudo-second-order kinetic simulation for the adsorption of TC (a) and CF (b) respectively.

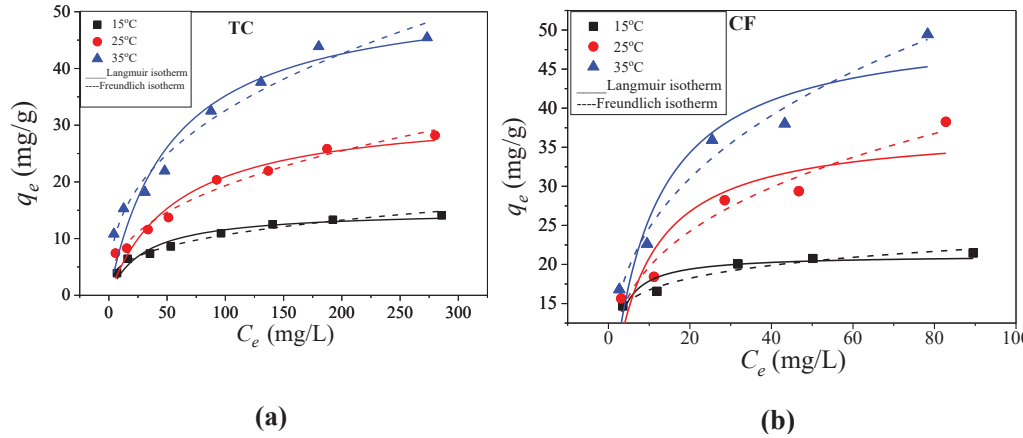


Fig. 9: Langmuir and Freundlich isotherm simulation for the adsorption of TC (a) and CF (b) respectively.

capacity and designing adsorption experiments. In this study, two classical isotherm models, Langmuir equation and Freundlich equation were used to fitting the experimental data.

The equations are as follows:

$$\text{Langmuir Equation} \quad q_e = \frac{q_m k_L C_e}{1 + k_L C_e} \qquad \ldots(7)$$

$$\text{Freundlich Equation:} \quad q_e = k_F C_e^{\frac{1}{n}} \qquad \ldots(8)$$

Where, $q_e$ equilibrium adsorption amount (mg/g); $q_m$ is the maximum adsorption capacity (mg/g); $C_e$ equilibrium concentration of the adsorbate in the solution (mg/L); $k_L$ is Langmuir isotherm constant (L/mg), related to the energy of adsorption); $k_F$ is the Freundlich isotherm constant (related to the adsorption capacity and strength of the adsorbent); $n$ isothermal constants. The results of the adsorption isotherms of Langmuir and Freundlich models for the adsorption of TC and CF on cornstalk biochar are shown in Fig. 9.

From Table 1, we can see that the adsorption of TC on cornstalk biochar was more in line with Freundlich isotherm,

Table 1: Langmuir and Freundlich isotherm parameters for adsorption of TC on cornstalk biochar at different temperatures.

| Temperature | Langmuir isotherm | | | Freundlich isotherm | | |
|---|---|---|---|---|---|---|
| | $q_m$ (mg/g) | $K_L$ (L/mg) | $R^2$ | $k_F$ | $n$ | $R^2$ |
| 288K | 14.98 | $3.376\times10^{-2}$ | 0.942 | 2.495 | 3.172 | 0.975 |
| 298K | 32.94 | $1.737\times10^{-2}$ | 0.926 | 3.076 | 2.505 | 0.976 |
| 308K | 53.9 | $1.877\times10^{-2}$ | 0.914 | 5.456 | 2.577 | 0.968 |

and the correlation coefficient is above 0.96. However, it can be seen from Langmuir isotherm that as the temperature increases, $q_m$ increases, which is an endothermic reaction.

The thermodynamic function of the reaction is calculated using the following equations:

$$\text{Gibbs equation: } \Delta G^\circ = RT \ln K \quad \ldots(9)$$

$$\text{Van't Hoff equation: } \Delta G^\circ = \Delta H^\circ - T\Delta S^\circ \quad \ldots(10)$$

Where: $\Delta G^\circ$ is the standard adsorption Gibbs free energy (J/mol), $\Delta S^\circ$ is the standard adsorption entropy change (J•mol-1•K$^{-1}$), $\Delta H^\circ$ is the standard adsorption entropy change (KJ/mol), and R is the gas molar constant (8.314 J•mol-1•K$^{-1}$), T is the thermodynamic temperature (K), and K is the equilibrium adsorption constant. In the actual calculation of thermodynamic parameters, the following method was used. At different temperatures and different $q_e$, the corresponding $C_e$ was calculated according to the Freundlich isotherm equation at different temperatures, and the corresponding K value was obtained. By using $q_e$ as the abscissa and $\ln(q_e/C_e)$ as the ordinate under different temperatures and different $q_e$, plot Fig.10(a), and then the corresponding K value was obtained, and $\Delta G^\circ$ to map T to Fig.10 (b) was used to obtain a straight line from the slope and intercept of the line $\Delta H^\circ$ and $\Delta S^\circ$ respectively, as given in Table 2.

It can be seen from Table 2 that the process of adsorbing TC by cornstalk biochar is spontaneous and an endothermic reaction. The positive value of $\Delta H^\circ$ indicates that the process absorbs heat, and the elevated temperature favours the occurrence of adsorption reaction, which is consistent with the experimental theoretical maximum equilibrium adsorption amount. $\Delta S^\circ$ is a positive value, indicating that the adsorption process is an entropy increase reaction. $\Delta G^\circ$ is a negative value, indicating that the reaction is a spontaneous reaction process, and $\Delta G^\circ$ decreases with increasing temperature, indicating that the higher the temperature, the more favourable the adsorption process of TC adsorption by cornstalk biochar.

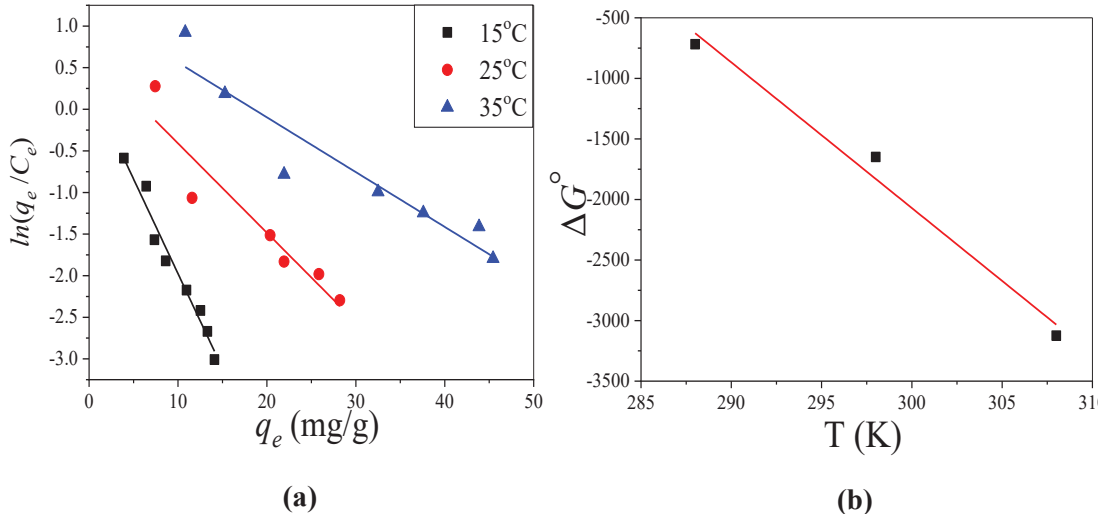


Fig. 10: Thermodynamic parameters (a, b) for TC adsorption on cornstalk biochar.

Table 2: Thermodynamic parameters at different reaction temperatures.

| Temperature | $\ln K$ | $\Delta G^\circ$ (kJ/mol) | $\Delta H^\circ$ (kJ/mol) | $\Delta S^\circ$ (J·mol$^{-1}$·K$^{-1}$) |
|---|---|---|---|---|
| 288K | 0.2998 | -0.718 | 34.02 | 120.30 |
| 298K | 0.6655 | -1.649 | 34.02 | 120.30 |
| 308K | 1.220 | -3.124 | 34.02 | 120.30 |

Table 3: Langmuir and Freundlich isotherm parameters of CF adsorption on cornstalk biochar at different temperatures.

| Temperature | Langmuir isotherm | | | Freundlich isotherm | | |
|---|---|---|---|---|---|---|
| | $q_m$ (mg/g) | $K_L$ (L/mg) | $R^2$ | $k_F$ | $n$ | $R^2$ |
| 288K | 21.20 | 0.538 | 0.830 | 12.552 | 8.021 | 0.953 |
| 298K | 37.56 | 0.124 | 0.752 | 9.873 | 3.334 | 0.947 |
| 308K | 50.51 | 0.103 | 0.861 | 11.488 | 3.015 | 0.974 |

For CF the thermodynamic function of the reaction was calculated using the equations (9) and (10). From Table 3, we can see that the adsorption of CF on corn straw biochar is more in line with Freundlich isotherm, and the correlation coefficient is above 0.94. However, it can be seen from Langmuir isotherm that as the temperature increases, $q_m$ increases, which is an endothermic reaction.

The positive value of $\Delta H^\circ$ indicates that adsorption of CF by cornstalk biochar is a spontaneous process and an endothermic reaction that absorbs heat, and the elevated temperature favours the occurrence of adsorption reaction, which is consistent with the experimental theoretical maximum equilibrium adsorption amount. $\Delta S^\circ$ is a positive value, indicating that the adsorption process is an entropy increase reaction. $\Delta G^\circ$ is a negative value, indicating that the reaction is a spontaneous reaction process, and $\Delta G^\circ$ decreases with increasing temperature, indicating that the higher the temperature, the more favourable the adsorption process of CF on cornstalk biochar adsorption.

### Effect of Natural Organic Matter on the Adsorption of TC and CF

We have checked the effect of the amount of natural material quantity on the adsorption of TC and CF as give in the graphs (a) and (b) of Fig. 11. The adsorption of TC at 20 mg/L was just 20.21 mg/g, while in the case of CF at 20 mg/L was increased to a value of 93.00 mg/g. Hence, we can conclude without any doubt that CF has a higher adsorption capacity than TC on the cornstalk biochar BC600.

## CONCLUSION

A simple pyrolysis process was used for the preparation of cornstalk biochar which can be used for relative adsorption of two antibiotics tetracycline (TC) and cefradine (CF). The dens morphology of geared up cornstalk biochar pyrolyzed at 600°C (BC600) had a more condensed configuration, which is responsible to make biochar developed greater hydrophobic and carbon-rich with increasing pyrolytic temperature. The uptake of TC and CF decreased step by step with higher pH whilst the uptake of CF used to be certainly greater than that of TC at a low adsorbate concentration. Based on the effects of pH effect, the zeta potential of biochar and distribution kinds of TC/CF beneath exclusive solution pH, impact of Coulombic force between biochar and TC/CF on the adsorption have to be neglectable. The π-π electron-donor-acceptor (EDA) interaction between CF and BC600 used to be higher than TC, and resilient a relatively greater adsorption potential of CF on BC600. Kinetics statistics can be fitted out higher by means of the use of the pseudo-second-order kinetic model, indicating a possible chemisorption process to some extent. Isotherms learn about advised that both ground adsorption and partitioning contributed to the uptake of TC and CF onto BC600.

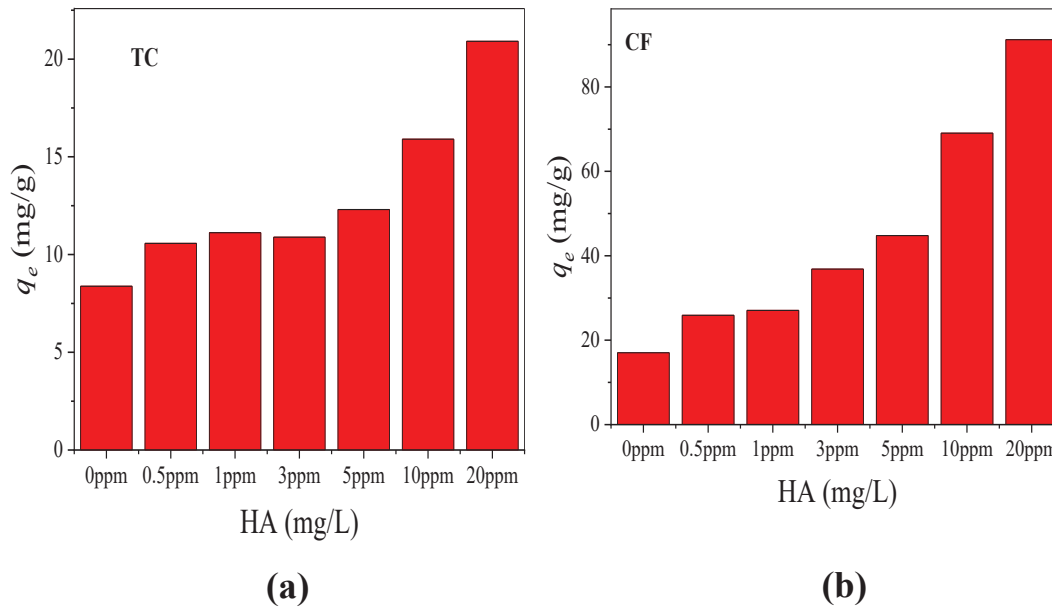


Fig. 11: Effect of humic acid (HA) on the adsorption of TC (a) and CF (b).

## ACKNOWLEDGEMENT

The authors thank for the financial support from National Natural Science Foundation of China (No. 51509088), Henan province, University Scientific and Technological Innovation Team (No. 18IRTSTHN009), and Henan Key Laboratory of Water Environment Simulation and Treatment (No. 2017016).

## ABBREVIATIONS

TC - Tetracycline
CF - Cefradine
EDA - Electron-donor-acceptor
PPCPs - Pharmaceutical and personal care products
DI water - Deionized water
Biochar - BC
SEM - Scanning electron microscope
EDX - Energy dispersive X-ray
BET - Brunauer, Emmett and Teller
FTIR - Fourier transform infrared spectroscopy
$R^2$ - Correlation coefficients

## REFERENCES

Ahmad, M., Rajapaksha, A. U., Lim, J. E., Zhang, M., Bolan, N., Mohan, D. and Ok, Y. S. 2014. Biochar as a sorbent for contaminant management in soil and water: A review. Chemosphere, 99: 19-33.

Ahmadzadeh, S., Rezayi, M., Karimi-Maleh, H. and Alias, Y. 2015. Conductometric measurements of complexation study between 4-Isopropylcalix[4]arene and $Cr^{3+}$ cation in THF-DMSO binary solvents. Measurement: Journal of the International Measurement Confederation, 70: 214-224.

Al-Wabel, M. I., Al-Omran, A., El-Naggar, A. H., Nadeem, M. and Usman, A. R. A. 2013. Pyrolysis temperature induced changes in characteristics and chemical composition of biochar produced from Conocarpus wastes. Bioresource Technology, 131: 374-379.

Ali, I., Asim, M. and Khan, T. A. 2012. Low cost adsorbents for the removal of organic pollutants from wastewater. Journal of Environmental Management, 113: 170-183.

Avilez, H.V.R. 2012. Remoción de Cianuro en Relaves Auríferos Utilizando Biochar Producido a Partir de Tallos de Gliricida Sepium., Vol. 66.

Bai, Y., Meng, W., Xu, J., Zhang, Y. and Guo, C. 2014. Occurrence, distribution and bioaccumulation of antibiotics in the Liao River Basin in China. Environmental Sciences: Processes and Impacts, 16(3): 586-593.

Carvalho, W. S., Martins, D. F., Gomes, F. R., Leite, I. R., Gustavo da Silva, L., Ruggiero, R. and Richter, E.M. 2011. Phosphate adsorption on chemically modified sugarcane bagasse fibres. Biomass and Bioenergy, 35(9): 3913-3919.

Chen, B. and Chen, Z. 2009. Sorption of naphthalene and 1-naphthol by biochars of orange peels with different pyrolytic temperatures. Chemosphere, 76(1): 127-133.

Chen, Y. di, Ho, S. H., Wang, D., Wei, Z. Su, Chang, J. S. and Ren, N. qi. (2018). Lead removal by magnetic biochar derived from persulfate-ZVI treated sludge together with one-pot pyrolysis. Bioresource Technology, 247: 463-470.

Chen, X., Chen, G., Chen, L., Chen, Y., Lehmann, J., McBride, M. B. and Hay, A. G. 2011. Adsorption of copper and zinc by biochars produced from pyrolysis of hardwood and corn straw in aqueous solution. Bioresource Technology, 102(19): 8877-8884.

Chun, Y., Sheng, G., Chiou, G. T. and Xing, B. 2004. Compositions and sorptive properties of crop residue-derived chars. Environmental Science and Technology, 38(17): 4649-4655.

Cornelissen, G. and Gustafsson, Ö. 2005. Importance of unburned coal carbon, black carbon, and amorphous organic carbon to phenanthrene sorption in sediments. Environmental Science and Technology, 39(3): 764-769.

Da-li, S., Sheng-peng, H. and Xiu-bin, W. 2018. Nutrient resource quantity of crop straw and its potential of substituting. Journal of Plant Nutrition and Fertilizers, 24(01): 1-21.

Figueroa, R.A., Leonard, A. and Mackay, A.A. 2004. Modeling tetracycline antibiotic sorption to clays. Environmental Science and Technology, 38(2): 476-483.

Gao, L., Shi, Y., Li, W., Liu, J. and Cai, Y. 2012. Occurrence, distribution and bioaccumulation of antibiotics in the Haihe River in China. Journal of Environmental Monitoring, 14(4): 1248-1255.

Ge, J. and Qu, J. 2003. Degradation of azo dye acid red B on manganese dioxide in the absence and presence of ultrasonic irradiation. Journal of Hazardous Materials, 100(1-3): 197-207.

Ho, Y. S. and McKay, G. 1999. Pseudo-second order model for sorption processes. Process Biochemistry, 34(5): 451-465.

Jing, X.R., Wang, Y.Y., Liu, W.J., Wang, Y. K. and Jiang, H. 2014. Enhanced adsorption performance of tetracycline in aqueous solutions by methanol-modified biochar. Chemical Engineering Journal, 248: 168-174.

Kim, H. Y., Jeon, J., Hollender, J., Yu, S. and Kim, S. D. 2014. Aqueous and dietary bioaccumulation of antibiotic tetracycline in *D. magna* and its multigenerational transfer. Journal of Hazardous Materials, 279: 428-435.

Kim, S., Eichhorn, P., Jensen, J. N., Weber, A.S. and Aga, D. S. 2005. Removal of antibiotics in wastewater: Effect of hydraulic and solid retention times on the fate of tetracycline in the activated sludge process. Environmental Science and Technology, 39(15): 5816-5823.

Kulshrestha, P., Giese, R.F. and Aga, D.S. 2004. Investigating the molecular interactions of oxytetracycline in clay and organic matter: Insights on factors affecting its mobility in soil. Environmental Science and Technology, 38(15): 4097-4105.

Lagergren, S. 1898. Zurtheorie der sogenannten adsorption gelösterstoffe. Kungliga Svenska Vetenskapsakademiens. Handlinga, 24: 1-39.

Lee, J. W., Hawkins, B., Day, D. M. and Reicosky, D. C. 2010. Sustainability: The capacity of smokeless biomass pyrolysis for energy production, global carbon capture and sequestration. Energy and Environmental Science, 3(11): 1695-1705.

Lehmann, J. 2007. A handful of carbon. Nature, 447(7141): 143-144.

Li, W. H., Yue, Q. Y., Gao, B. Y., Ma, Z. H., Li, Y. J. and Zhao, H. X. 2011. Preparation and utilization of sludge-based activated carbon for the adsorption of dyes from aqueous solutions. Chemical Engineering Journal, 171(1): 320-327.

Liu, H., Yang, Y., Kang, J., Fan, M. and Qu, J. 2012. Removal of tetracycline from water by Fe-Mn binary oxide. Journal of Environmental Sciences, 24(2): 242-247.

Luo, J., Im, J. H., Mayer, M. T., Schreier, M., Nazeeruddin, M. K., Park, N. G. and Grätzel, M. 2014. Water photolysis at 12.3% efficiency via perovskite photovoltaics and Earth-abundant catalysts. Science, 345(6204): 1593-1596.

Monsalvo, V. M., Mohedano, A. F. and Rodriguez, J. J. 2011. Activated carbons from sewage sludge. Application to aqueous-phase adsorption of 4-chlorophenol. Desalination, 277(1-3): 377-382.

Peng, X., Liu, X., Zhou, Y., Peng, B., Tang, L., Luo, L. and Zeng, G. 2017. New insights into the activity of a biochar supported nanoscale zerovalent iron composite and nanoscale zero valent iron under anaerobic or aerobic conditions. RSC Advances, 7(15): 8755-8761.

Polubesova, T., Zadaka, D., Groisman, L. and Nir, S. 2006. Water remediation by micelle-clay system: Case study for tetracycline and sulfonamide antibiotics. Water Research, 40(12): 2369-2374.

Qu, J. 2008. Research progress of novel adsorption processes in water purification: A review. Journal of Environmental Sciences, 20(1): 1-13.

Rokhina, E. V., Makarova, K., Lahtinen, M., Golovina, E. A., Van As, H. and Virkutyte, J. 2013. Ultrasound-assisted $MnO_2$ catalyzed homolysis of peracetic acid for phenol degradation: The assessment of process chemistry and kinetics. Chemical Engineering Journal, 221: 476-486.

Song, G., Guo, Y., Li, G., Zhao, W. and Yu, Y. 2019. Comparison for adsorption of tetracycline and cefradine using biochar derived from seaweed *Sargassum* sp. Desalination and Water Treatment, 160: 316-324.

Sun, Y., Gao, B., Yao, Y., Fang, J., Zhang, M., Zhou, Y. and Yang, L. 2014. Effects of feedstock type, production method, and pyrolysis temperature on biochar and hydrochar properties. Chemical Engineering Journal, 240: 574-578.

Teixidó, M., Pignatello, J.J., Beltrán, J.L., Granados, M. and Peccia, J. 2011. Speciation of the ionizable antibiotic sulfamethazine on black carbon (Biochar). Environmental Science and Technology, 45(23): 10020-10027.

Wang, S., Zhou, Y., Gao, B., Wang, X., Yin, X., Feng, K. and Wang, J. 2017. The sorptive and reductive capacities of biochar supported nanoscale zero-valent iron (nZVI) in relation to its crystallite size. Chemosphere, 186: 495-500.

Yang, F., Sun, L., Xie, W., Jiang, Q., Gao, Y., Zhang, W. and Zhang, Y. 2017. Nitrogen-functionalization biochars derived from wheat straws via molten salt synthesis: An efficient adsorbent for atrazine removal. Science of the Total Environment, 607-608: 1391-1399.

Yang, F., Sun, L., Zhang, W. and Zhang, Y. 2017. One-pot synthesis of porous carbon foam derived from corn straw: atrazine adsorption equilibrium and kinetics. Environmental Science: Nano, 4(3): 625-635.

Yang, F., Zhang, W., Li, J., Wang, S., Tao, Y., Wang, Y. and Zhang, Y. 2017. The enhancement of atrazine sorption and microbial transformation in biochars amended black soils. Chemosphere, 189: 507-516.

Yao, Y., Gao, B., Fang, J., Zhang, M., Chen, H., Zhou, Y. and Yang, L. 2014. Characterization and environmental applications of clay-biochar composites. Chemical Engineering Journal, 242: 136-143.

Zheng, H., Wang, Z., Zhao, J., Herbert, S. and Xing, B. 2013. Sorption of antibiotic sulfamethoxazole varies with biochars produced at different temperatures. Environmental Pollution, 181: 60-67.

Zhou, Y., Zhang, L. and Cheng, Z. 2015. Removal of organic pollutants from aqueous solution using agricultural wastes: A review. Journal of Molecular Liquids, 212: 739-762.

Zhu, X., Liu, Y., Zhou, C., Luo, G., Zhang, S. and Chen, J. 2014. A novel porous carbon derived from hydrothermal carbon for efficient adsorption of tetracycline. Carbon, 77: 627-636.

Nature Environment and Pollution Technology
An International Quarterly Scientific Journal

p-ISSN: 0972-6268
(Print copies up to 2016)
e-ISSN: 2395-3454

Vol. 19 | No. 4 | pp. 1391-1398 | 2020

Original Research Paper

https://doi.org/10.46488/NEPT.2020.v19i04.005

Open Access Journal

# Effective Removal of Cr(VI) from Aqueous Solution Using Modified Orange Peel Powder: Equilibrium and Kinetic Study

**L. P. Liang*, Q. Wang*, F. F. Xi*, W. S. Tan*, Y. T. Zhang*, L. B. Cheng*, Q. Wu*, Y. Y. Xue* and X. Meng**†**

*School of Civil Engineering, College of Life Science, College of Textile and Garment, Shaoxing University, Shaoxing, 312000, P.R.China

**Key Laboratory of Clean Dyeing and Finishing Technology of Zhejiang Province, Shaoxing University, Shaoxing, 312000, P.R.China

†Corresponding author: Xu.Meng; Mengxu0@163.com

**Nat. Env. & Poll. Tech.**
**Website: www.neptjournal.com**

*Received:* 27-12-2019
*Revised:* 19-01-2020
*Accepted:* 30-03-2020

**Key Words:**
Adsorbent
Adsorption
Chromium ion
Orange peel
Wastewater treatment

## ABSTRACT

A new adsorbent modified from orange peel (OP) was successfully synthesized by ethylenediamine crosslinking method to remove Cr(VI) from wastewater. The modified orange peel powder (MOPP) was investigated in a batch adsorption system, including both equilibrium adsorption isotherms and kinetics. Effects of several factors, including adsorbent dose, initial pH and Cr(VI) concentration were studied. The data indicated that the pH was not an essential factor that affected the adsorption process, it has a wide pH range from 4 to 10, and high adsorbent dose and lower Cr(VI) concentration could increase the Cr(VI) removal efficiency. Equilibrium data were analysed using the Langmuir, Freundlich and Temkin isotherm models and found to be well represented by the Langmuir isotherm model. The maximum capacity ($q_{max}$) obtained from Langmuir model was 52.08 mg/g at pH 6.0. The kinetics of adsorption followed the pseudo-second-order kinetic equation. The results suggest that MOPP is an inexpensive and efficient adsorbent for removing Cr(VI) from aqueous solution.

## INTRODUCTION

The chromium ion is ubiquitous in surface and groundwater since it is widely used in industries such as plastics, pigments, wood preservatives, electroplating, leather tanning, cement, mining, dyeing and fertilizers (Altundogan et al. 2005, Gu et al. 2013). Chromium is mainly present in the form of trivalent chromium and hexavalent chromium in the aquatic environment, in which Cr(III) tend to form precipitation, low mobility and low toxicity. On the contrary, Cr(VI) is soluble in water, easy to migrate and toxic, which is one of the three internationally recognized carcinogenic metals and one of the eight most harmful chemicals to human beings (Hu et al. 2016). Hexavalent chromium can precipitate some proteins in human blood, causing anaemia, nephritis, neuritis and other diseases. Long-term contact with hexavalent chromium can also cause respiratory tract inflammation and induce lung cancer (Kotaś et al. 2000). According to the recommendation of the World Health Organization (WHO), the maximum allowable limit of hexavalent chromium in drinking water is 0.05 mg/L. Therefore, considering the protection of aquatic environments and requirement on the discharge limits, it is of significant importance to reduce the Cr(VI) concentration in various sources before they are discharged into water (Zhou et al. 2015).

At present, the removal methods of hexavalent chromium in sewage include chemical precipitation, ion exchange, reverse osmosis, electrochemical generation, and photocatalytic oxidation. However, these processes are difficult to be accepted due to their high cost, low efficiency, secondary pollution and unsuitability for multiple pollutants. Among these methods, adsorption technology is one of the most effective methods to remove heavy metals in water. Recently, the search for low-cost adsorbents that have metal-binding capacity has intensified. Materials locally available in large quantities such as natural materials, agricultural wastes or industrial by-products can be used as low-cost adsorbents. Some of the reported biosorbents include crab shell, wheat straw, rice straw, grape bagasse, orange waste and so on. However, to use the biomass directly may suffer from lack of specificity and poor adsorption capacity. It is observed that appropriate modification of the raw adsorbents by crown esters, amines, polyethylamine and sulphur bearing groups can eliminate the drawbacks and improve their performances significantly (Mukhopadhyay et al. 2006).

The orange peel (OP) is a quite abundant agricultural waste which can be reused as adsorbent. The valuable waste material orange peel (OP) principally consists of cellulose, pectin, hemicellulose, lignin, chlorophyll pigments and

other low molecular weight hydrocarbons (Feng et al. 2008). Cellulose, hemicellulose, and lignin structures have a large number of easily available hydroxyl groups that can be used for the synthesis of functional polymers (Nakamura et al. 1992). World's orange production is estimated to be > 60 million tons per year (Fernandez et al. 2014). OP is abundant in juice industry residues, but many of them abandoned as waste without proper utilization. In general, the adsorption capacity of crude fruit waste is very low. Hence, in recent years, using such fruit residues as functional polymers has attracted much interest. For example, Feng et al. (2008) prepared a chemically modified orange peel adsorbent by hydrolysis of the graft copolymer, which was synthesized by the interaction of methyl acrylate and cross-linked orange peel. The results showed that the modified orange peel successfully adsorbed 289 $mg.g^{-1}$ of Copper (II). Liang et al. (2009) succeeded in adsorbing 204.50 $mg.g^{-1}$ $Pb^{2+}$ in the solution by chemically modifying the original orange peel by introducing sulphur groups with the carbon disulphide treatment in alkaline medium.

This work aimed to prepare a new adsorbent which modified the orange peel (OP) by ethylenediamine crosslinking method and to study the adsorption capacity of Cr(VI). The effects of biosorbent dosage, pH, and initial Cr(VI) concentration on Cr(VI) removal in solution were investigated. Besides this, adsorption isotherms and kinetics were also discussed and different adsorption models were used to evaluate the experimental data and to illustrate the possible adsorption mechanism.

## MATERIALS AND METHODS

### Materials

All the chemicals used in this study were of pure analytical grade. Stock solutions of heavy metals were prepared by dissolving $K_2Cr_2O_7$ in double-distilled water and then diluted to desired concentrations. The adsorbent used in this study was prepared by collecting the fruits from a local market in Shaoxing, Zhejiang, China. N, N-dimethylformamide ($C_3H_7NO$), epichlorohydrin ($C_3H_5ClO$), ethylenediamine ($C_2H_8N_2$), triethylamine($C_6H_{15}N$), and all the other reagents were purchased from the Sinopharm Group Chemical Reagent Co., Ltd., China. All these chemicals were of analytical grade and used as received.

### Preparation of Cationic Adsorbent

The OP was first washed with double distilled water to remove dirt and other particulate matter, and then dried at 60°C inside a convection oven for 24 h. The dried sample was ground and sieved to the desired mesh size (100-250 mesh). To 8 g of OP were added 20 mL of epichlorohydrin and 16 mL of N, N-dimethylformamide (DMF) in a 250-mL three-neck round-bottom flask at 85°C for 1 h. Next, 6 mL of ethylenediamine was added and the mixture was stirred for 1 h at 85°C. Finally, 15 mL of 99% triethylamine (w/w) was added and stirred for 3 h at 85°C. The primary product was washed with double distilled water until the eluant was neutral, and then dried overnight at 60°C and sieved to obtain particles. The prepared MOPP was stored in a desiccator for further use.

### Batch Experiments

Batch equilibrium studies were carried out by adding a fixed amount of MOPP to 250-mL sealed conical flasks containing 100 mL of different initial concentrations of Cr(VI) solution. The flasks were placed in a shaking thermostat machine at a speed of 150 r/min. Aqueous samples (5 mL) were withdrawn at equilibrium and filtered using a 0.45-μm filter. The adsorption capacities of MOPP were calculated under different environmental conditions to understand their effects on the reaction. The equilibrium adsorbed concentration, $q_e$ ($mg.g^{-1}$), was determined according to the following equation:

$$q_e = \frac{(C_0 - C_e)V}{W} \quad \ldots(1)$$

Where, $C_0$ and $Ce$ ($mg.L^{-1}$) represent the liquid-phase concentrations of Cr(VI) initially and at equilibrium, respectively; $q_e$ ($mg.g^{-1}$) is the equilibrium adsorption capacity; $V$ (L) is the volume of the solution, and $W$ (g) is the mass of the adsorbent. In addition, all the adsorption experiments were conducted in duplicate, and the mean values were calculated. The results were reproducible at most 5% error.

## RESULTS AND DISCUSSION

### Scanning Electron Microscopy Analysis

The morphology of OP and MOPP is presented in Fig. 1 (SEM image). The surface of the OP has well-structured layers without a well-defined direction, cavities and channels can be observed. These features are typical for adsorption materials. When comparing the SEM images of OP and MOPP, structural changes are evident with the latter showing a more porous and irregular surface. This led to physical and chemical cross-linking on the surface of adsorbent to enhance adsorption (Singh et al. 2014). Based on this fact, it can be determined that MOPP present an adequate morphology for metal adsorption.

### FTIR Spectroscopy Analysis

Fourier transform infrared spectroscopy (FTIR) was used to identify the functional groups responsible for Cr(VI) uptake.

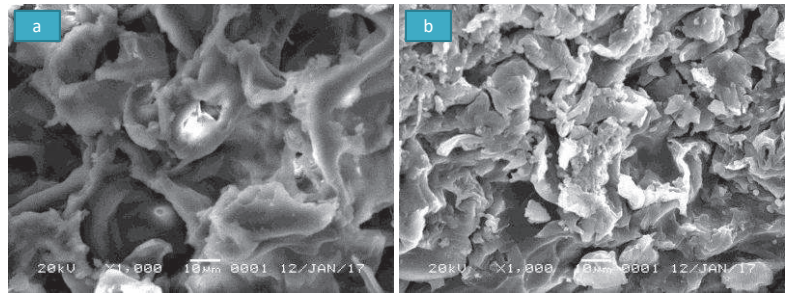


Fig. 1: SEM images of OP (a) and MOPP (b) of magnifications of 1000 times.

The infrared spectra of OP and MOPP are shown in Fig. 2. In OP spectrum, at a wavelength of about 3420 $cm^{-1}$, the broad and strong absorption peak corresponds to the O-H tensile vibration of alcohols, which stretching vibration region is from 3750$cm^{-1}$ to 3000$cm^{-1}$. The compositions of OP, like hemicellulose, cellulose, pectin and lignin including phenols and carboxylic acids indicate the presence of "free" hydroxyl groups on the surface of the adsorbent (Gnanasambandam et al. 2000). The peak at 2912 $cm^{-1}$ is caused by the C-H stretching vibration on the saturated carbon in the aliphatic acids. The peak observed at 2368 $cm^{-1}$ may be is the area of triple bond and a cumulative double bond. The absorption of carboxyl group occurs most often in the region of 1755-1670 $cm^{-1}$, therefore, the peak in the spectrum is corresponding to the tensile vibration of the bond caused by non-ionic oxycarbyl (-COOH, -COCH3) (Say et al. 2003). The peaks at 1644 $cm^{-1}$ and 1520 $cm^{-1}$ are located in the double bond telescopic vibration region, which mainly includes the stretching vibration of carbon-carbon double bond, carbon-nitrogen double bond, nitrogen-nitrogen double bond, etc. The 1060 $cm^{-1}$ peak may be caused by the stretching vibration of C-OH of ethanol group and carboxylic acid (Sengil & Ozacar 2009). Compared with OP, the spectrum of MOPP after modification can be seen that the peak caused by the C-H stretching vibration is not obvious. Carboxyl peak was disappeared around 1752 $cm^{-1}$ and a new peak was discovered at 1647 $cm^{-1}$. This shows that some functional groups have been successfully modified.

### Effect of solution initial pH

Solution pH is an important controlling parameter that strongly influences the adsorption of metals onto the solid-liquid interface (Chen et al. 2010). Batch adsorption experiments were carried out by varying the pH between 4.0 and 10.0 under optimized conditions of 200 $mg.L^{-1}$ initial concentration and 1 $g.L^{-1}$ MOPP to identify the Cr(VI) uptake capacity of the adsorbent, and the results are shown in Fig. 3. At this pH range, the Cr(VI) sorption capacity of MOPP was all above 22.32 $mg.L^{-1}$, and the maximum adsorption occurred at pH 6.0 (25.76 $mg.g^{-1}$). It could be seen from the figure that pH was not a considerable factor in this study, which makes it economical for wastewater treatment. The most effective pH was found to be 6.0 and it was used in further studies.

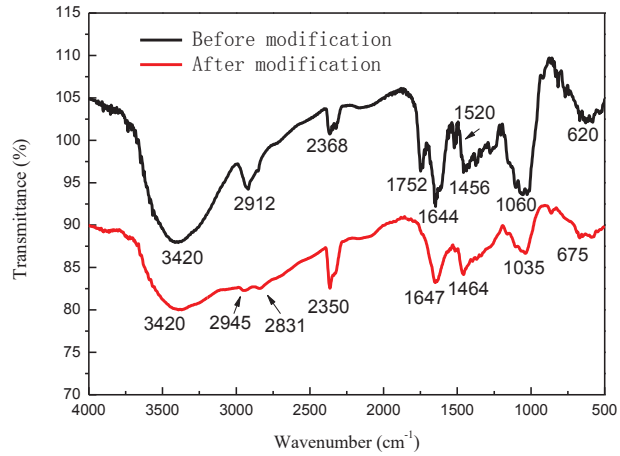


Fig. 2: FT-IR spectra of orange peel before and after modification by ethylenediamine.

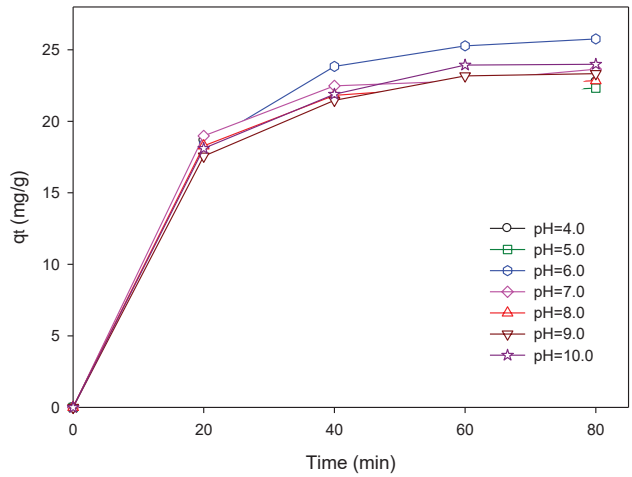


Fig. 3: Effect of pH on the kinetics of Cr(VI) removal by cation adsorbent.

### Effect of adsorbent dose

The effect of the adsorbent dosage on the removal of Cr(VI) in solution was investigated under the conditions of pH 6 and 200 mg.L$^{-1}$ solution concentration. The results are shown in Fig. 4. The removal amount of Cr(VI) ions increased significantly from 23.22 to 28.01 mg.g$^{-1}$, with adsorbent concentration increasing from 1 to 3 g.L$^{-1}$. With increasing adsorbent concentration, greater surface area and more adsorption sites became available for adsorption, and almost all the Cr(VI) ions were adsorbed when the concentration was increased to 3 g.L$^{-1}$. So, it could be concluded that further increasing the concentration, and when it reached 3 g.L$^{-1}$, had a negligible effect on Cr(VI) removal.

### Effect of Contact Time and Initial Concentration

The adsorption of Cr(VI) onto MOPP at different initial concentrations was studied as a function of time to determine the point of equilibrium under the condition of pH 6 and 2 g.L$^{-1}$ MOPP, as shown in Fig. 5. The adsorption capacity increased with increasing Cr(VI) ions concentration in the medium, and when the initial Cr(VI) concentration increased from 50 to 600 mg.L$^{-1}$, the Cr(VI) uptake capacity of the MOPP increased from 5.39 to 59.43 mg.g$^{-1}$. This may be attributed to the higher initial Cr(VI) concentration leading to faster and more strongly binding sites compared to lower concentrations of Cr(VI) at the same dose of adsorbent (Baral et al. 2009). It was also observed that adsorption of Cr(VI) ions onto MOPP was rather quick, and after 60 min, complete adsorption equilibrium was obtained. For the sake of the combined experiments, all further studies were carried out for 90 min. The initially higher rate was probably due to the high affinity of the interacting groups on the surface of MOPP. Once the exterior surface reached saturation, the Cr(VI) ions penetrated through the pores and were adsorbed inside them. Besides, the curves were single, smooth, and

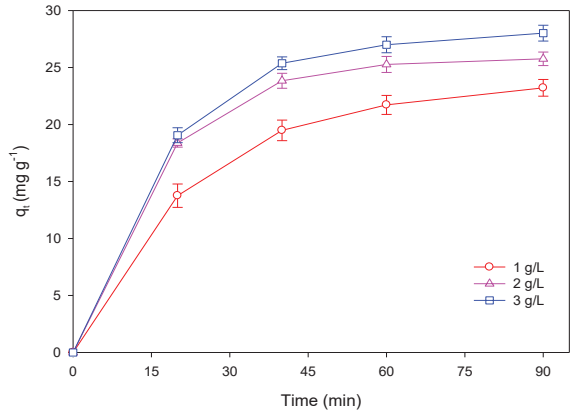


Fig. 4: Effect of cation adsorbent dose on the kinetics of Cr(VI) removal by cation adsorbent.

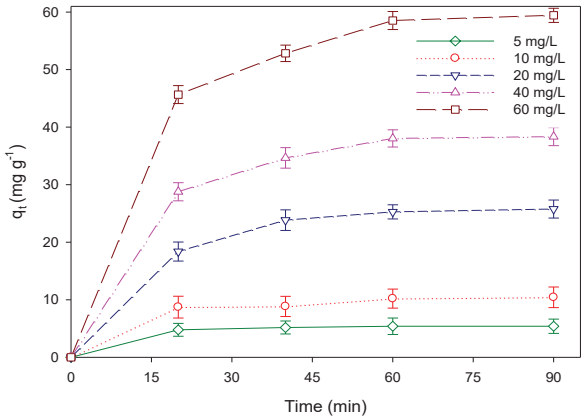


Fig. 5: Effect of initial Cr(VI) concentration on the kinetics of Cr(VI) removal by cation adsorbent.

continuous toward saturation, indicating the formation of monolayer coverage of Cr(VI) on the MOPP surface (Lugo-Lugo et al. 2012).

## Adsorption Kinetics Study

Adsorption kinetics is one of the most essential characteristics which govern the solute uptake rate; it represents the adsorption capacity of the adsorbent and therefore, determines its potential applications. It could be seen from Fig. 6(a) and (b) that with the increase of initial concentration, more Cr(VI) was adsorbed onto the MOPP, also the time to achieve adsorption equilibrium was prolonged. However, it still can be concluded that all the adsorption processes proceed rapidly and this observed rapid kinetics has significant practical importance as it could be used for the scale-up to a larger system.

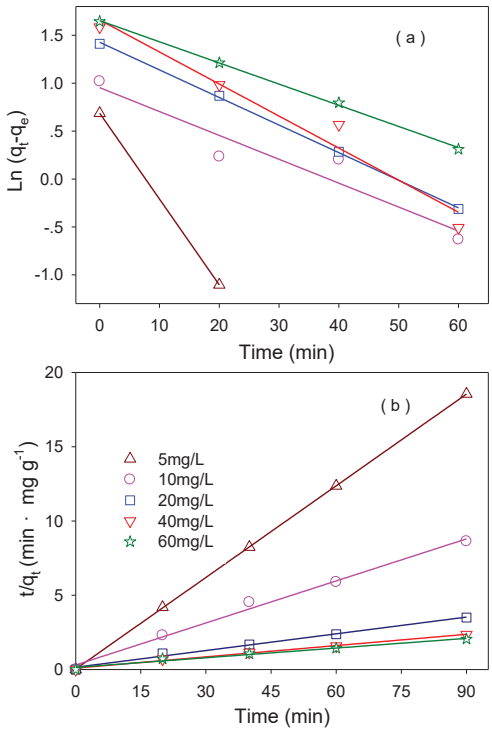


Fig. 6: Simulated results of pseudo-first-order kinetics (a); pseudo-second-order kinetics (b) at different initial Cr(VI) concentrations.

The kinetic experiments were carried out and data were fitted into the pseudo-first-order, pseudo-second-order and intraparticle diffusion models respectively. The pseudo-first-order model is represented by the following equation (Chairat et al. 2006):

$$\log(q_e - q_t) = \log q_e - \frac{k_1}{2.303} t \qquad \ldots(2)$$

Where, $q_e$ (mg.g$^{-1}$) and $q_t$ (mg.g$^{-1}$) are the amounts of Cr(VI) adsorbed at equilibrium (mg.g$^{-1}$) and at time t (min), respectively, and $k_1$ is the rate constant of pseudo-first-order adsorption process (min$^{-1}$). Values of $k_1$ and equilibrium adsorption density $q_e$ at 25°C were calculated from the plots of log($q_e$ - $q_t$) versus t for different initial concentrations of Cr(VI). The pseudo-second-order kinetic model can be expressed as (Ho et al. 1998):

$$\frac{t}{q_t} = \frac{1}{k_s q_e^{\,2}} + \frac{1}{q_e} t \qquad \ldots(3)$$

Where, $k_2$ (g mg$^{-1}$ min) is the rate constant for the pseudo-second-order adsorption kinetics. Values of $k_2$ and $q_e$ for different initial concentrations of Cr(VI) were calculated from the slope and intercept of the linear plot of $t/q_t$ versus $t$. The plot of $t/q_t$ versus $t$ at 25°C is shown in Fig. 6 (b).

The modelled parameters from pseudo-first and pseudo-second-order adsorption kinetic equations and the intraparticle diffusion equation are given in Table 1. The linear plots of $t/q_t$ versus $t$ indicated a good agreement between the experimental and calculated $q_e$ values for different initial Cr(VI) concentrations. Furthermore, the correlation coefficients of the pseudo-second-order kinetic model ($R^2$ = 0.9802) were greater than that of the pseudo-first-order model ($R^2$ = 0.9105), which indicated that the pseudo-second-order was more suitable for describing the adsorption of Cr(VI) on MOPP. This strongly suggested that the reaction between Cr(VI) and MOOP was chemical adsorption or chemisorption (Suksabye et al. 2008). A similar phenomenon has been observed in Cr(VI) adsorption by used coir pith (Suksabye et al. 2008), *Leersia hexandra* biomass (Li et al. 2009), and ethylenediamine-modified rice hull (Tang et al. 2003).

**Adsorption Isotherm Analysis**

Modelling of adsorption isotherm data is important for predicting and comparing composite adsorption properties of the adsorbent. It provides a comprehensive understanding of the nature of the interaction (Mahmoodian et al. 2015). In this study, three important isotherms were applied to fit the equilibrium data: the Langmuir, Freundlich and Temkin isotherms.

Based on the assumption that all the adsorption sites are equivalent and adsorption in active sites is independent of whether the adjacent is occupied, the Langmuir adsorption model can be expressed as (Bhugun et al. 1997):

$$\frac{1}{q_e} = \frac{1}{q_m} + \frac{1}{K_L q_m C_e} \quad \ldots(4)$$

Where, $q_e$ is the amount of adsorbate adsorbed per unit mass of adsorbent at equilibrium ($mg.g^{-1}$), $q_m$ is the monolayer capacity of the adsorbent ($mg.g^{-1}$), and $K_L$ is the adsorption constant ($L\ mg^{-1}$). According to this equation, a plot of $1/q_e$ versus $1/C_e$ gives a straight line of slope $1/q_m$ and intercepts $1/(q_m K_L)$.

The well-known logarithmic form of the Freundlich isotherm is expressed by the following equation (Elzinga et al 1999):

$$Lnq_e = LnK_F + \frac{1}{n} LnC_e \quad \ldots(5)$$

Where, $K_F$ and n are Freundlich constants related to adsorbent capacity and the sorption intensity of the adsorbent, respectively. Temkin isotherm takes into account sorbate-adsorbent interactions and assumes that fall in the heat of adsorption is linear rather than logarithmic. The Temkin isotherm can be expressed in its linear form (Samia et al. 2016) as:

$$q_e = BLnA + BLnC_e \quad \ldots(7)$$

Table 1: Comparisons of rate constants and calculated $q_e$ by the pseudo-first-order kinetics, pseudo-second-order kinetics at different initial Cr(VI) concentrations.

| ρ Cr(VI) ($mg.L^{-1}$) | Experiment | Pseudo-first-order kinetics | | | Pseudo-second-order kinetics | | |
|---|---|---|---|---|---|---|---|
| | $q_e$($mg.g^{-1}$) | $R^2$ | $q_e$ | $K_1$(g $mg^{-1}$ $min^{-1}$) | $R^2$ | $q_e$ | $K_2$ (g $mg^{-1}$ $min^{-1}$) |
| 5 | 4.8533 | 1.0000 | 4.8529 | 0.2063 | 1.0000 | 4.8614 | 1.6088 |
| 10 | 10.4322 | 0.9105 | 8.9681 | 0.0573 | 0.9923 | 10.5932 | 0.0285 |
| 20 | 25.7601 | 0.9995 | 26.6747 | 0.0663 | 0.9913 | 26.6667 | 0.0093 |
| 40 | 38.3487 | 0.9606 | 45.6457 | 0.0769 | 0.9930 | 39.5257 | 0.0069 |
| 60 | 43.9631 | 0.9989 | 44.9159 | 0.0509 | 0.9802 | 46.0829 | 0.0034 |

Table 2: Langmuir, Freundlich and Temkin model constants and correlation coefficients for Cr(VI) removal by cation adsorbent at 25°C.

| Temperature | Langmuir | | | Freundlich | | | Temkin | | |
|---|---|---|---|---|---|---|---|---|---|
| | $R^2$ | $q_m$ | $K_L$ (L.$mg^{-1}$) | $R^2$ | $K_F$($mg^{1-n}L^n g^{-1}$) | N | $R^2$ | A (L.$mg^{-1}$) | B |
| 25°C | 0.9915 | 52.0833 | 0.0606 | 0.9626 | 3.1606 | 0.6763 | 0.9826 | 1.8125 | 26.8822 |

Table 3: Adsorption capacities of various adsorbents for Cr(VI).

| Adsorbent ($g.L^{-1}$) | Major reaction conditions | $Q_m$ ($mg.g^{-1}$) | Source of information |
|---|---|---|---|
| MOPP | $[Cr(VI)]_0$ = 200 $mg.L^{-1}$,$[Adsorbent]_0$ = 2 $g.L^{-1}$, T = 293-303 K, pH = 6, reaction time = 90 min | 52.08 | The data from this paper |
| Wheat straw | $[Cr(VI)]_0$ = 11 $mg.L^{-1}$,$[Adsorbent]_0$ = 1g.$L^{-1}$, T = 298 K, pH = 2, reaction time = 60 min | 9.19 | (Samia et al. 2016) |
| aminated rice straw-grafted-poly | $[Cr(VI)]_0$ = 100 $mg.L^{-1}$,$[Adsorbent]_0$ = 0.5 $g.L^{-1}$, T = 333 K, pH = 2, reaction time = 60 hours | 140.39 | (Lin et al. 2018) |
| Corn cob ash | $[Cr(VI)]_0$ = 500 $mg.L^{-1}$,$[Adsorbent]_0$ = 20g.$L^{-1}$, T = 297-299K, pH = 6.2, reaction time = 24 hours | 4.2 | (Singh et al. 2014) |
| Orange peel powder | $[Cr(VI)]_0$ = 500 $mg.L^{-1}$,$[Adsorbent]_0$ = 20g.$L^{-1}$, T = 297-299 K, pH = 6.2, reaction time = 24 hours | 10.2 | (Singh et al. 2014) |
| Sawdust | $[Cr(VI)]_0$ = 5 $mg.L^{-1}$,$[Adsorbent]_0$ = 10 $g.L^{-1}$, T = 298 K, pH = 6, reaction time = 6 hours | 3.3 | (Srivastava et al. 1986) |
| Sugar cane bagasse | $[Cr(VI)]_0$ = 100 $mg.L^{-1}$, $[Adsorbent]_0$ = 4 $g.L^{-1}$,T = 298 K, pH = 1.2, reaction time = 24 hours | 13.4 | (Sharma et al. 1994) |

Where, $A$ is the equilibrium binding constant corresponding to the maximum binding energy (L.mg$^{-1}$) and $B$ is the Temkin constant related to the heat of adsorption.

From the plot of $Lnq_e$ versus $LnC_e$, the intercept and slope give the values of $K_F$ and $n$. Fig. 7(a)(b) shows Langmuir and Freundlich adsorption isotherms of MOPP at 25°C. It was clear from Fig. 7(a)(b) that data fitted better to Langmuir model in comparison to the Freundlich model. This indicated the monolayer adsorption on the homogeneous surface of the MOPP adsorbent with identical binding sites. The constants A and B were calculated from the slope and intercept of $q_e$ versus $LnC_e$. From linear regression, the $R^2$ values of 0.8746 for MOPP (Table 2), were also lower than Langmuir values. Therefore, the adsorption of MOPP was found to be well represented by the Langmuir adsorption isotherms, and the maximum adsorption capacity of MOPP was 52.08 mg.g$^{-1}$ calculated by it. In addition, we compared the adsorption capacity of other materials to Cr(VI), and found that MOPP has a good removal effect. The specific information is given in Table 3.

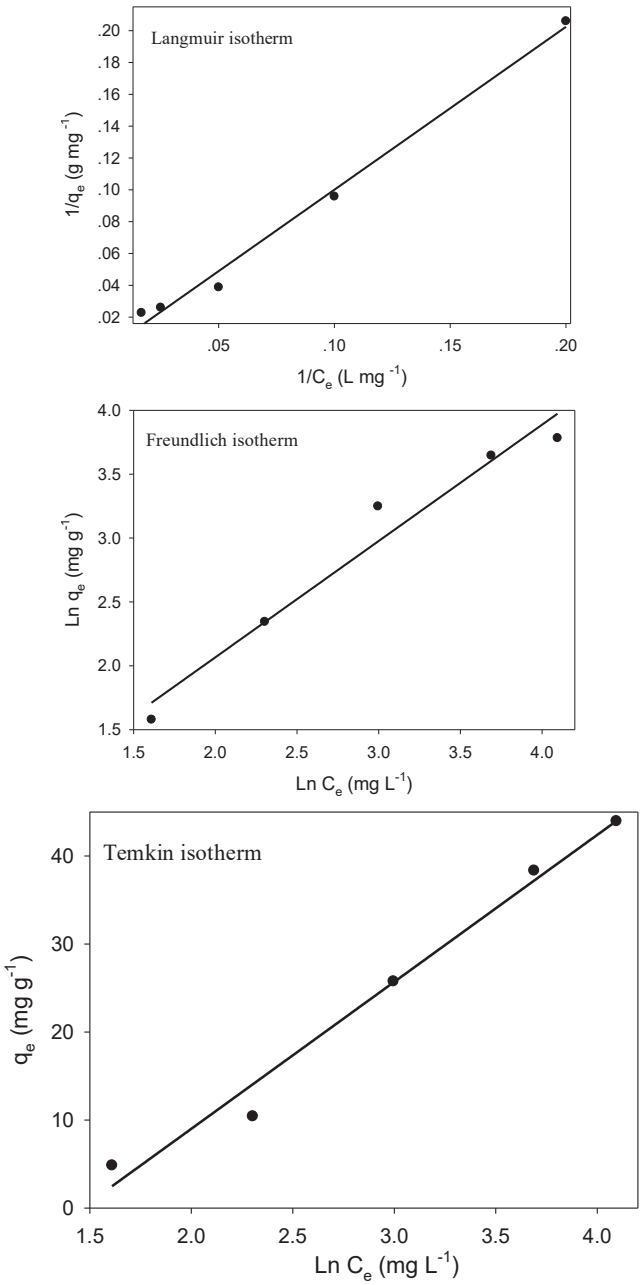


Fig. 7: Simulated results of Langmuir (a), Freundlich (b), Temkin (c) isotherm for Cr(VI) removal by cation adsorbent at 25°C.

## CONCLUSION

The potential of modified orange peel (MOPP) for removing Cr(VI) from aqueous solutions was studied in the present work. Batch experiments showed it an effective adsorbent for removal Cr(VI) from aqueous solution. The amount of Cr(VI) adsorbed was found to vary with initial solution pH, initial Cr(VI) concentrations, contact time, and adsorbent dose. Acidic pH was found to enhance the Cr(VI) removal the least. After fitting and analysing the data, it was found that the adsorption reaction between MOPP and Cr(VI) accorded with pseudo-second-order kinetics and was also presented well by the Langmuir adsorption isotherms. The maximum monolayer adsorption capacity of Cr(VI) was 52.08 mg.g$^{-1}$ at an optimum pH of 6.0. Based on the results, it could be concluded that MOPP is an effective and efficient adsorbent for the removal of Cr(VI) from aqueous solutions.

## ACKNOWLEDGEMENTS

The authors gratefully acknowledge the financial support of the National Natural Science Foundation of China (Grant No. 41807468), Zhejiang Provincial Natural Science Foundation of China (Grant No. LY18E080018), Shaoxing Public Welfare Project (Grant No. 2017B70042), State Key Laboratory of Pollution Control and Resource Reuse Foundation, (Grant No. PCRRF18021).

## REFERENCES

Altundogan, H.S. 2005. Cr(VI) removal from aqueous solution by iron (III) hydroxide-loaded sugar beet pulp. Process Biochem., 40(3-4): 1443-1452.

Baral, S.S., Das, N., Chaudhury, G.R. and Das, S.N. 2009. A preliminary study on the adsorptive removal of Cr(VI) using seaweed, *Hydrilla verticillata*. J. Hazard. Mater., 171(1-3): 358-369.

Bhugun, I. and Anson, F.C. 1997. A generalized treatment of the dynamics of the adsorption of Langmuirian systems at stationary or rotating disk electrodes1. J. Electroanal. Chem., 439(1): 1-6.

Chairat, M., Rattanaphani, S., John, B.B. and Rattanaphani, V. 2006. Adsorption kinetic study of lac dyeing on cotton. Dyes Pigm., 76(2): 435-439.

Chen, S., Yue, Q., Gao, B. and Xu, X. 2010. Equilibrium and kinetic adsorption study of the adsorptive removal of Cr(VI) using modified wheat residue. J. Colloid Interface Sci., 349(1): 256-264.

Elzinga, E.J., Grinsven, J.J.M.V. and Swartjes, F.A .1999. General purpose Freundlich isotherms for cadmium, copper and zinc in soils. Eur. J. Soil. Sci., 50(1): 139-149.

Feng, N., Guo, X. and Liang, S. 2008. Adsorption study of copper (II) by chemically modified orange peel. J. Hazard. Mater., 164(2-3): 1286-1292.

Fernandez, M.E., Nunell, G.V., Bonelli, P.R. and Cukierman, A.L. 2014. Activated carbon developed from orange peels: Batch and dynamic competitive adsorption of basic dyes. Ind. Crops. Prod., 62: 437-445.

Gnanasambandam, R. and Proctor, A. 2000. Determination of pectin degree of esterification by diffuse reflectance Fourier transform infrared spectroscopy. Food Chem., 68(3): 327-332.

Gu, H., Rapole, S.B., Huang, Y., Cao, D.M., Luo, Z.P., Wei, S. and Gao, Z. 2013. Synergistic interactions between multi-walled carbon nanotubes and toxic hexavalent chromium. J. Mater. Chem. A., 1(6): 2011-2021.

Ho, Y.S. and Mckay, G. 1998. The kinetics of sorption of basic dyes from aqueous solution by sphagnum moss peat. Can. J. Chem. Eng., 76(4): 822-827.

Hu, J., Lin, Y. and Zhu, G. 2016. Review on migration and transformation mechanisms of chromium in the subsurface and remediation techniques for chromium- contaminated sites. Environ. Eng., 34(S1): 1053-1056.

Kotaş J. and Stasicka, Z. 2000. Chromium occurrence in the environment and methods of its speciation. Environ. Pollut., 107(3): 263-283.

Li, J., Lin, Q., Zhang, X. and Yan, Y. 2009. Kinetic parameters and mechanisms of the batch biosorption of Cr(VI) and Cr (III) onto *Leersia hexandra* Swartz biomass. J. Colloid Interface Sci., 333(1): 71-77.

Liang, S., Guo, X., Feng, N. and Tian, Q. 2009. Application of orange peel xanthate for the adsorption of $Pb^{2+}$ from aqueous. J. Hazard. Mater., 170(1): 425-429.

Lin, C., Luo, W., Lou, T., Zhou, Q., Li, H. and Jing, L. 2018. A study on adsorption of Cr(VI) by modified rice straw: Characteristics, performances and mechanism. J. Cleaner Prod., 196: 626-634.

Lugo-Lugo, V., Barrera-Díaz, C., Ureña-Núñez, F., Bilyeu, B. and Linares-Hernandez, I. 2012. Biosorption of Cr (III) and Fe (III) in single and binary systems onto pretreated orange peel. J. Environ. Manage., 112: 120-127.

Mahmoodian, H., Moradi, O., Shariatzadeha, B., Salehf , T.A., Tyagi, I., Maity, A., Asif, M. and Gupta, V.K. 2015. Enhanced removal of methyl orange from aqueous solutions by poly HEMA-chitosan-MWCNT nano-composite. J. Mol. Liq., 202: 189-198.

Mukhopadhyay, B., Sundquist, J. and White, E. 2006. Hydro-geochemical controls on removal of Cr(VI) from contaminated groundwater by anion exchange. Appl. Geochem., 22(2): 380-387.

Nakamura, S., Amano, M., Saegusa, Y. and Sato, T. 1992. Preparation of aminoalkyl celluloses and their adsorption and desorption of heavy metal ions. J. Appl. Polym. Sci., 45(2): 265-271.

Samia, R., Mounir, B. and Salah, H. 2016. Neuro-fuzzy modeling of Cu(II) and Cr(VI) adsorption from aqueous solution by wheat straw. Desalin. Water Treat., 57(14): 1-16.

Say, R., Emir Diltemiz, S., Garipcan, B., Patir, S. and Denizli, A. 2003. Novel methacryloylamidophenylalanine functionalized porous chelating beads for adsorption of heavy metal ions. Adv. Polym. Technol., 22: 355-364.

Sengil, I., Ayhan and Ozacar, M. 2009. Competitive biosorption of $Pb^{2+}$ $Cu^{2+}$ and $Zn^{2+}$ ions from aqueous solutions onto valonia tannin resin. J. Hazard. Mater., 166(2-3): 1488-1494.

Sharma, D.C. and Forster, C.F. 1994. A preliminary examination into the adsorption of hexavalent chromium using low-cost adsorbents. Bioresour. Technol., 47(3): 257-264.

Singh, R. 2014. Comparison of hexavalent chromium adsorption from aqueous solutions by various biowastes and granulated activated carbon. Indian Chem. Eng., 56(1): 12-28.

Srivastava, H.C.P., Mathur, R.P. and Mehrotra, I. 1986. Removal of chromium from industrial effluents by adsorption on sawdust. Environ. Technol., 7(1-12): 55-63.

Suksabye, P., Nakajima, A., Thiravetyan, P., Baba, Y. and Nakbanpote, W. 2008. Mechanism of Cr(VI) adsorption by coir pith studied by ESR and adsorption kinetic. J. Hazard. Mater., 161(2-3): 1103-1108.

Tang, P.L., Lee, C.K., Low, K.S. and Zainal, Z. 2003. Sorption of Cr(VI) and Cu(II) in aqueous solution by ethylenediamine modified rice hull. Environ. Technol., 24(10): 1243-1251.

Zhou, J., Wang, Y., Wang, J., Qiao, D., Long, D. and Ling, L. 2015. Effective removal of hexavalent chromium from aqueous solutions by adsorption on mesoporous carbon microspheres. J. Colloid Interf. Sci., 462(8): 200.

Nature Environment and Pollution Technology
An International Quarterly Scientific Journal

p-ISSN: 0972-6268
(Print copies up to 2016)
e-ISSN: 2395-3454

Vol. 19 | No. 4 | pp. 1399-1410 | 2020

Original Research Paper

https://doi.org/10.46488/NEPT.2020.v19i04.006

Open Access Journal

# Correlation Analysis Between $PM_{2.5}$ Concentration and Meteorological, Vegetation and Topographical Factors in the Urbanized Ecosystem in Beijing, China

**Haiying Feng*† and Haixia Feng****
*School of Materials and Mechanical Engineering, Beijing Technology and Business University, Beijing 100048, China
**Beijing Key Laboratory of precision forestry, Beijing Forestry University, Beijing 100083, China
†Corresponding author: Haiying Feng; hyfeng8808@163.com

Nat. Env. & Poll. Tech.
Website: www.neptjournal.com

*Received:* 02-03-2020
*Revised:* 01-04-2020
*Accepted:* 15-06-2020

**Key Words:**
$PM_{2.5}$
Correlation analysis
Air quality
Water pressure
Topographical conditions

## ABSTRACT

With the economic growth and massive industrialization, the air quality of China in general and industrial regions in specific has saturated with different health hazard pollutants. Among the pollutants, $PM_{2.5}$ is posing some serious threats to the society. In this study we evaluated the correlation between $PM_{2.5}$ concentration and 12 different meteorological, vegetation and topographical factors in Beijing, China. We used the Difference Index (DI) method and dark pixel method to retrieve the $PM_{2.5}$ concentration of 30m and 1km spatial resolution. Spearman correlation analysis method was used to analyse the correlation between $PM_{2.5}$ concentration and three types of 12 factors. The results showed that the forest land can play a major role in decreasing the $PM_{2.5}$ concentration in the air, as in this study a significant drop of (18.78%) was observed in $PM_{2.5}$ concentration in the regions having coniferous forest. Moreover, the $PM_{2.5}$ reduction rate was positively correlated with forest vegetation coverage (FVC). Our results demonstrated that relative humidity, air pressure and water vapour pressure were positively correlated with $PM_{2.5}$, while air temperature and wind speed were negatively correlated. The altitude and slope showed a weak negative correlation with $PM_{2.5}$ concentration, while, aspect was very weakly correlated with the $PM_{2.5}$ concentration. The findings of this study could help design the urban green space planning and air pollutioncontrol in the heavily populated urban ecosystems.

## INTRODUCTION

In recent decades China has experienced an exponential infrastructural and developmental growth. With the economic growth and massive industrialization, the air quality of China, in general, and industrial regions in particular have saturated with different health hazard pollutants. Among the pollutants, the $PM_{2.5}$ is posing some serious threats to society. The distribution of $PM_{2.5}$ is affected by the emission, diffusion and propagation conditions of air pollution sources. Moreover, the atmospheric chemical reactions, under specific conditions, diffusion of pollen and other particles in the air also facilitate its distribution. Recently, many research studies have been focused on the $PM_{2.5}$ spatial distribution and related factors (Wang 2019), as it provides a reference for the effective control and management of atmospheric particles.

The diffusion and propagation of $PM_{2.5}$ is a very complex system, which is affected by many factors. Some studies established a direct correlation of spatial distribution of $PM_{2.5}$ with meteorological factors, such as wind speed and air pressure etc. (Feng 2019). Table 1 exhibits the findings of some studies that are conducted to assess the correlation between temperature and particle concentration in 10 years (Yang 2009, Li 2011, Liu 2015, Deng 2012. Wang 2019a, Hou 2019). It can be seen that the correlation between the same factors with $PM_{2.5}$ concentration may be different in different regions. The correlation of the same region, factor and different time is not completely consistent.

The leaves, branches and trunks of plants have microstructure, rough texture, and secretions such as the wax layer that can absorb $PM_{2.5}$ in its surface. The complex three-dimensional structure of forest vegetation, coniferous and broad-leaved forests canopy, and groove like tissue on leaves surface having a certain degree of humidity and roughness, that can effectively intercept and retain fine $PM_{2.5}$ found in the air (Zhang 2019). In addition, vegetation cover and types and canopy shading and transpiration play an important role in the construction of a suitable environment for particle deposition, effectively avoiding the environment that is not conducive to $PM_{2.5}$ deposition (Liu 2015). Nowak et al. (2006) showed that trees can remove air pollutants and improve urban air quality. The estimated total annual pollutant removal can reach up to 711 thousand tons in the urban ecosystem using trees. Liu et al. (2014) studied the correlation between $PM_{2.5}$ concentration and forest area in the Fifth Ring Road of Beijing and their results showed that $PM_{2.5}$ concentration was negatively correlated with air temperature and positively correlated with relative humidity.

Table 1: Comparison of correlation result between temperature and particles.

| Correlation | Author | Research area | Study period | Result |
|---|---|---|---|---|
| Temp-$PM_{2.5}$ concentration | Li-Jinjuan | Guiyang | July 2008 - Apr. 2009 | Positive correlation (+) |
| | Yang-Rongshi | Guiyang | Mar 2008 - Nov 2009 | Weak correlation |
| | DENG Li-qun | Chengdu | Aug. 2008 - Sept. 2009 | Weak correlation |
| | Liu Ningwei | Liaoning | Jun. 2012-May. 2013 | Negative correlation (-) |
| | Wang Qian | Fuzhou | Nov. 2012 | Negative correlation (-) |
| | Hou Zhonxin | Qingdao | 2014 - 2016 | Positive correlation (+) |

Vegetation cover is an important index to measure the state of vegetation and plays an effective role in the concentration of $PM_{2.5}$ (Nowak 2006, Yu et al. 2019). Above ground vegetation biomass is the most direct expression of the structure and function of the forest ecosystem, which can reflect the environmental quality of the ecosystem (Zhang & Buren 2020). Wind directly affects the propagation of $PM_{2.5}$, air temperature and air pressure play an important role in the diffusion, and dilution and transport of $PM_{2.5}$ (Wang et al. 2019). In addition, the $PM_{2.5}$ has certain hygroscopic property (Han & Wang 2016). The relative humidity and water vapour pressure reflect the moisture content and stability of the atmosphere (Wang et al. 2020) and play a significant role in the distribution and concentration of $PM_{2.5}$. Therefore, this study selected 5 meteorological factors including air temperature (temp), relative humidity (RH), wind speed (V_wind), air pressure (p) and water vapour pressure (e). At the same time, the terrain conditions affect climate and vegetation growth. Zhang (2019) studied the concentration of particles and the geographical topography in Zhangzhou of 2017-2018, found that the geographical topography of this city is not conducive to the dilution and diffusion of air pollutants. Terrain factors, such as altitude and slope, affect the meteorological conditions (e.g. temperature and wind) and vegetation growth to a certain extent. This study focused to estimate the influence of terrain factors including altitude, slope, position and direction on the distribution of $PM_{2.5}$.

In this study, we evaluated the correlation of atmospheric particulate $PM_{2.5}$ concentration with 3 types of 12 factors (Table 2).

## MATERIALS AND METHODS

### Overview of the Study Area

Beijing, the capital of China (39°28'-41°03'N，115°25'-117°30'E) is spanning over an area of 16410.54 $km^2$. It is surrounded by mountains on the north, east and west side. The terrain is high in the northwest and low in the southeast, with the warm and humid zone and semi-humid continental monsoon climate. Frequent haze in winter and $PM_{2.5}$ are the main pollutants throughout the year. Beijing has set up 35 ground air quality monitoring stations and 17 meteorological stations (Fig. 1). The zonal vegetation types in Beijing are warm temperate deciduous broad-leaved forests and temperate coniferous forests (Feng et al. 2015). The results of the Eighth National Forest Resources Inventory from 2009 to 2013 showed that the forest coverage rate of Beijing is 35.84%, with the total area of forest land of 1013500 hectares, and the forest area of 588100 hectares.

### Data Acquisition and Processing

This paper aims to correlate the temporal and spatial distribution of $PM_{2.5}$ with meteorological, topographical, vegetation and other factors using data obtained from multiple sources

Table 2: Influence factors of $PM_{2.5}$ concentration.

| Type | Factor |
|---|---|
| Vegetation | Forest land type |
| | Forest vegetation coverage |
| | Biomass |
| Meteorology | Temperature |
| | Relative humidity |
| | Wind speed |
| | Air pressure |
| | Water vapour pressure |
| Topography | Altitude |
| | Slope |
| | Aspect, |
| | Slope position |

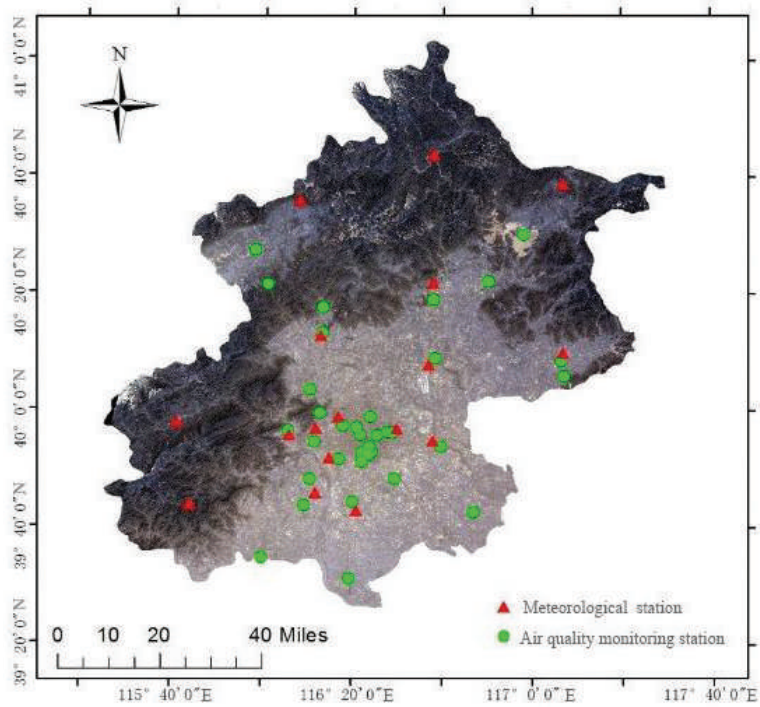


Fig.1: Monitoring station distribution map of the study area.

(Table 3). The data acquisition and analysis were carried out on the days with less cloud and better remote sensing image acquisition effect. The satellite remote sensing data were acquired of the year 2016 for dates including March 1, May 6, June 8, June 9, June 10, July 24, August 4, October 19, December 6, December 14, December 18 and December 19 in 2016, respectively. All the spatial data were unified as WGS_1984_UTM_Zone_50N coordinate system.

## Inversion of $PM_{2.5}$ Concentration

At present, most researchers use the data of ground monitoring stations and Geographic Information System (GIS) spatial interpolation to obtain the spatial-temporal distribution of $PM_{2.5}$. This kind of method is greatly influenced by the number and distribution of sampling points. There are 35 air quality monitoring stations in our study area. The monitoring stations are unevenly distributed in the area as are

Table 3: Summary of data involved in this paper.

| No. | Data | Source | Application |
|---|---|---|---|
| 1 | $PM_{2.5}$ hourly data for 2016 | Beijing environmental protection monitoring centre | $PM_{2.5}$ concentration inversion and accuracy verification |
| 2 | Meteorological data in 2016 | MICAPS | Interpolation diagram of temperature, relative humidity, wind speed, air pressure and water pressure factors |
| 3 | MOD09GQ surface reflectance data | NASA official database website | Obtain Vegetation cover inversion (250m) |
| 4 | Landsat8 Remote sensing image | Geospatial data cloud official website | Obtain particle concentration and vegetation coverage distribution (30M) |
| 5 | Global biomass inversion data | National integrated earth observation data sharing platform | Establishment of biomass distribution map database (1km) |
| 6 | NPP-VIIRS_SDK Landmark reflectivity and calibration data | NOAA Official data website | Inversion of $PM_{2.5}$ distribution by AOD(750m) |
| 7 | DEM data of Beijing | Cold and dry area scientific data centre | Altitude, slope and aspect distribution map (1km) |

more concentrated in the central area as compared to suburbs (Fig. 1). The accuracy of $PM_{2.5}$ concentration obtained by this method was poor. According to the research of Su et al. (2015) the correlation coefficient "r" between aerosol optical thickness (AOD) data retrieved from NPP_VIIRS (National Polar-orbiting Partnership_Visible Infrared Imaging Radiometer Suite) 750m surface reflectance data and AERONET (AErosol RObotic NETwork) ground aerosol remote sensing data is 0.7920. In this paper, we used this method to retrieve AOD by using the surface reflectance and calibration data of VIIRS sensor of NPP satellite, through altitude correction, using 6S model, establishing look-up table, and resampling it to 1km resolution. According to the transit time of the NPP satellite on the same day, we selected the closest ground monitoring station to collect the $PM_{2.5}$ concentration data for model fitting. Due to the seasonal difference of AOD, the four seasons including Spring (March-May), Summer (June-August), Autumn: (September-November), Winter (December- February) were respectively fitted as per the division of meteorology to retrieve the concentration and distribution of $PM_{2.5}$ on that day in Beijing. The model accuracy of four seasons are 0.9299 (spring) , 0.8181 (summer) , 0.8958 (autumn) and 0.8597 (winter) respectively. To analyze the effect of vegetation on the concentration of $PM_{2.5}$ we followed our previous work (Feng et al. 2018) and used near-infrared and infrared bands of Landsat 8 data to establish the remote sensing Difference Index (DI), and inversed the 30m particle concentration distribution. The comparison of $PM_{2.5}$ distribution maps which was retrieved using the aerosol inversion method (VIIRS data) and the difference index method (Landsat data) on March 1, 2016 is given in Fig. 2

## Vegetation Data Acquisition

**Quantification of forest land type:** Based on the sub-compartments survey data of 2016 in Beijing obtained from Beijing forestry bureau, we carried out a geographical analysis of the land type of forest in the study area. According to Technical Regulations for Forest Resources Planning and Design in China, the land classification of the data was

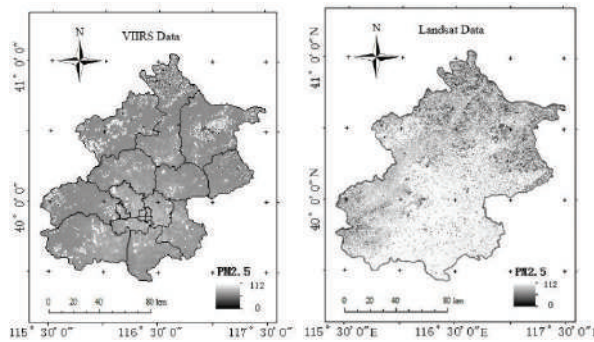


Fig. 2: $PM_{2.5}$ distribution obtained by from VIIRS and Landsat data.

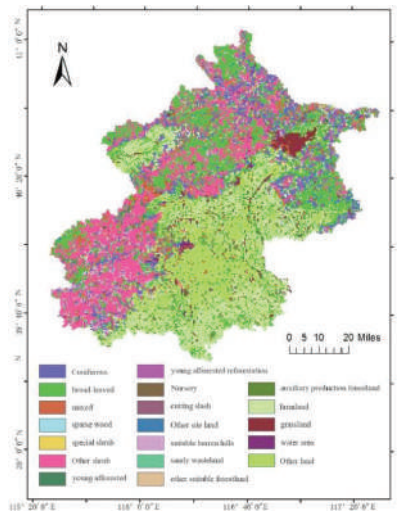


Fig. 3: Forest resource distribution of Beijing.

carried out to generate 1km resolution grid map of the forest resources found in our study area (Fig. 3).

As the forest land is a qualitative factor, it needs to be quantified and assigned for statistical analysis. According to the available data, there are very few data about young afforested land, sandy wasteland, other suitable forestlands, cutting slash and burned blank, therefore, in the statistical analysis, they are classified into the first level classification of young forest and suitable forest land and site land (Table 4). To intuitively analyze the impact of forest land on $PM_{2.5}$, four second level non-forest lands were classified into one category. The water areas in non-forest land were not included in the statistical analysis.

**Vegetation coverage and aboveground biomass data acquisition:** In this paper, MODIS (Moderate-resolution Imaging Spectroradiometer) 09GQ surface reflectance data from 2016 were used to obtain vegetation coverage (250m), while the MRT (MODIS Reprojection Tool) was used to re-project and splice the mod09 data. Cutting and band operation were carried out in ENVI to calculate vegetation coverage FVC, which was then resampled in ArcGIS software to 1km resolution. Due to the small change of vegetation coverage in a short period, the data with good inversion effect of May 6 (spring), July 24 (summer), October 17 (autumn) and December 19 (winter) for the year 2016 were selected as the coverage data of each season (Fig. 4).

Based on the above-ground biomass data of global 1km forest provided by the national integrated earth observation data-sharing platform, the biomass distribution map of Bei-

Table 4: Assignment of forest land types.

| | Land type | Twice classification | Assignment |
|---|---|---|---|
| 1 | Closed forest land | Coniferous forestland | 111 |
| | | broad-leaved forestland | 112 |
| | | mixed forestland | 113 |
| 2 | Sparse wood land | sparse wood land | 120 |
| 3 | Shrub forestland | special shrub | 130 |
| | | Other shrub | |
| 4 | Young forest | young afforested forestland | 140 |
| | | young afforested reforestation forestland | |
| 5 | Nursery land | Nursery land | 150 |
| 6 | Site land | cutting slash | 160 |
| | | burned b lank | |
| | | Other site land | |
| 7 | Suitable Forestland | suitable barren hills | 170 |
| | | sandy wasteland | |
| | | other suitable forestland | |
| 8 | Auxiliary production forestland | auxiliary production forestland | 180 |
| 9 | Non-forestland | farmland | 200 |
| | | water area | |
| | | unused land | |
| | | Other land | |

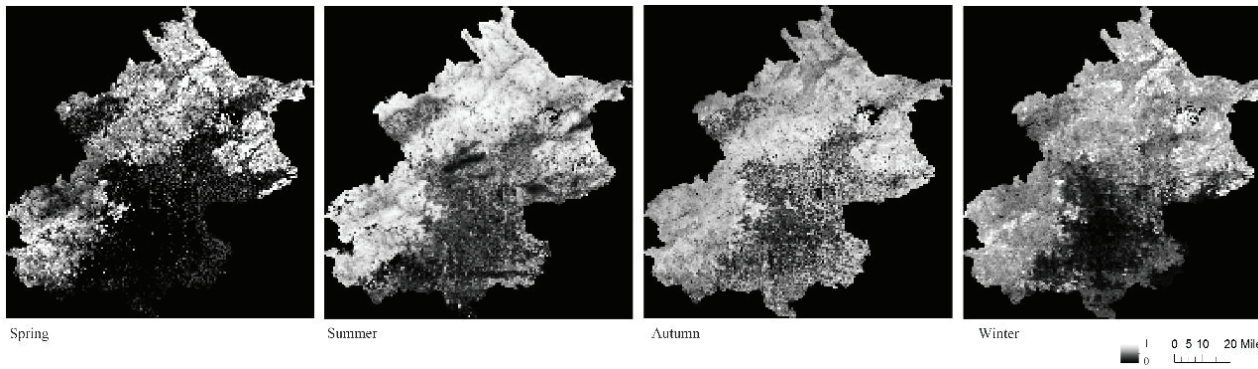


Fig. 4: FVC distribution of four seasons in Beijing.

jing (Fig. 5) was generated after cutting. According to the acquisition time of the measured data, the biomass data were only used for summer and autumn seasons.

**Forest profile data acquisition:** To analyze the impact of vegetation on the concentration of $PM_{2.5}$, three large forest areas, Tiantan Park, Orson centre and northern mountain area, were selected to obtain the vegetation coverage and analysed it on a high-resolution scale.

In ERDAS software, two sections of horizontal and vertical lines were drawn, which run through the forest area and extend to two pixels outside the forest area. The $PM_{2.5}$ concentration and the forest vegetation coverage on the section line were extracted based on Landsat data. To facilitate viewing, we enlarged the vegetation coverage value by 300%.

**Calculation of $PM_{2.5}$ reduction rate in forest area:** In the equation (3) t is the $PM_{2.5}$ concentration of air particles in the forest area, and $x_b$ is the concentration outside the forest area. The $PM_{2.5}$ concentration at the two ends of the profile line is taken as $x_b$, then the reduction rate of $PM_{2.5}$ ( $\rho$ ) can be calculated by the following formula:

$$\rho = (x_b - x_f)/x_b \quad \ldots(1)$$

We calculated the reduction rate of each point on the section line of Fig. 6, and fit the scatter diagram model with the extracted vegetation coverage value using the extended model to predict the reduction rate when the vegetation coverage exceeds 90% (extending forward to vegetation coverage = 1). In the modelling, 30% of data were used to verify the accuracy of the model ($R^2$ i = 0.649).

**Meteorological Data Acquisition**

The meteorological data were acquired from the MICAPS (Meteorological Information Combine Analysis and Process System) based on the data of 17 meteorological stations in Beijing. The daily average data corresponding to the time in the inversion model of $PM_{2.5}$ was selected for statistical analysis. The relative humidity data were obtained by querying the temperature and dew point. The spherical variogram of the Kriging interpolation tool of ArcGIS was used to interpolate the data of 5 meteorological factors into Beijing. Then we resampled the data to 1km. The distribution of five meteorological factors is shown in Fig. 6 (Data of 1st March 2016).

**Acquisition and Quantification of Terrain Data**

Using the DEM (Digital Elevation Model) data of 1km spatial resolution downloaded from the scientific data centre in the arid area of the cold region website (http://westdc.westgis.ac.cn), the altitude data of Beijing were obtained after cutting. 3D analysis tools in ArcGIS were used to extract the slope and aspect data. In the forest resource survey, the slope position was usually divided into six categories: ridge, upper, middle, flat, lower and valley to study the influence of site conditions on vegetation growth. The distribution of atmospheric particles in a small range was not very different due to their existing forms. Therefore, the slope position was divided into three categories upper, middle and lower (Zhao et al. 2014). The slop direction data was transformed into the vector in ArcGIS. After that, we extracted the maximum elevation (Hmax) and the minimum elevation (Hmin) of each

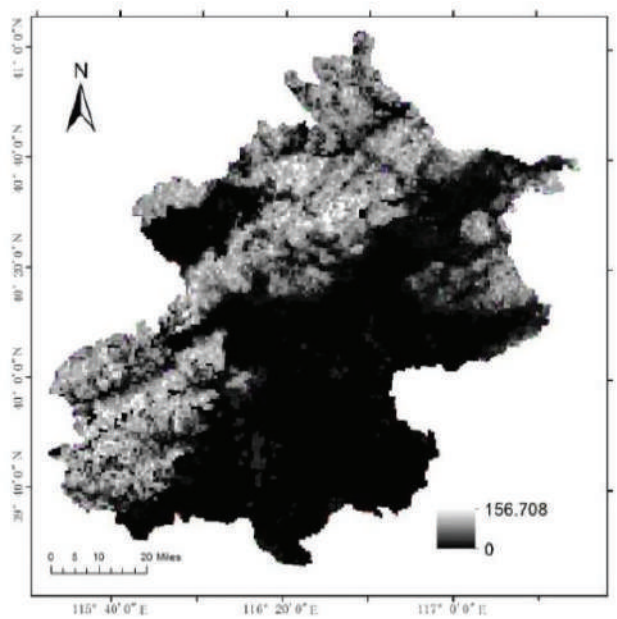


Fig. 5: Biomass distribution of Beijing.

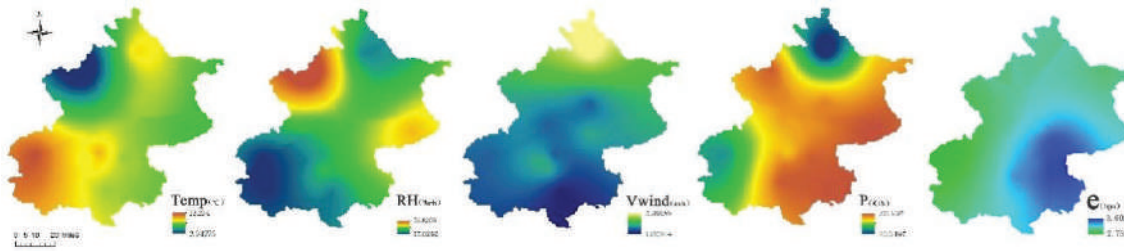

Fig. 6: Meteorological factor in 1km size (1st March 2016).

slope and calculated the critical values of the upper, middle and lower slopes of each slope according to the formula (2) and (3) to generate the slope map of the study area.

$$H_{mid-up} = (H_{max} - H_{min}) * 0.75 + H_{min} \quad \ldots(2)$$

$$H_{mid-low} = (H_{max} - H_{min}) * 0.25 + H_{min} \quad \ldots(3)$$

The slope direction and slope position are qualitative factors. To carry out correlation analysis, they were assigned and quantified respectively (Fig. 7, Table 5, Table 6).

### Sample Data Collection

Using the create random points tool in ArcGIS, 3000 random sampling points were created in Beijing, and the minimum allowable distance was set as 1km (Fig. 8). $PM_{2.5}$ concentration data and 12 kinds of impact factors data on the sampling points were extracted for statistical analysis. After removing the data that failed to acquire due to the quality of remote sensing image and abnormal data whose deviation from the average is more than three times of the standard deviation, 20473 groups of valid data were obtained.

### Spearman Correlation Analysis Method

Spearman correlation analysis can provide the common changing trend of two random variables under the linear or non-linear correlation, and the conclusion can still be obtained under the condition of unclear overall distribution and lack of overall information (Cameriere et al. 2019). The calculation formula is:

$$r = 1 - \frac{6\sum d_i^2}{n(n^2-1)} \quad \ldots(4)$$

$$d_i = x_i^1 - y_i^1 \quad \ldots(5)$$

Where, r is the correlation coefficient, n is the number of samples. Suppose that the original data $x_i$, $y_i$ have been arranged in the order of large to small, $x_i^1$, $y_i^1$ is the rank of $x_i$, $y_i$, and $d_i$ is the difference of the rank of $x_i^1$, $y_i^1$. The absolute value range of correlation coefficient 'R' (0~1) is used to judge the correlation strength, the larger the value, the stronger the correlation (Table 7).

## RESULTS

### Analysis of the Impact of Vegetation on $PM_{2.5}$

It can be seen from the comparison between the left and right graphs of Fig. 9 that at the forest edge (including the vegetation blank area in the middle of the forest), the concentration of $PM_{2.5}$ decreased significantly while in the interior of the forest this change was smaller.

The reduction rate of $PM_{2.5}$ concentration (Fig. 10) was not in a simple linear correlation with the vegetation coverage. As with an increase of vegetation coverage, a decrease in the reduction rate of $PM_{2.5}$ was observed, but when the vegetation coverage was too high (>83%), a decrease in the reduction rate took place.

The $PM_{2.5}$ concentration in all different forest land types was lower than that of non-forest land (Table 8). The most

Table 5: The classification and assignment of aspect.

| Slope direction | Flat slope | North | Northeast | East | Southeast | South | Southwest | West | Northwest |
|---|---|---|---|---|---|---|---|---|---|
| Range | -1 | 337.5~22.5 | 22.5~67.5 | 67.5~112.5 | 112.5~157.5 | 157.5~202.5 | 202.5~247.5 | 247.5~292.5 | 292.5~337.5 |
| assign-ment | 0 | 1 | 2 | 3 | 4 | 5 | 6 | 7 | 8 |

unit°

Table 6: The classification and assignment of TPI.

| Slope position | Upper | Middle | Lower |
|---|---|---|---|
| Assignment | 1 | 2 | 3 |

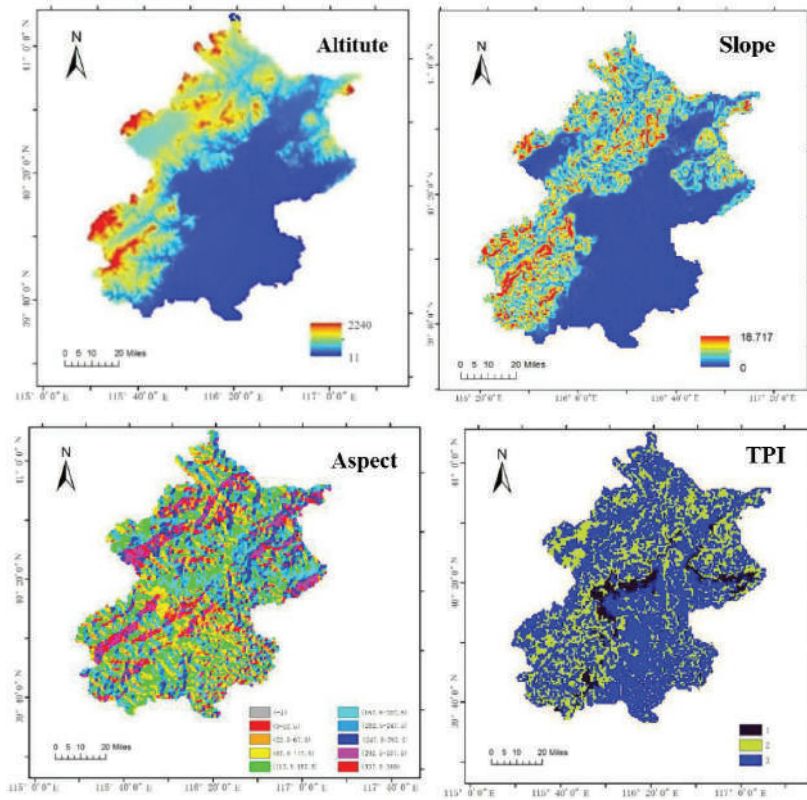


Fig. 7: Altitude, slope, aspect and TPI distribution of Beijing.

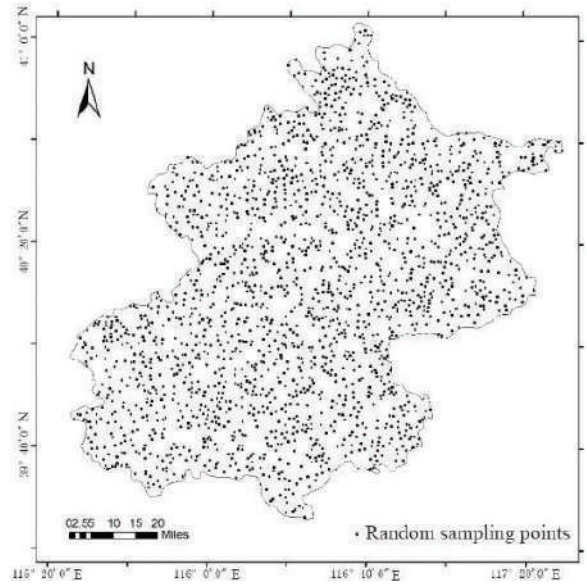


Fig. 8: Random sample points distribution.

Table 7: Correlation strength.

| R | 0.0~0.2 | 0.2~0.4 | 0.4~0.6 | 0.6~0.8 | 0.8~1 |
|---|---|---|---|---|---|
| Correlation strength | extremely weak | Weak | Moderate | Strong | extremely strong |

significant decrease was observed in the coniferous forest, with a decrease of 18.78% followed by Young Forestland (17.17%) and Mixed Forestland (15.54%).

### Correlation Analysis Between Influence Factors and $PM_{2.5}$

The correlation analysis results of daily average $PM_{2.5}$ concentration and meteorological factors and vegetation factors are given in Table 9 and Table 10, while Table 11 shows the correlation analysis result of annual average $PM_{2.5}$ concentration and terrain factors.

The correlation between air temperature and $PM_{2.5}$ was not completely consistent for the studied seasons. It was recorded negative in summer, autumn and winter while positive in spring. In terms of the correlation coefficient, the correlation between air temperature and atmospheric particulate was weak (< 0.4), among which the correlation

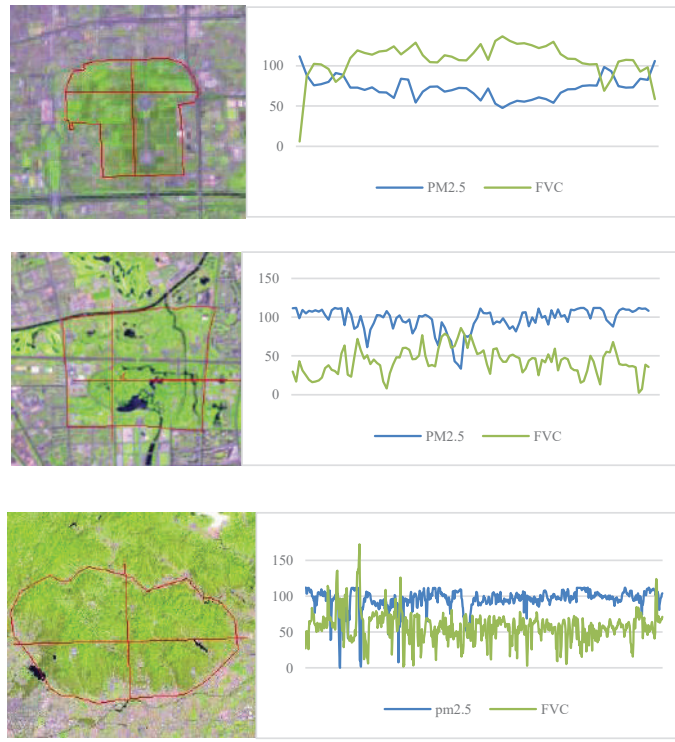


Fig. 9: $PM_{2.5}$ Concentration and FVC curve in profile (from top to bottom is Tiantan Park, Orson centre and northern mountain).

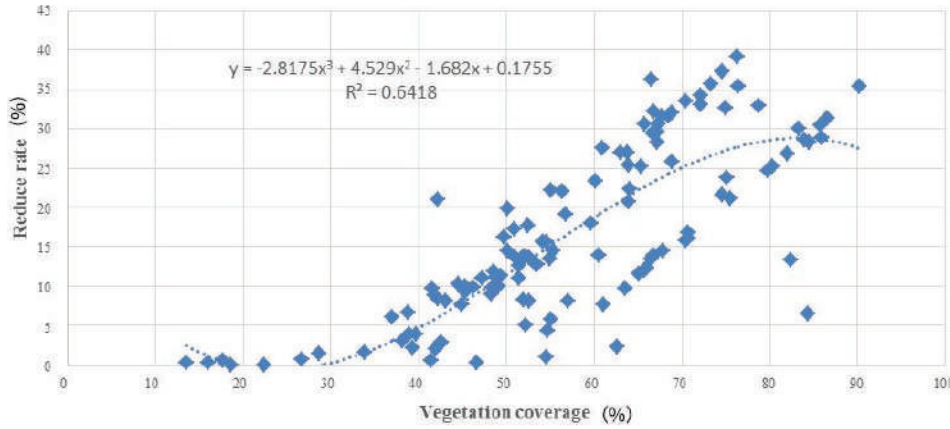


Fig. 10: The scatter plot of FVC-particle removal rate model.

coefficient in summer was the strongest (R = - 0.367).

The correlation between relative humidity and $PM_{2.5}$ was significantly positive in summer (R = 0.475) and winter (R= 0.368), while a weak correlation was observed for spring and autumn seasons, with the correlation coefficients less than 0.2.

Wind speed and $PM_{2.5}$ were negatively correlated in spring and winter, with the correlation coefficient greater than 0.4. In summer, the correlation was extremely weak (R < 0.1), while in autumn, the correlation between wind speed and atmospheric particles was not significant (sig > 0.05). Atmospheric pressure and $PM_{2.5}$ were positively correlated in spring (R = 0.434), summer (R = 0.581) and winter (R = 0.412). In summer, the correlation was extremely weak (R < 0.1), while in autumn, the correlation was not significant (sig > 0.05). Water vapour pressure was positively correlated with $PM_{2.5}$ for all four seasons, summer (R = 0.715), spring (R = 0.579), winter (R = 0.468) and autumn (R = 0.459).

There was a significant positive correlation between the concentration of $PM_{2.5}$ and forest land types for all four studied seasons (sig < 0.01, R > 0). According to the table of assignment of forest land type (Table 3), the assignment was

Table 8: Influence of forest land type on $PM_{2.5}$ concentration.

| Forest Land Type | $PM_{2.5}$ Annual Average ($\mu g/m^3$) | Drop |
|---|---|---|
| Coniferous Forestland | 60.9 | 18.78% |
| Young Forestland | 62.1 | 17.17% |
| Mixed Forestland | 63.3 | 15.54% |
| Broad-leaved Forestland | 63.9 | 14.73% |
| Shrub Forestland | 64.8 | 13.53% |
| Auxiliary Production Forestland | 67.5 | 9.93% |
| Site Land | 68.5 | 8.59% |
| Suitable Forestland | 72.1 | 3.80% |
| Non-forestland | 75.0 | 0.00% |

Table 9: Correlation analysis between meteorological factors and $PM_{2.5}$.

| Factor | Spring | | Summer | | Autumn | | Winter | |
|---|---|---|---|---|---|---|---|---|
| | R | Sig | R | Sig | R | Sig | R | Sig |
| Air Temperature | 0.163** | 0.000 | -0.367** | 0.000 | -0.111** | 0.000 | -0.075** | 0.000 |
| Relative Humidity | -0.145** | 0.000 | 0.475** | 0.000 | 0.151** | 0.000 | 0.368** | 0.000 |
| Wind Speed | -0.419** | 0.000 | 0.089** | 0.000 | 0.033 | 0.069 | -0.405** | 0.000 |
| Air Pressure | 0.434** | 0.000 | 0.581** | 0.000 | -0.045 | 0.013 | 0.412** | 0.000 |
| Water Vapor Pressure | 0.579** | 0.000 | 0.715** | 0.000 | 0.459** | 0.000 | 0.468** | 0.000 |

Table 10: Correlation analysis between forest factors and $PM_{2.5}$.

| Factor | Spring | | Summer | | Autumn | | Winter | |
|---|---|---|---|---|---|---|---|---|
| | R | Sig | R | Sig | R | sig | R | sig |
| Forest Land Type | 0.342** | 0.000 | 0.299** | 0.000 | 0.401** | 0.000 | 0.241** | 0.000 |
| Vegetation Coverage | -0.470** | 0.000 | -0.534** | 0.000 | -0.450** | 0.000 | -0.447** | 0.000 |
| Biomass | | | -0.503** | 0.000 | -0.508** | 0.000 | | |

Table 11: Correlation analysis between terrain factors and particulates.

| Factor | R | Sig |
|---|---|---|
| Altitude | -0.266** | 0.000 |
| Slope | -0.264** | 0.000 |
| Aspect | -0.054** | 0.001 |
| Slope position | 0.023** | 0.001 |

Sig is the value of the significance test. **When the confidence (double test) is 0.01, the correlation is significant.

gradually increasing from closed forest land to non-forest land, indicating that forest has a decreasing effect on the $PM_{2.5}$ concentration. Vegetation coverage, biomass and $PM_{2.5}$ concentration showed a significant negative correlation, with a higher correlation coefficient for summer (-0.503) and autumn (-0.508).

In this study, a weak correlation was observed between terrain factors and $PM_{2.5}$ concentration. Altitude was negatively correlated with $PM_{2.5}$ concentration (R = -0.266) while, the correlation between $PM_{2.5}$ and the slope direction (R = -0.054), and slope position (R = 0.023) concentration was poor.

## DISCUSSION

### Analysis of Impact of Vegetation on $PM_{2.5}$ and Correlation

Results of this study showed how different factors can affect the $PM_{2.5}$ concentration in an area. Our study outcomes showed that the coniferous forest can significantly reduce $PM_{2.5}$ concentration. The special leaf shape and three-dimensional microstructure of coniferous forest land has a larger contact area and can effectively intercept and retain fine atmospheric particles in the air. Moreover, the coarse texture and secretion promote the adsorption of particulates, which can cause a stronger $PM_{2.5}$ reduction effect than mixed, broad-leaved and other forest lands (Yu 2019). In terms of time, the negative correlation between vegetation coverage, biomass and $PM_{2.5}$ were larger in summer and autumn, which may be related to the growing season of main tree species in Beijing, concentrated in late spring to early autumn, thus all physiological functions of vegetation reached the best state, and the effect on $PM_{2.5}$ could have improved (Bai et al. 2020).

When the forest vegetation coverage was greater than 0.83, a decrease in the $PM_{2.5}$ concentration was observed. The dense canopy and complex morphological structure where the vegetation coverage is too high affect the air turbulence in the forest area, which is not conducive to the diffusion of atmospheric particles (Zhang et al. 2018). Moreover, when the vegetation coverage is dense, the microclimate has high humidity and low temperature in the forest area. The hygroscopicity of atmospheric particles makes it easier to gather in the area with higher humidity (Liu et al. 2016).

### Correlation Analysis Between Meteorological Factors and $PM_{2.5}$

Overall, the temperature was negatively correlated with the $PM_{2.5}$ concentration, as the surface temperature increases, the convection between the surface and the upper cold air gets stronger. As a result, the turbulence is enhanced, which could be conducive to the diffusion of atmospheric particles (give a reference for this statement). In winter, the correlation coefficient value was very small, which may be related to the frequent inversion phenomenon in winter. Inversion in meteorology refers to the abnormal phenomenon that the air temperature over the ground increases with the height under certain weather conditions. At the same time, the atmospheric structure of inversion layer is stable, which is not conducive to the diffusion of atmospheric particles (Wang & Ni 2019). The correlation in spring was positive, which may be related to the increase of dust, vegetation floating pollen and other particles in the atmosphere, so temperature increase causes the acceleration of atmospheric flow, increasing particulate concentration. Air particles have obvious hygroscopicity, and the high humidity air often causes the agglomeration of the air particles, resulting in the heavy pollution of the air particles (Long et al. 2017).

Wind speed has an important influence on the diffusion, dilution, transportation and propagation of atmospheric particles. In a certain range, the greater the wind speed, the faster the diffusion and propagation of atmospheric particles. When the wind speed is high, an area with a lot of dust on the ground could produce fugitive dust. Besides, Beijing is located in the monsoon climate zone, therefore, in the summer monsoon blows from the ocean to the land, bringing the moisture content along with. The hygroscopicity of atmospheric particles causes the concentration of atmospheric particles to rise to a certain extent. In the area with high air pressure, the atmospheric convection and diffusion of atmospheric particles are weak, hence the concentration value is high.

Water vapour pressure was significantly correlated with $PM_{2.5}$. This is because when the water vapour pressure is high, the water vapour content in the atmosphere causes the partial pressure of water vapour to be high, and water vapour is easy to attach to the fine atmospheric particles to form the pollution of atmospheric particles (Bao et al. 2017).

### Correlation Analysis Between Terrain Factors and $PM_{2.5}$

Due to vertical movement of particles with air convection, their concentrations become lower at higher altitude. In addition, with the increase of altitude, the air temperature also decreases, which is not conducive for the diffusion of particles (Wang 2019b). In our results, a weak negative correlation was observed between slope and $PM_{2.5}$ concentration; the steeper the slope is, the lower the concentration of atmospheric particles. The possible reason is that the slope affects the air movement, to a certain extent. As the air collision and turbulence phenomenon at the steep slope is more frequent than that at the flat slope and the particles diffuse quickly with the airflow (Zhang 2019).

## CONCLUSION

The findings of this study concluded that forest especially coniferous forest can reduce $PM_{2.5}$ concentration as compared to the non-forest land. The reduction rate of $PM_{2.5}$ was maximum when the forest vegetation coverage was around 0.83. Overall, relative humidity, air pressure and water vapour pressure were positively correlated with $PM_{2.5}$ concentration, while forest vegetation coverage, biomass, air temperature, wind speed, altitude were negatively correlated. The findings of this study could help design the urban green space planning and air pollutioncontrol in the heavily populated urban ecosystems.

## ACKNOWLEDGEMENT

This research is support by Key Research and Development Project of Shan Dong Province (GG201809190147) and Starting Foundation of Beijing Technology and Business University (QNJJ2019-50).

## REFERENCES

Bai, Y.J., Zhu, Y.J., Ma, J.Y., Liu, Peng., Yang, R.Z., Li, C. and Cha, T.S. 2020. Seasonal variation of canopy conductance and environmental regulation of urban green space. J. Journal of Ecology, 39(01): 120-129.

Bao, J., Xu, J., Tang, J., Xie, G., Liu, H.T., Sun, L.C. and Yang, H.M. 2017. Study on the nucleation and growth characteristics of fine particles in flue gas promoted by water vapor phase transition. J. Engineering Science and Technology, 49 (05): 171-177.

Cameriere, R., Scendoni, R., Lin, Z., Milani, C., Palacio, L.A., Velandia, T.M. and Ferrante, L. 2019. Analysis of frontal sinuses for personal identification in a Chinese sample using a new code number. J. Journal of Forensic Sciences, 65(1): 46-51.

Deng, L.Q. 2012. Pollution characteristics of atmospheric particulates in Chengdu from August to September in 2009 and their relationship with meteorological conditions. J. China Environmental Science, 32(08): 1433-1438.

Feng, H.Y., Feng, Z.K. and Feng, H.X. 2018. A new method of $PM_{2.5}$ concentration inversion based on difference index. J. Spectroscopy and Spectral Analysis, 38(10): 3012-3016.

Feng, X.I. 2019. Spatio-Temporal distribution characteristics of $PM_{2.5}$ pollution and the influence of meteorological factors in Hefei City from 2014 to 2017. J. Anhui Journal of Preventive Medicine, 25(05): 335-338.

Feng, Z.K., Mao, H.Y. and Li, H. 2015. Spatial correlation between vegetation distribution and inhalable particulate matter in the capital circle. J. Journal of Agricultural Engineering, 31(1): 220-227.

Han, Y.N. and Wang, G.H. 2016. Chemical composition, hygroscopic properties and optical characteristics of water-soluble substances in $PM_{2.5}$ in rural areas of North China. J. Journal of Earth Environment, 7(1): 44-54.

Hou, Z.X. 2019. Correlation analysis of $PM_{2.5}$ and meteorological elements in Qingdao. J. Environmental Science and Management, 44(1): 93-97.

Li, J.J. 2011. Pollution characteristics of atmospheric particles in Guiyang city and the correlation analysis with the main meteorological factors. J. Journal of Southwest University (Natural Science Edition), 33(1): 91-95.

Liu, X.H.,Yu, X.X., Zhang, Z.M. and Liu, M.M. 2014. Ruan Qingcao. Characteristics of $PM_{10}$, $PM_{2.5}$ pollution in forest belt and its relationship with meteorological conditions. J. Journal of Ecology, 33(7): 1715-1721.

Liu, N.W. 2015. Relationship between atmosphere particle concentration and atmosphere variables in the Central Part of Liaoning, China. J. Journal of Desert Research, 35(6):1659-1665.

Liu, Q.W. 2015. Is forest haze treatment a miracle or a cure for disease. Interview with Yu Xinxiao, project leader of "Research on regulation function and technology of forest to $PM_{2.5}$ and other particulate matters". J. Green China, 22: 38-42.

Liu, Y.C., Wu, Z.J., Tan, T.Y., Wang, Y.J., Qin, Y.H., Zheng, J. and Li, M. 2016. Hu min. estimation of effective hygroscopic parameters and water content based on measured chemical components of $PM_{2.5}$: Theoretical model and case analysis. J. Chinese Science: Geoscience, 46(7): 976-985.

Long, I., Zhao, X.L.,Tan, H. and He, J.L. 2017. Research progress of airborne sensitized pollen and atmospheric particulate matter. J. Environmental Science and Technology, 40(12): 112-118.

Nowak, D. J. 2006. Institutionalizing urban forestry as "biotechnology" to improve environmental quality. J. Urban Forestry & Urban Greening, 5(2): 93-100.

Nowak, D. J., Crane, D.E. and Stevens, J.C. 2006. Air pollution removal by urban trees and shrubs in the United States. J. Urban Forestry & Urban Greening, 4(3): 115-123.

Su, C.L. 2015. Retrieval of aerosol optical depth using NPP VII R S data. J. Journal of Remote Sensing, 19(6): 977-982.

Wang, C.L., Zhang, J., Zheng, Y., Zhao, T.Q., Lou, Y.M. and Zheng, H. 2019. The characteristics of $PM_{10}$, $PM_{2.5}$ mass concentration change and its response to meteorological factors in Zhengzhou City. J. Environmental Protection Science, 45(6): 76-83.

Wang, K.H. and Ni, T. 2019. Analysis and Research on two heavy pollution processes in Shouxian, Anhui Province in winter 2016. J. Journal of Atmospheric Science, 42(6): 944-952.

Wang, Q. 2019a. Correlation analysis of air particle concentration and meteorological factors in Moso Bamboo Forest in autumn. J. Modern Agricultural Science and Technology. 19: 133-135.

Wang, Y.X., Zhang, Y.J., Meng, I.Y., Zhang, Y., Cao, S.H. and Zhao, J.W. 2020. Characteristics of air quality in heating period and its relationship with meteorological conditions in Shijiazhuang. J. Science and Technology and Engineering, 20(1): 381-387.

Wang, Z.B. 2019b. Spatio-temporal evolution patterns and influencing factors of $PM_{2.5}$ in Chinese urban agglomerations. J. Acta Geographica Sinica, 74(12): 2614-2630.

Yang, R.S. 2009. Discussion on pollution characteristics of $PM_{10}$ and the relationships between meteorological factors in the Western urban part of Guiyang City. J. Journal of Guizhou University (Natural Sciences), 26(2): 123-127.

Yu, X.X. 2019. Regulation of forest vegetation on $PM_{2.5}$ and other particulate matter. J. China Flower Horticulture, 19: 14-15.

Yu, Z., San, Li., Chuan, Zou., Xiao, J.M. and Guocai, Z. 2019. Analysis of $PM_{2.5}$ concentrations in Heilongjiang Province associated with forest cover and other factors. J. Journal of Forestry Research, 30(1): 269-276.

Zhang, B.B. 2019. A study of mutative factors to $PM_{2.5}$ in green spaces with different arrangements of plants in winter. J. Journal of Chinese Urban Forestry, 17(5): 25-30.

Zhang, G., Zheng, N., Zhang, J.S. and Meng, P. 2018. Characteristics of turbulent micrometeorology in canopy of artificial forest. J. Journal of Applied Ecology, 29(6): 1787-1796.

Zhang, J.Y. and Buren, S. 2020. Temporal and spatial distribution characteristics of aboveground biomass of vegetation in semi-arid grassland type watershed and its influencing factors. J. Journal of Ecology, 39(2): 364-375.

Zhang, K.L. 2019. Analysis of particle concentration and geographical, topographical and meteorological conditions in Zhangzhou City. J. Channel Science, 10: 43-47.

Zhang, K.L. 2019. Analysis of particle concentration and geographical, topographical and meteorological conditions in Zhangzhou City. J. Channel Science, 10: 43-47.

Zhao, J.K., Ji, D.Z., Wang, D., Li, S. and Yang, F.H. 2014. The effect of slope position and fertilization on spring maize yield in black soil area. J. Journal of Northeast Agricultural University, 45(5): 8-12.

Nature Environment and Pollution Technology
An International Quarterly Scientific Journal

p-ISSN: 0972-6268
(Print copies up to 2016)
e-ISSN: 2395-3454

Vol. 19 | No. 4 | pp. 1411-1421 | 2020

Original Research Paper

https://doi.org/10.46488/NEPT.2020.v19i04.007

Open Access Journal

# Analysis of Watershed Characteristics of Nalagarh Watershed, Himachal Pradesh for Optimization of Recharge Structures and Management of Groundwater

**Reena Ahuja* and Naval Kishore**†**
*Centre for Advanced Study (CAS), Department of Geology, Panjab University, Chandigarh, India
**Department of Geology, Panjab University, Chandigarh, India
†Corresponding author: Naval Kishore; naval@pu.ac.in

**Nat. Env. & Poll. Tech.**
**Website: www.neptjournal.com**

*Received:* 17-12-2019
*Revised:* 09-01-2020
*Accepted:* 01-02-2020

**Key Words:**
Geoinformatics
Morphometric analysis
Rainwater harvesting
Utilizable runoff
Watershed

## ABSTRACT

The study involves the study of Nalagarh watershed in Himachal as a topographically delineated hydro-geological entity which is allowing the entire surface runoff of its sub-watersheds to channelize through defined streams and drainage network to certain points in the watershed. Geomorphic analysis of Nalagarh watershed has enabled the study of qualitative and quantitative parameters of the watershed for efficient utilization and optimizing the management of its surface and groundwater resources. As Nalagarh valley has recently witnessed the highest industrial growth in the district and State of Himachal Pradesh, the study becomes all the more impertinent. The watershed has been delineated into 13 micro watersheds, based on the geomorphic analysis. To use the surplus monsoon runoff, a detailed study has been carried out for the computation of utilizable runoff and the number of structures that can be planned for its utilization. To effectively plan the rainwater harvesting structures, the morphometric analysis has been done.

## INTRODUCTION

Nalagarh valley (243 km) represents some of the southern-most expanses of Solan district belonging to the fast-industrial belt of Baddi, Barotiwala, and Nalagarh (BBN). The valley has been rated as the fastest industrial growth in the last decade owing to the special packages of incentives granted by the Central government which act as a catalyst in uplifting industrial development in the state, particularly in the BBN area (Herojeet et al. 2013). Especially, the Baddi area is a fast-developing industrial hub with polluting and non-polluting industries, along with the development of domestic and commercial infrastructures to support the industry. In the industrial complex, there are more than 10,000 industrial units out of which 2500 are the pharmaceutical and food processing units and 5000 small and big units; some of them are textile units. The water supply to the industrial complex and other allied infrastructure depends entirely on the development of groundwater resources (HPEC 2011). The deep tube wells are being constructed by all the industrial units to meet their water demand. The utilization of groundwater is very high in the area due to the large number of industrial units and the resident population engaged as workforce in these units (Ahlawat & Kumar 2009, Bhatti 2013, Biswas 1991, Herojeet et al. 2013). The objectives of the study are:

1. Nalagarh watershed of Solan district is likely to encounter the multiplicity of water problems in the future. To study the total model of the recharge potential, the present study entails a detailed study of existing geology, subsurface lithology and the computation of non-committed monsoon runoff.
2. To use the surplus monsoon runoff available in the watershed a detailed study has been done for the computation of utilizable runoff and the number of structures that can be planned for its utilization.
3. To effectively plan the rainwater harvesting structures the present study involved morphometric analysis of the watershed by calculating linear parameters such as number and order of streams, bifurcation ratio, stream length ratio, basin length and areal parameters such as drainage density, frequency ($km^2$), form factor, circulatory ratio, elongation ratio. In the computation of the number of water conservation/recharge structures, various thematic maps have been prepared through visual interpretation of satellite data.

## THE STUDY AREA

### Location

The Nalagarh watershed area (243 sq.km) falls under the Solan District of Himachal Pradesh, between 76°43'12" E

longitude and 31°3'00" N latitude and includes the industrial town of Baddi. Sirsa watercourse is the main watercourse that flows through the central part of the Nalagarh valley. Large-and small-scale industrial development along with urbanization has taken place randomly all over the Sirsa river catchment area in the last two decades. This results in the high industrial as well as domestic load in the Sirsa watershed. Hence, it is necessary to determine the Sirsa river quality for irrigation purposes. Nalagarh valley forms a south-eastern slim prolongation of a great outermost Himalayan intermountain valley space. It lies between northern latitudes of 30°52' to 31°04' and eastern longitudes of 76°40' to 76°55'. The valley has a common border with Haryana towards south-east, i.e. Kalka-Pinjor area and with Punjab towards the south-west, i.e. Ropar district. Sirsa river is a perennial river which flows south-westerly in the area and joins Sutlej 10 kilometres upstream of Ropar (Fig. 1). There are various perennial and impermanent streams rising from the NE flank passing through the industrial belt usually loaded with industrial and sewage discharges and transverse flow across the valley, to join the Sirsa River (CGWB 2009). The vital streams among them are Chikni River, Phula River, Ratta River, Balad River and Surajpur Choe. The discharge in the streams fluctuates depending on the climatic conditions. During the monsoon, the streams are flooded and carry an extensive amount of sediment and deposited it in the flood plain of the valley.

## Regional Geology and Drainage

Nalagarh valley is mainly drained by the Sirsa River which enters the Himachal Pradesh in Solan district near Baddi and flows down to the Sutlej river in Punjab. The main tributaries of the Sirsa River in the study area are the Balad River and Ratta River along with minor tributaries. Sirsa River is a perennial river which flows north-westerly in the study area and joins Sutluj river, a few km upstream of Ropar. The study area is crisscrossed by many small to large khads, which join the Sirsa river at various places. The catchment area of the Balad River is 113.22 sq. km, Ratta River 30 sq. km and catchment area of Sirsa River 31.11 sq. km (Fig. 2) in the study area.

The study area of Baddi Industrial Complex lies between the Ratta River, Balad River and Sirsa River. Both the Ratta River and Balad River are tributaries of the Sirsa River. Sirsa River forms the western boundary of the study area and runs from south-east to northwest direction. Ratta River forms the northern boundary of the project area and runs from east to west direction. It meets Sirsa River in the northwestern part of the area. Balad River flows from northeast to southwest direction and forms the eastern boundary of the project. These Rivers were formed in the last phase of the upheaval of the Himalayas. All the tributaries khads of the Sirsa river flow from north-eastern directions and are almost parallel to each other. The tributaries show parallel to sub-parallel drainage pattern. The drainage developed in the area displays a dendritic pattern and conspicuously shows bad topography on the road section. A few southwest to northeast flowing seasonal nalas (small channels) of small magnitude from the outer Siwalik range of south-west flank also meets the main rivers in the valley areas. The valley-fill deposits have been deposited in sets of terraces by the Sirsa River. These deposits have been dissected to low lying plains and flood plains by various tributaries, nalas of the Sirsa river. The master slope of the study area is towards the northwest direction. However, the ground slope in the south-eastern part is from the flanks towards the Sirsa river. The Nalagarh valley has been carved

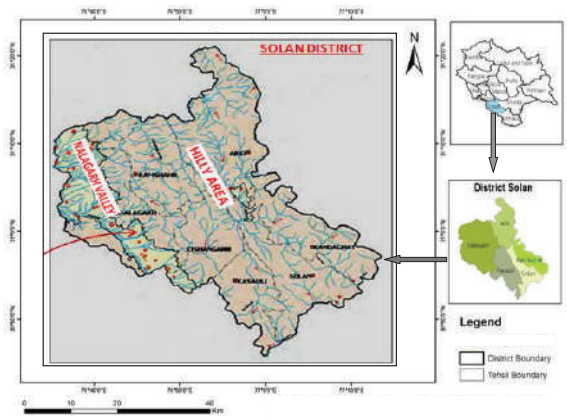


Fig. 1: Location map of the Nalagarh basin (arrow pointing towards Nalagarh watershed).

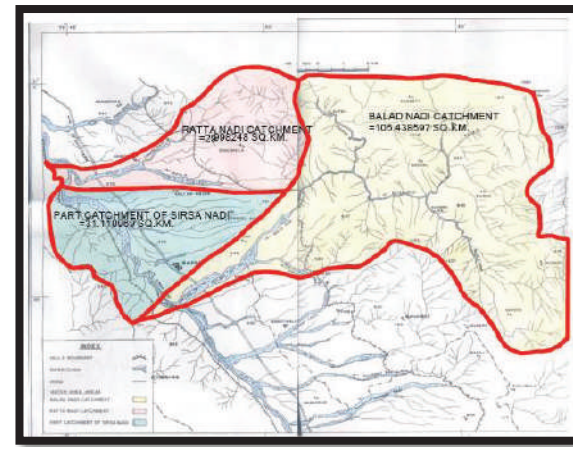


Fig. 2: Catchment area of Ratta River, Balad River and Sirsa River District Solan (H.P).

out in the Siwalik terrain of outer Himalayas and forms a part of the Sutlej Sub-Basin of Indus Basin. The valley is aligned in the northwest-southeast direction in conformity with the trend of main Himalayas in this part. The geology of the area is complex due to the neo-tectonic activity it has undergone. In terms of absolute relief, there is a sudden drop from the north-eastern to south-western into the dun. Relief of the dun ranges between 450 and 600 m, however, there are large variations between the different areas, related to local and regional tectonic conditions and unequal deposition and erosion. The regional variation in the absolute relief is correlated with the regional tectonic frame while in the local areas, variation in the deposition has been important. As a result of en echelon, faulting and tilting of the faulted block, the absolute relief within the dun is higher in the north-east and the south-east than in the north-west and south-west. In this dun, a large number of lower orders, geologically young tributaries fairly entrenched on the alluvial fans, have further broken the topography and produced a more complicated pattern of variations of local relief as the lithology of the area comprises valley-fill deposits of river terraces of immense thickness. These are horizontally bedded/stratified clay beds with lenses of fine sand and gravel. The geological sequence exposed in the area is given in Table 1. The geological map of Solan district is given in Fig. 3. The valley deposits are mainly fluvio-lacustrine in their characteristic. The deposits along the cutting of the nalas show thick clays with beds of boulders, gravels, sands and clay in the valley area. The sediments are more clayey and with lenses of fine sand along the Nalagarh section, which indicates that the sediments have been deposited under fluvio-lacustrine environment and more of the sediments are fine-grained and have been contributed by the River Satluj. The deposits again change to alternate beds of clay and boulders, cobbles, pebbles, gravels, sand and clayey towards the upstream sides of the nalas. The valley-fill deposits are coarser comprising of boulders, cobbles and pebbles, etc. towards the peripheral zone of the valley and from the recharge zone. The braided pattern of drainage in these zones also indicates recharge zones of the valley. The sediments continue to become finer until they blend into clay deposits. The horizontal layering of clay deposits also indicates that the deposits are lacustrine. The upper part of the Pinjore-Nalagarh dun along the foot of Himalaya is characterized by alluvial fans and colluvial deposits crisscrossed by a large number of small and large streams or choes. On the other hand, the south-western (lower) parts of dun are characterized by terraces that are open, wide and co-extensive with alluvial fans above. The growth of kankar was observed in the clay horizons due to the leaching of sub-surface water in the zone of aeration. The top of the terrace is covered with materials of cobble grade clays of fine grade.

The study area is of rectangular and runs parallel to the main strike direction of Siwalik formations. The area is carved between two semi-parallel hill ranges of Siwalik

Table 1: Geological sequence of the study area.

| Formation | Lithology | Age |
|---|---|---|
| Holocene deposits | River alluvium and the sediments along the present course | Recent |
| Pre Holocene deposit (River terraces) | Boulders, cobbles, pebbles with layers/lenses of sand/clay | Upper Pleistocene |
| Upper Siwalik (Boulder conglomerate) | Boulders, pebbles with sandstone and clay | Lower Pleistocene |

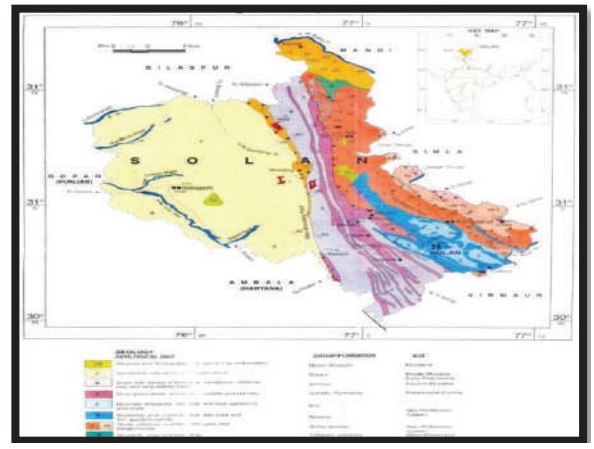


Fig. 3: Geology map of Solan.

formation in the southwestern side and the Kasauli formation on the north-eastern side. Most of the peaks of the ridge along the northeast flanks of the study area attain height more than 1000 m above mean sea level (MSL) and the Kasauli Dhar has the highest peak of 1926 m above mean sea level. The area under study has a higher elevation in the northwest and southeast direction. The topographic contour in the study area is given in Fig. 4. The slope of the area is from the northeast to southwest direction (CGWB 2007).

## Climate

The area has a humid to the semi-arid type of climate and experiences three distinct seasons. The monsoon starts towards the end of June and continues till the middle of September. During October and November, the climate is generally pleasant with very scanty precipitation. The winter lasts from December to February. The minimum day temperature is usually around 5ºC. A moderate amount of winter rains are received during this period. The spring months of March and April are generally summer months which are quite hot days and oppressive. At Chandigarh (the observatory closest to Nalagarh) the temperature ranges between 30.4ºC and 16.5ºC. The maximum daily temperature of 38.6ºC is observed in June and the minimum of 6.1ºC in January.

## Rainfall

The different parts of the area do not show any uniformity in the amount of rainfall throughout the year. The study area receives an annual average of 1100 mm rainfall which goes up to 1400 mm in the catchment of Balad River. The area thus receives about 1.32 million cu.m of rainfall which can be harnessed for recharging the aquifers. In order to have the increased sustainability of the aquifers to ensure the availability of groundwater to meet the demand for a longer period, the present project is of great significance. The five years (1999-2003) rainfall of the Nalagarh area under which the project area falls is given in Table 2. Due to high porosity and permeability, rainfall is generally absorbed in the soil as the soils are silty sand. Further, the study of data of the last twenty years has shown maximum rainfall recorded in 1988 as 1641 mm, and minimum rainfall recorded as 862 mm in 2006. While, the major share of precipitation, received in the district, i.e. around 70% is received from July to September.

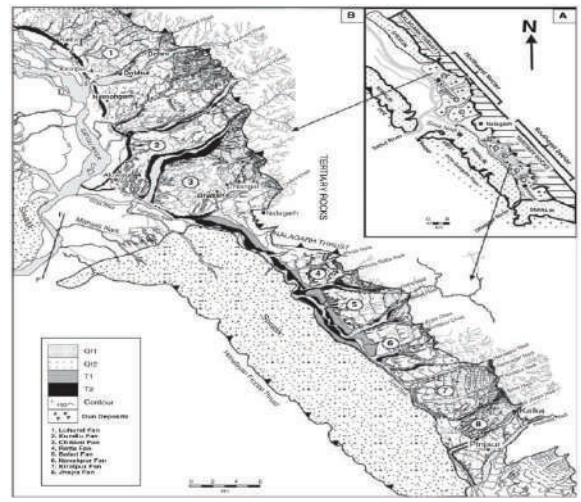


Fig. 4: Geological map of the study area, District Solan (Raivemann 2002).

Table 2: Rainfall (in mm) for the District Solan.

| Year | Rainfall in (mm) |
|---|---|
| 1999 | 1182.9 |
| 2000 | 937.4 |
| 2001 | 856.5 |
| 2002 | 908.9 |
| 2003 | 856.7 |

Table 3: Dynamic groundwater resources (Nalagarh valley) in MCM (CGWB 2007).

| | |
|---|---|
| Annual Replenishable Groundwater Resources | 77.07 |
| Net Annual Groundwater Draft | 10.25 |
| Projected Demand for Domestic and industrial Uses up to 2025 | 6.84 |
| Stage of Groundwater Development | 15% |

## Hydrogeology

In the valley area of Nalagarh, the groundwater occurs in porous consolidated alluvial formation (valley fills) comprising, sand, silt, gravel, cobbles/pebbles, etc. Groundwater occurs each underneath phreatic and confined conditions. Wells and tube wells are the primary groundwater abstraction structures. Groundwater is being developed in the area by medium to deep tube wells, dug wells, dug cum bored wells. Depth of open dug wells and dug-cum-bored well in the area ranges from 4.00 to 60.00 m bgl (below ground level) wherein depth to water level varies from near ground surface to more than 35 m bgl. The yield of the shallow aquifer is moderate having well discharges up to 10 lps.

In the Nalagarh valley area, there are 12-hydrograph network stations where depth to water level is monitored four times a year and groundwater quality once during pre-monsoon period. The depth to the water table shows a wide variation. During the pre-monsoon period (May 2006), it ranged between 3.02 and 38.2 m bgl, while during the post-monsoon period (Nov 2006) depth to water level ranged from 3.3 to 36.86 m bgl. Deeper water levels are observed mainly in the northwestern part and along the foothills. In major parts of the valley, the depth to water level is less than 15.00 m bgl. The fast pace of groundwater development (Table 3) is observed in recent years in valley areas and this has resulted in declining water levels. In the major part of the valley water level falls ranging from 0.05 to 6.20 metres has been observed in the past decade. There is thus a need to initiate water conservation and artificial recharge measures in such areas. In alluvial areas of Nalagarh valley, though there is scope for groundwater development as the stage of groundwater development is only 15% (HPEC 2011), however, there is a need to adopt a cautious and phased manner groundwater development approach because of depleting water levels in some parts. This decline can be ascribed to the fast pace of development in recent years, both in the agriculture sector and industrial sector. Fig. 5 shows the location of the wells of the Baddi block.

The water supply to the industrial complex and other allied infrastructure depends entirely on the development of groundwater resources. The deep tube wells are being constructed by all the industrial units to meet their water demand without consideration of the sustainability of aquifers. The water table is declining fast and about 11 m decline has been observed in the last 10 years (Fig. 6).

## Depth to Water Level

To study the variation in water levels, pre-monsoon water levels of the existing 56 groundwater structures were monitored. These include 27 tube wells, 26 dug wells, 2 artificial recharge wells and 1 hand pump. The depth to water level is deep in the vicinity of hills and it is shallow in the low-lying places and terraces. Based on the water levels recorded in the tube wells, the depth to water level map has been prepared (Fig. 6).

It is seen from the map that water levels in the area vary between 86 m (Well No. 8) to 2.5 m (Well No 44). Water levels are deep in the northeastern part and decrease towards the southwestern part of the area.

## Water Table Configuration

Based on the water level data, the water table elevation map has been prepared. The direction of groundwater flow, in general, is from east to west direction (Fig. 7). However, it is observed that from the central part of Balad River near village Koti, the flow directions are towards the Ratta River in the north of the area and towards Sirsa River in the west direction. The water table elevation varies from 448 m above msl in the east and 360 m above msl in the northwest direction.

## Allocation of Groundwater Resources for Future Utilization

The net annual groundwater availability is to be proportioned among domestic, industrial and irrigation uses. Among these, as per the National Water Policy 2002, the requirement for domestic water supply is to be accorded priority. The requirement for domestic and industrial water supply is to be kept based on the population as projected to the year 2025. The water available for irrigation use is obtained by deducting the allocation for domestic and industrial use, from the net annual groundwater availability.

## Recharge from Monsoon Rainfall

Recharge from rainfall has been computed by using two methods, water level fluctuation method, and rainfall infiltration factor method. Recharge computation through the water level fluctuation method has been done using the following relation:

$$R^{wtf} = h \times Sy \times A + D_G - Rgw \quad \ldots(1)$$

Where, $R^{wtf}$ = possible recharge by water table fluctuation method, h = the rise in water level in monsoon season, A = area of computation of recharge, Sy = specific yield, $D_G$= gross groundwater draft, Rgw = recharge from groundwater irrigation during monsoon season. The specific yield value in the case of valley-fill deposits which includes boulders, cobbles, gravels, sand, etc. has been taken as 0.16.

Rainfall recharge computed by this method has been normalized on the normal monsoon rainfall using the procedure

recommended by GEC-97 (CGWB 2009) using the relation:

$$R_{rf}\,(\text{Normal wtfm}) = NMR \times R^{wtf}/AMR \quad \ldots(2)$$

Where, $R_{rf}$ (Normal wtfm) = Normalized rainfall recharge

NMR = Normal monsoon rainfall

$R^{wtf}$ = Computed rainfall recharge

AMR = Actual monsoon rainfall in the year of assessment

As there is no draft data available for the last preceding years, hence recharge is normalized for the assessment year (2008-2009). Recharge computation by rainfall infiltration factor method during monsoon is given below:

Rainfall recharge during the monsoon period has been computed using normal monsoon rainfall (data obtained from Commissioner, Revenue Department, Govt. of H.P). The rainfall infiltration factor for valley fill has been taken as 0.22 as recommended by GEC 97 (CGWB 2009).

The equation used for computation of recharge is:

$$R_{rf}\,(\text{Normal rifm}) = NMR \times A \times RIF \quad \ldots(3)$$

Where, $R_{rf}$ (Normal rifm) = recharge from rainfall by rainfall infiltration factor method, NMR = normal monsoon rainfall, A = Area of the valley in hectare, RIF = rainfall infiltration factor

**Per Cent Deviation:** The results from the above two methods (water fluctuation and rainfall infiltration method) have been compared using per cent deviation using the following relation:

$$P.D = 100 \times \{R_{rf}\,(\text{Normal wtfm}) - R_{rf}\,(\text{Normal rifm})\}/R_{rf}\,(\text{Normal rifm}) \quad \ldots(4)$$

Where, P. D. = Percent deviation, $R_{rf}$ (Normal wtfm) = Recharge from (Normalized as computed water table fluctuation method), $R_{rf}$ (Normal rifm) = Recharge from rainfall as computed by Rainfall infiltration factor method.

After computation of the per cent deviation, the following criteria as recommended by the methodology (GEC '97) has been to compare the recharge from rainfall:

i. if $-20 \leq P.D. \leq +20$ then $R_{rf}$ (Normal) = $R_{rf}$ (Normal wtfm)

ii. if $P.D. < -20$ then $R_{rf}$ (Normal) = $0.8 \times R_{rf}$ (Normal rifm)

iii. if $P.D. > 20$ then $R_{rf}$ (Normal) = $1.2 \times R_{rf}$ (Normal rifm)

### Total Annual Recharge

The total annual recharge resource was computed as the arithmetic sum of recharge from the monsoon, non-monsoon rainfall and recharge from other sources during monsoon and non-monsoon season. Provision for natural discharges has been kept as 10%, as per GEC '97 methodology.

### Total Groundwater Resources of Nalagarh Valley

Net annual groundwater availability has been computed by deducting the unaccounted natural discharge taken as 10 % of the total annual recharge values calculated by rainfall infiltration factor method as per the criteria recommended by GEC-97 for recharge values calculated based on rainfall infiltration method. The stage of groundwater development has been computed using the relation:

$$\text{Stage of groundwater Development} = 100 \times \text{Gross groundwater draft for all uses } (D_G) \quad \ldots(5)$$

The stage of groundwater development of Nalagarh valley in Solan district is 50.85 % and falls under 'Safe' category.

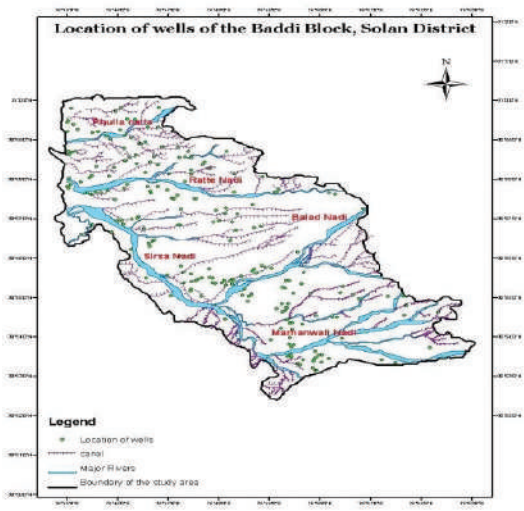


Fig. 5: Map of locations of wells of Baddi Block.

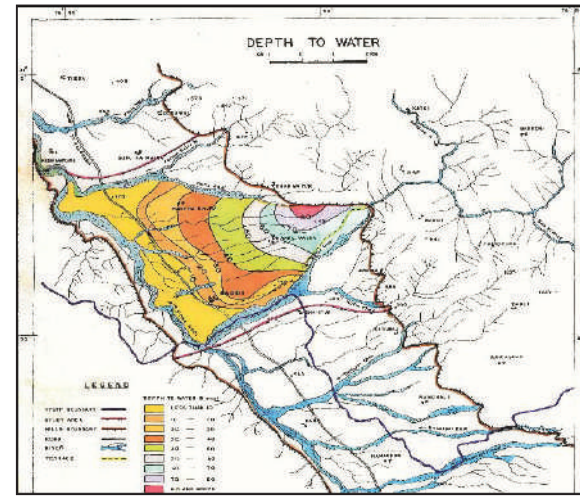


Fig. 6: Depth to water level map of the area.

Net groundwater availability for future use has been computed using the relation:

$$R = A-(B+C) \quad \ldots(6)$$

Where, R = Net annual groundwater available for future irrigation use

A = Net available groundwater resource
B = Gross groundwater draft for domestic and irrigation
C = Allocation for domestic and industrial water supply

## IN-STORAGE GROUNDWATER RESOURCES

The Baddi industrial complex is part of Nalagarh, which covers the area of 23849 ha. Central and State govt. agencies have carried out drilling in Nalagarh valley down to a depth of about 160 meters.

From the lithological logs of various tube wells, it has been observed that the aquifer consisting of sand, pebbles, gravel, boulder constitute about 27% and clay bed constitute 73% of the total aquifer system. The thickness of various granular zones ranges from 2 m to 6 m, whereas for the clay beds range from 2 m to 20 m. The average depth to the water level in the valley is about 20 m. An average specific yield of 16% has been considered uniformly for the study area.

### Methodology for Estimation of In-storage Groundwater Resource

The static groundwater resource of the area has been estimated based on the similar approach as adopted for the estimation of dynamic groundwater resources. The thickness of aquifer material below the zone of fluctuation and specific yield has been used to estimate the resources. The details of the methodology and formulae are given as under:

$$IR = A \times H \times SY \quad \ldots(7)$$

Where, IR = In-storage resources in ham

A = Area of the valley in ha

H = Thickness of aquifer sediments below the zone of fluctuation up to explored depth (explore depth - pre-monsoon water level in m)

SY = Specific yield of the aquifer in fraction

The salient features of the in-storage groundwater resource assessment are given in Table 4. The thickness of aquifer sediment has been estimated based on the study of the litholog of the area and only the aquifer part has been considered for estimation of resources. The total in-storage groundwater resources of Nalagarh valley are 158167 ham.

## MORPHOMETRIC ANALYSIS

The analysis of drainage morphometry is normally essential for the assessment of hydrological qualities of the surface water basin. The Sirsa watershed has been analysed through detailed morphometric analysis (Chadha & Neupane 2011, Eesterbrooks 1969). In this region, a large number of drainage systems originate from the Sirsa River. Following geomorphologic procedures, the catchment area of Sirsa watershed and the surrounding basins was delineated by direct tracing of the drainage tributaries from topographic maps (scale 1:50000). Drainage system boundaries were identified. This was accompanied by a systematic digitizing of the traced tributaries and basin systems in the Geographic Information System (GIS) by using Arc-GIS 10 software. Along these lines, a drainage system map was produced including three significant catchment areas in the region. Topographic maps in combination with remotely sensed data and Landsat images were used to delineate the existing drainage system, thus identifying precisely water divides. This was achieved using Geographic Information System (GIS) to provide computerized data that can be manipulated for different calculations and hydrological measures.

The obtained morphometric analysis can help in determining: 1) stream behaviour, 2) morphometric setting of streams within the drainage system and 3) interrelation between connected streams. The study used an imperial approach of morphometric analysis that can be used in assessments of rainwater harvesting structures (Way 1978). The current study was accomplished using several approaches for drainage system analysis. The study aimed to analyse the major morphometric elements of Baddi watershed in Nalagarh district. It treated the characterization of streams' behaviour (e.g. meandering, frequency, etc), their setting with regard to the catchment and their relation to each other (e.g. patterns, junctions, etc). This provided valuable information that can be used in different water assessments and selecting sites for water harvesting. Additionally, the morphometric analysis can be applied to similar drainage systems in the larger watersheds of Himachal Pradesh.

## MATERIALS AND METHODS

Morphometric analysis of a drainage system needs a delineation of all existing streams and reaches. Of the several methods of drainage system delineation, two procedures have been followed in the present study. These are the manual and automated system delineation. The manual sampling of the drainage network has been adopted from topographic maps, Survey of India open series map No. H43K13 of a scale of 1:50000 in combination with computerized tools, and Geographic Information System (GIS). The digital analysis has been carried out for Landsat Imagery using GIS software Arc GIS 10 and ERDAS Imagine Software and the Geo-informatics based multi-criteria evaluation has been done using

Weighted Overlays and AHP methods. For the unconnected drainage systems, satellite images were analysed using ERDAS Imagine software. These images can give information on the surface features, and able to detect buried stream networks. This can be achieved by applying thermal bands with 90m spatial resolution (i.e., capability to differentiate objects on the satellite image) in these images. The applied method in stream delineation was done digitally in GIS (Arc View software) system. Various digital applications were undertaken, including band combination, colour slicing, filtering and related measuring tools. Hence, all tributaries of different extents and patterns were digitized.

## RESULTS, DATA ANALYSIS AND DISCUSSION

**Drainage patterns:** The arrangement of streams in a drainage system constitutes the drainage pattern, which in turn

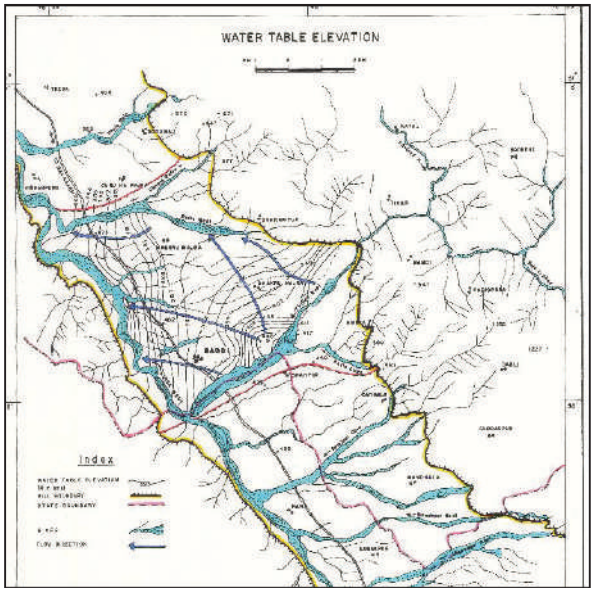


Fig. 7: Water table elevation map.

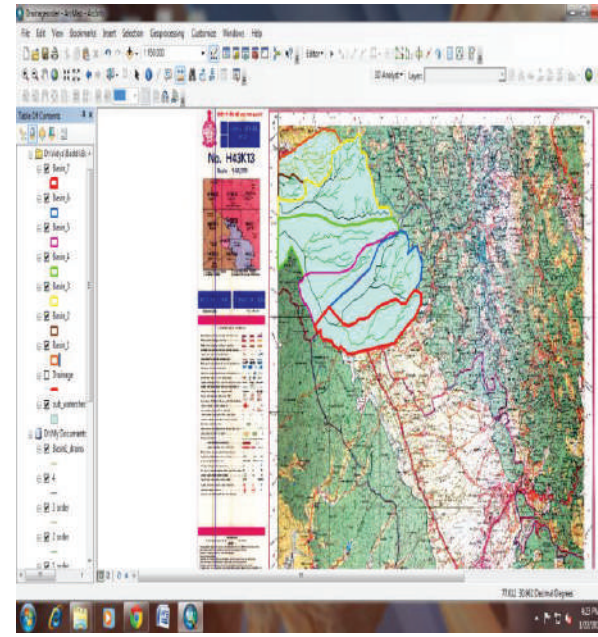


Fig. 8: Snapshot of the Arc view showing the division of the sub-watersheds of the Nalagarh watershed.

Table 4: Salient features of groundwater resource estimation for Nalagarh valley.

| | |
|---|---|
| Recharge from rainfall during monsoon | 6283.55 ham |
| Recharge from other sources during monsoon | 168.43 ham |
| Recharge from rainfall during non-monsoon | 1825.88 ham |
| Recharge from other sources during non-monsoon | 336.85 ham |
| Annual groundwater recharge | 861471 ham |
| Provision for natural discharge | 861.47 ham |
| Net groundwater availability | 7753.24 ham |
| | |
| Existing groundwater draft for irrigation | 2021.11 ham |
| Existing groundwater draft for domestic and industrial water supply | 1921.26 ham |
| Existing groundwater draft for all uses | 3942.37 ham |
| Provision for domestic and industrial supply to 2025 | 1921.26 ham |
| Net groundwater availability for future irrigation development | 3810.87 ham |
| Stage of groundwater development | 50.85 |
| Category | Safe |
| Total in-storage groundwater resources of Nalagarh valley | 158167 ham. |

Table 5: Linear and aerial parameters of Nalagarh watershed.

| Micro Watershed No. | Area | No. of streams | Bifurcation Ratio (Avg) Nu/Nu+1) | Drainage Density | Frequency | Form Factor | Elongation Ratio | Basin Length in km |
|---|---|---|---|---|---|---|---|---|
| 1 | 60 | 85 | 8 | 1.41666 | 2.666 | 0.32 | 0.032 | 15 |
| 2 | 124 | 628 | 6 | 5.6 | 1.625 | 0.04 | 0.1412 | 89 |
| 3 | 147 | 980 | 2.16 | 6.6 | 13.51 | 0.09 | 0.11 | 124 |
| 4 | 76 | 693 | 7.2 | 9.11 | 1.0524 | 0.04 | 0.03 | 42 |
| 5 | 77 | 452 | 3.12 | 7.5 | 5.8 | 0.04 | 0.22 | 42 |
| 6 | 80 | 147 | 2.83 | 5.03 | 1.83 | 0.03 | 1.01 | 50 |
| 7 | 110 | 397 | 3.21 | 2.6 | 3.6 | 0.014 | 0.13 | 87 |
| 8 | 41 | 571 | 3.15 | 1.8 | 14.2 | 14.2 | 1.65 | 19 |
| 9 | 42 | 450 | 2.95 | 3.2 | 10.14 | 0.0711 | 1.4 | 24 |
| 10 | 24 | 356 | 3.9 | 2.1666 | 14.1 | 0.074 | 1.3 | 18 |
| 11 | 23 | 294 | 5.3 | 4.325 | 2.78 | 0.0707 | 1.27 | 18 |
| 12 | 41 | 287 | 3.282 | 2.3 | 7.1 | 0.08 | 1.108 | 22 |
| 13 | 19 | 168 | 2.179 | 2.55 | 8.8 | 0.1319 | 1.1 | 12 |

reflects mainly structural/or lithologic controls of the underlying rocks (Herojeet et al. 2013). The area of study holds within a miscellany of drainage patterns; however, dendritic drainage pattern is the most dominant type and occupies more than 95% of the area. Although having a difference in stream lengths and angle of connection, yet they are, in general, characterized by a treelike branching system, which is a dendritic drainage pattern that indicates homogenous and uniform soil and rocks (Way 1978, Saud 2009, Sharma et al. 2010). All the parameters calculated for the watershed are given in Table 5, Table 6, Table 7 and Table 8 and a snapshot of Arc view analysis is given in Fig. 8.

**Drainage density (D):** Drainage density is a measure of the length of the stream channel per unit area of the drainage basin. Mathematically, it is expressed as $D = \sum L$ (total length of all stream)/A (area of the basin). In this study, the drainage density map was obtained using the digital data from the obtained drainage map. This was accomplished using the GIS system (Arc View software), which is capable of measuring the actual stream lengths and numbers. Therefore, the drainage system was classified into frames of fixed area (5 km × 5 km). This classification relies on the visual density of streams in the area. Hence, the overall length of streams in each frame (25 $km^2$) was measured using Arc View software.

**Drainage frequency (F):** A similar mathematical relation to that applied in drainage density and stream frequency was also done by counting the number of streams in a specified area. Taking into consideration, this morphometric relation, several workers used stream frequency rather than drainage density (length density). Therefore, some hydrologic studies consider the density of drainage (Sharma et al. 2010), while others deal with drainage frequency. Stream frequency is expressed by the equation: F = N (number of streams)/A (area of the basin).

**Meandering ratio (Mr):** It is calculated to indicate the ratio between straight to curved lengths of the primary (major) stream within the drainage system. It shows how the real stream length is larger than the straight one, which is indicative of stage maturity (Chadha & Neupane 2011, Eesterbrooks 1969).

## CONCLUSIONS

- This industrial area of Nalagarh is highly prone and vulnerable to surface and groundwater pollution, thus water quality monitoring in a close network is essential.
- Proper waste/effluent disposal measures are required to be adopted by all the industrial units established in the watershed and state authorities need to monitor it vigilantly.
- There is a need to protect, rejuvenate and rehabilitate traditional water harvesting structures like ponds and tanks to use these for rainwater harvesting and recharging shallow aquifers through the rainwater runoff collected through the drainage network in the watershed. It is estimated that it is possible to construct 22500 point recharge structures, 1500 storage/percolation tanks and about 10500 check dams, in order to effectively capture the runoff to be recharged.
- In hilly and mountainous terrain, traditional groundwater

Table 6: Water available for recharge in Baddi of Nalagarh watershed for all micro-watersheds.

| S. No. | Name of the class | Area covered (in hectares) | Area covered in square meters | Runoff Coefficient | Average annual rainfall in mm | Intensity of rainfall in meters | Runoff potential (C*I*A) in $m^3$ | MCM |
|---|---|---|---|---|---|---|---|---|
| 1 | Natural vegetation | 16442.00 | 164420004.3 | 0.1 | 851 | 0.851 | 13992142 | 13.99214 |
| 2 | Agriculture | 36868.24 | 368682398.8 | 0.4 | 851 | 0.851 | 125499489 | 125.4995 |
| 3 | Open area | 18331.24 | 183312405.3 | 0.16 | 851 | 0.851 | 24959817 | 24.95982 |
| 4 | Dry river bed | 2291.41 | 22914050.66 | | 851 | 0.851 | 0 | 0 |
| 5 | Water body | 5564.84 | 55648408.75 | | 851 | 0.851 | 0 | 0 |
| 6 | Settlement | 6902.28 | 69022732.19 | 0.5 | 851 | 0.851 | 29369173 | 29.36917 |
| | | | | | | Water available for recharge = | 193820621 | 193.8206 |

Table 7: Different recharge structures for the Nalagarh watershed.

| Utilizable runoff (MCM) | Sub-surface barriers | Percolation tanks | Check dam | Point recharge structure |
|---|---|---|---|---|
| 193.8206 | 640 | 1500 | 10500 | 22500 |

Table 8: Unit recharge/structure/annum

| Conservation structure | Unit recharge/structure/annum |
|---|---|
| Sub-surface | 0.3 |
| Percolation tank | 0.2 |
| Check dam | 0.03 |
| Point recharge structure | 0.02 |

sources, viz. springs, bowries, etc. need to be developed and protected for better health and hygiene with proper scientific intervention.

- Springs need to be inventoried and studied for optimum utilization of their discharge either by fracturing, horizontal drilling, or by constructing galleries, etc.
- Rooftop rainwater harvesting practices can be adopted in hilly areas and urban areas since the district receives a fair amount of rainfall. Construction of rooftop rainwater harvesting structures should be made mandatory in all new infrastructural, construction projects and rainwater harvesting in rural areas should be promoted.
- Traditional water storage systems are required to be revived.
- People's participation is a must for any type of developmental activities. Proper awareness for utilization and conservation of water resources is needed.

## REFERENCES

Ahlawat, K. and Kumar, A. 2009. Analysis of industrial effluents and its comparison with other effluents from residential and commercial areas in Solan H.P. International Journal of Theoretical and Applied Sciences, 1(2): 42-46

Al Saud, M. 2009. Morphometric analysis of Wadi Aurnah Drainage System, Western Arabian Peninsula, Open Hydrology Journal, 3, 1-10, Space Research Institute of Kingdom of Saudi Arabiathe, 2009.

APHA 1998. Standard Methods for the Examination of Water and Wastewater, 19th Ed., American Public Health Association, Washington DC, USA.

Bhatti, R. and CGWB 2013. Report on groundwater pollution of industrial area of Baddi District Solan (H.P). Northern Himalayan Region, Dharamshala, Ministry of Water Resources (GOI), pp 66, 73-87.

Biswas, A.K. 1991. Water For Sustainable Development in the 21st Century. 7th World Congress in Water Resources, Rabat, Morrocco, pp. 13-18.

Central Groundwater Board, Ministry of Water Resources, Government of India 2009. Reprint of original report 1998, Detailed Guidelines for Implementing the Groundwater Estimation Methodology.

CGWB 1998. Report on Groundwater Management Study in Solan District, Himachal Pradesh, Northern Himalayan Region, Dharamshala, pp. 1-71.

CGWB, Ministry of Water Resources (GOI) 2007. Groundwater Information Booklet, Solan District, Himachal Pradesh, Northern Himalayan Region, Dharmsala.

Chadha, D.K. and Neupane, B.R. 2011. Significance of geomorphic analysis of watershed for optimization of recharge structures. UNESCO and Global Hydrogeological Solutions, pp. 8-13.

Eesterbrooks, D. 1969. Principles of Geomorphology. McGraw-Hill Inc., NY.

Herojeet, R.K., Rishi, M.S. and Sidhu, N. 2013. Hydrochemical characterization, classification and evaluation of groundwater regime in Sirsa Watershed, Nalagarh Valley, Himachal Pradesh, India. Civil Environ Res, 3(7): 47-57.

Raiverman, V. 2002. Foreland sedimentation in Himalayan Tectonic Regime: A Re-look at the Orogenic Process. Bishen Singh Mahendra Pal Singh, Dehradun, 378 p.

Sharma, S.K., Rajput, G.S., Tignath, S. and Pandey, R.P. 2010. Morphometric analysis and prioritization of a watershed using GIS. Journal of Indian Water Resources Society, 30(2):33-39.

The High-Powered Expert Committee (HPEC), 2011. For Estimating the Investment Requirements for Urban Infrastructure Services, March 2011. Report on Indian Urban Infrastructure and Services.

Way, D. 1978. Terrain Analysis. NY: Mc-Graw-Hill Inc 1978.

Nature Environment and Pollution Technology
An International Quarterly Scientific Journal

p-ISSN: 0972-6268
(Print copies up to 2016)
e-ISSN: 2395-3454

Vol. 19 | No. 4 | pp. 1423-133 | 2020

Original Research Paper

https://doi.org/10.46488/NEPT.2020.v19i04.008

Open Access Journal

# Groundwater Modelling Using Visual Modflow in Tirupur Region, Tamilnadu, India

**K. Arumugam*†, T. Karthika*, K. Elangovan**, R.K. Sangeetha* and S. Vikashini*****

*Department of Civil Engineering, Kongu Engineering College, Perundurai-638 060, India
**Department of Civil Engineering, PSG College of Technology, Coimbatore-641 004, India
***Department of Pharmacy Practice, Nandha College of Pharmacy, Erode-638 052, India
†Corresponding author: K. Arumugam; sixface@kongu.ac.in

**Nat. Env. & Poll. Tech.**
**Website: www.neptjournal.com**

*Received:* 04-02-2020
*Revised:* 26-02-2020
*Accepted:* 05-03-2020

**Key Words:**
Aquifer
Groundwater modelling
Modflow
Hydrology

## ABSTRACT

Most of the textile and dying process industries in Tirupur region do not have proper wastewater treatment plants and they discharge the effluents in unlined channels and streams. Due to the issue, the groundwater in Tirupur is highly polluted. For analysing groundwater condition, groundwater modelling is used. For groundwater hydrologist, groundwater models are a vital tool. Nowadays, a lot of computer programs have been used for modelling groundwater. Visual MODFLOW software uses a finite difference method for solving the complexity. They can be used for simulating the behaviour of composite aquifers as well as the effects of irregular boundaries and different processes such as solute transport and groundwater flow. This paper evaluates the impact of industrial effluent in groundwater value in Tirupur region by five different scenarios.

## INTRODUCTION

Groundwater replication is an important assignment in groundwater managing system. Precise simulations of groundwater give information required for managing groundwater resources. A groundwater simulation model, like the modular 3-dimensional model of groundwater flow (MODFLOW) was developed by the United States Geological Survey (Michael et al. 1988). Groundwater modelling is a diplomat scale model of a groundwater aquifer condition which is useful for predicting the effects of hydrological changes such as abstraction of groundwater for irrigation, and industrial development on the performance of the local aquifer (Kujur & Akhtar 2014). Visual MODFLOW is one of the most accepted modelling programs for groundwater in subsistence due to well structure programs, applicable to groundwater modelling and applicable for modifications (Zheng 1990). Simulation of groundwater is an important task in groundwater managing. The parameter of hydraulic conductivity is strongly influencing the simulation of groundwater (Tung et al. 2003).

A systematic understanding of the spatial variation of hydraulic conductivity is useful for constructing an accurate deterministic model of groundwater. The hydraulic conductivity reconstruction field from many experimental data of hydraulic head raises problem not only about the complexity of the diffusion equation but need to report for physical aspects of the area such as boundary conditions, geology and effective recharge. The reconstruction of the hydraulic conductivity field from numerous experimental hydraulic head data, an inverse problem, raises the issue not only of the complexity of the diffusion equation that links the two variables, but need to account for the physical aspects of the site under study, includes the boundary conditions, the effective recharge, and the geology (Roth et al. 1998). Hydro-geological parameters can be predicted using the methods with trial and error or techniques of optimization (Detwiler et al. 2002, Tung et al. 2002, Abdulla et al. 2000).

Site investigations are indispensable for model development. The outcome consequences depend on the quantity and quality of the data of the area available to define input boundary parameters conditions (Wang & Anderson 1982). Rigorous application of fertilizers and pesticide, industrial effluent and too much groundwater abstraction are few examples of activities that lead to groundwater pollution which have resulted in the deterioration of water resources in various regions (Baalousha 2010). The development of textile industries is seriously vulnerable due to the immense environmental damage caused by the textile processing industries in Tirupur to the Noyyal river and its groundwater system

(Arumugam et al. 2015). The standard for the fundamental hypothesis of the model is the conservation of masses. For the development of models, field investigations are important consequences that depend on the quantity and quality of the available field data to define input parameters and the conditions of the boundary (Kujur & Akhtar 2014). The groundwater and surface water are not a separate mechanism in the water cycle. All the surface water features (estuaries, reservoirs, wetlands and lakes) interact with groundwater. The exchanges take several forms. Surface water contamination can cause the degradation of groundwater features (Dowlatabadi & Zomorodian 2015). The evaluation of groundwater pollution risk requires two important factors, viz. contamination probability and the impact of contamination when a site has a high contamination probability but has a low impact of contamination, the risk is low. However, when both contamination impact and contamination probability are high, the risk is high (Baalousha 2010).

## MATERIALS AND METHODS

The study area is an industrial hub for the textile segment and forms one of the most significant exporting centres of cotton textiles in India. It is characterized by an undulating topography with the height ranging from 290 to 323 meter above the mean sea level and slopes gradually towards east. The geographical extent of the study area is about 450 $km^2$ and lies between latitudes 11°11'00" N to 11°12'30" N and longitudes 77°13'00" E to 77°30'30" E (Fig. 1). Dendritic drainage pattern has been found. The study area is extracted from the toposheets No.58 E/4 and 58 E/8. The related data are extracted from IRS 1D 23.5m resolution with the aid of Earth Resource Data Analysing System in addition to Arc View GIS 3.2a software. The geomorphologies revealed the study area is duri crust, shallow buried pediments, pediments, shallow pediments, etc. (Arumugam et al. 2016). The various types of soils are red calcareous, non-calcareous and brown soil. Temperature variation of the study region ranges from 19°C to 38°C and receive scanty rains due to the leeward side of the Western Ghats with the annual average rainfall of 650 mm.

Land use and land cover maps are considered as an essential component for modelling and considerate the earth as a system. Land cover maps are currently being developed from national to global scales. Satellite imagery (IRS 1D 23.5m) has been utilized for mapping of land use/land cover. Due to fast textile industrialization/dying activities in Tirupur region, the discharge of industrial effluent is speedily increasing. Most of the effluents discharged in the region are untreated with high concentrated physico-chemical parameters. They are directly affecting the quality of groundwater in the study area. The scope of the investigation is to analyze the impact of industrial effluent to groundwater quality level by five different scenarios. The steps involved to carry out the analysis are:

- Sample collection and analysing the observation wellhead measurement data, meteorological information, geological data, quality measurement statistics, pumping data and digital map for the region.
- Determining the horizontal movement of groundwater with the help of the developed regional groundwater model through fixing the proper boundary condition and the parameter optimization.
- Predicting the quality of groundwater for the forthcoming years by using visual MODFLOW software in different scenarios.

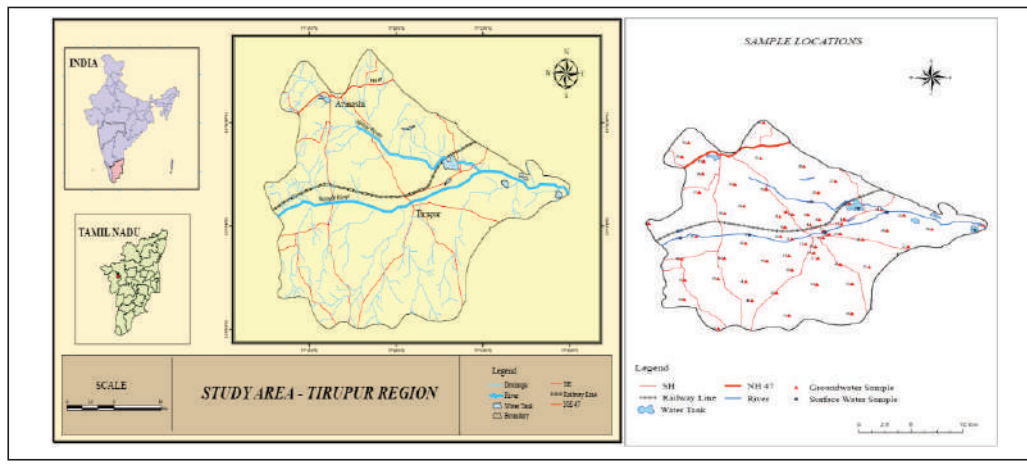


Fig. 1: Location of the study area.

**Aquifer parameters:** The aquifer properties such as transmissivity (T), horizontal hydraulic conductivity ($k_h$) and well yield was composed in the vicinity of the study region. The aquifer thickness, weathered and fractured zone in the study varies from 10 to 30 m below the ground. The level of groundwater reaches the lowest in the location, during summer season after which it starts increasing to reach the highest peak, after the end of the winter season. The rise and fall of the groundwater level depend upon the duration, quantity and intensity of precipitation, depth of weathered rocks, and specific yield of the bedrock and the wide-ranging of the slope of the fresh rock formation towards the drainage conduit.

MODFLOW is a computer program which is originally developed by the U.S. Geological Survey that simulates three-dimensional groundwater flow using a finite difference method. The MODFLOW 4.2 was used here. The partial differential equation of groundwater flow (McDonald & Harbaugh 1988) used in MODFLOW is as given below.

$$\frac{\partial}{\partial x}(K_{xx}\frac{\partial h}{\partial x})+\frac{\partial}{\partial y}(K_{yy}\frac{\partial h}{\partial y})+\frac{\partial}{\partial z}(K_{zz}\frac{\partial h}{\partial z})-W=Ss\frac{\partial h}{\partial t} \quad \ldots(1)$$

Where, $K_{xx}$, $K_{yy}$ and $K_{zz}$ are hydraulic conductivity values along the x, y and z coordinate axis which are assumed to be parallel to the major axis of hydraulic conductivity ($Lt^{-1}$), while *h* is the potentiometric head (L). W is a volumetric flux per unit volume that represents sources and sinks of water ($t^{-1}$), t is the time, and $S_s$ the specific storage of the permeable material ($L^{-1}$).

**Solute transport equation and model boundary conditions:** The equation represents the associate/movement of the flux of solute mass through the control volume. This states that the summation of all the mass, which consumes or else creates solute with the volume. They must be equal to a change in the reflection of the solute with the control volume.

$$\frac{\partial C}{\partial t}=\left[\frac{\partial}{\partial x}\left(D_x\frac{\partial C}{\partial x}\right)+\frac{\partial}{\partial y}\left(D_y\frac{\partial C}{\partial y}\right)+\frac{\partial}{\partial z}\left(D_z\frac{\partial C}{\partial z}\right)\right]$$
$$-\left[\frac{\partial}{\partial x}(V_xC)+\frac{\partial}{\partial y}(V_yC)+\frac{\partial}{\partial z}(V_zC)\right] \quad \ldots(2)$$

Where, Vx, Vy, and Vz are seepage velocity in x, y and z direction, m/s ($Lt^{-1}$), Dx, D and Dz are dispersion coefficient $m^2$/sec ($L^2T^{-1}$), t is time in seconds (T) and C is solute concentration mg/$m^3$ ($ML^{-3}$). Visual MODFLOW provides contaminant transport modelling and three-dimensional groundwater flow using MT3DMS, MODPATH and RT3D. It involves property and boundary conditions, the graphic design of the model grid, run the groundwater flow visualize mode, path-line and contaminant transport simulations, parameter estimation technique Win PEST, display and interpretation of model output manual method of calibration, in 3D space.

**Model formulation and grid design:** The conceptual model of the hydrogeologic structure was derived from the comprehensive study of the borehole lithology, geology, and fluctuations of water level from the study wells (Fig. 2). The model grid covering 450 $km^2$ was discretized into cells (80 rows × 80 columns (Fig. 3) and three upright layers based on lithology.

The aquifer top and bottom were derived from the lithology of boreholes. The vicinity of one grid is equal to 0.07 $km^2$. The upright cross-section of the system next to 29$^{th}$ row and 33$^{rd}$ column are revealed in Fig. 4 and Fig. 5 respectively. The depth of the topsoil stratum varies from 0-14 m, the lower partly weathered rock bed varies from 0-37 m and the bottom rock vary from 0-71 m.

**Model boundary conditions:** The study region consists of river (Noyyal) boundary at the middle intersected by its tributaries and is surrounded by the variable head boundary (study wells). The boundary of the river is assigned in the top cover based on the river point and river bottom in the region, both in starting and end points, are entered. The var-

Fig. 2: Model formulated of the study area.

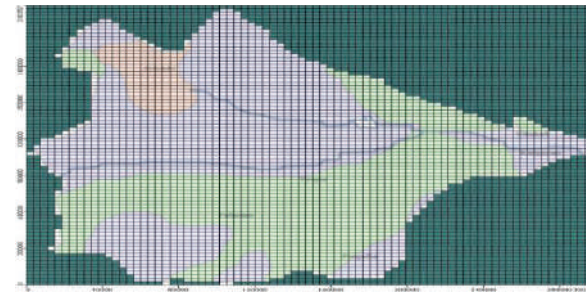

Fig. 3: Discretization of the study area.

iable head boundary is predetermined based on the monthly water level data collected (2014 to 2018) from PWD. 700 mm/yr is assigned as recharge for the entire top stratum of the model and 180 mm/yr is assigned as evapotranspiration. The control of river water level is restricted to 4 km around the location. As a result, the effective cell is taken within the river boundary and linking all the observation wells and pumping wells (Fig. 6).

**Initial head and concentration:** The initial head value at the initial stress period from the study wells around the study area was taken for the simulation purpose. The initial head for the different grids in the study area is revealed (Fig. 7).

Parameter concentrations at the initial stress period from the observation wells in the study area are accounted for as an initial concentration head for simulation (Fig. 8).

The recharge concentration of parameters is assigned in the study region based on point of injection of effluents from the industries after the treatment from a common ef-

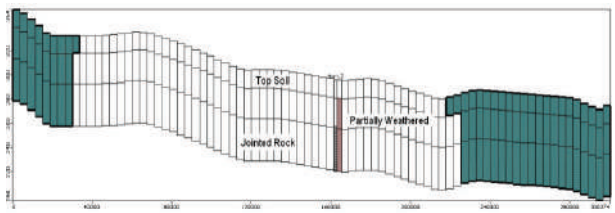


Fig. 4: Cross-section along the 29th row.

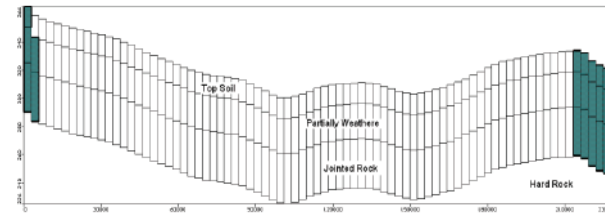


Fig. 5: Cross-section along the 33rd column.

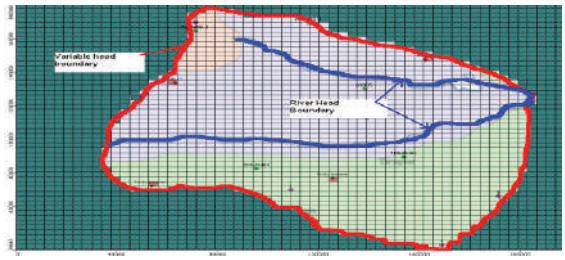


Fig. 6: Model boundary conditions of the study area.

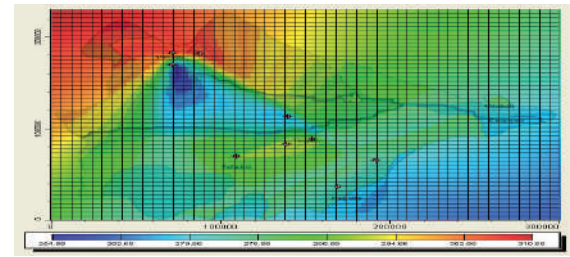

Fig.7: Initial water level head for the study area.

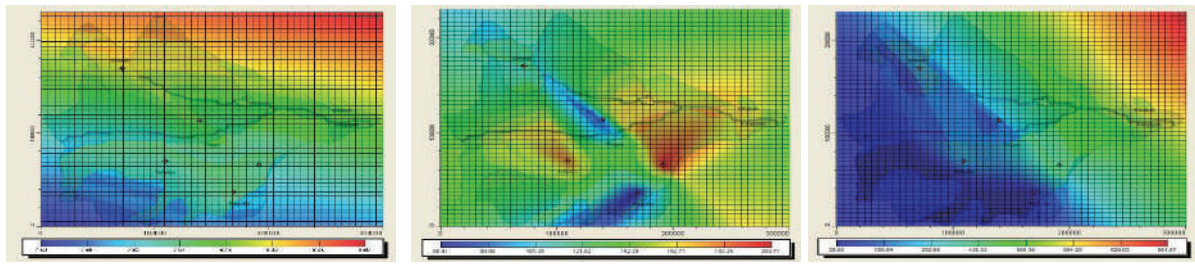

a) pH b) Mg c) $NO_3$

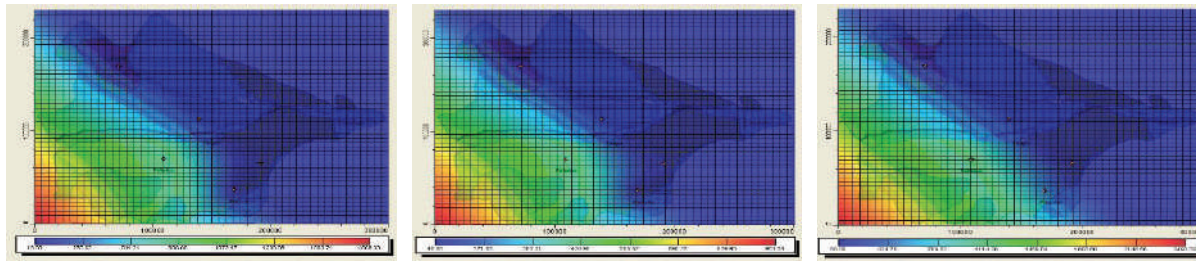

d) K e) Ca f) Na

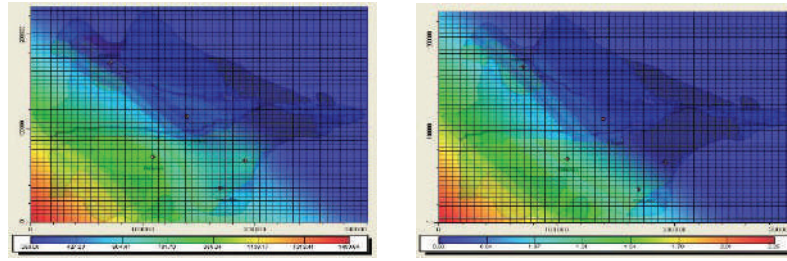

g) Cl h) F

Fig. 8: Initial concentration level for the study area.

fluent treatment plant. Particles are assigned to obtain the pathway from the point of injection. Dispersion coefficient is assigned for both the longitudinal and the layer boundary for the total model.

**Model calibration:** The calibration of groundwater is accomplished by a trial and error modification of the model input data to adjust the model output. The Win PEST provides automotive calibration progression by adopting the prediction factor such as recharge parameters, conductivity and specific yield. The calibration is done for the model data from 2014 to 2018. They are illustrated in Figs. 9 -14.

The reaction of groundwater from the different observation wells in the model calibration and the response of the concentration stage (pH, Mg, $NO_3$, K, Ca, Na, Cl and F) from the observation wells in the model calibration and validation have been done for the wells 1 to 5.

**Model validation:** The model validation periods were done for the periods from 2014 to 2018 (Fig. 15). The concert of the model acceptably predicts the exact aquifer state and reflects the same as in groundwater point and their concentration. As a result, the present model is appropriate for predicting and forecasting the groundwater eminence for the scenarios.

## RESULTS AND DISCUSSION

**Groundwater quality scenarios:** The validated model is used for predicting the groundwater quality for ten years (2021 to 2030) for the subsequent five different scenarios

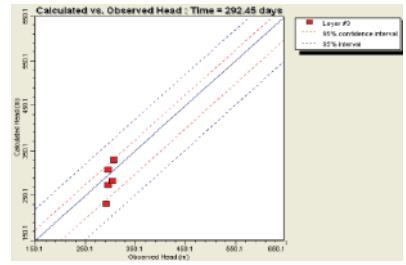


Fig. 9: Predicted head and observed- calibrated on 292nd day.

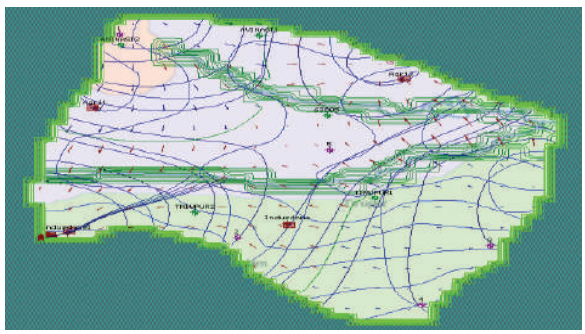

Fig. 10: Model output under steady simulation.

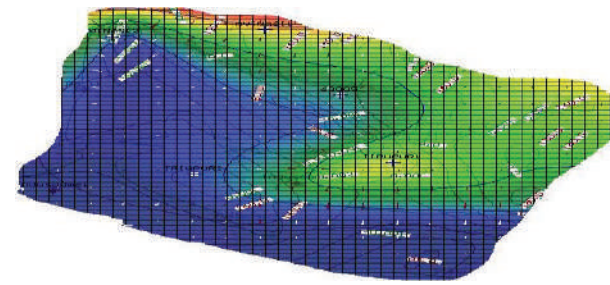

Fig. 11: Model output responses to head level.

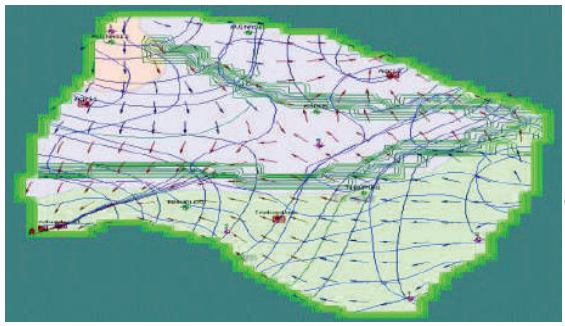

Fig. 12: Model output responses to velocity head.

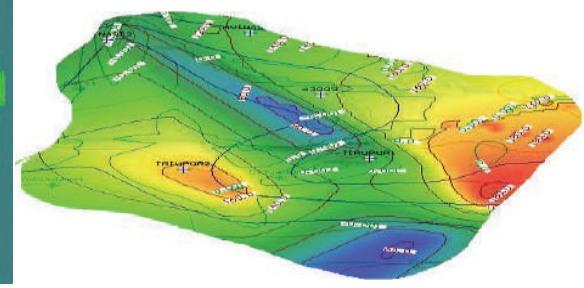

Fig. 13: Model output concentration in the top layer.

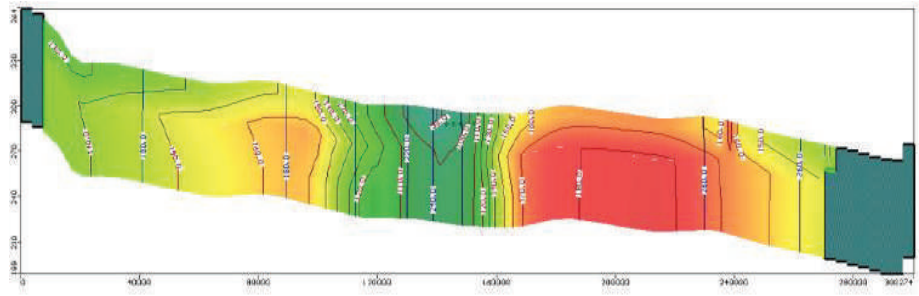

Fig. 14: Model output response to concentration level.

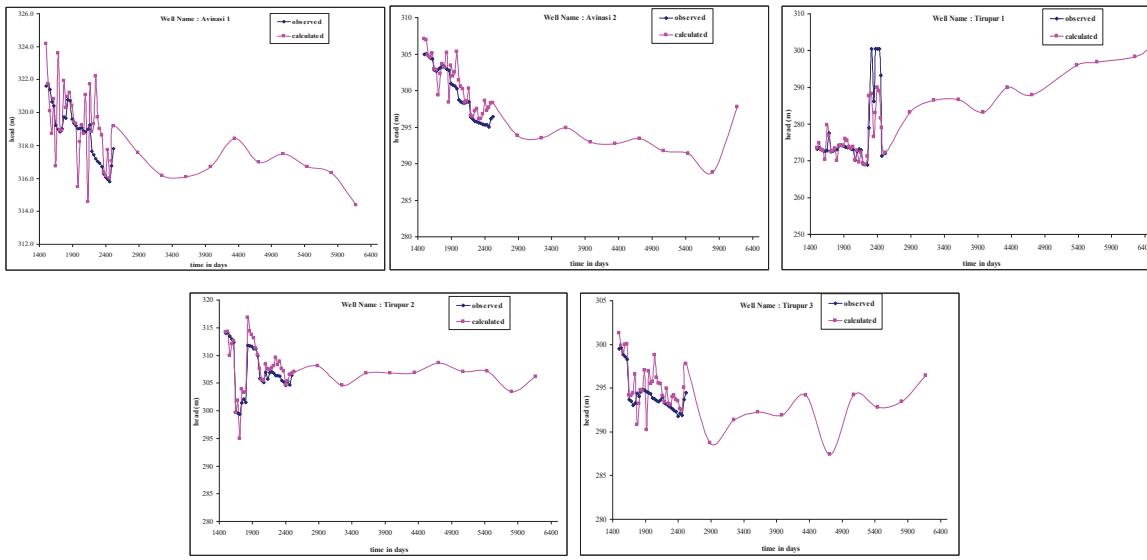


Fig. 15: Response of the groundwater level at diverse observation wells during the validation phase.

namely: The constant level of pumping and the discharge of effluent are same (Scenario number: 1); The pumping rate is reduced using 20 per cent and the discharge of effluent is in the same level (Scenario number: 2); the same level of pumping rate is continued and the discharge of effluent is condensed to 20 % (Scenario number: 3); The same level of pumping rate is continued and the discharge of effluent is reduced to 50 % (Scenario number: 4) and the same level of pumping rate is continued and the discharge of effluent reduced to 100 % (Scenario number: 5). The five different scenarios and their results regarding the observation wells are illustrated in Figs. 16 to 22.

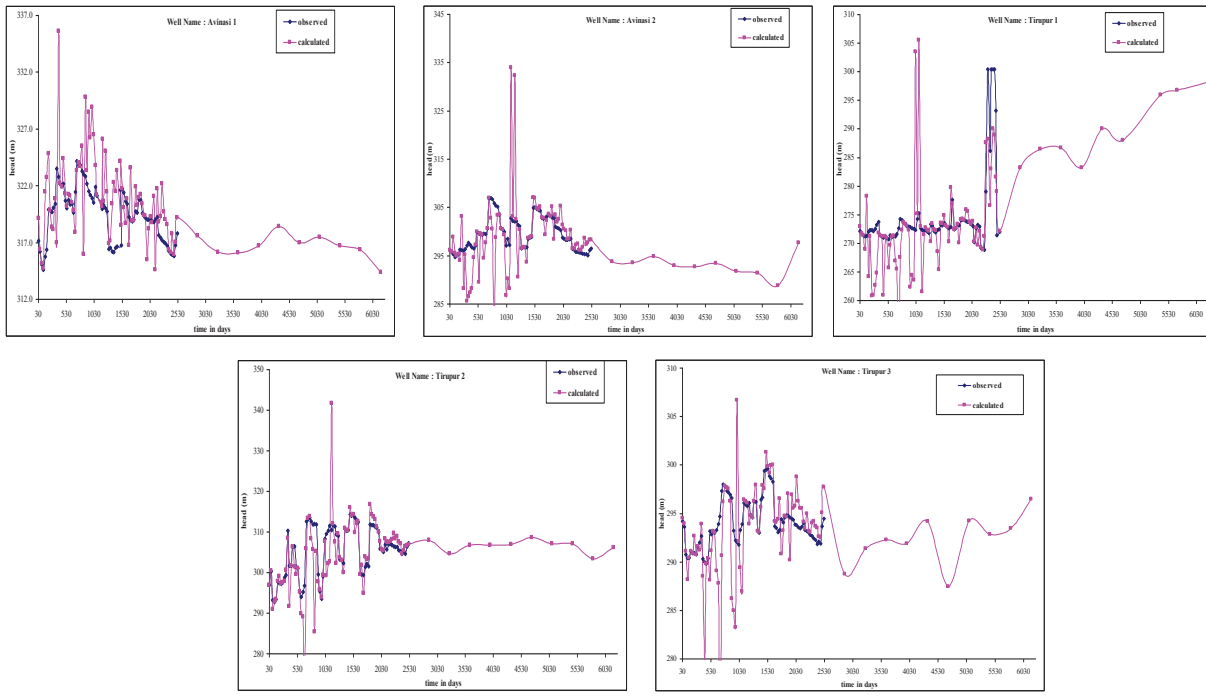


Fig. 16: Groundwater level at different study wells for the scenarios at a constant pumping rate.

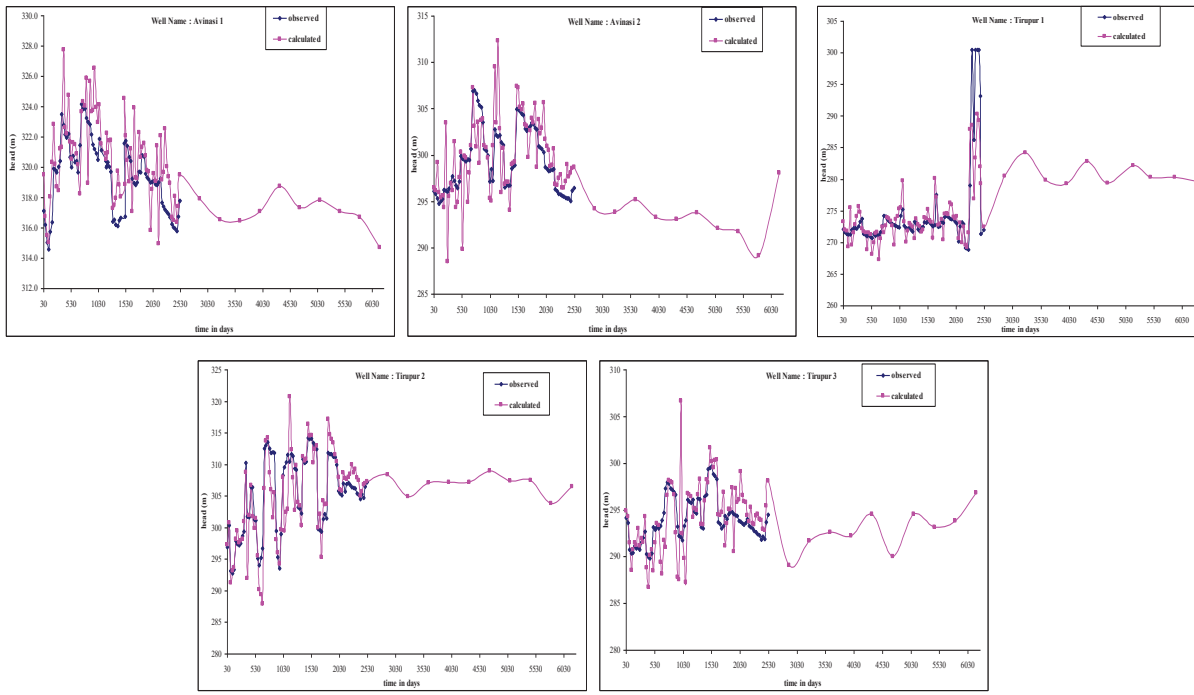


Fig. 17: Groundwater level at observation wells for scenario 2.

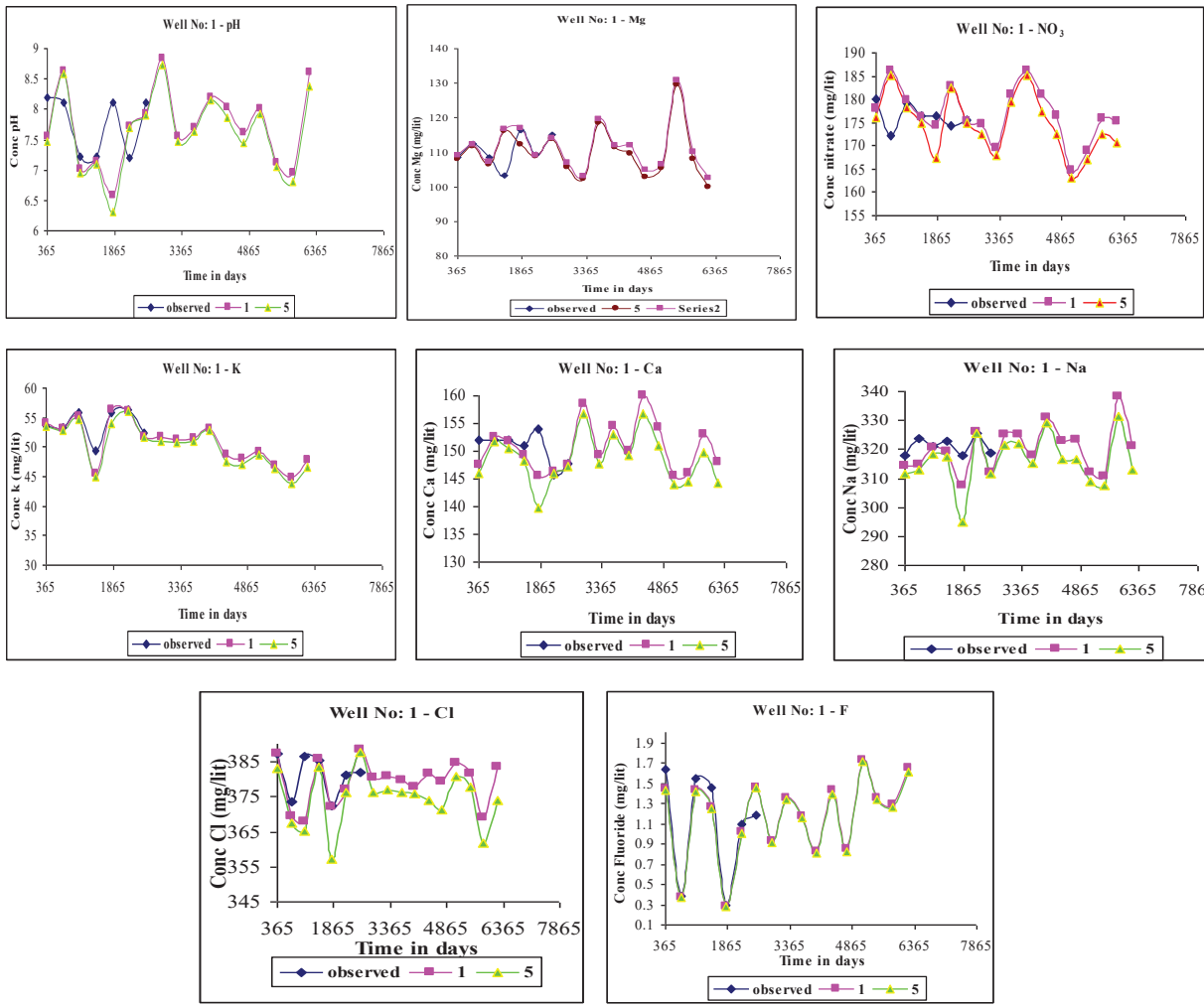


Fig. 18: Responses to concentration level at observation well number 1, for the scenarios 1 and 5.

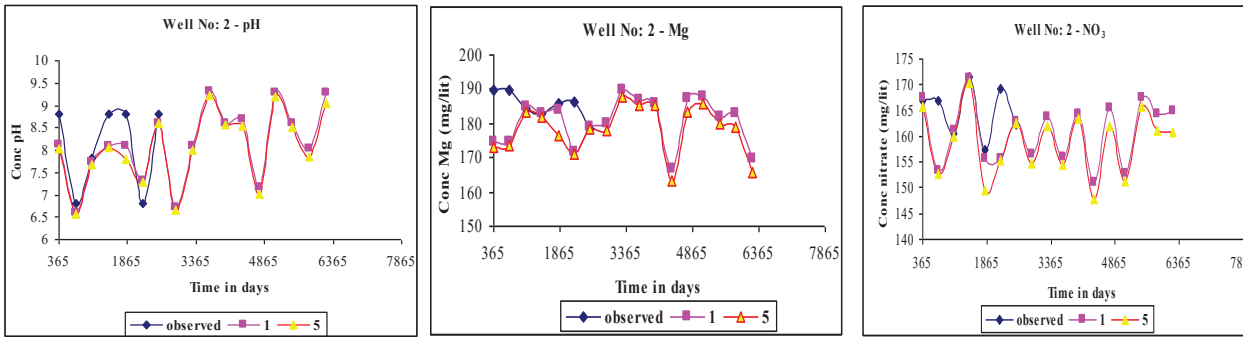


Fig. 19 Cont....

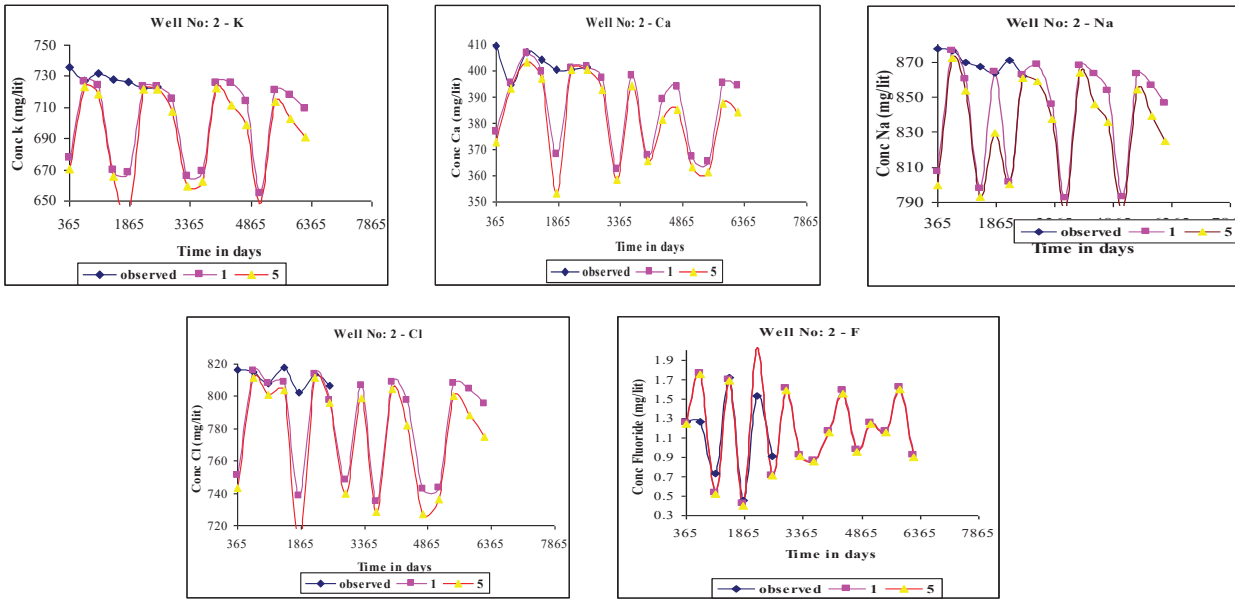


Fig. 19: Responses to concentration level at observation well number 2, for scenarios 1 and 5.

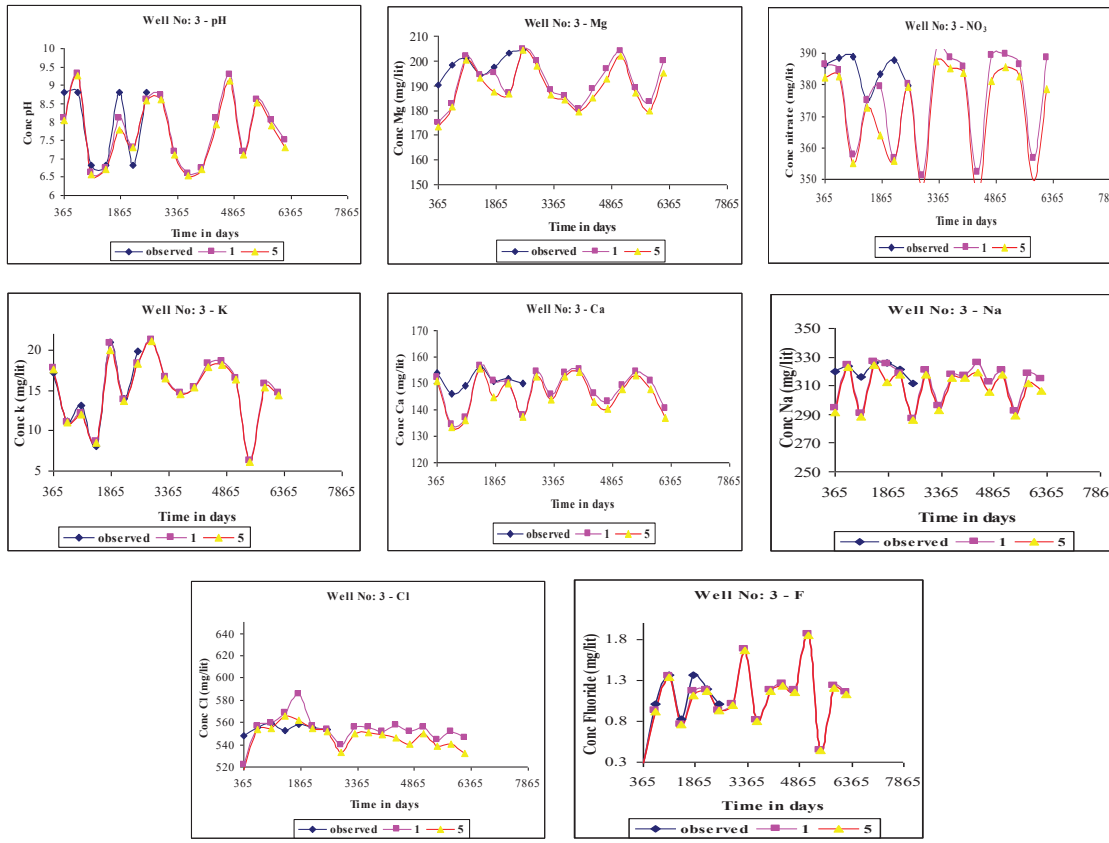


Fig. 20: Responses to concentration level at observation well number 3, for scenarios 1 and 5.

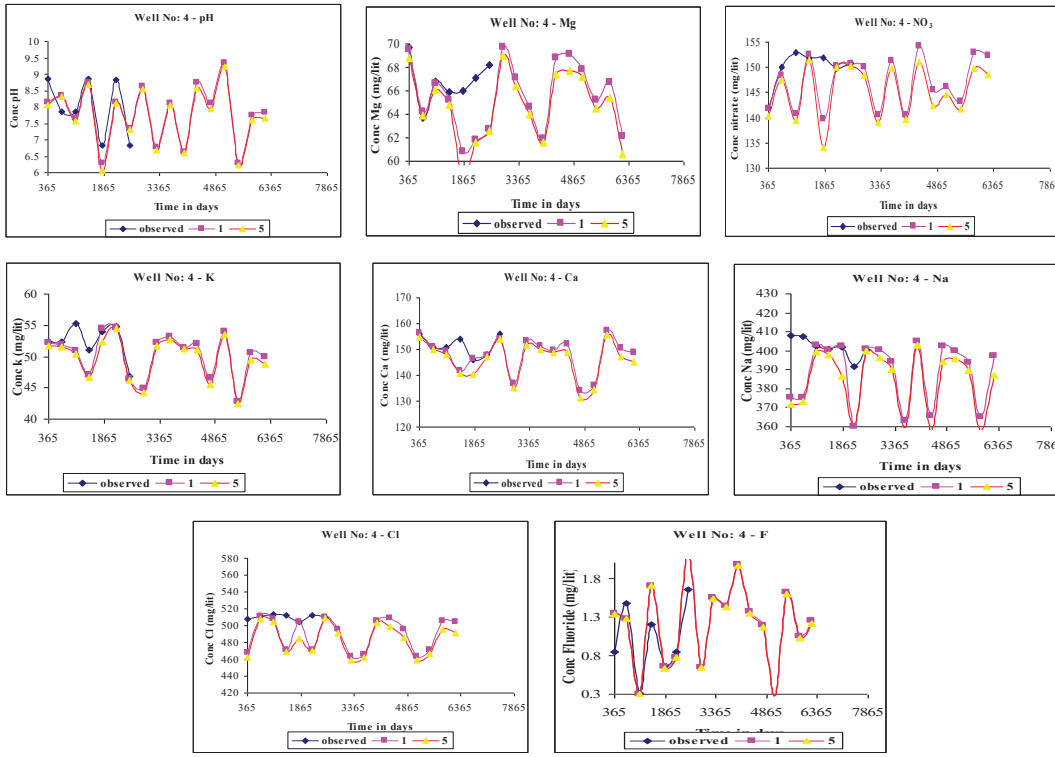


Fig. 21: Responses to concentration level at observation well number 4, for scenarios 1 and 5.

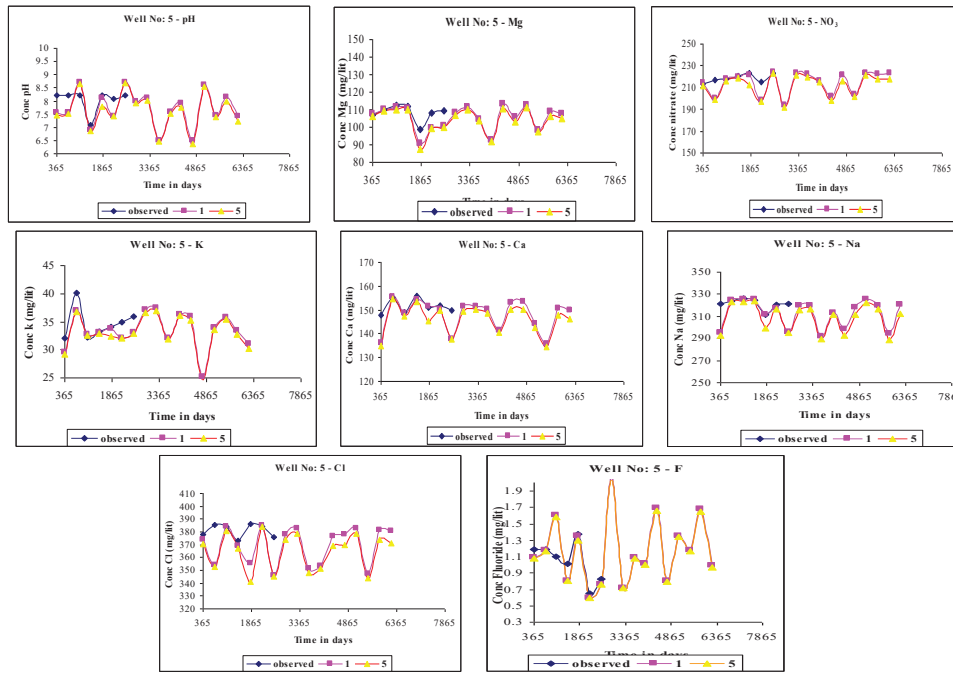


Fig. 22: Responses to concentration level at observation well number 5, for the scenario1 and 5.

The groundwater level is not much disturbed owed to different scenarios except scenario 2, in which the pumping velocity is condensed by 20 per cent results in the elevation of the groundwater level in all the observation wells. The forecasted groundwater level too reflects the same trend of water level for the data of the past seven years.

## CONCLUSION

The model response to scenario 1 for water quality forecasting for the next ten years from 2021 to 2030 indicates the real risk in the groundwater quality. Unfortunately, it is not suitable for both domestic and irrigation purposes. Uniform nature of the trend is followed in all the observation wells. The model exactly predicted the quality level in the well 1, 2 and 5 satisfactorily. In the wells 3 and 4, the model response to scenario 2 to 4 is very negligible. So, the exact value is much less comparing to the previous scenario. It indicates that the present condition in the Noyyal River does not change by reducing the concentration to some percentage. The model response to scenario 5 is negligible. Less than 2% reduction is observed in the wells 1, 2 and 5. In the wells 3 and 4, there is less than 0.5% change in concentration level. It is concluded that the present condition in Tirupur region will change if there is no injection of industrial effluent.

## REFERENCES

Abdulla, F. A., Al-Khatib M. A. and Al-Ghazzawi, Z.D. 2000. Development of groundwater modelling for the AZROQ basin. Environ. Geology, 40(1/2): 11-18.

Arumugam, K., Elangovan, K. and Kartic Kumar, M. 2016. Assessment of groundwater quality in Tirupur Environs, Tamil Nadu, India. International Journal of Engineering Research & Technology, 4(20): 1-6.

Arumugam, K., Rajesh Kumar, A. and Elangovan, K. 2015. Evolution of hydrochemical parameters and quality assessment of groundwater in Tirupur Region, Tamil Nadu, India. Int. J. Environ. Res., 9(3): 1023-1036.

Baalousha, H.M. 2010. Mapping groundwater contamination risk using GIS and groundwater modelling. A case study from the Gaza Strip, Palestine. Arab. J. Geosci., DOI 10.1007/s12517-010-0135-0.

Detwiler, R. L., Mehl, S., Rajaram, H. and Cheung, W.W. 2002. Comparison of an algebraic multigrid algorithm to two iterative solvers used for modelling groundwater flow and transport. Ground Water, 40(3): 267-272

Dowlatabadi, S. and Zomorodian, S.A. 2016. Conjunctive simulation of surface water and groundwater using SWAT and MODFLOW in Firoozabad watershed. KSCE Journal of Civil Engineering, 20(1): 485-496

Kujur, A.R. and Akhtar, H. 2014. Application of groundwater modelling in the development of sustainable water resources framework. International Journal of Scientific and Research Publications, 4(6): 1-4

Michael, G. McDonald and Arlen, W. Harbaugh 1988. A modular three-dimensional finite-difference ground-water flow model. Preceding Publications. DOI-10.3133/twri06A1

Roth, C., Chiles, J. P. and De Fouquet, C. 1998. Combing geostatistics and flow simulators to identify transmissivity. Adv. Water Resources, 21(7): 555-565.

Tung, C.P. and Chou, C. A. 2002. Application of Tabu search to groundwater parameter zonation. J. Am. Water Resour. Assoc., 38(4): 1115-1126.

Tung, C.P., Tang, C.C. and Lin, Y.P. 2003. Improving groundwater-flow modelling using optimal zoning methods. Environmental Geology, 44: 627-638

Wang, H.F. and Anderson, M. P. 1982. Introduction to Ground Water Modeling: Finite Difference and Finite Element Methods. W.H. Freeman and Company, San Francisco. 237.

Zheng, C. 1990. MT3D, A Modular Three-dimensional Transport Model. United States Environmental Protection Agency and SS Papadopulos and Associates, Rockville, MD.

Nature Environment and Pollution Technology
An International Quarterly Scientific Journal

p-ISSN: 0972-6268
(Print copies up to 2016)
e-ISSN: 2395-3454

Vol. 19 | No. 4 | pp. 1435-1442 | 2020

Original Research Paper

https://doi.org/10.46488/NEPT.2020.v19i04.009

Open Access Journal

# Spatial and Temporal Changes and Driving Factors of Desertification in the Source Region of the Yellow River, China

**Q. G. Liu*† and Y. F. Huang****
*Department of Tourism and Geography, Hefei University, Hefei 230601, China
** Department of Biology Food and Environment, Hefei University, Hefei 230601, China
†Corresponding author: Q. G. Liu; qgliuhf@163.com

**Nat. Env. & Poll. Tech.**
**Website: www.neptjournal.com**

*Received:* 03-12-2019
*Revised:* 21-01-2020
*Accepted:* 01-03-2020

**Key Words:**
Yellow river
Desertification
Spatial and temporal changes
Remote sensing

## ABSTRACT

The source region of the Yellow River, located in the north-eastern edge of the Qinghai-Tibet Plateau, is an important water conservation region and ecological barrier of the Yellow River. In this paper, based on remote sensing technology, multi-period Landsat remote sensing images in the source region were taken as the main information source. With the assistance of field investigation, we monitored the spatial and temporal changes of desertification in the source region from 2000 to 2019. The results show that the area of desertification in the source region has accounted for 9.36% of the total area, of which the light desertification land is the major portion. The desertification is mainly distributed between the southern margin of Madoi Valley basin and the northern margin of Heihe Valley basin, and is distributed on the river valleys, lakesides, ancient rivers and piedmont proluvial fan, showing the form of patches, sheets and belts. The growth rate of desertification in the source region was 87.47% from 2000 to 2010. With a high growth rate, the process of desertification was represented by the rapid spread of desertification. From 2010 to 2019, the growth rate of desertification was 37.32%, which was relatively slow. But the moderate desertification land maintained a straight linear growth trend, showing an increasing trend of desertification degree. Through the analysis of the driving factors of desertification in the source region of the Yellow River, this paper argues that the special geographical location, climatic factors, rodent damages and human activities are the main causes of desertification.

## INTRODUCTION

Desertification is one of the major ecological and environmental problems facing China. The source region of the Yellow River is located in the northeast of the Qinghai-Tibet Plateau, which is the transition zone from the Qinghai-Tibet Plateau to the Loess Plateau. It is an important water conservation region and ecological barrier of the Yellow River, and also a sensitive area of climate changes. Due to the harsh natural conditions and fragile ecological environment, and the impact of global climate changes and human activities, since the 1980s, many ecological and environmental problems have emerged in the source region of the Yellow River, such as desertification, grassland degradation, glacial recession, permafrost melting, and the flow interruption of the Yellow River. The overall eco-environment in the source region of the Yellow River is deteriorating, and desertification is the most serious ecological and environmental problems. A series of ecological and environmental problems dominated by land desertification, have seriously affected the sustainable economic development and social stability of the source region and had a certain impact on the middle and lower reaches of the Yellow River (Cheng 1998, Zeng et al. 2003, Wang et al. 2004).

At present, the research on desertification is relatively weak in the source region of the Yellow River, which has affected the governance of desertification and the reconstruction of eco-environment in alpine regions. Monitoring and assessment of desertification is an important way to scientifically and effectively prevent desertification. Remote sensing with a wide range of observations, a large amount of information, a fast update of data and high accuracy (Kang & Liu 2014, Ma et al. 2016), has been widely used in the monitoring and assessment of desertification. Based on RS image processing technology, this paper used Landsat TM/ETM+ remote sensing images from 2000 to 2019, analysed the spatial and temporal changes of desertification in the source region of Yellow River since 2000, explored the driving factors of desertification. Base on the analysis of the development trend of desertification, this paper provides a relevant scientific and theoretical basis for the restoration of desertification and eco-environment management in the source region of the Yellow River.

## STUDY AREA

The source region of the Yellow River generally refers to the river basin above Duoshixia (Institute of Geography, CAS

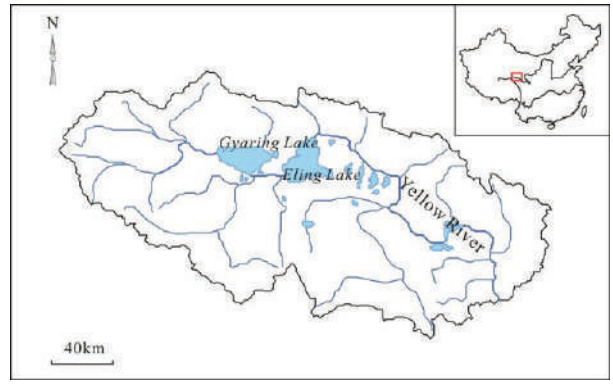


Fig. 1: Geographic location of the study area in China.

1990). To more completely study the desertification in the source region of the Yellow River, our study focused on the river basin above Tehetu Township. The study area is located between 33°42'~35°20' N and 95°52'~99°29' E, with an area approximately $3.7\times10^4$ km$^2$ (Fig. 1). The source region of the Yellow River is bounded by Kariqiong Mountain in the west, Bayan Har Mountain in the south, Buqing Mountain in the north and Amne Machin Mountain in the east. It belongs to Qinghai Province, includes most parts of Madoi County and a part of Darlag County and Maqen County in Golog Tibetan Autonomous Prefecture, as well as includes a part of Qumarleb County and Chindu County in Yushu Tibetan Autonomous Prefecture.

The source region of the Yellow River is high in the northwest and low in the southeast, and the elevation of most areas is 4,100-4,600m. The central area is relatively open, with numerous lakes and marshes, surrounded by icebergs and snow-capped peaks. The landform shows the characteristics of inter-distribution of low mountains, wide valleys and lake basins. The source region is a typical continental alpine climate, characterized by cold and dry weather, the sharp difference in temperature, much wind and snow, and violent climate changes. The annual mean temperature is -3.5°C, annual mean precipitation is 312 mm, and annual mean evaporation is 1,240-1,327.9 mm. The temperature and precipitation decrease from southeast to northwest, and the trend of precipitation increasing with altitude is also obvious. Alpine cold meadow (ACM) and alpine cold steppe (ACST) are the main vegetation types in the source region of the Yellow River.

## MATERIALS AND METHODS

**Desertification land classification:** The classification of desertification land is an objective reflection of the degree of land degradation. In this paper, based on the existing standards and methods for the division of desertification (Wang et al. 1998), through field investigation and laboratory analysis, and combined with the changes of vegetation, soil and other factors, the desertification land in the source region of the Yellow River can be divided into light desertification land (LDL), moderate desertification land (MDL), severe desertification land (SDL) and extremely desertification land (EDL). All types of desertification were mainly distinguished by the degree of land degradation.

***LDL***: the area of quicksand is under 5%, and there is almost no wind-sand flow. The vegetation coverage is over 30%, mainly distributed in fixed coppice sandbags and sporadic grassland. Most of the surface remains in the state of native grassland. There is a small amount of wind erosion and wind deposition, and the surface appears spot-like quicksand, which is equivalent to fixed sand.

***MDL***: the area of quicksand is 5-25%, and the wind-sand flow is not obvious. Semi-fixed sand and semi-naked gravel are distributed in patches. The vegetation coverage is 20-30%, and there are some sporadic sand dunes. Grassland has been significantly degraded, and the important constructive species of native vegetation has taken a secondary position, while the sandy vegetation has become the main species. Flaked quicksand and coppice dune have appeared in large numbers, which is equivalent to semi-fixed sand.

***SDL***: the area of quicksand is 25-50%, the wind-sand flow and the quicksand texture are obvious, with irregular patch distribution, and the sand dunes are clearly visible. The vegetation coverage is 10-20%, and there are coppices in the topsoil. The native vegetation no longer exists, sandy grass coppices are dominant species, and the wind erosion and wind landform are obvious.

***EDL***: the area of quicksand is over 50%, and large areas of sand land are distributed continuously. Sand dune, dune ridge and other landforms are obvious. The vegetation coverage is under 10%. The original surface form has been completely destroyed and replaced by quicksand.

**Data sources and processing:** In this paper, Landsat TM images obtained in 2000 and 2010, and Landsat ETM+ images obtained in 2019 were used to establish databases for desertification monitoring. To reduce the influence of seasonal aspect and cloud cover on monitoring, remote sensing images with cloud cover less than 10% in summer and autumn were selected as far as possible. ATCOR atmospheric correction module of PCI image processing software was used for radiation correction to obtain surface reflectance images. The geometric correction was based on the topographic map with a scale of 1:50,000, control points were selected from the topographic map, and the quadratic polynomial re-sampling was selected to correct them. The correction accuracy was controlled within 0.5 pixels, and the ground resolution was controlled within 30m×30m. Then, with the support of ARC/INFO software, based on the data of soil, vegetation and meteorology in the source region of the Yellow River, the human-computer interactive interpretation was used to extract the data.

**Desertification difference index model:** In this paper, the normalized differential vegetation index (NDVI) reflecting vegetation coverage was adopted to indicate the desertification degree, because vegetation coverage is generally considered as a good indicator of desertification. The NDVI was calculated using reflectance data from infrared and near-infrared bands of Landsat TM/ETM+ images after radiation and geometric correction. The surface albedo of the study area was estimated by using Landsat TM data inversion model (1) established by Liang (2000).

$$\text{albedo} = 0.356\rho_{TM1} + 0.130\rho_{TM3} + 0.373\rho_{TM4} + 0.085\rho_{TM5} + 0.072\rho_{TM7} - 0.0018 \quad \ldots(1)$$

Based on the spatial characteristics of Albedo-NDVI, a desertification difference index model in the study area was established. The model was used to obtain multi-temporal desertification index images. The detailed process was referred to relevant literature (Zeng et al. 2006). The desertification difference index model can be expressed as:

$$\text{DDI} = 1.3437\text{NDVI-albedo} \quad \ldots(2)$$

**Monitoring information extraction:** According to the data obtained from two field surveys in 2018 and 2019, combined with the map data of the vegetation type, soil type and geology of the study area, through the means of visual interpretation, the typical sample areas of different desertification types were selected and determined on Landsat ETM+ images obtained in 2019. With the support of image processing software, the connection between the typical sample areas and the desertification difference index images was established to determine the position of the typical sample areas on the desertification difference index images. The DDI values of different desertification types were calculated, and the monitoring indicators of different desertification types were finally determined (Table 1). Based on the monitoring indicators given in Table 1, the spatial distribution characteristics of desertification in 2000, 2010 and 2019 were obtained. Using the change monitoring tool in ENVI software, the raster data of desertification distribution during our study period were statistically analysed, the transfer matrix of desertification was obtained, and the temporal changes of desertification were further analysed.

## RESULTS AND ANALYSIS

**The spatial changes of desertification:** In this paper, the remote sensing monitoring results of desertification in 2000, 2010 and 2019 in the source region of the Yellow River were obtained. Based on the monitoring results in 2019, the current situation and spatial distribution characteristics of desertification in the source region were analysed. In 2019, the area of desertification in the source region has reached 3,519.97km$^2$, accounting for 9.36% of the total area, among which the LDL was the largest, accounting for 45.82% of the total area of desertification, the MDL followed, accounting for 26.20%. The area of the SDL was close to that of the EDL, accounting for 13.80% and 14.18% respectively. According to the China Desertification Census data in 2015, the total area of desertification on the Qinghai-Tibet Plateau reached 313,274.62 km$^2$, accounting for 13.96% of the total area of the plateau. According to the above data, the area ratio of desertification in the source region of the Yellow River is slightly lower than the average level of the whole Qinghai-Tibet Plateau.

However, the distribution of all types of desertification in the source region was relatively concentrated. Except for a small area of desertification to the west of the Eling Lake, most of the rest were distributed to the east of the Eling Lake. From the perspective of geomorphic units, desertification was concentrated between the southern margin of Madoi wide valley basin and the northern margin of Heihe River wide valley basin. It was in the form of patches, sheet and bands, distributed along the low mountains and hills that run northwest to southeast, and distributed in the river valleys, lakesides, ancient rivers and piedmont proluvium fans, etc.

According to the administrative division, the distribution of desertification in the source region was concentrated in Madoi County. The area of desertification in Madoi County accounted for 85.07% of that in the source region. All types of desertification in Madoi County were more than 78% of those in the source region. In order of proportion, from large to small, they were LDL, MDL, SDL and EDL respectively. The LDL and the MDL were the main ones, and the SDL

and the EDL also occupy a large proportion. The proportion of desertification land in Madoi County was much higher than the average level of Qinghai-Tibet Plateau. The area of desertification in Maqen County accounted for 11.71% of that in the source region. The remaining three counties, Qumarleb County, Chindu County and Darlag County, had a very small area of desertification. Overall, the average degree of desertification in the source region was not the highest in the Qinghai-Tibet Plateau. However, from the local area, the degree of desertification and damage in the source region was relatively high.

**The dynamic changes of desertification in the 2000s:** The monitoring results of desertification from 2000 to 2010 (Table 2 and Table 3) show that the area of desertification in the source region increased from 1,474.71km$^2$ to 2,768.61km$^2$, with a growth rate of 87.47% and an annual mean growth rate of 21.87%. Among them, the SDL increased the fastest, with an annual mean growth rate of 69.52%. The MDL and the LDL were followed, with an annual mean growth rate of 28.62% and 25.32%, respectively. The EDL increased more slowly, with an annual mean growth rate of only 0.71%. It can be seen that the changes of desertification in the source region in the 2000s, not only showed the rapid spread of desertification but also showed that the degree of desertification increased year by year.

The dynamic analysis of desertification mentioned above only reflected the overall situations of desertification in the source region of the Yellow River. In fact, in the process of dynamic changes of desertification, the expansion and reversal of desertification were two coexisting processes at the same time, and the final result of desertification depends on which process was dominant. The expansion of desertification indicated its spread and aggravation, while the reversal of desertification indicated improving in natural environmental conditions, weakening in human activities, and reducing in the area of desertification in the source region. To effectively analyse the process of desertification in the source region, according to the characteristics of the dynamic changes of desertification, the desertification in the 2000s was divided into three types: expansion type, reversal type and stabilization type. The expansion type refers to the region where the area of desertification expanded and degree of desertification increased. The reversal type refers to the region where the process of desertification reversed, the area of desertification reduced and the degree of desertification weakened. The stabilization type refers to the region where the desertification was maintaining its initial state.

The monitoring results of two-time phases in 2000 and 2010 were analysed by GIS spatial superposition, taking 2000 as the benchmark, and this paper concluded that the area of expansion type desertification was 1,938.8km$^2$ from 2000 to 2010, of which 1,401.54km$^2$ was transferred from the original non-desertification, and the remaining 537.26km$^2$ was from the original desertification aggravated by different degrees. The area of expansion type desertification accounted for 36.43% of the total area of desertification. The area of reversal type desertification was 319.73km$^2$, accounting for 21.68%. The area of stabilization type desertification was 617.72km$^2$, accounting for 41.89%. In the 2000s, the annual mean expansion rate of desertification was 32.86%, while the annual mean reversal rate was only 5.42%, and

Table 1: Desertification detecting indicator in the source region of the Yellow River.

| Desertification type | LDL | MDL | SDL | EDL |
|---|---|---|---|---|
| DDI value | 51-63 | 43-50 | 34-42 | 23-33 |

Table 2: Desertification land in the source region of the Yellow River from 2000 to 2010 (unit: km$^2$).

| Desertification type | 2000 | 2010 | Area Change | Change rate % | Annual change rate % |
|---|---|---|---|---|---|
| EDL | 417.34 | 429.11 | 11.77 | 2.82 | 0.70 |
| SDL | 95.21 | 360.00 | 264.79 | 278.10 | 69.52 |
| MDL | 295.43 | 633.61 | 338.18 | 114.47 | 28.62 |
| LDL | 666.73 | 1,341.89 | 675.16 | 101.26 | 25.32 |
| Total | 147.71 | 2,764.61 | 1,289.90 | 87.47 | 21.87 |

Table 3: Transfer Matrix of desertification land conversion in the source region of the Yellow River from 2000 to 2010 (unit: km$^2$).

| 2000 | 2010 | | | | | |
|---|---|---|---|---|---|---|
| | Water area | EDL | SDL | MDL | LDL | Non-desertification |
| Water area | 1,411.92 | 5.92 | 4.45 | 4.88 | 6.88 | 36.81 |
| EDL | 12.02 | 267.65 | 65.72 | 38.65 | 21.46 | 11.84 |
| SDL | 2.18 | 23.74 | 31.09 | 24.11 | 11.47 | 2.62 |
| MDL | 6.24 | 59.00 | 80.67 | 91.74 | 46.65 | 11.13 |
| LDL | 12.97 | 45.35 | 107.55 | 220.96 | 227.24 | 52.84 |
| Non-desertification | 65.83 | 27.45 | 70.52 | 253.27 | 1,028.19 | 33,196.91 |

Table 4: Desertification land in the source region of the Yellow River from 2010 to 2019 (unit: $km^2$).

| Desertification type | 2010 | 2019 | Area Change | Change rate % | Annual change rate % |
|---|---|---|---|---|---|
| EDL | 429.11 | 499.10 | 69.99 | 16.31 | 1.63 |
| SDL | 360.00 | 486.10 | 126.10 | 35.03 | 3.50 |
| MDL | 633.61 | 922.07 | 288.46 | 45.53 | 4.55 |
| LDL | 1,341.89 | 1,612.70 | 270.81 | 20.18 | 2.02 |
| Total | 2,764.61 | 3,519.97 | 755.36 | 37.32 | 2.73 |

Table 5: Transfer matrix of desertification land conversion in the source region of the Yellow River from 2010 to 2019 (unit: $km^2$).

| 2010 | 2019 | | | | | |
|---|---|---|---|---|---|---|
| | Water area | EDL | SDL | MDL | LDL | Non-desertification |
| Water area | 1,401.59 | 13.24 | 9.42 | 16.72 | 10.72 | 59.30 |
| EDL | 10.97 | 300.11 | 65.84 | 35.92 | 13.35 | 2.92 |
| SDL | 15.05 | 92.44 | 129.01 | 89.54 | 32.58 | 1.38 |
| MDL | 16.07 | 52.62 | 156.89 | 261.22 | 145.26 | 1.55 |
| LDL | 15.53 | 26.29 | 106.87 | 400.22 | 789.36 | 3.62 |
| Non-desertification | 41.03 | 14.40 | 18.07 | 118.45 | 621.43 | 32,498.74 |

the annual mean expansion rate was six times of the annual mean reversal rate. Therefore, in the 2000s, the process of desertification in the source region not only shows the rapid spread of desertification but also shows the increasing degree of desertification year by year, reflecting the serious degradation of land and the worsening of eco-environment in the source region during this period.

**The dynamic changes of desertification in the 2010s:** In Table 4 and Table 5, the monitoring results of desertification from 2010 to 2019 show that desertification in the source region was further expanded in the 2010s. From 2010 to 2019, the desertification expanded by 755.36$km^2$, with an annual mean expansion rate of 2.73%, which was lower than that in the 2000s. In the 2010s, the changes of desertification were characterized by the rapid growth of MDL and SDL. The annual mean expansion rate of EDL reached 1.63%, exceeding that in the 2000s.

Taking 2010 as the benchmark, the desertification in the 2010s was divided into three types: expansion type, reversal type and stability type. The area of expansion type desertification was 1,607.69$km^2$, of which 772.37$km^2$ was transferred from the original non-desertification, and the remaining 835.32$km^2$ was aggravated by different degrees. In the 2010s, the annual mean expansion rate of desertification was 5.82%, while the annual mean reversal rate was 1.63%, and the annual mean expansion rate was about four times of the annual mean reversal rate. From the above analysis, it shows that although the expansion rate of desertification in the 2010s was lower than that in the 2000s, the desertification in the source region still maintained a trend of continuous expansion in the 2010s, with the aggravation of the desertification as the main factor. In the 2010s, the desertification in the source region was in the stage of development to strong development, which was consistent with the overall situations of desertification development in the whole Qinghai-Tibet Plateau. If the situations should be not controlled, the desertification in the source region will expand further.

## DRIVING FACTORS OF DESERTIFICATION

Desertification is a complex process of land degradation. Its expansion and reversal are influenced by both natural conditions and human activities. When natural conditions deteriorate and the intensity of human activities exceeds the environmental carrying capacity, desertification will intensify and expand. On the contrary, when natural conditions improve and human activities are effectively controlled, desertification can be reversed. Due to the special geographical location of the source region, the climate changes, rodent damages and human activities are the main causes of desertification.

**Climatic factors:** The source region of the Yellow River is located in the hinterland of the Qinghai-Tibet Plateau. Under special geographical conditions, it has formed a special climate. Climate changes in the source region are an important cause of desertification. There are two main aspects of climate change, one is rising temperatures, and the other is declining precipitation. According to meteorological data, the annual mean temperature in the source region has been increasing slowly in the past 60 years (Fig. 2), and the temperature increased by 0.382°C per 10a. The variation trends of annual mean temperature are bounded by 1986. Before 1986, the temperature decreased by 0.149°C per 10a.

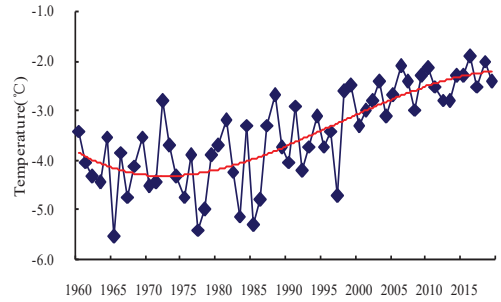


Fig. 2: The change of annual mean temperature from 1960 to 2019.

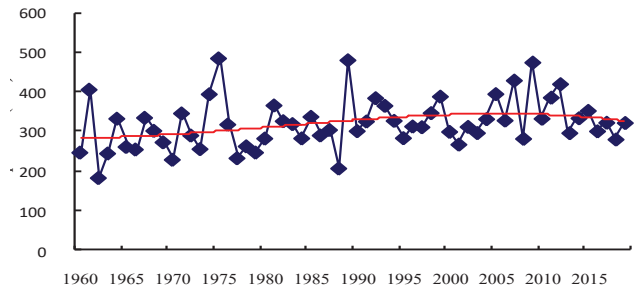


Fig. 3: The change of annual mean precipitation from 1960 to 2019.

Since 1986, the temperature increased by 0.557°C per 10a. Therefore, the increasing stage of annual mean temperature in the source region mainly occurred after 1986. The change of annual mean precipitation in the source region is also obvious (Fig. 3), and the inter-annual change is over 300mm. The annual mean precipitation in the source region is 312 mm, and the annual mean evaporation is over 1,240 mm, causing serious water shortage. Since 2000, the five-year drought has caused changeable windy weather and accelerated the process of desertification.

An important consequence of climate change is the impact on the permafrost environment. There is a large area of permafrost in the source region of the Yellow River. Permafrost has an important influence on the growth of alpine meadow vegetation. On the one hand, the permafrost can effectively prevent surface water and soil water from infiltrating, thereby increasing the water content of the plant root area. On the other hand, the permafrost has the function of gathering nutrients from the upper layers, because lower soil temperature is conducive to the accumulation of organic matter. Many studies have shown that the mean temperature of the upper permafrost has increased by 0.2-0.3°C in the past 60 years due to climate warming, resulting in large-scale thawing of permafrost, and even the disappearance of permafrost in some areas. As a result, the water content of plant roots decreased, swamps and lakes dried up, soil structure and composition changed, and finally, desertification intensified.

Another important consequence of climate change is the impact on the water environment. According to the survey data, the lake area decreased by 0.54% from 1970 to 1980, while the lake area decreased by 9.3% from 1980 to 1990. The water level of the lake generally decreased by 2-3m, and the lake shrank about 20-30m. From 1990 to 2019, the area of swamp and lake both decreased by about 10%, while the reduction of river area was the highest, reaching over 22%. The area of swamp shrank by nearly 200 $km^2$, and the number of lakes decreased by 49.

**Rodent damages:** Rodent damages are the main biological disasters that destroy the grassland ecology in the source region of the Yellow River. The rodent damages in the source region have a long history, but they have been especially serious since 1985. The main rodents in the source region are *Myospalax baileyi* and *Ochotona curzoniae*, among which *Ochotona curzoniae* is the most widely distributed and the most harmful. According to statistics, the area of the grassland affected by rodent damages in the source region is $149.95\times10^4 hm^2$, accounting for 65.20% of the natural grassland. The average density of rodent holes is 3,750-7,050/$hm^2$,

and the serious area is 19,860/hm$^2$. Rodents feed on the roots and stems of plants, and cut off the roots, causing large areas of grassland to wither and die, resulting in degradation and desertification of grassland. More than 50% of the "black soil type" degraded grassland in the source region is caused by rodent damages. According to the measurement, the water content of the surface soil of the secondary bare land on the shady and sunny slopes affected by rodent damages is 22.18% and 29.27% lower than that of the native grassland respectively. These rodent holes and "black soil beach" in the grassland become the breach of wind erosion, creating conditions for wind erosion, and accelerating degradation and desertification of grassland.

**Human activities:** Human activities are one of the important factors affecting the ecological environment in the source region, which are closely related to the changes of desertification. Especially in the process of economic development, human factors have become the leading factors affecting the changes of desertification (Chen et al. 2016). Unreasonable human activities destroy the surface ecosystem and lead to desertification.

The industrial structure of the source region is dominated by animal husbandry. Most of the economic income of herdsmen depends on animal husbandry, and expanding the number of livestock is the main way of economic growth. Since the end of 1960s, the animal husbandry in the source region has developed rapidly, the number of livestock has multiplied, and the grassland has been in the state of overloading, resulting in the continuous degradation of the grassland. In the source region, the area of grassland is small in winter and spring, the grazing time is long, and the overloading is more serious. Especially in the beach near the water source, the middle and lower part of the hillside and the two sides of the river valley, the overloading of grassland is frequent, which aggravates the load of grassland in winter and spring. According to the investigation of Wang (2001) on the grassland in the source region of the Yellow River, the theoretical stocking rate of the local grassland was 667,000 sheep units in winter and 3,048,900 sheep units in summer. From 2000 to 2019, the overloading rate of grassland in summer and winter in the source region reached 66.98% and 100% respectively. In winter and spring, the quantity of forage grass is the low quantity and poor quality, and in summer and autumn, the amount of forage is many quantities and high quality, which leads to the vicious cycle of livestock being fat in autumn, thin in winter and death in spring.

Another reason for the destruction of natural resources and the ecological environment by human activities is the improper use of water and soil resources, excessive mining, and indiscriminate digging. The source region of the Yellow River is rich in natural resources. Gold, salt and other minerals, as well as wild animals such as *Gymnocypris przewalskii*, *Vulpes corsac* and *Vulpes vulpes* are the main objects for local residents to engage in sideline business. According to the data of the grassland general station of Qinghai province, since 1980, sand gold production has started in the area around Daqing Mountain, and thousands of gold miners from other places have flocked to the area to collect gold and salt, catch fish and hunt natural enemies of wild rodents. Excessive mining, indiscriminate digging and illegal hunting have destroyed large areas of grassland vegetation, reduced the natural enemies of rodents, damaged the ecosystem, and further led to soil erosion and desertification. The grassland on both sides of the river has degenerated, the function of water conservation has declined, which has artificially aggravated the land desertification.

## DISCUSSION AND CONCLUSIONS

**Distribution of desertification land:** The area of desertification land in the source region of the Yellow River accounts for 9.36% of the total area, which is about 4.59% lower than that in the whole Qinghai-Tibet Plateau. However, the desertification land in the source region of the Yellow River is concentrated in Madoi County. The area of desertification land in Madoi County accounts for 14.3% of the total area, which is higher than that in the whole Qinghai-Tibet Plateau. The proportion is higher in the Huanghe Township and Heihe Township, where the desertification is concentrated. Therefore, on the whole, the area of desertification land in the source region is small, but the distribution of desertification land is relatively concentrated. In some areas, the proportion of desertification land is high, and the degree of desertification is also high.

**The general situation of desertification expansion:** During the 20 years from 2000 to 2019, the area of desertification land in the source region of the Yellow River increased by 2,045.26km$^2$. Among them, LDL accounts for 46.25%, MDL accounts for 30.64%, SDL accounts for 19.11%, and EDL accounts for the smallest proportion, only 4%. The results show that the desertification in the source region is increasing rapidly, among which LDL and MDL are expanding significantly. Since the 2000s, the process of desertification in the source region has presented a trend of rapid development, but the development of desertification in different periods showed different characteristics. In the 2000s, the growth rate of desertification was high, and the process of desertification was characterized by the rapid spread of desertification land. In the 2010s, the growth rate of desertification slowed down relatively, but MDL maintained a linear growth trend. In the past 20 years, although there is a certain reversal of desertification in some areas, on the whole, the source region is dominated by the expansion of desertification.

**The results of driving force analysis of desertification:** In the past 20 years, the desertification in the source region was attributed to the unreasonable exploitation and utilization of grassland resources under the background of the warming and drying trend of the alpine ecological environment, which further exacerbated the process of grassland degradation and land desertification. Due to the combined action of natural and human factors, many lakes and wetlands in the source region have shrunk or even dried up, causing a series of ecological environment problems such as grassland degradation, land desertification and soil erosion.

## ACKNOWLEDGEMENT

This research was financially supported by the Project of Anhui Education Department (No. SK2018A0603). The work was facilitated by the Qinghai Department of Lands, Environment and Resources and the Project of Scientific Research and Development Foundation of Hefei University (No. 20RW06ZDA).

## REFERENCES

Chen, L., Ding, W., Geng, Y. and Zhao, C. 2016. Dynamic change trend of desertification in Dulan County during 1975-2015. Desert and Oasis Meteorology, 10(5): 64-71.

Cheng, G. 1998. Some understandings about the eco-environmental protection and buildings in the source region of Yangtze and Yellow rivers. Advance in Earth Sciences, 13(suppl.): 1-5.

Institute of Geography, CAS. 1990. The Atlas of Qinghai-Tibetan Plateau. Science Press, pp. 77-79.

Kang, W. and Liu, S. 2014. A review of remote sensing monitoring and quantitative assessment of aeolian desertification. Journal of Desert Research, 34(5): 1222-1229.

Liang, S. 2000. Narrowband to broadband conversions of land surface albedo I: Algorithms. Remote Sensing of Environment, 76: 213-238.

Ma, Y., Sha, Z., Chen, X. and Fu, G. 2016. Desertificated land changes in Gonghe basin from 1990 to 2010. Journal of Arid Land Resources and Environment, 30(2): 176-181.

Wang, G. 2001. Eco-environmental degradation and causal analysis in the source region of the Yellow River. Environmental Geology, 40(7): 884-890.

Wang, G., Ding, Y., Wang, J. and Liu, S. 2004. Land ecological changes and evolutional patterns in the source regions of the Yangtze and Yellow rivers in recent 15 years. Acta Geographica Sinica, 59(2): 163-173.

Wang, T., Wu, W. and Wang, X. 1998. Remote sensing monitoring and assessing sandy desertification: An example from the sandy desertification region of northern China. Quaternary Sciences, 2: 108-118.

Zeng, Y., Feng, Z. and Cao, G. 2003. Land-cover change and its impacts on environment in the upper reach of the Yellow River, northeast Qinghai-Tibetan Plateau. Mountain Research and Development, 23(4): 353-361.

Zeng, Y., Xiang, N. and Feng, Z. 2006. Albedo-NDVI space and remote sensing synthesis index models for desertification detection. Scientia Geographica Sinica, 26(1): 75-81.

Nature Environment and Pollution Technology
An International Quarterly Scientific Journal

p-ISSN: 0972-6268
(Print copies up to 2016)
e-ISSN: 2395-3454

Vol. 19 | No. 4 | pp.1443-1452 | 2020

Original Research Paper

https://doi.org/10.46488/NEPT.2020.v19i04.010

Open Access Journal

# Effects of Different Tillage Measures on Soil Microbes and Enzymatic Activity

**Binglin Huang, Mengxue Wang†, Xinjun Jin, Yuxian Zhang and Guohua Hu**
Agronomy College of Heilongjiang Bayi Agricultural University, Daqing, 163319, China
†Corresponding author: Mengxue Wang; wangmengxue1978@yeah.net

**Nat. Env. & Poll. Tech.**
**Website: www.neptjournal.com**

*Received:* 15-12-2019
*Revised:* 28-12-2019
*Accepted:* 01-03-2020

**Key Words:**
Tillage
Inter-tillage
Soil microorganisms
Soil enzymes

## ABSTRACT

To reveal the effects of different tillage measures on soil microbes, enzyme activities and nutrients, eight different treatments were combined with different tillage methods to study the effects of different tillage measures on soil microbes, enzyme activities and nutrients. The results showed that in the flowering stage, the number of bacteria in the soil was higher than that in PT1 (ploughing + early ridging), RT1 (rotary tillage + early ridge) decreased by 22.6%. PT2 (ploughing + early subsoiling) was more than RT2 (rotary tillage + early subsoiling), PT3 (ploughing + conventional subsoiling) than RT3 (rotary tillage + conventional subsoiling), PCK (rotary tillage + conventional ridging) than RCK (rotary tillage + conventional ridging) increased by 13%, 22.9%, and 3.5%, respectively. The bacteria, fungi and actinomycetes in the whole rotary tillage treatment (rotary tillage) were higher than the tillage treatment (ploughing). Except for the invertase, the urease, phosphatase and catalase activities of the ploughing treatment were higher than those of the rotary tillage. When entering the pod-forming period, the number of soil bacteria, fungi and actinomycetes in rotary tillage were higher than tillage, the soil sucrase activity in rotary tillage was higher than that in ploughing. RT1 was significantly higher than PT1 and PT2 by 11.1% and 11.7%, but the soil urease, phosphatase and catalase activities were higher in ploughing than rotary tillage. The available nitrogen and the available potassium were opposite. At the stage of tillage, the number of bacteria, fungi, actinomycetes, urease activities and sucrase activities in the rotary tillage were higher than ploughing, while the activities of phosphatase and catalase were higher under ploughing. In the mature stage, the soil urease and catalase activities were higher in the tillage treatment, while the phosphatase and sucrase activities were opposite. On the whole, advance inter-tillage improved the soil environment to some extent on both tillage measures, especially T2 (subsoiling).

## INTRODUCTION

Soil microorganisms is the generic term for all tiny organisms in the soil that are invisible or unclear to the naked eye, including bacteria, actinomycetes, fungi, etc. (Zhang et al. 2009). Soil microorganisms is the main active ingredient of the soil, gets involved with a variety of metabolic activities (Ryan & Adley 2010), promotes the cycle and transformation of soil organic matters and nutrients, and involves themselves in biochemical processes such as humus formation, so it plays a vital role in the crop productivity and the stabilization of soil ecosystem (Lucas et al. 2015). Produced by the interaction of microorganisms and crop roots, the soil enzyme is also one of the most important active ingredients of soil (Zhao et al. 2015). Getting involved in all biochemical processes of soil, the soil enzyme's activity level reflects the relative intensity of biochemical processes in soil. It can quickly respond to the effects that the short-term tillage measures have on soil quality and reflect the soil quality changes (Sui et al. 2016, Chen et al. 2014). The soil tillage method directly or indirectly affects the physical and chemical properties of the soil, mainly affecting the soil nutrient content and its effectiveness (Wang et al. 2015). The content level of soil nutrients reflects the soil health status and affects the circulation of energy and material in the whole ecosystem, guiding the decomposition and transformation of organic carbon (Yu et al. 2017, Chen et al. 2011), and the soil nutrient contents will directly affect the normal growth and development of crops (Zhang & Wu 2018). Tillage measures are the main factors affecting the soil environment. Soil microorganisms and enzymatic activities are particularly sensitive to their responses. At the same time, microorganisms and various soil enzymes play an important mediation role in the transformation of soil nutrients. Appropriate tillage measures can enrich the diversity of microbial community structures and improve the activities of various enzymes in the soil, thus favourable for the normal transformation and accumulation of soil nutrients, which in turn helps protect the soil environment and increase the crop yield.

As one of the three major black soil belts in the world, with a total area of 7×104 $km^2$ (Yu et al. 2017), northeast China's soil environment has been seriously damaged due to

the unduly pursuit of high crop yields, and improper tillage measures and field management methods, and the organic matters and total nitrogen content in the black soil has been decreasing year after year (Wu et al. 2017). Therefore, to look for a suitable tillage measure is particularly important for keeping the ecological environment of soil. According to the research report, no tillage + straw mulching can increase the organic matters on the soil surface, improve the composition and diversity of soil microbial community, thus optimizing the growing environment of crop roots (Wang et al. 2018). Other researches show that no tillage + straw mulching improves the enzymatic activity of the surface layer in a better way than traditional tillage (Peng et al. 2018). But the long-term no-tillage will increase the soil hardness, reduce the total porosity of the soil, and affect the growth of aerobic microorganisms and roots. The studies where the protective tillage, combined with other technical measures influence the ecological environment of soil and crop yields are frequently reported, but there are fewer reports on traditional farming combined with other technical measures.

In this study, a test was conducted in Heshan Farm Science Park, Heihe City, Heilongjiang Province to learn the effects of different tillage methods combined with different inter-tillage methods on soil microorganisms and enzymatic activities. The problems to be solved in this study are: (1) the effects of different tillage methods on soil microorganisms and enzymatic activities, (2) the effects of the same tillage methods and different inter-tillage methods on soil microorganisms and enzymatic activities, (3) according to the effects of different tillage measures on soil microorganisms and enzymes, the tillage and inter-tillage measures that are appropriate for the area can be determined.

## MATERIALS AND METHODS

### Overview of the Experimental Site

The experiment was carried out in Heshan Farm Science Park, Heihe City, Heilongjiang Province (48°43'N-49°03'N, 124°56'E-126°21'E), where the annual average temperature is ≥10°C, the annual effective accumulative temperature is from 2000 to 2300°C, and the frost-free period is 115-120 days, belonging to the continental climate in the cold temperate zone, where the rainy season is mostly concentrated in summer, with an annual rainfall of 500-600mm. The local soil type is dominated by the black soil, the cultivated land is faintly acidic, with the fertile soil and the balanced soil fertility. The 0-20cm basic physical and chemical properties in the experimental site are as given in Table 1.

### Experiment Design

The experiment was carried out from October 2017 to October 2018, adopting the split-plot experiment design (Table 2). Among them, the main factors were ploughing and rotary tillage and the different inter-tillage methods were the second factors. That was, two different tillage methods were designed in the early period (the crop straws were returned to the field): Ploughing (P) and rotary tillage (R). After sowing, each tillage method was equipped with 4 different inter-tillage measures. As a whole, the comprehensive setting was conducted from different depths of deep scarification, different deep scarification and earthing up time, different deep scarification and earthing up number, a total of 8 treatments were designed, as given in Table 2. Deep scarification refers to a technique in which the deep scarification machines

Table 1: Basic physical and chemical properties of the soil of the test site.

| Bulk weight ($g.cm^{-3}$) | Available nitrogen ($mg.kg^{-1}$) | Available phosphorus ($mg.kg^{-1}$) | Available potassium ($mg.kg^{-1}$) | Organic matter ($g.kg^{-1}$) | pH |
|---|---|---|---|---|---|
| 1.19 | 138.9 | 20.79 | 179.35 | 14.3 | 6.25 |

Table 2: Different tillage methods.

| Tillage measures | Treatments | Stage | | | |
|---|---|---|---|---|---|
| | | 4-5 days after the broadcast | V2-V3 stage | V4-V5 stage | V6-V7 stage |
| Ploughing | PT1 | Soil dressing | | Middle ridging | Large banking up |
| | PT2 | 25-30 cm subsoiling | | 30-35 cm subsoiling + Mid-banking up | Large banking up |
| | PT3 | | 25-30cm Sub-soiling | | Large banking up |
| | PCK | | Soil dressing | Mid-banking up | Large banking up |
| Rotary tillage | RT1 | Soil dressing | | | Large banking up |
| | RT2 | 25-30 cm Subsoiling | | 30-35 cm Subsoiling + Mid-banking up | Large banking up |
| | RT3 | | 25-30 cm Sub-soiling | | Large banking up |
| | RCK | | Soil dressing | Mid-banking up | Large banking up |

and tools are drawn by a cultivator to loosen the soil at different depths, improve the structure of the plough layer, and enhance the capacity of soil moisture conservation and drought resistance and drainage. Soil dressing: The width of the cultivator earthing knife is 20-30°. Mid-banking up: The width of the cultivator earthing knife is 80-90°, and the large banking up: The width of the cultivator earthing knife is 110~120°. Three times of earthing inter-tillage (common mode in rural areas) are set as contrast (CK).

The soybean was sowed with fertilizer on May 4, 2018. The local main variety Heihe 43 provided by the local seed company was selected. Each row area was 45 m, the row width was 62.5 cm, 8-row areas, repeated twice, and the harvest occurred on September 28, 2018. The preceding crop was corn, and the fertilization amount was consistent with the local fertilization level. There was 54 $kg \cdot hm^{-2}$ of pure nitrogen fertilizer, pure $P_2O_5$ 67.5 $kg \cdot hm^{-2}$ and pure $K_2O$ 30 $kg \cdot hm^{-2}$, and the other field managements were consistent with the local production.

### Soil Sampling and Analysis

**Soil sampling:** The soil sampling was conducted 4 times during the flowering period, pod-setting period, seed filling period, and mature period of soybean. 0-20 cm soil was sampled between the rows with a soil auger with a diameter of 5 cm. Six points were sampled randomly in the shape of "S" in each plot, with crop residues and stones removed, finally they were mixed evenly and put into the sealed pockets and immediately brought to the laboratory for the treatment. Some soil samples were stored under 4°C for the measurement and analysis of soil microbial quantity, others were air-dried, ground and sieved out from the soil by a 2-mm soil screen (organic matters sieved by a 0.25 mm soil sieve) to remove straw residues and plant roots, and finally, they were used to measure the soil enzymatic activity and soil nutrients.

**Analysis of soil enzymatic activity:** The determination of soil enzymatic activity is based on the method of Guan Songyin (Bao 1999). The activity of invertase was determined by 3,5-dinitro salicylic acid, expressed as the quantity of mg of glucose in 1 g of soil after 24 hours. The activity of urease was determined by sodium phenol colourimetry, expressed as the quantity of mg of ammonia nitrogen released from 1 g of soil after 24 hours. The phosphatase activity was determined by the disodium phenyl phosphate colourimetric method, expressed as the quantity of mg of phenol released in 1 g of soil after 24 h. The soil catalase activity was determined by the permanganimetric method, and all the treatments were repeated thrice.

**Analysis of soil microbial quantity:** The soil microorganisms were inoculated by spread-plate method (Pan 2015). The fungus was cultivated in Martin medium and its quantity was determined. The composition of the medium was 10 g of glucose, 5 g of peptone, 1 g of $KH_2PO_4$. 0.5 g of $MgSO_4.7H_20$, 1 L of distilled water, 18 g of agar, 3.3 mL of 10 g/L Bengal red solution. 0.3 mL of 10 g/L streptomycin solution was added into per 100 mL culture medium, at the using time after sterilization. The actinomycetes were cultivated in the modified Gao's No.1 culture medium and its quantity was determined. The composition of the medium was starch 20 g, $KNO_3$ 1 g, $K_2HPO_4$ 0.5 g, $MgSO_4 \cdot 7H_2O$ 0.5 g, NaCl 0.5 g, $FeSO_4 \cdot 7H_2O$ 0.01 g, distilled water 1 L, agar 18 g, pH 7.2-7.4 at the using time after sterilization. 0.3 mL of 30 g/L $K_2Cr_2O_7$ solution was added per 100 mL of medium to inhibit the growth of fungi and bacteria (7.2-7.4). The bacteria were cultivated in the beef extract-peptone medium and then their quantity was determined (Medium composition: beef extract 3 g, protein 5 g, distilled water 1 L, agar 18 g, pH 7.0-7.2). All the treatments were repeated thrice. The fungus was cultivated under 28°C for 3 to 4 days, the bacteria were cultivated at 28°C for 2 to 3 days, and the actinomycetes were cultivated under 37°C for 6 to 8 days. After the completion of the cultivation, the number of bacterial colonies was determined by the plate count. Computational formulas are as follows:

CFU (forming unit of bacterial colonies/mL) = 3 repeated average quantity of bacterial colonies × dilution ratio.

### Data Analysis

Data processing was conducted by Excel 2010, and the effects that each treatment has on soil microbial quantity and enzymatic activity are compared using one-way variance (ANOVA). All statistical analyses are completed by SPSS 17.0 and the plotting adopts Origin 2018.

## RESULTS AND ANALYSIS

### Effects of Different Tillage Measures on Soil Microbial Quantity

**Effects on the bacterial population:** As shown in Fig. 1, the soil bacterial population reaches $10^5$ orders of magnitude. Different tillage measures have significant effects on bacteria. In the flowering period, T1 and T2 are significantly higher than CK with the same tillage method, and T3 is less significantly different from CK. Among them, PT1 and PT2 are significantly higher than PCK by 17.05% and 28.41%. RT1 and RT2 were significantly higher than RCK by 56.48% and 17.65%. PT2 is higher than PT3 by 24.47% and RT2 is higher than RT3 by 35.16%, indicating that the deep scarification or earthing up in advance contributes to the increase of the soil bacterial population. In the pod-setting period, except for

PCK and RT1, the bacterial population treated respectively increased in some degree, and in the same tillage method, T1, T2 and T3 were significantly higher than CK, which was consistent with that in the flowering period. In the seed filling period, the bacterial population treated respectively tends to decrease to some degree, compared with the previous period. And with the same tillage method, the bacterial population is consistent with the previous trend, i.e., T1 and T2 are significantly higher than T3 and CK treatment. In the same inter-tillage method, the bacterial population treated by the rotary tillage is higher than that treated by the ploughing. Among them, RT1 is increased by 13.29% compared with PT1, and RT2 is increased by 12.78% compared with PT2, both of which reach a significant level, indicating that the rotary tillage combined with other tillage measures is more conducive to bacterial survival, and RT1 has been kept at a higher level. This may be caused by the earthing up ahead of time in the RT1 treatment, increasing the soil temperature during the flowering period, and creating a more suitable soil environment for the bacteria.

**Effect on the number of fungi:** As shown in Fig. 2, the soil fungi number reaches $10^4$ orders of magnitude. In the flowering period, the fungi number in the rotary tillage was higher than that in the ploughing on the whole. By the same tillage, T1, T2 and T3 all show a decreasing trend. In the ploughing, PT1, PT2 and PT3 are decreased by 12.71%, 21.82% and 14.48%, compared with PCK. RT1, RT2, RT3 are significantly lower than RCK by 20.91%, 47.76% and 28.35% respectively. The fungi number by the earthing-up treatment with the two ploughing methods (T1, CK) is higher than that of deep scarification (T2, T3), indicating that the deep scarification is more conducive to reducing the fungi number in the soil and creating a better soil environment for the soil than earthing up, in the pod-setting period and seed filling period, the two have the same variation tendency. In the same cultivating conditions, the fungi number produced by ploughing is lower than that produced by the rotary tillage, and both tillage methods show CK>T1>T3>T2. In the seed filling period, PT1 is decreased by 12.67% compared with PCK, while RT1 is decreased by 4.69%, compared with RCK. Compared with PT3, PT2 is decreased by 17.91%. Compared with RT3, RT2 is decreased by 27.63%, which is similar to the result in the flowering period, showing that deep scarification can reduce the soil fungi number and make the soil microbial community structure more reasonable.

**Effect on the actinomycete number:** As shown in Fig. 3, the soil actinomycete number reaches $10^5$ orders of magnitude. In the flowering period, the soil actinomycete number treated by the tillage is higher than that treated by the rotary tillage. In the tillage, PT1, PT2 and PT3 are significantly increased by 32.5%, 37.68% and 27.3% compared with PCK. In rotary tillage, RT1 and RT2 are less different from RCK, RT2 is significantly higher than RCK by 50%. In the seed filling period, the two tillage methods have the same trend, i.e., T2>T1>T3>CK. In ploughing, PT1, PT2 and PT3 are significantly higher than PCK by 28.4%, 38.62% and 11.36%. Similarly, in rotary tillage, RT2 is significantly increased by 17.61% compared with RCK, while RT1 and PT3 are less significantly different from RCK, but the actinomycete number treated by the rotary tillage is higher than that treated by the ploughing, which may be because the rotary tillage has less soil disturbance than ploughing. In the

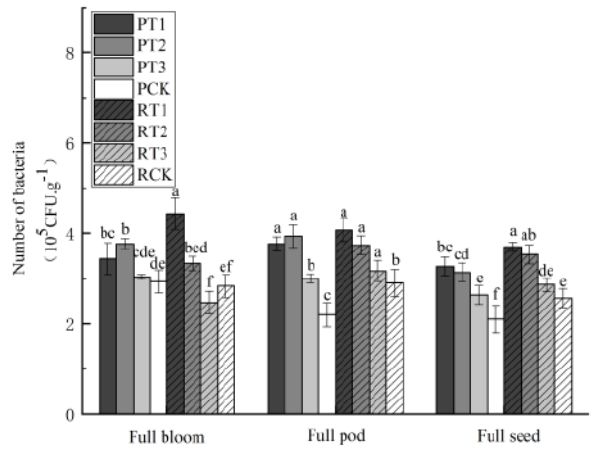


Note: Different letters indicate significant difference among treatments ($P < 0.05$).

Fig. 1: Effects of different tillage measures on soil microbial population.

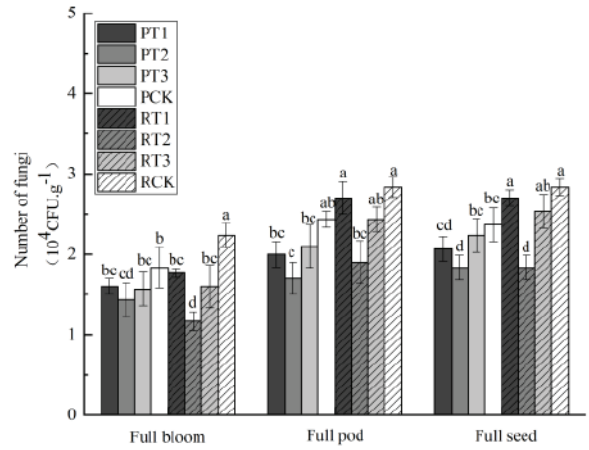


Fig. 2: Effects of different tillage measures on soil fungal population.

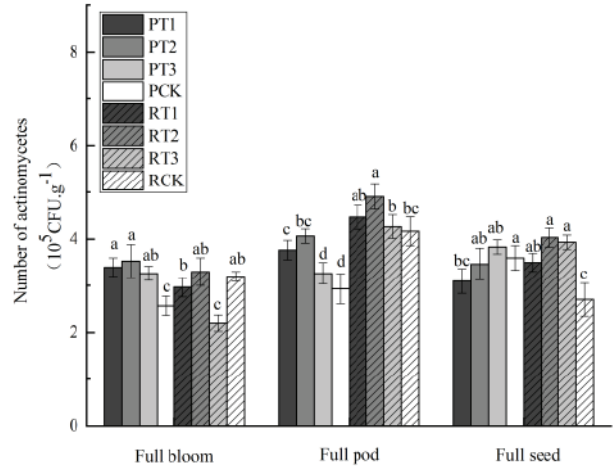


Fig. 3: Effects of different tillage measures on soil actinomycetes population.

seed filling period, the actinomycete number with the two tillage methods is decreased compared with the pod-setting period, especially PT1 and PT2 are decreased significantly compared with those in the previous period, both of which are lower than PCK. In rotary tillage, RT1, RT2 and RT3 are significantly higher than RCK by 29.63%, 49.37% and 45.66%. In general, the actinomycete number treated by the rotary tillage is higher than that treated by the ploughing in the later period, which is consistent with bacteria but opposite to the fungus, indicating that the rotary tillage may be more conducive to creating a more reasonable soil microbial community structure.

### Effects of Different Tillage Measures on Soil Enzymes

**Effect on soil urease:** Soil urease is often an important indicator used to characterize the soil nitrogen supply. As shown in Fig. 4, different tillage measures have a significant impact on it. During the flowering period, both tillage measures show a consistent variation trend (T2>T3>T1>CK). In the same tillage, PT2 is increased by 15.91%, 3.99% and 14.14% compared to PT1, PT3 and PCK. Compared with RT1, RT3 and RCK, RT2 is increased by 6.81%, 5.64% and 8.22%. Generally, the urease activity by the tillage is higher than that by the rotary tillage, which may be because the ploughing improves the soil's respiratory ability, accelerates the metabolism between rhizosphere and microorganisms, and increases the rate of secretory urease. During the pod-setting period, the basic trends of the two tillage measures are the same, T1 and T2 are higher than CK, and the urease activity of each treatment is generally improved. In the seed filling period, the urease activity of each treatment in rotary tillage has no significant difference. But the urease activity treated

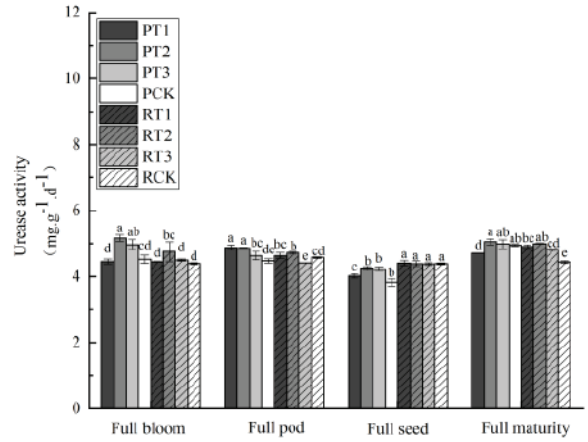


Fig. 4: Effects of different tillage measures on soil urease activity.

by rotary tillage is significantly higher than that treated by the ploughing; the urease activity in the mature period of soybean is increased compared with that in the seed filling period. That may be because the soybean roots break away from the putrefactive root nodules, and then release the rhizobia, which increases the activity of soil urease. Moreover, the urease activity treated by PT2 and RT2 is high all the time, indicating that the deep scarification is positively significant in improving and keeping the soil urease activity.

**Effects on soil phosphatase:** Soil phosphatase has a positive effect on the increase of the availability of soil phosphorus. As shown in Fig. 5, soil phosphatase activity gradually increases with the progress of soybean growth period. In the flowering period, the soil phosphatase activity treated by ploughing is higher than that treated by the rotary tillage but the differences are not significant. Similarly, whether treated by the ploughing or the rotary tillage, the treatment difference with the same tillage measures is not significant. In the soybean pod-setting period, except for RT1 and RT2, the phosphatase activity treated by each method is improved significantly. In the seed filling period, the soil phosphatase activity increases greatly, and the treatment difference is significant. Among them, the soil phosphatase activity treated by the tillage is higher than that treated by the rotary tillage, but the changing trend treated by each method is similar. That is, T2>T3>T1>CK. In the tillage, PT1, PT2 and PT3 increase by 11.26%, 53.62% and 26.38%, reaching a significant level compared with PCK. In rotary tillage, RT1, RT2 and RT3 increase by 5.96%, 25.5% and 12.21% compared with PCK. In the mature period, the variation trend in this period is consistent with that in the seeding filling period, and the phosphatase activity reaches the highest value. What differs from the seeding filling period is that the phosphatase activity treated by the deep scarification is lower than that treated by the earthing up, probably it is because the deep scarification improves the total porosity of the soil, the

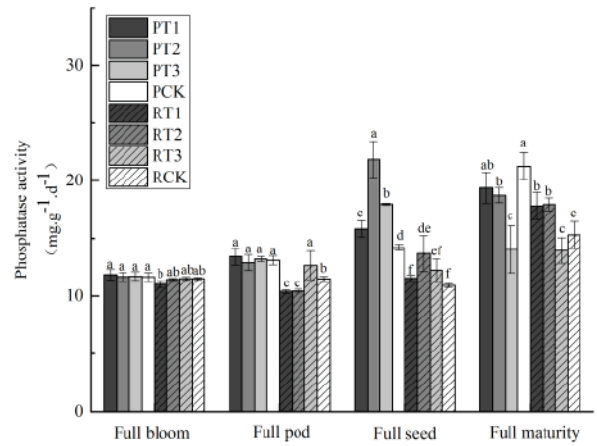


Fig. 5: Effects of different tillage measures on soil phosphatase activity.

thermal conductivity of soil decreases, causing the surface soil temperature to be closer to the surface temperature, thus affecting the soil phosphatase activity.

**Effect on soil invertase:** Widely distributed in soil, the soil invertase is often used to characterize the degree of soil maturity. It can catalyse and boost the sucrose in the soil to hydrolyse into glucose and fructose. As shown in Fig. 6, the soil invertase is significantly affected by the tillage methods. In the flowering period, the invertase activity gained by the ploughing is higher than that gained by the rotary tillage. The difference between two tillage methods may be caused because the crop stalks are returned to the field and the ploughing makes the soil respiration and the mineralization rate of organic matter stronger than those gained by the rotary tillage, allowing roots and microorganisms to secrete more active enzymes. By ploughing, PT1 and PT2 are significantly higher than PCK by 10.88% and 14.77%, respectively. PT1 and PT2 are both significantly higher than PT3, but the difference between PT1 and PT2 is not significant. By the rotary tillage, RT1 is significantly increased by 10.77 %, compared to RCK. RT2 is increased significantly by 19.92%, 27.92% and 31.19%, compared to RT1, RT3 and RCK, indicating that the advanced inter-tillage is beneficial to the increase of the activity of soil invertase, especially the effect through the advanced deep scarification is more significant. The variation tendencies in the pod-setting period, the seed filling period, and the mature period are basically similar. Both tillage measures show T2>T1>T3>CK. Under the same inter-tillage conditions, the invertase activity gained by the rotary tillage is higher than that gained by the ploughing, which may be related to a higher mineralization rate of organic matter in the flowering period. A large quantity of organic carbon is mineralized and decomposed, which causes the soil sucrose to be decreased relatively, thus the invertase activity is indirectly reduced. Especially in the mature period, the activity of invertase treated by the ploughing is lower than that treated by the rotary tillage. Among them, RT2 is increased by 27.56%, compared to PT2; RT1 is increased by 27.46%, compared to PT1, RT3 is increased by 29.47%, compared to PT3; and RCK is increased by 24.02%, compared to PCK, and all of them reach a significant level, indicating that the rotary tillage is more conducive to the improvement of invertase activity.

**Effect on soil catalase:** Catalase can transform hydrogen peroxide into $H_2O$ and $O_2$ through the enzymatic reaction, thereby removing the harm of hydrogen peroxide to soil and soybean roots. Therefore, the activity level of catalase seriously affects the soil environment and the health of soybean roots. As shown in Fig. 7, two different tillage measures have a significant effect on catalase. Generally speaking, in the same inter-tillage treatment, the catalase activity treated by the ploughing is higher than that treated by the rotary tillage. In the flowering period of soybean, through the same tillage method, on the whole, each treatment is not significantly different from CK, and the soil catalase activity treated by each method is higher. It is probably because the soybean roots grow and develop more quickly in the previous and middle period of soybean growth. The root metabolism is relatively strong, causing an increase of secretions. The metabolic activities of microorganisms and enzymes are active during this period, which leads to an increase in soil catalase activity. In the seed filling period, through the same tillage treatment, T1 treatment is significantly higher than other treatments. Among them, PT1 is significantly higher than PCK by 25.7%, RT1 is significantly higher than RCK by 10.3%, and the difference through other treatments are

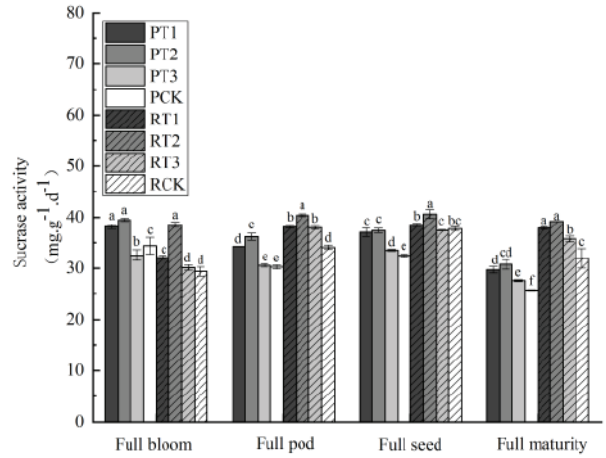


Fig. 6: Effects of different tillage measures on soil sucrose activity.

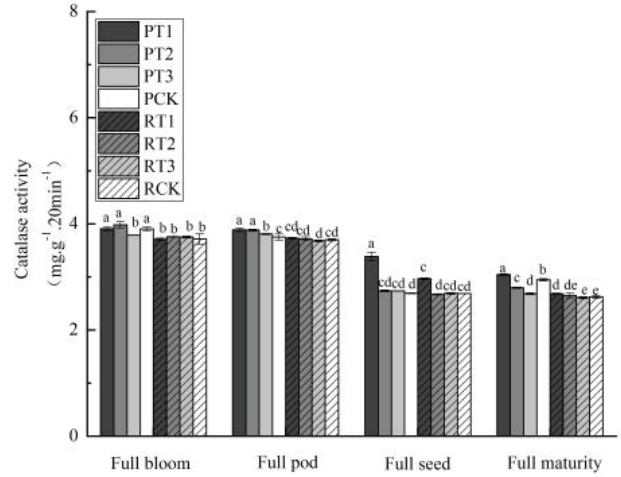


Fig. 7: Effects of different tillage measures on soil catalase activity.

not significant. In the mature period, the changing trend of soil catalase is the same as that in the seed filling period, and the soil catalase of PT1 and RT1 has a higher activity, which may be caused by the fact that, with the abundant rain this year, the soil treated by deep scarification (T2, T3) retains more water, which is not conducive to the metabolism of roots and soil microbes, resulting in the decrease of the activity. However, the earthing up treatment (T1, CK) just avoids this situation. The fact that PT2 and RT2 (addition of soil for V4 to V5) are higher than T3 can further indicate that the earthing up can increase the soil catalase activity.

## DISCUSSION

The soil microbial quantity, soil enzyme activity and nutrient have a great impact on the growth and development of soybean (Wei et al. 2018, Gai et al. 2019), and different farming measures will all affect greatly the soil environment (Zhang et al. 2019). Soil microbes are the main decomposers of soil micro-environment, and play a positive role in the transformation of soil nutrients and increase of soil moisture retention (Wei et al. 2018, Gai et al. 2019, Zhang et al. 2019, Li et al. 2018). A study by Vida et al. (2016) shows that the rotary tillage is more conducive to the increase of soil microbial quantity than the ploughing, and the microbial community structure can be improved. The study of Zhang (2018) indicates that deep scarification helps to improve the living environment of soil microbes, thereby contributing to the increase of soil microbial quantity, and thus affecting the improvement of genetic and functional diversity of soil microbes. Similarly, this experiment shows that in the flowering period of soybean, the quantity of soil bacteria and actinomycetes by the ploughing is higher than that by the rotary tillage. But the fungi hold the opposite direction, this is because, in the early period of soybean growth, the ploughing can cause the soil gap big and the soil temperature and humidity to be increased. Therefore, the mineralization rate of soil organic carbon is increased, which is beneficial to the survival of microorganisms. After entering the pod-setting period and seed filling period of soybean, the quantity of soil bacteria, fungi and actinomycetes produced by the rotary tillage is higher than that of actinomycetes. It is because the rotary tillage has less soil disturbance than the ploughing, and the mineralization speed of organic carbon through the ploughing in the early period is too fast. The relatively loose soil layer increases the soil moisture and weakens the circulation of soil air. Therefore, the rotary tillage can provide a more stable habitat, which is inconsistent with the study of Jia et al. (2018), maybe which is caused by the differences in rainfall and other issues in different years. Similarly, through the same tillage method, the microorganisms treated by the advanced inter-tillage (T1, T2) are higher than CK, which is because the advanced deep scarification or earthing up can increase the soil temperature in the soybean seedlings period and achieve the purpose of soil moisture conservation. Therefore, it provides a suitable habitat for the soil microorganisms. On the other hand, the quantity of microorganisms treated by the deep scarification (T2, T3) is also higher than that treated by the earthing up (T1, CK). It is because the deep scarification can change the surface weeds into the soil layer, which not only improves the permeability of the soil but also provides more nutrients for the soil microorganisms, contributing to the increase of the number of soil microorganisms.

The soil enzymes get involved in the circulation of materials and the flow of energy in the soil environment. The activity level of soil enzymes reflects the relative intensity

of various biochemical processes in the soil (Martin et al. 2006). Its activity is one of the important indicators to comprehensively evaluate the change of soil quality and detect the activity and quantity of soil microorganisms (Zhou et al. 2018, Li et al. 2018). The studies of Li et al. (2018) indicate that, compared with the ploughing, the rotary tillage can increase the soil enzymes in the soil surface layer (0~20 cm), but for the soil enzymes in the 20~40 cm soil layer, the case is opposite. The studies of Ding et al. (2017) and others show that the rotary tillage combined with other technical measures increases the activity of soil enzymes, compared with ploughing. But the study of Zhang & Wu (2018) shows that the activities of soil urease, phosphatase, invertase and catalase treated by the ploughing are higher than those treated by the rotary tillage, which is the same as the results of this experiment. In this experiment, except for the invertase, the enzymatic activities of soil urease, phosphatase and catalase in each period all indicate that the ploughing > rotary tillage, which may be caused by the fact that the ploughing can turn the preceding crops and other plant residues into the deeper soil layer, which not only increases the permeability and fertility of the soil, but also breaks the plough sole to create greater habitat for soybean roots and microorganisms, thus contributing to the improvement of soil enzyme activity. The invertase shows an opposite rule because invertase is often positively related to the content of soil organic matter. The soil ploughing increases the mineralization rate of soil organic carbon, accelerates soil respiration, decreases the content of organic matter, which reduces the catalytic substrate of the invertase, resulting in a decrease in the activity. The study of Zhang (2017) shows that the soil deep scarification in different tillage measures increases the activity of soil enzyme, but the catalase activity decreases, which is consistent with the experimental result. Similarly, in the experiment, under the same farming conditions, except for catalase, the enzyme activity through the deep scarification treatment is also improved to some extent, compared to the earthing up treatment. Luo (2009) also has a similar report. It is probably because the deep scarification reduces the unit density and hardness of the soil, making the damp heat condition of soil more reasonable, and thus provides a better growing environment for soybean roots and soil microorganisms, which in turn makes the roots and the metabolic activities of microbes more active, and finally, the enhancement of organisms' secretion increases the enzyme activity. The experiment also shows that the enzyme activity gained by the advanced inter-tillage (T1, T2) is increased more greatly than that gained by the corresponding treatment (CK, T3), indicating that the advanced inter-tillage and the "release the coldness" and the soil moisture conservation in the early period are beneficial to the rooting of soybeans and also play a positive role in the improvement of the soil environment.

## CONCLUSIONS

The tillage method affects the soil environment greatly, and then the growth and development of the soybean are affected, ultimately affecting the increase in yield. The frequent disturbance to the soil is not conducive to the growth of microorganisms, resulting in a decrease of the bacteria, fungoid and actinomycetes in the soil. Among them, the quantity of the bacteria, fungi and actinomycetes through the ploughing and treatment of PT1 in the maturity period reduces respectively by 11.7%, 23.4% and 11.4%, compared with the treatment of RT1 by the rotary tillage.

Compared with the microorganism, except for the invertase, the ploughing increases the activity of various enzymes in the soil than the rotary tillage, as well as the activities of the urease, phosphatase and catalase. PT2 treated by ploughing increases by 1.12%, 4.32%, 5.47% respectively than that treated by the rotary tillage in the mature period, but the invertase PT2 reduces by 21.6%, compared to RT2.

Besides, the advanced inter-tillage improves the soil environment significantly, the number of the soil microorganisms and the activity of enzymes are improved in different degrees, at the same time, deep scarification has a greater improvement than soil heaping, especially deep scarification reduces the number of the soil fungi and increases the number of bacteria, a more rational soil microbial community structure is created.

Therefore, no matter which tillage method is used, the properly advanced inter-tillage (especially deep scarification) after sowing can be conducted, which will have a positive effect and significant role in the improvement of the soil environment.

## ACKNOWLEDGMENTS

This work was supported by the "National Key R&D Projects" (2018YFD1000905), "Natural science foundation of Heilongjiang province"（C2017049), "Key Scientific Research Projects of Heilongjiang Farms and Land Reclamation administration (HKKY190206-1)" and "School start-up plan" (XBD-2017-03).

## REFERENCES

Bao, S.D. 1999. Soil Agrochemical Analysis. China Agriculture Press, Beijing, 37-154.

Chen, C., Lv, C.H., Fan, L. and Wu, H. 2011. Effects of land use change on soil organic carbon. Acta Ecologica Sinica, 31(18): 5358-5371.

Chen, C., Wu, J.G. and Yang, Z.Y. 2014. Effects of different manures and

their mixed application on the dynamic changes of soil enzymes activity for black soil. Journal of Water and Soil Conservation, 28(06): 245-250.

Ding, S.J., Xiong, S.P., Ma, X.M. Zhang, J.J. and Wang,X.C. 2017. Effects of tillage and nitrogen application rate on soil nitrogen transformation and yield in a winter wheat/summer maize multiple cropping system. Europe PMC, 28(01): 142-150.

Gai, Z.J., Wu, J.Y., Zhang, J.T. Liu, J.Q., Cai,L.J. and Du, J.X. 2019. Effects of continuous rotation and no-till of soybean-corn on soil nutrients and crop yield. Chinese Agricultural Science Bulletin, 35(05): 100-106.

Gong, Z.T. 1999. Chinese Soil Taxonomy. Science Press, Beijing, 404-409.

Jia, F.M., Zhang, S.H. and Wei, Y.D. 2018. Variation of soil nutrients and soil microbial activities of different tillage systems in farmland. Research of Soil and Water Conservation, 25(05): 112-117.

Li, H.Y., Zhang, J.G., Yao, T., Yang, X.Z, Gao, Y.M., Li, C.Q., Li, Y. and Feng, Y. 2018. Soil nutrients, enzyme activities and ecological stoichiometric characteristics in degraded alpine grasslands. Journal of Soil and Water Conservation, 32(05): 287-295.

Li, L.N., Xi, Y.G., Chen, E., He, L.P., Wang, L., Xiao X.J. and Wang, L. 2018. Effects of tillage and green manure crop on composition and diversity of soil microbial community. Journal of Ecology and Rural Environment, 34(04): 342-348.

Li, Z., Jing, W., Guo, Z.F. and Zhao, Y.G. 2018. Rotary tillage in rotation with plowing tillage improves soil properties and crop yield in a wheat-maize cropping system. PLOS ONE, 13(6): 198-193.

Lucas, W.M., Maria, J.L.B., Eiko, E.K. and Siu, M.T. 2015. Land-use system shapes soil bacterial communities in Southeastern amazon region, Applied Soil Ecology, 95: 151-160.

Luo, A. 2009. Effect of different tillage on soil physical chemistry and biology character and yield of soybean. Heilongjiang Bayi Agricultural University, Daqing.

Martin, D.L., Jose, R. and Jose, C.G.H. 2006. Post-fire vegetation succession in Mediterranean gorse shrublands. Acta Oecologica, 30(1): 54-61.

Pan, J. 2015. The dynamic study on soil microbial diversity of suburb plastic greenhouse in Huhhot. Inner Mongolia Agricultural University, Huhhot.

Peng, Z.K., Li, L.L., Xie, J.H., Deng, C.C., Eunicee, E., Wang, J.B., Hu, J.H., Shen, J.C. and Kang, C.R. 2018.
Effects of different tillage practices on water consumption structure and water use efficiency during crop growth period in arid farmland. Journal of Water and Soil Conservation, 32(5): 214-221.

Ryan, M.P. and Adley, C.C. 2010. *Sphingomonas paucimobilis*: A persistent Gram-negative nosocomial infectious organism. Journal of Hospital Infection, 75(03): 153-157.

Sui, P.X., Zhang, X.Y., Wen, X.F., You, D.B., Tian, P. and Qi, H. 2016. Effects of tillage and straw management on nutrient contents and enzyme activities of brown soil. Chinese Journal of Ecology, 35(08): 2038-2045.

Vida, K., Fayez, R. and Mohammad, A. 2016. Tillage effects on soil microbial biomass, SOM mineralization and enzyme activity in a semi-arid calcixerepts. Agriculture, Ecosystems & Environment, 232(16): 73-84.

Wang, B.S., Cai, D.Y., Wu, X.P., Li, J., Liang, G.P., Yu, W.S., Wang, X.L., Yang, Y.Y. and Wang, X.B. 2015. Effects of long-term conservation tillage on soil organic carbon, maize yield and water utilization. Journal of Plant Nutrition and Fertilizer, 21(06): 1455-1464.

Wang, X.L., Ma, K., Wang, Z.Q., Li, Y. and Wei, C.H. 2018. Effects of no-tillage, mulching and organic fertilization on soil microbial composition in winter wheat field. Chinese Journal of Eco-Agriculture, 12-23.

Wei, C.Z., Nong, Y.Q., Cen, Y.Q., Chen, H.S., Wei, J.J., Li, J.T. and Lu, J.M. 2018. Effects of tea and soybean intercropping on soil microbial community and enzyme activity. Acta Agriculturae Boreali-Occidentalis Sinica, 27(04): 537-544.

Wu, L.F., Li, B.B., Qin, Y. and Ed, G. 2017. Soil $CO_2$ emission and carbon budget of a wheat/maize annual double-cropped system in response to tillage and residue management in the North China plain. International Journal of Agricultural Sustainability, 15(03): 253-263.

Yu, Z.L., Qiu, L.F. and L.L. 2017. Influence of land use changes on soil organic carbon distribution in agricultural soils. Acta Agriculturae Zhejiangensis, 29(05): 806-811.

Zhang, B.W. 2018. Effects of subsoiling on soil properties and bacterial community structure in black soil region. Inner Mongolia Agricultural University, Huhhot.

Zhang, D.X. and Wu Q. 2018. Effects of different tillage method on soil nutrient content and enzyme activities. Jiangsu Agricultural Sciences, 46(11): 234-237.

Zhang, F., Huang, F.Q. and Xiao, X.P. and Wu, J.M. 2009. Short-term influences of winter crops on microbial biomass carbon, microbial biomass nitrogen and $C_{mjc}$-to-$C_{org}$ in a paddy soil. Acta Ecologica Sinica, 29(02): 734-739.

Zhang, G.Y., Lv, B.B., Zhang L.P., Liu, Z., Fan, Q.L., Wei, M.F., Yao, Z., Yuan, J.W. and Cai, Y.J. 2019. Effect of long-term no-tillage with stubble on soil fertility and diversity of prokaryotic microbiome in dryland wheat soils on the Loess Plateau. Chinese Journal of Eco-Agriculture, 27(03): 358-368.

Zhang, W.C. 2017. Effects of tillage methods on soil physical and chemical properties and maize of yield formation. Heilongjiang Bayi Agricultural University, Daqing.

Zhao, Y.L., Guo, H.B., Xue, Z.W., Mu, X.Y. and Li, C.H. 2015. Effects of tillage and straw returning on microorganism quantity, enzyme activities in soils and grain yield. Chinese Journal of Applied Ecology, 26(06): 1785-1792.

Zhou, D.X., Li, L., Li, J., Ning, Y.C., Cao, X., Wu, X.H. and Rong, G.H. 2018. Effects of different fertilization treatments on soil microbial biomass and enzyme activities in maize-soybean rotation system. Chinese Journal of Ecology, 37(06): 1856-1864.

Nature Environment and Pollution Technology
An International Quarterly Scientific Journal

p-ISSN: 0972-6268
(Print copies up to 2016)
e-ISSN: 2395-3454

Vol. 19 | No. 4 | pp. 1453-1463 | 2020

Original Research Paper

https://doi.org/10.46488/NEPT.2020.v19i04.011

Open Access Journal

# Study on the Efficiency of the Synchronous Alkali-ultrasonic Pretreatment of the Low Organic Matter Sludge and its Influence on the Microbial Population in the Anaerobic Digestion System

**Shihu Liu*(**), Lei He*, Pengcheng Zhao*, Xuejie He*, Xingxing Zhuo* and Jian Zhou*†**

*Key Laboratory of the Three Gorges Reservoir's Eco-Environments, Chongqing University, Chongqing, 400045, P.R. China

**Chongqing Drainage Co. Ltd, Chongqing, 400045, P.R. China

†Corresponding author: Jian Zhou; liushihucq@126.com

**Nat. Env. & Poll. Tech.**
**Website: www.neptjournal.com**

*Received:* 10-12-2019
*Revised:* 03-01-2020
*Accepted:* 28-03-2020

**Key Words:**
Sludge
Alkali treatment
Ultrasound treatment
Anaerobic digestion
Archaea group

## ABSTRACT

To solve the problem of the low anaerobic digestion efficiency of the minimal organic matter sludge, the study proposes the synchronous alkali-ultrasonic pretreatment technology of the low organic sludge. The research results show that the collaboration between alkali and ultrasonic has significant effects on pretreatment efficiency. The pretreatment efficiency of the sorts is as follows: synchronous alkali-ultrasonic treatment > alkali-ultrasonic stepwise treatment > ultrasonic-alkali stepwise treatment > ultrasonic treatment > alkali treatment. The synchronous alkali-ultrasonic treatment system has strong processing effectiveness. Compared with the control group (the raw sludge), the concentrations of the supernatant SCOD and VFAs of the low organic matter sludge after the pretreatment increases by 15.4 times and 59.64 times respectively, and the supernatant that is easily biodegradable organic matter increases by 19.1%. The gas production after alkali-ultrasonic synchronous pretreatment of the anaerobic digestion system of the sludge increases 58% higher than the control group (without pretreatment ). The results of the high-throughput sequencing of 16S rRNA in the anaerobic digestion system of the sludge, at the genus level, show that the dominant functional bacteria in the system mainly includes vadinHA17, *Peptoclostridium*, Peptostreptococcaceae, *Tissierella, Syntrophomonas*, Synergistaceae and *Aminobacterium*. The dominant functional bacteria genera in the systematic archaea group mainly include *Methanosaeta* (70.33%), Unclassified (2.74%), *Methanosarcina* (15.49%), *Methanobacterium* (5.31%), *Methanospirillum* (2.18%), ARC26 (1.04%), *Methanobrevibacter* (1.62%). The abundance of functional bacteria at the genus level was higher than that in the control group.

## INTRODUCTION

The anaerobic digestion of the surplus sludge in urban sewage treatment plants is considered to be the most effective way for sludge treatment and recycling due to its potential for energy recovery and environmental hazards reduction. The biogas generated through anaerobic digestion can be used to generate electricity, which can offset about 25%~30% of the electricity consumption in the whole sewage treatment plant (Carrere et al. 2010). At present, the sewage treatment scale of the urban sewage plants in China has been up to 210 million $m^3$/d, and the sludge treatment scale has reached 37000 t/d. However, the organic content of the sludge (VSS/TSS) in China is usually 20%~50%, far lower than 70%~80% in developed countries (He et al. 2007), and the sand content in the sludge is 30%~46%. The low organic sludge has severely restricted the application and development of the sludge anaerobic digestion technology.

Sludge pretreatment by alkali technology, namely dosing alkaline reagents, could induce the depolymerization of the refractory organic in the sludge through the solvation and saponification of reagents and facilitate the enzymatic reaction with the extracellular hydrolase. Moreover, it provides additional alkalinity for the anaerobic digestion system and improves the activity of the methane bacteria and the stability of the anaerobic digestion system. NaOH is considered to be the most effective reagent for the cell decomposition and sludge dissolution (Jang & Ahn 2013). The low pH environment can only destroy the EPS but not the cell structure in the sludge. The high pH environment can destroy the cell wall and produce the saponification reaction with the lipids contained in the cell membrane and dissolve it. When the pH is 12, the COD dissolution rate can reach 43.5%, and the rise in the rate of SCOD slows down when the pH continues to increase (Delgèns et al. 2000). However, the excessive high metal ions will inhibit microbial metabolism and reduce the

methane production capacity of the system (Li et al. 2012). Generally, it may be solved by coordination with other methods. For example, when the temperature is raised to 140°C (pH=12, contact 30min), the COD dissolution rate can be increased by 51%. However, the thermo-alkali technology has some problems such as high energy consumption and equipment corrosion.

The ultrasonic technology for sludge pretreatment mainly uses the cavitation effect of the low-frequency ultrasonic wave to generate resonance in the sludge to form the cavitation bubbles. The strong jet flow formed by the burst of the bubbles creates a huge shear force in the liquid to destroy the flocs and microbial cells (Neis et al. 2000). The higher frequency ultrasonic generates a large number of hydroxyl radicals, which can enhance the chemical reaction, while the lower frequency ultrasonic generates a relatively stronger shock wave, that can cause a cracking effect (Zhang et al. 2008). It is generally observed that when the ultrasonic frequency is at 20kHz~41kHz, the cracking effect in the sludge is the most effective, and the sludge particle size is significantly reduced. During the ultrasonic pretreatment of the sludge, the SCOD dissolution rate enhances with the increasing action time and power density. However, when the action time of the sludge is more than 45 min or the power is higher than 0.8 W/mL, the effect begins to weaken (Huan et al. 2009).

When alkali and ultrasonic pre-treat the sludge individually, the upper limit of SCOD/TCOD is 50%. When alkali treatment is first followed by ultrasonic treatment, SCOD/TCOD improves to 70% (Kim et al. 2010). Alkali pretreatment has the vital role on the subsequent ultrasonic pretreatment efficiency of the sludge, and adding alkaline makes soluble cell metabolic product in the supernatant, and the ultrasonic destroys some of the matters (Ni et al. 2009). However, it will not fundamentally change the compositions and chemical structures of the organic matters in the sludge supernatant (Chen et al. 2003, Wang et al. 2019). The above studies on the pretreatment technologies are all based on the high organic matter sludge as the research object. There are few reports on the enhanced pretreatment of the low organic matter sludge.

Aimed at the problem of the low anaerobic digestion performance of the low organic matter sludge, this study proposes alkali-ultrasonic pretreatment technology by investigating the low organic matter sludge in an urban sewage plant as the research object. Through setting the control group (without pretreatment, alkali treatment, ultrasonic treatment, ultrasonic-alkali stepwise treatment, alkali-ultrasonic stepwise treatment), that investigates the alkali-ultrasonic pretreatment efficiency in the low organic matter sludge, adopts the three-dimensional fluorescence to analyse the dissolvable organic matter in the low organic matter sludge. At the same time, it studies the anaerobic digestion efficiency of the sludge before and after the synchronous alkali-ultrasonic pretreatment , furthermore, uses the 16S rRNA high-throughput sequencing technology to explore the influence of the anaerobic digestion of the sludge on the microbial population in the system. The study will open a new way to improve the anaerobic digestion efficiency of the low organic matter sludge.

## MATERIALS AND METHODS

**Experimental sludge quality:** The experimental sludge was taken from the residual sludge in the second sedimentation tank of a municipal sewage plant. The characteristics of raw sludge are given in Table 1.

**3D-EEM and FRI technology:** The organic matters can be divided into five parts (Table 2) by using the 3D-EEM (Excitation-Emission Matrix) and FRI (Fluorescence Regional Integration) technologies according to the difference of the excited emission wavelengths. The biological acceptability and biodegradability of the matters in the Fluorescence Area I and II are outstanding. The matters in Fluorescence Area III and V usually have poorer biological acceptability and biodegradability. And the matters in Fluorescence Area IV are the microbial metabolic by-products usually, protein complexes, which generally have positive effects on biodegradability (Meng et al. 2011). Therefore, the contents of the organic matters with better biodegradability in the sludge DOM can be reflected in Area I, II and IV, and the contents of the organic matters with the worse biodegradability in the sludge supernatant can be reflected in Area III and V.

Table 1: Experimental sludge quality.

| Index | Concentration | Index | Concentration |
|---|---|---|---|
| pH | 7.61±0.2 | Soluble protein (mg/L) | 40.28±3.6 |
| TSS (g/L) | 26.22±3.5 | Soluble polysaccharide (mg/L) | 7.54±0.2 |
| VSS (g/L) | 6.06±4.4 | VFAs (mg/L) | 0.08±0.003 |
| VSS/TSS (%) | 23.11±5.6 | DNA (mg/L) | 2.22±0.2 |
| SCOD (mg/L) | 242.46±12.6 | Ammonia nitrogen (mg/L) | 39.15±1.7 |
| TCOD (mg/L) | 16767.00±32.7 | Phosphate (mg/L) | 1.53±0.2 |

Table 2: Ex/Em wavelengths of fluorescence region of liquid-phase organic matter after different alkali and ultrasonic pretreatment s of the sludge.

| Area number | Typical matter | Ex/Em wavelengths |
|---|---|---|
| Ⅰ | Tyrosine-protein | 200nm~250nm/200nm~330nm |
| Ⅱ | Tryptophan-protein | 200nm~250nm/330nm~380nm |
| Ⅲ | Fulvic acid-organic matter | 200nm~250nm/380nm~500nm |
| Ⅳ | Soluble microbial by-products | 250nm~280nm/200nm~380nm |
| Ⅴ | Humic acid-organic matter | 250nm~400nm/380nm~500nm |

**16S rDNA high-throughput sequencing:** 1) DNA extraction. An appropriate amount of the sludge mixture was taken and centrifuged at a high speed 5000r/min, 4°C for 5min. The centrifuged sludge was stored in a refrigerator at -20°C for DNA extraction. Genome DNA of the sludge samples is extracted by using Bead Beater and three times repeated freeze-thaw method in boiling water and liquid nitrogen (Wang et al. 2018). After the genome DNA extraction, the extracted genome DNA is detected by 1% agarose gel electrophoresis. 2) Construction of 16S rDNA gene bank.

The V1-V3 Areas of the 16S rDNA gene are amplified by using bacterial capture primers 27F (5'-AGAGTTTGATCMTGGCTCAG-3') and 533R(5'-TTACCGCGGCTGCTGGCAC-3'). The different samples are distinguished by adding labels. Amplification is performed on GeneAmp®9700 (ABI) PCR instrument. The loading amount is 20 μL, including 0.4M forward and reverse primers, 1μL DNA template, 250 nM dNTP and 1×FastPfu Buffer. PCR operation conditions are as follows: electrophoresis at 95°C for 2min, electrophoresis at 95°C for the 30s, and full operation for 25 times. Renaturation at 55°C for the 30s, extension at 72°C for 30s. All samples were carried out following the formal test conditions, with 3 replicates for each sample. The PCR products were detected and quantified by using the QuantiFluor™-ST blue fluorescence quantification system (Promega Company). After adjusting the sequence to an appropriate level, PCR amplification products were sequenced by using standard Illumina platform. Mothur and QIIME programs were used to aggregate valid sequences with the same classification.

**The particle size distribution of the sludge:** The Mastersizer 2000 laser particle size analyser was used to determine the particle size distribution of the sludge. The parameters of the instrument were as follows: the matter measurement range 0.02-2000 um, the recurrence rate >0.5%, the accuracy rate >1%, the data collection speed 1000 times/s. The measurement of a sample can be completed every 15s. The instrument can calculate the cumulative volume fraction and the average particle size of the sample automatically.

**Study on efficiency of the synchronous alkali-ultrasonic pretreatment of the low organic matter sludge:** Parallel experiments (set control groups) were used to investigate the efficiency of the alkali-ultrasonic synchronous pretreatment (pH=10, ultrasonic frequency 28kH, power density 0.4 W/mL, contact reaction time 30min) of the low organic matter sludge, and 5 control groups were set in parallel at the same time. Control group 1: without pretreatment; Control group 2: alkali treatment (pH=10, reaction time 30min); Control group 3: ultrasonic treatment (ultrasonic frequency 28kH, power density 0.4 W/mL, contact time 30min); Control group 4: ultrasonic-alkali stepwise treatment (ultrasonic frequency 28kH, power density 0.4 W/mL, contact time 15min; pH=10, reaction time 15min); Control group 5: alkali-ultrasonic stepwise treatment (pH=10, reaction time 15min; ultrasonic frequency 28kH, power density 0.4 W/mL, contact time 15min). The supernatant SCOD, soluble protein, soluble polysaccharide, VFAs, DNA and other indicators of the sludge before and after pretreatment were tested to characterize the efficiency of the pretreatment.

**Study on the organic matter conversion rules in the synchronous alkali-ultrasonic pretreatment system of the low organic matter sludge:** The liquid phase organic matter species of the synchronous alkali-ultrasonic pretreatment system of the low organic matter sludge and the control group (without pretreatment) were tested by the three-dimensional fluorescence spectroscopy technology to analyse the organic matter conversion rules. Besides, the laser particle size analyser was used to test the indexes such as the particle size and the distribution of the sludge, of the synchronous alkali-ultrasonic pretreatment system of the low organic matter sludge and the control group (without pretreatment).

**Study on the influence of the synchronous alkali-ultrasonic pretreatment of the low organic matter sludge on the anaerobic digestion system and the microbial population:** The treatment efficiency of the anaerobic digestion system (SRT 30d) of the synchronous alkali-ultrasonic pretreatment of the low organic matter sludge (pH=10, ultrasonic frequency 28 kHz, power density 0.4 W/mL, contact reaction time 15min) and the control group (without pretreatment without pretreatment) is investigated by the parallel experiments. The influence of 16S rRNA high-throughput sequencing on the microbial population is analysed by using the structure of the microbial population and the functional bacteria of archaea group in the synchronous alkali-ultrasonic pretreatment system of the

low organic matter sludge and the control group (without pretreatment).

## RESULTS AND DISCUSSION

Study on the efficiency of the synchronous alkali-ultrasonic pretreatment of the low organic matter sludge: The experimental results of the influences of the alkali and ultrasonic treatment methods on the pretreatment efficiency of the low organic matter sludge are shown in Fig. 1.

As presented in Fig. 1, the alkaline and ultrasonic treatment methods have a significant influence on the pretreatment efficiency of the low organic matter sludge. After pretreatment with synchronous alkali-ultrasonic treatment, the SCOD in the sludge supernatant increases to 7496 mg/L, which is enhanced by 15.44, 10.36, 1.05, 0.91 and 0.59 times compared with the control groups (without pretreatment 456 mg/L, alkaline treatment 660 mg/L, ultrasonic treatment 3644 mg/L, ultrasound-alkali stepwise treatment 3916 mg/L and alkali-ultrasonic stepwise treatment 4700mg/L). The VFAs of the sludge supernatant increase to 505.14mg/L, which is 59.64, 14.64, 2.03, 1.31 and 0.61 times higher than those of the control groups (without pretreatment 8.33mg/L, alkali treatment 32.30mg/L, ultrasonic treatment 166.69mg/L, ultrasound-alkali stepwise treatment 218.60mg/L and alkali-ultrasonic stepwise treatment 314.49mg/L). The soluble proteins increase by 23.25, 9.44, 1.10, 0.79 and 0.39 times respectively, and the soluble polysaccharides elevate by 14.13, 4.81, 0.33, 0.17 and 0.11 times respectively. The order of processing efficiency is as follows: synchronous alkali-ultrasonic treatment > ultrasound-alkali stepwise treatment > alkali-ultrasonic stepwise treatment > ultrasonic treatment > alkali treatment. The synchronous alkali-ultrasonic treatment system has a strong treatment efficiency.

The sludge can promote the dissolution of EPS and the microbial cytoplasm under the action of alkali (Jang & Ahn 2013). Low frequency ultrasonic wave can have stronger cavitation effect, which can break the cell wall and promote the transfer of the organic matters from the sludge to the liquid phase to a greater extent (Neis et al. 2000). During the synchronous alkali-ultrasonic action, the addition of alkali makes the flocculation structure of the sludge to become enlarged, so that the cavitation bubbles generated by ultrasonic reaction have a larger reaction area with EPS and microorganisms. And the change of the reaction sequence between ultrasonic and alkali significantly weakens this effect (Ni et al. 2009).

**Study on the organic matter conversion rules in the synchronous alkali-ultrasonic pretreatment system of the low organic matter sludge:** The liquid phase 3D-EEM spectra and FRI analysis integral results after the low organic matter sludge treated by the different pretreatment systems are shown in Fig. 2.

As presented in Fig. 2, after the low organic matter sludge is pre-treated in different methods, it significantly promotes the dissolution of the easily degraded organic matter in the sludge. The total fluorescence intensity of the sludge supernatant increases to 24.58×107 (a.u.) after the synchronous alkali-ultrasonic pretreatment of the low organic matter sludge, while the control groups are without pretreatment 5.63×107 (a.u.), alkali pretreatment 10.82×107 (a.u.), ultrasonic pretreatment 15.41×107 (a.u.), ultrasound-alkali stepwise pretreatment 21.83×107 (a.u.), and alkali-ultrasonic stepwise pretreatment 22.19×107 (a.u.). The fluorescence intensities of the Areas

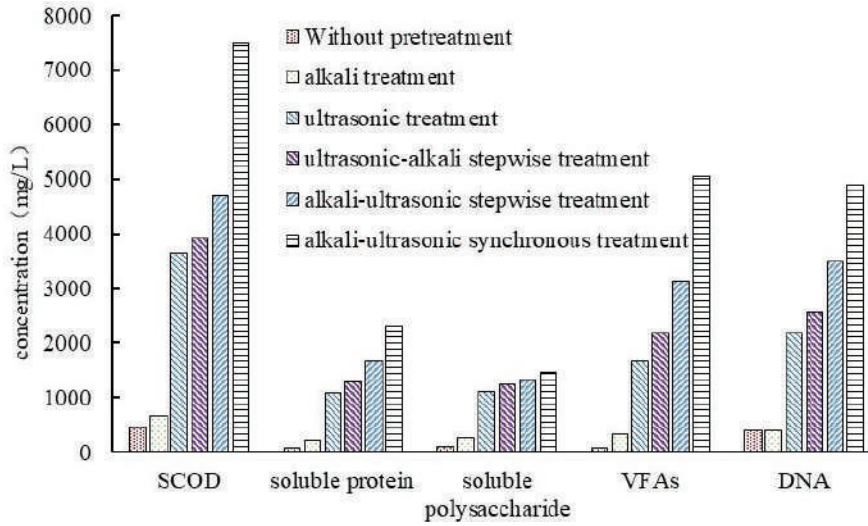


Fig. 1: Influence on the pretreatment efficiency of different alkaline and ultrasonic treatment methods of the sludge.

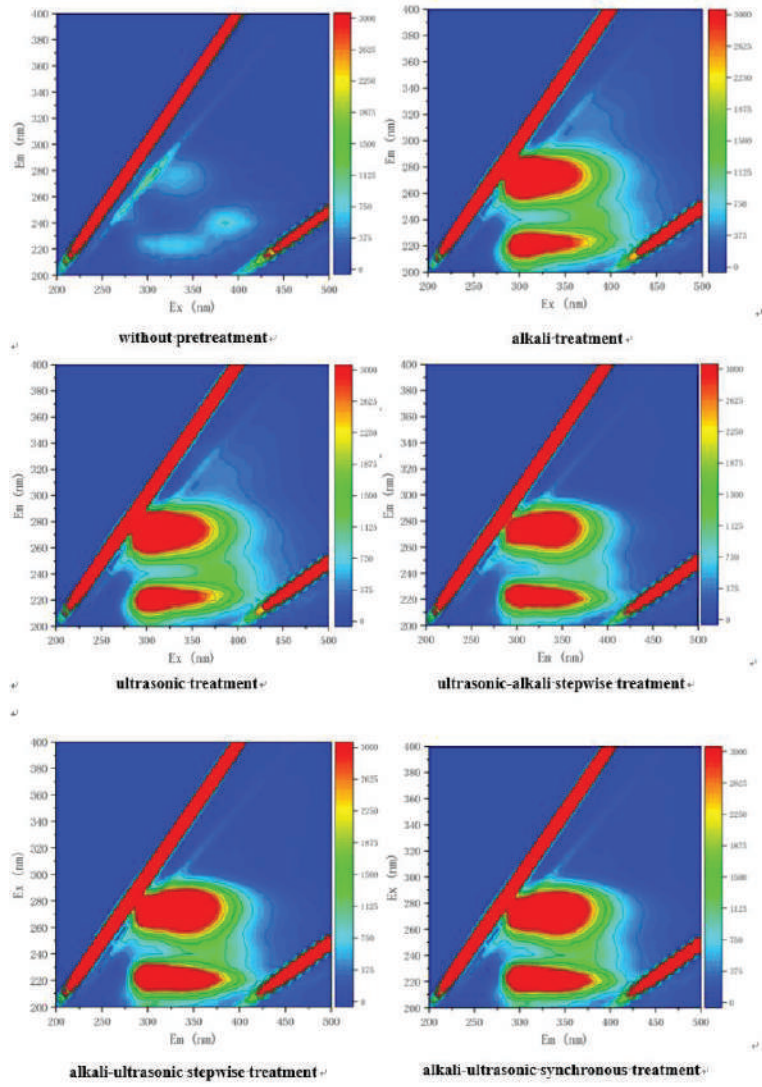


(a)

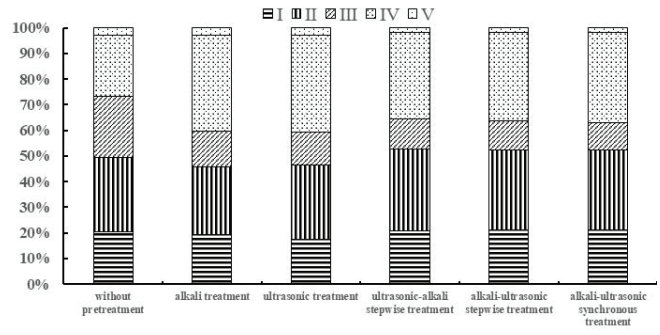


(b)

Fig 2: (a) Liquid phase three-dimensional fluorescence spectra and (b) FRI analysis integral diagram of different sludge pretreatment systems.

of easily biodegradable matters (Area I, II and IV) (Sun et al. 2016) account for 80.74%, 81.12%, 86.64%, 86.00% and 87.35%, higher than the control group (73.34%) by 10.1%, 10.6%, 18.1%, 17.3%, 19.1% , respectively.

These results show that the actions of alkali and ultrasonic in different methods have not only affected the pretreatment of the sludge flocculation and the breakage of the cell wall to make organic matter dissolute but also promote fulvic acids, quinones, humic acid, other organic matter such as polycyclic aromatic hydrocarbons and other large molecule organic matters to transfer into small molecule organic matters by the alkaline hydrolysis "catalyst" function and the ultrasonic cavitation effect, which have certain modification effect on the soluble organic matters (Ni et al. 2009). The organic dissolution and modification effects of the synchronous alkali-ultrasonic pretreatment method are best. The dissolvable organic matters are mainly tyrosine, tryptophan and microbial products and other easily biodegradable organic matters. However, the fluorescence peak types are the same, which indicate that alkali and ultrasonic pretreatment s will not fundamentally change the composition of the organic matters in the sludge supernatant (Chen et al. 2003).

**Study on the sludge morphology changes in the synchronous alkali-ultrasonic pretreatment system of the low organic matter sludge:** The experimental results of the influence of different pretreatment methods on the particle size distribution of the sludge are given in Table 3 and Fig. 3. Pretreatment has significant influence on the sludge morphology. After the synchronous pretreatment with alkali, ultrasonic and alkali-ultrasonic of the sludge, the average particle size of the sludge (D[4,3]) decreases from 80.279 μm without pretreatment to 76.858 μm, 36.003 μm and 30.241 μm, which decrease by %55.2 ,%4.3 and %62.3 respectively. The addition of alkali makes the negative charge on the surface of the sludge particles

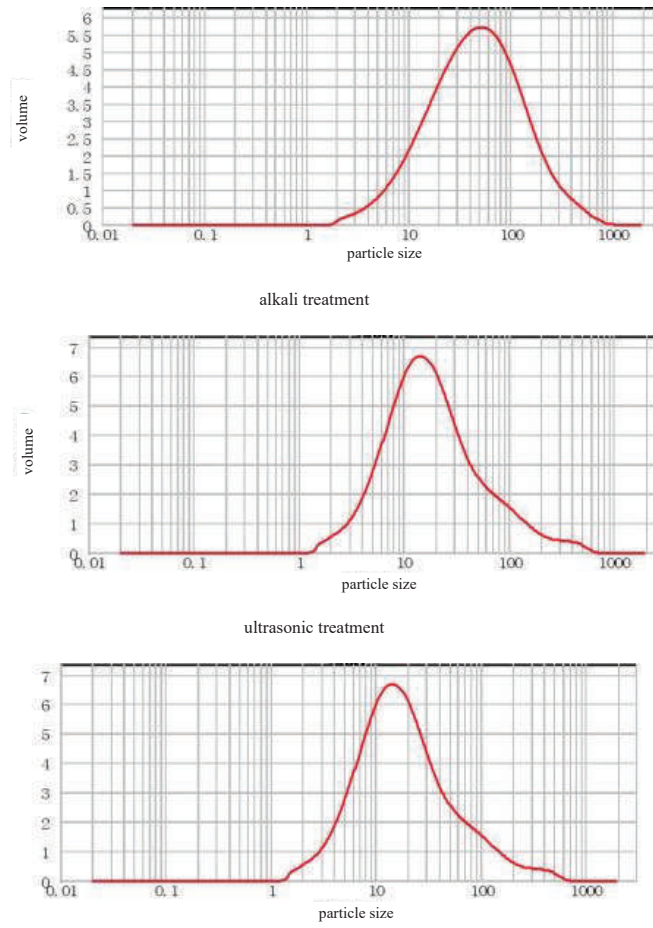


Fig. 3: The sludge particle size distribution change diagram of different alkali and ultrasonic pretreatment methods of the sludge.

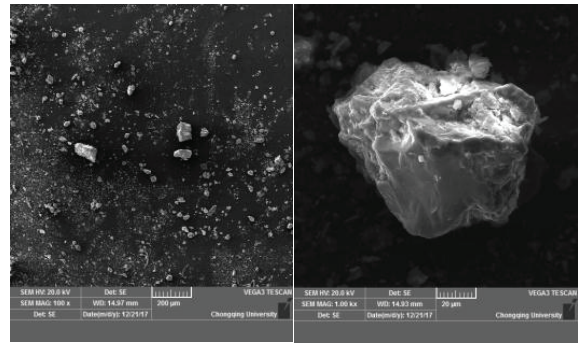

raw sludge

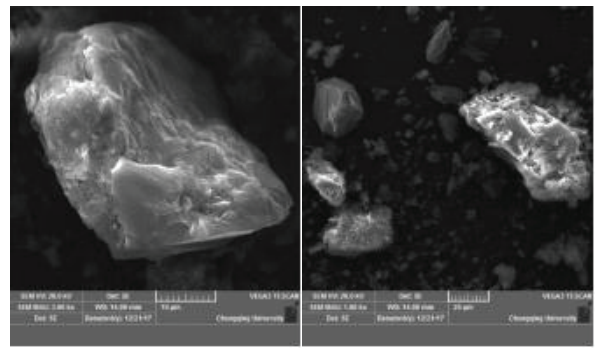

alkali treatment ultrasonic treatment

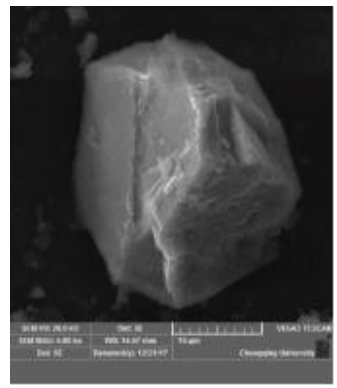

Synchronous alkali-ultrasonic treatment

Fig. 4: SEM diagram before and after treatment of different pretreatment methods of the sludge.

Table 3: Particle size distribution statistics.

| Sample | Control group | Alkali treatment | Ultrasonic treatment | Synchronous alkali-ultrasonic treatment |
|---|---|---|---|---|
| d(0.1)/μm | 11.45 | 11.228 | 5.375 | 7.151 |
| d(0.5)/μm | 47.823 | 46.823 | 16.608 | 17.835 |
| d(0.9)/μm | 179.647 | 172.599 | 80.426 | 54.984 |
| D[3,2]/μm | 26.01 | 25.576 | 11.566 | 13.803 |
| D[4,3]/μm | 80.279 | 76.858 | 36.003 | 30.241 |

gradually increase, and the produced electrostatic force makes the extracellular polymer structure widen (Penaud et al. 1999). The cavitation and the shearing actions of the ultrasonic wave on the sludge promote the disintegration of the microbial flocculation. The combined actions greatly improve the dissolution of the large granular sludge and reduce the average particle size of the sludge.

The SEM results of the different pretreatment methods of the sludge are shown in Fig. 4. In the control group (raw sludge), the particle sizes of the sludge are different and the appearance is rough. The improvement effect of the alkali treatment on the surface appearance of the inorganic sand is not obvious. After the ultrasonic treatment, the sludge surface becomes smooth, and a large number of the organic matters in the sludge adhere to the sand and gravel. The ultrasonic wave causes vibration of water molecules, microorganisms and other solutes, which causes the organic matter to be detached from the sand and gravel, making the particle size smaller and the surface become smooth (Dai et al. 2017).

**Influence of the synchronous alkali-ultrasonic pretreatment on the anaerobic digestion system efficiency of the low organic matter sludge:** The BMP test results of the synchronous alkali-ultrasonic pretreatment of the sludge anaerobic digestion system with low organic matter sludge and the control group (without pretreatment ) are shown in Fig. 5. The gas production effect of the synchronous alkali-ultrasonic pretreatment sludge anaerobic digestion system is significantly improved compared with the raw sludge system without pretreatment . After the synchronous alkali-ultrasonic pretreatment , the SCOD and the VFAs in the sludge supernatant increase from 2040 mg/L and 305.87 mg/L to 10840 mg/L and 1303.80 mg/L respectively, and decrease to 808 mg/L, 49 mg/L, 4090 mg/L and 51 mg/L after 30 d operation. The gas production increases by 58% from 250 mL to 396 mL.

**Analysis of the microbial population in the anaerobic digestion system of the low organic matter sludge:** The 16S rRNA high-throughput sequencing results of the sludge samples S1 in the control group (the raw sludge anaerobic digestion system) and S2 in the experimental group (the synchronous alkali-ultrasonic pretreatment sludge anaerobic digestion system) are provided in Table 4. According to the analysis results of the biological population OUT, abundance and diversity, the anaerobic digestion system of the sludge in the experimental group gets 44,864 Tags, and the anaerobic digestion system of the control group gets 44,818 Tags. After the pretreatment , the sludge enters the anaerobic digestion system, and its biodiversity (Shannon index) decreases from 5.24 to 5.00.

The phylum biological population of the anaerobic digestion system of the sludge without pretreatment and after alkali-ultrasonic synchronous pretreatment is shown in Fig. 6. The 36 species phylum population were detected in the anaerobic digestion system of the unpretreated sludge, among which the abundances of 9 species are higher than 1%, Firmicutes (16.06%), Bacteroidetes (15.24%), Actinobacteria (16.13%), Chloroflexi (16.19%), Hydrooxidize Bacteria WS6 (13.09%), Proteobacteria (13.93%), Synergistetes (1.15%), Saccharibacteria (0.65%) and Planctomycetes (1.44%) respectively. The 32 species phylum populations are detected in the anaerobic digestion system of the sludge after the synchronous alkali-ultrasonic pretreatment. The microbial diversity decreases, among which the abundances of 9 phylum populations are higher than 1%, Firmicutes (35.98%), Bacteroidetes (13.34%), Actinobacteria (11.48%), Chloroflexi (10.51%), Hydrooxidize Bacteria WS6 (6.97%), Proteobacteria (4.64%), Synergistetes (8.22%), Saccharibacteria (1.60%) and Planctomycetes (1.06%).

The abundances of Firmicutes and Synergistetes in the experimental group increase by 1.24 times and 6.15 times re-

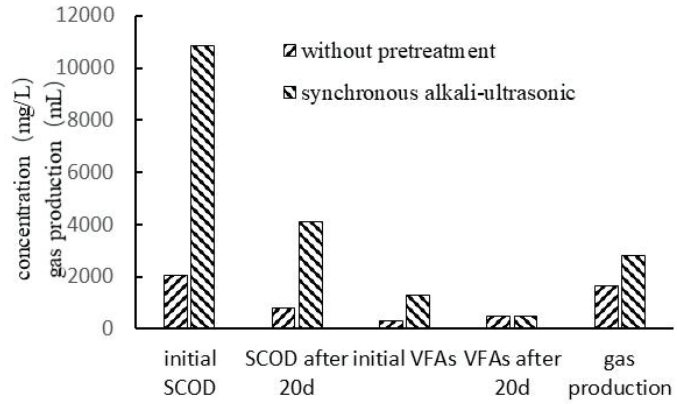


Fig. 5: Influence on the anaerobic digestive system efficiency of synchronous alkali-ultrasonic pretreatment of the low organic matter sludge.

spectively compared with those of the control group. Under the Firmicutes, the microbial genera can degrade the complex carbohydrates including cellulose into the small molecules such as acetic acid and butyric acid (Zhang & Lynd 2005). Synergistetes usually grow interactively with ethanotropic methanogens in the anaerobic digestion system to enable high-efficient operation of the anaerobic digestive system (Ahring 2003).

The genus microbial population of the anaerobic digestion system of the raw sludge and the sludge after the synchronous alkali-ultrasonic pretreatment are shown in Fig. 7. The dominant functional bacterial taxa in the system mainly include vadinHA17, *Peptoclostridium*, Peptostreptococcaceae, *Tissierella*, *Syntrophomonas*, Synergistaceae and *Aminobacterium*. Among them, vadinHA17, *Peptoclostridium*, Peptostreptococcaceae and *Tissierella* have the functions of producing acetic acid, propionic acid, butyric acid and other short-chain fatty acids (Ariesyady et al. 2007). The abundances in the test group are 8.91%, 6.32%, 3.37% and 3.23% respectively, which are largely improved compared with those in the control group (8.28%, 0.1%, 5.48% and 0.1%). The *Syntrophomonas* and Synergistaceae bacterial genera have the function of transforming fatty acids and other small molecular matters into acetic acid, hydrogen and carbon dioxide (Iino et al. 2007). The abundances of the experimental group are 3.08% and 3.06% respectively, which are significantly improved compared with those in the control group (1.22% and 0.1%). *Aminobacterium* has the function of amino acid degradation. The abundance of the experimental group (3.84%) is significantly improved compared with that of the control group (0.1%).

**Analysis of the archaea population in the anaerobic digestion system:** The results of the archaea OTU, abundance and diversity samples sequencing analysis are given in Table 5. The control group gets 32,288 Tags and the experimental group gets 42,585 Tags. After the synchronous alkali-ultrasonic pretreatment, the biodiversity (Shannon index) of the sludge in the anaerobic digestion system decreases from 3.39 to 2.32.

Table 4: Results of OUT, abundance and diversity samples sequencing depth analysis.

| Sample ID | Sequences | Ace | Chao | Shannon | Coverage |
|---|---|---|---|---|---|
| Control group (Samples of the system without pretreatment ) (S1) | 44818 | 757 | 759 | 5.24 | 0.9994 |
| Experimental group (Synchronous alkali-ultrasonic pretreatment of the sludge anaerobic digestion system samples) (S2) | 44864 | 714 | 737 | 5 | 0.99909 |

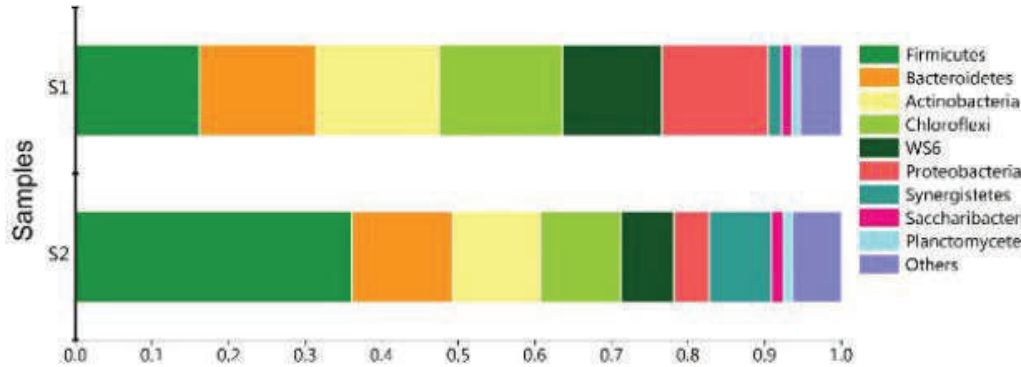


Fig. 6: Histogram of the phylum biological population in the anaerobic digestion system of the raw sludge and the sludge with the synchronous alkali-ultrasonic pretreatment.

Table 5: Results of archaea population OTU, abundance and diversity samples sequencing depth analysis.

| Sample ID | Sequences | Ace | Chao | Shannon | Coverage |
|---|---|---|---|---|---|
| Control group (Samples of anaerobic digestion system of raw sludge) (S1) | 42585 | 320 | 320 | 3.39 | 0.99976 |
| Experimental group (Samples of sludge anaerobic digestion system after synchronous alkali-ultrasonic pretreatment ) (S2) | 32288 | 227 | 216 | 2.32 | 0.99854 |

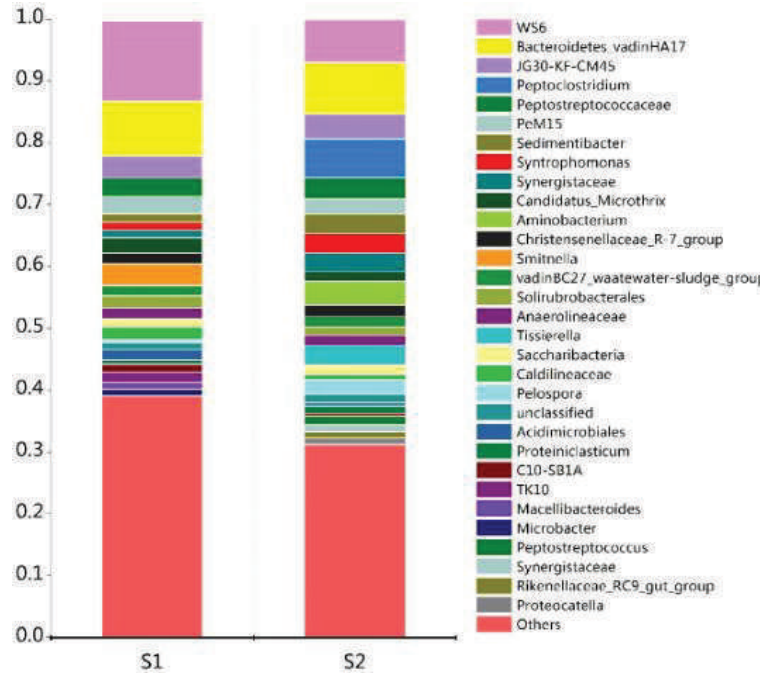


Fig. 7: Histogram of the genus biological population in the anaerobic digestion system of the raw sludge and the sludge with the synchronous alkali-ultrasonic pretreatment.

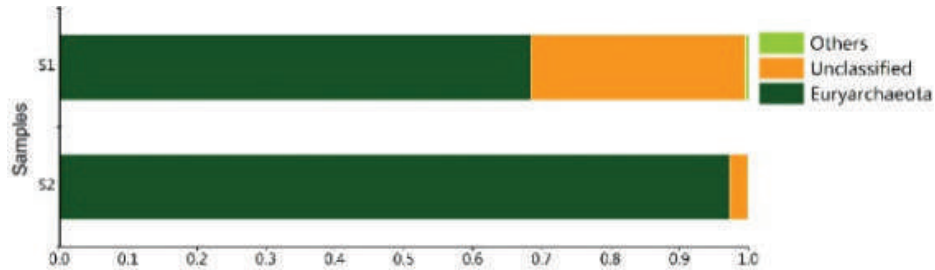


Fig. 8: Histogram of the phylum archaea populations in the anaerobic digestion system of the raw sludge and the sludge with the synchronous alkali-ultrasonic pretreatment.

The results of the phylum analysis of the system archaea organisms in the control group and the experimental group are shown in Fig. 8. The abundance of Euryarchaeota in the experimental group is 97.25%, an increase of 42% compared with 68.40% in the control group. Methanogens mainly belong to the microbial bacteria of Eurycloea, which is beneficial to improving the efficiency of the anaerobic digestion system.

The genera and species of archaea in the control group and the experimental group are shown in Fig. 9. The dominant functional genera in the experimental group are mainly *Methanosaeta* (70.33%), Unclassified (2.74%), *Methanosarcina* (15.49%), *Methanobacterium* (5.31%), *Methanospirillum* (2.18%), ARC26 (1.04%) and *Methanobrevibacter* (1.62%). Among them, *Methanosaeta* and *Methanosarcina* are acetotrophic methanogens (Sun et al. 2008), whose abundances are higher than those of the control group (54.5%, 0.22%). However, the abundances of $H_2$+$CO_2$ nutritive methanogens, such as *Methanobacterium* and *Methanospirillum*, have little changes compared with those of the control group, which may be related to the improvement of the abundances of the acetic acid bacteria in the hydrolytic acidification process.

## CONCLUSIONS

After the synchronous alkali-ultrasonic pretreatment of the low organic matter sludge, the dissolution of the large-particle sludge is enhanced. The average particle size of the sludge is

reduced. The dissolution and modification effects on the sludge organic matter are best. After the pretreatment, the concentrations of supernatant SCOD and VFAs increase by 11.36 times and 59.64 times respectively compared with those of the unpretreated system. The dissolved organic matters are mainly the biodegradable organic matters such as tyrosine, tryptophan and microbial products. The biodegradable matters are 19.1% higher than those of the unpretreated system, and their gas production is 58% higher than that of the unpretreated system.

The biological diversity of the anaerobic digestion system and the diversity of archaea are significantly reduced by the synchronous alkali-ultrasonic pretreatment of the low organic matter sludge, among which the abundances of Firmicutes and Synergistetes increase by 1.24 times and 6.15 times respectively compared with those of the control group. The dominant functional bacteria, such as vadinHA17, *Peptoclostridium*, Peptostreptococcaceae, *Tissierella*, *Syntrophomonas*, Synergistaceae, *Aminobacterium*, increase significantly. The dominant functional bacteria of the system archaea biological population genera mainly include *Methanosaeta* (70.33%), Unclassified (2.74%), *Methanosarcina* (15.49%), *Methanobacterium* (5.31%), *Methanospirillum* (2.18%), ARC26 (1.04%) and *Methanobrevibacter* (1.62%). The abundance of the functional bacteria is significantly higher than that of the control group.

## REFERENCES


Ahring, B.K. 2003. Perspectives for anaerobic digestion. Adv. Biochem. Eng. Biotechnol., 81: 1-30.

Ariesyady, H.D., Ito, T. and Okabe, S. 2007. Functional bacterial and archaeal community structures of major trophic groups in a full-scale anaerobic sludge digester. Water Res., 41(7): 1554-1568.

Carrere, H., Dumas, C., Battimelli, A., Batstone, D.J., Delgenes, J.P., Steyer, J.P. and Ferrer, I. 2010. Pretreatment methods to improve sludge anaerobic degradability: A review. J. Hazard. Mater., 183(1-3): 1-15.

Chen, W., Westerhoff, P., Leenheer, J.A. and Booksh, K. 2003. Fluorescence excitation-emission matrix regional integration to quantify spectra for dissolved organic matter. Environ. Sci. Technol., 37(24): 5701-5710.

Dai, X., Xu, Y. and Dong, B. 2017. Effect of the micron-sized silica particles (MSSP) on biogas conversion of sewage sludge. Water Res., 115: 220-228.

Delgèns, J.P., Penaud, V., Torrijos, M. and Moletta, R. 2000. Investigations on the changes in anaerobic biodegradability and biotoxicity of an industrial microbial biomass induced by a thermochemical pretreatment. Water Sci. Technol., 41(3): 137-144.

He, P.J., Lü, F., Zhang, H., Shao, L.M. and Lee, D.J. 2007. Sewage sludge in China: Challenges toward a sustainable future. Water Practice and Technology, 2(4): wpt2007083. doi10.2166/wpt.2007.083

Huan, L., Yiying, J., Mahar, R.B., Zhiyu, W. and Yongfeng, N. 2009. Effects of ultrasonic disintegration on sludge microbial activity and dewaterability. J. Hazard. Mater., 161(2-3): 1421-1426.

Iino, T., Mori, K., Tanaka, K., Suzuki, K. and Harayama, S. 2007. *Oscillibacter valericigenes* gen. nov., sp. nov., a valerate-producing anaerobic bacterium isolated from the alimentary canal of a Japanese corbicula clam. Int. J. Syst. Evol. Microbiol., 57(Pt 8): 1840-1845.

Jang, J.H. and Ahn, J.H. 2013. Effect of microwave pretreatment in presence of NaOH on mesophilic anaerobic digestion of thickened waste activated sludge. Bioresour. Technol., 131: 437-442.

Kim, D.H., Jeong, E., Oh, S.E. and Shin, H.S. 2010. Combined (alkaline+ultrasonic) pretreatment effect on sewage sludge disintegration. Water Res., 44(10): 3093-3100.

Li, H., Li, C., Liu, W. and Zou, S. 2012. Optimized alkaline pretreatment of sludge before anaerobic digestion. Bioresour. Technol., 123: 189-194.

Meng, F., Zhou, Z., Ni, B.J., Zheng, X., Huang, G., Jia, X., Li, S., Xiong, Y. and Kraume, M. 2011. Characterization of the size-fractionated biomacromolecules: tracking their role and fate in a membrane bioreactor. Water Res., 45(15): 4661-4671.

Neis, U., Nickel, K. and Tiehm, A. 2000. Enhancement of anaerobic sludge digestion by ultrasonic disintegration. Water Sci. Technol., 42(9): 73-80.

Ni, B.J., Fang, F., Xie, W.M., Sun, M., Sheng, G.P., Li, W.H. and Yu, H.Q. 2009. Characterization of extracellular polymeric substances produced by mixed microorganisms in activated sludge with gel-permeating chromatography, excitation-emission matrix fluorescence spectroscopy measurement and kinetic modeling. Water Res., 43(5): 1350-1358.

Penaud, V., Delgenès, J.P. and Moletta, R. 1999. Thermo-chemical pretreatment of a microbial biomass: influence of sodium hydroxide addition on solubilization and anaerobic biodegradability. Enzyme and Microbial Technology, 25(3-5): 258-263.

Sun, J., Guo, L., Li, Q., Zhao, Y., Gao, M., She, Z. and Wang, G. 2016. Structural and functional properties of organic matters in extracellular polymeric substances (EPS) and dissolved organic matters (DOM) after heat pretreatment with waste sludge. Bioresour. Technol., 219: 614-623.

Sun, Y., Zuo, J., Chen, L. and Wang, Y. 2008. Eubacteria and Archaea community of simultaneous methanogenesis and denitrification granular sludge. J. Environ. Sci. (China), 20(5): 626-631.

Wang, Y., Gong, B., Lin, Z., Wang, J., Zhang, J. and Zhou, J. 2018. Robustness and microbial consortia succession of simultaneous partial nitrification, ANAMMOX and denitrification (SNAD) process for mature landfill leachate treatment under low temperature. Biochem. Eng. J., 132: 112-121.

Wang, Y., Lin, Z., He, L., Huang, W., Zhou, J. and He, Q. 2019. Simultaneous partial nitrification, anammox and denitrification (SNAD) process for nitrogen and refractory organic compounds removal from mature landfill leachate: Performance and metagenome-based microbial ecology. Bioresour. Technol., 294: 122166.

Zhang, G., Zhang, P., Gao, J. and Chen, Y. 2008. Using acoustic cavitation to improve the bio-activity of activated sludge. Bioresour. Technol., 99(5): 1497-502.

Zhang, Y.H. and Lynd, L.R. 2005. Cellulose utilization by *Clostridium thermocellum*: Bioenergetics and hydrolysis product assimilation. Proc. Natl. Acad. Sci., U.S.A., 102(20): 7321-7325.

Nature Environment and Pollution Technology
An International Quarterly Scientific Journal

p-ISSN: 0972-6268
(Print copies up to 2016)
e-ISSN: 2395-3454

Vol. 19 | No. 4 | pp. 1465-1474 | 2020

Original Research Paper

https://doi.org/10.46488/NEPT.2020.v19i04.012

Open Access Journal

# Ethylenediaminetetraacetic Dianhydride (EDTAD) Modified Coconut Frond for Removal of Pb(II) Ions: Kinetics, Isotherm and Thermodynamic

**Nur Ain Mohd Nizam Prushotman*, Megat Ahmad Kamal Megat Hanafiah**†, Noorul Farhana Md Ariff*** and Shariff Ibrahim*****

*Faculty of Applied Sciences, Universiti Teknologi MARA, 26400, Jengka, Pahang, Malaysia
**Institute of Science (IOS), Universiti Teknologi MARA, 40450, Shah Alam, Selangor, Malaysia
***Faculty of Applied Sciences, Universiti Teknologi MARA, 40450, Shah Alam, Selangor, Malaysia
†Corresponding author: Megat Ahmad Kamal Megat Hanafiah; makmh@uitm.edu.my

**Nat. Env. & Poll. Tech.**
**Website: www.neptjournal.com**

*Received:* 15-12-2019
*Revised:* 23-1-2020
*Accepted:* 28-03-2020

**Key Words:**
Adsorption
Coconut frond
EDTA dianhydride
Lead removal

## ABSTRACT

Ethylenediaminetetraacetic dianhydride modified coconut frond (ECFP) was prepared, characterized and applied as a potential adsorbent to remove Pb(II) ions from aqueous solutions. Factors influencing adsorption such as pH of the solution, adsorbent dosage, Pb(II) concentration, contact time, and temperature were investigated. The optimum conditions for adsorption of Pb(II) ions were at pH 4 and dosage of 0.02 g. Adsorption reached its equilibrium state in 30 min for all Pb(II) concentrations. Chemisorption was suggested as the rate-limiting step as the adsorption process correlated well with the pseudo-second-order kinetics model. Based on adsorption isotherm results, Langmuir model fitted the experimental data well, and the maximum adsorption capacity was 84.03 $mg.g^{-1}$ at 300 K. Based on the thermodynamic study, Pb(II) adsorption occurred spontaneously with the enthalpy and entropy changes recorded were 0.0615 kJ $mol^{-1}$ and 241.28 J $K^{-1}$ $mol^{-1}$, respectively. It was found that the nature of adsorption was endothermic as the $\Delta H^{o}$ value obtained was positive.

## INTRODUCTION

The release of non-bioessential heavy metals in the aquatic system has resulted in a serious environmental pollution issue. Lead (Pb) is listed as one of the harmful pollutants by World Health Organization due to its high propensity for biological accumulation, non-biodegradability and very toxic even presents at a low concentration (Bai et al. 2019, Cao et al. 2019). At Pb(II) ions concentration above 0.05 $mg.L^{-1}$ in drinking water, one might experience acute lead poisoning symptoms such as anaemia, hepatitis, nephritic syndrome, and encephalopathy. Excess exposure to Pb(II) ions might damage central nervous and gastrointestinal systems, liver and kidneys. For this reason, the United State Environmental Protection Agency (USEPA) had set the maximum standard concentration of Pb(II) ions in drinking water of 300 $\mu g.L^{-1}$ (Hu & Qiu 2019). Due to these reasons, various methods such as ion exchange, chemical precipitation, membrane filtration, and adsorption have been used to remove Pb(II) ions from wastewater (Cao et al. 2019).

In Malaysia, coconut (*Cocos nucifera*) is the third most important industrial crop after oil palm and rubber. In 2001, about 151 000 ha of land in Malaysia were used for coconut plantation and the value reduced gradually due to competition with oil palm plantation. As a result, the coconut industry revitalizing plan was carried out for replanting coconut trees between 2008 and 2015. This consequently raised another environmental issue, which was related to the disposal of coconut waste, as large quantities of coconut fronds were produced during pruning and silvicultural practices (Njoku et al. 2014, Shafie et al. 2012).

Ethylenediaminetetraacetic dianhydride (EDTAD) is a revivification of ethylenediaminetetraacetic acid (EDTA) with two additional anhydride groups on each molecule of EDTA. EDTAD is a biodegradable and powerful complexing agent due to the presence of carboxylic and amine groups (Júnior et al. 2009, Yu et al. 2008, Zhang et al. 2011). Several researchers had used EDTAD in modifying low-cost biomaterials such as neem leaf powder (Hanafiah et al. 2013), *Aloe vera* rind powder (Hanafiah et al. 2018), sugarcane bagasse (Júnior et al. 2009) and baker's yeast biomass (Xia et al. 2015, Yu et al. 2008, Zhang et al. 2011) to improve their adsorption performance. In this study, the adsorption behaviour of Pb(II) ions onto EDTAD modified coconut frond which included the effects of pH, dosage, concentration, contact time, and temperature were evaluated.

## MATERIALS AND METHODS

**Materials:** Coconut fronds were collected from a coconut tree plantation located in Kelantan, Malaysia. The fronds were washed thoroughly, cut into small pieces, dried and washed with tap water to remove insoluble impurities before with deionized water. The fronds were dried in an oven at 333 K overnight before being ground and sieved by using a mechanical grinder to obtain the average particle size of 125-250 µm. The dried coconut frond powder was boiled in deionized water for 30 min to destroy microbes, washed and dried again in an oven overnight at 333 K. Ethylenediaminetetraacetic dianhydride (EDTAD) treatment was performed according to the method proposed by Hanafiah et al. (2013). Five grams of dried untreated coconut frond powder (UCFP) was added into the mixture of 0.50 g of EDTAD and 400 mL N, N-dimethylacetamide (DMAc) in a three-neck round bottom flask equipped with a condenser. The mixture was refluxed at 343 K for 24 h. The mixture was filtered and rinsed with 0.10 M NaOH thoroughly. The wet coconut frond powder was further rinsed with DMAc before finally rinsed with 4 L deionized water until the constant pH was obtained. The EDTAD treated coconut frond powder was dried in an oven at 333 K overnight and designated as ECFP.

**Characterizations of ECFP:** UCFP and ECFP were characterized by using an Attenuated Total Reflectance-Fourier Transform Infrared (ATR-FTIR) spectrometer (PerkinElmer, Spectrum 100, USA). Determination of $pH_{zpc}$ of ECFP was done according to the method reported by Hanafiah et al. (2018) with some modification. A volume of 50 mL (0.01 M) $KNO_3$ was placed into different 100 mL conical flasks. The initial pH of this solution ($pH_o$) was adjusted from 2 to 10 by adding drops of 0.10 M HCl or NaOH solutions. A weight of 0.10 g ECFP was added into each flask and shaken in a water bath shaker for 24 h at 120 stroke $min^{-1}$ at 300 K. ECFP was filtered and the final pH of $KNO_3$ solutions ($pH_f$) was measured using a pH meter.

**Batch adsorption experiments**: The analytical grade of 1000 $mg.L^{-1}$ stock solution of Pb(II) was obtained from Merck (Germany). Working concentration solutions of Pb(II) ions were prepared by appropriate dilutions. All adsorption experiments were done using 50 mL of 10 $mg.L^{-1}$ Pb(II) solutions (otherwise stated) and 0.02 g ECFP at 300 K and the shaking rate was 120 stroke $min^{-1}$. The effect of pH on adsorption of Pb(II) ions onto ECFP was done by adjusting the initial pH from 1 to 5 by adding drops of 0.10 M HCl and NaOH solutions. The effect of ECFP dosage on adsorption of Pb(II) ions was performed by varying the weight of ECFP (0.02 to 0.10 g) in Pb(II) ions solutions at pH 4. The mixtures were shaken for 90 min. In the kinetic study, the concentration of Pb(II) ions solutions was varied from 10 to 30 $mg.L^{-1}$ and the solutions were shaken at different time intervals (1, 3, 6, 10, 20, 30, 60, 90 and 120 min). The pH and the ECFP dosage were fixed at 4 and 0.02 g, respectively. Similar pH and adsorbent dosage were used in isotherm study, but the concentrations of Pb(II) ions were varied (5, 10, 15, 20, 25, 30, 40 and 75 $mg.L^{-1}$). The mixtures were then shaken for 90 min at 300 K. In the thermodynamic study, 5, 10, 15, 20, 25, 30, 40 and 75 $mg.L^{-1}$ Pb(II) ions solutions were shaken with 0.02 g ECFP for 90 min at different temperatures (303, 313 and 323 K). All experiments were done in duplicate. The mixtures were then filtered, and the final concentrations were analysed using an Atomic Absorption Spectrometer (AAS, PerkinElmer PinAAcle 900T, USA). The amount of adsorbed Pb(II) ions, $q_e$ ($mg.g^{-1}$) and the removal percentage (%) of Pb(II) ions were calculated using eqs. (1) and (2), respectively.

$$q_e = \frac{C_i - C_f}{m} \times V \quad \ldots(1)$$

$$\text{Removal (\%)} = \frac{C_i - C_f}{C_i} \times 100 \quad \ldots(2)$$

Where, $C_i$ and $C_f$ are initial and final concentrations of Pb(II) ions ($mg.L^{-1}$), respectively, m is the weight of ECFP (g) and V is the volume of Pb(II) ions solutions (L).

## RESULTS AND DISCUSSION

**Characterizations of ECFP:** Fig. 1 showed the FTIR spectra of UCFP, ECFP and Pb(II) loaded ECFP. A strong and broad band was observed at 3323 $cm^{-1}$ in the FTIR spectra of UCFP. This might be attributed to the presence of O-H groups from cellulose, hemicellulose and lignin. Other peaks were observed at 1727, 1607, 1368, 1033, 898, and 562 $cm^{-1}$ suggesting the presence of C=O, -NH, C-O, C-H, and =C-H. The presence of a new peak at 1736 $cm^{-1}$ in ECFP could be attributed to the introduction of ester groups, as suggested by Pereira et al. (2010). Thus, it might suggest that EDTAD was successfully introduced onto UCFP by forming an ester with -OH groups from coconut frond (Júnior et al. 2009). After the adsorption of Pb(II) ions, the intensity of the peaks at 3323 and 1033 $cm^{-1}$ was reduced, suggesting that -OH and C-O-C groups took part in the binding of Pb(II) ions during the adsorption process. Besides, there was a shift of peak at 1603 to 1593 $cm^{-1}$ suggesting that a bond might be formed between Pb(II) ions and -NH groups.

The pH of zero point charge or $pH_{zpc}$ was measured to determine the pH where the adsorbent had a zero net surface charge. Basically, at $pH=pH_{zpc}$, there were balance charges on the adsorbent surface. In general, at $pH < pHzpc$, an adsorbent surface tended to carry positive charges, while at $pH > pH_{zpc,}$ the adsorbent surface was negatively charged.

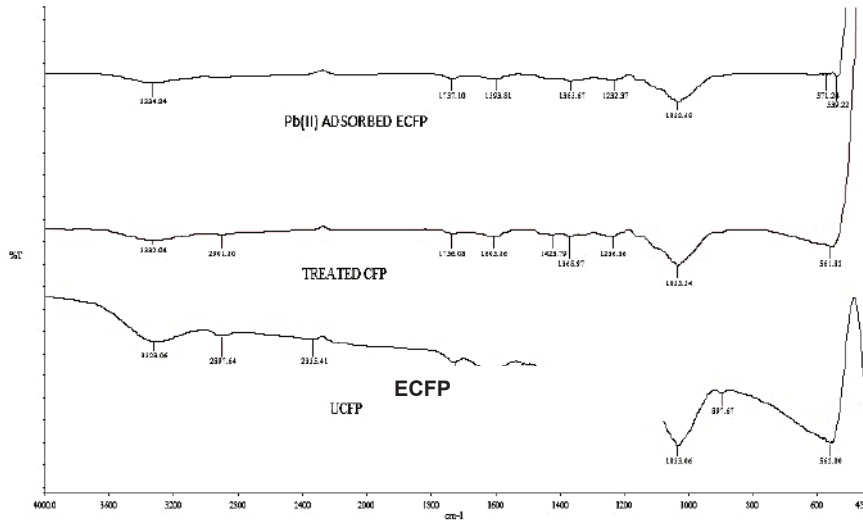


Fig. 1: FTIR spectra of UCFP, ECFP and Pb(II) ions adsorbed onto ECFP.

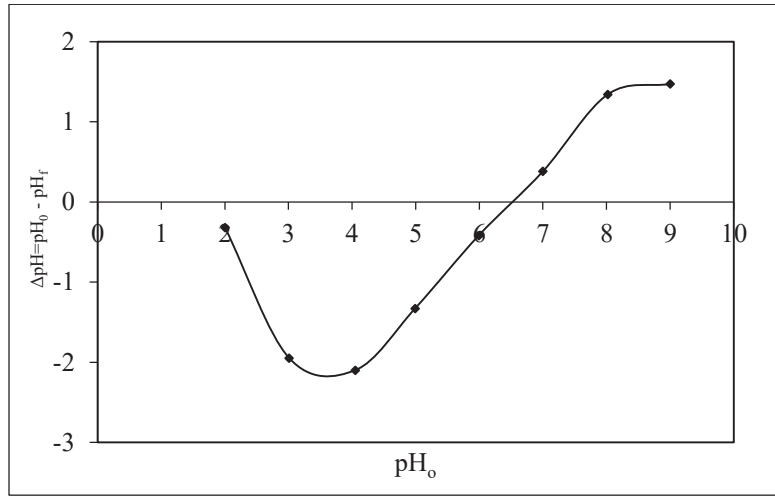


Fig. 2: $pH_{zpc}$ plot of ECFP.

Therefore, the adsorption of a cationic metal is favoured when the pH was higher than $pH_{zpc}$ (Srivastava et al. 2015). Fig. 2 shows the plot of $pH_{zpc}$ of ECFP. The $pH_{zpc}$ of ECFP was found at 6.4, based on the intersection point of the $pH_o$-axis. This indicated that when the pH of the solution was higher than 6.4, Pb(II) ions could have easily been attracted to the ECFP surface as more negative charges surrounded the adsorbent surface.

**Effect of pH on adsorption of Pb(II) ions onto ECFP**: The pH of a solution is a critical parameter in the adsorption of metal ions onto an adsorbent. The variation of pH might influence the affinity between adsorbent and adsorbate. To study the effect of initial pH on adsorption of Pb(II) ions onto ECFP, the initial pH of Pb(II) solution was varied from 1 to 5. Fig. 3 showed that low adsorption capacity, $q_e$ was recorded at pH 1 (4.43 $mg.g^{-1}$). This could be explained by electrostatic repulsion of positively charged Pb(II) ions with positively charged adsorbent due to protonation of functional groups on the adsorbent surface or excessive cations from sorbed $H^+$ ions on the adsorbent surface itself (Ali et al. 2011, Faghihian et al. 2005, Torres-Blancas et al. 2013, Zhang et al. 2016)

The $q_e$ value increased gradually with the increasing of initial pH of Pb(II) ions, where 7.25, 14.48, 22.20 and 23.45 mg.g-1 were recorded at pH 2, 3, 4 and 5, respectively. Basically, the increase of pH could lead to the reduction of repulsive force of the adsorbent surface towards the adsorbate

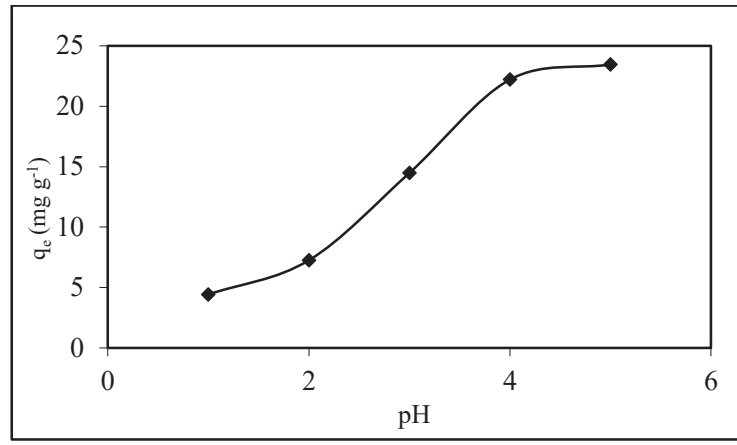


Fig. 3: Effect of pH on adsorption of Pb(II) ions onto ECFP (adsorbent weight: 0.02 g; volume: 50 mL; shaking rate: 120 stroke $min^{-1}$; equilibrium time: 90 min; Pb(II) concentration: 10 $mg.L^{-1}$).

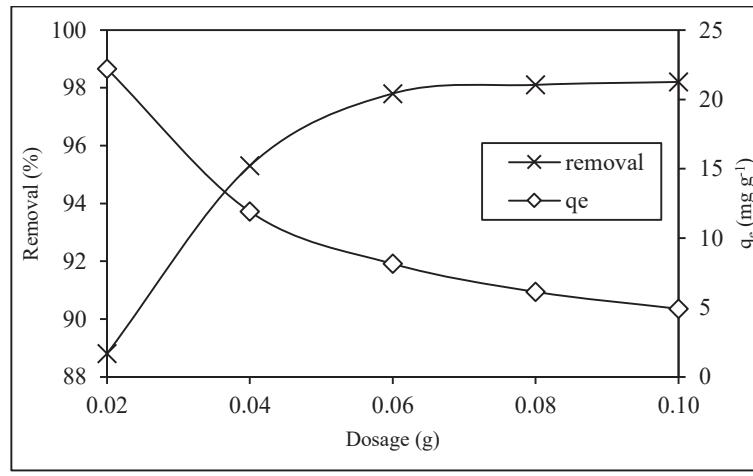


Fig. 4: Effect of adsorbent dosage on Pb(II) adsorption by ECFP (volume: 50 mL; pH: 4; shaking rate: 120 stroke $min^{-1}$; equilibrium time: 90 min; Pb(II) concentration: 10 $mg.L^{-1}$).

ion (Ali et al. 2011, Bhatnagar & Sillanpää 2009, Galhoum et al. 2015, Gok 2014) and thus promoted more adsorption sites as for the adsorption of metal ions. Furthermore, the number of protons ($H^+$) decreased with the increase of pH and thus reduced the competition between metal ions and $H^+$ for the adsorption sites (Miraoui et al. 2015, Torab-Mostaedi et al. 2015).

**Effect of adsorbent dosage on adsorption of Pb(II) ions onto ECFP:** The dosage of adsorbent was an important parameter as it strongly influenced the capacity of biosorption at a given initial concentration (Asgari et al. 2012). The dependence of adsorption of Pb(II) ions on the dosage of ECFP was shown in Fig. 4. The per cent of Pb(II) removal increased from 88.80 to 98.20 % for the adsorbent dosage of 0.02 g to 0.08 g, respectively. This could be attributed to the increase of surface area due to the increase of adsorbent weight or higher number of adsorption sites for a fixed concentration of Pb(II) (Mu et al. 2013). But, beyond dosage 0.08 g, there was no appreciable change in the percentage removal of Pb(II) because the number of Pb(II) ions became the limiting factor. The amount of Pb(II) ions adsorbed on the other hand showed the opposite trend. As more ECFP increased, the amount of Pb(II) ions adsorbed reduced. This was mainly due to the higher number of unsaturated adsorption sites when the dosage was increased, as stated in eq. (1).

**Adsorption rate and kinetic models:** Fig. 5 showed the effect of different concentrations on the adsorption rate of Pb(II) ions onto ECFP. Generally, the plots showed that the adsorption of Pb(II) ions involved two phases; the rapid adsorption pattern, and the slower, gradual adsorption rate

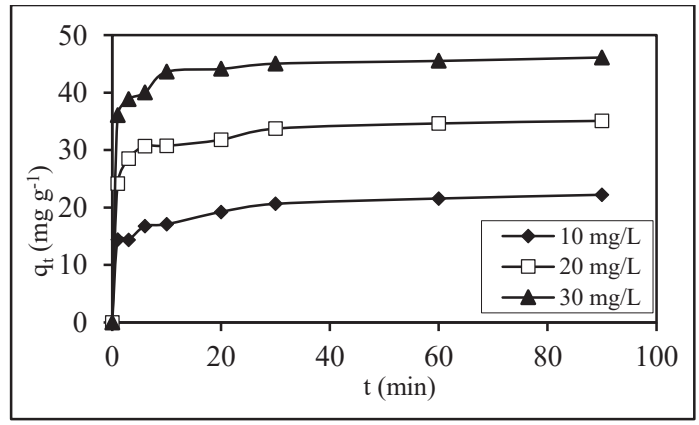


Fig. 5: Effect of contact time on different concentrations of Pb(II) ions for the adsorption of Pb(II) ions by ECFP (volume: 50 mL; pH: 4; shaking rate: 120 stroke $min^{-1}$; adsorbent dosage: 0.02 g).

until equilibrium uptake was achieved. At the beginning of the adsorption stage, a high amount of metal ions was adsorbed due to the high number of available active sites on the surface of the biosorbent. The actives sites were quickly occupied by the Pb(II) ions that led to a small difference in the change of adsorption rate after 10 min. Based on Fig. 5, it can be concluded that the amount of Pb(II) ions adsorbed increased proportionally with the initial concentration of Pb(II) ions. The amount of 10, 20 and 30 $mg.L^{-1}$ Pb(II) ions adsorbed were 22.20, 35.10 and 46.15 $mg.g^{-1}$, respectively. This situation could be explained by the increase in the driving force of the concentration gradient. The increase of driving force had overcome all the mass transfer resistance of metal ions from the aqueous phase to the solid phase, and subsequently provided a higher collision probability between metal ions and the active sites (Zhu et al. 2015). Overall, adsorption of Pb(II) ions onto ECFP showed relatively rapid adsorption process as equilibrium was achieved in less than 30 min for all Pb(II) concentrations. When the concentration of Pb(II) ions was low, the ratio of Pb(II) ions to the number of available adsorption sites was also low. Therefore, the adsorption sites seemed to take up the available Pb(II) ions much quickly since there was less competition among adsorbates ions (Gupta & Bhattacharyya 2008).

The rate of the adsorption of the metal ions is the momentum of the molecules to move from the aqueous solution to the adsorbent surface. In general, the adsorption process is governed by one or more mechanisms. Basically, adsorption process consists four stages (Srivastava et al. 2015), i.e; (i) the transfer of the solute from the solution to the boundary layer that surrounds the adsorbent surface, (ii) the transportation of the solute from the boundary layer to the adsorbent surface, (iii) the transfer of solute to the intraparticle sites from the adsorbent surface and (iv) the binding of solute ions to the available sites in the internal surface of the adsorbent.

Kinetics is the utmost important information for the adsorption study. A full-scale batch adsorption process can be obtained from the kinetics study. In addition, by applying certain adsorption kinetics models to the experimental data, one would gain a better understanding of the adsorption mechanism and the potential rate-limiting step (Sadeek et al. 2015, Zhang et al. 2016). Moreover, the rate of adsorption obtained through the kinetic study may help in optimizing the reactor dimension and residence time in any particular adsorption system (Sadeek et al. 2015). In this study, the pseudo-first (Ho & McKay 1998) and pseudo-second (Ho & McKay 2000) order kinetic models were used to determine the adsorption for the adsorption of Pb(II) ions onto ECFP and the linearized equations are given as follows:

$$\log(q_e - q_t) = \log q_{e,cal} - \frac{k_1}{2.303} t \qquad \ldots(3)$$

$$\frac{t}{q_t} = \frac{1}{k_2 q_{e,cal}^2} + \frac{1}{q_{e,cal}} t \qquad \ldots(4)$$

Where, t is time (min), $q_{e,cal}$ is the calculated adsorption capacity at equilibrium ($mg.g^{-1}$), $q_t$ is the concentration of the analyte at time t ($mg.g^{-1}$), $k_1$ is pseudo-first-order rate constant ($min^{-1}$) and $k_2$ is pseudo-second-order rate constant (g $mg^{-1}$ $min^{-1}$). Figs. 6 and 7 showed the plots of pseudo-first-order and pseudo-second-order kinetic models for the adsorption of 10, 20 and 30 $mg.L^{-1}$ Pb(II) ions onto ECFP at 300 K, respectively. The results analysed from both kinetics models are presented in Table 1.

In general, both pseudo-first and pseudo-second-order plots showed relatively good linearity ($R^2 > 0.85$), yet the pseudo-second-order kinetics model had a better agreement with the experimental data. This could be noticed from the values of $R^2$ that were almost unity (0.9990 to 0.9999) for

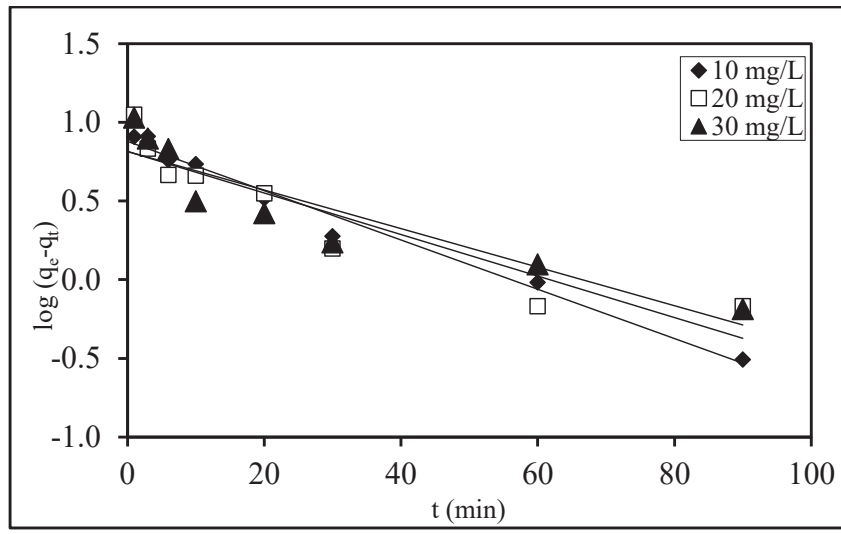


Fig. 6: Pseudo-first-order plots for the adsorption of Pb(II) ions onto ECFP (volume: 50 mL; pH: 4; shaking rate: 120 stroke $min^{-1}$; adsorbent dosage: 0.02 g; temperature: 300 K).

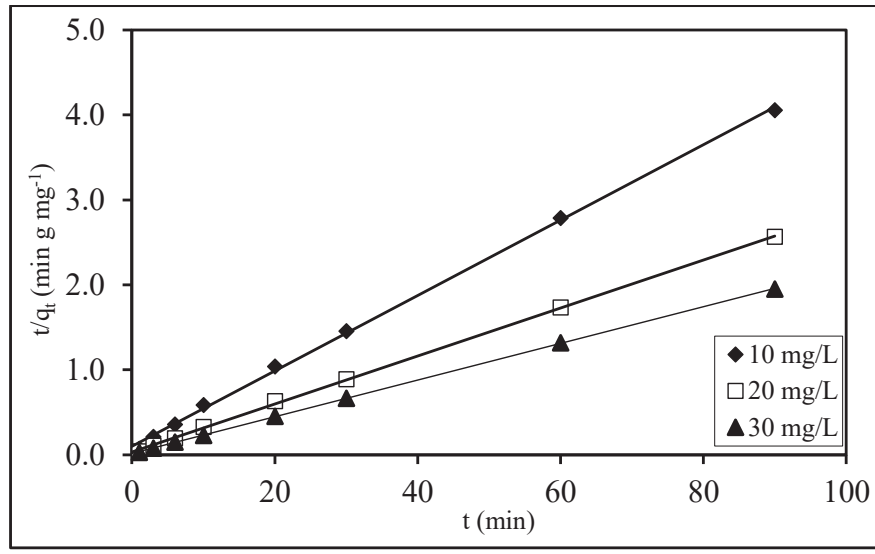


Fig. 7: Pseudo-second-order plots for the adsorption of Pb(II) ions onto ECFP (volume: 50 mL; pH: 4; shaking rate: 120 stroke $min^{-1}$; adsorbent dosage: 0.02 g; temperature: 300 K).

Table 1: Pseudo-first and pseudo-second-order parameters for adsorption of Pb(II) ions onto ECFP.

| [Pb(II)] ($mg.L^{-1}$) | $q_{e,exp}$ ($mg.g^{-1}$) | Pseudo-first-order | | | Pseudo-second-order | | | |
|---|---|---|---|---|---|---|---|---|
| | | $k_1$ ($mg.min^{-1}\ g^{-1}$) | $q_{e,cal}$ ($mg.g^{-1}$) | $R^2$ | h ($mg.g^{-1}\ min^{-1}$) | $k_2$ ($mg.min^{-1}\ g^{-1}$) | $q_{e,cal}$ ($mg.g^{-1}$) | $R^2$ |
| 10 | 22.24 | $3.62 \times 10^{-2}$ | 7.56 | 0.982 | 10.06 | $1.98 \times 10^{-2}$ | 22.52 | 0.999 |
| 20 | 35.12 | $3.04 \times 10^{-2}$ | 6.53 | 0.862 | 30.12 | $2.41 \times 10^{-2}$ | 35.33 | 0.999 |
| 30 | 46.84 | $2.83 \times 10^{-2}$ | 6.54 | 0.850 | 64.94 | $3.03 \times 10^{-2}$ | 46.30 | 0.999 |

all concentrations, and the qe,cal values were very close to those recorded from the batch adsorption study. Due to this reason, chemisorption might govern the adsorption process, where metal ions bonded to the adsorbent through valance force, either by covalent bond through sharing of electrons or ion exchange mechanism (Galhoum et al. 2015, Gok 2014, Pasquier & Largitte 2016, Toor & Jin 2012, Wang et al. 2013).

**Equilibrium and isotherm study:** The equilibrium or adsorption isotherm describes the interaction of adsorbate with the adsorbent. It represents the distribution of different initial concentrations of solute at a constant temperature in the aqueous phase and solid phase. As adsorption isotherm provides that information, it turns as the most vital study in optimizing the adsorbent-adsorbate system, mechanistic pathways and understanding the adsorbent surface properties (Galhoum et al. 2015, Rangabhashiyam et al. 2014, Zhang et al. 2016).

To study the adsorption isotherm for the adsorption of Pb(II) ions onto ECFP, the initial concentration of Pb(II) ions was varied from 5 to 75 mg.$L^{-1}$. The mixtures were shaken for 90 min to ensure the equilibrium state. At the low concentrations of Pb(II) ions (<30 mg.$L^{-1}$), the sharp slope could be observed as presented in Fig. 8, an indication of a high-efficiency adsorbent for the adsorption of low metal ion concentrations. As the concentration of Pb(II) ions increased to 40 mg.$L^{-1}$, the slope reduced drastically. This condition was associated with the saturation of adsorption sites due to the increase in the ratio of the number of Pb(II) ions to the number of adsorption sites.

In general, the application of suitable isotherm models onto the experimental data is important as it can provide valuable information about the distribution of adsorption sites on the adsorbent surface, adsorption characteristic and affinity of adsorbent-adsorbate in the adsorption system. Several mathematical models can be applied to the experimental data such as two-parameter isotherm models which include Langmuir (Langmuir 1916) and Freundlich (Freundlich 1906). The linearized equations for Langmuir and Freundlich models are given in eqs. (5) and (6), respectively.

$$\frac{C_e}{q_e} = \frac{1}{bQ_{max,cal}} + \frac{C_e}{Q_{max,cal}} \quad \ldots(5)$$

$$\log q_e = \frac{1}{n}\log C_e + \log K_F \quad \ldots(6)$$

Where, $q_e$ is the equilibrium adsorption capacity (mg.$g^{-1}$), $Q_{max,cal}$ is the maximum adsorption capacity (mg.$g^{-1}$), $C_e$ is the equilibrium concentration of the adsorbate (mg.$L^{-1}$), b is the equilibrium constant (L $mg^{-1}$), $K_F$ is a Freundlich constant (mg.$g^{-1}$) and n is a constant related to the heterogeneity of the adsorbent surface and its affinity for the adsorbate.

Figs. 9 and 10 showed Langmuir and Freundlich plots for adsorption of Pb(II) ions onto ECFP and the parameters for the isotherm models were listed in Table 2. In general, both isotherm models recorded high $R^2$ values (>0.92). Based on the agreement of experimental and theoretical values of $Q_{max}$, Langmuir isotherm model seemed to have a better fitting to the experimental data compared to Freundlich isotherm model. This condition might explain the monolayer coverage of Pb(II) ions on the ECFP surface.

Adsorption thermodynamics: To study the effect of different temperature on adsorption of Pb(II) ions, solutions ranged from 0 to 75 mg.$L^{-1}$ was stirred with ECFP at 303, 313 and 323 K for 90 min. Fig. 11 showed the isotherm plot for the adsorption of Pb(II) ions at 303, 313 and 323 K. In general, adsorption of Pb(II) onto ECFP was more favourable

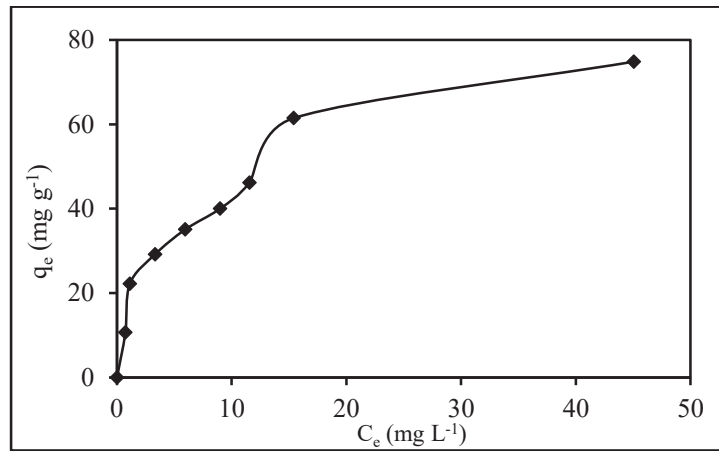


Fig. 8: Adsorption isotherm plot for adsorption of Pb(II) ions onto ECFP (volume: 50 mL; pH: 4; shaking rate: 120 stroke $min^{-1}$; adsorbent dosage: 0.02 g; temperature: 300 K).

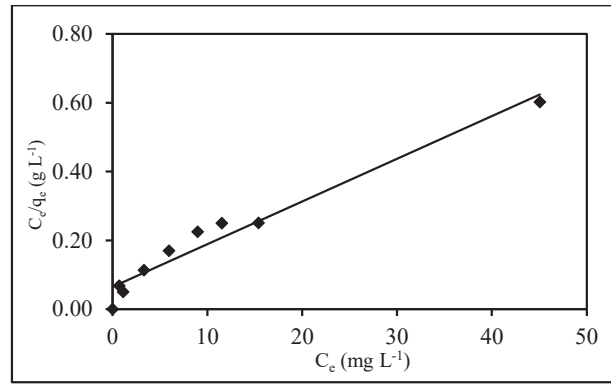


Fig. 9: Langmuir plot for adsorption of Pb(II) ions onto ECFP (volume: 50 mL; pH: 4; shaking rate: 120 stroke $min^{-1}$; adsorbent dosage: 0.02 g; temperature: 300 K).

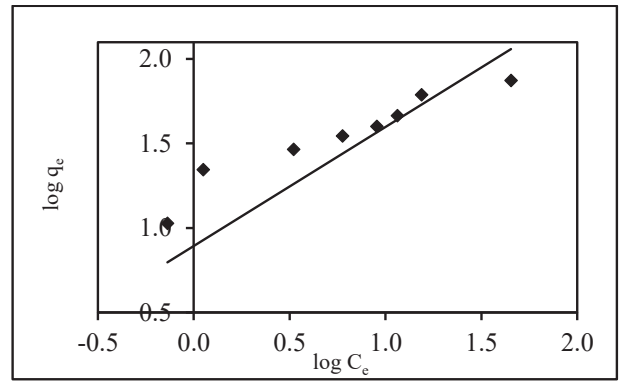


Fig. 10: Freundlich plot for adsorption of Pb(II) ions onto ECFP (volume: 50 mL; pH: 4; shaking rate: 120 stroke $min^{-1}$; adsorbent dosage: 0.02 g; temperature: 300 K).

Table 2: Langmuir and Freundlich isotherm parameters for adsorption of Pb(II) ions onto ECFP.

| Temperature (K) | $q_{e,exp}$ ($mg.g^{-1}$) | Langmuir | | | Freundlich | | |
|---|---|---|---|---|---|---|---|
| | | $q_{max}$ ($mg.g^{-1}$) | b ($L.mg^{-1}$) | $R^2$ | $K_f$ | n | $R^2$ |
| 303 | 74.85 | 84.03 | 0.15 | 0.974 | 16.29 | 2.31 | 0.927 |

at higher temperatures as the recorded adsorption capacities increased with increasing temperatures, which also suggested an endothermic adsorption behaviour.

The thermodynamic parameters such as enthalpy ($\Delta H°$), entropy ($\Delta S°$), and Gibb's free energy ($\Delta G°$) were calculated to determine the adsorption process by using the following equations:

$$K_c = \frac{C_{ad}}{C_e} \quad \ldots(7)$$

$$\ln K_c = \frac{-\Delta H^o}{RT} + \frac{\Delta S^o}{R} \quad \ldots(8)$$

$$\Delta G^o = -RT \ln K_c \quad \ldots(9)$$

Where, $K_c$ is the equilibrium constant, $C_{ad}$ is the concentration of Pb(II) ions adsorbed on solid at equilibrium ($mmol.L^{-1}$), $C_e$ is the equilibrium concentration of Pb(II) ions in the solution ($mmol.L^{-1}$), R is the gas constant (8.314 J $K^{-1}$ $mol^{-1}$) and T is the temperature in Kelvin. Fig. 12 showed the Van't Hoff plot for the adsorption of Pb(II) ions onto ECFP at 303, 313 and 323 K. The calculated values for $\Delta H°$, $\Delta S°$, and $\Delta G°$ were listed in Table 3. In general, all $\Delta G°$ values for the adsorption of Pb(II) at 303, 313 and 323 K were negative, an indication of spontaneous adsorption process at those temperatures. The positive $\Delta H°$ value recorded in this study indicated that adsorption of Pb(II) ions onto ECFP was endothermic, where adsorption was more favourable at a higher temperature. Meanwhile, the positive $\Delta S°$ value suggested that this process was an entropy-driven process where a higher degree of freedom of the ions was obtained at a higher temperature.

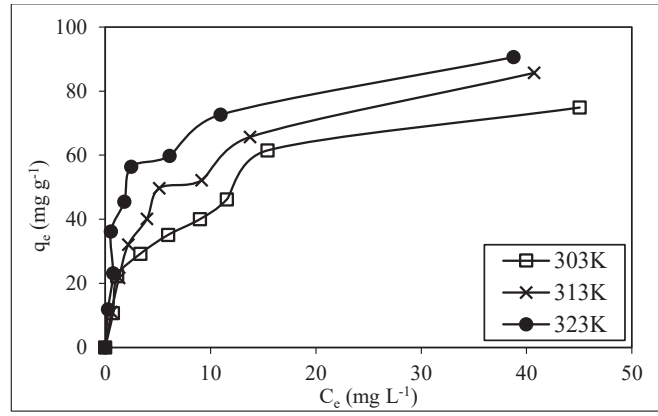


Fig. 11: Adsorption isotherm plots of Pb(II) ions onto ECFP at 303, 313 and 323 K (volume: 50 mL; pH: 4; shaking rate: 120 stroke $min^{-1}$; adsorbent dosage: 0.02 g).

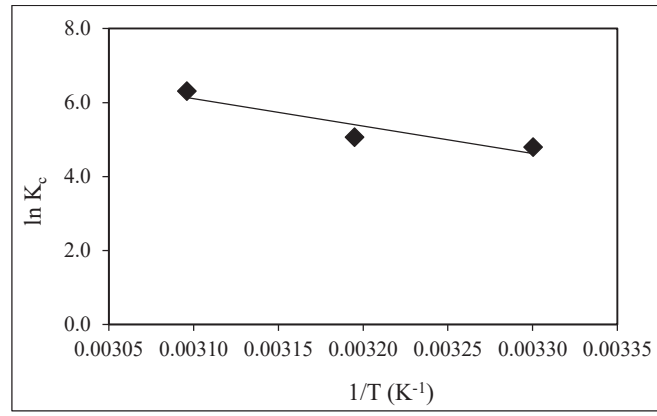


Fig. 12: Van't Hoff plot for adsorption of Pb(II) ions onto ECFP (adsorbent weight: 0.02 g; volume: 50 mL; pH: 4; shaking rate: 120 stroke $min^{-1}$, Pb concentration: 5-75 mg.$L^{-1}$; equilibrium time 90 min).

Table 3: Thermodynamic parameters for adsorption of Pb(II) ions onto ECFP.

| Temperature | $\Delta G^o$ (kJ $mol^{-1}$) | $\Delta H^o$ (kJ $mol^{-1}$) | $\Delta S^o$ (J $mol^{-1}$) |
|---|---|---|---|
| 303 | -13.14 | 0.0615 | 241.28 |
| 313 | -13.16 | | |
| 323 | -16.95 | | |

## CONCLUSION

The current work revealed the potential application of ECFP as an adsorbent for removing Pb(II) ions from aqueous solutions. The amount of Pb(II) ions adsorbed was reduced in a highly acidic condition and the optimum adsorption pH range was 4 to 5. The satisfactory adsorption capacity was recorded from the Langmuir isotherm model with the $q_{max}$ value of 84.03 mg.$g^{-1}$ being recorded. The potential functional groups responsible for adsorbing Pb(II) ions as revealed by the FTIR spectra were hydroxyl, amino, carbonyl, aromatics and ether. Adsorption process could be considered rapid due to the short time taken to reach equilibrium stage for all concentrations of Pb(II) ions. Based on the thermodynamic study, Pb(II) ions were more favoured to be adsorbed at a higher temperature, suggesting an endothermic adsorption behaviour.

## REFERENCES

Ali, O.I.M., Osman, H.H., Sayed, S.A. and Shalabi, M.E.H. 2011. The removal of some rare earth elements from their aqueous solutions on by-pass cement dust (BCD). Journal of Hazardous Materials, 195: 62-67.

Asgari, G., Roshani, B. and Ghanizadeh, G. 2012. The investigation of kinetic and isotherm of fluoride adsorption onto functionalize pumice stone. Journal of Hazardous Materials, 217-218: 123-132.

Bai, J., Chao, Y., Chen, Y., Wang, S. and Qiu, R. 2019. The effect of interaction between *Bacillus subtilis* DBM and soil minerals on Cu(II) and Pb(II) adsorption. Journal of Environmental Sciences (China), 78: 328-337.

Bhatnagar, A. and Sillanpää, M. 2009. Applications of chitin- and chitosan-derivatives for the detoxification of water and wastewater-A short review. Advances in Colloid and Interface Science, 152(1-2): 26-38.

Cao, Y., Xiao, W., Shen, G., Ji, G., Zhang, Y., Gao, C. and Han, L. 2019. Carbonization and ball milling on the enhancement of Pb(II) adsorption by wheat straw: Competitive effects of ion exchange and precipitation. Bioresource Technology, 273: 70-76.

Faghihian, H., Amini, M.K. and Nezamzadeh, A.R. 2005. Cerium uptake by zeolite A synthesized from natural clinoptilolite tuffs. Journal of Radioanalytical and Nuclear Chemistry, 264(3): 577-582.

Freundlich, H. 1906. Über die adsorption in läosungen. Journal of Physical Chemistry, 57: 385-470.

Galhoum, A.A., Mahfouz, M.G., Abdel-Rehem, S.T., Gomaa, N.A., Atia, A.A., Vincent, T. and Guibal, E. 2015. Diethylenetriamine-functionalized chitosan magnetic nano-based particles for the sorption of rare earth metal ions [Nd(III), Dy(III) and Yb(III)]. Cellulose, 22(4): 2589-2605.

Gok, C. 2014. Neodymium and samarium recovery by magnetic nano-hydroxyapatite. Journal of Radioanalytical and Nuclear Chemistry, 301: 641-651.

Gupta, S.S.G. and Bhattacharyya, K. 2008. Immobilization of Pb(II), Cd(II) and Ni(II) ions on kaolinite and montmorillonite surfaces from aqueous medium. Journal of Environmental Management, 87: 46-58.

Hanafiah, M.A.K.M., Jamaludin, S.Z.M., Khalid, K. and Ibrahim, S. 2018. Methylene blue adsorption on aloe vera rind powder: Kinetics, isotherm and mechanisms. Nature Environment and Pollution Technology, 17: 1055-1064.

Hanafiah, M.A.K.M., Ismail, M., Ngah, W.S.W., Wan Mat Khalir, W.K.A. and Zakaria, H. 2013. Adsorption behavior of methylene blue on ethylenediaminetetraacetic dianhydride modified neem (*Azadirachta indica)* leaf powder. Key Engineering Materials, 594-595(December): 270-274.

Ho, Y.S. and McKay, G. 1998. A comparison of chemisorption kinetic models applied to pollutant removal on various sorbents. Process Safety and Environmental Protection, 76(4): 332-340.

Ho, Y.S. and McKay, G. 2000. The kinetics of sorption of divalent metal ions onto sphagnum moss peat. Water Research, 34: 735-742.

Hu, C. and Qiu, M. 2019. Characterization of the biochar derived from peanut shell and adsorption of Pb(II) from aqueous solutions. Nature Environment and Pollution Technology, 18: 225-230.

Júnior, O.K., Gurgel, L.V A., de Freitas, R.P. and Gil, L.F. 2009. Adsorption of Cu(II), Cd(II), and Pb(II) from aqueous single metal solutions by mercerized cellulose and mercerized sugarcane bagasse chemically modified with EDTA dianhydride (EDTAD). Carbohydrate Polymers, 77(3): 643-650.

Langmuir, I. 1916. The constitution and fundamental properties of solids and liquids. Journal of American Chemical Society, 38: 2221-2295.

Miraoui, A., Didi, M.A. and Villemin, D. 2015. Neodymium(III) removal by functionalized magnetic nanoparticles. Journal of Radioanalytical and Nuclear Chemistry, 307: 963-971.

Mu, N., ALOthman, Z. A. and Khan, M. R. 2013. Removal of malathion from aqueous solution using De-Acidite FF-IP resin and determination by UPLC–MS/MS: Equilibrium, kinetics and thermodynamics studies. Talanta, 115: 15-23.

Njoku, V.O., Islam, M.A., Asif, M. and Hameed, B.H. 2014. Preparation of mesoporous activated carbon from coconut frond for the adsorption of carbofuran insecticide. Journal of Analytical and Applied Pyrolysis, 110(1): 172-180.

Pasquier, R. and Largitte, L. 2016. A review of the kinetics adsorption models and their application to the adsorption of lead by an activated carbon. Chemical Engineering Research and Design, 109: 495-504.

Pereira, F.V., Gurgel, L.V.A. and Gil, L.F. 2010. Removal of $Zn^{2+}$ from aqueous single metal solutions and electroplating wastewater with wood sawdust and sugarcane bagasse modified with EDTA dianhydride (EDTAD). Journal of Hazardous Materials, 176: 856-863.

Rangabhashiyam, S., Anu, N., Giri Nandagopal, M.S. and Selvaraju, N. 2014. Relevance of isotherm models in biosorption of pollutants by agricultural byproducts. Journal of Environmental Chemical Engineering, 2(1), 398-414.

Sadeek, S.A., Negm, N.A., Hefni, H.H.H. and Wahab, M.M.A. 2015. Metal adsorption by agricultural biosorbents: Adsorption isotherm, kinetic and biosorbents chemical structures. International Journal of Biological Macromolecules, 81: 400-409.

Shafie, S.M., Mahlia, T.M.I., Masjuki, H.H. and Ahmad-Yazid, A. 2012. A review on electricity generation based on biomass residue in Malaysia. Renewable and Sustainable Energy Reviews, 16(8): 5879-5889.

Srivastava, S., Agrawal, S.B. and Mondal, M.K. 2015. Biosorption isotherms and kinetics on removal of Cr(VI) using native and chemically modified *Lagerstroemia speciosa* bark. Ecological Engineering, 85: 56-66.

Toor, M. and Jin, B. 2012. Adsorption characteristics, isotherm, kinetics, and diffusion of modified natural bentonite for removing diazo dye. Chemical Engineering Journal, 187: 79-88.

Torab-Mostaedi, M., Asadollahzadeh, M., Hemmati, A. and Khosravi, A. 2015. Biosorption of lanthanum and cerium from aqueous solutions by grapefruit peel: equilibrium, kinetic and thermodynamic studies. Research on Chemical Intermediates, 41: 559-573.

Torres-Blancas, T., Roa-Morales, G., Fall, C., Barrera-Díaz, C., Ureña-Nuñez, F. and Pavón Silva, T. B. 2013. Improving lead sorption through chemical modification of de-oiled allspice husk by xanthate. Fuel, 110: 4-11.

Wang, F., Zhao, J., Wei, X., Huo, F., Li, W., Hu, Q. and Liu, H. 2014. Adsorption of rare earths (III) by calcium alginate-poly glutamic acid hybrid gels. Journal of Chemical Technology and Biotechnology, 89(7): 969-977.

Wang, Y., Wang, X., Wang, X., Liu, M., Wu, Z., Yang, L., Xia, S. and Zhao, J. 2013. Adsorption of Pb(II) from aqueous solution to Ni-doped bamboo charcoal. Journal of Industrial Engineering Chemistry, 19: 353-359.

Xia, Y., Yao, Q., Zhang, W., Zhang, Y. and Zhao, M. 2015. Comparative adsorption of methylene blue by magnetic baker's yeast and EDTAD-modified magnetic baker's yeast: Equilibrium and kinetic study. Arabian Journal of Chemistry, 12(8): 2448-2456.

Yu, J., Tong, M., Sun, X. and Li, B. 2008. Enhanced and selective adsorption of $Pb^{2+}$ and $Cu^{2+}$ by EDTAD-modified biomass of baker's yeast. Bioresource Technology, 99(7): 2588-2593.

Zhang, L., Zeng, Y. and Cheng, Z. 2016. Removal of heavy metal ions using chitosan and modified chitosan : A review. Journal of Molecular Liquids, 21: 175-191.

Zhang, Y., Zhu, J., Zhang, L., Zhang, Z., Xu, M. and Zhao, M. 2011. Synthesis of EDTAD-modified magnetic baker's yeast biomass for $Pb^{2+}$ and $Cd^{2+}$ adsorption. Desalination, 278(1-3): 42-49.

Zhu, H.X., Cao, X.J., He, Y.C., Kong, Q.P., He, H. and Wang, J. 2015. Removal of $Cu^{2+}$ from aqueous solutions by the novel modified bagasse pulp cellulose: Kinetics, isotherm and mechanism. Carbohydrate Polymers, 129: 115-126.

Nature Environment and Pollution Technology
An International Quarterly Scientific Journal

p-ISSN: 0972-6268
(Print copies up to 2016)
e-ISSN: 2395-3454

Vol. 19 | No. 4 | pp. 1475-1482 | 2020

Original Research Paper

https://doi.org/10.46488/NEPT.2020.v19i04.013

Open Access Journal

# Evaluation of Health Level of Land-use Ecosystem Based on GIS Grid Model

**Wei He*(**)†, Zheng Li*(**) and Dingqian Jing*(**)**

*College of Geography and Resources Science, Sichuan Normal University, Chengdu 610101, People's Republic of China

**Key Lab of Land Resources Evaluation and Monitoring in Southwest, Ministry of Education, Sichuan Normal University, Chengdu 610101, People's Republic of China

†Corresponding author: Wei He; scdlwhe@sicnu.edu.cn

Nat. Env. & Poll. Tech.
Website: www.neptjournal.com

*Received:* 18-03-2020
*Revised:* 17-4-2020
*Accepted:* 15-06-2020

**Key Words:**
Land-use
GIS grid model
Spatial exploratory analysis
Geographic detector

## ABSTRACT

The evaluation of health level of land-use ecosystem provides important support for the regional health and social-economic sustainable development. To measure and study the granularity characteristics and spatial differentiation law of ecological health level of land-use in Yibin City, based on PSR model, taking kilometre grid as an evaluation unit, spatial exploration method was used to reveal its spatial differentiation law, and the decisive force of each factor was visualized through the factor detector. The results show that: (1) The health level of the land-use ecosystem in Yibin City is generally good, and the regional development is relatively balanced, but there are significant differences between the municipal districts and suburban counties. The average index of comprehensive health level of land-use ecosystem fluctuates around 0.60, the land for health level accounts for 46.07% of the total area, the land for sub-health level accounts for 29.78%, the land for unhealthy level accounts for 24.15%. (2) The health level of land-use ecosystem had a strong spatial correlation, which was mainly positive, and there was a significant spatial agglomeration pattern, dominated by HH type or LL type clusters. (3) The difference of human activities was the main factor that affects the spatial differentiation of ecological health level of land-use in the whole city, followed by the difference of natural system resilience, and the other factors were soil properties, landform and policy regulation. Finally, it was concluded that tightening the upper limit of capacity, holding the ecological bottom line, insisting on the intensive utilization of land, optimizing the spatial layout of "production, life and ecology", adjusting the industrial structure, and developing ecotourism will become the necessary measures for Yibin city to improve the ecological health level of land-use and build a famous ecological city of landscape culture.

## INTRODUCTION

The health level of land-use ecosystem refers to a state in which the land under the jurisdiction can maintain the normal operation of self-structure and functions when used by people. So that the symbiosis process among land, human, biology and external environment can be continuously developed (Zhang et al. 2011). In recent years, with prominent problems such as resource depletion and environmental pollution, the ecological health of land-use, as a new goal of land ecological environment protection and sustainable development, has attracted much attention. Therefore, it is an urgent task for regional health and sustainable development of the social economy to evaluate the ecological health of land-use and formulate reasonable control measures.

Since the end of the 20th century, there are few studies on the evaluation of health level of land-use ecosystem at home and abroad, mainly focusing on the connotation, mechanism, level and regulation of ecological health of land-use (Gao et al. 2017, Zhang & Shi 2010), based on single land ecosystem and basic administrative areas such as city, county (district), township (town, sub-district) (Wei 2017), involving cities (Ma et al. 2014), wetlands (Zhu et al. 2012) grasslands (Zhao et al. 2017) and rivers (Hao et al. 2014), using building an index evaluation system of land-use ecological health based on vitality-organization-resilience (VOR) theory from the aspects of vitality, organization, resilience and function (Liu et al. 2017).

Yibin City, a hilly area in the upper reaches of the Yangtze River, was taken as the research object. Based on the PSR model of "human-land interaction" considering the interaction between land ecosystem and human activities, the grid model was used to transform the remote sensing data, land-use data and panel data in a unified way to expand the single ecosystem to a composite ecosystem while realizing the compatibility of multiple data and the refinement of spatial accuracy of evaluation, to establish an appropriate ecological health evaluation system for land-use. The ecological health level of land-use in each grid was measured taking kilometre grid as the basic measure unit; ESDA space exploration

technology was used to reveal the spatial differentiation law of land-use ecological health level in grid scale, and factor detector was used to show the decisive power of each factor directly. The purpose of this paper is to enrich the research content of land-use ecological health evaluation and to provide targeted countermeasures for improving the ecological health level of regional land-use.

## RESEARCH AREA, DATA SOURCES AND PREPROCESSING

### Overview of Research Area

Yibin City, located in the southeast of Sichuan Province, between 103°36′E and 105°20′E, 27°50′N and 29°16′N, has two districts and eight counties, with a total area of 13,000 km$^2$ (Fig. 1). It is the transition from Sichuan basin to Yunnan-Guizhou Plateau, with the terrain dominated by middle and low mountains and hills, alternated valleys and flatlands, and the landscape distribution pattern, which is high in the southwest and low in the northeast (Liu et al. 2017, Zhao et al. 2015). In 2018, Yibin city's population totalled 5.5429 million, with a GDP of 152.594 billion yuan, the urbanization rate has reached 48.5%. With the development of social economy, also increases the pressure of regional resources and environment, and brings new challenges to the sustainable development of regional land ecology. Therefore, under the background of the planning strategy of regional land ecological development, it is of practical significance to carry out the research on the evaluation of health level of the land-use ecosystem in the city for the restoration and protection of the land ecological environment and the establishment of ecological protective screens.

### Data Source and Pre-processing

Social and economic statistics in this study are mainly from the information published in Yibin Statistical Yearbook. The data of land-use status were interpreted by Landsat ETM + and OLI images downloaded from the data centre for resources and environmental sciences of Chinese Academy of Sciences (http://www.resdc.cn), with a spatial resolution of 30m × 30m. Considering the needs of research, the land-use types were determined as cultivated land, forest land, grassland, urban construction land, rural residential land, water area, independent industrial and mining district and land for transportation. DEM data came from ASTER-GDEMV2 digital elevation data with a resolution of 30m provided by NASA (search.earthdata.nasa.gov). The tool of creating fishnet in ArcGIS 10.2 was used to generate the grid of 1km × 1km, and there were a total of 13,307 grids generated in Yibin City.

## MATERIALS AND METHODS

### Construction of PSR Evaluation Index System

The internal health of the land ecosystem is related to people's survival and sustainable development of society.


Fig. 1: Geographical location of the study area

The interaction between land ecosystem and human activities must be considered comprehensively when establishing the indicator system. Based on the PSR model (Zhao et al. 2015, Xu et al. 2010), build the evaluation index system for the health level of the land-use ecosystem in Yibin City.

"Pressure" refers to the defect of land and resources and the impact of human activities on land and surrounding environment, which is measured by terrain fragmentation, soil erosion, population density and stress index of human activities (He et al. 2015). "State" refers to the energy and activity of land ecosystem (Jiang et al. 2009), which is measured by Landscape diversity index (Chen 2007), ecological resilience (Pan et al. 2004), ecosystem service values (Xie et al. 2008). "Response" refers to the policy measures taken by human beings for land ecological restoration, mainly including the amount of environmental protection investment and the proportion of the tertiary industry in GDP. Details are provided in Tables 1 and 2.

## Spatial Exploratory Analysis

Spatial exploratory analysis is a kind of data spatial descrip-

Table 1: Ecosystem health evaluation index system.

| Target layer | Criterion layer | | | Index layer | Formulas | Safety trend | Weight |
|---|---|---|---|---|---|---|---|
| Land ecosystem healthw | Pressure | | P1 | Soil erosion | - | Negative | 0.089 |
| | | | P2 | Terrain fragmentation | $P2 = 1/\cos\alpha$ | Negative | 0.177 |
| | | | P3 | Population density (person/km²) | $P3 = r_i / m_i$ | Negative | 0.102 |
| | | | P4 | Stress index of human activities | $P4 = \sum_{i=1}^{n} t_i * q_i / A$ | Negative | 0.081 |
| | State | Vitality | S1 | Normalized differential vegetation index | $S1 = \frac{NIR - R}{NIR + R}$ | Positive | 0.090 |
| | | Organization | S2 | Landscape diversity index | $S2 = -\sum_{i=1}^{n} \frac{t_i}{A} \ln\left(\frac{t_i}{A}\right)$ | Positive | 0.089 |
| | | Resilience | S3 | Ecological resilience | $S3 = S * \sum_{i=1}^{n} \frac{t_i * p_i}{A}$ | Positive | 0.087 |
| | | Function | S4 | Ecosystem service values | $S4 = \sum_{i=1}^{n} t_i * v_i$ | Negative | 0.087 |
| | Response | | R1 | Investment in environmental protection (104 yuan) | – | Positive | 0.097 |
| | | | R2 | Proportion of tertiary industry in GDP (%) | $R2 = S/GDP$ | Positive | 0.101 |

Note: $n$ = Number of land-use types; a =Average slope of cell grid; $r_i$ = Population of each district and county; $m_i$ = Area of the administrative region; $t_i$ = Area of the i[th] type of land-use; $q_i$ = Stress intensity parameters of human activities of the i[th] type of land-use; R = Reflection value of red band; *NIR*= Reflection value of infrared band; $V_i$ = Ecosystem service value of the unit area of the i[th] type of land-use; $p_i$ = Resilience score of the i[th] type of land-use; $A$ =Total area of evaluation unit; $S$ = Output value of the tertiary industry.

Table 2: Comparison of relevant parameters of land-use type.

| Types of land-use / Relevant index parameters | Cultivated land | Forest land | Grass-land | Urban construction land | Rural residential area | Water area | Independent industrial and mining district and land for transportation |
|---|---|---|---|---|---|---|---|
| Stress intensity of human activities | 0.55 | 0.10 | 0.23 | 0.95 | 0.68 | 0.12 | 0.68 |
| Parameters of ecological resilience | 0.50 | 0.90 | 0.60 | 0.40 | 0.40 | 0.80 | 0.40 |
| Ecosystem service value ($10^4$ yuan/ km$^2$) | 7.93 | 173.00 | 20.00 | 0.00 | 0.00 | 732.00 | 0.00 |

tion and visual analysis method which emphasizes the spatial correlation measure as the core and aims at revealing the spatial interaction mechanism of research objects, divided into global autocorrelation and local autocorrelation. Global spatial autocorrelation is mainly used to explore the distribution characteristics of attribute data values in the whole regional space. The global Moran's I index is a desirable measure of response distribution, which is between -1 and 1. If it is greater than 0, it means positive correlation; if it is less than 0, it means a negative correlation. Local spatial autocorrelation is mainly used to analyze the distribution pattern of attribute values of each unit in the heterogeneous space, and measure the degree of local spatial correlation between each region and its surrounding regions. The larger local Moran's I statistic represents the spatial agglomeration of regional units with similar observations, while smaller values represent spatial agglomeration of regional units with different values (Liu et al. 2018).

The calculation formula of global Moran´s I index is as follows:

$$I = n\sum_{i=1}^{n}\sum_{j=1}^{n} w_{ij}\left(x_i - \bar{x}\right)\left(x_j - \bar{x}\right) \Big/ \sum_{i=1}^{n}\sum_{j=1}^{n} w_{ij}\sum_{j=1}^{n}\left(x_i - \bar{x}\right)^2 \quad \ldots(1)$$

The calculation formula of local Moran's I index is as follows:

$$I_i = \left(x_i - \bar{x}\right)\sum_{j=1}^{n} w_{ij}\left(x_j - \bar{x}\right) \Big/ \frac{1}{n}\sum_{i}\left(x_i - \bar{x}\right)^2 \quad \ldots(2)$$

Where, $w_{ij}$ is the weight matrix based on the spatial adjacency principle; $x_i$ and $x_i$ are evaluation values of the $i^{th}$ and $j^{th}$ unit; $\bar{x}$ is the mean of the $n^{th}$ evaluation value.

### Geographical Detector Analysis

The geographical detector is a kind of econometric statistical analysis method proposed by Wang et al. (2002) of Chinese Academy of Sciences to check the spatial differentiation of single-variable and to detect the causal relationship between two variables by checking the consistency of spatial distribution of two variables, mainly including factor detector, risk detector, ecological detector and interaction detector. The factor detector was used to detect and identify the driving force of the spatial differentiation law of the comprehensive evaluation index of land ecosystem health in Yibin City, which was, in essence, comparing the total variance of the factor index in different categories and regions with the total variance in the whole region. The calculation formula is as follows:

$$P_{D,F} = 1 - \frac{1}{n * \sigma_F^2}\sum_{i=1}^{m} n_{D,i} * \sigma_{F_{D,i}}^2 \quad \ldots(3)$$

Where, $P_{D,F}$ = Detection index of influence factor $D$ on the spatial differentiation law of comprehensive health level of the land ecosystem in Yibin City.

$n_{D,i}$ = Number of samples in the secondary area
$n$ = Number samples in the whole region;
$s^2_F$ =Variance of spatial differentiation rule of comprehensive evaluation index of land ecosystem health;
$M$ = Number of samples in the secondary region;
$\sigma^2_{F_{D,i}}$ = Variance in the secondary region;

$P_{D,F}$ is between 0 and 1, the larger the value is, the greater the influence of the index on the spatial differentiation of land-use ecological health level.

## RESULTS AND ANALYSIS

### Analysis of Health Level of Land-use Ecosystem

To reflect the health level of the land-use ecosystem of each district and county in Yibin City, the health indexes of the land-use ecosystem within the grid were put on the ArcGIS

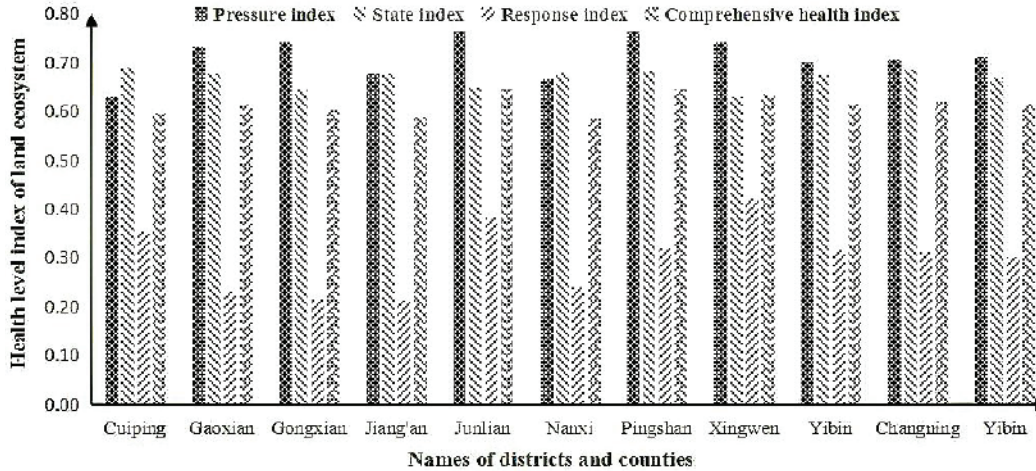


Fig. 2: Health level index of land-use ecosystem in each district and county of Yibin.

Table 3: Classification of the health status of land-use ecosystem.

| Health status | Classification standard | Area km$^2$ | Area percentage (%) | Regional characteristics |
|---|---|---|---|---|
| Healthy | [0.63，0.73] | 6131 | 46.07 | Reasonable ecological structure, strong system vitality, small external pressure, no ecological abnormality, perfect ecosystem function, stable system and sustainable state |
| Sub-healthy | [0.59，0.63) | 3962 | 29.78 | Relatively reasonable ecological structure, stable system, large external pressure, more ecologically sensitive areas, a small number of ecological abnormalities, basic ecological functions, and sustainable state |
| Unhealthy | [0.38，0.59) | 3214 | 24.15 | Defects in the ecological structure, low system vitality, high external pressure, many ecological abnormalities, weak ecological function to meet the needs of maintaining the ecosystem, and degradation of the ecosystem |

platform, and the average index of the health level of each district and county was obtained by using the summary statistical data tool (Fig. 2). Fig. 2 shows the comprehensive health status, as well as pressure, state and response subsystems of the land ecosystem of each district and county in Yibin City. In 2018, the average index of comprehensive health level of the land-use ecosystem in Yibin City fluctuated around 0.60. Junlian County, Pingshan County and Xingwen County exceeded the city's average, with the highest value of 0.65 (Pingshan County and Xingwen County); other districts and counties were slightly lower than the average level, with the lowest of 0.59 (Nanxi District).

It is necessary to deal with the differences in ecological health degree of land-use in the study area at different levels to clarify them. Natural breaks (Jenks) method in ArcGIS was used to divide the values of ecosystem health level into different discrete classes by comparing and analysing the GVF (the Goodness of Variance Fit) value. The comprehensive index of land-use ecosystem health level in Yibin City was divided into three levels, which respectively represent different health conditions, in order of healthy, sub-healthy and unhealthy. The regional characteristics of each level refer to the definitions of areas with different health level of the land ecosystem (Xu et al. 2010) (Table 3).

According to the classification standard, the health level of the land-use ecosystem of Yibin City was classified and evaluated.

It is observed from Fig. 4 that the areas with unhealthy land ecosystem were 6,131 km$^2$, accounting for 24.15% of the total. These are mainly concentrated in the transition area between the plain and hilly area in the northeast of Yibin City and the plateau and basin in the south. Where there were unreasonable ecological structure and low vitality, large areas of abnormal ecological environment, and damaged ecosystem to some extent.

The area of regions in sub-healthy level was larger than that in unhealthy level, accounting for 29.78% of the total area, which was mainly distributed in Cuiping District, Nanxi district and Jiang'an County, indicating that although there were many sensitive areas in the land ecosystem of the city, they had normal ecological functions and sustainable ecological economy.

The area of regions in healthy level was 6,131 km$^2$, accounting for 46.07% of the total area, which was mainly distributed in the middle and west of Pingshan County, the middle and south of Junlian county and Xingwen County. The main work in these places is to maintain and prevent.

## Spatial Exploratory Analysis on Health Level of Land-use Ecosystem

Moran's I was selected as the evaluation standard of the spatial difference law for the health level of the land-use ecosystem by using the spatial exploratory analysis method, revealing the characteristics of the spatial agglomeration pattern. The LISA cluster map was drawn at the significance level of 5% (Fig. 4B) according to Moran's I index of health level of the land-use ecosystem. The ecosystem by using the spatial exploratory analysis method revealed the characteristics of the spatial agglomeration pattern. The LISA cluster map was drawn at the significance level of 5% (Fig. 4B) according to Moran's I index of health level of the land-use ecosystem.

Fig. 4 A shows that Moran's I value of health level of the land-use ecosystem in Yibin City was 0.447179 in 2015. According to the distribution of Moran scattered points, the relationship between each region and a geographical phenomenon or attribute value in the surrounding region can be qualitatively determined. Points with strong spatial positive correlation will fall into the HH ("high-high") and LL ("low-low") quadrants, i.e., the health level of the areas around those with high health level will be high, the same to areas with low level, which are homogeneous; points with strong spatial negative correlation will fall into the LH ("low- high") and HL ("high-low") quadrants, that is, the health level of the region is opposite to that of the surrounding areas, which are heterogeneous. According to the distribution of attribute values, the health level of the land-use ecosystem in Yibin City has a strong spatial correlation.

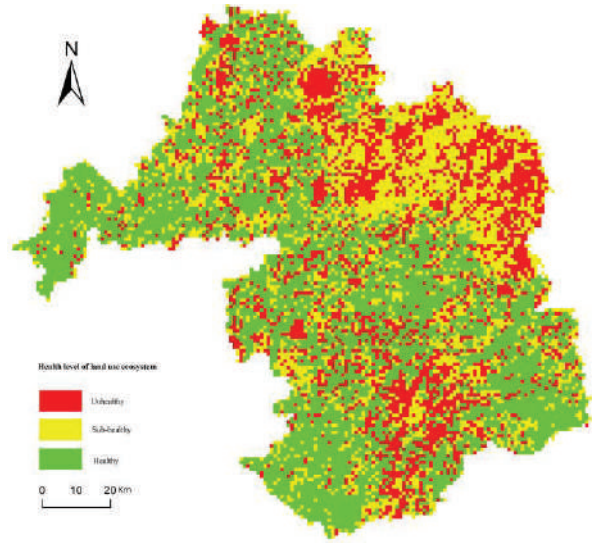


Fig. 3: Ecological health of the land-use in Yibin City.

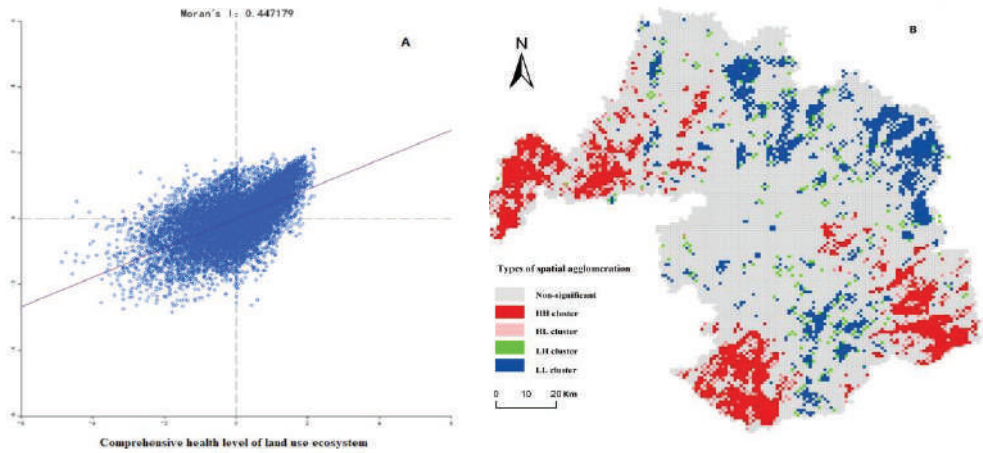


Fig. 4: Moran scatter diagram A and LISA cluster Diagram B of ecological health level of land-use in Yibin City.

It is observed from Fig. 4B that the health level of the land-use ecosystem in Yibin City was mostly non-significant in space, and those with spatial correlation were mainly positive, mainly high-value or low-value clusters. HH (high-high cluster) is distributed in the east and west of Pingshan County, the middle and south of Xingwen County, and the middle and west of Junlian County. In the future development, the ecological protection project should be put in the first place, to ensure the ecological non-degradation of the whole county.

LL (low-low cluster) is scattered in the northeast and south of Yibin City, mainly including Cuiping District, Nanxi District, Jiangan County, Yibin County and Gongxian County. The LL type area should develop new leading industries according to local conditions based on ecological economy and optimization of the land-use structure.

## Analysis of the Influencing Factors of Spatial Differentiation of Health Level of Land-use Ecosystem

The ecological health level of land-use is the result of the combined action of regional natural factors and human factors. Resilience and function" index system was selected as the geographic exploration variables of the spatial differentiation of the ecological health level of land-use, calculated the decisive power values of each influencing factor on the spatial differentiation of health level of land-use ecosystem respectively.

It is observed from Table 4 that value of the geographic detector of stress from human activities is 0.350, which is far greater than other factors, indicating that the difference of human activities is the main reason for the spatial dif-

Table 4: Geographical exploration results of spatial differentiation determination of health level of land-use ecosystem by various influencing factors.

| | Index level | Threshold values | | | P value |
|---|---|---|---|---|---|
| | | Level I areas | Level II areas | Level III areas | |
| P1 | Soil erosion | [0,0.330) | [0.330,0.667) | [0.667,1] | 0.208 |
| P2 | Terrain fragmentation | [0,0.842) | [0.842,0.931) | [0.931,1] | 0.064 |
| P3 | Population density (person / km²) | [0,0.561) | [0.561,0.769) | [0.769,1] | 0.184 |
| P4 | Stress index of human activities | [0,0.085) | [0.085,0.500) | [0.500,1] | 0.350 |
| S1 | Normalized differential vegetation index | [0,0.675) | [0.675,0.916) | [0.916,1] | 0.032 |
| S2 | Landscape diversity index | [0,0.210) | [0.210,0.730) | [0.730,1] | 0.296 |
| S3 | Ecological resilience | [0,0.0017) | [0.0017,0.110) | [0.110,1] | 0.318 |
| S4 | Ecosystem service value | [0,0.028) | [0.028,0.237) | [0.237,1] | 0.315 |
| R1 | Investment in environmental protection (104 yuan) | [0,0.225) | [0.225,0.553) | [0.553,1] | 0.054 |
| R2 | Proportion of tertiary industry in GDP (%) | [0,0.364) | [0.364,0.633) | [0.633,1] | 0.005 |

ferentiation of ecosystem health level. By the end of 2018, the area of cultivated land and construction land in Yibin City had reached 36.69% and 7.02% respectively, but there were significant differences among districts and counties. The different pressure of human activities on land leads to the destruction of regional ecological environment and the imbalance of the ecological system. Therefore, it is urgent to control the population, reduce the direct destruction of land by human activities.

The difference in resilience of the natural system is the secondary reason that affects the spatial differentiation of ecosystem health level. The values of ecological resilience, ecosystem service value and landscape diversity index were 0.318, 0.315 and 0.296, respectively, indicating that the ecological health status was affected by the resilience of the system itself. Although Yibin has a large proportion of arable land and construction land, there are various types of land. In particular, the area of grassland and forest land accounts for 41.74% of the total area of the region, which strong self-regulation and self-restoration capacity of the ecosystem. In the process of future development, should adjust the structure of land-use, optimize the spatial layout of "production, life and ecology", activate the stock, strictly observe the "red line" of cultivated land, increase the ecological land, adhere to the road of sustainable development, and promote the internal resilience of the ecosystem.

Soil properties, terrain factors and policy regulation are the other reasons for the spatial differentiation of ecosystem health level. The hilly landform brings about different regional natural geographical characteristics, and different types of soil erosion and terrain fragmentation, as a consequence, the above factors lead to obvious differences in the feedback of land ecosystem. Therefore, the city must implement a strict ecological environment protection system, severely crack down on the destruction of the ecological environment, vigorously develop science and technology, actively adjust the industrial structure, increase the proportion of the tertiary industry, reduce the pollution and damage of the primary and secondary industries to the soil, to build the ecological protection barrier of the upper reaches of the Yangtze River.

## DISCUSSION AND CONCLUSIONS

Evaluating the health level of the land-use ecosystem is the premise and foundation of planning for land space renovation. For spatial exploratory analysis, geographical detector model was used to explore the spatial distribution characteristics of the ecosystem health status of land-use in Yibin City, and its spatial differentiation law was explained by combining quantitative and qualitative methods. Based on the existing research results, firstly, the PSR model and the theory of vitality, organization, resilience and function were organically combined and improved to establish a comprehensive health assessment index system of land ecological security in line with the actual situation of Yibin. Then, the health indexes were calculated by 1km × 1km grid, and the spatial differentiation law was revealed by ESDA method. Finally, the decisive power of each factor was displayed by factor detector. All the above is the inheritance and development of previous research results. From the comparison of the results of this study, the temporal and spatial evolution law of health level of the land-use ecosystem is more in line with the regional reality (Huang et al. 2019), which also confirms that human activities are the important factors affecting land ecological security (Wei et al. 2020).

However, there are still many shortcomings: First, the evaluation index system is not perfect. The ecosystem is complex but was measured only by 10 indicators, neglecting NPP, soil pollution and other factors reflecting its attributes. At the same time, due to the availability of data, the response indexes were less, which needs to be further improved.

Second, the stress intensity of human activities, ecological resilience and ecosystem service value were the factors determined by reference to the existing research results. If the reference standards are different, the calculated values will be different. Therefore, it needs to be corrected according to the actual situation of Yibin City. Third, to facilitate the transformation and compatibility of multiple data, enrich the attribute dimensions of evaluation units, and refine the spatial accuracy of evaluation area, the grid of 1km × 1km was used as the basic evaluation unit, but the influence of administrative boundaries, data accuracy, and data processing convenience on the grid size was not considered. Fourth, adding the content of time series analysis may reveal the temporal and spatial evolution of health assessment of land-use ecosystem.

Following conclusions can be drawn from the study.

1. The health level of the land-use ecosystem in Yibin City is generally good, and the regional development is relatively balanced, but there are significant differences between the municipal districts and suburban counties. The average index of comprehensive health level of the land-use ecosystem in Yibin City fluctuates around 0.60, and the land for health level accounts for 46.07% of the total area, the land for sub-health level accounts for 29.78% of the total area, the land for unhealthy level accounts for 24.15% of the total area. The main reason is that the land-use structure of the central city and suburban counties is different, and the impact of human activities on the land ecosystem is also different. The large area of urban construction land and the small amount of ecological land lead to the poor ability of self-regulation and self-recovery in the ecosystem.
2. The health level of the land-use ecosystem in Yibin City was mostly non-significant in space, and those with spatial correlation were mainly positive, mainly high-value or low-value clusters. HH type was distributed in the east and west of Pingshan County, the middle and south of Xingwen County, the middle and west of Junlian County, and LL type was scattered in the northeast and south of Yibin City.
3. The difference of human activities was the main factor that affects the spatial differentiation of health level of the land-use ecosystem in the whole city, followed by the difference of natural system resilience, and the other factors were soil properties, landform and policy regulation. Finally, it was concluded that tightening the upper limit of capacity, holding the ecological bottom line, insisting on the intensive utilization of land, optimizing the spatial layout of production, life and ecology, adjusting the industrial structure, and developing ecotourism will become the necessary measures for Yibin City to improve the ecological health level of land-use and build a famous ecological city of landscape culture.

## REFERENCES


Chen, P. 2007. Assessment of regional ecological health based on remote sensing and GIS landscape scale: a case study of the new area of bay cities. Acta Scientiae Circumstantiae, 27(10): 1744-1752.

Gao, J.Z., Xia, M.L., Meng, Z. and Liu, Y.Z. 2017. Diagnosis of land-use and ecological health under PSR framework. Jiangsu Agricultural Sciences, 45(11): 240-243.

Hao, L.X., Sun, R.H. and Chen, L.D. 2014. River ecosystem health assessment in Haihe River Basin. Environmental Science, 35(10): 3692-3701.

He, X., Jiang, G.H., Zhang, R.J., Ma, W.Q. and Zhou, T. 2015. Spatial and temporal change analysis of land-use ecological health based on PSR model taking Pinggu District of Beijing as an example. Journal of Natural Resources, 12: 2057-2068.

Huang, L.J. and Yang, P. 2019. Spatio-temporal evolution characteristics and influencing factors of land ecological security in the Yangtze River Economic Belt. Resources and Environment in the Yangtze Basin, 28(8): 1780-1790.

Jiang, W.G., Pan, Y.Z., Hou, P., Li, X., Ji, W. and Zheng, J.R. 2009. Comprehensive assessment of wetland ecosystem health in Dongting Lake area. Geographical Research, 28(6): 1665-1672.

Liu, J.X. and He, W. 2018. Study on spatial differentiation and evolution mechanism of rural areas in Sichuan Province. Journal of Sichuan Normal University (Natural Science Edition), 41(01): 122-130.

Liu, X.B., Zhen, Y. and Chen, Y.J. 2017. Characteristics of precipitation change in Yibin City in recent 60 years. Journal of Neijiang Teachers College, 32(4): 73-77.

Ma, M.R., Han, H., Wang, H.B., Yang, J. and Qu, W.H. 2014. Ecosystem health assessment of Chongming County Based on RS and GIS. Ecological Science, 33(4): 788-796.

Pan, Y.Z., Shi, P.J., Zhu, W.Q., Gu, X.H., Fan, Y.D. and Li, J. 2004. Remote sensing quantitative measurement of ecological assets of terrestrial ecosystems in China. Scientia Sinica, 34(4): 375-384.

Wang, J.A., He, C.Y., Dong, Y.C., Gao, L. and Xu, W. 2002. Analysis of driving forces of land-use change in urban-rural transition area of Beijing. Advance in Earth Sciences, 17(2): 201-208.

Wei, F. 2017. Ecosystem health assessment at township, town and sub-district level. Wei Fang: Lanzhou Jiaotong University.

Wei, Y.C., and Zhang, L.Q. 2020. Spatiotemporal pattern and obstacle factors of land eco-security early warning in Henan province. Research of Soil Land Water Conservation, 27(3): 238-246.

Xie, G.D., Zhen, L., Lu, C.X., Xiao, Y. and Chen, C. 2008. A value-based approach to ecosystem services based on expert knowledge. Journal of Natural Resources, 23(5): 911-919.

Xu, M.D., Li, J., Peng, J., Niu, J. and Cao, L. 2010. Ecosystem health assessment based on RS and GIS. Ecology and Environmental Sciences, 19(8): 1809-1814.

Zhang, J., Zou. T., Lu, X., Yi, K., Tong, Z. and Liu, X. 2011. The application of fuzzy comprehensive evaluation in land-use and ecological health evaluation. Science and Technology Innovation Herald, 29(19): 34-39.

Zhang, X.Q. and Shi, P.J. 2010. Assessment of urban ecosystem health in Lanzhou based on PSR model. Journal of Arid Land Resources and Environment, 24(3): 77-82.

Zhao, M., Yu, J., Chen, P.M., Feng, X. and Nie, Y.K. 2015. Research progress of ecosystem health assessment in the gulf. Journal of Anhui Agricultural Sciences, 35: 8-11.

Zhao, Y.T., Li, W.L., Chen, D., Yu, C., Zhao, X.L. and Xu, J. 2017. Dynamic evaluation of grassland ecosystem health in Alpine pastoral area - taking Gannan as an example. Practaculture Science, 34(1): 16-29.

Zhu, W.H., Guo, Y.L., Sun, P., Miao, C.Y. and Cao, G.L. 2012. Health assessment of wetland ecosystem in the lower reaches of Tumen River. Acta Oecologica, 32(21): 6609-6618.

Nature Environment and Pollution Technology
An International Quarterly Scientific Journal

p-ISSN: 0972-6268
(Print copies up to 2016)
e-ISSN: 2395-3454

Vol. 19 | No. 4 | pp. 1483-1490 | 2020

Original Research Paper

https://doi.org/10.46488/NEPT.2020.v19i04.014

Open Access Journal

# Causes of Air Pollution in Bangladesh's Capital City and Its Impacts on Public Health

**Kudrat-E-Khuda (Babu)†**
Department of Law, Daffodil International University, Dhaka, Bangladesh
†Corresponding author: Kudrat-E-Khuda (Babu); kekbabu@gmail.com

**Nat. Env. & Poll. Tech.**
**Website: www.neptjournal.com**

*Received:* 14-04-2020
*Revised:* 03-05-2020
*Accepted:* 25-06-2020

**Key Words:**
Air pollution
Dhaka city
Air quality
Human health

## ABSTRACT

Air is one of the precious natural resources which is essential for living beings. Pollution in the urban areas like Cairo, Delhi, Mexico and Dhaka far surpasses the acceptable limits set by the World Health Organization (WHO). Urban air pollution in the South Asian region is approximated to cause more than 300,000 deaths and billions of cases of respiratory disease per year. In Bangladesh, about 200,000 people die each year due to air pollution as the WHO estimates in 2018. The air in Dhaka city, the capital of Bangladesh, has worsened to a level that the city has been identified as one of the most polluted cities in the world. Taking the problem with utmost importance into consideration as it is related to public health, air pollution is being treated as one of the priority issues. The level of pollution in the roadside environment is deeply connected with the density of motor vehicles plying on the roads. This situation is expected to worsen further in the upcoming days due to the increasing number of motor vehicles resulted from rapid economic growth and industrialization. This paper aims to provide the present status of air pollution in Dhaka city and some specific recommendations for making the city a better living place by reducing its air pollution.

## INTRODUCTION

Man is responsible, in many ways, for the present status of the environmental disasters that are on the rise all over the world. It is a common scenario and true feature that air pollution is one of the most concerning and alarming issues in the present world among the variety of manmade disasters. Generally, air pollution can be described as a condition of the atmosphere where different elements are present at concentrations that are higher than the normal ambient concentrations producing an effect measurable on humans, animals, vegetation or materials (Alam 1999). Here the term 'substances' refers to any chemical compound or elements which are natural or manmade and may be airborne. Theses chemical compounds or elements are nothing but exist as solid particles, liquid drops or gases. There are many substances in the atmosphere which may be harmful or benevolent. However, the term 'measurable effect' logically does not focus on those substances which cause unwanted effects. It is of no doubt that air is becoming more worsened day by day, and both human activities and natural phenomena are responsible for it. In Bangladesh, vehicular and industrial emissions are the two great sources of air contamination (EEA 2016). Particularly, the cities are subject to much air pollution as they have more vehicles plying on the road and industries than the rural areas. In the current years, air pollution has been given the best priority among environmental issues not only in Asian countries but also in the other countries of the world. In many parts of the world, exposure to air pollution, at present, has become the prime threat to human health. In particular, in cities, the urban population has been victimized of respiratory and other airborne diseases due to the emission issues that have increased the death rate significantly (WHO 2018). Dhaka is the capital of Bangladesh and also the centre point of most of the commercial activity, and is facing this problem acutely. Being centre of the country, it has a vast number of industries in and around the city, i.e. ready-made garment (RMG) manufacturing industries, different types of mills, industries, factories along with chemicals industries, brickfields and so on (Mahmud 2011). Moreover, the city has too much population causing it polluted which is a matter of great concern. In contrast, other cities of Bangladesh like Rajshahi, Khulna, Bogura and Chattagram have much lesser health-related problems caused by air pollution. The increasing numbers of motor vehicles, industrial development on a random basis and continuous housing have made ambient atmospheric conditions deteriorated. The result of this study will assist decision-maker in formulating national policies to combat air pollution.

## MATERIALS AND METHODS

All the relevant data and information were collected and used from primary and secondary sources of air pollution.

The information from different books, journals, booklets, proceedings, newsletters, souvenirs, and consultancy report that are available in the libraries of Daffodil International University, Bangladesh was compiled for the study. Maximum necessary support was taken from internet searching. The study presents a synopsis of several monitoring and surveys conducted by the author on ambient concentrations of lead, black smoke, nitrogen oxides, (NOx), Ozone ($O_3$) particular matters, carbon monoxide (CO) and sulphur dioxide ($SO_{2)}$. The selected data (collected from the selected stations between 2018 and 2019) reveal that the ambient air of the capital city of Bangladesh (Dhaka) is polluted more than 55 per cent of the year. The Air Quality Index observed in different locations of the Dhaka city shows that the roadside environment of 70% areas is severely polluted while that of 30% is heavily polluted as per the WHO's standards. The level of pollution in the roadside environment is deeply connected with the density of different types of motor vehicles moving on the roads regularly. This situation is expected to worsen further in the upcoming days due to the increasing number of motor vehicles resulted from rapid economic growth and industrialization. The present study provides some considerable recommendations to reduce air pollution in Dhaka, the capital city of Bangladesh.

## RESULTS AND DISCUSSION

**Air pollution in Dhaka city:** The industrial and vehicular emissions are the two main great sources of air pollution in Dhaka city. The industrial emission sources like thousands of ready-made garment factories (RMG), chemical industries, brick kilns, pharmaceutical industries, etc. produce not only an enormous amount of smokes but also dust, different types of gases, fumes, etc. which are mainly responsible for air pollution. Moreover, the tanneries at Hazaribag in Dhaka city emit ammonia ($NH_3$), chlorine (Cl), hydrogen sulphide ($H_2S$) and some other chemicals which are the highly poisonous and the cause of public health complaints. The number of vehicles is also increasing day by day in the capital city of Bangladesh as the population is increasing and the unabated urbanization is going on, all this lead to a rise in air pollution (Begum et al. 2011). The baby-taxies, tempos, mini-trucks, motorcycles and other vehicles with two-stroke engines are the prime source of air pollution in Dhaka city, which are recently observed by the scientific research conducted by the specialists of the Department of Environment (DoE), Bangladesh along with other relevant organizations in Bangladesh. Currently, more than 500000 motor vehicles including about 65,000 baby-taxies are plying in Dhaka city alone (Franchini 2019). In addition, a high number of trucks and mini-buses, which are overloaded, poorly maintained and very old are also plying on the streets emitting gases and smoke. Indeed, more than 80 % of vehicles playing on the streets of Dhaka city daily are defective and these types of vehicles emit black smoke far beyond the limits. Vehicles using petrol and diesel emit black smoke which contains unburned fine carbon particles. In particular, the quality standards of air vary from one place to another place due to its geographical location. Areas with more industrial and commercial institutions are highly contaminated than the residential areas. The areas Mohammadpur, Farmgate, Manik Mia Avenue, Tejgaon, Mohakhali, Gabtoli, Mirpur, Bonosree, etc. are the worst affected areas in Dhaka city. Generally, 400 micrograms/cubic meter is the allowable limit for the concentration of suspended particulars in air. But the concentration of suspended particulars goes up to 3,000 micrograms/cubic meter (at the Farmgate area of the Dhaka city) as per the study conducted in 2019. This study found that the presence of $SO_2$ in the air at the Farmgate area of Dhaka city is more than three times than the usual permissible limit. The presence of 100 micrograms $SO_2$ in the air is the maximum permissible limit for per cubic meter. However, the presence of 385 microgram sulphur-dioxide was found in the air of Farmagte area. Correspondingly, in the Tejgaon Industrial area, the similar picture of the air pollution was also found where the maximum concentration of suspended particles was 1,849 micrograms/cubic meter (in January of 2018) though the permissible limit is 500 micrograms/cubic meter. Generally, the months from December to March are considered as the dry months in Bangladesh and during this period the capital city Dhaka has the highest concentration of air pollution.

**Air pollutants level in 2018 in Dhaka city:** In March 2018, the average emission of air pollutants at Bangladesh Agricultural Research Council, Farmgate, Sangsad Bhaban and Darussalam Road, Mirpur in association with Standard Air Quality in Bangladesh are presented in Fig. 1.

**Traffic volume in Dhaka city:** Currently, Dhaka city is the most polluted city in the world as per the report released by Switzerland-based IQ Air and the seventh most populated city in the world (Fig. 3). More than 20 million people live here and the population is increasing randomly as people are coming here from different parts of Bangladesh for jobs and work. This overpopulated city has been declared as the most polluted urban city worldwide, and its traffic volume is the largest relative to other cities of Bangladesh. Fig. 2 and Fig. 4 show how the number of vehicles is increasing in Dhaka each year. The non-motorized vehicles in particular in road intersections, are significantly responsible for the severe congestion and thus enhance emission problems. Of total trips, the contribution of non-motorized transport

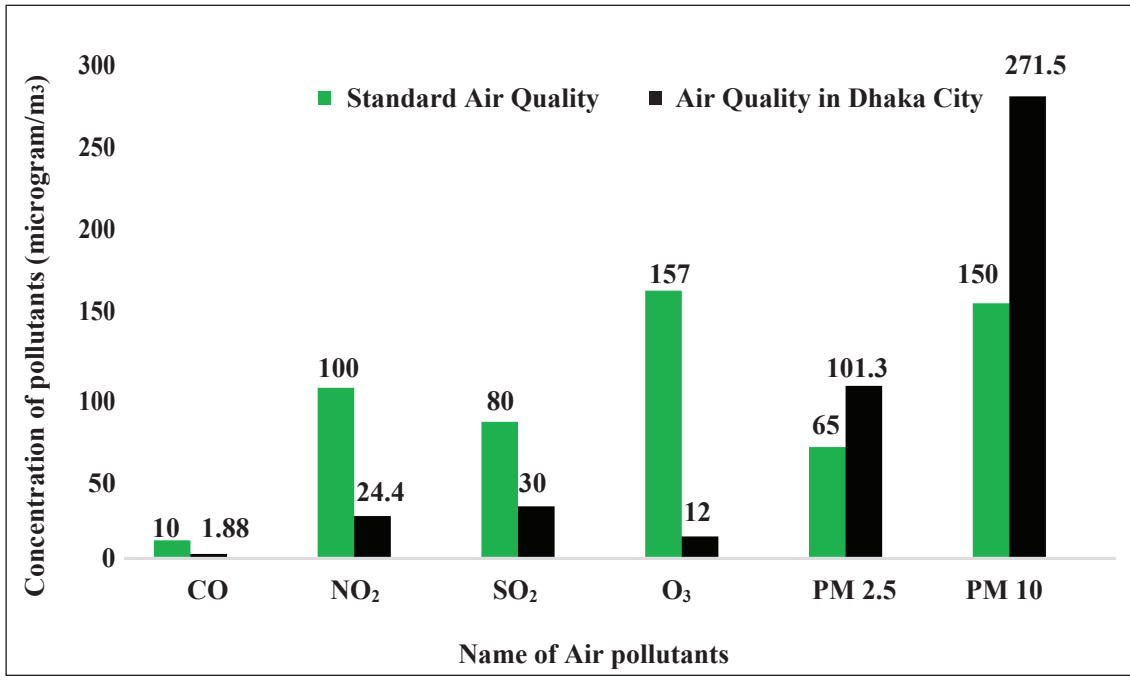


(Source: Department of Environment, Bangladesh)

Fig.1: Average ambient of air pollutants in Dhaka City.

Fig. 2: Traffic jam in Dhaka city.

(NMT) is 80% while that of motorized transport (MT) is only 5.9%.

**Air particulate matter and gaseous pollutants:** The continuous air quality monitoring station was first set-up in 2018 by the Department of Environment at the premises of the Parliament Building, the most important public institution in the country which is located in the centre of the city, in an attempt to monitor air quality and control air pollution in Dhaka city. It was observed that concentration of pollutants in the air was high during October to April and the PM was mostly constituted of $PM_{10}$ and $PM_{2.5}$.

Over the period from November 2019 to January 2020, the author found the presence of the Pb in the air of Dhaka city at 14.6 μg/$m^3$, though the maximum allowable limit for Pb in air, as per the WHO guideline (1 year average), is 0.51 μg/$m^3$.

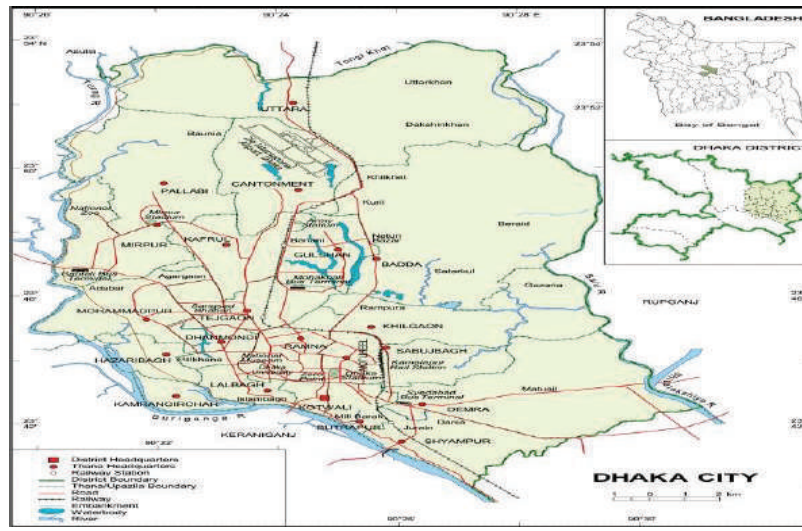


Fig. 3: Map of the Dhaka City (The area of Dhaka is 1,353 km$^2$, of which Dhaka City Corporation occupies 276 km$^2$. The city is situated between 23°42′ and 23°54′ north latitude and 90°20′ and 90°28′ east longitude).

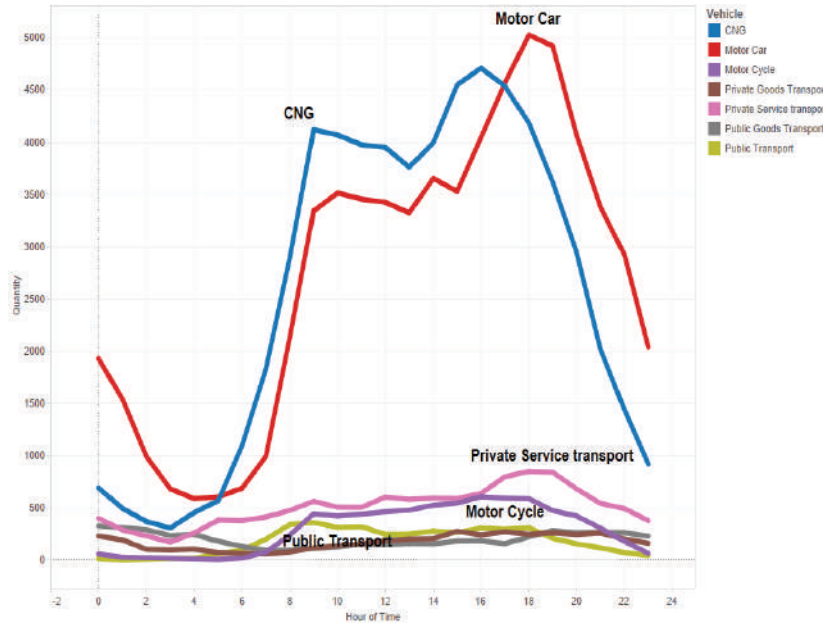


Fig. 4: Number of vehicles is increasing in Dhaka each year.

**Dhaka city air quality index:** According to an article published in the *Dhaka Tribune* on January 30, 2020, air is graded as "hazardous" in nature. The article states that the Dhaka city has earned the top position among the cities with worst air in the Air Quality Index. United News of Bangladesh in another report terms the city to be 'dangerous' with an AQI score of 408. Around 301 and 500, an AQI level includes emergency health alarms and is much more likely to affect the community as a whole.

To make the public anticipation about the air pollution problems clear, some calculations have been carried out as per the collected data as well as the projected air quality standards, to provide some AQI numbers. On the basis of Air Quality Rating, the index is measured for every single pollutant. For a number of pollutants, AQI is obtained from the geometric mean of the Air Quality Ratings. The findings

are abridged in Table 1. It has been found in the observation that the roadside environment of 70% areas, if we take the WHO's standards into consideration, is severely contaminated while that of 30% is heavily contaminated. Even, if we take the standards set by the Government of Bangladesh into consideration, severe contamination is found in all areas. As per the guidelines of WHO, Mohakhali, Jatrabari and Panthopath are the most polluted areas where the AQI is above 200. The AQI is above 100 even at roads besides residential areas like Dhanmondi and Jigatola.

**Suspended particulate matters (SPM) in Dhaka city air:** With the increasing industrialization, urbanization and infrastructure construction, the air is becoming more polluted day by day. In dry season, air pollution reaches its peak. The vehicular emissions, the industrial emissions and the waste burning are highly responsible for air pollution. Particulate matters $PM_{10}$ refer to those substances which are of 10 μm in size and these are considered as the rigorous health exposures (Flossmann et al. 2018). Brick kilns, cement, steel and ceramic factories are the sources from where $PM_{10}$ is emitted. Per year, among the sources, a cement factory emits most contributing 130 tones $PM_{10}$ while a brick kiln adds 83 tons. Along with this, a steel re-rolling mill and a ceramic factory also contribute 17 tons and 20 tons of $PM_{10}$ every year. As per the report of the State of Global Air 2019, approximately 72% of domestic households use solid fuels that also leads to air pollution. A survey was carried out at several places including those of busy roads of Dhaka city where the department took 8 hours measurements. The survey shows SMP concentrations of 660-2450 μg/m$^3$ at the area of Farmgate of Dhaka city though the minimum SMP concentrations, as fixed for the Standard for Commercial Area, is 400 μg/m$^3$. During the dry season (from December to March), the SMP trends are highly elevated because of increment in dust and the open burning.

## THE VARIOUS AIR POLLUTANTS AND THEIR EFFECTS ON HUMAN HEALTH

Air is one of the natural resources that are essential for animals and human beings. It is impossible to survive for human beings without air. So, the pollution of air can interfere with human health, and it is only in recent times that mankind has realized to what extent this interference is sustainable (Chafe et al. 2014). Mr. Md Shahab Uddin, the Environment, Forests and Climate Change Minister of Bangladesh said on 25 November 2019 to the journalists that Dhaka city has the most polluted air in the world because

Table 1: Air quality levels in the roads of Dhaka City.

| Standard | Category of Air Quality | Range of the Estimated Value of AQI | Average AQI for the Category | Number of Locations in Category |
|---|---|---|---|---|
| AQI Calculated on the basis of Bangladesh Standard | Severely Polluted | 209-454 | 318 | 49 (100%) |
| Calculated AQI on the basis of WHO Standard | Severely Polluted | 131-215 | 167 | 34 (70%) |
| | Heavily Polluted | 102-124 | 114 | 14 (30%) |
| | Polluted | 99 | - | 1 |

Source: Biswas (2020).

Fig. 5: The common scenario of air pollution in Dhaka city.

the level of air pollution has been increasing here day by day (The Independent, 27 November 2019). Taking the problem with utmost importance into consideration as it is related to public health, air pollution is being treated as one of the priority issues. Contamination in the urban areas like the New Delhi of India, Linfen of China, Faisalabad of Pakistan and Dhaka far surpasses the acceptable limits set by the WHO. An epidemiological study shows that air pollution is liable for the tens of thousands of extra deaths as well as the billions of dollars of loss of productivity each year in the developing countries like Bangladesh (Faiz et al. 1996). As per the recent estimates of the World Bank, more than 450000 people die and billions of cases of respiratory diseases occur in the South Asian region along with Dhaka due to the urban air pollution where the children and old men are the most vulnerable to the air pollution. In 2018, WHO estimated that about 200000 people died in Bangladesh each year due to the polluted air. Moreover, indoor and outdoor air pollution killed more than one lac people in 2017 in South Asia, as per the study report conducted by the US-based Institute for Health and Evaluation as well as the Health Effects Institute. As per a medical report, in Bangladesh perspective, four of the top 10 death-causing diseases are directly related to air pollution, i.e. stroke (5%); lung cancers (13%); chronic obstructive pulmonary disease (7%); chemic heart disease (6%), and the lower respiratory tract infections (7%). Besides, the effects of different types of air pollutants on human health are as below.

i. **Carbon dioxide:** $CO_2$ plays an important role in the planetary temperature structure as it is the major absorber of infrared radiation.

ii. **Carbon monoxide:** The high concentration of CO in blood makes it difficult for our heart to pump blood through the blood vessel that takes blood away from the heart to all parts of our body.

iii. **Hydrocarbons: HC**s cause convulsion of the central nervous system and may also form $O_3$ (ozone) with the oxides of nitrogen.

iv. **Lead:** Pb is liable for the kidney and irreversible brain damage. Pb is more dangerous for young children.

v. **Sulphur dioxide:** Sulphur dioxide is a colourless gas having a sharp odour. It irritates the eyes (Gonzalez et al. 2013). It also affects the functions of the lungs along with the respiratory system (Li et al. 2015). Moreover, it also causes cough, aggravation of asthma and mucus secretion (Padula et al. 2013).

vi. **Ozone:** The excess $O_3$ in the air affects human health in different ways. It is responsible for asthma, premature birth and the lung malfunctioning (Zaidi et al. 2011, Yamamoto et al. 2014). Ozone also affects cardiac development (Kannan et al. 2007). It is increasing the hospital admissions for asthma in children, especially in the South Asian countries along with Bangladesh (Lin et al. 2017).

vii. **Oxides of nitrogen:** NOx affect directly and indirectly human health and cause eye irritation, headache and breathing problems, and chronically reduce the function of our lungs and corrode teeth (Nishimura et al. 2013). Besides, NOx can affect human beings indirectly by damaging the ecosystems as they rely on the land and in water harming the plants and animals (Mc et al. 2007). An estimated 70,000 deaths occur from exposure to $NO_2$ whereas in Bangladesh it is estimated that 3000 premature deaths occur each year from exposure to PM and NOx (Faruque 2017). As per the study conducted in Hong Kong, 10 $\mu g/m^3$ increase in NOx corresponded to an adjusted OR of 1.25 (95% CI 1.16 to 1.36) for diagnosed asthma in 6 to 13 years old babies (Liu et al.2014).

## STEPS TO REDUCE AIR POLLUTION IN DHAKA CITY

Among the 17 Sustainable Developments Goals (SDGs), there are two specific goals related to the air and environment and these two SDGs are SDG 3 and SDG 11 that must be addressed if we want to materialize the importance of the air control management because a clear reference has been made in the duo goals about the air pollution. This issue not only mentioned the duo goals but it has multiple drivers and related sustainability impacts linking around 14 out of United Nations 17 SDGs. These goals, related objectives and indicators are linked with multiple drivers**,** while the best outcome to ensure the clean air can be achieved via the integrated approach of air quality management. Otherwise, the dream behind the SDGs will remain quite meaningless and unfulfilled. The Bangladesh government along with the Dhaka City Corporations can consider the following recommendations to reduce the air pollution in Dhaka city.

- The air of Dhaka city usually becomes severely polluted in December-March. Therefore, air pollution varies from one season to another season. So, the air control strategy needs to be unique and it will not be like the other overall management policies of the government.
- For the developing strategy for air quality control, the priority pollutants need to be determined soon. Determining pollutants and health hazards resulting from poor air quality of a particular area or location can help form a solution to that area or location.
- Along with other pollutants in the air, the increasing level of dust pollutants is gradually becoming a serious health threat to the residents of Dhaka city which is of

great concern nowadays. For that reason, a cost-effective control system should be set-up immediately that includes assimilating control measures in light of reducing the sources of dust and waste points. To meet the SDG objectives and indicators, other dominant source points like construction sites, brickfields, the total transportation system of Dhaka city, etc. should be taken into consideration.

- To reduce air pollution, the citizens of Dhaka city can play an important role individually or unitedly. People can play a vital role to reduce air pollution by driving less and driving wisely; using fuel-efficient vehicles, public transport, walking, cycling and so on.
- However, to ensure a better response in city air quality management, it is must to develop an integrated system. Regarding the air quality management, the Bangladesh government has some effective strategies and guidelines but there is no adequate monitoring and implementation programs. But these are very important not only to mitigate the air pollution but also to allow the owners of source points for getting the information they need to monitor and improve and upgrade their system further.
- Generally, the decision-makers of Bangladesh typically follow a traditional method to the air control system. In the manufacturing fields, this system primarily lays a set of standards for polluters. This could be a positive achievement for just only industrial sector, but the government can extend the process towards punishing all kinds of polluters and provide economic stimuli to mitigate emissions.
- While a limited incentive system is currently in operation, it may be extended to involve numerous initiatives and activities such as tax incentives related to pollution, waste-treatment subsidies, waste disposal rebate schemes, etc.
- It is true that the air control management policy mostly depends on the regulatory authorities of Bangladesh working within the missions-visions and network of the SDGs, declared by the UN and we should promote greater public involvement in the system.
- The Bangladesh government, different types of mass media along with environmental activists and organizations should encourage the mass people of Dhaka city along with the other people of the country to contribute something good from their positions to make the Dhaka city as the green city, as the living city as well as air-pollution free city. The proper direction, counselling and motivation from the government level and other concerned levels can motivate the people of Dhaka city to reduce less air pollution.
- Finally, the Bangladesh government should identify the real causes of air pollution in Dhaka city as per the given directions of the Supreme Court of Bangladesh. On 27 November 2019, the High Court Bench of Bangladesh Supreme Court directed the authorities concerned to identify the causes of air pollution.

## CONCLUSION

Air is one of the precious natural resources and it is impossible for human beings to live without it. It is well known that fresh air is good to improve blood pressure and heart rate; it makes us happier; fresh air strengthens our immune system; it cleans our lungs; it gives us more energy and a sharper mind. But the pollution of air can interfere with human activities, and it is only in recent times that mankind has realized to what extent this interference is sustainable. All the air pollutants are hazardous to health; for instance, short-term exposure to $SO^2$ to humans causes aggravation of asthma and chronic bronchitis. Moreover, different types of air pollutants affect human health in different ways. Those pollutants are also responsible for the lung infection, pulmonary infection and sometimes increase death rate. So, air pollution in Dhaka city has become the most important issue in the present context. The present study reveals that 70 per cent of the city's roadsides are severely polluted. Consequently, its impacts on the health of the city dwellers are very alarming. The presence of PM, $SO_2$ and Pb levels in the air of Bangladesh exceeds the acceptable limits set by WHO resulting pollution. The ambient level of $NO_2$ is, as defined by the air quality standard, regularly lower than the acceptable limit. Though the available time-series data are insignificant, accessible air quality indicators suggest that air of Dhaka city is getting worse day by day. Some positive measures, such as replacement of 2-stroke 3-wheelers with 4-stroke and the introduction of unleaded gasoline, have improved air quality but are still insufficient to track and control motor vehicles' pollution. Limited capacity of roads in comparison with growing traffic volumes and lack of traffic management have also hampered the air quality.

## ACKNOWLEDGEMENTS

The author is thankful to Mrs. Eva Armin (a former student of Bangabandhu Sheikh Mujibur Rahman Agricultural University, Bangladesh); Professor Dr. M. Habibur Rahman (BUET, Bangladesh) and A. Al-Muyeed (DUET, Bangladesh) for sharing their necessary information and facilities required for this work.

## REFERENCES


Alam, B., Rahman, H. and Jaigirdar, A. 1999. Ambient air quality at roadside in Dhaka City. J. of Poll. Res., 18(2): 65-72.

Biswas, K. 2020. Impact of unleaded gasoline introduction on the concentration of lead in the air of Dhaka, Bangladesh. J. of Air & Waste Manag. Asso., 53(11): 1355-1362.

Begum, A., Hossain, A. and Saroar, G. 2011. Sources of carbonaceous materials in the airborne particulate matter of Dhaka. Asian, J. of Atmo. Env., 5(4): 237$_2$246.

Chafe, Z.A., Brauer, M. and Smith, K.R. 2014. Household cooking with solid fuels contributes to ambient $PM_{2.5}$ air pollution and the burden of disease. Env. Health Pers., 122(12): 1314-1320.

EEA, European Environment Agency. 2016. Air quality in Europe-2016 report, Luxembourg Publications Office of the European Union. Retrieved from http://www.eea.europa.eu

Faiz, A., Weaver, C.S. and Walsh, M.P. 1996. Air Pollution from Motor Vehicles: Standards & Technologies for Controlling Emissions. WB Publishers., pp.11-12.

Faruque, A. A. 2017. Environmental law: global and Bangladesh context. New Warsi Book Corporation., pp. 374.

Flossmann, F.I., Hall, W.D. and Pruppacher, H.R. 2008. A theoretical study of the wet removal of atmospheric pollutants: Part-I. The redistribution of aerosol particles captured through nucleation and impaction scavenging by growing cloud drops. J. of Atmos. Sci., 42(1): 583-606.

Franchini, M. and Mannucci, P.M. 2019. Impact on human health of climate changes. Euro. J. of Int. Med., 26(1): 1-5.

Gonzalez., Pertega, S. and Garnelo, L. 2013. Truck traffic related air pollution associated with asthma symptoms in young boys: A cross sectional study. J. of Pub. Health., 127(3): 275-281.

Kannan, S., Misra, D.P. and Dvonch, J.T. 2007. Exposures to airborne particulate matter and adverse perinatal outcomes: A biologically plausible mechanistic framework for exploring potential. Env. Health Perspec., 11)114): 1636-1642.

Lin, Y., Zhou L. and Xu, J. 2017. The impacts of air pollution on maternal stress during pregnancy. Sci Rep., 7: 40956 DOI: 10.1038/srep40956

Liu, F., Zhao, Y. and Liu. Y.Q. 2014. Asthma and asthma related symptoms in 23326 Chinese children in relation to indoor and outdoor environmental factors: The Seven Northeastern Cities (SNEC) study. Sci. Total Env., 497(498): 10-17.

Mahmud, I. 2011. Air pollution cost TK 124 billion a year in Dhaka city, Bangladesh Independent News. Retrieved from: http:// www.bdinn.com

Mc, C., Culligan, P. and Nieuwenhuijsen, M. J. 2007. Respiratory effects of exposure to diesel traffic in persons with asthma. N. Engl. J. Med., 357(23): 2348-2358.

Nishimura, K., Galender, J.M. and Roth, L.A. 2013. Early life air pollution and asthma risk in minority children. Ame. J. of Respir. Crit. Care Med., 188(3): 309-318.

Padula, A. M., Ira B. and Tager, S. L. 2013. The Association of Ambient Air Pollution and Traffic Exposures with Selected Congenital Anomalies in the San Joaquin Valley of California. Am. J. Epidemiol., 177(10): 1074-1085.

Staff Reporter 2019. Identify causes of air pollution in capital. The Independent, 2019, November 27, 2019, Retrieved from http://www.theindependentbd.com/printversion/details/225366.

World Health Organization (WHO). World Report 2018: Annual review of human rights around the globe. Retrieved from: http://www.hrw.org

Yamamoto, S., Phalkey, R. and Malik, A. 2014. A systematic review of air pollution as a risk factor for cardiovascular disease in South Asia: Limited evidence from India and Pakistan. Int. J. Hyg. Environ. Health, 217(2-3): 133-144.

Zaidi, S.M., Moin, O. and Khan, J.A. 2011.Second-hand smoke in indoor hospitality venues in Pakistan. Int. J. of Tuberc Lung Dis., 15(7): 972-977.

Nature Environment and Pollution Technology
An International Quarterly Scientific Journal

p-ISSN: 0972-6268
(Print copies up to 2016)
e-ISSN: 2395-3454

Vol. 19 | No. 4 | pp. 1491-1497 | 2020

Original Research Paper

https://doi.org/10.46488/NEPT.2020.v19i04.015

Open Access Journal

# Nature of Waste and Disposal Practices Among Different Business Holders Around Industrial Area of Rosslyn, Pretoria, South Africa

**J.O. Olowoyo†, L. Mpagane and S. Nyathi**
Department of Biology, Sefako Makgatho Health Sciences University, Pretoria, South Africa
†Corresponding author: J.O. Olowoyo; woleolowoyo@yahoo.com

**Nat. Env. & Poll. Tech.**
**Website: www.neptjournal.com**

*Received:* 09-12-2019
*Revised:* 06-02-2020
*Accepted:* 16-04-2020

**Key Words:**
Waste disposal
Management
Recycling

## ABSTRACT

Waste disposal and management is a serious concern especially in most of the developing countries. Both big and small business holders may influence the quality of their immediate environment. The present study investigated the nature of waste and attitude of different business units towards waste disposal practices around the industrial area of Rosslyn, Pretoria, South Africa. Mixed method approach was used to carry out the research. 138 questionnaires were administered to owners of small and medium-sized business units and managers of big companies. Questionnaires were used to collect information on the nature of waste and attitude towards waste disposal and management. It was noted that the industrial area in Rosslyn is dominated largely by small and medium-sized business enterprises. The level of education of most of the small-sized business units was below matric level. The most common types of waste generated were papers, plastics and discarded food in some disposable materials. The small business holders did not consider waste separation as an important issue and also the purchase of different waste bins for wastes separations. The small business holders believed that it is the responsibility of the government to provide different waste bins. From the companies that render services to big companies, metals are separated for recycling mainly because they can be sold to other companies. Concern for the environment or human did not have any impact on waste management. The study concluded that though there are waste bins in the study area, these seem inadequate thus leading to improper waste management systems around the industrial area in Rosslyn. Workers and small companies' holders did not see any reason why they should be concerned about proper waste management. Campaigns and education on waste management should be intensified to change attitudes towards proper waste management.

## INTRODUCTION

Municipal solid waste disposal has become one of the major challenges both in developed and developing countries all over the world (Wang et al. 2018). This is as a result of urbanization and various developmental projects embarked upon in these countries (Harris-Lovett et al. 2018). Nyakaana (2012) reported that the increase in urban, economic and industrial activities, as well as the resultant population increase, has led to an increase in the quantity of solid waste generated.

In most of the urban city centres, discarded materials such as papers, glasses, bottles and leftover food items in disposable plates littering the roads that tend to accumulate over a prolonged period if not collected have become a permanent feature of most of these cities (Banjo et al. 2009). Hazra & Goel (2009) and Moghadama et al. (2009) also noted that improper bin collection systems, poor route planning, insufficient bins, poor roads and unwillingness to pay for the removal services have accounted for this phenomenon.

In general, if wastes are not properly collected, transferred and disposed at an approved waste disposal sites, they may decompose, produce methane or pollute both the water and soil within the area (Oyelola et al. 2009). Improper waste disposal may also lead to unsanitary conditions such as leaching of the waste, the spread of odours thereby increasing the risk and spread of diseases and reduction in the aesthetic value of the urban city centre (Edjabou et al. 2012). In some countries, solid wastes are disposed of in open dumpsites creating environmental and community health issues (Singh 2019). Studies have shown that pathogenic bacteria such as *Salmonella dysenteriae*, *Citrobacter freundii*, *Proteus vulgaris* and *Escherichia coli* have been found in solid waste in major cities when waste is not disposed of (Kirama & Mayo 2016).

Waste production and management is now considered a serious problem in urban areas, especially from developing countries. Different countries have developed different approaches to address the problems associated with municipal waste management and disposal. In China, fees are attached to the disposal of solid waste which is payable by an individual or the company involved in the generation of waste (Zhang et al. 2012). Also in China, there is a 'polluter pay principle'

that has been known to influence the generation and disposal of municipal solid waste. In Nigeria, individuals may buy waste bins and contact privately-owned companies which are paid for to assist in the disposal of waste. Waste collected is later disposed of in a dumpsite. Some have also resorted to burning of the wastes. In South Africa, registered houses and companies are supplied with waste bins and are billed at the end of the month for waste management and disposal.

There is a general belief that disposal and management of waste is the sole responsibility of the government (UN-Habitat 2010, Vidanaarachchi et al. 2006). However, if wastes are properly disposed of and managed, it may provide not only job opportunities especially in developing countries but also means of livelihood (Vergara & Tchobanogious 2012). Medina (2007) had earlier reported that over 2% of the world's population depends on waste collection, processing and recycling as a means of livelihood.

Over the years, research on waste disposal and management was conducted largely on households within the residential areas with a focus on the nature of waste, family income and the effect of education on waste generation and disposal (Sujauddin et al. 2008, Ekere et al. 2009). Minimum attention has been paid to waste generation and management around industrial areas (Singh 2019, Chu et al. 2019). South Africa like any other developing countries in the world is facing rapid urbanization and more than half of South Africa's population is urbanised. This may increase the generation of waste in South Africa as noted in other developing countries. In South Africa, wastes are usually collected on a specific day of the week depending on the location and area. However, it is not uncommon to see waste littering the streets, especially around the industrial areas. Waste bins are provided and collected around these areas on some specific days just as noted within the residential areas.

The study proposed three hypotheses, Hypothesis 1: Knowledge regarding waste separation and its economic benefit has a positive effect on different business units handling waste. The American Oxford dictionary 2010 edition defines knowledge as "skills acquired by a person through experience or education; the theoretical or practical understanding of a subject". Van Kien (2015) further added that knowledge may also be received through experience leading to contextual information which will assist in providing insight for evaluating and integrating new information through experience. Thus, it is assumed that, the higher the knowledge, the higher the changes in behaviour (Van Kien 2015). Prior knowledge will include appropriate information and importance of waste separation. Dijk et al. (2015) noted that effective education of workers would improve the working conditions of workers and when the educated, the trained worker becomes an integral part of workplace safety programs. We, therefore, assumed that those that are educated or well informed about waste disposal practices will tend to adhere to proper waste management options.

Hypothesis 2: Health and environmental concerns have a positive and significant effect on business units' disposal of waste. Concerns over the overall impact of the work environment may influence attitudes towards safety practices.

Hypothesis 3: Financial implication of waste management and disposal may adversely affect people's behaviour about waste management. The additional cost implication of managing and disposing of waste may influence people's decision on waste management.

The focus of the present study is therefore to investigate both the small business owners and big business owners' attitudes towards waste generation, management and disposal. The study will also attempt to determine factors that may bring about a change in the attitude of business holders in supporting waste disposal and management methods prescribed by the government.

## MATERIALS AND METHODS

### Study Site

The study was conducted around the industrial area of Rosslyn, Pretoria, South Africa. Rosslyn is an industrial area best known for its automotive industries such as BMW and Nissan and also the South African Breweries. There are other smaller industries (formal and informal) operating in this area providing subsidiary services to these big industries. These include roadside food vendors, roadside mechanics and several other retail shops among others. The area usually witnesses an influx of people coming from surrounding areas working and seeking for a job or buying items from the small retail shops around the area. The area was chosen because of the observed presence of different types of waste that are usually noticed when passing through the area (Fig. 1). Business owners were observed in their natural setting on their self-consciousness among others towards proper waste disposal (Kawulich 2005). Yusuf et al. (2019) also noted that population, economic activities and areas are factors that may account for waste generation. The study also checked these factors among the different business units in this area.

In the present research work, business units having more than 25 employees are referred to as big companies (28), 4-9 employees as medium-sized companies (46) and those with 3 or less employee are regarded as small size business units (64). Some of the small-sized business units are using illegal structures to carry out their businesses around the industrial area used for the study.


Fig. 1a and b: Waste discarded along the busy road in Rosslyn.

A mixed-method approach was used for the study (Creswell & Plano Clark 2011). The method assisted in gaining a deeper and broader understanding of the rationale underlying their attitudes towards waste disposal and management (Creswell 2015). Different business units (Small, medium-sized and big units) were invited to participate in the study around the industrial area of Rosslyn, Pretoria, South Africa. These included food vendors by the roadside, mechanics, retail shops, firms providing services to bigger industries and the big sized companies. This was done to ascertain the perception of these small and "informal" business owners on the importance of proper waste disposal and management. A total of 138 questionnaires were administered to all the business units that agreed to participate in the study.

The questionnaire was designed to understand the perceptions and attitudes of different business units on waste disposal methods and their involvement in managing and disposing of waste correctly. To do this effectively, the questionnaire contained information on the educational level of the business owner, prior information on waste management, awareness and importance of recycling, types of waste that can be reused, nature of waste generated, type of waste generated, attitude towards waste management, the importance of sorting waste, issues around waste and the environment, waste and human health, willingness to pay for additional waste bins and the use of waste bins among others.

## RESULTS AND DISCUSSION

### Type of Wastes Generated by the Different Small Business Holders

The data gathered during the study showed that paper was the most generated waste followed by plastic, metals and construction waste (Fig. 2). Other types of waste generated

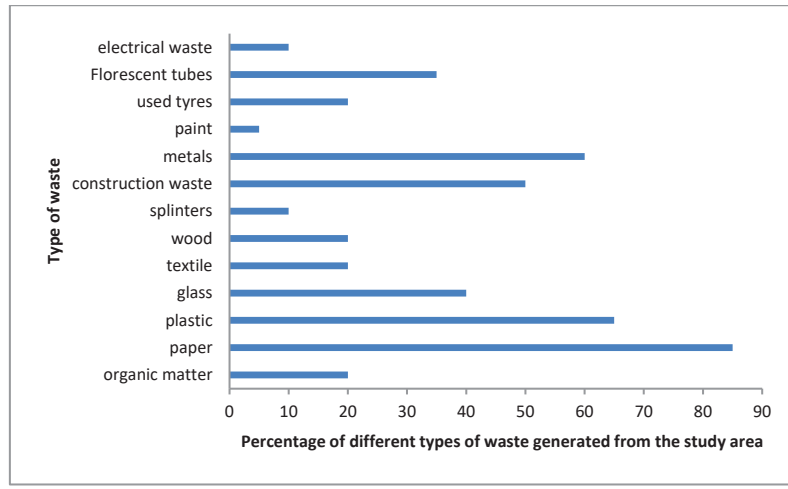


Fig. 2: Different types of waste generated from the study area by all the industries interviewed.

around this area include glasses, decomposing food items (leftover food items), textile, wood and used tyres. The use of paper in offices and communication may account for the reason why the paper was the most generated waste from all the companies. In addition, most of the companies around the industrial area in Rosslyn that agreed to participate in this study were more of medium to low size business units and they may not be able to afford the use of modern communication gadgets at their workplaces. The use of an electronic method for communication and transaction seems to be low or unacceptable in some of the industries. Our results are in agreement with the findings of Casares et al. (2005) where it was observed in a study from Spain that paper and cardboard, plastic, wood, and metals were the most common types of waste. Koolivand et al. (2017) also noted in a separate study conducted in Iran that metals, organic waste and paper and cardboard constituted about 80.9% of total waste generated while paper accounted for 49.53% of the total solid waste generated. The type of wastes generated by different industries as observed in our study depends on the type of industrial processing activities (Salihoglu 2010).

However, there are differences in the type and volume of wastes generated by the different business units interviewed in our study. This is mainly due to the nature of their work. For instance, the small business units generated more waste in terms of organic waste, disposable materials, plastic bags and leftover food items. From the small business units, paper as a form of waste generation was not common when compared to the middle and big sized industries. As noted in our study, the medium-sized industries generated more waste in terms of paper than the big sized industries except for some restaurants. Similar to the food vendors, the waste from the restaurants are plastic bags, disposable plates and leftover food items. All the restaurants interviewed are forced to dispose of their waste properly due to the impression that this may have on their customers. However, other medium-sized industries like those providing services to the big sized industries have papers as the most dominant waste from their businesses. The nature, size and quantity of waste generated by small business holders might have affected their attitudes towards waste separation. In most cases, it is generally assumed that only recyclable waste should be separated for recycling purposes. However, in some other countries, organic wastes are also purchased from household for organic farming thus favouring increased participation in waste separation from all stakeholders. The study of Vicente & Reis (2008) indicated among other that factors that affect recycling habits include the composition of household material and disposal method.

## Waste Management System from the Companies and Small Business Holders

Most of the companies and both the medium and small-sized business units surveyed (72.9%) admitted that they do not separate their waste or follow any waste management system. However, 85% of the big companies such as metal smelting companies that usually provide services to other big companies such as BMW and Nissan do separate their waste. The remaining 15% that do not separate their waste mentioned that they do not deal with metals or anything that can be recycled and therefore have no reason to separate their wastes. Those that separate their waste have different types of bin properly labelled for a specific type of waste. Afroz et al. (2008) in a study of factors affecting willingness to recycle which was carried out in Dhaka, Bangladesh showed that willingness to participate in waste recycling was as a result of economic benefits and awareness. This is similar to our findings where it was noted that companies that separate their waste did so for the economic profit and the information they had received about recycling.

From the companies that are willing to separate their waste, it was noticed that they had prior information about waste recycling and since these are registered companies they may be compelled to follow certain environmental law that indicates compliance.

The small and medium business holders that were interviewed had little or no knowledge about recycling and believed that they do not generate waste that can affect the environment and the type of waste they generate cannot be used for other purposes. Kamara (2006) had earlier reported that participation in domestic waste disposal and recycling in the Tshwane metropolitan area was low due to the level of awareness as regards sorting, recycling and disposal of domestic waste. Mohai (1985) noted that decisions and attitudes towards the environmental protection effort depend on degrees of personal efficacy and resource availability. The report of the findings of Kumar & Nandini (2013) from a study conducted in Karnataka, India also noted that most individuals are not willing to separate their waste because they have enough spaces either on the road or open spaces where it can be deposited and it is largely the duty of the municipality or the government.

Furthermore, on waste separation, all the medium and small business units are not willing to buy different bins for waste separations.

However, since the questionnaire shed more light on the importance of waste separation the respondents from medium-sized companies are willing to do it, if the government can provide bins for this purpose.

Separation of wastes was also considered as labour intensive especially from food vendors and those with small businesses. Most of those interviewed argued that it will generally be difficult for them to separate waste while trying to attend to their customers or when they are tired

in the evening and about to go home. One of the respondents said, "It is easier to just put it all in a waste plastic and throw it in the big bin outside". Another respondent replied, "Government should employ people that will help us to separate the waste and by so doing will provide job opportunities for the other".

This view is similar to those reported by Li (2003) in a study carried out in China where it was reported that households with more family member have more time to do recycling because they can distribute the household works between the household members while larger family size, households may face more waste and are therefore more willing to recycle.

On the other hand, most of the smaller companies reported that once the waste bin provided by the government is full, wastes are usually discarded in a black or green plastic bag and deposited next to the already full waste bins (Fig. 3). The food vendors and others selling perishable goods reported that they do not have a waste bin rather a waste plastic bag which is usually deposited next to government waste bin when it is full. They reported that due to stealing of the government waste bin, most of the business owners around the area have resulted to the use of black or green plastic waste bags and are usually placed in a conspicuous place for removal by the responsible authorities (Figs. 3a and 3b).

Except for some big companies that are involved in the waste separation, none of the small business holders is willing to buy a big waste bin, hence the deposition and littering of the business area around this area (Figs. 4a and 4b). It was also observed and reported that, if the waste that littered the environment are not collected on time, some of the small business units have resorted into illegal burning of these wastes (Figs. 5a and 5b). The unavailability of waste bin provided by the government may be a serious cause for concern if wastes are to be properly deposited in this area. Dauda et al. (2015) noted in a study from Berekun Municipality, Ghana that inadequate bins and long distance are major factors for solid waste management in the area. Scharfe (2010) mentioned that solid waste disposal and management have been neglected and given low priority from most African countries.

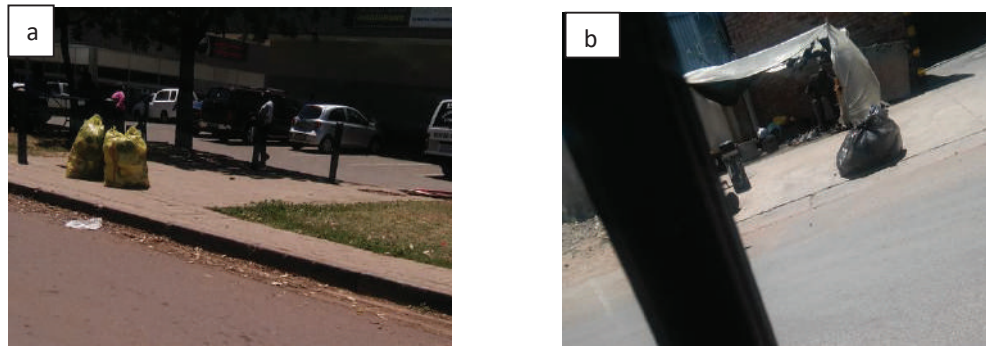


Fig. 3a and b: Waste wrapped properly on the streets of Rosslyn when the waste bin was full and not collected.


Fig. 4a and b: Waste deposited around the waste bin provided by the government and (b) littered waste around the industrial area of Rosslyn

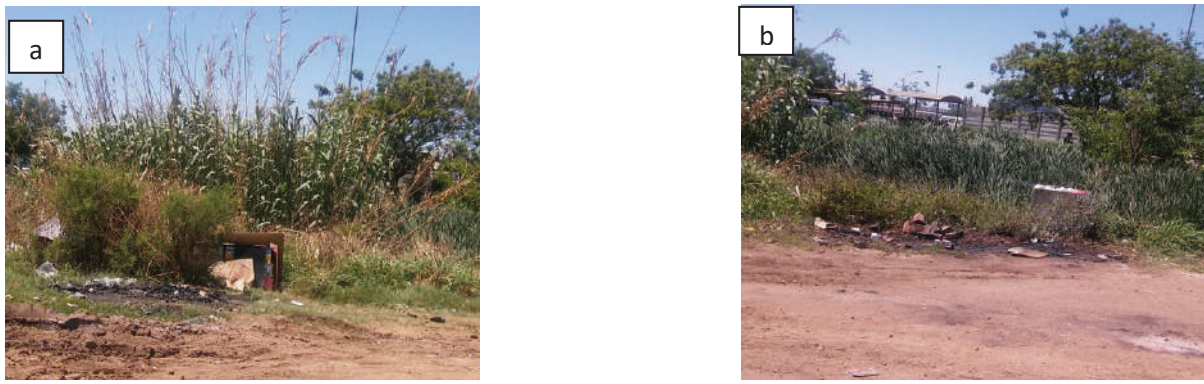


Fig. 5a and b: Illegal burning of waste around the industrial area of Rosslyn.

**Willingness to Pay for Waste Removal from Individual Business Centres**

Those operating and providing services to big companies mentioned that they are levied monthly for waste removal and management. They are not willing to pay an extra amount for the service they've paid for. None of the small business owners interviewed is willing to pay more on waste removal. Some of those interviewed reiterated that "We are currently struggling to make a living, we cannot pay anything, and government must remove the waste".

The major reason for not willing to pay according to the small business owners interviewed was that they have low income and have big families to cater for. A similar observation was noticed in the study conducted by Dauda et al. (2015) in Ijebu Ode, Nigeria where respondent indicated that it is the responsibility of the government to pay for the collection and management of waste.

## CONCLUSIONS

The present study investigated the attitudes of different business units on the disposal and management of waste around an industrial area of Rosslyn in Pretoria, South Africa. Three hypotheses were formulated to understand the attitude towards waste disposal and management. It was noted from the study that knowledge about waste disposal did not have any influence on small business units because most of the small business units believed that proper waste disposal was not their duty. Concerns for health and environment was of no issue from all the groups studied but some considered it important to dispose of waste properly just because of the health implication. None of the business units will accept an increase or introduction of fees for proper waste disposal. Improper waste management is a major problem in the area used for the present study. Most of the small business units termed as either small or medium in the present study constructed illegal structures and are not registered hence the difficulty on the part of the government to either charge them for waste management or provide waste bins for them individually. Papers were seen littering the entire area with several illegal burning of waste. It was discovered from the study that the type and composition of waste depend largely on the type, size and their processes. Papers and leftover food were common forms of waste generated in the area. Knowledge and awareness on the reuse of waste especially the organic waste is still very low among those interviewed. The area is largely dominated by both the small and medium-sized companies that are without waste bins hence the littering of the areas with different types of waste. Small company's holders did not see any reason why they should be concerned about proper waste management. The government should intensify effort on producing enough waste bins that are properly locked or chained to an object to prevent theft. Campaigns and education on proper waste management, disposal and recycling (organic and inorganic) should be intensified to change attitudes towards proper waste management.

## REFERENCES

Afroz, R., Hanaki, K and Kurisu, K.H. 2008. Factors affecting waste generation and willingness to recycle: a study in a waste Management Program in Dhaka city, Bangladesh. FEB Working Paper Series No. 0803, 2-17.

Banjo, A.D., Adebambo, A.A.R. and Dairo, O. S. 2009. Inhabitants' on domestic waste disposal in Ijebu Ode, Southwest Nigeria. African Journal of Basic & Applied Sciences, 1(3-4): 62-66.

Casares, M.L., Ulierte, N., Mataran,A., Ramos, A. and Zamorano, M. 2005. Solid industrial waste and their management in Asegra (Granada Spain). Waste Management, 25(1): 1075-1082.

Chu, Z., Wang, W., Zhou, A. and Huang, W. 2019. Charging for municipal solid waste disposal in Beijing. Waste Management, 94: 85-94.

Cresswell, J.W. and Plano Clark, V.L. 2011. Designing and Conducting Mixed Methods Research. 2nd ed., Los Angeles, CA: Sage.

Creswell, J.W. 2015. Educational research: Planning, Conducting, and Evaluating Quantitative and Qualitative Research. 5th ed., Boston, MA: Pearson.

Dauda, S., Mariwah, S. and Agyapong, R. 2015. Residents' perceptions and attitudes towards urban solid waste management in the Berekum Municipality, Ghana. Oguaa Journal of Social Sciences, 7(2): 25-37.

Dijk, F.J., Bubas, M., and Smits, P.B. 2015. Evaluation studies on education in occupational safety and health: Insipiration for development economies. Annals of Global Health, 81(4): 548-560.

Edjabou, M.E., Moller, J. and Christensen, T.H. 2012. Solid waste characterization in Keteo, a rural town in Togo, West Africa. Waste Management and Research, 30(7): 745-749.

Ekere, W., Mugisha, J. and Drake, L. 2009. Factors influencing waste separation and utilization among households in the Lake Victoria Crescent, Uganda. Journal of Waste Management, 29: 3047-3051.

Harris-Lovett, S., Lienert, J. and Sedlak, D.L. 2018. Towards a new paradigm of urban water infrastructure: identifying goals and strategies to support multi-benefit municipal wastewater treatment. Water, 10(9): 1127.

Hazra, T. and Goel, S. 2009. Solid waste management in Kolkata, India: Practices and challenges. Waste Management, 29(1): 470-478.

Kamara, A.J. 2006. Household Participation in Domestic Waste Disposal and Recycling in the Tshwane Metropolitan Area: An Environmental Education Perspective. Dissertation. University of Southern Africa, South Africa.

Kawulich, B.B. 2005. Participant observation as a data collection method [81 paragraphs]. Forum Qualitative Sozialforschung/Forum: Qualitative Social Research, 6(2), Art. 43. Available:http://www.qualitative-research.net/index.php/fqs/article/view/466/996 [Accessed: 21 September 2019].

Kirama, A. and Mayo, A.W. 2016. Challenges and prospects of private sector participation in solid waste management in Dar es Salaam City, Tanzania. Habitat International, 53: 195-205.

Koolivand, A., Mazandaranizadeh, H., Binavapoor, M., Mohammadtaheri, A. and Saeedi, R. 2017. Hazardous and industrial waste composition and associated management activities in Caspian industrial park, Iran. Environmental Nanotechnology, Monitoring & Management, 7: 9-14.

Kumar, M. and Nandini, N. 2013. Community attitude, perception and willingness towards solid waste management in Bangalore city, Karnataka, India. International Journal of Environmental Sciences, 4(1): 87-95.

Li, S. 2003. Recycling behaviour under China's social and economic transition. Environment and Behaviour, 35(6): 784-801.

Medina, M. 2007. The world's scavengers: Salvaging for sustainable consumption and production. AltaMira Press, Lanham.

Moghadama, M.R.A., Mokhtaranib, N and Mokhtaranic, B. 2009. Municipal solid waste management in Rasht City, Iran. Waste Mnagement, 29: 485-489.

Mohai, P. 1985. Public Concern and Elite Involvement in Environmental-Conservation Social Science Quarterly. 4(66): 820.

Oyelola, O.T., Babatunde, A. I. and Odunlade, A. K. 2009. Health implications of solid waste disposal: Case study of Olusosun dumpsite, Lagos, Nigeria. International Journal of Pure and Applied Sciences. 3(2): 1-8.

Salihoglu, G. 2010. Industrial hazardous waste management in Turkey: Current state of the field and primary challenges. Journal of Hazard Matter: 177(1-3): 42-56.

Scharfe, D. 2010. Integrated Waste Management Plan, Centre & South Waste Services Board/ Waste Diversion Ontario and Stewardship Ontario.

Singh, A. 2019. Managing the uncertainty problems of municipal solid waste disposal. Journal of Environmental Management 240: 259-265.

Sujauddin, M., Huda, M.S. and Rafiqul Hoque, A.T.M. 2008. Household solid waste characteristics and management in Chittagong, Bangladesh. Journal of Waste Management, 28: 1688-1695.

UN-Habitat. 2010. Solid Waste Management In The Worlds' Cities. Nairobi: UN-Habitat.

Van Kien 2015. Nearly %50 of the public official candidates have lobbied. *Tien Phong*, Issue April 15 2015. Accessed 12 May 2015. http://www.tienphong.vn/xa-hoi/chi-so-papi-2014-gan-50-phai-lot-tay-de-vao-cong-chuc-847508.tpo [Google Scholar]

Vergara, S.E. and Tchobanoglous, G. 2012. Municipal solid waste and the environment: A global perspective. Annual Review of Environment and Resources 37(1): 277-309.

Vicente, P. and Reis, E. 2008. Factors influencing households' participation in recycling. Waste Management & Research, 26: 140-146.

Vidanaarachchi, C.K., Yuen, S.T.S. and Pilapitiya, S. 2006. Municipal solid waste management in the Southern Province of Sri Lanka: problems, issues and challenges. Journal of Waste Management, 26: 920-930.

Wang, H., Fan, X., Wang, Y.N., Li, W., Sun, Y., Zhan, M. and Wu, G. 2018. Comparative leaching of six toxic metals from raw and chemically stabilized MSWI fly ash using citric acid. Journal of Environmental Management, 208: 15-23.

Yusuf, R.O., Adeniran, J.A., Mustapha, S.I. and Sonibare, J.A. 2019. Energy recovery from municipal solid waste in Nigeria and its economic and environmental implications. Environmental Quality Management, 28 (3): 33-43

Zhang, H.W. 2012. Research on current situation and counter measures of disposal of rural domestic garbage in Shandong province. China High-Tech Enterprises 24: 105-107.

Nature Environment and Pollution Technology
An International Quarterly Scientific Journal

p-ISSN: 0972-6268
(Print copies up to 2016)
e-ISSN: 2395-3454

Vol. 19 | No. 4 | pp.1499-1505 | 2020

Original Research Paper

https://doi.org/10.46488/NEPT.2020.v19i04.016

Open Access Journal

# Temporal and Spatial Analysis of Alpha and Beta Activity Concentration at Al-Tuwaitha Site, Baghdad

**Wedyan G. Nassif*, Basim I. Wahab*, Monim H. Al-Jiboori*† and Abdulrahhman B. Ali****
*Atmospheric Sciences Department, College of Science, Mustansiriyah University, Baghdad, Iraq
**Remote Sensing and GIS Department, College of Science, University of Baghdad, Baghdad, Iraq
†Corresponding author: Monim H. Al-Jiboori; mhaljiboori@gmail.com

**Nat. Env. & Poll. Tech.**
**Website: www.neptjournal.com**

*Received:* 14-02-2020
*Revised:* 12-03-2020
*Accepted:* 21-05-2020

**Key Words:**
Airborne radioactivity
Alpha/beta particles
Contamination rose

## ABSTRACT

Temporal and spatial analysis of air particulates sampling collection from the in and outside the Al-Tuwaitha, south of Baghdad, was carried out to measure daily gross alpha and beta activity concentrations (AAC and BAC) during the period from January to April of 2017. The results show that most frequencies are within the interval 1-1.49 Bq/m$^3$ for AAC and 3-3.49 Bq/m$^3$ for BAC. Also, the radioactivity levels within the site for both AAC and BAC were found to be higher than those around the outside. Across all air samples at the studied site, the monthly arithmetic means were 3.0 ± ٠٫٥ and 6.7 ± 0.9 Bq/m$^3$ for both AAC and BAC. It was found that a hotspot for both AAC and BAC in air layer with values of 4.0 and 8.5 Bq/m$^3$ respectively situated at ITR-5000 reactor northwest of the site, which is a major source of radioactive contamination, but with wind action. This contamination disperses according to its prevailing direction that is southeast. 6.7 ± 0.9

## INTRODUCTION

In air near the surface, most of the radioactive materials (e.g. uranium and thorium series and the isotope of potassium) at nuclear locations, nuclear weapons testing, or nuclear accidents are continuously emitting harmful ionizing radiations containing energetic charged particles such as alpha and beta. One of these common locations is Al-Tuwaitha nuclear research centre, which was used for nuclear activities, so contains significant amounts of radioactive materials. Alpha and beta particles have adverse health effects on human and animals (somatic and genetic) (Peirce et al. 1998).

Knowledge of the radioactivity levels in the surface air of Al-Tuwaitha site is an important prerequisite for planning work areas and for anticipated future uses of the remediated site when inhaled or ingested (Chesser et al. 2009).

In recent years, several local and international studies about the contaminated location for Al-Tuwaitha have been carried out by many Iraqi researchers. They investigated the radioactivity in analysing the different soil samples (Zaboon et al. 2013, Jarjies et al. 2013) taken from various places at the site and also an assessment of radiation hazards for plants species growth (Mansour et al. 2017). For example, Zaboon et al. (2013) analysed 201 soil samples collected by the Ministry of Science and Technology and then using geographical information system (GIS) they presented maps of radioactive doses contamination. They determined the highest radiation dose rate with 140 mrad/hr as a hotspot in the site.

Unfortunately, there are a few studies that investigate the analysis of measurements of gross alpha and beta activity concentration (will be symbolled as AAC and BAC, respectively) in the surface air layer at Al-Tuwaitha site. Salih et al. (2018) presented the results of AAC and BAC for selected places within and around the site, which showed that it has natural nuclides that are the daughters of the thorium and the uranium series. These radioactive decays are radon isotope escaping from the soil and ascending into the air. While in the present study, a further attempt to reanalyse the measurements published in this reference with absolutely different analysis from the scope of its objective aims. Here the purpose of this paper is to present the (1) spatial analysis of both AAC and BAC, (2) frequency distributions for specified intervals of these concentrations, (3) AAC and BAC roses, (4) daily variation during the study period, (5) comparison between AAC inside and outside of the studied site as well as for BAC, and finally (6) finding a simple empirical relation between AAC and BAC.

## MATERIALS AND METHODS

### Air Radioactivity

Radioactivity is the term used to describe the disintegration of atoms. Some materials are unstable. Therefore, their nuclides

disintegrate or decay, the atom can release energy in the form of radiation (Eisenbud & Gesell 1997). We frequently receive internal exposure from these elements taking into our bodies through the air we breathe. Continuous particulate air monitors are used for measuring releases of airborne particle radioactivity (APR) from the facility, for protection of plant personal, monitoring the air in the reactor containing structure to detect leakage from the reactor systems and to control ventilation fans when the APR has exceeded the defined threshold.

The activity concentration of a radionuclides alpha and beta is the activity of these in a radioactive substance in an air divided by the volume of the air. The change in counting and background rates represents the number of spontaneous nuclear transformations taking place in the relevant number of radionuclides in a time interval (Δ) divided by this time.

$$\mathrm{AAC/BAC} = \frac{\text{counting rate (alpha/beta)} - \text{background rate (alpha/beta)}}{\Delta t * V * E_f} \quad \ldots(1)$$

Where, $E_f$ is the filter efficiency. Thus, the unit of activity concentration in SI is the Becquerel per cubic meter ($Bq/m^3$), whereas 1 Bq = 1 disintegration/sec. Bq is a unit to express the strength of radioactivity.

## Al-Tuwaitha Site

Al-Tuwaitha site as the foundation of Iraq's nuclear research centre is located about 18 km southeast of Baghdad and 1 km east of the Tigris river, which covers an area about 1.3 $km^2$. Geographically, it is situated at latitude 33°10"-33°15" N, longitude 44°29"-44°35" E and 32 m above mean sea level (Fig. 1).

The site was established in 1967 for legitimate nuclear activities until its final closure in 2003. Large earthen beams (approximately 2.6 km length and 30 m high) were placed around the key distinct nuclear key facilities to fortify them. These facilities were comprised of 90 buildings dedicated to two reactors (Osiraq and IRT-5000), fuel fabrication, plutonium separation uranium enrichment, radioactive waste treatment and storages, several research laboratories and many others (Chesser et al. 2009) as shown in Fig. 2. Most of these were seriously bombarded during the Gulf War in 1990 in Iraq and then subjected to subsequent looting.

## Material and Data

The data used in this study can be broadly classified into two types: counting alpha/beta rates and wind directions. Observational data for alpha and beta particles were achieved through several steps: first, collection of air samples drawn from the ambient atmosphere in and out the site using high volume particulate sampling (HVPS) 3000 fixed at 1 m high. This device was operated with a typical airflow rate of between 10 and 15 $m^3$/hour. The instrument was put 20 m away from the building with a sampling period of 1 hour with collection efficiency 99%. The process of aspiration was done

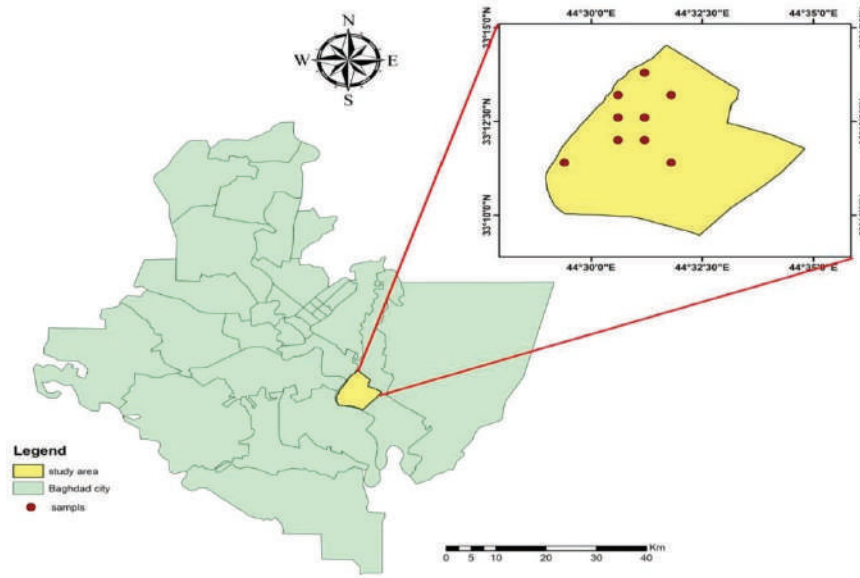


Fig. 1: Map of Al-Tuwaitha site showing some measurement locations (•) plotting by ArcGIS.


Fig. 2: Aerial satellite image for Al-Tuwaitha nuclear research site.

using an air filter type no. 373030, glass fibre with radius 2.75 cm. The number of samples is 50 taken at various places to cover inside (45) and outside (5), which can be considered as background levels of alpha and beta particles. Second, the above filters were analysed by alpha-beta sample counter Ludlum (model 3030, American originated) to measure simultaneous alpha and beta particles. The feature of this instrument with its other structures can be found in reference (Ludlum measurements 2020) for more details. Before using the device, calibration and quality control check were done using standard sources supplied by the manufacturer.

After ending the aspiration time (1 hour) by HVPS, all filters removed and put in Ludlum for 1 minute to count alpha and beta rates. This step was repeated 3 times and then the average value was calculated. Mean of these rates were substituted in Equation (1) to compute AAC and BAC.

## RESULTS AND DISCUSSION

### Frequencies for AAC and BAC

Daily activity concentrations of alpha and beta measured in the atmosphere of Al-Tuwaitha site are classified to several intervals with constant length of 0.5 and 1 Bq/m$^3$ for alpha and beta reported in X-axis of Figs. 3a and 3b respectively, which show the frequency distributions for the AAC and BAC values. Highest frequencies are found at the third interval

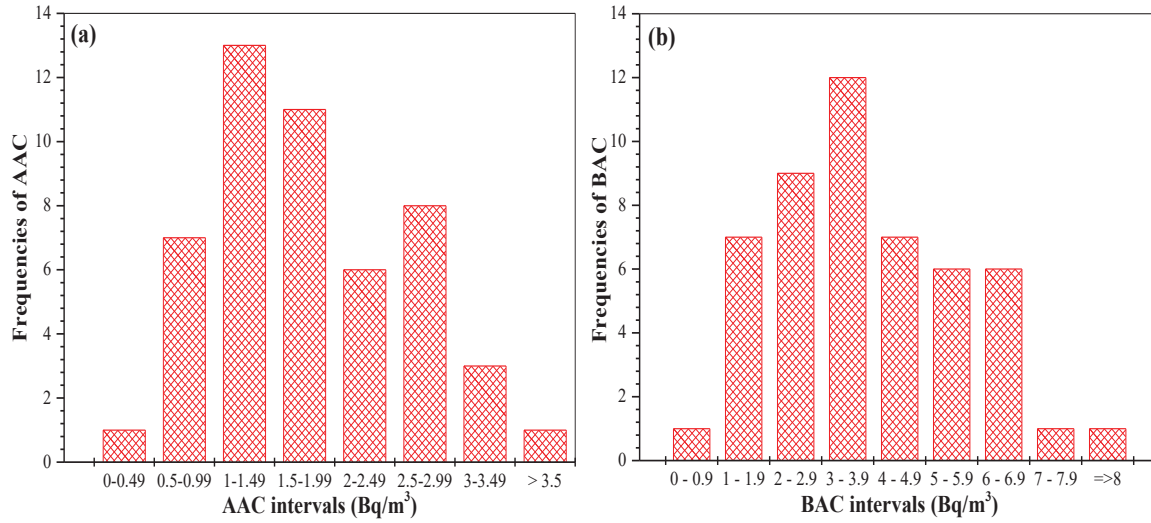


Fig. 3: Frequency distributions for (a) alpha and (b) beta activity concentrations at Al-Tuwaitha.

(1-1.49) Bq/m$^3$ with 13 times for AAC (Fig. 3a) while at fourth one (3-3.9) Bq/m$^3$ for BAC (Fig. 3b). Other intervals have lower frequencies at the beginning and ending of the intervals with a time. Finally, values of intervals for BAC are larger than that of AAC.

## Temporal Analysis of AAC and BAC

Daily variations of AAC and BAC during the study period for both in and outside the site are presented in Fig. 4a and Fig. 4b, respectively. Most of the measurements were taken in the site, so the data points are connected by a line while plotting scatter for data measuring out of the site. At some days, two measures were made for two places on the same day at different times. Thus, their values were averaged to be one. Generally, these figures have some interesting indications: first, values of both AAC and BAC measured at the site are larger than those for outside along the recording period. Another is that all AAC and BAC across the whole site have large values in January and gradually decrease to be minimum in April. Lastly, the behaviours of AAC and BAC are approximately similar but with different magnitudes, whereas BAC has large values. The same results were also recorded in the air of Tehran nuclear research centre (Arkian et al. 2006).

Now we are going to analyze these results by taking averages of AAC and BAC values over each month with calculating standard deviation as illustrated in Table 1. Winter months represented by January and February have large AAC/BAC values for both in and outside comparing to spring months (March and April). Large AAC and BAC values in the site across all months are fair respect to those recorded around the site. As shown in the last row of Table 1, the total average of all months of AAC and BAC in the site 1.84±0.5 and 4.0±1.1 Bq/m$^3$ are larger than those of outside (1.2±0.4 and 2.7±0.8 Bq/m$^3$), respectively.

According to the above discussion, the AAC and BAC behaviours are almost the same, and therefore now trying to examine the relationship between their values. Fig. 5 shows the linear relation between them which is very good in the air layer with correlation coefficient ($R^2$ Δ0.9). This implies that radionuclides (alpha and beta) present due to man-made sources in the site might be responsible for radioactive contamination of the air at the site. The results obtained above show that AAC and BAC values in the site are mostly higher than those of values surrounding the site.

## Spatial Analysis

To execute spatial analysis, digital map layers including

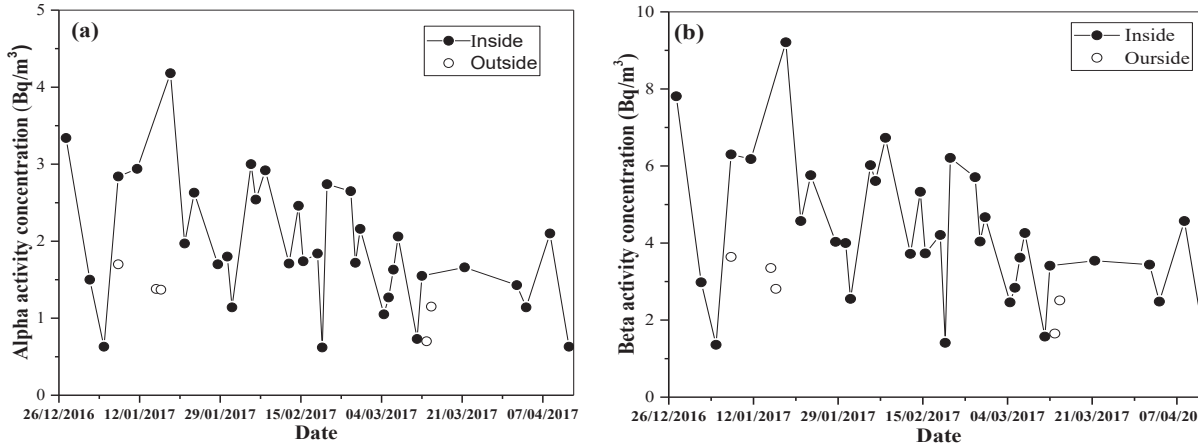


Fig. 4: Daily variations of (a) alpha and (b) beta activity concentrations in- and outside Al-Tuwaitha site.

Table 1: Monthly averages of AAC and BAC with their standard deviations within and outside of Al-Tuwaitha nuclear site.

| Months | Alpha activity concentration (Bq/m$^3$) | | | | Beta activity concentration (Bq/m$^3$) | | | |
|---|---|---|---|---|---|---|---|---|
| | Inside | St. dev. | Outside | St. dev. | Inside | St. dev. | Outside | St. dev. |
| January | 2.4 | 1 | 1.5 | 0.2 | 5.2 | 2.3 | 3.3 | 0.4 |
| February | 2.1 | 0.7 | - | - | 4.6 | 1.5 | - | - |
| March | 1.4 | 0.4 | 0.9 | 0.3 | 3.0 | 0.9 | 2.1 | 0.6 |
| April | 1.3 | 0.6 | - | - | 2.9 | 1.3 | - | - |
| Average | 1.8 | 0.5 | 1.2 | 0.4 | 4.0 | 1.1 | 2.7 | 0.8 |

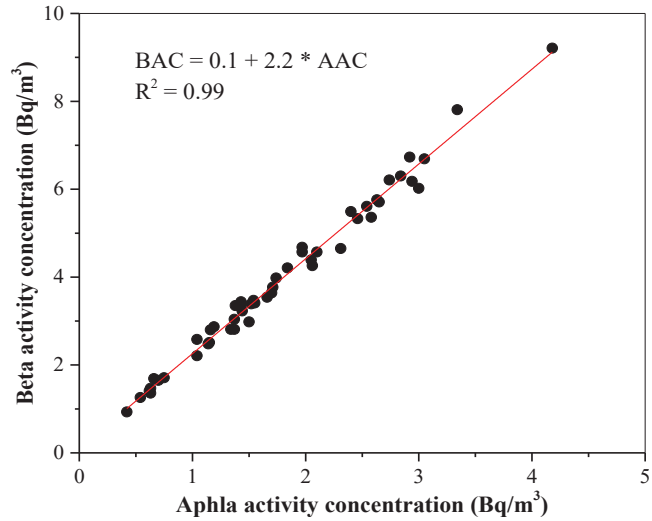


Fig. 5: Correlation of AAC and BAC in the air layer.

contours for AAC and BAC were created by GIS. The mapping procedure had started by converting geographic coordinates for all sample locations to universal transverse Mercator coordinates. These samples were indicated by point shapefile (vector), so it was converted to raster through interpolation using Kriging methods in ArcGIS version 10.4.1 software. Kriging technique is the most relevant method compared to other interpolation techniques in which the process of using points with known values to predict values at other unmeasured points as well as it aims to minimize the variance of the error (Al-Timimi et al. 2012). However, data are interpolated to display a continuous surface as a visual display.

The spatial interpolation maps of both AAC and BAC in the study area are shown in Fig. 6a and Fig. 6b, respectively. The patterns of contours in these two figures appear almost the same. There is a clear hotspot with the value of 4.0 Bq/m$^3$ for AAC (Fig. 6a) and 8.7 Bq/m$^3$ for BAC (Fig. 6b) centred over contaminated facility (e.g. Osiraq and IRT-5000), while a small value of both AAC and BAC to the west and moderate values to the east. Highest values of them are concentrated in the northwest. The location of the contaminated hotspot has serious problem especially

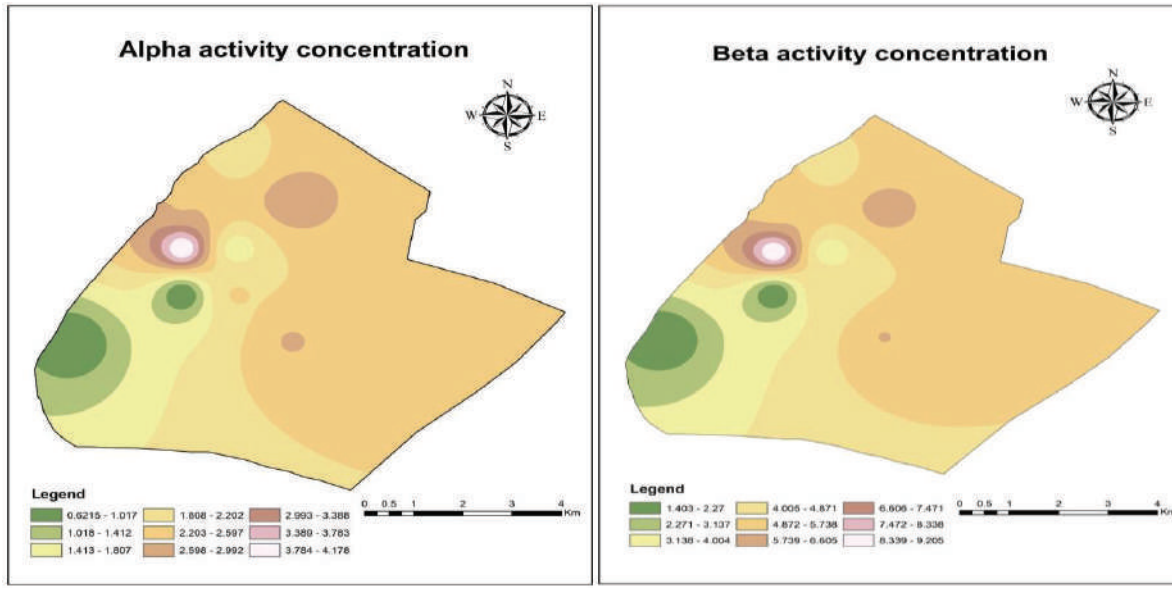


Fig. 6: Spatial analysis map for the distribution of AAC (left) and BAC (right).

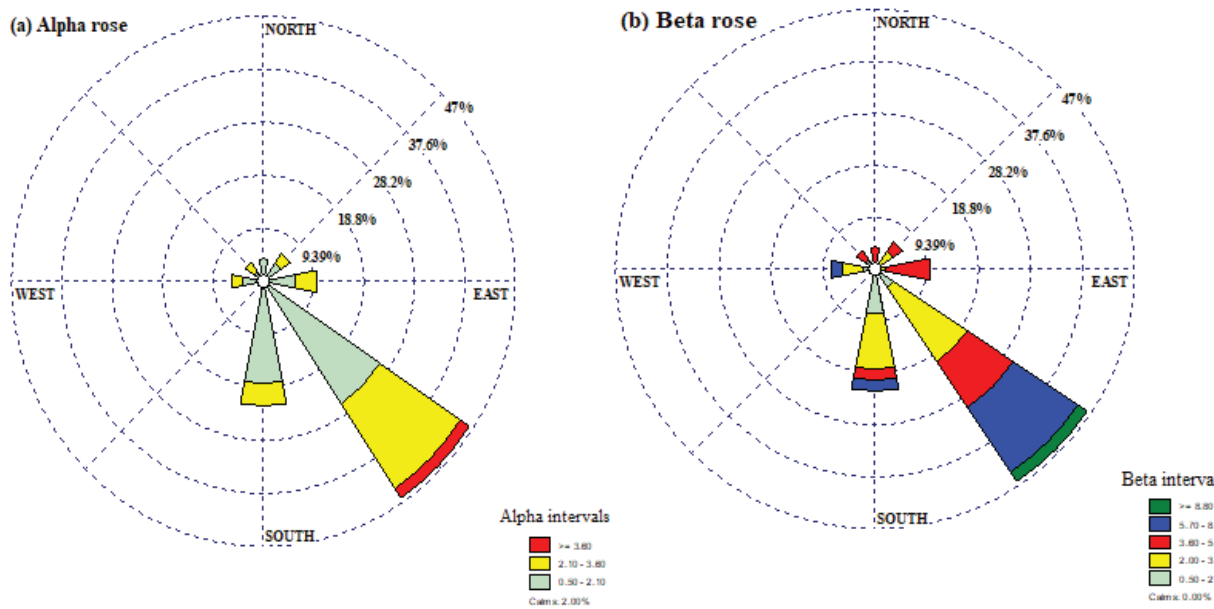


Fig. 7: Contamination roses for (a) alpha and (b) beta activity concentration at Al-Tuwaitha site.

when the prevailing wind direction is frequently coming from the northeast as will be shown in the next subsection.

### ACC and BAC Roses

A contamination rose is a graphical presentation of alpha and beta activity concentrations associated with each wind direction. This was drawn on a circular plot using eight directional sectors resolution. From these plots, it can be used to find the wind directional AAC and BAC, major source regions of the contamination of interest and help in identifying the direction associated with higher or lower concentrations (Said 2011).

Daily data of wind directions associated with measured AAC and BAC were drawn to depict the frequencies of the times that contamination levels exceeded background levels. The AAC and BAC roses were created with WRPOLT View-version 8.0.2 (Lakes Environmental 2018), as shown in Fig. 7a and Fig. 7b, respectively. These figures were generated by the frequency of AAC and BAC for each direction of wind some particular concentration. Thus, the western area of Al-Tuwaitha site has higher frequencies of high AAC and BAC as illustrated in Fig. 7a and Fig. 7b respectively, while low frequencies are from outside the site with north and northwest. This indicates that the areas associated with northwest and north directions, which have major sources of the radioactivity of alpha and beta, have a great impact on the southeast areas. Inversely, areas on the southwest direction have relatively low AAC and BAC.

## CONCLUSIONS

The gross alpha and beta activity concentrations were detected in the collected aerosol samples. The primary conclusion is that AAC and BAC in Al-Tuwaitha nuclear site show high levels with hotspot over ITR 5000 compared to the surrounding areas of the site. Across all sampling collections, values of BAC are larger than AAC. Monthly means of AAC and BAC in winter were higher than in spring because of the atmospheric stability on the radioactive nuclides. Wind directions have an important role in distribution and dispersion aerosols as carriers of these nuclides. To the best of our knowledge is to investigate the influences of meteorology in the dispersion and transport of radioactivity.

National and international standards considering sampling sites and measuring laboratories should be accurately applied to provide high quality assurance and quality control of the air radioactivity monitoring system.

## ACKNOWLEDGMENTS

The authors are grateful to Mustansiriyah University for the acceptance of this work.

## REFERENCES

Al-Timimi, Y. K., George, L. E. and Al-Jiboori, M. H. 2012. Drought risk assessment in Iraq using remote sensing and GIS techniques. Iraqi Journal of Sciences, 53(4): 1078-1082.

Arkian, F., Salahinejad, M. and Amidi, J. 2006. Analysis of gross alpha, gross beta activities and beryllium-7 concentrations in surface air: their variation and statistical prediction model. Iranian Journal Radiat. Res., 4(3): 155-159.

Chesser, R. K., Rodgers, B. E., Bondarkov, M., Shubber, E. and Phillips, C. J. 2009. Piecing together Iraq`s nuclear legacy. Bulletin of the Atomic Scientists, 19-26.

Eisenbud, M. and Gesell, T. 1997. Environmental Radioactivity: From Natural, Industrial and Military sources (4th ed.). Academic Press, pp. 656.

Jarjies, A., Abbas, M., Fernandes, H. M., Wong, M. and Coates, R. 2013. Prioritization methodology for the decommissioning of nuclear facilities: A study case on the Iraq former nuclear complex. Journal of Environmental Radioactivity, 119: 70-78.

Lakes Environmental. 2018. WRPLOT View, Wind Rose Plots for Meteorological Data. (L. E. Software, Producer) Retrieved from http://www.weblakes.com/products/wrplot/index.html.

Ludlum measurements 2020. Int. measurements. LUDLUM MODEL 3030 Alpha-Beta Sample Counter manual: 2020.

Mansour, H.L., Al-Bakhat, Y.M. and Karkosh, H.N. 2017. Measurement of radioactivity levels and assessment of radiation hazards for plants species grown at scrap yard (B) at Al-Tuwaitha nuclear site (Iraq). Nuclear, 2(4): 94-98.

Peirce, J.J., Weiner, R.F. and Vesilind, P.A. 1998. Environmental Pollution and Control (4th ed.). Butterworth-Heinemann, pp. 392.

Said, A. Y. 2011. Air quality trends and pollution roses in selection cities of Canada. University of Windsor, Canada.

Salih, N. A., Al-bakhat, Y. M., Al-Rahmani, A. A., Murbar, O. M., Ameen, N. H. and Majed, N. M. 2018. Assessment of radiological air contamination for selected places at Al-Tawaitha nuclear site during winter and spring. Baghdad Science Journal, 15(3): 278-286.

Zaboon, A. T., Al-Obaidy, A. M. and Al-Sharaa, H. M. 2013. Radioactive doses contamination in Al-Tuwaitha nuclear site using GIS techniques. Engineering & Technology Journal, 31 Part A(9): 1612-1615.

Nature Environment and Pollution Technology
An International Quarterly Scientific Journal

p-ISSN: 0972-6268
(Print copies up to 2016)
e-ISSN: 2395-3454

Vol. 19 | No. 4 | pp. 1507-1515 | 2020

Original Research Paper

https://doi.org/10.46488/NEPT.2020.v19i04.017

Open Access Journal

# Assessment of Heavy Metal Concentration in Tissues of Three Owl Species From Visakhapatnam, India

**Sanchari Biswas*†, Ch Ramakrishna* and Y A Maruthi****

*Department of Environmental Science, GITAM (Deemed to be University), Visakhapatnam-530045, Andhra Pradesh, India

**Department of Biotechnology and Bio Sciences, Krishna University, Machilipatnam-521001, Andhra Pradesh, India

†Corresponding author: Sanchari Biswas; biswasanchari@gmail.com

**Nat. Env. & Poll. Tech.**
**Website: www.neptjournal.com**

*Received:* 16-12-2019
*Revised:* 29-12-2019
*Accepted:* 03-01-2020

**Key Words:**
Heavy metals
Owls
Environmental monitoring
Birds as indicators

## ABSTRACT

The occurrence of heavy metals into the environment through various natural and anthropogenic sources is inevitable due to their persistent nature. This study investigated the concentration of heavy metals lead (Pb), zinc (Zn) and chromium (Cr) in liver, kidney, muscle and bones of three different species of owls namely Indian Eagle Owl *(Bubo bengalensis*), Barn Owl (*Tyto alba*) and Spotted Owlet (*Athene brama*) from Visakhapatnam, Andhra Pradesh, India. Given their sentinel role, birds can be used as suitable and reliable indicators in monitoring the quality of the environment. From the study, it was observed that *Bubo bengalensis* accumulated the highest concentration of metals followed by *Athene brama* and *Tyto alba*. On an average, the concentration of Zn (1.67±1.40 µg/g) was higher than Pb (0.079±0.05 µg/g) and Cr (0.99±1.11 µg/g). Among all the species, Spotted Owlet (*Athene brama*) recorded the highest concentration of Zn in bone (3.98 µg/g) whereas in the bone of Indian Eagle Owl (*Bubo bengalensis*) 2.44 µg/g of chromium (Cr) was reported. Pearson's correlation of the data showed significant positive correlations in the absorption of metals by the tissues. Kruskal-Wallis ANOVA was applied to validate the results and check whether the groups originated from the same population. Additionally, Principle Component Analysis (PCA) revealed that Pb showed a strong relationship with both Zn and Cr and might be due to the differences of sources of these elements in the environment.

## INTRODUCTION

Over the past few years, heavy metals have been accumulating in our environment due to the various anthropogenic point and non-point sources. Heavy metals are persistent and tend to accumulate in living forms. In some cases, heavy metals can change into a more toxic form through biochemical processes (Grúz et al. 2018). Due to the biomagnification properties of certain elements like organic forms of arsenic and mercury, when they get biomagnified over the food-chain, they jeopardize the health of living forms (De Luca et al. 2001, Grúz et al. 2018). It was reported by Denneman & Douben (1993) that birds were first used for monitoring the environmental conditions in the early 1960s because birds are more susceptible and tend to react to environmental changes. Battaglia et al. (2005) reported that using sentinel species aids in producing significant data to monitor environmental quality. They also stated that the prolonged exposure to the contaminants in certain species is due to their biological habits which if analysed would generate relevant data apart from that originating from water and soil. Tertiary consumers are good indicators in determining the extent of environmental contamination in the ecosystem across the food web (Sanchari et al. 2016, Biswas et al. 2019). It stated that birds have been used as bioindicators for monitoring environmental pollutants (Gragnaniello et al. 2001, Muralidharan et al. 2004) specifically heavy metals (Mochizuki et al. 2002) since they are easy to access, broadly distributed in ecosystems, sensitive to toxins and on higher trophic level of food chains**.** Guitart et al. (2010) concluded that when compared to wild animals, wild birds like waterfowl and raptors were the victims of poisoning. Additionally, apart from buzzards, little owls (Battaglia et al. 2005) and Indian Eagle Owls, which feed on a wide range of prey, can provide sufficient information regarding biomonitoring of the environment (Kim & Koo 2007). Different birds including Eagle Owls have been frequently used as biomonitors to monitor heavy metal burden in the environment (Nighat et al. 2013, Guitart et al. 2010, Grúz et al. 2018).

Heavy metals can accumulate in different tissues including liver, kidney and feathers of the birds (Deng et al. 2007, Jayakumar & Muralidharan 2011, Biswas et al. 2019). Birds can excrete metals via different routes like feathers and excreta (Furness 1996, Boncompagni et al. 2003, Mustafa et al. 2015) or into eggs (Burger et al. 1993, Grúz et al. 2018). Studies by various authors suggest that heavy metals influence reproductive health of some birds (Janssen et al.

2003, Dauwe et al. 2004) increased chances of diseases and increased reproductive failure (Furness 1996) and shifts in behaviour patterns. Therefore, monitoring of heavy metals in the environment not only provides species-specific information but can also aid in providing area-specific information about the changes in contaminant levels in the environment (Jayakumar & Muralidharan 2011). Studies done in the Indian context are limited. However, some of the studies carried out have recorded important levels of metals from various areas in southern and northern India (Jayakumar & Muralidharan 2011, Kaur et al. 2014, Sharma & Vashishat 2017, Gaba & Vashishat 2018, Manjula et al. 2015, Biswas et al. 2019). Visakhapatnam, Andhra Pradesh, India is home to diversified avifauna but is presently facing the consequences of development and urbanisation. Owls belong to the Strigidae family and are regarded as birds of prey which usually prey on rodents or small mammals. Due to their foraging habits, owls can fly up to long distances to search for food. The present study was carried out to investigate the concentration of certain heavy metals in three species of owls and establish some data because studies done in the region remain limited.

## MATERIALS AND METHODS

**Study area and sampling:** In India, owls are protected species under The Wildlife Protection Act 1972 (Schedule IV). As per bioethical concerns, domesticating or killing of any protected species is a strictly punishable offence. Hence, the present study involved the collection of dead birds (Owls) as reported by locals from residential areas and opportunistic findings of electrocution kill. Visakhapatnam is a situated along the Eastern Ghats which hosts a variety of flora and fauna. At the same time, it is also a fast-growing hub, budding with development and urbanization. A total of 27 samples including adults, sub-adults and juveniles were collected from Simhachalam, (17.7664° N, 83.2508° E), Kambalakonda (17.7664° N, 83.3496° E) and old post office or port area, (17.6940° N, 83.2922° E) on an opportunistic basis represented in Fig. 1. The samples collected were transported to the lab in ice box.

**Necropsy of specimens:** The samples were removed from ice storage and thawed for an hour. Necropsy of all samples were carried out individually. Birds (owls) in which rigor mortis had set in were also considered for post-mortem. The specimen was placed on the post mortem tray in the dorsal position and external observations were made in order to find discharges from mouth and cloaca if any. The breast feathers were plucked gently in order to reveal the epidermis where incision lines were made with scalpel and the breast tissue was cut open. On reaching the sternum, the abdominal tissue was further cut to reveal the visceral contents. Observations were carried out to check clots, exudate and fluids. The liver and pair of kidneys were procured after removing them with help of forceps and scissors. A small amount of breast tissue was also removed from the bird. The femur bone was cut with the help of stout scissor and all the contents were wrapped in aluminium foil, labelled respectively and stored in deep freezer at -20°C for the next experimental procedures.

**Apparatus and reagent:** All the laboratory apparatus used in the experiment were cleansed with Millipore Sigma extran® MA 03 solution to decontaminate them. All chemicals and reagents used in the present study were of Merck grade which included nitric acid, $HNO_3$ (69% Emplura Merck), perchloric acid, $HClO_4$ (60% Emparta ACS) and hydrogen peroxide $H_2O_2$ (30% Emplura Merck).


Fig. 1: Map showing sampling points and study area (source: https://earth.google.com/web)

**Acid digestion procedure:** All tissues were thawed initially and then oven-dried at 80°C for 24 hours. With the help of mortar and pestle, each tissue was then powdered. The acid digestion process was initiated by following the procedure suggested by Muralidharan et al. (2004). After weighing, 1-5 g of powdered sample was transferred to Teflon beakers to which 10 mL $HNO_3$ was added slowly. The mixture was then placed on a hot plate and heated for about 30 min until a thin solution was obtained. This was followed by pipetting 5 mL of $HClO_4$. The mixture was further heated for 15 mins until the solution turned clear. After cooling the solution, finally 2 mL of $H_2O_2$ was added and reheated till a final transparent solution was obtained. The Hydrogen peroxide ($H_2O_2$) was added to result in digestion of excessive organic matter present if any. All samples were finally digested and filtered using Whatman No. 1 filter paper. Millipore water (18.2 Ohms, Elga PURE Waterlab) was used to fill up the volume till 25 mL. All solutions obtained were stored in pre-cleaned polythene vials and refrigerated for analysis.

**Analysis of heavy metals:** The Inductively Coupled Plasma Mass Spectrometry (ICPMS), Agilent 770s, Agilent Technologies, Japan was employed to analyse heavy metals namely Pb, Zn and Cr. Calibration standards manufactured by NIST (National Institute of Standard Technology), U.S were used for calibration of each metal. The standards of the elements (Pb, Zn, Cr) were prepared according to 0.5 ppb, 1 ppb, 5 ppb, 10 ppb, 25 ppb, 50 ppb, 100 ppb respectively. To obtain accuracy in results, the samples were run in triplicates and mean (±SD) was considered. The results obtained were expressed in ppm (µg/g).

## RESULTS

Opportunistically, a total of 27 Owls were collected from Simhachalam, Kambalakonda and Old post Office (Port Area) which are represented in Table 1 along with their current conservation status according to IUCN (2019). Heavy metal concentrations of Pb, Zn and Cr were determined and the results have been expressed in dry weight (because dry weight values are more consistent compared to wet weight) (Adrian & Steven 1979, Biswas et al. 2019). Metal concentrations differed among various tissue of birds and among the species which are represented in Table 2 and Fig. 2 respectively. Among all the species studied, Indian Eagle Owl (*Bubo bengalensis*) was recorded to have the highest metal content (1.33±1.10 µg/g) followed by Spotted Owlet (*Athene brama*) (1.21±1.63 µg/g) and Barn Owl (*Tyto alba*) (0.19±0.15 µg/g) as represented in Fig. 3 and Fig. 4.

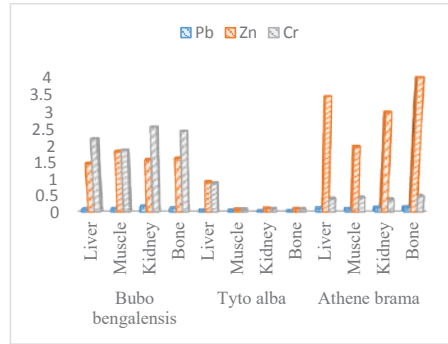


Fig. 2: Concentration of all metals (expressed in µg/g) in various tissues of owls.

Table 1: Sampling locations of owls and their current population trend (IUCN 2019).

| Common Name | Scientific Name | Sampling Area & GPS Location | Sample Size | Population Trend, IUCN 2019 |
|---|---|---|---|---|
| Indian Eagle Owl | *Bubo bengalensis* | Simhachalam 17.7664° N, 83.2508°E | 7 | Stable |
| Barn Owl | *Tyto alba* | Old Post Office (Port area) 17.6940° N, 83.2922° E | 9 | Stable |
| Spotted Owlet | *Athene brama* | Kambalakonda 17.7664° N, 83.3496° E | 11 | Stable |

The accumulation of metals in organs followed the order muscle>kidney>bone>liver which are represented in Fig. 5. Within metals, Zn was reported to be the highest (1.67±1.40 µg/g) compared to Cr (0.99±1.11 µg/g) and Pb (0.58±0.05 µg/g) which are represented in Fig. 6. Between species, the accumulation of metals by the organs was highest in *Bubo bengalensis* followed by *Athene brama* and *Tyto alba*.

**Statistical analysis:** In the PCA analysis, 3 PCAs for 3 different species were computed, and the variances explained by them were 67.35%, 97.83% and 100% for *Athene brama* (Table 3) respectively, 85.77%, 100% and 100% in *Tyto alba* (Table 4) followed by *Bubo bengalensis* as 68.66%, 97.53% and 100% (Table 5). In *Tyto alba*, Cr falls in component I, Zn and Pb showed a strong relationship and falls in component II. Whereas in *Bubo bengalensis*, Pb and Cr showed a strong relationship which falls under component I. Zn does not show any relationship with remaining metals and falls under Component IV. In *Athene brama*, it was observed that Cr did not show any relationship with the other heavy metals and falls under component I, and Zn and Pb show a strong relationship and falls under Component II.

Pearson's Correlation Coefficient (r) analysis was conducted in order to understand the relation between two variables namely organs (tissues) and metals accumulated by them. Significant positive correlations were obtained between the metals and organs (Table 6; Table 7; Table 8)

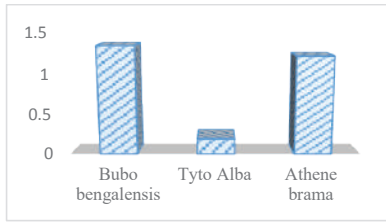


Fig. 3: Metal accumulation among species.

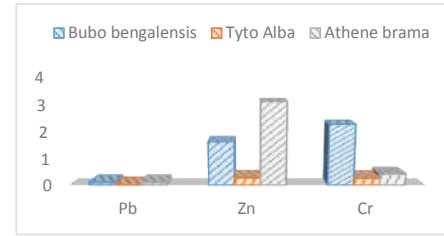


Fig. 4: Mean concentrations of all metals expressed in µg/g.

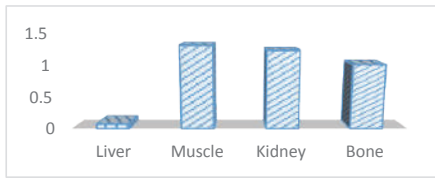


Fig. 5: Mean metal accumulation by organs (concentration expressed in µg/g).

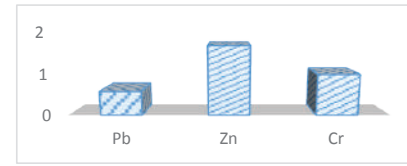


Fig. 6: Mean metal concentration (expressed in µg/g).

Table 2: Concentration of heavy metals in different organs of *Bubo bengalensis, Tyto alba* and *Athene brama* (expressed in µg/g).

| Bird | Organs | Zn | Cr | Pb |
|---|---|---|---|---|
| Indian Eagle Owl *(Bubo bengalensis)* | Muscle | 1.84±0.87 | 1.88±0.95 | 0.09±0.03 |
| | Liver | 1.48±1.32 | 2.21±0.93 | 0.08±0.03 |
| | Kidney | 1.58 | 2.56±1.34 | 0.16±0.07 |
| | Bone | 1.63±1.44 | 2.44±1.25 | 0.11±0.06 |
| Barn Owl *(Tyto alba)* | Muscle | 0.068±0.87 | 0.071±0.95 | 0.029±0.03 |
| | Liver | 0.91±1.32 | 0.87±0.93 | 0.034±0.03 |
| | Kidney | 0.098±1.44 | 0.092±1.34 | 0.008±0.07 |
| | Bone | 0.089±1.95 | 0.086±1.25 | 0.007±0.06 |
| Spotted Owlet *(Athene brama)* | Muscle | 1.98±0.87 | 0.440.95 | 0.08±0.03 |
| | Liver | 3.44±1.32 | 0.41±0.93 | 0.11±0.03 |
| | Kidney | 2.98±1.44 | 0.38±1.34 | 0.12±0.07 |
| | Bone | 3.98±1.95 | 0.49±1.25 | 0.13±0.06 |

Table 3: Explanation for the variation of elements in Spotted Owlet (*Athene brama).*

| Component | Variance % | Cumulative % |
|---|---|---|
| 1 | 67.35% | 67.35% |
| 2 | 30.47% | 97.83% |
| 3 | 2.17% | 100.00% |

respectively. In case of Lead, significant positive correlations were observed between muscle and kidney, (r=0.99), muscle and bone (r=0.98), and kidney and bone (r=0.98). For Zinc, significant positive correlations were obtained between liver and kidney (r=0.94), liver and bone (r=0.98), muscle and kidney (r=0.90), muscle and bone (r=0.83) and kidney and bone (r=0.99). In case of Chromium, significant positive correlations were obtained between liver and kidney (0.90), liver and bone (0.93), muscle and kidney (0.91), muscle and bone (0.99), kidney and bone (0.99) and where $p<0.05$ suggests that kidney and liver are the organs where most of the metals were absorbed. According to Kirubhanandhini et al. (2019), liver and kidney are good indicators for providing us with data about the metal contaminated environment.

To check the level of metal contamination among the tissues of various species in the present study, Kruskal-Wallis Test and Principal Component Analysis (PCA) using Origin Lab 2019 were conducted to understand the differences of metal accumulation among the 3 different species. The Kruskal-Wallis test was used to determine whether three or more independent samples originate from the same population and is a nonparametric test. When significant test results are obtained, it means that at least one sample differs from another. The p-value for Indian Eagle Owl (*Bubo bengalensis)* was 0.91 and for Spotted Owlet (*Athene brama)* was 0.86

Table 4: Explanation for the variation of elements in Barn Owl (*Tyto alba).*

| Component | Variance % | Cumulative % |
|---|---|---|
| 1 | 85.77% | 85.77% |
| 2 | 14.22% | 100.00% |
| 3 | 0.00% | 100.00% |

which confirmed that groups are not significantly different (Fig. 7, Fig. 8). The p-value was 0.45 for Barn Owl (*Tyto alba*) which confirmed that groups are significantly different (Fig. 9). The graphical form of Principal Component Analysis (PCA) obtained for three different Owl species are also represented in Fig.10, Fig.11 and Fig.12.

## DISCUSSION

Zinc: Being the 23rd abundant element found naturally on Earth's crust, zinc is naturally found in soils and sediments (Ullah et al. 2014). Zinc is an essential element required in the human body for growth and protection from renal toxicosis (Malik & Zeb 2009, Grúz et al. 2018). Zn also plays a role in the activation of enzymes and gene regulation expression but higher levels of zinc can impart physiological changes leading to decline in the population of birds (Gaba & Vashishat 2018, Kushwaha 2016). Zinc mobility into the environment is from manmade as well as natural sources (Ullah et al. 2014, Mustafa et al. 2015).

The average concentration of Zn when compared to other metals in the study was found to be highest 1.67 µg/g and Spotted Owlet (*Athene brama*) recorded the maximum accumulation of Zn content in bone (3.98 µg/g) followed by liver (3.44 µg/g), kidney (2.98 µg/g) and muscle (1.98 µg/g) when compared to Barn Owl and Indian Eagle Owl. Indian

Table 5: Explanation for the variation of elements in Indian Eagle Owl (*Bubo bengalensis).*

| Component | Variance % | Cumulative % |
|---|---|---|
| 1 | 68.66% | 68.66% |
| 2 | 28.87% | 97.53% |
| 3 | 2.47% | 100.00% |

Table 6: Correlation among the different organs for lead (Pb), $p<0.05$.

| | Liver | Muscle | Kidney | Bone |
|---|---|---|---|---|
| Liver | 1 | | | |
| Muscle | 0.135324 | 1 | | |
| Kidney | 0.113724 | 0.999763 | 1 | |
| Bone | 0.278397 | 0.989305 | 0.985895 | 1 |

Table 7: Correlation among the different organs for zinc (Zn), $p<0.05$.

| | Liver | Muscle | Kidney | Bone |
|---|---|---|---|---|
| Liver | 1 | | | |
| Muscle | 0.721359 | 1 | | |
| Kidney | 0.948101 | 0.904135 | 1 | |
| Bone | 0.982437 | 0.837917 | 0.990781 | 1 |

Table 8: Correlation among the different organs for chromium (Cr), $p<0.05$.

| | Liver | Muscle | Kidney | Bone |
|---|---|---|---|---|
| Liver | 1 | | | |
| Muscle | 0.903585 | 1 | | |
| Kidney | 0.937505 | 0.99619 | 1 | |
| Bone | 0.917254 | 0.999453 | 0.998528 | 1 |

| | |
|---|---|
| X-Function | Kruskal-Wallis ANOVA |
| User Name | Manu's |
| Time | 30-11-2019 14:08:17 |
| Data Filter | No |

*Input Data*

| | Data | Range |
|---|---|---|
| A | [Book1]Sheet1!A | [1*:3*] |
| Liver | [Book1]Sheet1!C1"Liver" | [1*:3*] |
| Muscle | [Book1]Sheet1!D1"Muscle" | [1*:3*] |
| Kidney | [Book1]Sheet1!B"Kidney" | [1*:3*] |
| Bone | [Book1]Sheet1!C"Bone" | [1*:3*] |

*Descriptive Statistics*

| | N | Min | Q1 | Median | Q3 | Max |
|---|---|---|---|---|---|---|
| A | 3 | 0.08 | 0.08 | 1.48 | 2.21 | 2.21 |
| "Liver" | 3 | 0.09 | 0.09 | 1.84 | 1.88 | 1.88 |
| "Muscle" | 3 | 0.16 | 0.16 | 1.58 | 2.56 | 2.56 |
| "Kidney" | 3 | 0.11 | 0.11 | 1.63 | 2.44 | 2.44 |

*Ranks*

| | N | Mean Rank | Sum Rank |
|---|---|---|---|
| A | 3 | 5.33333 | 16 |
| "Liver" | 3 | 6.33333 | 19 |
| "Muscle" | 3 | 7.33333 | 22 |
| "Kidney" | 3 | 7 | 21 |

*Test Statistics*

| Chi-Square | DF | Prob>Chi-Square |
|---|---|---|
| 0.63846 | 3 | 0.91036 |

Null Hypothesis:The samples come from the same population.
Alternative Hypothesis: The samples come from different populations
: At the 0.05 level, the populations are NOT significantly different.

Fig. 7: Kruskal-Walis ANOVA of Indian Eagle Owl (*Bubo bengalensis*).

| | |
|---|---|
| X-Function | Kruskal-Wallis ANOVA |
| User Name | Manu's |
| Time | 30-11-2019 14:12:58 |
| Data Filter | No |

*Input Data*

| | Data | Range |
|---|---|---|
| A | [Book1]Sheet1!A | [1*:3*] |
| Liver | [Book1]Sheet1!C1"Liver" | [1*:3*] |
| Muscle | [Book1]Sheet1!D1"Muscle" | [1*:3*] |
| Kidney | [Book1]Sheet1!B"Kidney" | [1*:3*] |
| Bone | [Book1]Sheet1!C"Bone" | [1*:3*] |

*Descriptive Statistics*

| | N | Min | Q1 | Median | Q3 | Max |
|---|---|---|---|---|---|---|
| A | 3 | 0.11 | 0.11 | 0.41 | 3.44 | 3.44 |
| "Liver" | 3 | 0.08 | 0.08 | 0.44 | 1.98 | 1.98 |
| "Muscle" | 3 | 0.12 | 0.12 | 0.38 | 2.98 | 2.98 |
| "Kidney" | 3 | 0.13 | 0.13 | 0.49 | 3.98 | 3.98 |

*Ranks*

| | N | Mean Rank | Sum Rank |
|---|---|---|---|
| A | 3 | 6.33333 | 19 |
| "Liver" | 3 | 5.66667 | 17 |
| "Muscle" | 3 | 6 | 18 |
| "Kidney" | 3 | 8 | 24 |

*Test Statistics*

| Chi-Square | DF | Prob>Chi-Square |
|---|---|---|
| 0.74359 | 3 | 0.86291 |

Null Hypothesis:The samples come from the same population.
Alternative Hypothesis: The samples come from different populations
: At the 0.05 level, the populations are NOT significantly different.

Fig. 8: Kruskal-Walis ANOVA of Spotted Owlet (*Athene brama*).

| | |
|---|---|
| X-Function | Kruskal-Wallis ANOVA |
| User Name | Manu's |
| Time | 30-11-2019 14:28:03 |
| Data Filter | No |

*Input Data*

| | Data | Range |
|---|---|---|
| A | [Book1]Sheet1!A | [1*:3*] |
| Liver | [Book1]Sheet1!C1"Liver" | [1*:3*] |
| Muscle | [Book1]Sheet1!D1"Muscle" | [1*:3*] |
| Kidney | [Book1]Sheet1!B"Kidney" | [1*:3*] |
| Bone | [Book1]Sheet1!C"Bone" | [1*:3*] |

*Descriptive Statistics*

| | N | Min | Q1 | Median | Q3 | Max |
|---|---|---|---|---|---|---|
| A | 3 | 0.034 | 0.034 | 0.87 | 0.91 | 0.91 |
| "Liver" | 3 | 0.029 | 0.029 | 0.068 | 0.071 | 0.071 |
| "Muscle" | 3 | 0.008 | 0.008 | 0.092 | 0.098 | 0.098 |
| "Kidney" | 3 | 0.007 | 0.007 | 0.086 | 0.089 | 0.089 |

*Ranks*

| | N | Mean Rank | Sum Rank |
|---|---|---|---|
| A | 3 | 9 | 27 |
| "Liver" | 3 | 4.66667 | 14 |
| "Muscle" | 3 | 7 | 21 |
| "Kidney" | 3 | 5.33333 | 16 |

*Test Statistics*

| Chi-Square | DF | Prob>Chi-Square |
|---|---|---|
| 2.58974 | 3 | 0.45929 |

Null Hypothesis:The samples come from the same population.
Alternative Hypothesis: The samples come from different populations
: At the 0.05 level, the populations are NOT significantly different.

Fig. 9: Kruskal-Walis ANOVA of Barn Owl (*Tyto alba*).

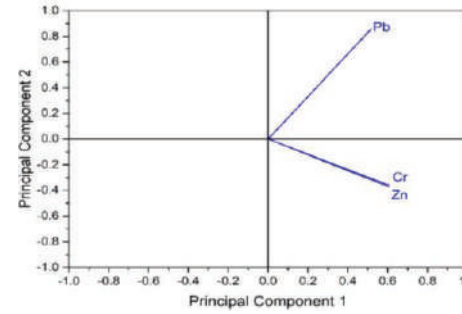


Fig. 10: Principal Component Analysis (PCA) of metals in Barn Owl (*Tyto alba*).

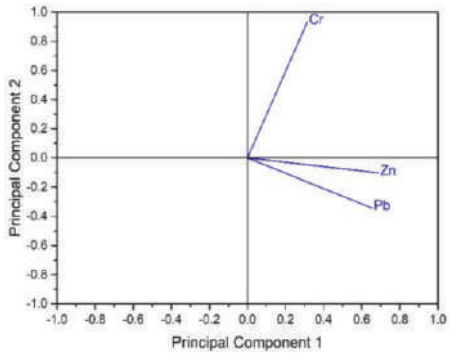


Fig. 11: Principal Component Analysis (PCA) of metals in Spotted Owlet (*Athene brama*).

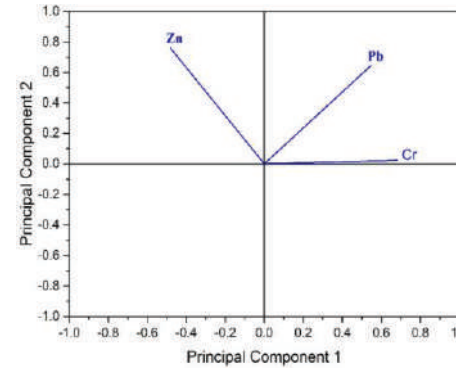


Fig. 12: Principal Component Analysis (PCA) of metals in Indian Eagle Owl (*Bubo bengalensis*).

Eagle Owl (*Bubo bengalensis*) recorded higher Zn content in the muscle (1.84 µg/g) followed by bone (1.63 µg/g), kidney (1.58 µg/g) and liver (1.48 µg/g). Compared to these two species of owls, Barn Owl (*Tyto alba)* recorded the lowest Zn levels (0.91-0.068 µg/g) in its organs. In India, studies done on same species of birds namely Barn Owl and Spotted Owlet by Gaba & Vashishat (2018) in Punjab yielded much higher concentrations of Zn (189.33-48.83 µg/g) in excreta

samples of Spotted Owlet, and 111.07 µg/g (Zn) in Barn Owl. Denneman & Douben (1993) reported a much higher level of Zn (535 µg/g) in feathers of Barn Owls from the Netherlands whereas (Grúz et al. 2018) reported 157.21-110.64 µg/g of Zn in owls from Hungary. A study done in Korea (Kim & Koo 2007) recorded 120 µg/g of Zn in Indian Eagle Owl, 225 µg/g Zn in Brown Hawk Owl and 66.4 µg/g in Collared Scoops Owl. A study done in Punjab province of Pakistan by Nighat et al. (2013) detected 90.74 µg/g of Zn in Spotted Owlet feathers whereas, in case of Indian Eagle Owl, no Zn content was detected. The present study was in agreement with the findings of Mustafa et al. (2015) who reported 1.10-13.26 µg/g of Zn in Black Kite (*Milvus migrans*) tissues from Sargodha district, Punjab, Pakistan. Black Kites belong to the Family *Accripiridae* and also falls under birds of prey or raptors which make them similar to Owls in feeding habits.

Chromium: Chromium is a trace element and an essential microelement for animals (Kirubhanandhini et al. 2019), but tissue concentration exceeding 4 µg/g dry weight is a warning for growing contamination (Outridge & Scheuhammer 1993, Boncompagni et al. 2003). Usually, Cr enters the body of the birds by nutrition (Grúz et al. 2018). Studies by various workers have reported that concentration of Cr more than 2.80 mg/kg in feathers of birds can lead to adverse effects (Burger & Gochfeld 2000, Grúz et al. 2018) and also can affect the development of the foetus and reproductive failure in mallards (Kertész & Fáncsi 2003). Some of the sublethal effects of Cr in birds include retarded growth, anaemia and male gonad damage which might also claim the life of an organism (US Fish & Wildlife Service 1986).

The mean concentration of chromium (Cr) was reported to be 0.994 µg/g and Indian Eagle Owl (*Bubo bengalensis*) recorded the highest concentration of Cr content in kidneys (2.56 µg/g) followed by bone (2.44 µg/g), liver (2.21 µg/g) and muscle (1.88 µg/g) in comparison to Spotted Owlet and Barn Owl. Spotted Owlet (*Athene brama*) recorded 0.49 µg/g in bone, followed by 0.44 µg/g in muscles, 0.41 µg/g in liver and 0.38 µg/g in kidney. The content of Cr recorded in Barn Owl was the lowest (0.086-0.87 µg/g) in its organs compared to the other two species of owls. In India, various studies have been carried out with respect to Cr in birds. Gaba & Vashishat (2018) have reported Cr in the range of 3.52-12.05 µg/g in excreta of Barn Owl and Spotted Owlet from Punjab, India. Another study by Kirubhanandhini et al. (2019) reported Cr concentrations in the range from 10.83-18.10 µg/g in muscle, liver and kidney tissues of Cattle Egret. Manjula et al. (2015) have reported an even higher level of Cr in Black Kite from Tiruchi, Chennai. However, the present study reported high levels of Cr compared to the study done by Grúz et al. (2018) who reported Cr in the range of 0.76±0.42 µg/g in owls (Long-eared Owl, Barn Owl and Tawny Owl) from Hungary. The present study was also in agreement with the findings of Deng et al. (2007) which reported Cr concentrations (0.96±0.34 µg/g) in liver tissues of Green Finch and 0.94±0.07 µg/g in the kidney of Green Finch and 0.69±0.06 µg/g in brain of the same. The present study also agreed with the findings of Boncompagni et al. (2003) who reported 0.94 µg/g Cr in feathers of Little Egret from Karachi and 0.47 µg/g Cr in feathers of Little Egret from Taunsa, Pakistan.

Lead: Grúz et al. (2018) stated that lead has the tendency to accumulate in calcium-rich tissues, bones, feathers and hair (Metcheva et al. 2006) and is not degradable. Studies by Burger et al. (1993) suggest that lead level above 4 mg/kg leads to reproductive failure and feeding behaviour in species like gulls. Lead affects the well-being of an organism directly by influencing procreation, circulatory and nervous systems (Gochfeld 2000, US Fish & Wildlife Service 1986, Kirubhanandhini et al 2019). However, Beyer et al. (1988) stated that symptoms of lead poisoning in birds vary among species.

The average concentration of lead recorded in the present study was 0.58±0.05 µg/g and Spotted Owlet (*Athene brama*) recorded the highest Pb content (0.13 µg/g) in bone followed by kidney (0.12 µg/g) and liver (0.11) µg/g. Compared to this, Indian Eagle Owl (*Bubo bengalensis*) recorded 0.16 µg/g in kidney and 0.11 µg/g in bone. The level of Pb in Barn Owl (*Tyto alba*) was found comparatively much lower (0.007-0.034) µg/g compared to the other two species. Studies carried out by Gaba & Vashishat (2018) on heavy metal content in excreta of Barn Owl and Spotted Owlet from Punjab district depicted quite high and alarming levels of lead (Pb) 25.91 µg/g which was under the toxic range and above the normal range as stated by the authors. Grúz et al. (2018) from Hungary have reported Pb in owls (Long-eared Owl, Tawny Owl and Barn Owl) in the range from 1.71-2.47 µg/g. In a similar study done by Kim & Koo (2007) in Korea in Eagle Owl, Brown Hawk Owl and Collared Scoops Owl has reported Pb in the range of 1.64-5.06 µg/g respectively. Whereas in a study done by Nighat et al. (2013) in Indian Eagle Owl (*Bubo bengalensis*), Pb was reported to be 17.9 µg/g, and in Spotted Owlet (*Athene brama*) to be 6.44 µg/g. Denneman & Douben (1993) reported quite high concentration (170 µg/g) of Pb in primary feathers of Barn Owls from Netherlands. However, the findings of the present study were in agreement with the levels of lead (Pb) reported by Kirubhanandhini et al. (2019) in muscles of Cattle Egret (0.28 µg/g), and with Gushit et al. (2016) in Red Cheeked Cordon Blue tail feathers (0.28 µg/g). When compared to similar investigations outside India, the present findings

agreed with that of Deng et al. (2007) (0.45±0.06 µg/g) in Greenfinch liver and (0.27± 0.06 µg/g) in Greenfinch brain and with that of Battaglia et al. (2005) who reported 0.35 µg/g Pb in liver, 0.50 µg/g in kidney, 0.88 µg/g in bone, and 0.10 µg/g in muscles. As the literature suggests, the Pb levels in the present findings were below the levels capable of imparting toxicity.

## CONCLUSION

As the results suggest, the Zn, Pb and Cr reported in the present study were at background levels which have been established for birds in the wild, and were definitely below the concentration of metals capable of imparting toxicity. However, differences in the concentration of heavy metal among the three species of owls throw light on the fact that environmental contamination is taking place in the environment which is inhabited by these owls. Differences in the metal contents among the 3 species of owls might have resulted due to differences in feeding habits and the availability of food resources based on the type of environment. A detailed study on their feeding guilds might be sufficient enough to provide further details in determining the source of environmental pollutants. Based on the results, it is unlikely to conclude that the extent of metal contamination threatens the life of the birds. However, owing to the fact that Visakhapatnam has many industries including petroleum industry, the presence of heavy metals in the environment is thus eminent (Biswas et al. 2019). Besides this, the presence of the heavy metals in the tissues of wild birds can also be contributed to the various point and non-point sources of pollution, which can be either natural or anthropogenic in origin and might continue to multiply through food chain leading to biomagnification.

## ACKNOWLEDGEMENT

The authors are thankful to GITAM (Deemed to be University) for providing the necessary facilities. The first author is also thankful to University Grants Commission (UGC) for providing Rajiv Gandhi National Fellowship which funded the present study. The first author also extends thanks to Bay of Bengal Lab, Andhra University, Visakhapatnam for analysis of samples.

## REFERENCES

Adrian, W. J. and Stevens, M. L. 1979. Wet versus dry weights for heavy metal toxicity determinations in duck liver. Journal of Wildlife Diseases, 15(1): 125-126.

Battaglia, A., Ghidini, S., Campanini, G. and Spaggiari, R. 2005. Heavy metal contamination in little owl (*Athene noctua*) and common buzzard (*Buteo buteo*) from northern Italy. Ecotoxicology and Environmental Safety, 60(1): 61-66.

Beyer, W. N., Spann, J. W., Sileo, L. and Franson, J. C. 1988. Lead poisoning in six captive avian species. Archives of Environmental Contamination and Toxicology, 17(1): 121-130.

Biswas, S., Ramakrishna, Ch and Maruthi, Y. A. 2019. Concentration of arsenic, lead, nickel in house crows (*Corvus splendens*) of Visakhapatnam city. Proceedings of the Zoological Society of India, 18(1): 59-64.

Boncompagni, E., Muhammad, A., Jabeen, R., Orvini, E., Gandini, C., Sanpera, C., Ruiz, X. and Fasola, M. 2003. Egrets as monitors of trace-metal contamination in wetlands of Pakistan. Arch. Environ. Contam. Toxicol., 45(3): 399-406.

Burger, J. and Gochfeld, M. 1993. Lead and cadmium accumulation in eggs and fledgling seabirds in the New York Bight. Environmental Toxicology and Chemistry, 12(2): 261-267.

Burger, J. and Gochfeld, M. 2000. Metal levels in feathers of 12 species of seabirds from Midway Atoll in the northern Pacific Ocean. Science of the Total Environment, 257(1): 37-52.

Dauwe, T., Janssen, E., Kempenaers, B. and Eens, M. 2004. The effect of heavy metal exposure on egg size, eggshell thickness and the number of spermatozoa in blue tit *Parus caeruleus* eggs. Environmental Pollution, 129(1): 125-129.

De Luca-Abbott, S. B., Wong, B. S., Peakall, D. B., Lam, P. K., Young, L., Lam, M. H. and Richardson, B. J. 2001. Review of effects of water pollution on the breeding success of waterbirds, with particular reference to ardeids in Hong Kong. Ecotoxicology, 10(6): 327-349.

Deng, J., Liao, B., Ye, M., Deng, D., Lan, C. and Shu, W. 2007. The effects of heavy metal pollution on genetic diversity in zinc/cadmium hyper accumulator *Sedum alfredii* populations. Plant and Soil, 297(1-2): 83-92.

Denneman, W.D. and Douben, P.E.T. 1993. Trace metals in primary feathers of the barn owl (*Tyto alba guttatus*) in the Netherlands. Environ. Pollution, 82(3): 301-310.

Furness, R.W. 1996. Cadmium in Birds. Environmental Contaminants in Wildlife: Interpreting Tissue Concentrations. Lewis, Boca Raton, 389-404.

Gaba, Y. and Vashishat, N. 2018. Estimation of heavy metal residues in excreta of spotted owlet (*Athene brama*) and barn owl (*Tyto alba*) from agro ecosystems of Punjab. Journal of Entomology and Zoology Studies, 6(3): 525-529.

Gochfeld, J. B. M. 2000. Effects of lead on birds (Laridae): A review of laboratory and field studies. Journal of Toxicology and Environmental Health, Part B: Critical Reviews, 3(2): 59-78.

Gragnaniello, S., Fulgione, D., Milone, M., Soppelsa, O., Cacace, P. and Ferrara, L. 2001. Sparrows as possible heavy-metal biomonitors of polluted environments. Bulletin of Environmental Contamination and Toxicology, 66(6): 719-726.

Grúz, A., Déri, J., Szemerédy, G., Szabó, K., Kormos, É., Bartha, A. and Budai, P. 2018. Monitoring of heavy metal burden in wild birds at eastern/north-eastern part of Hungary. Environmental Science and Pollution Research, 25(7): 6378-6386.

Guitart, R., Sachana, M., Caloni, F., Croubels, S., Vandenbroucke, V. and Berny, P. 2010. Animal poisoning in Europe. Part 3: wildlife. The Veterinary Journal, 183(3): 260-265.

Gushit, J.S., Turshak, L.G., Chaskda, A.A., Abba, B.R. and Nwaeze, U.P. 2016. Avian feathers as bioindicator of heavy metal pollution in urban degraded woodland. Ewemen Journal of Analytical & Environmental Chemistry, 2(2): 84-88.

IUCN 2019. www.iucnredlist.org

Janssen, C. R. and Heijerick, D. G. 2003. Algal toxicity tests for environmental risk assessments of metals. In: Reviews of Environmental Contamination and Toxicology, pp. 23-52.

Jayakumar, R. and Muralidharan, S. 2011. Metal contamination in select species of birds in Nilgiris District, Tamil Nadu, India. Bull. Environ. Contam. Toxicol., 87: 166-170.

Kaur, T. K., Vashishat, N. and Manoj, K. 2014. Heavy metal contamination in excreta of avian species from Ludhiana district of Punjab. International Journal of Advanced Research, 2(7): 873-879.

Kertész, V. and Fáncsi, T. 2003. Adverse effects of (surface water pollutants) Cd, Cr and Pb on the embryogenesis of the mallard. Aquat. Toxicol., 65(4): 425-433.

Kim, J. and Koo, T.H. 2007. Heavy metal concentrations in diet and livers of black-crowned night heron *Nycticorax Nycticorax* and grey heron *Ardea Cinerea* Chicks from Pyeongtaek, Korea. Ecotoxicology, 16(5): 411-416.

Kirubhanandhini, V., Muralidharan, S., Ganesan, K. and Shashikant, S.J. 2019. Elemental contamination in various species of birds from select states in India. Asian Journal of Engineering and Applied Technology, 8(2): 45-49.

Kushwaha, S. 2016. Heavy metal concentrations in feathers of critically endangered long-billed vultures (*Gyps indicus*) in Bundelkhand Region, India. International Journal of Life Sciences and Scientific Research, 2(4): 365-375.

Malik, R. N. and Zeb, N. 2009. Assessment of environmental contamination using feathers of *Bubulcus ibis* as a biomonitor of heavy metal pollution, Pakistan. Ecotoxicology, 18(5): 522-536.

Manjula, M., Mohanraj, R. and Devi, M. P. 2015. Biomonitoring of heavy metals in feathers of eleven common bird species in urban and rural environments of Tiruchirappalli, India. Environmental Monitoring and Assessment, 187(5): 267.

Metcheva, R., Yurukova, L., Teodorova, S. and Nikolova, E. 2006. The penguin feathers as bioindicator of Antarctica environmental state. Sci. Total Environ., 362(1-3): 259-265.

Mochizuki, M., Hondo, R. and Ueda, F. 2002. Simultaneous analysis for multiple heavy metals in contaminated biological samples. Biological Trace Element Research, 87(1-3): 211-223.

Muralidharan, S., Jayakumar, R. and Vishnu, G. 2004. Heavy metals in feathers of six species of birds in the District Nilgiris, India. Bulletin of Environmental Contamination and Toxicology, 73(2): 285-291.

Mustafa, I., Ghani, A., Arif, N., Asif, S., Khan, M. R., Waqas, A. and Malik, I. U. 2015. Comparative metal profiles in different organs of house sparrow (*Passer domesticus*) and black kite (*Milvus migrans*) in Sargodha District, Punjab, Pakistan. Pakistan Journal of Zoology, 47(4).

Nighat, S., Iqbal, S., Nadeem, M.S., Mahmood, T. and Shah, S.I. 2013. Estimation of heavy metal residues from the feathers of Falconidae, Accipitridae, and Strigidae in Punjab, Pakistan. Turk. J. Zool., 37: 488-500.

Outridge, P.M. and Scheuhammer, A.M. 1993. Bioaccumulation and toxicology of chromium: Implications for wildlife. Rev. Environ. Contam. Toxicol., 130: 31-77.

Sanchari, B., Ramakrishna, C.H. and Maruthi, Y.A. 2016. Extent of heavy metal accumulation in house crows of coastal zone. Life Sciences International Research Journal, 3(2): 158-161.

Sharma, C. and Vashishat, N. 2017. Assessment of heavy metals in excreta of house crow (*Corvus splendens*) from different agroecosystems of Ludhiana. Journal of Entomology and Zoology Studies, 5(4): 1891-1895.

Ullah, K., Hashmi, M. Z. and Malik, R.N. 2014. Heavy-metal levels in feathers of cattle egret and their surrounding environment: A case of the Punjab Province, Pakistan. Archives of Environmental Contamination and Toxicology, 66(1): 139-153.

US Fish and Wildlife Service. 1986. Chromium Hazards to Fish, Wildlife, and Invertebrates: A Synoptic Review. (Biological Report). Washington, USA: R. Eisler.

Nature Environment and Pollution Technology
An International Quarterly Scientific Journal

p-ISSN: 0972-6268
(Print copies up to 2016)
e-ISSN: 2395-3454

Vol. 19 | No. 4 | pp. 1517-1526 | 2020

Original Research Paper

https://doi.org/10.46488/NEPT.2020.v19i04.018

Open Access Journal

# Effect of Variable Compression Ratios on Performance and Emission Phenomena of DI CI Engine Fuelled with Palm Stearin Biodiesel-Diesel Blends

**V. Hariram*†, N. Balakarthikeyan*, S. Seralathan** and T. Micha Premkumar***

*Department of Mechanical Engineering, Hindustan Institute of Technology & Science, Hindustan University, Chennai, India

**Department of Aeronautical Engineering, Hindustan Institute of Technology & Science, Hindustan University, Chennai, India

†Corresponding author: V. Hariram; connect2hariram@gmail.com

**Nat. Env. & Poll. Tech.**
**Website: www.neptjournal.com**

*Received:* 27-05-2020
*Revised:* 25-06-2020
*Accepted:* 25-07-2020

**Key Words:**
Palm stearin wax
Transesterification
Biodiesel
Engine performance

## ABSTRACT

Rapid depletion of fossil fuels and escalating crude oil prices led the researchers to ascertain alternative feedstock as a substitute for mineral diesel. Biodiesel produced from non-edible sources was one among them. In the present investigation, palm stearin wax, a residue of palm oil extraction was used as a value-added feedstock for the production of biodiesel. Palm stearin biodiesel (PSBD) was derived from this feedstock using single stage transesterification process involving methanol and sodium hydroxide as a catalyst. PSBD was blended with mineral diesel at 20% (D80PSBD20) and 50% (D50PSBD50) in volume basis. The effect of variable compression ratios on the performance and emission phenomena of direct injection CI engine was analysed for test fuel blends. The tests were carried out for compression ratios 17:1, 17.5:1 and 18:1. Among all the fuel blends, D80PSBD20 blend showcased better performance characteristics along with reduced exhaust emissions at compression ratio of 18:1.

## INTRODUCTION

The increase in usage of internal combustion engine based automobile vehicles led to a dramatic increase in the demand for fossil fuels. Due to the escalating crude oil price and reduced availability of the fossil fuels led to explore the usage of vegetable-based bio-oil as a substitute fuel for compression ignition (CI) engine in the mid-1930s. The use of straight vegetable oil in CI engine created drastic deterioration on the engine's performance due to enlarged molecular size, higher density and increased kinematic viscosity (Arcaklioglu & Celikten 2005). Detailed investigations were conducted to reduce the kinematic viscosity of vegetable oils which includes heating, thermal cracking, transesterification, pyrolysis and others. Among these approaches, transesterification process emerged as a feasible and cost-effective methodology. According to pollution and renewable sources, the production capacity of biodiesel was getting increased day by day. Biodiesel was extracted from the feedstocks of either edible or non-edible oils. As the demand for edible oil for the cooking purpose already exists, non-edible oils were seen as the prime source for the production of biodiesel (Hariram et al. 2018). In the transesterification process, the mono-alkyl esters are converted into fatty acid methyl esters. Biodiesel produced from waxes is classified into two, such as animal waxes and plant waxes. Therefore, the palm stearin biodiesel extracted from the feedstock of the palm stearin wax obtained from palm oils is grouped as a plant wax. Based on the free fatty acid (FFA) content, the transesterification process is grouped into single-stage transesterification and double stage transesterification. As the FFA content of the palm stearin bio-oil was below two, single-stage transesterification was carried out to produce palm stearin biodiesel (Canakci et al. 2006). In general, three parameters influence the yield of biodiesel namely catalyst concentration, methanol to oil molar ratio, and reaction duration and these parameters were optimized to produce optimal yields. Ahmad et al. (2019) reported on the biodiesel production by transesterification process from flaxseed oil with a yield of 99.5%. The yield was determined at an optimum catalyst concentration, molar ratio and reaction duration of 0.51% catalyst, 5.9:1 and 33 minutes respectively. Anand et al. (2019) reported an optimum yield of biodiesel using Indian sardine fish as feedstock. The yield was 96.57% for process parameters namely, 20 vol. % methanol, 1.25 wt % KOH and reaction duration of 25 minutes. The characterization was also done using the GC-MS analysis.

Compression ratio (CR) is one of the key performance parameters for the CI engine. CR is responsible for the peak in-cylinder pressure and temperature during the combustion

of the hydrocarbon fuel. The variation of CR from the factory set value significantly affects the combustion, performance and emission phenomenon of the CI engine. Rosha et al. (2019) reported the combustion, performance and emission characteristics on CI engine with varying compression ratio using the palm-biodiesel blend. Palm-biodiesel B20 blend gave an optimal performance characteristic on increasing the compression ratio up to 18CR. The increase in CR reduced the CO, HC and smoke emissions to 47.8%, 41.0% and 35.7% respectively but increased the NOx emission to 41.1%. Mustafa et al. (2009) observed that the performance and emission of an engine fuelled with frying palm oil led to a better performance and emission values as predicted by ANN.

Ganesh et al. (2018) studied the emissions of palm stearin biodiesel involving six different blends namely, B20, B40, B60, B80 and B100. Palm stearin biodiesel reported lesser emissions (HC, CO, $CO_2$, $NO_x$ and smoke) compared to diesel. Hosamani & Katti (2018) studied the combustion, performance and emission characteristics of variable compression ratio (VCR) direct injection (DI) CI engine fuelled with *Simarouba* and *Jatropha* oil at various compression ratios and load conditions. Saravanan et al. (2019) analysed the performance and emission characteristics of VCR DI CI engine fuelled with rapeseed and *Madhuca* biodiesel blends. Anantha Kumar et al. (2016) investigated the performance and emission characteristics of VCR engine fuelled with diesel, waste plastic oil blended fuels with three blends such as 2.5%, 7.5% and 12.5%. The brake thermal efficiency enhanced by increasing the CR from 12CR to 20CR.

Raheman & Ghadge (2007) investigated the emission and performance characteristics of *Madhuca indica* biodiesel blends fuelled in Ricardo E6 engine. The investigation revealed that B20 blend was a suitable alternative to control air pollution. Praveena et al. (2020) analysed the performance and emission characteristics of DI CI engine fuelled with the grapeseed biodiesel blends. The test was conducted with various load conditions to predict the emissions of CO, $NO_x$, $CO_2$, HC and smoke. The UBHC got reduced by 20.7% compared to diesel fuel.

On reviewing the literature, it was observed that fuel sourced from non-edible feedstocks proved to be a promising substitute for the mineral diesel fuel. Numerous researchers have proved the utility on the usage of vegetable-based biodiesel in CI engines, but its effect on varied compression ratio needs exploration. In this study, palm stearin wax, derived as a residue during the extraction of palm oil, was used as a potential feedstock for biodiesel production. The palm stearin wax oil was subjected to a single stage transesterification process to transform it as palm stearin biodiesel (PSBD). PSBD was blended with mineral diesel in various proportions and its effect on the performance and emission phenomenon was analysed. Furthermore, the influence of the variations of the compression ratio on the emission and performance characteristics was studied.

## MATERIALS AND METHODS

### Materials

Palm stearin wax residue obtained after palm oil extraction was purchased from a local vendor in near Ambattur in the city of Chennai, Tamil Nadu, India. To carry out transesterification process, 99% pure sodium hydroxide and laboratory-grade methanol were procured from Praxor Scientific Corporation, Chennai and Hydrova Chemical and Systems,

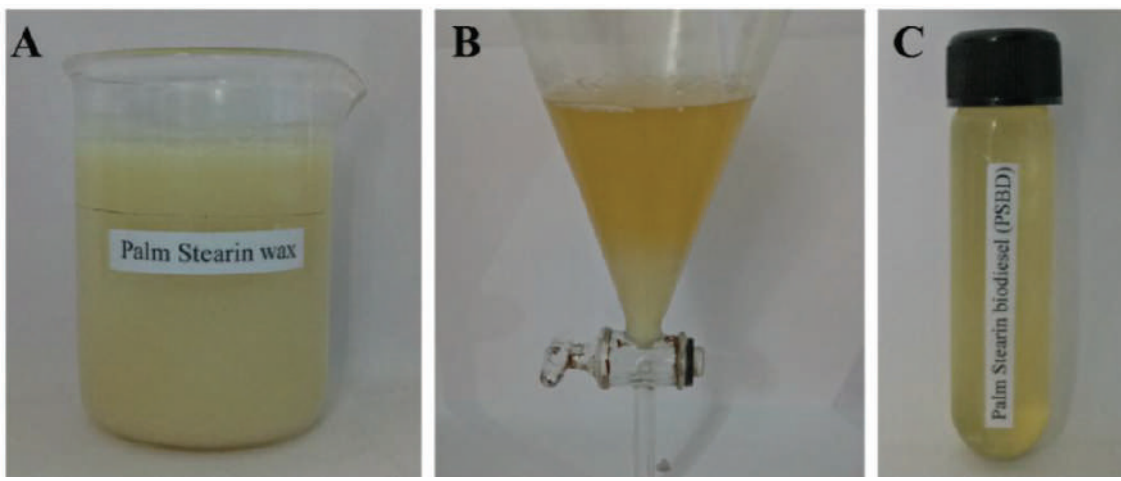


Fig 1: Bio-oil feed stock and PSBD.

Chennai respectively. Mineral diesel was purchased from a local petrol refilling station. All the chemical reagents procured were of analytical grade. Whatman's filter paper was procured from Swastik Scientific Company, Chennai, India to filter the biodiesel obtained during the transesterification process.

**Biodiesel Production**

Using titration method, the acid value of palm stearin wax oil was found to be 1.72. Therefore, single stage transesterification process using sodium hydroxide and methanol was adopted as it was widely reported by many researchers for the conversion of bio-oil with lower free fatty acid content into biodiesel. The transesterification process was carried out at Antonin Lavoisier Laboratory, Hindustan Institute of Technology and Science, Chennai, India. Initially, the palm stearin wax oil (Fig. 1A) was preheated upto 60°C and allowed to react with known concentrations of methanol and sodium hydroxide. The chemical reaction and the catalytic change in the reaction chamber were recorded carefully. On analysing the obtained data, it was noticed that the optimum conditions for biodiesel formation were 6:1 methanol to oil molar ratio, 62°C reaction temperature and 70 minutes of reaction time. The transesterification process was initiated using two litres inverted round bottom conical flask with holder arrangement.

Firstly, 0.72% of sodium hydroxide was thoroughly mixed with 400 mL of methanol for 20 minutes and kept at an agitation speed of 350 rpm for the formation of sodium methoxide solution. 500 mL of palm stearin wax oil heated up to 65°C for 45 minutes and later blended with sodium methoxide solution. The solution was agitated for 60 minutes at 450 rpm during which the reaction temperature was maintained between 65°C and 70°C. Then, the entire mixture was transferred into an inverted conical flask and a settling period of 12 hours was allowed. After six hours of settling, a ring formation appeared which separated the palm stearin biodiesel from glycerol. After 12 hours, the lower knob of the settling flask was opened to remove the glycerol (Hariram et al. 2015). The palm stearin biodiesel (PSBD) thus obtained was washed thoroughly with distilled water to remove the presence of methanol and glycerol. Later, the PSBD solution was heated up to 75°C to remove any moisture content. By the approach, 92.5% of palm stearin biodiesel was obtained (Fig. 1C).

**Physio-chemical Properties of Test Fuels**

Palm stearin biodiesel and its fuel blends were assessed for its physicochemical properties namely density, calorific value, kinematic viscosity, flash and fire point (Table 1). The density of PSBD was reduced to 0.882 g/m$^3$ from 0.941 g/m$^3$ at 15°C through transesterification process. The kinematic viscosity also showcased a significant reduction from 5.27 mm$^2$/s to 2.41 mm$^2$/s at 35°C. The calorific value showed a substantial increase up to 37122 kJ/kg from 21543 kJ/kg. The high flash and fire point values as 164°C and 242°C respectively reduced volatility of the PSBD. Table 1 lists the properties of PSBD which was compared with mineral diesel and other test fuel blends to understand its suitability in CI engine and all met the expected ASTM D6751 standards (Hariram et al. 2016).

**Experimental Procedure**

The experimentations were conducted at the standard operating condition and the average of three trials was used to analyse the test results. The test fuel blends used in this experiment were mineral diesel (100% commercial diesel), D80PSBD20 (mixture of 80% mineral diesel and 20% of PSBD) and D50PSBD50 (mixture of 50% mineral diesel and 50% PSBD). All the test fuel blends were prepared on the volume basis in a separate conical flask with almost care and agitated for 20 minutes to ensure thorough mixing of the test fuels.

Fig. 2 represents the layout of the experimental setup. Table 2 portrays the technical specification of the test engine. The performance and emission test of various fuel blends were carried out using Kirloskar 240 PE, 4-stroke, constant speed (1500rpm), water-cooled, computerized DI CI engine equipped with an eddy current dynamometer. Calibrated transmitters were used to restrain the air and fuel flow. Cali-

Table 1: Comparison of test fuel properties.

| Properties | Palm stearin wax oil | Palm stearin biodiesel (PSBD) | Mineral diesel | D80 PSBD20 | D50 PSBD50 |
|---|---|---|---|---|---|
| Density @ 15°C (g/m$^3$) | 0.941 | 0.882 | 0.832 | 0.841 | 0.879 |
| Kinematic viscosity @ 35°C (mm$^2$/s) | 5.27 | 2.41 | 2.57 | 2.45 | 2.54 |
| Calorific value (kJ/kg) | 21543 | 37122 | 42955 | 40329 | 41243 |
| Flash point (°C) | - | 164 | 48 | 127 | 135 |
| Fire point (°C) | - | 242 | 140 | 168 | 181 |

brated thermocouples were used to measure the temperature. Load on the engine was measured using a load cell. Rotameter was used to measure the flow of water. The tests were performed on three parameters namely compression ratios, fuel blends and various loads. Initially, the investigation was carried out using diesel as fuel at different load conditions.

The outcomes obtained by diesel fuel at different compression ratios and load conditions formed the baseline for further tests using different test fuels. The engine was run for 5 minutes to accomplish a constant operating condition which was the pertinent condition to run the engine. The load test was conducted by changing the loads from no load to full load (i.e., no load, low load, part load and full load conditions). Moreover, the test was conducted at various compression ratios, i.e. 17:1, 17.5:1 and 18:1 with varied fuel blends and diesel at various load conditions. The compression ratio was changed using the tilting block arrangement during the engine operation. Engine load was increased from low load to high load and then decreased from high load to low load to maintain the compression ratios and investigations of repeatability. The exhaust gas analyser was used to analyse emissions namely, CO, HC, $CO_2$, and $NO_x$ and the smoke meter was used to measure smoke opacity. The square root technique was used to predict the overall uncertainty of the experiments conducted and it was 1.89% as shown below.

Overall uncertainty (UC) = square root of (uncertainty of BSFC)$^2$ + (uncertainty of BTE)$^2$ + (uncertainty of BP)$^2$ + (uncertainty of CO)$^2$ + (uncertainty of $NO_X$)$^2$ + (uncertainty of HC)$^2$ + (uncertainty of smoke)$^2$ = 1.89%

## RESULTS AND DISCUSSION

### Performance Characteristics

**Brake thermal efficiency:** Fig. 3 depicts variations of brake thermal efficiency at various compression ratios for different load conditions involving fuel blends D80PSBD20, D50PSBD50 and mineral diesel. The brake thermal efficiency (BTE) of all test fuels was observed to be low at no-load conditions for the case 17.5CR. As the load is increased to part load, the BTE of all the blends increased. This may be due to an increase in the prevailing combustion temperature inside the combustion chamber. Fig. 3 portrayed that 17.5CR showed a higher value of BTE for all blends at full load conditions in comparison with other compression ratios. At 17.5CR, the maximum BTE (41.8%) was produced by diesel fuel at full load condition. This is due to its high calorific value (45.5MJ/kg), lower density, high viscosity and good air-fuel mixture ratio leading to complete combustion within the combustion chamber. At 17.5CR, the D50PSBD50 fuel blend showed a lower BTE value which was due to its fuel density, viscosity and calorific value phenomenon. Later, the compression ratio was reduced to 17CR and the BTE values of all fuel blends decreased at no-load conditions with respect

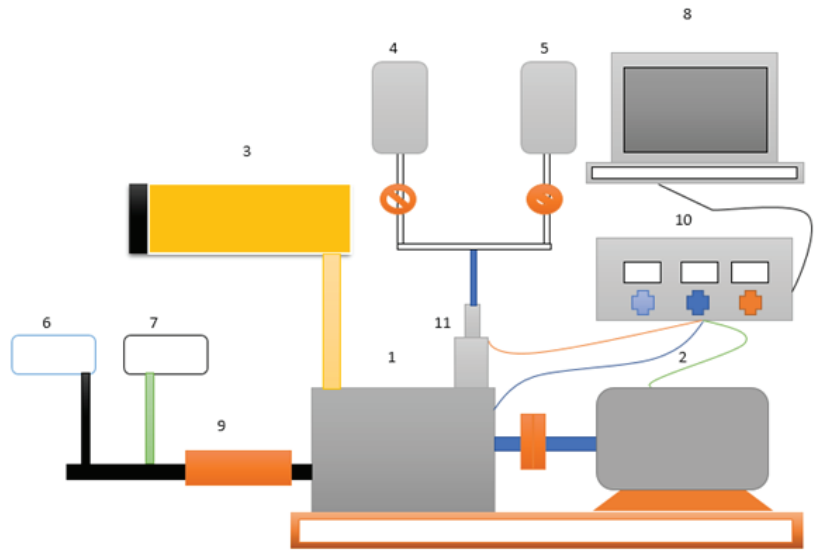


Fig. 2: Experimental setup.

Table 2: Test engine specification.

| Model and Make | 240 PE / Kirloskar make |
|---|---|
| Stroke | 110 mm |
| Bore | 87.5 mm |
| Factory set Compression ratio | 17.5 |
| Loading | Eddy current dynamometer |
| Rated power | 3.5 kW @ 1500 rpm |
| Injection timing | 23°bTDC |
| Swept volume | 661.45 cc |

to 17.5CR. This demonstrated the incomplete combustion phenomena with lower combustion temperature at low load conditions. Augmentation of the engine loading led to an increase in the combustion temperature and D80PSBD20 blend produced peak BTE. Similarly, BTE of all fuel blends at all load conditions increased on increasing the compression ratios to 18CR. This may be due to a decrease in combustion chamber volume leading to an increase in temperature within the combustion chamber. At 18CR, BTE of the D80PSBD20 and D50PSBD50 increased at low load with other CR ratios. At full load conditions, D80PSBD20 blend gave a better BTE at 18CR as 41.79% which was due to high combustion temperature within the combustion chamber. Higher blend (D50PSBD50) possessed low calorific value, lower combustion temperature, lower atomization and high density leading to poor brake thermal efficiency (Cenk et al. 2011).

**Brake specific fuel consumption:** The variations of brake specific fuel consumption (BSFC) at various engine loads for test fuels namely mineral diesel, D80PSBD20 and D50PSBD50 are presented in Fig. 4. Irrespective of the compression ratios, the BSFC were higher for all fuel blends at low load conditions. BSFC was inversely proportional to the brake thermal efficiency. Upon increasing the load condition up to the part load, the BSFC of biodiesel blends decreased significantly. D80PSBD20 gave the least BSFC (0.27 kg/kWh) among blended fuel for 17.5CR at all load conditions. This may be due to lower density and complete combustion in the combustion chamber. D50PSBD50 blend showed high BSFC values at all load conditions which may be due to low combustion temperature within the combustion chamber. Also, its density was high and calorific value was low compared to D80PSBD20 blend. Upon increasing the load to part load and later to full load condition, the BSFC values decreased representing an increase in the combustion temperature inside the combustion chamber. At 17CR, the mineral diesel gave a better BSFC value of 0.27 kg/kWh.

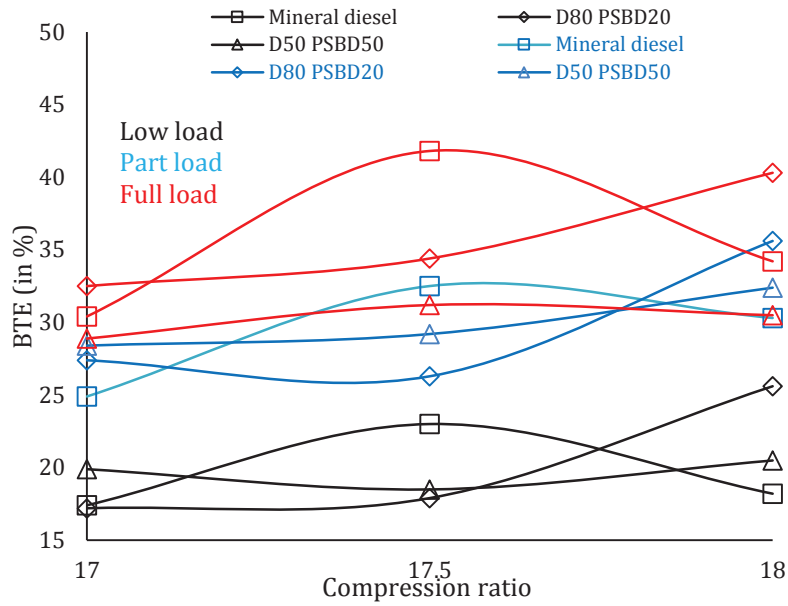


Fig. 3: Variation of BTE at various compression ratios.

Later, as the compression ratio was changed to 18CR, the whole process showed a significant effect. At low load conditions, BSFC of blended fuels were lesser compared to similar blends at other CRs. At full load condition, D80PSBD20 blend gave the low BSFC value as 0.25 kg/kWh which was achieved with low calorific value and low density of D80PSBD20 fuel as listed in Table 1. D50PSBD50 blend consumed more fuel at full load conditions involving various compression ratios. This is due to lower calorific value and higher density leading to poor atomization resulting in poor performance of BSFC.

## Emission Characteristics

**CO emission:** Carbon monoxide emission relates to the product of incomplete combustion. The pattern of CO emission under various compression ratios at different load condition is depicted in Fig. 5. At low load conditions, irrespective of the compression ratios, high CO emissions were observed which indicated the incomplete combustion process in the combustion chamber. The CO emission was lowered when increasing the load conditions up to part and full load condition. At 17.5CR, lowest CO value was observed as 0.025% for D80PSBD20 blend. D50PSBD50 had a slightly higher CO emission compared to D80PSBD20 blend at full load condition. All the CO emissions were still lesser compared to mineral diesel. On the other hand, at 17CR, the values of CO were comparatively higher at all load conditions. This was due to higher combustion

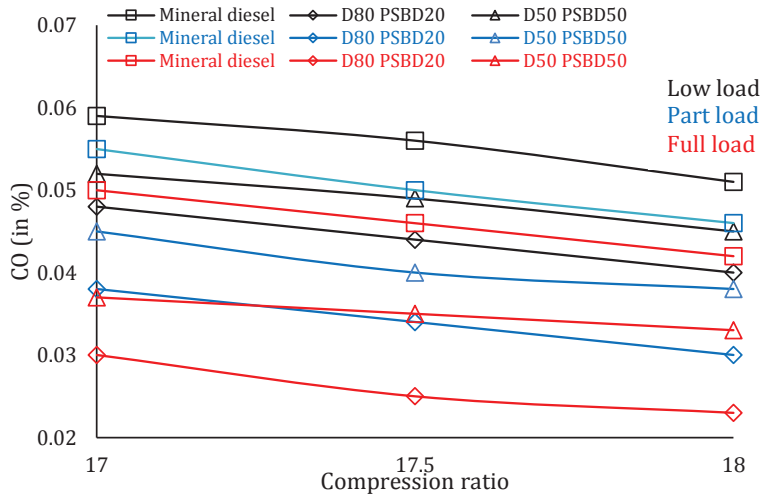


Fig. 5: Variation of CO emission at various compression ratios.

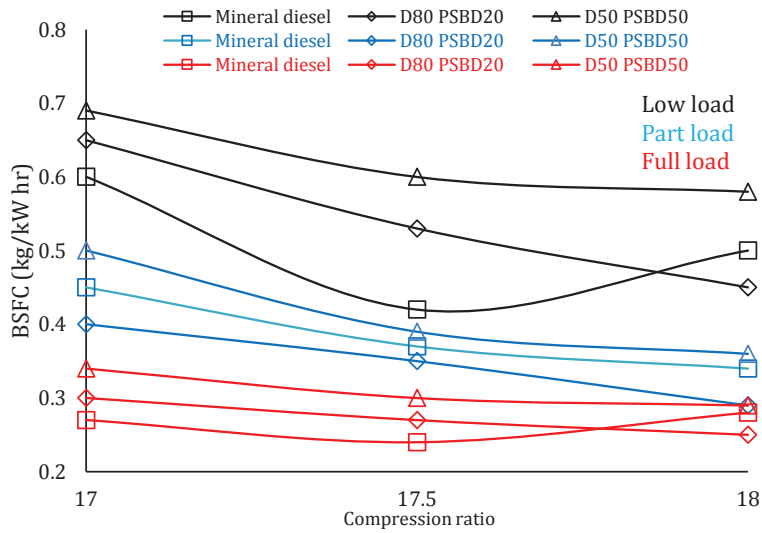


Fig. 4: Variation of BSFC at various compression ratios.

volume available in the combustion chamber leading to poor combustion (Hariram et al. 2016). At 18CR, the minimum CO emission recorded was 0.023% at full load condition fuelled with D80PSBD20 blend. This is due to a comparatively effective combustion process within the cylinder. Other fuel blends reported higher CO values compared to D80PSBD20 blend. This was due to higher fuel density, oxygen shortage at high speed condition, insufficient heat in cylinder along with lesser time available to ensure complete combustion.

**UBHC emission:** Due to low combustion temperature and nature of fuel mixture, i.e. lean or rich, unburned hydrocarbons are released from the VCR DI CI engine. The unburned hydrocarbon (UBHC) emission of all tested blends under various compression ratios at different load conditions is presented in Fig. 6. In general, it was observed that irrespective of compression ratios, D80PSBD20 blend gave the lowest UBHC emissions at varied loading conditions. At 17.5CR, D50PSBD50 blend had a higher UBHC value which represents insufficient combustion due to low combustion temperature inside the combustion chamber. Higher UBHC emission was observed for mineral diesel which may be due to poor atomization and volatility nature of the fuel. At 17CR, all fuel blends had a higher value of UBHC emissions compared to 17.5CR at all load conditions which again portrayed the insufficient combustion temperature prevailing inside the combustion chamber. The UBHC emissions were higher at low load conditions for all three fuel blends. By increasing the loading conditions, the UBHC emissions reduced. Similarly, by increasing the compression ratios to 18CR, the UBHC emissions reduced at all loading conditions. This was due to high combustion temperature, high cylinder pressure, high atomization and perfect air-fuel mixture. D50PSBD50 blend achieved lower UBHC emission as 78ppm at 18CR. But still was higher compared to D80PSBD20 blend UBHC emission. This was due to higher density and lower viscosity of the D50PSBD50 fuel blend.

**$NO_x$ emission:** The $NO_x$ emissions for all compression ratios at different load conditions are represented in Fig. 7. Nitrogen oxide was produced due to oxidation inside the cylinder as a result of high temperature. Oxygen content and in-cylinder temperature were the main factors to produce $NO_x$. Irrespective of the loading conditions, D80PSBD20 produced the highest $NO_x$ emissions among the tested fuel blends. $NO_x$ emission increased from no load to full loading conditions as the combustion chamber temperature increased due to complete combustion. $NO_x$ emission was observed to increase with an increase in CRs. The reason for lower emissions at 17CR was due to fall in combustion pressure and temperature inside the combustion chamber. The reason for mineral diesel and D50PSBD50 producing lower $NO_x$ was lack of oxygen content present inside the combustion chamber. The $NO_x$ emissions increased with increase in CR as prevailing conditions in the combustion chamber increased temperature. But, D80PSBD20 blend displayed a significant increase in $NO_x$ emissions due to increased compression ratio leading to better combustion resulting with an increase in in-cylinder temperature. On the other hand, D50PSBD50 blend produced the minimum $NO_x$ emissions (at part load 765ppm and full load condition 758ppm) as higher density

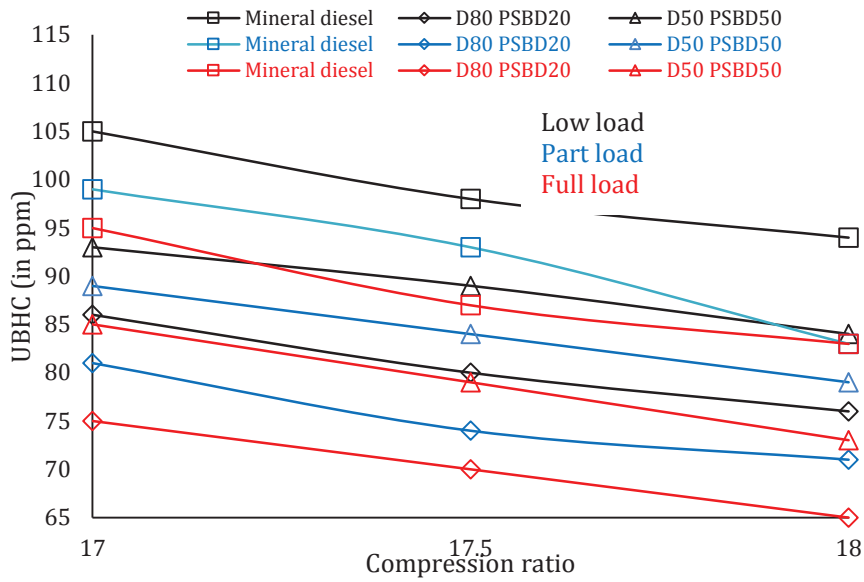


Fig. 6: Variation of UBHC emission at various compression ratios.

along with slightly lower calorific value resulted with reduced the in-cylinder temperature (Anand et al. 2011).

**$CO_2$ emission:** The variations of $CO_2$ emission for various compression ratios at different load conditions are highlighted in Fig. 8. $CO_2$ emission was derived as a product of complete combustion in the combustion chamber.

Significantly at 17.5CR, the $CO_2$ emission was investigated at low load, part load and full load fuelled with mineral diesel, D80PSBD20 and D50PSBD50. At low load condition, the diesel produced high $CO_2$ emission compared to other fuel blends. Upon increasing the load, $CO_2$ emissions of these three blends increased in the same pattern and the diesel fuel produced the maximum $CO_2$ emission as 580g/kWh. The escalation of $CO_2$ emission for the diesel fuel was due to prevailing high temperature inside the cylinder and perfect air supplied into the combustion chamber. On decreasing the compression ratio to CR17, the $CO_2$ emission of all tested fuels lowered at all load conditions. At low and part load conditions, $CO_2$ emission was low due to insufficient oxygen content present inside the combustion chamber leading to incomplete combustion. But, higher $CO_2$ emission was observed at full load condition for diesel

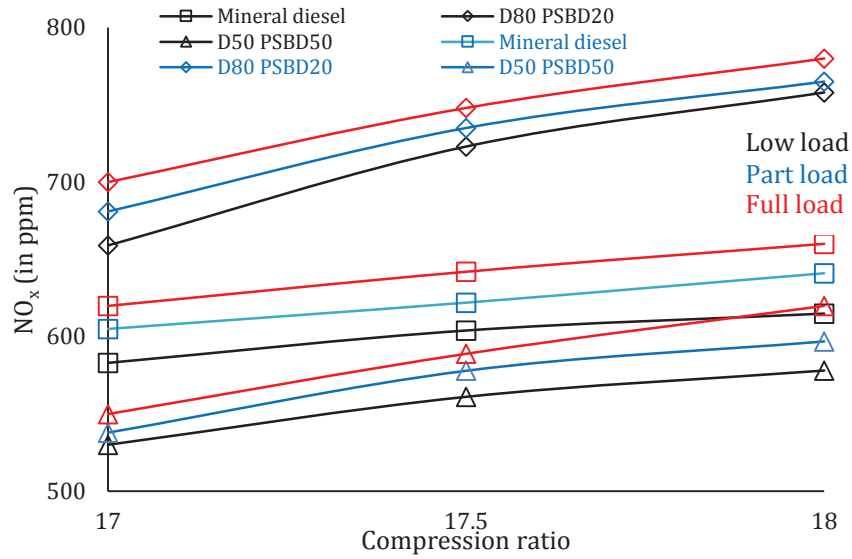


Fig. 7. Variation of $NO_x$ emission at various compression ratios.

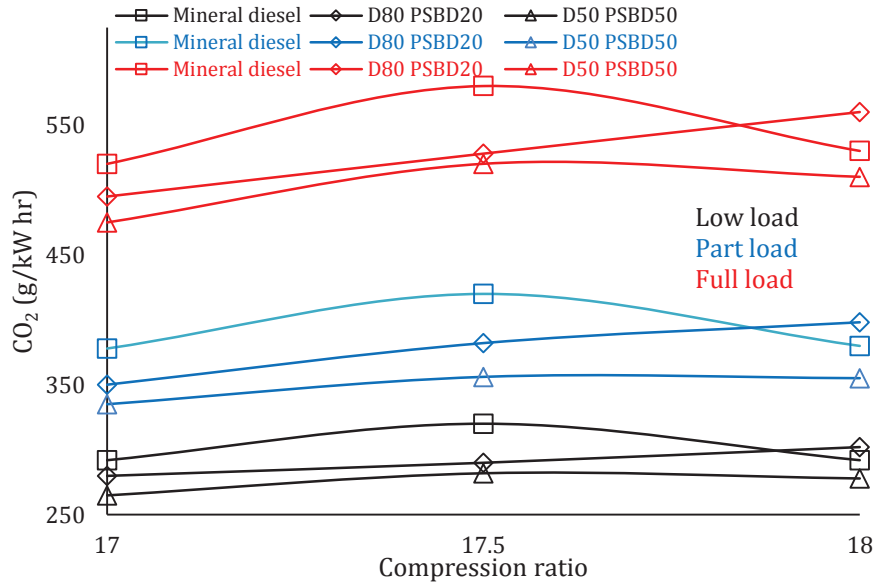


Fig. 8. Variation of $CO_2$ emission at various compression ratios.

fuel as 520g/kWh. Lack of oxygen content, higher density and poor atomization process led the D50PSBD50 blend to produce lower $CO_2$ emission. In general, D80PSBD20 fuel blend produced higher $CO_2$ emissions at all maximum load conditions irrespective of compression ratios. At 18CR, the $CO_2$ emission reached the maximum value for D80PSBD20 fuel blend due to higher pressure created in the combustion chamber by this compression ratio leading to complete combustion.

**Smoke emission:** Fig. 9 denotes the smoke opacity for various compression ratios at different load conditions and fuel blends. In general, the smoke opacity declined with increase in compression ratios for biodiesel blends as well as diesel. Also, the soot emissions reduced with increase in loading conditions for all CRs. At 17.5CR, high smoke opacity was observed for mineral diesel at all load conditions.

On the other hand, D80PSBD20 showed the lowest smoke opacity values at all load conditions. The lower smoke opacity value was due to the availability of oxygen content in the cylinder leading to perfect combustion. At 17CR, the smoke opacity values were higher for all fuel blends with respect to 17CR. Similarly, smoke opacity values of all fuel blends were lesser at 18CR at all load conditions compared to other CRs. At 18CR, the volume of the combustion chamber decreased resulting with increased pressure in combustion chamber leading to better combustion. Diesel fuel produces high soot emissions at various load conditions and increasing the CR led to a slight reduction in soot formation. D80PSBD20 reduced the smoke emission significantly at all conditions and various compression ratios. D50PSBD50 blend produced comparatively a higher soot formation with respect to D80PSBD20. This was due to the blend's physiochemical property in terms of having a higher density and poor volatility leading to a high smoke emission from the engine (Hariram et al. 2017).

## CONCLUSION

An attempt was made in the present experimental investigations to understand the capability of using palm stearin wax as a value-added feedstock for producing palm stearin biodiesel (PSBD). Single stage transesterification process was adopted based on the FFA content which yielded 92% of PSBD. The fuel blends namely D80PSBD20 and D50PSBD50 were tested in the CI engine and benchmarked with mineral diesel at CR17.5 at all loads. Investigations were carried out at compression ratios 18 and 17 under similar conditions and conclusions drawn from this study were listed below.

- D80PSBD20 showcased a higher BTE value as 40.3% for CR18 tested at full load condition whereas mineral diesel exhibited BTE as 41.8% at part load conditions for CR17.5. D50PSBD50 blend exhibited poor BTE at all load conditions as well as at all compression ratios.
- Increase in engine load reduced the BSFC of all test fuels at all compression ratios. At full load condition, D80PSBD20 exhibited lower BSFC (0.25 kg/kW hr) for CR18 which was 10.72% lower than diesel. At part load, D80PSBD20 showcased BSFC as 0.35 kg/kWh for CR17.5.

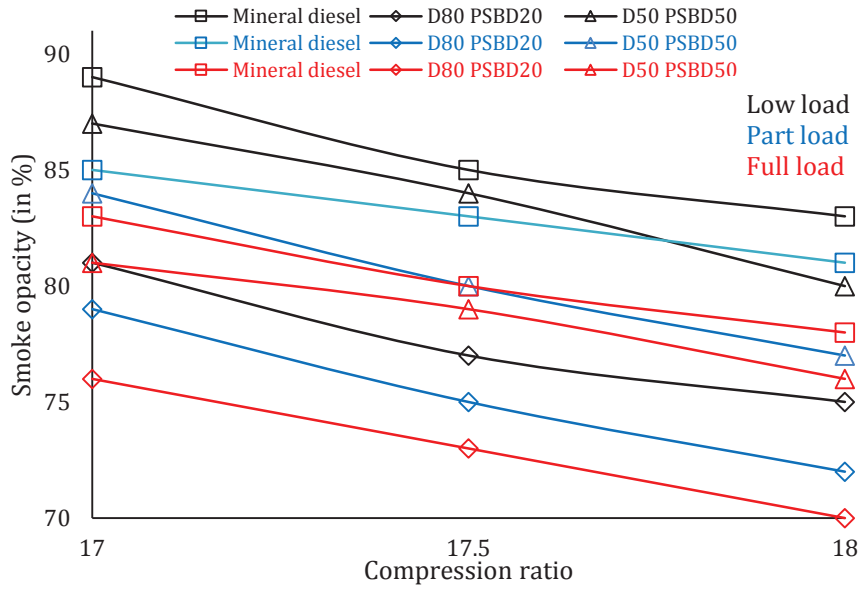


Fig. 9: Variation of $CO_2$ emission at various compression ratios.

- UBHC emission reduced significantly with an increase in compression ratios. D80PSBD20 exhibited lower UBHC emission (65ppm) for CR18 at full load condition. D80PSBD20 showcased a notable increase in UBHC emission around 6% to 8% as the CR was increased from 17 to 18.
- Smoke and carbon-monoxide emissions showed a decreasing trend with the increase in compression ratios. At full load, D80PSBD20 emitted 0.025% of CO at CR17.5 whereas it reduced to 0.023% at CR18. On the other hand, reducing the compression ratio to CR17 increased the CO emission up to 0.030%.
- $NO_x$ emission was observed at a higher level for all test fuels at CR18. D50PSBD50 produced lower $NO_x$ for CR17 at low and part load conditions.

## REFERENCES


Ahmad, T., Danish, M., Kale, P., Geremew, B., Adeloju, S.B., Nizami, M. and Ayoub, M. 2019. Optimization of process variables for biodiesel production by transesterification of flaxseed oil and produced biodiesel characterizations. Renewable Energy, 139: 1272-1280.

Anand Kumar, S.A., Sakthinathan, G., Vignesh Radhakrishnan, Rajesh J Banu and Ala'a Al Muhtaseb 2019. Optimized transesterification reaction for efficient biodiesel production using Indian oil Sardine fish as feedstock. Fuel, 253: 921-929.

Anand, K., Sharma, R.P. and Pramod Mehta, S. 2011. Experimental investigations on combustion, performance and emissions characteristics of neat karanja biodiesel and its methanol blend in a diesel engine. Biomass and Bioenergy, 35(1): 533-541.

Anantha Kumar, S., Jayabal, S. and Thirumal, P. 2016. Investigation on performance, emission and combustion characteristics of variable compression engine fuelled with diesel, waste plastics oil blends. J. Braz. Soc. Mech. Sci. Eng., DOI: 10.1007/s40430-016-0518-6.

Arcaklioglu, E. and Celikten, I. 2005. A diesel engine's performance and exhaust emissions. Applied Energy, 80: 11-22.

Canakci, M., Erdil, A. and Arcakliogl, E. 2006. Performance and exhaust emissions of a biodiesel engine. Appl. Energy., 83: 594-605.

Cenk, Sayin., Metin and Gumus 2011. Impact of compression ratio and injection parameters on the performance and emissions of a DI diesel engine fuelled with biodiesel-blended diesel fuel. Appl. Therm. Eng., 31: 3182-3188.

Ganesh, R., Manikandan, K. and Jishu Chandran 2018. Emission analysis of palm stearin biodiesel fuelled diesel engine. International Journal of Ambient Energy, DOI:10.1080/01430750.2018.1517692.

Hariram, V. and Bharathwaaj, R. 2016. Application of zero-dimensional model for predicting combustion parameters of CI engine fuelled with biodiesel-diesel blends. Alexandria Engineering Journal, 55: 3345-3354.

Hariram, V. and Vasanthaseelan, S. 2015. Optimization of base catalysed transesterification and characterization of *Brassica napus* (canola seed) for the production of biodiesel. International Journal of ChemTech Research, 8(9): 418-423.

Hariram, V., Prakash, S., Seralathan, S. and Micha Premkumar, T. 2018. Data set on optimized biodiesel production and formulation of emulsified *Eucalyptus teriticornisis* biodiesel for usage in compression ignition engine. Data in Brief, 20: 6-13.

Hariram, V., Seralathan, S., Dinesh Kumar, M., Vasanthaseelan, S. and Sabareesh, M. 2016. Analysing the fatty methyl ester profile of palm kernel biodiesel using GC/MS, NMR and FTIR techniques. Journal of Chemical and Pharmaceutical Sciences, 9(4): 3122-3128.

Hariram, V., Seralathan, S., Kunal Bhutoria and Harsh, H. Vora. 2018. Experimental study on combustion and performance characteristics in a DI CI engine fuelled with blends of waste plastic oil. Alexandria Engineering Journal, 57: 2257-2263.

Hariram, V., Seralathan, S., Micha, P. and Penchala, T 2017. Reduction of exhaust emission using a nano-metallic enriched lemongrass biodiesel blend. energy sources, part A: Recovery. Utilization and Environmental Effects, 39(21): 2065-2071.

Hosamani, B.R. and Katti, V.V. 2018. Experimental analysis of combustion characteristics of CI DI VCR engine using a mixture of two biodiesel blends with diesel. Engineering Science and Technology, DOI: 10.1016/j.jestch.2018.05.015.

Mustafa Canakci, Ahmet Necati Ozsezen, Erol Arcaklioglu and Ahmet Erdil 2009. Prediction of performance and exhaust emissions of a diesel engine fuelled with biodiesel produced from waste frying palm oil. Expert Systems with Applications, 36: 9268-9280.

Praveena, V., Leenus Jesu Martin, M. and Edwin Geo, V. 2020. Effect of EGR on emissions of a modified DI compression ignition engine energized with Nano emulsive blends of grapeseed biodiesel. Fuel, 267: 117317.

Raheman, H. and Ghadge, S.V. 2007. Performance of compression ignition engine with mahua (*Madhuca indica*) biodiesel. Fuel, 86: 2568-2573.

Rosha, P., Mohapatra, S.K., Mahla, S.K., Cho, H., Chauhan, B.S. and Dhir, A. 2019. Effect of compression ratio on combustion, performance, and emission characteristics of compression ignition engine fuelled with palm (B20) biodiesel blend. Energy, 178: 676-684.

Saravanan, A., Murugan, M., Sreenivasa Reddy, M. and Satyajeet Parida. 2019. Performance and emission characteristics of variable compression ratio CI engine fuelled with dual biodiesel blends of rapeseed and mahua. Fuel, 263: 116751.

Nature Environment and Pollution Technology
An International Quarterly Scientific Journal

p-ISSN: 0972-6268
(Print copies up to 2016)
e-ISSN: 2395-3454

Vol. 19 | No. 4 | pp. 1527-1535 | 2020

Original Research Paper

https://doi.org/10.46488/NEPT.2020.v19i04.019

Open Access Journal

# An Evaluation of the Green Performance of Chinese New Energy Enterprises From the Perspective of Social Responsibility

**Le Yang and Yue Zhang†**
Henan University of Engineering, Zhengzhou, Henan, China, 451191
†Corresponding author: Yue Zhang; zhangyue0106@163.com

**Nat. Env. & Poll. Tech.**
**Website: www.neptjournal.com**

*Received:* 12-05-2020
*Revised:* 27-08-2020
*Accepted:* 21-10-2020

**Key Words:**
Energy enterprises
Social responsibility
Green performance

## ABSTRACT

To evaluate the green performance of Chinese new energy enterprises, a performance evaluation system entailing four dimensions of social responsibility, management of liabilities, market-related responsibility, safety, and environmental responsibility was constructed. This system was subsequently applied to analyze and assess the green performances of 18 energy enterprises in China with their social responsibility. Results show that the green performances of most of the energy enterprises with social responsibility are hierarchically based. Specific countermeasures were proposed for promoting the health of energy enterprises and their sustainable development. These measures to be implemented by energy enterprises include establishing and perfecting systems for managing liabilities, sustaining the market, strengthening responsibility for security, and making diligent efforts to fulfil their environmental responsibilities.

## INTRODUCTION

In recent years, from the 18th National Congress of the Communist Party of China, the first proposed "beautiful China", the integration of ecological civilization into the overall layout of "five in one", to the concept of "green mountains and green waters are golden mountains and silver mountains" entered the United Nations. The construction of ecological civilization has been elevated to an unprecedented height. Green development measures are taking root across China. Since the 19th National Congress of the Communist Party of China, China has entered a new era of socialism with Chinese characteristics. The economy has shifted from a high-speed growth stage to a high-quality development stage. The development concept of innovation, coordination, green, openness, and sharing is deeply rooted in the hearts of the people, and corporate social responsibility has also been included in the overall situation of deepening reform. The modern energy system is the essential requirement of the new era of energy development, and the new energy industry is also the main engine that promotes the high-quality development of China's economy.

As the economy enters the stage of high-quality development in China, stakeholders have higher expectations for the quality of social responsibility reports. Enterprises also need a standard to improve the quality of report compilation. The quality rating of social responsibility reports has become an important issue. The energy industry differs from other industries. The particularity of energy industry entails more risks relating to safety and security, with frequent occurrences of accidents (Yongtae & Meir 2010). The energy industry supports China's economic and social development. However, environmental problems, wastage of resources, and security issues are common during the process of developing energy enterprises, leading to great security risks (Berman & Bui 2001). Therefore, an evaluation of the green performance of energy enterprises with social responsibility will contribute to the promotion of sustainable development of energy enterprises and providing measurable indicators for evaluating corporate social responsibility (Nahyun et al. 2015). When energy enterprises promise to protect the environment and staff safety and save resources (Christopher et al. 2015), it will have great practical benefits to promote economic development, social stability and sustainable development.

This study takes China's new energy companies in the economic development transition stage as the research object and aims to establish a performance evaluation system that includes four dimensions of social responsibility, i.e. responsibility management, market-related responsibility, and safety and environmental responsibility. The system was subsequently used to analyze and evaluate the relationship between the green performance of China's 18 energy companies and their social responsibilities.

## PAST STUDIES

The *Academy of Management Journal* devoted a thematic issue to corporate social responsibility and its editors identified research trends according to the papers published in this leading management journal (Wang et al. 2016).

They observed an increase in the number of articles on corporate social responsibility over recent decades and how works examining a non-U.S. context or data have gained significance to the point that they are comparable in scale to those in the U.S. setting. Amos (2018) reviewed scholarly papers focused on corporate social responsibility in developing countries in international journals and found that those applied empirical research methodologies increased steadily in the period 2006–2014. Specifically, attention to corporate social responsibility is slowly gaining traction in the Middle East (Al-Abdin et al. 2018) and is a very highly probable topic in the literature of transition economies and emerging markets (Piepenbrink & Nurmammadov 2015). Additionally, there was a noticeable concentration of papers in corporate social responsibility related journals, with the *Journal of Business Ethics* publishing as many articles as the nonspecialized journals.

At present, due to the differences in the understanding of the concept of corporate social responsibility by scholars, the academic circles mainly have two views on the connotation of corporate social responsibility. In general, there are two kinds of social responsibility in a broad sense and social responsibility in a narrow sense.

Most scholars believed that corporate social responsibility should be social responsibility in a broad sense. Carroll (1979) designed the corporate social responsibility pyramid. He divided corporate social responsibility into economic responsibility at the bottom level, legal responsibility at the second level, ethical responsibility at the third level, and charity responsibility at the final level. In 2010, the International Organization for Standardization (ISO) issued the *ISO26000 Social Responsibility Guide*, which covers nine aspects of social responsibility. The guide proposes that social responsibility should be fully integrated into the organization and integrated with the organization's strategy, philosophy, and planning. Lu & Abeysekera (2014) also believed that the content of corporate social responsibility is multifaceted, but there are differences in corporate social responsibility in different industries in terms of legislative provisions. The Shenzhen Stock Exchange's *Guidelines for Social Responsibility of Listed Companies* issued in September 2006 pointed out that social responsibility in a broad sense. It refers to the comprehensive development of the country and society, the natural environment and resources, as well as shareholders, creditors, employees and customers.

In terms of corporate social responsibility evaluation research, most of the existing studies are limited to the evaluation process, and it is rare to discuss the corporate behaviour decision-making based on corporate social responsibility performance. The reason may be that it is difficult to obtain evaluation data, and the challenge of quantitative indicators (Oliveira et al. 2018). Ferramosca & Verona (2019) applied the combination of bibliometric analyses on a sample of 2,583 corporate social responsibility studies derived from Scopus (1973–2018). First, it is found that the interdisciplinary character of corporate social responsibility. Second, it recognized numerous topics in the history of corporate social responsibility research and demonstrated how these topics emerge, vanish, or become steady over time. Third, the patterns of evolution in terms of topics are reflected in scientific journal specialization and coauthorship collaborations. Finally, it provided the latest evaluation on the state of the art in this field, highlighting the hottest topics. Imed et al. (2020) re-examined this issue using a newly available comprehensive innovation database on 20 countries and found support for the view that corporate social responsibility performance fosters innovation. This effect of corporate social responsibility is reflected in corporate innovation through its environmental and social dimensions. Jesús et al. (2020) used the 101 projects as a reference and analyzed the application of sustainability and other factors in the corporate social responsibility index. He found that the commitment to corporate social responsibility can also be achieved by improving shareholders' profitability or return on equity and investors consider not only financial risks but also sustainability factors.

The study on the field of new energy has begun to increase, but the study on the social responsibility of new energy enterprises has only appeared in recent years. Tan (2015) took Longyuan Wind Power New Energy listed company as an example to analyze the current status of the corporate social responsibility, focusing on three aspects, i.e. social responsibility performance, social responsibility management and social responsibility reporting. The study on the level of corporate social responsibility information disclosure in the electricity, coal, water, food and beverage, petrochemical and plastic industries found that a sound governance environment, corporate scale, and profitability have a significant positive impact on corporate social responsibility information disclosure (Liu & Zhang 2017). Han (2015) explored the impact of capacity utilization changes brought about by capacity reduction on the efficiency of industrial investment in China and found that the increase in capacity utilization has a positive effect on industrial investment efficiency, and it can also bring about non-surplus industries positive externalities.

## MATERIALS AND METHODS

Green performance is evaluated based on externally conducted assessments of green development and its task index. Stakeholders of energy enterprises include

shareholders, creditors, employees, the government, customers, the ecological environment, and communities (Du et al. 2020). This study drew on stakeholder theory applied to the actual situations of 18 energy enterprises listed in November 2016. A system for evaluating green performance was constructed based on the following four dimensions of social responsibility: liability management, market-related responsibility, safety, and environmental responsibility.

The system for evaluating the green performances of energy enterprises with their social responsibility comprised 4 level-one indicators, 12 level-two indicators, and 20 level-three indicators. The level-one indicators were the management of liabilities (*A*), market-related responsibility (*B*), security-related responsibility (*C*), and environmental responsibility (*D*). The level-three indicators were related to the basic score index. Each three-level indicator entailed either a score of five points or a score of zero, with 100 being the highest mark. The details of the indicators are shown in Table 1.

## RESULTS ANALYSIS

### The Dimension of Liability Management

Out of the 18 surveyed energy companies, 11 had established separate social responsibility management agencies. Therefore, each of these companies (PingZhuang Energy, Jizhong Energy, Xishan Coal and Electricity, Yanzhou

Table 1: The green performance evaluation index of social responsibility.

| Level-one indicators | Level-two indicators | Level-three indicators | Scoring criteria |
|---|---|---|---|
| Liability management (A) | Institutions; Report continuity; Report content | Organization of social responsibility management (A1) | A score of 5 for the establishment of a special administrative agency; otherwise, a score of 0 |
| | | The number of pages of the social responsibility report (A2) | A score of 5 for numbers more than or equal to the average of 33 pages; otherwise, a score of 0 |
| | | Disclosure of the social responsibility report for three consecutive years (A3) | A score of 5 for continuously issuing social responsibility reports for 3 consecutive years |
| | | Complete disclosure with inclusion of negative information (A4) | A score of 5 for disclosure of both positive and negative information; otherwise, a score of 0 |
| | | Comprehensibility of the social responsibility report (A5) | A score of 5 if the social responsibility report is comprehensible and comparable; otherwise, a score of 0 |
| Market-related responsibility (B) | Responsibility score; Employees' basic rights and interests; The government's responsibility | Earnings per share (B1) | A score of 5 for earnings more than or equal to average earnings for the industry; otherwise, a score of 0 |
| | | HeXun social responsibility report score (B2) | A score of 5 for a rating that is more than or equal to the overall rating of the industry |
| | | Safeguarding of employees' basic rights and interests (B3) | A score of 5 for a labor contract and social security coverage rate equal to 100% |
| | | Taxes paid on schedule (B4) | A score of 5 for taxes paid on schedule; otherwise, a score of 0 |
| | | Disclosure of relevant data to stakeholders (B5) | A score of 5 for more detailed data disclosure; otherwise, a score of 0 |
| Security-related responsibility (C) | Security certification; Safety concept; Accident rate | Certification of safety system (C1) | A score of 5 for passing authentication; otherwise, a score of 0 |
| | | Occupational safety training (C2) | A score of 5 for occupational safety training; otherwise, a score of 0 |
| | | Mortality rate per million tons (C3) | A score of 0 for a rate that is above the average rate of the industry; otherwise, a score of 5 |
| | | Safety administration (C4) | A score of 5 for investments in rectification; otherwise, a score of 0 |
| | | Disclosure of relevant information on safe production (C5) | A score of 5 for detailed disclosure on safe production, investments, and other relevant information |
| Environmental responsibility (D) | Environmental certification; Conservation of resources; Environmental protection | Environmental management system certification (D1) | A score of 5 for certification; a score of 0 for failure to obtain certification or lack of disclosure. |
| | | Environmental protection consciousness (D2) | A score of 5 for green initiatives and investments; otherwise, a score of 0 |
| | | Coal gangue utilization rate (D3) | A score of 5 if this rate exceeds the average rate for the industry; otherwise, a score of 0 |
| | | Mine water utilization rate (D4) | A score of 5 if this rate exceeds the average rate for the industry; otherwise, a score of 0 |
| | | Recovery rate (D5) | A score of 5 if this rate exceeds the average rate for the industry; otherwise, a score of 0 |

Coal, Shanghai Datun Energy, Shanxi Coal International, Yunnan Coal Energy, China Shenhua Energy, Haohua Energy, Shanxi Lu'an Environmental Energy, and China Coal Energy) scored 5 points. The remaining seven companies each obtained a score of 0 because they had not established an agency for managing social responsibility.

The average number of pages in social responsibility reports for the 18 energy enterprises was 34. Seven of these companies issued reports that were more than 34 pages in length. These companies were Jizhong Energy, Yanzhou Coal, Shanxi Coal International, Yunnan Coal Energy, China Shenhua Energy, Shanxi Lu'an Environmental Energy, and China Coal Energy whose social responsibility reports were respectively 49, 88, 47, 36, 116, 57, and 53 pages long. Consequently, these companies each scored 5 points, whereas the remaining 11 companies each scored 0.

All 18 energy companies released social responsibility reports for three consecutive years 2013, 2014, and 2015. Consequently, all of the companies scored 5 points.

Whereas all 18 companies announced positive developments, few enterprises released any negative information. However, the social responsibility reports of three companies contained both positive news as well as more detailed negative information relating to their productive and operational processes, such as accidents in coal mines and the death toll from accidents. These three companies, namely China Shenhua Energy, Haohua Energy, and Shanxi Lu'an Environmental Energy each scored 5 points, whereas the remaining 15 companies each scored 0.

Eight of the enterprises produced social responsibility reports that were relatively easy to understand compared with those of other companies because they contained a large number of tables and charts and provided comparisons and analyses of extensive historical data (Claudiu et al. 2014). These eight companies were Jizhong Energy, Yanzhou Coal, Shanxi Coal International, Yunnan Coal Energy, China Shenhua Energy, Haohua Energy, Shanxi Lu'an Environmental Energy, and China Coal Energy. Therefore, each of these companies scored 5 points, while the remaining 10 companies each scored 0.

### The Dimension of Market-Related Responsibility

EPS, which refers to the ratio of the after-tax profit to the total number of shares, is an important financial indicator for measuring the profitability of enterprises. In 2015, the average EPS value in the energy industry was 0.29 RMB. Of the 18 companies, six demonstrated EPS values that were above the industry's average. These companies were Jizhong Energy, Lanhua Sci-Tech Venture, China Shenhua Energy, Haohua Energy, Shanxi Lu'an Environmental Energy, and Yitai Coal, and their respective EPS values were 0.32, 0.46, 2.26, 0.31, 0.52, and 1.06. Whereas each of these companies scored 5 points, the remaining 12 companies, with lower than average EPS values, each scored 0.

The Hexun social responsibility report score is a relative authority score developed by HeXun that depends on the responsibility of an enterprise's shareholders, employees, suppliers, customers, and the environment. The shareholders' responsibility encompasses corporate profitability, solvency and returns and is measured using a series of financial and accounting indicators. In 2015, the energy industry's average social responsibility score was 16.05. The scores of five companies, namely Lanyan Holding, Xishan Coal and Electricity, Yanzhou Coal, China Shenhua Energy, and Shanxi Lu'an Environmental Energy were above the industry's average score at 51.49, 17.10, 16.10, 27.89, and 16.07, respectively. Therefore, these companies each scored 5 points, whereas the remaining 13 companies, whose scores were below the industry average, each scored 0.

The labour contract signing rate and the social security coverage rate for all 18 companies were at the 100% level. Consequently, all of the enterprises scored 5 points. All of the 18 energy companies paid their taxes on schedule. Therefore they all scored 5 points. Four out of the 18 companies disclosed relevant data to stakeholders. These companies, namely Jizhong Energy, Yanzhou Coal, China Shenhua Energy, and Shanxi Lu'an Environmental Energy each scored 5 points, whereas the remaining 14 companies each scored 0.

### The Dimension of Security Responsibility

Out of the social responsibility reports issued by the 18 surveyed energy companies, only that of China Shenhua Energy disclosed that the company's security system was certified. Therefore, this was the only company that scored 5 points, whereas each of the 17 other companies scored 0.

All 18 energy companies scored 5 points for occupational safety training. In 2015, the mortality rate per million tons of coal was 0.162 within the energy industry. All 18 of the energy enterprises demonstrated mortality rates below this average and therefore scored 5 points.

Only two companies, the Shenhuo Group and Yitai Coal did not disclose information on their security costs and rectification of security risks. Therefore, these companies both scored 0, whereas all of the remaining 16 companies, which disclosed security governance information, scored 5 points.

Ten companies, namely Pingzhuang Energy, Jizhong Energy, Lanyan Holding, Xishan Coal and Electricity, Yanzhou Coal, Shanxi Coal International, Yunnan Coal Energy, China Shenhua Energy, Shanxi Lu'an Environmental Energy, and China Coal Energy disclosed more detailed

information than other companies regarding the management of safe production, safe production inputs and other safety-related data. Each of these 10 companies scored 5 points, whereas the remaining eight companies each scored 0.

**The Dimension of Environmental Responsibility**

The social responsibility reports of the 18 companies revealed that five companies, namely Jizhong Energy, Xishan Coal and Electricity, Yanzhou Coal, China Shenhua Energy, and Shanxi Lu'an Environmental Energy had obtained certification of their environmental management systems. Therefore, these five companies each scored 5 points, whereas the remaining 13 companies each scored 0, as their environmental management systems had not been certified.

Only one company, Yitai Coal, scored 0, as it did not disclose its environmental philosophy or any investments relating to environmental protection. The other 17 companies, which provided information on their environmental protection concepts, and also disclosed the purposes and quantities of their environmental investments, all scored 5 points. Data on the utilization of coal gangue and mine water, and recovery rates, were extracted from the companies' social responsibility reports as well as from their annual financial reports and official websites. The specific data compiled are shown in Table 2.

For coal enterprises within China's energy industry, the standard rate of coal gangue utilization is 75%. The coal gangue utilization rates of seven out of the 18 energy companies were below 75%. Therefore, these companies, namely Pingzhuang Energy, the Shenhuo Group, Lanhua Sci-Tech Venture, Shanghai Datun Energy, China Shenhua Energy, Shanxi Lu'an Environmental Energy, and Yitai Coal, each scored 0. All of the remaining 11 companies evidenced ratios above 75% and therefore scored 5 points.

Again taking the example of coal enterprises, the standard rate of mine water utilization was 70%. Five of the companies (Pingzhuang Energy, China Shenhua Energy, Shanxi Lu'an Environmental Energy, Xinji Energy, and Yitai Coal) evidenced mine water utilization rates below 70% and accordingly scored 0. The remaining 13 companies, which evidenced rates over 70%, each scored 5 points.

The standard recovery rate for the coal industry is 75%. Among the 18 energy companies, the Shenhuo Group, Lanyan Holding, Shanghai Datun Energy, and Kailuan Clean Coal had recovery rates below the industry's standard and their scores were therefore 0. The rates of the remaining 14 companies were above this standard, so they all scored 5 points.

Tables 3 and 4 show the specific index scores of the 18 surveyed energy enterprises. Whereas Table 3 shows the

Table 2: Utilization ratios for coal gangue and mine water and recovery rates.

| S. No. | Company code | Corporate name | Coal gangue utilization ratio (%) | Mine water utilization ratio (%) | Recovery rate (%) |
|---|---|---|---|---|---|
| 1 | 000780 | Pingzhuang Energy | 60.00 | 30.03 | 77.14 |
| 2 | 000933 | The Shenhuo Group | 71.50 | 91.00 | 45.00 |
| 3 | 000937 | Jizhong Energy | 80.50 | 77.40 | 94.00 |
| 4 | 000968 | Lanyan Holding | 86.38 | 83.00 | 68.00 |
| 5 | 000983 | Xishan Coal and Electricity | 76.00 | 100.0 | 91.13 |
| 6 | 600123 | Lanhua Sci-Tech Venture | 74.00 | 72.00 | 78.90 |
| 7 | 600188 | Yanzhou Coal | 100.0 | 92.35 | 81.62 |
| 8 | 600508 | Shanghai Datun Energy | 49.60 | 76.00 | 57.00 |
| 9 | 600546 | Shanxi Coal International | 80.00 | 80.00 | 83.00 |
| 10 | 600792 | Yunnan Coal Energy | 92.00 | 90.50 | 75.00 |
| 11 | 600997 | Kailuan Clean Coal | 79.15 | 84.10 | 50.47 |
| 12 | 601088 | China Shenhua Energy | 20.14 | 67.50 | 89.19 |
| 13 | 601101 | Haohua Energy | 95.30 | 87.00 | 85.63 |
| 14 | 601666 | Pingdingshan Tianan Coal Mining | 100.0 | 80.00 | 85.00 |
| 15 | 601699 | Shanxi Lu'an Environmental Energy | 56.00 | 68.00 | 100.0 |
| 16 | 601898 | China Coal Energy | 98.80 | 75.40 | 89.10 |
| 17 | 601918 | Xinji Energy | 97.00 | 66.52 | 79.60 |
| 18 | 900948 | Yitai Coal | 66.40 | 41.00 | 80.00 |

Table 3: Green performance scores of the top-ranked nine surveyed companies.

| Evaluation indicator | Ping-zhuang Energy | Shen-huo Group | Jizhong Energy | Lanyan Holding | Xishan Coal and Electricity | Lanhua Sci-Tech Venture | Yanzhou Coal | Shanghai Datun Energy | Shanxi Coal Inter-national |
|---|---|---|---|---|---|---|---|---|---|
| $A_1$ | 5 | 0 | 5 | 0 | 5 | 0 | 5 | 5 | 5 |
| $A_2$ | 0 | 0 | 5 | 0 | 0 | 0 | 5 | 0 | 5 |
| $A_3$ | 5 | 5 | 5 | 5 | 5 | 5 | 5 | 5 | 5 |
| $A_4$ | 0 | 0 | 0 | 0 | 0 | 0 | 0 | 0 | 0 |
| $A_5$ | 0 | 0 | 5 | 0 | 0 | 0 | 5 | 0 | 5 |
| $B_1$ | 0 | 0 | 5 | 0 | 0 | 5 | 0 | 0 | 0 |
| $B_2$ | 0 | 0 | 0 | 5 | 5 | 0 | 5 | 0 | 0 |
| $B_3$ | 5 | 5 | 5 | 5 | 5 | 5 | 5 | 5 | 5 |
| $B_4$ | 5 | 5 | 5 | 5 | 5 | 5 | 5 | 5 | 5 |
| $B_5$ | 0 | 0 | 5 | 0 | 0 | 0 | 5 | 0 | 0 |
| $C_1$ | 0 | 0 | 0 | 0 | 0 | 0 | 0 | 0 | 0 |
| $C_2$ | 5 | 5 | 5 | 5 | 5 | 5 | 5 | 5 | 5 |
| $C_3$ | 5 | 5 | 5 | 5 | 5 | 5 | 5 | 5 | 5 |
| $C_4$ | 5 | 0 | 5 | 5 | 5 | 5 | 5 | 5 | 5 |
| $C_5$ | 5 | 0 | 5 | 5 | 5 | 0 | 5 | 0 | 5 |
| $D_1$ | 0 | 0 | 5 | 0 | 5 | 0 | 5 | 0 | 0 |
| $D_2$ | 5 | 5 | 5 | 5 | 5 | 5 | 5 | 5 | 5 |
| $D_3$ | 0 | 0 | 5 | 5 | 5 | 0 | 5 | 0 | 5 |
| $D_4$ | 0 | 5 | 5 | 5 | 5 | 5 | 5 | 5 | 5 |
| $D_5$ | 5 | 0 | 5 | 0 | 5 | 5 | 5 | 0 | 5 |
| Total score | 50 | 35 | 85 | 55 | 70 | 50 | 85 | 45 | 70 |

Table 4: Green performance scores of the nine lower-ranked surveyed companies.

| Evaluation indicator | Yunnan Coal Energy | Kailuan Clean Coal | China Shenhua Energy | Haohua Energy | Pingdin-gshan Tianan Coal Mining | Shanxi Lu'an Environmental Energy | China Coal Energy | Xinji Energy | Yitai Coal |
|---|---|---|---|---|---|---|---|---|---|
| $A_1$ | 5 | 0 | 5 | 5 | 0 | 5 | 5 | 0 | 0 |
| $A_2$ | 5 | 0 | 5 | 0 | 0 | 5 | 5 | 0 | 0 |
| $A_3$ | 5 | 5 | 5 | 5 | 5 | 5 | 5 | 5 | 5 |
| $A_4$ | 0 | 0 | 5 | 5 | 0 | 5 | 0 | 0 | 0 |
| $A_5$ | 5 | 0 | 5 | 5 | 0 | 5 | 5 | 0 | 0 |
| $B_1$ | 0 | 0 | 5 | 5 | 0 | 5 | 0 | 0 | 5 |
| $B_2$ | 0 | 0 | 5 | 0 | 0 | 5 | 0 | 0 | 0 |
| $B_3$ | 5 | 5 | 5 | 5 | 5 | 5 | 5 | 5 | 5 |
| $B_4$ | 5 | 5 | 5 | 5 | 5 | 5 | 5 | 5 | 5 |
| $B_5$ | 0 | 0 | 5 | 0 | 0 | 5 | 0 | 0 | 0 |
| $C_1$ | 0 | 0 | 5 | 0 | 0 | 0 | 0 | 0 | 0 |
| $C_2$ | 5 | 5 | 5 | 5 | 5 | 5 | 5 | 5 | 5 |
| $C_3$ | 5 | 5 | 5 | 5 | 5 | 5 | 5 | 5 | 5 |
| $C_4$ | 5 | 5 | 5 | 5 | 5 | 5 | 5 | 5 | 0 |
| $C_5$ | 5 | 0 | 5 | 0 | 0 | 5 | 5 | 0 | 0 |
| $D_1$ | 0 | 0 | 5 | 0 | 0 | 5 | 0 | 0 | 0 |
| $D_2$ | 5 | 5 | 5 | 5 | 5 | 5 | 5 | 5 | 0 |
| $D_3$ | 5 | 5 | 0 | 5 | 5 | 0 | 5 | 5 | 0 |
| $D_4$ | 5 | 5 | 0 | 5 | 5 | 0 | 5 | 0 | 0 |
| $D_5$ | 5 | 0 | 5 | 5 | 5 | 5 | 5 | 5 | 5 |
| Total score | 70 | 45 | 90 | 70 | 50 | 85 | 70 | 45 | 35 |

nine top-ranked companies, Table 4 shows the remaining nine lower-ranked companies in no particular order, listed according to their stock code numbers. The scores in these two tables reflect the green performance evaluations of the 18 surveyed companies with social responsibility.

The application of this classification scheme to the scores of the 18 surveyed energy companies resulted in the following groups. The first group of achievers comprised four companies: Jizhong Energy, Yanzhou Coal, China Shenhua Energy, and Shanxi Lu'an Environmental Energy. The group of leaders comprised five companies: Xishan Coal and Electricity, Shanxi Coal International, Yunnan Coal Energy, Haohua Energy, and China Coal Energy. The third group of pursuers comprised seven companies: Pingzhuang Energy, Lanyan Holding, Lanhua Sci-Tech Venture, Shanghai Datun Energy, Kailuan Clean Coal, Pingdingshan Tianan Coal Mining, and Xinji Energy. The final group of starters consisted of two companies, namely the Shenhuo Group and Yitai Coal.

When the scores for green performance ratings of corporate social responsibility were combined, the scores of Jizhong Energy, Yanzhou Coal, China Shenhua Energy, and Shanxi Lu'an Environmental Energy were all above 80. Of these companies, China Shenhua Energy had 90 points in total, demonstrating the best green performance relating to social responsibility. Two of the companies, the Shenhuo Group and Yitai Coal, attained only 35 points, indicating that their green performance relating to social responsibility was poor and that there was an urgent need for these companies to establish and develop improved systems for managing social responsibility. The performances of five companies, namely Xishan Coal and Electricity, Shanxi Coal International, Yunnan Coal Energy, Haohua Energy, and China Coal Energy were relatively good, but these companies still need to make sustained efforts. Seven companies, namely Pingzhuang Energy, Lanyan Holding, Lanhua Sci-Tech Venture, Shanghai Datun Energy, Kailuan Clean Coal, Pingdingshan Tianan Coal Mining, and Xinji Energy demonstrated relatively poor performances, indicating that they need to attach more importance to the development of social responsibility and to act in practical ways to promote its enforcement and enhance their performance levels.

## DISCUSSION

### The Dimension of Liability Management

From the perspective of liability management, whereas energy companies release social responsibility reports in time, most are unwilling to disclose negative information. The quality of social responsibility reports issued by energy companies was uneven in terms of the number of pages of the reports, their content, and their readability (Li et al. 2019). Moreover, they demonstrated striking contrasts in terms of the integrity of their content.

The results for the $A_1$ indicator (establishment of an organization for managing social responsibility) showed that 11 out of the 18 surveyed companies have performed relatively well, with more than half of the energy enterprises having prioritized the establishment of agencies for managing social responsibility. However, seven of the 18 companies still needed to prioritize the establishment of agencies to manage social responsibility.

The results for the $A_2$ indicator (number of pages of social responsibility reports) revealed the extent of disclosure of energy companies in their social responsibility reports, with the reports of seven companies exceeding 34 pages. Whereas the report content on social responsibility for these seven companies was good, as reflected in their scores, the remaining 11 companies scored lower for their report content, indicating that they needed to devote more attention to their social responsibility reports.

For the $A_3$ indicator (continuous disclosure of social responsibility reports for three consecutive years), the results indicated that each of the 18 surveyed companies scored 5 points, and this performance needs to be sustained.

The results for the $A_4$ indicator (complete disclosure, including negative information) indicated that the information reported by most of the energy enterprises was incomplete. Only three companies, namely China Shenhua Energy, Haohua Energy, and Shanxi Lu'an Environmental Energy scored 5 points, as they comprehensively disclosed positive as well as negative information. Thus, the information disclosed by most of the energy enterprises was incomplete. This situation indicates an urgent need for improvement.

For the $A_5$ indicator (comprehensibility of the responsibility reports), the results showed that eight of the surveyed companies performed relatively well. Thus, more than half of the energy companies attached less importance to their social responsibility reports.

### The Dimension of Market-Related Responsibility

From the perspective of market-related responsibility, energy companies did well in protecting their employees' basic rights and interests and in paying taxes on schedule. However, most energy companies did not publish comprehensive data and information to all concerned stakeholders.

For the $B_1$ indicator, the results showed that the EPS of six companies exceeded the current year's average EPS of 0.29, and the EPS of China Shenhua Energy was the highest at 2.26. Twelve companies had below-average EPS values, with that of Xinji Energy being especially low at -0.11. These

findings indicate that the economic benefits of the energy enterprises were not very promising.

The results for the $B_2$ indicator (the HeXun social responsibility report score) showed that the majority of companies (13) scored below the industry average, with only one-third (5) of the companies demonstrating scores above the average score for the industry.

For the $B_3$ indicator (safeguarding employees' basic rights and interests), the results showed that all of the surveyed companies scored 5 points. The labour contract signing rate and social security coverage reached the 100% level, indicating that energy companies performed well in terms of safeguarding their employees' basic rights and interests.

The results for the $B_4$ indicator (taxes paid on schedule) indicated that all of the surveyed firms scored 5 points, indicating that the 18 companies performed well in terms of paying their taxes and that they did so in a timely way.

For the $B_5$ indicator (disclosure of relevant data to stakeholders), the results showed that only four companies (22% of the sample) made detailed disclosures to each stakeholder. The disclosure of the remaining 14 companies to stakeholders was inadequate.

**The Dimension of Responsibility for Security**

From the perspective of responsibility for safety, energy enterprises diligently conducted safety training for their employees, and the accident mortality rate was controlled at a level below the average. Most companies attached great importance to safety governance, which included investments to improve safety and rectification of safety risks, with more than half of the companies also disclosing relevant safety data. However, less attention was given to certification of the safety system, so increased efforts to develop certified safety systems are necessary.

For the $C_1$ indicator (certification of safety systems), the results showed that only China Shenhua Energy had obtained certification of their safety system and that none of the other energy companies had obtained this certification. Therefore, strengthening the authentication work for security systems is an urgent priority.

The results for the $C_2$ indicator (occupational safety training of employees), showed that all of the companies scored 5 points, indicating that these 18 companies conducted occupational safety training for their employees. Although the number and scale of training sessions differed, energy companies performed quite well in protecting their employees' basic rights and interests.

For the $C_3$ indicator (mortality rate per million tons), the results showed that all of the companies scored 5 points. The mortality rates per million tons for all 18 companies were lower than the industry's average rate, indicating that energy enterprises had sufficient controls in place relating to accidental mortalities.

For the $C_4$ indicator (safety administration), the results showed that 16 companies (89% of the sample) invested in safety costs relating to production, management activities, and rectification of hidden dangers impacting on safety. Thus, most of the energy enterprises attached great importance to the work of safety management.

For the $C_5$ indicator (disclosure of relevant information on safety production), the results indicated that 10 companies performed relatively well. However, disclosure of safe production management, safe production inputs, and other related data information was incomplete.

**The Dimension of Environmental Responsibility**

In terms of environmental responsibility, most coal companies performed relatively poorly in the area of certification of their environmental management systems. The utilization rates of coal gangue and mine water and the recovery rate of half of the companies were above the industry standard. Nevertheless, these rates were below the industry's standard for many enterprises. Of the 18 companies, China Shenhua Energy attained the highest score, but the utilization ratios of coal gangue and mine water were inadequate. Consequently, energy enterprises need to pay more attention to protecting the environment.

For the $D_1$ indicator (environmental management system certification), the results showed that only five companies had obtained certification of their environmental management systems. Consequently, energy enterprises need to accelerate their efforts to obtain certification of their environmental management systems.

The results for the $D_2$ indicator (environmental awareness) indicated that most of the energy enterprises demonstrated awareness of the need for environmental protection, with only one company, Yitai Coal, obtaining a score of 0. This finding indicates that China's energy enterprises are performing reasonably well in the area of environmental awareness. However, there is still a need to strengthen efforts in the area of environmental protection.

For the $D_3$ indicator (the coal gangue utilization ratio), the results showed that 11 companies demonstrated ratios that exceeded the industry standard. Of these companies, Yanzhou Coal and Pingdingshan Tianan Coal Mining had the highest coal gangue utilization ratios. The remaining seven companies had ratios below the industry standard, with the ratio of China Shenhua Energy being the lowest.

The results for the $D_4$ indicator (the mine water utilization ratio) showed that the ratios for 13 companies were above the industry standard, with that of Xishan Coal and Electricity being the highest. The ratios of the remaining five companies were below the industry standard, and that of Pingzhuang Energy was the lowest.

The results for the $D_5$ indicator (the recovery rate) indicated that the recovery rates of 14 companies were above the industry standard, with that of Shanxi Lu'an Environmental Energy being the highest. The recovery rates of the remaining four companies were below the industry standard, and that of the Shenhuo Group was the lowest.

## CONCLUSIONS

A system for evaluating the green performance of energy enterprises was constructed based on four dimensions of social responsibility: liability management, market-related responsibility, responsibility for security, and environmental responsibility. The green performances of 18 energy enterprises with their social responsibility were subsequently analyzed and evaluated.

Based on the application of an established classification standard and the scores of the 18 surveyed energy companies, four companies were identified as achievers. These companies were Jizhong Energy, Yanzhou Coal, China Shenhua Energy, and Shanxi Lu'an Environmental Energy. Although China Shenhua Energy demonstrated the best green performance, it still needs to make considerable efforts to improve the utilization ratios of coal gangue and mine water.

Most of the energy companies' green performances relating to social responsibility were categorized at a medium level, with significant variations among them. The energy companies that demonstrated excellent green performances relating to social responsibility should make efforts to sustain their advantages, while companies whose green performance was the poor need to prioritize and strengthen their social responsibility to promote their health along with their benign and sustainable development.

## ACKNOWLEDGEMENT

This study was supported by the Humanity and Social Science Youth Foundation of the Ministry of Education of China (Grant No.18YJC630254), Henan Young Teachers Program of China (2019GGJS238), and Henan Soft Science Project of China (202400410377).

## REFERENCES

Al-Abdin, A., Roy, T. and Nicholson, J. D. 2018. Researching corporate social responsibility in the Middle East: The current state and future directions. Corporate Social Responsibility and Environmental Management, 25(1): 47-65.

Amos, G.J. 2018. Researching corporate social responsibility in developing-countries context: A systematic review of the literature. International Journal of Law and Management, 60: 284-310.

Berman, E. and Bui, T.M. 2001. Environmental regulation and labor demand: evidence from the south coast air basin. Journal of Public Economics, 79(5): 264-295.

Carroll, A.B. 1979. A three-dimensional conceptual model of corporate performance. Academy of Management Review, 4(4): 497-505.

Christopher, S.G., Robert, C.A. and Gregory, L. 2015. The environmental and economic effects of regional bio-energy policy in the southeastern U.S. Energy Policy, 85(11): 334-346.

Claudiu, C. 2014. Environmental efficiency of investments in renewable energy: comparative analysis at macroeconomic level. Renewable and Sustainable Energy Reviews, 3(7): 554-564.

Du, Y.C., Wang R.X. 2020. Impact of corporate governance ability on capital gains in mixed-ownership enterprises. Transformations in Business & Economics, 19(2): 92-113.

Ferramosca, S. and Verona, R. 2019. Framing the evolution of corporate social responsibility as a discipline (1973-2018): A large-scale scientometric analysis. Corporate Social Responsibility and Environmental Management, 27(3): 1-26.

Han, G.G. 2015. Analysis of the effect of capacity reduction on China's industrial investment efficiency. Management Modernization, 35(6): 28-30.

Imed, C.A, Boushra, H.A., Hatem, R.B. and Samir, S.C. 2020. Does corporate social responsibility influence corporate innovation? International evidence. Emerging Markets Review, 278(2): 498-513.

Jesús, M.F., Gracia, R.M. and Carmen, R.S. 2020. Corporate social responsibility and crowd-funding: The experience of the colectual platform in empowering economic and sustainable projects. Sustainability, 12(13): 5251

Li, W., Li, Z., Liu, S. and Huang, M. 2019. The economic-environmental impacts of China's action plan for soil pollution control. Sustainability, 11(8): 2322-2334.

Liu, X. and Zhang, C. 2017. Corporate governance, social responsibility information disclosure, and enterprise value in China. Journal of Cleaner Production, 142: 1075-1084.

Lu, Y. and Abeysekera, I. 2014. Stakeholders' power, corporate characteristics, and social and environmental disclosure: evidence from China. Journal of Cleaner Production, 64: 426-436.

Nahyun, K., Jon, J.M. and Hai, Y. 2015. Environmental pressure and the performance of foreign firms in an emerging economy. Journal of Business Ethics, 4(6): 1-16.

Oliveira, R., Zanella, A. and Camanho, A.S. 2019. The assessment of corporate social responsibility: The construction of an industry ranking and identifification of potential for improvement. European Journal of Operational Research, 278(2): 498-513.

Piepenbrink, A. & Nurmammadov, E. 2015. Topics in the literature of transition economies and emerging markets. *Scientometrics*, 102(3): 2107-2130.

Tan, J.S. 2015. Research on social responsibility of new energy enterprises. Modern Corporate Culture, 5: 74-75.

Wang, H., Tong, L., Takeuchi, R. and George, G. 2016. Corporate social responsibility: An overview and new research directions. Academy of Management Journal, 59(2): 534-544.

Yongtae, K. and Meir, S. 2010. Do corporations invest enough in environmental responsibility? Journal of Business Ethics, 105(3): 114-129.

Nature Environment and Pollution Technology
An International Quarterly Scientific Journal

p-ISSN: 0972-6268
(Print copies up to 2016)
e-ISSN: 2395-3454

Vol. 19 | No. 4 | pp. 1537-1545 | 2020

Original Research Paper

https://doi.org/10.46488/NEPT.2020.v19i04.020

Open Access Journal

# Applicability of the Surface Water Extraction Methods Based on China's GF-2 HD Satellite in Ussuri River, Tonghe County of Northeast China

**Wenfeng Gong*, Tiedong Liu*†, Yan Jiang** and Philip Stott*****
*College of Forestry, Hainan University, Haikou 570228, China
**College of Hydraulic and Electrical Engineering, Heilongjiang University, Harbin 150086, China
***School of Animal and Veterinary Sciences, The University of Adelaide, Roseworthy 5371, Australia
†Corresponding author: Tiedong Liu; 54626320@qq.com

**Nat. Env. & Poll. Tech.**
**Website: www.neptjournal.com**

*Received:* 03-12-2019
*Revised:* 20-12-2019
*Accepted:* 01-03-2020

**Key Words:**
Surface water extraction
GF-2 satellite
Water index
Support vector machine

## ABSTRACT

Surface water is the most important and common water resource on earth. Accurate and effective mapping and detecting of surface water have been made possible by remote sensing technology, high-resolution satellite data, playing an important role in surface water monitoring and mapping, which has become the current hot research for water information extraction in recent decades. Therefore, in this paper, we tested and analysed four models to extract water bodies using China's GF-2 HD satellite (GF-2) image, including Normalized Difference Water Index (NDWI), Modified Shadow Water Index (MSWI), Support Vector Machine (SVM) and Object-Oriented Method (OOM). The results showed applying water extraction models can map surface water with an overall accuracy of 0.8935, 0.9256, 0.9467 and 0.9357, respectively. SVM owns the highest overall accuracy value of 0.9467, followed by OOM. SVM performed significantly better at surface water extraction with kappa coefficients improved by 9.00%, 5.00%, and 2.00%, respectively, which yielded the best results and used to map surfaces water bodies in the study region, while index methods (NDWI and MSWI) are mostly classified into the water and non-water information based on a threshold value, with higher total omission and commission errors at 12.45%, 25.64%, 6.38% and12.87%, respectively. Therefore, we proposed SVM as the best algorithm to identify water body and effectively detect surface water from the GF-2 image.

## INTRODUCTION

Surface water is one of the vital components of the earth's environment, which is not only the essential for the survival of living beings (Vorosmarty et al. 2000), but also is the important basic information for land use/cover change (LUCC), climate changes, seasonal changes, and environmental changes throughout of the world (Alamgir et al. 2016, Araral & Wu 2016). Therefore, knowledge of the spatial distribution of surface water is imperative for assessment of water resources, watershed changes, land surface water management and environmental monitoring (NRC 2008, Sun et al. 2012). Besides, timely monitoring and delivering data on the dynamics of surface water are essential for policy and decision-making processes (Frey et al. 2010), especially for monitoring floods risk at an emergency.

Remote sensing has advantages of the macroscopic, real-time, periodic repeatability, dynamic access to the land surface information (Lu et al. 2011), which can provide low-cost and reliable information for environmental changes at local, regional, and global scales, with their long-collected repeatable and even real-time data (Melesse et al. 2007, Lee et al. 2018). Waterbody information, as an important constituent of remote sensing image, has become the vital national geo-information and can be automatically or semi-automatically extracted by integrating remote sensing data with geographic information systems (GIS). Meanwhile, in recent decades, accurate and effective extracting water from remote sensing data has become indispensable ways for the development and utilization of water resources (Du & Zhou 1998), which also becomes an important branch of remote sensing applications.

Due to the ease of processing and obtaining satellite image data (Masocha et al. 2018), numerous surface water extraction algorithms have been developed and applied for remotely sensed imageries (Borton 1989), which focused on the following satellite sensors with the different spatial, temporal and spectral resolution, including the Moderate-Resolution Imaging Spectro-radio-meter (MODIS) (Khandelwal et al. 2017, Ovakoglou et al. 2016), Satellite Pour l' Observation dela Terre (SPOT) (Ji et al. 2009), Advanced Spaceborne Thermal Emission and Reflection Radiometer (ASTER) (Huang et al. 2008 ), Advanced Very High Resolution Radiometer (AVHRR) (Zhou et al. 1996), Thematic Mapper

series data (MSS,TM,ETM+ and OLI) (Acharya et al. 2018, Alanazi & Ghrefa 2013, Alesheikh et al. 2007, Senay et al. 2016, Wang et al. 2018, Yang et al. 2010, Zhang et al. 2016), and others (Lu et al. 2011, Peng et al. 2018, Wang et al. 2012). Besides, although many studies have been conducted most of large surface water are limited to small water bodies, such as small ponds, narrow rivers, and shallow water at the edge of rivers, which accurately cannot be extracted due to the limited spatial resolution.

In the recent decade, with the improvement of the spatial resolution, visiting time and spectral resolution of remote-sensing images, more and more high-resolution satellite data can be widely applied to extract and map surface water, such as Chinese Gaofen-1/2, Quick-Bird, WorldView, IKONOS, Rapid Eye and so on (Sawaya et al. 2003, Wasowski et al. 2012, Tatar et al. 2018). In addition, the study on water body extraction from GF-1/2 series images has become a hot research topic in China (Chen et al. 2015, Li et al. 2015, Peng et al. 2018, Song et al. 2015), though several studies have tested the performance of water indices using GF-2 sensor in China (Liu et al. 2019, Zou et al. 2019). However, this new and advanced sensor has, unfortunately, not been exploited to map surface water at county scales in Northeast China, especially at Ussuri River between China and Russia.

Hence, in this paper, the algorithms have been proposed for identifying water bodies with GF-2 including water body index methods (Normalized Difference Water Index, NDWI, Modified Shadow Water Index, MSWI), supervised classification methods (Support Vector Machine method, SVM) and others methods (Object-Oriented Method, OOM). The objectives of this study are: to apply the different methods to obtain the surface water information by comparing with water body index, SVM and OOM, to detect and map land surface water in Northeast China region qualitatively and quantitatively, to achieve the suitable method to extract surface water from the evaluation accuracy.

## MATERIALS AND METHODS

### Study Region

The Ussuri River is the boundary river between China and Russia (Fig. 1). The study area is located at the confluence of the Heilongjiang (Amur) River and Ussuri River, which belonged to transboundary regions and located between 47°53' N-48°10' N latitude and 132°47' E-133° 9' E longitude. It belongs to the continental monsoon climate with the annual precipitation of 532.7 mm, the average accumulated temperature is 2435 degrees. The study region is covered by

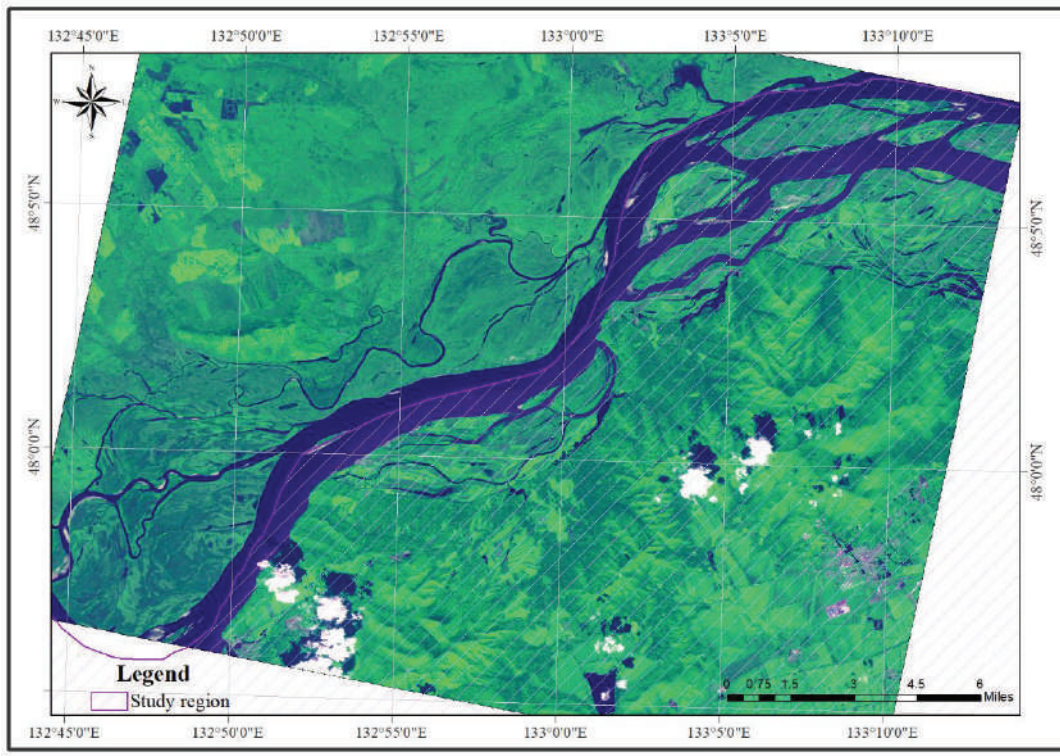


Fig. 1: Geographic location of the study region.

marsh plain with black soil, which is suitable for all kinds of crop cultivation, and there are a small number of mountainous areas scattered in the plain, covered with forest and elevation range from 45 m to 65 m, the regional terrain is high in the southwest and low in the northeast.

**GF-2 Image Preprocessing**

In the study, the GF-2 images (L1A products) containing a panchromatic image with a resolution of 0.8 m and multi-spectral image with a resolution of 4m, were acquired on September 12th, 2015. The parameters of the data within the study area collected are given in Table 1. Meanwhile, the high-resolution satellite imagery of GF-2 had a good quality of small cloudy and was orth-rectified by using the rational polynomial coefficient (RPC) model within remote sensing software ENVI 5.3. The average root mean square (RMS) value was less than 0.5 pixels for each image. Meanwhile, each image was projected to UTM (Zone 53N) with WGS-84 datum, the ground control points were obtained from the same aerial photograph image and Google map, the multi-special data were calibrated with the radiometric calibration tool in ENVI from raw digital number (DN) to surface reflectance values, and then the atmospheric correction was applied using the Fast Line-of-Sight Atmospheric Analysis of Spectral Hypercubes (FLAASH) module.

**Normalized Difference Water Index (NDWI)**

Using the Landsat TM image, the normalized-difference water index (NDWI) is a normalized ratio index between green and NIR bands (Yao et al. 2015), which was first formulated by McFeeters to detect surface waters in wetland environments and measure surface water dimensions (Mcfeeters 1996). While all negative NDWI values were categorized as non-water and all positive values as water by imposing a threshold value of zero for the value of NDWI. The NDWI was calculated as follows:

$$NDWI = \frac{TM2 - TM4}{TM2 + TM4} \quad \ldots(1)$$

Where, *TM2* represents the reflectance in green band of Landsat TM image, *TM4* is the reflectance in NIR band of Landsat TM image. In this paper, *TM2* and *TM4* correspond to the reflectance of *B2* (Green band) and *B4* (NIR band) on GF-2 image, respectively.

**Modified Shadow Water Index (MSWI)**

To discriminate the water body and mountain shadow, the shadow water index (SWI) was firstly proposed by Chen Wenqian (Chen et al. 2015), which successfully eliminated the most shadow information. While to completely separate the shadow and water body, according to the former researcher, the model of MSWI was applied for the extraction of water bodies from GF-2, which is defined in Eq. 2.

$$MSWI = (B_1 - B_4) / B_4 \begin{cases} < N(Shade) \\ \geq N(Waterbody) \end{cases} \quad \ldots(2)$$

Where, $B_1$ and $B_4$ represent the reflectance in the blue band and NIR band on GF-2 image, respectively. $N$ is the experimental threshold of the water body in the study region, which can discriminate between water and non-water and need a lot of experiments and visual comparison.

**Support Vector Machine (SVM)**

SVM is a supervised learning system and is based on recent improvements in statistical learning theory (Cristianini & Shawe 2000). Due to this method with the advantage of minimizer errors and maximiser, the geometric characteristics of edge areas, multi-class support vector machine (SVM) classification for water body extraction and coastline detection has been commonly used by many researchers (Nath et al. 2010, Sarp & Ozcelik 2016, Zhang et al. 2013). However, the research for water extraction on GF-2 image is less, therefore,

Table 1: The major parameters of the GF-2 image.

| Parameter | Resolution panchromatic/resolution multi-spectral camera | |
|---|---|---|
| Spectral range | Panchromatic | 0.45-0.90μm |
| | Multi-spectral | 0.45-0.52μm |
| | | 0.52-0.59μm |
| | | 0.63-0.69μm |
| | | 0.77-0.89μm |
| Spatial resolution | Panchromatic | 0.8 m |
| | Multi-spectral | 4 m |
| Width | | 45 km |
| Revisit period (when sideway) | | 5 days |

in this paper, SVM with kernel function and regularization parameters was used as a quantitative method to extract the water body form the GF-2 image.

### Object-Oriented Method (OOM)

In contrast to pixel-based image classification techniques, object-based image analysis methods provide additional information that can be used to improve the discrimination of land cover classes (Yan et al. 2006), which were discussed by several researchers for water body extraction (Kaplan et al. 2017, He et al. 2016, Yue et al. 2010), especially using object-oriented segmentation and classification methods for automated delineation of lakes (Johansson et al. 2013, Rishikeshan et al. 2018, Selmes et al. 2011). While using Feature Extraction (FE) module remote software ENVI 5.3 in this study area, an object-oriented classification method was utilized to segment the GF-2 image into small objects and to obtain the water body information.

## RESULTS AND DISCUSSION

### Water Maps Analysis

Visually, applying by the four water extraction methods in the study region, the Fig. 2 not only shown the similar patterns of water bodies but also lighted the differences between water and non-water areas. NDWI separates water and non-water objects well at the large scale of surface water region, which can keep the integrity of large river water information with a clear and accurate boundary outline. However, in the region of shadows and artificial building areas, dark shadows and water were often misidentified by water indices of NDWI (Yao et al. 2015), where the accuracy of water information acquiring was low and could not eliminate the effects of shadows. In this paper, a series of experimental thresholds of MSWI between water and non-water areas were firstly tested to generate the water body, then combing MSWI with DEM data to extract water body from the GF-2 image in the study region. It seems that MSWI can effectively distinguish water from non-water surfaces and keep the continuity and integrity for a large water body in some degree, which can eliminate some shallows of building-up land and unused land with lower commission errors. However, the discontinuities outline of the small river still occurs. NDWI and MSWI images classified into the water and non-water information based on threshold value selection, the threshold value of water region for NDWI is greater than zero, whereas threshold value on MSWI is near to -0.5. The extraction results of NDWI and MSWI models are not very good, because they not only can often mistakenly identify shadow as water bodies, but also can completely omit some of the small water regions (small ponds, narrow rivers, and shallow water) from GF-2 images using a lower threshold. SVM, based on the image pixel level and spectral characteristics of remote sensing image,

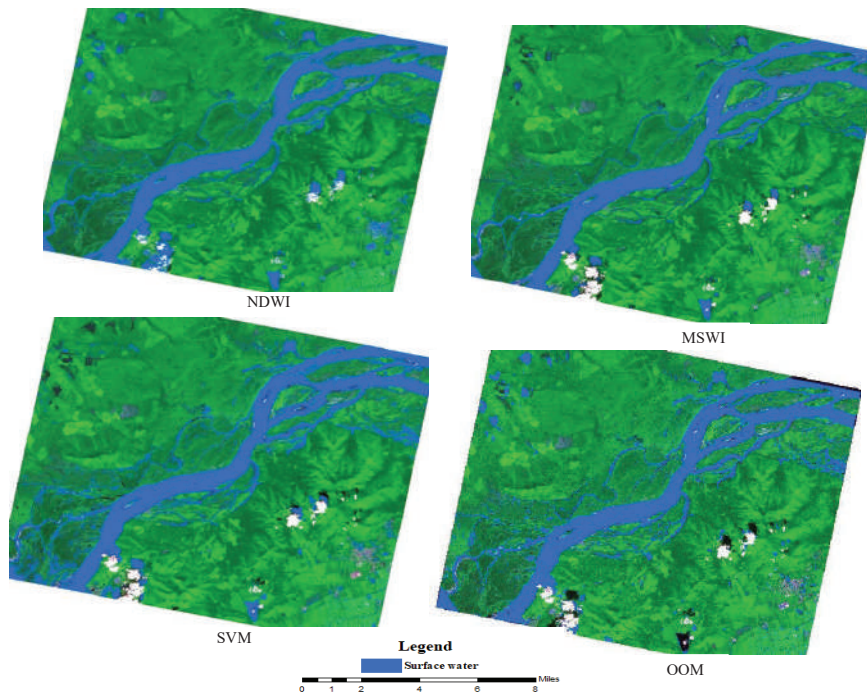


Fig. 2: Results of surface water information extraction for 4 methods from GF-2 image.

is applied to extract the water body by selecting the training samples. Comparing to the NDWI and MSWI, SVM can well and effectively offer a complete water map for study area from the GF-2 by lowering the mixing of water and non-water in small rivers, small ponds, bare land and shallow areas. Besides, it can increase the accuracy of the water body extraction by fewer impacts on shadows and artificial building areas. OOM, using the spectral and spatial texture information during the process of multi-scale segmentation (Sun et al. 2018), keeps the maximum homogeneity between water and non-water information, and exactly identify water body with slightly smoother in water boundary, which avoids the phenomenon of "salt and pepper" and can detect the small ponds and rivers. However, the phenomenon of broken lines for small river still occurred. Furthermore, SVM and OOM methods can extract small ponds and small waters with complete shapes from GF-2 data, whereas NDWI and MSWI can mostly omit them.

**No-water Information Analysis**

In this paper, the unused land (mining wasteland), building-up land and shadow area were selected as the typical samples to analyse the impact on water body extraction methods. A total of 200 pure pixels were selected from the GF-2 imagery for each type, which are shown in Fig. 3. As far as the unused land is concerned, the commission errors of NDWI were most serious, in which some land was almost mistakenly classified by water body, whereas a part of unused land was misclassified as surface water by MSWI. In contrast, the performance of SVM and OOM is better than that of NDWI and MSWI. In fact, the influence on water body extraction accuracy of NDWI and MSWI, a suitable threshold value selection is applied. In order to modify the classification errors in water extraction, in next step, the best way for NDWI and MSWI is to select the optimum threshold values. The Fig. 3 showed that nearly all the regions of built-up land were mistakenly identified as water bodies with the worst commission errors by using NDWI, followed by MSWI. It is possible to describe built-up areas as surface water due to the similar positive index values, while SVM and OOM are superior to that of NDWI and MSWI. It seems that SVM and OOM can effectively suppress the built-up land noises which were easily misidentified by NDWI and MSWI, and OOM showed the best results for the artificial construction, whereas a very small number of building shadows were wrongly identified as water bodies. From various water body extraction models in this study, the shadow areas are wrongly classified into water information at different levels. Compared with all the methods, the NDWI had mistaken all the shadow regions into water bodies and showed the worst water extraction accuracy, followed by MSWI. On the contrary, the OOM showed the highest accuracy by mistakenly classifying shadows into surface water on shadow regions, the presence of shadows in the images may cause misclassification due to similar spectral reflectance patterns as water body areas (Sarp & Ozcelik 2016), while it indicated that the OOM was more vulnerable to shadow pixels than the other method in some way.

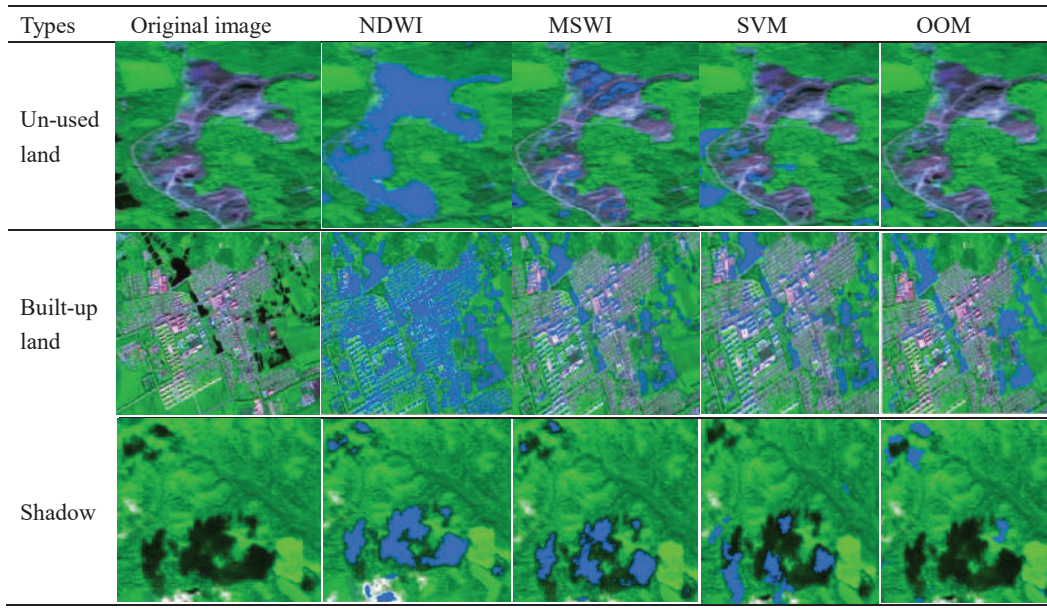


Fig. 3: Detail contrast of water extraction results from no-water objects.

### Water Extraction Accuracy

To test the accuracy of the water extraction in different models, we used images with the Gram-Schmidt spectral sharpening method to obtain the higher resolution image of 0.8 m. According to the scope of the research region within Chinese territory, combing the field survey data of water and non-water with GPS information (Garmin) of the study area, we examined 60 selected check-points (Fig. 4). Meanwhile, the water extraction information was applied to the ArcGIS 10.3 as the background data, we imported the field data into the ArcGIS software as the ground truth in shape format, based on the confusion matrix method, four accuracy measures are applied to evaluate the performance of water indices including overall accuracy and kappa coefficient. Compared to the results of different water extraction methods, the accuracy evaluations of the GF-2'S results are listed in Table 2.

The Table 2 shows that the accuracy assessment of water extraction methods, in which the SVM gave the highest overall accuracy of 94.68 % and with Kappa coefficient at 0.87, followed by OOM, with overall accuracy and Kappa coefficient of 93.57% and 0.85, respectively, while the NDWI showed the worst overall accuracy at 89.35%, with Kappa coefficient of 0.78. In addition, the SVM showed the best performance with the highest accuracy in water extraction, followed by the OOM, which have the 1.11% and 0.02 higher than those of the OOM for overall accuracy and Kappa coefficient, respectively. Meanwhile, the third highest accuracy was the MSWI at 92.56% of overall accuracy and at 0.82 of the Kappa coefficient.

The properties of surface water vary with seasonal and even daily changes, due to the angle of the sun, radiation hours and atmospheric composition impacts (Feyisa et al. 2014, Yang et al. 2015a, 2015b). Compared with other water extraction methods in this test site,the NDWI can quickly extract water body information form the GF-2 image , wherea performed the worst surface water extraction accuracy at 89.35%. In addition, the surface water total errors of omission and commission were lowest at 12.45% and 25.64%, respectively (Table 3). Especially in the region of building areas, shadows and unused land were wrongly identified as surface water. According to the previous research (Ji et al. 2015, Xiong et al. 2018, Masocha et al. 2018), it seems that NDWI was suitable for simple water body extraction in multi-spectral 30m resolution image of Landsat TM and

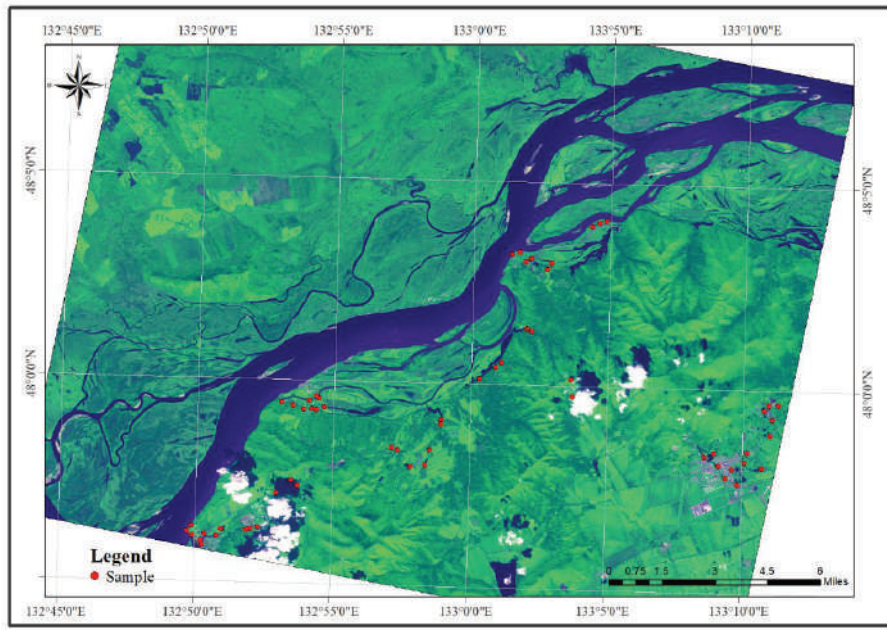


Fig. 4: Distribution map of survey sample in the study region.

Table 2: Accuracy comparison of five classification methods.

| Methods | NDWI | MSWI | SVM | OOM |
|---|---|---|---|---|
| overall accuracy /% | 89.35 | 92.56 | 94.68 | 93.57 |
| Kappa coefficient | 0.78 | 0.82 | 0.87 | 0.85 |

Table 3: Water extraction accuracy assessment for the study region E: errors (C, commission; O, omission).

| Number | Land surface water information extraction methods | Ec | Eo |
|---|---|---|---|
| 1 | NDWI | 25.64% | 12.45% |
| 2 | MSWI | 12.87% | 6.38% |
| 3 | SVM | 6.75% | 5.31% |
| 4 | OOM | 6.43% | 6.15% |

moderate-resolution image of MODIS data by band calculations; whereas it could realize the surface water automation extraction under the demands of lower accuracy, we can conclude that NDWI was not recommended to obtain water body in GF-2 images.

The total omission and commission errors of MSWI at 6.38% and 32.87%, respectively, compared to the NDWI, the MSWI not only extracted the small and tiny water bodies with the faster speed but also kept the complete shape of water that conformed to the actual geographical distribution, which can quickly obtain the surface water from remote sensing data and is suitable for hydrological emergency monitoring. However, this algorithm cannot distinguish between shadow pixels and water pixel in some regions. Also, the water extraction accuracy mainly relies on the experimental threshold value selection which is influenced by the subjective judgment of the researcher. Demands for lower accuracy of water monitoring and water emergency like flood risks, we propose this method for extracting surface water.

SVM, with the total omission and commission errors of 5.31% and 6.75%, respectively, can improve the water extraction accuracy and speed from GF-2 images, we propose this method as the best way to identify water bodies and effectively detect surface water in the study region. Great influence on water extraction speed of this model is related to the number of sample selections, while some region associated with classifying mixed pixels of shadow occurred the small omission errors.

The total omission and commission errors of OOM were similar to that of SVM, the water extraction results of OOM also could supply the demands for the department of water administration in detecting surface water. However, during the water extraction procession from high-resolution remote sensing image, applying the segmentation level and the merging level was mostly evaluated by the experimental threshold, comparing with SVM, which is greatly affected by manual interventions and cost more time with lower inefficiency. Therefore, it was not available for water body extraction and detecting surface water in the emergency. Although applying the Chinese high-resolution images to study water body extraction was relatively less, in the future, we would make full use of the spatial, spectral and texture attributes of GF-2 multi-spectral high-resolution and apply new algorithm to extract water body, especially focused on the panchromatic image.

## CONCLUSIONS

In this paper, the boundary river of Ussuri River of Tongjiang section between China and Russia was taken as the research region. Using GF-2 multi-spectral high-resolution remote sensing imagery of China government, we conducted the study by applying four methods for surface water extraction. Our results showed that all the models can extract large water body information to some degree, the results of NDWI models are not very good because some small water bodies could not be effectively extracted from GF-2 images. On the countrary, the performances of surface water extraction of study region indicate that the methods of SVM and OOM are suitable for detecting and updating surface water bodies from GF-2 images when compared to the other indices.We can conclude that NDWI methods are suitable for surface water extraction from Landsat TM or MODIS images.

Compared with classification results of a water body, SVM algorithms can extract surface water information more accurately than the other methods, which gives the highest overall accuracy of 94.68 % and with Kappa coefficient at 0.87, followed by OOM. While the NDWI can quickly extract water body information form the GF-2 image, which owes the highest omission and commission errors of 12.45% and 55.64%, respectively, followed by MSWI. Therefore, we proposed the SVM method as the best way to identify the water body and to effectively detect surface water in the study region. Further study is needed in GF-2 image for water information extraction in the future, we would make full use of the spatial, spectral and texture attributes of GF-2 multi-spectral high-resolution and apply new algorithm to extract water bodies, especially focused on the panchromatic image.

## ACKNOWLEDGEMENT

We appreciate the staff of the platform for Wuzhishan Ecological Station, 3S laboratory of Hainan University and Key Laboratory of Germplasm Resources of Tropical Special Ornamental Plants of Hainan Province and Haikou Urban Forestry Engineering Techn ology Development and Research

Center. We We thank International English teacher Steve Harding for his assistance in language editing. We also want to express our respect and thanks to the anonymous reviewers and the editors for their helpful comments in improving the quality of this paper. This research was supported by National High Technology Research and Development Program 863 (Grant No.2012AA102001), Natural Science Foundation of Hainan University (Grant No. KYQD (ZR) 20058 and 1863), and Natural Scientific Foundation of Heilongjiang Province (Grant No. D201410).

## REFERENCES

Acharya, T., Subedi, A. and Lee. D. 2018. Evaluation of water indices for surface water extraction in a Landsat 8 Scene of Nepal. Sensors, 18: 2580; doi:10.3390/s18082580.

Alamgir, A., Khan, M.A., Manino, I., Shaukat, S.S. and Shahab, S. 2016. Vulnerability to climate change of surface water resources of coastal areas of Sindh, Pakistan. Desalin. Water. Treat., 57: 18668-18678.

Alanazi, H.A. and Ghrefat, H.A. 2013. Spectral analysis of multispectral Landsat7ETM+ and ASTER data for mapping land cover at Qurayah Sabkha, Northern Saudi Arabia. J. Indian. Soc. Remote Sens., 41(4): 833-844.

Alesheikh, A.A., Ghorbanali, A. and Nouri, N. 2007. Coastline change detection using remote sensing. Int. J. Environ. Sci. Technol., 4: 61-66.

Araral, E. and Wu, X. 2016. Comparing water resources management in China and India policy design: institutional structure and governance. Water Policy, 18: 1-13.

Borton, I.J. 1989. Monitoring floods with AVHRR. Remote Sens. Environ., 30(1): 89-94.

Chen, W.Q., Ding, J.L., Li, Y.H. and Niu, Z.Y. 2015. Extraction of water information based on China-made GF-1 remote sense image. Resources Science, 37(6): 1166-1172.

Cristianini, N. and Shawe, T.J. 2000. An Introduction To Support Vector Machines and Other Kernel Based Learning Methods. Cambridge University Press. http://dx.doi.org/10.1017/CBO9780511801389.

Du, Z.Y. and Zhou, C.H. 1998. Automatically water extraction remote sensing information for water bodies. Journal of Remote Sensing, 4: 264-269.

Feyisa, G.L., Meilby, H., Fensholt, R. and Proud, S. R. 2014. Automated water extraction index: a new technique for surface water mapping using Landsat imagery. Remote Sens. Environ., 140: 23-35.

Frey, H., Huggel, C., Paul, F. and Haeberli, W. 2010. Automated detection of glacier lakes based on remote sensing in view of assessing associated hazard potentials. Grazer Schriften der Geographie und Raumforschung, 45: 261-272.

He, Y.R., Zhang, X.X. and Hua, L.Z. 2016. Object-based distinction between building shadow and water in high resolution imagery using fuzzy-rule classification and artificial bee colony optimization. J. Sens., https://doi.org/10.1155/2016/2385039.

He, Z.Y., Zhang, X.C., Huang, Z.C. and Jiang, H.X. 2004. A water extraction technique based on high-spatial resolution remote sensing images. J. Zhejiang. Univ. (Sci. Edu.), 31(6): 701-707.

Huang, H.B., Zhao, P., Chen, Z.Y. and Guo. W. 2008. Research on the method of extracting water body information from ASTER Remote Sensing image. Remote Sensing Technology and Application, 23(5): 525-528.

Ji, L., Geng, X., Sun, K., Zhao, Y. and Peng, C. 2015. Target detection method for water mapping using Landsat 8 OLI/TIRS imagery. Water, 7: 794-817.

Ji, L., Zhang, L. and Mylie, B. 2009. Analysis of dynamic thresholds for the normalized difference water index. Photogramm. Eng. Rem. S., 75(11): 1307-1317.

Johansson, A.M. and Brown, I.A. 2013. Adaptive classification of supra-glacial lakes on the West Greenland Ice Sheet. IEEE J. Sel. Top. Appl. Earth Obs. Remote Sens., 6: 1998-2007.

Kaplan, G. and Avdan, U. 2017. Object-based water body extraction model using Sentinel-2 satellite imagery. Eur. J. Remote Sens., 50(1):143-150.

Khandelwal, A., Karpatne, A., Marlier, M.E., Kim, J., Lettenmaier, D.P. and Kumar, V. 2017. An approach for global monitoring of surface water extent variations in reservoirs using MODIS data. Remote Sens. Environ., http://dx.doi.org/10.1016/j.rse.2017.05.039.

Lee, J.K., Acharya, T.D. and Lee, D.H. 2018. Exploring land cover classification accuracy of Landsat 8 image using spectral index layer stacking in hilly region of South Korea. Sens. Mater., 30: 1-15.

Li, Y.H., Ding, J.L. and Yan, R.H. 2015. Extraction of small river information based on China-made GF-1 remote sense images. Resources Science, 37(2): 408-416.

Liu, S.T., Wang, M.X., Yang, S.W., Yan, M.Z. and Yang, L.H. 2019. Extraction accuracy and stability analysis of different water body index models in GF-2 images. Bulletin of Surveying and Mapping, 8: 135-139.

Lu, S.L., Wu, B.F., Yan, N.N. and Wang, H. 2011. Water body mapping method with HJ-1A/B satellite imagery. Int. J. App. Earth Obs., 13: 428-434.

Masocha, M., Dube, T., Makore, M., Shekede, M.D. and Funani, J. 2018. Surface water bodies mapping in Zimbabwe using Landsat 8 OLI multispectral imagery: A comparison of multiple water indices. Physics and Chemistry of the Earth, Parts A/B/C, 106: 63-67.

Mcfeeters, S. K. 1996. The use of normalized difference water index (NDWI) in the delineation of open water features. Int. J. Remote Sens., 17(7): 1425-1432.

Melesse, A.M., Weng, Q., Thenkabail, P.S. and Senay, G.B. 2007. Remote sensing sensors and applications in environmental resources mapping and modelling. Sensors, 7: 3209-3241.

Nath, R.K. and Deb, S.K. 2010.Water-body area extraction from high resolution satellite images-an introduction, review, and comparison. Int. J. Image Process., 3: 353-372.

National Research Council, 2008. Integrating Multiscale Observations of U.S. Waters. The National Academies Press, Washington, DC, USA.

Ovakoglou, G., Alexandridis, T.K., Crisman, T.L., Skoulikaris, C. and Vergos, G.S. 2016. Use of MODIS satellite images for detailed lake morphometry: application to basins with large water level fluctuations. Int. J. Appl. Earth Obs., 51: 37-46.

Peng, B.F., Chen, Z.F., Li, J.H., Luo, W.J., Gan, J. and Zeng, R.L. 2018. Monitoring water quality of Dongting Lake region based on GF-1 image. Geographical Research. DOI: 10.11821/dlyj201809002

Rishikeshan, C.A. and Ramesh, H. 2018. An automated mathematical morphology driven algorithm for water body extraction from remotely sensed images. Isprs. J. Photogramm., 146: 11-21.

Sarp, G. and Ozcelik, M. 2016. Water body extraction and change detection using time series: A case study of Lake Burdur, Turkey. Journal of Taibah University for Science, 11: 381-391.

Sawaya, K.E., Olmanson, L.G., Heinert, N. J., Brezonik, P.L. and Bauer, M.E. 2003. Extending satellite remote sensing to local scales: land and water resource monitoring using high-resolution imagery. Remote Sensing of Environment, 88(1-2): 144-156.

Selmes, N., Murray, T. and James, T.D. 2011. Fast draining lakes on the green land ice sheet linked to routing of surface water. Geophys. Res. Lett. 38. https://doi.org/10.1029/2011GL047872.

Senay, G.B., Friedrichs, M.K., Singh, R.K. and Velpuri, N.M. 2016. Evaluating Landsat 8 evapotranspiration for water use mapping in the Colorado River Basin. Remote Sens. Environ.,185: 171-185.

Song, Y.B., Jin, Y.T. and Lang, F. 2015. Water extraction based on multispectral data of GF-1 satellite. Journal of North China Institute of Aerospace Engineering, 25(1): 16-19.

Sun, F., Sun, W., Chen, J. and Gong, P. 2012. Comparison and improvement of methods for identifying waterbodies in remotely sensed imagery. Int. J. Remote Sens., 33: 6854-6875.

Sun, Na., Zhu, W.N. and Cheng, Q. 2018. GF-1 and Landsat observed a 40-year wetland spatiotemporal variation and its coupled environmental factors in Yangtze river estuary. Estuar. Coast. Shelf. S., 207: 30-39.

Tatar, N., Saadatseresht, M., Arefi, H. and Hadavand. A. 2018. A robust object-based shadow detection method for cloud-free high resolution satellite images over urban areas and water bodies. Advances in Space Research, 61(11): 2787-2800.

Vorosmarty, C.J., Green, P., Salisbury, J. and Lammers, R.B. 2000. Global water resources: Vulnerability from climate change and population growth. Science, 289: 284-288.

Wang, Q.Y., Chen, R.X., Xu, J. and Chen, X.L. 2012. Research on methods for extracting water body information from HJ-1A/B Data. Science Technology and Engineering, 12(13): 3051-3056.

Wang, X.B., Xie, S.P., Zhang, X.L., Chen, C., Guo, H., Du, J.K. and Duan, Z. 2018. A robust multi-band water index (MBWI) for automated extraction of surface water from Landsat 8 OLI imagery. Int. J. Appl. Earth Obs., 68: 73-91.

Wasowski, J., Lamanna, C., Gigante, G. and Casarano, D. 2012. High resolution satellite imagery analysis for inferring surface–subsurface water relationships in unstable slopes. Remote Sensing of Environment, 124: 135-148.

Xiong, L.H., Deng, R., Li, J., Liu, X.L., Qin, Y., Liang, Y.H. and Liu, Y.F. 2018. Subpixel surface water extraction (SSWE) using Landsat 8 OLI Data. Water, 10. doi:10.3390/w100506531.

Yang, K., Li, M.C., Liu, Y.X., Cheng, L., Huang, Q.H. and Chen, Y.M. 2015a. River detection in remotely sensed imagery using Gabor filtering and path opening. Remote Sens., 7: 8779-8802.

Yan, G., Mas, J., Maathuis, B.H.P., Zhang, X.M. and Van, D.P. 2006. Comparison of pixel-based and object oriented image classification approaches-a case study in a coal fire area, Wuda, Inner Mongolia, China. Int. J. Remote Sens., 27(18): 4039-4055.

Yang, S.W., Xue, C.S. and Liu, T. 2010. A method of small water information automatic extraction from TM remote sensing images. Acta Geodaetica et Cartographica Sinica, 39(6): 611-617 (in Chinese).

Yang, Y.H., Liu, Y.X., Zhou, M.X., Zhang, S.Y., Zhan, W.F., Sun, C. and Duan, Y.W. 2015b.Landsat 8 OLI image based terrestrial water extraction from heterogeneous back-grounds using a reflectance homogenization approach. Remote Sens. Environ., 171: 14-32.

Yao, F.F., Wang, C., Dong, D., Luo, J.C., Shen, Z.F. and Yang, K.H. 2015. High-resolution mapping of urban surface water using ZY-3 multi-spectral imagery. Remote Sens., doi: 10.3390/rs70912336.

Yue, Y., Gong, J. and Wang, D. 2010. The extraction of water information based on SPOT5 image using object-oriented method. In: 2010 18th International Conference on Geoinformatics, pp. 1-5, IEEE.

Zhang, F., Tiyip, T., Kung, H., Johnson, V. C., Wang, J. and Nurmemet, I. 2016. Improved water extraction using Landsat TM/ETM images in Ebinur Lake, Xinjiang, China. Remote Sensing Applications: Society and Environment, 4: 109-118.

Zhang, H., Jiang, Q.G. and Xu, J. 2013. Coastline extraction using support vector machine from remote sensing image. Journal of Multimedia, DOI: 10.4304/jmm.8.2.175-182.

Zhou, C.H., Du, Y.Y. and Luo, J.C.1996. A description model based on knowledge for automatically recognizing water from NOAA/AVHRR. Journal of Natural Disaster, 5(3): 100-108.

Zou, C., Yang, X.Z., Dong, Z.Y. and Wang. D. 2019. A fast water information extraction method based on GF-2 remote sensing image. Journal of Graphics, 40(1): 99-104.

Nature Environment and Pollution Technology
An International Quarterly Scientific Journal

p-ISSN: 0972-6268
(Print copies up to 2016)
e-ISSN: 2395-3454

Vol. 19 | No. 4 | pp. 1547-1555 | 2020

Original Research Paper

https://doi.org/10.46488/NEPT.2020.v19i04.021

Open Access Journal

# Comparison of Lead Tolerance and Accumulation Characteristics of Fourteen Herbaceous Plants

**Xiongfei Cai, Xinjie Yu, Li Lei, Bin Xuan, Ji Wang†, Lingyun Zhang and Shijie Zhao**
School of Geographic and Environmental Sciences, Guizhou Normal University, Guiyang, 550025, China
†Corresponding author: Ji Wang: chuliu0610@163.com

**Nat. Env. & Poll. Tech.**
**Website: www.neptjournal.com**

*Received:* 08-12-2019
*Revised:* 02-01-2020
*Accepted:* 28-03-2020

**Key Words:**
Lead tolerance
Accumulation characteristics
Phytoremediation
Herbaceous plants

## ABSTRACT

To compare lead (Pb) tolerance and accumulation characteristics, 14 herbaceous plants were treated with different concentrations of lead (0 mg·kg$^{-1}$, 500 mg·kg$^{-1}$, 1000 mg·kg$^{-1}$, 1500 mg·kg$^{-1}$, 2000 mg·kg$^{-1}$) through an indoor pot experiment. Results indicated that the shoot dry weights (DWs), tolerance index (TI) and root tolerance index (RTI) of 14 herbaceous plants decreased with the increase of lead concentration. After comprehensive evaluation, *Campsis grandiflora*, *Polygonum lapathifolium*, *Lolium perenne*, and *Poa annua* were confirmed as tolerant plants to be cultivated in lead-zinc mining area. Moreover, shoots of the *Rudbeckia hirta* could effectively absorb the lead (I I) with the bioconcentration factor (BCF) of 2.29. The translocation factor (TF) of 6 herbaceous plants were larger than 1.0. They are: *Polygonum lapathifolium* (3.04) > *Medicago sativa* (2.49) > *Rudbeckia hirta* (1.72) > *Talinum paniculatum* (1.44) > *Capsicum annuum* cv. 276 (1.36) > *Trifolium repens* (1.21. Finally, after integration the BCF, TF and repair potential indices, we found that *Rudbeckia hirta* had a good restoration potential and its lead cumulation in the shoot was the highest (2.576 mg per plant) when the concentration was up to 1000 mg·kg$^{-1}$. Therefore, *Rudbeckia hirta* could be identified as a pioneer species of Pb-hyperaccumulator.

## INTRODUCTION

Lead is the most prevalent heavy metal contaminant and a human carcinogen (Ozkan et al. 2005, Guo et al. 2016). Over the past 50 years, approximately 783 thousand tons of lead have been reported to be entering the environment, especially the soil (Cui et al. 2013). Soil lead pollution disrupts the normal function of the ecosystem and poses a huge risk to human health. Cleaning up contaminated soil is a major challenge in environmental engineering.

Despite soil remediation techniques are numerous, most of them require high cost, intensive labour and may cause irreversible soil disturbances (Bhargava et al. 2012). Phytoremediation can provide efficient, cost-effective, and environmentally friendly remediation methods for the decontamination of heavy metal-polluted soils. Therefore, screening hyperaccumulators and tolerant species is a key step in the phytoremediation of soils (Mahdavian et al. 2017). Nowadays scientists found that the hyper-accumulators are mostly small biomass plants, and the most suitable hyper-accumulators are often the dominant plants in contaminated areas (Gao et al. 2014, Qin et al. 2013). Some studies show that the families of Gramineae, Compositae, Leguminosae, Cruciferae, *Cyperus*, and Pteridaceae in metal mining areas are prominent in accumulation and translocation (Nie et al. 2004). *Sesbania drummondii* (Sahi et al. 2002, Sharma et al. 2004), *Hemidesmus indicus* (Chandra et al. 2005), *Arabis paniculata* (Tang et al. 2009), and *Plantago orbignyana* (Bech et al. 2011) have been successfully used for phytoremediation of lead-zinc mines in some areas (Srivastava et al. 2014, Li et al. 2015). However, only a few studies focus on lead tolerant plants in southwestern China. As the distribution of plant resources is regional and temporal, screening out hyperaccumulators of high biomass and strong resistance for phytoremediation become practical.

We have selected 14 plant species in the southwest of China based on previous research to carry out seed germination indoor and experiment on plants' response to lead stress. The objectives of the study included: (1) evaluate and compare the effect of different application rates of lead on the growth; and (2) finding more hyperaccumulators through the evaluation and comparison of lead tolerance and accumulation traits of 14 plant species.

## MATERIALS AND METHODS

### Pot Experiment

Seeds of fourteen plant species were collected from areas surrounding Xiangbao mountain (Lat. 26°11'-27°22'N, Long. 106°07'-107°11'E) in Guiyang city because there is a decades-year-old coal mine. The species sampled were

from 6 families and 14 genera, including *Cynodon dactylon* (L.) Pers., *Lolium perenne* L., *Poa annua* L., *Aster ageratoides* Turcz. var. *laticorymbus* (Vant.) Hand.-Mazz., *Rudbeckia hirta* L., *Cosmos sulphureus* Cav., *Gynura bicolor* L., *Capsicum annuum* cv.276, *Trifolium repens*, *Medicago sativa* L., *Calendula officinalis*, *Bidens pilosa* L., *Polygonum lapathifolium* L. and *Talinum paniculatum* (Jacq.) Gaertn. Seeds were germinated in an incubator at 25±1 . After 7 days, seedlings were planted in individual pots. Soils were taken from the nearby farmland of Guizhou Normal University. Soil properties were as follows, pH: 7.36, organic matter: 31.24 $g \cdot kg^{-1}$, nitrogen (N): 213.52 $mg \cdot kg^{-1}$, phosphorus (P): 4.53$mg \cdot kg^{-1}$ and potassium (K): 4.27 $mg \cdot kg^{-1}$. Fertilization was not necessary during the growth stage. Five seedlings were planted in a 15cm×18cm pot with 1kg of soil, which contains lead (heavy metal) acetate [$Pb(CH_3COO)_2 \cdot 3H_2O$; 0, 500, 1000, 1500 and 2000 $mg \cdot kg^{-1}$]. After 90 days of treatment, plant samples were drawn for observations.

### Chemical Analysis

The plant samples were divided into roots and shoots before rinsed thoroughly with tap water and distilled water to remove adhering soil particles and sewage. Shoot height (the distance between the base of the tallest leaf and the tip of the lamina) and root length were measured. For dry weight determination, the cleaned samples were oven-dried at 105°C for 15 min and 70°C until constant weight. After their weight was recorded, dried plant samples were ground to pass a 1 mm mesh sieve, and wet digested in an $HNO_3/HClO_4$ (5:1) mixture (Wu et al. 2010). The samples were analysed on an atomic absorption spectrophotometer, model ZEEnit 700P. The accuracy of the method was verified by analysing certified reference material (GBW 07604 - Poplar leaves) from the National Centre for Standard Materials (Beijing China).

### Data Processing

One-way analysis of variance (ANOVA) was used to test the effects of the different valuables on the measured factors. Duncan's multiple range test was used to compare means when a significant variation was highlighted by the analysis of variance. SPSS 22.0 software and Origin 9.1 software were used for data processing. Bioconcentration factor (BCF), translocation factor (TF), single index of lead tolerance factor (SILTF) and metal accumulation in the shoot of plants (MASP) were calculated based on the following formulas:

$$BCF = [Metal]shoot/\ [Meter]soil \quad \ldots(1)$$

$$TF = [Metal]shoot\ /\ [Metal]root \quad \ldots(2)$$

$$SILTF=[Determination\ of\ indicators]average/\ [Control\ determination] \quad \ldots(3)$$

$$MASP = [Metal]shoot \times [Biomass]shoot \quad \ldots(4)$$

### Evaluation Methods

A comprehensive evaluation of lead tolerance of plants was conducted with Membership Function Method and Standard Deviation Coefficient (Li et al. 2009, Li et al. 2015). Related formulas can be expressed as follows:

(1) Using membership function to standardize the indicators:

$$\mu(X_{ij}) = (\overline{X}_{ij} - X_{j\min})/(X_{j\max} - X_{j\min}) \quad \ldots(5)$$

where $\mu(X_{ij})$ is the membership function of index j of class i; $\overline{X}_{ij}$ is the average measured value of index j of class i, $X_{j\min}$ and $X_{j\max}$ and denote the minimum and maximum values of index j.

(2) Determination of weight:

$$V_{ij} = \sqrt{\sum_{i=1}^{m}[\mu(X_{ij}) - \mu(\overline{X}_{ij})]^2} \,/\, \mu(\overline{X}_{ij}) \quad \ldots(6)$$

$$W_{ij} = V_{ij} \,/\, \sum_{j=1}^{n} V_{ij} \quad \ldots(7)$$

Where, $V_{ij}$ is the standard deviation coefficient of each index; $W_{ij}$ is the weight coefficient of each index.

(3) The calculation of D, the comprehensive evaluation value:

$$D = \sum_{j=1}^{n}[\mu(X_{ij}) \cdot W_{ij}] \quad \ldots(8)$$

Where, D refers to the comprehensive evaluation value of all indices. It is used to measure the lead tolerance.

## RESULTS

### Tolerance Analysis of Pb

Different shoot dry weights (DWs) under changing lead concentrations are given in Table 1. Under the lead concentration of 500 $mg \cdot kg^{-1}$, DWs of 14 plant species do not change significantly, indicating that the plants were free of this level of poison. The shoot biomass of *Rudbeckia hirta*, *Cosmos sulphureus*, *Gynura bicolor*, *Capsicum annuum* cv.276 and *Bidens pilosa* decreased considerably under 1,000, 1,500 and 2,000 $mg \cdot kg^{-1}$ of lead concentrations. The shoot biomass of *Cynodon dactylon*, *Lolium perenne*, *Poa annua*, *Aster ageratoides* and *Trifolium repens* decreased substantially under 1,500 and 2,000 $mg \cdot kg^{-1}$ of lead concentrations. In contrast, no significant change was observed in the shoot biomass of *Medicago sativa*, *Calendula officinalis*, *Polygonum lapathifolium* and *Talinum paniculatum* under all lead concentrations.

The tolerance index (TI) is the ratio of shoot dry weights of the treatment group to the control group. TI greater than

Table 1: Shoot dry weights under different lead concentrations.

| Species | Shoot dry weight under different lead concentrations ($g \cdot pot^{-1}$) | | | | |
|---|---|---|---|---|---|
| | CK | 500 $mg \cdot kg^{-1}$ | 1000 $mg \cdot kg^{-1}$ | 1500 $mg \cdot kg^{-1}$ | 2000 $mg \cdot kg^{-1}$ |
| *Cynodon dactylon* | $3.23 \pm 0.08^{a}$ | $3.06 \pm 0.25^{a}$ | $3.18 \pm 0.21^{a}$ | $2.17 \pm 0.13^{b}$ | $1.97 \pm 0.27^{b}$ |
| *Lolium perenne* | $2.73 \pm 0.04^{a}$ | $2.97 \pm 0.16^{a}$ | $2.31 \pm 0.25^{a}$ | $1.89 \pm 0.32^{b}$ | $1.39 \pm 0.21^{c}$ |
| *Poa annua* | $1.88 \pm 0.45^{a}$ | $1.82 \pm 0.13^{a}$ | $1.53 \pm 0.12^{a}$ | $0.89 \pm 0.19^{b}$ | $0.67 \pm 0.10^{b}$ |
| *Aster ageratoides* | $2.31 \pm 0.25^{a}$ | $2.07 \pm 0.12^{a}$ | $1.82 \pm 0.13^{b}$ | $0.98 \pm 0.31^{c}$ | - |
| *Rudbeckia hirta* | $3.97 \pm 0.23^{a}$ | $2.19 \pm 0.04^{ab}$ | $1.32 \pm 0.12^{b}$ | $1.61 \pm 0.17^{b}$ | $1.13 \pm 0.18^{c}$ |
| *Cosmos sulphureus* | $2.03 \pm 0.02^{a}$ | $1.86 \pm 0.16^{a}$ | $1.21 \pm 0.06^{b}$ | $1.09 \pm 0.24^{b}$ | $1.31 \pm 0.07^{b}$ |
| *Gynura bicolor* | $1.51 \pm 0.09^{a}$ | $1.36 \pm 0.17^{a}$ | $1.25 \pm 0.03^{ab}$ | $1.1 \pm 0.26^{b}$ | $0.96 \pm 0.19^{b}$ |
| *Capsicum annuum cv.276* | $3.02 \pm 0.30^{a}$ | $2.78 \pm 0.35^{a}$ | $2.36 \pm 0.12^{b}$ | $1.73 \pm 0.11^{c}$ | - |
| *Trifolium repens* | $1.98 \pm 0.17^{a}$ | $2.17 \pm 0.36^{a}$ | $1.85 \pm 0.23^{a}$ | $1.3 \pm 0.15^{b}$ | $0.95 \pm 0.18^{c}$ |
| *Medicago sativa.* | $1.77 \pm 0.16^{a}$ | $1.58 \pm 0.17^{a}$ | $1.35 \pm 0.03^{a}$ | $1.27 \pm 0.23^{ab}$ | $1.15 \pm 0.22^{b}$ |
| *Calendula officinalis* | $2.56 \pm 0.24^{a}$ | $2.1 \pm 0.31^{a}$ | $1.83 \pm 0.06^{a}$ | $1.95 \pm 0.28^{a}$ | $1.69 \pm 0.32^{b}$ |
| *Bidens pilosa* | $5.53 \pm 0.39^{a}$ | $5.41 \pm 0.32^{a}$ | $6.33 \pm 0.45^{b}$ | $5.1 \pm 0.27^{a}$ | $4.17 \pm 0.19^{c}$ |
| *Polygonum lapathifolium* | $1.87 \pm 0.03^{a}$ | $1.85 \pm 0.24^{a}$ | $0.99 \pm 0.15^{b}$ | $1.32 \pm 0.09^{ab}$ | $1.27 \pm 0.06^{ab}$ |
| *Talinum paniculatum* | $0.61 \pm 0.04^{a}$ | $0.55 \pm 0.12^{a}$ | $0.6 \pm 0.15^{a}$ | $0.65 \pm 0.11^{a}$ | $0.63 \pm 0.06^{a}$ |

Note: Different letters indicate a significant difference between the different treatments of the same plant (mean±S.D, $p < 0.05$, $n = 5$).

0.5 indicates the plant grows well and has a good tolerance (Wu et al. 2017). The root tolerance index (RTI) is the ratio of the average root length of each treatment group to the control group. Generally, RTI greater than 0.9 indicates that the root growth of the plant is not significantly inhibited (Chehregani et al. 2009). Therefore, TI and RTI can be used as an important index of plant heavy metal tolerance.

According to the TI and RTI values under different lead concentration (Table 2), it is shown that *Cynodon dactylon*, *Lolium perenne*, *Cosmos sulphureus*, *Gynura bicolor*, *Calendula officinalis* and *Polygonum lapathifolium* had good tolerance for lead stress, and their TI and RTI values were greater than 0.5 and 0.9 in all treatments. As the lead concentration increased in the treatment group, both TI and RTI of these 14 plants gradually declined. TI of *Poa annua*, *Rudbeckia hirta* and *Trifolium repens* gradually decreased with the increase of lead concentrations to 0.5. But most of the plants showed significant damage at the lead concentration of 2000 $mg \cdot kg^{-1}$, and the RTI values gradually began to be less than 0.9; furthermore, *Aster ageratoides*, *Capsicum annuum* cv.276 were killed at the lead concentration of 2000 $mg \cdot kg^{-1}$. When evaluated from DW, TI and RTI together, the Polygonum lapathifolium showed a strong tolerance and no obvious signs of damage under all treatments.

## Characteristics of Lead Accumulation

The lead concentration in shoot and root of 14 herbaceous plants were analysed by variance analysis (Fig. 1). The aerial part results demonstrated that most plants were significantly affected by the increase in lead concentrations. However, the lead concentration in shoots of *Rudbeckia hirta*, *Trifolium repens* and *Polygonum lapathifolium* increased and then stabilise before slowly declining. Therefore, the lead concentration in shoots did not maintain growth but slowed down or even declined when it exceeded the tolerance concentration, due to inhibition effects. At the initial concentration, no significant difference was observed on the lead concentration in shoots and roots. As lead concentrations increased, most roots have higher lead concentration than shoots.

Under the treatments of 1000 $mg \cdot kg^{-1}$ and 1500 $mg \cdot kg^{-1}$, no significant change of lead concentration in shoots was observed, except for *Cynodon dactylon*, *Cosmos sulphureus*, *Capsicum annuum* cv.276, and *Medicago sativa*. When the treatment exceeded 500 $mg \cdot kg^{-1}$, *Cynodon dactylon*, *Aster ageratoides*, *Rudbeckia hirta*, *Gynura bicolor*, *Capsicum annuum* cv.276 and *Trifolium repens* would have a substantially higher lead concentration in shoots compared with the control group. When the treatment exceeded 1000 $mg \cdot kg^{-1}$, *Lolium perenne*, *Poa annua*, *Cosmos sulphureus*, *Medicago sativa* and *Calendula officinalis* would have a substantially higher lead concentration in shoots compared with the control group. It is not until the treatment exceeding 1500 $mg \cdot kg^{-1}$ when *Bidens pilosa* and *Polygonum lapathifolium* started to show significantly higher lead concentration in shoots than that in the control. The lead accumulation in shoots of the *Rudbeckia hirta* and *Capsicum annuum* cv.276 passed the critical value of 1000 $mg \cdot kg^{-1}$ when they were treated with 1,000 $mg \cdot kg^{-1}$ of lead concentration. It was noted that the lead concentration in the shoots of *Rudbeckia hirta* had already exceeded the critical value when it was under the

Table 2: Tolerance index and root tolerance index of 14 species of plants under different lead gradient.

| Species | Tolerance index and Root tolerance index | | | | | | | |
|---|---|---|---|---|---|---|---|---|
| | 500/mg·kg$^{-1}$ | | 1000/mg·kg$^{-1}$ | | 1500/mg·kg$^{-1}$ | | 2000/mg·kg$^{-1}$ | |
| | TI | RTI | TI | RTI | TI | RTI | TI | RTI |
| *Cynodon dactylon* | 0.95 | 0.96 | 0.98 | 0.96 | 0.67 | 0.94 | 0.61 | 0.92 |
| *Lolium perenne* | 1.09 | 1 | 0.85 | 0.96 | 0.69 | 0.96 | 0.51 | 0.94 |
| *Poa annua* | 0.97 | 0.97 | 0.81 | 0.97 | 0.47 | 0.92 | 0.36 | 0.92 |
| *Aster ageratoides* | 0.90 | 0.98 | 0.79 | 0.98 | 0.42 | 0.93 | - | - |
| *Rudbeckia hirta* | 0.55 | 1 | 0.33 | 0.96 | 0.41 | 0.93 | 0.28 | 0.89 |
| *Cosmos sulphureus* | 0.92 | 1.02 | 0.60 | 1.05 | 0.54 | 0.96 | 0.65 | 0.91 |
| *Gynura bicolor* | 0.90 | 0.99 | 0.83 | 0.98 | 0.73 | 0.95 | 0.64 | 0.95 |
| *Capsicum annuum cv.276* | 0.92 | 1.02 | 0.78 | 1.04 | 0.57 | 1 | - | - |
| *Trifolium repens* | 1.10 | 1 | 0.93 | 1.02 | 0.66 | 0.93 | 0.48 | 0.86 |
| *Medicago sativa* | 0.89 | 0.93 | 0.76 | 0.98 | 0.72 | 0.95 | 0.65 | 0.88 |
| *Calendula officinalis* | 0.82 | 1 | 0.71 | 0.96 | 0.76 | 0.95 | 0.66 | 0.92 |
| *Bidens pilosa* | 0.98 | 1 | 1.14 | 1.03 | 0.92 | 1 | 0.75 | 0.86 |
| *Polygonum lapathifolium* | 0.99 | 0.99 | 0.53 | 0.99 | 0.71 | 0.99 | 0.68 | 0.97 |
| *Talinum paniculatum* | 0.90 | 1 | 0.98 | 0.94 | 1.07 | 0.91 | 1.03 | 0.85 |

500 mg·kg$^{-1}$ treatment, with the highest average lead concentration of 1783 mg·kg$^{-1}$.

The bioconcentration factor (BCF) and translocation factor (TF) of 14 plants under different concentrations are shown in Fig. 2. The results indicated that *Lolium perenne*, *Aster ageratoides*, *Bidens pilosa* and *Polygonum lapathifolium* showed no significant change in BCF under all treatments. Except for *Cynodon dactylon* and *Capsicum annuum* cv.276, BCF of other plants decreased with the increase of lead treatment. TF of *Poa annua* and *Aster ageratoides* showed no significant difference at all concentrations. However, TF of *Lolium perenne*, *Rudbeckia hirta*, *Cosmos sulphureus*, *Gynura bicolor* and *Trifolium repens* decreased with the increase of lead treatment.

Among 14 plants, only *Rudbeckia hirta*'s BCF was more than 1.0 at both the concentrations of 500 mg·kg$^{-1}$ and 1000 mg·kg$^{-1}$. When the *Capsicum annuum* cv.276 was treated with 1500 mg·kg$^{-1}$ lead concentration, *Medicago sativa* was treated at 1000 mg·kg$^{-1}$, and *Rudbeckia hirta*, *Trifolium repens* and *Talinum paniculatum* were treated at 500 mg·kg$^{-1}$, their TFs were more than 1.0, indicating that lead transport capacity of plants was closely related to their tolerance.

Different capital letters meant a significant difference of translocation factors at 0.05 level among treatments

### Comprehensive Evaluation of Lead Tolerance for 14 Plants

The lead tolerance of 14 plant species was sorted according to the standard deviation coefficient. Six indicators of plant height, root length, shoot and root biomass and lead absorption were considered. Besides, lead tolerance coefficients, subordination and D value of comprehensive evaluation were calculated (Table 3). Based on the results, the comprehensive lead tolerance for 14 plants were as follows: *Trifolium repens* > *Polygonum lapathifolium* > *Lolium perenne* > *Poa annua* > *Aster ageratoides* > *Bidens pilosa* > *Cosmos sulphureus* > *Cynodon dactylon* > *Medicago sativa* > *Gynura bicolor* > *Capsicum annuum* cv. 276 > *Rudbeckia hirta* > *Calendula officinalis* > *Talinum paniculatum*.

Among 14 herbaceous plants, *Rumex acetosa* showed a strong tolerance. Shi et al. (2007) used four indicators, including lead concentration in shoots, lead concentration in roots, RTI and BCF, to evaluate the lead tolerance of 3 gramineous forages. They reached the following conclusion of lead tolerance orders: *Lolium perenne* > *Poa annua* > *Cynodon dactylon*. According to the comprehensive evaluation results, the uptake of lead in the root systems of *Trifolium repens* and *Polygonum lapathifolium* was low at various concentrations. They showed a strong resistance to lead. In contrast, the advantages of *Lolium perenne* and *Poa annua* included higher capacity in lead absorption and adaptation. Therefore, these plants with exclusion and accumulation characteristics could be cultivated together as tolerant plants in the lead-zinc mining area.

## DISCUSSION

Tolerance mechanisms for heavy metals vary in different plants. Even the same species of plants will react in differ-

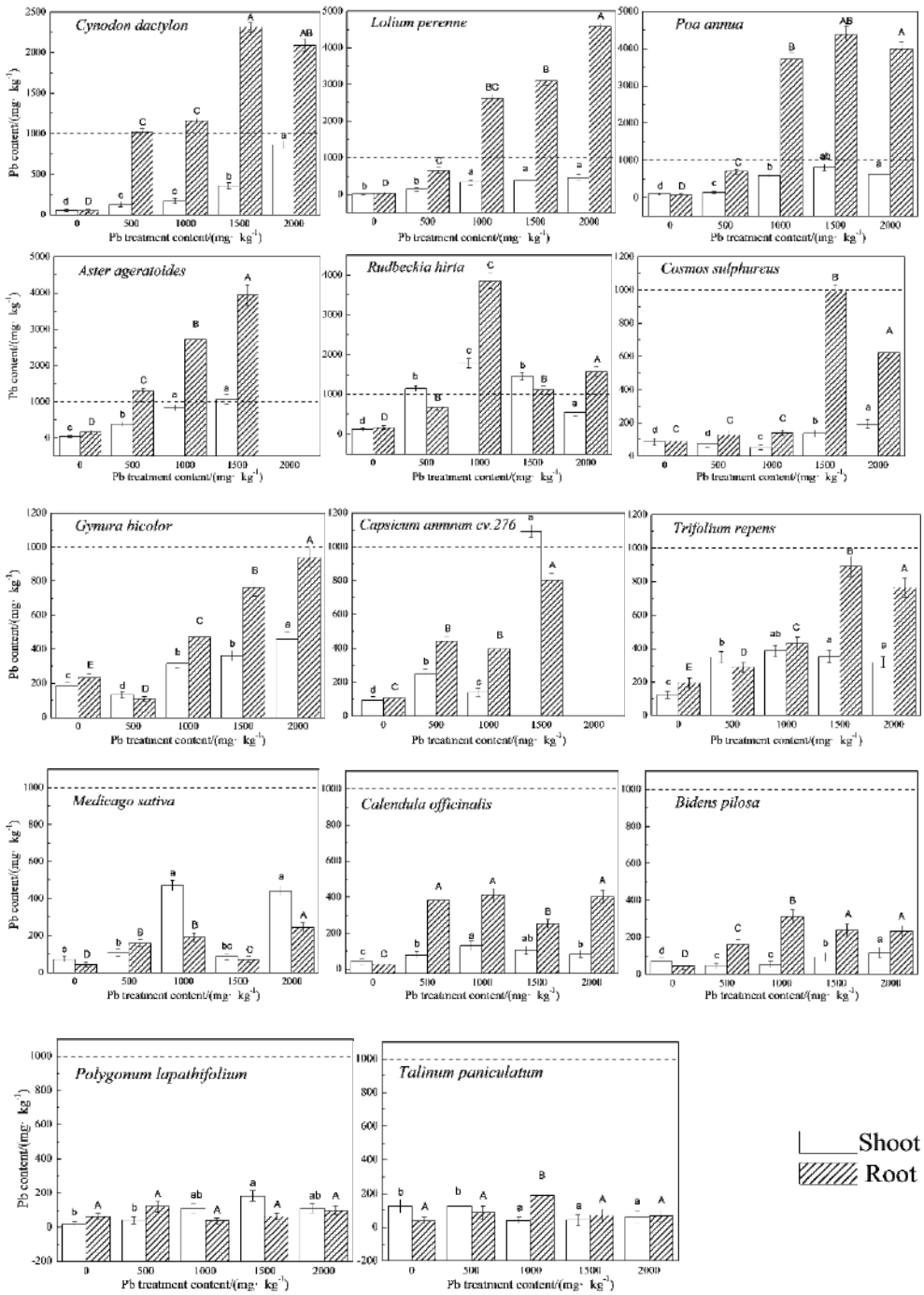


Note: Different small letters meant a significant difference of shoot lead content at 0.05 level among treatments; Different capital letters meant a significant difference of root lead content at 0.05 level among treatment

Fig. 1: Shoot and root lead accumulation under different lead concentrations.

ent ways at different concentrations of heavy metals. The biomass of *Trifolium repens* and *Lolium perenne* increased at 500 mg·kg$^{-1}$ of lead treatment, indicating that low lead concentration could promote growth. Liu et al. (2006) have also found that lead concentrations below 200 mg·kg$^{-1}$ will promote the root growth of cucumber seedlings. It might be caused by organic acids excreted by the plants under the stimulus of heavy metals at low concentrations. Organic

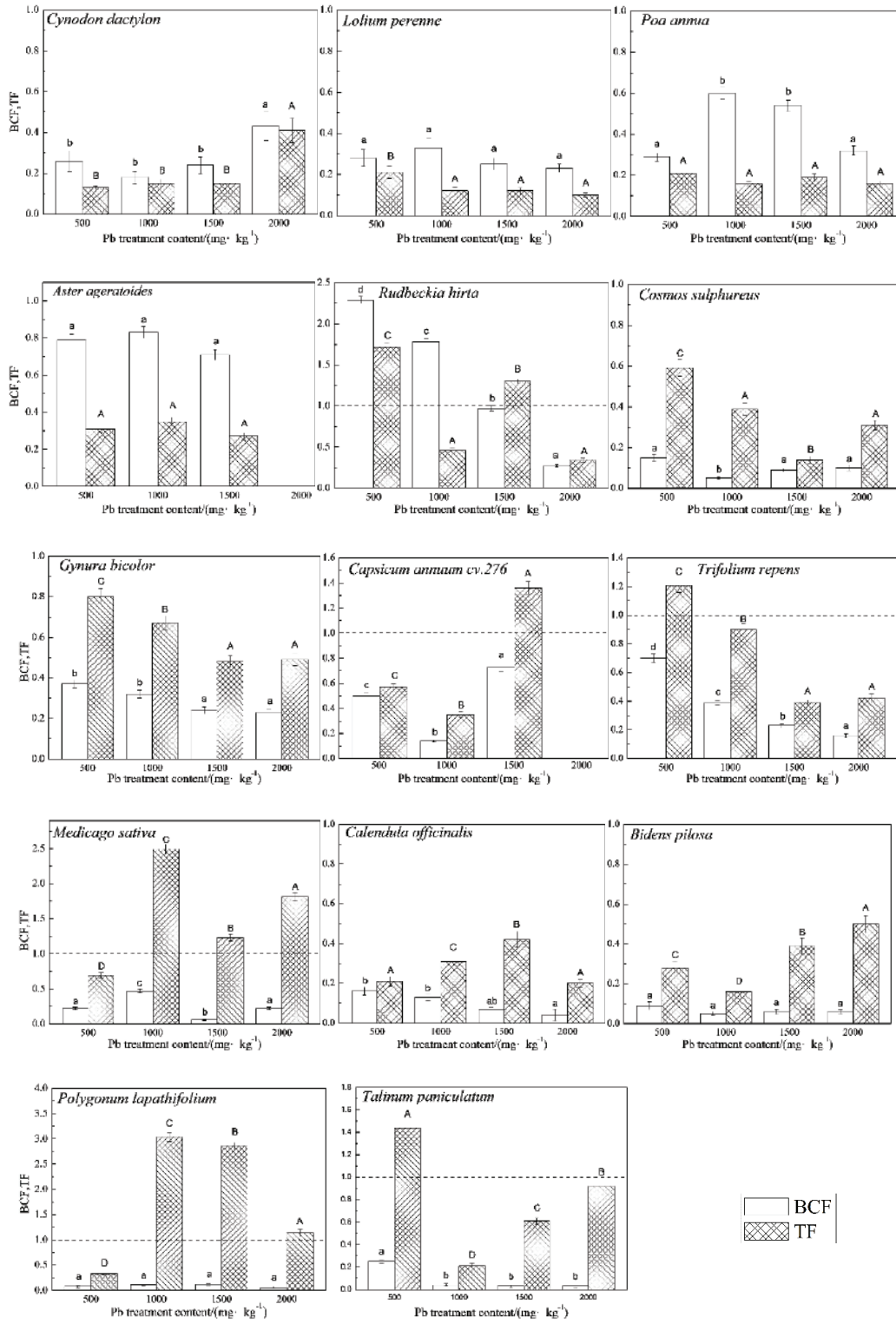


Note: Different small letters meant a significant difference in shoot bioaccumulation factors at 0.05 level among treatments;

Fig. 2: Shoot bioaccumulation and translocation factors under different Pb concentrations.

Table 3: The single lead tolerances coefficient, subordination value and D value of comprehensive evaluation.

| Plants | Resistance to each index lead coefficient | | | | | | Membership function value | | | | | | D values |
|---|---|---|---|---|---|---|---|---|---|---|---|---|---|
| | Plant height | Root length | Shoots biomass | Root biomass | Shoots lead absorption | Root lead absorption | μ(1) | μ(2) | μ(3) | μ(4) | μ(5) | μ(6) | |
| *Cynodon dactylon* | 0.87 | 0.70 | 0.80 | 0.89 | 5.71 | 26.03 | 0.639 | 0.450 | 0.597 | 0.625 | 0.323 | 0.576 | 0.504 |
| *Lolium perenne* | 0.89 | 0.72 | 0.78 | 0.83 | 22.28 | 56.98 | 0.722 | 0.533 | 0.549 | 0.555 | 0.559 | 0.477 | 0.568 |
| *Poa annua* | 0.96 | 0.70 | 0.65 | 0.82 | 3.15 | 37.46 | 0.576 | 0.440 | 0.569 | 0.564 | 0.501 | 0.581 | 0.542 |
| *Aster ageratoides* | 0.85 | 0.70 | 0.76 | 0.97 | 3.26 | 3.21 | 0.574 | 0.560 | 0.442 | 0.582 | 0.411 | 0.486 | 0.486 |
| *Rudbeckia hirta* | 0.96 | 0.70 | 0.79 | 0.86 | 2.50 | 2.63 | 0.480 | 0.628 | 0.574 | 0.587 | 0.694 | 0.457 | 0.569 |
| *Cosmos sulphureus* | 0.86 | 0.70 | 0.39 | 0.54 | 8.48 | 8.99 | 0.625 | 0.600 | 0.322 | 0.331 | 0.535 | 0.355 | 0.450 |
| *Gynura bicolor* | 0.84 | 0.71 | 0.74 | 0.58 | 2.11 | 11.11 | 0.435 | 0.550 | 0.436 | 0.172 | 0.524 | 0.697 | 0.523 |
| *Capsicum annuum* cv.276 | 0.95 | 0.73 | 0.67 | 1.18 | 1.27 | 4.39 | 0.591 | 0.880 | 0.264 | 0.273 | 0.398 | 0.338 | 0.411 |
| *Trifolium repens* | 1.00 | 0.73 | 0.95 | 0.87 | 1.12 | 4.53 | 0.516 | 0.671 | 0.527 | 0.619 | 0.410 | 0.573 | 0.528 |
| *Medicago sativa* | 0.94 | 0.72 | 0.77 | 0.60 | 1.56 | 2.16 | 0.400 | 0.500 | 0.502 | 0.459 | 0.487 | 0.476 | 0.474 |
| *Calendula officinalis* | 0.84 | 0.64 | 0.70 | 0.75 | 12.95 | 12.00 | 0.533 | 0.500 | 0.612 | 0.610 | 0.527 | 0.492 | 0.531 |
| *Bidens pilosa* | 0.85 | 0.74 | 0.73 | 0.90 | 3.52 | 3.18 | 0.364 | 0.600 | 0.534 | 0.585 | 0.495 | 0.661 | 0.557 |
| *Polygonum lapathifolium* | 1.26 | 0.68 | 0.76 | 0.74 | 4.17 | 4.05 | 0.698 | 0.417 | 0.576 | 0.521 | 0.300 | 0.474 | 0.454 |
| *Talinum paniculatum* | 0.85 | 0.68 | 1.00 | 1.24 | 0.63 | 2.33 | 0.584 | 0.600 | 0.580 | 0.356 | 0.462 | 0.343 | 0.444 |
| Weights | | | | | | | 0.10 | 0.08 | 0.08 | 0.12 | 0.30 | 0.32 | |

acids will stimulate the root growth of plants. However, when lead concentration becomes high, the plant biomass begins to decline due to growth inhibition. In this experiment, when the lead concentration of the treatment reached 2000 $mg \cdot kg^{-1}$, the biomass of *Cynodon dactylon*, *Poa annua*, *Trifolium repens*, *Rudbeckia hirta*, *Calendula officinalis*, *Bidens pilosa* and *Gynura bicolor* dropped sharply to 63.68%, 43.70%, 53.54%, 32.22%, 64.34%, 68.87% and 51.97% of the biomass of CK, respectively. Studies show that when the soil contains a high concentration of lead, the uptake of lead in plants will reach saturation. As the lead absorbed by roots is difficult to transport to the shoots due to the root adsorption, passivation or precipitation in cells, the toxicity accumulate and inhibit the absorption of macroelements such as K, Ca, Mg, and trace elements, such as Fe, Cu, Zn. As a result, plants grow slowly or die from the lack of nutrients (Seregin et al. 2008, Akinci et al. 2010, Wang et al. 2010 and Liu et al. 2016).

A hyperaccumulator is a plant capable of growing in soils with very high concentrations of metals, absorbing these metals through their roots, and concentrating extremely high levels of metals in their tissues (Brooks et al. 1997, Sun et al. 2008). According to Baker (1981), there are three indicators to define a Pb-hyperaccumulator: (a) the threshold value of metal accumulated in the shoots of the plant is up to 1000 $mg \cdot kg^{-1}$; (b) both bioconcentration factor (BCF) index, the proportion in the shoot of the plant to the soil, and translocation factor (TF) index, the proportion of metal concentration in shoots to roots, are greater than 1; and (c) the hyperaccumulator should have great tolerance capability; the shoot biomass of a hyperaccumulator should not decrease significantly when the concentration of heavy metals reach the critical value. Among 14 plants tested in this experiment, only *Rudbeckia hirta* meet the three conditions. Current hyperaccumulator plants have disadvantages such as small biomass, slow growth and low translocation capacity of heavy metals. Therefore, the total accumulation of heavy metals at the part of the plant above ground is a key factor

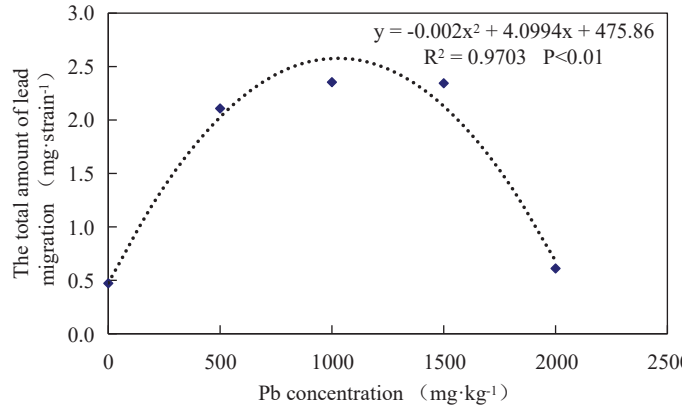


Fig. 3: Total lead concentration accumulated in shoots of *Rudbeckia hirta* versus different treatments.

to evaluate the potential of a hyperaccumulator (Monni et al. 2000, Lasat et al. 1988).

It can be seen from Fig. 3 that the total amount of lead in shoots of the *Rudbeckia hirta* is as per the binomial fitting curve and $R^2 = 0.9703$. According to the fitting curve, there was a sharp increase in the total accumulation of lead in shoots of the *Rudbeckia hirta* and then the percentage gradually went down. In the vicinity of 1000 mg·kg$^{-1}$, the cumulative total reached a saturated state, and after reaching the critical value, the cumulative amount begins to decrease. According to the fitting equation, when the soil lead concentration was 1025 mg·kg$^{-1}$, the lead concentrations in shoots of the *Rudbeckia hirta* was the highest at 2.576 mg·strain$^{-1}$, which was significantly higher than that of the control. Wang et al. (2005) have studied the total concentration of lead in *Bidens maximowicziana* Oett. at the same concentration. They found that the total amount of lead in the ground above was 0.3262 mg·strain$^{-1}$. Our experiment result on *Rudbeckia hirta* is 7.8 times than that of *Bidens maximowicziana* Oett, indicating that the tolerance and absorption of *Rudbeckia hirta* are better than that of *Bidens maximowicziana* Oett.

This study first proposes *Rudbeckia hirta* as a pioneer hyperaccumulator. We need to further confirm its function in the restoration of contaminated land and reduction of heavy metals' impacts on human health. Further research needs to be done for better understanding of the tolerance mechanism and restoration ability of *Rudbeckia hirta*.

## CONCLUSIONS

Among fourteen herbaceous plants in this experiment, the lead tolerance ability of *Trifolium repens* was the strongest and *Calendula officinalis* was the worst; the bioconcentration factor of *Rudbeckia hirta* was above 2.29, indicating that it can effectively absorb lead in soil； the translocation factor of the six plants were greater than 1.0, and their transport capacity was: *Polygonum lapathifolium* (3.04) > *Medicago sativa* (2.49) > *Rudbeckia hirta* (1.72) > *Talinum paniculatum* (1.44) > *Capsicum annuum* cv.276 (1.36) > *Trifolium repens* (1.21).

Through the comprehensive evaluation of lead tolerance, *Trifolium repens*, *Polygonum lapathifolium*, *Lolium perenne*, *Poa annua* can be used as a tolerant plant to cultivate in the lead-zinc mining district. *Rudbeckia hirta* satisfies the requirements of the hyperaccumulator plant, which is a pioneer species of Pb-hyperaccumulator plant. According to the repair potential index, *Rudbeckia hirta* has the best remediation potential. When the soil lead concentration was about 1000 mg·kg$^{-1}$, the total amount of lead accumulation in shoots was 2.576 mg·strain$^{-1}$.

## ACKNOWLEDGEMENTS

This work was supported by The Key Project of Science and Technology Foundation, Guizhou Province (Qian Sci. Co. JZ, [2014], NO.2012), Guizhou Provincial Science Technology Support Program, Guizhou Province (Qian Sci. Co.[2017], No.2580), and Technology Foundation, Guizhou Province (Qian Sci. Co., [2019], NO.1231).

## REFERENCES

Akinci, I. E., Akinci, S. and Yilmaz, K. 2010. Response of tomato (Solanum lycopersicum L.) to lead toxicity: Growth, element uptake, chlorophyll and water content. Afr. J. Agric Res., 5: 416-423.

Baker, A. J. M. 1981. Accumulators and excluders-strategies in the response of plants to heavy metals. J. Plant Nutr., 3: 643-654.

Brooks, R. R., Lee, J. and Reeves, R. D. 1997. Detection of nickliferous rocks by analysis of indicator plants. Journal Geochemical Exploration, 7: 49-77.

Bech, J., Duran, P., Roca, N., Poma, W., Sánchez, I., Barceló, J., Boluda, R., Roca-Pérez, L. and Poschenrieder, C. 2011. Shoot accumulation of several trace elements in native plant species from contaminated soil

in the Peruvian Andes. J. Geochem., 113(1): 106-111.
Bhargava, A., Carmona, F.F., Bhargava, M. and Srivastava, S. 2012. Approaches for enhanced phytoextraction of heavy metals. J. Environ. Manage., 105: 103-120.
Chehregani, A., Noori, M. and Yazdi, H. L. 2009. Phytoremediation of heavy-metal-polluted soil: Screening for new accumulator plants in Angouran mine (Iran) and evaluation of removal ability. Ecotox. Environ. Safe., 72(5): 1349-1353.
Cui, S., Zhang, T. G., Zhao, S. L., Li, P., Zhou, Q. X., Zhang, Q. R. and Han, Q. 2013. Evaluation of three ornamental plants for phytoremediation of Pb-contaminated soil. Int. J. Phytoremediat., 15(4): 299-306.
Chandra, S. K., Kamala, C. T., Chary, N. S., Balaram, V. and Garcia, G. 2005. Potential of Hemidesmus indicus for phytoextraction of lead from industrially contaminated soil. Chemosphere, 58: 507-514.
Gao, H. Z., Guo, W. Z. and Bi, J. 2014. Study on lead tolerance and enrichment characteristics of 20 plants. Chinese Agricultural Science Bulletin, 30(19): 19-24 (in Chinese).
Guo, X. H., Zhu, G. L. and Wei, X. Z. 2016. Absorption, enrichment and transport of heavy metal lead in soil by five herbaceous plants. Research of Soil and Water Conservation, 23(1): 183-186 (in Chinese).
Li, Y., Liu, G. B. and Gao, H. W. 2009. Study on comprehensive evaluation of drought resistance of Medicago sativa L. Germplasm at seedling stage. Acta Agrestia Sinica, 17(6): 807-812 (in Chinese).
Li, H. F., Wang, Y., Yuan, Q. H. and Zhao, G. Q. 2015. Effects of lead stress on growth, physiology, and lead ion accumulation and transportation in gramineous forages. Acta Prataculturae Sinica, 24(9): 163-172 (in Chinese).
Liu, S. C., Xiao, L. T. and Liao, B. H. 2006. Relationship between lead stress and growth and endogenous phytohormones of cucumber seedlings. Journal of Agro-Environment Science, 25(3): 592-596 (in Chinese).
Liu, Y. J., Zhu, X. M. and Lin, L. J. 2016. Physiological responses and lead accumulation of the winter weed Capsella bursa-pastoris under lead stress. Journal of Agro-Environment Science, 35(1): 29-36 (in Chinese).
Lasat, M. M. and Fuhrman, M.1988. Phytoextraction of radiocesium-contaminated soil: evaluation of cesium bioaccumulation in the shoots of three plant species. J. Environ. Qual., 27: 160-165.
Monni, S. and Salemaa, M. 2000. Copper resistance of Calluna vulgaris originating from the pollution gradient of a Cu-Ni smelter in southwest Finland. Environ. Pollut., 109: 211-221.
Mahdavian, K., Ghaderian, S. M. and Torkzadeh-Mahani, M. 2017. Accumulation and phytoremediation of Pb, Zn, and Ag by plants growing on Koshk lead-zinc mining area, Iran. Journal of Soil & Sediments, 17: 1310-1320.
Ozkan, M. H., Gurkan, R., Ozkan, A. and Akcay, M. 2005. Determination of manganese and lead in roadside soil samples by FAAS with ultrasound Assisted leaching. J. Anal. Chem., 60(5): 469-474.
Nie, J. H., Liu, X. M. and Wang, Q. R. 2004. Preparation of lead enrichment plant varieties. Chinese Journal of Agricultural Engineering, 20(4): 255-258 (in Chinese).
Qin, L., Zu, Y. Q., Li, Y. and Wang, J. 2013. Heavy metal contents and accumulation characteristic of seven wild plants from the slagheap surrounding of Huize lead-zinc tailings. Journal of Agro-Environment Science, 32(8): 1558-1563 (in Chinese).
Shi, R. J. and Lu, Y. G. 2007. Characteristics of lead uptake by four herbaceous in acid yellow soil. Journal of Soil and Water Conservation, 21(3): 73-76 (in Chinese).
Seregin, I. V. and Kosevnilove, A. D. 2008. Roles of root and shoot tissues in transport and accumulation of cadmium, lead, nickel and strontium. Russ. J. Plant Physiol., 55: 1-22.
Sun, Y. B., Zhou, Q. X. and Diao, C. Y. 2008. Effects of cadmium and arsenic on growth and metal accumulation of Cd-hyperaccumulator (Solanum nigrum L.). Bioresource Technol., 99: 1103-1110.
Sahi, S. V., Bryant, N. L., Sharma, N. C. and Singh, S. R. 2002. Characterization of a lead hyperaccumulator shrub, Sesbania drummondii. Environ. Sci. Technol., 36: 4676-4680.
Sharma, N. C., Gardea-Torresday, J. L. and Parson, S. V. 2004. Chemical speciation of lead in Sesbania drummondii. Environ. Toxicol. Chem., 23: 2068-2073.
Srivastava, J., Kalra, S. J. S. and Naraian, R. 2014. Environmental perspectives of Phragmites australis (Cav.) Trin. Ex. Steudel. Appl. Water Sci., 4: 193-202.
Tang, Y. T., Qiu, R. L., Zeng, X. W., Ying, R. R., Yu, F. M. and Zhou, X. Y. 2009. Lead, zinc cadmium accumulation and growth simulation in Arabis paniculata Franch. Env. Exp. Bot., 66: 126-134.
Li, Y., Zu, Y. Q., Fang, Q. X., Chen, H. Y. and Schvartz, C. 2013. Characteristics of heavy-metal tolerance and growth in two ecotypes of Oxyria sinensis Hemsl. grown on huize lead-zinc mining area in Yunnan Province, China. Commun. Soil Sci. Plan., 44(16): 2428-2442.
Yang, M. Y., Liang, Y. Y., Zeng, D. B., Chen, T., Chen, H., Liu, T. R. and Xing, J. Y. 2014. Effects of lead stress on accumulation capacity and physiological metabolism of ryegrass. Journal of Northwest A&F University (Nat. Sci. Ed.)., 42(12): 97-101.
Wu, C., Liao, B., Wang, S. L., Zhang, J. and Li, J. T. 2010. Pb and Zn accumulation in a Cd-hyperaccumulator (Viola baoshanensis). Int. J. Phytoremediat., 12(6): 574-585.
Wu, B. Y., Shao, B. J., Zhao, H. E., Wang, X. M. and Mei, L. 2017. Cd accumulation and tolerance characteristics of 11 species in Sedum sensu lato. Acta Scientiae Circumstantiae, 37(5): 1947-1956.
Wang, X. L., Chang, Q. S., Hou, X. L., Lei, M. and Ma, Q. X. 2010. Heavy metal enrichment of plants at lead-zinc mines in south China. Ecology and Environmental Sciences, 19(1): 108-112 (in Chinese).
Wang, H. Q., Li, H. and Lu, S. J. 2005. Bidens maximowicziana's absorption and restoration potential to lead in soil. Environmental Science, 26(6): 143-147 (in Chinese).

Nature Environment and Pollution Technology
An International Quarterly Scientific Journal

p-ISSN: 0972-6268
(Print copies up to 2016)
e-ISSN: 2395-3454

Vol. 19 | No. 4 | pp.1557-1565 | 2020

Original Research Paper

https://doi.org/10.46488/NEPT.2020.v19i04.022

Open Access Journal

# Variability and Modelling of Soil Moisture, Salt and Organic Matter Content in a Gravel-Sand Mulched Jujube Orchard

**Wenju Zhao*†, Jiazhen Hu*, Zongli Li** and Jie Sheng***

*College of Energy and Power Engineering, Lanzhou University of Technology, Lanzhou 730050, China

**General Institute for Water Resources and Hydropower Planning and Design, Ministry of Water Resources, Beijing, 100120, China

†Corresponding author: Wenju Zhao; wenjuzhao@126.com

**Nat. Env. & Poll. Tech.**
**Website: www.neptjournal.com**

*Received:* 19-12-2019
*Revised:* 23-01-2020
*Accepted:* 28-03-2020

**Key Words:**
Gravel-sand mulched soil
Soil properties
Agriculture
Jujube orchard

## ABSTRACT

Characterization of the variability of soil moisture, salt content and organic matter content (SOM) is of great significance in agricultural production management and sustainable soil utilization. We present a case study of the variability and modelling with the depth of soil moisture, salt and SOM in a gravel-sand mulched jujube orchard, using Geostatistics and Kriging interpolation. Soil moisture, salt and SOM were measured in 256 samples collected from a gravel-sand mulched jujube orchard in the 0-10, 10-20, 20-30 and 30-50 cm. Soil moisture, salt and SOM were more variable in the surface soil, due to several environmental factors, the coefficients of variation (CV) of soil were lower than 23%, indicating weak to moderate variation. The coefficient of variation of moisture and organic matter decreased with the depth and the salinity increased with the depth. There is a significant correlation between each soil layer, which decreases with the increase of the soil layer. The accuracy of the function model with depth as an independent variable and soil properties as a dependent variable is higher than 0.88. To master the relationship among soil depth, salinity, soil moisture and organic matter content can provide theoretical value for agricultural comprehensive management.

## INTRODUCTION

Soil moisture, salt and organic matter content (SOM) are important components of soil. Soil moisture, salinity and SOM can provide a theoretical basis for soil dynamic change, ecological environment management and soil salinization. Under the background of global change, the problem of soil desertification, salinization and productivity decline caused by scarce precipitation and intense evaporation is increasingly serious. Characterizing soil moistures variability in space and time is critical to managing water resources, and optimize agricultural practices (Mascaro et al. 2019). The spatial distribution of soil salt can reflect the status and degree of soil salinization (Chervan et al. 2019). SOM is an important factor to characterize soil fertility and soil quality (Wright et al. 2005). Therefore, mastering the spatial pattern of soil moisture, salt and SOM is beneficial to the rational utilization of soil resources and the sustainable production of dryland crops (Liu et al. 2006, Ahmed et al. 2010).

Many scholars have studied soil moisture, salt and organic matter (referred to as SOM). Researches on soil moisture and salt mainly focus on the analysis of the spatial distribution (Hao et al. 2015, Yang et al. 2017). The relationship between different vegetation, soil quality or utilization type and soil moisture and salt (Selim et al. 2013, Zhang et al. 2018), and the coupling relationship between moisture and salt (Ding et al. 2015). Some studies on the spatial variation of moisture, salt and nutrients in surface soil have a certain rule, among which the spatial variation of soil salt is affected by structural factors (Gaston et al. 2001, Shen et al. 2015). Wang et al. (2012) collected soil samples to analyse the variation of soil moisture content and salinity with depth. Liu et al. (2011) found that SOM had a significant effect on soil moisture content under natural and air-dried conditions, which was beneficial to soil moisture retention. Moreover, Zhang et al. (2012) found that the spatial distribution of SOM was mainly affected by terrain indices, soil texture and soil genetic types.

The spatial variation of soil properties mainly includes the variation of the horizontal direction and vertical direction, the spatial variability of soil properties in different soils in the vertical direction and its main influencing factors are not the same. The effect and interaction of various processes in the soil profile can produce variable soils (Liu et al. 2014, Harguindeguy et al. 2018). Gravel and sand are commonly used as mulch in the semi-arid loessal regions of northwestern China to conserve the sporadic and limited rainfall for reliable crop production (Feng et al. 2018, Lü et al. 2013). Gravel-sand mulches on soil surfaces can improve soil conditions, conserve moisture, reduce the accumulation of

surface salinity (Zhao et al. 2017b, Wang et al. 2011, Qiu et al. 2014), improve orchard survival and fruit production, solve land use, and improve the environment (Zhao et al. 2016). Soil moisture is used in hydrological models to determine infiltration and runoff rates at the local scale (Al Bitar et al. 2012). SOM is important in nutrient availability and often varies spatially due to its dependence on other soil attributes (Kosmas et al. 2000). In precision agriculture, information on spatial and temporal soil variability is essential to assist farmers in making agronomic decisions for farm management (Aliah Baharom et al. 2015).

However, most scholars focus on the spatial variation of single soil properties. There are few studies on the variability and modelling of soil moisture, salt and organic matter content in a gravel-sand mulched jujube orchard. The objectives of the study were (i) to obtain a more intuitive understanding of salinity, moisture, SOM by 3-D maps by Surfer12.0 and SEM; (ii) to analyse a function model with depth as independent variable and moisture, salinity, SOM as the dependent variable.

## MATERIALS AND METHODS

### Study Area

The study was conducted in a jujube orchard in Jingtai County near the Lanzhou University of Technology experimental station in the middle of the western portion of China's Gansu province on the east side of the Hexi corridor, at the junction of provinces of Gansu, Ningxia, and Inner Mongolia (Fig. 1). Brown desert soil and sierozem are the predominant soils in this area. The climate is intermediate between continental monsoon and non-monsoon regions, with a mean annual temperature of 8.2°C, fluctuating from -27.3 to 36.6°C from the winter to summer seasons. The mean annual precipitation is 185 mm, with a rainy season (accounting for approximately 61.4% of the annual rainfall) from July to September. The mean annual evaporation is 3038 mm, with annual average evaporation to precipitation ratio of 16.

### Test Treatments

A total of 256 soil samples were collected at sampling points established every 4 m along two perpendicular transects of a randomly selected 32×32 m plot in a gravel-sand mulched jujube orchard (Fig. 2). The locations of the sampling points were determined using GPS. Each sample was a thorough mixture of core samples collected from the 0-10, 10-20,20-30, and 30-50 cm layers, named S1, S2, S3, and S4, respectively.

### Research Methods

The electrical conductivity was measured using a conduc-

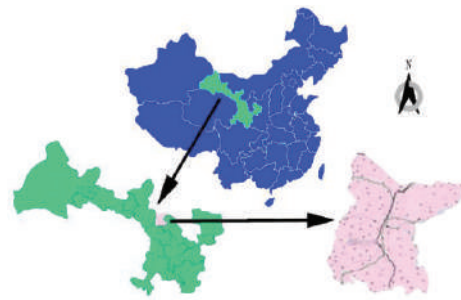

Fig. 1: Study area and the soil sampling locations in the study area situated in Gansu, China.

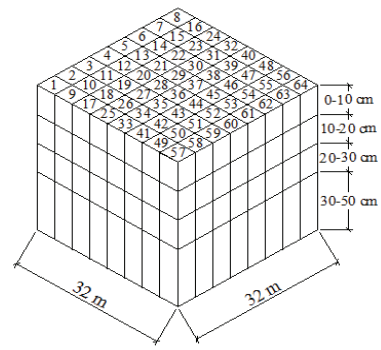


Fig. 2: Distribution of soil sampling points.

tivity meter (FG3-ELK, Mettler, Switzerland). The volume percentages of the particle-size classes were measured by a Mastersizer 2000 (Malvern Instruments, Malvern, England). Particles within the size range of 0.002 to 2.0 mm were categorized into 64 levels of increasing logarithmic intervals. The soil microcosm was analysed by SEM (s-4800, Hitachi, Japan) to obtain a more intuitive understanding of the PSDs. The determination of soil organic matter was carried out by potassium dichromate oxidation-external heating.

### Data Analysis

The relationship between the conductivity and soil salinity was calculated as described by Yao et al. (2006).

$$y = 2.9995x - 0.2269 \quad \ldots(1)$$

Where, $x$ is the conductivity (ms/cm) of the 5:1 moisture: soil solution and $y$ is the salinity (g/kg), with a coefficient of determination ($R^2$) of 0.988. The above formula is applicable to soil samples with no measured ion composition (Wraith 2004).

$$CV = \frac{\sigma}{\bar{\theta}} = \frac{\sqrt{\frac{1}{n-1}\sum_{i=1}^{n}(\theta_i - \bar{\theta})^2}}{\bar{\theta}} \quad \ldots(2)$$

Where, s is the standard deviation, and CV is the coefficient of variation. Then $\theta_i$ is the soil moisture content of the $i$ measuring point, and $\bar{\theta}$ is the average value of the soil moisture content of all the measuring points.

Fractal features can be described by the fractal dimension or fractal dimensionality of particle size. Soil D was calculated as described by (Tyler et al. 1990).

$$\frac{V(r < R_i^{'})}{V_T} = (\frac{R_i^{'}}{R_{\max}})^{3-D} \quad \ldots(3)$$

where r is size; $R_i$ is the mean particle size of two sieved particle sizes, $R_i$ and $R_{i+1}$; $V(r < R_i)$ is the accumulated mass of particles smaller than $R_i$ ; $V_T$ is the mass sum of soils containing all particle sizes; $R_{max}$ is the mean diameter of the largest particles; and 3-D is the slope of the linear regression line with $\log\frac{V(r < R_i^{'})}{V_T}$, and $\log\frac{R_i^{'}}{R_{\max}}$ as the y- and x-axes variables, respectively. D was obtained by the logarithmic transformation of Eq. 3.

Based on the regionalized variables theory and intrinsic hypothesis, the semivariogram, g($h$), was estimated by Pham (2016).

$$\gamma(h) = \frac{1}{2N(h)}\sum_{i=1}^{N(h)}[Z(x_i + h) - Z(x_i)]^2 \quad \ldots(4)$$

Where, $N(h)$ is the number of pairs of observations. $Z(x_i)$ (and) $Z(x_i + h)$ separated by a distance h. Only isotropic semivariograms were considered (Wang et al. 2008).

$$N = (\frac{tS}{xd})^2 \quad \ldots(5)$$

Where, $N$ is the number of sampling points, $t$ is the significance level corresponding to the distribution value ($t$-distribution table obtained by the investigation), $S$ is the sample standard deviation, $x$ is the mean model and $d$ is the estimation accuracy.

Coefficient of determination ($R^2$) between the measured and predicted values was used to evaluate the performance of the regression models.

$$R^2 = \left[\frac{\sum_{i=1}^{n}(o_i - \bar{o})(p_i - \bar{p})}{\left[\sum_{i=1}^{n}(o_i - \bar{o})^2\right]^{0.5}\left[\sum_{i=1}^{n}(p_i - \bar{p})^2\right]^{0.5}}\right]^2 \quad \ldots(6)$$

Where, $O_i$ and $P_i$ are measured and predicted values, respectively, $\bar{o}$ and $\bar{p}$ are the average measured and predicted values, respectively, and $n$ is the number of observations in the validation data set.

## RESULTS AND DISCUSSION

### Analysis of Spatial Variation of Soil Moisture, Salt and SOM Content

A statistical analysis of soil moisture, salt and SOM content is provided in Table 1. With the deepening of soil depth, the CV of different soil properties is different. In this study, coefficients of variation (CV) ≤10% indicate weak spatial variability, 10%<CV<100% indicate moderate variability, and CV ≤100% indicate strong variability (Cambardella 1994). The CV of three soil factors were lower than 23%, indicating weak to moderate spatial variation. There are not only differences in soil moisture, salt and SOM content, but also differences in the degree of variation.

The variation of the soil moisture with the depth depends on the moment in which the soil sampling is done. Because it has rained a few days before, the soil moisture will surely be higher in the upper layers. The CV of moisture ranged from 11.07 to 22.34% and tended to increase with depth (Choi 2007). The significant differences in soil types, land use types, terrain indices may result in the variability of SOM. The CV of organic-matter contents ranged from 5.56 to 11.89% and tended to increase with depth. Average soil salinity increased with depth, the CV of salinity ranged from 8.68 to 18.59% and tended to decrease with depth. This result indicated that the vertical distribution of soil moisture, salt and SOM is not only restricted by soil texture, bulk density and other factors but also affected by environmental factors such as rainfall, evaporative land use type and vegetation (Brye 2010).

### Spatial Distribution and SEM Observations of Soil Moisture, Salt and SOM Content

The author used surfer 12.0 to draw the spatial distribution,

Table 1: A statistical analysis of soil moisture, salt and SOM content

| Depth (cm) | Soil properties | Maximum | Minimum | Mean | SD | Kurt | Skew | CV (%) |
|---|---|---|---|---|---|---|---|---|
| 0-10 | salinity (g/kg) | 1.03 | 0.46 | 0.80 | 0.15 | -0.47 | -0.65 | 18.59 |
| | moisture (g/kg) | 11.60 | 7.60 | 9.81 | 1.09 | -0.98 | -0.31 | 11.07 |
| | organic matter (g/kg) | 5.75 | 4.25 | 4.95 | 0.27 | 0.89 | 0.22 | 5.56 |
| 10-20 | salinity (g/kg) | 1.12 | 0.55 | 0.88 | 0.14 | -0.39 | -0.72 | 15.90 |
| | moisture (g/kg) | 11.20 | 6.80 | 9.17 | 1.26 | -1.10 | -0.28 | 13.71 |
| | organic matter (g/kg) | 4.73 | 3.52 | 4.12 | 0.32 | -0.78 | -0.01 | 7.81 |
| 20-30 | salinity (g/kg) | 1.18 | 0.67 | 0.99 | 0.11 | 1.91 | -1.39 | 10.77 |
| | moisture (g/kg) | 11.00 | 5.20 | 8.06 | 1.53 | -0.91 | -0.12 | 18.98 |
| | organic matter (g/kg) | 3.73 | 2.61 | 3.26 | 0.25 | -0.37 | -0.28 | 7.60 |
| 30-50 | salinity (g/kg) | 1.30 | 0.88 | 1.12 | 0.10 | 0.27 | -0.50 | 8.68 |
| | moisture (g/kg) | 10.80 | 4.10 | 7.22 | 1.61 | -0.40 | 0.01 | 22.34 |
| | organic matter (g/kg) | 3.61 | 2.41 | 2.86 | 0.34 | -0.48 | 0.69 | 11.89 |

Note: SD standard deviation, CV coefficient of variation, Skew skewness, Kurt kurtosis.

before kriging interpolation, the data for soil moisture, salinity and organic matter content soil salinity were transformed to a normal distribution. After interpolation, the measured data of soil can be converted into more data. The Kriging interpolation maps (Fig. 3) showed the horizontal and vertical distribution in each layer. Soil moisture at each layer showed irregularly distribution with peaks, which may be related to the topography in the sampling area, the result was consistent with Xing et al. (2015).

The distribution of salinity is irregular with peaks and valleys. With the increase of depth, the number of peaks decreases and the distribution is more uniform. The distribution of soil salt content in horizontal and vertical planes was highly consistent with those of soil water content (Li et al. 2018). Moisture, salinity and SOM were most variable in the 0-10 cm layer. The decrease in the number of peaks with the depth may have been due to the irrewwgular surface topography in the orchard. The distributions were significantly affected by the terrain, rainfall, evaporation and cultivation, human factors, tended to gradually stabilize with depth (Zhao et al. 2017c).

SEM has helped the intuitive observation of the texture distribution of soil and the change rule of pore space

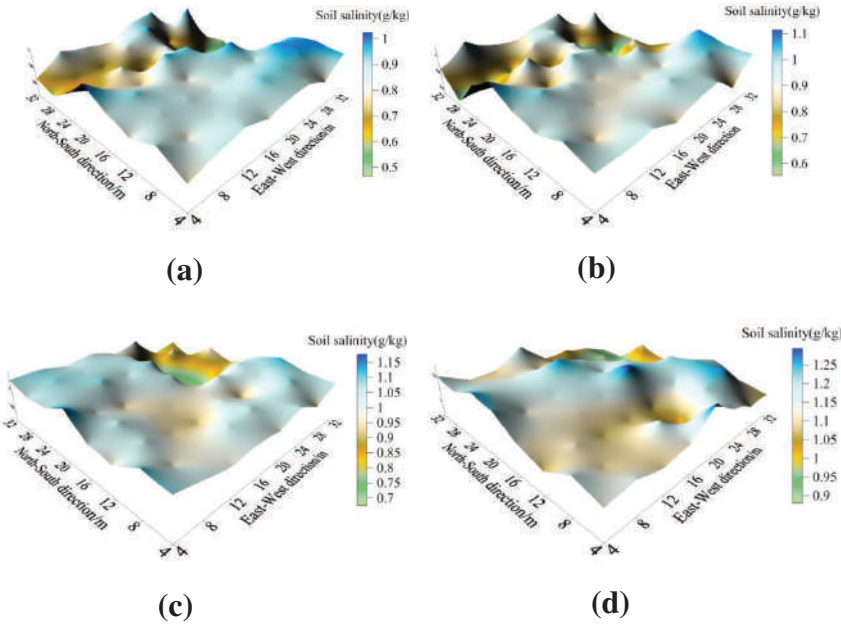

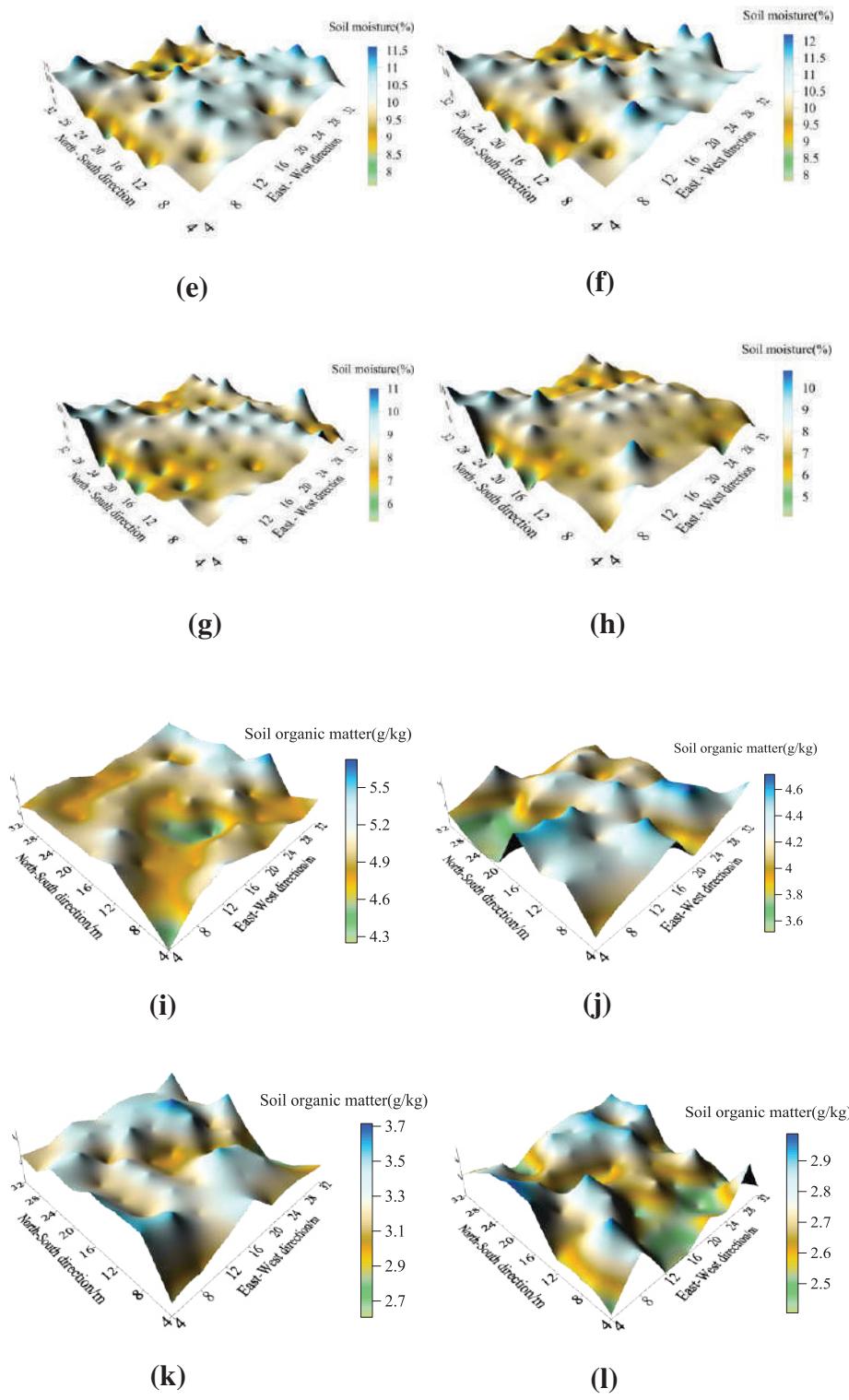


Fig. 3: Spatial distribution of soil salinity, moisture and organic matter content in 0-50 cm layers. (a) salinity: 0-10 cm; (b) salinity: 10-20 cm; (c) salinity: 20-30 cm; (d) salinity: 30-50 cm; (e) moisture: 0-10 cm; (f) moisture: 10-20 cm; (g) moisture: 20-30 cm; (h) moisture: 30-50 cm; (i) organic matter: 0-10 cm; (j) organic matter: 10-20 cm; (k) organic matter: 20-30 cm; (l) organic matter: 30-50 cm.

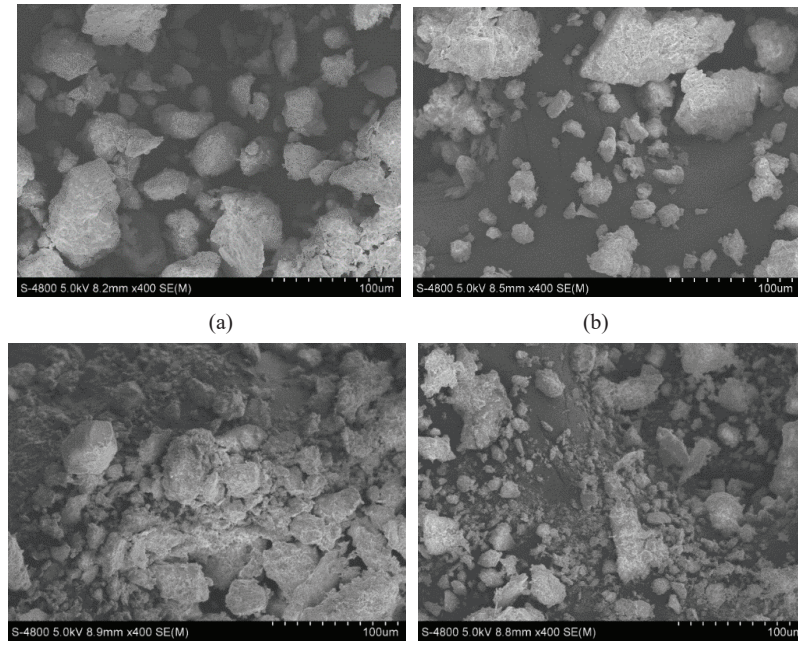


Fig. 4: Scanning electron micrograph of soil particle-size distribution in each layer. (a) S1; (b) S2; (c) S3; (d) S4.

Table 2: The correlation analysis of soil moisture, salt and SOM content in different soil layers.

| | depth/cm | 0-10 | 10-20 | 20-30 | 30-50 |
|---|---|---|---|---|---|
| salinity | 0-10 | 1 | | | |
| | 10-20 | 0.928** | 1 | | |
| | 20-30 | 0.584** | 0.649 | 1 | |
| | 30-50 | 0.307* | 0.299* | 0.568** | 1 |
| moisture | 0-10 | 1 | | | |
| | 10-20 | 0.782** | 1 | | |
| | 20-30 | 0.593** | 0.610** | 1 | |
| | 30-50 | 0.566** | 0.520** | 0.667** | 1 |
| organic matter | 0-10 | 1 | | | |
| | 10-20 | 0.518** | 1 | | |
| | 20-30 | -0.645* | 0.567** | 1 | |
| | 30-50 | -0.412 | 0.504* | 0.639** | 1 |

Note: * Correlation is significant at 0.05 level; ** Correlation is significant at 0.01 level.

(Markgraf et al. 2007). Fig. 4 can be seen that soil texture changes with depth, the texture is uneven at 0-10cm, but uniform within 10-50cm. It can be seen that there are several large particles in S1, mainly due to the gravel-sand mulch on the surface. The gravel-sand mulch had gradually degenerated due to natural or artificial damage, so the interface between the soil and gravel was indistinct, with an uneven texture and large particle size sand in S2. Particle sizes were homogeneous in S3-S4. The development degree of macropores decreases with the increase of soil depth. Therefore, the larger the soil bulk density, the smaller the soil moisture content, the smaller the salt immersion range and the higher the soil salt content.

## Correlation Analysis of Different Soil Properties

To describe the soil moisture, salt and SOM and the correlation with soil layers accurately, analysed by SPSS, the correlation was significant when the absolute value of the correlation coefficient was high. There is a significant

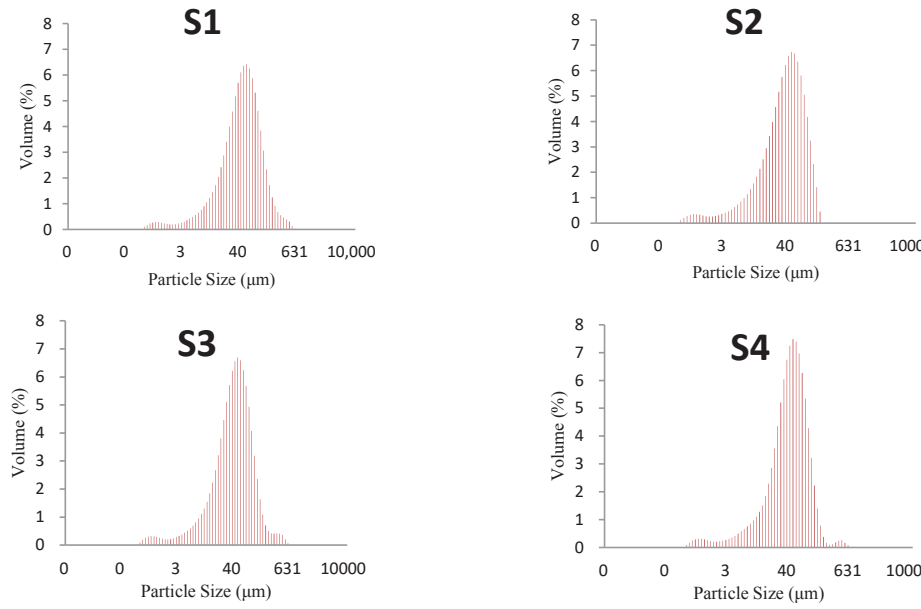


Fig. 5: Frequency distribution of volume content of the soil particles of the various layers.

correlation between the soil layers, and decreased with the increase of soil interval, from the correlation analysis of soil moisture, salt and SOM content in different soil layers (Table 2). The correlation of each soil properties was different, the correlation coefficients were 0.928 to 0.568 for salinity and 0.782 to 0.566 for moisture, respectively, which decreased with depth. The correlation coefficient between the 20-30 cm was the highest, followed by 10-20 cm and 30-50 cm for organic matter.

Moisture, salinity, SOM analysis has improved with remote sensing technology and developed by applying the remote-sensing optical method, which can provide timely, accurate and efficient information for salinization, agricultural production (Finn et al. 2011, Farifteh et al. 2006, Anne et al. 2014). The monitoring accuracy, however, is higher for surface soil than for subsoil. Thus, an effective method that can accurately evaluate and predict the moisture, salinity, SOM of deeper soil from routinely available surface-soil data can be developed in our future work, which would save human and material resources (Zhao et al. 2017b).

The soil particles were classified as clay (0-0.002 mm), silt (0.002-0.05 mm), and sand (0.05-2 mm) (Pieri et al. 2006). The frequency curve of soil particle size distribution can directly reflect the distribution of particle size, and the uniform and smooth curve indicates the uniform volume distribution of particle size fraction. As shown in Fig. 5, the curve distribution of S1 was relatively uniform, and the volume of sand particles is large. The particles in S2 are finer (e.g. < 0.1mm), where the powder has a high volume fraction. Most particles in other layers were mainly distributed between 0.002 and 0.05mm.

Fractal dimension (D) of soil particle size calculated from Eq.1 and Fig. 5 for each layer, D varied between 2.54 and 2.82. From the results of the correlation analysis of each variable in Table 3, there was a significant correlation between the different parameters. The D was negatively correlated with moisture content and positively correlated with organic matter content and salinity. Therefore, D can be used to some extent as a quantitative indicator of the status of soil moisture and salt in the gravel-mulched field

Table 3: Correlations analysis of different soil properties.

| | D | salinity | moisture | organic matter |
|---|---|---|---|---|
| D | 1 | | | |
| salinity | 0.327 | 1 | | |
| moisture | -0.356 | -0.996** | 1 | |
| organic matter | -0.242 | -0.97* | 0.983* | 1 |

Notes: D, fractal dimension; *Correlation is significant at 0.05 level; **Correlation is significant at 0.01 level.

Table 4: Modelling with depth and the measured value of each soil characteristics.

| Soil properties | Equation | $R^2$ |
|---|---|---|
| salinity | $y = 0.745x^{0.008}$ | 0.979 |
| moisture | $y = 10.969-0.117x + 0.001x^2$ | 0.882 |
| organic | $y = 6.25-0.141x + 0.018x^2$ | 0.924 |

Notes: $R^2$ is the coefficient of determination. Units of x, y are %.

(Zhao et al. 2017a). From the soil in Table 3, we find that moisture and salt are highly correlated. This is different from the correlation between soil moisture and salt in the wetland studied by Xu et al. (2013). It may be affected by climate, distance from moisture area and soil type.

### Soil Moisture, Salt, SOM and its Relationship with Soil Depth

Measured values of soil moisture, salinity and organic matter content were changeable in different depths. To find out the values of them more conveniently and efficiently, the author analysed the function model with depth as the independent variable and soil properties as the dependent variable and selected the best model of each soil properties (Table 4). Soil moisture, SOM all fitted to the quadratic equation, the salinity fitted to the exponential equation, and the $R^2$ were all higher than 0.88 in a gravel-sand mulched jujube orchard, which indicated the result of the fitting were precision.

Although moisture, salinity and SOM can be measured by experiments, soil sampling and laboratory analysis are time-consuming, labour intensive and expensive (Corwin et al. 2016). Our current research can directly calculate the values of moisture, salinity and SOM at different depths through the model, and the accuracy is high. Therefore, it can increase agricultural output value and reduce salinization. We plan to study the precision effects of the terrain on moisture and salinity and the effect of SOM where jujube is planted with sand mulching in further.

## CONCLUSION

The soil of a gravel-sand mulched jujube orchard was analysed by Geostatistics and Kriging interpolation. The CV of soil was lower than 23%, indicating weak to moderate spatial variation. The CV of salinity tended to decrease with depth, the CVs of moisture and organic-matter contents increased with depth. Kriging interpolation was performed by Surfer software and three-dimensional spatial distribution map of soil moisture, salt and organic matter content was drawn. The soil microstructure was scanned by SEM. The change of moisture, salinity and SOM in the 0-10cm layer was the largest, and the number of peaks decreases with depth. There is a significant correlation between soil layers, and decreased with the increase of soil interval, from the correlation analysis of moisture, organic matter content, salinity. D was correlated negatively with moisture, organic matter content, and positively with salinity. The author analysed a function model with depth as a variable, the $R^2$ were all higher than 0.88.

This study has contributed to our understanding of the variability of soil moisture, salinity and organic matter content in a gravel-sand mulched jujube orchard. The results can be effectively applied to ecological hydrology to prevent soil salinization and improve agricultural production value.

## ACKNOWLEDGMENTS

This study was supported by the National Natural Science Foundation of China (51869010). Guidance Program for Industrial Support of Colleges and Universities in Gansu Province (2019C-13), the Lanzhou University of Technology Hongliu first-class discipline funding.

## REFERENCES

Ahmed, O., Inoue, M. and Moritani, S. 2010. Effect of saline water irrigation and manure application on the available water content, soil salinity, and growth of wheat. Agr. Water Manage., 97(1): 165-170.

Al Bitar, A., Leroux, D., Kerr, Y. H., Merlin, O., Richaume, P. and Sahoo, A. 2012. Evaluation of SMOS soil moisture products over continental U.S. Using the SCAN/SNOTEL Network. IEEE T. Geosci. Remote., 50(5): 1572-1586.

Aliah Baharom, S. N., Shibusawa, S., Kodaira, M. and Kanda, R. 2015. Multiple-depth mapping of soil properties using a visible and near infrared real-time soil sensor for a paddy field. Engineering in Agriculture, Environment and Food, 8(1): 13-17.

Anne, N.J.P., Abd-Elrahman, A.H., Lewis, D.B. and Hewitt, N.A. 2014. Modelling soil parameters using hyperspectral image reflectance in subtropical coastal wetlands. Int. J. Appl. Earth Obs., 33: 47-56.

Brye, K.R. and Gbur, E.E. 2010. Regional differences in soil carbon and nitrogen storage as affected by land use and soil moisture regime. Soil Sci., 175(7): 339-348.

Cambardella, C.A., Moorman T.B. and Novak J M. 1994. Field-scale variability of soil properties in Central Iowa soils. Soil Sci. Soc. Am. J., 58: 1501-1511.

Chervan, A.M., Ustinova, A.M. and Tsyrybko, V.B. 2019. Spatiotemporal changes of soil salinization in the Soligorsk mining region. Eurasian Soil Sci., 52(8): 998-1006.

Choi, M. and Jacobs, J.M. 2007. Soil moisture variability of root zone profiles within SMEX02 remote sensing footprints. Adv. Water Resour., 30(4): 883-896.

Corwin, D. and Lesch, S.M. 2016. Validation of the ANOCOVA model for regional-scale $EC_a$ to $EC_e$ calibration. Soil Use Manage., 33(2): 178-190.

Ding, M., Watkins, E., Hartl, M. and Daemen, L. 2015. Water signatures and their thermal stability in bedded salt for nuclear waste storage: An incoherent inelastic neutron spectroscopy study. Environ. Sci. Tech. Let., 2(11): 308-313.

Farifteh, J., Farshad, A. and George, R.J. 2006. Assessing salt-affected soils using remote sensing, solute modelling, and geophysics. Geoderma, 130(3-4): 191-206.

Finn, M.P., Lewis, M., Bosch, D.D. and Giraldo, M. 2011. Remote sensing of soil moisture using airborne hyperspectral data. GISci. Remote. Sens., 48(4): 522-540.

Feng, H., Chen, J., Zheng, X., Xue, J., Miao, C., Du, Q. and Xu, Y. 2018. Effect of sand mulches of different particle sizes on soil evaporation during the freeze-thaw period. Water, 10(150). https://doi.org/10.3390/w10050536.

Gaston, L., Locke, M. and Zablotowicz, R. 2001. Spatial variability of soil properties and weed populations in the Mississippi Delta. Soil Sci. Soc. Am. J., 65(2): 449-459.

Hao, Y.Y., Xu, X., Ren, D.Y. and Huang, Q.Z. 2015. Distributed modelling of soil water-salt dynamics and crop yields based on HYDRUS-EPIC model in Hetao Irrigation District. Trans. Chin. Soc. Agric. Eng., 31(11): 110-116.

Harguindeguy, Stéphanie, Pierre C. and Martine P.G. 2018. Colloidal mobilization from soil and transport of uranium in (sub)-surface waters. Environ. Sci. Pollute. R., 26(2): 5294-5304.

Kosmas, C., Gerontidis, S. and Marathianou, M. 2000. The effect of land use change on soils and vegetation over various lithological formations on Lesvos (Greece). Catena, 40(1): 51-68.

Li, Y. and Liu, X.Z. 2018. Distribution of soil water, salt and water drop penetration time (WDPT) under two-point-source trickle irrigation with sewage water. Nature Environment & Pollution Technology, 17(3): 679-690.

Liu, J.L., Ma, X.Y. and Zhang, Z.H. 2014. Temporal stability of soil moisture in an orchard. J. Basic Sci. Eng., 22: 698-704.

Liu, Z.F., Fu, B.J. and Liu, G.H. 2006 Soil quality: Concept, indicators and its assessment. Acta Ecol. Sinica., 26(3): 901-913.

Lü, H., Yu, Z., Horton, R., Zhu, Y., Zhang, J., Jia, Y. and Yang, C. 2013. Effect of gravel-sand mulch on soil water and temperature in the semiarid loess region of northwest China. J. Hydrol. Eng., 18(11): 1484-1494.

Liu, X.D., Qiao, Y.N. and Zhou, G.Y. 2011. Controlling action of soil organic matter on soil moisture retention and its availability. Chin. J. Plant Ecol., 35(12): 1209-1208.

Markgraf, W. and Horn, R. 2007. Scanning electron microscopy-energy dispersive scan analyses and rheological investigations of south-Brazilian soils. Soil Sci. Soc. Am. J., 71(3): 851-859.

Mascaro, G., Ko, Ara, Vivoni and Enrique, R. 2019. Closing the loop of satellite soil moisture estimation via scale invariance of hydrologic simulations. Sci. Rep-UK, 9(1): 16123.

Pieri, L., Bittelli, M. and Pisa, P.R. 2006. Laser diffraction, transmission electron microscopy and image analysis to evaluate a bimodal gaussian model for particle size distribution in soils. Geoderma, 135: 118-132.

Pham, T. 2016. The semi-variogram and spectral distortion measures for image texture retrieval. IEEE T. Image Process., 25(4): 1556-1565.

Qiu, Y., Xie, Z., Wang, Y., Ren, J. and Malhi, S.S. 2014. Influence of gravel mulch stratum thickness and gravel grain size on evaporation resistance. J. Hydrol., 519: 1908-1913.

Selim, T., Berndtsson, R. and Persson, M. 2013. Simulation of soil water and salinity distribution under surface drip irrigation. Irrig. Drain., 62(3): 352-362.

Shen, H. and Jilili, A. 2015. Spatial distribution of soil moisture and salinity and their influence factors in the farmland of Manas River catchment, Northwest China. Chin. J. Appl. Ecol., 26(3): 769-776.

Tyler, S.W. and Wheatcraft, S.W. 1989. Application of fractal mathematics to soil water retention estimation. Soil Sci. Soc. Am. J., 53(4): 987-996.

Wang, Y.J., Xie, Z.K., Malhi, S.S., Vera, C.L., Zhang, Y.B. and Guo, Z.H. 2011. Effects of gravel-sand mulch, plastic mulch and ridge and furrow rainfall harvesting system combinations on water use efficiency, soil temperature and watermelon yield in a semi-arid Loess Plateau of northwestern China. Agr. Water Manage., 101(1): 88-92.

Wang, C., Zuo, Q. and Zhang, R.D. 2008. Estimating the necessary sampling size of surface soil moisture at different scales using random combination method. J. Hydrol., 352 (3-4): 309-321.

Wang, Z., Li, G., Li, X., Shan, S., Zhang, J., Li, S. and Fan, J. 2012. Characteristics of moisture and salinity of soil in Taklimakan Desert, China. Water Sci. Techonl., 66(6): 1162-1170.

Wraith, J. M. 2004. Soil water dynamics. Vadose Zone J., 3(4): 1490-1490.

Wright, A. L. and Hons, F.M. 2005. Soil carbon and nitrogen storage in aggregates from different tillage and crop regimes. J. Soil Sci. Soc. Am. J., 69(1): 141-147.

Xing, X.G., Zhao, W.G., Liu, Y. and Ma, X.Y. 2015. Spatial variability of soil moisture in kiwi field under different sampling density conditions. J. Trans. Chin. Soc. Agric. Mach., 8: 143-150.

Xu, L., Li., Y.H., Haimit, Y. and Li., L. 2013. Spatial variability of soil moisture and salinity in different plant communities in Ebinur Lake Wetland. Bulletin Soil Water Conserv., 33(6): 279-284.

Yang, Y., Dou Y., Liu, D. and An, S.S. 2017. Spatial pattern and heterogeneity of soil moisture along a transect in a small catchment on the Loess Plateau. J. Hydrol., 550: 466-477.

Yao, R.J., Yang, J.S. and Liu, G.M. 2006. Spatial variability of soil salinity and moisture and their estimations by co kriging method - A case study in characteristic field of Yellow river delta. J. Soil Water Conserv., 20(5): 133-138.

Zhang, D. M., Zhao, W.Z. and Zhang, G.F. 2018. Soil moisture and salt ionic composition effects on species distribution and diversity in semiarid inland saline habitats, northwestern China. Ecol. Res., 33: 505-515.

Zhang, S.W., Huang, Y.F., Shen, C.Y., Ye, H.C. and Du, Y.C. 2012. Spatial prediction of soil organic matter using terrain indices and categorical variables as auxiliary information. J. Geoderma., 171(2): 35-43.

Zhao, Y.G., Li, Y.Y., Wang, J., Peng H.C. and Li, Y. 2016. Buried straw layer plus plastic mulching reduces soil salinity and increases sunflower yield in saline soils. Soil Till. Res., 155: 363-370.

Zhao, W.J., Cui, Z. and Ma, H. 2017a. Fractal features of soil particle-size distributions and their relationships with soil properties in gravel-mulched fields. Arab. J. Geosci., 10: 211.

Zhao, W.J., Cui, Z, Zhang, J.Y. and Jin, J. 2017b. Temporal stability and variability of soil-water content in a gravel-mulched field in northwestern China. J. Hydrol., 552: 249-257.

Zhao, W. J., Sheng, J., Li, Z. L., Ma, H. and Yu, P. 2017c. Spatial variability of soil salinity in a gravel-sand mulched jujube orchard at different scales. J. Irrig. Drain. Eng., 143: 0401700911-0401700918.

Nature Environment and Pollution Technology
An International Quarterly Scientific Journal

p-ISSN: 0972-6268
(Print copies up to 2016)
e-ISSN: 2395-3454

Vol. 19 | No. 4 | pp. 1567-1576 | 2020

Original Research Paper

https://doi.org/10.46488/NEPT.2020.v19i04.023

Open Access Journal

# Bioremediation of Diesel Oil Contaminated Soil by a Novel Isolated Potential Oil Degrading *Staphylococcus argenteus* MG2 Bacteria Using Biostimulation Method

**Mahima Golani*† and Krishnan Hajela****
*PMB Gujarati Science College, Indore, M.P., India
**School of Life Sciences, Devi Ahilya University, Indore, M.P., India
†Corresponding author: Mahima Golani; go.mahi@yahoo.com

**Nat. Env. & Poll. Tech.**
**Website: www.neptjournal.com**

*Received:* 28-12-2019
*Revised:* 16-01-2020
*Accepted:* 01-02-2020

**Key Words:**
Bioremediation
Diesel oil
Hydrocarbons
Oil degradation
Biostimulation
*Staphylococcus argenteus* MG2

## ABSTRACT

The potential oil-degrading isolate *Staphylococcus argenteus* MG2 was used for bioremediation of oil-contaminated soil. Hydrocarbon degradation by the soil microorganisms was evaluated in a soil experimentally contaminated with diesel oil. The effects of six different biological treatments on hydrocarbon degradation were determined during a 50 days incubation period to evaluate biostimulation via inorganic fertilizers (NPK) or manure (compost) with and without inoculum of *Staphylococcus argenteus* MG2. Eight soil samples were used: (S) uncontaminated control soil; (CS) contaminated soil; (CSF) contaminated soil + N-P-K fertilizer; (CSC) contaminated soil + compost; (CSI) contaminated soil + Inoculum; (CSFI) contaminated soil + N-P-K fertilizer + Inoculum; (CSCI) contaminated soil + compost + Inoculum; (SCSCI) sterile (oil) contaminated soil + compost + Inoculum. Percentage of oil degradation during bioremediation treatment of 50 days was found to be (CS) - 32%, (CSF) - 70.80%, (CSC) - 75%, (CSI) - 84.40%, (CSFI) - 91%, (CSCI) - 93%, (SCSCI) - 94% respectively. Results showed that not only inorganic nutrients NPK and compost stimulated hydrocarbon biodegradation but inoculation of *Staphylococcus argenteus* MG2 also enhanced hydrocarbon degradation. The microbial count was found to be higher in SCSCI soil sample. The germination percentage and growth of leguminous plant (*Vigna radiata*) in the treated soil was also notably greater. It may be concluded that the *Staphylococcus argenteus* MG2 bacteria possess remarkable oil-degrading properties and can be effectively employed in the bioremediation of oil-contaminated soils and can be used for agriculture purpose.

## INTRODUCTION

The pollution of soil by petroleum products has become a widespread problem and among the technologies available to deal with contaminated soils, bioremediation based on the metabolic activities of microorganisms has certain advantages (Van Gestel et al. 2003). The useful properties of the soil such as soil fertility, water holding capacity, permeability and binding capacity get lost due to the contamination of soil by oil (Vasanthavigar et al. 2010). Microbial bioremediation is the only way to preserve our nature to overcome these environmental problems (Chithra et al. 2014). Lipase producing strains played a key role in the enzymological remediation of polluted soil (Lin et al. 2012). In bioremediation process, lipase is a new aspect in environmental management (Nakamura et al. 1994). Bioremediation is emerging as the cost-effective treatment method for the hydrocarbon contaminated soil (Namkoong et al. 2002). Bioremediation has become an important aspect among different treatment techniques for removal of polyaromatic hydrocarbons and its biodegradation was achieved either by bacteria (Arulazhagan & Vasudevan 2011, Hamamura et al. 2013), fungi (Hadibarata et al. 2009, Cerniglia & Sutherland 2010) or algae (Munoz et al. 2003, Chan et al. 2006).

Bioremediation of hydrocarbon contaminated soils exploit the ability of microorganisms to degrade the organic contamination which has been established as an efficient, economic, versatile and environmentally sound treatment (Norris et al. 1994). The most applicable bioremediation process is biostimulation of the indigenous microorganisms by addition of nutrients, as the input of large quantities of carbon sources cause a rapid loss of the available pools of major inorganic nutrients, such as N and P (Morgan et al. 1989). In various studies, the effects of biostimulation with mainly NPK fertilizers have reported positive effects on oil decontamination in cold ecosystems (Atlas 1981, Margesin & Schinner 1999a). Ex-situ treatment method can help in the clean-up of diesel contaminated soil sites (Thilakar et al. 2013). Compost and inorganic nutrients like N and P stimulated hydrocarbon biodegradation. Lipase activity was found to be the most applicable parameter for analysing the

hydrocarbon degradation in soil (Riffaldi et al. 2006). Recent research works have shown that lipase is closely related to the organic pollutants present in the soil. Total hydrocarbons from contaminated soil got substantially reduced due to lipase activity. Research undertaken in this area is likely to progress the knowledge in the bioremediation of oils spill (Margesin & Schinner 1999a, Riffaldi et al. 2006).

The objectives of this study were to isolate a potential oil-degrading strain which could be used in bioremediation of oil-contaminated sites and to find out the efficiency of the microbial isolates during the bioremediation process. This was achieved by evaluating six biological treatments of soil consisting in biostimulation via inorganic fertilizers (NPK) or manure (compost) with and without inoculum of *Staphylococcus argenteus* MG2 a potential lipase producing bacterium. Hydrocarbon degradation by the indigenous soil microorganisms along with oil-degrading bacteria and fertilizers was evaluated in a soil experimentally contaminated with diesel oil. The germination percentage and growth of a fast-growing leguminous plant (*Vigna radiata*) in the treated soil was also observed.

## MATERIALS AND METHODS

### Screening of Lipase Producing Bacteria

The screening of lipolytic bacteria was done by enrichment culture technique from different samples in Tributyrin medium containing 0.5% (w/v) peptone, 0.3% (w/v) yeast extract, 1% (v/v) Tributyrin. The lipolytic activity of isolated colonies was observed by spot inoculation on Tributyrin agar medium plates and incubated at 37ºC for 48 h (pH- 7 & 9) and zone of clearance was observed due to hydrolysis of tributyrin by lipase (Golani et al. 2019).

### Identification of Selected Isolate

The selected bacterial isolate MG2 was identified following the criteria laid down by Bergey's Manual of Determinative Bacteriology (Holt et al. 1994) and the biochemical tests. The isolate was further identified up to species level and confirmed based on 1500bp of 16S rDNA gene sequence analysis by Microbial Type Culture Collection Centre and Gene Bank (MTCC), Institute of Microbial Technology, (IMTECH), Chandigarh, India and culture was deposited also. The 16S rDNA nucleotide sequence of the isolate MG2 determined in this study has been deposited in the (NCBI, US) Gene Bank database.

### Collection of Soil Sample

The soil sample was collected from the Botanical garden of Nasia Road, Indore. The characteristic features of the soil were analysed.

### Design of Bioremediation Experiments

Eight pans were prepared, each containing 1 kg of sieved soil at 50% of its water holding capacity (WHC); each pan, except treatment S, was spiked at 10 g of diesel oil/kg soil and treated as follows:

Two pans were taken as controls:

1. S (control): uncontaminated soil (Soil without oil): this pan was used to monitor the level of biological activities in soil.
2. CS (contaminated soil): in this pan, only oil was added and contained no further addition to evaluate hydrocarbon degradation by the indigenous soil microorganisms.

Rest of six pans were used for bioremediation treatments:

3. CSF: this pan was treated with N, P and K nutrients, added as 0.5g $(NH_4)H_2PO_4$ and 2.5g $KNO_3$/kg soil at a C:N:P:K ratio in the soil of 4:1:0.16:0.84.
4. CSC: this pan was added with 50 g of manure compost from Indore Biotech plant $kg^{-1}$ soil on the dry weight basis. The compost had a pH of 7.8 and contained 17.2% organic C, 9.9 $mg.g^{-1}$ nitrogen and 2.8 $mg.g^{-1}$ phosphorus.
5. CSI: this pan was inoculated with 10 mL inoculum of *Staphylococcus argenteus* MG2 a potential lipase producing bacterium to evaluate hydrocarbon degradation by the indigenous soil microorganisms along with oil-degrading bacteria.
6. CSFI: this pan was treated with N, P and K nutrients, added as 0.5g $(NH_4)H_2PO_4$ and 2.5g $KNO_3$ at a C:N:P:K ratio in the soil of 4:1:0.16:0.84 and was inoculated with 10 mL inoculum of *Staphylococcus argenteus* MG2 to evaluate hydrocarbon degradation by the indigenous soil microorganisms along with oil-degrading bacteria and chemical fertilizers.
7. CSCI: this pan was added with 50 g of manure compost from Indore Biotech plant kg-1 soil on the dry weight basis and was inoculated with 10 mL inoculum of *Staphylococcus argenteus* MG2 to evaluate hydrocarbon degradation by the indigenous soil microorganisms along with oil-degrading bacteria and biological fertilizers.
8. SCSCI: soil of this pan was sterilized to kill the soil indigenous microorganisms and then was added with 50 g of manure compost from Indore Biotech plant $kg^{-1}$ soil on a dry weight basis and was inoculated with 10 mL inoculum of *Staphylococcus argenteus* MG2 a potential lipase producing bacterium to evaluate hydrocarbon degradation with inoculated oil-degrading bacteria and biological fertilizers.

The pans were incubated in the dark at 25°C for 50 days.

The water content of the pans was adjusted and maintained at 50% of the WHC during the whole incubation period. Pan contents were thoroughly mixed on every second day for assurance of sufficient aerobic condition.

Chemical and biological analyses were performed at the end of 10, 20, 35, 50 days by sampling 3 soil subsamples from each pan (Riffaldi et al. 2006).

### Chemical Analysis

**Soil pH:** 10 g of soil sample was collected from each experimental pot after completion of their treatment period and mixed with sterile distilled water in a beaker stirred and allowed to stand for 30 minutes. The soil pH was then determined with a glass electrode of digital pH meter.

**Total petroleum hydrocarbons content (estimation of the percentage of diesel oil):** Diesel oil degradation from each experimental pot soil except control after completion of their treatment period was studied by gravimetric analysis (Chang 1998, Marquez-Rocha et al. 2001). One g of the soil was taken from each pot. Petroleum ether and acetone were taken in the ratio 1:1 and mixed with the soil sample in a separating funnel. Bacterial activities were stopped by adding 1% 1N HCl. The mixture was shaken for about 30 minutes and then left undisturbed for about 10 minutes. The upper solvent along with oil was separated from the lower soil extract. The solvent with the oil layer was taken in a preweighed clean beaker. The extracted oil was passed through anhydrous sodium sulphate to remove moisture. The petroleum ether and acetone were evaporated on a water bath and then kept in the hot air oven at 100ºC for 10 minutes until the beaker gets dry. The quantity of residual oil left after biodegradation was estimated by weighing the quantity of oil in a tared beaker. The percentage of diesel oil degraded was determined from the following formula:

$$\% \text{ of diesel oil degraded} = \frac{\text{Weight of diesel oil degraded}}{\text{Weight of diesel oil present originally}} \times 100$$

Where, the weight of diesel oil degraded = original weight of diesel oil - weight of residual diesel oil obtained after evaporating the extractant.

### Standard Plate Count of Oil Degrading Microorganisms

The number of oil-degrading microorganisms from each experimental pot soil after completion of their treatment of time period interval was determined by the standard plate count method for viable cells as described (Margesin & Schinner 1999b), using oil agar plates (minimal medium) with 1% diesel oil as the sole source of carbon. Ten g of the diesel contaminated soil samples along with control were weighed and then added in 100 mL sterile distilled water. Serial dilutions of the soil samples were prepared up to $10^{-6}$. A 0.1 mL of appropriate dilution was plated in above mentioned medium plates by spread plate method. Enumerations were made with triplicates. Colony-forming units (cfu) were counted after 7 days at 28°C. No significant growth was observed on control plates without diesel oil. Some oil-degrading fungi and actinomycetes producing maximum zone of hydrolysis around the colony were observed during this soil bioremediation experiment.

### Germination and Plantation Tests in Soil During Bioremediation Treatment of Soil Contaminated with Diesel Oil

After fifty days of bioremediation treatment of soil contaminated with diesel oil was used to check that which quality of soil is appropriate for the plantation. In our study, *Vigna radiata* (Green gram or mung) was chosen for the seed germination test as it is a fast-growing and common leguminous plant which is available locally also. Healthy and uniform sized seeds of Green gram (*Vigna radiata*) were taken in sterile Petri plates for washing with sterile distilled water and then surface sterilized in 1% $HgCl_2$ for about 5 minutes followed by washing in sterile distilled water thrice under the aseptic condition to remove traces of $HgCl_2$. The surface-sterilized 8 seeds were then sowed in each of the 8 experimental pot which contained treated and untreated soil samples, i.e., 1. (S) uncontaminated control soil; 2. (CS) contaminated soil; 3. (CSF) contaminated soil + N-P-K fertilizer; 4. (CSC) contaminated soil + compost; 5. (CSI) contaminated soil + Inoculum; 6. (CSFI) contaminated soil + N-P-K fertilizer + Inoculum; 7. (CSCI) contaminated soil + compost + Inoculum; 8. (SCSCI) sterile (oil) contaminated soil + compost + Inoculum respectively. After a few days of watering, the germination of the seeds was noted. Growth of the plants, height of the stem, number of leaves and pods were also observed during the plant development. The germination percentage was calculated by the following formula:

$$\text{Germination (\%)} = \frac{\text{Number of seeds germinated}}{\text{Total number of seeds}} \times 100$$

### Statistical Analyses

All results were expressed as the mean ± standard deviation (± SD). The experiment was conducted at least 3 times, and each treatment had 3 replicates. Thus, for most data points, the n = 3. The Graph Pad PRISM (Version-5) software was used for statistical evaluations. Differences between untreated and treated groups were tested by two-way analysis of

variance (ANOVA). Differences at $p < 0.001$ were considered highly significant and $p < 0.01$ were considered significant while $p > 0.05$ were considered as non-significant (ns).

## RESULTS

### Screening of Lipase Producing Bacteria

The lipolytic activity of the isolates was determined by measuring the zone of lipid hydrolysis on the tributyrin agar plate. Among the 72 lipolytic isolates, MG2 (pH-7) showed maximum zone of hydrolysis (2.57 mm) around the colony and was also able to grow at pH 9 with maximum lipase activity (3.12 mm) which shows its alkali tolerant nature and was selected for further studies.

### Identification of Selected Isolate

The selected bacterium MG2 was negative towards citrate utilization, indole test, methyl red Voges-Proskauer tests, $H_2S$ production, urea hydrolysis, oxidase and haemolytic activity test. The strain was catalase positive.

The strain showing the maximum zone of hydrolysis was designated as MG2. Using consensus primers, the 1.5 kb 16SrDNA fragment was amplified using *Taq* DNA Polymerase by PCR technique. The morphological, cultural, physiological and biochemical characteristics, as well as phylogenetic trees made using Neighbour Joining method (Saitou & Nei 1987), suggested that the isolate MG2 was close to a novel bacterium *Staphylococcus argenteus*. Hence, this strain was identified and named as *Staphylococcus argenteus* MG2.

The 16S rDNA nucleotide sequence of the isolate *Staphylococcus argenteus* MG2 determined in this study has been deposited in the (NCBI, US) Gene Bank database under the accession number KY082046. The culture identified as *Staphylococcus argenteus* MG2 has been deposited in Microbial Type Culture Collection Centre and Gene Bank (MTCC), Institute of Microbial Technology, (IMTECH), Chandigarh, India, under the accession number MTCC-12820 (Golani et al. 2019).

### Characteristics of the Soil Sample

The main features of experimental soil analysed were, Sand-69.0 (%), Slit- 17.2 (%), Clay- 13.8 (%), WHC- 50.0 (%), CaCO3- 17.6 (%), Organic- 1.38 (%), pH- 7.5.

### Chemical Analysis

**Soil pH:** The soil pH remained in the neutral to the slightly alkaline range (7-8) during the whole incubation period independent of fertilization which is shown in Fig. 1.

**Total petroleum hydrocarbons content (estimation of the percentage of diesel oil):** Total petroleum hydrocarbons (TPH) content during the bioremediation trials is reported in Fig. 2. Both treatment and time had a significant influence on the residual hydrocarbon content. When CS was statistically compared for degradation of oil with other treated samples, then p-value was found to be highly significant ($p<0.001$) for all. There was a little loss of hydrocarbons (15%) of CS in the first incubation period i.e. on the 10th day, probably due to hydrocarbon degradation only by the indigenous soil

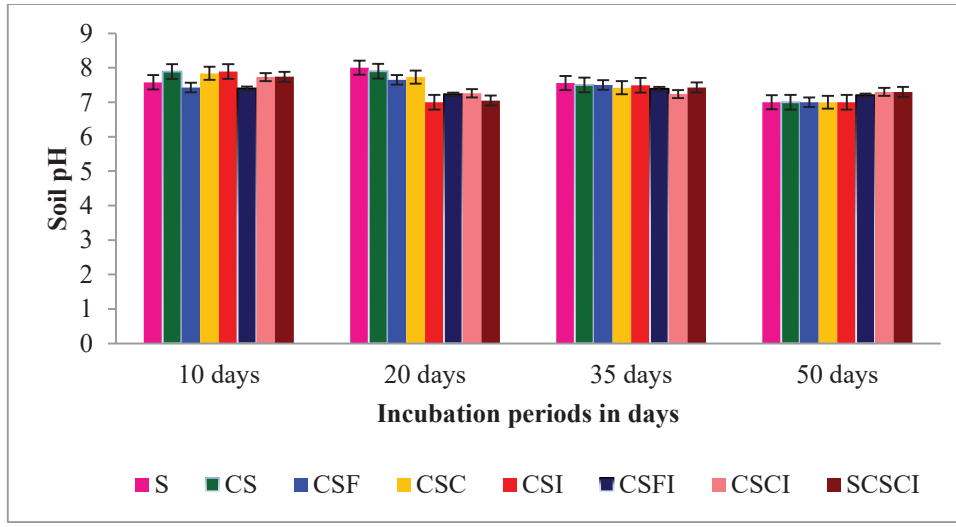


Fig. 1: Soil pH during bioremediation treatment of soil contaminated with diesel oil.

microorganisms. Such a loss was significantly lower relative to the other trials on the same date. The percentage of oil degradation of biologically treated samples (CSF-52%, CSC-58%) was higher than CS. The difference suggests, since the first incubation phases, biodegradation by a microbial community present in the biologically treated samples was enhanced by the addition of biological nutrients which was significant as compared to natural attenuation. In CSI, the % of oil degradation was 74.4% which was significantly higher ($p<0.001$) than CSF and CSC because of the addition of inoculum of *Staphylococcus argenteus* MG2, a potential lipase producing bacterium.

On the contrary, the decrease of TPH was highest for all the biologically active (CSFI-83.10%, CSCI-83.90%, SCSCI-84.10%) samples with the inoculum of *Staphylococcus argenteus* MG2. The oil degradation by *Staphylococcus argenteus* MG2 was not surprising not only because it was isolated from oil-spilled soil, but also because it is known to possess a more competent and active hydrocarbon degrading enzyme system. It is known to be fast-growing and is capable of degrading a wide variety of organic compounds. This biodegradation was also enhanced by a microbial community present in the biologically treated samples due to the addition of biological nutrients in CSFI and CSCI while in SCSCI the oil degradation by *Staphylococcus argenteus* MG2, a potential lipase producing bacterium, was found to be more competent and addition of compost also enhanced its activity.

On the 50th day, CS (32%) and CSF (70.8%), CSC (75%) was not significantly different either for initial or final TPH concentrations. The occurrence that CSF, CSC treatment presented an effect comparable to that in the contaminated but untreated soil, suggests a poor contribution of nutrients added to the soil in stimulating the indigenous microbial community. Probably, CSF and CSC treatment would have been more effective if nutrients had been added to the soil periodically rather than only at the initial experimental phase. In CSI treatment, the final biodegradation of oil was 84.4% because of the addition of inoculum of *Staphylococcus argenteus* MG2.

After 50th day, SCSCI treatment presented the lowest TPH concentration, corresponding to a TPH degradation of 94%, which was slightly higher than that of CSCI (93%) & CSFI (91%) which concludes the most effective biotreatment in hydrocarbon decay and confirms that the *Staphylococcus argenteus* MG2 is a potential lipase producing bacterium for the degradation of TPH. The compost may have facilitated the degradation of TPH because it plays an important role in supplementing continuously nutrient and carbon sources. Overall results indicated that the degradation of TPH was faster in all the inoculum added treated soil samples than others.

**Standard plate count of oil degrading microorganisms on diesel oil agar plate:** The number of oil-degrading microorganisms from each experimental pot soil after completion of their treatment of time period interval was determined by the standard plate count method for viable cells as described

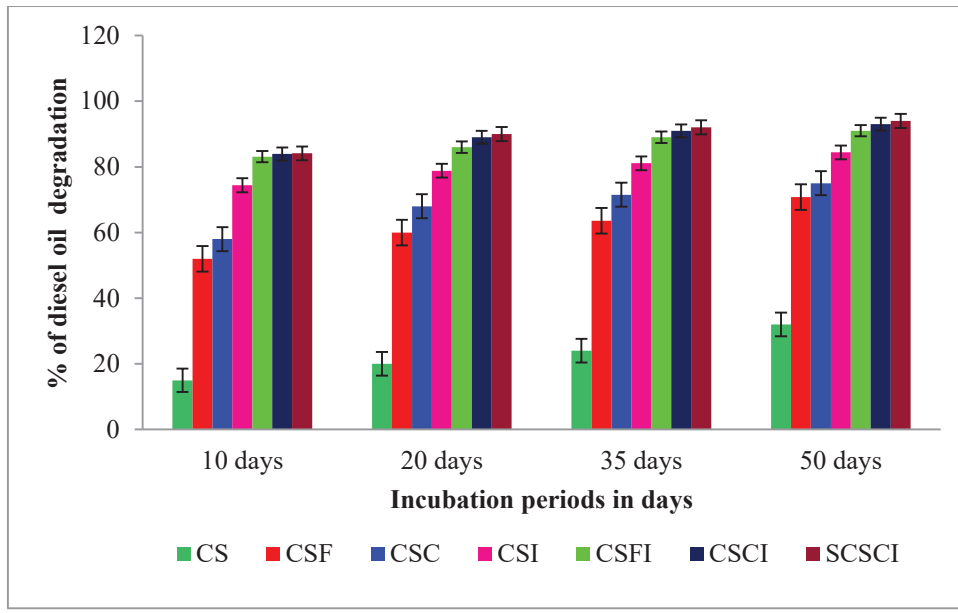


Fig. 2: Percentage of diesel oil degradation during bioremediation treatment of soil contaminated with diesel oil (10g/kg soil) in 50 days ($p<0.001$).

(Margesin & Schinner 1999b), using oil agar plates with 1% diesel oil as the sole source of carbon. Microbial count on diesel oil agar plate during the bioremediation trials are reported in Figs. 3 and 4. The oil-degrading microbial count in (S) uncontaminated control soil was found to be lesser via out the incubation period than CS, CSF and CSC because S was not contaminated by diesel oil which provides carbon source for microorganisms to grow.

Microbial community present in the biologically treated samples was enhanced by the addition of biological nutrients. In CSI the number of oil-degrading microorganisms was higher than CS, CSF and CSC because of the addition of inoculum of *Staphylococcus argenteus* MG2.

On the contrary, the oil-degrading microbial count was higher for the biologically active samples (CSFI, CSCI) which were inoculated with *Staphylococcus argenteus* MG2. This microbial count was also higher because of the microbial community present in the biologically treated samples due to the addition of biological nutrients in CSFI and CSCI while in SCSCI treatment the oil-degrading microbial count was

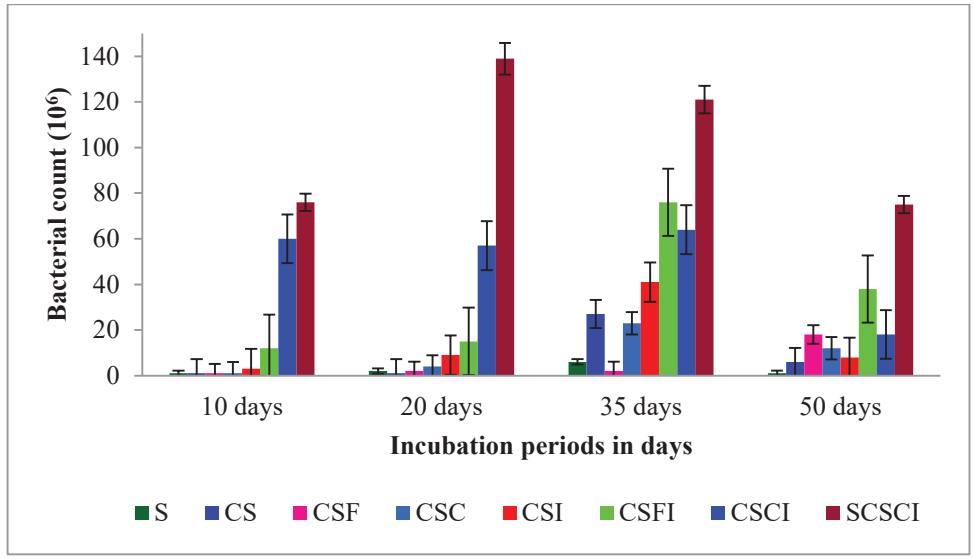


Fig. 3: Oil degrading bacterial count (CFU/g of soil) on diesel oil agar plate during bioremediation treatment of soil contaminated with diesel oil.

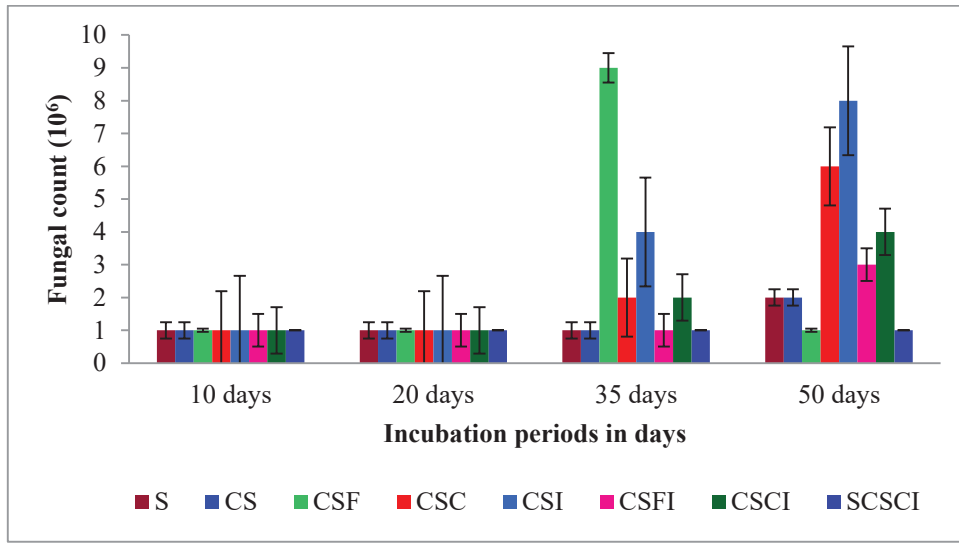


Fig. 4: Oil degrading fungal count (CFU/g of soil) on diesel oil agar plate during bioremediation treatment of soil contaminated with diesel oil.

Table 1: Effect of bioremediation treatment of soil contaminated with diesel oil on the growth of plant of *Vigna radiata.*

| S. No. | Soil sample | Seed germination (%) | No. of plants | Average height of plants (feet) a, b, c, d | Average No. of leaves a, b, c, d | Average No. of pods a, b, c, d |
|---|---|---|---|---|---|---|
| 1 | S | 100 | 8 | 7.053 ±0.050 | 41 ±1 | 0 ±0 |
| 2 | CS | 50 | 4 | 6.458 ± 0.052 ns | 30 ±0.577*** | 0.66 ±0.577 ns |
| 3 | CSF | 50 | 4 | 4.000 ± 0.05*** | 30 ±0.577*** | 1.66 ±0.577** |
| 4 | CSC | 62.5 | 5 | 6.466 ± 0.0577 ns | 36 ±1*** | 2.00 ±0** |
| 5 | CSI | 50 | 4 | 6.200 ±0.05 ns | 20 ±1*** | 0.33 ±0.577 ns |
| 6 | CSFI | 62.5 | 4 | 6.400 ±0.05 ns | 28 ±1*** | 2.33 ±0.577*** |
| 7 | CSCI | 87.5 | 6 | 6.045 ±0.0473 ns | 45 ±1.527*** | 3.66 ±0.577*** |
| 8 | SCSCI | 100 | 8 | 6.962 ±0.033 ns | 59 ±1*** | 6.66 ±0.577*** |

a. The results are expressed as the mean ± SD of three independent experiments conducted in triplicates.
b. Differences between untreated and treated growth of plants were tested by two-way analysis of variance (Anova).
c. differences at ***, $p < 0.001$ were considered highly significant and **, $p < 0.01$ were considered significant and $p > 0.05$ were considered as non-significant (ns)
d. ANOVA was performed taking S as a control for all the observations.

highest than all other samples because of the inoculation of potential oil-degrading *Staphylococcus argenteus* MG2. It is known to be fast growing in oil-contaminated soil and is capable of degrading a wide variety of organic compounds. Addition of compost also played an important role in supplementing continuously nutrient and carbon sources. It was also observed during the whole experiment that the microbial growth in SCSCI appeared in 2 days while other soil samples required 4-5 days. It was also noted that the fungal count was not found to be significant than bacterial count. Microbial growth was found to be good in SCSCI which was followed by CSCI and CSFI respectively.

**Germination and plantation tests in soil during bioremediation treatment of soil contaminated with diesel oil:** After fifty days of bioremediation treatment of soil contaminated with diesel oil was used to check that which quality of soil is appropriate for the germination of seeds and growth of plant. *Vigna radiata* (Green gram or mung) was chosen for the seed germination test. The surface-sterilized 8 seeds were then sowed in each experimental pot (8 in number) which contained treated and untreated soil samples, i.e., 1. (S) uncontaminated control soil; 2. (CS) contaminated soil; 3. (CSF) contaminated soil + N-P-K fertilizer; 4. (CSC) contaminated soil + compost; 5. (CSI) contaminated soil + Inoculum; 6. (CSFI) contaminated soil + N-P-K fertilizer + Inoculum; 7. (CSCI) contaminated soil + compost + Inoculum; 8. (SCSCI) sterile (oil) contaminated soil + compost + Inoculum respectively.

The present investigation led to the preliminary assessment and comparison of effect in treated and untreated samples by the germination test. The germination percentage (Table 1) in the 1. (S) was 100% while in 2. (CS) the germination percentage was 50%. In 3. (CSF) and 5. (CSI), the germination percentage was also 50% while in 4. (CSC) percentage was 62.5%. The germination percentage in 6. (CSFI) was 62.5% while in 7. (CSCI) was 87.5%. In 8. (SCSCI) the seed germination percentage was 100%.

Growth of the plant, height of the plant, and the number of leaves and pods were also observed during the plant development in various soil samples which is shown in Fig. 5.

Effect of bioremediation treatment of soil contaminated with diesel oil on the growth of plant of *Vigna radiata* is reported in Table 1. Results were similar to the germination of seeds. When S was statistically compared for growth of the plant with other treated samples, then p-value was found to be highly significant ($p<0.001$) for SCSCI except the height of plant (ns).

## DISCUSSION

Overall results of biotreatment in hydrocarbon decay indicated that the degradation of TPH was faster in all the *Staphylococcus argenteus* MG2 inoculum added treated soil samples than others. The compost may have facilitated the degradation of TPH because it plays an important role in supplementing continuously nutrient and carbon sources. The result agrees with the studies of Namkoong et al. (2000) and Riffaldi et al. (2006) who found that the degradation of TPH was significantly enhanced by the addition of organic amendments. Margesin et al. (1999) reported that after 116 days, the initial hydrocarbon contamination of 5 mg/g soil dry weight got reduced to 1.15 and 0.538 mg/g soil dry weight in the unfertilized and fertilized soil, respectively. This correlates to decontamination percentages of 77 and 89%,

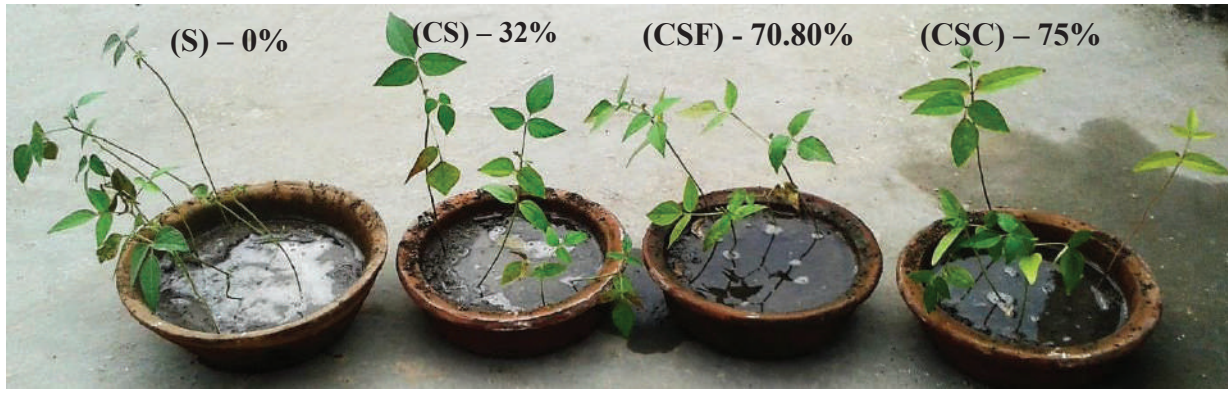


(a)

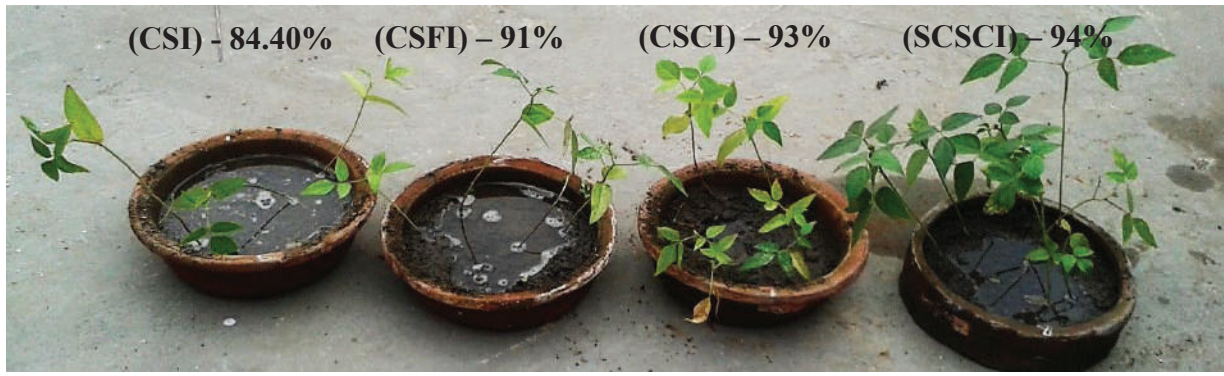


(b)

Fig. 5: (a), (b) Growth of the plant *Vigna radiata* during bioremediation treatment of soil contaminated with diesel oil.

respectively. In our results, after 50th day, SCSCI treatment corresponds to a TPH degradation of 94%, which was higher than the earlier mentioned results.

The biostimulation resulted in increased counts of oil degraders significantly. Margesin et al. (1999) observed that bioremediation treatment by adding inorganic nutrients enhanced hydrocarbon degradation by the indigenous soil microorganisms significantly as compared to natural attenuation. Our results are in accordance to Margesin et al. (2001) who concluded that in the fertilized soil all biological parameters (microbial numbers and lipase activity) got enhanced and correlated significantly with each other as well as with the residual hydrocarbon concentration which shows the importance of biodegradation. The effect of biostimulation of the indigenous soil microorganisms reduced with time. The microbial activities in the unfertilized soil fluctuated around background levels during the whole study.

A germination and plantation test in the soil during bioremediation treatment of soil contaminated with diesel oil was performed to check that which quality of soil is appropriate for the germination of seeds and growth of *Vigna radiata* (Green gram or mung) plant. The germination percentage in the 1. (S) was 100% because it was not contaminated with oil while in 2. (CS) the germination percentage was found to be 50% which clearly indicates that the contamination of oil in soil inhibits the germination of seeds. In 3. (CSF) and 5. (CSI), the germination percentage was also 50% while in 4. (CSC) percentage was found to be 62.5%. These results reveal that the addition of compost provides nutrients to the soil required for germination of seeds. The germination percentage in 6. (CSFI) was 62.5% while in 7. (CSCI) was 87.5% which clearly shows that the addition of compost and inoculation of *Staphylococcus argenteus* MG2 enhanced the seed germination percentage. In 8. (SCSCI) the seed germination percentage was 100%. It means that not only the addition of compost provides nutrients but also the inoculation of potential oil-degrading bacteria *Staphylococcus argenteus* MG2 degrades oil and thereby releases simple fatty acids which enhanced the seed germination percentage. Initially, the growth of plants was found to be good in (S) uncontam-

inated control soil but after 1.5 months the deterioration of plants was fast than other samples and number of pods was zero because no one fertilizer or compost was added in soil. The number of plants, leaves and pods was found to be higher in SCSCI soil sample followed by CSCI soil sample.

Similar results were obtained by other scientists when the experiment was performed in selected plants such as winter wheat, soybean and sunflower. Growth parameters such as germination percentage, fresh weight and plant height were observed (Yanqing et al. 2012).

From the results obtained above, it can be understood that biostimulation can effectively be used to combat pollution. The findings of other researchers also support the fact that biostimulation could indeed be a solution for degrading environmental pollutants (Miller 2010).

## CONCLUSION

To conclude, the results confirmed that the bioremediation mediated by *Staphylococcus argenteus* MG2 from SCSCSI (sterile oil-contaminated soil + compost + inoculum) sample and CSCSI have been very effective and the degradation of TPH was significantly enhanced by the treatment with compost and can be used to reclaim the oil-contaminated soil for agricultural purpose in the oil-contaminated soil.

The above experiment indicates that bioremediation can be used effectively to treat oil-contaminated soil. Bioremediation usually lowers the costs as compared to chemical treatment processes for various contaminated sites. It is also less disturbing to the environment. The present study has shown that the *Staphylococcus argenteus* MG2 bacteria isolated from the oil-spilled site possess the capacity to produce lipase, therefore it was used for the degradation of oil-contaminated soil. The effectiveness of the bioremediation was studied by finding out the germination percentage of a fast growing leguminous plant (*Vigna radiata*). It was observed that the germination percentage in the treated soil was notably greater. The results also prove that biostimulation is an effective method of reducing the environmental pollution. Thus, the present study concludes that microbial degradation can be regarded as a key component in the clean-up strategy for petroleum hydrocarbon remediation.

## ACKNOWLEDGEMENT

The financial assistance provided by University Grant Commission, Bhopal (MS-29/103042/12-13/CRO) and facilities provided by the Management & Principal of PMB Gujarati Science College and School of Life Sciences, DAVV, Indore is gratefully acknowledged.

## REFERENCES

Arulazhagan, P. and Vasudevan, N. 2011. Role of nutrients in the utilization of polycyclic aromatic hydrocarbons by halotolerant bacterial strain. J. Environ. Sci., 23: 282-287.

Atlas, R.M. 1981. Microbial degradation of petroleum hydrocarbons: An environmental perspective. Microbiol. Rev., 45: 180-209.

Cerniglia, C.E. and Sutherland, J.B. 2010. Degradation of polycyclic aromatic hydrocarbons by fungi. In: Handbook of Hydrocarbon and Lipid Microbiology, pp. 2079-2110.

Chan, S.M.N., Luan, T., Wong, M.H. and Tam, N.F.Y. 2006. Removal and biodegradation of polycyclic aromatic hydrocarbons by *Selenastrum capricornutum*. Environ. Toxicol. Chem., 25: 1772-1779.

Chang, R. 1998. Chemistry, 6th Ed., McGraw Hill Company, Inc., pp. 962-963.

Chithra, S. and Shenpagam, N.H. 2014. Isolation and identification of oil degrading bacteria from oil contaminated soil and comparison of their bioremediation potential. Global J. for Res. Analysis, 3: 181-184.

Golani, M., Hajela, K. and Pandey, G.P. 2019. Isolation and identification of a novel lipase producing *Staphylococcus argenteus* MG2 bacterium from oil spilled soil. Int. J. of Advance and Innovative Research, 6(1) (XIV): 20-30.

Hadibarata, T. and Tachibana, S. 2009. Microbial degradation of n-eicosane by filamentous fungi. In: Interdisciplinary Studies on Environmental Chemistry and Environmental Research in Asia. (Eds. Y. Obayashi, T. Isobe, A. Subramanian, S. Suzuki and S. Tanabe) Terrapub Tokyo, pp. 323-329.

Hamamura, N., Ward, D.M. and Inskeep, W.P. 2013. Effects of petroleum mixture types on soil bacterial population dynamics associated with the biodegradation of hydrocarbons in soil environments. FEMS Microbiol. Ecol., 85: 168-178.

Holt, J.G., Krieg, N.R., Sneath, P.H.A., Staley, J.T. and Williams. S.T. 1994. Bergey's Manual of Determinative Bacteriology. Ninth Edition, Williams and Wilkins Baltimore, Group 17, Gram-Positive Cocci, pp. 527-558.

Lin, J.F., Lin, Q., Li, J., Fei, Z.A., Li, X.R., Xu, H., Qiao, D.R. and Cao, Y. 2012. Bacterial diversity of lipase-producing strains in different soils in southwest of China and characteristics of lipase. Afr. J. Microbiol. Res., 6(16): 3797-3806.

Margesin, R. and Schinner, F. 1999a. Biological decontamination of oil spills in cold environments. J. Chem. Technol. Biotechnol., 74: 1-9.

Margesin, R. and Schinner, F. 2001. Bioremediation (natural attenuation and biostimulation) of diesel oil contaminated soil in an alpine glacier sking area. Appl. Env. Microbiol., 67: 3127-3133.

Margesin, R. and Schinner, F. 1999b. A feasibility study for the in situ remediation of a former tank farm. World J. Microbiol. Biotechnol., 15: 615-622

Margesin, R., Zimmerbauer, A. and Schinner, F. 1999. Soil lipase activity-a useful indicator of oil biodegradation. Biotech. Techniques, 13: 859-863.

Marquez-Rocha, F.J., Hernandez-Rodriguez, V. and Lamela, M.T. 2001. Biodegradation of diesel oil in soil by a microbial consortium. Water Air Soil Pollut., 128: 313-320.

Miller, H. 2010. Biostimulation as a form of bioremediation of soil pollutants. MMG 445 Basic Biotechnology, eJournal, 6(1): 7-12.

Morgan, P. and Watkinson, R.J. 1989. Hydrocarbon degradation in soils and methods for soil biotreatment. Crit. Rev. Biotechnol., 8: 305-333.

Munoz, R., Guieysse, B. and Mattiasson, B. 2003. Phenanthrene biodegradation by an algal-bacterial consortium in two-phase partitioning bioreactors. Appl. Microbiol. Biotechnol., 61: 261-267.

Nakamura, K.M., Yoda and Fukase, T. 1994. Treatment process for drainage containing fats and oils. Japan Patent. JP-06246295.

Namkoong, W., Hwang, E.Y., Park, J.S. and Choi, J. K. 2002. Bioremediation of diesel contaminated soil with composting. Environ. Pollut., 119: 23-31.

Norris, R.D. 1994. Handbook of Bioremediation. CRC Press Boca Raton Fla.

Riffaldi, R., Levi-Minzi, R., Cardelli, R., Palumbo, S. and Saviozzi, A. 2006. Soil biological activities in monitoring the bioremediation of diesel oil-contaminated soil. Journal Water, Air, and Soil Pollution, 170: 3-15.

Saitou, N. and Nei, M. 1987. The neighbour-joining method: A new method for reconstructing phylogenetic trees. Molecular Biology and Evolution, 4: 406-425.

Thilakar, J.R. and Rathi, J.J. 2013. Bioremediation of diesel contaminated soil by oil degrading bacteria (*Pseudomonas* sp.) using biostimulation method. J. Microbiol. Biotech. Res., 3(5): 18-26.

Van Gestel, K., Mergaert, J., Swings, J. and Coosemans, J. 2003. Bioremediation of diesel oil contaminated soil by composting with biowaste. Environ. Pollut., 125: 361-368.

Vasanthavigar, M., Srinivasamoorthy, K., Ganthi, R.R., Vijayaraghavan, K. and Sarma, V.S., 2010. Characterisation and quality assessment of groundwater with a special emphasis on irrigation utility: Thirumanimuttar sub-basin, Tamil Nadu, India. Arabian Journal of Geosciences, 5(2): 245-258.

Yanqing, Z., Ziling, S., Jianping, C., Cui, L., Bo, Q. and Qinghai, W. 2012. Effects of oil-contaminated soil on the seed germination and seedling growth of selected crops. World Automation Congress (WAC). IEEE Conference Publications, 1-4.

Nature Environment and Pollution Technology
An International Quarterly Scientific Journal

p-ISSN: 0972-6268
(Print copies up to 2016)
e-ISSN: 2395-3454

Vol. 19 | No. 4 | pp. 1577-1584 | 2020

Original Research Paper

https://doi.org/10.46488/NEPT.2020.v19i04.024

Open Access Journal

# Haematological and Serum Biomarker Responses in *Heteropneustes fossilis* Exposed to Bisphenol A

**Bhawna Srivastava and P. B. Reddy*†**
Department of Zoology, DAV College, Kanpur, U.P., India
*PG Department of Zoology, Govt. Art and Science College, Ratlam, M.P., India
†Corresponding author: P. B. Reddy; reddysirr@gmail.com

**Nat. Env. & Poll. Tech.**
**Website: www.neptjournal.com**

*Received:* 08-01-2020
*Revised:* 17-02-2020
*Accepted:* 09-03-2020

**Key Words:**
Biomarkers
BPA
*Heteropneustes fossilis*
Haematology
Serum biochemistry

## ABSTRACT

The present investigation was carried out for 21 days to explore the sub-lethal toxicity of bisphenol A (BPA) of concentration 0.714, 1.428 and 2.142 mg/L (1/10, 1/20 and 1/30 % of 96 h $LC_{50}$) on haematological and serum biochemical parameters of *Heteropneustes fossilis*. Routine haematological parameters like total erythrocyte count (TEC), total leukocyte count (TLC), haemoglobin content (Hb), haematocrit (Hct), erythrocyte indices, total serum protein, alanine aminotransferase (ALT), and aspartate aminotransferase (AST), albumin, globulin, uric acid, and creatinine were examined as toxicological endpoints. The findings of this study revealed that BPA had a negative effect on both the haematological and serum biochemical parameters of *Heteropneustes fossilis*. The study revealed a significant decrease in red blood cell count, haemoglobin concentration and haematocrit percentage (anaemia) while white blood cell count showed a significant increase in all treatment groups ($p < 0.0001$). The erythrocyte indices like MCV and MCH in the exposed groups reduced in a dose-dependent manner but BPA treatment increased MCHC values ($p > 0.05$). The results of serum biochemistry in BPA exposed fish showed enhanced serum AST, ALT, urea, uric acid and creatinine but decreased serum total protein and albumin. This might be due to the possible disruption of haemopoietic tissue or impairment of liver and kidney function. Based on the results, we conclude that BPA is toxic to *Heteropneustes fossilis* and its occurrence in the environment may threaten the health of aquatic species. Accordingly, it suggests that haematological and serum biochemical parameters could be effectively used as reflective bioindicators in ecotoxicological studies.

## INTRODUCTION

Bisphenol A (BPA), a synthetic chemical substance and extensively used in the production of synthetic plastic polymers, has appeared as a universal pollutant in the aquatic environment (Pal & Reddy 2018). Because of its widespread use, BPA is released into aquatic environs through sewage and affects the aquatic organisms (Krishnapriya et al. 2017, Faheem et al. 2019, Hassan et al. 2020).

Fish species are very sensitive to aquatic pollution and specific haematological and biochemical biomarkers of fish were demonstrated as direct indicators for assessing the ecological status of an aquatic environment. Many investigations have been conducted using fish as an experimental model for assessing contaminant-induced toxicity (Reddy 2012a,b, Reddy & Baghel 2012, Reddy & Rawat 2013, Reddy 2018, Sharma et al. 2019). The affinity between BPA and haemoglobin, as well as erythrocytes, is an important factor in understanding the mechanism of the BPA toxicity (Sangai et al. 2018). Like other toxicants, BPA can exert toxic effects on survival of fish and its accumulation in tissues may affect the metabolic processes like glycolysis, protein and lipid profile of the organism and cause oxidative stress (Javed et al. 2017). The energy requirements of organisms increase in stress condition and biomolecules like glucose, fats, and proteins pull together to meet the energy demand depending on the intensity of stress (Javed et al. 2017).

The study of serum biochemistry reflects the metabolic condition of several biochemical processes and the health status of the organism. A number of researchers used haematological and serum biochemical parameters effectively as reflective bioindicators in ecotoxicological studies (Lavanya et al 2011, Atli et al. 2015, Javed et al. 2017, Narra et al. 2017, Pandit & Kumari 2018, Ullah et al. 2019). These studies reveal internal alterations before the animal show any external signs of toxic stress (Osman et al. 2010). The *in vivo* research work of Roy et al. (2011) confirmed the degenerative effects of Bisphenol A on the liver of *Heteropneustes fossilis.* Hussein & Eid (2013) found significant disruptive hepatotoxic changes in the liver of mice. Aiswarya & James (2016) found a significant decrease in RBC, and Hb concentrations and an increase in WBC content in *H. fossilis*

exposed to 0.1g/L of BPA for 72 hours. The 28 days treatment with various sublethal concentrations of BPA significantly altered histopathological changes in liver, kidney, and serum biochemical parameters of *H. fossilis* in a dose-dependent manner (Pal & Reddy 2018). Several ecological stressors may alter serum biochemical parameters in fish. Serum biochemical parameters like AST, ALT, ALP, glucose, urea, creatine, total protein and albumin of fish serum may reflect health status and several biochemical pathways in the metabolism (Yousef et al. 2006, Pal & Reddy 2018, Nourian et al. 2019).

The present research on alteration in haematological and serum biochemistry has a more extended scope because of its probable advantage in the health diagnosis of the individual. Accordingly, many animal models under different experimental and ecological conditions are conducted to explain the toxic mechanisms of BPA but most of them are from mammalian models. Therefore, the current study assessed the use of a series of biomarkers in *H. fossilis* to measure the health status of fish exposed to different sublethal concentrations of Bisphenol A also and to determine most potentially used parameter as a biomarker of BPA intoxication and fish health status. The haematological and biochemical parameters bioindicators used in this study will provide necessary information on the impact of Bisphenol A (BPA) on fish health. With this perspective, we incorporated haematological and serum biochemical parameters as health indicators.

## MATERIALS AND METHODS

The ethical committee of the University approved the experimental design and all procedures used in the present study.

**Materials:** Healthy and adult *Heteropneustes fossilis* were collected from local fishponds and acclimatized to the laboratory backgrounds for 15 days. *Bisphenol-A*2, 2-Bis (4-hydroxyphenyl) propane (CAS No: 80-05-7. EC No: 201-245-8. Purity: 99.99%) was obtained from Chemex Chemicals, Mumbai (India).

**Experimental design**: The after acclimatized fish were categorized into four sets comprising of three replicates containing eight fish (average weight is 35.96g) in each aquarium of 40L capacity. The selection of sublethal concentrations of BPA for this experiment is based on our earlier study (Pal & Reddy 2018). One control group and three exposed sets containing three concentrations, i.e., 0.714mg/L (1/10th), 1.428mg/L (1/20th) and 2.142mg/L (1/30th) respectively of $LC_{50}$ value (7.14mg/L) (Pal & Reddy 2018). Both control sets and BPA treated groups were maintained under the same environmental conditions during the experimental period. No fish mortality was recorded during the experimental period. The fish were exposed under normal laboratory conditions for 21 days. Aquarium water along with BPA was entirely substituted once every two days by transferring the fish into freshly prepared BPA solutions. Control and experimental fish received a commercial prawn fish feed (Univar cure, Thane, MH, India).

**Collection of blood sample:** At the end of experimentation, fish was stopped feeding 24 h before blood sampling. Blood samples were collected from three fish of each experimental group randomly by puncturing the caudal veins with the help of a heparinized 2cm disposable syringe. The blood sample was mixed lightly and used for the estimation of haematological indicators like erythrocyte count (RBC), haemoglobin concentration (Hb), haematocrit (HCT), white blood cell (WBC) count, mean corpuscular volume (MCV), mean corpuscular haemoglobin (MCH) and mean corpuscular haemoglobin concentration (MCHC).

**Biochemical analysis:** Blood samples were collected by puncturing the caudal region of fish without rinsing the heparinised and stored in clean and dry Eppendorf tubes. The blood samples were allowed for 1h to clot at room temperature followed by 30min incubation at 4°C. Serum was obtained by centrifuging the blood samples at 3000g for 10 min at 4°C. Plasma total proteins, serum albumin, and globulin values were estimated by using a commercial kit obtained from Qualigens Fine Chemicals, Mumbai. Plasma glucose was assessed using a commercially available kit from Diatek, Kolkata. Serum creatinine and uric acid were estimated by the standard procedures given in the commercial kit supplied by Tulip Diagnostics (P) Ltd, Mumbai. All serum values were analysed statistically by Students' *t*-test by Microsoft Excel add-in program. Serum glutamic oxaloacetic transaminase/aspartate aminotransferase (SGOT/AST EC 2.6.1.1) and serum glutamic pyruvic transaminase/alanine aminotransferase/serum glutamic pyruvic transaminase (SGPT/ALT EC 2.6.1.2) were determined by the protocol given by Reitman & Frankel (1957) using a commercial diagnostic kit (Merck, Germany).

## RESULTS

The sublethal concentrations of BPA did not cause mortality in *H. fossils* during the experimental period. Increased mucus secretion, altered swimming behaviour, and irritability were important changes noticed in some exposed fish during the experimental period. These alterations were severed at the end experimental periods and in fish exposed to higher doses.

**Haematological parameters:** The mean values of haematological parameters of *H. fossils* exposed to various sublethal concentrations of BPA are given in Table 1. Results revealed that RBCs, HB and HCT were decreased significantly in fish exposed to BPA in all exposed fish in a dose-dependent

manner when compared to the control group ($p < 0.05$).

The RBC count reduced significantly ($p < 0.05$) in the fish of Group II, III and IV with counts of 1.16 ± 0.08, 1.09 ± 0.07, 1.65 ± 0.94 ± 0.06 and 1.31 ± 0.09 count × $10^6$ $mm^3$ for the control respectively. In contrast, the total WBC count was elevated significantly ($p < 0.05$) in all experimental fish in a dose-dependent manner. Similarly, a significant reduction in HB% and Hct% were found between the treated and control fish ($p < 0.05$). Haematological indices like MCV, MCH, and MCHC are vital biomarkers in the diagnosis of anaemia type. The MCV and MCHC are the indicators of erythrocyte size and shape. Their values reflect the normal or abnormal cell division during erythropoiesis. In the present experiment, both MCV and MCH values in *H. fossilis* were increased in all experimental fish compared to the control group ($p > 0.05$). Conversely, MCHC values decreased in exposed fish compared to the control ($p < 0.05$).

**Biochemical parameters:** The mean values of serum biochemical parameters of *H. fossilis* exposed to various sublethal concentrations of BPA for 21 days are given in Table 2. Significant differences were observed in serum total protein, albumin, globulin, creatine, uric acid, AST and ALT levels of fish exposed to BPA compared to control fish produced lowest values of those variables as compared with those of the control in dose dependent-manner ($p < 0.05$) (Table 2).

Results evidently revealed a significant increase in plasma glucose (mg/L) concentrations in dose-dependent manner ($p < 0.05$). Conversely, the total plasma protein levels of *H. fossilis* exposed to sublethal concentrations of BPA shown a significant reduction ($p < 0.05$) compared to the control group. Likewise, both albumin, globulin and A:G ratio was also declined expressively in dose-dependent manner ($p < 0.05$). The renal biomarkers of both urea and creatine levels were significantly ($p < 0.05$) increased in all experimental fish exposed to BPA. The activities of alanine aminotransferase (SGPT) and AST (SGOT) were significantly increased ($p < 0.05$) in all BPA exposed fish in dose dependent manner.

## DISCUSSION

Haematological and serum biochemical parameters in fish have proved to be a valuable tool in ecotoxicological

Table 1: Mean values (± standard error) of haematological parameters of *H. fossilis* exposed to BPA.

| Parameter | (Group I Control) | Group II | Group III | Group III |
|---|---|---|---|---|
| RBC (×$10^6$/$mm^3$) | 1.31 ± 0.09 | 1.16 ± 0.08* | 1.09 ± 0.07* | 0.94 ± 0.06** |
| WBC (×$10^3$/$mm^3$) | 188.4 ± 19.22 | 202.5 ± 19.4* | 219.7 ± 22.3* | 236.8 ± 23.8* |
| Hb (g/dl) | 9.7 ± 0.9 | 9.0 ± 0.8 | 8.4 ± 0.7* | 7.2 ± 0.6** |
| Hct (%) | 33.2 ± 3.1 | 27.6 ± 2.1* | 22.3 ± 2.4* | 16.4 ± 1.4** |
| MCV (fl/cell) | 172.30 ± 3.7 | 179.4 ± 5.2* | 186.5 ± 6.5 | 194.7 ± 3.6** |
| MCH (pg/cell) | 53.45 ± 2.6 | 56.6 ± 3.1* | 63.6 ± 2.2 | 69.6 ± 1.8** |
| MCHC (g/dl) | 268.8 ± 8.2 | 255.6 ± 7.7 | 228.8 ± 6.8* | 198.7 ± 6.8** |

Values are characterized as (mean ± SE) of six individual values. *Indicate values, those are significantly different from control and exposure ($p < 0.05$).

Table 2: The serum biochemistry of *H. fossilis* exposed to sublethal concentrations of Bisphenol A.

| Parameter | Group I Control | Group II | Group III | Group III |
|---|---|---|---|---|
| Plasma protein(µg/mL) | 9.77±0.95 | 8.34±0.24* | 6.56±0.63* | 4.58±0.61** |
| Plasma glucose (mg/dL) | 98.2±2.11 | 106.8±2.87* | 124.5±3.69** | 143.5±4.56** |
| Albumin (g/dL) | 2.58± 0.08 | 2.18± 0.06* | 2.07± 0.05 | 1.82± 0.04** |
| Globulin (g/dL) | 3.23± 0.23 | 3.08± 0.22 | 2.84 ± 0.18* | 2.46± 0.2** |
| A:G ratio | 0.80± 0.02 | 0.70± 0.01* | 0.72± 0.02* | 0.74± 0.01 |
| Creatinine (mg/L) | 1.89 ± 0.02 | 2.1 ± 0.03* | 3.4 ± 0.03** | 4.9 ± 0.05** |
| Uric acid (mg/L) | 5.71 ± 0.9 | 9.9 ± 0.8* | 10.7 ± 0.8** | 14.6 ± 1.2** |
| AST (SGOT) (U/L) | 61.45± 1.1 | 72.3± 2.5* | 86.6± 2.5 | 119.7± 3.7** |
| ALT (SGPT) (U/L) | 30.2± 1.5 | 36.3± 2.5* | 42.3 ± 3.1 | 51.4± 3.4** |

Means within the same row carrying different *superscripts are significant at $p < 0.05$.

research for evaluating the health status of fish exposed to various pollutants (Saravanan et al. 2011, Krishnapriya et al. 2017, Kumar et al. 2019). BPA intoxication in fish known to induce negative impacts on fish health (Canesi & Fabbri 2015, Cano-Nicolau et al. 2016, Pal & Reddy 2018, Wang et al. 2019).

In the present study, the total erythrocyte count, the Ht, and Hb percentage, and the secondary indices of RBCs of *Heteropneustes fossilis* exposed to BPA were significantly lower than that of the control group. The reduced RBC count generally also leads to low Ht and Hb levels (Javed et al. 2016). The reduction in RBC count, Hb and Ht specifies the anaemic condition of the exposed fish, which could be due to the damage of haemopoietic tissue (kidney/spleen) or inhibition of erythropoiesis. The dose-dependent decrease in haemoglobin concentration in experimental fish might be the consequence of injury or cellular damage or suppression of haemopoietic tissue of the fish (Kumar & Banerjee 2016). The obvious haemorrhage or haemolysis caused microcytic anaemia, as regenerating small and immature erythrocytes formed in response to BPA stress, constitute the majority of cells in outer circulation (Clauss et al. 2008). The anaemia in experimental fish might be due to decreased erythropoiesis caused by the intoxication of BPA on haematopoietic tissues (kidney/spleen). The results of the present study are in agreement with the result of Keum et al. (2005) in Korean rockfish, *Sebastes schlegeli*, Aiswarya & James (2016) in *H. fossilis*, and Yaghoobi et al. (2017) in yellowfin seabream (*Acanthopagrus latus*) and Krishnapriya et al. (2017) in *Labeo rohita*, exposed to various sublethal concentrations of Bisphenol A. The reduction in RBCs, Ht and Hb levels in BPA exposed *H. fossilis* indicate hypochromic microcytic anaemia (Narra et al. 2017) which might be due to both the inhibition of haemosynthesis, erythropoiesis or osmoregulatory dysfunction or rapid erythrocyte destruction in the haematopoietic organ (Narra et al. 2017, Kumar Maurya et al. 2019, Yonar et al 2020). In the same way, the substantial reduction in Hct value indicates the anaemic condition of the fish due to BPA toxicity, which is a common reaction in fish under stress conditions (Krishnapriya et al. 2017). The reduction in secondary indices of RBC specifies the shrinkage of RBCs due to the toxic stress prompted by BPA. The significant decrease in Hb percentage may perhaps lead to a reduction in MCHC value (Sarma 1990). The present experiment also exposed that the sublethal concentrations of the BPA may affect the Hb synthesis in *H. fossilis* resulting in a significant decrease of MCHC value. The higher values of MCV and MCH in the present study indicate the macrocytic condition and low values as microcytic conditions (Javed et al. 2016). In the present study, BPA exposure induced macrocytic anaemia as MCV values showed higher levels as compared to the control fish. The macrocytic anaemia occurs when a cell is unable to produce an adequate amount of DNA quickly as compared to cell growth (Javed et al. 2016). Our results are in agreement with the findings of Aiswarya & James (2016) and Yaghoobi et al (2017). The study of Keum et al. (2005) has demonstrated that BPA can induce adverse impacts on haematological parameters and serum biochemical parameters in the Korean rockfish, *Sebastes schlegeli*. The results of Krishnapriya et al. (2017) have shown that BPA exposure modifies the haematological and biochemical parameters in fish, *L. rohita.* Similarly, the study of Yaghoobi et al. (2017) also showed an inverse correlation of BPA with RBC, Ht, Hb, and secondary indices in yellowfin seabream (*Acanthopagrus latus*). Kumar Mourya et al. (2019) found a significant reduction in the RBC count, Hb and Hct percentage in *H. fossilis* exposed to the industrial wastewater at various concentrations.

Leucocytes play a major role in the non-specific immunity of the fish defence system. Assessment of total leucocyte count (TLC) is acknowledged as an important tool for assessing fish health conditions (Maceda-Veiga et al. 2010). WBCs mainly involve in nonspecific immunity of fish. In the present experiment, the BPA intoxication caused a significant increase in the total WBC count of experimental fish in a dose-dependent manner, which might be a general immune response and a protective reaction to BPA stress. Another possible reason for an increase in total WBCs count is due to the BPA induced toxic stress which might stimulate the leucocytosis/lymphopoiesis from lymphomyeloid tissue for effective defence against BPA toxicity. The higher values of total WBC might be due to increasing lymphopoiesis and/or higher release of lymphocytes from lymphomyeloid tissue. Such response in fish happens due to tissue damage by the accumulation of toxic materials, which consequently stimulated the non-specific immune system to produce more number of leucocytes. The increase in total leucocytes count in the present experiment may be endorsed to an adaptive higher immune response to protect the fish effectively from the BPA induced stress. Our results are in agreement with the results of Kumar & Banerjee (2016) in *Clarias batrachus* exposed to sublethal concentrations of arsenic. The reduction in erythrocyte count and Hb concentration along with increased WBC count were also observed when the same fish was exposed to different concentrations of BPA (Aiswarya & James 2016 and Pal & Reddy 2018). Srinivasa Rao et al. (2018) also found decreased values of RBC, Hb, Hct, and increased values of WBC in the *fish Ctenopharyngodon idella* exposed to lethal and sublethal concentrations of synthetic pyrethroid deltamethrin and 11% Decis.

Serum biochemistry in fish is extensively used in the assessment of dietary status, health status, and the compe-

tence of fish for adaptation to the external environment (Fırat et al. 2011, Acharya & Mohanty 2014, Sharma et al. 2017, Pandit & Rani 2019). In the present experiment, all the serum biochemical variables in fish were significantly affected by BPA treatment. In the present study, BPA treatment caused the elevation of glucose level and inhibition of total serum proteins in a dose-dependent manner in *H. fossilis*. The increase in plasma glucose level reflects the enhanced glycogenolysis and inhibited glycolytic pathway in BPA treated fish. Our outcomes are analogous with those of Pal & Reddy (2018), Sisodia et al. (2018), in BPA exposed *H. fossilis* and El-Sayed et al. (2007) in Nile tilapia exposed to deltamethrin. The elevated levels of glucose in the present study might be due to the stress caused by BPA, which enhanced the synthesis of adrenocorticotropic hormone (ACTH), glucagon, and decline in the synthesis of insulin (El-Sayed et al. 2007, Provvisiero et al. 2016). As a result, glycogen from hepatic tissue is rapidly converted into glucose and entered into blood circulation. Accordingly, the clarification of this BPA induced temporary stress effect in all experimental groups of *H. fossilis* may be endorsed to either reduction in the synthesis of the above-cited hormones or to higher energy demand, that stimulates the use and consumption of glucose (El-Sayed et al. 2007).

The protein synthesis is of great indicative importance as it is involved in the synthesis of enzymes, hormones and antibodies. Therefore, the effects of BPA on plasma total protein levels of *H. fossilis* have taken into consideration to assess the toxic effects of BPA. Serum total protein, albumin, and globulin experiments in fish are used to monitor the health status, liver disorder and impaired kidney function (Banaee 2013). In the present study, the values of serum total protein, albumin, and globulin were reduced significantly in fish exposed to BPA. The reduction in total serum protein, albumin, and globulin contents may be due to undernourishment and chronic liver disease as in rainbow trout (*Oncorhynchus mykiss*) exposed to diazinon (Banaee et al. 2011). Other researchers also found in the reduction of serum total protein, albumin and globulin in the fish exposed to various pollutants (Bhanu & Deepak 2015, Javed & Usmani 2015, Javed et al. 2017, Banaee et al. 2019). The reduction in the serum total protein concentration is accredited to low synthesis or increased loss of plasma proteins (hypoproteinemia) as in yellowfin sea bream, *Acanthopagrus latus* (Hedayati et al. 2011). Loss of protein, both albumin and globulin, occurs with haemorrhage and external injuries. The decrease of total serum protein, albumin, and globulin and albumin/globulin ratio particularly at the higher BPA doses reflects the hepatic dysfunction and immunosuppressive effect of the BPA. The decrease in total protein content of exposed fish perhaps due to either ceased metabolism or use it to create new cells or enzymes to reduce the stress. Our results are in agreement with the findings of El-Sayed et al. (2007) in Nile tilapia, *Oreochromis niloticus* exposed deltamethrin and Hedayati et al. (2011) in yellowfin sea bream, *Acanthopagrus latus* exposed to mercury chloride. The decrease of total serum protein content in the present experiment could be due to the conversion of blood and structural proteins to meet the higher energy demands on exposure to different BPA concentrations. However, some researchers endorsed to liver disorder or/and renal excretion for the reduction of serum protein in fish (Mutlu et al. 2015). The reduction in serum total protein, albumin and globulin may perhaps also be due to a higher haemodilution under the toxic stress of BPA (Kumar et al. 2011).

It is observed that BPA exposure significantly increased serum AST, ALT, urea and creatinine values. The obtained outcomes perhaps due to the toxic effects of BPA, which is known to induce several pathological processes in different fish organs (Pal & Reddy 2018, Manisha Sisodia et al. 2018, Faheem et al, 2019). It is well-known fact that AST, and ALT, are often used as a diagnostic tool to identify the damage in various tissues caused by pollutants (McGill 2016, Lala & Minter 2018). The higher AST and ALT activities point out the higher rate of transamination of proteins and subsequent consumption of free amino acids in the glycogenic pathway. Pal & Reddy (2018) and Manisha Sisodia et al. (2018) have given evidence that even a moderately elevated level of AST in serum is linked with liver damage. Similarly, urea and creatinine are traditional diagnostic tools for renal structural integrity and function. The reactive oxygen species (ROS) formed during BPA metabolism in can enhance the permeability of hepatic cells which results in leakage of AST, and ALT, enzymes into the blood circulation (Hamed & Abdel-Tawwab 2017, Pal & Reddy 2018, Sisodia et al. 2018, Mahdavinia et al. 2019, Faheem et al. 2019). Faheem et al. (2019) reported a similar increase in serum AST and ALT activities in *Catla catla* exposed to BPA. Alterations in AST and ALT activities directly point out cellular damage in hepatic tissue (Pal & Reddy 2018, Sisodia et al. 2018).

The values of serum creatinine and uric acid in vertebrates reflect the status of renal health, function, and muscle health and purine metabolism (Hamed & Tawwab 2017). Glomerulus damage, impair metabolism of carbohydrates and increased damage of muscle tissue may cause increased creatinine levels in the blood (Hadi et al. 2009). In the present study, a significant increase was recorded in serum creatinine and uric acid level of BPA exposed fish specifies that BPA affects muscle and purine (nucleic acid) metabolism as in C*hanna punctatus* exposed to industrial effluent (Javed et al. 2016). This increase may also be due to the damage of

renal tubules. Degeneration and necrosis of glomerulus and a decrease in haematopoietic tissue in *Catla catla* after BPA exposure was reported by Faheem et al. (2019). This decrease in haematopoietic tissue may be a cause of an increase in serum uric acid. Similar results were reported in Nile tilapia (*Oreochromis niloticus*) exposed to copper sulphate (Mutlu et al. (2015), BPA exposed Nile tilapia, *Oreochromis niloticus* (Abdel-Tawwab & Hamed 2018) and in *Catla catla* (Faheem et al. 2019). The toxic effect of BPA in the kidney is endorsed to its role in declining glomerular filtration rate (GFR) that is specified by a substantial increase in serum creatinine (Abdelkhalek et al. 2017). Faheem et al. (2019) observed a significant increase in serum urea and creatinine after BPA treatment in *Catla catla*. Jyothi & Narayan (2000) found a significant elevation in serum urea and creatinine after pesticide intoxication in a freshwater catfish, *Clarias batrachus*. Hamed et al. (2019) found a significant reduction in RBC's count, Hb, Ht, MCHC, platelets, and WBC's count and increase of creatinine, uric acid, AST, ALT, ALP, glucose, cholesterol, total protein, albumin, globulin, and A/G ratio in Nile tilapia (*Oreochromis niloticus)* exposed to microplastics for 15 days. The results confirm that BPA caused functional and structural damage in the kidney, which was reflected in the increased urea and uric acid levels with impairment in their excretion.

## CONCLUSIONS

The current study thus confirmed that haematological parameters are very responsive parameters for evaluating toxic responses of the fish following exposure to BPA. BPA intoxication reveals the anaemic condition in fish species. We believe that alterations in haematological indices and serum biochemistry may be a protective mechanism against BPA toxicity. Overall, the present study offers supplementary shreds of evidences for the usage of serum biomarkers in assessing the health of fish. The study also confirms the appropriateness of *H. fossilis* as experimental species and underlining the need for additional research to validate the presence of xenobiotics or other environmental toxins.

## REFERENCES

Abdelkhalek, N.K., Eissa, I.A., Ahmed, E., Kilany, O.E., El-Adl, M., Dawood, M.A., Hassan, A.M. and Abdel-Daim, M.M. 2017. Protective role of dietary *Spirulina platensis* against diazinon-induced oxidative damage in Nile tilapia, *Oreochromis niloticus*. Environmental Toxicology and Pharmacology, 54: 99-104.

Abdel-Tawwab, M. and Hamed, H.S. 2018. Effect of bisphenol A toxicity on growth performance, biochemical variables, and oxidative stress biomarkers of Nile tilapia, *Oreochromis niloticus* (L.). Journal of Applied Ichthyology, 34(5): 1117-1125.

Acharya, G. and Mohanty, P.K. 2014. Haematological and serum biochemical parameters in different sexes of walking catfish, *Clarias batrachus* (Linnaeus, 1758). International Journal of Science and Research, 3(8): 1914-1917.

Aiswarya, K.S. and James, R. 2016. Effect of Bisphenol A on certain haematological parameters of *Heteropneustes fossilis*, Bloch. International Journal of Emerging Trends in Science and Technology, 3(08): 4493-4497.

Atli, G., Ariyurek, S.Y., Kanak, E.G. and Canli, M. 2015.Alterations in the serum biomarkers belonging to different metabolic systems of fish (*Oreochromis niloticus*) after Cd and Pb exposures. Environmental Toxicology and Pharmacology, 40(2): 508-515.

Banaee, M. 2013. Physiological dysfunction in fish after insecticides exposure. In: Insecticides-Development of Safer and More Effective Technologies. IntechOpen.

Banaee, M., Sureda, A., Mirvaghefi, A.R. and Ahmadi, K. 2011. Effects of diazinon on biochemical parameters of blood in rainbow trout (*Oncorhynchus mykiss*). Pesticide Biochemistry and Physiology, 99(1): 1-6.

Banaee, M., Tahery, S., Nematdoost Haghi, B., Shahafve, S. and Vaziriyan, M. 2019. Blood biochemical changes in common carp (*Cyprinus carpio*) upon co-exposure to titanium dioxide nanoparticles and paraquat. Iranian Journal of Fisheries Sciences, 18(2): 242-255.

Bhanu, A.P. and Deepak, M. 2015. Impact of cypermethrin on biochemical aspects of clinical importance in the blood of freshwater fish *Cyprinus carpio*. Journal of Entomology and Zoology Studies, 3: 126-128.

Canesi, L. and Fabbri, E. 2015. Environmental effects of BPA: Focus on aquatic species. Dose-Response, 13(3): 1559325815598304.

Cano-Nicolau, J., Vaillant, C., Pellegrini, E., Charlier, T.D., Kah, O. and Coumailleau, P. 2016. Estrogenic effects of several BPA analogs in the developing zebrafish brain. Frontiers in Neuroscience, 10: 112.

Clauss, T.M., Dove, A.D. and Arnold, J.E. 2008. Hematologic disorders of fish. Veterinary Clinics of North America: Exotic Animal Practice, 11(3): 445-462.

El-Sayed, Y.S., Saad, T.T. and El-Bahr, S.M. 2007. Acute intoxication of deltamethrin in monosex Nile tilapia, *Oreochromis niloticus* with special reference to the clinical, biochemical and haematological effects. Environmental Toxicology and Pharmacology, 24(3): 212-217.

Faheem, M., Khaliq, S. and Lone, K.P. 2019. Effect of Bisphenol-A on serum biochemistry and liver function in the freshwater fish, *Catla catla*. Pakistan Veterinary Journal, 39(1): 71-75.

Fırat, Ö., Cogun, H.Y., Yüzereroğlu, T.A., Gök, G., Fırat, Ö., Kargin, F. and Kötemen, Y. 2011. A comparative study on the effects of a pesticide (cypermethrin) and two metals (copper, lead) to serum biochemistry of Nile tilapia, *Oreochromis niloticus*. Fish Physiology and Biochemistry, 37(3): 657-666.

Hadi, A., Shokr, A. and Alwan, S. 2009. Effects of aluminum on the biochemical parameters of fresh waterfish *Tilapia zillii*. Journal of Science and its Applications, 3(1): 33-41.

Hamed, H.S. and Abdel-Tawwab, M. 2017. Ameliorative effect of propolis supplementation on alleviating bisphenol-A toxicity: Growth performance, biochemical variables, and oxidative stress biomarkers of Nile tilapia, *Oreochromis niloticus* (L.) fingerlings. Comparative Biochemistry and Physiology Part C: Toxicology & Pharmacology, 202: 63-69.

Hamed, M., Soliman, H.A., Osman, A.G. and Sayed, A.E.D.H. 2019. Assessment the effect of exposure to microplastics in Nile Tilapia (*Oreochromis niloticus*) early juvenile: I. Blood biomarkers. Chemosphere, 228: 345-350.

Hassan, S., Ali, R., Shah, D., Sajjad, N. and Qadir, J. 2020. Bisphenol A and phthalates exhibit similar toxicogenomics and health effects. In: Handbook of Research on Environmental and Human Health Impacts of Plastic Pollution (pp. 263-287). IGI Global.

Hedayati, A., Safahieh, A., Savari, A., Movahedinia, A., Zare, P. and Bagheri, T. 2011. Serum biochemical change induced by in vitro sub chronic

mercury chloride in yellowfin sea bream (*Acanthopagrus latus*). Iranica Journal of Energy and Environment, 2(3): 208-214.

Hussein, R.M. and Eid, J.I. 2013. Pathological mechanisms of liver injury caused by oral administration of bisphenol A. Life Science Journal, 10(1): 663.

Javed, M. and Usmani, N. 2015. Stress response of biomolecules (carbohydrate, protein and lipid profiles) in fish *Channa punctatus* inhabiting river polluted by Thermal Power Plant effluent. Saudi Journal of Biological Sciences, 22(2): 237-242.

Javed, M., Ahmad, I., Ahmad, A., Usmani, N. and Ahmad, M. 2016. Studies on the alterations in haematological indices, micronuclei induction and pathological marker enzyme activities in *Channa punctatus* (spotted snakehead) perciformes, channidae exposed to thermal power plant effluent. SpringerPlus, 5(1): 761.

Javed, M., Ahmad, M.I., Usmani, N. and Ahmad, M. 2017. Multiple biomarker responses (serum biochemistry, oxidative stress, genotoxicity and histopathology) in *Channa punctatus* exposed to heavy metal loaded wastewater. Scientific Reports, 7(1): 1675.

Jyothi, B. and Narayan, G. 2000. Pesticide induced alterations of non-protein nitrogenous constituents in the serum of a freshwater catfish, *Clarias batrachus* (Linn.). Indian Journal of Experimental Biology, 38(10): 1058-61.

Keum, Y.H., Jee, J.H., Lee, O.H., Park, S.I. and Kang, J.C. 2005. In vivo effects of bisphenol A exposure on haematological parameters in Korean rockfish, *Sebastes schlegeli*. Journal of Fish Pathology, 18(3): 293-300.

Krishnapriya, K., Shobana, G., Narmadha, S., Ramesh, M. and Maruthappan, V. 2017. Sublethal concentration of bisphenol A induces haematological and biochemical responses in an Indian major carp *Labeo rohita*. Ecohydrology and Hydrobiology, 17(4): 306-313.

Kumar Maurya, P., Malik, D.S., Kumar Yadav, K., Gupta, N. and Kumar, S. 2019. Haematological and histological changes in fish *Heteropneustes fossilis* exposed to pesticides from industrial wastewater. Human and Ecological Risk Assessment, 25(5): 1251-1278.

Kumar, A., Ahirwal, S.K., Bhatt, R. and Singh, I.J. 2019. Certain haematological and biochemical changes in blood of rohu (*Labeo rohita*) in relation to sex, reproductive status and environmental factors. Journal of Entomology and Zoology Studies, 7(3): 1484-1490.

Kumar, N., Prabhu, P.A.J., Pal, A.K., Remya, S., Aklakur, M., Rana, R.S., Gupta, S., Raman, R.P. and Jadhao, S.B. 2011. Anti-oxidative and immuno-haematological status of Tilapia (*Oreochromis mossambicus*) during acute toxicity test of endosulfan. Pesticide Biochemistry and Physiology, 99(1): 45-52.

Kumar, R. and Banerjee, T.K. 2016. Arsenic induced haematological and biochemical responses in nutritionally important catfish *Clarias batrachus* (L.). Toxicology Reports, 3:148-152.

Lala, V. and Minter, D.A. 2018. Liver Function Tests. In: Stat Pearls. Stat Pearls Publishing.

Lavanya, S., Ramesh, M., Kavitha, C. and Malarvizhi, A. 2011. Hematological, biochemical and ionoregulatory responses of Indian major carp *Catla catla* during chronic sublethal exposure to inorganic arsenic. Chemosphere, 82(7): 977-985.

Maceda-Veiga, A., Monroy, M., Viscor, G. and De Sostoa, A. 2010. Changes in non-specific biomarkers in the Mediterranean barbel (*Barbus meridionalis*) exposed to sewage effluents in a Mediterranean stream (Catalonia, NE Spain). Aquatic Toxicology, 100(3): 229-237.

Mahdavinia, M., Alizadeh, S., Vanani, A.R., Dehghani, M.A., Shirani, M., Alipour, M., Shahmohammadi, H.A. and Asl, S.R. 2019. Effects of quercetin on bisphenol A-induced mitochondrial toxicity in rat liver. Iranian Journal of Basic Medical Sciences, 22(5): 499.

McGill, M.R. 2016. The past and present of serum aminotransferases and the future of liver injury biomarkers. EXCLI Journal, 15: 817.

Mutlu, E., Aydın, S. and Kutlu, B. 2015. Alterations of growth performance and blood chemistry in Nile tilapia (*Oreochromis niloticus*) affected by copper sulfate in long-term exposure. Turkish Journal of Fisheries and Aquatic Sciences, 15(3): 481-488.

Narra, M.R. 2017. Haematological and immune upshots in *Clarias batrachus* exposed to dimethoate and defying response of dietary ascorbic acid. Chemosphere, 168: 988-995.

Narra, M.R., Rajender, K., Reddy, R.R., Murty, U.S. and Begum, G. 2017. Insecticides induced stress response and recuperation in fish: Biomarkers in blood and tissues related to oxidative damage. Chemosphere, 168: 350-357.

Nourian, K., Baghshani, H. and Shahsavani, D. 2019. The Effect of Vitamin C on Lead-induced Plasma Biochemical Alterations in Fish, *Cyprinus carpio*. Iranian Journal of Toxicology, 13(2): 25-29.

Osman, A.G., Koutb, M. and Sayed, A.E.D.H. 2010. Use of haematological parameters to assess the efficiency of quince (Cydonia oblonga Miller) leaf extract in alleviation of the effect of ultraviolet - A radiation on African catfish *Clarias gariepinus* (Burchell, 1822). Journal of Photochemistry and Photobiology B: Biology, 99(1): 1-8.

Pal, S. and Reddy, P.B. 2018. Bisphenol A induced histopathological and biochemical alterations in the liver and kidney of stinging cat fish *Heteropneustes fossilis*. Trends in fisheries Research, 7(1): 67-74.

Pandit, D.N. and Kumari, V. 2018. Lead Induced Alterations in Serum Biochemical Features of an Indian Air-Breathing Catfish, *Clarias batrachus* (Linnaeus). Int. J. Chem. Sci., 16(4): 294.

Pandit, D.N. and Rani, U. 2019.Toxicity of tricyclazole on certain serum biochemical markers of an Indian paddy-field fish, *Channa punctatus* (Bloch). International Journal of Fisheries and Aquatic Studies, 7(6): 246-250.

Provvisiero, D., Pivonello, C., Muscogiuri, G., Negri, M., de Angelis, C., Simeoli, C., Pivonello, R. and Colao, A. 2016. Influence of bisphenol A on type 2 diabetes mellitus. International Journal of Environmental Research and Public Health, 13(10): 989.

Reddy, P.B. 2012a. Histopathological studies as potential and direct biomarkers of pollution. Trends in Life sciences, 1(1): 27-31.

Reddy, P.B. 2012b. Evaluation of potential biomarkers for effluent induced hepatotoxicity. International Journal on Applied Bioengineering, 6(2): 22-27.

Reddy, P.B. 2018. Study on the toxic effects of wastewater in catfish (*Heteropneustes fossilis)*. Life Sciences International Research Journal, 5(2): 165-174.

Reddy, P.B. and Baghel, B.S. 2012. Impact of Industrial wastewater on the Chambal River and Biomarker responses in fish due to pollution at Nagda. MP India. DAV International Journal Sciences, 1(1): 86-91.

Reddy, P.B. and Rawat, S.S. 2013. Assessment of aquatic pollution using histopathology in fish as a protocol. International Research Journal of Environment Sciences, 2(8): 79-82.

Reitman, S. and Frankel, S. 1957. A colorimetric method for the determination of serum glutamic oxaloacetic and glutamic transaminases. American Journal of Clinical Pathology, 28: 56-63.

Roy, S., Kalita, C.J. and Mazumdar, M. 2011. Histopathlogical effects of Bisphenol A on liver of *Heteropneustes fossilis* (Bloch). The Ecoscan, 1: 187-190.

Sangai, N.P., Patel, C.N. and Pandya, H.A. 2018. Ameliorative effects of quercetin against bisphenol A-caused oxidative stress in human erythrocytes: an in vitro and in silico study. Toxicology Research, 7(6): 1091-1099.

Saravanan, M., Kumar, K.P. and Ramesh, M. 2011. Haematological and biochemical responses of freshwater teleost fish *Cyprinus carpio* (Actinopterygii: Cypriniformes) during acute and chronic sublethal exposure to lindane. Pesticide Biochemistry and Physiology, 100(3): 206-211.

Sarma, P.R. 1990. Red cell indices. In: Clinical Methods: The History, Physical, and Laboratory Examinations. 3rd edition. Butterworths.

Sharma, N.K., Akhtar, M.S., Pandey, N.N., Singh, R. and Singh, A.K. 2017. Sex specific seasonal variation in haematological and serum biochemical indices of *Barilius bendelisis* from Central Himalaya, India. Proceedings of the National Academy of Sciences, India Section B: Biological Sciences, 87(4): 1185-1197.

Sharma, P., Chadha, P. and Saini, H.S. 2019. Tetrabromobisphenol A induced oxidative stress and genotoxicity in fish *Channa punctatus*. Drug and Chemical Toxicology, 42(6): 559-564.

Sisodia, Manisha, Khare, Meena and Kanhere, R.R. 2018. Biochemical effects of Bisphenol A (BPA) in Asian stinging fish *Heteropneustes fossilis*. International Journal of Researches in Biosciences, Agriculture and Technology, (VII)(1): 10-18.

Srinivasa Rao, G., Naik, K.B., Satyanarayana, S. and Rao, N.G. 2018. Haematological changes induced by the deltamethrin a synthetic pyrethroid technical grade and 11% EC (Decis) in the fish *Ctenopharyngodon idella* (Valenciennes). Journal of Innovations in Pharmaceutical and Biological Sciences, 5: 128-134.

Ullah, S., Li, Z., Arifeen, M.Z.U., Khan, S.U. and Fahad, S. 2019. Multiple biomarkers based appraisal of deltamethrin-induced toxicity in silver carp (*Hypophthalmichthys molitrix*). Chemosphere, 214: 519-533.

Wang, Q., Yang, H., Yang, M., Yu, Y., Yan, M., Zhou, L., Liu, X., Xiao, S., Yang, Y., Wang, Y. and Zheng, L. 2019. Toxic effects of bisphenol A on goldfish gonad development and the possible pathway of BPA disturbance in female and male fish reproduction. Chemosphere, 221: 235-245.

Yaghoobi, Z., Safahieh, A., Ronagh, M.T., Movahedinia, A. and Mousavi, S.M. 2017. Hematological changes in yellowfin seabream (*Acanthopagrus latus)* following chronic exposure to bisphenol A. Comparative Clinical Pathology, 26(6): 1305-1313.

Yonar, S.M., Yonar, M.E., Pala, A., Sağlam, N. and Sakin, F. 2020. Effect of trichlorfon on some haematological and biochemical changes in *Cyprinus carpio*: The ameliorative effect of lycopene. Aquaculture Reports, 16: 100246.

Yousef, M.I., Awad, T.I. and Mohamed, E.H. 2006. Deltamethrin-induced oxidative damage and biochemical alterations in rat and its attenuation by Vitamin E. Toxicology, 227(3): 240-247.

Nature Environment and Pollution Technology
An International Quarterly Scientific Journal

p-ISSN: 0972-6268
(Print copies up to 2016)
e-ISSN: 2395-3454

Vol. 19 | No. 4 | pp. 1585-1592 | 2020

Original Research Paper

https://doi.org/10.46488/NEPT.2020.v19i04.025

Open Access Journal

# Water Environment Quality Analysis Based on Information Diffusion Theory and Fuzzy Neural Network

**Hai-tao Chen, Ke-ke Xie and Wen-chuan Wang†**

School of Water Resources, North China University of Water Resources and Electric Power, Zhengzhou City, Henan Province, 450045, PR China

†Corresponding author: Wen-chuan Wang; zzchenhaitao@126.com (Hai-tao Chen)

**Nat. Env. & Poll. Tech.**
**Website: www.neptjournal.com**

*Received:* 26-12-2019
*Revised:* 16-01-2020
*Accepted:* 30-03-2020

**Key Words:**
Information diffusion theory
Fuzzy neural network
Water quality analysis
Mathematical modelling

## ABSTRACT

Reservoirs play a key role in many infrastructure functions for people like flood control, irrigation, and water supply. In this work, we focused on the water quality evaluation model for Shimen Reservoir. Based on the monthly changes of factors such as pH, nitrate, ammonia nitrogen ($NH_3$-N) and total nitrogen (TN) in 2013 and 2014, the information diffusion theory and fuzzy neural network technology were utilized to evaluate the water quality comprehensively. The probability distribution of these four factors in the reservoir was analysed and the water quality of the reservoir evaluated. The results show its reliability and these two methods can provide a basis for water quality control of Shimen Reservoir. Furthermore, the methods can be universally applied to the analysis and research of water quality in other regions..

## INTRODUCTION

The Shimen Reservoir is a large-scale water conservancy project with flood control, irrigation, and urban water supply as its main function, taking into account the functions of power generation and fish farming. Therefore, it is important to ensure the basic stability of the water quality of the reservoir. At present, there are many methods for water quality evaluation, and more methods such as single factor evaluation method, comprehensive evaluation method and Nemerow index method are used. The single-factor index method is simple to calculate, but it can only reflect the change of a single factor, so many scholars combine single-factor evaluation with other methods to get better results. Song (2018) used a single factor evaluation method combined with an improved grey correlation to evaluate water quality. Wu (2019) evaluates the groundwater environment in Pinghai Bay, Putian City based on a single factor and fuzzy mathematics comprehensive evaluation method.

Information diffusion theory can dig out more information when the amount of data is insufficient and the samples are insufficient. It can be well combined with artificial neural network models and applied to many fields. Currently, mainly involved in meteorological disasters, signal processing, geological disasters, surveying and mapping, etc. Liu et al. (2019) applied entropy information diffusion theory to the risk assessment of agricultural drought and flood disasters in the middle and lower reaches of the Yangtze River. Zhong et al. (2019) evaluation of flash flood risk was based on information diffusion method. Wang et al. (2016) used information diffusion theory to study flood and drought disaster risk characteristics in southern China. Lu et al. (2014) applied information diffusion technology in the probability analysis of grassland biological disaster risk. Besides, it is involved in some aspects such as thunderstorms, pests, typhoons and crop yields.

Regarding water environment issues, some scholars have applied the information diffusion theory. Li (2007) used the information diffusion technology to study the river health risk estimation model under the condition of incomplete information. The inspection of reservoir water quality is very complicated. Therefore, grasping the changes in the content of each element in the reservoir can better analyse the water quality and maintain the normal use of the reservoir. This paper analyses the risk probability of each element's pollution index through a combination of single factor index and information diffusion theory. It is of great significance to prevent the pollution index from exceeding the standard and the water quality to be stable.

The T-S fuzzy neural network model is an organic combination of fuzzy logic and neural networks. It inherits the advantages of both fuzzy logic and neural networks. It can represent highly nonlinear complex systems with

fewer fuzzy rules, which is very suitable for water quality evaluation. Mo et al. (2017) evaluated the water quality of the main rivers in Qinzhou based on the T-S fuzzy network model. Zhang et al. (2018) combined fuzzy neural network with LSSVM-MC to predict comprehensive water quality. Zhao (2018) uses neural networks to study early warning of aquaculture and transportation environment. This paper uses a fuzzy neural network to evaluate the water quality of the Shimen Reservoir.

## MATERIALS AND METHODS

### Single Factor Index

The single factor evaluation method is to determine the category of comprehensive water quality of the water body by the category of the single index with the worst water quality. This method is simple to calculate and can directly reflect the pollution of a single factor. With reference to the "Environmental Quality Standard for Surface Water" (GB3838-2002) Category V water standard(2002), the formula is:

$$P_i = C_i/S_i \quad \ldots(1)$$

Where, $C_i$ is the measured value of type i pollutant, and $S_i$ is the evaluation standard of type i pollutant.

When $P_i \leq 1$, it means that the water body is not polluted; when $P_i > 1$, it means that the water body is polluted.

The standard index for PH value is:

$$PH_j \leq 7.0$$
$$SPH_j = |7.0 - PH_j| / (7.0 - PH_{sd}) \quad \ldots(2)$$

$$PH_j > 7.0$$
$$SPH_j = |PH_j - 7.0| / (PH_{su} - 7.0) \quad \ldots(3)$$

Where, $PH_{sd}$ is the lower limit of the evaluation standard; $PH_{su}$ is the upper limit of the evaluation standard; and $PH_j$ is the measured value of PH.

According to the standard limit value of the supplementary project for centralized drinking water and surface water sources, the standard value of nitrate (in N) is 10 mg/L.

### Information Diffusion Theory

Information diffusion is a kind of fuzzy mathematical processing method for set-valued samples. In order to make up for the lack of information, it is considered to preferentially use the fuzzy information of samples, so as to set-valued samples.

The information diffusion method can turn a sample with observations into a fuzzy set, that is, a single-valued sample into a set-valued sample. The most commonly used model is the normal diffusion model.

Suppose that the set of actual observation samples is X, the sample series is $X=\{x_1,x_2,...,x_n\}$, and the discourse domain is $U=\{u_1,u_2,...,u_m\}$. A single-valued observation sample can carry the information spread to all points in U.

$$f_i(u_j) = \frac{1}{h\sqrt{2\pi}} \exp\left[-\frac{(x_i - u_j)^2}{2h^2}\right] \quad \ldots(4)$$

Where, $h$ is the information diffusion coefficient, which is determined according to the maximum value b, the minimum value a, and the number of samples n in the sample set. □ =

$$\begin{cases} 0.8146 \times (b-a), n = 5 \\ 0.5690 \times (b-a), n = 6 \\ 0.4560 \times (b-a), n = 7 \\ 0.3860 \times (b-a), n = 8 \\ 0.3362 \times (b-a), n = 9 \\ 0.2986 \times (b-a), n = 10 \\ 2.6851 \times \frac{(b-a)}{n-1}, n \geq 11 \end{cases} \quad \ldots(5)$$

Set

$$C_i = \sum_{j=1}^{m} f_i(u_j), i = 1, 2, \quad , m \quad \ldots(6)$$

Where, $C_i$ is the normal diffusion information sum of the observation sample $x_i$.

The membership function of the corresponding fuzzy subset is:

$$g_i = \frac{f_i(u_j)}{C_i}, i = 1, 2, \ldots, n; j = 1, 2, \ldots, m \quad \ldots(7)$$

Assume that after performing the above processing on all the samples, the number of samples with an observed value of $u_j$ is inferred to be $q(u_j)$.

Let

$$q(u_j) = \sum_{i=1}^{n} g_i(u_j) \quad \ldots(8)$$

$$Q = \sum_{j=1}^{m} q(u_j) \quad \ldots(9)$$

Q is the sum of the number of sample points at each $u_j$ point.

Table 1: Standard value of basic items for environmental quality standard for surface water (unit in mg/L).

| Classification standard valueitems | Class Ⅰ | Class Ⅱ | Class Ⅲ | Class Ⅳ | Class Ⅴ |
|---|---|---|---|---|---|
| pH (dimensionless) | 6～9 | | | | |
| $NH_3$-N | 0.15 | 0.5 | 1.0 | 1.5 | 2.0 |
| TN (N for lakes and reservoirs) | 0.2 | 0.5 | 1.0 | 1.5 | 2.0 |

$$p(u_j)=\frac{q(u_j)}{Q} \quad \ldots(10)$$

Where $p(u_j)$ is the frequency value at which the sample point falls at $u_j$, which can be used as an estimate of the probability. Its transcendence probability is:

$$p(u \geq u_j)=\sum_{k=1}^{m} p(u_k) \quad \ldots(11)$$

Where, $P(u \geq u_j)$ is the probability of exceeding .

**T-S Fuzzy Neural Network**

The T-S fuzzy system can be defined by the "if-then" rule form. In the case of the rule $R_i$, the fuzzy reasoning is as follows:

$$R_i: if\ x_1 is A_1^i, x_2 is A_2^i, \cdots, x_k is A_k^i, then\ y_i = p_0^i + p_1^i x_1 + \cdots + p_k^i x_k \quad \ldots(12)$$

Where $A_j^i$ is the fuzzy set of the fuzzy system; $p_j^i$ is the fuzzy system parameter; $y_i$ is the output obtained according to the fuzzy rules, the input part (the if part) is fuzzy, and the output part (the then part) is determined. The fuzzy inference output is a linear combination of the inputs.

T-S fuzzy system is a kind of fuzzy system with strong adaptive ability. The model can not only update automatically but also continuously modify the membership function of the fuzzy subset. It consists of an antecedent network and an after ware network.

***Antecedent network***

The first layer is the input layer. Assume that the input quantity $x = [x_1, x_2, \ldots x_k]^T$, and the number of nodes in this layer is k.

The second layer is the fuzzification layer. The membership degree of each input variable $x_j$ is calculated according to the fuzzy rules.

$$u A_j^i = \exp\left(-\frac{(x_j - c_j^i)^2}{b_j^i}\right) \quad \ldots(13)$$

Where, $c_j^i$ and $b_j^i$ are the center and width of the membership function respectively; k is the input parameter; n is the number of fuzzy subsets.

The third layer is the fuzzy rule layer. The fuzzy operator is used as the multiplication operator to perform fuzzy calculations for each membership degree.

$$\omega_i = u A_j^1(x_1) * u A_j^2(x_2) * \quad * u A_j^K(x_K) \quad \ldots(14)$$

The fourth layer is used to normalize the applicability of each rule. The calculation expression is:

$$\overline{\omega_i} = \frac{\omega_i}{\sum_{i=1}^{n} \omega_i} \quad \ldots(15)$$

***After ware network***

The first layer is the input layer, which is used to provide the constant term of the fuzzy rule follower.

The role of the second layer is to calculate each postscript of the rule.

$$y_i = p_0^i + p_1^i x_1 + \quad + p_k^i x_k \quad \ldots(16)$$

The third layer calculates the output value of the fuzzy model based on the fuzzy calculation results to achieve clear calculations.

$$y_c = \sum_{i=1}^{n} \left(p_0^i + p_1^i x_1 + \quad + p_k^i x_k\right) \overline{\omega_i} \quad \ldots(17)$$

***Algorithm learning***

The model's error analysis, coefficient correction, and parameter correction methods are as follows:

Error calculation:

$$e = \frac{1}{2}(y_d - y_c) \quad \ldots(18)$$

Where $y_d$ is the expected output of the network; $y_c$ is the actual output of the network; e is the error between the expected output and the actual output.

Coefficient correction:

$$p_j^i(k) = p_j^i(k-1) - \alpha \frac{\partial e}{\partial p_j^i} \quad \ldots(19)$$

$$\frac{\partial e}{\partial p_j^i} = (y_d - y_c)\omega_i \Big/ \sum_{i=1}^{n} \omega_i x_j \quad \ldots(20)$$

Where, $p_j^i$ is the neural network coefficient, $x_j$ is the learning efficiency of the network, $x_j$ is the network input parameter, and $\omega_i$ is the membership product of input parameters.

Parameter correction:

$$c_j^i(k) = c_j^i(k-1) - \beta \frac{\partial e}{\partial c_j^i} \quad \ldots(21)$$

$$b_j^i(k) = b_j^i(k-1) - \beta \frac{\partial e}{\partial b_j^i} \quad \ldots(22)$$

Where, $c_j^i$ and $b_j^i$ are the centre and width of the membership function, respectively.

Empirical formula for the number of nodes in the hidden layer:

$$M = \sqrt{I + O} + a \quad \ldots(23)$$

Table 2: T-S fuzzy neural network construction parameter table.

| I | O | M | Recommended M value |
|---|---|---|---|
| 2 | 1~3 | 4~8 | 8 |
| 3 | 1~4 | 5~9 | 8 |
| 4 | 1~5 | 6~10 | 10 |
| 5 | 1~5 | 8~12 | 10 |
| 6 | 1~3 | 9~14 | 12 |

Where, M is the number of nodes in the hidden layer; I is the number of nodes in the input layer; O is the number of nodes in the output layer

**Survey of Research Area**

Shimen Reservoir is located at 122°45'00""east longitude and 40°22'00""north latitude. It is a large-scale water conservancy project with flood control, irrigation, and urban water supply as its main function while taking into account power generation and fish farming functions. The maximum dam height is 47 meters, the dam is 350 meters long, the annual runoff is 117 million cubic meters, and the total storage capacity is 102.2 million cubic meters. The reservoir provides an average of 25 million cubic meters of industrial and urban domestic water and 36 million cubic meters of agricultural water to Yingkou and Gaizhou. Reservoir operation has played a huge benefit and harm removal benefits

## RESULTS AND ANALYSIS

In this paper, the monthly pH, nitrate, ammonia nitrogen, and total nitrogen contents of Shimen Reservoir in 2013 and 2014 were selected to ensure the stability of the water environment of the reservoir. The feasibility of the information diffusion theory and T-S neural network in the analysis of reservoir water quality was verified. The main research contents are as follows:

(1) After determining the single factor index of each element, use information diffusion technology to process each single factor index to analyse the occurrence probability of pH, nitrate, ammonia nitrogen and total nitrogen in Shimen Reservoir.

(2) The T-S fuzzy neural network was used to evaluate the water quality of the Shimen Reservoir in 2013 and 2014.

Table 3: Probability of exceeding the pH single factor index.

| Single factor index | Probability |
|---|---|
| 0 | 1.000000 |
| 0.1 | 0.831928 |
| 0.2 | 0.502622 |
| 0.3 | 0.287776 |
| 0.4 | 0.215550 |
| 0.5 | 0.161780 |
| 0.6 | 0.065910 |
| 0.7 | 0.005141 |
| 0.8 | 0.000040 |
| 0.9 | 0.000000 |
| 1.0 | 0.000000 |

**Water Quality Analysis of Shimen Reservoir Based on Information Diffusion Theory and Single Factor Index**

The single factor index corresponding to the four factors was calculated from Equations 1-3. According to the information diffusion theory, each single factor index is used as the information diffusion sample for diffusion. $X_1$, $X_2$, $X_3$ and $X_4$ are information diffusion samples of pH, nitrate, ammonia nitrogen, and total nitrogen, respectively. With reference to the "Environmental Quality Standard for Surface Water" (GB3838-2002), the set [0,1] of one-dimensional space can be used to take points at equal intervals as the discourse of each factor. Set the discrete domain of PH as: $U_1 = \{0,0.1,0.2,...,1\}$; the discre≤te domain of nitrate as: $U_2 = \{0,0.1,0.2,...,1.4\}$; the discrete domain of NH3-N as: $U_3 = \{0,0.025,0.05,...,0.325\}$ and the discrete domain of TN as: $U_4 = \{1.0,1.6,1.7,...,2.5\}$. Then the control points of PH, nitrate, NH3-N and TN are $m_1$=11, $m_2$=15, $m_3$=14, $m_4$=16. The number of samples is n = 24. According to formula 4-11, the diffusion coefficients of each factor can be obtained as $h_1 = 0.064209$, $h_2 = 0.075883$, $h_3 = 0.019496$, $h_4 = 0.093395$. Surpassing probability of each factor is given in Tables 3-6, and the probability density and surpass probability of the four elements in Figs. 1-4.

It can be seen from the Figs. 1-4 that the probability of the corresponding single factor index of four elements in Shimen Reservoir appears. The maximum probability of pH is $SPH_j = 0.1$, which is 32.93%. Nitrate has the highest probability at 46.13%; $NH_3$-N has the highest probability at 18.99% and TN has the highest probability at 23.78%.

It can be seen from Fig. 1 and Table 3 that the transcendental probability curve of pH is on the side less than 1. Therefore, the pH value of the Shimen Reservoir is relatively stable.

It can be known from Table 5 and Fig. 2 that the single factor exponential distribution of nitrate is distributed on the side of Pi≤1.

Table 4: Probability of exceeding the nitrate single factor index.

| Single factor index | Probability |
|---|---|
| 0 | 1.000000 |
| 0.1 | 0.999637 |
| 0.2 | 0.981154 |
| 0.3 | 0.783971 |
| 0.4 | 0.322698 |
| 0.5 | 0.074134 |
| 0.6 | 0.042579 |
| 0.7 | 0.041663 |
| 0.8 | 0.040967 |
| 0.9 | 0.031620 |
| 1.0 | 0.009881 |
| 1.1 | 0.000688 |
| 1.2 | 0.000009 |
| 1.3 | 0.000000 |
| 1.4 | 0.00000 |

Table 5: Probability of exceeding the $NH_3$-N single factor index.

| Single factor index | Probability |
|---|---|
| 0 | 1.000000 |
| 0.025 | 0.985991 |
| 0.05 | 0.911267 |
| 0.075 | 0.761674 |
| 0.1 | 0.571740 |
| 0.125 | 0.398739 |
| 0.15 | 0.258229 |
| 0.175 | 0.164238 |
| 0.2 | 0.078687 |
| 0.225 | 0.015765 |
| 0.25 | 0.000952 |
| 0.275 | 0.000014 |
| 0.3 | 0.000000 |
| 0.325 | 0.000000 |

That is, the nitrate content of the water body meets the standard.

From Table 6 and Fig. 3, when $P_i'' \leq 0.075$, the content of $NH_3$-N conforms to type I water, and the probability of occurrence is $P \geq 76.17\%$; when $0.075 < P_i \leq 0.25$, the $NH_3$-N content accords with the water of class II, and the probability of occurrence at this time is $76.17\%'' \leq P'' \leq 0.09\%$. That is, most of the ammonia nitrogen content in the water body meets the standards of Class I and II water.

It is clear from Table 7 and Fig. 3 that the single factor index of total nitrogen in the water body is greater than 1. Therefore, the biggest cause of water pollution may be excessive nitrogen content.

## Water Quality Evaluation of Shimen Reservoir Based on T-S Fuzzy Neural Network

Table 6: Probability of exceeding the TN single factor index.

| Single factor index | Probability |
|---|---|
| 1.0 | 1.000000 |
| 1.1 | 1.000000 |
| 1.2 | 0.999999 |
| 1.3 | 0.999912 |
| 1.4 | 0.997685 |
| 1.5 | 0.978861 |
| 1.6 | 0.904393 |
| 1.7 | 0.813638 |
| 1.8 | 0.690715 |
| 1.9 | 0.498245 |
| 2.0 | 0.260474 |
| 2.1 | 0.103946 |
| 2.2 | 0.043997 |
| 2.3 | 0.013959 |
| 2.4 | 0.003121 |
| 2.5 | 0.000000 |

The basic steps and evaluation results of Shimen reservoir water quality evaluation based on T-S fuzzy neural network are as follows:

(1) Selected network structure: The construction of the fuzzy neural network determines the number of input and output points of the fuzzy neural network according to the dimensions of the training samples. Selected four indicators of pH, nitrate, $NH_3$-N and TN, so the number of input nodes is 4. Water quality levels I-V are represented by numbers 1-5, and the number of output nodes is 1. It can be known from Table 2 that the number of nodes in the hidden layer is 10, so a 4-10-1 network structure is formed.

(2) Generate training samples: In this paper, 400 sets of training samples are generated by interpolating water quality index standard data "Environmental Quality Standard for Surface Water" (GB3838-2002) with the evenly spaced distribution. Obtain water quality level indicators based on network predictions. When the predicted value is less than 1.5, the water quality level is Class I; when the predicted value is 1.5 to 2.5, the water quality level is Class II; when the predicted value is 2.5 to 3.5, the water quality level is Class III; when the predicted value is 3.5 to 4.5 When the predicted value is greater than 4.5, the water quality level is Category V.

(3) Network training and testing: The training sample is used to train the fuzzy neural network 100 times. The training result is shown in Fig. 5. Fifty sets of data were drawn from a random sample to verify the accuracy of the model. The verification results are shown in Fig. 6.

It can be seen from Fig. 6 that the error between the actual water quality level and the model output water quality level is small, and it can play an accurate prediction role.

(4) Water quality evaluation: Select the content of pH, nitrate, $NH_3$-N and TN from month to month from 2013 to 2014. The trained T-S fuzzy neural network was used to evaluate the Shimen reservoir. The evaluation results are shown in Fig. 7. It can be seen from the figure that the water quality level of Shimen Reservoir is basically maintained at Class III and IV, and the water environment is relatively stable.

## CONCLUSIONS

(1) 24 sample data are selected in this paper. The nitrate, $NH_3$-N, TN and pH in Shimen Reservoir were evaluated based on single factor index and information diffusion theory. The results show that the pH, nitrate and ammonia nitrogen in Shimen Reservoir are stable and meet

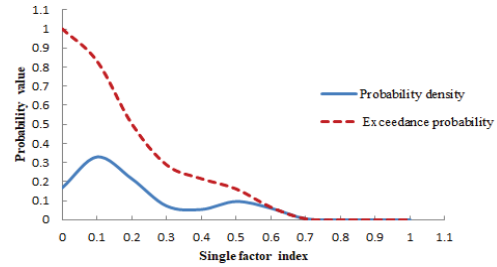


Fig.1: Probability distribution of the pH single factor index.

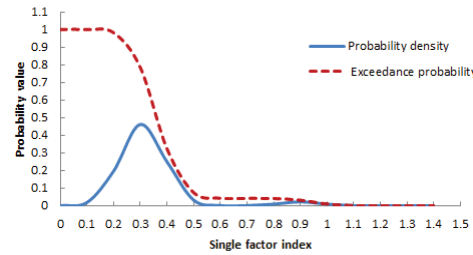


Fig. 2: Probability distribution of the nitrate single factor index.

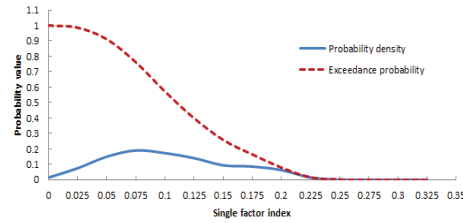


Fig.3: Probability distribution of the $NH_3$-N single factor index.

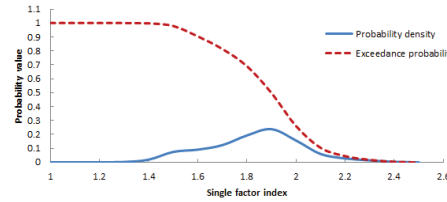


Fig.4: Probability distribution of the TN single factor index.

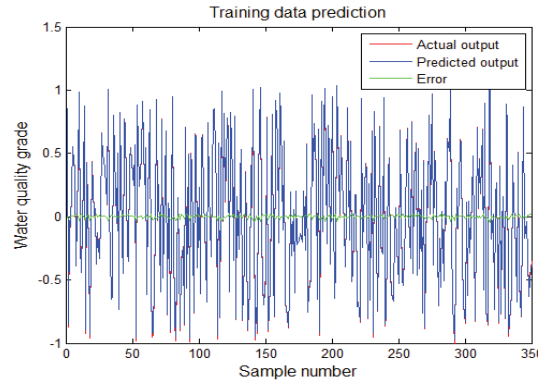


Fig. 5: Prediction simulation results of training data of fuzzy neural network model.

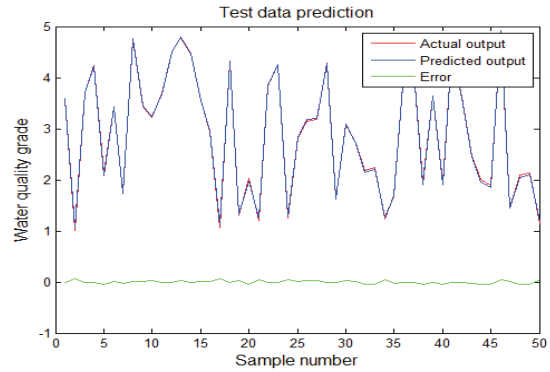


Fig. 6: Prediction simulation results of fuzzy neural network test data.

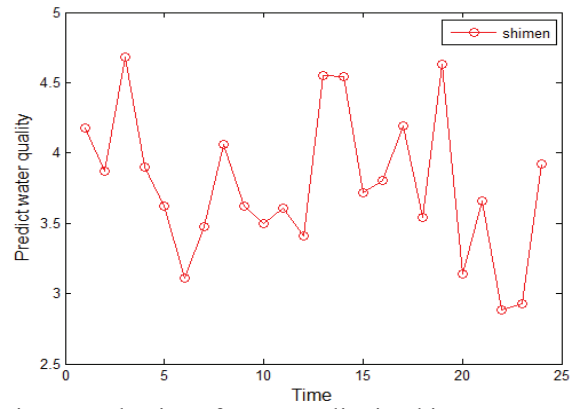


Fig. 7: Evaluation of water quality in Shimen Reservoir by the fuzzy neural network.

national standards, but the total nitrogen contents are significantly higher than the standard.

(2) Analysis of water quality of Shimen Reservoir from 2013 to 2014 based on T-S fuzzy neural network. The results show that the comprehensive water quality of Shimen Reservoir is good and stable.

(3) It is feasible to use information diffusion technology combined with single factor index to evaluate water quality. The analysis results are clear and have guiding significance for the water quality control of Shimen Reservoir. T-S fuzzy neural network fuzzy takes single factor prediction as input and comprehensive evaluation

as output. It has effectively evaluated the water environment quality of the Shimen Reservoir and obtained good evaluation results.

## REFERENCES

GB3832-2002 Environmental Quality Standard for Surface Water [S]. National Environmental Protection Agen. Standards Press of China, Beijing.

Ji, Q. 2017. Evaluation of *Matsucoccus sinensis* Hazarb based on information diffusion theory. Hubei Agricultural Sciences. 56(02): 273-275.

Jia, Z.H. and Li, X.G. 2017. Analysis on variation characteristics of Dagu river based on T-S fuzzy neural network. Environmental Science and Management. 42(01): 50-54.

Jin, B., Du, Z.X. and Xue, S.C. 2018. Operation reliability assessment of straddle monorail vehicle based on T-S fuzzy neural network. Urban Mass Transit, 21(08): 77-81+85.

Li, M. 2007. The Study of risk estimation model of river health by incomplete information. Xi'an University of Technology.

Liu, Y., You, M., Zhu, J., Wang, F. and Ran, R. 2019. Integrated risk assessment for agricultural drought and flood disasters based on entropy information diffusion theory in the middle and lower reaches of the Yangtze River, China. International Journal of Disaster Risk Reduction, 38: 101194.

Lu, H., Yang, L.Z. and Gao, J.M. 2014. The application of information diffusion technique in probabilistic analysis to grassland biological disasters risk. Ecological Modelling, 272: 264-270.

Luo, B.L., Zhang, C. and Huang, W.H. 2009. Flooding Risk Assessment of Rice Production Based on Information Diffusion in Hunan Province. Chinese Journal of Agrometeorology.30(3): 458-462.

Mo, C.X., Ruan, Y.L., Mo, G.Y. et al. 2017. Water quality assessment of main rivers in Qingzhou city based on T-S fuzzy neural network. Pearl River, 38(8): 80-83.

Song, R.W. 2018. Application of single factor evaluation method and improved grey correlation degree in water quality evaluation. Shaanxi Water Resources. 3: 103-107.

Wang, Y., Zhang, Q. and Han, L.Y. 2016. Risk characteristics of flood and drought disasters in southern China based on information diffusion theory. Journal of Arid Meteorology, 34(06): 919-926.

Wu, M. 2019. Assessment of groundwater environment for Pinghai Bay, Putian City based on single factor evaluation method and fuzzy comprehensive evaluation method. Heilongjiang Environmental Journal, 43(03): 49-54.

Zhang, Z.Y., Zhang, X.P., Zhang, L. et al. 2018. Integrated water quality prediction based on LSSVM-MC and fuzzy neural network. Jiangxi Science, 36(02): 331-334+339.

Zhao, Y.T. 2018. Research on environment early-warning of aquaculture and transportation based on fuzzy neural network. Shanghai Ocean University.

Zhong, M., Wang, J., Gao, L. et al. 2019. Fuzzy risk assessment of flash floods using a cloud-based information diffusion approach. Water Resources Management, 33(7): 2537-2553.

Nature Environment and Pollution Technology
An International Quarterly Scientific Journal

p-ISSN: 0972-6268
(Print copies up to 2016)
e-ISSN: 2395-3454

Vol. 19 | No. 4 | pp. 1593-1598 | 2020

Original Research Paper

https://doi.org/10.46488/NEPT.2020.v19i04.026

Open Access Journal

# Influence of Government Subsidies for Green Technology Development on the Performance of Chinese New-Energy Automobile Enterprises

**Hongjun Xiong* and Yi Shen**†**

*School of Business, Shanghai Dianji University, Shanghai 201306, China

**Higher Education Research Institute, Shanghai University of Engineering Science, Shanghai 201620, China

†Corresponding author: Yi Shen Email: hnshenyi1990@163.com

**Nat. Env. & Poll. Tech.**
**Website: www.neptjournal.com**

*Received:* 08-06-2020
*Revised:* 10-09-2020
*Accepted:* 27-09-2020

**Key Words:**
Green Technology
New energy vehicles
Government subsidies
Foton automobile
New-energy resources
Financial performance

## ABSTRACT

Recently, facing situations of insufficient energy and harsh environmental conditions, new-energy vehicles begin to enter people's lives. But considering many factors such as price and market acceptance development of new-energy automobile market must not lack government incentives. In recent two years, the government's subsidy for green technology development to new-energy automobile enterprises has entered the post-subsidy era. To explore the sustainable development of new-energy automobile enterprises, Foton automobile was selected as the research object and the scale of government subsidy for green technology development to Foton automobile was clearly defined, the performance was analyzed by using multiple regression method. Results show that government subsidy and tax return for green technology development have a positive effect on Foton automobile's performance, environmental regulation stringency has a significant positive moderating effect. Referring to the conclusions, some suggestions were put forward for Foton automobile's future development and the development of new-energy automobile industry.

## INTRODUCTION

As the international environment continues to change and various advanced technologies continue to change, environmental and energy issues are becoming more and more prominent and countries are attaching more and more importance to environmental protection. Traditional cars need to consume a large amount of oil and emit carbon monoxide, carbon dioxide, hydrocarbon chemicals and other waste gas, polluting the air environment. In such an environment, new-energy vehicles emerge as the times require (Chu et al. 2018). However, as new-energy vehicles need the support of high-end technologies, there is no advantage in price, and the market acceptance of new-energy vehicles is not high compared with traditional cars at present. Therefore, the development of new-energy vehicles enterprises and industries requires a series of subsidies and policy support for green technology development from the government.

In 2010, China's government issued a new-energy subsidy policy to support green technology development. In recent years, with the change of market conditions, the government subsidy policy for green technology development has been changing constantly in the continuous process. In 2016, the Ministry of Finance exposed the "subsidy fraud" of some auto companies. Starting from 2018, relevant government departments' support measures for relevant enterprises are significantly lower than before, which can be described as entering the "post-subsidy era".

As early as 2011, the production and sales volume of new-energy vehicles in China was very low, which was only 820,000 units. According to the overall automobile production in 2011, the proportion of new-energy vehicles was less than 1‰. By 2018, however, tremendous changes had taken place. The annual sales volume reached 1.27 million, accounting for 4.5% of the total automobile production and sales volume, and the production and sales volume increased by more than 150 times. From 2011 to 2018, both the production and sales volume, as well as the proportion of total automobile production and sales volume in China, showed an amazing development speed.

The ministry of industry and information technology has released the audit report on the promotion and application of new-energy vehicles for the first time since May 2017. According to the latest report, the number of new-energy vehicles receiving government subsidies for green technology development totaled 615,100, and the number of subsidies to be liquidated reached 62.4 billion RMB. The specific situation is shown in Table 1.

Table 1: New-energy vehicles to promote the application of clearing table.

| Year of the vehicle | Enterprise declaration and promotion (unit) | Liquidation fund (ten thousand RMB) | Number of promotions approved by the expert group (unit) | Subsidy funds to be liquidated (ten thousand RMB) | Time of public notice | Batch |
|---|---|---|---|---|---|---|
| 2016 | 94,072 | 641,482 | 85,094 | 585,936 | 2017.05.17 | First |
| 2016 | 71,446 | 320,804 | 71,199 | 314,263 | 2017.09.07 | Second |
| 2016 | 57,816 | 1,684,109 | 57,494 | 1,676,431 | 2017.11.28 | Third |
| 2016 | 51,016 | 1,246,311 | 50,208 | 1,233,058 | 2018.05.25 | Fourth |
| 2017 | 230,616 | 960,115 | 161,667 | 664,099 | 2018.05.25 | Fourth |
| 2016 | 10,952 | 266,020 | 10,876 | 264,500 | 2018.09.25 | Fifth |
| 2017 | 85,717 | 274,872 | 78,011 | 244,319 | 2018.09.25 | Fifth |
| 2015 | 30,936 | 330,055 | 29,034 | 300,088 | 2019.03.19 | Sixth |
| 2016 | 72,614 | 968,440 | 71,546 | 957,937 | 2019.03.19 | Sixth |
| Total | 705,185 | 6,692,208 | 615,129 | 6,240,631 | | |

The cumulative sales volume of new-energy vehicles in China increased continuously from the first quarter of 2016 to the third quarter of 2019. The quarterly sales volume of new-energy vehicles fluctuated and increased from the first quarter of 2016 to the fourth quarter of 2018, and showed the characteristic of quarterly change from 2017 to 2018, which meant that the sales volume kept rising from the first quarter to the fourth quarter. In addition, it could be found that the sales volume in the second and third quarters of 2019 was lower than that in the same period of 2018, which was most likely due to the serious decline of government subsidies for new-energy vehicles during this period. It could be seen that government subsidies for green technology development had played a positive role in promoting the overall performance of the industry.

Had new-energy automobile enterprises used government subsidies to enhance their strength? Did government subsidies and policy support for green technology development promote the pace of development of each enterprise and the whole industry? What would companies need to do to cope with future subsidy declines? Therefore, it is of great significance for both the government and enterprises to study the influence of government subsidies for green technology development on the performance of new-energy automobile enterprises.

## PAST STUDIES

Government subsidies mainly referred to the free monetary and non-monetary economic subsidies provided by the government to enterprises. The purpose was to promote the upgrading and development of enterprises and industries, to optimize the allocation of social resources, and to promote the balance of social supply and demand. Government subsidies were generally free and conditional. Therefore, government subsidies did not affect the ownership of enterprises, and enterprises in turn had no obligation to repay the assets to relevant departments in the future. But enterprises would be limited in their use of government subsidies. At present, subsidies for green technology development of the Chinese government to the new-energy automobile enterprises were mainly in the form of direct subsidies and tax incentives. In 2012, the government just issued a new energy vehicle subsidy policy, vigorously advocating the purchase of new energy vehicles, and adopting different subsidy rules according to different models. In 2013, the subsidy rate was reduced by 5%, and in 2014, the subsidy rate was reduced by 10%. In 2017, the subsidy policy was substantially adjusted to further improve the subsidy rules from requirements of energy consumption, mileage and power battery standards. The requirements of electric passenger cars were strictly stipulated to avoid cheating and compensation. In addition to large subsidies to businesses, consumers could enjoy exemption from vehicle purchase tax when they buy a car. In addition, electric vehicles in new energy vehicles could also enjoy an additional exemption from consumption tax. At the same time, new-energy automobile manufacturers, if they met the requirements for the recognition of high-tech enterprises, might pay enterprise income tax at a tax rate of 15%, and allow additional deductions based on research and development expenses (Han 2019).

It was found that government subsidy would slow down the growth of enterprises in terms of performance and scale, which would have a negative influence on the performance of enterprises (Fredrik 2000). Okamuro & Nishimura (2015) pointed out that government subsidy could improve innovation performance. Research showed that non-tax subsidies had a greater influence on the cost of debt and social performance than tax subsidies. Government subsidies to university-industry research collaborations through financial subsidies could improve innovation performance, and financial subsidy from the government would slow down the growth of enterprises in terms of performance and scale, which would have a negative influence on the performance of

enterprises (Beason 2015). In addition, supporting measures of relevant departments could also promote development pace of some small and medium-sized enterprises that attached importance to advanced technology (Du & Huang 2020). Although direct replenishment funds of relevant subsidy policies were relatively limited, the atmosphere in the industry tended to be optimistic due to the encouragement of government departments, which indirectly introduced capital from outside the industry into the industry. Relevant subsidy measures further encouraged the enthusiasm of technological innovation of relevant enterprises and guide their development direction (Xu et al. 2016, Kolkis 2019). Support policies of relevant departments could positively affect the financial performance of enterprises with little force (Roper & Hewitt-Dundas 2015, Votinov et al. 2020).

Government subsidies would cause enterprises to become dependent on subsidy funds and even lead to non-productive investment behaviours, which would reduce the financial performance of enterprises and hinder the improvement of the innovation ability of enterprises (Syed & Kamel 2018, Miguel et al. 2020). Due to the information asymmetry between government and enterprises, and the motivation of enterprises to maximize profits, enterprises could apply for subsidies without conducting research and development, namely, showing the problem of enterprises cheating for subsidies.

## MATERIALS AND METHODS

In the study, 79 enterprises' data on two core explanatory variables of government subsidy (*Gov*) and tax return (*Tax*) in 2018, the moderating variable of environmental regulation stringency (*ERS*), and the control variables of total asset size (*Size*), listed age (*Age*), and revenue growth rate (*Rgr*) were selected. The explained variable was analyzed by a cross-sectional regression method. The regression analysis of the performance (*Perf*) was carried out. Because of the cross-sectional data, data of different enterprises were independent of each other. Therefore, before regression, stability test can be avoided, and only some data need to be logarithmically processed. The processed variables can be shown as government subsidies (*Gov*), tax returns (*Tax*), and total asset size (*Size*). The selection and definition of specific indicators are shown in Table 2.

## RESULTS ANALYSIS

**Scale of government subsidy for green technology development granted to Foton automobile:** According to the data of the enterprise's annual report and quarterly report, the number of government subsidies for green technology development Foton automobile received from 2012-2019 is shown in Table 3.

The number of government subsidies that Foton received from 2012 to 2015 was increasing. In 2012, it received a total of 33.90 million RMB of government subsidies, and in 2015, it reached 90.23 million RMB, achieving an increase of 166.29%. Since 2016, the number of government subsidies received by Foton automobile had been declining. The subsidy in 2018 was only 22.35% of that in 2015. In 2019, the number of government subsidies for green technology development received was close to that in 2018.

According to the annual report of Foton automobile, the ways included financial allocation and tax refund. In terms of financial allocation, the subsidies received by Foton automobile in 2012-2015 mainly included automobile

Table 2: Definition of variables.

| Variable | Variable name | Variable symbol | Variable explain |
|---|---|---|---|
| Dependent variable | Performance | Perf | Market value/total assets |
| Independent variable | Government subsidies | Gov | Log(government subsidies) |
| | Tax refund | Tax | Log(tax refund) |
| Moderating variable | Environmental Regulation Stringency | ERS | Strict degree of regional environmental regulation |
| Control variable | Total asset size | Size | Log(total assets) |
| | Listed age | Age | Observed year and established year impairment |
| | Revenue growth rate | Rgr | Main revenue of the current period-main revenue of the previous period)/main business income of the previous period |

Table 3: Amount of Government subsidy for green technology government of Foton automobile from 2012 to 2019.

| Year | Amount (ten thousand RMB) | Year | Amount (ten thousand RMB) |
|---|---|---|---|
| 2012 | 33895.24 | 2016 | 85719.75 |
| 2013 | 46777.66 | 2017 | 37443.37 |
| 2014 | 72737.32 | 2018 | 20169.14 |
| 2015 | 90230.06 | 2019 | 19805.21 |

R&D subsidies, automobile basic research fund subsidies, energy-saving automobile subsidies for green technology development, etc. After 2016, the government subsidies for green technology development received by Foton automobile mainly focused on automobile R&D, production and sales.

**Regression result:** The correlation between independent variables and dependent variables is given in Table 4. Government subsidy (*Gov*), tax return (*Tax*), and total asset size (*Size*) have a significant positive relation with revenue growth rate (*Rgr*). In addition, total asset size (*Size*) has a significant positive relation with listed age (*Age*).

According to index and relative data, the regression result is given in Table 5. It shows that the influence of government subsidies (*Gov*) on performance (*Perf*) is significantly positive at 5% level, and the coefficient is 0.07, which can be shown in equation (1).

$$Perf = 0.89 + 0.07Gov + 0.57Size - 0.11Age + 1.22Rgr \quad (1)$$

The influence of tax return (*Tax*) on performance (*Perf*) is significantly positive at 5% level, and the coefficient is 0.06, which can be shown in equation (2)

$$Perf = 0.31 + 0.06Tax + 1.45Size + 0.15Age + 0.58Rgr \quad (2)$$

When the moderating variable of environmental regulation stringency (*ERS*) is introduced, the influence of government subsidies (*Gov*) on performance (*Perf*) is significantly positive at 1% level, and the coefficient is 0.23, which can be shown in equation (3). It means that under the situation of environmental regulation, new-energy automobile enterprises tend to get better performance by using government subsidies, which shows lager coefficient and higher significance level.

$$Perf = 1.32 + 0.23Gov + 1.11ERS \times Gov + 0.89Size - 1.24Age + 0.98Rgr \quad (3)$$

The influence of tax return (*Tax*) on performance (*Perf*) is significantly positive at 1% level under environmental regulation, and the coefficient is 0.14, which can be shown in equation (4). It means that under the situation of environmental regulation, the coefficient is larger and the significant level is improved. Due to tax return, new-energy automobile enterprises get more capital in green technology development. Strict regulation may constrain enterprise behaviour.

$$Perf = 0.67 + 0.14Tax + 0.53ERS \times Tax + 0.66Size + 0.35Age + 1.21Rgr \quad (4)$$

Under environmental regulation, the influence of government subsidies (*Gov*) on performance (*Perf*) is significantly positive at 5% level, and the coefficient is 0.35. The influence of tax return (*Tax*) on performance (*Perf*) is significantly positive at 5% level, and the coefficient is 0.10, which can be shown in equation (5).

$$Perf = 0.78 + 0.35Gov + 1.10Tax + 0.89ERS \times Gov + 0.25ERS \times Size - 0.12Age + 0.84Rgr \quad (5)$$

Through the analysis, the following results are drawn. Firstly, the government subsidies for green technology development of China's new-energy automobile industry are characterized by large overall subsidies and large differences in the number of government subsidies received by different enterprises. And relevant documents show that the government subsidies to new-energy automobile enterprises will be withdrawn shortly. At present, China had issued several policies to encourage new-energy automobile enterprises to strengthen technological transformation and upgrading and increased support and government subsidies. However, from the actual effect, it was not ideal. It was mainly reflected in the fact that the core technology of new-energy enterprises had not made great progress, and the problems such as the endurance and security of new-energy technology have not been completely solved (Samanta et al. 2019). At the same time, after obtaining government subsidies, some enterprises did not fully invest in green technology research and development, but invested their funds in real estate, stock market, etc., resulting in a large amount of capital waste, which was not conducive to the whole industry

Secondly, after a specific empirical analysis, it is found that government subsidies for green technology development have a significant positive influence on the performance of relevant enterprises. At the significance level of 5%, the

Table 4: Correlation between independent variables and dependent variables of the samples.

| | Gov | Tax | ERS | Size | Age | Rgr |
|---|---|---|---|---|---|---|
| Gov | 1 | -0.07 | 0.16 | 0.01 | -0.09 | 0.24** |
| Tax | -0.07 | 1 | 0.08 | -0.04 | 0.02 | 0.12* |
| ERS | 0.16 | 0.08 | 1 | 0.13 | 0.05 | 0.21* |
| Size | 0.01 | -0.04 | 0.13 | 1 | 0.17* | 0.32** |
| Age | -0.09 | 0.02 | 0.05 | 0.17* | 1 | 0.05 |
| Rgr | 0.24** | 0.12* | 0.21* | 0.32** | 0.05 | 1 |

Note: *, ** and *** indicate that the parameter estimates are significant at the level of 1%, 5%, and 10%, respectively.

Table 5: Regression results.

| Independent variable | Model (1) | Model (2) | Model (3) | Model (4) | Model (5) |
|---|---|---|---|---|---|
| | Coefficient (t) | | | | |
| c | 0.89*** | 0.31** | 1.32 | 0.67** | 0.78* |
| | (5.68) | (2.47) | (0.56) | (2.12) | (1.69) |
| Gov | 0.07** | | 0.23*** | | 0.35** |
| | (2.44) | | (4.67) | | (2.29) |
| Tax | | 0.06* | | 0.14*** | 0.10** |
| | | (1.88) | | (6.43) | (2.44) |
| ERS*Gov | | | 1.11** | | 0.89* |
| | | | (2.40) | | (1.74) |
| ERS*Tax | | | | 0.53* | 0.25* |
| | | | | (1.73) | (1.87) |
| Size | 0.57*** | 1.45** | 0.89** | 0.66*** | 0.53*** |
| | (3.78) | (2.14) | (2.39) | (5.12) | (7.32) |
| Age | -0.11* | 0.15** | -1.24* | 0.35** | 0.12* |
| | (-1.77) | (1.99) | (-1.85) | (2.15) | (1.72) |
| Rgr | 1.22** | 0.58** | 0.98* | 1.21 | 0.84** |
| | (2.01) | (2.25) | (1.91) | (1.26) | (2.47) |

Note: *, ** and *** indicate that the parameter estimates are significant at the level of 1%, 5%, and 10%, respectively.

coefficients of government subsidies and tax refunds are 0.06 and 0.02, respectively. This means that government subsidies for green technology development can promote new-energy automobile enterprises to continue to carry out technology research and development, to improve their technological level and enhance their competitive strength. Finally, sustainable development ability may be gained (Dou et al. 2019, Elston 2019).

Thirdly, through a case study of Foton automobile, it is found that the government subsidies for green technology development have a significant positive effect on the profitability, operation ability and growth ability, but it has no obvious effect on the debt-paying ability. In general, government subsidies for green technology government have a significant positive influence on the performance, and to some extent, government subsidies have improved the performance of Foton automobile. From the performance point of view, profit and growth can reflect the sustainable competitive advantage of new-energy automobile enterprises. Foton automobile can continue to invest in R&D, continuously launch green products and innovate and upgrade green technology by obtaining government subsidies for green technology development, to not only make continuous profits but also to promote its rapid growth. At the same time, it can also drive the whole new-energy automobile industry to transform into green technology and green energy.

Fourthly, after introducing the moderating variable of environmental regulation stringency, the influence of both government subsidies and tax return on performance is enhanced, which may explain that environmental regulation may have a strict requirement of using the subsidies. New-energy automobile enterprises should use these subsidies in green technology development, to improve the core competitiveness and sustainable development capacity. With relative regulations, most enterprises may have capital embezzlement, which may lead to a vicious cycle.

## CONCLUSION

It can be concluded that government subsidies for green technology development have a significant positive effect on the performance of new-energy automobile enterprises. To sum up, government subsidies for green technology development have a significant positive influence on Foton automobile's performance, which to some extent improves its' performance.

Through the analysis of this study, it can be found that development position shown and disclosed by some companies is not true. Therefore, enterprises should be aware of this situation. While receiving and applying government subsidies for green technology development, attention should be paid to research, development and innovation. A series of measures should be adopted to improve operating conditions and strength, to achieve independent and sustainable development.

Due to the emergence of many failure cases, China's subsidies to new-energy automobile enterprises are becoming less and less. Enterprises should be able to make good use of subsidies to promote their development, rather than relying on government subsidies for green technology

development. It can be found that government subsidies for green technology development can play a positive role in promoting the performance of enterprises. It also takes into account the decline and withdrawal of government subsidies. What's more, the government should introduce relevant environmental regulations in succession, because requirements of these regulations may supervise enterprises to increase green technology development input, and standardize the use of government subsidies. In addition, what enterprises need to do is increasing R&D input, to get sustainable development ability. Therefore, investors in the market should conduct in-depth research and analysis on the performance of the intended investment enterprises, and consider the factor of government subsidies, so as to reduce investment risks to some extent.

## ACKNOWLEDGEMENT

This study was supported by Grant from the Development Center of Shanghai Municipal People's Government (2019-U-A02).

## REFERENCES

Beason, R. 2015. Growth economies of scale, and targeting in Japan. The Review of Economics and Statistics, 25(2):286-295.

Chu, Y.L., Wang, J.W. and Cheng, Z. 2018. China's "mercantilist" government subsidies, the cost of debt and firm performance. Journal of Banking and Finance, 40(86): 37-52.

Dou, Y., Masulis, R. W. and Zein, J. 2019. Shareholder wealth consequences of insider pledging of company stock as collateral for personal loans. The Review of Financial Studies, 32(12): 4810-4854.

Du, Y.C. and Huang, R.K. 2020. Research on the core competitiveness of pharmaceutical listed companies based on fuzzy comprehensive evaluation. Journal of Intelligent and Fuzzy Systems, 38(6): 6971-6978.

Elston, J. 2019. Corporate governance: What we know and what we don't know. Journal of Industrial and Business Economics, 46(2): 147-156.

Fredrik, B. 2000. Capital subsidies and the performance of firms. Small Business Economics, 10(3): 183-193.

Han, X.N. 2019. Effect assessment of new energy vehicle subsidy policy: A case study of BYD. Guide to Economic Research, 15(9): 149-153.

Kolkis, S. 2019. Benchmarking the sustainability of urban energy, water and environment systems and envisioning a cross-sectoral scenario for the future. Renewable and Sustainable Energy Reviews, 103: 529-545.

Miguel, M., Carolina, B. and Kepa, M. 2020. How to improve supplier selection for complex items using Product Engineering: perspectives from the industry. DYNA, 95(3): 270-275.

Okamuro, H. and Nishimura, J. 2015. Not just financial support, another role of public subsidy in university–industry research collaborations. Economics of Innovation and New Technology, 24(7): 633-659.

Roper, S. and Hewitt-Dundas, N. 2015. Knowledge stocks, knowledge flows and innovation: evidence from matched patents and innovation panel data. Research Policy, 44(7): 1327-1340.

Samanta, N., Guha, S.K. and Majumdar, A. 2019. Evolution of corporate governance in India and its influence on the growth of the financial market: An empirical analysis (1995-2014). Corporate Governance International Journal of Business in Society, 19(1): 230-245.

Syed, A.T. and Kamel, F. 2018. Exploring the relationships of strategic entrepreneurship and social capital to sustainable supply chain management and organizational performance. International Journal of Productivity and Performance Management, 67(9): 2046-2070.

Votinov, M., Smirnova, O. and Liubchenko, M. 2020. The main directions of the humanization of industrial objects in urban environment. Tehnicki Glasnik-Technical Journal, 14(1): 60-65.

Xu, F.J., Du, Y.C. and Yu, Y.B. 2016. Research on relationship between ownership structure and financial performance of agricultural listed corporations in china. Agro Food Industry Hi-Tech, 27(6): 10-15.

Nature Environment and Pollution Technology
An International Quarterly Scientific Journal

p-ISSN: 0972-6268
(Print copies up to 2016)
e-ISSN: 2395-3454

Vol. 19 | No. 4 | pp. 1599-1605 | 2020

Original Research Paper

https://doi.org/10.46488/NEPT.2020.v19i04.027

Open Access Journal

# Physicochemical Properties of *Jatropha podagrica* Biodiesel Blends and Their Effects on Tractor Engine Performance and Emission

**S. Nuanual*, P. Maneechot*, P. Thanarak*, A. Phuruangrat** and S. Artkla***†**

*School of Renewable Energy and Smart Grid Technology (SGTech), Naresuan University, Phitsanulok, 65000, Thailand

**Department of Materials Science and Technology, Faculty of Science, Prince of Songkla University, Hat Yai, Songkhla, 90112, Thailand

***Faculty of Liberal Arts and Science, Roi-Et Rajabhat University, 113 Moo 12, Koh Koae Selaphum, Roi Et, 45120, Thailand

†Corresponding author: Surachai Artkla; surachaiartkla@hotmail.com

**Nat. Env. & Poll. Tech.**
**Website: www.neptjournal.com**

*Received:* 23-10-2019
*Revised:* 18-11-2019
*Accepted:* 16-01-2020

**Key Words:**
Engine performance
Biodiesel
Energy
*Jatropha podagrica*

## ABSTRACT

Jatropha biodiesel produced from *Jatropha podagrica* oil by alkaline-catalysed transesterification was blended with diesel in the ratios of 88:12 wt% (B88) and 12:88 wt% (B12). The fuel properties, consumption rate and exhaust gas emission characteristics of *J. podagrica* biodiesel, diesel and their blends were assessed. The results showed that *J. podagrica* seed oil have similar fatty acid profile with those of *Jatropha curcas* cultivated in Thailand and other South-East Asian countries. Blending of *J. podagrica* biodiesel and diesel enhanced the fuel properties of the blends, similar to those of the diesel. However, the B88 blend emitted lesser pollutants when compared to B12 and petrol diesel, making it very ideal for use as a promising alternative to the petrol diesel used in the mini tractor for farming activities. The results from the current study form a basis for further research on the use of B88 as a fuel source.

## INTRODUCTION

Global energy demand is growing as a result of rapid economic and population growth (Salvi & Panwar 2012). The worldwide primary energy demand is estimated to increase by 1.5% per annum from 2007 to 2030 with an overall increase of 40% (Elango & Senthilkumar 2011). Currently, the world's economy is mostly dependent on fossil fuels, a situation which has raised serious concerns due to the limited reserves and the negative effects of fossil fuel combustion (Borugadda & Goud 2012). Energy security, environmental health, and greenhouse gases (GHGs) concerns associated with fossil fuel combustion have resulted in the development of environmentally friendly and renewable alternative energy sources (Abbaszaadeh et al. 2012).

In recent years, utilization of biofuel has attracted global attention, especially in the transportation industry, because of its general compatibility with conventional liquid transport fuel from fossil sources (Salvi & Panwar 2012). Biodiesel is a vital renewable clean biofuel that shares similar characteristics with petrol diesel, making it a promising alternative (Ibeto et al. 2012). Biodiesel is biodegradable, renewable, has low emissions, and not toxic (Atabani & Cesar 2014). It is produced from animal fats and vegetable oils (Aransiola et al. 2014). First generation biodiesel is produced from food-based oils such as rapeseed, soybean, and palm oils (Gülsen et al. 2014). However, biodiesel from these edible oil crops is not sustainable (Zhang et al. 2015). Continuous use of these edibles crops creates a food versus fuel crisis, resulting in an increase in their demand and price, adding up to the cost of biodiesel production (Larran et al. 2015). Consequently, biodiesel production from non-food oil crops has gain global attention (Atabani & Cesar 2014). Second generation biodiesel from non-food oil crops is more economical as these crops are found all over the world and can survive under all types of environmental conditions and lands without intensive husbandry (Atabani et al. 2013). In view of this, several researches have been done on Jatropha, a non-edible oil, as a potential substitute for petrol diesel.

Jatropha oil is relatively easy to store, transport, and safe to handle. However, the high viscosity of Jatropha oil causes insufficient atomization and incomplete combustion when used directly in diesel engines (Forson et al. 2004). Modification of the Jatropha oil through techniques such as heating, transesterification, and blending with petrol diesel has been used to eliminate atomization and combustion problems associated with high viscosity (Agarwal & Agarwal

2007). A combination of these techniques has been reported by several researchers as enhancing the fuel properties of Jatropha oil, comparable to that of petrol diesel (Agarwal & Agarwal 2007, Chauhan et al. 2011, Chen et al. 2013).

Notwithstanding the potential of Jatropha oil, research works have mainly focused on *Jatropha curcas*. However, there are other equally important Jatropha species yet to be exploited. Our study effort is aimed at using *Jatropha podagrica* oil as a substitute for diesel fuel with no engine modification. Our research highlights the physio-chemical properties of *J. podagrica* seed oil, and the performance and emission characteristics of *J. podagrica* biodiesel, Jatropha biodiesel-diesel blends in a mini-tractor (Kubota M7040, 4-stroke, 3-inches, 20 HP) engine. For comparison, diesel fuel was also tested and set as the benchmark. This is important because of the high energy consumption in the agriculture sector of Thailand. Tillage and other farm operations are expensive due to high fossil fuel consumption (Youssef et al. 2014), and on the other hand, is ecologically unfavourable (Borugadda & Goud 2012). Therefore, a fuel type that has less consumption rate, with fewer emissions will reduce farmers production cost and contribute immensely to environmental sustainability.

## MATERIALS AND METHODS

### Extraction of Jatropha Oil

Healthy whole *J. podagrica* seeds were collected from field crops in NongYaPlong District, Petchaburi, Thailand. The 50 kg of the unshelled seeds were thoroughly washed and dried under room temperature for 3 months. The seeds were then shelled and dried in a hot air oven at 60°C for 12 h. Approximately 40 kg of the dried kernels were finely milled with an SM 100, Rtsch, Rheinis-che StraBe 36-D-42781 (Haan, North Rhine-Westphalia, Germany) miller for 30 min. From the dried kernels, 39.2 kg dough was obtained and used for the oil extraction. The dough was continuously stirred in a distilled water for 15 min and the mixture filtered with a 5-micron filter to separate the solid waste from the solvent. The solvent was kept under room temperature for 12 h to enable the oil layer separate from the water. The oil layer was then strain and kept in a rotary evaporator to remove excess moisture. Finally, the Jatropha oil obtained was held in a 100-litre oxygen-free chamber for 3 months to precipitate smaller particles. After the 3 months storage, the yellowish brown-liquid oil (triglyceride) was filtered with 3-micron filter and transferred to the stock-solution chamber for transesterification.

### Fatty Acid Analysis

The fatty acid profile of the seed oil was evaluated using the gas chromatography (GC, Agilent 6890, Agilent Technologies Inc., CA, USA) fitted with a flame ionization detector (FID). The carrier gas was helium at the flow rate of 1 mL/min. The fatty acid compositions were identified with an HP-FFAP capillary column (25 m × 0.25 mm; 0.22 mm film thickness; Agilent Technologies Inc., CA, USA). The initial temperature of the oven was held at 180°C for 50 min and increased to 220°C at the rate of 10°C/min. The injector and FID temperatures were set at 220°C. The total oil volume of 10 µL was injected into the column at the flow rate of 1 mL/min.

### Transesterification Process

Alkaline-catalysed transesterification was carried out in this study as described by (Mofijur et al. 2013). The conditions for the transesterification process were 6:1 M ratio of *J. podagrica* oil to methanol, 1% potassium hydroxide (KOH) as a catalyst, a reaction time of 60 min, continuous stirring at a speed of 600 rpm, and a temperature of 60°C. The mixture was then kept in a separating funnel for 12 h to separate the biodiesel from glycerol and other impurities. The glycerol and other impurities were then disposed of. The methyl ester obtained was then placed in a rotary evaporator to evaporate the excess methanol and gently washed with distilled water at 60°C to remove the remaining impurities and glycerol. The washing was repeated severally till a neutral pH was attained. Finally, the biodiesel was dried in a rotary evaporator.

### Experimental Fuels

After the transesterification process, two Jatropha biodiesel-diesel blends were prepared in the ratios of 88:12 wt% (B88) and 12:88 wt% (B12). The blending was done at the speed of 2000 rpm with a homogenizer machine. The crude Jatropha oil, methyl ester, and petrol diesel were set as test fuels. The test fuels and blends were then tested in the mini-tractor (Kubota M7040, 4-stroke, 3-inches, 20 HP) engine.

### Physicochemical Properties of the Fuels

The standard methods of the Association of Official Analytical Chemists (AOAC 2006), were adopted to determine the physicochemical properties of the seed oil, methyl ester, diesel, and blends. Properties such as viscosity, density, acids value, specific gravity, iodine number, saponification values and free fatty acids were analysed. The calorific value, carbon residues, sulphur content, cloud point, pour point, and flash point were also evaluated as described by the American Society for Testing and Materials (ASTM) D240, D4530, D6667, D2500, and D93, respectively.

### Engine Performance Test

The mini-tractor (Kubota M7040, 4-stroke, 3-inches, 20 HP) engine was used to evaluate the test fuels and blends

for engine fuel consumption rate (mL/h) at various speeds (1,500-2,300 rpm) and exhaust emissions at the maximum speed of 2,300 rpm. The exhaust emission gases, nitrogen oxides (NOx), hydrocarbons (HCs), and carbon monoxide (CO), were measured with the exhaust gas analyser (BOSCH BEA-350).

### Statistical Analysis

One-way analysis of variance (ANOVA) and comparison of means (Tukey's test at 5% significance level) were done using SPSS version 17.0 (SPSS Inc., Chicago, IL). The mean values with their corresponding standard deviations were presented.

## RESULTS AND DISCUSSION

### Compositional Analysis of Fatty Acids in *J. podagrica* Oil

A total of 14.22 kg crude oil yield was realized, representing 28.4% by weight per kg of the unshelled Jatropha kernels. It is well known that the crude oil content of Jatropha is approximately 30-35% (Pandey et al. 2012). Forson et al. (2004) reported a 6.88 kg of oil from 32 kg of unshelled Jatropha seeds using a simple mechanical ram-press, which represented a 21.5% oil yield per kg of the unshelled seeds. The major fatty acid components of *J. podagrica* seed oil in the current study were the unsaturated fatty acids linoleic and oleic acids (Table 1). The study also revealed the presence of saturated fatty acids, mainly palmitic and stearic acids, in the seed oil. Several researchers have reported linoleic, oleic, palmitic, and stearic acids as the main fatty acid composition of *J. curcas* seed oil (Deng et al. 2010, Emil et al. 2010, Ilham & Saka 2010, Jain & Sharma 2010a, Jain & Sharma 2010b). *J. podagrica* seed oil in the current study share similar fatty acid profile with those of *J. curcas* cultivated in Thailand, Malaysia and Indonesia (Table 1).

### Physicochemical Properties of the Fuels

Transesterification of *J. podagrica* seed oil is very important in its consumption as fuel. Due to the low acid value of the seed oil in this study, alkaline transesterification was carried out. The physicochemical properties of raw *J. podagrica* seed oil, methyl ester, diesel, and blends are shown in Table 2. The viscosity of *J. podagrica* seed oil in the current study was reduced after the transesterification process. However, the value was still higher when compared to that of the diesel. A blend of the methyl ester and diesel further reduced the viscosity close to that of the diesel. The viscosity of the oil is a very important property in assessing its suitability as a liquid fuel. High viscosity inhibits the injection process and delays ignition of the engine (Ong et al. 2013). The low viscosity of the blend is very significant in enhancing its flow and atomization characteristics, making it very suitable as liquid fuel for diesel engines. Similar to viscosity, the density, acid value, specific gravity, cloud point, pour point, flash point, sulphur content, and carbon residue of the seed oil were reduced after transesterification. Blending the biodiesel with the diesel again caused a further reduction to these properties except for the sulphur content which increased slightly. However, transesterification of the seed oil helped to increase the calorific value. The value was further increased after blending with petrol diesel. Transesterification and further blending with diesel in this research enhanced the physicochemical

Table 1: Fatty acid composition of *J. podagrica* seed oil.

| Fatty acid composition (%) | *J. podagrica* (This study) | *J. curcas* (Thailand)* | *J. curcas* (Malaysia)* | *J. curcas* (Indonesia)* |
|---|---|---|---|---|
| Myristic acid (C14:0) | 0.10 | - | 0.10 | 0.10 |
| Palmitic acid (C16:0) | 13.80 | 15.20 | 14.20 | 14.50 |
| Heptadecanoic acid (C17:0) | 0.10 | 0.10 | 0.10 | 0.10 |
| Stearic acid (C18:0) | 7.80 | 6.80 | 7.00 | 7.00 |
| Arachidic acid (C20:0) | 0.30 | 0.20 | 0.20 | 0.20 |
| Palmitoleic acid (C16:1) | 0.70 | 0.70 | 0.70 | 0.70 |
| Oleic acid (18:1) | 44.50 | 44.60 | 44.70 | 42.40 |
| Linoleic acid (C18:2) | 32.50 | 32.20 | 32.80 | 34.60 |
| αLinolenic acid (C18:3) | 0.20 | 0.20 | 0.20 | 0.20 |
| Saturated fatty acids | 22.10 | 22.30 | 21.60 | 21.90 |
| Unsaturated fatty acids | 77.90 | 77.70 | 78.40 | 77.90 |

Source: (Emil et al. 2010, Supamathanon et al. 2011)

properties of the blends. The properties of the blends were comparable to that of the diesel (Table 2). Modification of vegetable oils to give them similar combustion properties as petrol diesel is very important in their use as a liquid fuel. Transesterification, pyrolysis, micro-emulsion, and blending are major processes for the modification of vegetable oils including that of Jatropha seed (Agarwal & Agarwal 2007). Several researchers have reported of the enhancement of vegetable oil after blending with diesel at various ratios (Agarwal & Agarwal 2007, Chen et al. 2013, Mofijur et al. 2013, Rehman et al. 2011).

## Fuel Consumption

The fuel consumption rate of the mini-tractor (Kubota M7040, 4-stroke, 3-inches, 20 HP) at different engine speeds used in the current study is given in Table 3. Fuel consumption increased as the engine speed was increased from 1,500-2,300 for the different fuel types. Jatropha biodiesel consumption was very high when compared to the other fuel types. The consumption rate of the other fuel types was however similar. The low B88, B12, and petrol diesel consumption, when compared to that of Jatropha biodiesel, may be attributed to their high calorific value (Chen et al. 2013). Agarwal & Agarwal (2007) reported that the low calorific value of seed oil from Jatropha results in high fuel consumption to maintain the level of energy input to engines. The decrease in the viscosity of B88 and B12 may have also contributed to the low consumption when compared to that of Jatropha biodiesel (Chauhan et al. 2010). Fuel atomization of the blends may have been significantly improved due to the

Table 2: Physicochemical properties of *J. podagrica* seed oil, methyl ester, diesel, and blend.

| Properties | Jatropha oil | Jatropha biodiesel | Diesel | B88 | B12 |
|---|---|---|---|---|---|
| Viscosity (cP, 40°C) | 42.8 | 5.23 | 3.50 | 3.80 | 3.60 |
| Density (20°C, kg/m$^3$) | 0.90 | 0.88 | 0.84 | 0.87 | 0.85 |
| Acid value (mg KOH/g) | 2.13 | 0.52 | 0.12 | 0.32 | 0.12 |
| Specific gravity (g/cm$^3$) | 0.93 | 0.90 | 0.85 | 0.87 | 0.86 |
| Calorific value (MJ/kg) | 39.20 | 41.05 | 42.80 | 41.40 | 42.20 |
| Cloud point (°C) | 8 | 1 | - 10 | - 4.3 | -8 |
| Pour point (°C) | 5 | 2 | - 13 | - 8 | -10 |
| Flash point (°C) | 180 | 135 | 76 | 85 | 79 |
| Sulphur content (%) | 0.007 | 0.002 | 0.043 | 0.003 | 0.040 |
| Carbon residue (%, w/w) | 2.35 | 1.23 | 0.16 | 0.75 | 0.50 |
| Iodine number (g/100 g) | 86.80 | - | - | - | - |
| Saponification value (mg KOH/g) | 183.50 | - | - | - | - |
| Free fatty acids (FFA, %) | 2.10 | - | - | - | - |

Table 3: Fuel consumption rate of the mini-tractor (Kubota M7040, 4-stroke, 3-inches, 20 HP).

| Engine operation (RPM) | Jatropha biodiesel (mL/h) | B88 (mL/h) | B12 (mL/h) | Diesel (mL/h) |
|---|---|---|---|---|
| 1,500 | 520 | 502 | 502 | 502 |
| 1,600 | 525 | 501 | 501 | 500 |
| 1,700 | 550 | 543 | 542 | 542 |
| 1,800 | 630 | 590 | 590 | 589 |
| 1,900 | 670 | 632 | 632 | 632 |
| 2,000 | 730 | 699 | 699 | 698 |
| 2,100 | 770 | 764 | 763 | 762 |
| 2,200 | 850 | 809 | 809 | 808 |
| 2,300 | 910 | 858 | 875 | 875 |

low viscosity (Agarwal & Agarwal 2007). The difference in fuel density observed earlier (Table 2) may have also contributed to the variations in fuel consumption. The decrease in the fuel density results in less discharge of fuel for the same displacement of the plunger in the fuel injection pump (Chauhan et al. 2011). This leads to less fuel consumption as was observed in B88, B12 and diesel in comparison to Jatropha biodiesel in our current study.

**Gaseous Emissions**

The emissions levels of NOx (Fig. 1), HC (Fig. 2), and CO (Fig. 3) as a result of using the various fuel types were assessed by operating the engine at the maximum speed of 2300 rpm. The assessment revealed that Jatropha biodiesel and its blends emitted significantly ($p<0.05$) higher NOx when compared to petrol diesel. The NOx emission levels significantly ($p<0.05$) increased with an increase in the Jatropha biodiesel percentage. This may be attributed to the higher oxygen content in biodiesel when compared to petrol diesel. This causes complete combustion with the biodiesel and its blend increasing the combustion temperature and subsequent increase in NOx emissions (Mofijur et al. 2013). Similar observations have been reported by several researchers (Chauhan et al. 2011, Mofijur et al. 2013, Dhar et al. 2012). However, the emission levels of HC and CO were significantly ($p<0.05$) higher with the use of petrol diesel when compared to those of the Jatropha biodiesel and its blends. As the percentage of the petrol diesel increased, significantly ($p<0.05$) more HC and CO were emitted. The complete combustion that occurs with the use of biodiesel and blends with high biodiesel percentage leads to a decrease in the CO and HC emissions (Chauhan et al. 2011).

The performance of the engine and the level of pollutants it emits are very critical factors in the use of biodiesel and its blends as an alternative fuel to petrol diesel (Chen et al. 2013). The use of biodiesel and its blends as fuel for engines contributes less emissions of carbon monoxide, particulate matter, sulphur oxides, smoke, and polyaromatic hydrocarbons (Agarwal & Agarwal, 2007). However, petrol diesel combustion is one of the main contributors to environmental pollution worldwide. These pollutants have a serious impact on the health of the environment and humans (Mofijur et al. 2013). One of the major advantages of using biodiesel as an alternative fuel is that it can be blended with petrol diesel to enhance its performance as well as significantly reducing emission of pollutants (Chauhan et al. 2010). The successful use of biodiesel-petrol diesel blends at different ratios has been reported by several researches across the globe (Atabani & Cesar 2014, Mofijur et al. 2013, Rehman et al. 2011, Tsolakis et al. 2007). Among the different types of fuel in the current study, B88 and B12 share similar properties with the petrol diesel. However, B88 emits less pollutant, making

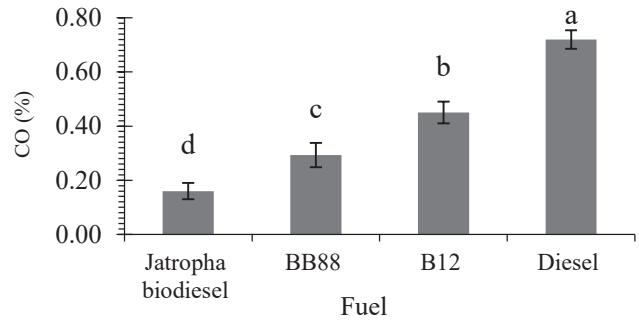


Fig. 1: Nitrogen oxides emissions for different fuel types at the maximum speed of 2300 rpm.

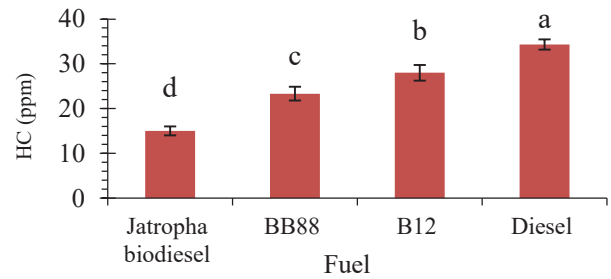


Fig. 2: Hydrocarbon emissions for different fuel types at the maximum speed of 2300 rpm.

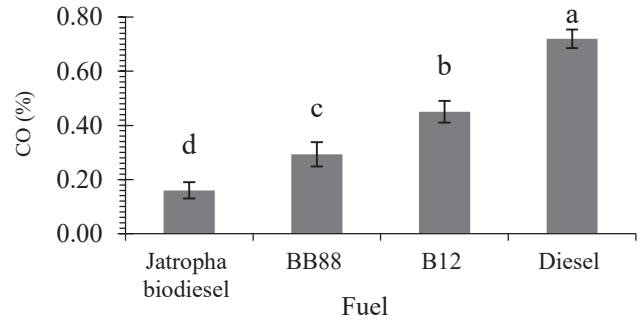


Fig. 3: Carbon monoxide emissions for different fuel types at a maximum speed of 2300 rpm.

it very ideal for use as a promising alternative to the petrol diesel in the mini tractor for farming purposes.

## CONCLUSION

Jatropha biodiesel-petrol diesel blend can be an alternative fuel for mini tractor during farming activities. The Jatropha biodiesel-petrol diesel blends in the current study share similar characteristics and properties with petrol diesel. However, B88 emits less pollutant when compared to B12 and petrol diesel, making it a potential alternative fuel. This study forms a strong basis for further research on the use of B88 as the fuel source for diesel engines.

## ACKNOWLEDGEMENTS

We acknowledge the financial support provided by the National Research Council of Thailand (NRCT). Equipment supports were from Scientific Equipment Center, Suranaree University of Technology, Nakhon Ratchasima, 30000, Thailand; Research Laboratory Equipment Center, Maha Sarakham University, Maha Sarakham, 44000, Thailand and the Faculty of Liberal Arts and Science, Roi-Et Rajabhat University (RERU), 45120, Thailand. The assistance of P. Sriprapakhan is also acknowledged.

## REFERENCES

Abbaszaadeh, A., Ghobadian, B., Omidkhah, M.R. and Najafi, G. 2012. Current biodiesel production technologies: A comparative review. Energy Convers. Manag., 63: 138-148.

Agarwal, D. and Agarwal, A.K. 2007. Performance and emissions characteristics of Jatropha oil (preheated and blends) in a direct injection compression ignition engine. Appl. Therm. Eng., 27: 2314-2323.

AOAC 2006. Official Methods of Analysis. 18th ed., Association of Official Analytical Chemists, Washington, DC, U.S.A.

Aransiola, E.F., Ojumu, T.V., Oyekola, O.O., Madzimbamuto, T.F. and Ikhu-Omoregbe, O.I.O. 2014. A review of current technology for biodiesel production: State of the art. Biomass Bioenergy, 61: 276-297.

Atabani, A.E. and César, A.D.S. 2014. *Calophyllum inophyllum* L. – A prospective non-edible biodiesel feedstock. Study of biodiesel production, properties, fatty acid composition, blending and engine performance. Renew. Sust. Energ. Rev., 37: 644-655.

Atabani, A.E., Mahlia, T.M.I., Anjum, B.I., H. H. Masjuki, H.H., Chong, W.T. and Lee, K.T. 2013. Investigation of physical and chemical properties of potential edible and non-edible feedstocks for biodiesel production, a comparative analysis. Renew. Sust. Energ. Rev., 21: 749-755.

Borugadda, V.B. and Goud, V.V. 2012. Biodiesel production from renewable feedstocks: Status and opportunities. Renew. Sust. Energ. Rev., 16: 4763-4784.

Chauhan, B.S., Kumar, N. and Cho, H.M. 2011. A study on the performance and emission of a diesel engine fuelled with Jatropha biodiesel oil and its blends. Energy, 37: 616-622.

Chauhan, B.S., Kumar, N., Du Jun, Y. and Lee, K.B. 2010. Performance and emission study of preheated Jatropha oil on medium capacity diesel engine. Energy, 35: 2484-2492.

Chen, L.Y., Chen, Y.H., Hung, Y.S., Chiang, T.H. and Tsai, C.H. 2013. Fuel properties and combustion characteristics of Jatropha oil biodiesel-diesel blends. J. Taiwan Inst. Chem. E., 44: 214-220.

Deng, X., Fang, Z. and Liu, Y.H. 2010. Ultrasonic transesterification of *Jatropha curcas* L. oil to biodiesel by a two-step process. Energ. Convers. Manage., 51: 2802-2807.

Dhar, A., Kevin, R. and Agarwal, A.K. 2012. Production of biodiesel from high-FFA neem oil and its performance, emission and combustion characterization in a single cylinder DICI engine. Fuel Process. Technol., 97: 118-129.

Elango, T. and Senthilkumar, T. 2011. Combustion and emission characteristics of a diesel engine fuelled with jatropha and diesel oil blends. Thermal Science, 15: 1205-1214.

Emil, A., Yaakob, Z., Satheesh Kumar, M., Jahim, J.M. and Salimon, J. 2010. Comparative evaluation of physicochemical properties of jatropha seed oil from Malaysia, Indonesia and Thailand. J. Am. Oil Chem. Soc., 87: 689-695.

Forson, F.K., Oduro, E.K. and Hammond-Donkoh, E. 2004. Performance of jatropha oil blends in a diesel engine. Renewable Energy, 29: 1135-1145.

Gülsen, E., Olivetti, E., Freire, F., Dias, L. and Kirchain, R. 2014. Impact of feedstock diversification on the cost-effectiveness of biodiesel. Appl. Energy, 126: 281-296.

Ibeto, C.N., Okoye, C.O.B. and Ofoefule, A.U. 2012. Comparative study of the physicochemical characterization of some oils as potential

feedstock for biodiesel production. ISRN Renew. Energ., 2012, Article ID 621518, 5 pages.

Ilham, Z. and Saka, S. 2010. Two-step supercritical dimethyl carbonate method for biodiesel production from *Jatropha curcas* oil. Bioresour. Technol., 101: 2735-2740.

Jain, S. and Sharma, M.P. 2010a. Biodiesel production from *Jatropha curcas* oil. Renew. Sust. Energ. Rev., 14: 3140-3147.

Jain, S. and Sharma, M.P. 2010b. Kinetics of acid base catalyzed transesterification of *Jatropha curcas* oil. Bioresour. Technol. 101: 7701-7706.

Larran, A., Jozami, E., Vicario, L., Feldman, S.R., Podestá, F.E. and Permingeat, H.R. 2015. Evaluation of biological pretreatments to increase the efficiency of the saccharification process using *Spartina argentinensis* as a biomass resource. Bioresour. Technol., 194: 320-325.

Mofijur, M., Masjuki, H.H., Kalam, M.A. and Atabani, A.E. 2013. Evaluation of biodiesel blending, engine performance and emissions characteristics of *Jatropha curcas* methyl ester: Malaysian perspective. Energy, 55: 879-887.

Ong, H.C., Silitonga, A.S., Masjuki, H.H., Mahlia, T.M.I., Chong, W.Y. and Boosroh, M.H. 2013. Production and comparative fuel properties of biodiesel from non-edible oils: *Jatropha curcas*, *Sterculia foetida* and *Ceiba pentandra*. Energ. Convers. Manage., 73: 245-255.

Pandey, V.C., Singh, K., Singh, J.S., Kumar, A., Singh, B. and Singh, R.P. 2012. *Jatropha curcas*: A potential biofuel plant for sustainable environmental development. Renew. Sust. Energ. Rev., 16: 2870-2883.

Rehman, A., Phalke, D.R. and Pandey, R. 2011. Alternative fuel for gas turbine: Esterified jatropha oil–diesel blend. Renew. Energ., 36: 2635-2640.

Salvi, B.L. and Panwar, N. L. 2012. Biodiesel resources and production technologies-A review. Renew. Sust. Energ. Rev., 16: 3680-3689.

Supamathanon, N., Wittayakun, J. and Prayoonpokarach, S. 2011. Properties of Jatropha seed oil from Northeastern Thailand and its transesterification catalyzed by potassium supported on NaY zeolite. J. Ind. Eng. Chem., 17: 182-185.

Tsolakis, A., Megaritis, A., Wyszynski, M.L. and Theinnoi, K. 2007. Engine performance and emissions of a diesel engine operating on diesel-RME (rapeseed methyl ester) blends with EGR (exhaust gas recirculation). Energy, 32: 2072-2080.

Youssef, M., Khoramivafa, M. and Mondani, F. 2014. Integrated evaluation of energy use, greenhouse gas emissions and global warming potential for sugar beet (*Beta vulgaris*) agroecosystems in Iran. Atmos. Environ., 92: 501-505.

Zhang, H., Zhou, Q., Chang, F., Pan, H., Liu, X.F., Li, H., Hu, D.Y. and Yang, S. 2015. Production and fuel properties of biodiesel from *Firmiana platanifolia* L. as a potential non-food oil source. Ind. Crops Prod., 6: 768-771.

Nature Environment and Pollution Technology
An International Quarterly Scientific Journal

p-ISSN: 0972-6268
(Print copies up to 2016)
e-ISSN: 2395-3454

Vol. 19 | No. 4 | pp. 1607-1615 | 2020

Original Research Paper

https://doi.org/10.46488/NEPT.2020.v19i04.028

Open Access Journal

# Wetland Plants' Chemical Ecology for Iron of A Ramsar Site in An Indo-Burma Hotspot: *In-Situ* Bioaccumulation and Phytoremediation Implications

**Prabhat Kumar Rai† and M. Muni Singh**
Department of Environmental Science, Mizoram University, Aizawl, Mizoram, India
†Corresponding author: Prabhat Kumar Rai; mzut127@mzu.edu.in

**Nat. Env. & Poll. Tech.**
**Website: www.neptjournal.com**

*Received:* 04-02-2020
*Revised:* 17-02-2020
*Accepted:* 05-03-2020

**Key Words:**
Invasive alien plants
Ramsar site
Phytoremediation
Bio-accumulation
Biodiversity

## ABSTRACT

Biogeochemistry of iron in wetlands is inextricably linked with chemical ecology of aquatic biota impacting the ecology of wetland plants and human health. Therefore, its bio-accumulation in plants is of extreme eco-technological relevance in quest of potential phytoremediation tools. To this end, the Fe concentrations in water and four invasive alien macrophytes (*Eichhornia crassipes*, *Lemna minor, Pistia stratiotes* and *Salvinia cucullata*) of Loktak lake (a Ramsar Site) were measured. Further, the outcome of the present research can assess the efficiency of these plants in Fe-phytoremediation. Concomitantly, to get an explicit Fe-macrophyte's chemical ecology scenario of Loktak lake, physico-chemical parameters as well as biodiversity attributes were also investigated. Results revealed that among the four plant species, *Pistia stratiotes* accumulated the highest amount of Fe concentration and thus act as the best bio-accumulator of Fe. Further, the extent of Fe bio-accumulation was as *Pistia stratiotes*>*Lemna minor*>*Eichhornia crassipes*>*Salvinia cucullata*. The study revealed the importance of the selected invasive wetland plants as the potential bio-agents of Fe accumulation.

## INTRODUCTION

Global wetland systems offer immense ecosystem services to humanity with their unique ecological/environmental features and biodiversity of floating and/or submerged macrophytes (Prasad et al. 2002, Bassi et al. 2014**,** Rai et al. 2018). However, recent decades witnessed a paradigm shift in wetland's health in view of the abrupt increase in environmental contaminants. In this respect, it has been well known that natural wetlands demonstrate a majestic chemical ecology in remediating the metallic contaminants. Thus, elucidating the complex chemical and ecological interactions existing in the wetland systems can pave the way for phytoremediation, hence ecological restoration (Valderrama et al. 2013, Evangelou et al. 2013, Singh & Rai 2016, Al-Baldawi et al. 2017, Rai & Kim 2019, Rai et al. 2020).

Several macrophytes of Indian Ramsar wetlands, e.g. *Phragmites australis* (of Hokersar wetlands in Kashmir Himalaya) have been identified for their phytoremediation potential of heavy metals (Chatterjee et al. 2011, Ahmad et al. 2014, Khatun 2016)**.** Moreover, in this context elucidation of mechanisms leading to integrated restoration/eco-management of Kolleru lake (a Ramsar wetland in Andhra Pradesh, India) abridged the chemistry with ecological restoration (Sharma & Sujatha 2016). Thus, the heavy metal pollution of global wetland systems and their phytoremediation attained considerable research attention (Feng et al. 2017, Rai 2018; Rai 2019, Rai et al. 2019).

The excess use of agrochemicals (including fertilizer and plant nutrients) contaminate soil, water and food crops/vegetables with heavy metals (Rai 2008, Alhashemi et al. 2011, Fatima et al. 2014, Rai et al. 2020). Also, the bioavailability of heavy metals is remarkably influenced by the geochemical factors in global wetlands (Fairbrother 2007). Moreover, the sediments of the wetland effectively sequester hydrophobic chemical pollutants which are readily available from various pollutant discharges (Rai et al. 2018).

Natural wetlands are the important sink for environmental pollutants in view of their complex physico-chemical and biogeochemical mechanisms operating inside wetlands (Jiao et al. 2014, Xin et al. 2014, Zhang et al. 2016). It has been well known that aquatic/wetland plants absorb emerging contaminants and nutrients from the water/sediments of natural wetlands in view of being interfaces with them (Xue et al. 2010, Rai et al. 2019). For a low level of environmental contamination, the aquatic plants (mostly invasive aliens) also act as ecological indicators (Pratas et al. 2012, Borisova et al. 2014, Rai & Singh 2020). Therefore, in environmental biotechnology, the screening of macrophytes for phytoremediation of metallic contaminants has also received tremendous attention (Sood et al. 2012, Borisova et al. 2014, Rai et al. 2019).

Phyto-technological investigations in global biodiversity hotspots especially from North East Indian sites are rarely investigated for pollution ecology of Ramsar wetland plants.

The sewage is eventually drained into the Ramsar wetland (Loktak lake) may also result in eutrophication as well as contamination of the lake with heavy metals of extreme human health concerns (Meitei et al. 2016, Rai 2018a). In Indian prospect, 26 Ramsar wetlands of ecological importance are listed (out of the current total of 37 wetlands under the Ramsar convention), facing the environmental perturbations in one form or other (Tombi & Shyamananda 1994; Ramsar secretariat 2013, Bassi et al. 2014, Rai 2018). The scientific investigations of Ramsar sites tend to provide their current global status in order to fill up the knowledge gap pertaining to their metals biogeochemistry and aquatic plants ecology.

Iron (Fe) plays a crucial role in various bio-systems (plants as well as animals) due to its involvement in biochemical pathways, metabolic machinery, respiratory functions (being an integral component of haemoglobin) and in DNA synthesis (Ghaly et al. 2008, Rai et al. 2018a). Nevertheless, Fe is also toxic in higher concentration ranges to living entities of the wetland ecosystem and propensity to cause human health risks in case of metals transfer through food chain. In the present study, considering the all the stress caused by the Fe (as other metallic contaminants were negligible), the authors aim to analyse and determine the amount of Fe accumulation in aquatic bodies as well as selected aquatic plants such as *Eichhornia crassipes*, *Lemna minor, Pistia stratiotes* and *Salvinia cucullata* of Loktak lake to know the efficiency of their bio-accumulation/phytoremediation. Physicochemical parameters not only affect the concentrations of metallic contaminants but also creating unique relationships among and within the biotic and abiotic components of the ecosystem (APHA 2005, Rai 2010). Henceforth, chemical/physicochemical parameters and ecological attributes (phytosociology/biodiversity) were also studied to have an integrated chemical as well as the ecological approach. It is worth mentioning that these selected wetland plants are invasive aliens, perturbing the aquatic biodiversity. Nevertheless, their controlled utilization as contaminant's hyperaccumulators can assist their sustainable management, concomitantly, decontaminating the organic/inorganic pollutants from the environment (Rai & Kim 2019).

## MATERIALS AND METHODS

### Study Area

Loktak lake (Ramsar site; Latitude of 24º25'-24 º42' N and Longitude of 93º46'-93º55'E) lies in the middle of the state Manipur situated in the north-eastern part of India.

### Sampling Sites

A total of four sampling sites were selected for analysis which is explicitly described in Fig. 1. The basis of the site selection was attributed to the source of pollution and other anthropo-

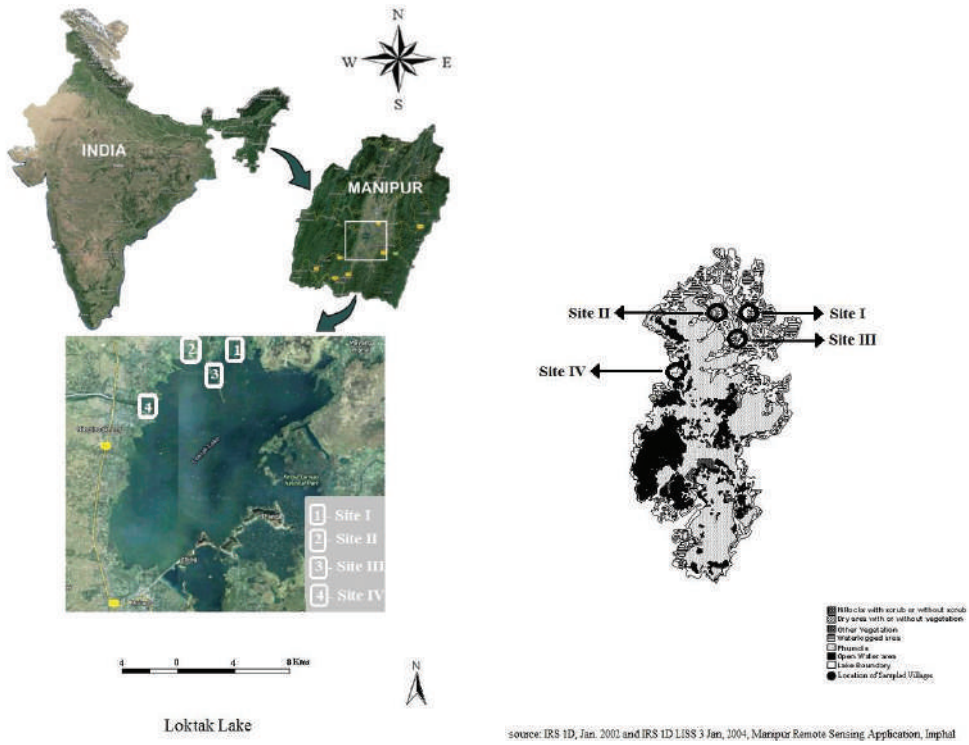


Fig. 1: Study area and location of study in Manipur, North East India (an Indo-Burma hotspot region).

genic disturbances in the vicinity of this Ramsar lake. The Sites are as follows. Site I (Loktak Nambul vicinity); Site II (Loktak Nambol vicinity, Nambol river carries waste of the Bishenpur municipal area); Site III (Loktak Yangoi vicinity, located at the confluence of Yangoi river); Site IV (Loktak proper, near National Hydro Power Corporation Limited of Loktak lake).

Water samples in triplicate (in 2L polythene bottles) were collected in the morning between 6:30 to 9:30 a.m. in rainy, winter and summer seasons from August 2013 to July 2015, and immediately brought to the laboratory for analysis. In addition to physicochemical parameters, we confined our quest on Fe as it was the only metal recorded above the permissible limit in natural water and wetland plants (Singh & Rai 2016). Other hazardous heavy metals like Hg, Cr, Pb, Hg, As (a metalloid) and Zn were recorded in negligible/ trace concentrations in water and wetland plants. Henceforth, this fact prompted us to carry out a detailed chemical and biological study in relation to screening the different wetland plants for their possible role in bio-accumulation and phytoremediation of iron (Fe).

### Phytosociological Analysis

Vegetation analysis was carried out by following the standard methods as outlined in Misra (1968), Kershaw (1973) and Mueller-Dombois & Ellenberg (1974). Harvest methods were adopted for phytosociological analysis on the macrophytes and quadrats (1m × 1m) were used. Macrophytic diversity has been calculated using the following indices.

Iron Analysis of Water and Wetland Plants

The water samples were filtered through 45 µm syringe filter and metals were determined by Microwave Induced Plasma Atomic Emission Spectrophotometer (MP-AES: Agilent-4100) available in Central Instrumentation Laboratory (CIL), Mizoram University, India. The fresh macrophytes samples were weighed and kept in the oven for drying and temperature was maintained at 802°C for 24 hours. The dried plant samples were again weighed and crushed it into powder. The powdered plant samples were then digested using the di-acid method as mentioned elsewhere (APHA 2005).

## RESULTS AND DISCUSSION

### Iron Accumulation in Water

The Fe concentrations of water at different sites during different seasons were measured and presented in Table 1. As mentioned before, the chemical, as well as physical (physico-chemical/water quality) parameters, play a vital role in bio-availability of heavy metals in water and wetland plants (Rai 2010), therefore, it was duly monitored in conjunction with ecological studies. Fig. 2(a-f) explicitly describe the seasonal variations in different water quality parameters recorded during the study period.

Pertaining to the metal concentrations (analysed in the year 2013-15), the highest value of Fe concentration was measured as 0.17 $mg.L^{-1}$ at Site IV during winter season of 2014 followed by 0.15 $mg.L^{-1}$ at Site II and Site IV during the winter season and 0.13 $mg.L^{-1}$ at Site II during the winter season of the same year 2014. The lowest value of 0.01 $mg.L^{-1}$ was observed at Site I during the rainy season and summer season of 2014, as demonstrated clearly in Fig. 3. Seasonal variations revealed that Fe accumulation in lake water is higher during the winter season. However, comparatively low values were measured during the rainy season (attributed to dilution) and summer season for all the sampling periods.

### Fe Accumulation in Plants

The four plant species samples were collected in triplicate from all the four sites in winter season. The trends of Fe concentrations are shown in Figs. 4-7. Results revealed that among the plants, the highest Fe concentration was measured 28.29 $mg.kg^{-1}$ in *Pistia stratiotes* at Site II followed by 13.01 $mg.kg^{-1}$ and 12.68 $mg.kg^{-1}$ in *Pistia stratiotes* at Site I and Site III, 12.74 $mg.kg^{-1}$ and 12.52 $mg.kg^{-1}$ in *Lemna minor* at Site I and Site II. The lowest value of 1.68 $mg.kg^{-1}$ was measured in *Salvinia cucullata* at Site I (Table 2). The highest value 28.29 $mg.kg^{-1}$ is higher than the permissible limit set by World Health Organisation (WHO), i.e. 20 $mg.kg^{-1}$. *Salvinia cucullata* has the lowest Fe as compared to the other plant species, i.e. *Eichhornia crassipes*, *Lemna minor* and *Pistia stratiotes*.

Table 1: Fe concentrations ($mg.L^{-1}$) of water from different study sites (average of three replicates).

| Study Sites | 2013-2014 | | | 2014-2015 | | |
|---|---|---|---|---|---|---|
| | Rainy | Winter | Summer | Rainy | Winter | Summer |
| Site I | 0.02 | 0.07 | 0.03 | 0.01 | 0.08 | 0.01 |
| Site II | 0.08 | 0.13 | 0.1 | 0.07 | 0.15 | 0.09 |
| Site III | 0.04 | 0.1 | 0.06 | 0.06 | 0.12 | 0.03 |
| Site IV | 0.08 | 0.17 | 0.06 | 0.05 | 0.15 | 0.07 |

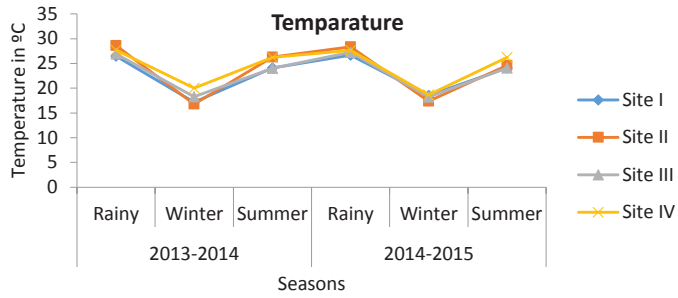


Fig. 2a

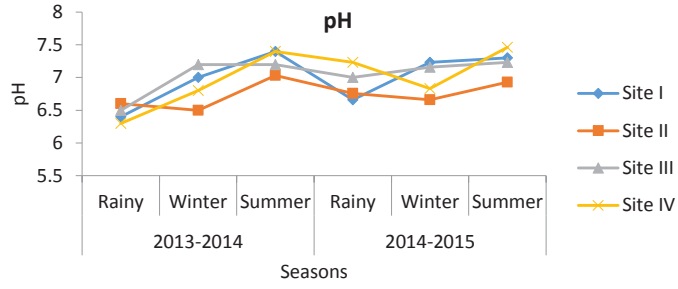


Fig. 2b

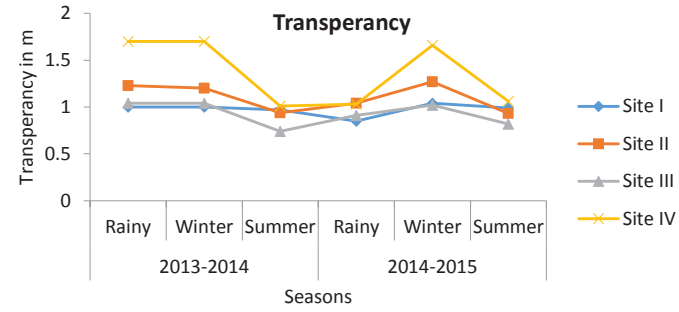


Fig.2c

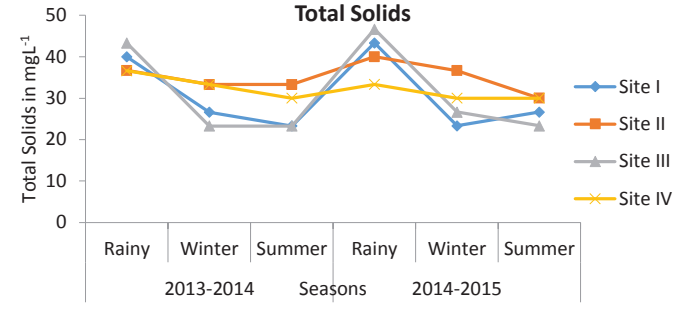


Fig. 2d

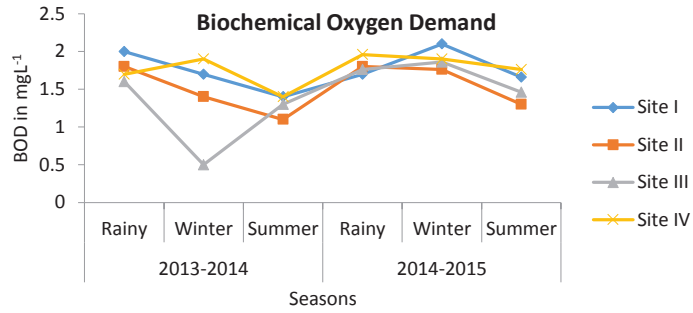


Fig. 2e

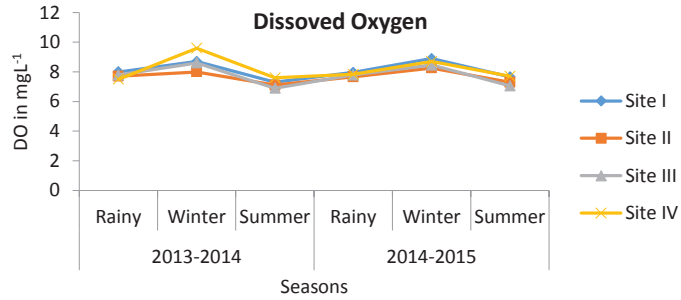


Fig. 2f

Fig. 2a-f: Seasonal variations in chemical/physicochemical/water quality parameters at all the four sites of the study area, i.e. Ramsar wetland (Loktak lake, N.E. India of biodiversity hot spot).

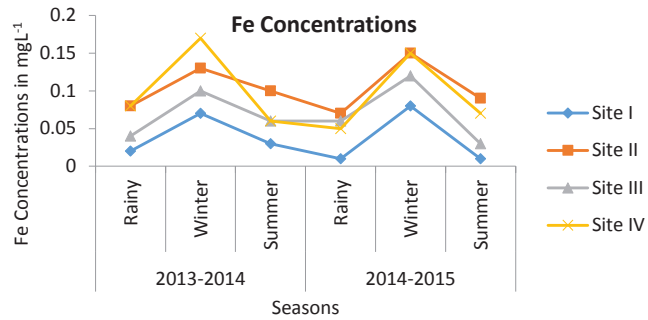


Fig. 3: Seasonal variations of Fe concentrations (in $mg.L^{-1}$) of water from different study sites.

Table 2: Fe concentrations (in $mg.kg^{-1}$) of plants from different study sites.

| Name of the plants/macrophytes | Site I | Site II | Site III | Site IV |
|---|---|---|---|---|
| *Eichhornia crassipes* | 0.72 | 9.77 | 9.07 | 0.53 |
| *Lemna minor* | 12.52 | 12.74 | 9.92 | 9.41 |
| *Pistia stratiotes* | 13.01 | 28.29 | 12.68 | 1.09 |
| *Salvinia cucullata* | 1.68 | 3.14 | 2.72 | 2.25 |

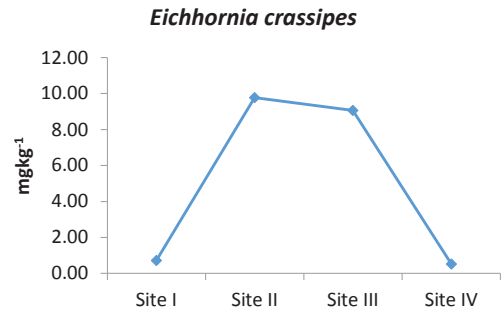


Fig. 4: Fe concentrations (in mg.kg$^{-1}$) in *Eichhornia crassipes* of different study sites.

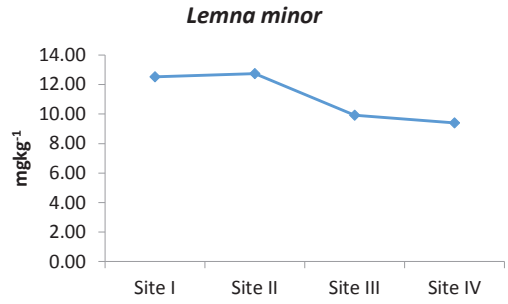


Fig. 5: Fe concentrations (in mg.kg$^{-1}$) in *Lemna minor* of different study sites.

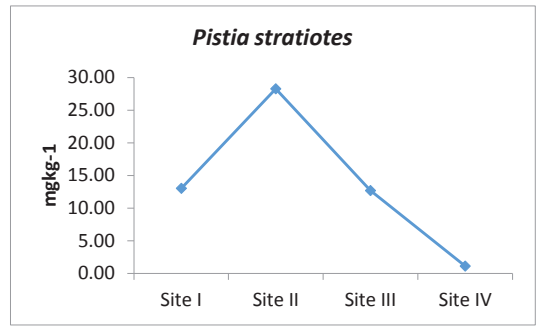


Fig. 6: F e concentrations (in mgkg$^{-1}$) in *Pistia stratiotes* of different study sites.

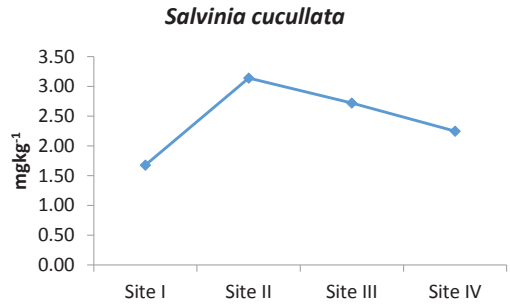


Fig.7: Fe concentrations (in mgkg$^{-1}$) in *Salvinia cucullata* of different study sites.

Table 3: Ecological/phytosociological attributes of wetland plants/macrophyte species in Ramsar (Loktak) lake.

| Parameter | Site I | Site II | Site III | Site IV |
|---|---|---|---|---|
| Number of Families | 8 | 11 | 9 | 15 |
| Number of Genera | 8 | 12 | 11 | 20 |
| Number of Species | 10 | 13 | 12 | 21 |
| Simpson Index of Dominance | 0.37 | 0.27 | 0.42 | 0.12 |
| Shannon-Weiner Diversity Index | 1.31 | 1.68 | 1.37 | 2.37 |

Table 4: Sorenson's Similarity Index between different sites of Ramsar (Loktak) lake.

| | Site I | Site II | Site III | Site IV |
|---|---|---|---|---|
| Site I | | | | |
| Site II | 0.87 | | | |
| Site III | 0.73 | 0.72 | | |
| Site IV | 0.65 | 0.71 | 0.61 | |

Table 5: Family-wise distribution of wetland plants/macrophyte species in Ramsar (Loktak) lake.

| Sl. No. | Family | Site I | Site II | Site III | Site IV |
|---|---|---|---|---|---|
| 1 | Amaranthaceae | 1 | 1 | 1 | 1 |
| 2 | Apiaceae | - | - | - | 1 |
| 3 | Araceae | 1 | 1 | 1 | 1 |
| 4 | Asteraceae | - | 1 | - | - |
| 5 | Azollaceae | 1 | 1 | 1 | 1 |
| 6 | Ceratophyllaceae | 1 | 1 | - | 1 |
| 7 | Convolvulaceae | - | - | 1 | 1 |
| 8 | Hydrocharitaceae | 1 | 1 | - | 2 |
| 9 | Lemnaceae | 2 | 2 | 2 | 2 |
| 10 | Menyanthaceae | - | 1 | - | 1 |
| 11 | Nymphaeaceae | - | - | - | 2 |
| 12 | Poaceae | - | 1 | 1 | 3 |
| 13 | Polygonaceae | - | - | 2 | - |
| 14 | Pontederiaceae | 1 | 1 | 1 | 1 |
| 15 | Potamogetonaceae | - | - | - | - |
| 16 | Salviniaceae | 2 | 2 | 2 | 2 |
| 17 | Trapaceae | - | - | - | 1 |

(-) Absent

From the present studies, it has been noted that *Pistia stratiotes* accumulate high amount of Fe concentration from the lake. The recorded trend of Fe bio-accumulation was as *Pistia stratiotes*>*Lemna minor*>*Eichhornia crassipes*>*Salvinia cucullata*. In this context, high concentrations of Fe in water samples might be attributed to the pollution caused by draining rivers and the domestic/urban waste from human settlements.

From the phytosociological/ecological studies of the different sites of Loktak lake, altogether a total of 24 wetland plant species belonging to 23 genera and 17 families were recorded. Of this, 10 species belonging to 8 genera and 8 families, 13 species belonging to 12 genera and 11 families, 12 species belonging to 11 genera and 9 families and 21 species belonging to 20 genera and 15 families were reported from Site I, Site II, Site III and Site IV respectively (Table 3). To

this end, among 24 plants recorded, *Alternanthera philoxeroides* Griseb., *Azolla pinnata* Lam., *Eichhornia crassipes* Linn., *Lemna minor* Linn., *Pistia stratiotes* Linn.,*Salvinia cucullata* Roxb., *Salvinia natans* Hoffm., and *Spirodela polyrhiza* (Linn) Schleid. were the plants with higher density at all the sites. Biodiversity/phytosociological attributes related data of macrophyte/wetland plant species is calculated in the study (Table 4). Shannon-Weiner diversity index for macrophyte species was highest at the Site IV i.e. 2.37 and lowest in the Site I i.e. 1.31. However, a reverse trend in the results was observed in the case of the Simpson index of dominance. The Simpson index of dominance was maximum at Site III i.e. 0.42 and minimum at Site IV i.e. 0.12. Table 5 shows the present dominance and diversity of wetland plants in this Ramsar lake. As the Simpson's index of dominance values decreases, Shannon-Weiner diversity increased which is quite appropriate in ecological perspective.

Pertaining to Fe bio-accumulation/remediation, many studies have documented the Fe accumulation and ability of these wetland plants from wastewaters which are rich in nutrients (Singh & Rai 2016). Ghaly et al. (2008) studied the accumulation of Fe by different aquatic plants including broad leaved cattail, soft stem bulrush, soft rush and wool grass plants from the contaminated water.

*P. stratiotes* has also been extensively used for removal of heavy metals other than Fe (Rai 2018a). The removal of heavy metals by *P. stratiotes* in the laboratory was tested (Miretzky 2010). Lu et al. (2011) reported that *Pistia* is a hyper-accumulator of Cu, Fe, and Pb. Also, *Pistia stratiotes* was found to be the best phytoremediator for Cu and Pb in removing 66.5% and 70.7% of these metals (Lone et al. 2008). To this end, remarkable advances in instrumentation assisted metals analysis in wetland plants (Feng et al. 2017). However, to our best of knowledge, the present study is the first report on *Pistia stratiotes* as a better tool as an ecological indicator of Fe.

## CONCLUSION

From the findings of the present study, it can be concluded that the water of the Loktak lake is contaminated with Fe to a reasonable extent and may further exacerbate in due course of time. However, the other heavy metals were well below the permissible limit in water sediments and biota. To this end, wetland plants can be a remarkable tool and this study revealed differential extent of Fe bio-accumulation among macrophytes (*Pistia stratiotes*>*Lemna minor*>*Eichhornia crassipes*>*Salvinia cucullata*). The present study can possibly be the first report on *Pistia stratiotes* as a better tool in relation to bio-accumulation of Fe. Henceforth, the wetland plants play an important role in indicating the Fe concentration of the water as well as the extent of accumulation in the plants itself. Interestingly, the studied macrophytes are actually invasive aliens, perturbing the aquatic ecology/biochemistry. Nevertheless, their controlled utilization as contaminant's hyperaccumulators can assist in their sustainable management, concomitantly, decontaminating the organic/inorganic pollutants from the total environment.

## ACKNOWLEDGEMENT

The author is thankful to Department of Biotechnology (BT/PR24917/NER/95/907/2017), New Delhi, India and Department of Science and Technology (WTI Nexus Project-TPN/33209-No. DST/TMD-EWO/WTI/2K19/EWFH/2019/190) for financial assistance. Thanks are due to University Grants Commission of India and Dr. M. Muni Singh.

## REFERENCES

Ahmad, S.S., Reshi, Z.A., Shah, M.A., Rashid, I., Ara, R. and Andrabi, S.M.A. 2014. Phytoremediation potential of *Phragmites australis*. Int. J. Phytoremediation, 16(7-12): 1183-1191.

Al-Baldawi, I.A., Abdullah, S.R.S., Anuar, N. and Mushrifah, I. 2017. Bioaugmentation for the enhancement of hydrocarbon phytoremediation by rhizobacteria consortium in pilot horizontal subsurface flow constructed wetlands. Inter. J. Environ. Sci. Technol., 14: 75-84.

Alhashemi, A.H., Karbassi, A.R., Kiabi, B.H., Monavari, S.M. and Nabavi, M.B. 2011. Accumulation and bioaccessibility of trace element in wetland sediments. African J. Biotechnol., 10: 1625-1638.

APHA, 2005. Standard methods for the examination of water and wastewater. American Water Works Association, Water Environment Federation, American Public Health Association. Washington, DC: pp.144.

Bassi, N., Kumar, M.D., Sharma, A. and Pardha-Saradhi, P. 2014. Status of wetlands in India: A review of extend, ecosystem benefits, threats and management strategies. J. Hydrol. Regional Studies, 2: 1-19.

Borisova, G., Chukina, N., Maleva, M. and Prasad, M.N.V. 2014. *Certophyllum demersum* L. and *Potamogeton alpines* Balb. From Iset' River, Ural Region, Russia differ in adaptive strategies to heavy metals exposure-A comparative study. Inter. J. Phytorem., 16: 621-633.

Chatterjee, S., Chetia, M., Singh, L., Chattopadhyay, L., Datta, S. and Mukhopadhyay, S.K. 2011. A study on the phytoaccumulation of waste elements in wetland plants of a Ramsar Site in India. Environ.Monit. Assess., 178: 361-371.

Evangelou, M.W.H., Ebel, M. and Schaeffer, A. 2007. Chelate assisted phytoextraction of heavy metals from soil. Effect, mechanism, toxicity, and fate of chelating agents. Chemosphere, 68: 989-1003.

Fairbrother, A., Wenstel, R., Sappington, S. and Wood, W. 2007. Framework for metals risk assessment. Ecotoxico. Environmen. Safety, 68: 145-227.

Fatima, M., Usmani, N., Hossain, M.M., Siddiqui, M.F., Zafeer, M.F., Firdaus, F. and Ahmad, S. 2014. Assessment of gentoxic induction and deterioration of fish quality in commercial species due to heavy-metal exposure in an urban reservoir. Archive Environ. Contamination Toxicol., 67: 203-213.

Feng, H., Qian, Y., Cochran, J.K., Zhu, Q., Hu, W., Yan, H., Li, L., Huang,

X., Chu, Y.S., Liu, H., Yoo, S. and Liu, C. 2017. Nanoscale measurement of trace element distributions in Spartina alterniflora root tissue during dormancy. Sci. Reports, 7: 40420.

Ghaly, A.E., Snow, A. and Kamal, M. 2008. Kinetics of Iron uptake by wetland plants. American J. Biochem. Biotechnol., 4: 279-287.

Jiao, W., Ouyang, W., Hao, F.H., Wang, F.L. and Liu, B. 2014. Long-term cultivation impact on the heavy metal behavior in a reclaimed wetland, Northeast China. Environmental Pollution, 147: 311-323.

Kershaw, K.A. 1973. Quantitative and Dynamic plant Ecology. Edward Arnold LTD., London.

Khatun, A. 2016. Evaluation of metal contamination and phytoremediation potential of aquatic macrophytes of East Kolkata Wetlands, India. Environ Health Toxicol 31:7.

Lone, M.A., He, Z. and Stoffella, P.J. 2008. Phytoremediation of heavy metal polluted soils and water: Progresses and perspectives. Journal Zhejiang University Science, B19: 210-220.

Lu, Q., He, Z.L., Graetz, D.A., Stoffela, P.J. and Yang, X. 2011. Uptake and distribution of metals by water lettuce (*Pistia stratiotes* L.) Environ. Sc. Poll. Res., 18: 978-986.

Meitei, M.D. and Prasad, M.N.V. 2016. Bioaccumulation of nutrients and metals in sediment, water,and phoomdi from Loktak lake (Ramsar site), northeast India: phytoremediation options and risk assessment. Environ. Monitoring Assess. 188: 329.

Miretzky, P., Saralegui, A. and Cirelli, A.F. 2010. Quantitative assessment of worldwide contamination of air, water and soil by trace elements. Nature, 279: 409-411.

Misra, R. 1968. Ecology Work Book, Oxford Publishing Company, Calcutta, pp. 242.

Mueller-Dombois, D. and Ellenberg, H. 1974. Aims and Methods of Vegetation Ecology. John Willey and Sons, USA., pp. 547.

Prasad, S.N., Ramachandra, T.V., Ahalya, N., Sengupta T., Kumar,A., Tiwari A. K., Vijayan V. S. and Vijayan, L. 2002. Conservation of wetlands of India-a review. Tropical Ecology, 43: 173-186.

Pratas, J., Favas, P.J.C., Paulo, C., Rodrigues, N. and Prasad, M.N.V. 2012. Uranium accumulation by aquatic plants from uranium-contaminated water in Central Portugal. Inter. J. Phytorem., 14: 221-234.

Rai, P.K. 2008. Mercury pollution from chlor-alkali industry in a tropical lake and its bio-magnification in aquatic biota: Link between chemical pollution, biomarkers and human health concern. Human Ecol. Risk Assess., 14: 1318-1329.

Rai, P.K. 2010. Seasonal Monitoring of heavy metals and physico-chemical characteristics in a lentic ecosystem of sub-tropical industrial region, India. Environ. Monit. Assess., 165: 407-433.

Rai, P.K. 2018a. Heavy metals phyto-technologies from a Ramsar wetland plants: Green approach. Chemistry and Ecology, 34(8): 786-796

Rai, P.K. 2019. Heavy metals/metalloids remediation from wastewater using free floating macrophytes of a natural wetland. Environ. Technol. & Innovation, 15: 100393.

Rai, P.K., Kumar, V., Lee, S.S., Naddem, R., Ok, Y.S., Kim, K.H. and Tsang, D.S.W. 2018. Nanoparticle-Plant interaction: implications in energy, environment, and agriculture. Environ. Int., 119: 1-19.

Rai, P.K., Lee, J., Kailasa, S.K., Kwon, E.K., Tsang, Y.F., Ok, Y.S. and Kim, K.H. 2018a. A critical review of ferrate (VI)-based remediation of soil and groundwater. Environ. Res., 160: 420-448.

Rai, P.K., Lee, S.S., Zhang, M., Tsang, Y.F. and Kim, K.H. 2019. Heavy metals in food crops: Health risks, fate, mechanisms and management. Environ. Int., 125: 365-385.

Rai, P.K. 2018. Phytoremediation of emerging contaminants in wetlands. CRC Press, Taylor & Francis, Boca Raton, USA, pp. 248.

Rai, P.K. and Kim, K.H. 2020. Invasive alien plants and environmental remediation: A new paradigm in sustainable restoration ecology. Restoration Ecology 28(1), 3-7.

Rai, P.K., Kim, K.H., Lee, S.S. and Lee, J.H. 2020. Molecular mechanisms in phytoremediation of environmental contaminants and prospects of engineered transgenic plants/microbes. Sci. Total Enviro. 705: 135858.

Rai, P.K. and Singh, J.S. 2020. Invasive alien plant species: their impact on environment, ecosystem services and human health. Ecol. Indicators, 111: 106020.

Ramsar secretariat 2013. The list of wetlands of international importance. The secretariat of the convention on wetlands, Gland, Switzerland.

Sharma, S. and Sujatha, D. 2016. Characterization of the water chemistry, sediment $^{13}C$ and $^{18}O$ compositions of Kolleru Lake-A Ramsar wetland in Andhra Pradesh, India. Environ. Monit. Assess., 188: 409.

Singh, M.M. and Rai, P.K. 2016. Microcosm investigation of Fe (iron) removal using macrophytes of Ramsar Lake: A phytoremediation approach. Inter. J. Phytoremed., 18(12): 1231-1236.

Sood, A., Uniyal, P.P., Prasanna, R. and Ahluwalia, A.S. 2012. Phytoremediation potential of aquatic macrophyte, *Azolla*. Ambio, 41: 122-137.

Tombi, H. and Shyamananda, R.K. 1994. Loktak. World Wide Fund, New Delhi.

Valderrama, A., Tapia, J., Penailillo, P. and Carvajal, D.E. 2013. Water phytoremediation of cadmium and copper using *Azolla* filiculoides Lam. In a hydroponic system. Water Environ Journal, 27: 293-300.

Xin, K., Huang, X., Hu, J.L., Li, C., Yang, X.B. and Arndt, S.K. 2014. Land use change impacts on heavy metal sedimentation in mangrove wetlands-a case study in Dongzhai Harbor of Hainan, China. Wetlands, 34: 1-8.

Xue, P., Li, G., Liu, W. and Yan, C. 2010. Copper uptake and translocation in a submerged aquatic plants *Hydrilla verticillata* (L.f) Royle. Chemosphere, 81: 1098-1103.

Zhang, G., Bai, J., Zhao, Q., Lu, Q., Jia, J. and Wen, X. 2016 Heavy metals in wetland soils along a wetland-forming chronosequence in the Yellow River Delta of China: Levels, sources and toxic risks. Ecol. Indicators, 69: 331-339.

Nature Environment and Pollution Technology
An International Quarterly Scientific Journal

p-ISSN: 0972-6268
(Print copies up to 2016)
e-ISSN: 2395-3454

Vol. 19 | No. 4 | pp. 1617-1626 | 2020

Original Research Paper

https://doi.org/10.46488/NEPT.2020.v19i04.029

Open Access Journal

# Comparison of Structural Stability and Erodibility of the Purple and Loess Soils Based on Le Bissonnais Method

**Y. Wang, Z. Wu, F.T. Li, Y. Deng, X.L. Liang† and G. Wang**

College of Water Conservancy and Hydropower Engineering, Sichuan Agricultural University, Ya'an 625014, Sichuan, People's Republic of China

†Corresponding author: X. L. Liang; wangyong2015@sicau.edu.cn

**Nat. Env. & Poll. Tech.**
**Website: www.neptjournal.com**

*Received:* 07-11-2019
*Revised:* 29-11-2019
*Accepted:* 16-01-2020

**Key Words:**
Purple soil
Loess soil
Soil aggregate
Stability index
Soil erodibility

## ABSTRACT

This paper aims to study structural differences and anti-erodibility properties of purple and loess soils in hilly terrains of southern and northern China. Yoder's method and Le Bissonnais method were used to determine the distribution of soil particle sizes, mean weight diameter (MWD), and geometric mean diameter (GMD). The sequences of water-stable aggregates in different sizes were as follows: On one hand, the sequence of purple soil aggregates was $W_{2\text{-}5mm}>W_{0.25\text{-}0.5mm}>W_{0.5\text{-}1mm}>W_{0\text{-}0.053mm}>W_{0.053\text{-}0.25mm}>W_{1\text{-}2mm}>W_{>5mm}$. On the other hand, the sequence of the loess soil was $W_{0\text{-}0.053mm}>W_{0.053\text{-}0.5mm}>W_{0.25\text{-}0.5mm}>W_{0.5\text{-}1mm}>W_{2\text{-}5mm}>W_{1\text{-}2mm}>W_{>5mm}$. Three LB treatments were carried out and the results were as follows: MWD and GMD of soil aggregates in the loess soil presented the trend of slow wetting (SW)>wetting stirring (WS)>fast wetting (FW), while those in the purple soil were WS>SW>FW. Under SW treatment, purple soil had higher erodibility factor (*K*) than loess soil, close to the result of Yoder's method. Yet under WS and FW treatments, *K* values of purple soil were much lower than that of loess soil ($P<0.05$). A significant difference in *K*, MWD, GMD, and soil organic matter (SOM) values was found between purple soil and loess soil ($P<0.05$). Slope positions greatly influence MWD, GMD, SOM content for the two soils ($P<0.01$), and the interaction between soil type and slope position showed an extremely significant positive correlation to MWD and GMD ($P<0.01$). Our study indicates that, under different breakdown mechanisms, purple soil has a more stable structure and higher anti-erodibility than loess soil. The results of this study will provide a theoretical basis for further understanding of the erosion mechanism of the main soils in China.

## INTRODUCTION

Soil structure plays an important role in maintaining soil functions. The structure's basic units are soil aggregates, which will decide the stability of the soil (Mikha & Rice 2004). Aggregate stability refers to the ability to resist external damage, which affects a variety of physical or chemical properties of the soil, such as nutrient storage, water infiltration and soil anti-erosion ability (Bernard & Roose 2002). Improving the stability of soil aggregates will effectively enhance soil quality and prevent environmental problems such as soil erosion and other forms of land degradation (Zhu et al. 2017). Soil erodibility is the intrinsic susceptibility of a soil to erosion by runoff and raindrop impact. It is an important quantitative parameter to evaluate the sensitivity of soil to erosion. The most commonly used soil erodibility term is the soil erodibility factor (K) of the Universal Soil Loss Equation (USLE) (Wang et al. 2014).

Purple soil is one of the most important soil resources in China. It is widely distributed in southern China and covers an area of 0.2 million km$^2$ (about two per cent of China's territory). It is a highly fertile soil but also weatherable and prone to water erosion. Soil erosion of the purple soil in the hilly areas will result in an adverse effect on soil quality and form coarse sand, which indicates desertification (Shi et al. 2012). Most widespread in northern China, loess soil covers about 10 per cent of the land surface of the Earth and approximately 5 to 10 per cent of China's territories. Due to its special structure, loess soil has very weak resistance of soils to erosion and may be easily dislodged by heavy rains. The Loessal Plateau is one of the areas in China where soil erosion by water is problematic, which is the result of its deep loess deposits (Liu 2013).

Some studies have demonstrated the soil erosion of loess soil and purple soil by the dynamic activity of erosive agents, respectively. Others have focused on the effects of tillage, land use, and vegetation etc. (An et al. 2013, Zeng et al. 2018, Kalhoro et al. 2017, Li et al. 2015, Tuo et al. 2017, Xu et al. 2016). For example, the FW treatment of the LB method is proved to be better than Yoder's method in determining aggregate stability, especially for land uses. So, it is recommended for future studies (An et al. 2013). Furthermore, with

the LB method, vegetation types had significant effects on soil aggregates during different rain conditions. Soil organic matter and clay contents were significantly related to the stability of soil aggregate (Zeng et al. 2018). Although external agents cause soil erosion, the structure and properties of the soil will determine how much it is eroded.

Most previous studies compared loess and purple rill erosion through measuring volume replacement (Chen et al. 2015, Chen et al. 2017, Xing et al. 2018). Yet few of them studied different soil structures and anti-erodibility in purple soil and loess soil. Therefore, the purposes of this study were (1) to compare the stability of the purple and loess soil aggregates by adopting Yoder's method and LB method, and (2) to examine soil anti-erodibility of the two soils, and discuss the similarities and differences of soil structures and anti-erodibility of purple soil and loess soil in different landscape positions.

## MATERIALS AND METHODS

**Soil location of this study:** To further the study, we have selected two areas, of which loess soil and purple soil are widely distributed, respectively (Fig. 1). One area is located in Suining County at the centre of Sichuan Basin (30°21'51" N,105°28'37" E). It is in the middle and lower reaches of the Jialing River and has the monsoon-influenced humid subtropical climate. Its annual average temperature is 18°C and the average annual precipitation is about 933 mm, concentrating from May to September. Its average annual evaporation is 897 mm. The parent material of the purple soil is the Jurassic Suining formation (J3s). Suining County is one of the main areas where purple soil is widely distributed. Located on steep slopes, most farmland is small in size and arable lands are prone to tillage erosion. The other area is located in Guyuan City of Ningxia province in China (36°01'43" N, 106°28'08" E). As part of the Loessal Plateau, it is a semi-arid region in the transitional climate zone (TCZ). Its annual average temperature is 7°C and the average annual precipitation is about 400 mm. Approximately 70% of annual precipitation falls as rain between June and September. The majority of the soils in the study area are loess soil. It is a result of cultivation and crop growth, which break down loessal parent material.

**Soil Samples and Experimental Procedures:** A straight slope was selected to study the purple soil and loess soil. It


Fig. 1: Location of the study area.

was 20 meters long and 5 meters wide, with a slope gradient of 15 degrees. The entire slope was divided into three segments: the upper (0-7m), the middle (7-14m), and the lower (14-20m). Five repetitions were performed to take core samples on each slope segment. For aggregate analyses, samples were collected from the surface layer (0-20 cm) with a flat spade, and placed in plastic containers that were rigid and impact-resistant. In this way, samples would not be disturbed during transportation to the laboratory. Subsequently, soil samples were air-dried, with large particles being gently peeled off so that the samples mainly consisted of 10-mm diameter small clods while the natural structure of soil was preserved. Debris, roots and other impurities on the samples' surface were also removed. The distribution of aggregates' size was measured by Yoder's method and LB method.

First of all, we conducted Yoder's method, 50 g of aggregates was carefully added to nests of sieves, with a pan underneath, having with 5 mm, 2 mm, 1 mm, 0.5 mm, 0.25 mm and 0.053 mm size arranged from top to bottom, respectively, on the shaker apparatus. Each sample was added to the top sieve and slowly wetted in tap water for about 20 min. The water level in the container was adjusted to ensure that the water just touches the base of this sieve. The aggregates would be saturated due to the capillary rise. Then, the nest was manually oscillated in the water. The rate of oscillation was 60 cycles per minute and the process lasted for 2 min. Aggregates retained in the sieves were transferred to beakers using tap water. The remained fraction on each sieve was weighed and recorded after drying at 105°C for 24 h.

Secondly, we took the LB method, in which slow wetting (SW), wet stirring (WS) and fast wetting (FW) were carried out after the samples were dried at 40°C for 24 h (Bissonnais 1996). Soil aggregates with size ranging from 3 to 5 mm were selected to measure their structural properties. The measurements were based on the three tests FW, WS and SW. (1) FW, 5 g of aggregates were immersed in 50 mL of deionized water in a 250 mL beaker for 10 minutes before the water was absorbed by a liquid transfer tube. (2) WS, 5 g of aggregates were immersed in 50 mL of alcohol in 250 mL conical bottles (concentration 99%). After 10 min, water was added to 200 ml of the conical bottle before the bottle was tightly closed with the stopper. The bottle was then carefully turned upside down for 20 times and was allowed to stand for 30 min. It could be observed that a coarse dispersion was precipitated. A straw was used to remove the excess water. (3) SW, firstly, 5 g of aggregates were placed on a wet filter paper with the tension of -0.3 kpa, and they were completely wetted for 30-40 min. Secondly, the wetted soil was moved to a screen with circular pores 50 μm in diameter and was immersed in alcohol, before being swayed up and down for 20 times (the maximum extent of a vibration was 2 cm). Finally, the soil was moved to an aluminium box, dried at 40°C and weighed. Besides, sieves with 2 mm, 1 mm, 0.5 mm, 0.25 mm, and 0.053 mm openings were used to perform dry screening for obtaining aggregates of varying sizes.

Wet oxidation with $K_2Cr_2O_7$ and the pipette method (Liu 1996) were adopted to measure the concentrations of soil organic matter (SOM; $g.kg^{-1}$) and soil particle-size fractions for each subsample. The basic soil physical and chemical properties for the purple soil and loess soil are listed in Table 1.

**Calculations:** Aggregate indices (MWD, mm) were calculated by:

$$\text{MWD} = \sum x_i \frac{m_i}{\sum m_i} \quad \ldots(1)$$

Where, $x_i$ is the mean particle diameter of the $i^{\text{th}}$ size class (mm) and the value of $m_i$ is calculated from the weight of aggregates retained on each sieve (g).

The corresponding expression of GMD (mm) is:

$$\text{GMD} = \exp\left\{\frac{m_i \ln x_i}{\sum m_i}\right\} \quad \ldots(2)$$

Where, $m_i$ is the weight of aggregates retained on each sieve (g) and $lnx_i$ is the natural log of the average particle diameter of the $i$th size classes (mm).

PAD (%) is calculated as follows:

$$\text{PAD} = \frac{W_T - W_S}{W_S} \times 100\% \quad \ldots(3)$$

Where, $W_T$ refers to the weight of aggregates >0.25 mm after dry sieving (g) and $W_S$ indicates the weight of aggregates of the same size after wet sieving (g).

Relative slaking index (RSI) and relative mechanical breakdown index (RMI) were used to describe the breakdown mechanism of soil aggregates. Their expressions are as follows (Zhang & Horn 2001):

$$\text{RSI} = \frac{\text{MWD}_{\text{SW}} - \text{MWD}_{\text{FW}}}{\text{MWD}_{\text{SW}}} \quad \ldots(4)$$

$$\text{RMI} = \frac{\text{MWD}_{\text{SW}} - \text{MWD}_{\text{WS}}}{\text{MWD}_{\text{SW}}} \quad \ldots(5)$$

Where, $\text{MWD}_{\text{SW}}$, $\text{MWD}_{\text{FW}}$ and $\text{MWD}_{\text{WS}}$ are the mean weight diameter values of the soils after slow wetting, fast wetting and wet stirring treatments, respectively. RSI and RMI evaluate the effects of slaking disaggregation and mechanical breakdown of soil aggregates, respectively.

Table 1: Basic properties of soil.

| Soil type | Slope position | Bulk Density ($g \cdot cm^{-3}$) | Moisture content (%) | Organic matter ($g \cdot kg^{-1}$) | Soil particle-size fraction (%) | | |
|---|---|---|---|---|---|---|---|
| | | | | | 0.05-2 mm | 0.002-0.05 mm | <0.002 mm |
| loessal soil | Upper | 1.22 | 15.21 | 4.30 | 17.91 | 69.08 | 13.01 |
| | Middle | 1.11 | 15.34 | 6.77 | 17.11 | 66.18 | 16.71 |
| | Lower | 1.32 | 15.16 | 9.92 | 18.79 | 67.66 | 13.56 |
| | Mean | 1.22±0.09A | 15.24±0.08A | 9.84±1.23A | 17.94±0.69A | 67.64±1.18A | 14.43±1.63A |
| purple soil | Upper | 1.34 | 20.01 | 8.49 | 24.89 | 45.75 | 29.37 |
| | Middle | 1.43 | 19.12 | 11.17 | 24.13 | 39.98 | 35.89 |
| | Lower | 1.41 | 18.33 | 12.67 | 24.61 | 41.64 | 33.75 |
| | Mean | 1.39±0.04B | 19.15±0.69B | 10.78±1.73A | 24.54±0.31B | 42.46±2.43B | 33.00±2.71B |

Note: The capital letters in the same column indicate that the structural characteristics of different soils are significantly different at the level of $P<0.05$. The same below.

$K$ was calculated as follows (Shi et al. 2012):

$$K = 7.954 \times \left\{ 0.0017 + 0.0494 \times \exp\left[ -0.5 \times \left( \frac{\log GMD + 1.675}{0.6986} \right)^2 \right] \right\} \quad \ldots(6)$$

**Statistical analysis:** All statistical analyses were performed with SPSS (version 21.0). Duncan's multiple-range test and both One Way and Two Way ANOVA were used to analyze the significance of the differences in soil properties between the loess and purple soils. Values with the different letters indicated a significant difference ($P<0.05$). Pearson's correlation coefficient was adopted to measure the statistical relationship between two continuous variables.

## RESULTS

**Properties of purple soil and loess soil in terms of soil aggregate size distribution and wet aggregate stability:** The soil aggregate size distribution at different positions of the experimental terrain is shown in Fig. 2. According to Fig.

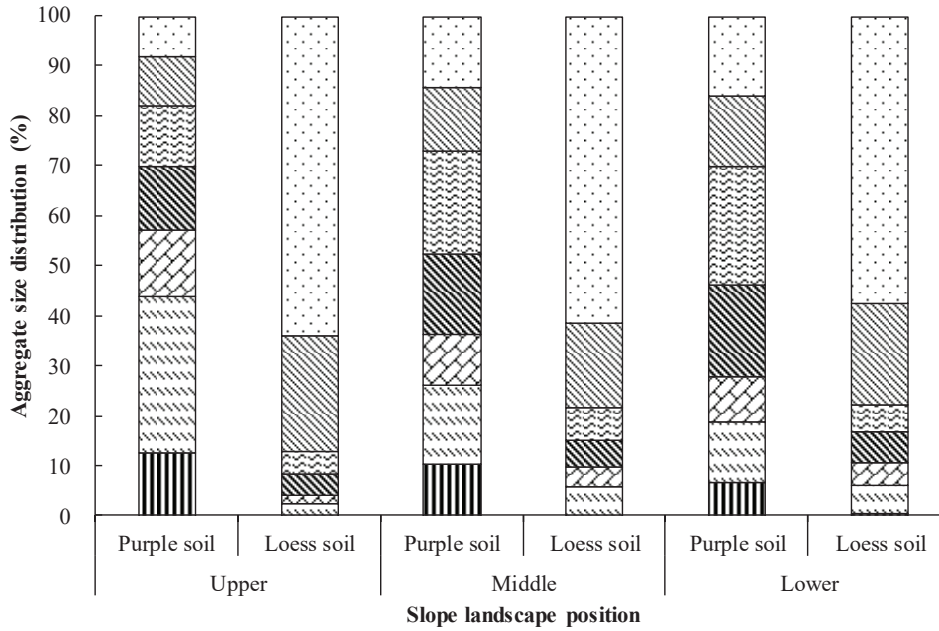


Fig. 2: Particle size distribution of purple and loess soils.

2, the most and second most dominant sizes of purple soil are 2~5 mm and 0.25~0.5 mm, respectively. The average contents of 2~5 mm and 0.25~0.5 mm large purple soil particles are 19.68% (11.29%~34.67%) and 18.76% (11.53%~23.73%), respectively. They are significantly higher than that of loess soil ($P$<0.05, 5.54%). By contrast, the dominant size of loess soil is 0~0.053 mm, with an average content of 60.93% (46.11%~68.91%), significantly larger than that of purple soil ($P$<0.05) in the same size fraction. Besides, loess soil has more 0.053~0.25 mm aggregates (15.36%~23.28%) than purple soil (less than 39.18%). The difference between purple soil and loess soil in soil aggregate size distribution is notable. For purple soil, the contents of different particle sizes decrease in the following order: 2-5 mm> 0.25-0.5 mm> 0.5-1 mm> 0-0.053 mm> 0.053-0.25 mm> 1-2 mm> 5 mm. The soils at the lower slope are more stable than soils at the slope as the content of water-stable aggregates (<0.25 mm) increases in the slope (from top slope to foot slope). As for loess soil, the contents of different particle sizes decrease in the following order: 0-0.053 mm> 0.053-0.5 mm> 0.25-0.5 mm> 0.5-1 mm> 2-5 mm> 1-2 mm> 5 mm, among which loess soil aggregates 0-0.053 mm in size are most widely distributed. Based on the result of Yoder's method, there are much more water-stable aggregates in purple soil than in loess soil.

**The properties of purple soil and loess soil in terms of aggregate stability based on Yoder's method and LB method:** To further analyse purple and loess soils, we have used Yoder's method to determine values including MWD, GMD, PAD and the percentage of aggregates larger than 0.25 mm ($R_{0.25}$) (Qi et al. 2011). The results are given in Table 2. The MWD and GMD of purple soil were significantly higher than those of loess soil after dry sieving, indicating stronger mechanical stability of purple soil than loess soil. Moreover, $R_{0.25}$ of purple soil is three times higher than that of loess soil. Based on Yoder's method, the MWD and GMD values of purple soil were significantly higher than those of loess soil, indicating better water-stability of aggregates in purple soil than in loess soil. $R_{0.25}$ of purple and loess soils are significantly different. Purple soil has significantly smaller PAD value than loess soil, but both values increase as the slope goes steeper. The CV of PAD in purple and loess soils are 24.71% and 2.32% respectively. It shows that the loess soil is more easily influenced by the Yoder's method, no matter on which kind of terrain positions.

The results of the LB method show differences in MWD and GMD values among treatments (Table 3). After the FW treatment, different soils show significantly different MWD and GMD values, even at the same slope position. MWD and GMD of purple soil increase by 36.19% and 36.59%, respectively, compared with loess soil. After the WS treatment, MWD and GMD of purple soil at the same slope position are 2.14mm and 1.63mm, respectively, which are strikingly different with those of loess soil (0.53 mm and 0.22 mm). Despite the above-mentioned differences, ($P$<0.05), there is no large significance between the two soils after SW treatment. The MWD values of loess soil at the same slope position show SW>WS>FW, while for purple soil at the same slope position the sequence is WS>SW>FW. The results of the LB (FW, SW and WS) method show that purple soil has higher aggregate stability than loess soil.

We have adopted the LB method to study the breakdown mechanism of the two types of soils and found significant differences between their soil aggregates at different terrain positions. The RSI values of purple soil are on an upward trend, while RSI values of loess soil, which are significantly higher, show a downward trend. The RMI values of loess soil are positive, and less than the RSI values. Moreover, RMI also

Table 2: The soil aggregate stability based on Yoder method.

| Soil types | Slope position | MWD (mm) | | GMD (mm) | | $R_{0.25}$ (%) | | PAD (%) |
|---|---|---|---|---|---|---|---|---|
| | | Dry | Wet | Dry | Wet | Dry | Wet | |
| Loess soil | Upper | 3.86 | 2.41 | 2.71 | 1.08 | 96.86 | 81.99 | 15.35 |
| | Middle | 4.55 | 1.71 | 2.94 | 0.59 | 93.62 | 73.13 | 21.89 |
| | Lower | 4.52 | 1.31 | 2.93 | 0.45 | 93.98 | 69.96 | 25.56 |
| | Mean±SD | 4.31±0.32A | 1.81±0.45A | 2.86±0.11A | 0.71±0.27A | 94.82±1.44A | 75.03±5.09A | 20.93±4.22A |
| Purple soil | Upper | 0.57 | 0.22 | 0.20 | 0.06 | 19.8 | 13.09 | 31.40 |
| | Middle | 0.66 | 0.37 | 0.26 | 0.08 | 33.34 | 21.59 | 31.99 |
| | Lower | 0.54 | 0.41 | 0.24 | 0.09 | 32.04 | 22.36 | 32.88 |
| | Mean±SD | 0.59±0.05B | 0.33±0.08B | 0.23±0.02B | 0.08±0.01B | 28.39±6.10B | 19.01±4.20B | 32.09±0.61A |

shows a downward trend. Therefore, loess soil aggregates are more prone to the slaking effect than the mechanical breakdown effect. Since the RMI values of purple soil are negative, its dominant breakdown mechanism is slaking.

**The comparison of K values based on Yoder method and the LB method:** Yoder's method shows the significant differences between the K values of purple and loess soils (Fig. 3). Purple soil has much lower K values than loess soil at the same slope position. LB method studies K values through three treatments. It is found that the K values of the two soils are similar after the SW treatment. This result suggests that the dominant aggregate breakdown mechanism of purple soil is clay swelling. After the WS treatment, purple soil has much smaller K values than loess soil. After the FW treatment, the K values of loess soil increase by 102.79% compared with that of purple soil. It can be concluded that purple soil has lower erodibility than loess soil, especially for WS and FW treatment. Moreover, loess soil has higher $K_{SW}$ than $K_{WS}$ but purple soil shows the opposite pattern, which is consistent with the results of $MWD_{SW}$ and $MWD_{WS}$. In general, loess soil is more susceptible to erosion than purple soil. As for purple soil, fast wetting, among all three treatments, does the most damage to its soil aggregates, while Yoder's method has done more damage to purple soil

Table 3: The soil aggregate stability based on the LB method.

| Soil type | Slope position | MWD (mm) | | | GMD (mm) | | | RSI | RMI |
|---|---|---|---|---|---|---|---|---|---|
| | | SW | WS | FW | SW | WS | FW | | |
| Purple soil | Upper | 1.53 | 2.32 | 1.18 | 0.97 | 1.85 | 0.66 | 0.23 | -0.52 |
| | Middle | 0.86 | 1.63 | 0.55 | 0.49 | 1.19 | 0.26 | 0.34 | -0.91 |
| | Lower | 1.35 | 2.48 | 0.72 | 0.75 | 1.84 | 0.36 | 0.48 | -0.74 |
| | Mean±SD | 1.25±0.28A | 2.14±0.37A | 0.82±0.27A | 0.74±0.20A | 1.63±0.31A | 0.43±0.17A | 0.35±0.10A | -72±0.16A |
| Loess soil | Upper | 1.93 | 0.64 | 0.59 | 1 | 0.25 | 0.22 | 0.69 | 0.65 |
| | Middle | 1.15 | 0.47 | 0.38 | 0.42 | 0.19 | 0.14 | 0.67 | 0.6 |
| | Lower | 1.05 | 0.5 | 0.32 | 0.47 | 0.2 | 0.13 | 0.61 | 0.48 |
| | Mean±SD | 1.38±0.39A | 0.54±0.07B | 0.43±0.12B | 0.63±0.26A | 0.21±0.03B | 0.16±0.04B | 0.66±0.03B | 0.58±0.07B |

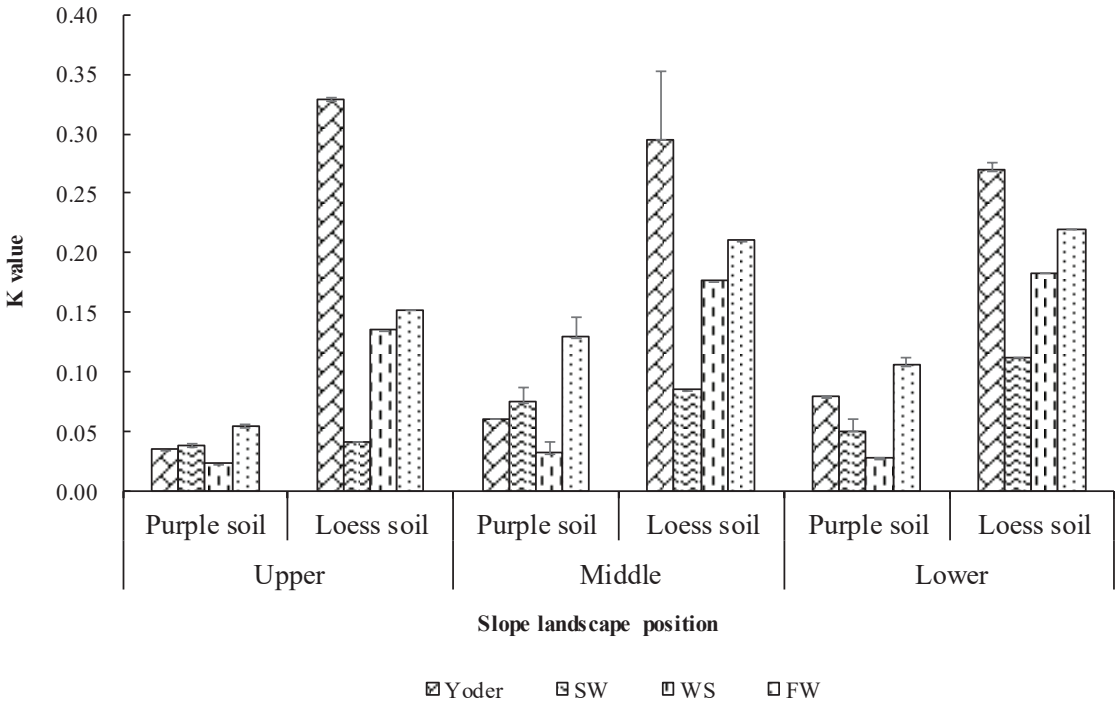


Fig. 3: Comparison of K values of purple soil and loess soils under different treatments.

aggregates than the LB method. Under Yoder's method, the overall effect of the crushing mechanism is greater than the individual effect on loess soil.

**Effects of slope position and soil types on the stability of soil aggregates:** Table 4 gives the correlations among MWD values. In terms of purple soil, a positive and significant correlation exists between the MWD values of the SW treatment and the MWD values of the WS and FW treatments. But no such significant correlations are found in MWD values of loess soil by both Yoder's method and LB method. Purple soil shows a significant positive correlation between soil clay swelling effect and mechanical breakdown effect, and soil clay swelling effect expresses a positive relationship with slaking effect. However, no significant relationship is observed in the breakdown mechanisms of loess soil.

As findings illustrated above (Table 5), soil types greatly influence soil properties including K value, MWD, $R_{0.25}$, SOM, RSI and RMI while slope position is highly related to SOM content, MWD and GMD values. However, only MWD and GMD values show significant and positive relationship with the interaction of soil type and slope position. No significant correlation exists between SOM content and values of K, $R_{0.25}$, RSI and RMI. Therefore, the interaction of soil type and slope position has a significant impact on SOM.

## DISCUSSION

Purple and loess soils are two typical erodible soils widely distributed in southern and northern China, respectively. They have distinct properties due to differences in climate, topography, elevation, and parent rock (Table 6). The wide difference in both latitude and topography of the two soils' geographical distribution results in different climates. Every summer, the southeast monsoon will blow from the ocean to the mainland. Monsoon also brings precipitation, the level of which decreases from east to west and from south to north. Therefore, the rainfall in the area of purple soil is 2~3 times heavier than in the area of loess soil and often lasts for a long time. There are broad differences between the breakdown mechanism of purple and loess soils (Table 3).

The purple soil is weathered from purplish rocks while loess soil is a young soil that develops weakly on the loess or secondary loess parent material. Since humus accumulation and tillage fracture and crumble the soil, they disrupt soil structure, accelerating surface runoff and soil erosion. Profile of purple soil is A-AC-C. The upper and lower layers are uniform without significant difference. Leaching and precipitation are rare, and a new body is not formed. By contrast, the soil profile of loess soil is A-C; the transition of horizons is obvious; the upper and lower layers are the organic layers

Table 4: Correlation analysis of MWD values of the purple soil and loessal soil under Yoder and LB method.

| Treatment | Purple soil | | | | Loess soil | | | |
|---|---|---|---|---|---|---|---|---|
| | SW | WS | FW | Yoder | SW | WS | FW | Yoder |
| SW | 1 | | | | 1 | | | |
| WS | 0.831* | 1 | | | 0.527 | 1 | | |
| FW | 0.835* | 0.618 | 1 | | 0.809 | 0.229 | 1 | |
| Yoder | 0.336 | -0.022 | 0.708 | 1 | -0.559 | -0.772 | -0.523 | 1 |

Notes: * Significant correlation at the $P<0.05$ level. ** Significant correlation at the $P<0.01$ level. The same below.

Table 5: Multivariate ANOVA of soil type and slope position.

| Index | Soil type | | Slope position | | Soil type*Slope position | |
|---|---|---|---|---|---|---|
| | *F* | *P* | *F* | *P* | *F* | *P* |
| K | 152.897 | <0.001** | 0.257 | 0.781 | 1.695 | 0.261 |
| MWD | 450.398 | <0.001** | 15.187 | 0.004** | 28.665 | 0.001** |
| GMD | 2243.445 | <0.001** | 193.636 | <0.001** | 224.568 | <0.001** |
| $R_{0.25}$ | 368.544 | <0.001** | 0.183 | 0.837 | 4.934 | 0.054 |
| SOM | 124.578 | <0.001** | 69.803 | <0.001** | 2.320 | 0.179 |
| RSI | 12.059 | 0.013* | 0.295 | 0.755 | 1.233 | 0.365 |
| RMI | 67.841 | <0.001** | 0.795 | 0.494 | 0.478 | 0.642 |

Table 6: Comparison of the main properties of purple and loess soils.

| Characteristic item | Purple soil | Loess soil |
|---|---|---|
| Regional distribution | Mainly distributed in the subtropical area of China (Sichuan, Yunnan, Guizhou, etc.) and most widely distributed in Sichuan Basin. | Mainly distributed in Semi-arid and arid areas in temperate and warm-wet zones (Shaanxi, Ningxia, etc.) and is the most widely distributed on Loess Plateau. |
| Climate condition | The annual average temperature is 14~18°C; the annual average precipitation is 1000~1500 mm; rainfalls concentrate in June-October, and the annual evaporation is 300~900 mm. | The annual average temperature is 7~16°C, and the annual average precipitation is 200~500 mm, mostly concentrating in July-September. Annual evaporation is 800~2200 mm. |
| Mechanism of soil | Purple soil is a lithogenic soil formed by weathering of purple shales in tropical and subtropical regions, mainly due to frequent weathering and erosion. | The parent material of loess is Quaternary aeolian loess. Its formation is mainly through light humus accumulation of grass, tillage maturation and soil erosion. |
| Profile morphology | The section structure is usually A-AC-C, with no obvious humus layer. The AC transition layer is below the surface layer and the parent layer is at the bottom. | The profile is A-C soil structure, with organic stratum on above and parent stratum on below. |
| Topsoil properties | The thickness of the plough layer in a farmland slope is 15~20 cm. Below plough layer is plough bottom layer and parent material layer. | The tillage layer is 10~15 cm thick, thinner than that of purple soil, and the loess parent material layer is below the tillage layer. |
| Mineral composition | The clay minerals of purple soil are mainly 2:1 hydromica, montmorillonite and chlorite. The primary minerals contain a lot of quartz, and the secondary minerals are mainly illite. | The mineral composition of loess is mainly quartz and feldspar, while the clay mineral is mainly hydromica, followed by chlorite and a small amount of kaolinite. |
| Architectural feature | The pore distribution is mainly macropore (>1.2 mm), and the degree of agglomeration is high. | Structurally loose, there are many voids between particles and large voids. |
| Soil particle-size fraction | The content of sand and clay in purple soil is higher, and the particles of different sizes are evenly distributed. | The silt content of loess soil is relatively high, and the particle size distribution is mainly concentrated in non-water-stable aggregates. |
| Chemical property | SOM contents range from 10 to 30 $g.kg^{-1}$. pH is from 5.5 to 8.0, and the content of $CaCO_3$ is less than 30 $g.kg^{-1}$. | SOM content is 3~10 $g.kg^{-1}$; pH is 8.0~8.5, and the content of $CaCO_3$ is 90~180 $g.kg^{-1}$. |

with 10~30 cm thick; and at parent material layer, where the precipitation is greater, the calcium carbonate has been leached slightly.

Influenced by human activities, the thickness of the purple soil layer is 15~25 cm, and the thickness of the tillage layer is relatively stable. The tillage layer of the loessal layer is about 15 cm thick. Some areas are less than 10 cm thick, and loess parent material is immediately below the tillage layer. The mineral composition of purple soil is mainly composed of hydromica and quartz. Purple soil has a stable aggregate structure, with higher contents of sand grains and clay than loess soil. The mineral composition of loess soil is mainly quartz and feldspar. Loess soil is loose in structure, with a relatively high content of silt (about 60%). The SOM content of purple soil ranges from 10 to 30 $g{\cdot}kg^{-1}$, and the pH from 5.5 to 8.0, with low content of $CaCO_3$ and very low content of nitrogen. The contents of phosphorus and potassium are rich. The SOM content of loess soil is from 3 to 10 $g{\cdot}kg^{-1}$, with the pH ranging from 8.0 to 8.5, the content of $CaCO_3$ 3~6 times higher than that of purple soil, and low content of nitrogen, zinc, and manganese. Although loess soil is rich in phosphorus and potassium, it is hard to be made into commercial use (Li 1991, Zhang 2002).

Soil stability is greatly affected by both external and internal factors. LB method identifies different disaggregation mechanisms of soil aggregates. The SW treatment simulates the capillary action inside the soil under the damage of light rain, which causes the soil clay to swell; the WS simulates the mechanical breakdown caused by splash erosion which damages the soil structure; and the FW treatment simulates the slaking of soil under heavy rains due to gas explosion nearby. In our study, the aggregate stability of both purple soil and loess soil was most severely damaged under the FW treatment, among all three treatments. Heavy rains were the main external factor for soil erosion in the study areas, and slaking is the main internal factor of soil aggregate disruption. The SW treatment has the least damage to loess soil, which is supported by the current findings by Guo et al. (2010). The study indicates that clay swelling has little effect on the aggregate stability of loess soil. By contrast, the WS treatment has the least damage to purple soil, indicating that mechanical breakdown of splash erosion will slightly affect the aggregate stability of purple soil. In mountainous areas with purple and loess soils, serious soil erosion is observed

in summer when heavy rains become frequent. It is recommended to plant hedgerows on the slopes to enhance soil stability and prevent soil losses (Wang et al. 2018).

Related researches showed that due to the difference in geographical location and parent material, the breakdown mechanisms of purple and loess soils were different (Wang et al. 2013). The slaking effect of loess soil was stronger than mechanical breakdown, which increased from the top to the bottom of the slope, but mechanical breakdown decreased in the opposite direction. The purple soil mainly expressed slaking rather than mechanical breakdown, because the high content of clay prevented further mechanical breakdown (Wang 2013). The high content of soil clay acted as a binder to enhance soil aggregate stability. During the wetting process, the clay enhanced the slaking and thus decreased soil aggregate stability (Yan 2008). That was the reason why the clay enhanced the stability of the agglomerate in the purple soil but reduced the stability in the loess soil. To sum up, the dissipation and mechanical effect of the LB method on loess soil is greater than that in purple soil, which affects its anti-erodibility.

There was a significant correlation between soil type and soil aggregate stability indexes. Since Yoder's method was a combination of various breakdown mechanisms, the binding effect of SOM was dwarfed by the slaking and clay swelling. As a result, the effect of SOM on soil aggregate stability became not obvious. Related researches showed that clay content significantly affected the binding effect of soil organic matter (Wang 2013). SOM promoted the stability of soil aggregates through its binding effects when the clay content was less than 25%, but the effects would be lost when the clay content was above 35%. According to a recent study, the MWD values of the loess soil gradually rose down the slope, while the purple soil followed the opposite trend. The clay content of purple soil was 29.37%~35.89%, and that of loess soil was 13.01%~16.71%. Therefore, SOM in loess soil promoted soil aggregate stability, but the binding effect of SOM in purple soil couldn't be reflected. Besides, as purple soil was located in a hilly area with frequent heavy rainfalls, strong water erosion occurred on the slope. Water erosion would carry the fine aggregates down the slope and caused the content of fine-grained soil at the lower slope significantly increased. Such a sorting effect on soil aggregates reduced MWD values (Zhang et al. 2014).

## CONCLUSION

Laboratory experiments were conducted to evaluate structural stability and erodibility of loess and purple soils. The results of this study showed that the structural stability and erodibility of purple soil is quite different from that of loess soil. Purple soil has a more stable structure and higher anti-erodibility than loess soil under different breakdown mechanisms (SW, WS and FW). After comparing three LB treatments, we found that MWD and GMD of the loess soil showed the trend of SW>WS>FW, yet that of the purple soil followed the trend of WS>SW>FW. Under the SW treatment, the $K$ value of purple soil was greater than that of loess soil and was close to the result of Yoder's method. Under WS and FW treatments, the $K$ value of the purple soil was significantly lower than that of the loess soil. This study demonstrated and provided a theoretical basis for further understanding of the erosion mechanism of the loess and purple soils in southern and northern China.

## ACKNOWLEDGEMENT

This work was supported by the CRSRI Open Research Program (CKWV2018489/KY), the National Natural Science Foundation of China (41701324), and the Scientific Research Foundation of the Education Department of Sichuan Province, China (17ZB0343). Yong Wang acknowledges the China Scholarship Council for supporting a Post-Doctoral Fellow program grant (201806915001).

## REFERENCES

An, S.S., Darboux, F. and Cheng, M. 2013. Revegetation as an efficient means of increasing soil aggregate stability on the Loess Plateau (China). Geoderma, 209-210: 75-85.

Bernard, B. and Roose, E. 2002. Aggregate stability as an indicator of soil susceptibility to runoff and erosion validation at several levels. Catena, 47(2): 133-149.

Bissonnais, Y.L. 1996. Aggregate stability and assessment of soil crustability and erodibility: I. Theory and methodology. European Journal of Soil Science, 47(4): 425-437.

Chen, X.Y., Huang, Y.H., Zhao, Y., Mo, B. and Mi, H.X. 2015. Comparison of loess and purple rill erosions measured with volume replacement method. Journal of Hydrology, 530: 476-483.

Chen, X.Y., Huang, Y.H., Zhao, Y., Mo, B., Mi, H.X. and Huang, C.H. 2017. Analytical method for determining rill detachment rate of purple soil as compared with that of loess soil. Journal of Hydrology, 549: 236-243.

Guo, M., Zheng, F.L., An, S.S., Liu, Y. and Darboux, F. 2010. Application of Le Bissonnais method to study soil aggregate stability in the Hilly-gully region. Science of Soil and Water Conservation, 8(2): 68-73.

Kalhoro, S., Xu, X., Chen, W., Hua, R., Raza, S. and Ding, K. 2017. Effects of different land-use systems on soil aggregates: a case study of the Loess Plateau (Northern China). Sustainability, 9(8): 1349.

Li, Z.M. 1991. Purple Soils in China. Science Press, pp. 1-122.

Li, Z.W., Zhang, G.H., Geng, R. and Wang, H. 2015. Rill erodibility as influenced by soil and land use in a small watershed of the Loess Plateau, China. Biosystems Engineering, 129: 248-257.

Liu, D.D. 2013. The coupling relationship of soil macro-structure with soil erosion resistance. Shanxi: Northwest A & F University, pp. 1-2.

Liu, G.S. 1996. Soil Physical and Chemical Analysis and Description of Soil Profiles. Chinese Standard Press, pp. 469-517.

Mikha, M.M. and Rice, C.W. 2004. Tillage and manure effects on soil and aggregate-associated carbon and nitrogen. Soil Science Society of America Journal, 68(3): 809-816.

Qi, Y.C., Wang, Y.Q., Liu, J., Yu, X.S. and Zhou, C.J. 2011. Comparative study on composition of soil aggregates with different land use patterns and several kinds of soil aggregates stability index. Transactions of the Chinese Society of Agricultural Engineering, 27(1): 340-347.

Shi, D.M., Chen, Z.F., Jiang, G.Y. and Jiang, D. 2012. Comparative study on estimation methods for soil erodibility K in Purple hilly area. Journal of Beijing Forestry University, 1: 32-38.

Tuo, D.F., Xu, M.X., Li, Q. and Liu, S.H. 2017. Soil aggregate stability and associated structure affected by long-term fertilization for a Loessial Soil on the Loess Plateau of China. Polish Journal of Environmental Studies, 26(3): 827-835.

Wang, B. 2013. Key factors and calculation of soil erodibility in the typical eroded black soil area of northeast China. Doctoral thesis, Northwest A & F University, Shanxi, pp. 70-71.

Wang, J.G., Kang, Q., Kuang, G.M., Guo, Y.B. and Li, D.Q. 2014. Spatial variability of soil erodibility (K-factor) in Jianshan watershed of Yunnan province. Ecology and Environmental Sciences, 4: 555-560.

Wang, R.Z., Chen, Y., Li, T., He, B.H., Xiang, M.H., Chen, X., Tang, H., Zhou, T. and Liu, X.H. 2018. Study on stability of soil aggregates in the sedimentation zone in front of hedgerows in purple soil area. Journal of Soil and Water Conservation, 32(2): 210-216.

Wang, S.S., Huang, X.Z., Shi, D.M., Guo, Y.J. and Li, Y.X. 2013. Study on soil aggregates stability of mulberry ridge in Rocky Desertification based on Le Bissonnais method. Acta Ecologica Sinica, 33(18): 5589-5598.

Xing, H., Huang, Y.H., Chen, X.Y., Luo, B.L. and Mi, H.X. 2018. Comparative study of soil erodibility and critical shear stress between loess and purple soils. Journal of Hydrology, 558: 625-631.

Xu, M.X., Li, Q. and Wilson, G. 2016. Degradation of soil physicochemical quality by ephemeral gully erosion on sloping cropland of the hilly Loess Plateau, China. Soil and Tillage Research, 155: 9-18.

Yan, F.L. 2008. Aggregate stability characteristic of red soils and its effects on erosion processes at hillslope. Doctoral Thesis, Huazhong Agricultural University, Hubei, pp. 56-57.

Zeng, Q.C., Darboux, F., Man, C., Zhu, Z. and An, S. 2018. Soil aggregate stability under different rain conditions for three vegetation types on the Loess Plateau (China). Catena, 167: 276-283.

Zhang, B. and Horn, R. 2001. Mechanisms of aggregate stabilization in Ultisols from subtropical China. Geoderma, 99(1-2): 123-145.

Zhang, F.R. 2002. Soil Geography. China Agricultural Press, pp. 234-243.

Zhang, J.H., Wang, Y. and Zhang, Z.H. 2014. Effect of terrace forms on water and tillage erosion on a hilly landscape in the Yangtze River Basin, China. Geomorphology, 216: 114-124.

Zhu, G.Y., Shangguan, Z.P. and Deng, L. 2017. Soil aggregate stability and aggregate-associated carbon and nitrogen in natural restoration grassland and Chinese red pine plantation on the Loess Plateau. Catena, 149: 253-260.

Nature Environment and Pollution Technology
An International Quarterly Scientific Journal

p-ISSN: 0972-6268
(Print copies up to 2016)
e-ISSN: 2395-3454

Vol. 19 | No. 4 | pp. 1627-1636 | 2020

Original Research Paper

https://doi.org/10.46488/NEPT.2020.v19i04.030

Open Access Journal

# Lockdown Impact on Particulate Matter and Role of Meteorological Parameters in the Transmission of Covid-19

**Manish Sharma*† and Pargin Bangotra***
*Satellite Remote Sensing Group, Department of Physics, School of Basic Sciences and Research, Sharda University, Greater Noida, India
†Corresponding author: Manish Sharma; manish.sharma@sharda.ac.in

**Nat. Env. & Poll. Tech.**
**Website: www.neptjournal.com**

*Received:* 01-08-2020
*Revised:* 05-09-2020
*Accepted:* 08-10-2020

**Key Words:**
COVID 19
Particulate matter
Meteorological parameters
Lockdown impact

## ABSTRACT

The coronavirus disease (COVID-19) was first noticed over Wuhan, China during December 2019. The spreading characteristics of COVID-19 infection from one person to another are resulting in a growing number of infected cases and created massive stresses across the world. The rapid dissemination of COVID-19 infection declares it as a pandemic. In India, till the mid of May 2020, there were around 75,048 confirm with 2440 number of death cases, specifically due to COVID-19. To break the chain of COVID-19, the Government of India had decided to implement the lockdown, first implemented on 23rd March 2020. Some of the significant benefits of lockdown resulted in the reduction in atmospheric pollutants of the cities across the world. The study is based on the fine and coarse particulate matters (PM) data corresponding to before lockdown and during lockdown periods. The efforts were made over Delhi (DEL) and one of the neighbouring cities, i.e. Gurgaon (GW) considering the duration 1st January 2020 to 15th May 2020 to understand the impact of lockdown on the particulate matter, i.e. PM ($PM_{1.0}$, $PM_{2.5}$ and $PM_{10}$). Our investigation shows the decline in PM concentration during the lockdown period. The impact of COVID-19 pandemic resulted in the rapid increase in the number of COVID-19 cases in DEL, India, and the inhabitants of about 14 million people. The significance of the particulate matter, temperature (°C) and relative humidity (%) on the dispersal of COVID-19 virus and its association to the total number of cases (TC), active cases (AC), recovered cases (RC) and death cases (DC) with special reference to DEL were also discussed.

## INTRODUCTION

In the existing scenario, the whole world is at the risk of the widespread global infection, i.e. COVID-19 declared as pandemic (WHO 2020) that affected more than 208 countries (Singh et al. 2020). According to the recent study conducted by Jain et al. (2020), there were approximately 4,369,933 COVID-19 cases all over the world out of which 98% were suffering from mild, 2 % with a severe infection while 15 % patient could not survive. The first case of the novel coronavirus, i.e. COVID-19 was initially reported in Wuhan city, China in December 2019 and after a few weeks, it started to progressively spread across bordering countries. As per the medical reports, COVID-19 has a severe impact on the respiratory system causing a range of breathing problems, from mild to critical and, more dangerous for the people's previous history of bronchitis, Chronic Obstructive Pulmonary Disease (COPD), heart disease, and diabetes. As per the World Health Organization (WHO), the people having age above 60 years, and children less than 10 years are severely affected by coronavirus (Donnelly et al. 2003). As per the medical experts, this type of disease is a bit similar to severe acute respiratory syndrome (SARS), mostly spread through the droplets, hand contact or some times by indirect contact also, but still, the exact reasons of the medium of transmission or the routes of transmission could not be recognized.

In India, till 13th May 2020, there were around 75,048 confirmed with 2440 number of death cases (MoHFW 2020). By seeing the criticality of this infection and its fast spread, the Government of India has decided to implement the lockdown in different phases which was first implemented on 23rd March 2020. As a preventive measure, various activities and operations related to the social gathering, travel, industries operations, transport including all three modes, commercials, construction, restaurants except the limited essential services like groceries, milk, fruits and vegetable, medicines, etc. were restricted. However, one of the positive impacts which has been observed in many cities and countries including China, Brazil, Barcelona, New York, Los Angeles, Zaragoza, Rome, Dubai, India, Beijing, Shanghai, etc., was the reduction of the pollutants during the period of lockdown (Bao & Zhang 2020, Saadat et al. 2020, Singh et al. 2020). Xu et al. (2020) reported the deterioration in the levels of

pollutants like $PM_{2.5}$, $PM_{10}$, $SO_2$, CO, and $NO_2$ during the lockdown period over China. With the various air pollution monitoring stations, the improvement in air quality was also observed in most of the Indian cities during the lockdown period (http://www.cpcbenvis.nic.in/). Before the lockdown, the pollutant level in most Indian cities was at very high (Aggarwal & Jain 2015, Kumar et al. 2013, WHO 2018).

The earlier study demonstrated the noticeable effect of meteorological parameters especially surface air temperature and relative humidity on particulate matters (Wang et al. 2020). Wu et al. (2020) are also in close agreement of the association between air quality and COVID-19 cases in China. Air pollution measured as particulate matter (PM) has also been shown to be detrimental to human health (Cohen et al. 2005, Donaldson et al. 2001) and lead to increased mortality rates (Dockery et al. 1993, Hales et al. 2010). Various pollutants have been included to define the air quality index, some of them are CO, ozone, $SO_2$, $NO_2$, $NH_3$, Pb, $PM_{2.5}$ and $PM_{10}$ (NAAQS). However, the most accountable pollutants responsible for poor air quality indexes in India are currently $PM_{2.5}$ and $PM_{10}$.

Saksena & Dayal (2000), in their study over DEL, considered PM as one of the hazardous pollutants responsible for chronic bronchitis, whereas, Goyal (2003) found it accountable for asthma. Therefore, considering the criticality of PM and the current lockdown situation, we have analysed the fine ($PM_{1.0}$ and $PM_{2.5}$) and coarse ($PM_{10}$) PM data for seven different places of Delhi (DEL) and Gurugram also known as Gurgaon (GW), India. Gurgaon is a city situated in the southwest of New Delhi. The 24 hours daily mean concentrations of PM ($PM_{1.0}$, $PM_{2.5}$ and $PM_{10}$) were analysed for the different sites over DEL, i.e. IIT-Delhi (IIT-DEL), Greater Kailash (GK), Lodhi Road (LR), Mahant Gurmukh Singh (MGS), Ramjas colony (RJ), Shantipath (SP), US Embassy (USE) and Gurgaon (GW) together with the corresponding temperature (T°C) and relative humidity (RH %) for the duration from 1st January 2020 to 15th May 2020. The resulting daily averages corresponding to the above locations were analysed and compared for before (1st January 2020 - 22nd March 2020) and during lockdown (23rd March 2020-15th May 2020) period. As the optimized T (°C) and RH (%) support the droplet stability in the local environment which may be favourable for the widespread transmission of the virus (Chen et al. 2020). As per the study conducted over different cities of Italy and China, it was noticed that the association between the high frequency of corona cases/mortality and the high level of atmospheric pollutants persistently for over four years (Down to Earth ). The efforts were also made over DEL to understand the linkage between PM, T (°C), and RH (%) and their synergic effect on COVID-19 cases corresponding to the total number of cases (TC), active cases (AC), recovered cases (RC) and death cases (DC) by considering the available data for period 1st April 2020 to 15th May 2020.

## DATA AND ANALYSIS TECHNIQUES

The present study examines the effect of lockdown on the air quality of Delhi (DEL) and Gurgaon (GW), India (Fig. 1). The data related to major pollutants, i.e. PM of size ≤ 2.5

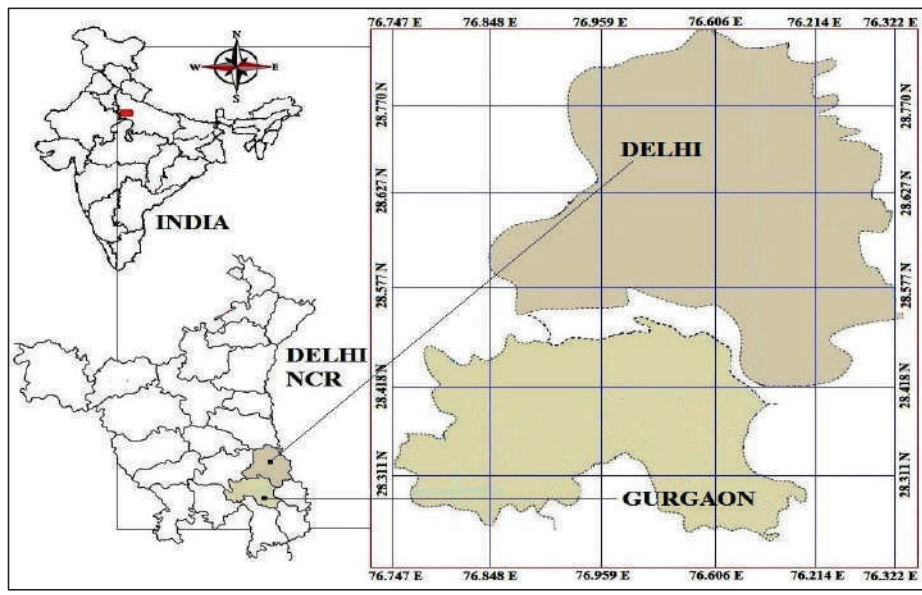


Fig. 1: Map of the studied region.

μm ($PM_{2.5}$), ≤ 10 μm ($PM_{10}$) and ≤1.0 ($PM_{1.0}$) along with meteorological parameters, i.e. T (°C), RH (%) were downloaded through the freely available data source, i.e. Purple Air Sensors (https://www.purpleair.com). The PurpleAir sensors are an "Internet of things" (IoT) air quality sensor or particulate sensor consisting of a network of elements. PurpleAir uses PMS5003 and PMS1003 laser particle counters. These sensors count suspended particles in sizes of 0.3, 0.5, 1.0, 2.5, 5.0 and 10 μm. These particle counts are processed by the sensor using a complex algorithm to calculate the $PM_{1.0}$, $PM_{2.5}$ and mass concentration in $\mu g.m^{-3}$.

The continuous 24-hour average PM with associated T (°C) and RH (%) data was procured for the period 1st January 2020 to 15th May 2020. The procured data cover seven different sites over Delhi, i.e. IIT-DEL, GK, LR, MGS, RJ, SP and USE, and two locations over GW (Fig. 1). In the case of the analysis over DEL and GW, the combined averages of all locations were taken. The data corresponding to TC as well as RC was collected from the source of New Delhi Television Limited (NDTV), an Indian television media company. (https://www.ndtv.com/coronavirus?pfrom=home-mainnavgation). To calculate the 2-tailed Bivariate Pearson correlations among PM, T (°C), RH (%), TC, AC, RC and DC, the statistical analysis model Statistical Package for the Social Sciences (SPSS) was used.

## RESULTS AND DISCUSSION

This section examines the variation in the mean concentration of PM associated to size 1 micron, 2.5 microns and 10 microns commonly recognized as $PM_{1.0}$, $PM_{2.5}$ and $PM_{10}$, over DEL and GW, Influence of Meteorology on PM and its association to TC and RC associated to COVID-19.

### Distribution of PM

The significant dissimilarity appears for fine ($PM_{1.0}$, $PM_{2.5}$) and coarse ($PM_{10}$) over DEL and GW in the box and whiskers charts view (Fig. 2).

The boxes here correspond to 50% of the distribution of the values (from 25% to 75%), while the square and line within the boxes indicate the mean and median values, respectively. The "x" and "–" symbols correspond to 1%/99% and min/max values, respectively. The dissimilar dispersal can be visible clearly from the distribution pattern of PM concentration ($PM_{1.0}$, $PM_{2.5}$ and $PM_{10}$) in the above two sites during the period 1st January 2020 to 15th May 2020. It was found the median PM concentration of 56.10 $\mu g.m^{-3}$ ($PM_{1.0}$), 85.72$\mu g.m^{-3}$ ($PM_{2.5}$) and 96.03 $\mu g.m^{-3}$ ($PM_{10}$) over DEL while lower median concentration of 29.66 $\mu g.m^{-3}$ ($PM_{1.0}$), 44.62 $\mu g.m^{-3}$ ($PM_{2.5}$) and 48.22 $\mu g.m^{-3}$ ($PM_{10}$) was observed over GW. The higher mean PM concentration of 69.22 $\mu g.m^{-3}$ (12.88-264.34 $\mu g.m^{-3}$), 111.75 $\mu g.m^{-3}$ (12.88-64.34 $\mu g.m^{-3}$) and 127.61$\mu g.m^{-3}$ (20.94-559.78 $\mu g.m^{-3}$) related to $PM_{1.0}$, $PM_{2.5}$ and $PM_{10,}$ respectively were observed over DEL. It was noticed that the low mean concentration of PM ($PM_{1.0}$, $PM_{2.5}$ and $PM_{10}$) over the site GW show better air quality as compare to DEL. All of the sizes of PM were exhibited dissimilar concentration that indicates the diverse sources over both the locations, i.e. DEL and GW. The higher mean concentration and prominent characteristic of $PM_{2.5}$ and $PM_{10}$ indicated in Box plot (Fig. 2), suggest road traffic (Mahato et al. 2020, Kumar et al. 2017) as well as industries, power plants and domestic emissions (Sahu et al. 2011a, Guttikunda et al. 2013) as the prime responsible factors.

In trend analysis (Figs. 3a & 3b), covering entire duration, i.e. 1st January 2020 to 15th May 2020, $PM_{10}$ exhibit a higher mean concentration of 127.61 $\mu g.m^{-3}$ (DEL) and 57.53 $\mu g.m^{-3}$ (GW), whereas $PM_{1.0}$ and $PM_{2.5}$, illustrate the mean concentration of 69.22 $\mu g.m^{-3}$ (DEL), 34.20 $\mu g.m^{-3}$ (GW) and 111.75 $\mu g.m^{-3}$ (DEL) and 53.10 $\mu g.m^{-3}$ (GW), respectively. The higher PM concentration during this period, evidently suggests the vehicular emission, industrial emission, and other forms of combustion process as the major sources of pollutants. After the execution of comprehensive lockdown through

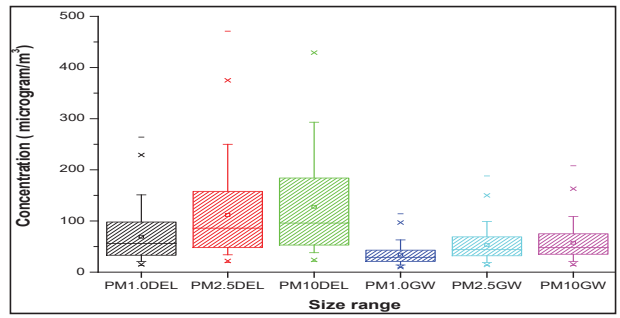


Fig. 2 Boxplots of daily concentrations of analysed pollutants over Delhi and Gurgaon; the median is shown by the middle line of the box. Concentrations are expressed in $\mu g.m^{-3}$ for $PM_{1.0}$, $PM_{2.5}$ and $PM_{10}$.

restricting various activities and operations related to social assembly, travel, industries operations, and transport started from 23rd March 2020, PM mass concentration in DEL (Fig. 3a), and GW (Fig. 3b) were significantly declined. Before the lockdown, it was noticed that the PM concentration in DEL as 94.72 $\mu g.m^{-3}$ ($PM_{1.0}$), 155.45 $\mu g.m^{-3}$ ($PM_{2.5}$) and 178.88 $\mu g.m^{-3}$ ($PM_{10}$) that drastically reduced to 30.96 $\mu g.m^{-3}$, 46.12$\mu g.m^{-3}$ and 50.69 $\mu g.m^{-3}$ by the percentage decrease of 67.31, 70.29 and 71.66, respectively due to the result of the lockdown. The significant decline in the concentration of PM, clearly confirms the influence of the transport and traffic movement in the air quality of DEL.

Before lockdown, low PM concentration has been observed corresponding to $PM_{1.0}$ (42.29 $\mu g.m^{-3}$), $PM_{2.5}$ (66.82 $\mu g.m^{-3}$), and $PM_{10}$ (72.62 $\mu g.m^{-3}$), in GW (Fig. 2b) as compared to DEL. The observed PM concentration ($PM_{2.5}$ and $PM_{10}$) was slightly towards the higher side of the prescribed limit given by NAAQS (http://cpcb.nic.in/airquality-Standard). The tremendous decline of 48.21 %, 51.82 % and 52.45 % in $PM_{1.0}$ (21.90 $\mu g.m^{-3}$), $PM_{2.5}$ (32.19 $\mu g.m^{-3}$) and (34.52 $\mu g.m^{-3}$) were witnessed the impact of lockdown over GW. The analysis related to before and after lockdown noticeably exposed a significant decline in the concentration of PM pollutants during lockdown (23rd March-15th May 2020) by strictly follow-up. Due to holdup of all type of movements, industrial emission and transportation on the road, the fine ($PM_{1.0}$ and $PM_{2.5}$) and coarse ($PM_{10}$) particulate were significantly reduced over both of the locations (DEL and GW) and approached within the limit of NAAQS ($PM_{2.5}$ = 60 $\mu g.m^{-3}$, $PM_{10}$ = 100 $\mu g.m^{-3}$, based on 24-hours average (Jain et al. 2020) demonstrating the noticeable improvement in air quality. The significant decrease in atmospheric pollution attributed to transportation and industrial emissions over Beijing, Shanghai, Guangzhou and Wuhan cities were also observed during the corona pandemic (Wang et al. 2020).

## Influence of Meteorology on PM

The previous studies demonstrated the effect of meteorological variables which has a major impact on air quality (Espinosa et al. 2004, Karar & Gupta 2006). The complete cycle of the formation of secondary pollutants has a great association with the pollutant release rate into the air from the origin, wind speed, turbulence level, air temperature, and precipitation (Bhaskar et al. 2010). Generally, T (°C) has substantial involvement in the air quality of the province, therefore, correlation analysis by considering the period of 1st March 2020-15th May 2020 between PM concentrations and T (°C) for the site DEL (Fig. 4) and GW (Fig. 5) were

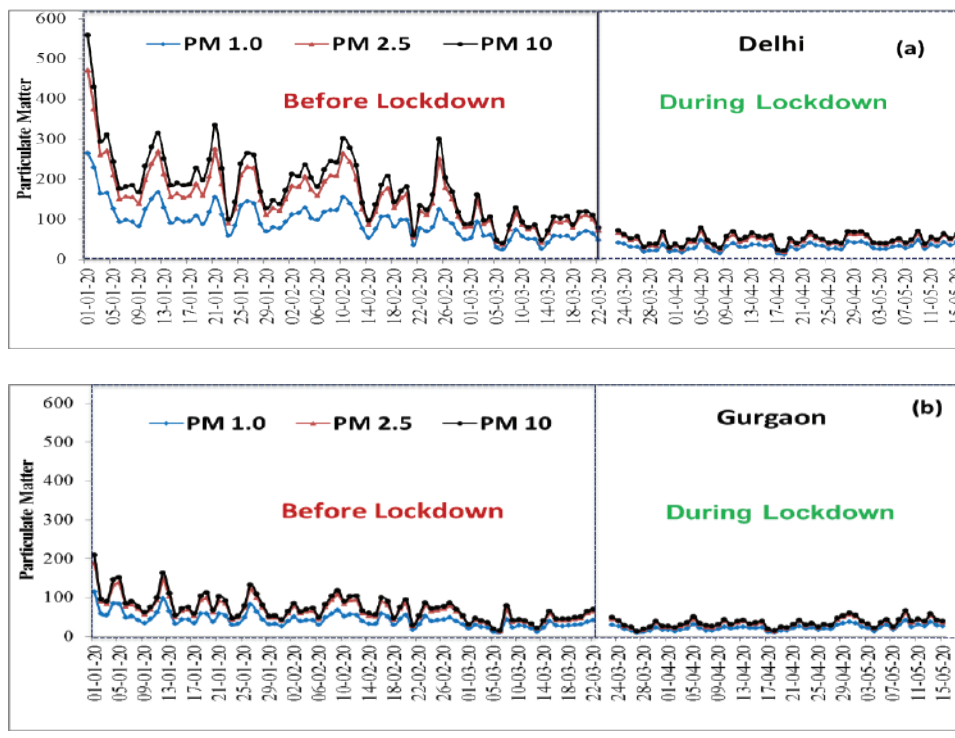


Fig. 3 (a, b). Trend analysis showing the effect of lockdown period on particulate matter in Delhi (a) and Gurgaon (b).

studied to understand the role of T (°C).

There was a significant negative correlation between T (°C) and $PM_{1.0}$ (0.72), $PM_{2.5}$ (0.73) and $PM_{10}$ (0.73) in DEL while over GW, it was found to be 0.54 ($PM_{1.0}$), 0.58 ($PM_{2.5}$) and 0.25 ($PM_{10}$). In the associated Fig. 4 and Fig. 5, the red, green and black dots indicate the data corresponding to $PM_{1.0}$, $PM_{2.5}$ and $PM_{10,}$ respectively. The regression analysis reveals a significant negative correlation (r) of T (°C) with PM in DEL whereas GW has a low negative correlation of 0.25 with $PM_{10}$. The regression slope obtained over DEL was -0.09 ($PM_{1.0}$), -0.05 ($PM_{2.5}$) and -0.04 ($PM_{10}$) which has the similar pattern as followed over GW with regression slope -0.16 ($PM_{1.0}$), -0.11 ($PM_{2.5}$) and -0.01 ($PM_{10}$), respectively. The complete period of observation indicates the declining characteristics of PM concentrations on the increase of the T (°C).

### PM Over Different Locations of DEL and GW

As long-range transport and dust also have a significant contribution to the accumulation or dispersion of pollutants at urban sites (Arif et al. 2018). Further, the concentration of $PM_{1.0}$, $PM_{2.5}$ and $PM_{10}$ for seven different locations of DEL and GW were analysed and impressed in the box and whisker plot to distinguish the possible impact of lockdown (Fig. 6a-c).

Before lockdown and during the lockdown period of the study have been distinguished by the letter B and A, respectively. Before lockdown, the mean concentration of $PM_{1.0}$ and $PM_{2.5}$ over IIT-DEL, GK, LR, MGS, RJ, SP and USE were 89.29±45.51 $\mu g.m^{-3}$, 57.07±32.70 $\mu g.m^{-3}$, 90.01±40.72 $\mu g.m^{-3}$, 70.35±28.33 $\mu g.m^{-3}$, 133.18±68.15 $\mu g.m^{-3}$, 97.53±49.39 $\mu g.m^{-3}$, 121.31±54.03 $\mu g.m^{-3}$ and 146.67±78.63 $\mu g.m^{-3}$, 85.04 ± 51.02 $\mu g.m^{-3}$, 162.04±91.42 $\mu g.m^{-3}$, 124.75±57.26 $\mu g.m^{-3}$, 218.38±144.20 $\mu g.m^{-3}$, 163±88.94 $\mu g.m^{-3}$, 191.09±94.03 $\mu g.m^{-3}$, respectively (Fig. 5a and Fig. 5b). However, the mean concentration of $PM_{1.0}$ in the above said locations was 166±89.47 $\mu g.m^{-3}$, 103.33±60.19 $\mu g.m^{-3}$, 187.32±116.52 $\mu g.m^{-3}$, 134.78±63.75 $\mu g.m^{-3}$, 283.46±161.89 $\mu g.m^{-3}$,

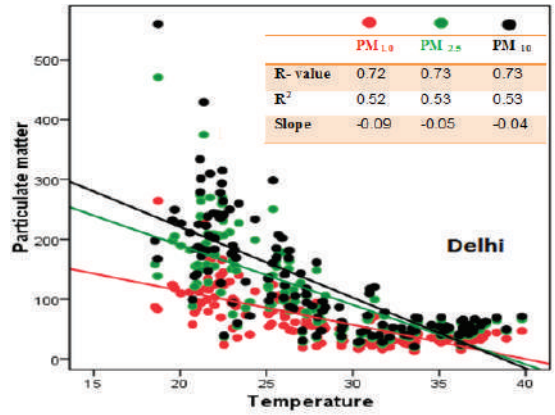


Fig. 4: Scatter plot among $PM_{1.0}$, $PM_{2.5}$ and $PM_{10}$ and T (°C) over DEL.

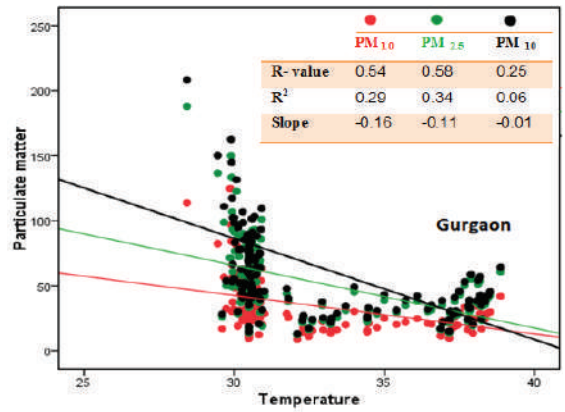


Fig. 5: Scatter plot among $PM_{1.0}$, $PM_{2.5}$ and $PM_{10}$ and T (°C) over GW.

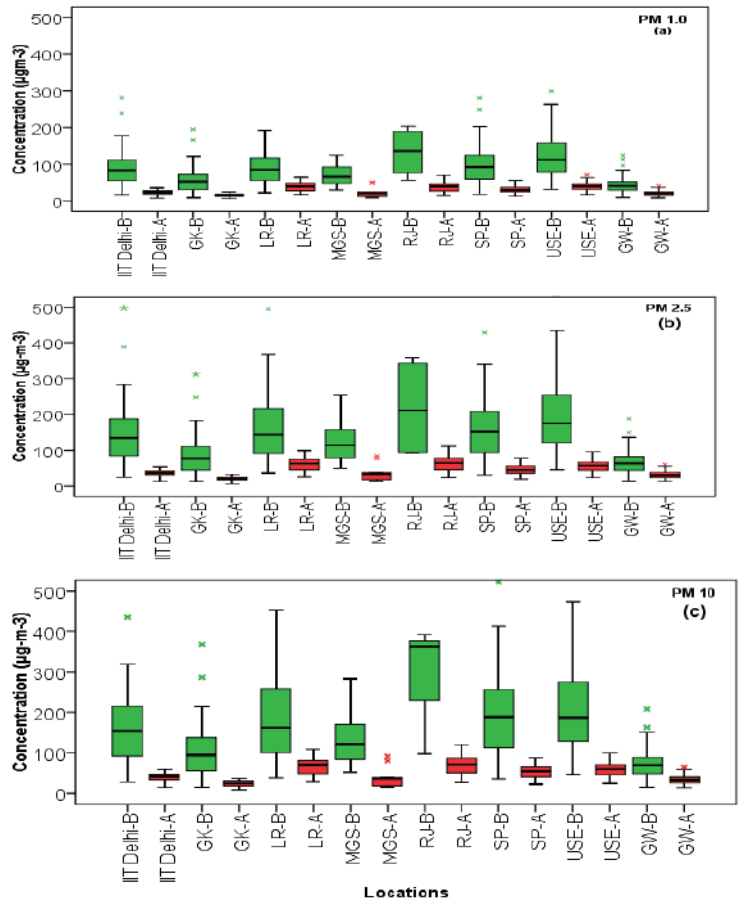


Fig.6. Boxplots of daily concentrations of analysed pollutants over different locations of Delhi and Gurgaon; the median is shown by the middle line of the box. Concentrations are expressed in µg.m$^{-3}$ for $PM_{1.0}$ (a), $PM_{2.5}$ (b) and $PM_{10}$ (c). (Letter "B" and "A" represent the boxes related to before lockdown and during lockdown respectively).

200.83±112.21 µg.m$^{-3}$, 205±105.07 µg.m$^{-3}$, respectively as depicted in Fig. 6c.

The GW region was observed the lower PM concentration, i.e. 43.31±20.25 µg.m$^{-3}$ ($PM_{1.0}$), 66.55±29.94 µg.m$^{-3}$ ($PM_{2.5}$), and 72.63±33.10 µg.m$^{-3}$ ($PM_{10}$) as compared to DEL during the span of before lockdown. The average $PM_{2.5}$ and $PM_{10}$ concentrations over the different study sites of DEL and GW regions were at higher side than the given limit of NAAQS ($PM_{2.5}$ = 40 µg.m$^{-3}$) and $PM_{10}$=60 µg.m$^{-3}$) (Jain et al. 2020). Before the lockdown situation, the highest $PM_{1.0}$ values were found over the RJ showing mean of 133.18 µg.m$^{-3}$ and is followed by USE, SP, LR, IIT, MGS and GW, respectively. The high interquartile range (RJ, USE, SP and LR) suggests that $PM_{1.0}$ hold quite different concentration demonstrating the large spread (56.95-203.85 µg.m$^{-3}$). The large upper whisker over the location IIT-DEL, SP and USE show that the $PM_{1.0}$ concentration varies amongst the most positive quartile group. The upper parts of the scale, i.e. positive quartile group corresponding to almost all locations except RJ shows the pronounced variability in the concentration of $PM_{1.0}$, but in the case of the least positive quartile group, the concentration spread is relatively less. However, the box plots associated with the before lockdown period, show large concentration distributions of $PM_{1.0}$ whereas the box plot accompanying during lockdown shows the slight dispersion that illustrates the extreme decline in the concentration of $PM_{1.0}$.

As per the previous studies, $PM_{2.5}$ comprises numerous unsafe constituents, which may enter into the lungs through the respiratory tract and hazardous to the human health, mainly to children and the elderly people (Daoru et al. 2018). The previously conducted study, expose the particulate matter as one of the prime reasons behind the destructive consequence on the human respiratory system by emphasizing to take

recurrent medical prescription (Anderson et al. 2012). The dissemination and variability of $PM_{2.5}$ concentration have been summarized in box plots as depicted in Fig. 6(b). The highest mean concentration of fine particulate matter $PM_{2.5}$ (218.37μg.m$^{-3}$) was observed over RJ during before lockdown period and 63.41 μg.m$^{-3}$ during the lockdown period. The extremely upper and lower whiskers (before lockdown) demonstrate the case of least quartile that corresponds to less pronounced behaviour of $PM_{2.5}$ concentration due to the less number of data (4 days) over RJ region. The localities LR, SP and USE unveil the large upper whisker and show the noticeable inconsistency in the concentration of $PM_{2.5}$.

As compared to the DEL region, the GW region (Fig. 6b) elucidate the low mean $PM_{2.5}$ concentration monitoring data, i.e. 73.51 μg.m$^{-3}$ (13.98 μg.m$^{-3}$-188.04 μg.m$^{-3}$) associated to prior lockdown (GW-B) that drastically reduced to 31.97 μg.m$^{-3}$ (12μg.m$^{-3}$-60.83 μg.m$^{-3}$) due to the impact of lockdown (GW-A). The lockdown impact was responsible for the sudden fall in $PM_{2.5}$ concentrations due to nationwide restriction on transport movement and industrial units that were associated with the emission of primary pollutants into the vicinity. Before the lockdown period, the corresponding locations of DEL and GW were high $PM_{2.5}$ concentration which supports the finding of ambient $PM_{2.5}$ concentrations greater than 60 μg.m$^{-3}$ over New Delhi (Singh et al. 2011, Tiwari et al. 2014). This might be due to the location of the site that is close to traffic and residential pollution sources (Gulia et al. 2018, Kumar et al. 2017). As per the above findings, a very diverse pattern of PM concentration has been observed in the studied region. Fig. 6(c) exposes the mean concentration of $PM_{10}$ by showing the highest value over RJ (283.46 μg.m$^{-3}$) trailed by USE (205.82 μg.m$^{-3}$) and SP (200.83 μg.m$^{-3}$) associated to before lockdown period that further started to deteriorate to 69.36 μg.m$^{-3}$ (RJ), 58.64 μg.m$^{-3}$ (USE) and 53.59 μg.m$^{-3}$ (SP) due to the lockdown effect. The location GW shows the mean concentration of 72.63 μg.m$^{-3}$ (before lockdown) and 34.28 μg.m$^{-3}$ (during lockdown) and both are very close to the prescribed limit of 60 μg.m$^{-3}$ given by NAAQS.

## COVID-19 and Associated Factor

DEL has been regarded as one of the epicentres for coronavirus in India and to understand the rapid increase in COVID-19 cases, it is important to understand the phenomenon and responsible factors for its spreading. The available data corresponding to COVID-19 along with T (°C), RH (%), and PM, the analysis over DEL has been conducted. The results of 2-tailed Bivariate Pearson correlation (Table 1), were applied among Total Cases (TC), Active Case (AC), Recovered Case (RC), $PM_{1.0}$, $PM_{2.5}$, $PM_{10}$, T (°C), and RH (%) over DEL for the period 1 April 2020 to 15 May 2020.

Based on forty-five days data for period 1$^{st}$ April 2020 to 15$^{th}$ April 2020, it was observed the average TC, AC, RC, DC as 3003±2393, 2137±1514, 821±877, 44±28 respectively. During this period the mean concentration of $PM_{1.0}$, $PM_{2.5,}$ and $PM_{10}$ were 31.42 μg.m$^{-3}$, 46.36 μg.m$^{-3}$ and 50.78 μg.m$^{-3}$, respectively. However, the average T (°C) and RH (%) were 34.72°C and 27.86 % respectively. The Pearson correlation results (Table 1) over DEL revealed the considerable correlation of T (°C) with TC (0.57, p = 0), AC (0.59, p = 0), RC (0.51, p = 0) and DC (0.58, p = 0) related to COVID-19 and clearly indicates the increase in total and active COVID-19 cases due to elevation of T (°C). Due to the unavailability of the data related to the other features

Table 1: Two-tailed Bivariate Pearson correlation among Total Cases (TC), Active Case (AC), Recovered Case (RC), $PM_{1.0}$, $PM_{2.5}$, $PM_{10}$, Temp, and RH over DEL. (** shows here that Correlation is significant at the 0.01 level (2-tailed) and * showing that Correlation is significant at the 0.05 level (2-tailed).

| 2-tailed bivariate Pearson correlation | | | | | | | | | | |
|---|---|---|---|---|---|---|---|---|---|---|
| | | TC | AC | RC | DC | PM 1.0 | PM 2.5 | **PM 10** | **Temp** | **RH** |
| **TC** | Pearson Correlation | 1.00 | 0.99** | 0.98** | 0.93** | 0.34* | 0.21 | 0.16 | 0.56** | 0.28 |
| | p-value | | 0.00 | 0.00 | 0.00 | 0.02 | 0.16 | 0.29 | 0.00 | 0.06 |
| **AC** | Pearson Correlation | 0.99** | 1.00 | 0.95** | 0.92** | 0.33* | 0.20 | 0.15 | 0.58** | 0.25 |
| | p-value | 0.00 | | 0.00 | 0.00 | 0.03 | 0.19 | 0.34 | 0.00 | 0.10 |
| **RC** | Pearson Correlation | 0.98** | 0.95** | 1.00 | 0.92** | 0.36* | 0.23 | 0.18 | 0.52** | 0.33* |
| | p-value | 0.00 | 0.00 | | 0.00 | 0.01 | 0.12 | 0.24 | 0.00 | 0.03 |
| **DC** | Pearson Correlation | 0.93** | 0.92** | 0.92** | 1.00 | 0.32* | 0.20 | 0.14 | 0.58** | 0.26 |
| | p-value | 0.00 | 0.00 | 0.00 | | 0.03 | 0.20 | 0.37 | 0.00 | 0.08 |
| **RH** | Pearson Correlation | 0.28 | 0.25 | 0.33* | 0.26 | 0.09 | 0.06 | 0.03 | -0.07 | 1.00 |
| | p-value | 0.06 | 0.10 | 0.03 | 0.08 | 0.55 | 0.70 | 0.85 | 0.65 | |

that contribute to affecting the rate of spread of COVID-19 infection within a DEL region, the analysis does not point out towards temperature as a single one factor responsible for the transmission of COVID-19. As the increase in the T (°C) over DEL during April and May is also associated to the seasonal weather phenomenon, so it is difficult to declare the accurate association of T (°C) with the TC. The important finding related to the worthy positive correlation (0.51, p = 0) of T (°C) and RC has been observed but the probability of a significant increase in RC with temperature alone is not reasonable to come at some conclusion.

There is a relationship between RH (%) and the COVID-19 virus persistence (Oliveiros et al. 2020 . Most viruses survive best at low RH (<40%) and extremely high RH (>90%). But, the relationship between the survival of the COVID-19 virus and relative humidity needs to be explicated (Paul et al. 2020). Here, the RH (%) shows the least correlation with TC (0.28, p = 0.06), AC (0.25, p = 0.10), and DC (0.26, p = 0.08) and moderate correlation with RC (0.33, p = 0.03). Such a good correlation of RH (%) with RC suggests the slight positive influence of RH on RC. The lower humidity supports the aerosol particles to reduce its size to stay suspended in the air for a longer time. As in the existing months (April to May 2020), the mean RH (%) is lower (27.86 %) and the infection spread may be due to the suspended aerosol particles. In the case of COVID-19 virus dissemination, these suspended aerosols particles may play a major role in the transmission of the virus from one to another but up to some inadequate distance. To avoid this infection, the Government of India, declared the guidelines to maintain the social distancing as a well minimum of 1-meter distance with another person which was helpful to avoid the possibility of infection and a large increase in the number of TC (0.28, p = 0.06).

The increase of RH (%) with the presence of droplets in the atmosphere supports the heavy aerosol particles to settle down on the ground surface. So, in this case, when the infected person, coughs or sneezes in an open area, the aerosol droplets due to its heaviness starts to settle down on the surface and further contribute to transmitting the COVID-19 virus through the surface contact.

Some earlier studies found the significant role of T (°C) and RH (%) responsible for the spread of many respiratory infectious diseases like influenza (Barreca et al. 2012, Lowen et al. 2007). Chen et al. (2020), reported that the cities with the prevalent transmission of COVID-19 virus were with high RH of 60-90% and low T (°C). To diagnose the influence of the concentration of particulate pollutants on the total number of COVID-19 cases, the spatio-temporal analysis (Fig. 7) was done.

It was found that there was 154 number of confirmed cases of COVID-19 on dated 1 April 2020 which corresponds to the particulate mass concentration of 21.96 $\mu g.m^{-3}$ ($PM_{1.0}$), 34.69 $\mu g.m^{-3}$ ($PM_{2.5}$) and 39.04 $\mu g.m^{-3}$ ($PM_{10}$). After 43 days (15$^{th}$ May 2020), the cases of COVID-19 in DEL reached up to a maximum number of 8470 with the increase of 98.02 %, and in the similar pattern the PM concentration also rapidly increased by 48 % ($PM_{1.0}$), 40.47 % ($PM_{2.5}$) and 38.02 % ($PM_{10}$). The increase in the number of COVID-19 cases with the increase of particulate matter mass concentration over DEL suggests the influence of fine and coarse particulate matter on TC. The influence of variable sizes of PM on TC, AC, RC and DC were demonstrated using the Pearson correlation (r) and Sig. 2-tailed, i.e. p-values.

The PM of different sizes, i.e. $PM_{1.0}$, $PM_{2.5}$ and $PM_{10}$ demonstrated the correlation (r) with TC, AC, RC and DC (Table 1). The $PM_{1.0}$ has the moderate correlation with TC (0.34, p = 0.02), AC (0.33, p = 0.02), RC (0.36, p = 0.01) and DC (0.32, p = 0.02) whereas $PM_{2.5}$ and $PM_{10}$ had least correlation value (r) with TC, AC, RC and DC as 0.21 (p = 0.15), 0.19 (p = 0.19), 0.23 (p = 0.12), 0.19 ( p = 0.19) and 0.16 (p = 0.29), 0.14 (p = 0.23), 0.18 (p = 0.23) and 0.13 (p = 0.36), respectively. Our studies indicate that $PM_{1.0}$ is relatively more associated with the various stages of COVID-19

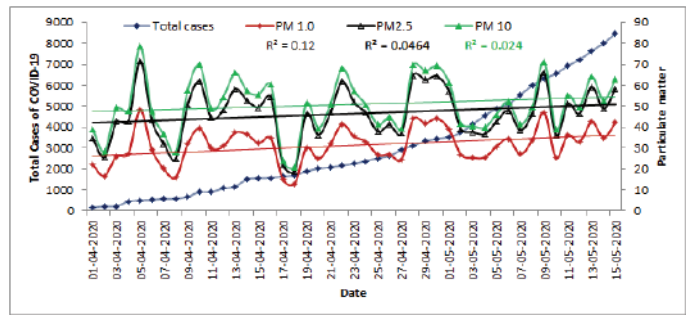


Fig. 7: Spatio-temporal observation between fine ($PM_{1.0}$, $PM_{2.5}$) and coarse ($PM_{10}$) particulate pollutants and TC of COVID-19.

patients, i.e. TC, AC, RC and DC as compared to $PM_{2.5}$ and $PM_{10}$. These findings suggest that, while direct COVID-19 infection is vital track of transmission, the role of $PM_{1.0}$ in virus transmission may play a significant character. The RH (%) was associated with the PM by signifying the correlation (r) as follows, i.e. 0.09 ($PM_{1.0}$), 0.05 ($PM_{2.5}$) and 0.03 ($PM_{10}$). Also the Sig. (2-tailed), i.e. p values of 0.54, 0.69 and 0.84 related to $PM_{1.0}$, $PM_{2.5}$ and $PM_{10}$ respectively, demonstrate the extremely less influence of RH (%) on PM over DEL during the study period.

## CONCLUSION

The paper validates the effect of lockdown over Delhi and Gurgaon on the particulate matter in air. This is the first study that attempts to demonstrate the effects of meteorological factors in COVID-19 in DEL. It has been observed that prominent effect of lockdown demonstrates the decline of 67.31%, 70.29 % and 71.66 % over Delhi and 48.21 %, 51.82 %, and 52.45 % over Gurgaon in $PM_{1.0}$, $PM_{2.5,}$ and $PM_{10}$, respectively. In this study, the particulate matter, temperature and relative humidity justify special attention. Relative humidity (RH %) was found as a substantial parameter that showed a significant correlation with COVID 19 recovered cases. For the study period selected, the COVID-19 recovered cases in Delhi were observed to be favoured by lower mean relative humidity (27.86°C) that was validated through the moderate correlation of 0.33 ($p = 0.03$) with the recovered cases. Such correlation suggests the influence of relative humidity on COVID-19 recovered cases. Based on the dual character of RH (%) on the dispersion of COVID-19 virus, the increase in the number of COVID-19 cases in July and August through surface transmission can be predicted.

However, it is essential to declare that the present study presents a preliminary investigation and as per our observation, an extensive study with long term data might enhance the understanding between meteorological conditions and the COVID-19 transmissibility.

## ACKNOWLEDGEMENT

We thank to PurpleAir for particulate pollutants data and New Delhi Television Limited (NDTV) for providing the COVID-19 updated. We are also thankful to the Editor of NEPT and two unknown referees for their valuable suggestions to improve the manuscript.

## ABBREVIATIONS

| | | | |
|---|---|---|---|
| COVID-19 | Coronavirus | SP | Shantipath |
| DEL | Delhi | GK | Greater Kailash |
| GW | Gurgaon | LR | Lodhi Road |
| PM | Particulate matter | WHO | World Health Organization |
| T | Temperature | TC | Total cases |
| RH | Relative Humidity | RC | Recovered cases |
| IIT-DEL | IIT-Delhi | AC | Active cases |
| USE | US Embassy | DC | Death cases |
| MGS | Mahant-Gurmukh Singh | NAAQS | National Ambient Air Quality Standards |

## REFERENCES

Anderson, J.O., Thundiyil, J.G. and Stolbach, A. 2012. Clearing the air: A review of the effects of particulate matter air pollution on human health. J. Med. Toxicol., 8(2): 166-175.

Arif, M., Kumar, R., Kumar, R., Eric, Z. and Gourav, P. 2018. Ambient black carbon, PM2.5 and PM10 at Patna: Influence of anthropogenic emissions and brick kilns. The Science of the Total Environment, 624: 1387-1400.

Aggarwal, P. and Jain, S. 2015. Impact of air pollutants from surface transport sources on human health: A modeling and epidemiological approach. Environ. Int., 83: 146–157. https://doi.org/10.1016/j.envint.2015.06.010.

Barreca, A.I. and Shimshack, J.P. 2012. Absolute humidity, temperature, and influenza mortality: 30 years of county-level evidence from the United States. American Journal of Epidemiology, 176(7): 114 - 122.

Bhaskar, B.V. and Mehta, V.M. 2010. Atmospheric particulate pollutants and their relationship with meteorology in Ahmedabad. Aerosol Air Qual. Res., 10: 301-315.

Bao, R. and Zhang, A. 2020. Does lockdown reduce air pollution? Evidence from 44 cities in northern China. Sci. Total Environ., 731: 139052. https://doi.org/10.1016/j.sci totenv.2020.139052.

Cohen, A.J., Anderson, H.R., Ostra, B., Pandey, K.D., Krzyznowski, M., Gutschmidt, N.K.K., Pope, A., Romieu, I., Samet, R.J.M. and Smith, K. 2005.The global burden of disease due to outdoor air pollution. J. Toxicol. Environ. Health A, 68: 1-7.

Chen, C. and Zhao, B. 2020. Makeshift hospitals for COVID-19 patients: Where health-care workers and patients need sufficient ventilation for more protection. J. Hosp. Infect. https://doi.org/10.1016/j.jhin.2020.03.008.

Chauhan A. and Singh R.P. 2020. Decline in $PM_{2.5}$ concentrations over major cities around the world associated with COVID-19. Environmental Research, 2020: 187.

Down to Earth (https://www.downtoearth.org.in/)

Daoru, L., Deng, Q., Zhou, Z., Lin, Y. and Tao, J. 2018.Variation trends of fine particulate matter concentration in Wuhan City from 2013 to 2017. Int. J. Environ. Res. Public Health, 15 (7): 1487.

Dockery, D., Pope, C., Xu, X., Spengler, J., Ware, J., Fay, M., Ferris, B. and Speizer, F. 1993. An association between air pollution and mortality in six U.S. cities. N. Engl. J. Med., 329: 1753-1759.

Donaldson, K., Stone, V., Seaton, A. and MacNee, W. 2001. Ambient particle inhalation and the cardiovascular system: potential mechanisms. Environ. Health Persp., 109: 523-527.

Donnelly, C.A., Ghani, A.C., Leung, G.M., Hedley, A.J., Fraser, C., Riley, S., Radded, L.A.J., Ho, L.M., Thach, T.Q., Chau, P., Chan, K.P., Lam, T.H., Tse, L.Y., Tsang, T., Liu, S.H., Kong, J.H.B., Lau, E.M.C., Ferguson, N.M. and Anderson, R.M. 2003. Epidemiological determinants of spread of causal agent of severe acute respiratory syndrome in Hong Kong. Lancet, 361(9371): 1761-1766.

Espinosa, A.J.F., Rodriguez, M.T. and Alvarez, F.F. 2004. Source charac-

terisation of fine urban particles by multivariate analysis of trace metal speciation. Atmos. Environ., 38: 873 - 886.

Gulia, S., Mittal, A. and Khare, M. 2018. Quantitative evaluation of source interventions for urban air quality improvement- A case study of Delhi city. Atmos. Pollut. Res., 9: 577-583.

Guttikunda, S.K. and Calori, G. 2013. A GIS based emissions inventory at 1 km × 1 km spatial resolution for air pollution analysis in Delhi, India. Atmos. Environ., 67: 101-111.

Goyal, P. 2003. Present scenario of air quality in Delhi: A case study of CNG implementation. Atmospheric Environment, 37: 5423-5431.

Hales, S., Blakely, T. and Woodward, A. 2010. Air pollution and mortality in New Zealand: Cohort study. J. Epidemiol. Community Health, 66: 468-473.

Jain, S. and Sharma, T. 2020. Social and travel lockdown impact considering coronavirus disease (COVID-19) on air quality in megacities of India: Present benefits, future challenges and ways forward. Aerosol Air Qual. Res., 20: 1222-1236.

Karar, K. and Gupta, A.K. 2006. Seasonal variations and chemical characterization of ambient $PM_{10}$ at residential and industrial sites of an urban region of Kolkata (Calcutta), India. Atmos. Res., 81: 36-53.

Kumar, P., Gulia, S., Harrison, R.M. and Khare, M. 2017. The influence of odd-even car trial on fine and coarse particles in Delhi. Environ. Pollut., 225: 20-30.

Kumar, P., Jain, S., Gurjar, B.R., Sharma, P., Khare, M., Morawska, L. and Britter, R. 2013. New Directions: Can a "blue sky" return to Indian megacities? Atmos. Environ., 71: 198-201. https://doi.org/10.1016/j.atmosenv.2013.01.055.

Lowen, A.C., Mubareka, S., Steel, J. and Palese, P. 2007. Influenza virus transmission is dependent on relative humidity and temperature. PLoS Pathogens, 3(10): 1470-1406.

Ministry of Health and Family Welfare, Government of India (https://www.mohfw.gov.in/).

Oliveiros, B., Caramelo, L., Ferreira, N.C. and Caramelo, F. 2020. Role of temperature and humidity in the modulation of the doubling time of COVID-19 cases. Preprint at Med RXIV, doi.org/10.1101/2020.03.05.20031872.

Paul J. Villeneuve and Mark S. Goldberg. 2020. Methodological considerations for epidemiological studies of air pollution and the SARS and COVID-19 coronavirus outbreaks. Environmental Health Perspectives, 128(9): 095001.

Saksena, S. and Dayal, V. 2000. Total exposure as a basis for the economic valuation of air pollution in India. Energy Environment Monitor, 13(2): 93-102.

Susanta Mahato, Swades Pal and Krishna Gopal Ghosh 2020. Effect of lockdown amid COVID-19 pandemic on air quality of themegacity Delhi, India. Science of the Total Environment, 730: 139086.

Sahu, S.K., Beig, G. and Parkhi, N.S. 2011. Emissions inventory of anthropogenic PM2.5 and PM10 in Delhi during commonwealth games 2010. Atmospheric Environment, 45: 6180-6190.

Singh, D.P., Gadi, R. and Mandal, T.K. 2011. Characterization of particulate-bound polycyclic aromatic hydrocarbons and trace metals composition of urban air in Delhi, India. Atmos. Environ., 45: 7653-7663.

Tiwari, S., Bisht, D.S., Srivastava, A.K., Pipal, AS., Taneja, A., Srivastava, M.K. and Attri, S.D. 2014.Variability in atmospheric particulates and meteorological effects on their mass concentrations over Delhi, India. Atmos. Res., 45(46): 145-146.

Xu, K., Cui, K., Young, L.H., Hsieh, Y.K., Wang, Y.F., Zhang, J. and Wan, S. 2020. Impact of the COVID-19 event on air quality in central China. Aerosol Air Qual. Res., 20: 915-929. https://doi.org/10.4209/aaqr.2020.04.0150.

Wang, P., Chen, K., Zhu, S., Wang, P. and Zhang, H. 2020. Severe air pollution events not avoided by reduced anthropogenic activities during COVID-19 outbreak. Resour. Conserv. Recycl., 158: 104814. https://doi.org/10. 1016/j.resconrec.2020.104814.

Wu, X., Nethery, R.C., Sabath, B.M., Braun, D. and Dominici, F. 2020. Exposure to air pollution and COVID-19 mortality in the United States. medRxiv 2020.04.05.20054502. https://doi.org/10.1101/2020.04.05.20054502.

World Health Statistics 2018. Monitoring health for the SDGs (https://www.who.int/gho/publications/world_health_statistics/2018/en/).

WHO 2020. Coronavirus disease (COVID-19) pandemic (www.who.int/emergencies/diseases/novel-coronavirus).

Nature Environment and Pollution Technology
An International Quarterly Scientific Journal

p-ISSN: 0972-6268
(Print copies up to 2016)
e-ISSN: 2395-3454

Vol. 19 | No. 4 | pp. 1637-1644 | 2020

Original Research Paper

https://doi.org/10.46488/NEPT.2020.v19i04.031

Open Access Journal

# Socio-Economic Utility of Coastal Flora Growing in and Around Mangrol Taluka (Junagadh) of Gujarat

**T. B. Chudasama and S. J. Vyas†**
Department of Life Sciences, Bhakta Kavi Narsinh Mehta University, Junagadh-362640, Gujarat, India
†Corresponding author: S. J. Vyas; vsuhas.13@gmail.com

**Nat. Env. & Poll. Tech.**
**Website: www.neptjournal.com**

*Received:* 03-12-2019
*Revised:* 14-12-2019
*Accepted:* 03-01-2020

**Key Words:**
Halophytes
Coastal flora
Environmental economics

## ABSTRACT

Halophytes are widely distributed throughout several regions due to the presence of the saline condition. The present paper reflects vegetation cover along with plant species of different kinds in the coastal area of Mangrol taluka of Gujarat, India. It consists of 25 plant species under 25 genera and 12 families of angiosperm. During the field survey, observations were made and plant characteristics and habitat of flora were studied. The main objectives of the present study are the identification, baseline survey and utility of saline plants in the area. The utility of the plants such as ecological and economic (such as medicinal, industrial and commercial, etc.) which can reflect their significance to the society. Majority of the plant species found are naturally occurring, but a few of them are agricultural plants used for various purposes. Due to increasing population growth, urbanization and especially over-demanding medicinal plants people are harvesting without any knowledge of regeneration and conservation, due to which many species are threatened. Because of this, it is very important to conserve plant species, which are extensively utilized in various purposes.

## INTRODUCTION

India has a coastline of about 7,516.6 km long with 2.02 million km $^2$ exclusive economic zone and 0.13 million km $^2$ continental shelf (Khoshoo 1996) and it covers nine states and two union territories. Gujarat coastal line has a length of approximately 1600 km; it constitutes about 24% of the total coastal length of India. Coastal zone is an important bi-ogeographically habitats of the Indian subcontinent (Rodgers & Panwar 1998). Coastal areas are vulnerable to be invaded by tides, and conventional saline-alkali land management measures can hardly achieve the desired results because of serious salinity problems, harsh natural conditions, simple ecosystem structure, poor stability, and fragile ecological environment (Zhang 2018). According to Stoker (1928), the critical level of salinity for plants is 0.5% of the dry weight. Though the fact that only a small group of higher plants can grow in the saline habitats was recognized many hundred years ago yet the name "halophyte" was assigned to such plants by Pallas in the early nineteenth century. Researches on biological diversity and its values, uses, loss, conservation and management during the last two decades has made a spectacular niche in the field of environmental science (Vyas & Joshi 2014). In recent years, however, the attention is being paid worldwide to accommodate the salt-tolerant species such as *Cressa, Suaeda, Trianthema, Salvadora,* to support animal life and providing useful pharmacological as well as economic aspects for human (Nikalje et al. 2018).

The local community around the coast relies on these basic resources, collecting and using many plant species for food, wood, fibre, fuel and medicine. Their high utility in economic and medicinal usage is an important contributing factor to their overexploitation. Salinity is among the major environmental crisis and serious threat to food, fuel and fibre production in the world. This problem, which extends to more than 100 countries, is encountered in all types of climate due to the consequence of both natural processes as well as human interference (Shabala & Munns 2017). The continual use of coastal plants over many years without any replanting, it has resulted in an accelerated decline in the loss of a wide range of threatened and endangered species. This kind of survey is necessary to explain the usefulness of coastal vegetation to the human community living around the coast.

## MATERIALS AND METHODS

### Study Area

Mangrol taluka of Junagadh district is situated on the extreme coast of Gujarat having dense vegetation of coastal flora. Nine villages of Mangrol taluka and three villages of Madiya taluka were surveyed for the present study 21°13'N to 21° 00'N and 69°59 ' E to 70° 13' E. Total area surveyed under the present study was approximately 40 km, along the coastline

of Mangrol taluka consisting of various villages on the coast.

### Data Collection

As described earlier, twelve villages were surveyed namely, Antroli, Diwasa, Sangavada, Shil, Lodge, Rahij, Maktupur, Mangrol, Khodada, Khambhadiya, Jujarpur and Chorvad. Plant species along the coast of 40 km around Mangrol taluka were observed and identified and recorded for the baseline study. The number of each species in all the surveyed villages was recorded along with their habitat in which they were found. Based on the number of species, they were distributed into families in which they belong and utility of all the species were studied.

## RESULTS

In the present investigation a total of 25 species of coastal flora belonging to 18 families were enumerated (Fig. 2) in the coastline of Mangrol taluka (Junagadh). As stated earlier, 12 villages namely Antroli, Diwasa, Sangavada, Shil, Lodge, Rahij, Maktupur, Mangrol, Khodada, Khambhadiya, Jujarpur and Chorvad located on the coastal belt were identified and selected for the current study. From these locations, four species which were found to be dominant in the majority of areas were noted to be *Cyprus conglomerates, Halopyrum mucronatum, Prosopis juliflora* and *Casuarinas equisitifolia.* Habitats of these plants are saline and hence can be considered as halophytic vegetation. Halophytic vegetation is growing in different parts of the habitat by facing several environmental stresses.

For this study, a maximum of 15 species was found in the village of Lodge, and at least 4 species were found in the village of Shil, in the coast between Antroli to Chorvad village. As shown in Fig. 2, it was interesting to observe and note that the species in the rocky area are higher than in any other habitats such as sand dunes and moist areas.

SD=Sand dunes, M=Marshy, RP=Rock poolsAmong the habitat of selected coastal sites, sand dunes were found to be more followed by rock pools and marshy region. In the coastal areas surrounding Mangrol taluka, 9 villages with sand dunes are given in Table 1 such as Antroli, Sangavada, Shil, Maktupur, Mangrol, Khodada, Khambhadiya, Jujarpur and Chorvad; 2 villages with rocky pool are Lodge and Rahij and 1 village with marshy space is located in Diwasa. According to the survey, highly coastal floras are found on rocky pools (Fig. 2), while vegetation is less common on sandy dunes and marshy places.

As shown in Table 2, the *Fabaceae* family is found to be most dominant than all other families. There are three types of plants found in the Fabaceae family, namely *Lotus garcini, Prosopis juliflora* and *Indigofera oblingifolia.* Two species are found in Convolvulaceae, Poaceae, Acanthaceae and Amaranthaceae family and in addition to this, 1 plant is found in all family found here.


Fig. 1: Map showing study area (Source: Google earth).

Table 1: The habitat in and around Mangrol taluka.

| Habitat | No. of habitat | Location |
|---|---|---|
| SD | 9 | Antroli, Sangavada, Shil, Maktupur, Mangrol, Khodada, Khambhadiya, Jujarpur, Chorvad |
| RP | 2 | Lodge and Rahij |
| M | 1 | Diwasa |

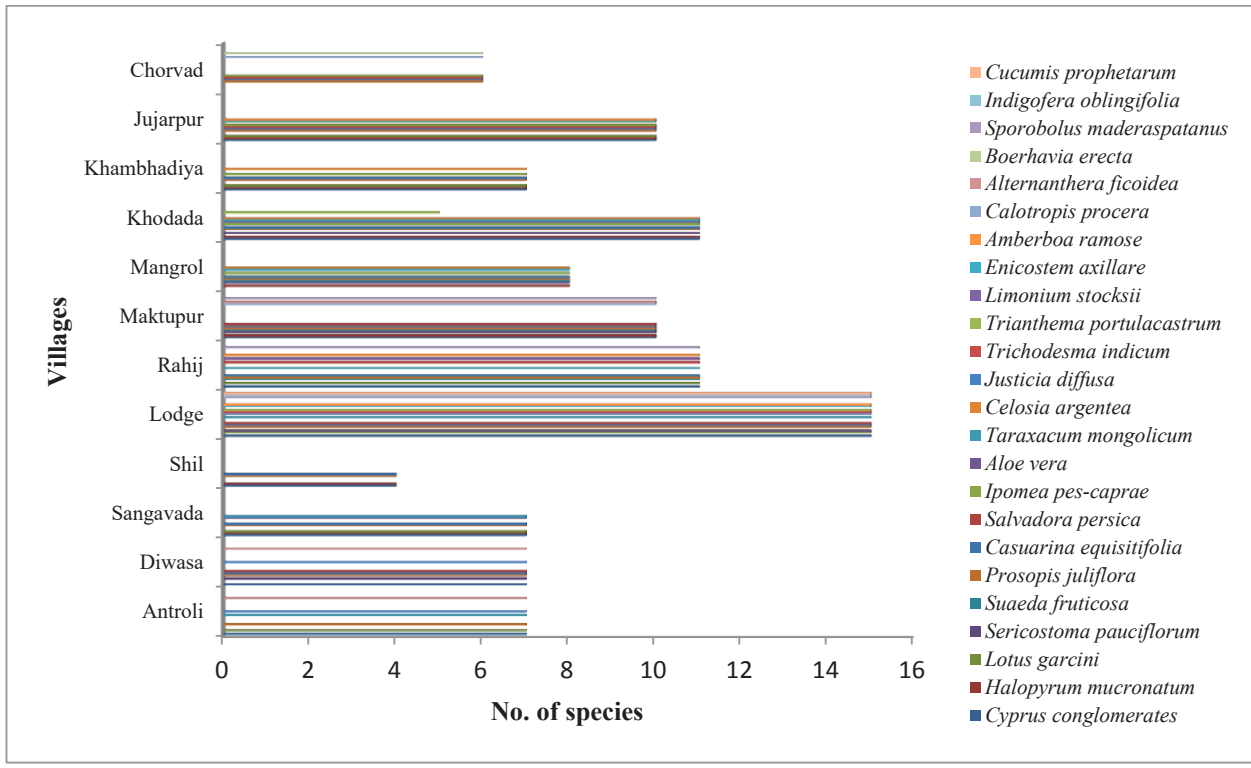


Fig. 2: Village-wise species richness.

Table 2: No. of Genera present in each family.

| Sr. No. | Family | No. of Genera |
|---|---|---|
| 1. | Fabaceae | 3 |
| 2. | Convolvulaceae | 2 |
| 3. | Poaceae | 2 |
| 4. | Acanthaceae | 2 |
| 5. | Amaranthaceae | 2 |
| 6. | Boraginaceae | 1 |
| 7. | Chenopodiaceae | 1 |
| 8. | Cucurbitaceae | 1 |
| 9. | Plumbaginaceae | 1 |
| 10. | Cyperaceae | 1 |
| 11. | Casuarinaceae | 1 |
| 12. | Salvadoraceae | 1 |
| 13. | Asphodelaceae | 1 |
| 14. | Asteraceae | 1 |
| 15. | Aizoaceae | 1 |
| 16. | Gentianaceae | 1 |
| 17. | Apocynaceae | 1 |
| 18. | Nyctaginaceae | 1 |

Table 3: Checklist of coastal flora showing scientific name, common name, family, habit & utility.

| S. No. | Plant name | Family | Habitat | Common name | Plant part used | Utility | References |
|---|---|---|---|---|---|---|---|
| 1 | *Cressa cretica* | Convolvulaceae | H | Rudravanti | Whole plant | enriches the blood and useful in constipation | (Chopra et al. 2006) |
| 2 | *Cyprus conglomeratus* | Cyperaceae | H | - | Whole plant | used as fodder for animals | (Keblawy 2011) |
| 3 | *Halopyrum mucronatum* | Poaceae | G | - | Whole plant | coastal dune stabilizer | (Khan et al. 1999) |
| 4 | *Lotus garcini* | Fabaceae | H | - | Leaves | Used in benefits of kidney, controls diarrhea, for sleep deficiency | (Ghulam 2002) |
| 5 | *Sericostoma pauciflorum* | Boraginaceae | S | Karvash, Matravalli | Whole plant | Diabetes, dysentery, urinary infection | (Thakar 1998) |
| 6 | *Suaeda fruticosa* | Chenopodiaceae | S | Shrubby seablight | Leaves<br>Whorl plant | Treatment of ophthalmia<br>Making soap and glass | (Wichens 2012) |
| 7 | *Prosopis juliflora* | Mimosaceae | T | Gando baval | Wood | Production of hard wood for mosaics, boards and sleepers, good quality firewood | (Gomes 1977) |
| 8 | *Casuarina equisitifoliys* | Casuarinaceae | T | Saru, she-oak | Root, stem | Treatment of dysentery | (World health organization 2009) |
| 9 | *Salvadora persica* | Salvadoraceae | T | Meswak tree, Piludi | Wood<br>Roots | Useful for fuel<br>Used as a toothbrushes | (Uphof 1959) |
| 10 | *Ipomea pes-caprae* | Convolvulaceae | C | Morning glory or goat's foot, Maryada vel | Stem<br>Leaves<br>Root | Made in ropes<br>Used to extirpate fungoid growth of ulcers<br>Relief in bladder diseases | (Burkill 1985) |
| 11 | *Aloe vera* | Asphodelaceae | H | Indian aloe, Kuvarpathu | Whole plant | Cosmetic & medicinal purpose, Used in commercially as an ingredient in yogurts, beverages, and some desserts | (Reynolds & Tom (Ed.) 2004) |
| 12 | *Taraxacum mongolicum* | Asteraceae | H | Dandelions | Whole plant | Treat inflammation, swollen lymph nodes, cysts and abscesses, as well detoxifying the kidney and liver | (Roger & George 2004) |
| 13 | *Cucumis prophetarum* | Cucurbetaceae | C | Spiked melon | Fruit | Used as an emetic | (Uphof 1959) |
| 14 | *Justicia diffusa* | Acanthaceae | H | Water willow | Leaves | Used in ophthalmic | (Chopra et al. 1986) |
| 15 | *Trichodesma indicum* | Boraginaceae | H | Undhaphuli, Indian borage | Leaves, root | treatment of cough | (Subban & AlarmalMangai 2012) |
| 16 | *Trianthema portulacastrum* | Aizoaceae | H | Black pigweed | Whole plant | Used as a vermifuge and is useful in rheumatism | (Aggarwal & Kaur 2017) |
| 17 | *Limonium stocksii* | Plumbaginaceae | H | Sea-lavender | Whole plant | Used as a food, pharmaceutical, cosmetics and other industrial products | (Akashi & Ayabe 2010) |
| 18 | *Enicostem axillare* | Gentianaceae | H | Mahmejo | Whole plant | Used as a laxative, stomachic and tonic | (Chopra et al. 1986) |

Table Cont....

| S. No. | Plant name | Family | Habitat | Common name | Plant part used | Utility | References |
|---|---|---|---|---|---|---|---|
| 19 | *Lapidagathis cristata* | Acanthaceae | H | Hiran-chaaro (pathar-kotar) | Whole plant | Antiallergic medicine & used as a fodder | (Panda 2002) |
| 20 | *Calotropis procera* | Apocynaceae | S | Auricula tree | Stem<br>Root<br>Seed capsules<br>Leaves | Termite proof stem used for roofing and building huts<br>Treatment of snakebites<br>Used as a stuffing material in mattresses<br>Treatment of asthma | (Von Maydell 1990) |
| 21 | *Alternanthera ficoidea* | Amaranthaceae | H | Calico plant | Whole plant | Bioagent in greywater treatment | (Abbasi & Tauseef 2018) |
| 22 | *Boerhavia erecta* | Nyctaginaceae | H | Erect spiderling, Satodi | Whole plant | Used as a vermifuge | Achigan-dako 2009) |
| 23 | *Sporobolus maderaspatanus* | Poaceae | G | - | Whole plant | Used as a forage | (Joshi 2011) |
| 24 | *Celosia argentea* | Amaranthaceae | H | Common cockscomb | Whole plant | It could purge the liver of pathogenic fire, improve eyesight, and eliminate nephelium | (Shen 1997) |
| 25 | *Indigofera oblingifolia* | Fabaceae | S | Jhil, Jhiladi | Leaves<br>Stem<br>Root | Treat skin rash & stomach pain<br>Treatment of mercurial salivation<br>Used as a purgative | (Chopra et al. 1986) |

H = herb, S = shrub, T = tree and G = grass and C = Climber

1: *Cressa cretica*

2: *Suaeda fruticosa*

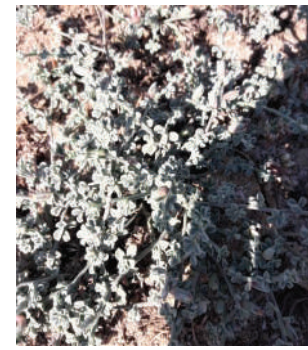

3: *Sericostoma pauciflorum*

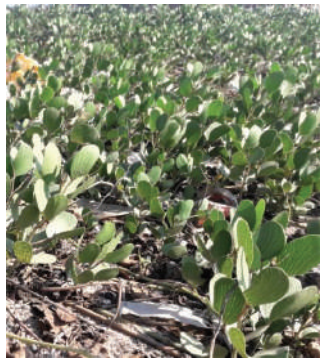

4: *Ipomea pes-caprae*

5: *Salvadora persica*

6: *Halopyrum mucronatum*

7: *Taraxacum mongolicum*

8: *Calotropis procera*

9: *Lotus garcini*

PLATE 1

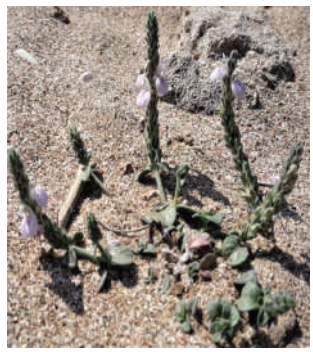

10: *Justicia diffusa*

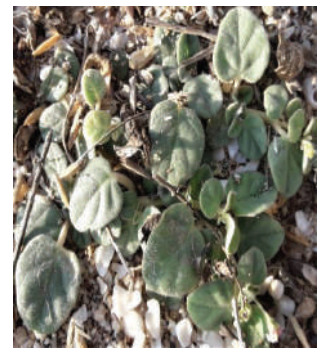

11: *Trianthema portulacastrum*

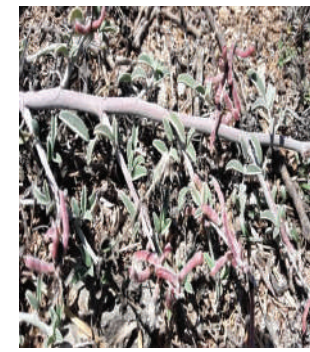

12: *Indigofera oblingifolia*

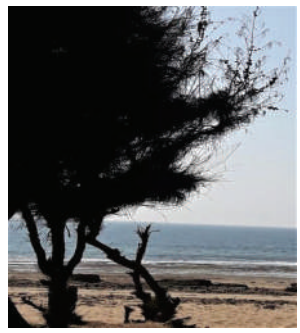

13: *Casuarinas equisitifoliys*

14: *Alternanthera ficoidea*

15: *Boerhavia erecta*

16: *Amberboa ramose*

17: *Prosopis juliflora*

18: *Cucumis prophetarum*

PLATE 2

19: *Limonium stocksii*

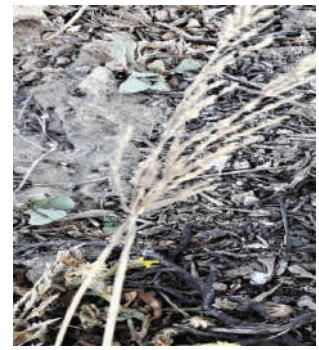

20: *Sporobolus maderaspatanus*

21: *Aloe vera*

22: *Trichodesma indicum*

23: *Celosia argentea*

24: *Enicostem axillare*

25: *Cyprus conglomerates*

PLATE 3

Fig. 3: Plant species of the study area (Plates 1-3).

Coastal vegetation is not commonly used for economic gain, but it also identified for ethnomedicinal, handicrafts and many other uses. Numerous reports have documented the utility of coastal flora in rural and tribal areas all over the world as a successful home remedy against different ailments (Hamburger & Hostettmann 1991, Hammiche & Maiza 2006, Hussain et al. 2003). Among the species, herbs were found to be more (14 sp.) followed by shrubs (4 sp.), trees (3 sp.), grass (2 sp.) and climbers (2 sp.) (Fig. 3). In the available literature, the vegetation of coastal flora was highly used in traditional and ethnobotanical interests were recorded after the critical screening.

## CONCLUSION

The present work reflected a detailed and comprehensive database and descriptive survey of coastal flora which compiled the economic and ecological utility of the plant species observed for identifying the potential of the Mangrol coast. Throughout the 40 km coastline of the study area, twenty-five

coastal species were observed and recorded for their utility. The interesting fact is to interpret that these 25 species were listed under 18 families, which showed the immense potential of all the species observed in various treatments of diseases. It also revealed that Mangrol taluka having a coastal belt in highly diversified in terms of plant species with reference to the coastal line based on the habitat. These plant species were recorded on different coastal habitats comprising of sandy, rocky and marshy.

## ACKNOWLEDGMENT

The authors would like to thanks Department of Forest, Development & Management, Gujarat state for providing the permission to carry out this research.

## REFERENCES

Abbasi, S.N. and Tauseef, S.M. 2018. Use of terrestrial weed *Alternanthera ficoidea* in treating greywater treatment in soil-less SHEFROL bioreactor. Water Sci. Technol., 77(8): 2005-2013.

Achigan-dako, E. 2009. Traditional Vegetables in Benin, Darwin initiative. International Foundation for Science, 2009.

Akashi, T. and Ayabe, S. 2010. Comprehensive Natural Products. Elsevier Science, Vol. 2

Burkill, H.M., 1985. The Useful Plants of West Tropical Africa Royal Botanic Gardens. London, 3, pp.101.

Chopra, R. N., Nayar, S. L. and Chopra, I. C. 1986. Glossary of Indian Medicinal Plants. Council of Scientific and Industrial Research, New Delhi.

Chopra, R.N., Nayar, S.L. and Chopra, I.C. 2006. Glossary of Indian Medicinal Plants. National Institute of Science Communication and Information Resources, New Delhi, pp. 80.

Ghulam, S. 2002. The Phytochemical and Phytopharmacological studies on *Saraca indica*, *Capparis decidua* and *Lotus garcinia*. Deptt. of Pharmacognosy, University of Karachi, Pakistan.

Gomes, P.A. 1977. Forragens Fartas Na Seca. 4th Ed. São Paulo, Nobel, pp. 223.

Hamburger, M. and Hostettmann, K. 1991. Bioactivity in plants: The link between phytochemistry and medicine. Phytochemistry, 30: 3864-3874.

Hammiche, V. and Maiza, K. 2006. Traditional medicine in Central Sahara: Pharmacopoeia of Tassili N'ajjer. Journal of Ethnopharmacology, 105: 358-367.

Hussain, N. A., Naseem, R., Sarwar, G., Mujeeb, F. and Jamil, M. 2003. Domestication/cultivation scope of medicinal crops on salt-affected soils. Conservation and Sustainable Uses of Medicinal and Aromatic Plants of Pakistan, 2-4: 37-43.

Joshi, A.J. 2011. Monograph on Indian halophytes. Ocean & Atmo. Sci. and Techno. Cell, 70-73.

Kaur, M. and Aggarwal, N.K. 2017. *Trianthema portulacastrum* L.- The noxious weed and its control. Adv. Plants Agric. Res., 6(3): 62-64.

Keblawy, A., Neyadi, S.S., Rao, M.V. and Marzouqi, A.H. 2011. Interactive effects of salinity, light and temperature on seed germination of sand dunes glycophyte *Cyprus conglomeratus* growing in the United Arab Emirates deserts. Seed Sci. & Technol., 39: 364-376.

Khan, M.A., Ungar, I.A. and Showalter, A.M. 1999. Effects of salinity on growth, ion content and osmotic relations in *Halopyrum mucronatum* (L). Stapf. J. Plant Nutr., 22: 191-204.

Khoshoo, T.N. 1996. Vesicular-arbuscular mycorrhizae of Hawaiian dune plants. Curr. Sci., 71: 506-513.

Nikalje, G.C., Srivastava, A.K., Pandey, G.K. and Suprasanna, P. 2018. Halophytes in biosaline agriculture: Mechanism, utilization, and value addition. Land Degradation and Development, 29(4): 1081-1095.

Panda, H. 2002. Medicinal Plants Cultivation and Their Uses. National Institute of Industrial Research.

Reynolds, T. and Tom (Ed.) 2004. Aloes: The genus Aloe (Medicinal and Aromatic Plants- Industrial Profiles. CRC Press.

Rodgers, W.A. and Panwar, H.S. 1998. Planning a Wildlife Protected Area Network in India. Wildlife Institute of India, Dehra Dun, India, Vol. 1.

Roger, P. and George, D. 2004. Encyclopedia of Medicinal Plants 1: Education and Health Library, pp. 398.

Shabala, S. and Munns, R. 2017. Salinity stress: physiological constraints and adaptive mechanisms. In: Shabala, S. (ed.) Plant Stress Physiology. 2nd edn. CABI, Wallingford. (2017): 24-63.

Shen, N. 1997. Shen Nong Ben Cao. Liaoning Science & Technology Press, Shenyang, pp. 40

Stoker, O. 1928. Das halophytes problem. Erg. Biol., 3: 265-353.

Subban, R. and Alarmal Mangai, S. 2012. Comparative corrosion inhibition effect of imidazole compounds of *Trichodesma indicum* (Linn) R. Br. on C38 Steel in 1 M HCl medium. Journal of Chemistry, 2012, 2013:1-4.

Thakar, J.K. 1998. Vanaspati Shashtra, 2nd edition. Pravin Prakashan, Rajkot, pp. 471-480.

Uphof. J. C. 1959. Dictionary of Economic Plants. Weinheim.

Von Maydell, H. 1990. Trees and Shrubs of the Sahel. Their characteristics and Uses. Deutsche Gesellschaft Technische usammenarbeit, Germany.

Vyas, S.J. and Joshi, A.J. 2014. Mineral composition in leaves of some halophytic species of 'Bhal' region in Gujarat. Research Journal of Biology, 2: 99-103.

Wichens, G.E., David, V. and Goodin, R. 2012. Plants for arid lands. In: Proceedings of the Kew International Conference on Economic Plants for Arid Lands held in the Joderell Laboratory, Royal Botanic Gardens, Kew, England, 23-27 July 1984.

WHO 2009. Medicinal Plants in Papua, New Guinea, World Health Organisation.

Zhang, G., Wang, C., Yang, H., Zhou, Z., Zhang, Y. and Zhao, L. 2018. Experimental research on improving the salt tolerance of plants in coastal saline soil - A case study of Huanghua City in Hebei Province of China. Nat. Env. & Poll. Tech., 17(2): 459-468.

Nature Environment and Pollution Technology
An International Quarterly Scientific Journal

p-ISSN: 0972-6268
(Print copies up to 2016)
e-ISSN: 2395-3454

Vol. 19 | No. 4 | pp 1645-1656 | 2020

Original Research Paper

https://doi.org/10.46488/NEPT.2020.v19i04.032

Open Access Journal

# Biosorption of Manganese by Amended *Aspergillus versicolor* from Polluted Water Sources

**A.H. El Maghrabi*, M.A. Marzouk**, M.A. Elbably*** and M.E.M. Hassouna*†**

*Department of Chemistry, Faculty of Science, 62514 Beni-Suef University, Egypt

**Department of Botany & Microbiology, Faculty of Science, Beni-Suef University, Egypt

***Department of Hygiene, Management & Zoonoses, Faculty of Veterinary Medicine, Beni-Suef University, Egypt

†Corresponding author: M.E.M. Hassouna; Mohamed.hassona@science.bsu.edu.eg; mhassouna47@hotmail.com

**Nat. Env. & Poll. Tech.**
**Website: www.neptjournal.com**

*Received:* 19-11-2019
*Revised:* 02-12-2019
*Accepted:* 16-01-2020

**Key Words:**
Biosorption
*Aspergillus versicolor*
Bioadsorbent
Mn(II)

## ABSTRACT

This study deals with the adsorption capacity of the powder of *Aspergillus versicolor* (Ascomycota) as a bioadsorbent for the removal of manganese ion from polluted water samples. The effect of various experimental parameters such as the effect of pH, quantity of the fungus powder, contact time with the manganese (II) ion solution and its concentration on the biosorption capacity was conducted to optimize them. Potato Dextrose Agar (PDA) plates amended with 100 ppm of Mn(II) ions were used for growing the fungus isolates and standard spread plate method was applied. The plates were incubated at 27°C for 4 to 7 days, then the grown fungi were killed by adding 0.5 N NaOH, washed with doubly distilled water, dried out in hot air oven and finally ground into a very fine powder. The results verify that the optimum pH value for manganese biosorption was 6. The rate of adsorption of manganese by *Aspergillus versicolor* was very fast reaching a maximum within 15 min at 31°C. Maximum removal efficiency occurred on the use of 0.3 g A. versicolor powder. The maximum metal uptake was relatively observed at 90 ppm manganese concentration. Manganese removal process decreased with increasing metal concentration. The desorption study showed that manganese was recovered up to 81.53% using 0.1 N HCl rendering the possibility of the adsorbent regeneration. Experimental results have been analysed using a Langmuir and Freundlich adsorption isotherm models. Surface morphology study of A. versicolor powder using SEM analysis, assured its irregular surface nature.

## INTRODUCTION

Heavy metals in the environment represent a significant and long-term environmental hazard (Saranya et al. 2017), even low concentration of metals can be toxic to organisms, including humans (Ramrakhiani et al. 2011). Industrial wastewater usually contains non-biodegradable heavy metal ions and many of them are soluble in aqueous media thus being available to living organisms (Ashraf 2017). Groundwater is considered as one of the major sources of drinking water especially in rural and semi-urban areas of Egypt (Akl et al. 2013). Manganese is often present in groundwater through natural leaches from soil rocks. The presence of such metal in waste stream and groundwater represents very serious concern since this metal is toxic to various life forms (Garba et al. 2016). Heavy metals and other constituents leach into the soil and damage the flora and fauna on the earth (Gayatri et al. 2017). The administration of water contaminated with heavy metals even in low dose has been found to cause kidney damage, liver damage and anaemia. Manganese is a common metallic element found in the earth's crusts (Kerani & Barbell 2014). According to the World Health Organization (WHO), the maximum acceptable drinking water limit of Mn is 0.05 mg/L. Abnormal concentration of manganese in the brain, especially in the basal ganglia, results in neurological disorders which are similar to Parkinson's disease (Okoniewska et al. 2007). Manganese presence in water may generate organoleptic and operational troubles including discolouration of water, unpleasant metallic taste and odour, increased turbidity and biofouling of pipelines as well (El Nemr et al. 2008, Khaled et al. 2015). Manganese can pollute water from dual sources, natural and manufactured (El-Waked et al. 2015). Manganese must be removed from water and wastewater for many reasons; first of them, it causes corrosion and pipe blockages. Thus, many methods have been developed for manganese removal such as precipitation, ion exchange, membrane technologies, adsorption, electrochemical processes, and also biological methods are commonly used (Shu et al. 2016). However, most of these methods are highly priced and complicated. Others can produce secondary pollution (Emmanuel & Rao 2009). Adsorption is one of the most accessible techniques for heavy metals elimination from wastewater. Diverse physicochemical characteristics like specific surface area,

pore structure, and surface chemistry of adsorbents control the adsorption efficiency, selectivity, equilibrium time, regeneration capability, and their stability in aqueous solutions have been studied (Islam et al. 2015). Microorganisms such as yeasts, fungi, bacteria and algae can adsorb heavy metals and radionuclides from their external environment (Jasmidia et al. 2017). The cell wall of the microorganisms essentially consists of negative surface charge membrane composition and various organic compounds such as carboxyl, acidic polysaccharides, lipid molecules, amino acids and other constituents, extracellular polymeric substances present on the outer surface of some microorganisms also contribute to biosorption of metal ions as those of polymers which retain negatively charged functional groups, such as carboxyl group, phosphate and sulphate. Several studies have been forwarded towards the use of fungal biomass such as *Rhizopusarrhizus, Saccharomyces cerevisiae* and *Aspergillus niger* for heavy metals removal (Veglio & Beolchini 1997). *Aspergillus niger* has been utilized in the biological decolourization of azo dyes from textile wastewater effluent (Salem et al. 2019). Heavy metal removal by fungus *Mucorrouxii* has been achieved by Khambhaty et al. (2009). Biosorption of hexavalent chromium ions by dead marine *Aspergillus niger* fungus has been reported by Wang & Chen (2009).

In the present study, *Aspergillus versicolor* powder has been used for Mn removal from polluted water. Aspergillus is defined as a group of conidial fungi, where fungi are in an asexual state. The influences of the experimental parameters such as the effect of pH, contact time, initial concentration, stirring time, adsorbent dosage, the temperature on adsorption were studied.

## MATERIALS AND METHODS

### Reagents

All reagents were of analytical pure grade. Standard manganese(II) solution (1000 ppm) and Mn(II) stock solutions were prepared by dissolving 0.2846 g of anhydrous $MnSO_4$ in DDW containing 2 mL conc. $H_2SO_4$ and accurately diluted to volume in 100 mL volumetric flask by 20% potassium tartrate solution.

1M formaldoxime prepared by dissolving 20.0 g of hydroxylamine hydrochloride in 450 mL of distilled water. Add 10 mL of formaldehyde solution (37%) and made up to 500 mL with distilled water. Doubly distilled water [DDW] was used in all the experiments.

### Preparation of Potato Dextrose Broth and Agar Media

Potato dextrose broth and agar media for *Aspergillus versicolor* fungus composed of 20 g of potato slices was boiled with 100 mL of doubly distilled water for 30 min, the filtrate was extracted by strain through many layers of cheesecloth and then the cloth was pressed for extracting the remaining liquid. Two g of dextrose was added. The filtrate was made to 100 mL. For agar plates, 1.5 g of agar was added to this mixture, the flask was closed with cotton plug and aluminium foil and this solution was autoclaved for 20 minutes at 121°C.

### Preparation of Fungal Biosorbents

*A. versicolor* was obtained from Assuit University Mycological Centre under the AUMC No. 90. It was grown on Czapek yeast extract agar (CYA). For fungal biosorption examination, Potato Dextrose Agar (PDA) plates were amended with 100 ppm of Mn(II) ions and the standard spread plate method was performed. The fungus was incubated for 4 to 7 days at 27°C (Wang & Chen 2009). After the incubation period, the fully grown fungi (resistant metal fungi) were killed by adding 0.5 N NaOH in a conical flask containing the fungal mat and preserved in a water bath for 15 minutes. The mat was washed with doubly distilled water for about 6-7 times till the pH reaches 7. The mat was then transferred to a sterile Petri dish and put in a hot air oven for 24 hours at 75°C. The dried dead fungal mat was powdered to smallest particle size using mortar and pestle; the smaller the particle size, the larger the surface area. Biomass has been crushed to inhibit particle aggregation for enhancing the biosorption capacity, then stored in a sterile container for further study.

### Instruments

UV/Vis spectrophotometer (Shimadzu UV/Vis, Perkin Elmer Lambada 3B spectrophotometer with 1cm Quartz cell) and Flame Atomic Absorption Spectrophotometer (AA 240FS, Agilent Technologies) were used for the determination of the residual manganese ions in the effluents samples after each adsorption processes. The pH measurements were made by the microprocessor pH meter (BT 500 BOECO, Germany), which was calibrated with two standard buffer solutions of pH 4 and 9. The morphology of the prepared samples was studied by Scanning Electron Microscopy (SEM) JEOL JEM-1200 EX.

### Adsorption of Manganese

Batch experiments were carried out by shaking stopper flasks containing specific concentration of $Mn^{2+}$ cations solution and specific amount of *Aspergillus versicolor* powder at 120 rpm for desirable time, temperature and initial pH. The suspensions were then filtered and the filtrates were analysed using flame atomic absorption spectrophotometer. The pH values of suspensions were adjusted with dilute HCl or NaOH solution. The experiments were carried out by varying the

initial metal ion concentration, contact time, amount of the adsorbent, and pH of the initial suspension. Removal percentage of the initial concentration was expressed by a specific biosorption q (mg/g), which is calculated by equation (1):

$$q = \frac{C_i - C_f}{Wt} \times V \quad \ldots(1)$$

Where, $C_i$ is the initial manganese concentration (ppm), $C_f$ is the final concentration (ppm), Wt is the dose of sorbents (g) and V is the volume of solution (mL). The equation was applied in the pH range 1-10; the optimum pH was found to be 6 (Fig. 1).

### Optimization of the Factors Affecting the Adsorption of Mn from Standard Solutions

**Optimization of the pH:** To study the effect of pH on the uptake % (adsorption) of manganese from aqueous media by *Aspergillus versicolor* dried powder, aliquots of 25 mL containing 100 ppm of the manganese ion were transferred to a set of 100 mL conical flasks each containing 0.3 g of the fungal powder. The pH of each flask was adjusted to a value in the range of 1-10, respectively, using 0.1M NaOH and 0.1M HCl solutions and stirred for 15 minutes. The contents of each flask were centrifuged and the residual manganese content in the supernatant solution was decanted, then filtered and the concentrations of metal ions were determined using both the spectrophotometric and the flame atomic absorption method.

**Optimization of biomass dose:** Aliquots equal to 100 ppm manganese were transferred to a set of 100 mL conical flasks. The pH of each flask was adjusted to the optimum value of 6. Varying amounts of *A. versicolor* powder in the range 0.05-0.5 g were added to each flask, respectively. The mixtures were stirred for 15 minutes, the residual manganese content in the supernatant solution separated by centrifugation, was determined by FAAS.

**Stirring time:** A set of 100 mL conical flasks, each of which loaded with the optimum biomass dose 0.3 g of *A. versicolor* powder and aliquots of 25 mL solution containing 100 ppm of manganese at the optimum pH of 6 were taken, and the incubation time was changed for different intervals of time (5-30 min) for each flask.

**Metal ion concentration range:** Applying the optimum conditions of the weight of *A. versicolor* powder, pH and stirring time in a group of flasks, aliquots of 25 mL solution containing varying concentrations of manganese in the range of 90-150 ppm were added to the flasks. The same procedure was applied and the residual manganese content was determined from which the uptake per cent was calculated.

**The Determination Methods:** ***The spectrophotometric method:*** In a 25 mL volumetric flask, 2 mL of 20% potassium tartarate solution (in case of the presence of traces of Al, Ti, Cr or U), about 10 mg of ascorbic acid (in case of the presence of traces of Fe (III)), and 20 mg of KCN (in case of presence of Ni, Co, Fe(III) or Cu) were added. Next, 1 mL of 1 M formaldoxime was added followed immediately by 1 mL 1 M NaOH more than the volume required for the neutralization. The solution was diluted with DDW and mixed thoroughly. After 10 minutes, the absorbance of the solution was determined at 455 nm against a blank solution as reference.

***FAAS method:*** The Mn lamp was adjusted at current 5.0 mA with optimum work range of 0.02-5 µg/mL at $_{max}$ equals 279.5 nm, slit width 0.2 nm, using an acetylene-nitrous oxide fuel-oxidant mixture.

**Desorption studies:** Reusability of the adsorbent was tested by regenerating the spent adsorbent following a modified literature procedure (Chen et al. 2011). The desorption process should yield the metal in a concentrated form, restore the biosorbent close to the original state for effective reuse with undiminished metal uptake and physical changes or damages to the biosorbent (Tella et al. 2014). The adsorbed manganese ions on the adsorbent surface are treated with 25 mL 0.1 M HCl and stirred for 1 h. The amount of manganese ions remained in the solution after filtration or centrifugation is measured using the recommended spectrophotometric and FAAS methods. The percentage desorption was calculated according to equation (2)

$$\text{Desorption } \% = \frac{C_r}{C_i} \times 100 \quad \ldots(2)$$

Where $C_r$ is the released metal concentration, and $C_i$ is the initially sorbed metal concentration.

## RESULTS AND DISCUSSION

The dried powdered biomasses have been introduced as a new field of bio-treatment technology, as an effective and relatively simple method for heavy metals recovery. Several studies have explained that inactive dried microbial biomass can passively bind metal ions via various physicochemical mechanisms (Dhankhar & Hooda 2011). It has been suggested that the pretreatment by manganese ions stimulates the surface characteristic groups by removing or masking them or by increasing the metal-binding sites (Asheh et al. 2003). The use of fungal biomass has been reported in literature for the removal of different heavy metals from wastewater, e.g. the uptake of chromium by *Aspergillus foetidus* (Prasenjit & Sumathi 2005), heavy metal biosorption using *Aspergillus niger* (Kapoor et al. 1999, Ahluwalia & Goyal 2007), heavy metal removal by fungus *Mucorrouxii* (Khambhaty et al. 2009) biosorption of hexavalent chromium by dead fungal biomass of marine *Aspergillus niger* (Wang & Chen 2009).

Different factors that affect the adsorption process have been extensively studied to improve the biosorption capacity Q (mg/g) of *A. versicolor* towards manganese ions from the aqueous solutions.

## Optimum pH

Earlier studies showed that the pH value has been observed as one of the important parameters which control the heavy metal biosorption (Blázquez et al. 2005, Dogan et al. 2006, Siddiquee et al. 2015). The variation of adsorption rates at different pH values is dependent on both the metal chemistry in solution and the surface chemistry of the sorbent (Iram et al. 2015). Adsorption of manganese by *A. versicolor* powder has been found to increase with the increase in pH value until it attains its maximum at pH 6. The biosorption of dried biomass increased with the solution pH due to the excess amounts of $OH^-$ ions within the solution, the binding sites on the fungal cell wall are negatively charged. The cell wall is made up of several components such as carboxyl, carbonyl, alcoholic and amino groups which determines the biosorption ability based on its protonation or unprotonation nature. This exerts an influential attraction between active sites and positively charged ions. Thus, it is most possible that at low pH values, the positively charged surface will not favour the binding with manganese ions due to columbic repulsion. With an increase in pH values, the surface becomes more and more negatively charged and thereby favouring manganese ion binding (Fig. 1, Table 1).

## Stirring Time

The kinetics of adsorption describing the shaking time in the removal of manganese is one of the characteristics defining the efficiency of biosorption rate. The results indicate that maximum biosorption capacity occurred after 15 minutes

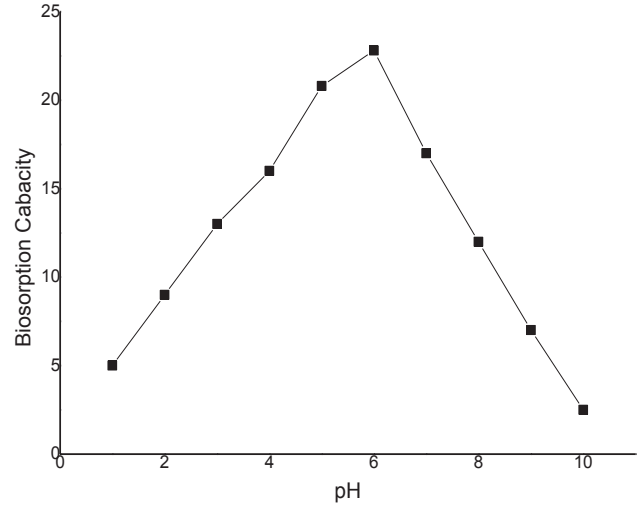


Fig. 1: Effect of Initial pH on biosorption capacity of manganese by *A. versicolor* resistant powder.

Table 1: Effect of initial pH on biosorption capacity of manganese by *Aspergillus versicolor* resistant powder, N=3.

| pH | Std. Deviation | q (mg/g) |
|---|---|---|
| 1.00 | 0.051 | 5.16±0.03 |
| 2.00 | 0.037 | 9.16±0.02 |
| 3.00 | 0.072 | 13.25±0.05 |
| 4.00 | 0.080 | 16.23±0.04 |
| 5.00 | 0.019 | 20.82±0.07 |
| 6.00 | 0.025 | 22.83±0.01 |
| 7.00 | 0.105 | 17.26±0.06 |
| 8.00 | 0.152 | 12.27±0.08 |
| 9.00 | 0.069 | 7.23±0.04 |
| 10.00 | 0.090 | 2.54±0.06 |

where the uptake was 22.83 mg/g for manganese ions. After this period, the equilibrium is reached (Fig. 2, Table 2).

**Biomass Dose**

The increase in biosorbent concentration from 0.05g to 0.5g results in an extensive increase in the metal adsorption. The increase of the adsorption surface area and the availability of free adsorption sites help in the removal of manganese. Maximum removal efficiency was observed at the biomass dosage concentration of 0.3 g *A. versicolor,* which achieves manganese removal of 22.83 mg/g, after this concentration equilibrium is reached (Fig. 3, Table 3).

**Effect of Initial Metal Ion Concentration**

The interest in processes of heavy metal removal by microorganisms has increased considerably in recent years due to the biotechnological potential of microorganisms in metal recovery (Soleimani et al. 2016 ). The maximum metal uptake was 22.83 mg/L at 90 ppm manganese concentration, which decreases with the increase of manganese concentration. At higher concentration, the available sites for sorption become fewer in comparison with the molecules of solute present. Hence, the removal of metal ions is strongly dependent upon the initial solute concentration, so heavy metal tolerant microorganisms such as *A. versicolor* instinctively use defence mechanisms on exposure to metal stress (Fiol et al. 2006 ) (Fig. 4, Table 4).

**Effect of Temperature**

Temperature is an essential and important factor in the biosorption process of metals. Metal adsorption onto the biosorbent is dependent on temperature; the increase in temperature has improved the manganese biosorption rate and decreased the contact time required for heavy metal removal. The temperature of the adsorption medium is con-

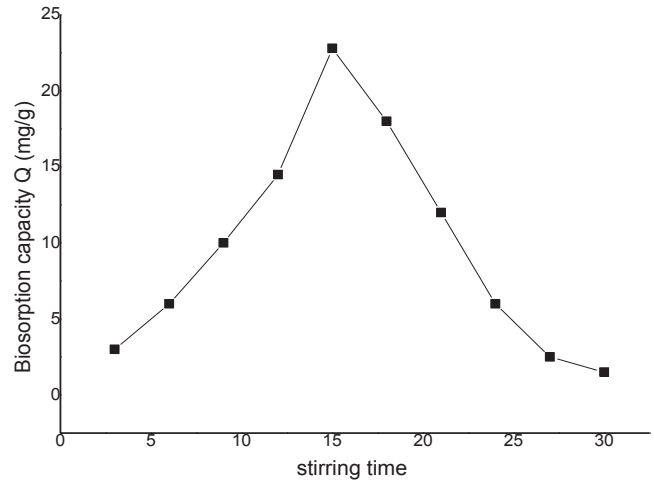


Fig. 2: Effect of stirring time on biosorption capacity of manganese by *A. versicolor* resistant powder.

Table 2: Effect of stirring time on biosorption capacity of manganese by *Aspergillus versicolor* resistant powder, N=3.

| Time of stirring (min) | Std. Deviation | q (mg/g) |
|---|---|---|
| 3.00 | 0.105 | 3.22±0.06 |
| 6.00 | 0.070 | 6.16±0.04 |
| 9.00 | 0.159 | 10.22±0.09 |
| 12.00 | 0.020 | 14.53±0.01 |
| 15.00 | 0.015 | 22.83±0.08 |
| 18.00 | 0.020 | 18.15±0.05 |
| 21.00 | 0.095 | 12.15±0.07 |
| 24.00 | 0.028 | 6.16±0.02 |
| 27.00 | 0.022 | 2.53±0.01 |
| 30.00 | 0.018 | 1.53±0.03 |

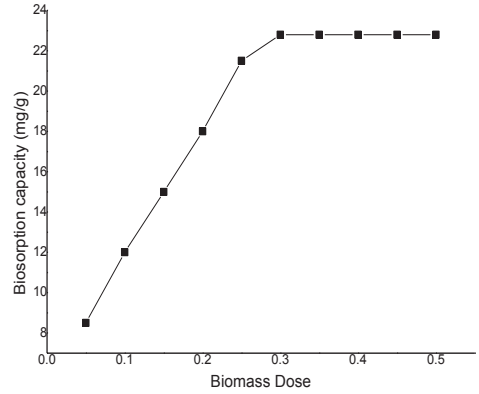


Fig. 3: Effect of biomass dose on biosorption capacity of manganese by *A. versicolor* resistant powder.er.

Table 3: Effect of biomass dose on biosorption capacity of manganese by *Aspergillus versicolor* resistant powder, N=3.

| Dose (g) | Std. Deviation | q (mg/g) |
|---|---|---|
| .050 | 0.020 | 8.54±0.01 |
| .100 | 0.035 | 12.14±0.02 |
| .150 | 0.115 | 15.45±0.06 |
| .200 | 0.032 | 18.30±0.02 |
| .250 | 0.085 | 21.55±0.05 |
| .300 | 0.047 | 22.83±0.03 |
| .350 | 0.078 | 22.82±0.04 |
| .400 | 0.085 | 22.83±0.01 |
| .450 | 0.075 | 22.83±0.06 |
| .500 | 0.040 | 22.85±0.02 |

sidered to be an important parameter for energy-dependent mechanisms in metal removal using the biosorbent. Maximum removal of manganese was found to be 22.93 mg/g at a temperature of 31°C. Temperature affects the cell wall stability components, its configuration and ionization of chemical moieties, and energy-independent mechanisms are likely to be affected due to temperature changes since the processes responsible for removal are largely physicochemical (Bayramoğu et al. 2003). Similar results have been recorded in the bioaccumulation of Cu(II) and Cr(VI) by *Streptococcus equisimilis* and *Aspergillus sp.* (Dehghani et al. 2016, Chen et al. 2011) (Fig. 5, Table 5).

## The Morphology of the Prepared Fungi

Scanning electron microscope (SEM) is a type of electron microscope that produces images of a sample by scanning it

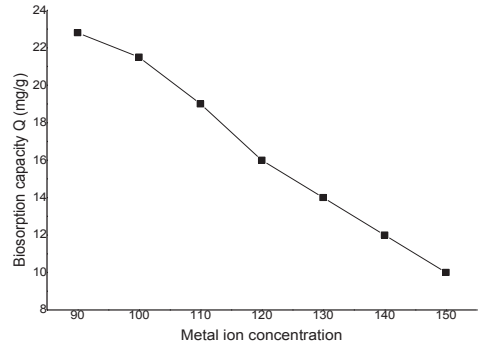


Fig. 4: Effect of metal concentration on biosorption capacity of manganese by *A. versicolor* resistant powder.

Table 4: Effect of metal concentration on biosorption capacity of manganese by *Aspergillus versicolor* resistant powder.

| Metal Concentration (ppm) | Std. Deviation | q (mg/g) |
|---|---|---|
| 90.00 | 0.030 | 21.56±0.01 |
| 100.00 | 0.144 | 19.28±0.08 |
| 110.00 | 0.142 | 16.57±0.08 |
| 120.00 | 0.305 | 14.54±0.17 |
| 130.00 | 0.172 | 12.44±0.09 |
| 140.00 | 0.104 | 10.30±0.06 |
| 150.00 | 0.025 | 16.79±0.05 |

with a focused beam of electrons. The micrographs showed that the fungi have an irregular surface (Fig. 6).

**Adsorption Isotherm Studies**

For the solid-liquid adsorption system, the adsorption behaviour can well be described as adsorption isotherm model (Tella et al. 2014). The adsorption isotherm means the distribution of adsorbate molecules between the solid phase and the liquid phase at equilibrium. Equilibrium is said to be reached when the concentration of adsorbate in bulk solution is in dynamic balance with that on the liquid adsorbate interface.

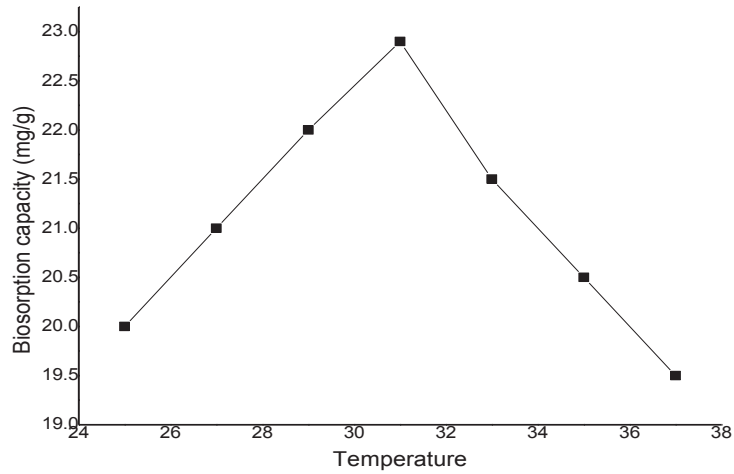


Fig. 5: Effect of temperature on biosorption capacity of manganese by *A. versicolor* resistant powder.

Table 5: Effect of temperature on biosorption capacity of manganese by *Aspergillus versicolor* resistant powder, N=3.

| Temperature (°C ) | Std. Deviation | q (mg/g) |
|---|---|---|
| 25.00 | 0.081 | 20.22±0.04 |
| 27.00 | 0.061 | 21.34±0.03 |
| 29.00 | 0.098 | 22.23±0.07 |
| 31.00 | 0.020 | 22.93±0.01 |
| 33.00 | 0.026 | 21.56±0.05 |
| 35.00 | 0.079 | 20.44±0.06 |
| 37.00 | 0.028 | 19.54±0.02 |
| 39.00 | 0.115 | 19.25±0.09 |
| 41.00 | 0.025 | 18.53±0.01 |

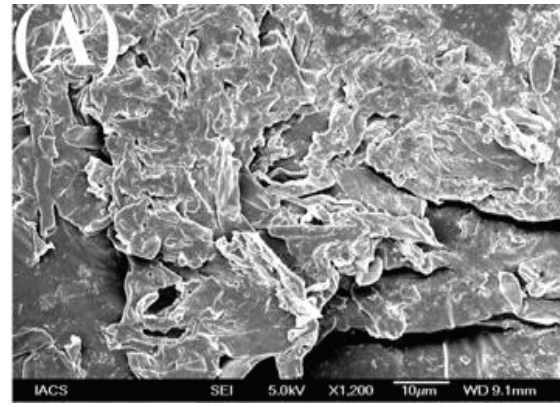


Fig. 6: Scanning electron micrograph of *Aspergillus versicolor* biomass

Table 6: Freundlich, Langmuir adsorption isotherm parameters.

Langmuir and Freundlich adsorption isotherm Parameters of manganese ions by *Aspergillus versicolor*.

| S. No. | Langmuir isotherm Parameters | | Freundlich isotherm parameters | |
|---|---|---|---|---|
| 1 | $Q_{max}$(mg/g) | 22.9 | 1/n | 0.826 |
| 2 | KL | 0.27 | KF | 1.9 |
| 3 | R2 | 0.999 | R2 | 0.999 |
| 4 | RL | 0.045 | | |

**Langmuir adsorption isotherm:** The equilibrium adsorption data for the concentrations of manganese ions were fitted into the linear form of Langmuir's isotherm equation to determine the distribution of manganese ions between the adsorbent and solution according to equation (3).

$$\frac{c_e}{Q_e} = \frac{1}{Q_m K_L} + \frac{c_e}{Q_e} \quad \ldots(3)$$

Where, $C_e$ is the equilibrium concentration of the manganese ions in solution ($mg.L^{-1}$), $Q_e$ is the equilibrium concentration of manganese ions on *A. versicolor* adsorbent ($mg.g^{-1}$), $Q_m$ and $K_L$ are Langmuir constants related to sorption capacity and the rate of adsorption respectively. Maximum adsorption capacity ($Q_m$) is the monolayer capacity of the adsorbent ($mg.g^{-1}$) and $K_L$ is the Langmuir adsorption constant. A plot of $C_e/Q_e$ against $C_e$ over the entire concentration range is a straight line with a slope of $1/Q_m$ and the intercept of $1/Q_mK_L$. The correlation coefficient ($R^2$) values reported were very close to 1 indicating that the adsorption follows the Langmuir adsorption isotherm. The quality of Langmuir isotherm can be determined by the magnitude of a dimensionless constant $R_L$ known as the separation factor expressed in equation (4).

$$R_L = \frac{1}{1+C_0 K_L} \quad \ldots(4)$$

Where, $C_o$ is the initial concentration of the manganese ions in $mg.L^{-1}$ and $K_L$ is the Langmuir constant described earlier. The adsorption process is favourable within the range $0<R_L<1$, unfavourable when $R_L>1$, becomes linear when $R_L=1$, and the process is irreversible when $R_L=0$. The value of $R_L$ is 0.045 for *A. versicolor*; hence the adsorption process is favourable (Fig. 7, Table 6).

**Freundlich adsorption isotherm:** The linear form of the Freundlich adsorption model equation (5) is:

$$\log e\, Qe = \log KF + \frac{1}{n} \log e c_e \quad \ldots(5)$$

Where, $Q_e$ is the quantity of manganese ions adsorbed at equilibrium per gram of the adsorbent ($mg.g^{-1}$), $C_e$ is the equilibrium concentration of the manganese ions in the solution ($mg.L^{-1}$), and $K_f$ and n are the Freundlich adsorption model constants related to the adsorption capacity and adsorption intensity, respectively. Log $Q_e$ was plotted against log $C_e$ and a straight line obtained giving the intercept of log $K_f$ and the slope of 1/n. The reported numerical value of 1/n is less than 1, (Fig. 8, Table 6).

## Selectively of the Adsorbent

The spiking of the manganese authentic samples with different concentrations of other metal ions, e.g. Ni(II) and Cu(II) proved that there is no complete selectivity for the resistant *A. versicolor* powder towards manganese ions, but it has an

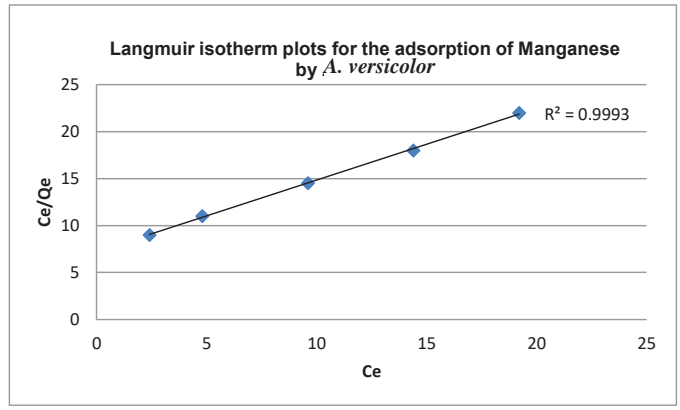


Fig. 7: Langmuir isotherm plots for the adsorption of manganese ions by *A. versicolor*.

Table 7: Effect of pH on desorption%, N=3.

| pH | Std. Deviation | Desorption % |
|---|---|---|
| 1.80 | 0.020 | 81.53±0.01 |
| 2.40 | 0.147 | 81.44±0.08 |
| 3.00 | 0.228 | 77.66±0.13 |
| 3.60 | 0.102 | 73.19±0.05 |
| 4.20 | 0.245 | 68.27±0.14 |
| 4.80 | 0.221 | 64.30±0.11 |
| 5.40 | 0.191 | 58.35±0.01 |
| 6.00 | 0.147 | 55.48±0.09 |
| 6.60 | 0.019 | 52.31±0.02 |
| 7.20 | 0.025 | 81.53±0.07 |

increased capacity towards the spiking ion more than the others. However, the resistant *A. versicolor* powder proved as efficient, low cost, available, economic biosorbent for removal of heavy metals, in general.

## Desorption Studies

**Effect of pH on desorption of iron:** In strong acidic media at pH range (1.8-2.4) *A. versicolor* resistant powder showed a high desorption percentage, but on increasing the pH values

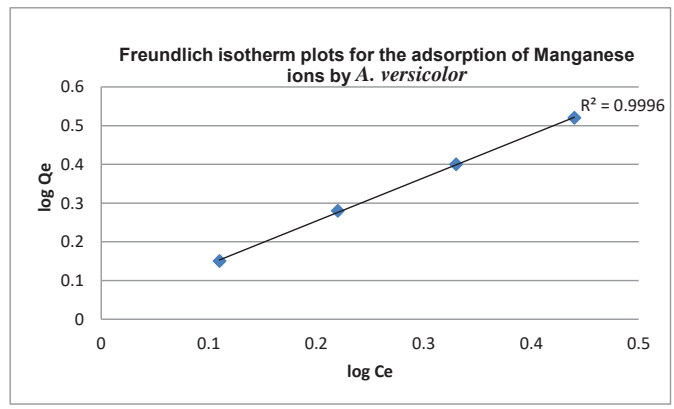


Fig. 8: Freundlich isotherm plots for the adsorption of manganese ions by *A. versicolor.*

Table 8: Effect of stirring time on desorption %, N=3

| Stirring time (min) | Std. Deviation | Desorption % |
|---|---|---|
| 20.00 | 0.032 | 81.54±0.01 |
| 25.00 | 0.075 | 65.23±0.04 |
| 30.00 | 0.161 | 52.44±0.09 |
| 35.00 | 0.258 | 44.41±0.14 |
| 40.00 | 0.158 | 38.34±0.09 |
| 45.00 | 0.294 | 34.58±0.17 |
| 50.00 | 0.025 | 33.55±0.01 |
| 55.00 | 0.133 | 32.49±0.07 |
| 60.00 | 0.136 | 32.81±0.08 |

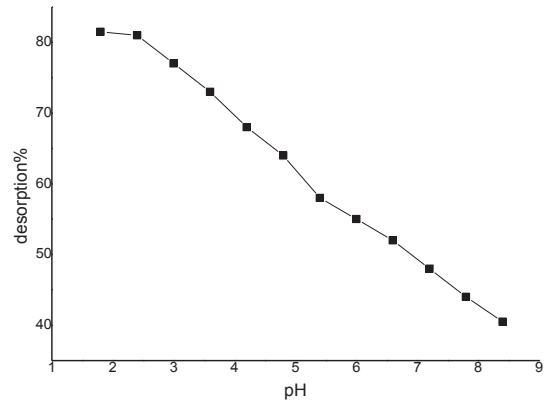


Fig. 9: Effect of pH on desorption (%) of manganese by *A. versicolor* resistant powder.

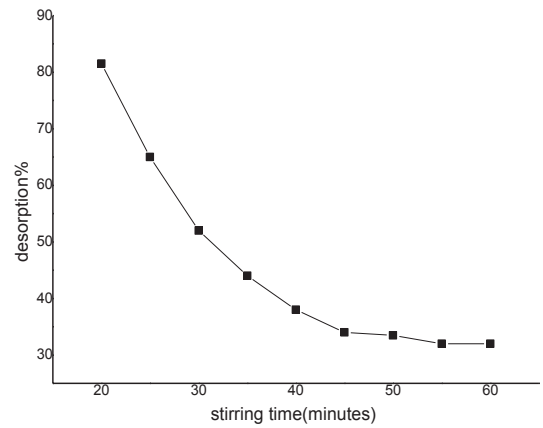


Fig. 10: Effect of stirring time on desorption (%) of manganese by *A. versicolor* resistant powder.

desorption percentage decreases (Fig. 9, Table 7).

**Stirring time**: The maximum desorption percentage was found to be 81.54 during the first 20 minutes, but then gradually decreased (Fig. 10, Table 8).

### Real Samples Analysis

Water samples collected from tap water, Bahr Youssef water, groundwater and Ibrahemia water were subjected to the adsorption procedure as mentioned previously and the residual manganese was analysed by two methods, viz. colourimetry and AAS (Table 9).

## CONCLUSION

Biosorption of manganese ion by *A. versicolor* resistant fungus is shown to be an effective bioremoval process. It could retain relatively high quantities of metal ions with increased capacity towards the adsorption of the amending metal ion,

Table 9: Analysis of real water samples after adsorption on *Aspergillus versicolor* powder, number of determinations N=3.

| Type of sample | Method of finish | *Aspergillus versicolor* | | |
|---|---|---|---|---|
| | | Measured Concentration | SD | Removal % |
| Drinking water | AAS | 0.19 | 0.228 | 88.24±0.13 |
| | Colorimety | 0.18 | 0.152 | 88.16±0.08 |
| Bahr youssef water | AAS | 1.11 | 0.025 | 87.97±0.01 |
| | Colorimety | 1.05 | 0.047 | 87.84±0.03 |
| Ground water | AAS | 1.22 | 0.161 | 87.57±0.09 |
| | Colorimetry | 1.21 | 0.305 | 87.53±0.17 |
| Ibrahimia water | AAS | 0.81 | 0.115 | 88.15±0.09 |
| | Colorimetry | 0.79 | 0.080 | 88.11±0.04 |

although its selective adsorption was not achieved. The kinetics of biosorption has rapidly enhanced with temperature increase and acidic pH. From the obtained statistical results, it can be seen that the models are suitable for predicting biosorption capacity of *A. versicolor* within the range of the studied variables.

## REFERENCES


Ahluwalia, S.S. and Goyal, D. 2007. Microbial and plant derived biomass for removal of heavy metals from wastewater. Journal of Bioresource Technology, 98(12): 2243-2257.

Akl, M.A., Yousef, A.M. and AbdElnasser, S. 2013. Removal of iron and manganese in water samples using activated carbon derived from local-agro-residues. Journal of Chemical Engineering Process Technology, 4(4): 154.

Asheh, S.A., Jumah, R., Banat, F. and Hammad, S. 2003. The use of experimental factorial design for analyzing the effect of spray dryer operating variables on the production of tomato powder. Journal of Food and Bioproducts Processing, 12(12): 0960-3085.

Ashraf, A. 2017. Removal of Mn[II] from water using chemically modified banana peels as efficient adsorbent. Journal of Environmental Nanotechnology, Monitoring & Management, 7(4): 757-763.

Bayramoğlu, G., Bektağ S. and Arica, M.Y. 2003. Biosorption of heavy metal ions on immobilized white-rot fungus *Trametes versicolor*. Journal of Hazardous Mater, 101(3): 285-300.

Blázquez, G., Hernáinz, F., Calero, M. and Ruiz-Nú˜nez, L.F. 2005. Removal of cadmium ions with olive stones: The effect of some parameters. Journal of Process Biochemistry, 40(8): 649-654.

Chen, C.Y., Yang, C.Y. and Chen, A.H. 2011. Biosorption of Cu(II), Zn(II), Ni(II) and Pb(II) ions by cross-linked metal-imprinted chitosans with epichlorohydrin. Journal of Environmental Management, 92(3): 796-802.

Dehghani, M.H., Sanaei, D., Ali, I. and Bhatnagar, A. 2016. Removal of chromium (VI) from aqueous solution using treated waste newspaper as a low-cost adsorbent: Kinetic modeling and isotherm studies. Journal of Ecological Engineering, 215(1): 671-679.

Dhankhar, R. and Hooda, A. 2011. Fungal biosorption- An alternative to meet the challenges of heavy metal pollution in aqueous solutions. Journal of Environmental Technology, 32(5): 467-491.

Dogan, C.E., Turhan, K., Akcin, G. and Aslan, A. 2006. Biosorption of Au(III) and Cu(II) from aqueous solution by a non-living *Cetraria islandica* (L.). Journal of Ach. Analytical Chemistry, 13(2): 229-236.

El Nemr, C.A., Khaled, A., Abdelwahad, O. and El Eikalily, A. 2008. Treatment of wastewater containing toxic chromium using new activated carbon developed from date palm seed. Journal of Hazardous Mater, 152(1): 263-275.

El-Waked, K.Z., El-Sayed, G.O., El-Abo, S.M. and Nassr, E.l. 2015. Removal of ferrous and manganese from water by activated carbon obtained from sugarcane bagasse. Journal of Desalination Water Treatment, 55(2): 179-186.

Emmanuel, E.A. and Rao, A.V. 2009. Comparative study on adsorption of Mn(II) from aqueous solutions on various activated carbon. Journal of Chemical Engineering, 6(2): 693-704.

Fiol, N., Villaescusa, I., Martinez, M., Miralles, N., Poch, J. and Serarols, J. 2006. Sorption of Pb(II), Ni(II), Cu(II) and Cd(II) from aqueous solution by olive stone waste. Journal of Separation and Purification Technology, 38(4): 132-140.

Garba, Z.N., Ugbaga, N.I. and Abdullahi, A.K. 2016. Evaluation of optimum adsorption conditions for Ni(II) and Cd(II) removal from aqueous solution by modified plantain peels (MPP). Journal of Basic and Applied Science, 135(5): 170-179.

Gayatri, Y., Shailaja, R.M. and Vijayalakshmi, B. 2017. Biosorption of lead by *Bacillus licheniformis* isolated from e-waste landfill, Hyderabad, Telangana, India. Journal of Bioassays, 13(1): 5240-5244.

Iram, S., Shabbir, R., Zafar, H. and Javaid, M. 2015. Biosorption of copper and lead by heavy metal resistant fungal isolates. International Journal of Scientific and Research Publications, 5(1): 255-266.

Islam, S. Md., Rahaman, S. Md. and Yeum, J.H. 2015. Phosphine-functionalized electrospun poly (vinyl alcohol)/silica nano fibers as highly effective adsorbent for removal of aqueous manganese and nickel ions, colloids and surfaces. Journal of Physicochemical Engineering Aspects, 484(1): 9-18.

Jasmidia, Z.M., Kembarenc, A., Sellyd, R. and Silalahie, A. 2017. Biosorption of manganese ions (II) by immobilized biomass on a mixture of silica gel and zeolite. Journal of Basic and Applied Research, 35(2): 102-112.

Kapoor, A. and Viraraghavan, T. and Roy, C.D. 1999. Heavy metal biosorption using *Aspergillus niger*. Journal of Bioresource Technology, 70(1): 95-104.

Kerani, D.S.L. and Barbell, B. 2014. Pyrolucite fluidized-bed reactor [PFBR]: A robust and compact process for removing manganese from groundwater. Journal of Water Research, 49(4): 475-483.

Khaled, Z., Waked, A.l., Abd, H., Monem, E.l, Mostara, M. and Kharil, H. 2015. Removing of divalent manganese from aqueous solution using glycine modified chitosan resin. Journal of Chemical Engineering, 3(4): 179-186.

Khambhaty, Y., Mody, K., Basha, S. and Jha, B. 2009. Kinetics, equilibrium and thermodynamic studies on biosorption of hexavalent chromium by dead fungal biomass of marine *Aspergillus niger*. Journal of Chemical Engineering, 145(3): 489-495.

Okoniewska, E., Lach, J., Karperzak, M. and Tveczaj, E. 2007. Removal

of manganese, iron and ammonium nitrogen on impregnated activated carbon. Journal of Desalination, 206(2): 251-258.

Prasenjit, B. and Sumathi, S. 2005. Uptake of chromium by *Aspergillus foetidus*. Journal of Mater Cycles Waste Management, 3(2): 88-92.

Ramrakhiani, L., Majumdel, R. and Khowala, S. 2011. Removal of hexavalent chromium by heat inactivated fungal biomass of *Termitonayces clypeatus*: Surface characterization and mechanism of biosorption. Journal of Chemical Engineering, 171(4): 1060-1068.

Salem, S.S., Mohamed, A., El-Gamal, M., Talat, M. and Fouda, A. 2019. Biological decolorization and degradation of azo dyes from textile wastewater effluent by *Aspergillus niger*. Egyptian Journal of Chemistry, 62(10): 1799-1813.

Saranya, A., Sasikala, S. and Muthuraman, G. 2017. Removal of manganese from ground/ drinking water at South Madras using natural adsorbents. International Journal of Recent Scientific Research, 8(6): 0976-3031.

Shu, J., Liu, R., Liu, Z., Chen, H. and Tao, C. 2016. Simultaneous removal of ammonium and manganese from electrolytic metal manganese residue leachate using phosphate salt. Journal of Cleaner Production, 135(1): 468-475.

Siddiquee, S., Rovina, K., Azad, S.A, Naher, L. and Suryani, S. 2015. Heavy metal contaminants removal from wastewater using the potential filamentous fungi biomass: A review. Journal of Microbial Biochemistry Technology, 243(6): 384-395.

Soleimani, N., Fazli, M.M., Ramazani, A and Mehrasbi, M. 2016. Application of live, dead, and dried biomasses of *Aspergillus versicolor* for cadmium biotreatment. Journal of Human Environmental Health Promotion, 6(2): 87-98.

Tella, A.C., Owalude, S.O., Ojekanmi, C.A. and Oluwafemi, O.S. 2014. Synthesis of copper-isonicotinate metal-organic frameworks simply by mixing solid reactants and investigation of their adsorptive properties for the removal of the fluorescein dye. Journal of New Chemistry, 35(7): 4494-4500.

Veglio, F. and Beolchini, F. 1997. Removal of metals by biosorption: A review. Journal of Hydrometallurgy, 44(3): 301-316.

Wang, J. and Chen, C. 2009. Biosorbents for heavy metals removal and their future. Journal of Biotechnology Advances, 27(2): 195-226.

Nature Environment and Pollution Technology
An International Quarterly Scientific Journal

p-ISSN: 0972-6268
(Print copies up to 2016)
e-ISSN: 2395-3454

Vol. 19 | No. 4 | pp. 1657-1662 | 2020

Original Research Paper

https://doi.org/10.46488/NEPT.2020.v19i04.033

Open Access Journal

# Adsorption of Acid Orange 7 in Aqueous Solution by Biochar from Peanut Shell Supported with Clay Mineral Kaolinite

**Keyuan Huang, Wangying Li, Yue Wang, Bin Liu, Ruolin Xu, Jing Dai, Xitong Zheng, Ningcan Yang, Muqing Qiu and Li Han†**

College of Life Science, Shaoxing University, Shaoxing, 312000, P.R. China

†Corresponding author: Li Han; 51778067@qq.com

**Nat. Env. & Poll. Tech.**
**Website: www.neptjournal.com**

*Received:* 29-10-2019
*Revised:* 18-11-2019
*Accepted:* 16-01-2020

**Key Words:**
Adsorption
Acid Orange 7
Kaolinite
Biochar

## ABSTRACT

Biochar was prepared from the peanut shell. Then, it was mixed with the clay mineral kaolinite and stirred under the magnetic stirrer. The biochar derived from peanut shell supported with clay mineral kaolinite (B@K) was obtained. Adsorption experiments of dye Acid Orange 7 by B@K were conducted. The characteristics of B@K were determined by the elemental analyzer, specific surface area meter, scanning electron microscopy, transmission electron microscopy, Fourier transform infrared spectroscopy, X-ray photoelectron spectrometer and the model axis-HS. The experimental results showed that a large number of oxygen-containing functional groups appear on the surface of B@K, which is beneficial for binding dye ions. The adsorption process fits well with the pseudo-second-order kinetic model. It indicated that the adsorption process was both physical adsorption and chemical adsorption. Chemical adsorption is the main adsorption process. Langmuir isotherm model can better describe the adsorption isothermal process of B@K on dye Acid Orange 7. The adsorption process is monolayer adsorption process.

## INTRODUCTION

With the development of the printing and dyeing industry, a large number of dyes in China will be applied to many plants every year (Hu et al. 2017a). Therefore, it also produces a large amount of dye wastewater into the environment. The printing and dyeing wastewater is one of the most difficult to be treated among the industrial wastewaters at present. The printing and dyeing wastewater has large water volume, high organic matter content, complex composition, difficult to be degraded, and so on (Hu et al. 2017b, Qiu et al. 2018). Moreover, dye wastewater concentration in a water body usually remains low, which will cause the destruction of the water system for the decreasing of the water transmittance by the dye wastewater (Hu et al. 2017c). Additionally, the products of dye wastewater degraded are mainly carcinogenic aromatic compounds. Effective treatment of this kind of wastewater will be very urgent (Rafatullah et al. 2010, Louis et al. 2018).

At present, the treatment methods of dye wastewater mainly include physico-chemical and biological methods (Hu et al. 2013). Among these methods, adsorption using activated carbon as an adsorbent is a commonly used treatment method for removing organic dyes in water. However, the high cost of activated carbon limits its application widely. Therefore, research on adsorbent containing lower costs and higher efficiency treatment is widely concerned by many researchers (Lu et al. 2012).

As a new type of efficient and inexpensive adsorbent, biochar is a better material. Biochar is a highly aromatized structure, and carboxyl group, phenolic hydroxyl group, carbonyl group and acid anhydride appear on the surface of biochar. Because of these structural characteristics, biochar is a good adsorption material. Raw materials for the preparation of biochar are very extensive (Kennedy et al. 2007, Wu 2007, Ling et al. 2011, Pardieu et al. 2016, Lefebvre et al. 2017). At present, the agricultural waste, the forestry waste and the industrial organic waste were applied into the preparation of biochar, and the biochar derived from these materials own good adsorption ability (Nautiyal et al. 2016, Khataee et al. 2018). Crop resources are abundant in China. Every year, a large amount of peanut shell was burned. It not only wastes of resources but also pollution of air. It is an urgent problem to develop clean and efficient technology and utilize these agricultural waste resources (Maria et al. 2018).

To improve the adsorption characteristics of biochar, it is usually modified by a clay mineral. In this study, the preparation of biochar from peanut shell supported with clay mineral kaolinite was explored. The biochar@kaolinite (B@K) was obtained. Then, the adsorption ability of B@K to remove dye Acid Orange 7 from aqueous solution was

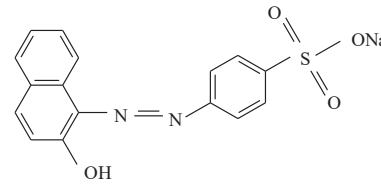


Fig. 1: The chemical structure of the dye Acid Orange 7.

tested. Additionally, the other goals of the study are: (1) study on the characteristics of B@K; (2) the adsorption kinetics and adsorption isotherms were discussed in details; (3) the adsorption mechanism was explored.

## MATERIALS AND METHODS

**Dyes and Chemicals:** The dye Acid Orange 7 was chosen as an object in this experiment. It was purchased from Shanghai Chemical Co. Ltd. in China. Its molecular formula is $C_{16}H_{11}O_4N_2SNa$. The chemical structure of the dye Acid Orange 7 is shown in Fig. 1.

**Preparation of B@K:** The peanut shells were washed with deionized water, and dried at 80°C for 24 h. The dried peanut shells were crushed and sieved into 80 meshes. 10 g of peanut shell powder was taken into a 200 mL reaction vessel containing 100 mL of distilled water and kept at 140°C for 24 h. After cooling, 80 meshes of biochar powder derived from peanut shells was obtained. 5 g of biochar power and 5 g of clay kaolinite were added to the 200 mL of a beaker containing 100 mL distilled water and stirred for 30 min on a magnetic stirrer. Then, they were dried at 80°C for 24 h to obtain the biochar derived from peanut shells supported with clay mineral kaolinite (B@K).

**Effect of contact time on the removal rate:** 0.5 g of B@K powder was added into a 250 mL Erlenmeyer flask containing 200 mL of 10 mg/L dye Acid Orange 7, and placed in an incubator at 25°C and 150 r/min. The contact time was 5, 10, 20, 40, 60, 90, 120, 180, 240, 360 and 480 min. The sample was taken from the supernatant, placed in a centrifuge tube and centrifuged at 8000 r/min for 5 min. Then, it was measured with a UV-1600 spectrophotometer at 485 nm.

**Effect of the initial concentration of dye on the removal rate:** 0.5 g of B@K powder was added into a 250 mL Erlenmeyer flask containing 200 mL of dye Acid Orange 7, and placed in an incubator at 25°C and 150 r/min. The contact time was 360 min. The initial dye concentration ranged from 5 to 80 mg/L. The sample was determined with a UV-1600 spectrophotometer at 485 nm.

**Analytical methods:** The value of pH was measured with a pH probe according to APHA standard method. The concentration of dye Acid Orange 7 was measured with a UV-1600 spectrophotometer at 485 nm.

The removal rate of dye Acid Orange 7 was calculated as follows:

$$Q = \frac{C_0 - C_t}{C_0} \times 100\% \quad \ldots(1)$$

Where, $C_0$ and $C_t$ (mg/L) are the initial and equilibrium concentrations of dye Acid Orange 7 in solution respectively. Q is the removal rate of dye Acid Orange 7. The elements of C, H, O and N were determined by Elemental Analyzer (Vario ELIII, Elementar, Germany). BET specific surface area was measured by the Specific Surface Area Meter (Autosorb-iQ3). The particle microstructure of B@K was determined by scanning electron microscopy (JEOL 6500F, Japan) and Transmission electron microscopy (JEM-F200, Japan) respectively. The functional groups on the surface of B@K were determined by Fourier transform infrared spectroscopy (Bruker Tensor 27). X-ray photoelectron spectrometer (Krato AXIS Ultra DLD, Japan) and the model Axis-HS (Kratos Analytical) were used to determine the surface composition.

The pseudo-first-order kinetic model and the pseudo-second-order kinetic models were applied in this study to elaborate the adsorption kinetics.

The pseudo-first-order rate is given as (Liu et al. 2016):

$$\ln(q_e - q_t) = \ln q_e - k_1 t \quad \ldots(2)$$

The pseudo-second-order rate is given as:

$$\frac{t}{q_t} = \frac{1}{k_2 q_e^2} + \frac{1}{q_e} t \quad \ldots(3)$$

Where, $q_e$ (mg/g) is the amount of adsorbed solute at equilibrium conditions, $q_t$ (mg/g) is the amount of adsorbed solute at any time t (min), $k_1$ ($h^{-1}$) and $k_2$ (g/mg/h) are the model rate constants respectively.

The Langmuir model and Freundlich model were used in this experiment. The Langmuir model and Freundlich model of linear forms are (Ding et al. 2016):

$$\frac{C_e}{q_e} = \frac{1}{K_L q_{max}} + \frac{C_e}{q_{max}} \quad \ldots(4)$$

$$\ln q_e = \ln K_F + \frac{1}{n} \ln C_e \quad \ldots(5)$$

Where, $C_e$ (mg/L) is the equilibrium concentration in the solution, $q_e$(mg/g) is the adsorbate adsorbed at equilibrium, $q_{max}$ (mg/g) is the maximum adsorption capacity, n is the Freundlich constant related to adsorption intensity, $K_L$ (L/mg) and $K_F$ ((mg/g)$^{1/n}$) are the adsorption constants for Langmuir and Freundlich models respectively.

**Statistical analyses of data:** All experiments were repeated in duplicate and the data of results were the mean and the standard deviation (SD). The value of the SD was calculated by Excel Software. All error estimates given in the text and error bars in figures are the standard deviation of means (mean ± SD). All statistical significance was noted at $\alpha$ =0.05 unless otherwise stated.

## RESULTS AND DISCUSSION

**Characteristics of B@K:** The elements C, H, O and N of B@K are 44.21%, 4.18%, 47.16% and 4.45% respectively. BET specific surface area of B@K is 6.15 $m^2$/g. The images of SEM and TEM are shown in Fig. 2.

From Fig. 2, it can be concluded that it was a layered and irregular structure. The irregular surface of B@K is beneficial to adsorb.

Fig. 3 is the FT-IR spectrum of B@K. There is a strong adsorption peak in the range from 3000 $cm^{-1}$ to 3700 $cm^{-1}$, which may refer to the stretching vibration of a hydroxyl radical group. It indicates that a large number of oxygen-containing functional groups appear on the surface of B@K, such as carboxyl groups, hydroxyl groups, carbonyl groups and so on. The peak at 1645 $cm^{-1}$ may correspond to stretching vibration of a carboxyl group, or an ester group, or an aldehyde C = O group. The peaks at 1400 $cm^{-1}$ and 1060 $cm^{-1}$ may correspond to the aromatic group and C-O-C group respectively. The peaks at 820 $cm^{-1}$, 562 $cm^{-1}$ and 472 $cm^{-1}$ may correspond to C-H stretching functional group, -COO- bending vibration functional group and $S_i$-O-$S_i$ functional group (Rebitanim et al. 2013).

The surface composition and chemical state of B@K were further investigated by XPS. The C1s XPS spectra of B@K are shown in Fig. 4. The C1s XPS spectra of B@K

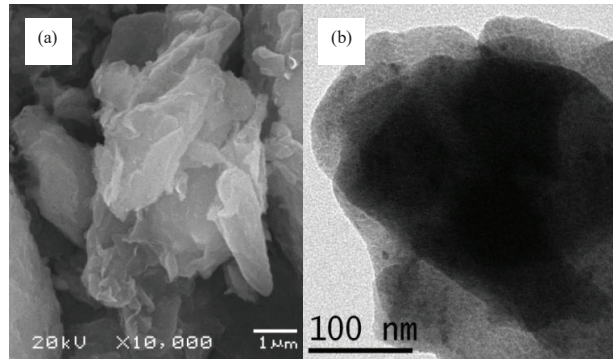


Fig. 2: SEM and TEM images of B@K, (a) SEM image, (b) TEM image.

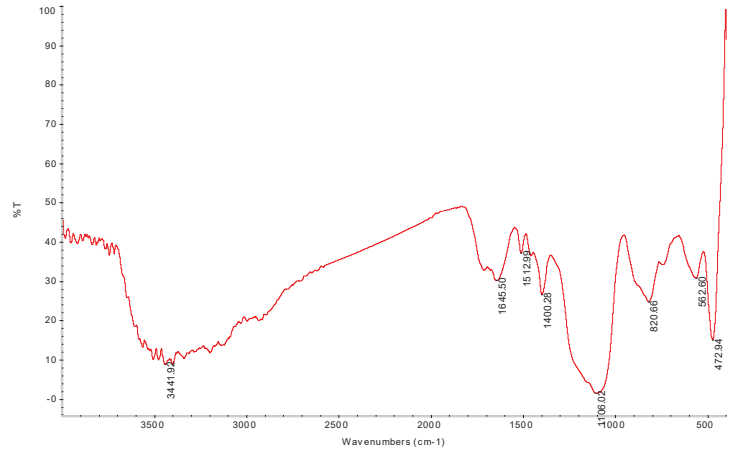


Fig. 3: FT-IR spectrum of B@K

can be the major component with peaks at 284.4 eV, which may be assigned to C/N-O, C-O or C-C bonds. These results suggest that B@K possess considerable amounts of oxygen/nitrogen containing groups on its surface, which is beneficial for binding dye ions (Mohamed et al. 2016).

**Effect of contact time on the removal rate:** Fig. 5 is the effect of contact time on the removal rate of dye Acid Orange 7.

As shown in Fig. 5, the adsorption process of dye Acid Orange 7 by B@K can be divided into three stages. At the first stage of 5 min, the removal rate of dye Acid Orange 7 is very fast. It is because the concentration of dye Acid Orange 7 on the surface of the B@K is the highest in the initial stage. The removal rate increases the action of mass transfer. From 5 to 360 minutes, the removal rate is faster, and the removal rate tends to increase slowly with the increase of contact time. When the adsorption process begins, the difference in the concentration of dye between the surface of B@K and liquid gradually decreases, resulting in a gradual decrease in the removal rate. After 360 min, the change of removal rate is very slow and the adsorption reaches an equilibrium state.

**Effect of initial concentration on the removal rate:** The effect of initial concentration of dye Acid Orange 7 on the removal rate is shown in Fig. 6. It can be seen that as the initial concentration of dye Acid Orange 7 increases, the amount of adsorption also gradually increases. This is mainly due to an increase in the difference in the initial concentration of dye Acid Orange 7.

**Sorption kinetics:** According to the data from Fig. 3, Eqn. 2 and Eqn. 3, parameters of the pseudo-first-order kinetic model and the pseudo-second-order kinetic model for the description of dye Acid Orange 7 adsorption onto B@K were calculated. They are given in Table 1.

From Table 1, it can be seen that the adsorption process fits well with the pseudo-second-order kinetics model according to the value of $R^2$ (0.9973 > 0.8622). It also indicates that the adsorption process is both physical adsorption and

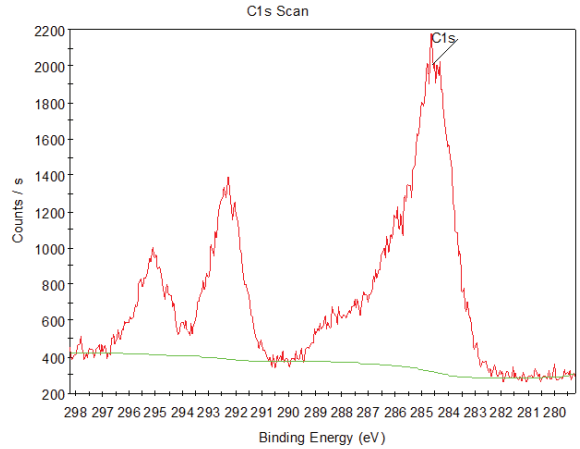


Fig. 4: XPS spectrum of B@K.

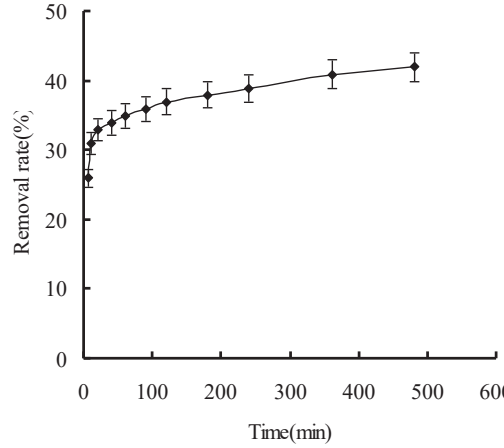


Fig. 5: Effect of contact time on the removal rate of dye Acid Orange 7 by B@K.

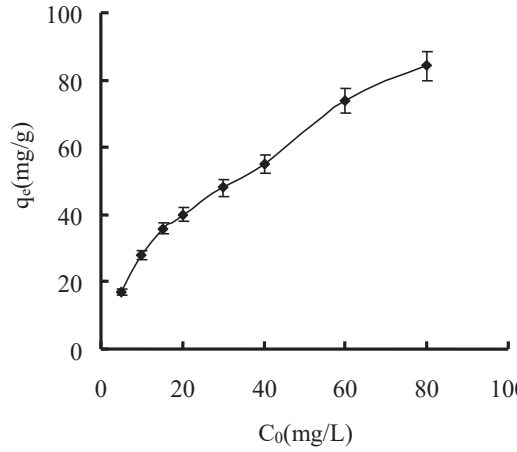


Fig. 6: Effect of the initial concentration of dye Acid Orange 7 on the removal rate by B@K.

chemical adsorption. Chemical adsorption is the main adsorption process.

**Sorption isotherms:** According to the data from Fig. 4, Eqn. 4 and Eqn. 5, parameters of Langmuir isotherm model and Freundlich isotherm model for the description of dye Acid Orange 7 adsorption onto B@K are given in Table 2.

From Table 2, the Langmuir isotherm model can better describe the adsorption isothermal process of B@K on dye Acid Orange 7 according to the value of $R^2$ (0.9836 > 0.9623). The adsorption process is monolayer adsorption process. As the initial concentration of dye increases, the amount of adsorption increases and gradually reaches equilibrium.

## CONCLUSIONS

(1) B@K was a layered and irregular structure. A large number of oxygen-containing functional groups appeared on the surface of B@K, which is beneficial for binding dye ions.

(2) The adsorption process fits well with the pseudo-second-order kinetics model. It indicates that the adsorption process is both physical adsorption and chemical adsorption. Chemical adsorption is the main adsorption process.

(3) Langmuir isotherm model can better describe the adsorption isothermal process of B@K on dye Acid Orange 7. The adsorption process is monolayer adsorption process. As the initial concentration of dye increases, the amount of adsorption increases and gradually reaches equilibrium.

## ACKNOWLEDGEMENTS

This work is supported by the financial support from the research fund program of national Nature Science Foundation of China (No. 21876115).

Table 1: Parameters of the pseudo-first-order kinetic model and the pseudo-second-order kinetic model for the description of dye Acid Orange 7 adsorption onto B@K.

| pseudo-first-order kinetic model | | | pseudo-second-order kinetic model | | |
|---|---|---|---|---|---|
| $k_1$ (min) | $q_e$ (mg/g) | $R^2$ | $k_2$ (mg/g·min) | $q_e$ (mg/g) | $R^2$ |
| 0.4815 | 13.18 | 0.8622 | 0.00292 | 15.46 | 0.9973 |

Table 2: Parameters of the Langmuir isotherm model and Freundlich isotherm model for the description of dye Acid Orange 7 adsorption onto B@K.

| Langmuir | | | Freundlich | | |
|---|---|---|---|---|---|
| $q_m$(mg/g) | $K_L$ | $R^2$ | $K_F$ | n | $R^2$ |
| 101.28 | 0.0645 | 0.9836 | 11.3265 | 2.1786 | 0.9623 |

## REFERENCES


Ding, G.Y., Wang, B.Y., Chen, L.Y. and Zhao, S.J. 2016. Simultaneous adsorption of methyl red and methylene blue onto biochar and an equilibrium modeling at high concentration. Chemosphere, 163: 283-289.

Hu, B.W., Chen, G.H., Jin, C.G., Hu, J., Huang, C.C., Sheng, J., Sheng, G.D., Ma, J.Y. and Huang, Y.Y. 2017a. Macroscopic and spectroscopic studies of the enhanced scavenging of Cr(VI) and Se(VI) from water by titanate nanotube anchored nanoscale zero-valent iron. J. Hazard. Mater., 336: 214-221.

Hu, B.W., Hu, Q.Y., Xu, D. and Chen, C.G. 2017b. The adsorption of U(VI) on carbonaceous nanofibers: A combined batch, EXAFS and modeling techniques. Sep. Pur. Tech., 175: 140-146.

Hu, B.W., Qiu, M.Q., Hu, Q.Y., Sun, Y.B., Sheng G.D., Hu, J. and Ma, J.Y. 2017c. Decontamination of Sr(II) on magnetic polyaniline/graphene oxide composites: Evidence from experimental, spectroscopic, and modeling investigation. ACS Sustain. Chem. Eng., 5: 6924-6931.

Hu, L.X., Yang, F., Lu, W.C., Hao, Y. and Yuan, H. 2013. Heterogeneous activation of oxone with CoMg/SBA-15 for the degradation of dye Rhodamine B in aqueous solution. Appl. Catal. B Environ., 134: 7-18.

Kennedy, L.J., Vijaya, J.J., Sekaran, G. and Kayalvizhi, K. 2007. Equilibrium, kinetic and thermodynamic studies on the adsorption of m-cresol onto micro- and mesoporous carbon. J. Hazard. Mater., 149: 134-143.

Khataee, A., Gholami, P., Kalderis, D., Pachatouridou, E. and Konsolakis, M. 2018. Preparation of novel $CeO_2$-biochar nanocomposite for sonocatalytic degradation of a textile dye. Ultrason. Sonochem., 41: 503-513

Lefebvre, L., Kelber, J., Jierry, L., Ritleng, V. and Edouard, D. 2017. Polydopamine-coated open cell polyurethane foam as an efficient and easy-to-regenerate soft structured catalytic support ($S_2CS$) for the reduction of dye. J. Environ. Chem. Eng., 5: 79-85.

Ling, S.K., Tian, H.Y., Wang, S.B., Rufford, T., Zhu, Z.H. and Buckley, C.E. 2011. KOH catalysed preparation of activated carbon aerogels for dye adsorption. J. Colloid Interf. Sci., 357: 157-162.

Liu, Na, Zhu, M.L., Wang, H. and Ma, H.Q. 2016. Adsorption characteristics of Direct Red 23 from aqueous solution by biochar. J. Mol. Liq., 223: 335-342.

Louis, L., Géraldine, A., Alissa, B. and David, E. 2018. Adsorption of dye with carbon media supported on polyurethane open cell foam. Catal. Today, 301: 98-103.

Lu, J., Lin, J.X., Zhao, X.L. and Cao, R. 2012. Photochromic hybrid materials of cucurbituril and polyoxometalates as photocatalysts under visible light. Chem. Commun., 48: 669-671.

Maria, A.Z., Marcelo, G., Daniele, P., Edson, L.F., Gabriela, C.C. and Guilherme L.D. 2018. New biochar from pecan nutshells as an alternative adsorbent for removing reactive red 141 from aqueous solutions. J. Clean. Prod., 171: 57-65.

Mohamed, E.M., Gehan, M.N., Nabila, M.E., Heba, I.B., Sandeep, K. and Tarek, M.A. 2016. Kinetics, isotherm, and thermodynamic studies of the adsorption of reactive red 195 A dye from water by modified Switchgrass Biochar adsorbent. J. Indus. Eng. Chem., 37: 156-167.

Nautiyal, P., Subramanian, K.A. and Dastidar, M.G. 2016. Adsorptive removal of dye using biochar derived from residual algae after in-situ transesterification: Alternate use of waste of biodiesel industry. J. Environ. Manage., 182: 187-197.

Pardieu, E., Chau, N.T.T., Dintzer, T., Romero, T., Favier, D., Roland, T., Edouard, D., Jierry, L. and Ritleng, V. 2016. Polydopamine-coated open cell polyurethane foams as an inexpensive, flexible yet robust catalyst support: a proof of concept. Chem. Commun., 52: 4691-4693.

Qiu, M.Q., Wang, M., Zhao, Q.Z., Hu, B.W. and Zhu, Y.L. 2018. XANES and EXAFS investigation of uranium incorporation on nZVI in the presence of phosphate. Chemosphere, 201: 764-771.

Rafatullah, M., Sulaiman, O., Hashim, R. and Ahmad, A. 2010. Adsorption of methylene blue on low-cost adsorbents: A review. J. Hazard. Mater., 177: 70-80.

Rebitanim, N.Z., Azlina, W.A., Ghani, K., Rebitanim, N.A. and Salleh, M.A.M. 2013. Potential applications of wastes from energy generation particularly biochar in Malaysia. Renew. Sus. Energ. Rev., 21: 694-702.

Wu, C. 2007. Adsorption of reactive dye onto carbon nanotubes: Equilibrium, kinetics and thermodynamics. J. Hazard. Mater., 144: 93-100.

Nature Environment and Pollution Technology
An International Quarterly Scientific Journal

p-ISSN: 0972-6268
(Print copies up to 2016)
e-ISSN: 2395-3454

Vol. 19 | No. 4 | pp. 1663-1668 | 2020

Original Research Paper

https://doi.org/10.46488/NEPT.2020.v19i04.034

Open Access Journal

# Decontamination Efficiency of Phenylethylene by an Activated Carbon-Based Adsorbent

**Wang Shouzhong, Zhou Zhen, Zhang Tong†, Fang Xiaojun and Miao Chaoyang**

*State Key Laboratory of Technologies in Space Cryogenic Propellants, Beijing Special Engineering Design and Research Institute, Beijing 100028, China

†Corresponding author: Zhang Tong; 1164177746@qq.com

**Nat. Env. & Poll. Tech.**
**Website: www.neptjournal.com**

*Received:* 08-11-2019
*Revised:* 25-11-2019
*Accepted:* 16-01-2020

**Key Words:**
Phenylethylene
Activated carbon
Oxidizing agent
Decontamination efficiency

## ABSTRACT

A sudden leak of phenylethylene is an urgent issue for the surrounding environment. To mitigate its negative effect, the decontamination efficiency of phenylethylene on an activated carbon (AC)-based adsorbent was investigated. Factors such as the particle size and the temperature, that could affect the adsorption ratio, were explored. Meanwhile, the efficiency of AC, pretreated with different $KMnO_4$ and NaClO concentrations, was examined. It was proven that the decontamination efficiency was higher for the 300-mesh AC compared to the 200-mesh AC. The introduction of the oxidizer, $KMnO_4$, had a negative effect on phenylethylene adsorption. Nevertheless, the NaClO-modified AC showed a positive influence on phenylethylene removal, while its decontamination gradually improved with the increase of the NaClO concentration. It was also found that the adsorption rate of phenylethylene was ascended with the temperature rise. After 1 h of adsorption with AC heated to 200°C, no phenylethylene desorption was observed.

## INTRODUCTION

Phenylethylene ($C_8H_8$) is a typical volatile organic compound (VOC) (Ren et al. 2013), which is mephitic, toxic and flammable. Phenylethylene is an important organic chemical and is widely used in the production of synthetic resin, synthetic rubber, and ion-exchange resin. Its strong irritation and the narcotic effect would greatly harm people's respiratory tracts and eyes. In recent years, several phenylethylene leakage accidents have occurred in China (Yu 2012, Zhou et al. 2016), such as the phenylethylene leakage at the Yangtze River in 2001, the phenylethylene leakage due to tank car turnover in Lueyang City in 2010, and the phenylethylene spill at Jiangyin Section of the Yangtze River in 2011.

In case of emergency, the firefighters shall take simple and efficient measures to decontaminate hazardous chemicals quickly and conveniently. The decontamination materials should apply to the existing equipment and have a wide source, low cost, large output, and high adsorption efficiency (Jiang et al. 2017, Wang et al. 2016). Decontamination generally consists of chemical methods and physical methods. In particular, the physical methods include flushing, adsorption, evaporation, and reverse osmosis, while the chemical methods include neutralization, catalysis and oxidation (Li et al. 2014, Liu et al. 2010, Yao et al. 2016, Zhou et al. 2017).

Regarding the adsorption method, the decontamination is achieved by using a certain adsorbent to concentrate the molecular pollutants on its surface or in the internal pores (Yu et al. 2019, Zhou et al. 2019, Zhou et al. 2015). The use of large Brunauer, Emmett and Teller (BET) and abundant micropores resulted in the adsorption capacity of AC up to 30-80 $mg.g^{-1}$ (Guo et al. 2010), employing mainly granular, powdered, and fibrous AC. In 2008 Pan et al. (2008) studied the adsorption of ammonia-modified AC and determined the porous structure and surface acid-base groups of several modified AC fibres, while the effect of the porous structure and the surface groups on the adsorption of phenylethylene was also discussed. Results showed that, after ammonia modification, the basic group content, the pore volume, and the BET features of the AC fibre surface increased, thus further improving the adsorption capacities of AC fibre on phenylethylene. In the study by Ren et al. (2013), AC and its modification were initially prepared from municipal sludge. The BET, acid-base group content, phenylethylene static adsorption, and desorption activation energy of AC were then compared before and after modification. It was demonstrated that the BET of sludge AC, modified by 0.1 M copper sulphate solution, was increased by 32% (705 $m^2.g^{-1}$) compared to the value prior to modification. The impregnation of the aluminium sulphate and copper sulphate solutions increased the surface acid group content of sludge AC, while the surface basic group content was reduced. Besides, the adsorption capacity of phenylethylene was increased more than two times compared to the precursor (211.4 and 178.8

mg.g$^{-1}$, respectively). The adsorption penetration time for phenylethylene was increased from 2 to 10 min and the desorption activation energy was extended from 2.94 to >6.00 kJ.mol$^{-1}$. Instead, Li et al. (2014) degraded phenylethylene by ozonation. Specifically, phenylethylene was effectively decontaminated by the ozone-coupled biological AC, whereas the decontamination rates of 1, 2, and 4 ppm phenylethylene were 100%, 60.6% and 57.9%, respectively.

The current study aimed to explore the decontamination behaviour of phenylethylene via AC in case of sudden leakage. The effect of particle size, thermal treatment, and oxidant modification on the phenylethylene adsorption on AC was investigated. Meanwhile, the second-order kinetic equation was used to illustrate the adsorption behaviour. The results of our investigation shed new light on the emergency disposal of sudden phenylethylene leakage.

## MATERIALS AND METHODS

### Reagents and Apparatus

Phenylethylene was procured from Tianjin Tianli Chemical Reagent (China). $KMnO_4$ and NaClO were obtained from Sinopharm Chemical Reagent (China). The abovementioned reagents were of analytical grade and dissolved in deionized water (18.2 MΩ Milli-Q, USA). AC was purchased from Jiangshan Lvyi Bamboo Charcoal (China) and was used after following purification process. After grinding and sieving, the AC was cleaned with deionized water before boiling. Afterwards, the solution was continuously stirred for 1 h and repeatedly flushed with deionized water to remove the surface impurity. Finally, the AC was dried for 12 h in a drying oven at 80°C. After being tested with the BET detector (ASAP 2460, Micromeritics, USA), the specific surface area of the adsorbent reached 873.1 m$^2$.g$^{-1}$ (Fig. 1).

Fig. 2 shows a self-made apparatus that was used during the current study. It mainly consisted of four parts, namely a decontamination chamber, a water treatment agent atomization injection system, a dry powder treatment agent injection system, and a foam injection system. The decontamination chamber consisted of a tank-8 (700 mm × 700 mm × 800 mm), an oil evaporating pan-21 (120 mm high), an air sac-7 (for balancing the chamber pressure during jet decontamination), a steam sampling tube-20, a filter-12, and a vapour concentration analyzer-13 (CEM200 Multi-Gas Emergency Detector, Beijing Taihua Hengyue Technology Development Co., Ltd.). The water treatment agent atomization injection system consisted of a sink-1, a liquid pump-2, a transfer tube-16, and a spray nozzle-3. The dry powder treatment agent injection system consisted of an air pump-4, a dry powder tank-5, a dry powder nozzle-6, a dry powder tube-18, and a compressed air tube-19. The foam injection system consisted of a foam concentrate tank-11, a foam concentrate tube-17, a foam pump-10, and a foam nozzle-9.

### Experimental Steps

1. After treating the dry powder tank-5 with vacuum, it was added in the tank, and the pressure was adjusted to 8 bar. Then, the nozzle above the experimental tank was connected to the dry powder tank. Boiling water of 50 mm in height was added to the liquid tray-21 and 15 mL of phenylethylene were sprayed on the surface of the boiling water to accelerate the evaporation.
2. The real-time monitoring was performed on the concentration of phenylethylene gas with the gas detector-13. When phenylethylene was substantially evaporated and

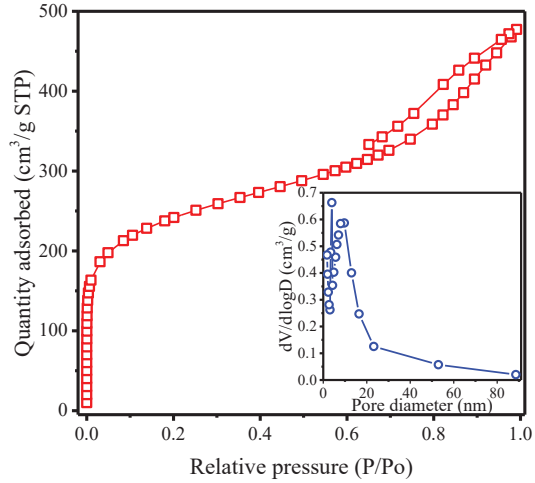


Fig. 1: Nitrogen adsorption-desorption isotherms and pore size distribution profiles (inset) of AC.

the concentration reached a constant level, the valve of the dry powder tank was opened to spray the dry powder.

3. The spraying was repeated 10 times, each of which lasted for about 2 s, and was completed in 3 min. The change in phenylethylene concentration was continuously monitored and when the concentration dropped to a constant level, the experiment was considered to be complete.

## RESULTS AND DISCUSSION

Effect of particle size: The 200 and 300-mesh AC are commonly used in the market and are applicable for firefighting equipment (Sun et al. 2017, Zhang et al. 2015). The 200 and 300-mesh AC powders were selected for this study as well to compare their effect on the phenylethylene decontamination. During the experiment, all the experimental conditions, including the amount of AC, the pressure of the dry powder tank, and the volatilization concentration of phenylethylene, were maintained constant. The real-time decontamination effect within five minutes is illustrated in Fig. 3.

The adsorption kinetics by the AC complied with the second-order kinetics, with insets showing the constants ($R^2$ >0.97), indicating that the chemical adsorption is the rate-limiting step of the decontamination process (Liang et al. 2018, Yan et al. 2017). The decontamination rate of the 300-mesh AC was 0.0127 $h^{-1}$, i.e. about 1.25 times higher than the decontamination rate of the 200-mesh AC (0.0102 $h^{-1}$). Moreover, the 300-mesh AC had a lower phenylethylene residual rate (0.21 vs. 0.26), which indicated that its decontamination capability was greater than that of the 200-mesh AC. The 300-mesh AC had also smaller particle size, higher BET, and better hovering property, leading to improved phenylethylene elimination (Yu et al. 2017, Zhou et al. 2018).

**Effect of oxidant modification:** Fang et al. (2017) and Hu et al. (2017) documented that the oxidant impregnation could improve the adsorption capacity of the adsorbent. Based on these data, the 300-mesh AC was impregnated with a $KMnO_4$ solution and a NaClO solution and then used for the decontamination of phenylethylene. Fig. 4 presents the adsorption kinetics of phenylethylene using the AC impregnated with 1.5 $g.L^{-1}$ and 3.0 $g.L^{-1}$ of the $KMnO_4$ solution. The kinetics followed the second-order kinetic equation ($R^2$ >0.99), which demonstrated that the impregnation with $KMnO_4$ did not change the type of the phenylethylene adsorption kinetics. The decontamination process was still dominated by the

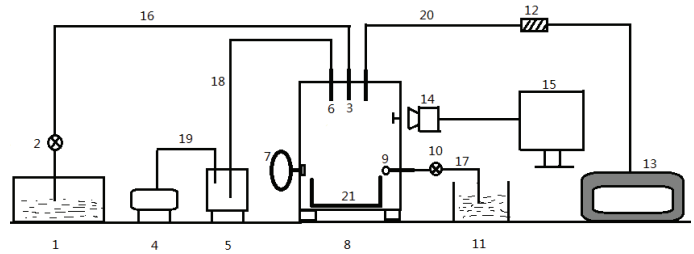


Fig. 2: Schematic diagram of the experiment.

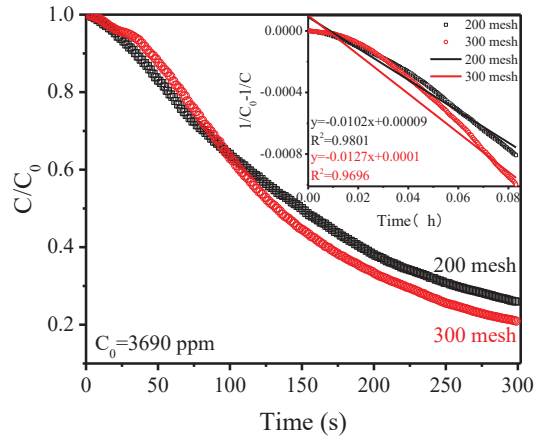


Fig. 3: Decontamination kinetics of phenylethylene on AC at different mesh number. The inset is the corresponding parameters of the second-order model.

chemical adsorption. It was proven that the decontamination efficiency of phenylethylene was the same when using AC impregnated with 1.5 g.L$^{-1}$ of $KMnO_4$ (0.0117 h$^{-1}$) and 3.0 g.L$^{-1}$ of $KMnO_4$ (0.0116 h$^{-1}$). Whereas, both of the impregnated AC manifested the inferior adsorption rate than their pristine predecessor (0.0127 h$^{-1}$), demonstrating that impregnation with $KMnO_4$ negatively affected the phenylethylene adsorption. The effect of the oxidation treatment on AC had two sides. Although the oxidant impregnation increased the number of the surface hydroxyl, carboxyl, and carbonyl groups, hence improving the decontamination efficiency, the oxidant could etch the surface and pore walls of AC and occupy partial pores. Such effects could concomitantly decrease the BET and the AC pore volume and reduce the adsorption sites (Fang et al. 2017, Zhou et al. 2016a, 2016b). In this study, $KMnO_4$ corroded the surface and pore walls of AC to such an extent that the negative impact predominated the positive effect.

According to previous reports, strong oxidants, such as nitric acid, easily damaged the pore walls, reduced the number of micropores, increased the number of mesopores and macropores, and reduced the BET, and the pore volume. Subsequently, they affected the adsorption efficiency (Gil & Grange 1997). Other studies (Wang et al. 2012) reported that the modification of AC with NaClO was relatively mild, indicating that the pore structure was slightly damaged, while the number of phenolic hydroxyl, carboxyl, ketonic, and ether surface oxygen-containing functional groups was increased (Rivera-Utrilla et al. 2011).

Hence, NaClO solutions with 5% effective chlorine and 10% effective chlorine were selected to treat AC, to carry out the decontamination test. Fig. 5 describes that the adsorption rate of 5% NaClO impregnated AC was significantly elevated from 0.0127 to 0.0200 h$^{-1}$, and further increased to 0.0217 h$^{-1}$ with the increase of NaClO concentration. This improvement substantiated that the impregnation with NaClO could gradually increase the active sites on the surface of AC and in turn the decontamination efficiency of phenylethylene.

**Effect of thermal modification:** Thermal treatment is an easily achievable physical method for controlling the surface functional groups and pore structures of AC (Fang et al. 2017). Herein, we investigated the decontamination efficiency of phenylethylene using AC treated at 100°C and 200°C and the obtained results are displayed in Fig. 6. The decontamination efficiency of phenylethylene after thermal modification was higher than that of pristine AC (0.0127 h$^{-1}$), while their decontamination efficiency gradually elevated with rising temperature (0.0175-0.0190 h$^{-1}$). The adsorption capacity of the adsorbent for a specific adsorbate was mainly determined by physical properties such as BET, micropore volume, and pore size distribution, as well as its chemical properties such as the surface groups (Zhen et al. 2017, Zhen et al. 2016). The high-temperature activation improved the lattice structure of the AC, removed parts of impurities adsorbed on the surface and in the pores, and also increased the number of micropores or mesopores, thus increasing the BET of AC. Meanwhile, the high-temperature activation also oxidized some functional groups on the surface of AC, released a number of oxygen-containing functional groups, and enhanced the hydrogen bonding force, thus improving the adsorption efficiency (Fang et al. 2017).

**Stability test:** The adsorbed adsorbates may desorb over a

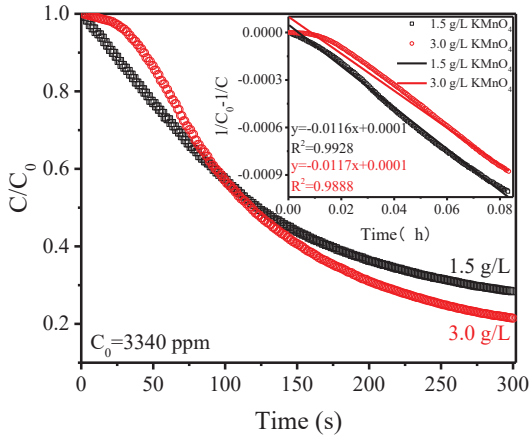


Fig. 4: Decontamination kinetics of phenylethylene on AC after 1.5 and 3.0 g/L $KMnO_4$ immersion. The inset is the corresponding parameters of the second-order model.

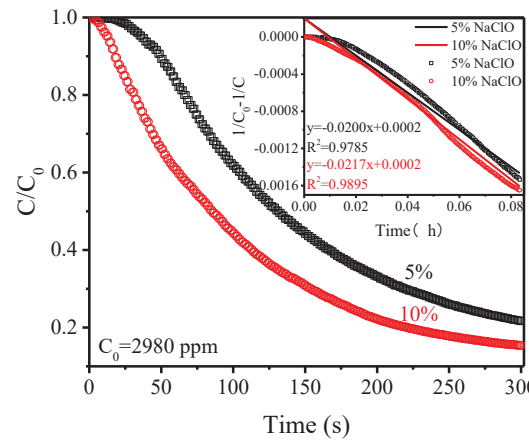


Fig. 5: Decontamination kinetics of phenylethylene on AC after 5% and 10% NaClO immersion. The inset is the corresponding parameters of the second-order model.

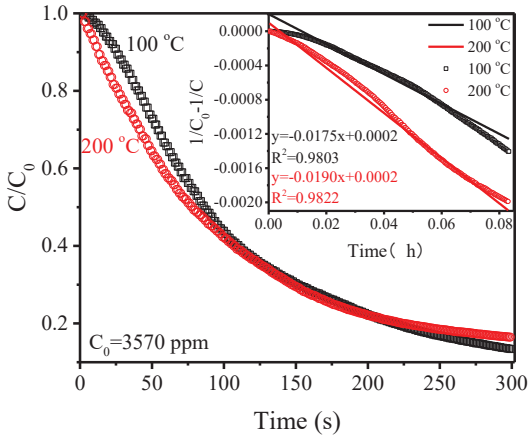


Fig. 6: Decontamination kinetics of phenylethylene on AC after 100 and 200°C heat treatment. The inset is the corresponding parameters of the second-order model.

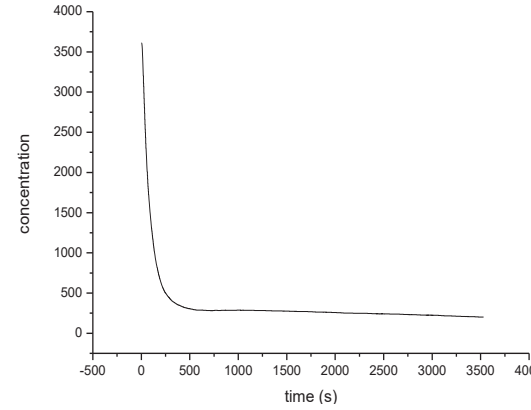


Fig. 7: Adsorption stability of phenylethylene on AC.

long time (Zhou et al. 2016a, Zhou et al. 2017). The 200°C treated AC was selected to decontaminate phenylethylene and test its adsorption stability on AC. Fig. 7 illustrates the content of phenylethylene with the concomitant increase of the adsorption time, where an apparent decrease could be observed at a rudimentary stage spanning between 0-400 s. Subsequently, an equilibrium period was achieved. Specifically, the concentration of the phenylethylene gas in the decontamination chamber did not significantly rise within 1 h, indicating that the phenylethylene molecule was tightly adsorbed on AC and was hard to be desorbed.

## CONCLUSIONS

Herein, the effect of the particle size, the oxidant modification, and the thermal treatment on the decontamination efficiency of phenylethylene was studied. The AC with a higher mesh number resulted in a greater decontamination efficiency. The modification of AC with $KMnO_4$ decreased the efficiency, while it was increased with the NaClO modification and was further elevated with the increase of the NaClO concentration. Thermal treatment enhanced the adsorption rate of phenylethylene, which escalated with the temperature rise. No phenylethylene desorption was detected 1 h after the AC adsorption.

## ACKNOWLEDGEMENTS

The work was subsidized by the National Science & Technology Pillar Program of China (2015BAK37B00).

## REFERENCES

Fang, H., Li, Z., Ma, D. and Dong, H.. 2017. Research progress in modification of activated carbon as adsorbent used in flue gas desulfurization. Energy for Metallurgical Industry, 36(6): 56-61.

Gil, A., Puente, G. D. L. and Grange, P. 1997. Evidence of textural modifications of an activated carbon on liquid-phase oxidation treatments. Microporous Materials, 12(1):51-61

Guo, C., Zhao, P. and Xiao, J. 2010. Application of several absorbing material to treat oil wastewater. Environmental Science and Management, 35(3): 96-98,102.

Hu, C., Lu, R., Huang, J. and Lv, X. 2017. Epoxidation of styrene by novel asymmetric Schiff base copper complex. Chemical Engineering, 45(10): 62-66.

Jiang, T., Ni, X., Wang, X. and Dong, C. 2017. A comparative study on the performances of multi-type agents used for emergency disposal of leaked methanol. Industrial Safety and Environmental Protection, 43(5): 62-65.

Li, T., Wang, Z., Bai, X. and Zhu, Y. 2014. Emergency treatment of styrene contamination in source water for waterworks. China Water & Wastewater, 30(13): 6-9,14.

Liang, Q., Luo, H., Geng, J. and Chen, J. 2018. Facile one-pot preparation of nitrogen-doped ultra-light graphene oxide aerogel and its prominent adsorption performance of Cr(VI). Chemical Engineering Journal, 338: 62-71.

Liu, J., Ma, W., Wang, M. and Huang, L. 2010. Cleaning of waste gas containing styrene using a fungal biofilter. Environmental Engineering, 28(05): 66-69,73.

Pan, H., Li, Z., Xia, Q. and Li, J. 2008. Adsorption of styrene on ammonia-treated activated carbon fibres. Journal of Functional Materials, 2: 324-327.

Ren, A., Fu, F., Qu, Y. and Guo, B. 2013. Adsorption properties of modified activated sludge carbon to styrene. Environmental Chemistry, 32(5): 833-838.

Rivera-Utrilla, J., Sánchez-Polo, M., Gómez-Serrano, V., Álvarez, P. M., Alvim-Ferraz, M. C. M. and Dias, J. M. 2011. Activated carbon modifications to enhance its water treatment applications. An overview. Journal of Hazardous Materials, 187(1): 1-23.

Sun, Z., Ding, Y., Geng, Z. and Gao, J. 2017. Comparison of adsorption properties of biomass based activated carbon for p-nitrophenol. Industrial Catalysis, 25(6): 74-77.

Wang, K. and Xu, Q. 2012. Effect of several different treatment methods on surface chemical properties of activated carbon. Chinese Journal of Environmental Engineering, 6(2): 373-380.

Wang, S., Dong, C., Ni, X. and Cong, H. 2016. Experimental study on effectiveness of composite dry powder in emergence disposal of leaked methanol. China Safety Science Journal, 26(5): 164-168.

Yan, L., Tu, H., Chan, T. and Jing, C. 2017. Mechanistic study of simultaneous arsenic and fluoride removal using granular $TiO_2$-La adsorbent. Chemical Engineering Journal, 313: 983-992.

Yao, J., Zhou, Z., Pang, Z. and Liu, B. 2016. Research progress of ultrasonic wave combined technology for water treatment. Contemporary Chemical Industry, 45(11): 2660-2665.

Yu, A. 2012. Establishing precautionary and emergency handling system for water pollution: Application in Nanjing chemical industrial park. Environmental Monitoring Management and Technology, 24(06): 6-10.

Yu, Y., Yan, L., Cheng, J. and Jing, C. 2017. Mechanistic insights into $TiO_2$ thickness in $Fe_3O_4$@$TiO_2$-GO composites for enrofloxacin photodegradation. Chemical Engineering Journal, 325: 647-654.

Yu, Y. Q., Zhou, Z., Ding, Z. X., Zuo, M. M., Cheng, J. M. and Jing, C. Y. 2019. Simultaneous arsenic and fluoride removal using {201} $TiO_2$-$ZrO_2$: Fabrication, characterization, and mechanism. Journal of Hazardous Materials, 377: 267-273.

Zhang, B., Tang, X., Yi, H. and Wang, Z. 2015. Study on NO adsorptive removal on modified activated carbon. New Chemical Materials, 43(7): 111-113,121.

Zhen, Z., Jilun, Y., Xing, Z., Zhaoxia, D. and Meimei, Z. 2017. Enhanced effluent quality of ceramic membrane ultrafiltration combined with UV/$TiO_2$ photocatalysis. Nature Environment and Pollution Technology, 16(3): 695-702.

Zhen, Z., Yao, J., Pang, Z. and Bo, L. 2016. Optimization of electrocoagulation process to eliminate $COD_{Mn}$ in micro-polluted surface water using response surface method. Journal of Dispersion Science and Technology, 37(5): 743-751.

Zhou, Y., Li, J., Chen, F. and Ning, Y. 2016. Study on the 3D fluorescence feature of styrene and emergent treatment of styrene pollutant in water. Spectroscopy and Spectral Analysis, 36(7): 2169-2172.

Zhou, Z., Yao, J., Liu, B., Pang, Z. and Zhang, X. 2017. Research progress on water treatment by $TiO_2$ photocatalysis. Chemistry & Bioengineering, 34(4): 1-5,9.

Zhou, Z., Yao, J., Pang, Z. and Liu, B. 2015. Review of research development in electrocoagulation technology in water treatment. Water Purification Technology, 34(5): 9-15,38.

Zhou, Z., Yao, J., Pang, Z. and Liu, B. 2016a. Optimization of electrocoagulation-ceramic micro-filtration membrane process by response surface method. Environmental Pollution & Control, 38(3): 39-44,49.

Zhou, Z., Yao, J., Pang, Z. and Liu, B. 2016b. Optimization of electrocoagulation process to eliminate $UV_{254}$ in micro-polluted surface water using response surface method. Technology of Water Treatment, 42(3): 32-36,42.

Zhou, Z., Yao, J., Pang, Z., Liu, B. and Zhang, X. 2017. Effect of transmembrane pressure and crossflow velocity on membrane fouling using magnetic flocculation pretreatment. Environmental Engineering, 35(6): 10-14.

Zhou, Z., Yu, Y., Ding, Z., Zuo, M. and Jing, C. 2018. Modulating high-index facets on anatase $TiO_2$. European Journal of Inorganic Chemistry, 2018(6): 683-693.

Zhou, Z., Yu, Y., Ding, Z., Zuo, M. and Jing, C. 2019. Competitive adsorption of arsenic and fluoride on {2 0 1} $TiO_2$. Applied Surface Science, 466: 425-432.

Nature Environment and Pollution Technology
An International Quarterly Scientific Journal

p-ISSN: 0972-6268
(Print copies up to 2016)
e-ISSN: 2395-3454

Vol. 19 | No. 4 | pp. 1669-1674 | 2020

Original Research Paper

https://doi.org/10.46488/NEPT.2020.v19i04.035

Open Access Journal

# Combined Treatment of Real Sugar Industry and Sago Wastewater Using Hybrid Upflow Anaerobic Sludge Blanket (HUASB) Reactor

**T. Kavimani*†, K. Balaji** and G. Gnanapragasam*****

*†Department of Civil Engineering, Government College of Engineering, Thanjavur, Tamilnadu, India
**Department of Civil Engineering, University College of Engineering, Anna University, Panruti, Tamilnadu, India
***Department of Chemical Engineering, VSB Engineering College, Karur, Tamilnadu, India
†Corresponding author: T. Kavimani; tkavimani@gmail.com

**Nat. Env. & Poll. Tech.**
**Website: www.neptjournal.com**

*Received:* 15-12-2019
*Revised:* 29-12-2019
*Accepted:* 03-01-2020

**Key Words:**
Biogas
HUASB reactor
Sago wastewater
Sugar industry

## ABSTRACT

This paper presents the performance of Hybrid Upflow Anaerobic Sludge Blanket (HUASB) reactor in treating combined real sugar industry and synthetic sago effluents. Sugar industry is one of the most important agricultural industries which discharge the effluent in a huge quantity that creates environmental problems. The disposal of untreated sugar industry effluent in soils and water bodies has received much attention since decades ago. So, in this study, it was decided to inoculate the HUASB reactor with seed sludge from the existing anaerobic digester treating sago wastewater and then it was started by using synthetic sago wastewater, and then it was fed with the combined real sugar industry and synthetic sago wastewater. The reactor was fed with the combined effluents of a real sugar industry and synthetic sago wastewater at different mixing ratios having the Chemical Oxygen Demand (COD) ranging from 4450 to 5360 mg/L with HRT of 24 hours. The pH, COD removal, volatile fatty acid (VFA), alkalinity and biogas production were monitored for various inlet of COD values. The inlet and outlet pH was between the range of 5.62 to 7.36 and 7.53 to 8.18 respectively. The VFA and alkalinity varied from 36 to 84 mg/L and 926 to 998 mg/L respectively. The biogas production varied from 10.6 to 13.2 L/d. The maximum COD removal of 94.4% and the biogas production of 13.2 L/d was reported at pH 8.11 at the mixing ratio of 60/40 (sago/sugar industry wastewater).

## INTRODUCTION

Sago is a main agro-based product found in various parts of the world. Products from tapioca like starch and sago introduced in India since1940s onwards. Processing of tapioca need 20,000-30,000 L of water per ton of sago; besides it produces same quantity of wastewater which is extremely organic, foul smelling and acidic. Most of the starch units generate effluent within the range of 200-300 $m^3$/d. Several studies reported that the sago industry wastewater may bring about drastic ecological imbalances in the nearby agro ecosystems if it is not treated properly (Murthy & Patel 1961, Saroja & Sastry 1972, Gnanapragasam et al. 2010, Senthilkumar et al. 2011).

Sugar industry contributes to the development of the economy in many countries, but arguably harms the environment (Ndobeni et al. 2019). The conversion of natural habitats for cane cultivation in coastal areas and tropical islands has led to critical environmental damage, loss of biodiversity and ecosystem services at landscape levels (Rein et al. 2011). These wastes not only represent a threat to the environmental quality but also possess a potential energy value which is not fully utilized despite the fact that they are cheap and abundant in most parts of the world (Hampannavar & Shivayogimath 2010).

Anaerobic treatment converts the wastewater organic pollutants into small amount of sludge and large amount of biogas as source of energy (Ayati & Ganjidoust 2006). Whereas aerobic treatment needs external input of energy for aeration. The upflow anaerobic sludge blanket (UASB) reactor is by far the most widely used high rate anaerobic treatment system for variety of wastewater (van Haandel & Lettinga 1994). The anaerobic biological sludge blanket systems proposed over recent years have elicited considerable interest because of their good removal efficiencies of organic substrates, their relatively simple layout and the low capital and operating costs. Granular biomass with high methanogenic activity and excellent settling properties can be cultivated in these reactors (Buzzini et al. 2006).

The investigation is on the feasibility of treatment of real sugar industry effluent under bench scale hybrid upflow anaerobic sludge blanket reactor of stressed loadings. Shortening the start-up time bears practical significance as

it can raise attractiveness of HUASB reactor applications by saving time and cost. After the start-up process the reactor were operated at various mixing ratio of real sugar industry and synthetic sago wastewater and COD, pH, VFA, alkalinity and biogas were monitored regularly.

## MATERIALS AND METHODS

### Biomass

In the present research, materials were collected from sago factory which is located in Salem. The unspecified microoraganims present in the granular sludge from the starch effulent were used in the study. The sludge was completely washed before loading and filtered in a mesh in order to minimize the inorganic components present in the granules. About 60000mg/L content of sludge was estimated as volatile suspended solids (APHA 2005).

### Wastewater

**Sugar industry:** Real sugar industry wastewater was collected from M.R.Krishnamurthy Co–operative sugar mill Ltd, Sethiyathope village, Chidambaram Taluk, Cuddalore District, Tamil Nadu, India. The characteristics were immediately analysed before feeding the reactor.

**Synthetic sago:** In this research synthetic sago wasterwater was prepared in which nitrogen and phosphorus were added along with starch and minerals in the ratio of 5:1:550. Ferric chloride, zinc sulphate, copper sulphate present as nutrients were added to the reactor at the concentration of 1.0ml/L (Bhatti 1995, Arshad et al. 2009).

### Experimental Setup

In this research study benchscale HUASB reactor was designed and fabricated using perspex tube (Fig 1). The reactor of about 20L volume has a total height of 1.42m with 1.17m as the effective height and 0.15m diameter. The upper most part of the reactor has solid-gas-liquid separater (GLSS) portion which is mainly for biogas collection in the form of inverted conical funnel. The gas produced from the reactor can be estimated by water displacement method. A peristaltic pump (20 ppm) was used to pump the substrate into the reactor with constant discharge flow. Bioballs as support media were used in this study and placed in top segment in the reactor. Totally 152 bioballs were kept in the reactor to prevent the escape of biogranules from the reactor. Five sampling ports at different heights were installed for ease of collection of samples for analysis. The reactor was operated at 30±3°C.

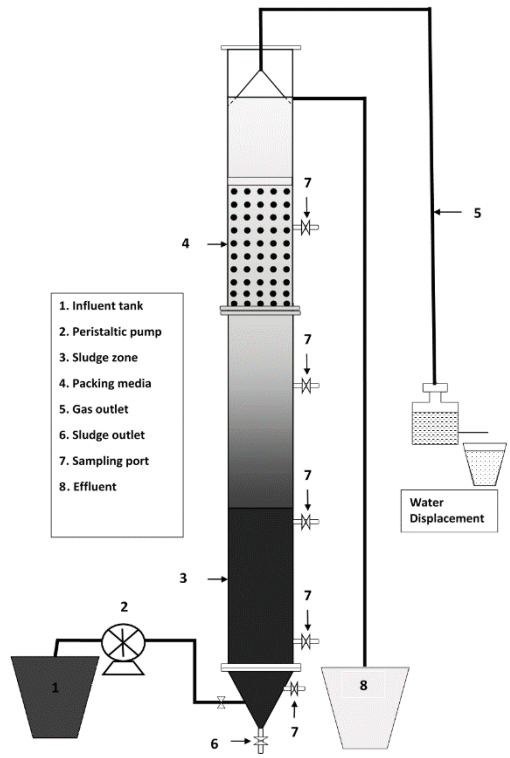


Fig. 1: Schematic representation of Bench Scale Hybrid Anaerobic Slude Blanket Reactor.

## RESULTS AND DISCUSSION

### COD Conversion and Removal Performance

After mixing the wastewater of sago and sugar industries, the COD values of influent and reactor outlet are presented in Fig. 2. The COD values range from 5360 to 4450 mg/L. The COD removal efficiency for different effluent mixing proportions at 24 h HRT is presented in Fig. 3.

The COD removal efficiency was in the range of 61.9-94.4 %. At effluent mixing ratio of 60/40 (sago 60 %, sugar 40 %), the overall COD removal efficiency was 94.4 %.

### pH, VFA and Alkalinity

The pH values of the inlet and outlet of HUASB reactor are presented in Fig. 4. The HUASB reactor effluent pH increased to a value beyond 7 and always remained so (range 7.53-8.18). The VFA values in HUASB reactor were in the range of 36-84 mg/L (Fig. 5) and VFA value increased when the sugar industry effluent proportion was increased. The HUASB reactor effluent alkalinity was in the range of 926-998 mg/L (Fig. 6).

### VFA/Alkalinity Ratio

The Fig. 7 shows VFA/Alkalinity ratio (VFA/AL) in the HUASB reactor. The effluent of HUASB reactor had VFA/AL ratio less than 0.089. It means that process in HUASB reactor is under stable condition.

Senthilkumar et al. (2009) reported that the VFA/Alk ratio for acidogenic and H UASB reactors is in the range of 1.3-1.5 and 0.04-0.09. A stable anaerobic treatment system requires a balance among all microorganisms. The maintenance of this balance is normally indicated by a low VFA concentra-

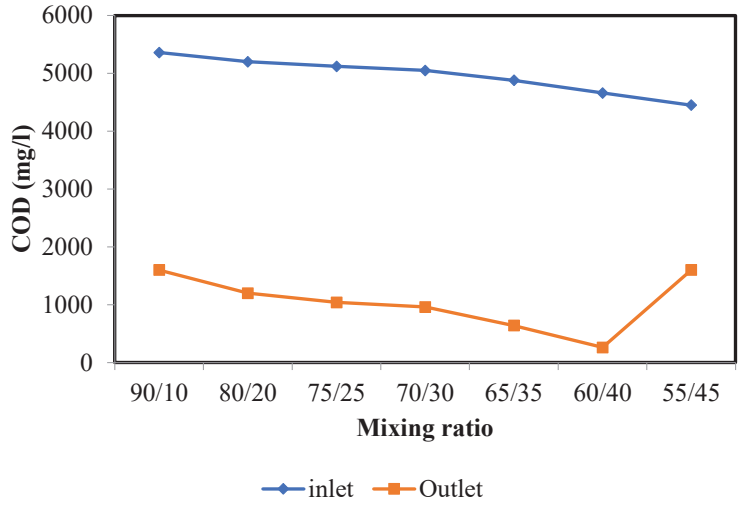


Fig. 2: COD values at various mixing ratios.

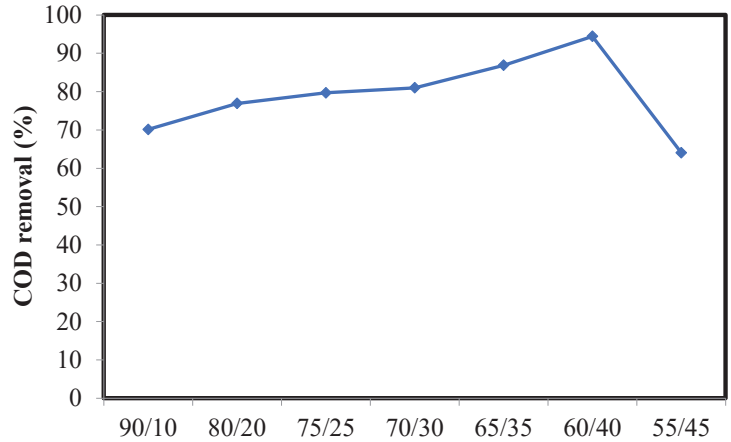


Fig. 3: COD removal efficiency at various mixing ratios.

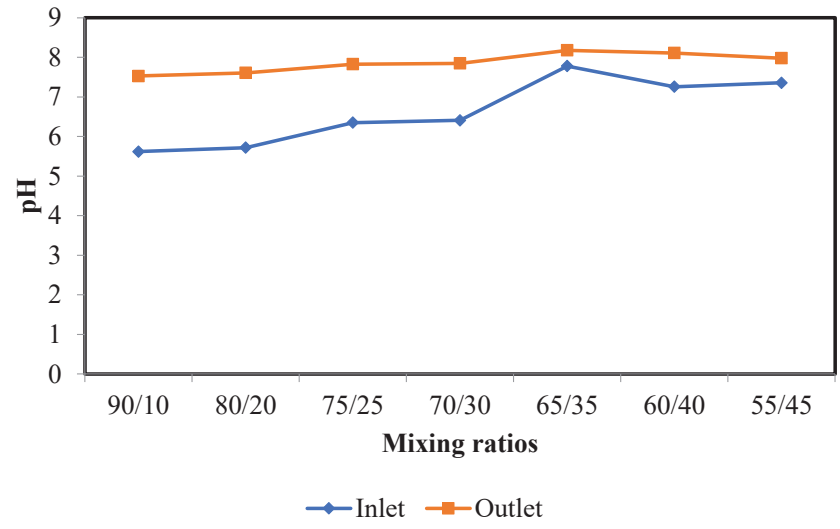


Fig. 4: pH values at various mixing ratios.

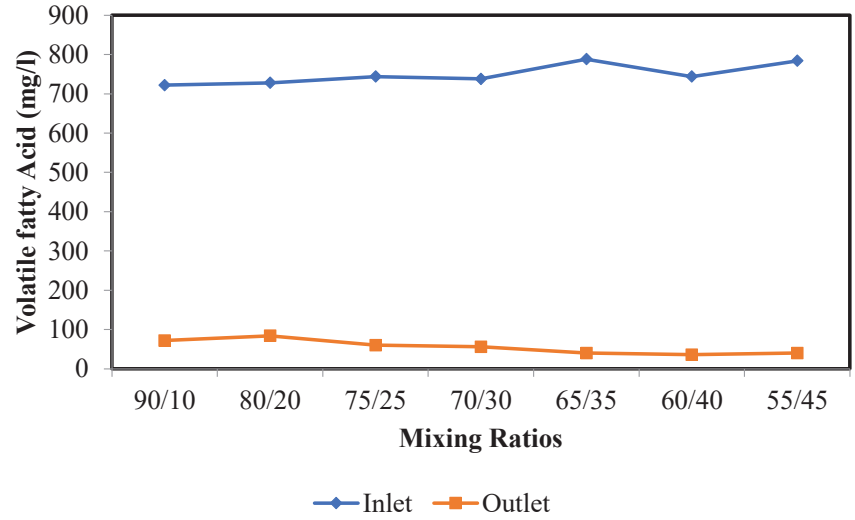


Fig. 5: VFA concentration at various mixing ratios.

tion, appropriate pH and VFA/Alk ratio. If a UASB reactor is stable, the VFA/Alk ratio of the reactor effluent must be lower than 0.4 (Behling et al. 1997). Sanchez et al. (2005) stated that the optimum ratio of VFA to alkalinity should be less than 0.3 or 0.4 for UASB reactor.

### Biogas Production

Fig. 8 shows the biogas production at various mixing ratios such as 90/10, 80/20, 75/25, 70/30, 65/35, 60/40 and 55/45 for HUASB reactor. The maximum biogas production of 13.2 L/d was achieved at the mixing ratio of 60/40.

## CONCLUSION

The bench-scale hybrid upflow anaerobic sludge blanket (HUASB) reactor was used to treat combined effluents of the real sugar industry and synthetic sago wastewaters. The maximum COD removal of 94.4% and the biogas production of 13.2 L/d at pH 8.11 was found at the mixing ratio of 60/40 (sago/sugar industry wastewater). The pH, VFA and alkalinity of the reactor effluent were under control for every 24 h of HRT which indicates the stability of the reactor. From the results obtained it was clear that HUASB reactor could be a very feasible alternative, eco-friendly and sustainable treatment system for the combined real sugar industry and sago wastewater.

## REFERENCES

APHA 2005. Standard Methods for the Examination of Water and Waste-

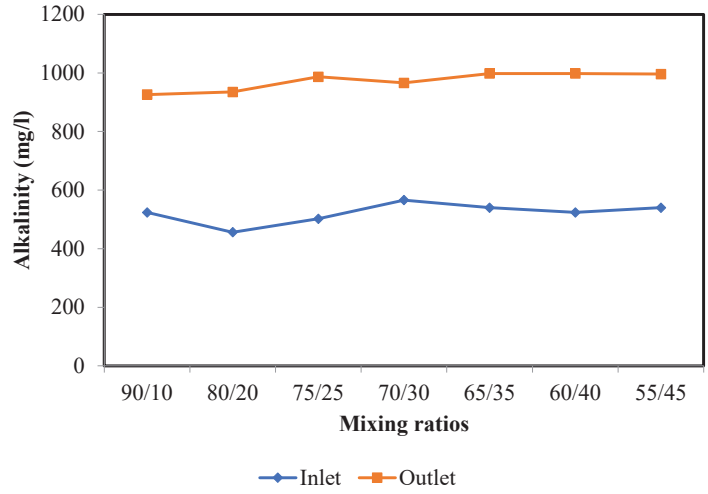


Fig. 6: Alkalinity at various mixing ratios.

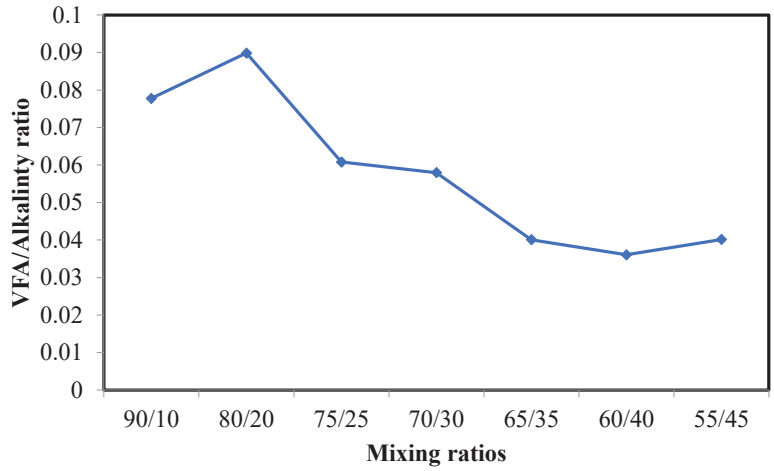


Fig. 7: VFA/Alkalinity at various mixing ratios.

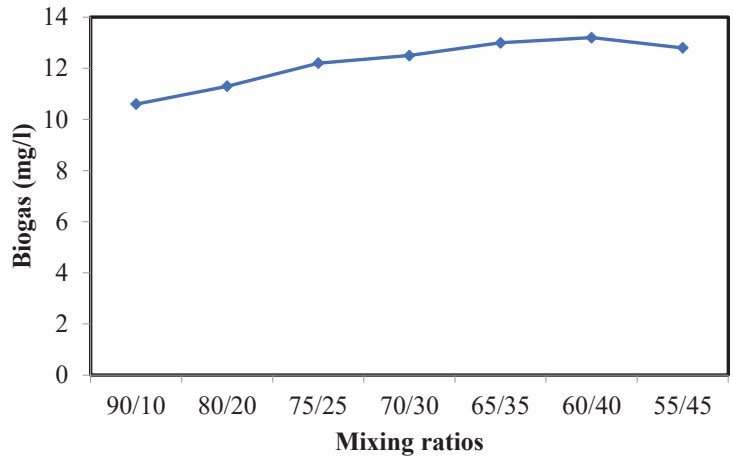


Fig. 8: Biogas production at various mixing ratios.

water, 20th edition. American Public Health Association, Washington DC, USA.

Arshad, A, Hashim, NH, Inthikhab, AQ and Athar, S 2009. Treatment feasibility of NSSC pulping effluent using UASB reactor, Journal of Water, Energy and Environment, 5: 57-60.

Ayati, B. and Ganjidoust, H. 2006. Comparing the efficiency of UAFF and UASB with hybrid reactor in treating wood fiber wastewater. Iranian Journal of Environmental Health Science and Engineering, 3(1): 39-44.

Behling, E., Diaz, A., Coline, G., Herrera, M., Gutierrez, E., Chacin, E., Fernandez, N. and Foster, C.F. 1997. Domestic wastewater treatment using a UASB reactor. Bioresource Technology, 61(3): 239-245.

Buzzini, A.P., Sakamoto, I.K., Varesch, M.B. and Pires, E.C. 2006. Evaluation of the microbial diversity in a UASB reactor treating from an unbleached pulp plant. Process Biochem., 41(1): 168-176.

Bhatti, ZI 1995. Problems encountered during the start-up of UASB reactor, Japanese Journal of Water Treatment and Biology, 31: 59-62.

Gnanapragasam, G., Senthilkumar, M., Arutchelvan, V., Sivarajan, P. and Nagarajan, S. 2010. Recycle in upflow anaerobic sludge blanket reactor on treatment of real textile dye effluent. World J. of Microbiology and Biotechnology, 26: 1093-1098.

Hampannavar, U.S. and Shivayogimath, C.B. 2010. Anaerobic treatment of sugar industry wastewater by upflow anaerobic sludge blanket reactor at ambient temperature. International Journal of Environmental Sciences, 1(4): 631-639.

Murthy, Y.S. and Patel, M.D. 1961. Treatment and disposal of sago wastes. Report Submitted to the Central Public Health Engineering Research Institute, India.

Ndobeni. A., Oyekola. O. and Welz. P. J. 2019. Organic removal rates and biogas production of an upflow anaerobic sludge blanket reactor treating sugarcane molasses. South African Journal of Chemical Engineering, 28: 1-7.

Rein, P.,Turner, P. and Mathias, K. 2011. Good Management Practices for the Cane Sugar Industry. Int. Fin. Corp. Pub., pp. 1-696.

Sanchez, E., Borja, R., Traviesco, L., Martin, A. and Colmenarejo, M.F. 2005. Effect of organic loading rate on the stability operational parameters and performance of a secondary upflow anaerobic sludge bed reactor treating piggery waste. Bioresource Technology, 96: 335-344.

Saroja, K. and Sastry, C.A. 1972. Report on Treatment of Sago Wastes. National Environmental Engineering Research Institute, India.

Senthilkumar, M., Arutchelvan, V., Kanakasabai, V., Venkatesh, K.R. and Nagarajan, S. 2009. Biomineralisation of dye waste in a two-phase hybrid UASB reactor using starch effluent as a co-substrate. International Journal of Environmental and Waste Management, 3: 354-365.

Senthilkumar, M., Gnanapragasam, G., Arutchelvan, V. and Nagarajan, S. 2011. Treatment of textile dyeing wastewater using two phase pilot plant UASB reactor with sago wastewater as co-substrate. Chemical Engineering Journal, 166: 10-14.

Van Haandel, A.C. and Lettinga, G. 1994. Anaerobic Sewage Treatment: A Practical Guide for Regions with a Hot Climate. John Wiley and Sons, New York.

Nature Environment and Pollution Technology
An International Quarterly Scientific Journal

p-ISSN: 0972-6268
(Print copies up to 2016)
e-ISSN: 2395-3454

Vol. 19 | No. 4 | pp. 1675-1682 | 2020

Original Research Paper

https://doi.org/10.46488/NEPT.2020.v19i04.036

Open Access Journal

# Removal of Lead from Drinking Water by Bioadsorption Technique: An Eco-friendly Approach

**Prasenjit Mondal†, B. P. Yadav and N. A. Siddiqui**
University of Petroleum and Energy Studies, Dehradun, U.K., India
†Corresponding author: Prasenjit Mondal; pmondal@ddn.upes.ac.in

**Nat. Env. & Poll. Tech.**
**Website: www.neptjournal.com**

*Received:* 09-12-2019
*Revised:* 06-01-2020
*Accepted:* 01-02-2020

**Key Words:**
Heavy Metal Concentration
Orange peels
Bio-adsorption
Bio-adsorbent

## ABSTRACT

India is the world's largest user of groundwater, accounting for 25 per cent of the world's extracted groundwater. Contamination of water bodies is the main problem for degrading the potable water quality in India. The contaminants, mainly cadmium, chromium, nickel, lead, zinc, copper, calcium, fluoride, nitrates, etc. have a significant impact on waters. There have been several advancements in technology for removal or reduction of these contaminants in water such as reverse osmosis, UV filtration, distillation and ion exchange. But these methods are not found to be eco-friendly and cost-effective. This paper elaborates various techniques of organic nature that can be used to reduce/remove the heavy metals from water bodies using orange peels as a bioadsorbent and detailed experimentation for the removal of lead ion concentration from water. In the present study, synthetic water with various heavy metals of known concentration was treated by a bioadsorbent (orange peels) by changing various parameters such as adsorbent particle size, dose, initial pH, etc. At pH 7, dose 0.5 g, and adsorbent particle size of 250 µm, a drastic reduction in the concentration of lead from 10 ppm to 0.213 ppm in 50 mL synthetic sample was observed.

## INTRODUCTION

Water stands first among the important fundamental requirements and also a basic nutrient having critical importance to human life (Howard et al. 2003) and is involved in almost every bodily function from digestion to excretion (Feldman et al. 1996). Water is transparent, colourless, odourless, and tasteless and covers almost 71% per cent of the earth's surface (Lindstrom 2012, Khyade & Swaminathan 2016). Coming to drinking water, it plays an important role in the life of every living organism (Vitousek et al. 1997). It boosts the metabolism and helps in breaking down the food but not all people get the quality drinking water (Congress 1995).

The problem we are facing currently is the pollution of water through various sources. Urbanization and industrialization are the main reasons for the pollution of water (Shiklomanov 1991, Czech et al. 2000, Le et al. 2010). With the increase in industrialization, there has been an increase in the high usage of different metals, chemicals and materials, etc. for the production of various products which resulted in producing waste which is being released into nearby water resources (Shukla et al. 2002). The chemicals, when mixed with water which is the source for drinking water in many areas, makes it toxic. Most of the people in many households are drinking the water which contains pathogens that may cause various diseases like typhoid, jaundice, diarrhoea, etc. (Niemczynowicz 1999). A filtering mechanism uses techniques like RO, activated carbon filters to filter the water to make it fit for drinking (Matilainen et al. 2010).

The present work mainly focused on the removal of lead ions from water, a persisting problem in India, by using organic methods such as orange peels.

### Heavy Metal Pollution in Water

Heavy metals have higher atomic weights and are approximately five times heavier than water. Many ecological and global public health concerns with the contamination by these metals have been emerged in recent years (Demirbas 2005). Heavy metals extensive use in several industrial, agricultural, domestic and technological applications has increased their exposure to the environment (Mulligan et al. 2001).

Pollution resulting from land runoff, precipitation, atmospheric deposition or land drainage is known as non-point source pollution (World Water Development Report 2017). Non-point sources are not easy to identify like the use of excess fertilizers or pesticides from agricultural lands or toxic chemicals from urban run-off and thus heavy metals find their way into water by industrial, agricultural, pharmaceutical, domestic effluents and atmospheric sources (Tarver 2008).

Heavy metals are naturally occurring in the earth's crust but the pollution caused by them is mainly due to the an-

thropogenic sources like mining, industrial production and using compounds containing metals (Annadurai et al. 2003). Some of the industrial sources include metal processing in refineries, coal burning in power plants, textiles, microelectronics, nuclear power stations and high tension lines, and combustion of petroleum (Hegazi 2013).

The metals like Co, Cu, Cr, Fe, Mg, Mn, Mo, Ni, Se and Zn are essential nutrients to the human body in adequate amounts. Insufficiency of these micronutrients in the human body results in a variety of ailments (Dobaradaran et al. 2017). Heavy metals are classified as human carcinogens (known or probable) according to the U.S. Environmental Protection Agency, and the International Agency for Research on Cancer (Howard et al. 2003). They are systemic toxicants which can induce multiple organ damage, even at lower levels of exposure (Pehlivan et al. 2008).

Heavy metals pollute the groundwater bodies and the surface water bodies like rivers, lakes, ponds. The primary metals like lead, arsenic, copper, cadmium, mercury and nickel are also known as trace elements, which are normally found in low concentrations. Surface water contamination is due to mining, dumping of solid wastes containing metal salts and discharge of effluents from battery and paint manufacturing, electroplating, viscous-rayon manufacturing, copper picking industries (Tokalioğlu et al. 2000).

### Previous Works on Heavy Metal Removal Techniques

The rapid growth in industries over the start of the 20th century has increased the demand for freshwater and thereby discharging the wastewater into the nearby water sources (Barlow & Clarke 2017). The discharged effluents from the industries contain harmful heavy metals like lead, chromium, cadmium, etc. in the form of dyes, coatings, pigments and so on and many of them are considered as hazardous to health because of their toxicity to human health. There are many methods available for the removal of these heavy metals from water such as reverse osmosis, chemical oxidation, adsorption, membrane separation, ion exchange, etc., out of which adsorption is considered as the simple and efficient method because of its ease of operation and versatility. The summative assessment on the removal of heavy metals from water by adsorption technique using organic wastes as adsorbents is listed in Table 1.

## MATERIALS AND METHODS

### Preparation of Adsorbent

Orange peels were used as adsorbents for the removal of

Table 1: Summative assessment on the removal of heavy metals from water using organic waste as adsorbent.

| S. No. | Objective | Brief Summary | Outcome | References |
|---|---|---|---|---|
| 1 | Water purification using different waste fruit cortexes for the removal of heavy metals. | Water can be purified by using different fruit cortices to remove heavy metals. They used the peels of fruits like kiwi, tangerine and banana and crushed them into powder to an optimum size of 1 mm and 2 mm. A water sample was made by taking 50 mL wastewater and 0.5 g of the crushed powder of particle size both 1 mm and 2 mm is added into the flask as adsorbent. It is then kept in a shaker at 158 rpm for 60 minutes. It was later filtered and then the concentration of the metals was analysed by Inductively Coupled Plasma (ICP) | It has shown that the particles of size 1 mm had better adsorption when compared to the particles of size 2 mm. Of the fruits used, kiwi fruit gave better adsorption results than banana. The order of adsorption capacity of the metal ions for banana was Cr < Cd <Zn and for Kiwi and tangerine, it was Cd < Cr < Zn. The capacity of adsorption will depend upon the pH, adsorbent dosage and the contact time. After conducting the experiments, the optimum value of pH was found to be 6.0 | (Al-Qahtani 2016) |
| 2 | Adsorption of heavy metals from water using banana and orange peels. | banana peels and orange peels for the removal of heavy metals like $Cu^{2+}$, $Zn^{2+}$, $Co^{2+}$, $Ni^{2+}$ and $Pb^{2+}$. Banana and orange peels, both were cleaned with double distilled water, dried and crushed into powder with particle size of 1-5 mm. The peels are treated with 0.4 mol/L Sodium Hydroxide, 0.4 mol/L Nitric Acid & distilled water. 15 g of banana peels and orange peels were soaked in 0.4 mol/L $HNO_3$ for 24 hours. "Synthetic solutions of $CuSO_4$, $CoSO_4$, $NiSO_4$, $ZnSO_4$ and $Pb(NO_3)_2$ are prepared". Experiments are done by adding 0.1gms of adsorbent in the 100 mL metal solution at a speed of 180rpm for 24 hours and centrifugation at 10,000rpm for 20 minutes, then later the concentration of metals were analysed by an atomic absorbance spectrophotometer (Varian Model 202FS) | The results from the experiments have shown that the maximum adsorption was at around pH 6-8 for banana and orange peels and the adsorption decreased with the increase in pH. The adsorption capacity was found to be 7.97 mg/g for lead, 6.88 mg/g for nickel, 5.80 mg/g for zinc, 4.75 mg/g for copper, and 2.55 mg/g for cobalt using banana peels. And for orange peels it was 7.75 mg/g for lead, 6.01 mg/g for nickel, 5.25 mg/g for zinc, 3.65 mg/g for copper and 1.82 mg/g for cobalt. The experiment also shown that maximum adsorption was attained at high pH with max level of lead by using banana peels was 7.97 mg/g and by using orange peels it was 7.75 mg/g. | (Annadurai, Juang et al. 2003) |

Table Cont....

Cont Table...

| S. No. | Objective | Brief Summary | Outcome | References |
|---|---|---|---|---|
| 3 | Removal of heavy metals from wastewater using agricultural and industrial wastes as adsorbents. | Synthetic wastewater with known concentrations of copper sulphate, nickel nitrate and iron sulphate metal solutions are made separately in double distilled water using Cu, Ni, Fe. The stock solution consisting of 20 mg/L as the adsorbent dose and concentration of metal (Cu, Ni, Fe) is around 10 mg/L. The agitation speed is 200rpm. The adsorbent doses of 20,30,40,50 and 60 mg/L are taken. The adsorbents and the metal ions are added and stabilized by agitating to attain pH of range 2-10 | water is purified by removing heavy metals using agricultural wastes like rice husk and industrial wastes like fly ash. First, The experiments are done and the results shown were that the agricultural waste rice husk found to be efficient in removing the metals like Fe, Pb and Ni whereas the industrial waste, fly ash has shown to be effective in removing i.e. adsorbing Cu and Cd. The experiments were also done by increasing the adsorbent concentration of rice husk and it was found that the Fe removal by using rice husk increased from 68.59% to 99.25%. Same when done for Pb, it was increased from 22.22 % to 87.17 %. When the concentration of fly ash was increased, the Cd removal increased from 25.21% to 73.5%. Same when done for Cu, the removal increased from 37.38% to 98.54%. The adsorption capacity was dependent on the level of pH, dosage of the adsorbent and the time of contact with the respective adsorbent. The contact time for attaining the desired level of metal ions was found to be 2 h and pH range was 6-7 for the effective adsorption. | (Hegazi 2013) |
| 4 | A laboratory study using maple leaves as a bio-sorbent for lead removal from aqueous solutions. | Lead was removed from aqueous by using maple leaves as a bio-sorbent. The materials used were one kg of maple leaves, salt, lead nitrate solution, Pb (II) and water. | 10 mg/L removed 98.2% Pb (II) ions than other concentrations and 0.5 g Maple leaves posed higher removal for Pb (II) ions. A sharp increase in bio-sorption occurred in the pH range 2.5–4.5. The maximum bio-sorption was 98.5% for Pb(II) ions at pH 6.3. Smaller particles (<75 μm) have greater Pb (II) removal capacity. | (Hossain et al. 2014) |
| 5 | Self-purification of the marine environment for heavy metals: A study on removal of lead and copper by cuttlebone. | Self-purification marine environment done by the cuttlefish to remove lead and copper. In this experiment, cuttlebone from cuttle fish was collected and washed with tap and deionized water and dried at 105°C for 24hrs and grinded to particles with sizes between 0.3-0.7mm. The solutions of lead and copper are prepared by dissolving the required amount of lead nitrate and copper nitrate Pent hydrate in de-ionized water. The pH values were modified and calibrated by using 0.1-1.0 M HCl and 0.1-1.0 M NaOH. Experiment was conducted in batch reactor on shaker at 120rpm at room temperature. The pH is maintained at 5 initially. Experiments were done with metal concentrations of 10, 20, and 50 mg/L and the adsorbent dose of 0.1 to 1.0 g/L with constant ion concentration of 50 mg/L initially. The adsorption was studied by keeping the range of pH between 2-7. Later, the concentration of metals was analysed by using AAS. | The results were that the capacity of cuttlebone to adsorb Pb and Cu were found to be 45.9 mg/g and 39.9 mg/g. The adsorption of Pb and Cu increased with an increase in pH and the max adsorption occurred when the pH was 7.0 and the adsorption was found to be 18.7 mg/g and 19.8 mg/g for Pb and Cu. And the maximum uptakes were found when at the pH values 5.0 and 5.5. | (Dobaradaran, Nabipour et al. 2017) |

Table Cont....

Cont Table...

| S. No. | Objective | Brief Summary | Outcome | References |
|---|---|---|---|---|
| 6 | Adsorptive removal of Arsenic from aqueous solution by waste litchi pericarps. | Litchi pericarps are washed with tap water and ultrapure water. They are dried at 70°C and then sized through a 60 mesh and stored in a polyethylene bottle. A stock solution of sodium arsenate $NaAsO_2$ (1,000 mg/L) was prepared with ultrapure water. Polyethylene tubes of 100 mL are taken with 50 mL of aqueous arsenic solution. Different adsorption capacities are observed with LPs (1–20 g/L) with varying initial arsenate concentration (0.01–100 mg/L) at 293.15 K. The pH is maintained between 2-11 by using 0.1 M HCl and 0.1 M NaOH solutions. The polyethylene centrifuge tubes were shaken in a vertical temperature oscillation incubator at 220 rpm for 5 to 180 min. These suspensions are filtered through 0.45 µm "cellulose acetate membrane filters". Arsenic filtrates are observed through AAS. | The removal rate increases from 24.0% to 97.74% as the adsorbent dose increases from 1.0 to 10.0 g/L. No further increase in the removal rate of As (III) is observed for LP additions from 10.0 to 20.0 g/L. Arsenic removal efficiency increases from 88% to 93% as the contact time increases from 10 to 60 min. The percentage removal rate increases by an increase in pH from 2 to 5, and then it decreases slightly with a further pH increase from 6-7. | (Li, Qi et al. 2016) |
| 7 | "Arsenic removal from aqueous solutions by adsorption on red mud". | Arsenic is removed from water by using red mud as an adsorbent. In this paper it is mentioned that mud was wet sieved through a 200 mesh screen and was washed for five times with distilled water. The suspension was filtered and was dried at 105°C, ground and sieved through a 200 mesh screen. Stock solutions of 1 As (III) were prepared by adding 1.320 g of $As_2O_3$ in 10 mL of 5M NaOH and made it up to 1 L with distilled water. Another stock solution of 1 g/L As(V) was prepared by adding $Na_2HSO_4.7H_2O$. Solutions with 125 to 1500 mg of arsenic and 5 mL of 0.1 M NaCl were made to 50 mL using distilled water. The red mud was added as an adsorbent into the solution and shaken at the rate of 800 cycles/min with a mechanical shaker. Later, the mixture was centrifuged at 10000 rpm for 10 mins | As (III) and As (V) adsorptions are obtained within 45 and 90 min respectively at 25°C, 133.5 µmol/L concentration and 20 g/L red mud dosage. As(III) and As(V) adsorptions take places at pH 9.5 and 3.2. The adsorption densities at these conditions are 4.31 and 5.07 µmol/g for As(III) and As(V). | (Altundoğan et al. 2000) |
| 8 | Removal of Pb(II) and Cd(II) from water by adsorption on peels of banana. | Banana peels were dried in sunlight for 5 days and in an oven at 70°C. The dried peels were sieved through 60 mesh screen. Standard solutions with desired concentrations (10-100 µgm/L) of lead nitrate and cadmium nitrate were prepared. Six solutions with concentrations of 30, 40, 50, 60,70 and 80 µgm/L of lead and cadmium were made with pH adjusted to 5 for lead and 3 for cadmium. Then adsorbent of 2.0 g for lead and 1.5 g for cadmium were added 50 mL of each solution which was agitated for half an hour. Later the concentration of the metals was analysed by AAS. | From the results, it was observed that banana peels were effective in removing cadmium compared to lead. 1 g of banana peels adsorbed 5.71 g of cadmium and 2.18 g of lead. Max adsorption of cadmium was observed at pH 3 and for the lead at pH 5. | (Anwar et al. 2010) |

lead from water. Orange peels were collected from the juice shops in Dehradun, India. They were washed with water for removal of any dirt and dried in a hot air oven for 4 h at 80°C and 6 h at 105°C (total of 10 hours). They were cut into pieces using a grinding machine and sieved to various sizes like 250 µm, 500 µm and 850 µm for the experimentation.

## Preparation of Stock Solution

1000 ppm stock solution was prepared and diluted with distilled water to make standard solutions of 5 ppm, 10 ppm, 15 ppm, 20 ppm and 25 ppm. The experiment was carried out using 10 ppm and 15 ppm stock solutions and rest were used as standards in atomic absorption spectroscopy.

## Equipment and Chemicals Used

pH was checked by using a digital pH meter. The metal solution was taken and the exact selected size and dose of adsorbent was added and stirred using a magnetic stirrer at 600 rpm for 30 min. The metal solution was given 2-h time for settling and filtered using a Waterman Filter paper of size

400 micron. The pH was adjusted to the required value (4, 6, 8) using 0.1 N HCl or 0.1 N NaOH solutions.

Size of adsorbent: 250 µm, 500 µm, 850 µm

Dose: 0.5 g, 1 g and 2 g

### Study of Process Parameters

Effects of various parameters like adsorbent particle size, pH and dose were studied by keeping agitation speed at 600 rpm for 30 min constant. For studying the effect of one parameter, the other three parameters were kept constant. Standard values of various heavy metals are mentioned in Table 2.

## RESULTS AND DISCUSSION

It is observed that the removal efficiency increases with increase in pH and is maximum at pH 7 and started decreasing from pH 8. The removal efficiency was tested at three different pH values starting from pH 4, pH 7 and pH 8. Anwar et al. (2010) mentioned that the pH of the stock solution is one of the most important factors that decides the extent of adsorption of heavy metal ions. As shown in Fig. 1, adsorption efficiency increases from pH 4 to pH 7 which is acidic and declined after pH 7 which is optimum pH. At lower pH, the hydrogen ions ($H^+$) compete with heavy metal cations for active adsorption sites. But beyond the optimum pH, the adsorption sites will not be activated and metal cations will react with ($OH^-$) ions and form metal hydroxide precipitate which makes adsorption uncertain (Anwar et al. 2010).

It was observed that at 0.5 g as the adsorbent dose 250µ size and pH 7, the maximum metal removal efficiency was observed, i.e. (97.87%) (Fig. 2). As the adsorbent size increases, the available surface area for adsorption decreases and its available active sites decrease, thereby decreasing the metal removal efficiency (Fig. 3).

Same experiments were carried out by preparing 15 ppm lead concentration stock solution in 50 mL distilled water.

It was observed that for 10ppm metal concentration stock solution at 0.5 g as adsorbent dose and 250 µ size and pH 7, the maximum metal removal efficiency was 97.87%, and for 15ppm metal concentration at 0.5 g as adsorbent dose and 250µ size and pH 7, the maximum metal removal efficiency was 96.57% (Fig. 4). As the adsorbent size increases,

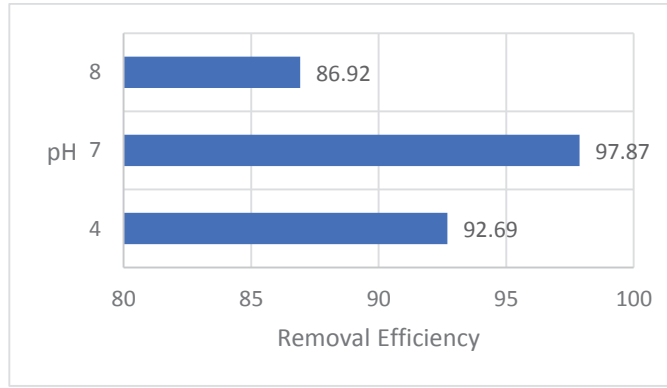


Fig. 1: Removal Efficiency with respect to varying pH at 10ppm lead concentration, adsorbent size-250µm and adsorbent dose-0.5g.

Table 2: Drinking water standards: IS 10500:2012.

| S. No. | Element | Acceptable Limit µg/L ( BIS 10500:2012) | PEL µg/L (BIS 10500:2012) |
|---|---|---|---|
| 1 | Arsenic | 10 | 50 |
| 2 | Cadmium | 3 | No relaxation |
| 3 | Chromium | 50 | No relaxation |
| 4 | Copper | 50 | 1500 |
| 5 | Iron | 300 | No relaxation |
| 6 | Lead | 10 | No relaxation |
| 7 | Mercury | 1 | No relaxation |
| 8 | Nickel | 20 | No relaxation |

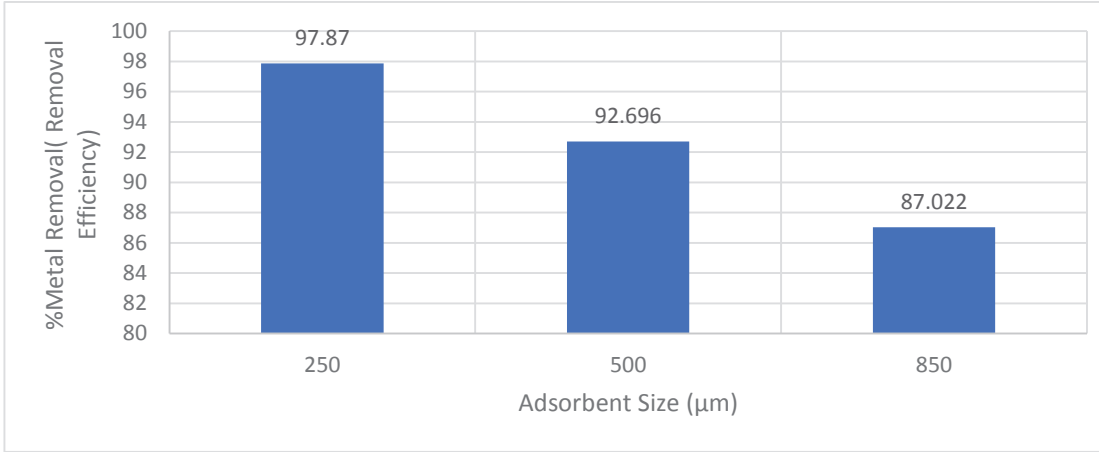


Fig. 2: Effect of adsorbent size for 10 ppm lead concentration at adsorbent dose-0.5g and pH 7.

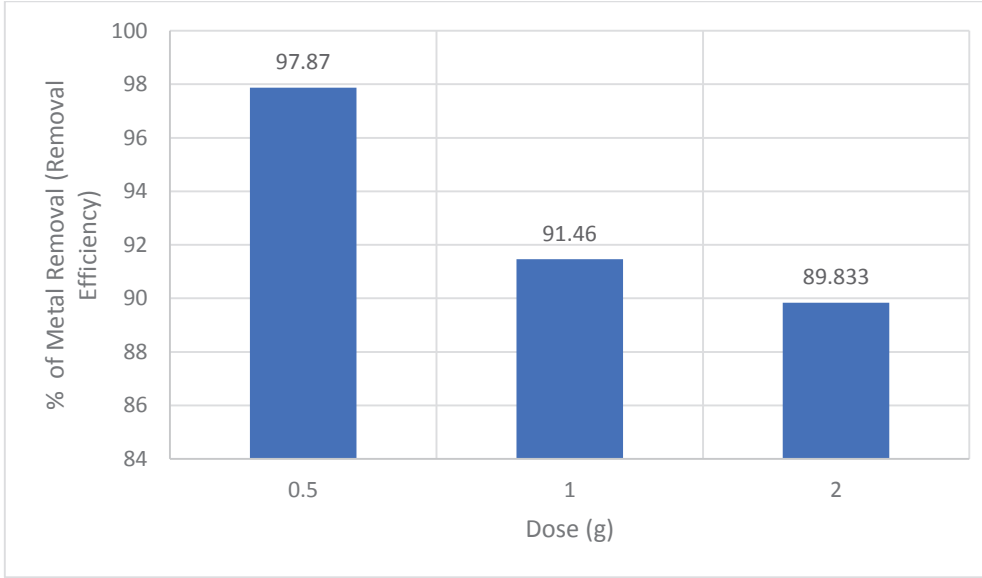


Fig. 3: Effect of adsorbent dose at adsorbent size-250µ and pH-7 on metal removal efficiency.

the available surface area for adsorption decreases and its available active sites decrease thereby decreasing the metal removal efficiency (Fig. 5).

## CONCLUSIONS

A total of 20 samples were collected and tested by atomic absorption spectroscopy. The following observations were made.

1. The removal efficiency was found to mainly depend on adsorbent particle size, adsorbent dose and pH.
2. The RPM of the magnetic stirrer was kept constant throughout (600 RPM for 20 mins). Particles having sizes in the range of 250-500 µm are expected to have greater adsorption tendencies as compared to larger particles because of the large surface areas of smaller particles allowing adsorption on the surface.
3. The optimum pH range can be between 5 and 7 for maximum adsorption of lead using orange peels. The minimum adsorption can be expected to occur at a pH of 3 because of its acidic nature. As the pH value increases, the adsorption capacity is also increased till a pH of 7 and it may remain stable in case of a further increase in pH.

From the above study it can be concluded that instead of using harmful chemicals for the removal of heavy metals

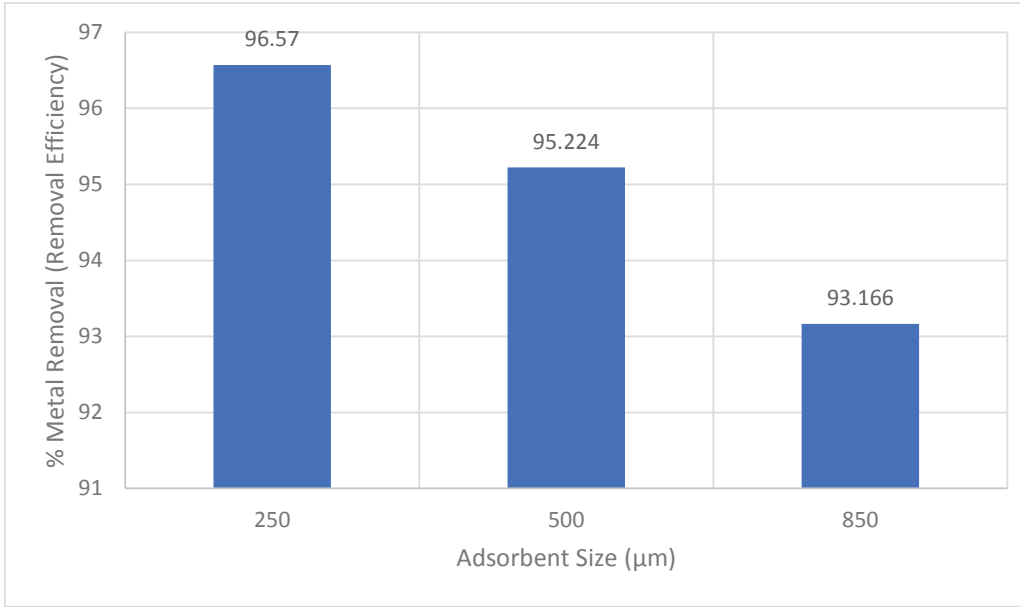


Fig. 4: Effect of adsorbent size at stock solution concentration of 15ppm at pH 7 and adsorbent dose of 0.5g.

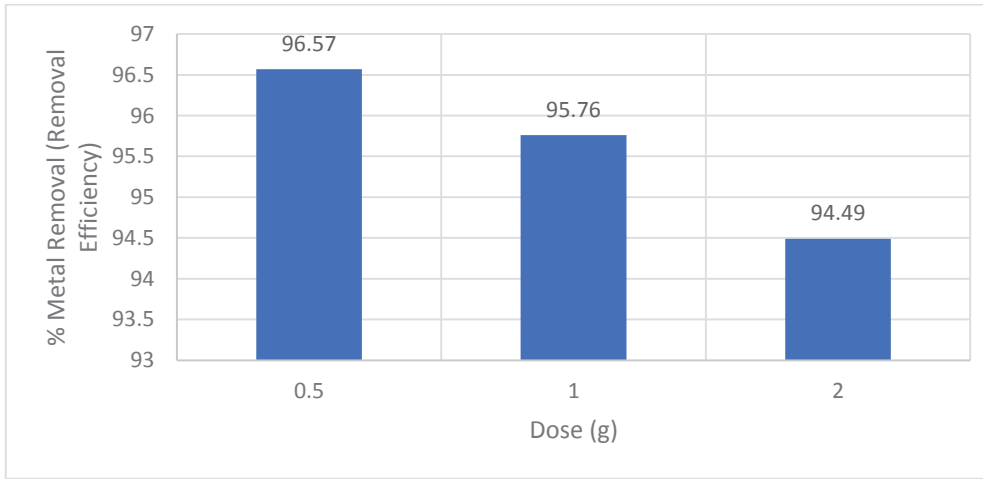


Fig. 5: Effect of adsorbent dose at adsorbent size-250µ and pH-7 on metal removal efficiency at 15 ppm concentration.

from water, organic wastes such as orange peels, banana peels and rice husk can be used for the same. Detailed analysis of experimental data has been carried out for maximum adsorption capacity. It was found that maximum adsorption efficiency is at pH 7.

## REFERENCES

Al-Qahtani, K. M. 2016. Water purification using different waste fruit cortexes for the removal of heavy metals. Journal of Taibah University for Science, 10(5): 700-708.

Altundoğan, H.S., Altundoğan, S., Tümen, F. and Bildik, M. 2000. Arsenic removal from aqueous solutions by adsorption on red mud. Waste Management, 20(8): 761-767.

Annadurai, G., Juang, R. and Lee, D. 2003. Adsorption of heavy metals from water using banana and orange peels. Water Science and Technology, 47(1): 185-190.

Anwar, J., Shafique, U., Salman, M., Dar, A. and Anwar, S. 2010. Removal of Pb (II) and Cd (II) from water by adsorption on peels of banana. Bioresource Technology, 101(6): 1752-1755.

Barlow, M. and Clarke, T. 2017. Blue Gold: The Battle Against Corporate Theft Of The World's Water. Routledge.

Congress, U. S. 1995. Office of Technology Assessment. Adolescent Health 1.

Czech, B., Krausman, P.R. and Devers, P.K. 2000. Economic associations among causes of species endangerment in the United States: associations among causes of species endangerment in the United States reflect the integration of economic sectors, supporting the theory and evidence that economic growth proceeds at the competitive exclusion of nonhuman species in the aggregate. BioScience, 50(7): 593-601.

Demirbas, A. 2005. Potential applications of renewable energy sources, biomass combustion problems in boiler power systems and combustion related environmental issues. Progress in Energy and Combustion Science, 31(2): 171-192.

Dobaradaran, S., Nabipour, I., Saeedi, R., Ostovar, A., Khorsand, M., Khajeahmadi, N., Hayati, R. and Keshtkar, M. 2017. Association of metals (Cd, Fe, As, Ni, Cu, Zn and Mn) with cigarette butts in northern part of the Persian Gulf. Tobacco Control, 26(4): 461-463.

Feldman, M., Cryer, B., McArthur, K.E., Huet, B.A. and Lee, E. 1996. Effects of aging and gastritis on gastric acid and pepsin secretion in humans: a prospective study. Gastroenterology, 110(4): 1043-1052.

Hegazi, H. A. 2013. Removal of heavy metals from wastewater using agricultural and industrial wastes as adsorbents. HBRC Journal, 9(3): 276-282.

Hossain, M., Ngo, H., Guo, W., Nghiem, L., Hai, F., Vigneswaran, S. and Nguyen, T. 2014. Competitive adsorption of metals on cabbage waste from multi-metal solutions. Bioresource Technology, 160: 79-88.

Hossain, M.A., Ngo, H. H., Guo, W., Zhang, J. and Liang, S. 2014. A laboratory study using maple leaves as a biosorbent for lead removal from aqueous solutions. Water Quality Research Journal, 49(3): 195-209.

Howard, G., Bartram, J., Water, S. and Organization, W.H. 2003. Domestic Water Quantity. Service Level and Health.

Khyade, V. B. and Swaminathan, M. S. 2016. Water: The pacemaker for life of earth. World Scientific News, 44: 93-125.

Le, C., Zha, Y., Li, Y., Sun, D., Lu, H. and Yin, B. 2010. Eutrophication of lake waters in China: Cost, causes, and control. Environmental Management, 45(4): 662-668.

Li, X., Qi, J., Jiang, R. and Li, J. 2016. Adsorptive removal of As (III) from aqueous solution by waste litchi pericarps. Water Science and Technology, 74(9): 2135-2144.

Lindstrom, B.R. 2012. America's Water Future and Deep Energy. Army War Coll Carlisle Barracks Pa.

Matilainen, A., Vepsäläinen, M. and Sillanpää, M. 2010. Natural organic matter removal by coagulation during drinking water treatment: A review. Advances in Colloid and Interface Science, 159(2): 189-197.

Mulligan, C., Yong, R. and Gibbs, B. 2001. Remediation technologies for metal-contaminated soils and groundwater: an evaluation. Engineering Geology, 60(1-4): 193-207.

Niemczynowicz, J. 1999. Urban hydrology and water management–Present and future challenges. Urban Water, 1(1): 1-14.

Pehlivan, E., Yanık, B., Ahmetli, G. and Pehlivan, M. 2008. Equilibrium isotherm studies for the uptake of cadmium and lead ions onto sugar beet pulp. Bioresource Technology, 99(9): 3520-3527.

Shiklomanov, I.A. 1991. The World's Water Resources: A New Appraisal and Assessmentfor the 21st century. A summary of the monograph World Water Resources prepared in the framework of the International Hydrological Programme, UNESCO.

Shukla, A., Zhang, Y.H., Dubey, P., Margrave, J. and Shukla, S. S. 2002. The role of sawdust in the removal of unwanted materials from water. Journal of Hazardous Materials, 95(1-2): 137-152.

Tarver, T. 2008. Just add water: Regulating and protecting the most common ingredient. Journal of Food Science, 73(1): R1-R13.

Tokalioğlu, Ş., Kartal, Ş. and Elci, L. 2000. Determination of heavy metals and their speciation in lake sediments by flame atomic absorption spectrometry after a four-stage sequential extraction procedure. Analytica Chimica Acta, 413(1-2): 33-40.

Vitousek, P. M., Mooney, H. A., Lubchenco, J. and Melillo, J. M. 1997. Human domination of earth's ecosystems. Science, 277(5325): 494-499.

Nature Environment and Pollution Technology
An International Quarterly Scientific Journal

p-ISSN: 0972-6268
(Print copies up to 2016)
e-ISSN: 2395-3454

Vol. 19 | No. 4 | pp. 1683-1688 | 2020

Original Research Paper

https://doi.org/10.46488/NEPT.2020.v19i04.037

Open Access Journal

# Solar Light Induced Photodegradation of Brilliant Green Dye by Barium Calciate ($BaCaO_2$) Nanoparticles

**K. Nagendra Naik*, K. Yogendra*† and K. M. Mahadevan****
*Department of P. G. Studies and Research in Environmental Science, Kuvempu University, Jnana Sahyadri, Shankaraghatta, Shimoga, Karnataka, India
**Department of Chemistry, Kadur P. G. Center, Kuvempu University, Kadur, Karnataka, India
†Corresponding author: Yogendra Kambalagere; yogendraku@gmail.com

**Nat. Env. & Poll. Tech.**
**Website: www.neptjournal.com**
*Received:* 11-01-2020
*Revised:* 28-01-2020
*Accepted:* 05-03-2020

**Key Words:**
Brilliant Green
$BaCaO_2$
Nanoparticles
Photocatalysis

## ABSTRACT

The study on photodegradation of Brilliant Green dye was done by barium calciate nanoparticles ($BaCaO_2$). The $BaCaO_2$ was prepared by solution combustion synthesis. The analytical instruments like SEM, XRD, EDAX, and UV-absorption spectroscopy were employed for characterization. All the experiments were accomplished under various irradiation conditions such as sunlight, UV light and dark conditions. The obtained results examined the percentage of degradation capacity of $BaCaO_2$ on Brilliant Green by differing the Brilliant Green concentration, pH and catalyst loading. The percentage of degradation was 98.93% in 20ppm of dye concentration at pH 6 with a constant catalyst concentration of 0.7g/100mL. This proves that the synthesized barium calciate nanoparticles are more efficient in removing Brilliant Green from the wastewater.

## INTRODUCTION

Recent industrial developmental activities are posing one or the other negative impacts on the environment, like the discharge of contaminants or discharge of coloured effluents directly into the environment. These coloured discharges impart severe pollution on the environment and cause health problems due to their toxicity and ability to sustain in nature (Arslan et al. 2000, Sauer et al. 2002). The dye effluents discharged into the water body decrease the aesthetic value of the water by colouring it. The sunlight penetration into the water body is blocked due to its colouring and inhibits the growth of useful biota (Yogendra et al. 2011). Due to low biodegradation characteristics and highly aromatic condition dyes have become prominent water pollutants (Madhusudhana et al. 2013, Daneshvar et al. 2004).

Recent studies have reported that wide ranges of metal oxide nanoparticles are being synthesized and their applications have made a unique contribution in the field of nanotechnology because of its unique and wide-ranging physicochemical properties (Di-Paola et al. 2003, Turchi et al.1990). Nowadays degradation of dye effluents using nanoparticles has attracted more attention of the scientific community (Mirkhani et al. 2009). The traditional methods like biological, physical and chemical are not so effective when compared to photocatalytic degradation. Advanced oxidation processes are promising alternatives for photodegradation of industrial effluents especially from the environmental point of view. Heterogeneous photocatalysis concentrates on the dissociation of dyes into simpler molecules of $CO_2$, $H_2O$ and mineral acids by using metal oxide nanoparticles as catalysts (Vinodgopal et al. 1996, Movahedi et al. 2009). Hence, this work is a novel, simple and fast method to degrade the Brilliant Green dye by $BaCaO_2$ nanoparticles under solar irradiation.

## MATERIALS AND METHODS

Brilliant Green is an easily available dye in the market (Sigma Aldrich, Mumbai, India (Fig. 1). The chemicals (99% A.R.), $Ba(NO_3)_2$, $Ca(NO_3)_2$ and $NH_2CONH_2$ were procured from Hi-Media Chemicals, Mumbai. Through visible spectrophotometer (Elico, SL 177) the absorbance was recorded at λmax.

**Nanoparticles synthesis:** $BaCaO_2$ nanoparticles were prepared using solution combustion methodology by redox mixtures of stoichiometric amounts of metal nitrates and fuel.

$$3Ba(NO_3)_2 + 3Ca(NO_3)_2 + 10NH_2CONH_2^- = BaCaO_2 + 10CO_2 + 20H_2O + 16N_2 \quad \ldots(1)$$

**XRD:** The XRD of $BaCaO_2$ is displayed in Fig. 2 as stated by Debye Scherrer's formula:

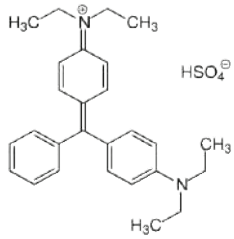


Fig. 1: Chemical structure of Brilliant Green.

$$D = K\lambda/\beta \cos\theta \quad \ldots 2$$

Where, K = Scherrer's constant, λ = X-ray wavelength, β = peak width at half-maximum, θ = Bragg's diffraction angle

In this work, the finely divided sample of $BaCaO_2$ by XRD studies was found to have a size varied from 25 nm to 60 nm with an average size of 40 nm.

**SEM:** Scanning Electron Microscope pictures of $BaCaO_2$ nanoparticles have shown scattered crystals with irregular shapes. The magnified images also have shown a sharp-edged uneven texture of the different nanoparticles with strong bonding of nanoparticles over one another (Fig. 3).

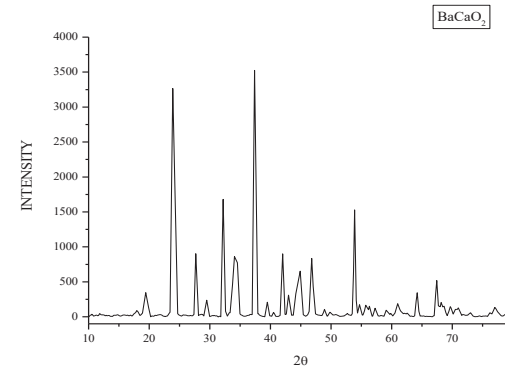


Fig. 2: XRD of synthesized $BaCaO_2$ nanoparticles.

**UV-Vis spectroscopy:** Optical absorption is a significant tool to get the optical energy band gap of the nanomaterials. The elemental absorption related to the electron jump from the valence band to the conductivity band. The spectrum reveals that the $BaCaO_2$ nanoparticle absorption in the visible radiation with a wavelength of 400 nm (Fig. 4). The value of optical band gap (OBG) was calculated from the TAUC's relation:

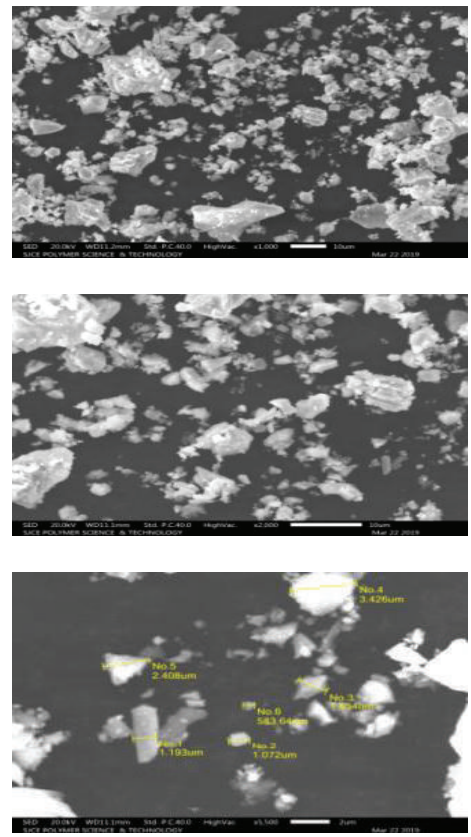


Fig. 3: Scanning Electron Micrographs of synthesized $BaCaO_2$ nanoparticles.

Table 1: Weight and atomic percentage of the elements in the barium calciate.

| Element | Weight % | Atomic % |
|---|---|---|
| C | 17.87 | 36.89 |
| O | 31.23 | 48.41 |
| Ca | 12.59 | 7.79 |
| Ba | 38.31 | 6.92 |

$$\alpha h\upsilon = B\,[h\upsilon - Eg]n$$

'hυ' = photon energy,

'B' = constant

'n' = power factor.

OBG of the $BaCaO_2$ nanoparticle was found to be 3.57eV.

**EDAX:** The EDAX analysis confirms the presence of $BaCaO_2$, carbon and oxygen in the nanoparticle sample. The vertical axis displays the number of x counts although, the horizontal axis displays energy in KeV (Fig. 5). The weight and atomic percentage (Table 1) of carbon, oxygen, calcium, and barium were found to be 17.87, 31.23, 12.59, 38.31 and 36.89, 48.41, 7.79, 6.92 which correspond to the spectrum without impurities peaks.

## Experimental Procedure

Using UV-visible absorption studies, the degradation of dye solutions was carried out. The spectral data noted using a spectrophotometer (Systronic UV-Visible) with 350-800 nanometre range. 492 nm was the maximum wavelength (λmax) of Brilliant Green. Solar irradiation is the main source for photocatalytic degradation experiments. The standard (20mg/L) dye solution was made by mixing 20 mg of Brilliant Green dye in 1 litre double distilled water. The dye solution then used for degradation experiments against $BaCaO_2$ nanoparticle. Different parameters such as pH levels, dye concentration and $BaCaO_2$ dosage were used to examine the degradation, and results were noted. pH balance of dye solution was maintained accurately by adding HCl or NaOH. Finally, the colour degradation percentage was calculated using the formula as follows.

$$\text{Decolorization} = \frac{V_0 - V_t}{V_0} \times 100$$

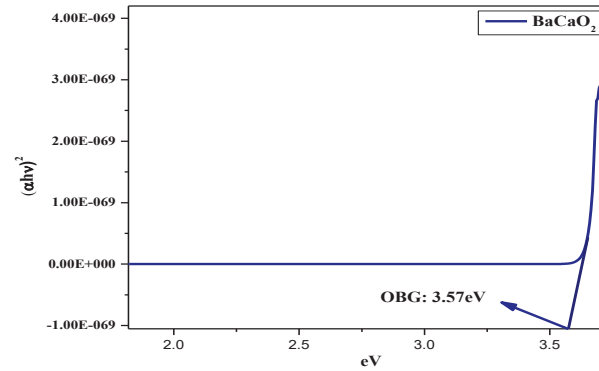


Fig. 4: UV-absorption spectra of synthesized barium calciate nanoparticles.

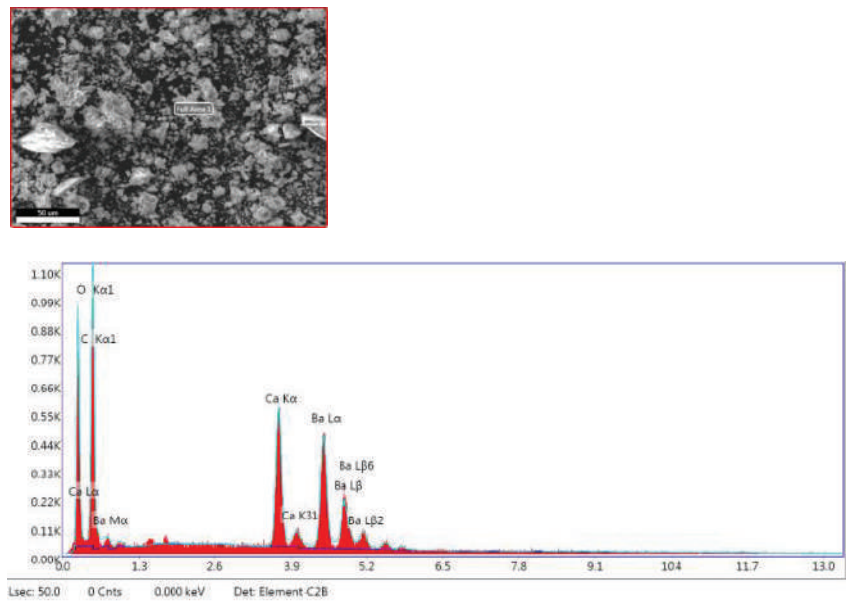


Fig. 5: Energy dispersive X-ray of synthesized $BaCaO_2$ nanoparticles.

Where, $V_0$ = initial absorbance of dye solution, $V_t$= absorbance at time 't'

## RESULTS AND DISCUSSION

### $BaCaO_2$ Dosage

$BaCaO_2$ dosage varied between 0.1 g and 1 g/100mL of selected dye solution and tested for its efficiency. The $BaCaO_2$ with the size 40 nm has shown 98.35% degradation. Since the photodegradation for the selected dye solution was highly successful at 0.7g/100mL within 2 hours (120 minutes), further experiments were continued with the effective dosage of 0.7 g for all the remaining parameters. The results are shown in Fig. 6.

The degradation of Brilliant Green was maximum at 0.7 g due to the availability of optimum active sites on $BaCaO_2$ surface area. In addition to this, the optimum sunlight into the solution and also a scattering of light by the catalyst also led to the photodegradation of the dye. Dosage level more than 0.7 g reduced the photodegradation due to overlying, overcrowding and collision with the ground state catalysts (Shanmugam 2006, Gandhi 2010, Thirugnanam 2017).

Hence, the dye molecules were degraded due to the high energy radicals formed in the reaction.

$$\text{Nanoparticles} + h\nu \rightarrow (\text{e-CB} + \text{h+VB}) \quad \ldots 1$$

$$e^{-CB} + O_2 \rightarrow O_2^{\bullet -} \quad \ldots 2$$

$$H_2O + O_2^{\bullet -} \rightarrow OOH^{\bullet} + OH^{-} \quad \ldots 3$$

$$2OOH^{\bullet} \rightarrow O_2 + H_2O_2 \quad \ldots 4$$

$$O_2^{\bullet -} + \text{Brilliant green} \rightarrow \text{Brilliant green-}OO^{\bullet} \quad \ldots 5$$

$$O\ OH^{\bullet} + H_2O + e^{-}CB \rightarrow H_2O_2 + OH^{-} \quad \ldots 6$$

Hydrogen peroxide can be generated in another path.

$$H_2O_2 + e^{-}CB \rightarrow OH^{\bullet} + OH^{-} \quad \ldots 7$$

$$H_2O_2 + O_2^{\bullet -} \rightarrow OH^{\bullet} + OH^{-} + O_2 \quad \ldots 8$$

$$OH^{\bullet} / O_2^{\bullet -} / \text{Nano-particles}^{\bullet +} + \text{Brilliant green} \rightarrow \text{Brilliant green degradation} \quad \ldots 9$$

### pH Effect on Brilliant Green

For pH experiments, the range was set to 2, 4, 6, 8 and 10 for dye solutions. The degradation rate for the dye solutions has shown a remarkable increase from 97.36% to 98.93% with a pH change from 2-6 and a reduction up to 98.28% at pH 10 (Fig. 7). An optimum degradation was achieved at pH 6. The time required to achieve the degradation was 120 minutes at the optimum dosage of 0.7g per 100 mL dye solution.

As the dye is a cationic compound which is very efficient in forming OH· radicals in acidic solution, OH· radicals are the main source of oxidation in carrying out photocatalytic degradation of Brilliant Green. Either positive or negative charge generate on the catalyst surface due to amphoteric effect and this is greatly influenced by changing pH value (Khan et al. 2017). In this reaction, the optimum amount of OH· radicals were generated at pH 6 in the solution. Acidic condition of solution less than pH 6 has noted a reduction in degradation. The basic condition has an inhibition effect on Brilliant Green a cationic dye due to overproduction of OH· radicals (Xiang et al. 2012, Liu 1999).

### Effect of Dye Concentration

Experiments were conducted by differing the Brilliant Green dye levels from 20-50 ppm. The results for $BaCaO_2$ are 98.93% for 20ppm, 93.39% for 30ppm, 88.7% for 40ppm and 87.36% for 50ppm, respectively (Fig. 8). This has proved that photodegradation capacity directly depends upon the concentration of dye solution. An increased path length at lower dye concentration directly influences the increased photodegradation. At higher dye concentrations the path length reduces and hence less absorption of a photon by the catalyst. This results in a reduced photodegradation rate.

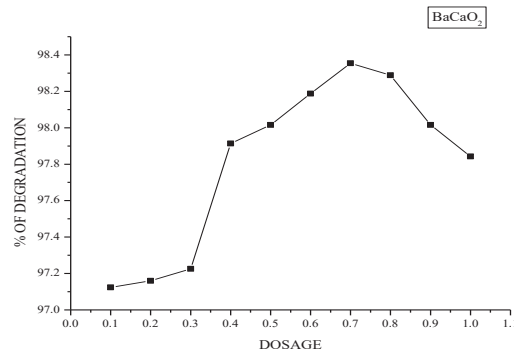


Fig. 6: Effect of catalyst concentration on Brilliant Green at 120 minutes (Brilliant Green=20 ppm, pH=6, $BaCaO_2$).

### Effect of Sunlight Irradiation

Under three different conditions, i.e. through sunlight alone, dye-dark-catalyst, dye-UV-catalyst and dye-sunlight-catalyst experiments were conducted to check the nanoparticle efficiency. In sunlight alone, without catalyst, the photodegradation of Brilliant Green was noted almost nil. 98.93% of degradation achieved at dye-sunlight-$BaCaO_2$ condition, 72% of degradation recorded at the dye-UV light-$BaCaO_2$ condition and 54.04% degradation observed at dye-dark-$BaCaO_2$ condition (Fig. 9). This clearly emphasizes the importance of different light conditions in the degradation of Brilliant Green dye.

The efficient photodegradation requires both sunlight as well as photocatalyst. The formation of electron-hole on the catalyst surface requires excitation of semiconductors. The sunlight gives the excitation energy to the semiconductors and thus efficient break down of organic dye molecule is achieved (Byrappa et al. 2006.)

## CONCLUSION

As per the results, synthesized $BaCaO_2$ has been proved to be photocatalytic and efficient in mineralizing the Brilliant Green. The proposed photocatalytic method proved to be very effective for the degradation of Brilliant Green, an industrial dye. For the degradation experiment, we have achieved 98.93% degradation at pH 6. With this result, we can say that the application of nano-sized materials is more suitable for degradation of dye effluents. This will certainly help in solving the problem of the textile effluent treatment process.

## ACKNOWLEDGEMENT

The authors would like to uphold their sincere thanks to the Department of Environmental Science, Kuvempu University and Government First Grade College, Shivamogga, Karnataka.

## REFERENCES

Arslan, I. A., Balcioglu and Bahnemann, D.W. 2000. Heterogeneous photocatalytic treatment of simulated dye house effluents using novel $TiO_2$-photocatalysts. Appl. Catal. B., 26: 193-206.

Byrappa, K., Subramani, A. K., Ananda, S.K., Lokanatha Rai, K., Dinesh, M. R. and Yoshimura, M. 2006. Photocatalytic degradation of Rhodamine B dye using hydrothermally synthesized ZnO. Bull. Mater. Sci., 29: 433-438.

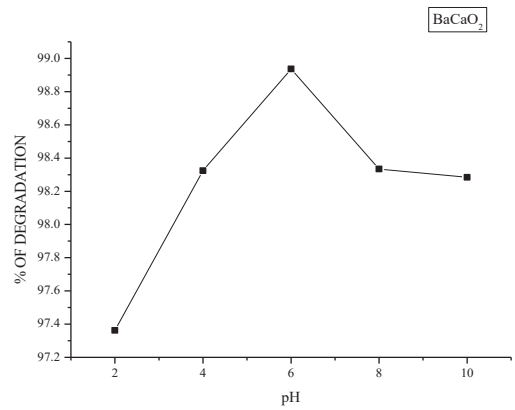


Fig. 7: Effect of pH on Brilliant Green at 120 minutes (Brilliant Green=20 ppm, $BaCaO_2$).

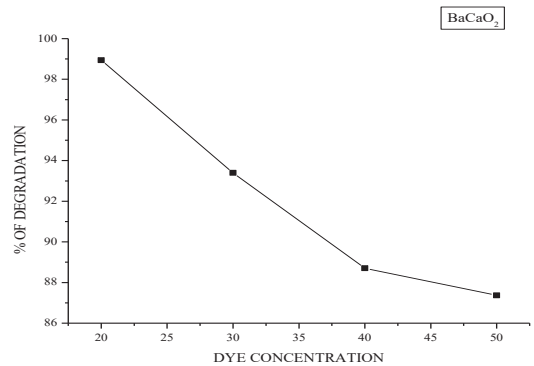


Fig. 8: Effect of dye concentration on the photodegradation of Brilliant Green [$BaCaO_2$ g/pH=0.7/4 and Brilliant Green= (20+30+40+50) ppm].

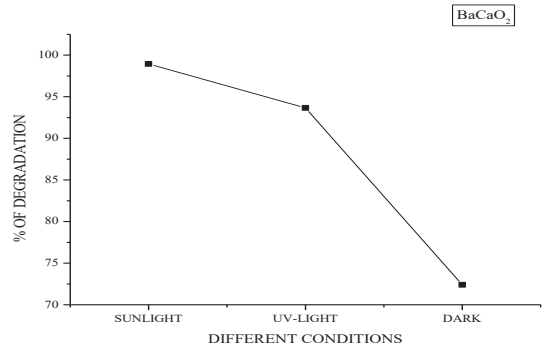


Fig. 9: Effect of sunlight irradiation with respect to the dark condition and UV condition on photocatalytic degradation of Brilliant Green in 120 minutes.

Daneshvar, N., Salari, D. and Khataee, A. R. 2004. Photocatalytic degradation of azo dye acid red 14 in water on ZnO as an alternative catalyst to $TiO_2$. J. Photochem. Photobiol. A, 162: 317-322.

Di-Paola, Augugliaro, V., Palmisano, L. Pantaleo, G. and Savinov, E. 2003. Heterogeneous photocatalytic degradation of nitrophenols. J. Photochem. Photobiol. A, 155: 207-214.

Gandhi, J., Dangi, R., Sharma, J. C., Verma, N. and Bhardwaj, S. 2010. Photocatalytic bleaching of malachite green and Brilliant Green dyes using ZnS-CdS as semiconductor: A comparative study. Der Chemica Sinica. 1: 77-83.

Khan, Mamun Reza, Kurny, A.S.W. and Fahmida Gulshan 2017. Parameters affecting the photocatalytic degradation of dyes using $TiO_2$: A review. Appl. Water Sci., 7: 1569-1578.

Liu, danxia, W., Jing, L., Liping, 1999. The roles of free radicals in amyotrophic lateral sclerosis: reactive oxygen species and elevated oxidation of protein, DNA, and membrane phospholipids. The FASEB Journal. 2318-2328.

Madhusudhana, N., Yogendra, K. and Mahadevan, K.M. 2013. Photocatalytic decolourization of textile effluent by using metal oxide nanoparticles. J. Sci. Art., 3: 303-318.

Mirkhani, Tangestaninejad, S., Moghadam, M., Habibi, M. H. and Rostami Vartooni, A. 2009. Photocatalytic degradation of azo dyes catalyzed by Ag doped $TiO_2$ photocatalyst. J. Iran Chem. Soc., 6: 578-587.

Movahedi, M., Mahjoub, A.R. and Janitabar-Darzi, S. 2009. Photodegradation of Congo Red in aqueous solution on ZnO as an alternative catalyst to $TiO_2$. J. Iran Chem. Soci., 6: 570-577.

Sauer, T., Neto, G. C., Jose, H. J and Moreira, R. F. P. M. 2002. Kinetics of photocatalytic degradation of reactive dyes in a $TiO_2$ slurry reactor. J. Photochem. Photobiol. A, 149: 147-154.

Shanmugam, N., Sathya, T., Viruthagiri, G., Kalyanasundaram, C. and Gobi, R. and Ragupathya, S. 2016. Photocatalytic degradation of Brilliant Green using undoped and Zn doped $SnO_2$ nanoparticles under sunlight irradiation. Appl. Surf. Sci., 360: 283-290.

Thirugnanam, N., Song, H. and Wu, Y. 2017. Photocatalytic degradation of Brilliant Green dye using CdSe quantum dots hybridized with graphene oxide under sunlight irradiation. Chinese Journal of Catalysis, 38: 2150-2159.

Turchi, S. and Ollis, D. F. 1990. Photocatalytic degradation of organic water contaminants: Mechanisms involving hydroxyl radical attack. J. Catal., 122: 178-192.

Vinodgopal, K., Wynkoop, D.E. and Kamat, P.V. 1996. Environmental photochemistry on semiconductor surfaces: Photosensitized degradation of a textile azo dye, acid orange 7, on $TiO_2$ particles using visible light. Environ. Sci. Technol., 30: 1660-1666.

Xiang, Q., Yu, J. and Jaroniec, M. 2012. Synergetic effect of $MoS_2$ and graphene as cocatalysts for enhanced photocatalytic $H_2$ production activity of $TiO_2$ nanoparticles. J. Am. Chem. Soc., 134: 6575-6578.

Yogendra, K., Suneel Naik, Mahadevan, K. M. and Madhusudhana, N. 2011. A comparative study of photocatalytic activities of two different synthesized ZnO composites against Brilliant Green dye in presence of natural solar light. Int. J. Environ. Sci. Res., 1: 11-15.

Nature Environment and Pollution Technology
An International Quarterly Scientific Journal

p-ISSN: 0972-6268
(Print copies up to 2016)
e-ISSN: 2395-3454

Vol. 19 | No. 4 | pp.1689-1694 | 2020

Original Research Paper

https://doi.org/10.46488/NEPT.2020.v19i04.038

Open Access Journal

# Operating Performance of China's Environmental Governance Industry Under the Impact of COVID-19

**Zhaohua Leng†**
School of Economics and Management, Ningbo University of Technology, Ningbo 315211, China
†Corresponding author: zhaohua.leng@163.com

**Nat. Env. & Poll. Tech.**
Website: www.neptjournal.com

*Received:* 12-07-2020
*Revised:* 10-10-2020
*Accepted:* 18-10-2020

**Key Words:**
COVID-19
Epidemic
Environmental governance
Financial performance

## ABSTRACT

With the continuous emergence of environmental problems in recent years, governments of various countries attach great importance to the application of key core technologies such as energy conservation and efficiency, low carbon environmental protection, resource recovery and recycling. The implementation of environmental management concepts is emphasized such as clean production and energy efficiency. As a result, the environmental governance industry has achieved rapid development. However, under the impact of COVID-19, the operation and development of environmental governance industry may be restricted. To explore COVID-19 influence on the operating performance of China's environmental governance industry, Dongzhu Ecological Environment was selected as the research object, and the operation performance of Dongzhu Ecological Environment was analyzed by using the factor analysis method. The results show that the operating performance of Dongzhu Ecological Environment gets up a lot, with the rise of the whole industry due to the epidemic. Additionally, some management implications were put forward that adopted by the environmental governance industry to better promote the coordinated development of economy, society and environment.

## INTRODUCTION

At the beginning of 2020, the new epidemic hit the whole world, severely cut off the flow of human, material, and resources, which brought a serious impact on China's economy and enterprises. As the epidemic spreads around the world, epidemic prevention and control work is carried out in an orderly manner, and the economic situation has undergone major changes. The market pattern is divided, and enterprises are faced with serious challenges in resuming work. The epidemic has dealt a blow to China's economy. Many cities in China have already begun blockades. It is difficult for workers to return to work, so they can only find jobs online, and enterprises cannot start to work offline. They have to bear certain rents and wages of employees and face severe challenges. As the epidemic situation in foreign countries is becoming more and more serious, especially the environmental management enterprises have been hit hard, and the impact of the epidemic on countries is sudden and long-term. Affected by the epidemic situation, the risk resonance and risk spillover effects of consumption, investment, production price index, import and export trade, and other macroeconomic fields have been greatly improved, and the risk transmission path has changed significantly.

In the face of the increasing demand for ecological and environmental protection, ecological repair should be focused on. The case study of Dongzhu Ecological Environment focuses on the ecological wetland field with "water treatment" as the core, and it systematically provides customers with the whole industrial chain solutions of ecological environment construction and restoration engineering from the aspects of planning, design, procurement, construction and maintenance. At the same time, it adheres to the business optimization and upgrading strategy and seeks breakthroughs in other niche areas of ecological restoration. The enterprise actively and deeply distributed water ecological management, mine rehabilitation and forest park projects, trying to gradually achieve the overall coverage of ecological rehabilitation industry and to improve its comprehensive strength and brand effect. In the current epidemic environment, it is of a certain value to ensure that environmental protection enterprises can effectively carry out their business, rapidly improve their business performance, and indeed make great efforts to improve the ecological environment and create a good living environment.

## PAST STUDIES

In recent years, with the continuous emergence of environmental problems, environmental governance has increasingly received extensive attention from the government and all sectors of society. With the dual opportunities of

policy support and market demand-driven, the environmental governance industry has achieved rapid development, and scholars have also conducted extensive research on its operating performance. Zhu & Gong (2014) and Wang & Huang (2016) took environmentally friendly listed companies as research objects and found that their operating performance is at a low level through the DEA evaluation model. It's negatively affected by the institutional environment in emerging markets (Alexandre & Renato 2020). Cheng & Yao (2018) evaluated the performance of ecological protection and environmental governance industry and found that the comprehensive performance of this industry shows a decreasing trend year by year, and indicators such as management costs, fixed assets and the number of employees did not reach the corresponding output level. Arrangement and operation rate of environmental protection equipment, number of R&D expenditure, environmental protection technology achievement awards, environmental investment, sewage charge were selected as evaluation indicators (Niu 2018, Ames et al. 2020). Discontinuous environmental events such as rewards and fines were regarded as indicators to reflect the accumulative performance of enterprises, and their environmental initiatives were reflected by the reputation index of enterprises (Baldo 2018). Due to defects and insufficiency of the traditional perspective of enterprise environmental performance evaluation, a new perspective was proposed based on the value chain theory to the internal value chain and external value chain of each link, respectively. Environmental performance evaluation and new evaluation system were built from three dimensions, namely evaluation index, evaluation method and environmental disclosure of value chain of environmental performance (Cardoso et al. 2019). Lv et al. (2018) believed that profitability and growth ability are the keys to improving the operating performance of listed companies in the environmental governance industry. He also proposed that the development of businesses in the form of operational projects can improve the environmental governance benefits and promote the diversification of profit models. Different scholars at home and abroad had put forward different evaluation methods for environmental performance evaluation. According to the summary of existing literature, the commonly used methods in domestic and foreign academic circles included analytic hierarchy process, data envelopment analysis, fuzzy comprehensive evaluation, grey relational degree, artificial neural network method and so on. Among them, the more subjective methods included AHP, and the more objective methods included data envelopment analysis, grey relational degree method (Niu 2007, Zhou & Huang 2018). Environmental performance evaluation of enterprises was put forward to combine enterprise goal establishment, with the management system and production management, and the key to choose environmental performance indicators and monitoring environmental activities and environmental performance evaluation was using the SPC technology to manage environmental performance, using the system capability index to monitor environmental risk, and analyzing the change of the risk to get the key area of environmental performance evaluation. The risk assessment method was adopted, the quantitative indicators of environmental performance evaluation were established. Different indicators had corresponding environmental risk assessment, which was used to identify the priority of indicators and the environmental factors (Schmidt & Sewerin 2019).

However, the existing studies on the operating performance of listed companies in the environmental governance industry mainly focus on a single dimension and lack systematic and comprehensive analysis. In the context of climate and social and ecological changes, the environmental governance industry faces higher challenges (Boyd 2018). Whether the business performance of this industry is impacted by the influence of COVID-19 and how the response effect is worth further exploring.

## MATERIALS AND METHODS

### Sample Selection and Data Sources

According to the listed companies published on the websites of Shanghai and Shenzhen stock exchanges in 2020, the study classifies the "environmental governance" listed companies and selects 12 ones as the research samples based on the availability of financial data of listed companies. Based on the data from 2019 to mid of 2020, the financial performance of Dongzhu Ecological Environment is compared. This study mainly relies on the Wind information and the CSMAR database to collect data and standardize the variables to eliminate dimensions.

### Modelling

The factor analysis method can be expressed by a mathematical model, with the $p$ variables $x_1, x_2, ..., x_p$. The mean value after standardization is 0, and the standard deviation is 1. $x_1, x_2, ..., x_p$ are expressed in linear form by using $k(k<p)$ factors, namely, $f_1, f_2, ..., f_k$ .

$$\begin{cases} x_1 = a_{11} f_1 + a_{12} f_2 + ... + a_{1k} f_k + \varepsilon_1 \\ x_2 = a_{21} f_1 + a_{22} f_2 + ... + a_{2k} f_k + \varepsilon_2 \\ ... \\ x_p = a_{p1} f_1 + a_{p2} f_2 + ... + a_{pk} f_k + \varepsilon_p \end{cases} \quad (1)$$

Equation (1) shows the linear equations of this method. The matrix expression is

$$x = af + e' \quad (2)$$

In the above formula, $f$ is the factor, and the correlation coefficient $f_j(j = 1, 2, ..., k)$ is 0. $a$ is the factor load matrix and $a_{ij} = 1, 2, ..., p; j = 1, 2, ..., k)$ is the factor load. $e'$ is a special factor, which is independent of $f_j(j = 1, 2, ..., k)$ .

### Index System Selection

Following the relevant provisions of the state-owned capital performance evaluation rules issued by the Ministry of finance, this study constructs a comprehensive evaluation index system of the financial performance of listed companies based on the principle of obtaining data objectively and comprehensively, drawing on the results of domestic and foreign scholars on financial performance evaluation (Table 1). Referring to Gu (2009), Zhang & Shen (2013), Tao et al. (2016) and Hou & Cao (2019), this study analyzes from the following aspects, solvency (liquidity ratio, quick ratio, asset-liability ratio), operational ability (turnover rate of accounts receivable, inventory turnover, the turnover rate of total assets), profitability (return on equity, return on invested capital, operating profit margin), growth ability (growth rate of total assets, the growth rate of net intangible assets, rate of capital accumulation).

## RESULTS ANALYSIS

### KMO and Bartlett Spherical Test

In this study, the KMO test and Bartlett spherical test are used to verify the correlation between the selected variables and explore whether they meet the factor analysis conditions. The test results show that the KMO values from 2019 to 2020 are 0.506 and 0.502, respectively, which are both greater than 0.5. The significance probability p-value (sig=0.00) of Bartlett's spherical test from 2019 to 2020 is 0.000, which all meet the test standards and can be factored in.

### Factor Analysis

The common factor is extracted, and the eigenvalue and contribution rate of the correlation matrix are obtained by using the rotation method of maximizing variance. The calculation results of the correlation matrix are provided in Table 2. It can be seen from the table that four eigenvalues meet the conditions from 2019 to 2020, and their cumulative variance contribution rate exceeds 75%.

Table 1: Operating performance evaluation index system construction of environmental governance industry.

| Primary index | Secondary index | Calculation formula |
|---|---|---|
| Solvency | Liquidity ratio | Current assets/current liabilities |
| | Quick ratio | Quick assets/current liabilities |
| | Asset liability ratio | Total liabilities/total assets |
| Operational ability | Turnover rate of accounts receivable | Operating income/average balance of accounts receivable |
| | Inventory turnover | Operating cost/average inventory balance |
| | Turnover rate of total assets | Operating income/average balance of assets |
| Profitability | Return on equity | Net profit/average net assets |
| | Return on invested capital | Operating profit/invested capital before interest and after-tax |
| | Operating profit margin | Operating profit/revenue |
| Growth ability | Growth rate of total assets | Total assets growth of the year/total assets at the beginning of the year |
| | Growth rate of net intangible assets | Increase in net intangible assets/net intangible assets at the end of last year |
| | rate of capital accumulation | Ending owner's equity/beginning owner's equity |

Table 2: Eigenvalues and the contribution rate of principal components.

| Year | Ingredients | Extract sum of squares load | | Rotate sum of squares load | |
|---|---|---|---|---|---|
| | | Cumulative variance contribution rate % | Total | Contribution rate of variance % | Cumulative variance contribution rate % |
| 2019 | 1 | 31.89 | 4.69 | 29.33 | 29.33 |
| | 2 | 51.73 | 3.12 | 19.48 | 48.81 |
| | 3 | 66.29 | 2.40 | 14.98 | 63.78 |
| | 4 | 76.32 | 2.01 | 12.54 | 76.32 |
| Mid of 2020 | 1 | 32.07 | 4.02 | 25.10 | 25.10 |
| | 2 | 50.71 | 2.96 | 18.51 | 43.61 |
| | 3 | 64.76 | 2.31 | 14.42 | 58.03 |
| | 4 | 74.28 | 1.80 | 11.23 | 69.25 |
| | 5 | 81.23 | 1.73 | 10.81 | 80.06 |
| | 6 | 87.70 | 1.22 | 7.64 | 87.70 |

**Model calculation:** This study adopts the regression analysis method to calculate the scores of principal factors $F_1$, $F_2$, $F_3$ and $F_4$, which represent profitability, debt repayment, growth and anti-risk ability. After taking the common factor rotation, the variance contribution rate is taken as the weight, and the weighted sum is sorted.

$$F_{2019} = (F_1 * 29.33\% + F_2 * 19.48\% + F_3 * 14.97\% + F_4 * 12.54\%) / 76.32\% \quad ...3$$

$$F_{2020} = (F_1 * 25.1\% + F_2 * 18.51\% + F_3 * 14.42\% + F_4 * 11.23\% + F_5 * 10.8\% + F_6 * 7.63\%) / 87.87\% \quad ...4$$

**Calculation results:** Table 3 shows the comprehensive scores and rankings of the financial performance of listed companies in the environmental governance industry from the beginning of 2019 to June 2020. From the comprehensive score, it can be seen that different strategic choices under the epidemic situation of Dongzhu ecological environment have had a greater impact on financial performance. In recent years, its financial performance has maintained rapid growth, and it gets better when the epidemic is controlled.

The empirical analysis concludes that despite the impact of the epidemic, the sales level of Dongzhu Ecological Environment has declined, as long as it adopts appropriate

Table 3: Comprehensive score and ranking of the financial performance of listed companies in environmental treatment industry from 2019 to mid of 2020.

| Period | Name | Stock code | F1 | F2 | F3 | F4 | F5 | F6 | Comprehensive score | Ranking |
|---|---|---|---|---|---|---|---|---|---|---|
| 2019 | Wangneng Environment | 002034 | 1.328 | 0.347 | 0.220 | 2.242 | | | 1.010 | 1 |
| | Lvyin Ecology | 002887 | 0.824 | -0.591 | 0.069 | -0.447 | | | 0.106 | 2 |
| | Kerong Environment | 300152 | 0.191 | -0.077 | 0.489 | -0.455 | | | 0.075 | 3 |
| | Sanfeng Environment | 601827 | -0.919 | 0.773 | -0.170 | 1.323 | | | 0.028 | 4 |
| | Tus Environment | 000826 | 0.612 | -0.426 | -0.340 | -0.321 | | | 0.007 | 5 |
| | Weiming Environment | 603568 | 0.037 | -0.396 | 0.573 | -0.332 | | | -0.029 | 6 |
| | Guozhen Environment | 300388 | 0.095 | -0.256 | 0.300 | -0.374 | | | -0.031 | 7 |
| | Poten Environment | 603603 | -0.196 | -0.037 | -0.037 | 0.121 | | | -0.072 | 8 |
| | Dongzhu Ecological Environment | 603359 | 0.278 | -0.935 | 0.078 | 0.188 | | | -0.086 | 9 |
| | Hanlan Environment | 600323 | -0.007 | -0.364 | -0.011 | -0.373 | | | -0.159 | 10 |
| | Misho Ecology | 300495 | -0.228 | -0.001 | 0.142 | -0.624 | | | -0.163 | 11 |
| | Yonker Environmental Protection | 300187 | 0.020 | -0.305 | -0.097 | -0.449 | | | -0.163 | 12 |
| Mid of 2020 | Lvyin Ecology | 002887 | 2.151 | -0.033 | 1.705 | 3.183 | 1.753 | 0.751 | 1.575 | 1 |
| | Sanfeng Environment | 601827 | -0.693 | 0.034 | 4.242 | -0.257 | 0.030 | -0.395 | 0.442 | 2 |
| | Kerong Environment | 300152 | 0.690 | 1.447 | -1.596 | 0.230 | 0.418 | 0.732 | 0.384 | 3 |
| | Dongzhu Ecological Environment | 603359 | 1.044 | -0.388 | 0.667 | 0.597 | -0.140 | -0.586 | 0.334 | 4 |
| | Wangneng Environment | 002034 | 0.231 | 0.598 | -0.592 | 1.514 | -0.239 | 0.001 | 0.259 | 5 |
| | Weiming Environment | 603568 | -0.385 | 1.613 | -1.644 | 0.661 | 1.173 | 0.471 | 0.230 | 6 |
| | Tus Environment | 000826 | 1.738 | -0.044 | 0.276 | -2.903 | -0.440 | 0.547 | 0.155 | 7 |
| | Hanlan Environment | 600323 | 0.647 | -0.596 | 0.696 | -0.291 | 0.154 | -0.045 | 0.151 | 8 |
| | Guozhen Environment | 300388 | -0.445 | 0.715 | -0.303 | 0.965 | 0.383 | -0.082 | 0.137 | 9 |
| | Yonker Environmental Protection | 300187 | -0.381 | -0.165 | 0.477 | -0.771 | -0.321 | 3.751 | 0.123 | 10 |
| | Poten Environment | 603603 | 0.601 | 0.202 | -0.283 | -0.031 | -0.143 | -0.488 | 0.104 | 11 |
| | Misho Ecology | 300495 | -0.195 | 0.407 | -0.146 | 0.874 | -0.131 | -0.095 | 0.093 | 12 |

cost reduction and sales strategies to produce products in response to the needs of the masses under the epidemic situation, the company can still reverse the market situation. After the epidemic, the group will far exceed the same industry group.

According to the factor analysis of listed companies in the environmental governance industry, Dongzhu Ecological Environment's internal resource capacity has met the relevant diversified strategic model. Based on the above comprehensive evaluation of financial performance, it can be concluded that its cost control and precision sales strategy can effectively resist the overall downward risk of the industry. Since the outbreak of the epidemic in 2020, its cost-control strategy has successfully seized rare opportunities for enterprises and achieved the reverse trend of financial performance. Combined with the quantitative and qualitative characteristics, it can be concluded from big data analysis that Dongzhu Ecological Environment's series of measures to rational production, reducing the expenses and production costs, and improving the inventory turnover rate. It is in line with the development requirements of the environmental governance industry.

### Management Implications

Full play should be given to its first-mover advantage in the field of ecological wetland restoration, to focus on its main business, and vigorously expands the market. At the same time, enterprises should actively deploy water ecological management, mine restoration and forest park projects to gradually achieve comprehensive coverage of the ecological restoration industry and enhance comprehensive strength and brand effect. Innovative business cooperation models should be actively explored, to seek comprehensive and in-depth cooperation opportunities with local design and construction companies with strong comprehensive strength. Through taking advantage of the partners' local advantages to jointly contract high-quality projects, enterprises' business development capabilities are expected to be further enhanced.

Resource integration of the industrial chain should be actively laid out, to explore opportunities for optimizing and upgrading the industrial chain in the field of ecological and environmental protection. Under the premise of the continuous and steady growth of the main business scope, plans are needed for the supplement of qualifications, to explore the extension of business opportunities in mine management and soil remediation. At the same time, business models should be actively explored in the field of ecological cultural tourism.

Through improving the corporate risk control mechanism, enterprises can actively improve the risk control mechanism and strengthen the construction of risk control departments. The first of the three tough battles is to "resolutely fight against major risks". The country must guard against risks, and enterprises must also guard against risks. Especially in the landscape engineering industry where enterprises are located, expansion capability of engineering business scale depends to a certain extent on the capital turnover, and financial risks are related to the sustainable development of the engineering construction business. Great importance should be attached to the construction of risk control department. The risk control centre may consist of the management department, final accounts review department, receivable clearing department, and general department. Employees are composed of professionals in law, auditing, fund management, finance, and business. To ensure the high quality of enterprises' contracted projects and to avoid the high risks of the project, steady and healthy growth of enterprises' performance can be escorted.

Internal environmental governance should be optimized, to improve the environmental governance level. On the one hand, enterprises must implement standardized management, act in strict accordance with relevant rules and regulations, integrate environmental governance into the entire internal operating process, and strengthen environmental governance from all aspects of the enterprise. On the other hand, enterprises must formulate an effective environmental supervision system, reward and punishment system to restrict and supervise their daily environmental governance behaviours, and then establish a complete environmental governance system to optimize internal environmental governance. Besides, enterprises must strengthen the learning of environmental governance, carry out corresponding environmental protection education and training, cultivate employees' awareness of environmental protection and responsibility, and realize green and sustainable development.

## CONCLUSION

Environmental governance is an important industry in the development of the national economy, which has important practical significance in the effective use of energy, reduction of environmental pollution, prevention of environmental emergencies and other aspects. This study takes Dongzhu ecological environment as the research object and analyzes its operating performance. The main conclusions are as follows: (1) under the impact of the COVID-19 epidemic, Dongzhu ecological environment has good risk response-ability and growth ability and has realized the overall business performance rising against the trend. (2) For listed companies in the environmental governance industry, resource advantages should be made full use to layout integration of industrial chain resources. Then, risk control mechanism should be

explored and the relative system must be established, with optimizing internal environmental governance, to achieve sustainable growth of operating performance.

## ACKNOWLEDGEMENT

This study was supported by the Scientific Research Fund of Zhejiang Provincial Education Department of China (No. Y201942995).

## REFERENCES

Alexandre, S.G. and Renato, J.O. 2020. Testing the institutional difference hypothesis: a study about environmental, social, governance, and financial performance. Business Strategy and the Environment, 1(7): 10-25.

Ames, J.B., Gaskin, J. and Goronson, B.D. 2020. Exploring antecedents and consequences of managerial moral stress. Business Ethics: A European Review, 28(3): 12272.

Baldo, D. 2018. Sustainability and CSR orientation through 'Edutainment' in tourism. International Journal of Corporate Social Responsibility, 3(1): 5-19.

Boyd, E. 2018. Navigating Amazonia under uncertainty: Past, present and future environmental governance. Philosophical transactions of the Royal Society of London. Biological Sciences, 363(1498): 1911-1917.

Cardoso, G., Carr, D.D. and Rogers, P. 2019. Does corporate governance matter for stock returns volatility in the Brazilian context? Corporate Governance: The International Journal of Business in Society, 19(6): 1236-1252.

Cheng, Y. and Yao, J. 2018. Ecological protection and environmental governance industry development efficiency evaluation and restrictive factors analysis. China Population Resources and Environment, 28(S2): 74-78.

Guo, Q.Y. 2009. Application of analytic hierarchy process in the research of enterprise competitiveness evaluation. China Management Information Technology, 1: 87-90.

Hou, J.J. and Cao Y.D. 2019. Are the contributions of technical standards to economic growth consistent: An empirical analysis based on the provincial level. Journal of Guizhou University of Finance and Economics, 1: 52-59.

Lv, Z. 2018. Research on the financial performance of listed companies in the ecological protection and environmental governance industry. Modern Economic Information, 36(18): 180-181.

Niu, J.L. 2018. Study on financial performance evaluation of Chinese new energy automobile company. Economic Practice, 6(10): 2-12.

Niu, Y.H. 2007. Adjustment of China's environmental governance strategy from export-oriented to domestic Demand. Journal of Nanchang Polytechnic, 4: 34-36.

Schmidt, T.S. and Sewerin, S.. 2019. Measuring the Temporal Dynamics of Policy Mixes: An Empirical Analysis of Renewable Energy Policy Mixes' Balance and Design features in Nine Countries. Research Policy, 48:1-13.

Tao, Y., Xu, F. J. and Du, Y.C. 2016. Strategic selection of listed companies in household appliance industry under the background of "Internet+": An empirical test based on comprehensive evaluation of financial performance. Monthly Journal of Accounting, 4: 6-16.

Wang, H. and Huang, Y.L. 2016. Research on technical efficiency evaluation of listed companies in energy-saving and environmental protection industry. Chinese Market, 17: 159-160.

Zhang, R.W. and Shen R. 2013. Operation performance analysis of listed companies in innovation-oriented manufacturing enterprises in China. Journal of Tianjin University (Social Science Edition), 5: 10-17.

Zhou, M. and Huang, Q.H. 2018. Research on strategic adjustment of B2C E-commerce listed companies based on the concept of "quality E-commerce". Western Journal, 7: 6-6.

Zhu, Y. and Gong, J.J. 2014. Financial analysis of ecological protection and environmental governance industry: taking "sound environment" as an example. Journal of Hubei University of Economics (Humanities and Social Sciences Edition), 11: 70-72.

Nature Environment and Pollution Technology
An International Quarterly Scientific Journal

p-ISSN: 0972-6268
(Print copies up to 2016)
e-ISSN: 2395-3454

Vol. 19 | No. 4 | pp. 1695-1699 | 2020

Original Research Paper

https://doi.org/10.46488/NEPT.2020.v19i04.039

Open Access Journal

# The Effect of Ejectors on Reduction of Indoor Air Pollution in the Welding Room

**Sattar Yunus*†, Makmur Saini**, Rizal Sultan***, Rusdi Nur**** and Ibrahim*****

*Department of Mechanical Engineering, Universitas Muslim Indonesia, Makassar, 90231, Indonesia
**Department of Energy Conversion, Ujung Pandang State Polytechnic, Makassar, 90245, Indonesia
***Department of Electrical, Ujung Pandang State Polytechnic, Makassar, 90245, Indonesia
****Department of Mechanical Engineering, Ujung Pandang State Polytechnic, Makassar, 90245, Indonesia
*****Department of Mechanical Engineering, Polytechnic of Industry, Makassar, 90213, Indonesia
†Corresponding author: Sattar Yunus; sattar.teknik@umi.ac.id

**Nat. Env. & Poll. Tech.**
**Website: www.neptjournal.com**

*Received:* 22-11-2019
*Revised:* 15-12-2019
*Accepted:* 01-03-2020

**Key Words:**
Indoor air pollution
Ejectors
Carbon monoxide
Nitrogen monoxide
Total suspended particles

## ABSTRACT

In this study, the ejector installation has been designed and processed according to the plan and further investigated the effect of the ejector's performance on reducing air pollutants in a welding chamber. This is done after gas and dust particles appear during the welding process. The measurement of air pollutants was carried out in two conditions. The first condition during the welding process was without using the ejector and the second condition is when the welding process continues and the ejector runs simultaneously. The measurements were made for carbon monoxide (CO) gas, nitrogen monoxide (NO) gas and total suspended particles. The ambient gas sampler was used in measuring CO and NO gases, while the Staflex air sampler measures dust particles. The results show that when the ejector is run or in the second condition, carbon monoxide and nitrogen monoxide and total dust particles are lower in concentration compared to the situation when the ejector is not running.

## INTRODUCTION

The rapid industrialization over the past two decades has caused many problems in the environment, including air pollution whose influence has started to be felt and even become a pivotal problem today and certainly requires special attention in the development of a country (Lima et al. 2009), including in the City of Makassar, South Sulawesi Province. It is one of the cities in Indonesia which has air pollution trends increasing from year to year (Sattar et al. 2012, Sattar et al. 2019). The increasing number of the population is not only happening in developed countries but also in developing countries that have caused widespread air pollution (WHO 2005). Urban air pollution affects the health, well-being and lives of hundreds of millions of people, women and children every day in Asia. It was reported that outdoor air pollution causes around 537,000 deaths annually, indoor air pollution causes more than double the number of deaths (WHO 2002); this means that indoor pollution causes a greater impact than outdoor pollution especially in indoor activities that directly produce gases and particles (dust) which are quite dangerous for those exposed.

Based on the discoveries of historical objects, it can be seen that the technique of connecting metal known today with welding has been known since prehistoric times, for example, the contrasting of copper-gold alloy metal and lead-tin disordering. According to the information, it has been known and practised in the span of 4000 to 3000 years BC and alleged sources of heat come from burning wood and charcoal. In the 19$^{th}$ century, welding technology developed rapidly due to the use of electrical energy (Suharno 2008). According to Deutsche Industrie Normen (DIN), welding is a metallurgical bond on alloy metal joints that is carried out in hot and liquid conditions, further explained that welding is a process where the same material and type are combined together so that a connection is formed through the chemical bonds produced from the use of heat and pressure (Suharno 2008). Since there is a heat source, it will produce gases and particles where the gases that arise are dust (particles) in large welding fumes ranging from 0.2 µm to 3 µm. The chemical composition of welding smoke dust depends on the type of welding and electrodes used. When the hydrogen type electrode is low, there will be fluorine (F) and potassium oxide ($K_2O$) in smoke dust. In electric arc welding without gas, the smoke will contain a lot of magnesium oxide (MgO). The gases that occur during welding are carbon monoxide (CO), carbon dioxide ($CO_2$), ozone ($CO_3$) and nitrogen monoxide gas (Wiryosumarto & Okumura 2004). In line with that when the welding process takes place, there are dangerous gases which need to be considered such as carbon monoxide gas

(CO). This gas has a high affinity for haemoglobin (Hb) which will reduce the absorption of oxygen, and the condition of the total suspended particles (TSP) also needs attention in the welding room (Harsono 1996).

In the effort to minimize the gases and harmful particles that arise in the room when welding takes place, a system or tool is required that can reduce gases or particles that occur. One method that can be done is by using the ejector method. The projector has succeeded used for polluted gas cleaning applications over the past few decades because of their ability to handle gases containing pollutants such as vapour, gas and solid/liquid aerosols up to 0.1 μm (Dutton et al. 1982, Subramarian et al. 2006). In line with this, it was stated that the ejector is one of the most important devices used in the industry. This device has two main tasks. One is to make a vacuum and remove gas and the other is to mix it in liquid. One of the tasks above or both can be considered in designing and using an ejector (Stefan & Hamjak 2008, Gamisansa 2002). In general, the main function of the ejector is to achieve maximum secondary flow in each of the main operating conditions given and to compress entangled masses in the ejector to the necessary release conditions (Chou 1996).

Based on this description, we will investigate in this study whether there is a reduction in the concentration of gases and particles in the air that arise specifically carbon monoxide (CO), nitrogen monoxide (NO) and total suspended particles (TSP) with tools that have been designed with the ejector method.

## MATERIALS AND METHODS

### Ejector Installation

The design of the ejector installation consisting of several core components such as cylindrical joints, reservoirs and other components has been done and completed the installation as shown in Fig. 1.

### Tools and Procedure Sampling

The implementation of the study is to examine the extent of the influence of the ejector tool that has been designed and made but will require direct testing to the actual environment, namely the industrial environment. As a testing phase, this tool is carried out in the student's welding practice room at the Makassar Industrial Engineering Polytechnic (ATI) Makassar, with the consideration that in the welding room when welding takes place there will be a range of air conditions with bad air condition, which certainly has an impact on welders or students who temporarily practice welding.

The entire air sampling process uses tools from the Environmental Engineering Centre and Makassar Class I Disease Control whose equipment is available and sufficient for sampling and also for the analysis of air samples that have been taken. The tool used for sampling air for gas is Ambient Gas Sampler (Impinger Model: MD-51MP), while TSP samples are used by the Staflex Air Sampler tool. Sampling was carried out in two air test conditions, namely:

1. Condition I (Ejector OFF): Retrieval and analysis of air samples when welding practices are taking place but the ejector has not operated. The data generated are as a control to see how much influence the ejector has.
2. Condition II (Ejector ON): Retrieval and analysis of air samples while ongoing welding practices and temporarily operated ejectors. Data generated will be compared with the data generated in the condition I.

### Sampling Implementation Procedures

Supply installation equipment systems with electric power, throat length used was 30 cm (Saini et al. 2018). The pump

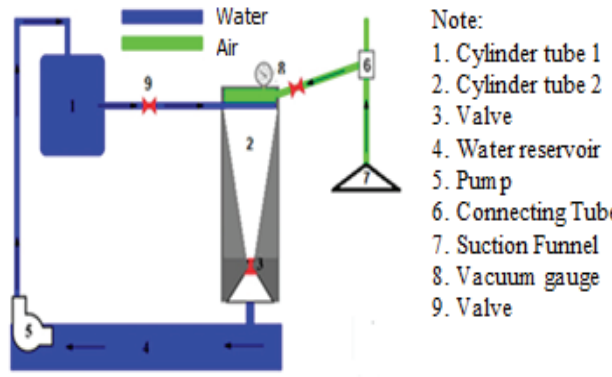


Fig. 1: Ejector installation design results.

engine (5) was operated to fill the reservoir (4). The valve (9) and valve (10) were opened and the valve (3) was closed until the cylinder (2) can be fully charged. The valve 9 and valve 10 were closed after the cylinder 2 was filled. The initial height of the reservoir water level (4) was measured and the ejector was run by the opening valve (3) and valve (10) so that the water is circulated continuously. The vacuum value was measured in the vacuum gauge (8) after opening the valve (10). Notes were taken and the level of water in the reservoir (4) was maintained. The throat ejector (3), which is 30 cm long, was set and used based on the results of previous tests. The ambient gas sampler tools and Staflex air samplers were operated and the time to start operating the tool in this step was recorded. Sampling tools were operated for 60 minutes, with three sampling times at 9-10, 10-11, 13-14 (in the case of students while doing welding, such as conditions when taking samples without running an ejector). After enough time, the ejector and the sampler were stopped. Air samples were taken to the BTKL-PP Laboratory for analysis.

## RESULTS AND DISCUSSION

The air measurements in the welding room for carbon monoxide are shown in Fig. 2. With the ejector condition not yet executed (OFF) the sampling at 9-10 a.m. showed CO concentrations of 2,384 ppm, at 11-12 a.m. of 2.43 ppm, and at 1-2 p.m. of 2,425 ppm. When the ejector is ON, at 09-10 a.m. CO concentration was 2,378 ppm, at 11-12 was 2.41 ppm, and at 1-2 p.m. was 2.39 ppm. Concentration when the ejector is carried out at all hours, the nine samples show a decrease in concentration, which more noticeably decreased at 1-2 p.m. This means that the longer the ejector is executed, the more carbon monoxide in the indoor air will be.

Based on the results of the air test for the nitrogen monoxide is shown in Fig. 3. With OFF ejector conditions at sampling at 9-10 a.m., NO concentration was 0.003 ppm, at 11-12 a.m. it was 0.004 ppm, while at 1-2 p.m. the concentration was 0.0045 ppm. Meanwhile, on the ejector ON condition at 9-10 a.m., NO concentration was 0.0025 ppm, at 11-12 a.m. it was 0.0039 ppm, while at 1-2 p.m. it was 0.0044 ppm. There appears to be a decrease in NO concentration when the ejector is run, but it is different from carbon monoxide which decreases a bit.

Based on the air measurement results in the welding room for the total suspended particles as shown in Fig. 4,

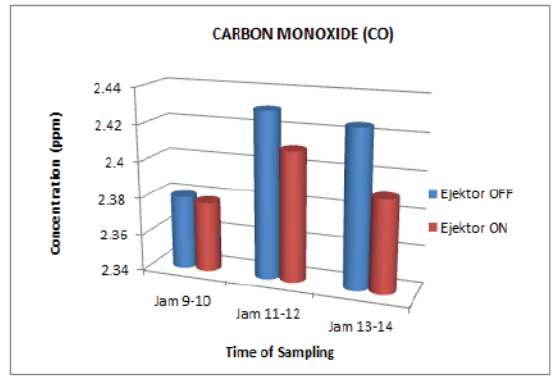


Fig. 2: Graph of CO concentration in the air when the ejector is OFF and ON.

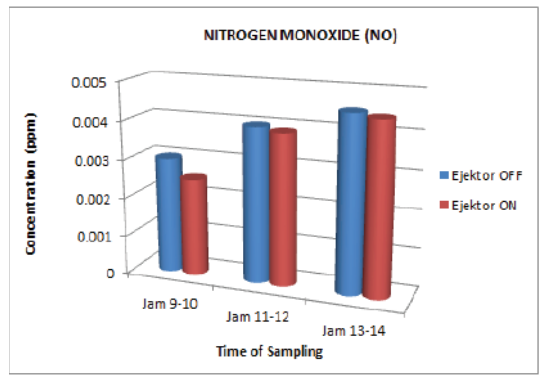


Fig. 3: Graph of the NO concentration in the air when the ejector is OFF and ON

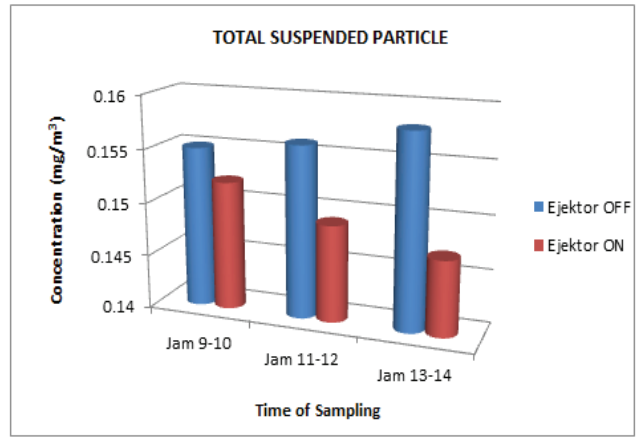


Fig. 4: Graph of TSP concentration in the air when the ejector is OFF and ON.

with the ejector not running, at 9-10 a.m. TSP concentration of 0.155 mg/$m^3$ was obtained, 11-12 a.m. it was 0.156 mg/$m^3$, while at 1-2 p.m. the concentration was 0.158mg/$m^3$. While the results of TSP measurements on the condition of the ejector ON at 9-10 a.m., the TSP concentration was 0.152mg/$m^3$, at 11-12 a.m. it was 0.149mg/$m^3$, while at 1-2 p.m. the concentration was 0.147 mg/$m^3$. There appears to be a decrease in TSP concentration when the ejector was run, also like carbon monoxide, a reduction was seen at 1-2 p.m. sampling.

Based on the graphs of the data shown in Fig. 2 and Fig. 4, it seems that there are differences that can be observed, namely in the carbon monoxide, where the highest concentration in the sampling hours is at 11-12 a.m. both when the ejector is not executed and when the ejector is executed. Whereas in TSP measurements it appears that when the ejector has not been executed, the trend of TSP concentration appears to increase, and when the ejector is carried out, the total dust concentration (TSP) trend is decreasing. From both CO and TSP measurements, it appears that the total dust concentration decreases more (suspended particles) due to the effect of the ejector (4.47 %), compared to carbon monoxide (CO) (0.78 %). One reason is that the particles have heavier mass than CO. In addition to larger sizes, the particles themselves can be categorized by diameter. If the diameter is smaller or equal to 2.5 microns, it is categorized as fine particles, if the diameter is between 2.5-10 microns it is categorized as coarse particles, whereas when the diameter is greater than 10 microns it is called total dust or total suspended particles (Sattar et al. 2014). The finer the particles have a higher impact on respiratory health (Rashid et al. 2014).

## CONCLUSIONS

In this study, the reduction and recovery of pollutant gases and total dust have been carried out by sucking from the air by vacuum into a tube. Then the pollutant gases and particles are being sent into water that continues to circulate. The conclusions in this study are: There is a reduction in the concentration of carbon monoxide gas and total suspended particles by the operation of the ejector. The longer the ejector is operated, more the carbon monoxide and total suspended particles will be reduced. Compared to carbon monoxide gas, the concentration of total suspended particles appears to have a greater degree of reduction in all hours of sampling. The greater the vacuum, the higher will be the ability to reduce the concentration of carbon monoxide gas and total suspended particles.

## ACKNOWLEDGEMENT

This research was carried out with funding support from the Directorate of Research and Community Service (DRPM) of the Ministry of Research, Technology and Higher Education through the Ujung Padang Polytechnic Unit of Research and Community Service (UPPM), therefore, we extend our full appreciation and gratitude to them.

## REFERENCES

Chou, S. K. 1986. Experimental studies on an air-air jet exhaust pump. ASHRAE Transactions. 4: 497-506.

Dutton, J. C., Mikkelsen, C.D. and Addy, A. L. 1982. A theoretical and experimental investigation of the constant area, supersonic-supersonic ejector. AIAA Journal, 20: 1392-1400.

Gamisansa, X., Sarrab, M. and Lafuente, F. J. 2002. Gas pollutants removal in a single and two-stage ejector venturi scrubber. Journal of Hazardous Materials, B90: 251-266.

Harsono, 1996. Technology of Welding Metal. Pradya Paramita Press, Jakarta.

Lima, E.A.P., Guimaraes, E.C., Pozza, S.A., Barrozo, M.A.S. and Coury, J.R. 2009. A Study of atmospheric particulate matter in a city of the central region of Brazil using time-series analysis. Int. J. Environment Engineering, 1: 1-9.

Rashid, M., Yunus, S., Mat, R., Baharun, S. and Lestari, P. 2014. $PM_{10}$

black carbon and ionic species concentration of urban atmospheric in Makassar of South Sulawesi Province, Indonesia. Atmospheric Pollution Research, 5: 610-615. doi: 10.5094/APR.2014.070.

Saini, M., Nur, R., Yunus, S. and Ibrahim, 2018. The influence of throat length and vacuum pressure on air pollutant filtration using ejector. AIP Conference Proceedings. doi.org/10.1063/1.5042939.

Sattar, Y., Rashid, M., Ramli, M. and Sabariah, B. 2014. Black carbon and elemental concentration of ambient particulate matter in Makassar Indonesia. IOP Conf. Series: Earth and Environmental Science, 18: 012099, doi: 10.1088/1755-1315/18/1/012099.

Sattar, Y., Rashid, M., Mat, R., Baharun, S. and Man, H.C. 2019. Characteristics of the $PM_{10}$ in the urban environment of Makassar, Indonesia. Journal of Urban and Environmental Engineering, 13(1): 198-2017: doi: 10.4090/juee. 2009. v13n1.198207.

Sattar, Y., Rashid, M., Mat. R. and Puji, L. 2012. A preliminary survey of air quality in Makassar City South Sulawesi Indonesia. Jurnal Teknologi (Sciences & Engineering), 57:123-136.

Stefan, E. and Harnjak, P. 2008. Ejector refrigeration: An overview of historical and present developments with emphasis on air-conditioning applications. International Refrigeration and Air Conditioning Conference, U.S.A., 1-8.

Subramarian, G., Natrajan, S.K., Adhimolane, K. and Natarajan, A.T. 2006. Comparison of numerical and experimental investigation of jet ejectors with blower. International Journal of Thermal Science, 84: 134-142.

Suharno, 2008. Principles of Welding Metal and Mettalurgy. UNS Press. Surakarta, Indonesia.

WHO 2002. The World Health Report 2002: Reducing Risks, Promoting Health Life. WHO, Geneva.

WHO 2005. Indoor Air Pollution and Health, Bonn.

Wiryosumarto, H. and Okumura, T. 2004. Technology of Welding Metal. Pradaya Paramita Press, Jakarta.

Nature Environment and Pollution Technology
An International Quarterly Scientific Journal

p-ISSN: 0972-6268
(Print copies up to 2016)
e-ISSN: 2395-3454

Vol. 19 | No. 4 | pp. 1701-1705 | 2020

Original Research Paper

https://doi.org/10.46488/NEPT.2020.v19i04.040

Open Access Journal

# Study on Quantification Method for the Risk of Soil-Plant-Human System Environmental Pollution Caused by Sewage Irrigation in Agriculture

**Xin Huang† and Lin Qiu**

School of Water Resources, North China University of Water Resources and Electric Power, Zhengzhou, Henan, 450046, China

†Corresponding author: Xin Huang; huangxin0013@163.com

**Nat. Env. & Poll. Tech.**
**Website: www.neptjournal.com**

*Received:* 05-12-2019
*Revised:* 27-12-2019
*Accepted:* 01-03-2020

**Key Words:**
Environmental pollution
Sewage irrigation
Agriculture
Risk model

## ABSTRACT

Long-term sewage irrigation can cause accumulation of contaminants in soil, which imposes severe damages to soil and plants and further triggers many chronic diseases in human bodies via the food chain. In this paper, the effect of sewage irrigation on changes in concentration of contaminants in soil and its relationship with the concentration of contaminants in the main agricultural plants are discussed, and a health risk assessment is performed on the contaminant exposure suffered by people in the sewage irrigation area. Based on this, an environmental pollution risk model for the soil-plant-human system was established for research on the acceptable irrigation concentration of contaminants in sewage and the safe service period of sewage irrigation. A practical example adopted in this paper proves that arsenic pollution caused by sewage irrigation to soil-plant-human body system in the irrigation area imposes a comprehensive risk degree of 0.40, the acceptable arsenic irrigation concentration is 0.086mg/L and the safe service period for this irrigation area is 150 years. Thus, the reclaimed water shall be subject to innocuous disposal under scientific guidance for agricultural irrigation.

## INTRODUCTION

With the rapid development of Chinese economy and increasingly improved living standards, water used for irrigation is growingly reduced due to the excessive industrial and domestic water demand, which causes a growing shortage of water used for agriculture (Bibliometric 2016). It has been a general practice in China that sewage was used for irrigation, which can provide fertilizer resources. Nevertheless, due to poor sewage processing capacity, high sewage processing cost and low awareness of environmental protection, a large volume of sewage that fails to pre-processing is used for irrigating farmland, significantly damaging water quality and causing environmental pollution (Zeng et al. 2015, Jiang et al. 2017). In recent years, scholars have made great efforts into studies of environmental pollution caused by sewage irrigation (Liu et al. 2015, Liu et al. 2016, Wu et al. 2018).

In this paper, the author will make a discussion over the effect of concentration of contaminants in sewage used for irrigation, on changes in concentration of contaminants in soil, the correlation between the concentration of contaminants in soil and those in the main agricultural plant. According to a survey performed on habits of people in sewage irrigation area, a quantification analysis on the process that how people are exposed to contaminants in the environment and a supporting health risk assessment has been performed, based on which, an environmental risk pollution model for the soil-plant-human system was established, whereby a study on the acceptable irrigation concentration of contaminants in sewage and the safe service period of sewage irrigation is made.

## MATERIALS AND METHODS

### Heavy Metal Accumulation in Soil Due to Sewage Irrigation in Farmland

The annual accumulation of heavy metals (annual residue) in soil is calculated with the formula (1):

$$W = K（B+R）\quad \ldots(1)$$

Where, $W$ is the annual accumulation of the heavy metal in soil, mg/kg; $B$ is the soil background value, mg/kg; $R$ is the annual input of the contaminant into soil, mg/kg; $K$ is the annual residual rate of the contaminant in soil, %.

Given the fact that historically annual production of pollution sources has been stable, the changes in heavy metal concentrations in local soil can be regarded as increasing in arithmetic progression. In the case that annual input of the contaminant into the soil is inaccessible and experimental data from local pot planting and community simulations are

not available, formula (2) can be used to predict the accumulation of the contaminant within a certain year and the safe service period during which sewage irrigation is tolerant in soil (Huang & Qiu 2017).

$$W = N_w \cdot x + W_0, \quad n = (S_i - W_0)/x, \quad x = (W_0 - B)/N_0 \qquad \ldots(2)$$

Where, $W$ is the predicted accumulation of the contaminant in soil within certain years, mg/kg; $N_w$ is the predicted sewage irrigation period; $x$ is the annual increment of the contaminant in soil, mg/kg; $W_0$ is the accumulation of the contaminant in the soil in the current year, mg/kg; $n$ is the safe period; $S_i$ is the environmental standards for soil, mg/kg; $B$ is the soil background value, mg/kg; $N_0$ is the period amid which sewage irrigation has been applied.

### Heavy Metal Concentration in Agricultural Plants Irrigated by Sewage

Reports from many scholars indicate that in a certain area, heavy metal concentration in the agricultural plants is correlated with heavy metal concentrations in soil (Li 2002, Liu & Jiang 2004, Li et al. 2006). In this study, correlation analysis has been performed on concentrations of heavy metals in soil from each sampling site and the concentrations of heavy metals in the main agricultural plants.

### Health Risk Assessment on Heavy Metal Exposure in Sewage Irrigation Area

The lifetime risk of chronic heavy metal poisoning imposed on people in sewage irrigation area ($G$) is characterized by three indicators, i.e., reference dose of heavy metal accumulation ($G_fM$), lifetime accumulation of heavy metal in people in sewage irrigation area ($U_{\text{lifetime}}$) and prevalence rate of heavy metal poisoning ($P$), as below:

$$G = \frac{U_{\text{lifetime}}}{G_f M} \times P \qquad \ldots(3)$$

Assuming that 80 years is the life expectancy of people in sewage irrigation area, i.e., safe period, and $U_{\text{lifetime}}$ is calculated by the following formula:

$$U_{\text{lifetime}} = U_{\text{diet (lifetime)}}$$

$$U_{\text{diet (lifetime)}} = \sum_{=1}^{80} \sum S_{(i,j)} \cdot h_{(i,j)}$$

Where, $U_{\text{diet (lifetime)}}$ is the lifetime exposure of heavy meal in diet for people in sewage irrigation area; $S_{(i,j)}$ is the total intake of food $j$ in the year $i$, kg/a; $h_{(i,j)}$ is the heavy metal concentration in food $j$ in the year $i$, mg/kg.

By performing epidemics surveys on arsenic poisoning of people in sewage irrigation area, and analysing people's cumulative exposure to arsenic, some scholars (Shang et al. 2002) have summarized the relationship between prevalence rate of arsenic poisoning in people ($P$, %) and the cumulative exposure of arsenic ($U$, mg).

### Quantification Model for Risk Caused by Sewage Irrigation on the Soil-Plant-Human and Analysis of Safe Period and Acceptable Irrigation Concentrations of Heavy Metals in Soil

After analysing the health risk caused by exposure to heavy metals, authors have further established a quantification model to study the environmental risk of heavy metal pollution on the soil-plant-human system in sewage irrigation area, as described in formula (4):

$$M_s = G / [M] \qquad \ldots(4)$$

Where, $M_s$ is the risk degree of pollution on the soil-plant-human system caused by sewage irrigation; $[M]$ the permissible risk degree. $M_s \geq 1$ means that the concentration of heavy metal in the sewage used for irrigation exceeds the environmental tolerance limit for such heavy metal and irrigation of farmland with this sewage will cause pollution of the soil-plant-human system; $M_s < 1$ means that the risk of soil-plant-human system pollution caused by a heavy metal contained in sewage used for irrigation is acceptable.

Given the said study on the risk caused by sewage irrigation to soil-plant-human system pollution and with reference to data from U.S. Environmental Protection Agency, the health risk analysis result obtained by formula (4) when the risk degree of chronic heavy metal poisoning to people in sewage irrigation area ($G$) is lower than the permissible risk of such heavy metal $[M]$ is acceptable (i.e., $G < [M]$). The safe period of sewage irrigation defined in this study means the period during which the cumulative heavy metal exposure risk imposed on existing residents in the sewage irrigation area is always lower than the permissible risk when sewage containing a certain concentration of a heavy metal containment is used for farmland irrigation on a long-term basis. Accordingly, the acceptable risk irrigation concentration of a heavy metal contaminant in the soil-plant-human system is defined as the maximum permissible concentration of heavy metal in the sewage used for irrigation when the cumulative heavy metal exposure risk imposed on existing residents in the sewage irrigation area is lower than the permissible risk of such heavy metal exposure. Thus, the acceptable risk irrigation concentration is not fixed but changed with the safe period required for a sewage irrigation area.

## THE CASE STUDY OF ENVIRONMENTAL POLLUTION CAUSED BY SEWAGE IRRIGATION IN AGRICULTURE IN YELLOW RIVER BASIN

### General Information

For the sewage irrigation area in the Yellow River Basin, there are detailed monitoring data. By 2018 sewage had been applied to irrigation in this area for 20 consecutive

years. Specific data are described as below. Topsoil depth is 15～45cm. Soil background values: cadmium (Cd) is 0.16 mg/kg, Hg is 0.09mg/kg, arsenic (As) is 8.9mg/kg and lead (Pb) is 16.25mg/kg. The annual volume of irrigation water is 4500$m^3$/$hm^2$. The main agricultural plant in this area is rice whose whole growth period is from April to September.

Scholars concluded that the residual accumulation rate of heavy metal in sewage irrigated soil is often higher than 90% through community or pot planting experiments (Huang & Wang 2009). Given the fact that heavy metals in sewage pose the most significant harm to environment and people in the irrigation area, arsenic (As) is taken as an example, in this study, to calculate the pollution risk imposed on the soil-plant-human system.

### Change in Concentration of Arsenic in Soil

It is assumed that the concentration of arsenic in soil is an arithmetic progression, from which, the cumulative concentration of arsenic in soil in 2018 can be obtained. The average annual increment of arsenic concentration in the soil can be calculated, $x = (W_0 - B)/N_0 = 0.295$mg/kg. It can be seen from formula (2) how the concentration of arsenic changes in soil irrigated by sewage in a certain year, $W = N_w \cdot x + W_0 = 0.295\ N_w + 8.9$ ($N_w$ = 1,2,3,...$w$).

### Determination of Concentration of Arsenic in the Soil-Plant System

Rice is the primary food taken by people in the irrigation area. According to the detected concentration of arsenic in rice harvested from sewage irrigation area and the concentration of arsenic in soil, the correlation equation between concentration of arsenic in rice, $a$ (mg/kg) and the concentration of arsenic in soil, $b$ (mg/kg) can be obtained by fitting, $a = 7.9\times10^{-3}b - 4.89\times10^{-2}$ ($r^2$=0.98).

### Calculation of Cumulative Arsenic Exposure in Human Body

Rice consumed by each adult (over 18 years old) per day in the sewage irrigation area is 505g, the annual rice intake for each adult is $S$ = 505g/d×365d = 184325g. According to Recommended Nutrition Supplies in Daily Diet (revised), the average food consumed by a minor is about 0.669 time of that by an adult.

The concentration of arsenic in rice is taken as the average concentration over such 20 years. The $h$ (0.131 mg/kg) can be calculated from the correlation between the concentration of arsenic in rice, $a$ (mg/kg), and the concentration of arsenic in soil, $b$ (mg/kg). Further, with c into relevant formulas, the arsenic exposures $U_{\text{adult}}$ and $U_{\text{minor}}$ in the diet of residents in sewage irrigation area in 2018 can be obtained, $U_{\text{adult}} = Sh = 24.147$mg, $U_{\text{minor}} = 0.669U_{\text{adult}} = 16.154$mg.

Residents of different ages are influenced by arsenic for different periods and the lifetime arsenic exposure for one person is different from that for another. Two cases are discussed in this study depending on how long each resident has been living in the sewage irrigation area. The first case applies to residents who were born in 2018 and have been living there since then, they are subject to the highest arsenic exposure risk, with the lifetime arsenic exposure caused by rice consumption from the soil-plant system.

$U_{\text{lifetime}} = 0.669\cdot\sum_{i=2019}^{2036} U_{\text{diet}\,(i)} + \sum_{j=2037}^{2098} U_{\text{diet}\,(j)} = 1.788$ g

The second case applies to residents who had lived in the soil-plant system for more than 20 years, with the highest arsenic exposure risk $U_{\text{current}} = 20\cdot U_{\text{adult}} = 0.483$ g

### Health Risk Caused by Arsenic Pollution

$G_f M$ is taken as 200g/d because no chronic poisoning reaction occurs when the human body intakes arsenic with a dose of 200～250g/d (Qiu & Wang 2003). According to the relationship between prevalence rate arsenic poisoning among people ($P$, %) and cumulative arsenic exposure ($U$), 2018 prevalence rate of arsenic poisoning among people in the irrigation area is 1%. According to Provisional Regulations on Classification of Regional Arsenic Poisoning Areas and Clinical Diagnosis, this area is classified as a mild regional arsenic poisoning area.

The arsenic exposure health risk $G_{\text{lifetime}}$ for residents born in 2018 is $G_{\text{lifetime}} = U_{\text{lifetime}}/G_f M \times P = 0.003$, and the arsenic exposure health risk $G_{\text{current}}$ for people who had been living in the irrigation area since sewage was used for irrigation is $G_{\text{current}} = U_{\text{current}}/G_f M \times P = 0.0008$.

For residents who had been living in the irrigation area for more than 20 years, the comprehensive risk of land-plant-human system pollution caused by sewage irrigation $M_s = G_{\text{current}}/[M] = 0.40$.

For residents who were born in 2018, the lifetime risk of land-plant-human system pollution caused by sewage irrigation $M_s = G_{\text{lifetime}}/[M] = 1.50 > 1$, which means that if the current sewage irrigation is continued without any improvement action, residents who were born in 2018 and would live in the irrigation area for their lifetime would be harmed.

### Analysis of Acceptable Risk Irrigation Concentration of Arsenic in Land-Plant-Human System and Safe Period

Given the available data about the irrigation area, from an analysis of annual sewage volume used for irrigation and average annual increment of arsenic concentration on soil,

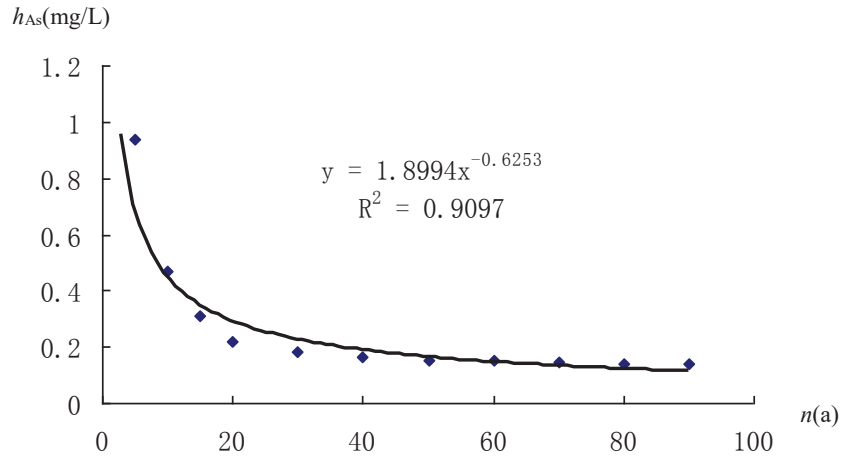


Fig. 1: The fit curve relationship between $n$, safe period of sewage irrigation, and $h_{As}$, acceptable risk irrigation concentration of arsenic in the soil-plant-human system.

it can be known that the average concentration of arsenic in sewage used for irrigating main agricultural plant in this area is 0.164 mg/L. This concentration would impose cumulative health risks at different degrees to people born in 2018 in this irrigation area. To have residents born in 2018 subject to a health risk caused by arsenic exposure of lower than [$M$], the acceptable risk irrigation concentration of arsenic in sewage is 0.086mg/L, as calculated from the model adopted for risk assessment of soil-plant-human system pollution. That is to say, when the concentration of arsenic in sewage used for irrigation is not higher than 0.086mg/L, all residents living in the irrigation area experience a health risk caused by arsenic exposure that is lower than [$M$] and the safe period of sewage irrigation is at least 150 years.

For the development of irrigation systems for an irrigation area, the effect of changes in contaminants contained in sewage and changes in management standards on safe service period of sewage irrigation should be clearly understood. A fit curve relationship between $n$, the safe period of sewage irrigation, and $h_{As}$, acceptable risk irrigation concentration of arsenic in the soil-plant-human system is plotted in Fig. 1.

With reference to the analysis of acceptable risk irrigation concentration of arsenic for residents born in 2018, the acceptable risk irrigation concentration of arsenic in sewage when the safe period is 150 years can be calculated from Fig. 1. As $n$, the safe period of sewage irrigation becomes longer, the acceptable risk irrigation concentration of arsenic, $h_{As}$, is stabilized around 0.086mg/L. The current average concentration of arsenic in sewage used for irrigation is 0.164mg/L, which in turn, with the help of the curve described in Fig. 1, can help calculate the safe period $n$=90.5 years. Without improvement actions, the safe period of sewage irrigation in this irrigation area cannot be increased.

## CONCLUSIONS

The practical example provided in this study indicates that the comprehensive risk of the soil-plant-human system pollution caused by 20-year sewage irrigation is 0.40, the acceptable risk irrigation concentration of arsenic in sewage is 0.086mg/L and the corresponding safe period is at least 150 years. The sewage irrigation has caused significant pollution on the soil-plant-human system and a procedure-based management system for sewage irrigation should be established and improved as soon as possible by specifying the sewage irrigation ways, times, optimum irrigation time and irrigation quota for the main agricultural plan that apply to different sewage types and different soil conditions, to achieve reasonable and proper sewage irrigation.

Despite soil's self-cleaning ability which helps degrade organic pollution in soil within a certain period, long-term irrigation with a large amount of sewage definitely can cause accumulation of contaminants, which imposes great harm to the soil-plant-human system. The sewage irrigation pollutes soil and further agricultural plant; contaminants contained in agricultural plant enter and accumulate in the human body via the food chain to trigger many chronic diseases. The theory and model presented in this paper can describe the pollution degree of the soil-plant-human system by sewage irrigation from a quantitative perspective. The influence of sewage irrigation on the soil-plant-human system is enduring and cumulative, and the mechanism of contaminant migration, transformation and accumulation is quite complicated. The study result presented in this paper can provide some reference for practices, but more deep studies should be pursued in the future. Next, more reasonable methods will be developed to describe the risk caused by sewage irrigation, and the indicators that characterize the risk of soil-plant-human system

pollution improved, and the standards for the classification of risks of soil-plant-human system pollution developed.

## REFERENCES

Bibliometric, S.M. 2016. Analysis of research on wastewater irrigation during 1991-2014. Irrigation and Drainage, 65(5): 644-653.

Huang, C.G. and Wang, X. 2009. China's farmland sewage irrigation development and its impact on crop research. Journal of Anhui Agricultural Sciences, 37(22): 10692-10693.

Huang, X. and Qiu, L. 2017. Theoretical exploration of risk analysis of sewage irrigation in farmland. Nature Environment and Pollution Technology, 16(1): 67-73.

Jing, X., Yao, G.J., Liu, D.H., Liang, Y.R., Luo, M., Zhou, Z.Q. and Wang, P. 2017. Effects of wastewater irrigation and sewage sludge application on soil residues of chiral fungicide benalaxyl. Environmental Pollution, 224: 1-6.

Li, H.Y. 2002. The relationship between the heavy metals Cd, Zn in Crop and soil properties, the total content of Cd and Zn. Ningxia Engineering Technology, 1(3): 221-223.

Liu, Y.L. and Jiang, X.Y. 2004. Evaluation of heavy metal pollution of soil and crops in Baima village Zhuzhou City. Soils, 36(5):551-556.

Li, Q.X., Huang, Y.Y., Zhao, Y.H. and Huang, Y.Z. 2006. Study on absorption of pollutants of irrigating water by several vegetables and their soil. Ecologic Science, 25(3): 216-221.

Liu, Y., Wang, H.F., Li, X.T. and Li, J.C. 2015. Heavy metal contamination of agricultural soils in Taiyuan, China. Pedosphere, 25(6): 901-909.

Liu, B.L., Ma, X.W., Ai, S.W., Zhu, S.Y., Zhang, W.Y. and Zhang, Y.M. 2016. Spatial distribution and source identification of heavy metals in soils under different land uses in a sewage irrigation region, northwest China. Journal of Soils and Sediments, 16(5): 1547-1556.

Qiu, F.G. and Wang, X.C. 2003. Assessing methods for health risks of reclaimed water. Environmental Pollution and Control, 25(1): 49-51.

Shang, Q., Ren, X.Q. and Li, J.R. 2002. Estimation of arsenic accumulative intake and residents' health effects in an air pollution area-relationship between arsenic accumulative intake level and arsenicism prevalence. Journal of Hygiene Research, 31(5): 926-929.

Wu, B., Guo, S.H., Li, X.J. and Wang, J.N. 2018. Temporal and spatial variations of polycyclic aromatic hydrocarbons (PAHs) in soils from a typical organic sewage irrigation area. Science of the Total Environment, 613: 513-520.

Zeng, X.F., Wang, Z.W., Wang, J., Guo, J.T., Chen, X.J. and Zhuang, J. 2015. Health risk assessment of heavy metals via dietary intake of wheat grown in Tianjin sewage irrigation area. Ecotoxicology, 24(10): 2115-2124.

Nature Environment and Pollution Technology
An International Quarterly Scientific Journal

p-ISSN: 0972-6268
(Print copies up to 2016)
e-ISSN: 2395-3454

Vol. 19 | No. 4 | pp. 1707-1712 | 2020

Original Research Paper

https://doi.org/10.46488/NEPT.2020.v19i04.041

Open Access Journal

# Evaluation of the Effect of Sewage Irrigation on Groundwater

**Xiuli Li*† and Xiaoyu Li****
*School of Water Conservancy, North China University of Water Resources and Electric Power, Zhengzhou 450045, China
**Hydrology Bureau of Yellow River Conservancy Commission, Zhengzhou 450004, China
†Corresponding author: Xiuli Li; lixiuli96@163.com

**Nat. Env. & Poll. Tech.**
**Website: www.neptjournal.com**

*Received:* 07-12-2019
*Revised:* 21-12-2019
*Accepted:* 28-03-2020

**Key Words:**
Sewage irrigation
Groundwater
Water quality evaluation
Fuzzy comprehensive evaluation
Evaluation standard

## ABSTRACT

In areas with water resources shortage, sewage irrigation can alleviate the contradiction between supply and demand for water. However, long-term use of sewage irrigation will affect soil, crops and groundwater. In this paper, irrigation water and groundwater in different irrigation source areas were sampled and analysed respectively to study the effect of sewage irrigation on groundwater. The irrigation water was evaluated for $Cl^-$, Cd, Pb, $Cr^{6+}$, As, Cu, $F^-$, TP, Hg and Zn as standards for irrigation water quality which along with Nemerow index method were used for comprehensive evaluation. The result of the evaluation is that the water quality of the reclaimed water, domestic sewage and mixed sewage meet the requirements of the agricultural irrigation, and the industrial sewage pollution index is relatively high and less suitable for agricultural irrigation. The fuzzy comprehensive evaluation method was adopted to evaluate groundwater quality, using Quality Standard for Ground Water (GBT14848-2017) as evaluation factor standard and ammonia nitrogen ($NH_3$-N), chloride ($Cl^-$), nitrate ($NO_3$-N) and nitrite ($NO_2$-N) as evaluation indicators. The results of the evaluation showed that the water quality of 2 monitor wells among the 11 monitor wells was within Category II, 6 within Category III, and 3 within Category IV. With regards to the influence of different irrigation sources on groundwater, the comprehensive evaluation results are reasonable as well. According to the comprehensive membership grades, it can be concluded that the influence of different water sources on groundwater quality, in turn, is reclaimed water < domestic sewage < mixed sewage < industrial sewage. The evaluation results are in line with the actual situation in the study area.

## INTRODUCTION

The shortage of water resources restricts the development of economy, and the limited water resources usually first meet the demand of domestic and industrial use, and then agriculture, which undoubtedly makes the phenomenon of agricultural water shortage more serious. China is a big agricultural country dominated by irrigation. According to the China Water Resources Bulletin, agricultural water consumption accounted for 61.4% of total water consumption in 2018. At present, the water shortage in agriculture is becoming more and more serious as agriculture water is being squeezed continuously to meet domestic and industrial water demand. The only way to solve agricultural water shortage is "increasing income and decreasing expenditure" to achieve the benign development of agriculture. Wastewater recovery is considered as a major way to solve the problem of agricultural water shortage. Using sewage effluent for irrigation, on the one hand, solves the problem of discharge of massive sewage generated in the process of domestic and industrial use of water resources in areas without sewage treatment plants, on the other hand, alleviates the problem of agricultural water shortage. However, there are still many problems concerning the use of sewage for agricultural irrigation. While some nutritive elements in the sewage can add to the content of nutrients in the soil, long-term use of sewage for irrigation will affect the soil and the quality of groundwater (Wen 2012). Massive pollutants and substances in the sewage that hardly decompose will remain in the soil, accumulate and enter into groundwater environment along with agricultural irrigation & water supply, which pollutes and influences the groundwater (Wan et al. 2015). Evaluating the quality of groundwater by testing and analysing the chemical indicators provides a scientific basis for the protection and sustainable exploitation of water resources.

## MATERIALS AND METHODS

### General Situation of the Study Areas

As there are quite many irrigation areas adopting sewage irrigation in the North China Plains, where there is a serious shortage of water, in this article, several irrigation areas in a city of North China Plain with a 10+ year history of using different water quality for irrigation were chosen and sam-

pled to study the influence of irrigation with different water quality on groundwater. Based on the different water quality of the sewage adopted in the irrigation areas, the irrigation areas are divided into domestic sewage irrigation area, mixed sewage irrigation area, industrial sewage irrigation area and reclaimed water irrigation area.

### Sample Collection and Water Analysis

In the study area, irrigation water sampling locations and groundwater sampling locations were set respectively based on the irrigation water sources and the actual situation of various irrigation areas. For irrigation water sources, the sampling locations were set at the intake of various irrigation areas; and for groundwater, 11 groundwater monitor wells in different places of the studied areas were chosen as sampling locations. The selection of sampling locations takes account of irrigation areas with different water quality, as 2 wells were chosen from the reclaimed water irrigation area, 2 from the domestic sewage irrigation area, 3 wells from the mixed sewage irrigation area, and 4 wells from the industrial sewage irrigation area.

To reduce water sample errors, pre-sampling and post-sampling were carried out strictly in line with Water Quality Sampling-Technical Regulation of the Preservation and Handling of Samples (HJ 493-2009). Respective analysis methods were adopted to test various indicators.

Major monitoring indicators for the irrigation water source test include $Cl^-$, Cd, Pb, $Cr^{6+}$, As, Cu, $F^-$, TP, Hg and Zn; and major monitoring indicators for the groundwater include: chlorine ions, ammonia nitrogen, nitrates, nitrite and heavy metals.

All indicators in the water samples were tested and analysed in strict accordance with respective methods. Table 1 provides the specific tests and analysis methods of each indicator.

## RESULTS AND ANALYSIS

**Evaluation of irrigation water quality:** The quality of all kinds of irrigation water in the study area was evaluated following Standards for Irrigation Water Quality (GB5084-2005). Indicators such as $Cl^-$, Cd, Pb, $Cr^{6+}$, As, Cu, $F^-$, TP, Hg and Zn were chosen as evaluation factors. Pollution index of every single indicator was calculated with the following calculation formula:

$$I = \frac{C_i}{C_0} \quad \ldots(1)$$

Where, $C_i$ implies the water quality indicator of various sampling locations; $C_0$ implies the standard limit of Standards for Irrigation Water Quality. Table 2 gives the calculation results of the pollution index of every single indicator of different irrigation water quality.

Based on the data from Table 2, various evaluation indicators of reclaimed water, domestic sewage, mixed sewage, industrial sewage were compared and analysed against the limits of Standards for Irrigation Water Quality: (1) all single indicators of reclaimed water are within the standards except for Cd which is 1.2 times that of the standard; (2) in domestic sewage, Pb is twice that of the standard, Hg reaches the critical value, and other indicators are within the standards; (3) in mixed sewage, $Cl^-$ is 1.34 times that of the standard, Cd is twice that of the standard, and other indicators are within the standards; (4) in industrial sewage, $Cl^-$ is 1.41 times that of the standard, Cd is 6.4 times that of the standard, Pb is 1.4 times that of the standard, $Cr^{6+}$ is 2.28 times that of the standard, Hg is 2 times that of the standard, and other indicators are within the standard.

Nemerow index method (Tang et al. 2019) was applied for the comprehensive evaluation, and the comprehensive index values were compared against pollution level standards to conclude the pollution levels of the water quality. The com-

Table 1: Analysis methods for various indicators.

| Item | Method | Item | Method |
|---|---|---|---|
| $Cl^-$ | Ion Chromatography | Pb | Inductively Coupled Plasma Mass Spectrometry |
| $F^-$ | | Zn | |
| TP | | Cu | |
| $NO_3$-N | | As | Atomic Fluorescence Spectrometry |
| $NH_3$-N | | Hg | |
| $NO_2$-N | Spectrophotometry | Cd | Graphite furnace Atomic Absorption Spectrometer |
| | | $Cr^{6+}$ | |

prehensive index PI used the following calculation formula:

$$PI = \sqrt{\frac{\bar{I}^2 + I_{max}^2}{2}} \quad \ldots(2)$$

$$\bar{I} = \frac{1}{n}\sum_{i=1}^{n} I_i \quad \ldots(3)$$

$$I = \frac{C_i}{C_0} \quad \ldots(4)$$

in which, $\bar{I}$ implies the average value of the pollution indexes of various indicators; $I_{max}$ implies the maximum value of pollution indexes; *PI* implies the comprehensive pollution index, and *n* implies the quantity of the indicators.

Based on the data from Table 2, the calculated comprehensive indexes are respectively: the comprehensive index of reclaimed water is 0.86, domestic sewage is 1.45, mixed sewage is 1.48, and industrial sewage is 4.69. The evaluation standards are PI<1.0 - unpolluted; 1.0≤PI<2.5 - slightly polluted; 2.5≤PI<5 - mediumly polluted, and; 5≤PI - heavily polluted. The comparison results between the comprehensive indexes of various water quality and the evaluation standards are reclaimed water -unpolluted, domestic sewage and mixed sewage-slightly polluted, industrial sewage-moderately polluted. Based on the results of the comprehensive evaluation, the water quality of reclaimed water, domestic sewage and mixed sewage basically conform to the requirement of agricultural irrigation, and the pollution index of industrial sewage is quite high and not much suitable for agricultural irrigation.

**Groundwater quality evaluation:** To a certain extent, irrigation with sewage alleviates the problem of agricultural water shortage. But if you do not pay attention to the safety of irrigation sewage, the groundwater could be polluted (Peng et al. 2014). The pollutants enter into groundwater environment mainly through intermittent and infiltrative contamination, and the harmful ingredients enter into the aquifer through the leaching of precipitation or irrigation water (Bao 2014). Once the groundwater is polluted, treatment for it is more difficult than that for surface water. That is why people are paying more and more attention to the quality of groundwater.

**Groundwater evaluation methods:** Fuzzy comprehensive evaluation method was adopted to evaluate groundwater quality. Establishing the membership relation between the evaluation factors and evaluation standards based on membership grade is a way of formulating the borders of water quality classification (Fang et al. 2019), which demonstrates the fuzziness of water quality grades and reflects the comprehensive water quality categories very well, and makes the evaluation results more reasonable. Quality Standard for Ground Water (GBT14848-2017) was adopted as an evaluation factor standard, see Table 3. In view of the situation of the irrigation areas and the principles for water quality evaluation, ammonia nitrogen ($NH_3$-N), chloride $Cl^-$, nitrate ($NO_3$-N) and nitrite ($NO_2$-N) were chosen as evaluation indicators. As the content of cadmium, lead, copper, zinc and mercury is relatively low in groundwater quality and lower than the detectable level, this time they were not included in the evaluation indicators.

Table 2: calculation results of pollution index of single indicators of different irrigation water quality.

| Indicator | $Cl^-$ | Cd | Pb | $Cr^{6+}$ | As | Cu | $F^-$ | TP | Hg | Zn |
|---|---|---|---|---|---|---|---|---|---|---|
| Standard Limit $C_0$ | 250.000 | 0.005 | 0.100 | 0.100 | 0.050 | 1.000 | 3.000 | 5.000 | 0.001 | 2.000 |
| Reclaimed Water $C_1$ | 84.600 | 0.006 | 0.000 | 0.012 | 0.000 | 0.000 | 0.644 | 0.000 | 0.000 | 0.000 |
| Pollution Index $I_1$ | 0.338 | 1.200 | 0.000 | 0.120 | 0.000 | 0.000 | 0.215 | 0.000 | 0.200 | 0.000 |
| Domestic Sewage $C_2$ | 86.200 | 0.003 | 0.200 | 0.004 | 0.000 | 0.025 | 0.826 | 1.820 | 0.001 | 0.117 |
| Pollution Index $I_2$ | 0.345 | 0.600 | 2.000 | 0.040 | 0.002 | 0.025 | 0.275 | 0.364 | 1.000 | 0.059 |
| Mixed Sewage $C_3$ | 335.000 | 0.010 | 0.080 | 0.052 | 0.005 | 0.078 | 0.982 | 0.610 | 0.000 | 0.610 |
| Pollution Index $I_3$ | 1.340 | 2.000 | 0.800 | 0.520 | 0.100 | 0.078 | 0.327 | 0.122 | 0.400 | 0.305 |
| Industrial Sewage $C_4$ | 285.350 | 0.032 | 0.140 | 0.228 | 0.167 | 0.103 | 0.765 | 0.350 | 0.002 | 0.396 |
| Pollution Index $I_4$ | 1.141 | 6.400 | 1.400 | 2.280 | 3.340 | 0.103 | 0.255 | 0.070 | 2.000 | 0.198 |

Table 3: Groundwater evaluation factor standard.

| Project | I | II | III | IV | V |
|---|---|---|---|---|---|
| $NH_3$-N | ≤0.02 | ≤0.1 | ≤0.5 | ≤1.5 | >1.5 |
| $Cl^-$ | ≤50 | ≤150 | ≤250 | ≤350 | >350 |
| $NO_3$-N | ≤2 | ≤5 | ≤20 | ≤30 | >30 |
| $NO_2$-N | <0.01 | ≤0.1 | ≤1 | ≤4.8 | >4.8 |

Major steps of Fuzzy comprehensive evaluation are:

(1) Define the target grades: Based on the different status of the evaluation objects, define m evaluation grades, which are recorded as:

$$V = \{v_1, v_2, \ldots, v_m\} \quad \ldots(5)$$

(2) Establish an evaluation indicator set: Based on the situation of the evaluation objects, choose n typical evaluation factors and form the indicator set:

$$U = \{u_1, u_2, \ldots, u_n\} \quad \ldots(6)$$

(3) Establish a membership grade function: Calculate the membership grade of each evaluation factor $u_i$ vs. evaluation grade $v_i$, and establish a fuzzy relation matrix R.

$$R = \begin{bmatrix} r_{11} & r_{12} & & r_{1m} \\ r_{21} & r_{22} & & r_{2m} \\ \vdots & \vdots & \ddots & \vdots \\ r_{a1} & r_{a2} & & r_{am} \end{bmatrix} \quad \ldots(7)$$

In the formula, $m$ implies evaluation grade and implies the number of evaluation indicators.

$$r_{i1} = \begin{cases} 1 & x \le x_1 \\ \dfrac{x_2 - x}{x_2 - x_1} & x_1 < x < x_2 \\ 0 & x > x_2 \end{cases} \quad \ldots(8)$$

$$r_{i2} = \begin{cases} 0 & x \le x_1 or x > x_3 \\ \dfrac{x - x_1}{x_2 - x_1} & x_1 < x \le x_2 \\ \dfrac{x_3 - x}{x_3 - x_2} & x_2 < x \le x_3 \end{cases} \quad \ldots(9)$$

$$r_{i3} = \begin{cases} 0 & x \le x_2 or x \ge x_4 \\ \dfrac{x - x_2}{x_3 - x_2} & x_2 < x \le x_3 \\ \dfrac{x_4 - x}{x_4 - x_3} & x_3 < x \le x_4 \end{cases} \quad \ldots(10)$$

$$r_{i4} = \begin{cases} 0 & x \le x_3 or x \ge x_5 \\ \dfrac{x - x_3}{x_4 - x_3} & x_3 < x \le x_4 \\ \dfrac{x_5 - x}{x_5 - x_4} & x_4 < x \le x_5 \end{cases} \quad \ldots(11)$$

$$r_{i5} = \begin{cases} 0 & x \le x_4 \\ \dfrac{x - x_4}{x_2 - x_1} & x_4 < x < x_5 \\ 1 & x > x_5 \end{cases} \quad \cdots(12)$$

In the formula, $X_1, X_2, \ldots X_5$ imply the boundary values of water quality standard grades of the evaluation factor indicators, and $X$ implies the measured values of various evaluation factors.

(4) Define the weights: as this article uses a multiple indicator system for a comprehensive evaluation, to reflect the interaction between indications more directly, entropy method (Xie 2016) is adopted to define the weights, i.e. defining the weights of various indicators based on the difference of the measured values of various indicators.

(5) Establish data matrix

$$S = \begin{bmatrix} x_{11} & & x_{1a} \\ \vdots & \ddots & \vdots \\ x_{n1} & & x_{na} \end{bmatrix}_{n \times a} \quad \ldots(13)$$

In the formula, $X_{ij}$ implies the value of Indicator #j of Plan #i, $n$ implies the quantity of evaluation samples, and $a$ implies the quantity of evaluation indicators.

(6) Calculate the specific gravity of Plan #i under Indicator #j in the indicators.

$$P_{ij} = \frac{x_{ij}}{\sum_{i=1}^{n} x_{ij}} (\text{j=1,2, } \cdots \text{a}) \quad \ldots(14)$$

(7) Define the entropy value of the evaluation factor $E_{ij}$

$$E_{ij} = -\left(\sum_{i=1}^{m} p_{ij} \ln p_{ij}\right) \Big/ \ln n \quad \ldots(15)$$

(8) Define the weight of evaluation factors

$$w_j = E_i \Big/ \sum_{j=1}^{a} E_i \quad \ldots(16)$$

Get the weight matrix A = ($w_1$, $w_2 \ldots w_a$)

(9) Define the evaluation grades: Composite calculation with weight matrix A and fuzzy relation matrix R to get the comprehensive membership grade vector B of the evaluation object.

$$B = A \bullet R = \left[b_1, b_2, \quad , b_m\right] \quad \ldots(17)$$

Normalization processing on vector B, and get the grade of the evaluation object based on the value of H.

$$H = \sum_{j=1}^{m} [(b_j \Big/ \sum_{j=1}^{m} b_j) \times j)] \quad \ldots(18)$$

**Results of the comprehensive evaluation:** Adopting Quality Standard for Ground Water (GBT14848-2017) as evaluation factor standard, the groundwater quality was divided into 5 grades. Fuzzy relation matrix R for the water quality samples of 11 groundwater monitor wells was established respectively, taking Monitor Well # 1 as an example.

$$R = \begin{bmatrix} 0.000 & 0.675 & 0.325 & 0.000 & 0.000 \\ 0.720 & 0.280 & 0.000 & 0.000 & 0.000 \\ 0.377 & 0.623 & 0.000 & 0.000 & 0.000 \\ 0.967 & 0.033 & 0.000 & 0.000 & 0.000 \end{bmatrix}$$

In the formula, Line 1 represents the relative membership grade values of ammonia nitrogen corresponding to 5 grades, which are Grade I to Grade V from the left to the right; Line 2 to Line 4 are $Cl^-$, $NO_3$-N, $NO_2$-N in turn.

The respective weights of the evaluation indicators, i.e. ammonia nitrogen ($NH_3$-N), chloride $Cl^-$, nitrate ($NO_3$-N) and nitrite ($NO_2$-N) were defined in the water quality samples with entropy evaluation method, which are 0.364, 0.165, 0.253 and 0.218 respectively.

Based on the water quality monitoring data of the 11 groundwater monitor wells chosen in the study area, fuzzy mathematics comprehensive evaluation model was applied to get the water quality evaluation results as given in Table 4.

According to the comprehensive evaluation results, among the water quality results of the 11 groundwater monitor wells from different irrigation water sources, the water in 2 monitor wells belongs to Water Category II, the water in 6 monitor wells belongs to Water Category III, and the water in 3 monitor wells belongs to Water Category IV. Taking monitor well #1 as an example, the comprehensive evaluation result on water quality of the #1 monitor well is within Category II, as among the single evaluation indicators, ammonia nitrogen is within Category III, while chloride, nitrate and nitrite are within Category II, therefore it is reasonable to tell with the fuzzy comprehensive evaluation that the water in # 1 monitor well belongs to Water Category II.

The monitor wells #1 and #2 are located in the reclaimed water irrigation area, and the fuzzy comprehensive evaluation result is Category II; #3 and #4 monitor wells are located in the domestic sewage irrigation area, and the fuzzy comprehensive evaluation result is Category III; #5-7 are located in the mixed sewage irrigation area, and the fuzzy comprehensive evaluation result is Category III, and; #8-11 are located in the industrial sewage irrigation area, and the fuzzy comprehensive evaluation result is Category III for #10, and Category IV for the rest of 3 wells. In terms of the effect of different irrigation water sources on the groundwater, the comprehensive evaluation results are reasonable as well. Based on comprehensive membership grades, we can tell that the effect levels of different irrigation water sources on the groundwater are, in turn, reclaimed water < domestic sewage < mixed sewage < industrial sewage, which is line with the pollution levels of the sewage on the water quality when irrigating. Therefore, the method of evaluating groundwater quality with fuzzy comprehensive evaluation is feasible.

The effect of irrigation with reclaimed water on the water quality of groundwater is relatively small; the impact of domestic sewage and mixed sewage is relatively big, and; the effect of industrial sewage on groundwater is quite high, in which the groundwater quality reaches Category IV, which causes severe pollution of the groundwater. From the comprehensive evaluation results, we can conclude that the groundwater in the study areas has been contaminated to different extent. Therefore, if sewage irrigation is adopted in places where there is a shortage of water resources, sewage water quality management should be strengthened, especially with regards to the discharge of industrial sewage which should not be discharged until it is up to the discharge standard, and domestic sewage should be treated and discharged in a concentrated way, to avoid serious impact on groundwater quality.

Table 4: Fuzzy comprehensive evaluation results of groundwater quality of various monitor wells.

| Minor well number | I | II | III | IV | V | H | Water quality classification |
|---|---|---|---|---|---|---|---|
| 1 | 0.425 | 0.457 | 0.118 | 0.000 | 0.000 | 1.694 | II |
| 2 | 0.451 | 0.549 | 0.000 | 0.000 | 0.000 | 1.549 | II |
| 3 | 0.408 | 0.326 | 0.100 | 0.000 | 0.165 | 2.188 | III |
| 4 | 0.291 | 0.353 | 0.327 | 0.030 | 0.000 | 2.096 | III |
| 5 | 0.417 | 0.099 | 0.319 | 0.000 | 0.165 | 2.398 | III |
| 6 | 0.365 | 0.393 | 0.077 | 0.000 | 0.165 | 2.208 | III |
| 7 | 0.367 | 0.331 | 0.137 | 0.000 | 0.165 | 2.266 | III |
| 8 | 0.218 | 0.044 | 0.351 | 0.222 | 0.165 | 3.074 | IV |
| 9 | 0.213 | 0.187 | 0.104 | 0.331 | 0.165 | 3.050 | IV |
| 10 | 0.218 | 0.098 | 0.263 | 0.422 | 0.000 | 2.889 | III |
| 11 | 0.218 | 0.137 | 0.109 | 0.172 | 0.364 | 3.327 | IV |

## CONCLUSIONS

Sewage irrigation can alleviate the shortage of irrigation water and solve the problem of shortage of water resources, but long-term use of untreated sewage for irrigation will cause problems such as soil pollution, impact on crop growth, groundwater quality decline and so on. Compared with dry farming, irrigation on crops with sewage can increase the yield of crops to a certain extent, but the impact on soil, crops and groundwater should not be ignored. As long as scientific irrigation method is adopted, sewage water is utilized properly, and the harm caused by sewage is controlled within the acceptable safety range, the sewage can be used in agricultural irrigation safely and efficiently. For different water sources, different soil types and different crops, suitable irrigation system and irrigation methods should be adopted. The establishment of a reasonable and comprehensive safety evaluation system will provide a theoretical basis for the proper management of sewage irrigation. Developing high efficiency and energy saving sewage treatment technology will reduce treatment cost and promote sewage irrigation.

Using sewage irrigation safely and properly can not only alleviate the contradiction between supply and demand for water resources but also protect the ecological environment and support the sustainable development of water resources.

## REFERENCES

Bao, Z. 2014. Research on pollution risk of heavy metals in soil and groundwater under reclaimed water irrigation. China University of Geosciences (Beijing), pp. 91-93.

Fang, Y.H., Zheng, X.L., Peng, H., Wang, H., Xin, J. and Zhang, B. 2019. Groundwater quality assessment based on optimization of fuzzy synthetic evaluation. Earth Science Frontiers, 26(4): 301-306.

Peng, S.Z., Cheng, S., Xu, J.Z. and Xiong, Y.J. 2014. Advances in safe utilization of poor-quality water. Water Resources Protection, 30(4): 1-6.

Tang, Y.Q., Li, Q.W., Zuo, W.L. and Wang, J. 2019. Analysis of applicability of Nemerow index method in evaluation of water quality of Beidaihe national wetland park. Environmental Engineering, 37(8): 195-199,189.

Wan, L., Zhang, M.Y., Lu, S. and Hu, K. 2015. Study progress on effect of polluted water irrigation on soil and problem analysis. Ecology and Environmental Sciences, 24(5): 906-910.

Wen, X.G. 2012. Study on groundwater environment impact by reclaimed water irrigation in Beijing NanHongmen. Tsinghua University, pp. 37-38.

Xie, F. 2016. The groundwater quality assessment and response of different irrigation water sources to groundwater in Jinghuiqu irrigation district. Northwest A&F University, pp. 27-31.

Nature Environment and Pollution Technology
An International Quarterly Scientific Journal

p-ISSN: 0972-6268
(Print copies up to 2016)
e-ISSN: 2395-3454

Vol. 19 | No. 4 | pp. 1713-1721 | 2020

Original Research Paper

https://doi.org/10.46488/NEPT.2020.v19i04.042

Open Access Journal

# Hydrochemical Characteristics and Water Quality Assessment of Surface Water and Groundwater in Agriculture Demonstration Base, Jiagou District, Northern Anhui Province, China

**Jie Ma*(***)(****)†, Linhua Sun*(***)(****), Song Chen*(***)(****), Zhichun Li **, Ting Gao *(***)(****), Hongbao Dai** and Haitao Zhang***

*School of Resources and Civil Engineering, Suzhou University, Suzhou, Anhui 234000, China
**School of Environment and Surveying Engineering, Suzhou University, Suzhou, Anhui 234000, China
***National Engineering Research Centre of Coal Mine Water Hazard Controlling, Suzhou, Anhui 234000, China
****Key Laboratory of Mine Water Resources Utilization, Suzhou, Anhui 234000, China
†Corresponding author: Jie Ma; ahszumajie@163.com

**Nat. Env. & Poll. Tech.**
**Website: www.neptjournal.com**

*Received:* 09-12-2019
*Revised:* 23-1-2020
*Accepted:* 28-03-2020

**Key Words:**
Rock-water interaction
Carbonate dissolution
Silicate weathering
Ion exchange
Irrigation suitability

## ABSTRACT

Jiagou district, located in Northern Anhui Province, China, has been taken as an agriculture demonstration base for several decades, but limited hydrochemical work has been conducted on the water resources. The objective of this research was to understand the controlling processes of hydrochemical evolution and the water quality for drinking and irrigation. Twenty-seven samples of surface water and groundwater have been collected and analysed for major ions. Although the values physicochemical parameters are subjected of spatial fluctuation in different water resources, calcium and bicarbonate is still the dominant ion in the cations and anions, respectively. The values of all the parameters are within the WHO maximum permissible limit for inhabitant drinking. The predominant water type is Ca-Mg-$HCO_3$ and Ca-$HCO_3$. The hydrochemical methods (Gibbs diagram, Mg/Na and $HCO_3$/Na versus Ca/Na diagram and ion ratios) suggest that rock-water interactions furnish the dominant major ion sources of the samples. Carbonate dissolution, silicate weathering and ion exchange have the predominant contribution to the origin of chemical solutes, as well as a slight function of halite dissolution. The USSL and Wilcox diagram reveal that all the samples have low salinity and low sodium water. It is of good quality suitable for irrigation, and it can be used for irrigation of most crops on most soils with less negative impacts.

## INTRODUCTION

The global common and thorny issue of water shortage and pollution has restricted the development of social and regional economic development (Jaeger et al. 2013, Hanasaki et al. 2013). The concentration and form of chemical compositions have a significant influence on the water quantity and quality, and also play an important role to ensure ecological environment and regional economic development (Ayadi et al. 2018). As the increasing utilization of water resources for life, agriculture and ecosystems, etc., a series of geological environmental problems, such as water scarcity, land subsidence, sea encroachment and soil salinization have been induced and the geo-environment deterioration was irreparable (Melloul & Goldenberg 1998, Andaryani et al. 2019, Xie et al. 2019).

Acting as the carrier and link during the water-rock interaction, water with abundant solutes generally can be considered as a remarkable indicator to explain the change of environment. Hence, identifying hydrochemical characteristics is an effective tool to assess the mechanism of controlling water chemistry and discuss the origin of ions. Meanwhile, the content of solute compositions can be employed to evaluate the suitability for irrigation.

The study area named Jiagou district is one of the most important agriculture bases in Northern Anhui Province. Local water resources have been used for resident drinking, agriculture irrigation and small-scale industries for a long time. It is widely known for high-quality fruit and vegetable products and agriculture products. Especially, Jiagou aromatic rice is the most famous local product and ever paid as tribute to royalty during the period of the Qing Dynasty (A.D. 1796-1820). But long-term pumping and inconsiderate exploitation of water resources, coupled with the planting of agriculture products, inevitably have led to the degradation of soil and water quality. However, no systematic and profound

researches on the hydrochemical characteristics and water quality assessment have been performed in the study region (Zhang et al. 2010).

Therefore, to understand the controlling processes of hydrochemical evolution and the water quality for drinking and irrigation, the present study initiated to describe the hydrochemical characteristics and illustrate the source of water for proposing the valuable information of the water quality status of the various water source. It can also contribute to the sustainable development of irrigation as well as effective management of water resources in this region.

## GEOLOGICAL AND HYDROLOGICAL CONTEXT

The study area, belonging to Huaibei plain, form a part of Suzhou city, Anhui Province and is located between latitudes 3391°' and 3396°' and longitudes 11700°' and 11707°' (Fig. 1). This region is characterized by a semi-humid monsoon climate, with annual average precipitation, evaporation and temperature as 866.1 mm, 988.0 mm and 14.5 , respectively. The overall terrain is mainly plain, topographic variation trend is that northwestern is higher than southeastern, and several mountains are scattered in the central section.

Geologically, the regional stratigraphic development includes Qingbaikou, Cambrian and Quaternary system, with the dominant distribution in NNE direction. The geological features are described as follows: (1) Qingbaikou system is chiefly characterized by limy dolomite and shaly sand. (2) Cambrian system is mostly constituted by limestone, marl, silty shale and arkosic quartz siltstone. (3) The quaternary system is mainly composed of unconsolidated silty clay, silty sand and fine sand.

Hydrogeologically, local water sources can be categorized into two types, including surface water (spring water and reservoir water) and groundwater. In terms of lithology and buried condition, the groundwater aquifer can be classified into two types, consisting of carbonate fractured aquifer and loose pored aquifer. Owing to a huge recharge area and the short distance supply-drainage condition, the water quantity of each aquifer is abundant with single well yield of 1000-5000 $m^3/d$, which is extensively utilized for agriculture product and resident use (Wang & Ma 2005). Meanwhile, the spring water and the reservoir water are employed for scenic landscape, irrigation and drinking water supply. Regardless of the water source, all of the water bodies have inherent features with nature pollution-free and 17 species minerals and trace elements. Consequently, Jiagou aromatic rice nourished by this excellent water resource is applauded for delicate fragrance, sweet and pure taste. On account of the superiority of the high content of protein and lysine, nowadays, it still has wide appeal and exports abroad in great demand.

## SAMPLING AND METHODS

The sampling campaign was carried out from June to October 2017. Surface water and groundwater samples were collected from different water bodies at multi-sampling points in Jiagou district, northern Anhui province, China (Fig. 1). Four spring samples, eighteen reservoir samples and five groundwater samples, marked as SW, RW and GW, respectively, were obtained for hydrochemical analysis.

Electrical conductivity (EC), total dissolved solids (TDS) and pH were directly measured in situ using portable pH, TDS, and EC meters at each sampling site. Preservation and transportation of the samples followed the standard methods.

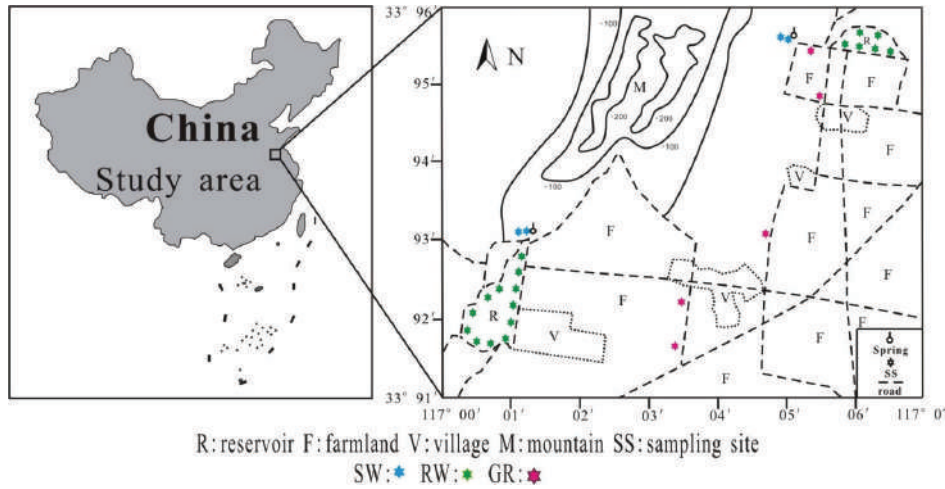


Fig. 1: Location of the study area and sampling sites.

The measurement of the parameters, which include calcium ($Ca^{2+}$), magnesium ($Mg^{2+}$), sodium ($Na^{+}$), potassium ($K^{+}$), chloride ($Cl^{-}$), sulphate ($SO_4^{2-}$) and bicarbonate ($HCO_3^{-}$) was conducted in the National Engineering Research Centre of Coal Mine Water Hazard Controlling, China. Major cations ($Ca^{2+}$, $Mg^{2+}$, $Na^{+}$ and $K^{+}$) were determined using the DIONEX-600 ion chromatography, and anions ($Cl^{-}$ and $SO_4^{2-}$) were analysed by the DIONEX-900 ion chromatography while $HCO_3^{-}$ was analysed by acid-base titration. All concentrations of the parameters are expressed in mg/L, except pH and EC.

Descriptive statistics were completed using Mystat 12.0 software. Piper, Gibbs and some traditional hydrochemical diagrams were conducted to elucidate the dominant factors and processes controlling the chemical characteristics. Drinking water quality was evaluated as per World Health Organization (WHO 1997). Irrigation suitability was evaluated using the USSL and Wilcox diagram.

## RESULTS AND DISCUSSION

### Major Ion Concentrations and Drinking Water Quality

Physicochemical characteristics of water sources are summarized in Table 1. As can be seen from Table 1, most of the coefficient of variations are less than 0.5, indicating that the majority of chemical constituents perform a low-medium spatial fluctuation. pH value of all the samples varies between 7.02 and 8.13, indicating a neutral to slightly alkaline conditions. TDS contents of spring water, reservoir water and groundwater range from 166.00 to 274.00, 94.00 to 167.00 and 149.00 to 262.00 mg/L, with an average concentration of 219.50, 129.61 and 216.00 mg/L, respectively. In-situ measured EC values (μS/cm) of spring samples, reservoir samples, and groundwater samples were in the range of 554.00 to 664.00, 296.00 to 515.00 and 512.00 to 699.00, with a mean value of 609.25, 365.11 and 571.20, respectively. It shows that the TDS, EC and pH values of samples are all within the maximum desirable limit according to WHO standard, indicating that the quality of all the water sources can meet the demand for inhabitant and suitable for drinking.

Among the cations of spring samples, the concentrations of $Ca^{2+}$, $Mg^{2+}$, $Na^{+}$ and $K^{+}$ range from 85.79 to 104.81, 13.80 to 16.20, 5.80 to 6.78, 0.60 to 1.62 mg/L, with an average value of 96.10, 14.98, 6.34 and 0.96 mg/L, respectively. Among the anions, the contents of $HCO_3^{-}$, $SO_4^{2-}$ and $Cl^{-}$ vary between 365.10 and 398.32, 23.19 and 26.82, 12.04 and 14.92 mg/L, with a mean of 388.46, 24.97 and 13.59 mg/L, respectively. As shown in the reservoir samples, the concentration of $Ca^{2+}$, $Mg^{2+}$, $Na^{+}$ and $K^{+}$ is ranging from 38.12 to 77.38, 11.70 to 15.31, 4.85 to 5.89, 0.81 to 2.18 mg/L, with an average concentration of 50.92, 13.63, 5.21 and 1.24 mg/L, respectively. While for the anions, the average concentration of $HCO_3^{-}$, $SO_4^{2-}$ and $Cl^{-}$ in the reservoir samples is 227.02, 24.66 and 9.61 mg/L, respectively. The concentrations of $Ca^{2+}$, $Mg^{2+}$, $Na^{+}$ and $K^{+}$ ions in groundwater samples vary from 80.28 to 104.91, 9.35 to 15.78, 4.53 to 9.95 and 0.57 to 0.74 mg/L, with a mean value of 88.46, 13.10, 7.27 and 0.64, respectively. As to the anions, the values of $HCO_3^{-}$, $SO_4^{2-}$ and $Cl^{-}$ vary in the range from 296.12 to 395.62, 17.99 to 29.91 and 7.05 to 17.78, with an average concentration of 342.84, 22.91 and 12.63, respectively. Apart from some calcium contents of the samples are between the maximum desirable limit and the maximum permissible limit described by WHO standard, the concentrations of other major ions are within the maximum desirable limit, which indicates that all the water sources are properly suitable for drinking. In view of the lower content of potassium and inherent homology between sodium and potassium, $Na^{+}$ and $K^{+}$ are merged into $Na^{+}$ in the following discussion.

Table 1: Summary statistics for concentrations of physicochemical parameters.

| Parameters | | $Ca^{2+}$ (mg/L) | $Mg^{2+}$ (mg/L) | $Na^{+}$ (mg/L) | $K^{+}$ (mg/L) | $HCO_3^{-}$ (mg/L) | $SO_4^{2-}$ (mg/L) | $Cl^{-}$ (mg/L) | TDS (mg/L) | EC (μS/cm) | pH |
|---|---|---|---|---|---|---|---|---|---|---|---|
| SW | Min | 85.79 | 13.80 | 5.80 | 0.60 | 365.10 | 23.19 | 12.04 | 166.00 | 554.00 | 7.02 |
| | Max | 104.81 | 16.20 | 6.78 | 1.62 | 398.32 | 26.82 | 14.92 | 274.00 | 664.00 | 7.27 |
| | Mean | 96.10 | 14.98 | 6.34 | 0.96 | 388.46 | 24.97 | 13.59 | 219.50 | 609.25 | 7.15 |
| | CV (%) | 8.40 | 9.00 | 7.20 | 47.60 | 4.10 | 7.00 | 10.90 | 27.60 | 10.20 | 1.90 |
| RW | Min | 38.12 | 11.70 | 4.85 | 0.81 | 156.09 | 19.61 | 6.41 | 94.00 | 296.00 | 7.49 |
| | Max | 77.38 | 15.31 | 5.89 | 2.18 | 291.91 | 30.80 | 19.44 | 167.00 | 515.00 | 8.13 |
| | Mean | 50.92 | 13.63 | 5.21 | 1.24 | 227.02 | 24.66 | 9.61 | 129.61 | 365.11 | 7.88 |
| | CV (%) | 20.50 | 9.20 | 5.00 | 36.20 | 16.10 | 11.80 | 45.20 | 20.80 | 15.60 | 2.90 |
| GW | Min | 80.28 | 9.35 | 4.53 | 0.57 | 296.12 | 17.99 | 7.05 | 149.00 | 512.00 | 7.10 |
| | Max | 104.91 | 15.78 | 9.95 | 0.74 | 395.62 | 29.91 | 17.78 | 262.00 | 699.00 | 7.20 |
| | Mean | 88.46 | 13.10 | 7.27 | 0.64 | 342.84 | 22.91 | 12.63 | 216.00 | 571.20 | 7.15 |
| | CV (%) | 11.20 | 21.00 | 34.90 | 9.80 | 12.60 | 19.00 | 37.30 | 24.50 | 13.50 | 0.70 |
| WHO 1997) | MDL | 75 | 30 | 50 | 100 | 200 | 200 | 250 | 500 | 750 | 7.0-8.5 |
| | MPL | 200 | 150 | 200 | 200 | 600 | 600 | 600 | 1500 | 1500 | 6.5-9.2 |

SW, RW, GW, MDL and MPL represent spring samples, reservoir samples, groundwater samples, the maximum desirable limit and the maximum permissible limit, respectively.

## Hydrochemical Facies

The hydrochemical facies were carried out using the Piper diagram (Fig. 2). According to the relative contents of each major ion, two main chemical types of the water sources have been identified: (1) Ca-$HCO_3$ (7 samples) and (2) Ca-Mg-$HCO_3$ (20 samples). The Ca-$HCO_3$ water types account for 75%, 5% and 60% of the spring samples, reservoir samples and groundwater samples, respectively. The Ca-Mg-$HCO_3$ types account for 25%, 95% and 40%, respectively.

Composition changes and hydrochemical characterization of the major ions can be described by the chemical ternary diagram (Palmer & Edmond 1992, Hou et al. 2009). On a ternary cation diagram, the plots falling towards $Na^+$ and $Ca^{2+}$-$Mg^{2+}$ manifest the dissolution of evaporite and carbonate, respectively. Similarly, on a ternary anion diagram, the plots falling towards $HCO_3^-$ and $Cl^-$+$SO_4^{2-}$ indicate the dissolution of carbonate and evaporite, respectively. In Fig. 2a and 2b, most of cation and anion plots fall towards $Ca^{2+}$ end-member and $HCO_3^-$ end-member, respectively, suggesting that carbonate dissolution are the dominant water-rock interactions with a relatively minor contribution from other reactions, such as silicate rocks, etc. It can properly prove that the flowing formation lithology of the watershed is mainly carbonate rocks.

## Mechanism and Processes Regulating Hydrochemistry

To ascertain the sources of dissolved chemistry components, Gibbs proposed two semi-log diagrams known as Gibbs diagrams of TDS versus Na/(Na+Ca) and TDS versus Cl/(Cl+$HCO_3$) to elucidate three major natural mechanisms controlling water chemistry: atmospheric precipitation, rock dominance, and the evaporation (Gibbs 1970). The distribution of sample plots (Fig. 3) showed that the ratios plotted in the rock dominance zone, suggesting the dominant influence is related to water-rock interaction, such as mineral weathering and dissolution.

The plots of Mg/Na and $HCO_3$/Na versus Ca/Na can be further used to identify the source of solutes during water-rock interaction: carbonate dissolution, silicate weathering and evaporation dissolution (Nagaraju et al. 2018). As can be seen in Fig. 4, the ratios of Mg/Na, $HCO_3$/Na and Ca/Na range from 1.46 to 2.59, 8.29 to 25.96, 3.18 to 10.5, respectively, reflecting that carbonate dissolution and silicate weathering are the main functions in the hydrochemistry evolution.

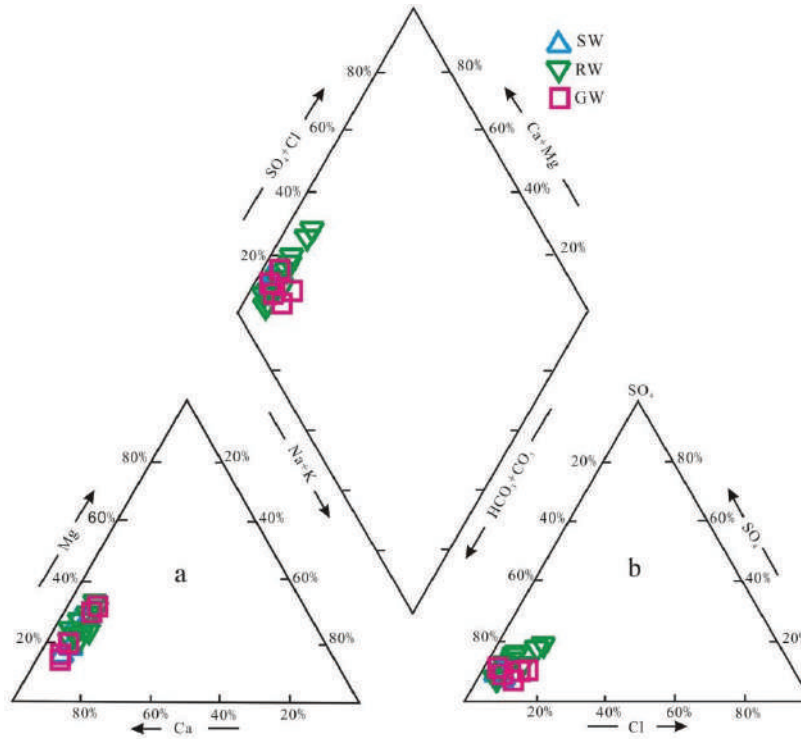


Fig. 2: Piper diagram for hydrochemical facies classification.

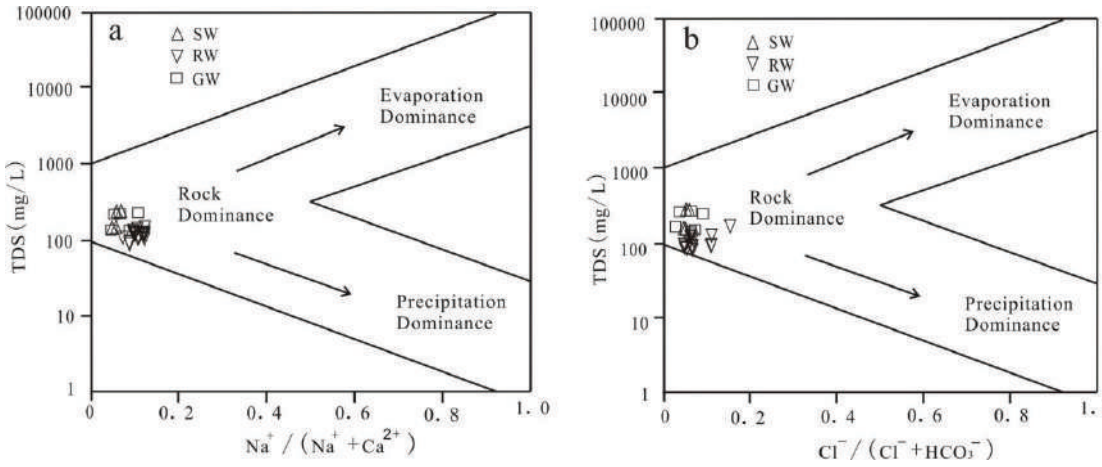


Fig. 3: Gibbs plots of TDS values versus $Na^+/(Na^+ + Ca^{2+})$ (a), TDS values versus $Cl^-/(Cl^- + HCO_3)$ (b).

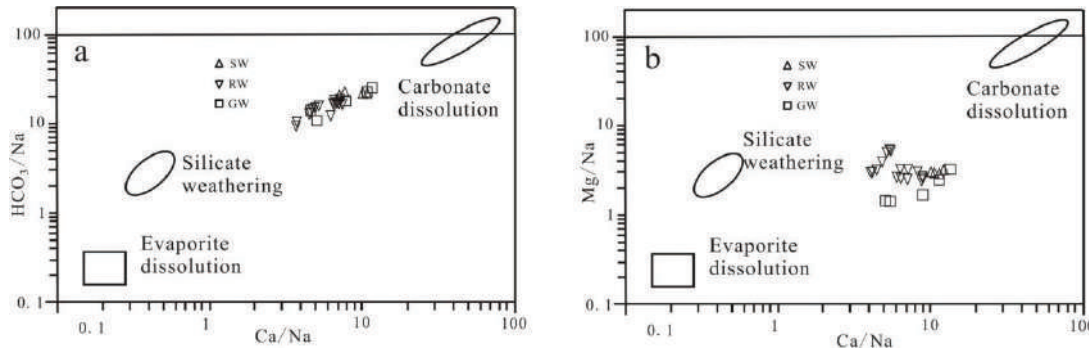


Fig. 4: $Na^+$ normalized $Ca^{2+}$-$HCO_3^-$ (a) and $Ca^{2+}$-$Mg^{2+}$ (b) plots.

## The Origin of Solutes

The ratio of Na/Cl has been proposed to identify the origin of $Na^+$ and Cl. If $Na^+$ and $Cl^-$ are mainly from the dissolution of halite, the expected ratio will be 1:1. Values exceeding 1 indicate the dissolution of silicate minerals and wastewater, whereas values much lower than 1 show the dissolution of carbonate minerals and ion exchange (Jalali 2005, Sun & Gui 2014). Local government has implemented strict laws and enforcement to protect the farmland under the pollution-free environment. So based on this actual condition, sodium and chlorine cannot be originated from the anthropogenic activities. As can be seen in Table 1, compared to the content of $Ca^{2+}$ and $HCO_3^-$, $Na^+$ and $Cl^-$ show a low to medium concentration, indicating the watershed undergone play a slight reaction of the dissolution of halite. Meanwhile, all the spring samples in Fig. 5a shows the excess of $Cl^-$ relative to $Na^+$, this feature suggest that apart from the dissolution of halite, the carbonate dissolution and/or ion exchange also occurred during the water-rock interaction. The plots of RW and GW deviated from the 1:1 relation can be explained by the interactions of water-rock, such as the weathering of silicate and the dissolution of carbonate and/or ion exchange.

As can be seen in Fig. 5b, the scatter plots of calcium and sulphate shows that all the samples deviate from the 1:1 line, indicating another source of calcium, which may be accounted for the process of cation exchange.

The plots of $(Ca^{2+}+Mg^{2+})$ versus $(HCO_3^-+SO_4^{2-})$ were used to illustrate the solute origin of $Ca^{2+}$, $Mg^{2+}$, $SO_4^{2-}$ and $HCO_3^-$, which are acquired from the simple dissolution of calcite, dolomite and gypsum with the expected ratio of 1:1. Points fall below the equiline, indicating the effect of silicate minerals weathering. Points fall above the equiline, implying the effect of carbonate minerals dissolution. In Fig. 5c, except for one groundwater sample, other points all fall around and below the equiline, reflecting the dominant water-rock interactions are the weathering of silicate minerals and the dissolution of calcite, dolomite and gypsum.

Dissolution of undesirable constituents in aquifer system cannot be controlled, but it is essential to understand the changes undergone by water during the runoff and infiltration. According to Schoeller (1977), ion exchange can be inferred by analysing the chloro-alkaline indices.

$$CA\text{-}I = [Cl^- - (Na^+ + K^+)] / Cl^-$$

$$CA\text{-}II = [Cl^- - (Na^+ + K^+)] / (SO_4^{2-} + CO_3^{2-} + HCO_3^-)$$

Positive values of CA indices indicate that $Na^+$ and $K^+$ in the water are exchanged with Mg and/or Ca in the host rocks, whereas negative values indicate there is a reverse cation exchange. As can be seen in Fig. 6, all the spring samples show positive chloro-alkaline values, 33% of the reservoir samples are positive and 67% negative, 20% of the groundwater samples are positive and 80% negative, respectively, which confirm that ion exchanges have an important

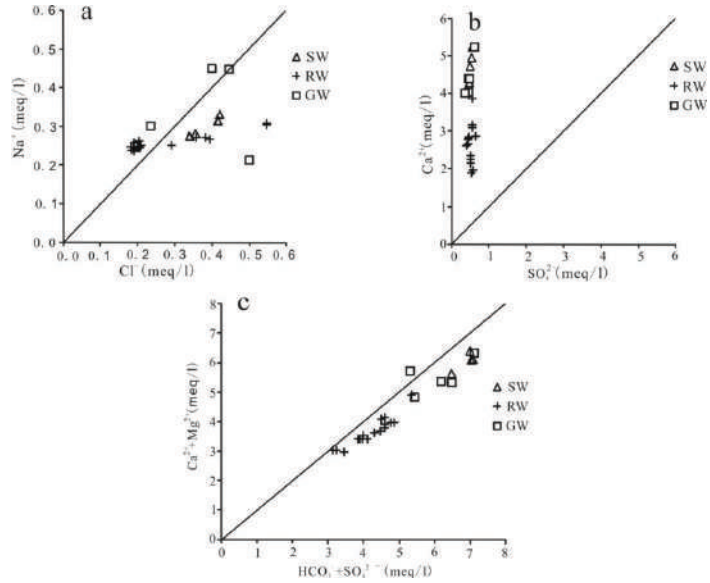


Fig. 5: Relationship between cations and anions of the samples in the study area.

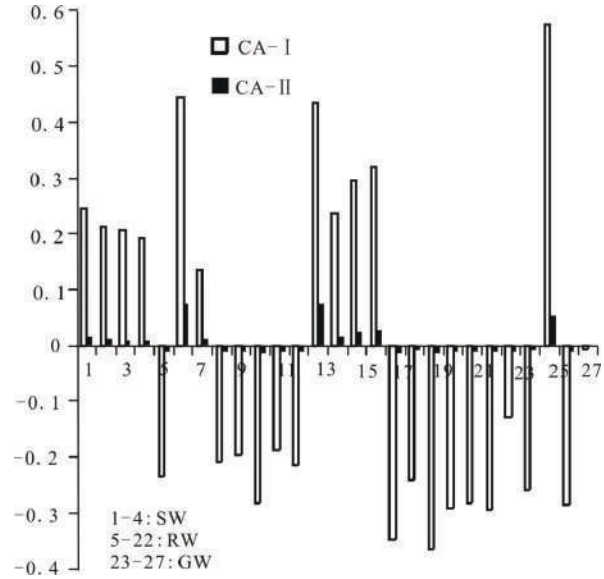


Fig. 6: Chloro-alkaline indices of the samples in the study area.

contribution to hydrochemical components.

## Irrigation Water Quality

As to evaluate the irrigation suitability, it is necessary to determine the parameters in terms of salinity and sodium hazard. Sodium adsorption ratio (SAR), sodium percentage (%Na) and electrical conductivity (EC) are the important parameters to assess the water quality for irrigation. The notable problem with a high sodium concentration is leading to degradation of soil structure and decreases on soil permeability. Regardless of the sodium content, samples with the EC less than 200 μS $cm^{-1}$ promotes soil crusting and reduces water penetration (Zaman et al. 2018).

In the study area, variation in EC was observed with the minimum value of 296.00 μS $cm^{-1}$ and the maximum value of 699.00 μS $cm^{-1}$. According to Wilcox classification (Kaur et al. 2017), all the water samples belonged to the good class for irrigation. The values of SAR were in the range from 0.14 to 0.28, according to Richards classification, 100% of the samples can be classified to excellent for irrigation. The

Table 2: Classification of samples for irrigation purposes.

| Parameters | Range | Classification | Number of samples | | |
|---|---|---|---|---|---|
| | | | SW | RW | GW |
| Salinity hazard (EC) | <250 | Excellent | 0 | 0 | 0 |
| | 250-750 | Good | 4 | 18 | 5 |
| | 750-2250 | Permissible | 0 | 0 | 0 |
| | 2250-3000 | Doubtful | 0 | 0 | 0 |
| | >3000 | Unsuitable | 0 | 0 | 0 |
| Sodium hazard (SAR) (Richard 1954) | <10 | Excellent | 4 | 18 | 5 |
| | 10-18 | Good | 0 | 0 | 0 |
| | 18-26 | Doubtful | 0 | 0 | 0 |
| | >26 | Unsuitable | 0 | 0 | 0 |
| Percent sodium (%Na) (Wilcox 1955) | <20 | Excellent | 4 | 18 | 5 |
| | 20-40 | Good | 0 | 0 | 0 |
| | 40-60 | Permissible | 0 | 0 | 0 |
| | 60-80 | Doubtful | 0 | 0 | 0 |
| | >80 | Unsuitable | 0 | 0 | 0 |

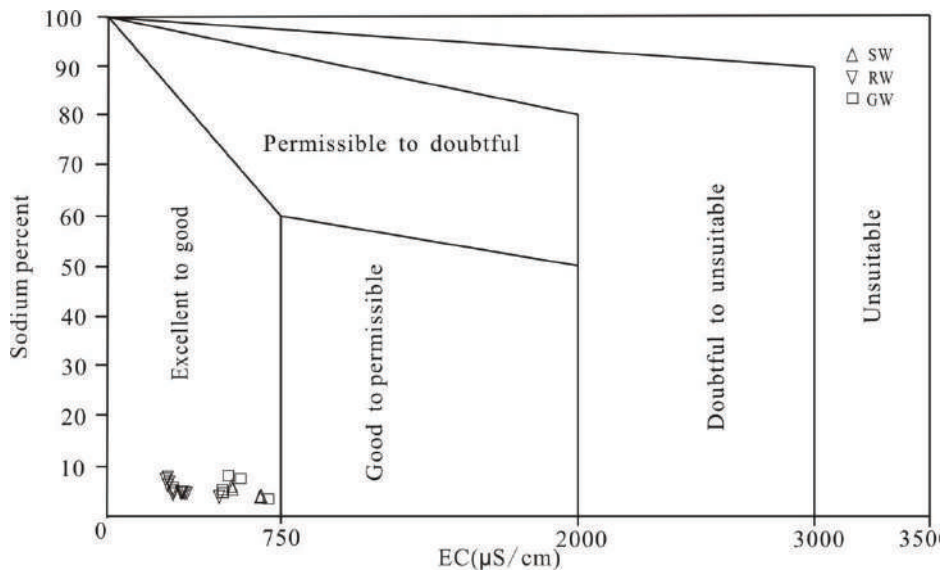


Fig. 7: Water classification based on per cent sodium and electrical conductivity (after Wilcox 1955).

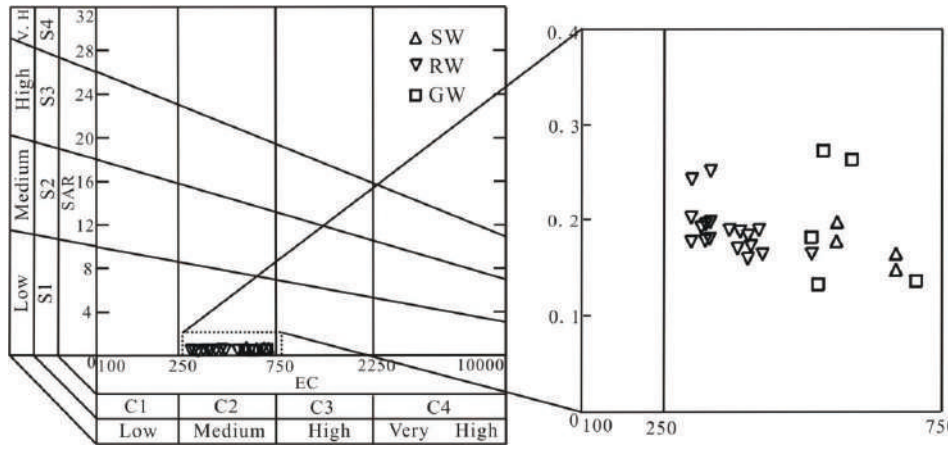


Fig. 8: Water classification based on the USSL diagram.

values of %Na varied from 3.8% to 9.2%, indicating all the samples had excellent suitability for irrigation (Table 2).

The general suitability categorization of waters for irrigation was evaluated using USSL and Wilcox diagram (Etteieb et al. 2017, Zouahri et al. 2015, Bhardwaj & Singh 2011). Wilcox proposed %Na and EC to assess the water quality using Wilcox diagram (Fig. 7). The scatter plots on Wilcox diagram illustrates that all the samples fall in excellent to good categories and can be properly used for irrigation. The USSL Staff presented SAR and EC to evaluate irrigation using USSL diagram (Fig. 8). The plots of data on the US salinity diagram show that all of the water samples fall in the category C2S1, indicating low sodium and medium salinity water. It can be used for irrigation of most crops on most soils with less negative impacts.

## CONCLUSIONS

The hydrochemical analysis of surface water and groundwater from Jiagou district, Northern Anhui Province, China reveals that the processes of water-rock interaction and suitability for irrigation. All the parameters concentration can meet the demand for inhabitant and suitable for drinking. Two main chemical types of the water sources have been identified: (1) Ca-$HCO_3$ (7 samples) and (2) Ca-Mg-$HCO_3$ (20 samples). Gibbs diagram suggests that the dominant influence is related to water-rock interaction. The plots of Mg/Na and $HCO_3$/Na versus Ca/Na, and the ion ratio of Na/Cl, $Ca^{2+}$/$SO_4^{2-}$, ($Ca^{2+}$+$Mg^{2+}$) /($HCO_3^-$+$SO_4^{2-}$) reflect that carbonate dissolution, silicate weathering have the predominant contribution to the origin of chemical solutes, with a slight function of halite dissolution. Meanwhile, ion exchange has an important contribution to hydrochemical components. Wilcox diagram illustrates that all the samples fall in excellent to good categories and the US salinity diagram show that all of the water samples fall in the category C2S1, indicating low sodium and medium salinity water. It is concluded that all the samples are suitable for drinking and irrigation purpose.

## ACKNOWLEDGEMENTS

This work was supported by the Natural Science Foundation of Anhui Province Education Department (NO. KJ2019A0667, KJ2019A0676 and KJ2019A0677), the Excellent Top-notch Talents Cultivation Foundation of Colleges and Universities, Anhui Province, China (gxbjZD2020091, gxgnfx2020106 and gxgnfx2020107) and the Key Science Project of Suzhou University (NO. 2019yzd01 and 2016ykf02).

## REFERENCES

Andaryani, S., Nourani, V., Trolle, D., Dehghani, M. and Asl, A.M. 2019. Assessment of land use and climate change effects on land subsidence using a hydrological model and radar technique. Journal of Hydrology, 578: 1-14.

Ayadi, Y., Mokadem, N., Besser, H., Redhaounia, B., Khelifi, F., Harabi, S., Nasri, T. and Hamed, Y. 2018. Statistical and geochemical assessment of groundwater quality in Teboursouk area (Northwestern Tunisian Atlas). Environmental Earth Sciences, 77: 349-368.

Bhardwaj, V. and Singh, D.S. 2011. Surface and groundwater quality characterization of Deoria district, Ganga plain, India. Environmental Earth Sciences, 63(2): 383-395.

Etteieb, S., Cherif, S. and Tarhouni, J. 2017. Hydrochemical assessment of water quality for irrigation: A case study of the Medjerda river in Tunisia. Applied Water Science, 7(1): 469-480.

Gibbs, R. J. 1970. Mechanisms controlling world's water chemistry. Science, 170: 1088-1090.

Hanasaki, N., Fujimori, S., Yamamoto, T., Yoshikawa, S., Masaki, Y., Hijioka, Y., Kainuma, M., Kanamori, Y., Masui, T., Takahashi, K. and Kanae, S. 2013. A global water scarcity assessment under shared socio-economic pathways-part 2: Water availability and scarcity. Hydrology and Earth System Sciences, 17(7): 2393-2413.

Hou, S.H., Xu, H. and An, Z.S. 2009. Major ion chemistry of waters in lake

Qinghai catchment and the possible controls. Earth and Environment, 37(1): 11-19. in Chinese.

Jaeger, W.K., Plantinga, A.J., Chang, H., Dello, K., Grant, G., Hulse, D., McDonnell, J.J., Lancaster, S., Moradkhani, H., Morzillo, A.T., Mote, P., Nolin, A., Santelmann. and Wu, J. 2013. Toward a formal definition of water scarcity in natural-human systems. Water Resources Research, 49(7): 4506-4517.

Jalali, M. 2005. Major ion chemistry of groundwaters in the Bahar area, Hamdam, western Iran. Environmental Geology, 47(6): 763-772.

Kaur, T., Bhardwaj, R. and Arora, S. 2017. Assessment of groundwater quality for drinking and irrigation purposes using hydrochemical studies in Malwa region, southwestern part of Punjab, India. Applied Water Science, 7(6): 3301-3316.

Melloul, A.J. and Goldenberg, L.C. 1998. Early-indicator signals of groundwater contamination: The case of seawater encroachment. Environmental Geology, 33(4): 279-288.

Nagaraju, A., Balaji, E., Sun, L.H. and Thejaswi, A. 2018. Processes controlling groundwater chemistry from Mulakalacheruvu area, Chittoor district, Andhra Pradesh, South India: a statistical approach based on hydrochemistry. Journal of the Geological Society of India, 91(4): 425-430.

Palmer, M.R. and Edmond, J.M. 1992. Controls over the strontium isotope composition of river water. Geochimica et Cosmochimica Acta, 56(5): 2099-2111.

Schoeller, H. 1977. Geochemistry of groundwater. An international guide for research and practice. UNESCO, 15: 1-18.

Sun, L.H. and Gui, H.R. 2014. Chemical and isotopic characteristics of groundwater from deep sandstone aquifer in northern Anhui Province, China: a case study. Asian Journal of Chemistry, 26(7): 1983-1987.

Wang, Z.L. and Ma, Q. 2005. Study on evaluation and utilization of karstic water resources in Jiagou-Fuliji water source site in the area to the north of Huai river. Groundwater, 27(5): 367-368, 387. in Chinese.

WHO, 1997. Guidelines For Drinking-Water Quality, Vol 1, Recommendations. World Health Organisation, Geneva.

Xie, X.F., Pu, L.J., Zhu, M., Xu, Y. and Wang, X.H. 2019. Linkage between soil salinization indicators and physicochemical properties in a long-term intensive agricultural coastal reclamation area, Eastern China. Journal of Soil and Sediment, 19(11): 3699-3707.

Zaman, M., Shahid, S.A. and Heng, L. 2018. Guideline for Salinity Assessment, Mitigation and Adaptation Using Nuclear and Related Techniques. Springer, Cham., pp. 113-131.

Zhang, C.L., Wang, Y.L. and Yuan, X.T. 2010. Study on soil and water quality of aromatic rice habitation Jiagou of Suzhou city. Journal of Suzhou University, 25(11): 48-50. in Chinese.

Zouahri, A., Dakak, H., Douaik, A., Khadir, M.E. and Moussadek, R. 2015. Evaluation of groundwater suitability for irrigation in the Skhirat region, northwest of Morocco. Environmental Monitoring and Assessment, 187(1): 4184-4198.

Nature Environment and Pollution Technology
An International Quarterly Scientific Journal

p-ISSN: 0972-6268
(Print copies up to 2016)
e-ISSN: 2395-3454

Vol. 19 | No. 4 | pp. 1723-1727 | 2020

Original Research Paper

https://doi.org/10.46488/NEPT.2020.v19i04.043

Open Access Journal

# Effectiveness of *Sagittaria lancifolia* as Detergent Phytoremediator

**H. Fitrihidajati†, F. Rachmadiarti, F. Khaleyla and E. Kustiyaningsih**
Department of Biology, Faculty of Mathematics and Natural Sciences, Universitas Negeri Surabaya Jl. Ketintang, Surabaya, East Java, Indonesia
†Corresponding author: H. Fitrihidajati; herlinafitrihidajati@unesa.ac.id

**Nat. Env. & Poll. Tech.**
**Website: www.neptjournal.com**

*Received:* 19-12-2019
*Revised:* 6-01-2020
*Accepted:* 30-03-2020

**Key Words:**
Phytoremediation
Detergent
*Sagittaria lancifolia*
Toxicity
*Xiphophorus maculatus*

## ABSTRACT

The extensive use of detergent causes a high level of it to contaminate water body. This study was aimed to determine the effectiveness of the *Sagittaria lancifolia* plant as a phytoremediator for water contaminated with detergents. *Sagittaria lancifolia* was planted in medium exposed to detergent at various levels (10, 50, 75 ppm) with two different detention times (7 and 14 days). Remediated water was tested of its toxicity using *Xiphophorus maculatus*. LAS removal rate, BOD, plant morphology, and mortality of *X. maculatus* were recorded. The result showed that *S. lancifolia* had a high level of LAS removal rate, the longer detention time (81.53 ± 0.37% at 14 days) with significantly lower BOD (27.48 ± 0.78mg/L). Plant leaves showed signs of necrosis and chlorosis during detergent exposure. Detergent water remediated for 14 days induced the lowest rate of mortality in *Xiphophorus maculatus*. Thus, *Sagittaria lancifolia* can be applied to remove the organic contaminant from the water body.

## INTRODUCTION

Water pollution is generally caused by anthropomorphic activities around water bodies. The higher human population leads to more waste disposed to the environment, causing pollution level to be increased. Waste can be originated from domestic or industrial activities. The domestic activities result in waste with high organic content. Without proper management, this type of waste can potentially contaminate water and endanger the aquatic organisms in ecosystems.

One of the causing factors of water pollution is detergent waste from domestic areas. Detergent is a soap compound formed through chemical processes. Generally, the main component composing detergent is natrium dodecyl benzene sulfonate (NaDBS) and sodium tripolyphosphate (STPP), both of which are difficult to be degraded naturally. NaDBS and STPP can form a precipitate with alkaline soil and transitional metals (Herlambang & Hendriyanto 2015). Surfactant types commonly used in detergent are anionic surfactant Alkyl Benzene Sulfonate (ABS) or Linear Alkylbenzene Sulfonate (LAS).

Detergent is a synthetic cleaner composed of petroleum derivative materials. Detergent is widely used due to its better cleaning ability compared to soap and not affected by water salinity. Generally, detergent contains surfactants, builders, fillers, and additives. Overuse of detergents can be dangerous to humans as it is a skin irritant. It can also endanger the environment; the decrease of water quality due to LAS affects the aquatic organisms living in it (Kamiswari 2013).

High level of detergent in water can lower oxygen level. At a concentration of 0.5 mg/L, detergent was found to form suds that inhibited oxygen diffusion to the water surface (Rochman 2016). Previous findings reported that average surfactant concentration in domestic wastewater could reach up to 10 mg/L (Scott & Jones 2000). The presence of excessive detergent is signified with soap foams on the water surface (Rochman 2009).

Phytoremediation is the application of plant to extract, accumulate, or detoxify pollutants. This technique is considered as a novel technique to cleanse the environment. Plants are ideal agent to improve land and water, because of their unique genetic properties, both form biochemical and physiological facets (Sidauruk & Sipayung 2015). The ability of aquatic plants to reduce water pollution has been studied extensively, including *Sagittaria lancifolia* (Melinda Paz-Alberto & Sigua 2013). *Sagittaria lancifolia* is a species of aquatic plants endemic to tropical regions, including Indonesia. A previous study found that this species was able to survive detergent-polluted water up to concentration 0.15 g/L (Adistiara et al. 2019) thus *S. lancifolia* was hypothesized to have potential in phytoremediation of detergent.

The safety of water after remediation using plants is rarely examined, whether it has become safe for water organisms or not. As fishes can show response to the presence

of pollutants in water, they can be used as a bioindicator of safe water. *Xiphophorus maculatus*, a species of tropical fish, was previously shown to have sensitivity towards contaminant potassium chloride (Santos Oliveira et al. 2018), but no previous study had examined the response of this species towards detergent. Thus, we examined the ability of *Sagittaria lancifolia* to remediate detergent-contaminated water and the safety of remediated water using *Xiphophorus maculatus* in this study.

## MATERIALS AND METHODS

This study was an experimental laboratory study. *Sagittaria lancifolia* used was taken from the original collection of Purwodadi Botanical Garden, Indonesia. The plants were acclimatized first for 14 days in an aquarium filled with 4 L of distilled water medium with additional nutrients. After that, plants were rinsed before put into the aquarium filled with 4 L aquatic planting medium added with various levels of detergent (10 ppm, 50 ppm, 75 ppm). Planting medium was first measured for its LAS level to ensure the detergent level. Control was planting medium without *S. lancifolia*. Each concentration of detergent was replicated thrice. Level of LAS was examined at two different detention times; 7 and 14 days. Water quality parameters like temperature and acidity were recorded at the end of the experiment.

Resulting water after phytoremediation using *S. lancifolia* was tested of its safety by performing toxicity test on *X. maculatus*. Fish sized ± 4-6 cm were first acclimatized in 10 L aquarium filled with 5 L water for three days. Fish were given commercial feed daily during acclimatization and then fasted for two days during the pre-treatment period. For treatment, as much as 10 fishes were put into a plastic container filled with 1.5 L water resulted from phytoremediation at various concentrations of the detergent. Each treatment was replicated three times. Mortality of fish was evaluated at 24 h, 48 h and 72 h.

Level of LAS removal and BOD were analysed statistically using one-way ANOVA and continued using the Duncan test. Leaf morphological change and fish mortality were analysed descriptively.

## RESULTS AND DISCUSSION

### Phytoremediation of the Detergent Using *Sagittaria lancifolia*

Results showed that *S. lancifolia* was able to remove LAS significantly compared to control (Table 1). Level of detergent in control did not change, but different initial detergent level resulted in significantly different LAS removal rate using *S. lancifolia*. The higher the detergent concentration at the start and the longer the detention time, the higher the rate of LAS removal by *S. lancifolia*. The temperature did not show much difference between phytoremediated and non-phytoremediated water, but pH was lowered slightly, from the range of 7 to 8 in phytoremediated water, both at 7 and 14 days detention time.

*Sagittaria lancifolia* was able to remove LAS from planting medium. At 75 ppm, *S. lancifolia* was able to

Table 1: Rate of LAS removal and BOD of detergent-contaminated water.

| Group | Detergent level (ppm) | LAS removal rate (%) | BOD (mg/L) |
|---|---|---|---|
| Control 7 days | 10 | $1.14 \pm 0.01^{a}$ | $29.37 \pm 0.38^{a}$ |
| | 50 | $1.27 \pm 0.02^{a}$ | $29.40 \pm 0.25^{a}$ |
| | 75 | $1.33 \pm 0.01^{a}$ | $29.57 \pm 0.16^{a}$ |
| Plant 7 days | 10 | $71.65 \pm 0.21^{b}$ | $26.90 \pm 0.69^{bc}$ |
| | 50 | $73.44 \pm 0.17^{c}$ | $28.08 \pm 0.42^{d}$ |
| | 75 | $77.43 \pm 0.85^{e}$ | $28.10 \pm 0.79^{d}$ |
| Control 14 days | 10 | $1.20 \pm 0.01^{a}$ | $29.22 \pm 0.15^{a}$ |
| | 50 | $1.61 \pm 0.01^{a}$ | $29.48 \pm 0.25^{a}$ |
| | 75 | $2.63 \pm 0.01^{a}$ | $29.60 \pm 0.44^{a}$ |
| Plant 14 days | 10 | $75.57 \pm 0.31^{d}$ | $25.55 \pm 0.94^{e}$ |
| | 50 | $76.53 \pm 0.56^{e}$ | $26.18 \pm 0.99^{be}$ |
| | 75 | $81.53 \pm 0.37^{f}$ | $27.48 \pm 0.78^{cd}$ |
| Standard* | | - | 100 |

(*) Standard based on Regulation of East Java Governor No. 72 year 2013.
Different letters indicated statistical difference based on Duncan test ($\alpha = 0.05$).

remove up to 77.43% of LAS at 7 days and 81.53% at 14 days of detention time. Similarly, BOD was also lowered significantly after using plants compared to control. LAS was taken from the medium by plant roots, which would then be translocated to the upper part of the plants (Grøn et al. 2000). Besides, LAS was also lowered through microorganism activity in roots of plants, which degraded LAS in the medium. Thus, a longer period of detention time, microorganisms could degrade the higher level of LAS, decreasing LAS in the medium. Aquatic plants also can effectively absorb various pollutants, such as heavy metals and organic contaminants, due to their hairy roots (Rachmadiati et al. 2018).

As LAS translocated to the upper part of the plant body, this resulted in alteration of plant organs. During the experiment period, morphological changes could also be observed from the leaves of *S. lancifolia.* Alteration of leaves morphology from 7 and 14 days course from 75 ppm detergent exposure is presented in Fig. 1.

The toxicity of LAS on *S. lancifolia* induced senescence to leaves, as indicated by chlorosis and necrosis. This change could be particularly clearly observed in 75 ppm detergent concentration. Leaf colour was turned from green to yellow to brown, while leaf surface was gradually shrivelled. LAS accumulation to leaf caused the change of lipid composition, resulting in lowered production of chlorophyll, plastoquinone, and carotenoid, as well as $NADP^+$ activity. This decrease would decrease electron transport to chloroplast and the disruption of the Calvin cycle, lowered metabolism and slowed plant growth (Sharma & Dubey 2005).

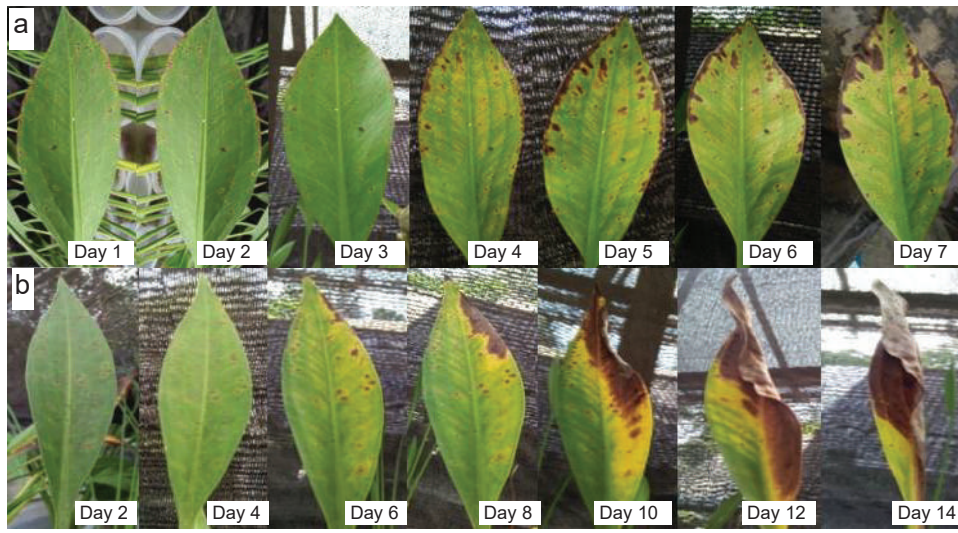


Fig. 1: Morphological change in *Sagittaria lancifolia* leaf during exposure to 75 ppm detergent for (a) 7 days and (b) 14 days.

Table 2: Mortality level of *X. maculate* in remediated detergent-contaminated water.

| Group | Detergent concentration (ppm) | Mortality (%) | | |
|---|---|---|---|---|
| | | 24 h | 48 h | 72 h |
| Control 7 days | 10 | 0 | 40 | 60 |
| | 50 | 0 | 60 | 40 |
| | 75 | 100 | 0 | 0 |
| Plant 7 days | 10 | 0 | 0 | 0 |
| | 50 | 0 | 20 | 0 |
| | 75 | 40 | 0 | 0 |
| Control 14 days | 10 | 0 | 40 | 60 |
| | 50 | 0 | 60 | 40 |
| | 75 | 100 | 0 | 0 |
| Plant 14 days | 10 | 0 | 0 | 0 |
| | 50 | 0 | 0 | 10 |
| | 75 | 0 | 20 | 0 |

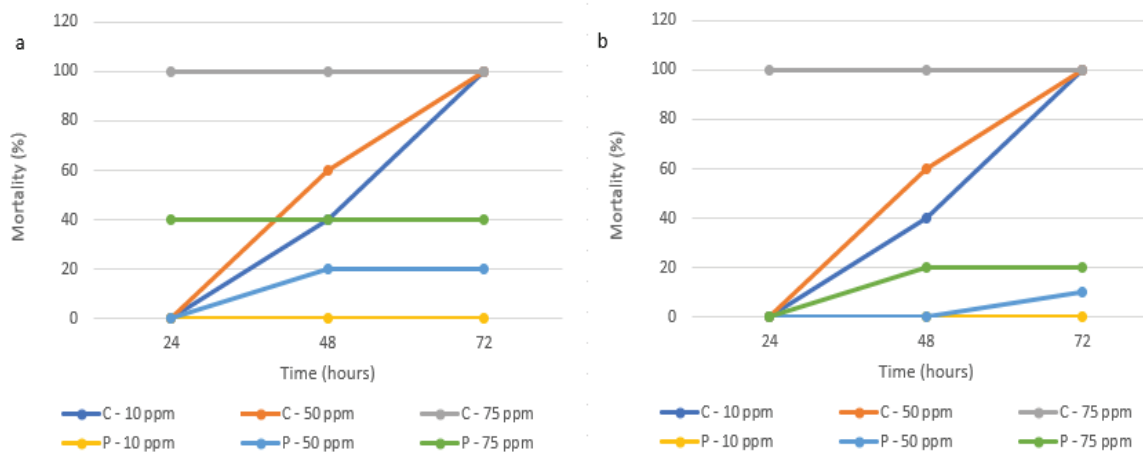


Fig. 2: Trends of *Xiphophorus maculatus* mortality in remediated water after (a) 7 days and (b) 14 days of detention time. C: control group, P: plants group.

### Toxicity Test of Remediated Water

Post-phytoremediation contaminated water was evaluated of its safety based on the mortality of *X. maculate*. Mortality level of *X. maculate* was varied based on the detergent level in the water and whether phytoremediation was performed or not. Level of *X. maculate* mortality in water after various treatments is presented in Table 2, while the trend of mortality is presented in Fig. 2.

*Xiphophorus maculatus* was found to have a higher mortality rate at the higher level of detergent concentration and shorter period of phytoremediation. Fish in control water had 100% mortality rate at 24 hours. Fish mortality in control water took longer time in the lower detergent concentration. This was in line with a previous study, in which 18 ppm detergent induced the mortality of *X. maculatus* longer than 54 ppm (Kamiswari et al. 2013).

In contrast with control, the mortality of *X. maculatus* was lower in water with phytoremediation of *S. lancifolia*. No mortality was found in 10 ppm detergent with phytoremediation for both 7 and 14 days. Contaminated water at initial detergent water of 75 ppm remediated for 7 days resulted in 40% mortality in the first 24 hours and no additional mortality during the next 48 hours. However, the same level of detergent remediated for 14 days resulted in 20% mortality at 48 hours and no additional mortality thereafter. This shows that the longer the phytoremediation period, the lower the detergent level remained in the water, as well as safer water.

Suds and foam caused by detergent could cause oxygen level in the water to reduce. This would in turn induce hypoxia in various water organisms, such as phytoplankton, aquatic plants and fishes. In fishes, hypoxia causes stress that disrupts physiological homeostasis, resulting in a complex process of physiological and biochemical changes to help fishes to cope with the stress. Hypoxia also affects nutrient metabolism (Abdel-Tawwab et al. 2019). When oxygen in water is below the level sufficient for aerobic glycolysis, fishes fail to maintain normal physiological function and metabolism (Richard 2011).

In addition to hypoxia, the surfactant can also induce stress if it enters fish metabolism. Fishes will mobilize triglycerides and protein to meet increased energy demand from stress-induced physiological changes and xenobiotic excretion (Alkahem et al. 1998). Behavioural abnormality can also indicate nervous impairment due to blocked nervous transmission, enzyme dysfunction, and/or disruption of the metabolic pathways (Siddiqui & Arifa, 2011). This change was found in the *X. maculatus* used in this study, as fish experienced stress from detergent. The failure to adapt to detergent-induced stress caused mortality to *X. maculatus*. Thus, this species could also be used as an indicator of organic pollutant.

## CONCLUSIONS

Based on the present study, it could be concluded that *Sagittaria lancifolia* has an ability of phytoremediation, as indicated by a high rate of LAS removal. At high concentration of detergent, phytoremediation for 14 days resulted in the lowest mortality. The plant could survive until detention time of 14 days, however, leaves showed signs of chlorosis and necrosis.

## REFERENCES

Alkahem, H.F., Ahmed, Z., Al-Akel, A.S. and Shansi, M.J.K. 1998. Toxicity bioassay and changes in haematological parameters of *Oreochromis niloticus* induced by trichloroform. Arab Gulf J. Sci. Res., 16: 581-585.

Abdel-Tawwab, M., Monier, M. N., Hoseinifar, S. H. and Faggio, C. 2019. Fish response to hypoxia stress: Growth, physiological, and immunological biomarkers. Fish Physiol. Biochem., 45: 997-1013.

Adistiara, V.Y., Kustiyaningsih, E. and Irawanto, R. 2019. Phytoremediation of domestic wastewater (detergent) with arrowhead and burhead plants in Purwodadi Botanic Garden. IOP Conference Series: Earth and Environmental Sciences. https://doi.org/10.1088/1755-1315/259/1/012002.

Grøn, C., Laturnus, F., Mortensen, G. K., Egsgaard, H., Samsøe-Petersen, L., Ambus, P. and Jensen, E. S. 2000. Plant uptake of LAS and DEHP from sludge amended soil. Persistent, Bioaccumulative, and Toxic Chemicals I: 99-111. https://doi.org/10.1021/bk-2001-0772.ch00.

Herlambang, P. and Hendriyanto, O. 2015. Fitoremediasi limbah deterjen menggunakan kayu apu (*Pistia stratiotes* L.) dan Genjer (*Limnocharis flava* L.) (In Indonesian). Jurnal Ilmiah Teknik Lingkungan, 7(2): 101-114.

Kamiswari, R., Thamrin, H. and Yuni, R. 2013. Pengaruh pemberian deterjen terhadap mortalitas ikan *Platy sp*. (In Indonesian). LenteraBio, 2(1).

Melinda Paz-Alberto, A. and Sigua, G.C. 2013. Phytoremediation: A green technology to remove environmental pollutants. Am. J. Clim. Change, 2: 71-86. https://doi.org/10.4236/ajcc.2013.21008.

Rachmadiati, F., Fitrihidajati, H., Purnomo, T., Yuliani, Y. and Wahyuningsih, D.A. 2018. *Azolla microphylla* and *Pistia stratiotes* as phytoremediators of Pb (Lead). Proceedings of the International Conference on Science and Technology (ICST 2018). https://doi.org/10.2991/icst-18.2018.20.

Richard, J.G. 2011. Physiological, behavioral and biochemical adaptations of intertidal fishes to hypoxia. J. Exp. Biol., 214: 191-199.

Rochman, F., Hamami, H. and Sapuan, I. 2016. Pembuatan IPAL limbah deterjen metode elektroflotasi skala pilot (In Indonesian). Jurnal Kimia Riset, 1(1): 58-67.

Rochman, F. 2009. Pembuatan IPAL mini untuk limbah deterjen domestik (In Indonesian). Jurnal Penelitian Eksakta, 8(2): 134-142.

Santos Oliveira, M., Faleiros, C. A., Brunetti, I. A., Garlich, N., Viana Da Silva, S. and DaCruz, C. 2018. Avaliação toxicológica do organofosforado triclorfon para o peixe *Xiphophorus maculatus* (Platy) utilizado como bioindicador. Congresso Brasileiro de Zootecnia. http://www.adaltech.com.br/anais/zootecnia2018/resumos/trab-1801.pdf

Sharma, P. and Dubey, R.S. 2005. Lead toxicity in plants. Brazilian Journal of Plant Physiology, 17: 1-19. http://dx.doi.org/10.1590/s1677-04202005000100004.

Sidauruk, L. and Sipayung, P. 2015. Fitoremediasi lahan tercemar di Kawasan industri Medan dengan tanaman hias (In Indonesian). Jurnal Pertanian Tropik, 2(2): 178-186.

Siddiqui, A. A. and Arifa, N. 2011. Toxicity of heavy metal copper and its effect on the behaviour of fresh water Indian cat fish, *Clarias batrachus* (Linn.). Current Biotica, 4(4): 405-411.

Scott, M.J. and Jones, M.C. 2000. The biodegradation of surfactants in the environment. BBA-Biomembranes, 1508(1-2): 235-251.

Nature Environment and Pollution Technology
An International Quarterly Scientific Journal

p-ISSN: 0972-6268
(Print copies up to 2016)
e-ISSN: 2395-3454

Vol. 19 | No. 4 | pp. 1729-1735 | 2020

Original Research Paper

https://doi.org/10.46488/NEPT.2020.v19i04.044

Open Access Journal

# Isolation of Fungi and Optimization of pH and Temperature for Cellulase Production

**Sheetal Barapatre†, Mansi Rastogi, Savita and Meenakshi Nandal**
Department of Environmental Sciences, Maharshi Dayanand University, Rohtak, Haryana, India
†Correspondence: Sheetal Barapatre; barapatresheetal26@gmail.com

**Nat. Env. & Poll. Tech.**
**Website: www.neptjournal.com**

*Received:* 01-02-2020
*Revised:* 21-02-2020
*Accepted:* 05-03-2020

**Key Words:**
*Aspergillus flavus*
Cellulase
Cellulose
FPase
Synergism

## ABSTRACT

The crystalline structure of cellulose makes it difficult to degrade and so most of the cellulosic waste in nature is disposed of by biomass burning. Cellulase enzyme system is potent enough to convert cellulose into glucose. Fungi are known to produce an array of hydrolytic enzymes. This study involves isolation of high potential cellulolytic fungal strains from the soil and optimizing pH and temperature conditions for enhanced cellulase production. The fungal strains were isolated from soil using serial dilution and pour plate techniques and screened using Congo red test and FPase method. Based on hydrolytic zones formation and cellulase enzyme production, *Aspergillus fumigatus, Aspergillus terreus* and *Aspergillus flavus* were found to show the highest potency for hydrolytic enzyme production at pH 5.8-6.0 and temperature range of 40°C-50°C.

## INTRODUCTION

Cellulose is a linear polysaccharide of glucose residues with β-1,4-glycosidic linkages. Copious availability of cellulose renders it a desirable raw material to produce imperative products for industrial use. Unfortunately, most of the cellulosic waste is often disposed of by biomass burning, which is not restricted to developing countries alone but is considered a global phenomenon. Cellulase enzyme system can convert cellulose to glucose economically and favourably. Cellulase enzyme system harbours three types of enzymes that are produced extracellularly: 1, 4-β-endoglucanase, 1, 4-β-exoglucanase, and β-glucosidase. Endoglucanase aids in the conversion of the crystalline cellulosic structure into a soluble polymer. While exoglucanase is responsible for cleavage of these polymers to produce tri and di-saccharides, β-glucosidase breaks these tri and di-saccharides to finally produce glucose (Shewale 1982, Woodward & Wiseman 1983). The synergistic effect of these three enzymes brings about this complex process effectively to produce glucose molecules (Ryu & Mandels 1980, Wood 1989, Samdhu & Bawa 1992). To make this possible, it is desirable to involve certain cellulase producing microorganisms (Béguin & Aubert 1994, Singh & Hayashi 1995, Lynd et al. 2002).

In-plant cell walls, cellulose is bound by lignin which makes it difficult to degrade the crystalline and complex structure of cellulose. Hence, there is a need to harness cellulase enzyme through economically feasible and effective techniques. Fungi are the most influential and dominant groups present in soils. They produce an array of hydrolytic enzymes and are more effective than bacteria in acidic soils and decomposing cellulose rooted in lignin. Fungi are filamentous and produce prolific spores. Therefore, they invade the substrate easily and are quite effective in composting of lignocellulosic waste. Also, they can stand a wide range of pH as compared to bacteria and hence are more preferred than bacteria for the decomposition of complex organic wastes. With regard to this, filamentous fungi are more appealing owing to their ease of cultivation and substantial yield of extracellular enzymes with significant prospective for industrial application (Mishra & Dadhich 2010). Also, these extracellularly produced enzymes are easily retrievable using the culture media (Abe et al. 2015). Other advantages associated with cellulase production through fungi include rapid enzyme production and the cost-benefit aspect.

Plants are capable of generating $4\times10^9$ tons of cellulose annually. Cellulases are mainly employed in the textile industry for bio-polishing of fabrics. They are also used to improve the nutritional value and digestibility of animal feeds and in de-inking of paper (Tolan & Foody 1999). The cellulases that are used in these cases are harnessed from fungal sources. The importance of cellulose as a replenishable energy source generates a dire need for keen industrial interest and research in the hydrolysis of cellulose (Bhat et al. 2000). Profita-

ble bioconversion of cellulosic resources is subject to the characteristics of cellulose, sources of cellulolytic enzyme and favourable circumstances for the catalytic activity and enzyme yield. The crystalline structure and insoluble nature of cellulose make it less susceptible to degradation. For the biotechnological implication of cellulases, the present study has been formulated to screen and isolate high potential fungal cultures for cellulases production.

## MATERIALS AND METHODS

**Isolation of cellulolytic fungi from soil:** For isolation of cellulose-degrading fungi, three random soil samples were collected from rice field of Kanheli village, Rohtak, Haryana by digging at a depth of 10 cm and stored in a sterile polythene bag at 4°C. Pure isolates of fungal strains were obtained by Pour Plate technique and streaking on PDA (Potato Dextrose Agar) medium supplemented with (CMC) Carboxymethylcellulose (Viji et al. 2015). Serial dilutions of the experimental soil samples using sterile distilled water were made up to $10^{-5}$ dilution. PDA media was prepared and autoclaved. 0.3% sodium azide was added to the media as an antibacterial solution to restrict the growth of bacterial colonies on agar plates. Around 50 µL of diluted soil samples were spread on the solidified agar plates. The Petri plates were then sealed and incubated at 28°C for 48 hours. Fungal colonies were found to appear on the agar plates. These plates were labelled as Fungal Master plates (Fig.1). The isolates were further inoculated on sterile PDA plates by point inoculation and incubated at 28°C for 48 hours to obtain pure fungal plates (Fig. 2). Streaking was done to purify the fungal colonies further (Fig. 3). Following media was used for plating:

$NaNO_3$ – 2g/L, $K_2HPO_4$ – 1g/L, KCl – 0.5g/L, $MgSO_4$.7H2O – 0.5g/L, Peptone – 2g/L, Agar – 15g/L, CMC – 0.5% = 5g/L, PDA – 39g/L (Neethu et al. 2012)

**Primary screening - Congo red test:** The pure fungal plates were flooded with Congo red solution (1%), and then the solution was discarded after 5 minutes. The plates were then counterstained with 1N NaCl solution and allowed to rest for 15 to 20 minutes. Clear hydrolytic zones could be seen around the fungal colonies indicating cellulose hydrolysis by the enzymes (Fig. 4). High potential cellulolytic fungi were selected depending on their ability to form clear and wider hydrolytic zones around the fungal colony.

**Secondary screening - Determination of exoglucanase (total cellulase):** Standard Filter Paper Assay (FPase) method described by Eveleigh et al. (2009) was used to determine the total cellulase activity of the isolated fungal strains. Cellulase activity is defined as 1 µmols of the substrate converted to

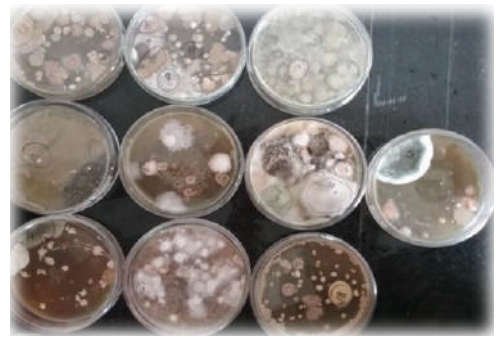

Fig. 1: Fungi Master plates

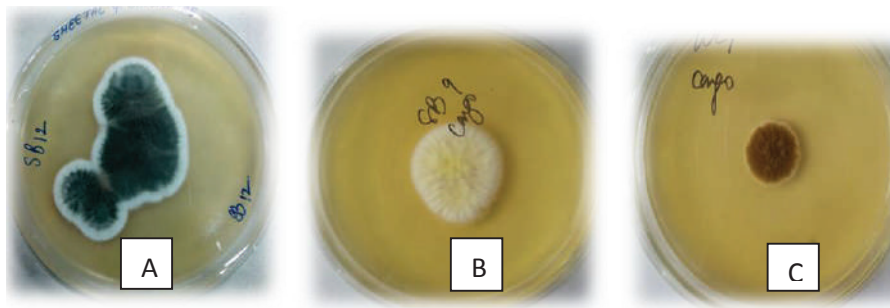


Fig. 2 (A-C): Purified fungal plates

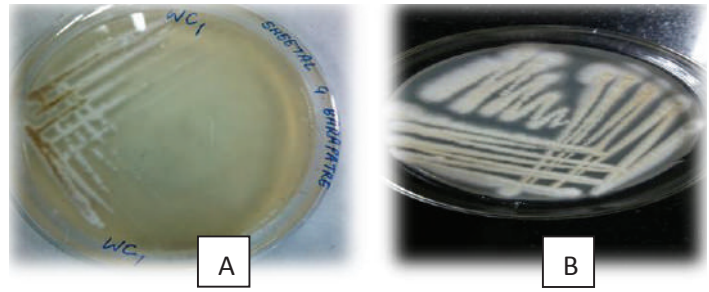


Fig. 3 (A-B): Streaked fungal plates

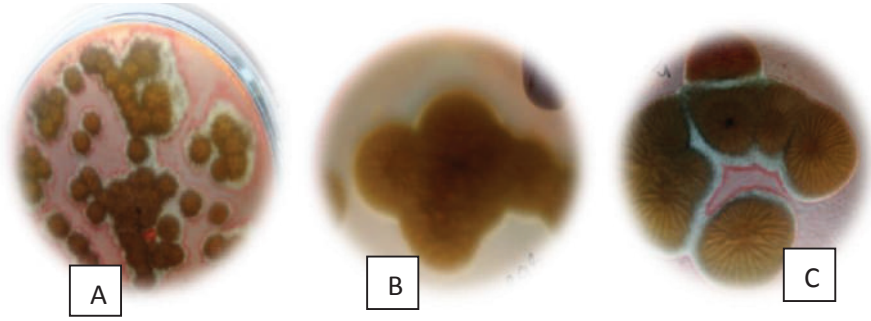


Fig. 4 (A-C): Plates showing Congo Red Test

glucose (Gilna & Khaleel 2011). 0.5 mL culture supernatant from each culture was added to 1 mL of sodium citrate buffer (pH 5.8). A 50 mg strip of Whatman No.1 filter paper (1.0 × 6.0 cm) was added to each tube and incubated at 50°C for 1 hour. Tubes were vortexed till filter paper settled at the bottom of the tube. Glucose standards, Enzyme blank and Substrate blank were prepared and incubated at 50°C for 1 hour. 3 mL of dinitrosalicylic acid (DNS) was added to each tube and mixed well (Fig. 5). The sample mixtures, glucose standards, enzyme blank and substrate blank were boiled together for 5 min in a water bath and then transferred to a cold water bath. Twenty mL of distilled water was added to all tubes and mixed properly. The absorbance values of these sample tubes were measured at 540 nm. Reagent blank was used to set the spectrometer at zero. Cellulase activity was expressed in Filter Paper Unit (FPU) per mL of undiluted culture filtrate (Mandels et al. 1976).

***Calculation***:

$$\text{FPU/mL} = \frac{0.37}{\text{Enzyme releasing 2 mg of glucose}}$$

**Determination of optimum pH for cellulase production:** Following buffers were used to maintain different pH values:

- 50 mM acetate buffer (for pH 3 and 4),
- 50 mM Sodium Citrate buffer (for pH 5.8)
- 50 mM Tris-base buffer (for pH 6)
- 50 mM sodium phosphate buffer (for pH 8-10).

0.5 mL culture supernatant pre-incubated at 50°C for 10

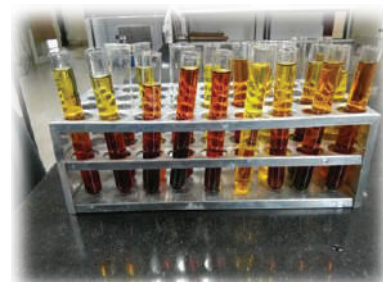

Fig. 5: Sample tubes for Filter Paper Assay

minutes was added to 0.5 mL buffer and incubated at 50°C for 30 minutes. 0.5 mL of DNS was added to terminate the reaction. The test tubes were then placed in a hot water bath for 5 minutes and then allowed to cool down. 2.5 mL of distilled water was added to all test tubes and the amount of reducing sugar liberated was determined by reading the absorbance at 540 nm (Mendel et al. 1969)

**Determination of optimum temperature for cellulase production:** To assess the effect of temperature on cellulase enzymatic activity, 0.5 mL sodium citrate buffer (pH 5.8) pre-incubated at 50°C for 10 minutes was combined with 0.5 mL of culture supernatant and incubated at 30°, 40°, 50° and 60° Celsius for 30 minutes. 0.5 mL DNS was added to stop the reaction and all mixtures were subjected to the hot water bath for 5 min. All test tubes were then allowed to cool down to room temperature and 2.5 mL of distilled

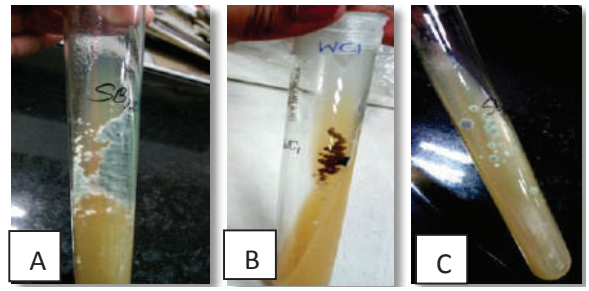


Fig. 6 (A-C): Fungal growth on media slants.

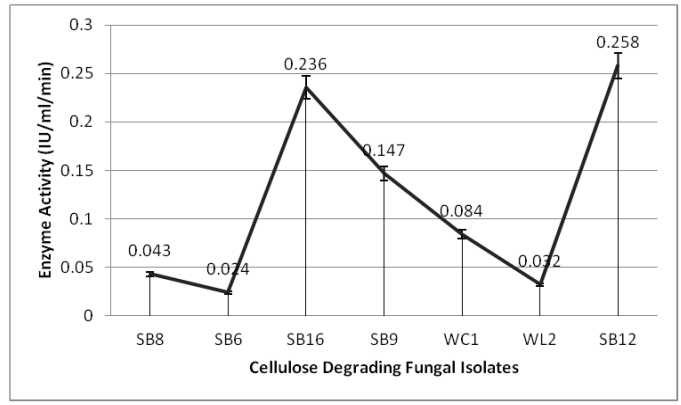


Fig. 7: Total cellulase activity of isolated fungal strains.

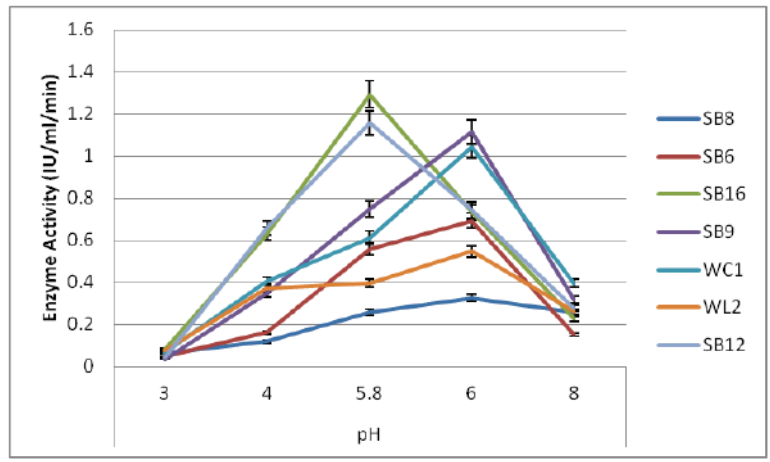


Fig. 8: Effect of pH on cellulase activity of isolated fungal strains.

Table 1: Hydrolytic zone diameter produced by isolated cellulolytic fungal strains.

| S. No. | Fungal Isolates | Fungal Colony Diameter (mm) | Fungal Colony + Zone Diameter (mm) | Hydrolysis Zone Diameter (mm) |
|---|---|---|---|---|
| 1 | WC1 | 13 | 16.3 | 3.3 |
| 2 | WL2 | 10.2 | 11.5 | 1.3 |
| 3 | SB6 | 14 | 16.5 | 2.5 |
| 4 | SB8 | 11.1 | 13.5 | 2.4 |
| 5 | SB9 | 15 | 18.6 | 3.6 |
| 6 | SB16 | 11 | 14.1 | 3.1 |
| 7 | SB12 | 6.2 | 9.4 | 3.2 |

Table 2: Effect of pH on cellulase activity of isolated fungal strains.

| Fungal Strains | Enzyme Activity (IU/mL/min) | | | | |
|---|---|---|---|---|---|
| | pH 3 | pH 4 | pH 5.8 | pH 6 | pH 8 |
| SB8 | 0.065±0.06 | 0.118±0.03 | 0.257±0.16 | 0.326±0.21 | 0.256±0.27 |
| SB6 | 0.048±0.06 | 0.161±0.21 | 0.559±0.19 | 0.693±0.14 | 0.151±0.02 |
| SB16 | 0.082±0.19 | 0.631±0.11 | 1.293±0.29 | 0.733±0.03 | 0.227±0.11 |
| SB9 | 0.036±0.27 | 0.348±0.21 | 0.748±0.17 | 1.115±0.16 | 0.318±0.24 |
| WC1 | 0.068±0.13 | 0.406±0.09 | 0.611±0.21 | 1.042±0.06 | 0.397±0.07 |
| WL2 | 0.077±0.24 | 0.372±0.11 | 0.397±0.26 | 0.546±12 | 0.261±0.02 |
| SB12 | 0.042±0.18 | 0.658±0.13 | 1.157±0.03 | 0.745±0.22 | 0.276±0.18 |

(n=3; Mean ± SD)

Table 3: Effect of temperature on cellulase activity of isolated fungal strains.

| Fungal Isolates | Enzyme Activity (IU/mL/min) | | | |
|---|---|---|---|---|
| | 30°C | 40°C | 50°C | 60°C |
| SB8 | 0.048±0.09 | 0.151±0.26 | 0.382±0.18 | 0.202±0.18 |
| SB6 | 0.051±0.12 | 0.183±0.04 | 0.341±0.23 | 0.107±0.26 |
| SB16 | 0.076±0.03 | 0.398±0.12 | 0.986±0.14 | 0.359±0.17 |
| SB9 | 0.047±0.11 | 0.912±0.03 | 0.415±0.27 | 0.361±0.19 |
| WC1 | 0.213±0.06 | 0.419±0.01 | 1.013±0.04 | 0.241±0.07 |
| WL2 | 0.061±0.17 | 0.554±0.15 | 0.361±0.16 | 0.253±0.08 |
| SB12 | 0.167±0.22 | 0.358±0.05 | 0.901±0.21 | 0.269±0.21 |

(n=3; Mean ± SD)

water was added to them. Absorbance was read at 540 nm (Balamurugan et al. 2011).

## RESULTS AND DISCUSSION

A total of 11 fungal strains (B1, WC1, WC3, WL1, WL2, SB6, SB9, SB12, SB16, SB8 and I12), were purified by Pour Plate technique and streaking on PDA media supplemented with CMC. CMC degradation was verified by staining the fungal plates with 1 mg/mL Congo red dye and counter-stained using 1N NaCl. Seven fungal strains (WC1, WL2, SB6, SB8, SB9, SB12, SB16) gave positive results in primary screening by forming visible hydrolytic zones around the fungal colonies. Table 1 shows the hydrolytic zone diameters formed by isolated fungal strains.

These 7 fungal strains were then subjected to secondary screening using enzymatic assay FPase for production of exoglucanase. FPase results revealed that the exoglucanase activity was observed to be highest for the isolated fungal

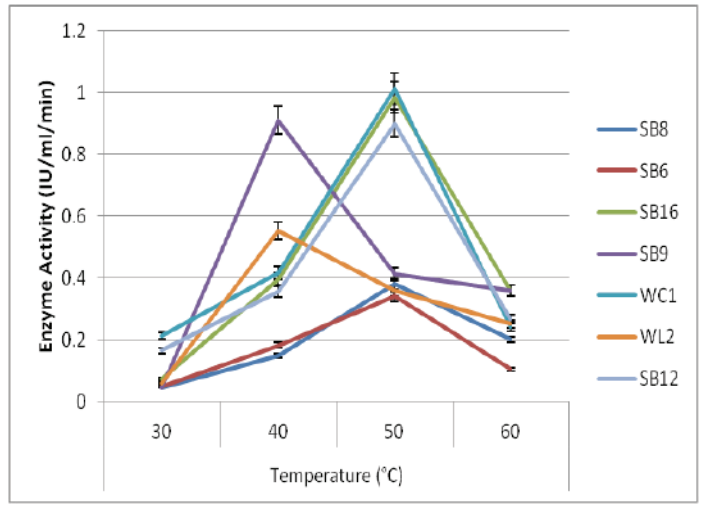


Fig. 9: Effect of temperature on cellulase activity of isolated fungal strains.

strains SB12 (0.258 IU/mL) followed by SB16 (0.236 IU/mL), SB9 (0.147 IU/mL) and WC1 (0.084 IU/mL) as depicted in Fig. 7.

The effect of pH on the activity of the cellulase enzyme was studied by varying pH in the range of 3 to 8 (Table 2). The maximum cellulase activities were noticed at pH 5.8-6.0 with SB16 (1.293 IU/mL), SB12 (1.157 IU/mL), SB9 (1.115 IU/mL) and WC1 (1.042 IU/mL) showing highest enzyme activity. On further increase in pH, a reduction in the cellulase activity was obtained (Fig. 8). The reason for decreasing production at higher pH was probably due to proteolytic inactivation of the cellulase. Hence, it is suggested that slightly acidic pH values favoured cellulase production, which is in agreement with earlier results of other researchers (Ander & Eriksson 1976).

The effect of different temperatures on cellulase production by fungal strains was evaluated by assessing the number of glucose molecules released over temperatures ranging from 30 to 60°C using DNS method (Table 3). Maximum cellulase activities were observed between 40-50°C with WC1 (1.013 IU/mL), SB16 (0.986 IU/mL), SB9 (0.912 IU/mL) and SB12 (0.901 IU/mL) showing highest enzyme activities (Fig. 9).

Based on hydrolytic zones formation and cellulase enzyme production, three fungal strains - SB12, SB9 and WC1 were selected as high potential cellulolytic strains. Then they were grown on media slants (Fig. 6) and sent for identification to Pathology Department, IARI, Pusa. The strains were identified as *Aspergillus fumigatus* (SB12), *Aspergillus terreus* (SB9) *and Aspergillus flavus* (WC1).

## CONCLUSION

This study suggests that *Aspergillus fumigatus, Aspergillus terreus and Aspergillus flavus* are potent cellulase producers and can contribute to cellulase production under optimized conditions of pH and temperature. The effect of pH and temperature on the synthesis of cellulase enzyme can be studied by optimizing these parameters. Fungi need optimum pH and temperature to achieve substantial growth and show cellulase enzyme production activity which can be rendered beneficial to be utilized for several industrial applications. In accordance with the results, considering the influencing factors, the optimal cultural process for *Aspergillus* species was considered as PDA media supplemented with CMC at pH 5.8-6.0 within a temperature range 40-50°C.

## REFERENCES

Abe, C.A.L., Faria, C.B., De Castro, F.F., De Souza, S.R., Santos, F.C.D., Da Silva, C.N. and Barbosa-Tessmann, I.P. 2015. Fungi isolated from maize (*Zea mays* L.) grains and production of associated enzyme activities. International Journal of Molecular Sciences, 16(7): 15328-15346.

Ander, P. and Eriksson, K.E. 1976. The importance of phenol oxidase activity in lignin degradation by the white-rot fungus *Sporotrichum pulverulentum*. Archives of Microbiology, 109(1-2): 1-8.

Balamurugan, A., Jayanthi, R., Nepolean, P., Pallavi, R. V. and Premkumar, R. 2011. Studies on cellulose degrading bacteria in tea garden soils. African Journal of Plant Science, 5(1): 22-27.

Béguin, P. and Aubert, J.P. 1994. The biological degradation of cellulose. FEMS Microbiology Reviews, 13(1): 25-58.

Bhat, M.K. 2000. Cellulases and related enzymes in biotechnology. Biotechnology Advances, 18(5): 355-383.

Eveleigh, D.E., Mandels, M., Andreotti, R. and Roche, C. 2009. Measurement of saccharifying cellulase. Biotechnology for Biofuels, 2(21): 1-8, doi: 10.1186/1754-6834-2-21.

Gilna, V.V. and Khaleel, K.M. 2011. Cellulase enzyme activity of Aspergillus fumigatus from mangrove soil on lignocellulosic substrate. Recent Research in Science and Technology, 3(1): 132-134.

Lynd, L.R., Weimer, P.J., Van Zyl, W.H. and Pretorius, I.S. 2002. Microbial cellulose utilization: Fundamentals and biotechnology. Microbiol. Mol. Biol. Rev., 66(3): 506-577.

Mandels, M. and Weber, J. 1969. Production of cellulases. Adv. Chem. Ser., 95: 391-414.

Mandels, M., Andreotti, R. and Roche, C. 1976. Measurement of saccharifying cellulose. Biotechnol. Bioeng. Symp., 6: 21-33.

Mishra, B.K. and Dadhich, S.K. 2010. Production of amylase and xylanase enzymes from soil fungi of Rajasthan. J. Adv. Dev. Res., 1(1): 21-23.

Neethu, K., Rubeena, M., Sajith, S., Sreedevi, S., Priji, P., Unni, K.N. and Benjamin, S. 2012. A novel strain of *Trichoderma viride* shows complete lignocellulolytic activities. Advances in Bioscience and Biotechnology, 3: 1160-1166.

Ryu, D.D.Y. and Mandels, M. 1980. Cellulases: Biosynthesis and applications. Enzyme and Microbial Technology, 2(2): 91-102.

Samdhu, D.K. and Bawa, S. 1992. Improvement of cellulase activity in *Trichoderma*. Applied Biochemistry and Biotechnology, 34-35(1): 175-192.

Shewale, J.G. 1982. β-Glucosidase: Its role in cellulase synthesis and hydrolysis of cellulose. International Journal of Biochemistry, 14(6): 435-443.

Singh, A., Hayashi, K., Hoa, T.T., Kashiwagi, Y. and Tokuyasu, K. 1995. Construction and characterization of a chimeric β-glucosidase. Biochemical Journal, 305(3): 715-719.

Tolan, J.S. and Foody, B. 1999. Cellulase from submerged fermentation. In: Recent Progress in Bioconversion of Lignocellulosics. Springer, Berlin, Heidelberg, pp. 41-67.

Viji, J. and Neelanarayanan, P. 2015. Efficacy of lignocellulolytic fungi on the biodegradation of paddy straw. International Journal of Environmental Research, 9(1): 225-232.

Wood T.M. 1989. Synergism between enzyme components of *Penicillium pinophilum* cellulase in solubilizing hydrogen ordered cellulose. Journal of Biochemistry, 260: 37-43.

Woodward, J. and Wiseman, A. 1983. Fungal and other β-dglucosidases: Their properties and applications. Enzyme and Microbial Technology, 4(2): 73-79.

Nature Environment and Pollution Technology
An International Quarterly Scientific Journal

p-ISSN: 0972-6268
(Print copies up to 2016)
e-ISSN: 2395-3454

Vol. 19 | No. 4 | pp.1737-1741 | 2020

Original Research Paper

https://doi.org/10.46488/NEPT.2020.v19i04.045

Open Access Journal

# Evaluation of Sugarcane and Soil Quality Amended by Sewage Sludge Derived Compost and Chemical Fertilizer

**P. Balaganesh*†, M. Vasudevan*, S. M. Suneethkumar**, S. Shahir*** and N. Natarajan******

*Department of Civil Engineering, Bannari Amman Institute of Technology, Sathyamangalam-638401, Tamil Nadu, India
**Department of Civil Engineering, ATME College of Engineering, Mysore-570028, Karnataka, India
***Department of Food Technology, Bannari Amman Institute of Technology, Sathyamangalam-638401, Tamil Nadu, India
****Department of Civil Engineering, Dr. Mahalingam College of Engineering and Technology, Pollachi-642003, Tamil Nadu, India
†Corresponding author: P. Balaganesh; balachem.aec@gmail.com

**Nat. Env. & Poll. Tech.**
**Website: www.neptjournal.com**

*Received:* 03-01-2020
*Revised:* 21-01-2020
*Accepted:* 05-03-2020

**Key Words:**
Sugarcane
Soil nutrients
Sludge
Compost
Chemical fertigation

## ABSTRACT

The impact of compost prepared from sewage sludge in addition/alteration to chemical fertilizer makes a unique direction for effective waste management with high crop productivity. The study aims to compare the quality, agronomic parameters of sugarcane amended by sewage sludge compost with that using optimum chemical fertilizer (NPK 150-50-90 kg/ha) in the two random fields near sewage treatment plant (STP) of our institute and also to predict the soil quality in that field before sowing and after ripening. Dimensional analysis, Brix, Pol, Purity, Sugar recovery and other necessary quality analysis were estimated for the sugarcane samples. Similarly, soil physico-chemical parameters such as pH, electrical conductivity, forms of nitrogen, organic carbon and other nutrients were also monitored. Obtained sugarcane purity of 89.2% from sludge derived compost (SDC) over the 82.8% using chemical fertilizer amendment leads to the sustainable management system. The % recovery of 12.23 of cane shows the optimum value for the compost amendment. The results scientifically reveal the suitability of sludge compost to the replacement of chemical fertilizers in terms of productivity and soil quality.

## INTRODUCTION

India's most important socio-economic crop is sugarcane which promotes the rural agricultural practices to the good income generating based category (Tripathi et al. 2017). Sugarcane is also one of the largest sowing cash crops in India. About 42 lakh farmers are involved in sugarcane farming. Quality and yield of sugarcane highly depend upon temperature, sunlight and moisture conditions. The hot climatic condition with sufficient moisture is the ideal condition for growth. Accumulation of sucrose content in the internodes of basal to the apex is commonly said to be ripening (Pathak et al. 2018). White sugar and jaggery are the two important products from sugarcane juice extraction. Sugarcane quality also depends upon various parameters such as soil characteristics, breeds, tillers, age of tillers, etc. Juice clarification process focuses on removing non-sugars and colouring contents. The major by-products are bagasse and molasses. They are used extensively for making various products (Kumar et al. 2015). In addition to this, invasion of sugarcane borer highly interferes with the quality of sugarcane (de S. Rossato Jr et al. 2013). By comprehending the aforementioned basic introduction, it is inevitable to devise a suitable research methodology for the problems of sugarcane cultivation. Sugarcane yield of our country is significantly low when we compare to the other countries with similar environmental conditions. This might be due to several factors and fertilizer usage balance is the notable one and cause low yield (Nawaz et al. 2017, Kumar et al. 2014), since sugarcane is a typical heavy feeding crop which consumes most of the vital nutrients in the soil and consequently increases the production cost (Nawaz et al. 2017). Deficiency in organic carbon poses a serious threat to the fertility of Indian soil (Gaind & Nain 2012). Suitable fertigation with sufficient nitrogen, phosphorus and potassium is the vital requirement for the sugarcane quality. To get good juice quality and high yield it is important to consider the potassium fertilizer high (Soomro et al. 2014). However, continuous chemical fertilizer usage for high sugarcane yield resulted in deprived soil health, altered chemical composition and available micronutrients. At the same time, organic amendment enhances the soil organic matter and other nutrients within less time by optimising the dosage (Lakshmi et al. 2011). Consistent application of nutrients to the soil is not feasible in all conditions. It depends upon the type of soil and atmospheric conditions. Many researchers made different trials using organic amendments, inorganic and integrated organic and inorganic amendments

to optimize the dosage for high sugarcane quality and yield economically (Nawaz et al. 2017). Managing the organic wastes effectively in our soil is the best way to enhance soil organic carbon with an economical approach. Besides, this also enhances the carbon sequestration potential (Gaind & Nain 2012). One of the best organic waste management techniques is composting. Composting is the process of converting organic wastes into humus like substances which is rich in nutrients. Microorganisms in the presence of air generally degrade the complex waste materials and yield compost, carbon dioxide and water (Atalia et al. 2015). Alternately, sewage sludge application on land is the best economical practice and in turn, it increases the water holding capacity, aeration, and organic matter and soil nutrients (Bhat & Agarwal 2013, Kootenaei et al. 2014), even though, many workers reported that sewage sludge application also results in heavy metal accumulation and cause metal contamination in edible crops (Singh et al. 2017). However, the limited proportion of sewage sludge as compost amendment up to 45% best suited for healthy soil conditioning and fertilizer for the plant growth (Chu 2017). Thereby, sugarcane quality analysis is very important for many things, especially for optimizing the cultivation process and production management. Xiao et al. (2017) analysed and reported the sugarcane quality indexes such as Brix %, pol %, purity and sugarcane recovery %. Brix (°Bx) is the sugar substance of a fluid arrangement. One degree Brix is 1 gram of sucrose in 100 grams of solution and speaks to the quality of the solution as rate by mass. The optical device refractometer used to find Brix under the refractive index principle. Pol (°Z) is another important quality index which is also sucrose content of the sugarcane juice. It is also said to be apparent sucrose. Purity is the ratio between pol and Brix.

So far, the synergistic approach of managing sewage treatment plant sludge as the composting substrate to enhance sugarcane quality not addressed well in our Indian conditions. By considering this need and above importance the main objectives of the study focussed to compare the quality, agronomic parameters of sugarcane amended by SDC with that using chemical fertilizer (NPK 150-50-90 kg/ha) and also to predict the soil quality in that field before sowing and after ripening, thus reporting the suitability of sludge compost to the replacement of chemical fertilizers in terms of productivity and soil quality.

## MATERIALS AND METHODS

### Investigational Location and Environmental Conditions

Sugarcane crop was sown during monsoon and post-monsoon seasons of 2018 at an investigational ranch near Sewage Treatment Plant (STP) located at Bannari Amman Institute of Technology, Sathyamangalam, Tamilnadu, India (Lat. 11.49520 and Long. 77.27640). The experimental soil type at the site was a clayey-loam.

### Co-compost Preparation

Dynamic sludge gathered from the sludge waste line of STP along with other organic fraction of municipal wastes segregated from the institute was fed into the non-destructive sheet-metallic canister to get ready in-vessel aerobic compost. The substances were blended altogether once per week. The moisture of substance and temperature were observed day by day (Lokeshwari et al. 2017). The canister was checked for a time of 40 days and tests were taken routinely to assess the maturity of SDC in terms of different vital physico-chemical parameters.

### STP Compost Amended Sugarcane Quality Analysis

Ten stalks from the field have been chosen randomly for analysis where STP compost amended. The average weight of a stalk is 1.5 kilogram and length ranges from 230 to 250 cm. The stalks were taken to Bannari Amman Sugars, crushed and filtered for analysis. Around five litres of juice was extracted from the crusher. The quality control lab analysed the quality parameters. Lead sulphate was added to the extract, and the sample taken to the optical device refractometer's cell compartment to find out the Brix value. Pol value was found by pouring the processed filtrate into the quartz plate of the polarimeter. Apparent purity found by taking the ratio between pol and Brix (Lingle et al. 2010).

The percentage of cane recovery was determined by the following equation.

$$\% \text{ Recovery Cane} = [\text{Pol}\% - \{(\text{Brix}\% - \text{Pol}\%) \times 0.4\}] \times 0.75 \quad \ldots(1)$$

### Agronomic Characteristics of Sugarcane

The agronomic investigation (germination %, tillers per plant, millable canes and cane yield) for the two field sugarcane samples carried out as per the methods suggested by Soomro et al. (2014). After 45 days of implant, the number of plantlets came out in every plot were counted and then by the formula below was converted into germination percentage.

$$\text{Germination } (\%) = \frac{\text{Number of germinated buds}}{\text{Total number of buds}} \times 100 \quad \ldots(2)$$

### Physico-Chemical Analysis

For the chemical analysis, 5 g of each soil sample and compost were extracted with 50 mL of 2M potassium chloride

(Shahandeh et al. 2011, Amponsah et al. 2014) solution for 2 hours using an orbital shaker. After settling, the supernatant was filtered through syringe filters (20 µm) and directly used for measuring pH (Elico LI120) and electrical conductivity (Elico CM 180). The presence of total organic carbon (TOC) and total nitrogen (TN) was analysed by TOC Analyzer (Shimadzu, TOC L, TNM L, Malaysia) with 6800°C combustion (catalytic oxidation) and non-dispersive infrared detection (NDIR) method (Vasudevan et al. 2019). It is a preferred method for estimating organic carbon in environmental samples over the conventional Walkley-Black method and loss-on-ignition (LOI) method for its comprehensive and accurate detection mechanism (Bautista et al. 2016). The aqueous concentration of phosphorus (P), nitrate-nitrogen ($NO_3$-N) and ammonia-nitrogen ($NH_4$-N) was estimated using UV-Visible spectrophotometer (Systronics PC based 2202) (Nartey et al. 2017, Benito et al. 2018). The concentration of potassium (K) was estimated by a digital flame photometer (Labtronics LT-65) (Sharma et al. 2017). All the experiments were in triplicate for analysing the statistical significance using (LSD) least significant difference test with 5% probability.

## RESULTS AND DISCUSSION

### Physico-Chemical Characteristics of the Matured SDC

The compost bin periodically assessed for its maturity and the final results were tabulated after 40 days of degradation (Table 1). The observed pH (7.35) was near to neutral and EC values (1.2 dS/m) were less than 4.0 dS/m. This reveals the maturity of stable compost (Gaind & Nain 2012). The suitability of SDC for the field application can be comprehended by the author guidelines (Ahmad et al. 2007) for the maturity of compost.

Table 1: Matured compost physico-chemical parameter values.

| Parameter | Mean Values |
|---|---|
| pH | 7.35 |
| EC (dS/m) | 1.2 |
| Moisture (%) | 18 |
| OM (%) | 42.66 |
| N (%) | 1.62 |
| $NO_3$-N (mg/kg) | 35.73 |
| $NH_4$-N (mg/kg) | 1.56 |
| OC (%) | 24.8 |
| C/N | 15.3 |
| P (%) | 0.62 |
| K (%) | 1.2 |

OM-Organic matter, OC-Organic carbon, N-nitrogen

### Amendment Impact on Sugarcane Quality

The study results of sugarcane quality amended by the SDC and chemical fertilizer (NPK 150-5-90 kg/ha) are shown in Fig. 1. The SDC Brix value of 19.21 % was sucrose content which is optimum for the sugar crystallization. Similarly, the polarimeter value of 17.14 pol % was apparent sucrose; the apparent purity 89.2% and the recovery % cane 12.23%. Whereas, chemical fertigated sugarcane quality differs in terms of Brix 20.6, pol 17.36, apparent purity 82.8% and recovery % cane 13.15%. These findings harmonize with the results of Soomro et al. (2014) and high enough when compared with the fertilizer dose of Bokhtiar et al. (2005) and Lingle et al. (2010). It reveals that the maximum apparent purity can be attained through the SDC amendment (89.2%). However, the Brix and pol values of SDC compost were slightly less when compared to chemical fertilizer and in turn, the recovery cane % also deprived to some extent.

### Impact of SDC Compost and Chemical Fertigation on Soil

The soil from the two fields was taken for analysis after SDC and chemical fertilizer amendment. The SDC amended soil yielded high quality sugarcane (89.2% purity) and optimum recovery cane % over the chemical fertigated sugarcane. The amendments compared to the feasibility of soil nutrient dynamics. Initially, the composite soil samples were taken from respective fields and assessed for physico-chemical characteristics before sowing. Similarly, after the ripening

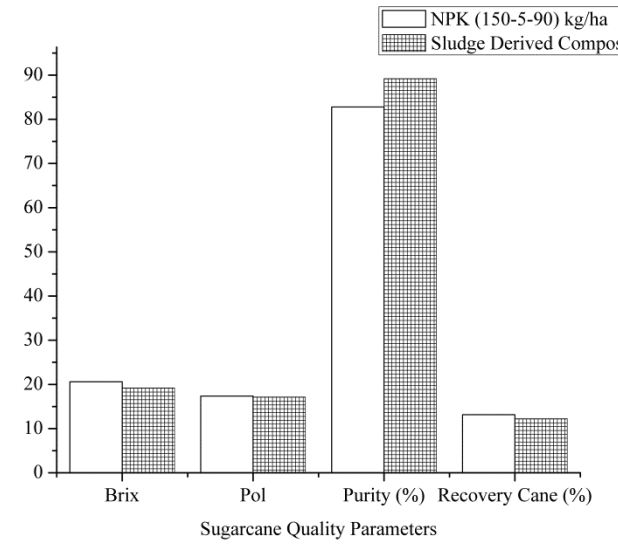


Fig. 1: Comparison of sugarcane quality parameters.

Table 2: Physico-chemical analysis of soil.

| Parameter | Sludge Derived Compost amended field | | NPK (150-50-90) kg/ha amended field | |
|---|---|---|---|---|
| | Before sowing | After harvesting | Before sowing | After harvesting |
| pH | 7.72 | 7.69 | 8.03 | 7.92 |
| EC (dS/m) | 0.62 | 0.9 | 0.81 | 0.8 |
| OC (%) | 0.42 | 0.45 | 1.52 | 1.58 |
| N (%) | 0.038 | 0.035 | 0.134 | 0.142 |
| C/N | 11.05 | 12.85 | 11.34 | 11.12 |
| P (ppm) | 3.9 | 3.81 | 4.22 | 4.96 |
| K (ppm) | 118 | 123 | 356 | 372 |

Table 3: Sugarcane agronomic characteristics.

| Amendment | Germination % | Tillers per plant | Millable canes/ha | Yield, t/ha |
|---|---|---|---|---|
| SDC | 66.24 | 3.92 | 132.6 | 148.72 |
| NPK (150-50-90 kg/ha) | 48.33 | 2.81 | 126.2 | 98.26 |

also, the soil parameters assessed for fertility. Generally, soil nutrients are highly consumed by sugarcane crop because it is a heavy fed crop, still due to the STP compost amendment, the soil quality after ripening did not deteriorate much. The SDC amended soil pH value of 7.69 is optimum for further crop production and slightly decreased with the initial pH level of 7.72. Whereas, before sowing chemical fertigated soil showed high level pH of 8.03 and decreased to 7.92 after ripening. These typical pH values were following the similar results of Teshome et al. (2010). Similarly, EC, OC %, N % along with P and K values also reveal that soil fertility is protected (Table 2).

### Agronomic Characteristics of the Sugarcane

The two fields near STP were periodically observed and the vital agronomic characteristics were tabulated (Table 3). The germination percentage of 48.33 was observed for chemical fertilizer amended field. This low value might be due to elevated nitrogen value. Rapid availability of nutrients enhanced the tillering values in both the fields and it also resulted in high millable canes (Sarwar et al. 2010). High yield and other parameters were observed for the SDC amendment.

## CONCLUSION

The implications of the findings of this research on the quality of sugarcane best suits for sustainable waste management policies. The juice quality extracted from the sugarcane stalks of sludge compost amendment field has higher apparent purity 89.2% over the chemical fertigated sugarcane stalks. The Brix, pol and recovery % of cane were optimum ranges with that of chemical fertilizer dose (NPK 150-50-90 kg/ha). The synergistic approach of waste management in terms of sludge derived compost amendment can be recommended for the high yield and quality sugarcane economically. This can be understood from the agronomic characteristic's variation. The co-compost prepared with STP sludge and other community wastes have the natural potential to hold vital nutrients in the soil for further cropping.

## ACKNOWLEDGEMENTS

This work was supported by the Management and staff of Bannari Amman Institute of Technology, Sathyamangalam and funded by Science and Engineering Research Board, Department of Science and Technology, Government of India under Swacch Bharat Mission [ECR/2016/001114/ES].

## REFERENCES

Ahmad, R., Jilani, G., Arshad, M., Zahir, Z.A. and Khalid, A. 2007. Bio-conversion of organic wastes for their recycling in agriculture: An overview of perspectives and prospects. Annals of Microbiology, 57(4): 471-479.

Amponsah, D., Godfred, E. and Sebiawu, D.O. 2014. Determination of the amount of the exchangeable ammonium-nitrogen in soil samples from the university of cape coast school farm. International Journal of Scientific & Engineering Research, 5(6): 731-36.

Atalia, K.R., Buha, D.M., Joshi, J.J. and Shah, N.K. 2015. Microbial biodiversity of municipal solid waste of Ahmedabad. J. Mater. Environ. Sci., 6(7): 1914-1923.

Bautista, F., García, E. and Gallegos, Á. 2016. The App SOC plus a tool to estimate and calculate organic carbon in the soil profile. Journal of Applied Research and Technology, 14(2): 135-39.

Bhat, M.A. and Agrawal, H.P. 2013. Evaluation of digested sludge as an amendment to chromium and lead contaminated Gangetic alluvial soils of India. Indian J. Agric. Sci., 83(1): 51-55.

Bokhtiar, S.M. and Sakurai, K. 2005. Effect of application of inorganic and organic fertilizers on growth, yield and quality of sugarcane. Sugar Tech., 7(1): 33-37.

Chu, S., Wu, D., Liang, L.L, Zhong, F., Hu, Y., Hu, X., Lai, C. and Zeng, S. 2017. Municipal sewage sludge compost promotes *Mangifera persiciforma* tree growth with no risk of heavy metal contamination of soil. Sci. Rep., 7(1): 13408.

de S. Rossato Jr. J.A., Costa, G.H., Madaleno, L.L., Mutton, M.J., Higley, L.G. and Fernandes, O.A. 2013. Characterization and impact of the sugarcane borer on sugarcane yield and quality. Agron. J., 105(3): 643-48.

Gaind, S. and Nain, L. 2012. Soil carbon dynamics in response to compost and poultry manure under rice (*Oryza sativa*)-wheat (*Triticum aestivum*) crop rotation. Indian Journal of Agricultural Sciences, 82(5): 410-415.

Kootenaei, F.G., Aminirad, H. and Ramezani, M. 2014. Composting of sewage sludge and municipal solid waste. Nature Environment and Pollution Technology, 13(3): 553-558.

Kumar, N., Singh, H., Kumar, R. and Kumari, G. 2014. Nutrient uptake, sugarcane yield and economics of high sugar early genotypes of sugarcane (*Saccharum* sp. hybrid complex) under various planting seasons and fertility levels in Bihar. Indian J. Agric. Sci., 84(4): 444-51.

Lingle, S.E., Johnson, R.M., Tew, T.L. and Viator, R.P. 2010. Changes in juice quality and sugarcane yield with recurrent selection for sucrose. Field Crops Research, 118(2): 152-157.

Lokeshwari, M., Vikas Mandi, Raghavendra, T., Amaranatha Reddy and Udayashankar B.C. 2017. Co-composting of municipal solid waste with sewage sludge for sustainable waste management in urban areas. Proceedings of ASCE India Conference on Urbanization Challenges in Emerging Economies, pp. 79-89. 12 -14 December 2017. New Delhi, India.

Marín-Benito, J.M., Barba, V., Ordax, J.M., Andrades, M.S., Sánchez-Martín, M.J. and Rodríguez-Cruz, M.S. 2018. Application of green compost as amendment in an agricultural soil: Effect on the behaviour of triasulfuron and prosulfocarb under field conditions. J. Environ. Manage., 207: 180-91.

Nartey, E.G., Amoah, P., Ofosu-Budu, G.K., Muspratt, A. and Kumar Pradhan, S. 2017. Effects of co-composting of faecal sludge and agricultural wastes on tomato transplant and growth. International Journal of Recycling of Organic Waste in Agriculture, 6(1): 23-36.

Nawaz, M., Chattha, M.U., Chattha, M.B., Ahmad, R., Munir, H., Usman, M., Hassan, M.U., Khan, S. and Kharal, M. 2017. Assessment of compost as nutrient supplement for spring planted sugarcane (*Saccharum officinarum* L.). J. Anim. Plant Sci., 27(1): 283-93.

Pathak, S.K., Singh, P., Singh, M.M. and Sharma, B.L. 2019. Impact of temperature and humidity on sugar recovery in Uttar Pradesh. Sugar Tech., 21(1): 176-81.

Rama Lakshmi, C.S., Sreelatha, T., Usha Rani, T., Rao, S.R.K. and Naidu, N.V. 2011. Effect of organic manures on soil fertility and productivity of sugarcane in north coastal zone of Andhra Pradesh. Indian J. Anim. Res., 45(4): 307-13.

Sarwar, M.A., Muhammad, I., Muhammad, T., Kafeel, A., Khan, Z.I. and Valeem, E.E. 2010. Appraisal of pressmud and inorganic fertilizers on soil properties, yield and sugarcane quality. Pak. J. Bot., 42(2): 1361-67.

Shahandeh, H., Wright, A.L. and Hons, F.M. 2011. Use of soil nitrogen parameters and texture for spatially-variable nitrogen fertilization. Precision Agriculture, 12(1): 146-63.

Sharma, D. and Yadav, K.D. 2017. Bioconversion of flowers waste: composting using dry leaves as bulking agent. Environmental Engineering Research, 22(3): 237-44.

Singh, V., Singh, J., Singh, S. and Singh, H. 2017. Effect of sewage sludge and fertilizers on accumulation of micronutrients and yield of cauliflower (*Brassica oleracea* var. *botrytis*) in an alluvial soil. Indian J. Agric. Sci., 85(7): 965-969.

Soomro, A.F. 2014. Effect of inorganic NPK fertilizers under different proportions on growth, yield and juice quality of sugarcane (*Saccharum officinarum* L.). Pure. Appl. Biol., 3(1): 10-18.

Teshome, Z., Abejehu, G. and Hagos, H. 2014. Effect of nitrogen and compost on sugarcane (*Saccharum officinarum* L.) at Metahara sugarcane plantation. Advances in Crop Science and Technology, 2(5): 1000153.

Tripathi, S., Singh, N., Mali, S., Naik, J.R. and Pritesh, S.M. 2017. Sugarcane/sugarcane juice quality evaluation by FT-NIR spectrometer. Int. J. Curr. Microbiol. Appl. Sci., 6(8): 3025-3032.

Umesh Kumar, P.K. and Chand, K. 2015. Application of response surface method as an experimental design to optimize clarification process parameters for sugarcane juice. J. Food Process Technol., 6(422): 1000422.

Vasudevan, M., Karthika, K., Gowthaman, S., Karthick, K., Balaganesh, P., Suneeeth Kumar, S.M. and Natarajan, N. 2019. Aerobic in-vessel co-composting of dewatered sewage sludge with mixed municipal wastes under subhumid and semiarid atmospheric conditions. Energy Sources, Part A: Recovery, Utilization, and Environmental Effects, 1-12.

Xiao, Z., Liao, X. and Guo, S. 2017. Analysis of sugarcane juice quality indexes. Journal of Food Quality, 2017: 1-6.

Nature Environment and Pollution Technology
An International Quarterly Scientific Journal

p-ISSN: 0972-6268
(Print copies up to 2016)
e-ISSN: 2395-3454

Vol. 19 | No. 4 | pp. 1743-1748 | 2020

Original Research Paper

https://doi.org/10.46488/NEPT.2020.v19i04.046

Open Access Journal

# Industrial Pollution Governance Efficiency and Big Data Environmental Controlling Measures: A Case Study on Jiangsu Province, China

**Jianwei Lu*(**)†**

*School of Information Engineering, Changzhou Institute of Industry Technology, Changzhou 213164, China

**Changzhou Ciyanglin Information Technology Co. Ltd., Changzhou, 213000, China

†Corresponding author: Jianwei Lu; 13925915@qq.com

**Nat. Env. & Poll. Tech.**
**Website: www.neptjournal.com**

*Received:* 05-07-2020
*Revised:* 31-10-2020
*Accepted:* 05-11-2020

**Key Words:**
Industrial pollution
Pollution governance
Environmental protection
Controlling measures

## ABSTRACT

Industrial economic development, which is characterized by high input, high pollution, high consumption, and low benefits, causes environmental pollution problems to be prominent due to the increase of industrial pollutants every year. Blind expansion of investment scale regardless of governance efficiency of industrial pollution can lead to a certain amount of resource wastage. Thus, improving the governance efficiency of industrial pollution is an important method to solve industrial pollution. In particular, applying big data on environmental protection for environmental pollution management can improve the efficiency and quality of pollution control, and ensure comprehensive examination and governance of environmental pollution. In this study, research on industrial pollution governance efficiency in foreign developed countries was reviewed. Furthermore, industrial pollution governance efficiency in Jiangsu Province, China was calculated and certain measures were proposed to prevent and control industrial pollution by applying big data on environmental protection. Results demonstrate that the trend in which industrial pollution governance of emerging technologies, such as big data, penetrate into environmental protection and human capital input can significantly decrease industrial wastewater and industrial solid wastes. Technological innovation makes remarkable contributions to industrial waste gas control. To increase industrial pollution governance efficiency, this study proposes certain measures, such as establishing a scientific and highly efficient big-data monitoring network system for ecological environment, fully utilizing block-chain technological advantages in industrial pollution control, constructing a perfect big-data sharing and processing platform for environmental protection, and increasing sharing and application values of big data on environmental protection. Research conclusions can provide important references to reduce industrial pollutant emissions, increase the efficiency of industrial pollution governance, increase applications of big-data on environmental protection, and construct and perfect a big-data sharing platform for environmental protection.

## INTRODUCTION

China's economic development model of "high consumption, high pollution, and low output" has been formed over a long period at great cost to the country's natural and ecological resources. Rapid industrial development has brought pollution problems in recent years, which has become one of the main factors that influence the living conditions of humans. Environmental damage caused by industrial pollution accounts for most pollution outcomes. Atmospheric, water and solid waste pollution are the major types of industrial pollution. Controlling industrial pollutant emissions and increasing the efficiency of industrial emission reduction is vital to improve economic development and raise people's standard of living. With the gradual maturity of big data technology, using big data on environmental protection to control environmental pollution not only can increase the control efficiency and quality but also can establish a perfect environmental governance system for comprehensive examination and management of environmental pollution.

Jiangsu is an economically developed province in China. Although it has achieved rapid economic growth, it faces significant threats from environmental pollution (Fig. 1). As industrialization is accelerated in Jiangsu Province, environmental pollution caused by industrial development has posed great threats to human health. Although various theoretical requirements and specific measures of ecological environmental protection have been implemented, the Province cannot avoid the intensifying pollution problems caused by economic development. Effects of industrial development on ecological environmental damage and natural resource consumption cannot be ignored even though it can drive economic development. Therefore, finding a new way to control environmental pollution caused by industrial development is necessary. Applications of big data on environmental protection are based on Internet

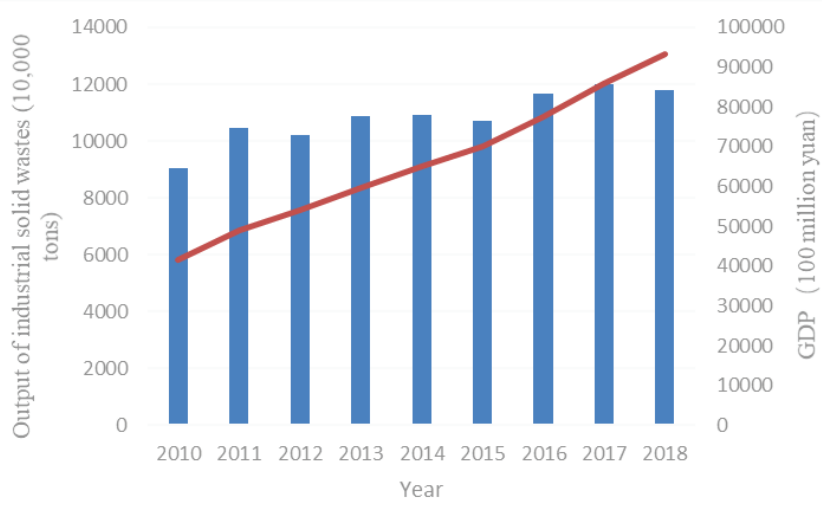


(Data source: *http://olap.epsnet.com.cn/*)

Fig. 1: GDP and output of industrial solid waste in Jiangsu Province in 2010-2018.

technology and the development of data technology, which lay a solid technological foundation for environmental pollution prevention and control. Big data sharing for environmental protection can help realize nationwide networking of environmental pollution problems, identify common environmental pollution problems, and offer centralized analysis and processing of such problems, thereby enabling an increase in environmental governance efficiency. Furthermore, big data sharing for environmental protection can provide real and reliable control in regions with serious environmental pollution, enable the public to learn advanced philosophies and techniques for environmental protection management in China, change environmental pollution status in local areas, and ensure comprehensive prevention and strong control of pollution-related problems.

## PAST STUDIES

Industrial pollution has intensified continuously in Western countries since the Industrial Revolution, and has brought major challenges as a result of the Second Industrial Revolution. Thus, ecological environmental governance has attracted close attention in many developed countries. Studies on industrial pollution control began early in Western countries and achieved certain outcomes. In particular, the increasing maturity of big data theory and extensive applications of big data on environmental protection has raised the complexity of industrial pollution control. Using big data on environmental protection to implement pollution control not only can increase environmental pollution controlling efficiency and quality, but also can set up a perfect environmental governance system for a comprehensive examination and management of environmental pollution behaviours. With respect to industrial environmental pollution improvement and applications of big data on environmental protection, Dellink & Ierland (2006) introduced a dynamic application general equilibrium model with bottom-up important emission reduction information on environmental theme and conducted an empirical study on effective emission reduction strategies in the Netherlands. Results showed that environmental pollution status can be improved effectively through technological measures of emission reduction, economic restructuring, and temporary economic slowdown. Larsson & Telle (2008) measured the validity of DEA to pollution governance efficiency of energy enterprises in Norway based on panel data. He found that after the European Union (EU) implemented the Regulations for Comprehensive Pollution Prevention and Control, pollution governance efficiency of energy enterprises was improved significantly. Moreover, advanced pollution governance technologies that were beneficial to reduce emissions of greenhouse gases and acid substances were proposed. Zhao et al. (2009) believed that industrial water pollution was intensifying day by day as a result of rapid economic development in China; thus, he proposed a factory-level clustering method to estimate the spatial distribution of industrial water pollution pressure in the next five years. Moreover, he evaluated regional effect and spatial fairness from the perspective of government and industries and proposed specific measures to relieve industrial pollution. Jia & Zhao (2012) constructed an evaluation model space for industrial pollution control performance and used it to

evaluate the industrial pollution control performance in 30 provinces in China in 2003-2010. According to evaluation results, China's pollution governing performance improved quickly, but the great regional imbalance of pollution governing performance occurred in the eastern, middle, and western parts of the country. Specifically, pollution-governing performance in middle and eastern China was significantly higher than that in the middle and western parts of the country. Kanada et al. (2013) analyzed the benefits of pollution control policies in Kawasaki, Japan, finding that aviation pollution control policy has a great impact on industrial energy resources, thereby significantly decreasing the energy intensity of the manufacturing industry. Maria & Patrik (2014) believed that industrial pollution accounted for a very high proportion of global pollution and analyzed the validity of industrial pollution-control measures through the issuance of licenses for industrial plants in Sweden. Cao & Ramirez (2020) deemed that the rapid industrialization in China led to serious deterioration of air quality, and created a method to measure government policies for air pollution control; he concluded that government policies did not influence industrial production greatly when it decreased air pollution. Thuy et al. (2020) pointed out that environmental pollution caused by wastewater from an industrial park in Vietnam was a new problem that brought great pressure to the government. Moreover, different calculation methods of sewage in the industrial park were assessed and specific measures to control industrial sewage were proposed. Main theoretical studies and applications of big data on environmental protection are introduced as follows. Wu et al. (2016) pointed out that big data are widely applied as one of the strongest driving forces to promote productivity and increase efficiency and supporting innovation; he also discussed the relationship between big data and the new generation of the green revolution. Bibri & Elias (2017) believed that big data constitutes an important method to optimize energy efficiency and relieve impacts on the environment. Big data applications can play a key role in improving environmentally sustainable development. Song et al. (2018) reviewed the latest developments in environmental management based on big data technology and found that big data applications on practical environmental performance evaluation can provide scientific references and guidance in formulating environmental protection policies. Shan (2018) classified environmental protection projects effectively based on big data techniques. According to experimental results, studies on environmental pollution classification based on big data technology can complete the classification of abundant environmental data in a short period at extremely high precision. It is vital to the further development of environmental protection projects. Cheng & Yuyu (2018) collected abundant search data on public networks through the big data method and discussed influences of public concerns on environmental performances of enterprises in heavy-pollution industries; he concluded that enterprises with higher public concern have better environmental performances, which are conducive to the promotion and maintenance of China's environmental protection measures. Applying big data mining method, Liu et al. (2020) determined the orientation trend of food delivery service providers and the expansion trend of environmental pollution loads in the Beijing-Tianjin-Hebei region. He pointed out that food delivery service platforms, which are the bridge between food delivery service providers and consumers, can enhance the environmental protection mechanism. He also suggested strengthening environmental protection awareness of the public, changing the consumption mode of people, and achieving coexistence between resource utilization and environmental protection. Existing studies have shown that research on industrial pollution governance in foreign developed countries has been mature, and emerging technologies such as big data have gradually penetrated the environmental protection field. In China, limited studies have focused on industrial pollution governance. Most studies have emphasized administrative technologies, methods and pollution control, but applications of new technologies such as big data to environmental protection fields have not been sufficiently examined. Thus, we have conducted a case study on Jiangsu Province, China. Industrial pollution governance effect in the province was estimated and specific measures were proposed from big data applications of environmental protection to explore how such applications in environmental protection can contribute to pollution prevention and control. In this way, the value of big data can be maximized in environmental protection. Policy suggestions are proposed to formulate corresponding environmental protection schemes with consideration of practical environmental pollution conditions in China.

## INTRODUCTION TO MODELS AND DATA SPECIFICATIONS

### Models

Based on the improvement of the Cobb-Douglas production function, this study constructed a model (Eq. 1) to study the influencing factors of industrial pollution governance efficiency.

$$E_t = \beta_0 I_t^{\beta_1} L_t^{\beta_2} T_t^{\beta_3} S_t^{\beta_4} \quad (1)$$

According to some scholars, the influences of various factors are often hysteretic for generally one or two phases. For instance, the increased investment may not bring produc-

tion ability immediately in the current phase and an increased workforce takes a process of training and adaptation. Thus, explanatory variables were treated for one-phase hysteresis. Moreover, natural logarithms of all data were collected to ensure data stationarity. Finally, the used model was obtained as follows (Eq. 2) :

$$LnE_{t+1} = \beta_0 + \beta_1 LnI_t + \beta_2 LnL_t + \beta_3 LnT_t + \beta_4 S_t + \phi_t \quad (2)$$

Where $E_{t+1}$ represents industrial pollution governance efficiency characterized by removal rate of industrial COD, the removal rate of industrial $SO_2$ and comprehensive utilization of industrial solid wastes (*SOLID*). $I_t$ denotes capital inputs and is characterized by the finished amounts of investments to industrial wastewater control ($I_{cod}$), industrial waste gas control ( $Iso_2$ ), and industrial solid control (*Isolid*). $L_t$ refers to labour inputs and is characterized by the number of staff in the environmental protection system (*Labour*). $T_t$ implies technological innovation and is characterized by number of patent authorizations to industrial enterprises (*Tech*). $S_t$ refers to the industrial structure and is characterized by the proportion of industrial value-added in GDP for a particular year (*Strc*). $b_0$ is a constant term. $b_1$, $b_2$, $b_3$, and $b_4$ are elasticity coefficients, and $f_t$ is the error term.

### Data Specifications

All data were collected from past *Environmental Statistics Yearbook of China* and *Statistical Yearbook of Jiangsu Province*, which were available on the EPS data platform. The data in 2001-2018 were used as the explained variable and the explanatory variable. To eliminate influences of price factors, we deflated the finished amounts of investments to industrial pollution governance according to the price index of investment in fixed assets in Jiangsu Province.

## RESULT ANALYSIS

Models were established according to Eqs. 1-2. Model regression results based on EViews 9.0 software are listed in Table 1.

Table 1 shows that the three models have good regression fitting. The adjusted R-squared is higher than 0.85 and the F statistics are significant at 1% level. Labour input in the environmental protection system causes positive significant effects on industrial wastewater and industrial solid wastes. This result is related to the fast labour implementation of the environmental protection system in Jiangsu Province. This condition fully reflects that Jiangsu Province pays attention to industrial environmental protection, introducing professional industrial environmental protection talent vigorously, and increasing the efficiency of industrial environmental pollution governance. Technological innovation has positive and significant effects on industrial waste gas governance, indicating that Jiangsu Province has achieved great technological breakthroughs in industrial $SO_2$ governance and applied new technologies extensively. Industrial structure, a control variable, has negative effects on industrial wastewater governance but has positive impacts on industrial waste gas control. The reason may be that the industrial restructuring of Jiangsu Province focuses on closure and transformation of factories with heavy dependence on coal, which is a main $SO_2$ source, but it ignores restructuring with consideration for industrial wastewater. Environmental governance investment exerts a slight impact on industrial pollutant governance efficiency, which might be related to the small investment scale of environmental pollution governance. As a result, increasing investment in industrial environmental pollution governance in the future is suggested.

Table 1: Regression results of the models.

| Variable | COD | $SO_2$ | SOLID |
|---|---|---|---|
| Labour | 0.891*** | 0.436 | 0.182** |
| Tech | 0.023 | 0.128*** | 0.015** |
| Strc | –0.512** | 1.987** | 0.184* |
| Icod | –0.875 | - | - |
| $Iso_2$ | - | 0.713* | - |
| *Isolid* | - | - | –0.856 |
| $b_0$ | –8.012* | –3.298 | –2.391*** |
| Adjusted R-squared | 0.901 | 0.887 | 0.851 |
| F-Measure | 43.987*** | 65.786*** | 27.629*** |

(*, **, and *** mean that T statistics are significant on 10%, 5%, and 1% levels, respectively.)

## INDUSTRIAL POLLUTION GOVERNANCE MEASURES BASED ON BIG DATA OF ENVIRONMENTAL PROTECTION

**Establishing a scientific and high-efficiency big data monitoring network system for the ecological environment:** The big data on environmental monitoring is the basis for scientific, accurate, and effective environmental protection. Coverage and index items of existing ecological environmental monitoring networks cannot meet demands for evaluation, assessment, and alarm of environmental quality. Networking layouts of surface water and underground water have yet to be integrated and the environmental monitoring network layouts of atmosphere, soil, acoustic environment, ecology, and radiation have to be perfected. To ensure authenticity, accuracy, and comprehensiveness of environmental monitoring data, economic and environmental management departments have to improve their 24-hour/7-day monitoring network system by observing the integrity, systematic character, and internal laws of the ecosystem. The application values of big data on environmental protection can only be developed as long as real, accurate, and representative environmental monitoring data are collected.

**Making full use of the advantages of block-chain technologies in industrial pollution management:** Internet technology is the main basis for big data at present. Internet and multimedia platforms are necessary for better environmental pollution control. With the support of Internet technology, acquiring big data on environmental protection can be achieved comprehensively and conveniently. The public can understand the current conditions of ecological environmental pollution governance through multimedia or mobile applications. In this way, universal participation in environmental pollution control is increased, thereby further promoting ecological environmental pollution management. In addition, big data on environmental protection should fully utilize the advantages of block-chain technology and attention should focus on development and applications of scientific research innovation, united efforts in technological breakthrough, settle down and applications and achievement transformation. This approach not only increases the quality of big data on environmental protection but also supports scientific decision-making in environmental management while promoting economic and social development.

**Constructing a big-data sharing and processing platform for environmental protection:** Big data on environmental protection requires data management based on monitoring equipment during the application process. A higher requirement for data storage function of monitoring equipment is proposed due to diversified and real-time data updates. To improve the innovation effect of environmental pollution governance, a perfect environmental protection data processing platform can be constructed by combining Hadoop and Spark technologies and through distributed processing of big data on environmental protection. The platform can be used for comprehensive processing of various types of abundant environmental protection data. At present, China's big data processing platform for environmental protection has a high automation level and can provide effective data management services to existing environmental protection business, thereby significantly increasing the application effect of environmental protection data. Establishing an adaptive big-data sharing and processing platform for environmental protection can improve the sharing, processing, and service functions of environmental protection data, and realize effective integration and processing of data information related to environmental protection. As a result, environmental protection departments in all regions have to work together to set up a common data information library to realize service functions of data storage, management, and maintenance. On this basis, explicit interfaces between data management and services can be provided effectively.

**Increasing big data sharing and application values of environmental protection:** The coming era of big data not only provides guarantees to acquire environmental protection data but also ensures reasonable use of environmental protection data, thereby developing the role of big data technology in promoting environmental pollution control. Targeted integration of big data is needed, which not only increases the sharing effect of environmental protection data but also raises the application efficiency of big data in environmental pollution management. Using big data technology for environmental protection in environmental pollution governance aims to strengthen integration and correlation of data, thereby enabling to increase utilization of such data and providing data support for environmental pollution prevention and control. Therefore, relevant workers have to pay attention to increase the application values of big data on environmental protection, including meteorological, air quality, and meteorological monitoring data. Applying these data to environmental pollution governance does not only combine them simply but also develops their values fully through research. Combining various types of data effectively in specific environmental pollution control can improve the use of data validity.

## CONCLUSIONS

Heavy industrial pollution remains in China. As a result, the environment has deteriorated and resources are increasingly

depleted as extensive development occurs. Controlling industrial pollution emission and increasing the efficiency of emission reduction are important in supporting the economy and increasing living standards. Applying big data on environmental protection for environmental pollution management can significantly increase the efficiency of pollution control. It not only avoids waste of environmental protection data but also greatly improves the accuracy of environmental protection. In this case study on Jiangsu Province, China, industrial pollution governance efficiency is estimated and relevant industrial protection control measures based on big data technology are proposed. Results show that the trend of industrial pollution control for emerging technologies (e.g., big data) in the environmental protection field and labour input can considerably decrease industrial wastewater and industrial solid waste. Technological innovation has significant effects on industrial waste gas control. Finally, some environmental protection measures based on big data technology are proposed, including establishing a scientific and high-efficiency big-data monitoring network system for the environment, fully utilizing block-chain technological advantages in industrial pollution control, constructing a perfect big-data sharing and processing platform for environmental protection, and increasing the sharing and application values of big data on environmental protection. Further in-depth research is proposed on the best investment scale for industrial pollution control, construction of a big-data platform for industrial environmental protection, and a big-data dynamic simulation of environmental pollution governance.

## ACKNOWLEDGMENT

This study is sponsored by QingLan Project of Jiangsu Province, the New Generation Information Technology Team of Changzhou Institute of Technology (Grant No.YB201813101005) and Scientific Research Project Supported by Enterprise (Project No. HKKJ2020-37)

## REFERENCES

Bibri, S.E. and Elias, S. 2017. The IoT for smart sustainable cities of the future: An analytical framework for sensor-based big data applications for environmental sustainability. Sustainable Cities & Society, 38: 230-253.

Cao, D. and Ramirez, C. D. 2020. Air pollution, government pollution regulation, and industrial production in china. Journal of Systems Science and Complexity,33(2): 1064-1079.

Cheng, Jun and Liu, Yuyu 2018. The effects of public attention on the environmental performance of high-polluting firms: based on big data from web search in China. Journal of Cleaner Production, 186(10), 335-341.

Dellink, R. and Ierland, E.V. 2006. Pollution abatement in the Netherlands: A dynamic applied general equilibrium assessment. Journal of Policy Modeling, 28(2): 207-221.

Larsson, J. and Telle, K. 2008. Consequences of the Ippc's bat requirements for emissions and abatement costs: A DEA analysis on Norwegian data. Environmental & Resource Economics, 41(4): 563.

Liu, G., Agostinho, F., Duan, H., Song, G., and Lega, M. 2020. Environmental impacts characterization of packaging waste generated by urban food delivery services. a big-data analysis in Jing-jin-ji region (China). Waste Management, 117: 157-169.

Maria, P. and Patrik, S. 2014. Industrial pollution control and efficient licensing processes: The case of Swedish regulatory design. Sustainability, 6(8): 5401-5422.

Kanada, M., Fujita, T., Fujii, M. and Ohnishi, S. 2013. The long-term impacts of air pollution control policy: Historical links between municipal actions and industrial energy efficiency in Kawasaki city, Japan. Journal of Cleaner Production, 58(1): 92-101.

Jia, R.Y. and Zhao, D.T. 2012. Modeling performance of industrial pollution control: Empirical study from the perspective of environmental regulation. Systems Engineering, 6: 5-13.

Shan, Y. 2018. Research on big data classification for environmental protection based on differential equation. Environmental Science and Management, 6: 126-129.

Song, M. L., Fisher, R., Wang, J. L. and Cui, L. B. 2018. Environmental performance evaluation with big data: Theories and methods. Annals of Operations Research, 270(2): 459-472.

Thuy, P. T., Tuan, P. T., Huyen, D. T. T. and Khai, N. M. 2020. Insights of environmental impact assessment reports for industrial parks: Wastewater quantity prediction aspect. Environmental Monitoring and Assessment, 192(4): 1-13.

Wu, J., Guo, S., Li, J. and Zeng, D. 2016. Big data meet green challenges: Big data toward green applications. IEEE Systems Journal, 10(3): 888-900.

Zhao, N., Liu, Y. and Chen, J. 2009. Regional industrial production's spatial distribution and water pollution control: A plant-level aggregation method for the case of a small region in China. Science of The Total Environment, 407(17): 4946-4953.

Nature Environment and Pollution Technology
An International Quarterly Scientific Journal

p-ISSN: 0972-6268
(Print copies up to 2016)
e-ISSN: 2395-3454

Vol. 19 | No. 4 | pp. 1749-1753 | 2020

Original Research Paper

https://doi.org/10.46488/NEPT.2020.v19i04.047

Open Access Journal

# Desulfurization of Fuel by [Bmim]$CoCl_3$ and Potassium Monopersulfate

**Jun Zhang, Hang Xu† and Yang Li**

Chemical Engineering and Pharmaceutics School, Henan University of Science and Technology, Luoyang 471023, China

†Corresponding author: Hang Xu; xhinbj@126.com

**Nat. Env. & Poll. Tech.**
**Website: www.neptjournal.com**

*Received:* 02-01-2020
*Revised:* 23-01-2020
*Accepted:* 30-03-2020

**Key Words:**
Functional ionic liquid
Desulfurization
Benzothiophene
Potassium monopersulfate

## ABSTRACT

Functional ionic liquid [Bmim]$CoCl_3$ was prepared with potassium monopersulfate compound (PMS) to form extraction catalytic oxidative desulfurization system for benzothiophene (BT) removal. The best reaction conditions for removing BT were as follows: m (ionic liquid) = 2 g, m(PMS) = 1.5 g, C (initial sulphur) = 500 ppm, T = 40°C ~ 50°C. The desulfurization rate could be reached at 92.4 %. The ionic liquid still had higher activity after 5 cycles of reuse which exhibited that there was only a slight difference in the amount of the oxidant. It was proved that [Bmim]$CoCl_3$ ionic liquid combined with oxidant PMS has an excellent desulfurization performance.

## INTRODUCTION

Over the past two decades, haze pollution events have taken place in many developing countries. Some Chinese cities are suffering from smog pollution in winter. The smog brings great harm to human health, especially causing two main types of diseases, i.e. respiratory disease and cardiovascular disease. There are many reasons for the formation of haze, of which the most important is the one caused by sulphur pollution. For example, cars that burn sulphur containing gasoline or diesel fuel emit sulphur dioxide, which forms sulphate, the main material of smog, under the reaction of nitrogen dioxide in the air (Xu et al. 2014). To reduce the air pollution caused by sulphur, the sulphur content in gasoline or diesel fuel is strictly controlled all over the world. In 2016, the Chinese government issued a national standard (GB 17930-2016 and GB 19147-2016) for gasoline and diesel with a sulphur content of less than 10 ppm, the same as the USA and European countries.

In petroleum, there are two kinds of sulphur containing compounds, i.e. aliphatic sulphur and aromatic sulphur. Aliphatic sulphur compounds have acceptable activity, which can be easily removed by hydrodesulfurization (HDS) method. The aromatic sulphur compounds have a stable structure, which are difficult to be treated (Chen et al. 2015). Thiophene sulphides have aromatic and steric hindrance, so they are more difficult to be removed than other sulphides. Extraction catalytic oxidative desulfurization (ECODS) has become the most promising deep desulfurization technology due to its mild reaction conditions, simple experimental operation and excellent desulfurization effect, especially for aromatic sulphur compounds (Shakirullah et al. 2010). The desulfurization mechanism of ECODS is as follows: (1) the sulphur compounds in fuel are extracted by extractant (mostly ionic liquid), and (2) the catalyst and oxidant in the extractant cooperate for desulfurization. When the sulphur compounds are oxidized to sulfone organics, they are removed by polar solvent (Lv et al. 2013). For example, Jiang et al. (2014) selected [$C_4$mpip]$FeCl_4$/$H_2O_2$ system to perform a 73% sulphur removal from diesel. The dibenzothiophene (DBT) was treated by [Bmim] Cl/2$ZnCl_2$/$H_2O_2$ system with nearly 100% sulphur removal (Yu et al. 2011). Gao used [$C_4$min] $HSO_4$/$H_2O_2$ system to achieve 88.5% DBT removal (Gao et al. 2010). According to the analysis of literature, DBT as target pollutant was studied a lot and all the oxidant was $H_2O_2$.

Benzothiophene (BT), one of the thiophene sulphides, as target pollutant was studied. Compared with DBT, BT structure is relatively stable and difficult to be removed (Li et al. 2009). In our previous research (Xu et al. 2017), $H_2O_2$ was not a good oxidant because of instability characteristics and high price. In this study, potassium monopersulfate compound (PMS) was selected as the oxidant. Functional ionic liquid [Bmim]$CoCl_3$ was prepared with PMS to form ECODS for BT removal.

## MATERIALS AND METHODS

### Preparation of [Bmim]$CoCl_3$

[Bmim]$CoCl_3$ was prepared by mixing 1-n-butyl-3-methylimidazolium chloride ionic liquid ([Bmim]Cl) and cobalt chloride hexahydrate ($CoCl_2 \cdot 6H_2O$) in the molar ratio of 1:1 at 110°C for 48 hours to form homogeneous phase and evaporation of water. [Bmim]$CoCl_3$ ionic liquid is viscous blue liquid and stored in a desiccator. All reagents were required in the experiment were of analytical grade and purchased from Shanghai Aladdin Reagent Co., Ltd.

### Extraction Catalytic Oxidation Desulfurization Process

Ionic liquid [Bmim]$CoCl_3$ and model oil (6 g, sulphur content: 500 ppm) were added to a 40 mL flask in a certain ratio. A constant temperature water bath was used to control a certain reaction temperature, and stirred vigorously for 30 minutes so that the ionic liquid and the oil were in full contact until the extraction reached equilibrium. A certain amount of 20 wt% of PMS solution was added to the reaction vessel and stirred vigorously until the oxidative desulfurization reaction was complete. In the process of reaction, the upper liquid was taken regularly to analyse the sulphur content. The sulphur content was determined by an ultraviolet-visible spectrophotometer and calculated by the external standard method (A=0.07418+0.05366BT, $R^2$=0.9998). The desulfurization rate in the model oil is calculated by the following formula:

$$R\ (\%) = \left(1 - \frac{[S]_t}{[S]_0}\right) \times 100 \qquad \ldots(1)$$

Where, R is the desulfurization rate, $[S]_0$ is the initial concentration of sulphur in the model oil, $[S]_t$ is the concentration of sulphur in the model oil at t time.

## RESULTS AND DISCUSSION

### Effect of [Bmim]$CoCl_3$ Ionic Liquid Dosage On Desulfurization Rate

Fig. 1 shows the curves of desulfurization rate with time under the different dosages of [Bmim]$CoCl_3$ ionic liquid dosages. The fixed reaction conditions are as follows: T = 50°C, m(simulated fuel) = 6 g, C(initial sulphur) = 500 ppm, m(PMS) = 1.5 g, t = 100 min.

From Fig. 1, the reaction can be divided into two stages. The first stage (-30 min~0 min) is the extraction process, in which the BT is extracted from the oil phase to the ionic liquid phase by the ionic liquid. As is apparent from Fig. 1, at this stage, the desulphurization rate increases with the increase of ionic liquid dosage. When the ionic liquid dosages are 0.5 g, 1 g, 2 g, 3 g and 6 g, the desulfurization rates are 2.8 %, 6.7 %, 14.7 %, 29.3 % and 40.3 %, respectively. The second stage (0 min~70 min) is the ECODS process. It can be seen from Fig.1 that when the dosage of [Bmim]$CoCl_3$ increases from 0.5 g to 2 g, the rate of desulfurization increases significantly. After 70 minutes, the desulfurization rate increases from 50.3% (0.5 g ionic liquid) to 92.4% (2 g ionic liquid). Especially in the initial stage of the reaction (0 min~15 min), the desulfurization rate increases significantly. After 15 minutes, the rate of increase in the desulfurization rate tends to be flat. Under the dosage of 2 g ionic liquid, from 15 minutes to 70 minutes, the desulfurization rate only increases by 15.1 % (77.3 % to 92.4 %). When the ionic liquid increases to 6 g continuously, the desulfurization rate increases rapidly at the initial stage of the second stage reaction, and the desulfurization rate reaches 86.1 % after 10 min reaction. The ionic liquid dosage increases from 2 g to 6 g, the desulfurization rate increases from 92.4 % to 93.7 % after

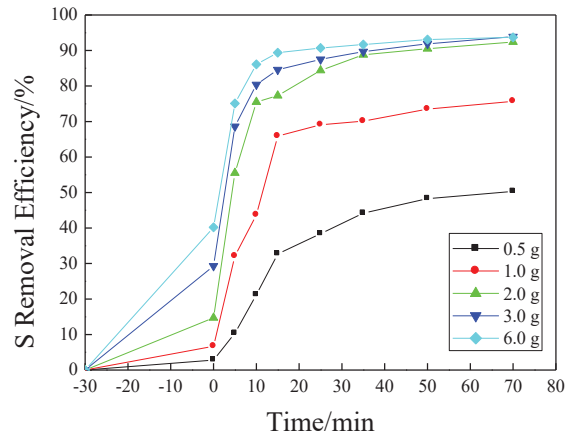


Fig. 1: Influence of the [Bmim]$CoCl_3$ dosage on S removal efficiency.

70 minutes. Therefore, considering the economic problems, the optimal dosage of [Bmim]/$CoCl_3$ ionic liquid is 2 g.

In the extraction stage, BT is extracted into the [Bmim]$CoCl_3$ ionic liquid phase firstly, and the extraction rate increases as the ionic liquid increases. After the addition of the oxidant PMS solution, cobalt ions catalyse the active component hydrogen ion in PMS to produce sulphate radicals which have strong oxidation ability to oxidize BT to oxidation products, such as $BTO_2$, and remove them. Therefore, with the increase of ionic liquid, the content of cobalt ions increases. The more sulphate radicals are formed to oxidize BT and the desulfurization rate increases. However, when the cobalt content of the system exceeds a certain value, the concentration of hydrogen ion does not increase, and the concentration of sulphate radicals does not increase significantly. Excess cobalt ions can be used as scavengers. Therefore, after the ionic liquid exceeds 2 g, the desulfurization rate increases less.

### Effect of Oxidant PMS Dosage on Desulfurization Rate

Fig. 2 shows the desulfurization rate versus time for different oxidant PSM dosages. The fixed reaction conditions are as follows: T = 50°C, m([Bmim]$CoCl_3$ ionic liquid) = 6 g, C(initial sulphur) = 500 ppm, t = 100 min (including 30 minutes' extraction time). It can be seen from the figure that the desulfurization rate of the PMS solution increases greatly. When the dosage of the PMS solution is in the range of 0.1 g to 1.5 g, the desulfurization rate increases as the amount of PMS increases. After 15 min reaction, when the dosage of the PMS solution increases from 0.1 g to 1.5 g, the desulfurization rate increases from 33 % to 91.9 % rapidly. When the dosage of PMS solution exceeds 1.5 g, the desulfurization rate shows a certain downward trend. The desulfurization rate is 77 % at 15 minutes, which is 14 % lower than the 1.5 g dosage.

Cause analysis: As an oxidant, PMS plays a vital role in the desulfurization process. As the amount of PMS increases, a large amount of sulphate radicals is produced, and the desulfurization rate is improved significantly. However, when the amount of PMS exceeds the optimum value, the strong acidity of hydrogen ion has a negative effect on the catalytic oxidation of cobalt ion. At the same time, hydrogen ion is also a scavenger for sulphate radicals, which is not conducive to reaction. Therefore, 1.5 g is the optimum dosage of the PMS solution.

### Effect of Reaction Temperature on Desulfurization Rate

Fig. 3 shows the desulfurization rate as a function of time at different temperatures. The fixed reaction conditions are: m (ionic liquid) = 2 g, m(PMS) = 1.5 g, C (initial sulphur) = 500 ppm, t = 100 minutes (including 30 min of extraction time).

It can be seen from Fig. 3 that both high temperature and low temperature are not conducive to desulfurization. Low temperature (30°C) is more conducive to desulfurization than high temperature (60°C). The optimum temperature range of the reaction is from 40°C to 50°C, which is close to room temperature. During the extraction phase (-30 min ~ 0 min), BT diffuses from the oil phase into the ionic liquid. When the extraction temperature is 30°C, 40°C, 50°C and 60°C, the desulfurization rates are 15.9%, 15.2%, 14.6%, 14.1%, respectively. The extraction of the desulfurization

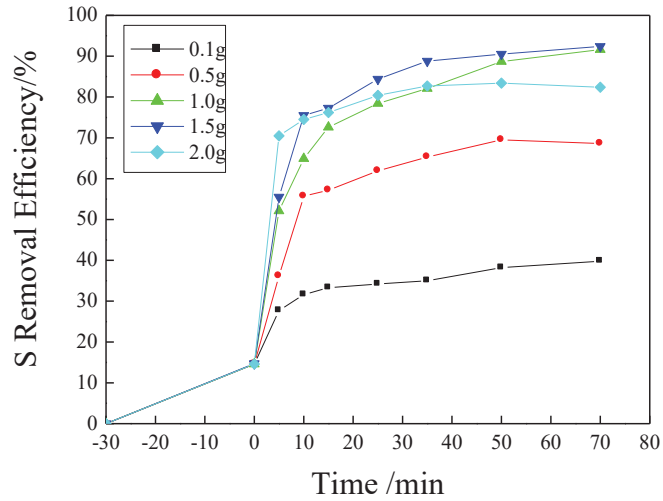


Fig. 2: Influence of the PMS dosage on S removal efficiency.

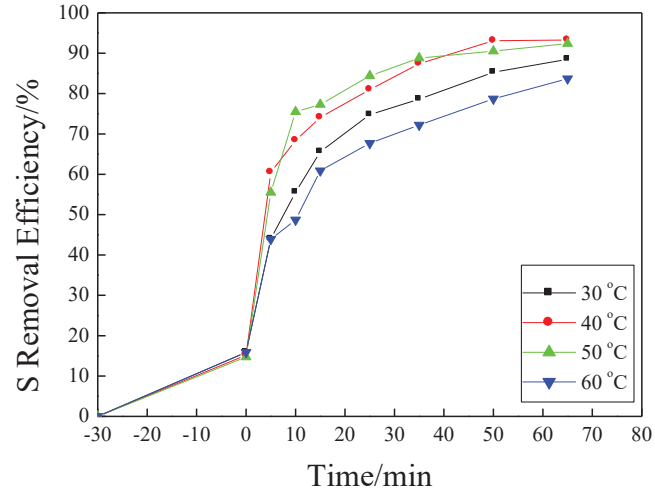


Fig. 3: Influence of temperature on S removal efficiency.

rate decreases slightly as the reaction temperature increases. In the ECODS phase (0 min ~ 70 min), the desulphurization rate at different reaction temperature is different after 15 min of reaction. When the reaction temperatures are 30°C, 40°C, 50°C and 60°C, the desulfurization rates are 65.7 %, 74.1 %, 84.9 % and 67.7 %, respectively.

Causes analysis: High temperature is not conducive to the catalytic oxidation process, PMS (decomposition temperature is 65°C) is unstable and easy to be decomposed at high temperature. However, high temperature helps to reduce the viscosity of the ionic liquid, which is beneficial to mix the ionic liquid and the oil phase. The ionic liquid [Bmim] $CoCl_3$ has a high viscosity at low temperature, which seriously hinders the mixing between the ionic liquid and the oil phase. Therefore, 40°C to 50°C is the optimum reaction temperature.

## Effect of Initial Concentration of BT on Desulfurization Rate

Fig. 4 shows the desulfurization rate versus time for different BT initial concentrations. The fixed reaction conditions are: m (ionic liquid) = 2 g, m(PMS) = 1.5 g, T = 50°C, t = 100 minutes (including 30 minutes' extraction time).

During the extraction phase (-30 min ~ 0 min), the initial sulphur content are 250 ppm, 500 ppm, 750 ppm, and 1000 ppm, the desulfurization rates are 18.3 %, 14.7 %, 11.5 %, and 8.7 %, respectively. In the ECODS phase (0 min ~ 70 min), after 70 min of reaction, the desulfurization rates of

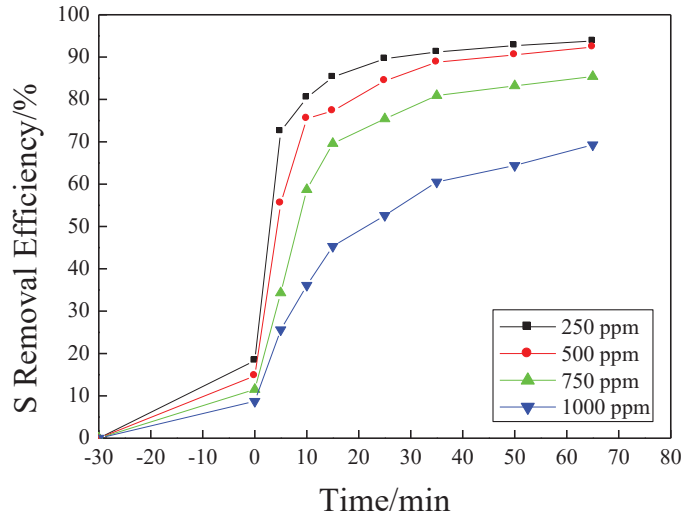


Fig. 4: Influence of initial S-content on S removal efficiency.

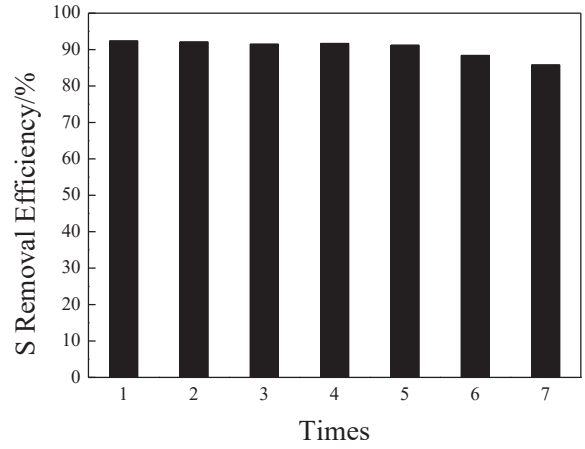


Fig. 5: Effect of recycling of used ionic liquid.

250 ppm, 500 ppm, 750 ppm, and 1000 ppm are 93.8 %, 92.4 %, 85.4 %, and 69.3 %, respectively. Therefore, in the case where the dosage of the ionic liquid and the PMS solution is constant, the desulfurization rate decreases as the initial sulphur content increases. However, in the entire reaction process, the overall removal of sulphur is increasing.

### Recycling Performance of Ionic Liquid [Bmim]$CoCl_3$

The recycling of ionic liquids is an important indicator for the industrialization of the system in the future. Separation and drying of ionic liquids after one reaction, then new BT model oil and PMS solution were added under the determined optimal reaction conditions, we have tested the performance of cyclic desulfurization. Figs. 3-5 show the recycling performance of ionic liquids. It can be seen from the figures that after repeated use for 5 times, the ionic liquid still maintains a good desulfurization performance, and the desulfurization rate is maintained above 90 %. At the 7th time, the desulfurization rate decreased slightly (85.8 %). It is proved that [Bmim]$CoCl_3$ ionic liquid has good performance.

## CONCLUSIONS

The best reaction conditions for removing BT were as follows: m(ionic liquid) = 2 g, m(PMS) = 1.5 g, C(initial sulphur) = 500 ppm, T = 40°C ~ 50 °C. The desulfurization rate could be reached at 92.4 %. The ionic liquid still had higher activity after 5 cycles of reuse which was exhibited that there was only a slight difference in the amount of oxidant. It was proved that [Bmim]$CoCl_3$ ionic liquid combines with oxidant PMS had excellent desulfurization performance once again.

## ACKNOWLEDGMENTS

This study was supported by the Nature Science Foundation of Henan Province (No: 202300410155) and Henan Provincial Science and Technology Foundation (No: 202102210236).

## REFERENCES

Chen, X.C., Guo, H.S., Ahmed, A.A., Guang, Y.W., Salem, S.A., Yu, G.R. and Yu, L. 2015. Brønsted-Lewis acidic ionic liquids and application in oxidative desulfurization of diesel fuel. Energy and Fuels, 29: 2998-3003.

Gao, H., Guo, C., Xing, J., Zhao, J. and Liu, H. 2010. Extraction and oxidative desulfurization of diesel fuel catalyzed by a Brønsted acidic ionic liquid at room temperature. Green Chemistry, 12: 1220-1224.

Jiang, W., Zhu, W.S., Chang, Y.H., Chao, Y.H., Yin, S., Liu, H., Zhu, F.X. and Li, H.M. 2014. Ionic liquid extraction and catalytic oxidative desulfurization of fuels using dialkylpiperidinum tetrachloroferrates catalysts. Chemical Engineering Journal, 250: 48-54.

Li, H.M., Zhu, W.S., Wang, Y., Zhang, J.T., Lu, J.D. and Yan, Y.S. 2009. Deep oxidative desulfurization of fuels in redox ionic liquids based on iron chloride. Green Chemistry, 11: 810-815.

Lv, H.Y., Ren, W.Z., Wang, H.O., Wang, Y., Chen, W. and Suo, Z.H. 2013. Deep desulfurization of diesel by ionic liquid extraction coupled with catalytic oxidation using an Anderson-type catalyst $[(C_4H_9)_4N]_4Ni$-$Mo_6O_{24}H_6$. Applied Catalysis A: General, 453: 376-382.

Shakirullah, M., Ahmad, W., Ahmad, I. and Ishaq, M. 2010. Oxidative desulphurization study of gasoline and kerosene: Role of some organic and inorganic oxidants. Fuel Process Technology, 91: 1736 -1741.

Xu, H., Zhang D.D. and Wu, F.M. 2017. Deep oxidative desulfurization of fuels based on $[C_4mimCl]CoCl_2$ ionic liquid oxone solutions at room temperature. Fuel, 208: 508-513.

Xu, S.H., Zhu, W.H., Zheng, D., Zhang, L., Liu, H., Yin, S., Zhang, M. and Li, H. 2014. Synthesis of metal-based ionic liquid supported catalyst and its application in catalytic oxidative desulfurization of fuels. Fuel, 136: 358-365.

Yu, G.R., Zhao, J.J., Song, D.D., Asumana, C., Zhang, X.Y. and Chen, X.C. 2011. Deep oxidative desulfurization of diesel fuels by acidic ionic liquids. Industrial and Engineering Chemistry Research, 50: 11690-11697.

Nature Environment and Pollution Technology
An International Quarterly Scientific Journal

p-ISSN: 0972-6268
(Print copies up to 2016)
e-ISSN: 2395-3454

Vol. 19 | No. 4 | pp. 1755-1762 | 2020

Original Research Paper

https://doi.org/10.46488/NEPT.2020.v19i04.048

Open Access Journal

# Performance of Semi-dry Anaerobic Digestion of Organic Solid Waste in Mesophilic Continuous Operation

**B. Sajeena Beevi*, G. Madhu** and Praseetha P. Nair***

*Department of Chemical Engineering, Govt. Engineering College, Thrissur-680 009, Kerala, India

**Division of Safety & Fire Engineering, School of Engineering, Cochin University of Science and Technology, Kochi-682 022, Kerala, India

†Corresponding author: B. Sajeena Beevi; sajeenanazer@gmail.com

**Nat. Env. & Poll. Tech.**
**Website: www.neptjournal.com**

*Received:* 07-05-2020
*Revised:* 20-06-2020
*Accepted:* 26-06-2020

**Key Words:**
Anaerobic digestion
Municipal solid wastes
Mesophilic condition
Biogas

## ABSTRACT

The purpose of this study was to evaluate the performance of anaerobic digestion of organic fraction of municipal solid waste to biogas in a mesophilic (32°C) continuous digester at a total solid concentration (TS) of 12%. The digester was operated with different organic loading rates and constant retention time. The performance of the reactor was evaluated using parameters like pH, volatile fatty acid (VFA), alkalinity, chemical oxygen demand (COD), total organic carbon (TOC), ammonia-N and biogas yield. During the reactor's start-up period (first phase), the process is stable and there is no inhibition occurred. In the second phase, the reactor was fed in continuous mode with different organic loading rates and constant retention time. The highest volatile solid (VS) degradation of 65.9%, with specific biogas production of 368 $L.kg^{-1}$ VS fed was achieved with organic loading rate (OLR) of 3.1 kg $VS.m^{-3}.d^{-1}$ and a retention time of 30 days.

## INTRODUCTION

Municipal solid waste (MSW) generation is significantly increasing in the Indian urban area and is creating enormous waste disposal problems in the recent past (Rao & Singh 2004). More than 90 % of the municipal solid waste generated in India is dumped in an unsatisfactory way, which creates environmental hazards to water, air and land. In general, the organic fraction of municipal solid waste (OFMSW) in India is about 40-60 % (Mufeed et al. 2008, Visvanathan et al. 2004). In Kerala, around 70% of the waste is compostable organics enabling a high level of recycling in the form of manure or fuel. Anaerobic digestion is widely being practiced as a major treatment option for disposal of organic fraction of municipal solid waste. It mainly combines with the energy recovery benefits, greenhouse gas mitigation and produces stable end products, which can be further upgraded as compost for soil applications (Forster-Carneiro et al. 2008, Walker et al. 2009).

Anaerobic digestion is a biological process wherein a diverse group of microorganisms convert the complex organic matter into a simple and stable end products in the absence of oxygen (De Baere 2000). The main advantages of this process are the low level of sludge generation, lower energy consumption and increased level of methane production. The main drawback is the slow rate of the process. Several research groups have developed anaerobic digestion processes using different organic substrates (Mata-Alvarez et al. 1992, Gallert et al. 2003). In general, anaerobic digestion systems are broadly categorized under wet (<10% total solids) or dry (>20% total solids), mesophilic (35-40°C) or thermophilic (>55°C), batch or continuous and single or two-stage systems (Yabu et al. 2011, Forster-Carneiro et al. 2008). The amenability of substrate for bio gasification, gas yield-organic loading relationships, bioprocess conversion efficiency and process inhibitory parameters vary from substrate to substrate, and also for different environmental and operating conditions such as pH, temperature, type and quality of the substrate, mixing, retention time etc. In this view, anaerobic digestion of solid waste is a process that is rapidly reaching to new advances especially in the area of dry anaerobic fermentation and has become a major focus of interest in waste management throughout the world. The purpose of this study was to analyse the performance of semi-dry anaerobic digestion of OFMSW in a single-stage pilot scale reactor in a continuous mode of operation at mesophilic condition (32°C). In this experiment, the optimization of the pilot scale reactor treating OFMSW was performed by testing different organic loading rates (OLRs). The study was started with a start-up phase (batch mode of operation) followed by continuous operation. In continuous operation, the effect of various organic loading rates on the stability

and performance of the reactor was evaluated at a constant retention time.

## MATERIALS AND METHODS

### Feedstock and Inoculum Preparation

Fresh organic fractions of MSW and inoculum were used as feed to the bioreactor. The organic fraction of MSW consists of food waste, fruit waste, vegetable waste from nearby vegetable market and household. The composition of the substrate was as follows: vegetable waste (35%), fruits (25%), food waste (37%) and paper (3%). The wastes were sorted and shredded, then mixed several times in laboratory and kept at 4°C until used for processing (Rodriguez et al. 2017, Kim et al. 2002). The inoculum used in this study was fresh cattle dung which contains all the required microbes essential for anaerobic digestion process. The percentage of inoculation for acidogenic fermentation of organic urban wastes is approximately 30% (w/w). The pH, total solids and volatile solids of the inoculum were 6.5, 26.2% and 82.5% respectively. The characteristics of the substrate and feed are given in Table 1.

### Experimental Set-up

The experiments were performed in a pilot scale reactor. The digester, made of transparent acrylic sheet, was designed for a total volume of 36.8 L and working volume (80% of total volume) of 29.4 L. The lower portion of the reactor was of conical shape making the discharge of drain leachate easy. A perforated plate was provided above this conical bottom. A bottom pipe was connected to collect the leachate produced and the pipe was connected to a peristaltic pump which was used for recirculation purpose. To obtain a homogeneous suspension, liquid from the bottom of the reactor was withdrawn by a peristaltic pump and recirculated through the top of the reactor. Waste is fed through a hopper connected on the top of the reactor. A wet gas meter (INSCIN) is provided at the gas outlet pipe to measure the biogas flow via a water seal. As per the required waste load, daily feeding was done from the top while almost the same quantity of the digestate was removed from the reactor through digestate outlet as shown in Fig. 1 in continuous operation. The system was operated in semi-continuous mode with feeding one time per day. Fig. 1 shows the experimental set-up.

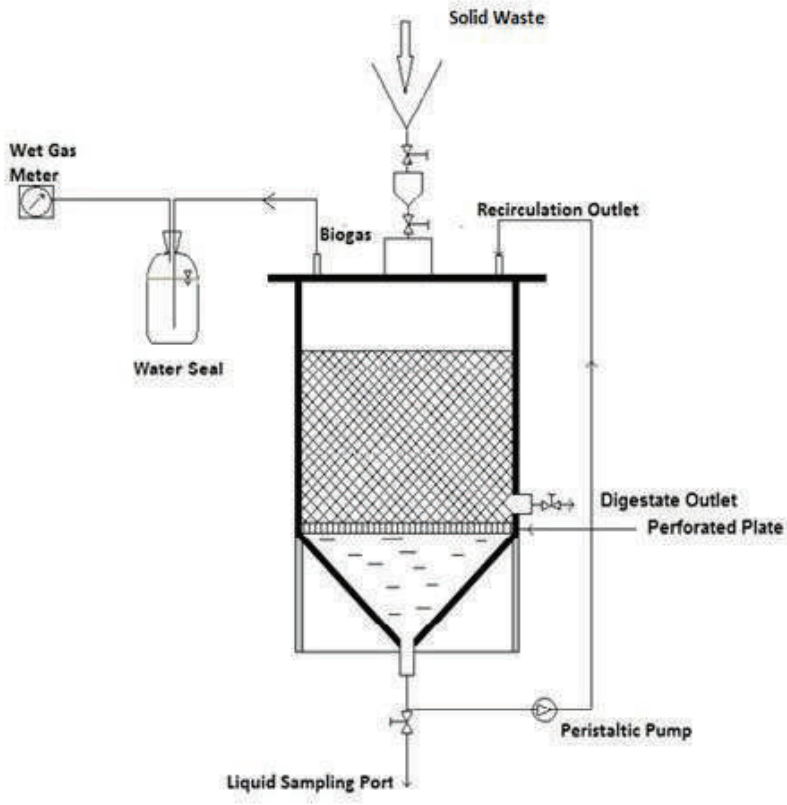


Fig. 1: Pilot-scale experimental setup of semi-dry anaerobic digester.

Table 1: Characteristics of the substrate and feed during the start-up of the pilot experiment.

| Parameter | OFMSW | Feed |
|---|---|---|
| pH | 6.12 | 6.65 |
| TS (%) | 19.02 | 12.30 |
| VS (%) | 85.65 | 85.12 |
| VFA (meq.$L^{-1}$) | 10.85 | 10.57 |
| COD (mg.$L^{-1}$) | 35230 | 36018 |
| TKN (g.$L^{-1}$) | 1.04 | 1.06 |
| TOC (g.$L^{-1}$) | 22.49 | 24.5 |

## Experimental Condition

In this experiment, the optimization of semi-dry anaerobic digestion at mesophilic temperature (32°C) was studied by varying the OLR. The study included both start-up operation as well as a continuous operation. The details of experimental conditions are given in the following subsections.

**Start-up operation**: Fresh organic fractions of MSW and inoculum were used as feed to the bioreactor. For the start-up operation, the prepared feedstock was loaded into the reactor after mixing it well with the inoculum. The reactor was initially loaded with 12 kg of feedstock and 3.6 kg of inoculum source. Water was added to obtain the desired total solid concentration. The total solid concentration of the feed was 12%. The system was operated without loading any additional feedstock for the first 50 days and it is considered as start-up phase. During the initial start-up phase, the system pH was neutralized using commercial caustic soda solution (6N NaOH) for quick onset of methanogenesis in the digester. To obtain a homogeneous suspension, leachate from the bottom of the reactor was recirculated by the peristaltic pump at the rate of 0.08 L/min for 6 hours daily.

Table 2: Operating conditions of pilot scale experimental reactor.

| Run | Loading rate (kg.$day^{-1}$) | OLR (kg VS.$m^{-3}$.$d^{-1}$) | Retention time (day) |
|---|---|---|---|
| Start up | - | - | 50 |
| Continuous 1 | 0.85 | 3.1 | 30 |
| 2 | 1.3 | 4.2 | 30 |
| 3 | 1.5 | 5.65 | 30 |

During this period, the system was continuously monitored for the fluctuations in process parameters such as biogas rate, ammonia-N, chemical oxygen demand (COD), total organic carbon (TOC), volatile fatty acids (VFA), alkalinity and pH. The pH of the digestate was analysed every 2 days, whereas all other parameters were analysed once in a week to interpret the process performance.

**Continuous operation**: The reactor was operated in a continuous mode from day 51 onwards by loading the reactor with designed OLRs. As detailed in Table 2, the feedstock was loaded into the reactor with different OLRs of 3.1, 4.2 and 5.65 kgVS.$m^{-3}$.$d^{-1}$ in three consecutive runs (1 to 3) with a constant retention time of 30 days. Each run was continued until the biogas yield attained to its steady-state, with no further increment, in the digester. To obtain a homogeneous suspension, leachate from the bottom of the reactor was re-circulated using the peristaltic pump at the rate of 0.08 L.$mt^{-1}$ for 6 hrs. At each feeding, one part of the fresh feedstock was mixed up with the two parts (wt./wt. basis) of the digestate collected from the reactor. As per the required waste load, daily feeding was done from the top while almost the same quantity of the digestate was removed from the reactor. Feeding and the digestate withdrawal were done once in a day. During this period, the system was continuously monitored for the fluctuations in process parameters such as biogas

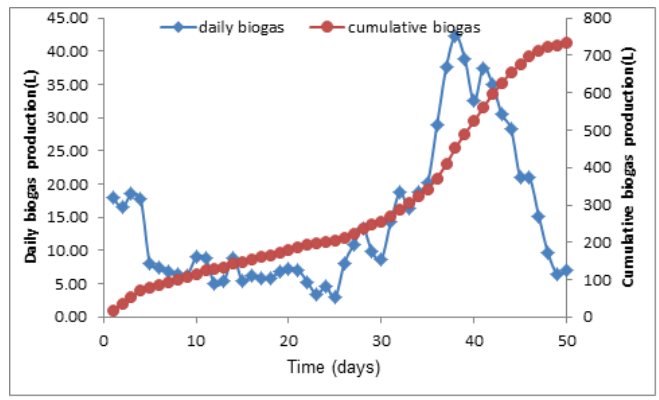


Fig. 2: Daily and cumulative biogas production during the start-up period.

rate, ammonia-N, COD, VFA, alkalinity and pH as well as other digestate parameters (TS, VS and TOC). The pH was measured every 2 days, whereas all other parameters were analysed once to twice a week to interpret the process performance. Operating Conditions of the pilot scale experimental reactor is shown in Table 2.

### Analytical Methods

The parameters analysed for the characterization of substrates were as follows: Total solids (TS), volatile solids (VS), pH, VFA, total Kjeldahl nitrogen (TKN), and total organic carbon (TOC). Following quantities were monitored during the digestion process: pH, VFA, alkalinity, $NH_3$-N, COD and TOC. All analytical determinations were estimated according to the procedures recommended by APHA (1998). pH was measured using a digital pH meter (μpH System 362). TS samples were dried in an oven at 105-110°C, and for VS, the ash waste was dried in a muffle furnace at 500±50°C. TKN and $NH_3$-N content were examined by the spectrophotometer (HITACHI, U-2900 UV/VIS spectrophotometer). VFA and alkalinity were determined using a simple titration method (Anderson & Yang 1992). TOC analysis was carried out using Shimadzu TOC-LCPH/CPN analyser for non-purgeable organic carbon as per the standard methods.

## RESULTS AND DISCUSSION

This study was conducted in two phases, namely the reactor start-up (Phase 1) and continuous operation (Phase 2).

### Phase 1: Performance of the Reactor During Start-up

Digestion during start-up ran for a period of 50 days. Biogas production is the primary indicator to evaluate the performance efficiency of the reactor. Fig. 2 indicates the daily and cumulative biogas production, where, the biogas production was high at the beginning which was due to the entrapped air inside the reactor. From Fig. 2, it is clear that the biogas production was low between 5$^{th}$ and 23$^{rd}$ days. This may be due to the reduction of pH. So after adjusting the pH value in

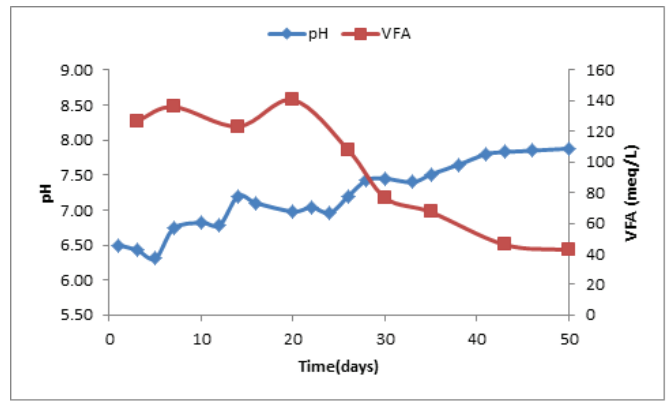


Fig. 3: Variation of pH and VFA during the start-up period.

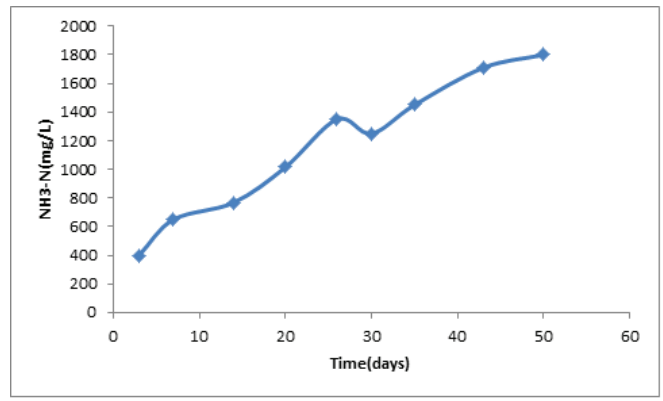


Fig. 4: Evolution of $NH_3$-N during the start-up process.

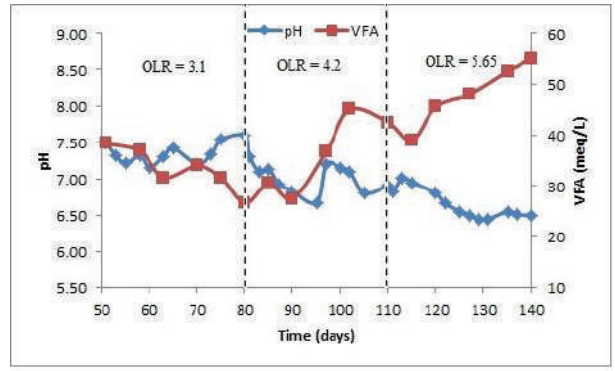


Fig. 5: Variation of pH and VFA during continuous loading.

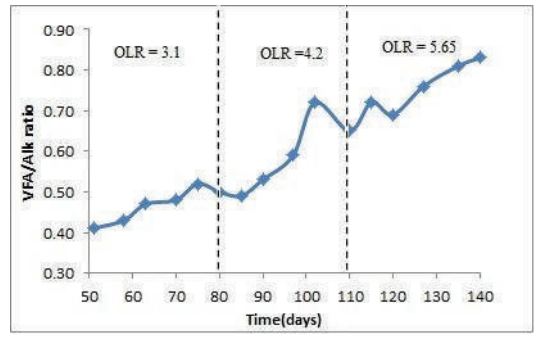


Fig. 6: VFA/Alk ratio in the digester during continuous loading.

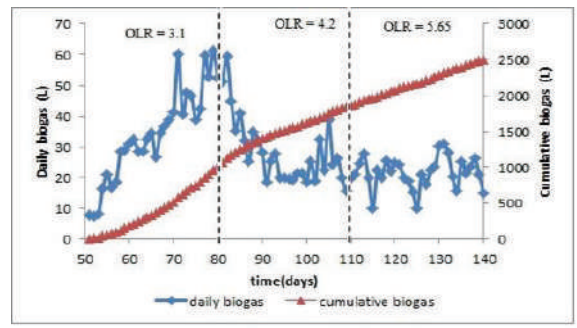


Fig. 7: Daily and cumulative biogas production during different OLRs.

the neutral range by the addition of 6N NaOH to the system, the production was increased. pH control favours the biodegradation process (Banks 2008). The highest volume of biogas produced (42.3 $L.d^{-1}$) was achieved at day 38. The biogas production rate decreased after day 39 indicating exhausting of readily accessible substrate for biogas production. The reactor system was run until the gas production rate peaked and then dropped below 06.5 L of gas per day. Then, the feeding and withdrawing mode of operation was started. During the start-up phase, approximately 735 L biogas was produced.

The pH and volatile fatty acid (VFA) variation during the start-up period are shown in Fig. 3. pH was initially 6.5, which started to decrease to 6.31. Therefore, small quantities of 6N NaOH were added to the reactor periodically during days 5-24 to maintain pH at the near-neutral range. This can be noted as small peaks during days 5-24 in Fig. 3. From day 26 onwards, pH started increasing slowly; therefore, NaOH was not added anymore. It became stable at around 7.8 during

days 41-50. The VFA generation in the beginning was high due to higher acidogenesis and lower methanogenic activity. The initial pH drop and high volatile fatty acid concentration show that the substrate contains some easily biodegradable constituent. VFA concentration was increased till 20$^{th}$ day and maximum VFA concentration of 140.5 meq.L$^{-1}$ was formed on the same day. After that VFA concentration was found decreased due to methanogenic activity in which the intermediate organic acids were started to convert into biogas. The concentration of VFA dropped from 140.5 meq.L$^{-1}$ to 42.5 meq.L$^{-1}$ in 30 days. The reason is that there was no waste feeding throughout the start-up phase (day 1-50).

The organic content of the substrate was measured in terms of COD and TOC. The significant increase in COD in leachate was observed at the beginning which was the sign of an active hydrolyse phase. The COD and TOC of the leachate were found decreasing due to the conversion of organic matter into biogas. The trend of ammonia-nitrogen ($NH_3$-N) during the start-up process is shown in Fig. 4. In this experiment, concentrations of $NH_3$-N were increasing due to the release of ammonia during the hydrolysis of protein. Ammonia nitrogen is an important parameter for the bu er capacity in an anaerobic reactor. With concentrations up to 1000 mg/L, ammonia nitrogen stabilizes the pH value. Ammonia nitrogen is released during the anaerobic hydrolysis of protein, causing an increase in the pH value. It is evident that the ammonia nitrogen concentration (>6000 mg.L$^{-1}$) indicates the inhibition of methanogens in an acclimated environment (Mata-Alvarez et al. 2000). In this study, the $NH_3$-N concentration increased from 400 mg.L$^{-1}$ to 1800 mg.L$^{-1}$. So it can be concluded that there was no inhibition of ammonia nitrogen during the AD process of this system during the start-up process.

**Phase 2: Continuous Operation**

In this operation, continuous feeding was applied in draw and feed mode. Experiments were conducted for three different organic loading rates of 3.1, 4.2 and 5.65 kg VS.m$^{-3}$.d$^{-1}$ in three consecutive runs with a constant retention time of 30 days.

**Effect of Organic Loading Rate on Stability Parameters of The Reactor**

(i) pH and VFA

In the anaerobic digestion process, methanogenic bacteria are more sensitive to environmental conditions than hydrolytic and acidogenic bacteria. The first criterion that was taken into account is the pH value. The pH indicates the stability of the system and its variation also depends on the buffering capacity itself. The pH is an indicator of good process performance and should be above 7.0 at all times in which case the process operates successfully. With OLR of 3.1 kg VS.m$^{-3}$.d$^{-1}$, the system stabilized its pH around 7.36 with a range of 7.15-7.6 as shown in Fig.5. When the OLR was increased from 3.1 to 4.2 kg VS.m$^{-3}$.d$^{-1}$, pH fell to 6.8 and regulated to an average of 7.01 (6.8-7.31). As a result of a further increase in OLR to 5.65 kg VS.m$^{-3}$.d$^{-1}$, a drastic decrease in pH was observed and pH dropped to the value of 6.5. The decline in pH in the starting days of each of the first two runs and most of the last run is linked to the destabilization of the system as a result of an increase in OLR. The reason is that when organic loading rate is increased, the acidogens also increase their activity and produce a high amount of VFA, as they are fast-growing. But, on the other hand, methanogens owing to their slow specific growth rate cannot utilize all the already produced VFA and need more time to build the required population size. Thus initial and a temporary decrease in pH occurred due to accumulation of VFA as a result of the imbalance in the microbial groups, is recovered when methanogens build their sufficient population. The decrease in pH is more pronounced while working with higher OLR, i.e., 5.65 kg VS.m$^{-3}$.d$^{-1}$. The reason is that the imbalance between acidogenic and methanogenic activity is more at high OLRs. The concentration of volatile fatty acids in the digestate was quite stable at an average value of 33.2 meq.L$^{-1}$ (range: 26.6-38.4 meq.L$^{-1}$) while operating at OLR of 3.1 kg VS.m$^{-3}$.d$^{-}$. When OLR was increased to 4.2 kg VS.m$^{-3}$.d$^{-}$, VFA concentration started to increase and reached a maximum value of 45 meq/L with an average value of 36.5 meq.L$^{-1}$ in this run. Finally, at an OLR of 5.65 kg VS.m$^{-3}$.d$^{-1}$, the VFA concentration increased to 55 meq. L$^{-1}$ because of increasing organic loading rate. This trend shows the destabilization of the reactor caused by an increase in OLR. It is important to note that at the start of each OLR, the VFA started to accumulate, which is related with the imbalance of activity of microbial groups and initial temporary destabilization of the reactor as a result of an increase in OLR as discussed above in the case of pH. Similarly, at the end of each of the first two OLRs, the concentration of VFA declined, which is a sign of stability of the system.

(ii) VFA to Alkalinity Ratio (VFA/Alk Ratio)

VFA/Alk ratio is a good indicator of digester functioning. It is shown in Fig. 6. With OLR of 3.1 kgVS.m$^{-3}$.d$^{-1}$, this parameter remained between 0.41 and 0.52 for most of the time. This is a good range of VFA/Alk ratio for a digester to work. But at OLR of 4.2 kg VS.m$^{-3}$.d$^{-1}$, the average value of VFA/Alk ratio increased to 0.59, which is still acceptable for an operating digester. However, at OLR of 5.65 kg VS.m$^{-3}$.d$^{-1}$, VFA/Alk ratio increased to a very harmful range (0.72-0.83) because at VFA/Alk ratio of 0.8, significant pH reduction and digester failure happen.

### Performance of Pilot Scale Reactor At Different Loading Rate

**Biogas production:** Biogas production was monitored daily. One of the main objectives of this research was to determine the performance of the AD process when operated at different loading rates. To evaluate this system on the effect of loading rate, biogas production, specific biogas production or biogas yield and VS reduction were taken as the indicators to assess the reactor performance of each loading rate. Fig. 7 shows the daily and cumulative biogas production during continuous loading. The average biogas production rate during runs 1, 2 and 3 was approximately 34 L/d, 28 L/d and 21.6 $L.d^{-1}$ respectively. It can be noted that at the end of OLR 3.1 and 4.2 kg $VS.m^{-3}.d^{-1}$, the gas production rate becomes stable. This is related to stable pH and VFA concentration of the system at the mentioned time. The decrease in the biogas production rate was almost linear with the increase in OLR during the first two runs. But, during run 3 (i.e. OLR 5.65 kg $VS.m^{-3}.d^{-1}$), the gas production rate did not decrease with the same rate as that of OLR. This could be explained from a drastic increase in the VFA/Alk ratio (or drop in alkalinity) during that run.

**VS removal and Specific biogas production:** Volatile solid reduction was taken into consideration as well to evaluate the reactor performance and stability of the digestate. VS degradation value of 65.9 % was achieved when operating at OLR of 3.1 kg $VS.m^{-3}.d^{-1}$. On the other hand, while loading rate 2 and 3 with increased OLR of 4.2 and 5.65 kg $VS.m^{-3}.d^{-1}$, VS removal were decreased to 55.2 % and 43.7 % respectively. Comparably, these VS reductions were lower with the result found by Castillo et al. (2006) who reported that VS reduction of 77.1% was obtained with the digestion time of 25 days. This lower value may be due to the reactor configuration. But, these results are similar to those obtained by Gallert & Winter (2003). They obtained VS removal of 65 % in a thermophilic system operating at OLR of 9.5 kg $VS.m^{-3}.d^{-1}$ and 18% TS. The highest specific biogas production observed was 368 L/kgVS fed at OLR of 3.1 kg $VS.m^{-3}.d^{-1}$. As the loading rate was increased, decreases in the biogas yields (229 L/kgVS and 130 L/kgVS) were observed at OLR of 4.2 and 5.65 kg $VS.m^{-3}.d^{-1}$ respectively. The overloading was marked by the fall in pH and gas yield. However, the specific biogas production of 368 L/kg VS at OLR of 3.1 kg $VS.m^{-3}.d^{-1}$ of this study is in line with the biogas yield values found in the literature. The biogas yield reported by various authors through dry anaerobic digestion of OFMSW at thermophilic conditions is in the range of 350-500 L/kg VS added (Pavan et al. 2000, Montero et al. 2010, Bolzonella et al. 2003). Similarly, biogas yield reported for water sorted organic fraction of municipal solid waste (WS-OFMSW) under mesophilic semi-dry anaerobic digestion was 423L/kg VS added (Li et al. 2010). It should be cautioned here that the optimum loading rate of 3.1 kg $VS.m^{-3}.d^{-1}$ observed here is not universal as the optimal rate depends upon the reactor configuration.

## CONCLUSIONS

The present study focused on the continuous operation of semi-dry anaerobic digestion of OFMSW under mesophilic condition. In this study, an effective start-up of the anaerobic digestion with inoculum was done successfully. During the continuous operation, when the loading rate was increased, the biogas production decreased. Specific biogas production or biogas yield dropped from 368L/kgVS to 130 L/kgVS when loading rates were increased from 3.1 to 5.65 kg $VS.m^{-3}.d^{-1}$. The highest VS degradation of 65.9% was obtained with OLR of 3.1 kg $VS.m^{-3}.d^{-1}$at a retention time of 30 days. From the present study, the optimum loading rate obtained for maximum biogas production was 3.1 kg $VS.m^{-3}.d^{-1}$.

## REFERENCES

Anderson, G.K. and Yang, G. 1992. Determination of bicarbonate and total volatile acid concentration in anaerobic digesters using a simple titration. Water Environ. Res., 64: 53-59.

APHA 1998. Standard Methods for the Examination of Water and Wastewater. 20th ed., American Public Health Association, Washington, DC, USA.

Banks, C. J. and Chesshire, M. 2008. A pilot-scale comparison of mesophilic and thermophilic digestion of source segregated domestic food waste. Water Science and Technology, 58(7): 1475-1481.

Bolzonella, D., Innocenti, L., Pavan, P., Traverso, P. and Cecchi, F. 2003. Semi-dry thermophilic anaerobic digestion of the organic fraction of municipal solid waste: Focusing on the start-up phase. Bioresource Technology, 86(2): 123-129.

Castillo, M.E., Cristancho, D.E. and Arellano, V A. 2006. Study the operational condition for anaerobic digestion of urban solid wastes. Waste Management, 26: 546-556.

De Baere, L. 2000. Anaerobic digestion of solid waste: State-of-the-art. Water Science Technology, 41: 83-290.

Forster-Carneiro, T., Perez, M. and Romero, L.I. 2008. Thermophilic anaerobic digestion of source-sorted organic fraction of municipal solid waste. Bioresource Technology, 99: 6763-6770.

Gallert, C., Henning, A. and Winter, J. 2003. Scale-up of anaerobic digestion of the biowaste fraction from domestic wastes. Water Research, 37: 1433-1441.

Kim, D. and Oh, S. 2011. Continuous high-solids anaerobic co-digestion of organic solid wastes under mesophilic conditions. Waste Management, 31(9): 1943-1948.

Li, Dong, Yuan, Zhenhong and Sun, Yongming 2010. Semi-dry mesophilic anaerobic digestion of water sorted organic fraction of municipal solid waste (WS-OFMSW). Bioresource Technology, 101: 2722-2728.

Mata-Alvarez, J., Mace, S. and Llabres, P. 2000. Anaerobic digestion of organic solid wastes. An overview of research achievement and perspectives. Bioresource Technology, 74: 3-16.

Mata-Alvarez, J., Llabres, P., Cecchi, F. and Pavan, P. 1992. Anaerobic digestion of the Barcelona central food market organic wastes: Experimental study. Bioresource Technology, 39: 39-48.

Montero, B., Garcia-Morales, J.L., Sales, D. and Solera, R. 2010. Evolution of butyric acid and the methanogenic microbial population in a thermophilic dry anaerobic reactor. Waste Management, 30(10): 1790-1797.

Mufeed, Sharholy, Kafeel, Ahmad and Gauhar, Mahmood 2008. Municipal solid waste management in Indian cities- A review. Waste Management, 28: 459-467.

Pavan, P., Battistoni, P., Mata-Alvarez, J. and Cecchi, F. 2000. Performance of thermophilic semi-dry anaerobic digestion process changing the feed biodegradability. Water Science and Technology, 41(3): 75-81.

Rao, M.S. and Singh, S.P. 2004. Bioenergy conversion studies of organic fraction of MSW: Kinetic studies and gas yield-organic loading relationships for process optimization. Bioresource Technology, 95: 173-185.

Rodriguez, C., Alaswad, A. and El-Hassan, Z. 2017. Mechanical pretreatment of waste paper for biogas production. Waste Management, 68: 157-164.

Visvanathan, C., Trankler, J., Joseph, K., Chiemchaisri, C., Basnayake, B.F.A. and Gongming, Z. 2004. Municipal Solid Waste Management In Asia, Asian Regional Research Program On Environmental Technology (ARRPET). Asian Institute of Technology Publications, ISBN: 974-417-258-1.

Walker, L., Charles, W. and Cord-Ruwisch, R. 2009. Comparison of static, in-vessel composting of MSW with thermophilic anaerobic digestion and combinations of the two processes. Bioresource Technology, 100(16): 3799-3807.

Yabu, H., Sakai, C., Fujiwara, T., Nishio, N. and Nakashimada, Y. 2011. Thermophilic two-stage dry anaerobic digestion of model garbage with ammonia stripping. J. Bioscience and Bioengineering, 111: 312-319.

Nature Environment and Pollution Technology
An International Quarterly Scientific Journal

p-ISSN: 0972-6268
(Print copies up to 2016)
e-ISSN: 2395-3454

Vol. 19 | No. 4 | pp. 1763-1766 | 2020

Original Research Paper

https://doi.org/10.46488/NEPT.2020.v19i04.049

Open Access Journal

# 16S rRNA Phylogenetic Analysis of Heavy Metal Tolerant Plant Growth Promoting Rhizobacteria

**Shuchita Verma*† and Baljeet Singh Saharan****
*Department of Microbiology, Microbial Resource Technology Laboratory, Kurukshetra University, Kurukshetra, Haryana-136119, India
**Department of Microbiology, CCS Haryana Agricultural University, Hisar-125004, India
†Corresponding author: Shuchita Verma; shuchitaverma86@gmail.com

**Nat. Env. & Poll. Tech.**
**Website: www.neptjournal.com**

*Received:* 11-12-2019
*Revised:* 21-12-2019
*Accepted:* 03-01-2020

**Key Words:**
PGPR
16S rRNA sequence
*Pseudomonas fluorescence*
Rhizosphere

## ABSTRACT

The present study was aimed to characterize the bacterial isolate DDI(I)1 isolated from the rhizospheric soil of *Ocimum* grown in New Delhi (India). The isolate exhibited multiple plant growth promoting activities namely ammonia production, production of phytohormones, hydrogen cyanide, solubilization of minerals, tolerance against heavy metals, etc. The isolate was morphologically and biochemically characterized and it was found that DDI(I)1 belongs to genus *Pseudomonas*. Further, 16S rRNA sequencing revealed that the isolate shared 99% homology with *Pseudomonas fluorescens*.

## INTRODUCTION

The rhizosphere is the region around the roots of plants where the nutrient availability is very high due to the release of plant photosynthates from the roots (Lynch 1991). This region is actively colonized by the bacterial community including beneficial bacteria known as PGPR, i.e. plant growth promoting rhizobacteria. PGPR promote the plant growth in different ways such as suppression of plant pathogens and production of useful compounds helping in increased crop yield. Due to these bacteria, we can reduce the use of chemical fertilizers (Saharan & Nehra 2011, Glick 2012). These are an eco-friendly way for sustainable agriculture and do not pose any threat to human and animal health (Saharan & Verma 2015).

Few examples of PGPR are *B. licheniformis* CECT5106, *B. pumilus* CECT5105, *Bacillus subtilis* A13, *Enterobacter cloacae* UW4 & CAL2, *P. fluorescens* Pf-5, *P. fluorescens* 2-79, *P. fluorescens* CHA0, *Pseudomonas putida* GR12-2 (Turner & Backman 1991, Jacobson et al. 1994, Shah et al. 1998, Li et al. 2000, Wang et al. 2000, Penrose & Glick 2001, Probanza et al. 2002). One of the most promising candidates as PGPR is *Pseudomonas fluorescens*. *Pseudomonas* and *Bacillus* confer plant growth enhancement and control of diseases against phytopathogens (Hamid & Ahmad 2010). *Pseudomonas fluorescence* inoculant stimulated chickpea growth and yield (Rokhzadi et al. 2008). A total of 140 PGPR strains of *Pseudomonas* were obtained from potatoes rhizosphere at Dehradun Valley, India (Deshwal et al. 2013). About 30 PGPR strains belonging to fluorescent *Pseudomonas* with PGP activities were isolated from the rhizosphere of rice and characterized by PCR-RAPD analysis (Reddy & Reddy 2009). The present study was aimed to characterize the isolate DDI(I)1 due to its multiple plant growth promoting traits it possesses.

## MATERIALS AND METHODS

### Collection of Soil Samples, Isolation and Screening for PGP Traits

Soil samples were collected from the rhizospheric soil of *Ocimum* sp. plants from different localities of Kurukshetra, Delhi and Haridwar. The intact soil of the roots was collected carefully in sterile plastic bags and stored at 4°C in the laboratory until their further use. The isolate was obtained from the rhizospheric soil of *Ocimum* grown in Delhi and further screened for various PGP traits. The isolate was found to possess multiple plant growth promotion activities such as solubilization of phosphorus, IAA production, HCN production, siderophore production, tolerance to heavy metals, etc.

These numerous activities render it a potential candidate for sustainable agriculture so the present study was undertaken to characterize this isolate DDI(I)1.

### Morphological and Phenotypic Characterization

Selected isolates were examined for the colony morphology. Different morphological characteristics such as colony size, colour, shape, margin, pigmentation, elevation, etc. were recorded for the chosen PGPR isolates. Gram staining procedure was also performed according to the Bergy's Manual (Holt 1994).

### Biochemical Characterization

The biochemical characterization of selected PGPR isolates was done according to the methods outlined by Cappuccino & Sherman (2010). Various methods such as IMViC test, catalase, gelatin liquefaction, oxidase, hydrogen sulfide production, etc. were performed.

### Molecular Characterization

**DNA extraction (Biopure™ Kits):** DNA was isolated from the bacterial sample by using Biopure kits for genomic DNA isolation. 16S rRNA gene was amplified using PCR by extracting DNA from a bacterial isolate. The primers used for the amplification of 16S rDNA gene were 16SF Universal 5'-AGAGTTTGA TCCTGGCTCAG-3' and 16SR Universal 3'-ACGGCTACCTTG TTACGA CTT-5'.

**Amplification of 16S rDNA gene:** PCR condition: Initial denaturation was done at 94°C for 5 min; denaturation (35cycles) at 94°C for 60 sec, annealing at 53°C for 45 sec; extension at 72°C for 90 sec and then the final extension at 72°C for 10 min. The amplified PCR products were electrophoresed by using 1% Agarose gel in TAE buffer and visualized by staining with ethidium bromide. PCR product was then purified by washing with sodium acetate and 70% of ethanol and eluted from the gel. Forward and reverse sequencing reactions of PCR amplicon were carried out on the ABI 3730XL sequencer to obtain the sequence. The assembled DNA sequence was then submitted to NCBI and phylogenetic tree was prepared.

## RESULTS AND DISCUSSION

### Morphological and Phenotypic Characterization

Isolate DDI(I)1 showed yellowish-green, small, round and raised colonies (Table 1). The isolate is a Gram negative, rod shaped bacterium.

### Biochemical Characterization

The isolate showed a positive test for citrate utilization, oxidase, nitrate reduction, gelatin liquefaction, glucose fermentation and negative test for indole, methyl red, Vogues Prauskeur reaction and hydrogen sulfide (Table 2). Based on the morphological, phenotypic and biochemical characterization, the isolate DDI(I)1 belongs to *Pseudomonas* genus.

### Molecular Characterization and Phylogeny

**16S rDNA sequencing of PGPR isolate DDI(I)1:** The molecular characterization of the isolate was done by 16S rRNA Gene Sequence Analysis. The 16S rDNA sequencing

Table 1: Morphological and phenotypic characterization of DDI(I)1.

| Characteristics | Reaction | Characteristics | Reaction |
|---|---|---|---|
| Colour | Yellowish green | Odour | None |
| Size | Small | Pigmentation | Yellowish green |
| Shape | Round | Surface | Smooth |
| Elevation | Raised | Gram staining | -ve |
| Margin | Irregular | Shape | Rods |

Table 2: Biochemical characterization of DDI(I)1.

| Biochemical test | Reaction | Biochemical test | Reaction |
|---|---|---|---|
| Indole | - | Oxidase | + |
| Methyl red | - | $H_2S$ | - |
| VP | - | Nitrate reduction | + |
| Citrate | + | Gelatin liquefaction | + |
| Catalase | + | Glucose fermentation | + |

was performed. Selected bacterial 16S rDNA was amplified in full length by PCR using primers, 16SF Universal (AGA GTT TGA TCC TGG CTC AG) and 16SR Universal (ACG GCT ACC TTG TTA CGA CTT). Based on 16S rDNA sequencing data, the isolate DDI(I)1 showed 99% homology with *Pseudomonas fluorescens* strain CB32.

To evaluate the phylogenetic analysis of 16S rDNA sequence, the resulting sequence was compared with the known sequences using the BLAST function of GeneBank in the National Centre Biotechnology information (http://www.ncbi.nlm.nih.gov). Multiple sequence alignments and consensus sequences were computed using the program CLUSTAL W programmed at European Bioinformatics (EBI) site (http://www.ebi.eic.uk/clustalw) and the phylogenetic tree was constructed using MEGA 5.05 software (Fig. 1).

**Sequence**

> GGAATCTGCCTGGATAGTGGGGGATAACGTTCGGAAACGAACGCTAATACCGCATACGTCCTACGGGAGAAAGCAGGGGACCTTCGGGCCTTGCGCTATCAGATGAGCCTAGGTCGGATTAGCTAGTTGGTGAGGTAATGGCTCACCAAGGCGACGATCCGTAACTGGTCTGAGAGGATGATCAGTCACACTGGAACTGAGACACGGTCCAGACTCCTACGGGAGGCAGCAGTGGGGAATATTGGACAATGGGCGAAAGCCTGATCCAGCCATGCCGCGTGTGTGAAGAAGGTCTTCGGATTGTAAAGCACTTTAAGTTGGGAGGAAGGGCAGTTACCTAATACGTAATTGTTTTGACGTTACCGACAGAATAAGCACCGGCTAACTCTGTGCCAGCAGCCGCGGTAATACAGAGGGTGCAAGCGTTAATCGGAATTACTGGGCGTAAAGCGCGCGTAGGTGGTTCGTTAAGTTGGATGTGAAATCCCCGGGCTCAACCTGGGAACTGCATTCAAAACTGTCGAGCTAGAGTATGGTAGAGGGTGGTGGAATTTCCTGTGTAGCGGTGAAATGCGTAGATATAGGAAGGAACACCAGTGGCGAAGGCGACCACCTGGACTGATACTGACACTGAGGTGCGAAAGCGTGGGGAGCAAACAGGATTAGATACCCTGGTAGTCCACGCCGTAAACGATGTCAACTAGCCGTTGGGAGCCTTGAGCTCTTAGTGGCGCAGCTAACGCATTAAGTTGACCGCCTGGGGAGTACGGCCGCAAGGTTAAAACTCAAATGAATTGACGGGGGCCCGCACAAGCGGTGGAGCATGTGGTTTAATTCGAAGCAACGCGAAGAACCTTACCAGGCCTTGACATCCAATGAACTTTCCAGAGATGGATTGGTGCCTTCGGGAGCATTGAGACAGGTGCTGCATGGCTGTCGTCAGCTCGTGTCGTGAGATGTTGGGTTAAGTCCCGTAACGAGCGCAACCCTTGTCCTTAGTTACCAGCACGTTATGGTGGGCACTCTAAGGAGACTGCCGGTGACAAACCGGAGGAAGGTGGGGATGACGTCAAGTCATCATGGCCCTTACGGCCTGGGCTACACACGTGCTACAATGGTCGGTACAGAGGGTTGCCAAGCCG

The given sequence was identified as *Pseudomonas fluorescens* strain 16S ribosomal RNA gene, partial sequence length: 1423

Score: 2109 bits (1142) Identities: 1142/1142(100%) Strand: Plus/Plus

**Phylogenetic analysis**

The phylogenetic analysis revealed that our isolate DDI(I)1 showed 99% homology with *Pseudomonas fluorescens* CB32. In a similar study, a psychrotolerant PGPR strain

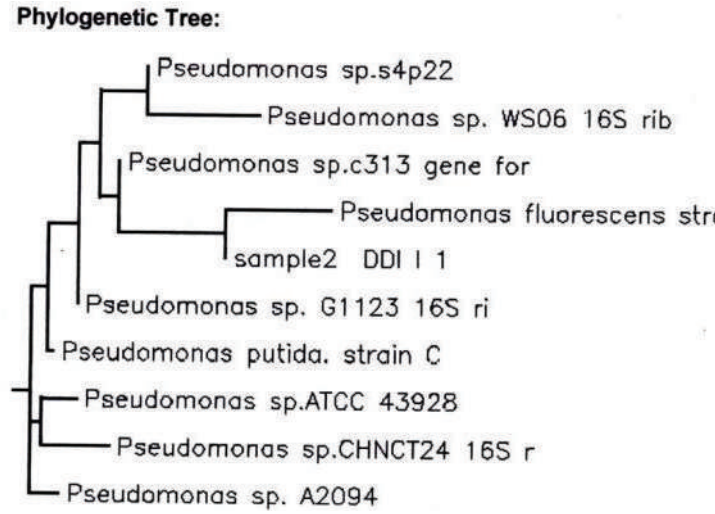


Fig. 1: Phylogenetic tree of DDI(I)1 based on 16S rDNA gene sequences.

PGERs17 was isolated from north-western Indian Himalayas and characterized the isolate which showed maximum homology (99%) with *Pseudomonas* sp. The phylogenetic tree revealed the close association of the isolate with *Pseudomonas vancouverensis* (ATCC 700688), *Pseudomonas alcaligenes* (ATCC 14909), *Pseudomonas tolaasii* (ATCC 33618) and *Pseudomonas agarici* (ATCC 25941) (Mishra et al. 2008). Isolate CV6 was characterized as *Pseudomonas fluorescens* as the potent biocontrol agent against *Phytophthora drechsleri* (Maleki et al. 2010). In another investigation, 10 bacterial isolates (AW1 to AW10) were selected from the wheat rhizosphere. Out of these, AW8 showed 98% homology with *Pseudomonas aeruginosa* (Rana et al. 2011).

## CONCLUSION

This present study suggested that the *P. fluorescens* DDI(I)1 can exhibit multiple plant growth promoting traits such as the production of ammonia, hydrogen cyanide production, siderophore production, solubilization of phosphorus, etc. The *P. fluorescens* DDI(I)1 bacterial strain was also found to exhibit heavy metal tolerance against copper, lead, nickel and zinc. Due to the multiple PGP traits exhibited by rhizospheric isolate, it may be useful as a bio-inoculant in sustainable agriculture.

## REFERENCES


Cappuccino, J.C. and Sherman, N. 2010. In: Microbiology: A Laboratory Manual, 10th Edn., New York. Benjamin/Cummings Pub. Co., pp. 125-179.

Deshwal, V.K., Singh, S.B., Chaubey, A. and Kumar, P. 2013. Isolation and characterization of *Pseudomonas* strains from potatoes rhizosphere at Dehradun valley, India. Int. J. Basic Appl. Sci., 2(2): 53-55.

Glick, B.R. 2012. Plant Growth-Promoting Bacteria: Mechanisms and Applications. Hindawi Publishing Corporation, Scientifica.

Hamid, A. and Ahmad, G. 2010. The effect of seed inoculation (*Pseudomonas putida* + *Bacillus lentus*) and different levels of fertilizer on yield and yield components of wheat (*Tritium aestivum* L.) activities. World Acad. Sci. Eng. Technol., 4: 1369-1373.

Holt, J.G., Krieg, N.R., Sneath, P.H.A., Staley, J.T. and Williams, S.T. 1994. Bergey's Manual of Determinative Bacteriology (ed. 9th). Williams and Wilkins Publishers, Baltimore Maryland, USA., pp. 786-788.

Jacobson, C.B., Pasternak, J.J. and Glick, B.R. 1994. Partial purification and characterization of 1-aminocyclopropane-1-carboxylate deaminase from PGPR, *Pseudomonas putida* GR12-2. Can. J. Microbiol., 40: 1019-1025.

Li, J., Daniel, H., Charles, T.C. and Glick, B.R. 2000. An ACC deaminase minus mutant of *Enterobacter cloacae* UW4 no longer promotes root elongation. Curr. Microbiol., 41: 101-105.

Lynch, J.M. and Whipps, J.M. 1991. Substrate flow in the rhizosphere. In: Keister DL, Cregan PB. (Eds.), The rhizosphere and plant growth. Beltsville Symposia in Agric. Res. vol 14. Springer, Dordrecht, The Netherlands.

Maleki, M., Mostafee, S., Mohammad, L. and Farzenah, M. 2010. Characterization of *Pseudomonas fluorescence* strains CV-6 isolated from cucumber rhizosphere in varamin as a potential biocontrol agent. Aust. J. Crop Sci., 4(9): 676-683.

Mishra, P.K., Mishra, S., Selvakumar, G., Bisht, S.C., Bisht, J.K., Kundu, S. and Gupta, H.S. 2008. Characterisation of a psychrotolerant plant growth promoting *Pseudomonas* sp. strain PGERs17 (MTCC 9000) isolated from north western Indian Himalayas. Ann. Microbiol., 58(4): 561-568.

Penrose, D.M. and Glick, B.R. 2001. Levels of ACC and related compounds in exudates and extracts of canola seeds treated with ACC deaminase-containing plant growth promoting bacteria. Can. J. Microbiol., 47: 368-372.

Probanza, A., Lucas Garcia, J.A., Palomino, M.R., Ramos, B. and Gutierrez Manero, F.J. 2002. *Pinus pinea* L. seedling growth and bacterial rhizosphere structure after inoculation with PGPR Bacillus (*B. licheniformis* CECT 5106 and *B. pumilus* CECT 5105). Appl. Soil Ecol., 20: 75-84.

Rana, A., Saharan, B., Joshi, M., Prasanna, R., Kumar, K. and Nain, L. 2011. Identification of multi-trait PGPR isolates and evaluating their potential as inoculants for wheat. Ann. Microbiol., 61: 893-900.

Reddy, P.K. and Reddy, M.S. 2009. Biochemical and PCR-RAPD characterization of *Pseudomonas fluorescens* produced antifungal compounds inhibit the rice fungal pathogens *in vitro*. J. Pure Appl. Microbiol., 3(1): 1-4.

Rokhzadi, A., Asharzadeh, A., Darvish, F., Nour-Mohammadi, G. and Majidi, E. 2008. Influence of plant growth promoting rhizobacteria on dry matter accumulation of Chickpea (*Cicer arietinum* L) under field conditions. J. Agric. Environ. Sci., 3(2): 253-257.

Saharan, B.S. and Nehra, V. 2011. Plant growth promoting rhizobacteria: A critical review. Life Sci. Med. Res., 21: 1-30.

Saharan, B.S. and Verma, S. 2015. Evaluation of rhizospheric bacteria from *Ocimum* sp. as potential PGPR. J. Microb. Biochem. Technol., 7(2): 088-095.

Shah, S., Li, J., Moffatt, B.A. and Glick, B.R. 1998. Isolation and characterization of ACC deaminase genes from two different plant growth-promoting rhizobacteria. Can. J. Microbiol., 44: 833-843.

Turner, J.T. and Backman, P.A. 1991. Factors relating to peanut yield increases after seed treatment with *Bacillus subtilis*. Plant Dis., 75: 347-353.

Wang, C., Knill, E., Glick, B.R. and Defago, G. 2000. Effect of transferring 1- aminocyclopropane-1-carboxylic acid (ACC) deaminase genes into *Pseudomonas fluorescens* strain CHAO and its gacA derivative CHA96 on their growth-promoting and disease-suppressive capacities. Can. J. Microbiol., 46: 898-907.

Nature Environment and Pollution Technology
An International Quarterly Scientific Journal

p-ISSN: 0972-6268
(Print copies up to 2016)
e-ISSN: 2395-3454

Vol. 19 | No. 4 | pp. 1767-1770 | 2020

Original Research Paper

https://doi.org/10.46488/NEPT.2020.v19i04.050

Open Access Journal

# Water Quality Evaluation by Monitoring Zooplankton Distribution in Wild Ponds, Noakhali, Bangladesh

**Najmus Sakib Khan*†, Md. Saiful Islam*, Jaber Bin Abdul Bari* and Naznin Akter Tisha****

*Department of Oceanography, Noakhali Science & Technology University, Noakhali-3814, Bangladesh

**Department of Fisheries & Marine Science, Noakhali Science & Technology University, Noakhali-3814, Bangladesh

†Corresponding author: Najmus Sakib Khan; nsakib.iium@gmail.com

**Nat. Env. & Poll. Tech.**
**Website: www.neptjournal.com**

*Received:* 11-11-2019
*Revised:* 02-12-2019
*Accepted:* 16-01-2020

**Key Words:**
Zooplankton
Water quality evaluation
Wild ponds
Wetland zooplankton index

## ABSTRACT

Pond water quality was evaluated by identifying and estimating zooplankton during monsoon in Noakhali, Bangladesh. Three wild ponds were chosen for monitoring zooplankton distribution which are not used for fish culture or any other commercial purposes. In this study, the Wetland Zooplankton Index (WZI) was employed to engage the zooplankton genera according to their specific WZI values. Two of the sampling ponds were found to have moderate water quality. Additionally, another pond was found with nearly good water quality. Total zooplankton was observed as 5541.67±176.77 ind/L, 9608.34±271 ind/L and 9541.67±176 ind/L in three different sampling ponds. There were four groups of zooplankton as Rotifera (6 genera), Copepoda (4 genera) and Cladocera (6 genera) identified in all the sampling ponds. The physicochemical water parameters as water temperature, water pH, total alkalinity, free $CO_2$, ammonia, nitrate and nitrite were also evaluated in sampling ponds.

## INTRODUCTION

The earthen ponds are recognized as most traditional living essentials in our society. In the southern part of Bangladesh, the ponds are used for drinking purposes and fish culture. Unfortunately, many household or roadside ponds and seasonal wetlands are not properly treated due to some misconceptions. In many cases, ponds and wetlands are used as local waste depositing points and it is very disastrous for us. The Noakhali district is consecrated with a lot of ponds and wetlands. In Noakhali, ponds and wetlands are used for aquaculture and daily household uses. Therefore, the potentiality of many ponds is deteriorated because of the misuse and mismanagement. Zooplankton are very sensitive to environmental changes in aquatic bodies. The prime environmental factor temperature initiates the growth and survival performance of zooplankton through seasonal change. Aquatic nitrogenous and phosphorus nutrients control the distribution and diversity of zooplankton (Rajkumar et al. 2014). The capability of aquaculture is determined by zooplankton assemblages in a pond. Zooplankton represents themselves as an obvious trophic connecting agents between fishes and phytoplankton. Recently, the biological assessment of water quality by using zooplankton was very well accepted and practised by scientists. Zooplanktons are proficient in quick response to even slight environmental changes (Sládeček 1973, Gannon & Sternberger 1978, Sinha & Sinha 1993, Joseph et al. 2011, Patra et al. 2011) Thus, the Wetland Zooplankton Index (WZI) was designed to evaluate the lake water quality in North America (Lougheed & Chow-Fraser 2002). This index was suggested as a scale from bad (0) to good (5) of water quality.

The present study was attempted to evaluate the contribution of zooplankton as a bioindicator to wild pond water quality.

## MATERIALS AND METHODS

A total of three mistreated wild ponds at Sonapur, Noakhali in Bangladesh were chosen for zooplankton sampling and water quality analysis. These ponds were ignored or not properly used by local people. This study was conducted from July 2018 to September 2018 and aimed at the analysis of the physicochemical water quality (water temperature, total alkalinity, total suspended solids, free $CO_2$, ammonia, nitrate, nitrite and phosphorus) and zooplankton assemblages in these three ponds. The water temperature and pH were measured directly on spot by thermometer and pH meter (HANNA-HI96107) respectively. While conducting the study, the total alkalinity (mg/L), total suspended solids (mg/L), free $CO_2$ (mg/L), ammonia (mg/L), nitrate (mg/L), nitrite (mg/L) and phosphorus (mg/L) were determined according to guidelines from the American Public Health Association (APHA 1995).

Zooplankton were collected from surface water through plankton net (mesh size: 25 µm) and preserved in 250 mL plastic containers with 5 % buffered formalin. Furthermore, zooplankton were observed at 16×10 and 16×40 magnification using a light microscope in a Sedgewick-Rafter counting cell. The density and diversity of zooplankton were determined by following Tonapi (1980) and Battish (1992). For ranking water quality by using zooplankton, Wetland Zooplankton Index: WZI = ČYiTiUi/ČYiTi (Yi = Individual/liter, Ti = Tolerance, Ui = Optimum) was employed (Lougheed & Chow-Fraser 2002).

## RESULTS AND DISCUSSION

The groups of zooplankton as Rotifera, Copepoda and Cladocera were represented with their genera specific abundance (Table 1). There are six genera of Rotifera and Cladocera and four genera of Copepoda listed from three sampling ponds (Table 1, Fig. 1). A total of 5541.67±176.77 ind/L, 9608.34±271 ind/L and 9541.67±176 ind/L of zooplankton were recorded in Pond A, Pond B and Pond C, respectively (Table 1, Fig.1). In the present study, Pond A, Pond B and Pond C were dominated by Cladocera, Copepoda and Rotifera respectively (Fig. 1). Many scientists have observed the density and distribution of zooplankton in wild, fish culture, seasonal and unused ponds. Hossain et al. (2015) reported Rotifera (6 genera), Cladocera (3 genera), Crustacean (3 genera) and Copepoda (2 genera) in different cultures, households and unused ponds. The groups of zooplankton as Rotifera, Crustacea, Cladocera were also studied by (Morris & Mischke 1999, Beaugrand et al. 2000, Mahar et al. 2000, Begum et al. 2007, Dirican et al. 2009, Jakhar 2013, Saha et al. 2017, Khan & Bari 2019). Wetland zooplankton index (WZI) was established as a water quality indicator by monitoring zooplankton distribution (Lougheed & Chow-Fraser 2002). In the present study, Pond A and Pond B were found with moderate water quality (Table 1). Furthermore, Pond C was found to have nearly good water quality (Table 1). Khalifa et al. (2015) studied the seasonal water quality of different lakes and found spring water quality is better than other seasons followed by autumn, winter and summer.

Table 1: Spatial distribution and wetland zooplankton index (Lougheed & Chow-Fraser 2002) of zooplankton during sampling periods.

| Zooplankton | Pond A Yi (ind/L) | Pond B Yi (ind/L) | Pond C Yi (ind/L) | Optimum Ui | Tolerance Ti |
|---|---|---|---|---|---|
| **Rotifera** | - | - | - | - | - |
| *Amuraeopsis* | - | 666.67 | 791.67 | 3 | 1 |
| *Ascomarpha* | - | 1166.67 | - | 1 | 1 |
| *Brachionus* | 500.00 | 666.67 | - | 2 | 1 |
| *Lepadella* | - | 1125.00 | - | 4 | 2 |
| *Plationus* | 958.34 | - | - | - | - |
| *Polyarthura* | - | 958.34 | 541.67 | 3 | 1 |
| **Copepoda** | - | - | - | - | - |
| *Heliodiaptomus* | 791.67 | - | 1208.34 | - | - |
| *Mesocyclops* | - | - | 1458.34 | - | - |
| *Neodiaptomus* | 1208.34 | - | 958.34 | - | - |
| *Thermocyclops* | 958.34 | 958.04 | 958.34 | - | - |
| **Cladocera** | - | - | - | - | - |
| *Alona* | - | 1125.00 | - | - | - |
| *Alonella* | 666.67 | 1458.34 | - | - | - |
| *Chydorus* | 458.34 | - | 666.67 | 4 | 2 |
| *Macrothrix* | | 1458.34 | 1041.67 | 5 | 3 |
| *Scapholeberis* | - | - | 958.34 | - | - |
| *Sinocephalus* | - | - | 958.34 | 5 | 3 |
| Total Zooplankton (Average ± Standard Error) | 5541.67±176 | 9608.34±271 | 9541.67±176 | | |
| WZI (Scale: 0-5) = ČYiTiUi/ČYiTi | 3.29 | 3.79 | 4.54 | | |
| Water Quality | Moderate | Moderate | Nearly good | | |

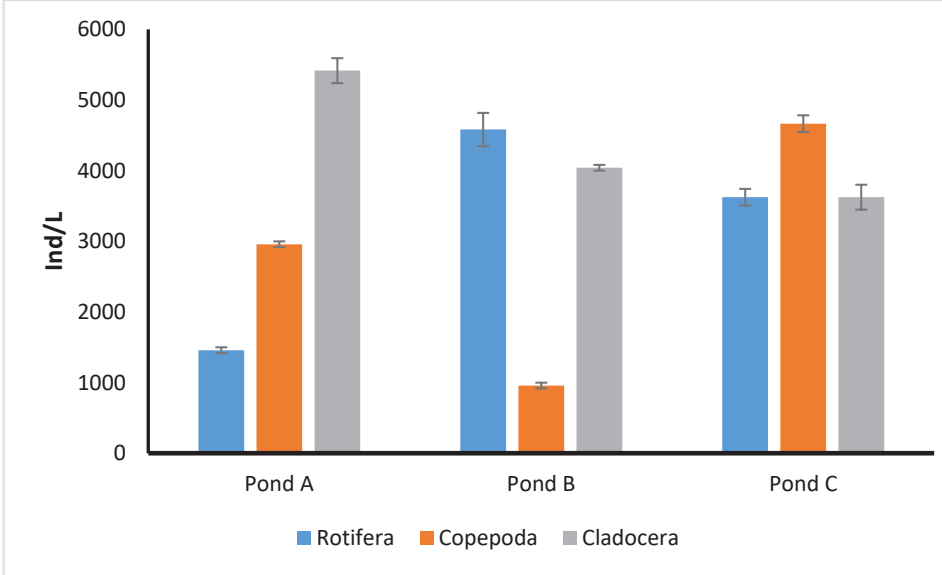


Fig.1: Group-wise zooplankton distribution in sampling ponds.

Several important physicochemical water quality parameters were also estimated in all the sampling ponds (Table 2). In the present study, the temperature was recorded from 29.05 to 30.03°C. The water temperature is the most important factor in the zooplankton distribution and diversity in ponds (Wetzel & Likens 2000). The fertility of pond water is indicated by pH (Sreenivasan 1976). The pH range (7.4-8.2) specifies the well buffering of water quality in sampling ponds which is favourable to the zooplankton growth. The total alkalinity and free $CO_2$ were recorded as 9.00- 18.16 mg/L and 4.90-12.05 mg/L respectively (Table 2). Rotifers showed a negative relationship with total alkalinity in fish culture ponds (Khan & Bari 2019). The water quality parameters recorded in this study were in agreement with many workers (Hegde & Bharti 1985, Boyd & Tucker 1998, Pulle & Khan 2003, Chowdhury & Mamun 2006, Joseph & Yamakanamardi 2011, Rashed-un-Nabi et al. 2011, Khan et al. 2020, Khan et al. 2019, Khan & Islam 2019, Waseeh et al. 2020).

The present study also focussed on to estimate dissolved phosphorus, dissolved inorganic nitrogen composed of ammonia ($NH_3$), nitrite ($NO_2$) and nitrate ($NO_3$) in the sampling ponds. The pond water quality was ranked with the concentrations of ammonia, nitrate, nitrite and phosphorus according to (Sládeček 1973) as in Table 3. In this study, all sampling ponds were found with moderate to poor water quality (Table 3).

Table 2: Physicochemical water quality of sampling ponds.

| Water Quality Parameters | Pond A | Pond B | Pond C |
|---|---|---|---|
| Temperature (°C) | 29.05-30.01 | 29.06-30.03 | 29.05-30.01 |
| pH | 8.1-8.2 | 7.4-7.6 | 7.8-8 |
| Total Alkalinity | 18.00-18.16 | 9.00-9.08 | 13.50-13.62 |
| $FCO_2$ | 11.09-12.05 | 4.90-7.99 | 7.99-8.05 |

Table 3: Dissolved inorganic nitrogen and phosphorus of sampling ponds.

| Water Quality Parameters | Pond A | Pond B | Pond C |
|---|---|---|---|
| $NH_4$ (mg/L) | 0.7-0.9 | 0.8-1.0 | 0.4-0.6 |
| Nitrate (mg/L) | 0.08-0.1 | 0.03-0.05 | 0.04-0.05 |
| Nitrite (mg/L) | 0.05 | 0.05 | 0.05 |
| $PO_4$ (mg/L) | 0.09-0.10 | 0.10-0.13 | 0.08-0.11 |
| Water quality rank (Sládeček 1973) | Moderate to Poor | Moderate to Poor | Moderate to Poor |

The chemical water quality determines the favourable conditions for life survival in ponds, lakes, rivers or any aquatic body (Khalifa et al. 2015). The chemical components of water, to evaluate the suitability of aquatic ecosystems, were studied by Fisher et al. (2008), Heikal (2010), Patra et al. (2011) and Belal (2012).

## CONCLUSION

This study was conducted to inaugurate preliminary water quality of wild ponds in Noakhali by using zooplankton as a bioindicator. The findings of this base study will be used for further comprehensive research on zooplankton distribution and physicochemical properties of water in freshwater wetlands.

## REFERENCES


APHA 1995. Standard Methods for the Examination of Water and Wastewater. American Public Health Association, Washington DC, USA, 19th Edition.

Battish, S.K. 1992. Freshwater Zooplankton of India. Oxford and IBH Publishing Co., New Delhi, 235.

Beaugrand, G.F., Ibanez, P.C. and Reid. 2000. Spatial, seasonal and long-term fluctuations of plankton in relation to hydroclimatic features in the English Channel, Celtic Sea and Bay of Biscay. Mar. Ecol. Prog. Ser., 93-102.

Begum, M., Hossain, M.Y., Wahab, M.A., Ahmed, Z.F., Alam, M.J. and Shah, M.M.R. 2007. Effects of iso-nutrient fertilization on plankton production in earthen ponds of Bangladesh. Pakistan Journal of Biological Sciences., 1221-1228.

Belal, D.M.H. 2012. Epipelic Diatoms as a Tool for Monitoring Pollution in River Nile from Aswan to Cairo. M.Sc. Thesis. Fac. Sci. Zagazig Univ., Egypt, pp. 109.

Boyd, C.E. and Tucker, C.S. 1998. Pond Aquaculture Water Quality Management. Kluwer Academic Publishers, Boston.

Chowdhury, A.H. and Mamun, A.A. 2006. Physio-chemical Conditions and plankton population of two fish ponds in Khulna. University Journal of Zoology, 25: 41-44.

Dirican, S., Musul, H. and Cilek, S. 2009. Some physico-chemical characteristics and rotifers of Camligoze Dam Lake, Susehri, Sivas, Turkey. Journal of Animal and Veterinary Advances, 8(4).

Fisher, M.R. and Williams W.P. 2008. The development of a biotic pollution index for the River Nile in Egypt. Hydrobiologia, 598: 17-34.

Gannon, J.E. and Sternberger, R.S. 1978. Zooplankton (especially crustaceans and rotifers) as indicators of water quality. Transactions of the American Microscopical Society, 97(1): 16-35.

Hegde, G.R. and Bharti, S.G. 1985. Comparative phytoplankton ecology of freshwater ponds and lakes of Dharwad, Karnataka State, India. In: Propc. Nat. Symp. Pure and Appl. Limnology (Ed.), 32: 24-29.

Heikal, M.T. 2010. Impact of water level fluctuation on water quality and trophic state of Lake Nasser and its Khors, Egypt. Egyptian Journal of Aquatic Biology & Fish., 14(1): 75-86.

Hossain, S., Rahman, M.M., Akter, M. and Bhowmik, S. 2015. Species composition and abundance of zooplankton population in freshwater pond of Noakhali district, Bangladesh. World Journal of Fish and Marine Sciences, 7(5): 387-393.

Jakhar, P. 2013. Role of phytoplankton and zooplankton as health indicators of aquatic ecosystem: A review. International Journal of Innovative Research & Studies, 2(12): 490-500.

Joseph, B. and Yamakanamardi, S.M. 2011. Monthly changes in the abundance and biomass of zooplankton and water quality parameters in Kukkarahalli Lake of Mysore, India. Journal of Environment Biology, 32: 551-557.

Khalifa, N., El-Damhogy, K.A., Fisher, M.R., Nasef, A.M. and Hegab, M.H. 2015. Using zooplankton in some environmental biotic indices to assess water quality of lake Nasser, Egypt. International Journal of Fisheries and Aquatic Studies, 2(4): 281-289.

Khan, N.S., Islam, M.S., Bari, J.B.A., Kamal, M.M. 2020. Monsoonal plankton distribution and physico-chemical water qualities in a rain-fed lake in Noakhali, Bangladesh. Bangladesh Journal of Fisheries, 32 (1): 179-184.

Khan, N.S. and Bari, J.B.A. 2019. The effects of physico-chemical parameters on plankton distribution in poultry manure and artificial formulated feed treated fish ponds, Noakhali, Bangladesh. International Journal of Fisheries & Aquatic Studies, 7(5): 01-07.

Khan, N.S. and Islam, M.S. 2019. State the organic pollution level in rain-fed ponds, Noakhali, Bangladesh. International Journal of Fisheries & Aquatic Studies, 7(5): 438-441.

Khan, N.S., Uddin, A., Bari. J.B.A. and Tisha, N.A. 2019. Evaluation the potentiality of ancient ponds by Palmer's algal pollution index, Noakhali, Bangladesh. International Journal of Fisheries and Aquatic Research, 4(4): 28-38.

Lougheed, V.L. and Chow-Fraser 2002. Development and use of zooplankton index of wetland quality in the Laurentian Great Lakes Basin. Ecological Applications, 12 (2): 474-486.

Mahar, M.A., Baloch, W.A. and Jafri, S.I.H. 2000. Diversity and seasonal occurrence of planktonic rotifers in Manchhar Lake, Sindh Pakistan. Pakistan J. Fish, 1: 25-32.

Morris, J.E. and Mischke, C.C. 1999. Plankton Management for Fish Culture Ponds. NCRAC Technical Bulletins.

Patra, A., Santra, K.B. and Manna, C.K. 2011. Ecology and diversity of zooplankton in relation to physico-chemical characteristics of water of Santragachi Jheel, West Bengal. Indian Journal of Wet Ecology, 5: 20-39.

Pulle, J.S. and Khan, A.M. 2003. Phytoplanktonic study of Isapur dam water. Eco. Env. Cons., 9: 403-406.

Rajkumar, M., Sun, J., Jenkinson, I.R. and Rahman, M.M. 2014. Seasonal variation in the structure of copepod assemblages in tropical marine and estuarine waters, Coleroon, Southeast India. Journal of the Marine Biological Association of the United Kingdom, 94(3): 521-533.

Rashed-un-Nabi, M., Mamun, A.A., Hedayetullah, M. and Mustafa, M.G. 2011. Temporal and spatial distribution of fish and shrimp assemblage in the Bakkhali river estuary of Bangladesh in relation to some water quality parameters. Marine Biology Research, 7(5): 436-452.

Saha, S., Goswami, S.N., Trivedi, R.K., Mandal, A. and Jana, S. 2017. A study of plankton diversity of three urban ponds in Kolkata of West Bengal State, India. International Journal of Advanced Biological Research, 7(44): 687-691.

Sinha, K.K. and Sinha, D.K. 1993. Seasonal Trends in physico-chemical factors and zooplankton in a fresh water pond of Munger, Bihar. J. Ecobiol., 5: 299-302.

Sládeček, V. 1973. System of water quality from the biological point of view. Arch. Biol. Beih. Ergeb. Limnol., 7: 1-218.

Sreenivasan, A. 1976. Limnological studies and primary production in temple pond ecosystem. Hydrobiologia, 48: 117-123.

Tonapi, G.T. 1980. Freshwater Biology. National Book Trust of India, New Delhi, pp. 341.

Waseeh, M.A., Rahman, A.A., Khan, N.S. 2020. Effects of artificial food additives in Vietnam Koi, *Anabus testudineus* (Bloch, 1792) pond culture system. International Journal of Fisheries and Aquatic Research, 5 (3): 50-54.

Wetzel, R.G. and Likens, G.E. 2000. The heat budget of lakes. In: Limnological Analyses, pp. 56-45, Springer, New York, NY.

Nature Environment and Pollution Technology
An International Quarterly Scientific Journal

p-ISSN: 0972-6268
(Print copies up to 2016)
e-ISSN: 2395-3454

Vol. 19 | No. 4 | pp. 1771-1774 | 2020

Original Research Paper

https://doi.org/10.46488/NEPT.2020.v19i04.051

Open Access Journal

# Geoelectrical Variations in Residential Area of Ojongbodu, Oyo, Southwestern Nigeria

**T.A. Adagunodo*† and O.P. Oladejo****
*Department of Physics, Covenant University, Ota, Nigeria
**Department of Physics, Emmanuel Alayande College of Education, Oyo, Nigeria
†Corresponding author: T.A. Adagunodo; theophilus.adagunodo@covenantuniversity.edu.ng

**Nat. Env. & Poll. Tech.**
**Website: www.neptjournal.com**

*Received:* 09-11-2019
*Revised:* 03-12-2019
*Accepted:* 16-01-2020

**Key Words:**
Geoelectrical variations
Lithological variations
Residential area
Structural failure

## ABSTRACT

This study is aimed at mapping the geoelectrical variations in the residential area of Ojongbodu, Oyo, Nigeria. Thirty vertical electrical sounding stations were occupying across the study area using PZ-02 Earth resistivity meter. Four subsurface layers involving topsoil, two weathered layers and bedrock were mapped, with clay being the most dominating soil type in the third layer, which is about 3.9 m below the first two layers. The thickness of the third layer itself is about 10.4 m. About 70% of the bedrock is fractured. The thickness of clay in the third layer cum fractured bedrock could aid development of differential settlements in buildings or total collapse of structures within the study area.

## INTRODUCTION

One of the human physiological needs on earth is shelter or building. It protects the man from the local environment and gives one feeling of well-being. Structures can be used for commercial, residential, industrial, institutional, entertainment and religious purposes. Unfortunately, a building that supposes to satisfy human's need has become worrisome to man as a result of its failure. The two causes of building failure, as identified by Sunmonu (2018) are structural and cosmetic failures. Structural failure occurs when addition or subtraction of material is made to the building, which affects both its stability and outlook. Cosmetic failure occurs when the effect is only on the outlook of the building. In other words, the building is considered to have failed when it could no longer fulfil its functions and be relied upon for safety again.

The alarming rate of building collapses in Nigeria today is very high (Sunmonu 2018). Most people believed that these collapses are due to usage of substandard material without considering the lithological variations. Electrical resistivity (ER) method has been a proven and reliable tool in the assessment of near-surface structures for civil engineering purpose (Olatinsu et al. 2018). It is considered as the best in comparison to the geotechnical investigation, because of its ability to produce 3-D subsurface imaging and its cost (Adewoyin et al. 2017).

In this study, the ER method involving Schlumberger array was used to determine the geoelectrical variations of each delineated lithology in the residential area of Ojongbodu, Oyo, Nigeria. This study aims to characterize the geoelectrical sequence of the study area, to map out the thickness of clayey zone to determine its civil engineering worthiness. Structural failure is not only peculiar to Nigeria, but it has also become a global concern. Some of the structural failure incidences across the globe have been documented in Omenihu et al. (2016), Sunmonu (2018), and Wikipedia-Structural Failure (2019). Among numerous studies that have employed geophysical approach for civil engineering investigations include Adewoyin et al. (2017), Adagunodo et al. (2018), and Olatinsu et al. (2018).

Nigeria is on the Pan-African mobile belt, which is an integral of the remobilized basement rocks of West Africa. The two major geological formations that spread in equal proportion are the sedimentary Basins (Upper Cretaceous in age) (Bayowa et al. 2019, Joel et al. 2019, Usikalu et al. 2018) and Basement rocks (Precambrian in age) (Olafisoye et al. 2012, Oladejo et al. 2013, Orosun et al. 2019). The study area resides over the Basement complex rocks of southwestern Nigeria (Fig.1). These Basement rocks are either igneous or metamorphic. Locally, some of the available rocks around the study area include older granite, quartzites, marble, laterites, and quartzofeldspathic biotite schists (Adagunodo et al. 2018).

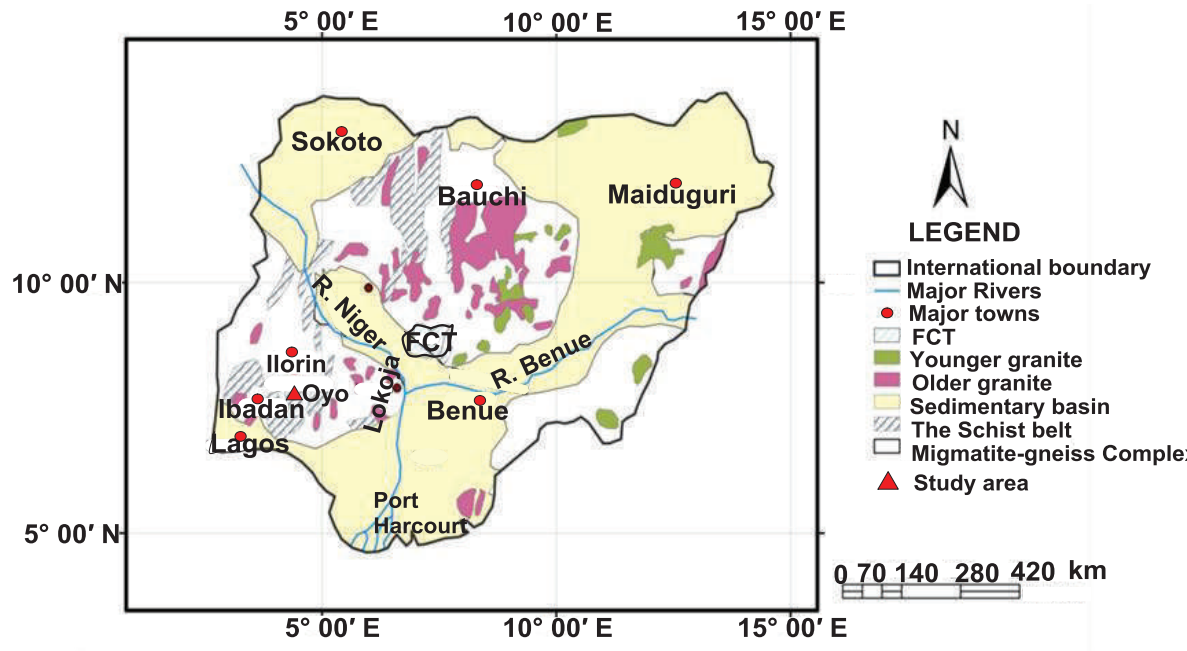


Fig. 1: Geological domains of Nigeria (Adapted from Adagunodo et al. 2019).

## MATERIALS AND METHODS

A PZ-02 Earth meter was used to acquire Vertical Electrical Sounding (VES) data from thirty different stations in the study area (Fig. 2). The field data acquisition was randomly collected to cover the study area, which is bounded by latitude 07°50'00" to 07°52'12" north and longitude 03°54'51" to 03°56'00" east. The apparent resistivity ($\rho_a$) was determined through the product of the measured resistance and the geometric factor (which is a function of the spacing of the electrode array used) as documented by Koefoed (1979). Partial curve matching involving the plot of apparent resistivity against the current electrode spacing was used to produce the first field thickness and resistivity of each layer (first layer parameters). An automated approach known as WinResist was used to produce the final layers parameters (from the field data and the first layer parameters), which are capable of revealing the geoelectrical sequences of the study area.

## RESULTS AND DISCUSSION

The geoelectrical parameters of each layer are revealed in Fig. 3. According to the classifications of Koefoed (1979), and Sunmonu et al. (2015), maximum of four subsurface layers were mapped. The prominent constituents of the topsoil in the study area are clay and laterites. These two soil types transcend to the second layer with the identification of the weathered layer, which could be interpreted as either sandy clay or clayey sand. In the third layer, about 65% of this layer is composed of clay, while the southern region is composed of weathered layer and compacted sands. The fourth layer constitutes the bedrock, which is composed of either fractured or fresh bedrock. About 70% of the study area is underlain by fractured bedrock, an indicative of incompetent location for the construction of mega structures. The mean thicknesses of topsoil, second and third layers are 1.3, 2.6 and 10.4 m, respectively. Clay is composed of minuscule particles that depict hard rock-like when dry, and a sticky mixture when wet. This property enables clay to swell and shrink during the rainy and dry seasons, respectively. The thickness of clay in the third layer could aid development of differential settlements in buildings or total collapse of structures within the study area. In order not to compromise the integrity of building foundations in the study area, mats are recommended for the construction of conventional shallow foundations. However, deep foundations such as piles or caissons are recommended for the construction of mega structures. This will enable the load of the buildings not to be transmitted directly on the clayey zone, which could result in vertical movement of the foundations during seasonal variations.

## CONCLUSION

This study has been able to reveal the heterogeneous nature of subsurface. Four layers that were delineated in the study area are topsoil, second and third layers, as well as the

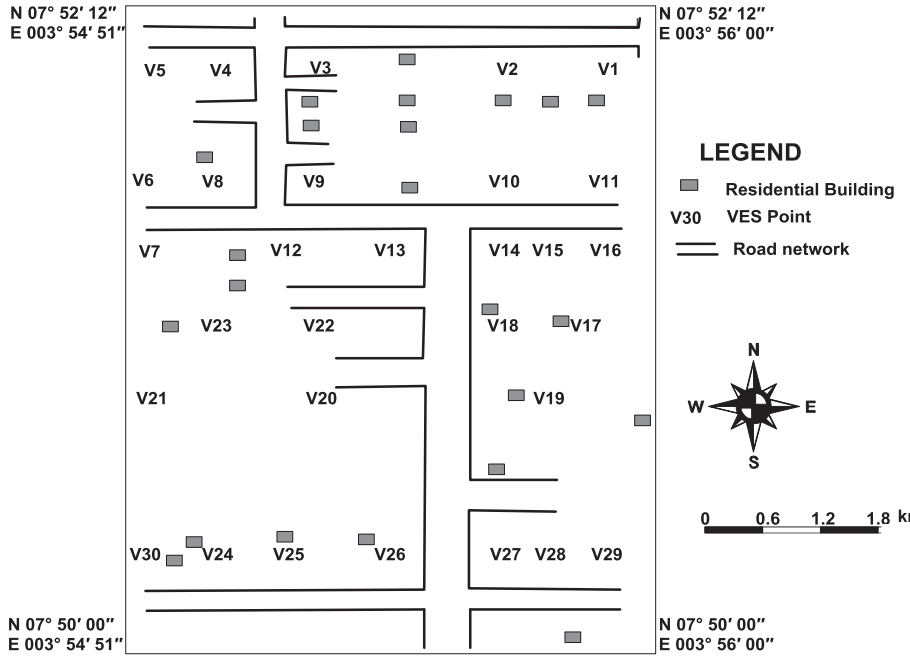


Fig. 2: VES stations within the study area.

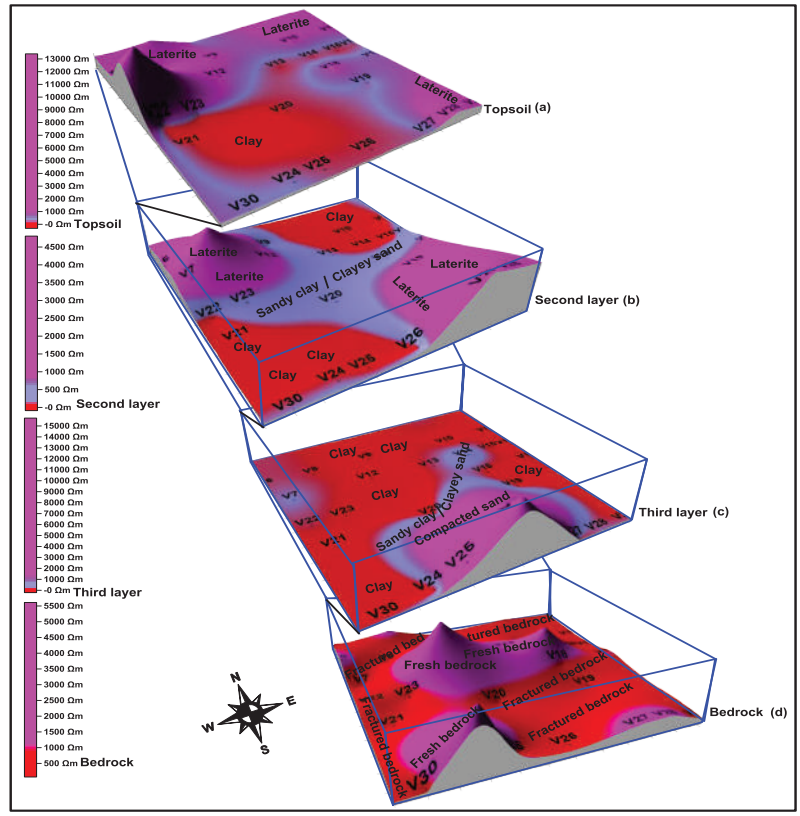


Fig. 3: Geoelectrical variations across each layer in the study area.

bedrock. Thick clay constitutes the third layer, while about 70% of the bedrock is fractured. Geoelectrical sequences in the study area have shown that competent hands (that is, certified builders) are only worthy of constructing buildings in the residential area of Ojongbodu, Oyo, Nigeria.

## ACKNOWLEDGEMENT

Partial support from Covenant University, Nigeria is appreciated.

## REFERENCES

Adagunodo, T.A., Sunmonu, L.A., Oladejo, O.P., Hammed, O.S., Oyeyemi, K.D. and Kayode, O.T. 2018. Site characterization of Ayetorohousing scheme, Oyo, Nigeria. IOP Conference Series: Earth and Environmental Science, 173: 012031.

Adagunodo, T.A., Sunmonu, L.A., Oladejo, O.P. and Olanrewaju, A.M. 2019. Characterization of soil stability to withstand erection of high-rise structure using electrical resistivity tomography. In: Kallel A. et al. (eds.). Recent Advances in Geo-Environmental Engineering, Geomechanics and Geotechnics, and Geohazards. Advances in Science, Technology and Innovation (IEREK Interdisciplinary Series for Sustainable Development).

Adewoyin, O.O., Joshua, E.O., Akinwumi, I.I., Omeje, M. and Joel, E.S. 2017. Evaluation of geotechnical parameters using geophysical data. J. Eng. Technol. Sci., 49(1): 95-113.

Bayowa, O.G., Adagunodo, T.A. and Oyedara, I.I. 2019. Reservoir classification and petrophysical evaluation of "BAO" Field, Niger Delta. Petroleum and Coal, 61(5): 1112- 1119.

Joel, E.S., Olasehinde, P.I., Adagunodo, T.A., Omeje, M., Akinyemi, M.L. and Ojo, J.S. 2019. Integration of aeromagnetic and electrical resistivity imaging for groundwater potential assessment of coastal plain sands area of Ado-Odo/Ota in Southwest Nigeria. Groundwater for Sustainable Development, 9: 100264.

Koefoed, O. 1979. Geosounding Principles, I. Resistivity Sounding Measurements. Elsevier Scientific Publishing, Comp. Amsterdam.

Oladejo, O.P., Sunmonu, L.A., Ojoawo, A., Adagunodo, T.A. and Olafisoye, E.R. 2013. Geophysical investigation for groundwater development at Oyo State Housing Estate Ogbomosho, Southwestern Nigeria. Research Journal of Applied Sciences, Engineering and Technology, 5(5): 1811-1815.

Olafisoye, E.R., Sunmonu, L.A., Ojoawo, A., Adagunodo, T.A. and Oladejo, O.P. 2012. Application of very low frequency electromagnetic and hydro-physicochemical methods in the investigation of groundwater contamination at Aarada waste disposal site, Ogbomoso, Southwestern Nigeria. Australian Journal of Basic and Applied Sciences, 6(8): 401-409.

Olatinsu, O.B., Oyedele, K.F. and Ige-Adeyeye, A.A. 2018. Electrical resistivity mapping as a tool for post-reclamation assessment of subsurface condition at a sand-filled site in Lagos, Southwestern Nigeria. SN Applied Sciences, 1:24.

Omenihu, F.C., Onundi, L.O. and Alkali, M.A. 2016. An analysis of building collapse in Nigeria (1971-2016): Challenges for Stakeholders. Annals of Borno, XXVI: 113-140.

Orosun, M.M., Usikalu, M.R., Oyewumi, K.J. and Adagunodo, T.A. 2019. Natural radionuclides and radiological risk assessment of granite mining field in Asa, North-Central Nigeria. MethodsX, 6C: 2504-2514.

Sunmonu, L.A. 2018. The good and the bad of faults: A geophysical perspective. Inaugural Lecture Series 25. Ladoke Akintola University of Technology, Nigeria. ISBN: 978-2902-82-9.

Sunmonu, L.A., Adagunodo, T.A., Adeniji, A.A., Oladejo, O.P. and Alagbe, O.A. 2015. Geoelectric delineation of aquifer pattern in crystalline bedrock. Open Transactions on Geosciences, 2(1): 1-16.

Usikalu, M.R., Oderinde, A., Adagunodo, T.A. and Akinpelu, A. 2018. Radioactivity concentration and dose assessment of soil samples in cement factory and environs in Ogun State, Nigeria. International Journal of Civil Engineering and Technology, 9(9): 1047-1059.

Wikipedia-Structural Failure, 2019. List of structural failures and collapses. Retrieved on July 6, 2019.

*... Continued from inner front cover*

- The text of the manuscript should run into **Abstract, Introduction, Materials & Methods, Results, Discussion, Acknowledgement** (if any) and **References** or other suitable headings in case of reviews and theoretically oriented papers. However, short communication can be submitted in running with **Abstract and References.** The references should be in full with the title of the paper.
- The figures should preferably be made on a computer with high resolution and should be capable of withstanding a reasonable reduction with the legends provided separately outside the figures. Photographs may be black and white or colour.
- Tables should be typed separately bearing a short title, preferably in vertical form. They should be of a size, which could easily be accommodated in the page of the Journal.
- References in the text should be cited by the authors' surname and year. In case of more than one reference of the same author in the same year, add suffix a,b,c,.... to the year. For example: (Thomas 1969, Mass 1973a, 1973b, Madony et al. 1990, Abasi & Soni 1991).

## List of References

The references cited in the text should be arranged alphabetically by authors' surname in the following manner: (Note: The titles of the papers should be in running 'sentence case', while the titles of the books, reports, theses, journals, etc. should be in 'title case' with all words starting with CAPITAL letter.)

Dutta, A. and Chaudhury, M. 1991. Removal of arsenic from groundwater by lime softening with powdered coal additive. J. Water Supply Res. Techno. Aqua., 40(1) : 25-29.

Hammer, D.A. (ed.) 1989. Constructed Wetlands for Wastewater Treatment-Municipal, Industrial and Agricultural. Lewis Publishers Inc., pp. 831.

Haynes, R. J. 1986. Surface mining and wetland reclamation. In: Harper, J. and Plass, B. (eds.) New Horizons for Mined Land Reclamation. Proceedings of a National Meeting of the American Society for Surface Reclamation, Princeton, W.V.

## Submission of Papers

- The paper can be submitted by e-mail as an attachment in a single WORD file at **contact@neptjournal.com**
- The paper can also be submitted online in a single WORD file through the journal's website: **www.neptjournal.com**

## Attention

1. Any change in the authors' affiliation may please be notified at the earliest.
2. Please make all the correspondence by e-mail, and authors should always quote the manuscript number.

**Note:** In order to speed up the publication, authors are requested to send the publication charges as soon as they get the 'initial acceptance' letter, and also correct the galley proof immediately after receipt. The galley proof must be checked with utmost care, as publishers owe no responsibility for mistakes. The papers will be put on priority for publication only after receiving the processing and publication charges.

# Nature Environment and Pollution Technology

**(Abbreviation: Nat. Env. Poll. Tech.)**

**(An International Quarterly Scientific Journal)**

Published by

**Technoscience Publications**

A-504, Bliss Avenue, Opp. SKP Campus

Balewadi, Pune-411 045, Maharashtra, India

In association with

**Technoscience Knowledge Communications**

Mira Road, Mumbai, India


For further details of the Journal please visit the website. All the papers published on a particular subject/topic or by any particular author in the journal can be searched and accessed by typing a keyword or name of the author in the 'Search' option on the Home page of the website. All the papers containing that keyword or author will be shown on the home page from where they can be directly downloaded.

**www.neptjournal.com**




Published for Proprietor, Printer and Publisher: Mrs. T. P. Goel, B-34, Dev Nagar, Tonk Road, Jaipur, Rajasthan, India; Editors: Dr. P. K. Goel and Prof. K. P. Sharma